PHYSICAL REVIEW

A journal of experimental and theoretical physics established by E. L. Nichols in 1893

Published by the American Institute of Physics for the

AMERICAN PHYSICAL SOCIETY

Officers

President

R. T. Birge
University of California
Berkeley, California

Vice-President

E. P. Wigner
Princeton University
Princeton, New Jersey

Secretary

K. K. Darrow
Bell Telephone Laboratories
Office:
Columbia University
New York 27, New York

Treasurer

G. B. Pegram
Columbia University
New York 27, New York

Local Secretary
for the Pacific Coast

William A. Nierenberg
University of California
Berkeley, California

Managing Editor

S. A. Goudsmit
Brookhaven National Laboratory
Upton, Long Island
New York

Editor

S. A. Goudsmit

1955–1956

W. A. Fowler
Kenneth Greisen
Charles Kittel
R. E. Marshak
W. K. H. Panofsky
V. F. Weisskopf

Manuscripts for publication should be submitted to the Brookhaven National Laboratory, Upton, Long Island, New York. Authors' institutions are requested to defray a publication charge of $10 per page which, if honored, entitles each author to 100 free reprints. Reprints must be sent with galley proofs.

Proof and all correspondence concerning papers in the process of publication should be addressed to the Publication Manager, American Institute of Physics, 57 East 55 Street, New York 22, New York.

Publication Price

United States and Canada . . . . . $

Elsewhere . . . . . $

Back Volumes[1]

Forty-four complete volumes of the *Physical Review* are available

Prior to 1913 . . . . . $

Thereafter . . . . . $

Single copies: $0.60 each, prior to 1913;

$1.50 each, January, 1913–December, 1944;

$0.60 each, January, 1945–December, 1946;

$1.50 each, thereafter.

General Index, 1913–1920: $3.00

1921–1930: $4.00 (Subscribers); $5.00 (Others)

1931–1940: $5.00 (Subscribers); $6.00 (Others)

Subscriptions, business and editorial communications should be addressed to the American Institute of Physics, 57 East 55 Street, New York 22, New York.

Changes of address for the *Physical Review* and *Review of Scientific Instruments* should be addressed to the Circulation Department, American Institute of Physics.

[1] For Bound Volumes of *Physical Review*, *Review of Scientific Instruments*, Publication

The Physical Review is published each [illegible] at Easton, Pennsylvania.

Entered as second-class matter March 4, 1921, at the Post Office at Lancaster, Pa., under the Act of March 3, 1879.

Acceptance for mailing at special rate of postage provided for in paragraph (d-2), section 34.40, P. L. and R., of 1948, authorized [illegible]

Copyright © 1955 by the American Physical Society

THE
PHYSICAL REVIEW

A journal of experimental and theoretical physics established by E. L. Nichols in 1893

SECOND SERIES, VOL. 100, NO. 6 DECEMBER 15, 1955

Double Scattering of Electrons with Magnetic Interaction. II. Depolarization*

H. MENDLOWITZ† AND K. M. CASE
H. M. Randall Laboratory of Physics, University of Michigan, Ann Arbor, Michigan
(Received September 2, 1955)

The depolarization occurring in attempts to measure the electron's gyromagnetic ratio by double-scattering experiments in a magnetic field is discussed. Formulas are found for the effects expected to be most significant. These are applied to estimate the possible accuracy obtainable. One part in 10^3 seems to be quite feasible. In addition, formulas are appended which permit rapid estimation of other depolarization effects.

I. INTRODUCTION

IN a previous paper[1] the change in asymmetry produced by a magnetic field acting between the two targets in a double scattering of electrons was discussed. The magnetic field was idealized as being perfectly homogeneous. It is, however, necessary to consider the effects of small inhomogenities in the constant magnetic field. These will tend to depolarize the beam of electrons coming from the first target and thus decrease the asymmetry to be found after a second scattering. If all particles take the same path, variations in the magnetic field will not cause depolarization. The polarization vector will merely be rotated. Depolarization occurs only when particles take different paths through the field.

In the following, the state of polarization will be discussed in terms of the field and orbit parameters. For simplicity we restrict ourselves to the case where the constant magnetic field is oriented along the plane determined by the incident beam and first scattered beam but perpendicular to the direction of the first scattered beam. Thus, the beam executes cyclotron-like motion between the two targets. This corresponds to case (2) discussed in I. The other case in I corresponds to the experiment of Louisell, Pidd, and Crane[2]; for those experimental conditions the time the particles spend in the field is short[3] so that depolarization is negligible.

In the situation to be considered there is a magnetic field that is essentially constant in the z-direction. The small radial decrease of the field is described by the index $n(0<n<1)$. In such a field a charged particle executes small oscillations about an equilibrium cyclotron orbit in the plane perpendicular to the z-direction. The frequencies of the radial and axial oscillations about the equilibrium orbit are[4]

$$\omega_r=\omega_L(1-n)^{\frac{1}{2}}, \tag{1}$$

and

$$\omega_a=\omega_L n^{\frac{1}{2}}, \tag{2}$$

where ω_r, ω_a are the radial and axial frequencies respectively. ω_L is the Larmor frequency

$$\omega_L=e\mathcal{H}_0(1-\beta^2)^{\frac{1}{2}}/(m_0c). \tag{3}$$

($\mathcal{H}_0$ is the magnitude of the field along the orbit axis.)

II. DEPOLARIZATION

In considering the depolarization of the beam due to small oscillations about the equilibrium orbit, the particles will be considered as Dirac particles and the effects of the anomalous moment will be neglected. The depolarization effects of the radial oscillations and oscillations perpendicular to the plane of the equilibrium orbit will be considered separately. It is demonstrated that the depolarization arising from the radial oscillations is small and independent of the number of revolutions executed by the particle. However, the depolarization due to the oscillations perpendicular to the plane of

* Supported in part by the U. S. Atomic Energy Commission.
† Now at National Bureau of Standards, Washington, D. C.
[1] H. Mendlowitz and K. M. Case, Phys. Rev. **97**, 33 (1955) (hereafter referred to as I).
[2] Louisell, Pidd, and Crane, Phys. Rev. **94**, 7 (1954).
[3] See discussion Eq. (30), reference 1.
[4] D. W. Kerst and R. Serber, Phys. Rev. **60**, 53 (1941); O. Klemperer, *Electron Optics* (Cambridge University Press, Cambridge, 1953); H. Mendlowitz, thesis, University of Michigan, 1954 (unpublished).

the orbit is not negligible, and places an upper limit on the number of revolutions between the two targets.

A. Radial Oscillation

We first consider the effect of the small radial oscillations. It has been shown,[1,5] that in the Foldy-Wouthuysen representation, the equation of motion for the spin wave function for a Dirac particle is given by

$$i\hbar\dot{\Phi}=-\mu\boldsymbol{\sigma}\cdot\mathfrak{IC}\Phi, \tag{4}$$

where $\mu=(e\hbar/2m_0c)(1-\beta^2)^{\frac{1}{2}}=(e\hbar/2mc)$. This equation describes the positive energy solutions in the case where the anomalous moment has been neglected.

It is found that the field that the particle sees when executing radial oscillations in the plane of the equilibrium orbit (xy-plane) is

$$\mathfrak{IC}=\mathfrak{IC}_z=\mathfrak{IC}_0+\mathfrak{IC}_r\sin\omega_r t, \tag{5}$$

and

$$\frac{\mathfrak{IC}_r}{\mathfrak{IC}_0}=-\frac{v_r(i)}{v_\theta(i)}\cdot\frac{n}{(1-n)^{\frac{1}{2}}}, \tag{6}$$

where $v_r(i)$ is the initial radial velocity and $v_\theta(i)$ is the initial orbital velocity.

Now let

$$\Phi(t)=U(t)\Phi_0, \tag{7}$$

where U is a unitary transformation matrix operating on the spin components of Φ, and Φ_0 is the spin wave function at time $t=0$. Then

$$U(t)=Q_P(t)\exp\left[\frac{i\omega_L}{\omega_r}\sigma_z\frac{\mathfrak{IC}_r}{\mathfrak{IC}_0}\sin^2\omega_r t\right]=Q_P(t)W(t), \tag{8}$$

where

$$Q_P(t)=\exp[i\omega_L\sigma_z t/2]. \tag{9}$$

The transformation matrix $U(t)$ for any given particle in the beam depends upon the amplitude of the oscillating field $\mathfrak{IC}_r$. The relavant parameter being $\mathfrak{IC}_r/\mathfrak{IC}_0$ which is seen to be a function of the initial orbit parameters as given in (6).

If the initial spin density matrix is given by

$$\rho^{(0)}=\tfrac{1}{2}[\mathbf{1}+\mathbf{a}\cdot\boldsymbol{\sigma}], \tag{10}$$

where $\mathbf{1}$ is a two-by-two unit matrix and $\boldsymbol{\sigma}$ is the Pauli spin vector, the degree of polarization can be defined as[6]

$$P=[\nu/(\nu-1)][\operatorname{trace}(\rho^{(0)})^2-1/\nu]=|a|^2. \tag{11}$$

ν being the number of accessible polarization states for the system. The degree of depolarization is then defined as

$$\text{D.P.}=\frac{P(\text{initial})-P(\text{final})}{P(\text{initial})}. \tag{12}$$

Since the Hamiltonian is Hermitian, $U(t)$ is unitary. Therefore, if all the particles travelled in the same orbit, they would obey the same Hamiltonian, and so

$$\rho^{(0)}(t)=U(t)\rho^{(0)}(0)U^+(t), \tag{13}$$

where $\rho(t)$ is the density matrix at time t and $\rho(0)$ is the density matrix at $t=0$. From this follows that

$$\operatorname{trace}[\rho^{(0)}(t)]^2=\operatorname{trace}[\rho^{(0)}(0)]^2, \tag{14}$$

and so the final degree of polarization is the same as the initial polarization. The depolarization vanishes. We see that even though the spin states of the individual particles precess about the field, the beam keeps the same polarization.

The case of interest is the one where the particles take different paths. This is caused by variations in the initial velocities. In this case, the initial density matrix does not describe a pure momentum state. We assume that we can average over the momentum states. We obtain from Eq. (8)

$$\begin{aligned}\rho^{(0)}(t)&=\langle U(t)\rho^{(0)}(0)U^+(t)\rangle\\&=Q_P(t)\langle W(t)\rho^{(0)}(0)W^+(t)\rangle Q_P^+(t),\end{aligned} \tag{15}$$

where the angular braces denote an average over the momentum states of the ensemble. Although the particles of the beam spend different times in the magnetic field (depending upon the amplitude of the small oscillation about the equilibrium orbit) the experiment is designed so that the number of revolutions is the same for all the particles of the beam. Therefore $\omega_L t$ is the same for each particle of the beam. $Q_P(t)$ is then the same for each electron in the ensemble. Therefore

$$\operatorname*{trace}_{\text{spin}}[\rho^{(0)}(t)]^2=\operatorname*{trace}_{\text{spin}}[\langle W\rho^{(0)}(0)W^+\rangle\langle W\rho^{(0)}(0)W^+\rangle]. \tag{16}$$

Let $W(t)$ be expressed as

$$W(t)=\exp\left[i\frac{\omega_L}{\omega_r}\sigma_z\frac{\mathfrak{IC}_r}{\mathfrak{IC}_0}\sin^2\omega_r t\right]=\exp[(i/2)\gamma\boldsymbol{\sigma}\cdot\mathbf{h}], \tag{17}$$

where $\mathbf{h}$ is the unit vector in the direction of $\mathfrak{IC}_0$, the main component of the field. Then

$$\begin{aligned}\langle W\rho^{(0)}(0)W^+\rangle=\tfrac{1}{2}\{&1+\boldsymbol{\sigma}\cdot\mathbf{a}\langle\cos\gamma\rangle+\boldsymbol{\sigma}\cdot\mathbf{h}(\mathbf{h}\cdot\mathbf{a})\\&\times[1-\langle\cos\gamma\rangle]+\boldsymbol{\sigma}\cdot(\mathbf{h}\times\mathbf{a})\langle\sin\gamma\rangle\},\end{aligned} \tag{18}$$

and

$$\begin{aligned}\operatorname*{trace}_{\text{spin}}[\rho^{(0)}(t)]^2=\tfrac{1}{2}+\{&(\mathbf{h}\cdot\mathbf{a})^2+[a^2+(\mathbf{h}\cdot\mathbf{a})^2]\\&\times[\langle\cos\gamma\rangle^2+\langle\sin\gamma\rangle^2]\}.\end{aligned} \tag{19}$$

The depolarization is

$$\text{D.P.}=\frac{[a^2-(\mathbf{h}\cdot\mathbf{a})^2]}{a^2}\{1-[\langle\cos\gamma\rangle^2+\langle\sin\gamma\rangle^2]\}. \tag{20}$$

If the initial polarization were such that the nonvanishing component of $\mathbf{a}$ was along the direction of $\mathbf{h}$, the depolarization given by (20) would be identically zero. However, in general, the other components do not usually vanish. Therefore, it is necessary to study the

[5] K. M. Case, Phys. Rev. **95**, 1323 (1954).
[6] U. Fano, Phys. Rev. **93**, 621 (1954).

behavior of the trigonometric functions as a function of time (number of revolutions) to know how the depolarization will vary with time. The argument of the function γ is given by (17) as

$$|\gamma| = \left|\frac{\omega_L}{\omega_r}\frac{\mathcal{H}_r}{\mathcal{H}_0}\sin^2\omega_r t\right| \leq \left|\frac{\omega_L}{\omega_r}\frac{\mathcal{H}_r}{\mathcal{H}_0}\right|, \tag{21}$$

so that, independent of time, the upper limit of γ is

$$|\gamma| \leq \left|\frac{\omega_L}{\omega_r}\frac{\mathcal{H}_r}{\mathcal{H}_0}\right| = \left|\frac{n}{1-n}\frac{v_r(i)}{v_\theta(i)}\right|. \tag{22}$$

The fall off index of the field, n, is much less than unity in the proposed experiment. The ratio of the initial radial velocity to the initial orbital velocity is much smaller than unity. We can therefore consider

$$\langle\sin\gamma\rangle \sim \langle\gamma\rangle, \tag{23a}$$

$$\langle\cos\gamma\rangle \sim 1-\langle\gamma^2\rangle/2, \tag{23b}$$

and

$$[\langle\cos\gamma\rangle^2+\langle\sin\gamma\rangle^2] \cong 1-\langle\gamma^2\rangle+\langle\gamma\rangle^2=[1-\langle(\gamma-\langle\gamma\rangle)^2\rangle]. \tag{23}$$

If this is substituted in into (20), we see that the depolarization is extremely small, of the order of small quantities squared. It is seen that no matter how much time the particles spend in the field, the depolarization arising from the radial oscillations is negligible. This is independent of the initial polarization of the beam.

B. Transverse Oscillations

The depolarization of the ensemble arising from small oscillations of parts of the beam in a direction transverse to the plane of the equilibrium orbits will now be considered. The particles oscillate in the z-direction and "see" an oscillating magnetic field in the radial direction given by

$$(\mathcal{H})_a = \mathcal{H}_a \sin\omega_a t, \tag{24}$$

where

$$(\mathcal{H}_a/\mathcal{H}_0) = -[v_z(i)n^{\frac{1}{2}}/v_\theta(i)]. \tag{25}$$

Here $v_z(i)$ is the initial velocity in the z-direction, $v_\theta(i)$ is the initial orbital velocity, and n is the fall off index of the "constant" magnetic field discussed above.

Each electron is considered as traveling in a cyclotron-like orbit but each "sees" a radial oscillating field of magnitude depending upon the amplitude of oscillations in the z-direction (initial z-velocity). The direction of the oscillating field that the electrons "see" is always in the same direction as the electron goes about in its orbit. Let us consider this the x-direction. This can be decomposed into two circular fields[7]

$$\mathcal{H}_x = \tfrac{1}{2}(\mathcal{H}_x, \mathcal{H}_y, 0) + \tfrac{1}{2}(\mathcal{H}_x, -\mathcal{H}_y, 0), \tag{26}$$

where

$$\mathcal{H}_x = \mathcal{H}_a \sin\omega_a t, \tag{27}$$

$$\mathcal{H}_y = \mathcal{H}_a \cos\omega_a t. \tag{28}$$

The depolarization arising from one of the circular fields in (26) will be considered. This will probably tend to depolarize the beam more than the superposition of both fields of (26) where one would tend to cancel the effects of the other. We now consider the following field $\mathcal{H}$ acting on the electron.

$$\mathcal{H}_z = \mathcal{H}_0, \tag{29a}$$

$$\mathcal{H}_x = \tfrac{1}{2}\mathcal{H}_a \sin\omega_a t, \tag{29b}$$

$$\mathcal{H}_y = \tfrac{1}{2}\mathcal{H}_a \cos\omega_a t, \tag{29c}$$

where $\mathcal{H}_a$ is different for different parts of the beam.

The equation of motion of the spin wave function is given by (4) and a solution in the form of (7) is assumed. This gives us

$$\frac{\partial U}{\partial t} = \frac{i\omega_L}{2}\left[\sigma_z + \frac{\mathcal{H}_a}{2\mathcal{H}_0}(\sigma_x \sin\omega_a t + \sigma_y \cos\omega_a t)\right]U. \tag{30}$$

The solution of (30) is given by (Appendix A)

$$U(t) = Q_P(t)W(t), \tag{31}$$

where $Q_P(t)$ is given by (9) and

$$W(t) = \exp[-\tfrac{1}{2}(\omega_L-\omega_a)\sigma_z t] \times \exp(\tfrac{1}{2}i\tau\sigma_z)\exp(\tfrac{1}{2}i\lambda\sigma_x t). \tag{32}$$

λ and τ are defined by

$$\lambda\cos\tau = (\omega_L-\omega_a), \tag{33a}$$

$$\lambda\sin\tau = \tfrac{1}{2}\omega_L\mathcal{H}_a/\mathcal{H}_0. \tag{33b}$$

For the case of interest, the fields will be held as uniform as possible so that

$$n \ll 1. \tag{34}$$

The initial velocity in the z direction will be very small compared to the orbital velocity because it is desired that the electrons execute a very large number of revolutions in a comparatively small distance δz, so that

$$v_z(i)/v_\theta(i) \ll 1. \tag{35}$$

From (2), (25), and (33), we have

$$\tan\tau \approx \tau \approx \mathcal{H}_a/(2\mathcal{H}_0) \ll 1. \tag{36}$$

Therefore, the term in $W(t)$ depending on σ_z can be expressed as

$$\exp(\tfrac{1}{2}i\tau\sigma_z) \approx 1+\tfrac{1}{2}i\sigma_z\tau.$$

The contributions of this term to $[\rho^{(s)}(t)]^2$ differ from unity by small quantities of the order of magnitude of τ, which is small for any part of the beam. It should also be noted that this quantity is independent of the time. In further considerations this will therefore be replaced

[7] Rabi, Ramsey, and Schwinger, Revs. Modern Phys. 26, 167 (1954).

by the unit matrix. $W(t)$ can now be given by

$$W(t)\approx\exp\{-\tfrac{1}{2}i[\lambda-(\omega_L-\omega_a)\sigma_z]\}. \quad (37)$$

From (33), we can write

$$\lambda\approx(\omega_L-\omega_a)+\frac{\omega_L^2}{(\omega_L-\omega_a)}\left(\frac{\mathcal{K}_a}{2\mathcal{K}_0}\right)^2,$$

so that

$$[\lambda-(\omega_L-\omega_a)]t\approx\tfrac{1}{2}(\mathcal{K}_a/2\mathcal{K}_0)^2\omega_L t=\gamma'. \quad (38)$$

Therefore

$$W(t)=\exp(\tfrac{1}{2}i\sigma_z\gamma')=\exp(\tfrac{1}{2}i\gamma'\sigma\cdot\mathbf{h}), \quad (39)$$

where $\mathbf{h}$ is the unit vector in the direction of the main field $\mathcal{K}_0$.

If the initial spin density matrix is given by (10), then the depolarization is given by

$$\text{D.P.}=\frac{[a^2-(\mathbf{h}\cdot\mathbf{a})^2]}{a^2}\{1-[\langle\cos\gamma'\rangle^2+\langle\sin\gamma'\rangle^2]\}, \quad (40)$$

where the angular braces denote the averaging over the initial momentum states of the particles in the beam. Although all the particles of the beam do not spend the same amount of time in the field, the experiment is designed so that all the particles make the same number of revolutions between the two scatterings, and therefore, the factor in (38) $\omega_L t$ is the same constant for all electrons. The only variation in γ' among the various electrons in the beam that is to be considered arises from the different initial velocities (radial fields).

If the particles spend a very long time in the field, we have (Appendix B)

$$\lim_{\omega_L t\to\infty}\langle\cos\gamma'\rangle=\lim_{\omega_L t\to\infty}\langle\sin\gamma'\rangle=0, \quad (41)$$

so that from (40) we see that if $\mathbf{a}$ is not parallel to $\mathbf{h}$ the depolarization can be very large. We could then expect the asymmetry in the double scattering experiment to decrease. The oscillations transverse to the equilibrium orbit cause depolarization of the beam and this places an upper limit on the number of revolutions that the electrons can execute between the two scattering events without eliminating the asymmetry.

III. DOUBLE SCATTERING WITH DEPOLARIZATION

We have shown that the major depolarization effects arise from the small oscillations about the equilibrium orbit in the direction of the main component of the magnetic field. Here we will show how the formula describing the double-scattering cross section is modified by the depolarization. The notation of I will be employed.

The most interesting case is the following. The initial incident beam on the first target IA (Fig. 1) is scattered into the direction AB at an angle θ_1 with the initial beam. The magnetic field is perpendicular to the plane IAB. If $\theta_1=90°$, then the magnetic field would be along

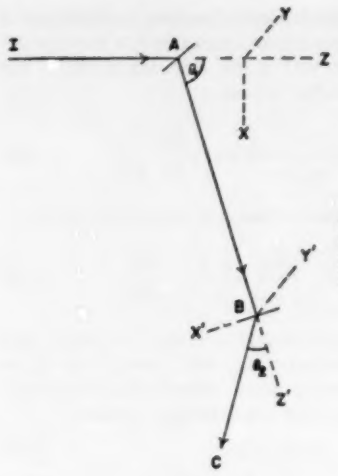

FIG. 1. Schematic diagram of a double-scattering experiment. In the case of interest $\theta_1=90°$.

IA. In the primed coordinate system, the magnetic field is along the x'-axis (Fig. 1).

If there is no depolarization, the density matrix describing the beam incident on the second target is given by Eq. (19) of I as

$$\rho''=P(t)Q(t)\rho'Q^{-1}(t)P^{-1}(t), \quad (42)$$

where $P(t)$ and $Q(t)$ are the transformation matrices related to the rotation of the space and spin states respectively. In this case, Q is given by Eq. (21) of I as

$$Q(t)=Q_P(t)Q_a(t), \quad (43)$$

where $Q_P(t)$ corresponds to the same angle of rotation as $P(t)$ and $Q_a(t)$ arises from the rotation due to the anomalous moment.

When the depolarization effects are included, $Q(t)$ is replaced by

$$Q(t)\to Q_P(t)Q_a(t)W(t)=R(t). \quad (44)$$

Equation (42) describing the beam (without depolarization) incident on the second target is now replaced by

$$\rho^{II}=P(t)R(t)\rho'R^{+}P^{-1}(t), \quad (45)$$

where ρ' does not describe a pure momentum state. In (44) only $W(t)$ depends upon the momentum distribution after the first scattering.

Instead of I Eq. (23) describing the beam after the second scattering, we have

$$\langle\rho^{II}\rangle=P(t)Q_P(t)VQ_a(t)\times\langle W(t)\rho'W^{+}(t)\rangle Q_a^{-1}(t)V^{+}Q_P^{-1}(t)P^{-1}(t). \quad (46)$$

We have made the following approximation. We considered ρ' as describing a pure momentum state which is an average of the various momentum states, but the averaging over the momentum states has been considered when calculating the spin density matrix of the beam incident on the second target [denoted by the

angular braces in (46)]. The scattering cross section is obtained by taking the trace over the spin states in (46). If $P(i)$ is a rotation corresponding to an integral number of revolutions, the cross section in the primed coordinate system is given by

$$d\sigma \sim 1-\delta\cos\varphi_2\langle\cos(\epsilon+\gamma')\rangle, \tag{47}$$

or

$$d\sigma \sim 1-\delta\cos\varphi_2[\cos\epsilon\langle\cos\gamma'\rangle-\sin\epsilon\langle\sin\gamma'\rangle]. \tag{48}$$

Without depolarization, we had from I, Eq. (32),

$$d\sigma \sim 1-\delta\cos\varphi_2\cos\epsilon. \tag{49}$$

The effect of the depolarization is given by the trigonometric functions of γ' which are functions of the number of revolutions executed between the two scatterers. From (41) we see that if the number of revolutions between scatterings is very large, the bracket in (48) tends to vanish. Thus the asymmetry will tend to vanish because of the depolarization of the beam.

IV. APPLICATION TO MEASURING THE GYROMAGNETIC RATIO g

In order that the amount of depolarization be small, we will limit the number of revolutions by requiring that

$$\langle\cos\gamma'\rangle \approx 1, \tag{50a}$$

$$\langle\sin\gamma'\rangle \sim \gamma' \ll 1, \tag{50b}$$

or

$$\tfrac{1}{2}(3\mathcal{C}_a/2\mathcal{C}_0)^2\omega_L t \ll 1. \tag{50c}$$

As an upper limit on $\langle\gamma'\rangle$ let us consider

$$\langle\gamma'\rangle \leq \pi/20,$$

so that

$$\frac{n}{8}\langle[v_s(i)/v_\theta(i)]^2\rangle\omega_L t \leq \frac{\pi}{20}. \tag{51}$$

The time for N revolutions is

$$t = 2\pi N/\omega_L, \tag{52}$$

so that (51) becomes

$$\frac{2\pi N n}{8}\langle v_s(i)/v_\theta(i)\rangle \leq \frac{\pi}{20}, \tag{53}$$

or

$$N \leq \langle[v_\theta(i)/v_s(i)]^2\rangle\frac{1}{5n}. \tag{54}$$

Thus we have an upper limit on the number of revolutions in terms of the experimental parameters, the initial velocities and the falloff index n.

Let us consider the case where the maximum velocity in the z direction (x' direction) is given by

$$v_s(i) = v_\theta(i)\sin(1°),$$

or

$$v_s(i)/v_\theta(i) \approx 0.017.$$

If this is the value taken as the average over the beam, then

$$N \lesssim 700/n. \tag{55}$$

For these values of N, (48) is effectively equal to (49), the double scattering cross section without depolarization.

Let us assume that we can measure ϵ of (49) to within ± 0.3 radian and we would like to measure g, the gyromagnetic ratio of the free electron, to one part in one hundred thousand. Let

$$\epsilon = \epsilon_0 \pm \Delta\epsilon, \tag{56}$$

and the number of revolutions be given by

$$N = N_0 \pm \Delta N. \tag{57}$$

Now

$$\tfrac{1}{2}g\omega_L t = \tfrac{1}{2}g2\pi N = 2\pi N + \epsilon,$$

so that

$$\tfrac{1}{2}g = 1 + \frac{\epsilon_0}{2\pi N_0} \pm \frac{\Delta\epsilon}{2\pi N_0} \pm \frac{\epsilon_0}{2\pi N_0}\frac{\Delta N}{N_0}. \tag{58}$$

We therefore require that

$$\frac{\Delta\epsilon}{2\pi N_0} \leq 10^{-5}, \tag{59a}$$

$$\frac{\epsilon_0}{2\pi N_0}\frac{\Delta N}{N} \leq 10^{-5}. \tag{59b}$$

We assume $\Delta\epsilon \sim 0.3$, which means that we must have

$$N \gtrsim 5000. \tag{60}$$

It was shown in I, Eq. (38), that

$$\epsilon = a\omega_L t/(1-\beta^2)^{\frac{1}{2}},$$

$$a = \alpha/2\pi,$$

α being the fine structure constant. Therefore, from (59b) we have

$$\frac{1}{(1-\beta^2)^{\frac{1}{2}}}\frac{\alpha}{2\pi}\frac{\Delta N}{N_0} \leq 10^{-5},$$

which, for one hundred kilovolt electrons, can be approximated by

$$\frac{\alpha}{2\pi}\frac{\Delta N}{N_0} \leq 10^{-5},$$

so that

$$\Delta N/N_0 \lesssim 10^{-2}. \tag{61}$$

Thus, one of the requirements on such an experiment is that the number of revolutions be of the order of 5000. This limits the fall-off index to be of the order of 0.1. Also it is necessary that the number of revolutions be known to within 1%.

V. CONCLUSION

Depolarization effects place certain restrictions on the accuracy with which the gyromagnetic ratio of a free electron can be determined by double scattering experiments in a magnetic field. However, with sufficient care it does seem possible to make the measurement to at least one part in 10^5. This is then another feasible method of checking the radiative corrections.

APPENDIX A

Here we show how we can obtain Eq. (32) from Eq. (30) in the text. We are given Eq. (30)

$$\frac{\partial U}{\partial t}=\tfrac{1}{2}i\omega_L\left[\sigma_z+\frac{3\mathcal{C}_a}{2\mathfrak{I}\mathcal{C}_0}(\sigma_x\sin\omega_a t+\sigma_y\cos\omega_a t)\right]U. \quad \text{(A-1)}$$

Let

$$U=\exp[\tfrac{1}{2}i\omega_L\sigma_z t]W=Q_P W, \quad \text{(A-2)}$$

so that

$$\frac{\partial W}{\partial t}=\frac{i\omega_L}{4}\frac{3\mathcal{C}_a}{3\mathcal{C}_0}\exp\left[-\frac{i}{2}(\omega_L-\omega_a)\sigma_z t\right]\sigma_y \times\exp\left[\frac{i}{2}(\omega_L-\omega_a)\sigma_z t\right]W. \quad \text{(A-3)}$$

We now express W as

$$W=\exp[-\tfrac{1}{2}i(\omega_L-\omega_a)\sigma_z]X, \quad \text{(A-4)}$$

and

$$\frac{\partial X}{\partial t}=\frac{i}{2}\left[\frac{\omega_L}{2}\frac{3\mathcal{C}_a}{3\mathcal{C}_0}\sigma_y+(\omega_L-\omega_a)\sigma_z\right]X. \quad \text{(A-5)}$$

Now let

$$\lambda\cos\tau=(\omega_L-\omega_a), \quad \text{(A-6)}$$

$$\lambda\sin\tau=\omega_L 3\mathcal{C}_a/(2\mathfrak{I}\mathcal{C}_0), \quad \text{(A-7)}$$

then

$$\partial X/\partial t=\tfrac{1}{2}i\lambda\exp(\tfrac{1}{2}i\tau\sigma_z)\sigma_z\exp(-\tfrac{1}{2}i\tau\sigma_z)X. \quad \text{(A-8)}$$

If we define Y such that

$$X=\exp(\tfrac{1}{2}i\tau\sigma_z)Y, \quad \text{(A-9)}$$

then

$$\partial Y/\partial t=\tfrac{1}{2}i\lambda\sigma_z Y, \quad \text{(A-10)}$$

so that

$$Y=\exp(\tfrac{1}{2}i\sigma_z t)Y_0. \quad \text{(A-11)}$$

Where Y_0 may be taken as a unit matrix. Therefore

$$U=Q_P(t)W(t), \quad \text{(A-12)}$$

where

$$W(t)=\exp[-\tfrac{1}{2}i(\omega_L-\omega_a)\sigma_z t] \times\exp[\tfrac{1}{2}i\sigma_z\tau]\exp[\tfrac{1}{2}i\lambda\sigma_z t], \quad \text{(A-13)}$$

which is Eq. (32).

APPENDIX B

We are interested in determining how the number of revolutions that the particles execute in the field will affect the average of the trigonometric functions given in Eq. (40) in the text. It is shown that as the number of revolutions becomes very large so that $\omega_L t\to\infty$ the average values of both the sine and cosine functions tend to vanish. Consider

$$\lim_{\omega_L t\to\infty}\langle\cos\gamma'\rangle, \quad \text{(B-1)}$$

$$\lim_{\omega_L t\to\infty}\langle\sin\gamma'\rangle, \quad \text{(B-2)}$$

where γ' is given by

$$\gamma'=\tfrac{1}{2}(3\mathcal{C}_a/3\mathcal{C}_0)^2\omega_L t=\tfrac{1}{2}\alpha^2\omega_L t, \quad \text{(B-3)}$$

and the maximum of

$$\alpha=\tfrac{1}{2}3\mathcal{C}_a/3\mathcal{C}_0\ll 1. \quad \text{(B-4)}$$

The average value of one of the trigonometric function is

$$\langle\cos\gamma'\rangle=\int_0^\infty P(\alpha^2)\cos(\tfrac{1}{2}\alpha^2\omega_L t)d(\alpha^2), \quad \text{(B-5)}$$

where $P(\alpha^2)$ is the probability over the beam that a given particle will "see" the fields denoted by the parameter α^2.

Let

$$\tfrac{1}{2}\alpha^2\omega_L t=\lambda, \quad \text{(B-6)}$$

so that

$$\langle\cos\gamma'\rangle=\frac{2}{\omega_L t}\int_0^\infty P\left(\frac{\lambda}{\omega_L t}\right)\cos\lambda d\lambda, \quad \text{(B-7)}$$

and

$$\langle\sin\gamma'\rangle=\frac{2}{\omega_L t}\int_0^\infty P\left(\frac{\lambda}{\omega_L t}\right)\sin\lambda d\lambda. \quad \text{(B-8)}$$

It is assumed that $P(\alpha^2)$ is a reasonable type probability function which is not too peaked at the origin and falls off rapidly for large α. Then

$$\int_0^\infty P\left(\frac{\lambda}{\omega_L t}\right)\left\{\begin{matrix}\cos\lambda\\ \sin\lambda\end{matrix}\right\}d\lambda,$$

is a bounded function, so that

$$\lim_{\omega_L t\to\infty}\left\{\begin{matrix}\langle\cos\gamma'\rangle\\ \langle\sin\gamma'\rangle\end{matrix}\right\}=0. \quad \text{(B-9)}$$

This tells us that the beam will tend to depolarize if it stays too long in these fields. This is expressed in the Eq. (40) of the text.

APPENDIX C

The fields causing depolarization considered in the main body of the text are analytically so simple that the integration problems could be handled very easily. For many questions, however, it is convenient to have the approximate formulas for more general situations obtained below.

Let us assume the Schrödinger equation for the spin function to be

$$i\hbar\partial\Phi/\partial t=[H_0(t)+H_1(t,\alpha)]\Phi, \tag{C1}$$

where $H_0(t)$ is independent of the orbital parameters α and H_1 is small.

If

$$\Phi(t)=U(t)\Phi(0), \tag{C2}$$

we obtain

$$U=Q(t)W(t,\alpha), \tag{C3}$$

where

$$i\hbar\partial Q/\partial t=H_0Q, \tag{C4}$$

and

$$i\hbar\partial W/\partial t=Q^{-1}H_1QW. \tag{C5}$$

Assuming $Q(t)$ known for Eq. (C4), $W(t,\alpha)$ is, correct to first order in H_1,

$$W(t,\alpha)=\mathbf{1}+W_1(t,\alpha), \tag{C6}$$

where

$$W_1(t,\alpha)=\frac{1}{i\hbar}\int_0^t Q^{-1}(t')H_1(t',\alpha)Q(t')dt'. \tag{C7}$$

Using (13), the definition (12), and the approximate formula for U we obtain

$$\text{D.P.}=\frac{-2\,\text{trace}\{[\rho(0)]^2[\langle W_1^2(t)\rangle-\langle W_1(t)\rangle^2]\}}{\text{trace}\rho^2(0)-\frac{1}{2}}$$
$$+\frac{2\,\text{trace}\{\langle\rho(0)W_1Q^{-1}\rho(0)QW\rangle-\langle\rho(0)W_1Q^{-1}\rangle\langle\rho(0)QW_1\rangle\}}{\text{trace}\rho^2(0)-\frac{1}{2}}. \tag{C8}$$

$\rho(0)$ is the initial spin density matrix. The angular braces denote averages with respect to α. Equation (C8) is correct to second order in H_1. (This follows somewhat indirectly from an assumed Hermiticity of H_1.) It may be remarked, that since the limitations on experiments are obtained by requiring the depolarization to be small, these could be derived directly using (C8) and

$$H_0=f(t)\boldsymbol{\sigma}\cdot\mathbf{h}, \tag{C9}$$

$$H_1(t,\alpha)=\mathbf{b}(t,\alpha)\cdot\boldsymbol{\sigma}, \tag{C10}$$

with $\mathbf{h}$ a constant unit vector, $f(t)$ a given function of time, and b a small, variable vector.

PHYSICAL REVIEW VOLUME 100, NUMBER 6 DECEMBER 15, 1955

Diffusion of Like Particles Across a Magnetic Field

ALBERT SIMON
Oak Ridge National Laboratory, Oak Ridge, Tennessee
(Received July 25, 1955)

It is shown that the diffusion rate across a magnetic field due to collision of like charged particles is derivable from the macroscopic equations of the plasma. However, it is necessary to include the off-diagonal terms in the stress tensor. The resultant diffusion rate does not obey Fick's law and is proportional to the inverse fourth power of magnetic field strength. This diffusion rate is usually smaller than that due to unlike particle collisions, but may sometimes dominate.

I. INTRODUCTION

MANY of the gross properties of a plasma may be obtained from a consideration of the hydrodynamical (or macroscopic) equations of the plasma.[1] Thus, for example, for a gas consisting of ions and electrons and assuming an isotropic stress tensor, one has the following momentum equation in the steady state

$$\nabla P=\mathbf{j}\times\mathbf{H}+\epsilon\mathbf{E}. \tag{1}$$

Here P is the gas pressure, H and E are the magnetic and electric field strengths respectively, j is the current and ϵ the charge density in the plasma. Note that a nonlinear term in the velocity is neglected. In addition to this equation, we have another expression representing the generalized Ohm's law:

$$\mathbf{E}+(\mathbf{v}\times\mathbf{H})/c=\mathbf{j}/\sigma+\nabla P_i/en. \tag{2}$$

[1] Lyman Spitzer, Jr., *Physics of Fully Ionized Gases* (Interscience Publishers, New York, to be published).

Again, steady state has been assumed and nonlinear terms neglected. The mass velocity of the plasma is denoted by $\mathbf{v}$, the ion partial pressure by P_i and the conductivity of the plasma by σ. The conductivity is defined as

$$\sigma\cong ne^2/mc\nu, \tag{3}$$

where n is the density of electrons, m the electron mass, and ν is the collision frequency for electron-ion impact.

As Spitzer has shown,[1] an expression for the diffusion rate across a magnetic field may be readily derived from Eqs. (1) and (2). Assuming that the density gradient and the electron field are in a single direction (say x) and the magnetic field is in the z-direction, one may eliminate $\mathbf{j}$ between Eqs. (1) and (2). The result is

$$v_x=-(c/\sigma H^2)(\nabla P-\epsilon E). \tag{4}$$

This has the usual form for diffusion in that Fick's law

is obeyed ($v \sim \nabla n$). The effective diffusion coefficient is

$$D = cnkT/\sigma H^2, \tag{5}$$

which is proportional to H^{-2} and to the cross section for electron-ion collisions. The mobility u has the usual form

$$u = eD/kT. \tag{6}$$

It is the purpose of this note to point out that the assumption of an isotropic stress tensor in Eq. (1) omits the effects due to like particle collisions and leads to a contradiction for the case of a gas consisting of one type of particle only (simple gas). Inclusion of the off-diagonal terms in the stress tensor removes the contradiction and yields a diffusion rate for collisions of like particles which is of an unusual form in that Fick's law is not obeyed and the diffusion coefficient is proportional to H^{-4}.

II. DIFFUSION IN A SIMPLE GAS

Consider a simple gas of charged particles. In this case, Eq. (2) does not exist. Equation (1) is still valid; however $\mathbf{v}$ and $\mathbf{j}$ are no longer independent and are related by

$$\mathbf{j} = \epsilon \mathbf{v}/c = ne\mathbf{v}/c. \tag{7}$$

As a result, Eq. (1) predicts that no mass flow occurs in the direction of a density gradient which is perpendicular to the magnetic field and hence that the diffusion rate is zero. It is also clear from the resulting form of the diffusion coefficient in Eq. (5) that like-particle collisions are not included in this expression; and hence the paradoxical result for a simple gas, which was just obtained, is not unexpected.

A very different result may now be obtained by including the off-diagonal terms of the stress tensor T_{ij} in Eq. (1) for a simple gas. Assume that the magnetic field is in the z-direction, that all quantities vary only in the x-direction and that the mass velocity in the direction of the magnetic field is constant everywhere. The resultant equation has the following three components:

$$\partial T_{xx}/\partial x = (nev_y/c)H + \epsilon E, \tag{8}$$

$$\partial T_{xy}/\partial x = -(nev_x/c)H, \tag{9}$$

$$\partial T_{xz}/\partial x = 0. \tag{10}$$

Chapman and Cowling[2] have derived the proper expressions for the stress tensor of a simple gas in a magnetic field. The relevant expressions are

$$T_{xx} = P - \frac{2\mu}{1+(16/9)\omega^2\tau^2}\left[\bar{e}_{xx} + \tfrac{1}{2}(\bar{e}_{xx}+\bar{e}_{yy}) \cdot \frac{16}{9}\omega^2\tau^2 + \bar{e}_{xy}\cdot\frac{4}{3}\omega\tau\right], \tag{11}$$

$$T_{xy} = -\frac{2\mu}{1+(16/9)\omega^2\tau^2}\left[\bar{e}_{xy} + \frac{1}{2}(\bar{e}_{yy}-\bar{e}_{xx})\cdot\frac{4}{3}\omega\tau\right], \tag{12}$$

$$T_{xz} = -\frac{2\mu}{1+(4/9)\omega^2\tau^2}\{\bar{e}_{xz} + \tfrac{2}{3}\omega\tau\bar{e}_{yz}\}, \tag{13}$$

where μ is the usual coefficient of viscosity in the absence of a magnetic field. Thus

$$\mu \cong \tfrac{2}{5}P\tau. \tag{14}$$

The mean free time between collisions is denoted by $\tau(=\lambda/v)$ and $\omega = eH/mc$. The symbol $\bar{e}_{ij}$ represents the symmetrical and traceless tensor $\nabla\mathbf{v}$. The usual case of interest is where $\omega\tau \gg 1$, which corresponds to a particle making very many gyrations between collisions. Clearly the opposite limit $\omega\tau < 1$ is of no interest since the magnetic field is then unimportant.

By our assumptions $\bar{e}_{xx} = \bar{e}_{xy} = 0$ and hence $T_{xx} \equiv 0$. Equation (10) is thus satisfied identically. It will be seen from the form of the final result that $\mu\bar{e}_{xy} \ll \omega\tau P$ and that $\bar{e}_{xy}/\bar{e}_{xx} \gg \omega\tau$. If one assumes these inequalities, the remaining tensor components can be written as

$$T_{xx} \cong P, \tag{15}$$

$$T_{xy} \cong -\frac{9}{16}\frac{\mu}{(\omega\tau)^2}\frac{dv_y}{dx}. \tag{16}$$

Solving Eq. (8) for v_y and substituting in Eq. (9), one obtains

$$v_x = \frac{c}{neH}\frac{d}{dx}\left\{\frac{9}{16}\frac{\mu}{(\omega\tau)^2}\frac{d}{dx}\left[\frac{c}{neH}\left(\frac{dP}{dx} - \epsilon E\right)\right]\right\}. \tag{17}$$

Assume a constant temperature in the gas and ignore the electric field. By virtue of the fact that $\tau \sim n^{-1}$ and hence that μ is independent of n, Eq. (17) can be rewritten as

$$v_x = \frac{3}{8}\frac{v^4}{\omega^4\tau}\frac{1}{n^2}\frac{d}{dx}\left\{n^2\frac{d}{dx}\left(\frac{1}{n}\frac{dn}{dx}\right)\right\}$$

or

$$v_x = \frac{3}{8}\frac{r_0^4}{\tau}\frac{1}{n}\left\{\frac{d^3n}{dx^3} - \frac{1}{n}\frac{d^2n}{dx^2}\frac{dn}{dx}\right\}, \tag{18}$$

where $r_0 = mvc/eH$ is the Larmor radius. Equation (18) is the desired result. The diffusion velocity due to like particle collisions is clearly proportional to H^{-4} and does not obey Fick's law. Instead, the diffusion rate depends on the second and third space derivatives of the particle density. An alternative form for Eq. (18) is

$$v_x = \frac{3}{8}\frac{r_0^4}{\tau}\frac{d}{dx}\left[\frac{1}{n}\frac{d^2n}{dx^2}\right]. \tag{19}$$

Equations (18) and (19) can be expected to give the proper form for the diffusion due to like particle collisions even in a nonsimple gas. An expression which

[2] S. Chapman and T. G. Cowling, *The Mathematical Theory of Nonuniform Gases* (Cambridge University Press, Cambridge, 1952), p. 338.

is identical to that given in Eq. (19), except for the factor $\frac{3}{4}$, has been obtained by Kruskal by the use of a model based on individual particle orbits.[3]

It remains now to justify the approximation made in deriving the results. All order of magnitude estimates of the various terms which have been used above rest on the following assertion. It is extremely unlikely that the ion density n, in any practical problem, can fall off faster than with an e-folding length equal to the Larmor radius r_0. In fact, the actual e-folding length should usually be considerably larger than this. Hence, order-of-magnitude estimates may be made by replacing each space derivative of n by the quantity $(\kappa r_0)^{-1}$, where κ is substantially larger than unity.

By combining this assertion with the result of Eq. (19), it is seen that

$$v_x = O[r_0/\tau\kappa^2], \tag{20}$$

where the symbol O denotes "of the order of."

Similarly, by Eqs. (8) and (15),

$$v_y = O\left[\frac{ckT}{eH}\frac{1}{\kappa r_0}\right] = O\left[\frac{r_0}{\tau}\frac{\omega\tau}{\kappa}\right]. \tag{21}$$

Hence

$$v_y/v_x = O[\omega\tau\kappa^2] \gg \omega\tau.$$

As a result, then,

$$\frac{\bar{e}_{xy}}{\bar{e}_{xx}} \cong \frac{\partial v_y/\partial x}{\partial v_x/\partial x} \gg \omega\tau,$$

as was asserted earlier. In addition,

$$\mu\bar{e}_{xy} \cong P\tau\partial v_y/\partial x = P\cdot O[\omega\tau/\kappa^2].$$

Hence $\mu\bar{e}_{xy} \ll \omega\tau P$ as was also asserted earlier.

III. COMPARISON OF DIFFUSION RATES

It is of interest to compare the rate of diffusion of ions due to ion-ion collisions with that due to electron-ion collisions in a plasma consisting of both types of particles (assumed in approximate space-charge neutrality). The rate due to ion-ion collisions is obtained from Eq. (19) and is of the order of magnitude

$$v = O[r_{0i}/\tau_i\kappa^2],$$

where r_{0i} is the Larmor radius of the ions and τ_i is the mean free time between ion-ion collisions. The ion diffusion rate due to electron-ion collisions is obtained from Eqs. (4) and (3), (assuming $E=0$) and is of the order of magnitude

$$v' = O\left[\frac{r_{0e}^2}{\tau_e\kappa r_{0i}}\right],$$

where r_{0e} is the electron Larmor radius and τ_e is the mean free time between electron-ion collisions. Hence,

$$\frac{v}{v'} = O\left[\frac{r_{0i}^2\tau_e}{r_{0e}^2\tau_i\kappa^2}\right] = O\left[\left(\frac{M}{m}\right)^{\frac{1}{2}}\frac{\lambda_e}{\lambda_i}\frac{1}{\kappa^2}\right],$$

where equal temperatures have been assumed for the electron and ion gas, and where M denotes the ion mass. For the case of equal temperatures, $\lambda_e \cong \lambda_i$ and

$$\frac{v}{v'} = O\left[\left(\frac{M}{m}\right)^{\frac{1}{2}}\frac{1}{\kappa^2}\right]. \tag{22}$$

Hence it is possible for the diffusion rate due to ion-ion collisions to be larger than that due to electron-ion collisions, since $(M/m)^{\frac{1}{2}}$ is of the order of 10^2. However, in most cases one might expect $\kappa \gg 1$ and then the self-diffusion rate will become comparable to or smaller than that due to electron-ion collisions.

A curious point which is worth noting is that if one were dealing with a truly simple gas with density varying only in the x-direction then the electric field E is related to the density by Poisson's law $dE/dx = 4\pi ne$. Upon substitution of this relation in Eq. (17), one now finds that a term proportional to dn/dx contributes to v_x. Hence, to this extent, Fick's law is obeyed. The coefficient of this term is still proportional to H^{-1}. Moreover, in a nonsimple gas, which is all that may be obtained in practice, the electric field gradient is no longer simply related to the density of one species of charged particle.

ACKNOWLEDGMENTS

The author wishes to take this opportunity to thank Dr. Lyman Spitzer for a prepublication copy of his forthcoming tract on *The Physics of Fully Ionized Gases*.

[3] Martin Kruskal (private communication).

Bremsstrahlung Differential Cross-Section Measurements for 0.5- and 1.0-Mev Electrons*†

J. W. Motz
National Bureau of Standards, Washington, D. C.
(Received August 19, 1955)

The bremsstrahlung cross section, differential in photon energy and angle, has been determined by measuring the x-rays emitted from thin targets of beryllium, aluminum, and gold, for incident electron energies of 0.5 and 1.0 Mev, with a 5-inch diameter, 4-inch long NaI(Tl) scintillation spectrometer at angles of 0, 10, 20, 30, 60, 90, and 120 degrees. The results show that in this energy region, the Bethe-Heitler-Sauter (Born approximation) theory underestimates the cross section. A comparison of the cross section for beryllium and aluminum gives evidence for electron-electron bremsstrahlung. The experimental values for the Heitler parameter $\phi_{\text{rad}}/\bar{\phi}$ with a gold target are 10 at 1.0 Mev and 9.5 at 0.5 Mev. The low-Z values for $\phi_{\text{rad}}/\bar{\phi}(1+1/Z)$ are 8.8 for beryllium and 8.4 for aluminum at 1.0 Mev and 6.8 for aluminum at 0.5 Mev. The accuracy of these values is estimated to be better than 20%. The corresponding Bethe-Heitler values for $\phi_{\text{rad}}/\bar{\phi}$ are 6.5 at 1.0 Mev and 5.5 at 0.5 Mev.

I. INTRODUCTION

INVESTIGATIONS of the elementary process of bremsstrahlung production have been few and incomplete. On the one hand, the present theory that has been developed to account for the important features of bremsstrahlung radiation depends on the Born approximation except in the extreme energy regions.[1] On the other hand, very few measurements of the bremsstrahlung cross section are available. These measurements mostly involve studies of the energy loss of electrons passing through a material, and in the low-energy region require corrections for the ionization energy loss.

With the development of scintillation spectroscopy, considerable progress has been made in measurements of photon energies and intensities. This technique of photon analysis has been utilized in the present work, which was undertaken to provide detailed experimental information about the bremsstrahlung differential cross section in the low-energy region from 0.5 to 1.0 Mev.

The bremsstrahlung cross section for electrons accelerated in the field of a nucleus has been evaluated by Bethe and Heitler,[2,3] by Sauter,[4] and by Gluckstern and Hull[5] on the basis of the Born approximation. From their results, the cross section at various stages of integration may be designated as

$$d\sigma_{k,\theta}(E_0,k,\theta), \quad [\text{Eq. (11), reference 4; Eq. (4.1), reference 5}]; \tag{1}$$

$$d\sigma_k(E_0,k), \quad [\text{Eq. (16), reference 3}]; \tag{2}$$

$$\phi_{\text{rad}}, \quad [\text{Eq. (28), reference 3}]; \tag{3}$$

where E_0 is the initial total electron energy, k is the photon energy, and θ is the angle between the directions of the incident electron and the emitted photon. Expression (1) is integrated over the direction of the emerging electron and represents the differential form of the cross section with respect to photon energy and angle, without screening. Expression (2) gives the cross section integrated over the direction of photon emission, and expression (3) defines a cross section for the energy lost by radiation, which is given by the quantity

$$\frac{1}{E_0}\int_0^{E_0-m} k\left(\frac{d\sigma_k}{dk}\right)dk.$$

In the relativistic region, experimental results have shown better than 10% agreement with the cross section given by expression (2). Such confirmation was obtained for the upper half of the bremsstrahlung spectrum at 60 Mev and 247 Mev by Curtis[6] and Fisher[7] respectively, who used a cloud chamber to measure the energy losses of electrons which passed through thin targets with high atomic number ($Z\approx 80$). In addition, experimental agreement[8] (not in absolute value) with the shape of the photon spectrum predicted by expression (2) has been obtained for electron energies covering a range from about 10 Mev to 300 Mev for both thick and thin high-Z targets.

In the region where the electron kinetic energy is of the order of the electron rest energy, the extent of agreement between existing measurements and the theoretical predictions has not been established. In this energy region the validity of the Born approximation

* Work supported by the U. S. Atomic Energy Commission.
† A preliminary report of this work was given by J. W. Motz and William Miller, Phys. Rev. **96**, 544 (1954).
[1] Theories not depending on this approximation have been given in the nonrelativistic region by A. Sommerfeld, Ann. Physik (5) **11**, 257 (1931), and in the extreme relativistic region by H. A. Bethe and L. C. Maximon, Phys. Rev. **93**, 768 (1954).
[2] H. Bethe and W. Heitler, Proc. Roy. Soc. (London) **146**, 83 (1934).
[3] W. Heitler, *The Quantum Theory of Radiation* (Oxford University Press, London, 1954), third edition, p. 242.
[4] F. Sauter, Ann. Physik (5), **20**, 404 (1934).
[5] R. L. Gluckstern and M. H. Hull, Jr., Phys. Rev. **90**, 1030 (1953).
[6] C. D. Curtis, Phys. Rev. **89**, 123 (1953).
[7] Philip C. Fisher, Phys. Rev. **92**, 420 (1953).
[8] H. W. Koch and R. E. Carter, Phys. Rev. **77**, 165 (1950); J. W. DeWire and L. A. Beach, Phys. Rev. **83**, 476 (1951); Motz, Miller, and Wyckoff, Phys. Rev. **89**, 968 (1953).

becomes more questionable, especially for high Z. Also, it is difficult to accurately evaluate the large effect of electron energy loss and scattering on the intensity and on the angular and energy distribution of the bremsstrahlung radiation in the measurements. Experiments which point up this uncertainty may be summarized as follows:

(a) Measurements[9] were made of electron energy losses due to radiation in cloud chamber gases ($Z=7$, 18, 36, and 54) and in high-Z absorbers[10] with initial electron kinetic energies in the energy region from about 1 to 5 Mev. The experimental values were factors of about 1.5 to 100 larger than theoretical predictions found from expression (3), although it was indicated[11] that at least some of the disagreement could be attributed to the effects of multiple scattering.

(b) In the same energy region, the total energy loss of electrons that were completely stopped in a high-Z thick target was measured with a calorimeter,[12] and the bremsstrahlung intensity produced in such a process was measured with an ionization chamber.[13] The results indicated about 10 percent agreement with theoretical estimates obtained from expression (3). These estimates included corrections for the electron energy loss due to ionization, but did not account for electron backscattering. In addition, different values (33 and 45.5 electron volts) for the energy required to produce an ion pair in air were used in the ionization chamber measurements.[12]

(c) Spectrometer measurements[14] of high-Z thick target bremsstrahlung spectra yielded results that were about a factor of two greater than theoretical estimates which were based on expressions (1) and (2), and which took account of electron backscattering.

The general lack of agreement in the above results indicates the need for more studies in this energy region. It would be particularly desirable to have measurements which do not involve such large corrections for electron multiple scattering before a comparison with the theory can be made.

In the present work, measurements are made of the angular and energy distribution of the bremsstrahlung from low- and high-Z targets for electrons with initial kinetic energies of 0.5 and 1.0 Mev. The bremsstrahlung radiation is measured directly with a scintillation spectrometer, and the targets are thin enough so that the electron scattering and energy loss is negligible. From these measurements, the bremsstrahlung differential cross section with respect to photon energy and angle is determined and compared with the theoretical predictions given by expression (1). A study of the cross section in this differential form constitutes a much more sensitive test of the theory than the integrated forms (2) and (3). Furthermore, this energy range lends itself nicely to such an angular distribution measurement because the radiation intensity is not peaked so sharply in the forward direction, and therefore is not so sensitive to small errors in the photon angle θ. For example, estimates made from expression (1) indicate that for small values of θ, there is only about a 10% difference in the photon intensity for a one-degree error in θ, while at higher energies the difference becomes much larger.

II. EXPERIMENTAL METHOD

A. Apparatus

The experimental arrangement for these measurements is shown schematically in Fig. 1. A beam of monoenergetic electrons is incident on a target of a specific thickness and atomic number Z. The bremsstrahlung emitted from the target at a given angle θ with respect to the incident electron direction, passes to a scintillation spectrometer through a 15-mil aluminum window in the target chamber and a $\frac{3}{8}$-inch diameter, 12-inch long brass collimator.

The electron beam is produced by the National

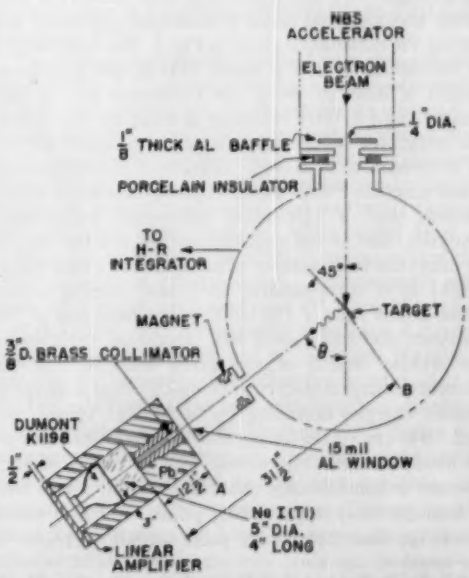

FIG. 1. Experimental arrangement for bremsstrahlung measurements. Initial electron kinetic energies were 0.5 and 1.0 Mev, and values of θ were 0, 10, 20, 30, 60, 90, and 120 degrees.

[9] H. Klarman and W. Bothe, Z. Physik **101**, 489 (1936); L. Leprince-Ringuet, Compt. rend. **201**, 712 (1935); D. Skobeltzyn and E. Stepanowa, Nature **137**, 234 (1936).

[10] J. J. Turin and H. R. Crane, Phys. Rev. **52**, 63 (1937); A. J. Ruhlig and H. R. Crane, Phys. Rev. **53**, 618 (1938).

[11] M. M. Slawsky and H. R. Crane, Phys. Rev. **56**, 1203 (1939).

[12] Ivanov, Walter, Sznelnikov, Taranov, and Abramovich, J. Phys. (U.S.S.R.) **4**, 319 (1941).

[13] Petrauskas, Van Atta, and Myers, Phys. Rev. **63**, 389 (1943); Buechner, Van de Graaff, Burrill, and Sperduto, Phys. Rev. **74**, 1348 (1948).

[14] Miller, Motz, and Cialella, Phys. Rev. **96**, 1344 (1955); K. Liden and N. Starfelt, Phys. Rev. **97**, 419 (1955); N. Starfelt and N. L. Svantesson, Phys. Rev. **97**, 708 (1955).

Bureau of Standards 1.4-Mev cascade-type accelerator.[16] The electron energy is determined from the electrostatic potential of the accelerator, which is measured with a high-resistance voltmeter[15] with an accuracy of approximately one percent. A lens-type magnet coil is used to focus the electrons toward the target position where geometry considerations indicate that the angular spread in the beam is less than 0.5°. In order to align the beam with the center of the target chamber and to prevent any shifting of the beam on the target, it was necessary to introduce a $\frac{1}{4}$-inch thick, $\frac{1}{4}$-inch diameter aluminum defining baffle before the entrance to the chamber. The beam position and size was determined from the visible darkening on exposed glass lantern slides. The slides indicated that the beam diameter at the target position was approximately $\frac{1}{8}$ inch for 1000 kilovolts, and $\frac{1}{4}$ inch for 500 kilovolts.

The target chamber is constructed out of a 14-inch diameter, 10-inch long brass cylinder with $\frac{5}{8}$-inch diameter ports. The ports are spaced at 10° intervals covering a range of θ values from 0° to 130°. Brass plates with O-rings seal the ports and ends of the cylinder. One end plate contains a bellows-type rotating seal which is used to turn a wheel for the target holders. The targets are mounted on 2-inch diameter thin aluminum frames which are automatically positioned in or out of the beam path at the center of the chamber with the aid of a Yardeny SL-3 Servo-Control unit.

The scintillation spectrometer consists of a 5-inch diameter 4-inch long NaI(Tl) crystal and a Dumont K1198 5-inch diameter photo-multiplier tube. These components were assembled in a steel cylindrical container and mounted inside a brass-lead collimator pot having the dimensions given in Fig. 1. The total weight of the collimator unit is about 1000 lb, and a counterweight is used to swing the collimator pot to any desired angle θ. With radiation incident on the crystal, the integrated pulses from the photomultiplier are fed in succession to a cathode follower, a nonoverloading linear amplifier[16] with an RC clipping time of 10 microseconds, and a 12-channel differential pulse-height analyzer. Also at the amplifier output, a scaler is used to count the total number of pulses above a base pulse-height level corresponding to 5 kev. During a run, there is less than a 2% shift in the base line of the analyzer, and less than a 10% maximum variation in the window width of any given channel. For the bremsstrahlung measurements which cover a range of photon energies extending up to 500 kev in one case and 1000 kev in the other, the window widths are set at about 10 kev. The actual window width of each channel is continuously calibrated during a run with a mercury relay type sliding pulser, which is motor driven so that the 60-cps pulse output increases in height at a rate that is constant to better than 1 percent. The over-all resolving time of the system as determined with a double pulse generator, is approximately 10 microseconds. The intensity of the bremsstrahlung radiation is controlled so that the total counting rate from the amplifier for all pulses larger than 5 kev does not exceed 900 counts per second. Therefore, the probability that 2 successive pulses in this energy range will be registered as a single pulse is less than 1%.

[15] E. E. Charlton and H. S. Hubbard, Gen. Elec. Rev. **43**, 272 (1940).

[16] R. L. Chase and W. A. Higinbotham, Rev. Sci. Instr. **23**, 34 (1952).

B. Procedure

With the accelerator operating at 500 and 1000 kilovolts, measurements were made at angles of θ equal to 0, 10, 30, 60, 90, and 120 degrees and 0, 10, 20, 30, and 90 degrees respectively.

The measurements were carried out according to the following procedure. The pulse-height distribution of the scintillation crystal was determined for a particular set of conditions: a given incident electron kinetic energy (500 or 1000 kev), a given target material and thickness, an integrated charge incident on the target, and a given angle θ. For each set of conditions, the pulse-height distribution was measured with the target foil in and out of the electron beam.

For a given incident electron energy E_0, the bremsstrahlung differential cross section with respect to photon energy and angle is determined by the quantity $P(k,\theta)/mn\Omega$, where $P(k,\theta)$ is the number of photons emitted from the target in the solid angle Ω per unit energy interval at energy k and angle θ for n electrons incident on m target atoms per cm^2. The photon flux $P(k,\theta)$ is directly related to the pulse-height distribution measured by the spectrometer. The method of determining each of the above quantities and estimates of the corresponding errors are discussed below.

C. Measurement of Electron Current

Electrons incident on the target are collected by the target chamber as shown in Fig. 1. This chamber is electrically insulated from the grounded section of the accelerator, and serves as a Faraday cup. Only a negligible fraction of the incident electrons can be backscattered out of the chamber because of the small solid angle (less than 0.01 steradian) subtended by the entrance aperture with respect to any point on the chamber wall. Target currents in a range from 10^{-10} to 10^{-6} ampere are measured with approximately 2 percent accuracy with a Higinbotham-Rankowitz type current integrator.[17] The input circuit to the integrator has the property of maintaining the chamber at ground potential. To assure the absence of spurious effects such as the external collection of charge produced by ionization in the air, the chamber potential was varied plus and minus 45 volts with respect to ground, and no change was observed in the target current. The in-

[17] W. A. Higinbotham and S. Rankowitz, Rev. Sci. Instr. **22**, 688 (1951).

tegrator was calibrated with currents in the specified range, which were determined with an accuracy of one percent. The area in the vicinity of the target chamber was surrounded with a ring of lead shielding stands which were grounded to minimize outside electrostatic disturbances. During a run, the target current appeared stable, and frequent checks were made of the zero-target-current setting.

D. Target Materials and Thicknesses

The target materials were selected to test the theory over a wide range of atomic numbers, and included beryllium, aluminum, and gold. The purity of these materials was determined by spectrochemical analysis. Various target impurities were detected in quantities not exceeding a fraction of one percent by weight. Because of the Z^2 dependence of the bremsstrahlung intensity, the relative contribution to the total radiation intensity from these impurities is primarily important for the low-Z targets. This contribution was estimated for the impurities in a given target by the use of the Z^2 impurity-target ratio, and was found to be less than 5% for all of the targets used in these measurements.

A detailed measurement of the bremsstrahlung differential cross section requires thin targets in which the electron energy loss and scattering is negligible. As an aid in the selection of such a thin target the angular spread of the electrons emerging from the target may be compared with the angular spread of the bremsstrahlung radiation. From the results of multiple scattering theory, Blanchard[18] has given a convenient expression for the mean square angle $\bar{\theta}_e^2$ of the electrons emerging from a given target. His results indicate that $\bar{\theta}_e^2 \approx 0.6Z\bar{\Delta}/T_0(T_0+1)$, where the average electron energy loss, $\bar{\Delta}$, is about 2 Mev per g per cm^2 in the present energy range,[19] and T_0 is the initial electron kinetic energy in Mev. For the bremsstrahlung radiation, angular distribution plots obtained with the Sauter theory[4] indicate that the angular spread can be approximated by a Gaussian distribution with a mean square angle $\bar{\theta}_k^2$ of $2/3T_0^2$. From these estimates, a rough guide which can be used in the selection of thin targets, is that $\bar{\theta}_e^2/\bar{\theta}_k^2 \ll 1$, or that the target thickness $t(\text{g/cm}^2) \ll (1/2Z)[(T_0+1)/T_0]$. In order to definitely establish the fact that the targets used in the present study are thin enough, measurements were made with two target thicknesses of gold and of aluminum (see below). The plots of the differential cross section, computed from the measurements for two thicknesses of the same material, agreed within the limits of the experimental error.

The average thickness of each target was determined with one percent accuracy from measurements of the target area and weight. In order to check the uniformity of each target thickness, the target was scanned in $\frac{1}{4}$-inch diameter segments with a polonium α-particle gauge, which measured the relative alpha-particle transmission through the foil. The maximum variation from the average foil thickness was found to be less than 10% over the whole target area and less than 3% over the limited area where the electron beam impinges on the target.

A summary of the targets used in these measurements is given as follows: a 0.22-mg/cm^2 gold foil, a 0.43-mg/cm^2 gold foil, a 0.63-mg/cm^2 aluminum foil, a 1.0-mg/cm^2 aluminum foil, and a 4.3-mg/cm^2 beryllium foil. Because each of these targets was tilted at an angle of 45° with respect to the direction of the incident electron beam (see Fig. 1), it is necessary to use a multiplying factor of 1.4 to obtain the effective target thickness.

E. Geometry Measurements

The important geometrical quantities involved in an absolute determination of the differential cross section are the angle θ (Fig. 1), and the solid angle Ω in which the photons emitted from the target are detected by the spectrometer.

The collimator axis of the spectrometer was set at given values of θ (see Sec. B) with the aid of an index plate. The accuracy of each setting was determined by comparing the angle between the collimator axis and electron beam direction with calibrated angles inscribed on a template. The maximum possible error in a specified θ value was less than 1 degree, and the corresponding error in the photon intensity $P(k,\theta)$ (Part II-B) was about 10%.

The solid angle Ω was determined from the geometry shown in Fig. 1. The area subtended by the spectrometer crystal with respect to the center of the chamber is mainly defined by the $\frac{1}{4}$-inch diameter collimator hole, which gives an angular resolution of about 1°. However, depending on the photon energy, there can be various degrees of photon penetration and scattering through the collimator walls. Such an effect would tend to increase the solid angle. In order to estimate how this effect depends on photon energy, measurements were made with gamma-ray sources, Cs^{137} (0.66 Mev), and Co^{60} (1.17 Mev, 1.33 Mev), placed at position A directly in front of the collimator and at the target position B (see Fig. 1). Because of the difference in solid angle at the two positions, there is a corresponding difference in the relative number of photons which strike the collimator wall. Therefore, if the pulse-height distribution curves measured at the two positions, are normalized to a given source-crystal distance by the use of the inverse square law, the percent change in the effective solid angle in the two cases can be found by the ratio of the curve areas. The results show that the effective solid angle is 14% larger for the Cs^{137} source, and 32% larger for the Co^{60} source, at position A

[18] C. H. Blanchard, in *Electron Physics*, National Bureau of Standards Circular 527 (U. S. Government Printing Office, Washington, D. C., 1954), p. 9.
[19] See reference 3, p. 368.

compared to position B. Additional measurements made with a calibrated Co^{60} source at the target position B (see Sec. G) indicate that the effective solid angle of detection for 1-Mev photons emitted from the target is approximately 10% larger than that computed by using an area equal to the $\frac{3}{4}$-inch diameter hole at the front crystal face. This solid-angle correction was used in the present measurements for 1-Mev photons, and on the basis of the results obtained above with the Cs^{137} and Co^{60} sources, the correction was assumed to have approximately the same dependence on photon energy as the photon penetration that is given by using the total photon absorption coefficient for brass.

F. Determination of the Photon-Flux

The radiation incident on the NaI(Tl) crystal can be separated into two components: (a) the normal background radiation which includes that produced by the electrons incident on the walls of the target chamber, and (b) the photons defined in Sec. B as $P(k,\theta)$, which pass from the target through the $\frac{3}{4}$-inch diameter collimator hole to the crystal as shown by the geometry in Fig. 1. Component (a) is measured with the target foil out of the electron beam, and component (b) is then the difference measured with the foil in and out of the electron beam. In addition to the target itself, other materials in the collimator line of sight can act as potential sources of radiation. These materials include the 15-mil aluminum window of the target chamber and a small region of the opposite chamber wall (Fig. 1). Radiation from the wall region is mainly accounted for by the measurements made with the foil moved out of the electron beam. To eliminate radiation from the window, an electron trap employing a permanent magnet deflects electrons traveling in the direction of the window. The effectiveness of the trap was checked in the following manner: A tantalum foil was placed over the inside area of the aluminum window for values of θ equal to zero degree (where the window is in the direct electron beam) and 20 degrees, and no appreciable difference was detected in the pulse-height distributions for a given target as compared to the cases with no tantalum foil.

The pulse-height distribution produced in the NaI(Tl) crystal by the incident radiation is measured with the differential analyzer, as described in Sec. A. If the pulse heights are calibrated in terms of photon energies, then the pulse height distribution can be expressed in terms of the number of pulses per unit energy interval at a given photon energy. Such a distribution is shown in Fig. 2 for the case where the initial electron kinetic energy is 1 Mev, θ is 30 degrees, the charge of the electrons is 3.5×10^{-6} coulomb, and the target is a 0.43-mg/cm^2 gold foil. The solid line (open circles) represents the pulse height distribution, $N(h)$, produced by the photon flux $P(k,\theta)$. The values for $N(h)$ are obtained from the counting rate difference for the

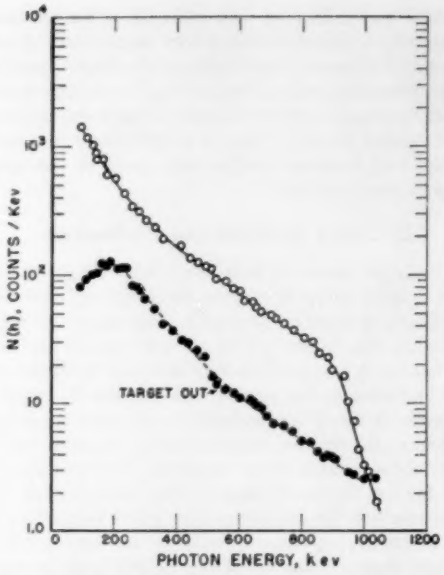

FIG. 2. Pulse-height distribution measured with 1-Mev electrons incident on 0.43-mg/cm^2 gold target for total electron charge of 3.5×10^{-6} coulomb and for θ equal to 30 degrees. The dashed line (closed circles) is the background distribution with the target removed from the electron beam, and the solid line (open circles) is the distribution given by the difference between the target in and out of the electron beam.

target positioned in and out of the electron beam. The dashed curve shows the target out data which indicates the relative contribution of background radiation over the entire energy range. The effect of the finite spectrometer resolution is shown by the extension of the $N(h)$ curve beyond the maximum photon energy expected for 1-Mev bremsstrahlung.

For a given photon flux $P(k)$, the pulse-height distribution $N(h)$ can be expressed as

$$N(h)=\int_0^{E_0-\mu} R(h,k)P(k)dk, \qquad (4)$$

where μ is the electron rest energy, and $R(h,k)$ is the spectrometer response function which represents the probability that a pulse is recorded in a unit pulse-height interval at height h for a photon of energy k. Approximate solutions of the integral equation for $P(k)$ have been considered for certain analytical response functions.[20,21]

In the present case, the pulse-height response of this large crystal spectrometer to monoenergetic photons has a Gaussian shape with a low-energy tail[22] which

[20] G. E. Owen and H. Primakoff, Phys. Rev. **74**, 1406 (1948); Rev. Sci. Instr. **21**, 447 (1950); J. P. Palmer and L. J. Laslett, Atomic Energy Commission Report AECU-1220, 1951 (unpublished).
[21] Theus, Beach, and Faust, J. Appl. Phys. **26**, 294 (1955).
[22] R. S. Foote and H. W. Koch, Rev. Sci. Instr. **25**, 746 (1954).

replaces the prominent Compton escape peak found with small crystals. Response curves were measured for the photons from sources of Co^{60} (1.17 Mev, 1.33 Mev),[23] Cs^{137} (0.662 Mev),[22] Hg^{203} (0.279 Mev),[22] and Cd^{109} (0.087 Mev).[22] Corrections were made for the background pulse-height distribution which was measured by plugging the collimator hole. The resulting response curves showed good agreement with the theoretical response curves obtained from Monte Carlo calculations by Berger and Doggett.[24] For example, with the gamma rays from thin sources of Cs^{137} and Co^{60} placed at target position B, the response curves gave values of the photo-fraction (defined as the ratio of the photopeak area to the total area under the pulse-height distribution curve) equal to 0.79 and 0.65 (1.33-Mev Co^{60} gamma rays only), compared to the theoretical values of 0.82 and 0.67 respectively. In addition, the measurements indicated that with the source placed at the closer position A (Fig. 1), there was about a 10 percent decrease in the photo-fraction due to the increased scattering in the collimator. The shapes of these curves, which have half-widths that are inversely proportional to $k^{\frac{1}{2}}$ for photon energies below 2 Mev,[22] can be represented as a single universal curve, if the peak values are normalized to one and the abscissas are plotted in terms of the quantity $(h/k-1)\sqrt{k}$. Such a universal shape is plotted in Fig. 3 for the above photon energies. The data shows that the ratio of tail height to peak of the response curve, decreases with photon energy. In the present case, it is a good approximation to assume that the tail height is constant with pulse height for a given photon energy, and a functional relationship can then be obtained between the tail height and photon energy.

With the above information, the response function $R(h,k)$ can be constructed in the form of a matrix with indices h and k, and Eq. (4) can be solved for $P(k)$ by numerical inversion.[20] The matrix elements are determined by adjusting the values obtained from Fig. 3, so that for a given k, $\int_0^\infty R(h,k)dh$ is equal to the detector efficiency. In practise, the matrix elements are summed over h for pulse-height intervals of both 25 and 50 kev. (These intervals were found to be small enough to cause no distortion in the shapes of the computed spectra.) The detector efficiency is given by the quantity $(1-e^{-\mu(k)t})$, where $\mu(k)$ is the total absorption coefficient[25] and t is the length of the NaI(Tl) crystal. If this response matrix is now applied to a given input photon spectrum, a set of simultaneous linear equations is determined which relate the photon spectrum to the corresponding pulse-height distribution.

The accuracy with which values of the photon flux

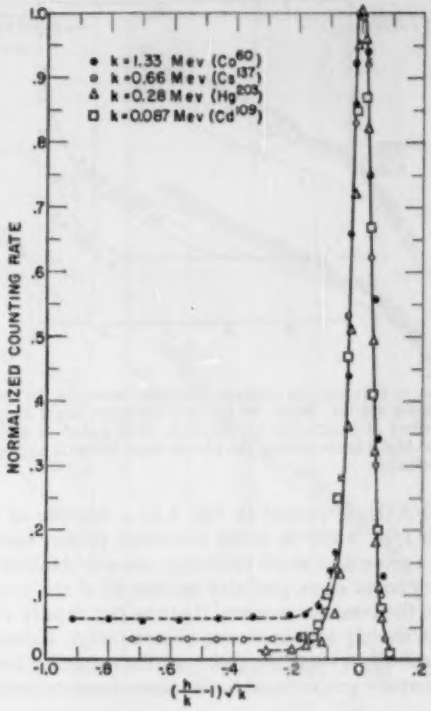

FIG. 3. Universal spectrometer response curves for monoenergetic photons. The measured counting rate is plotted as a function of the pulse height h and the photon energy k. Small fluctuations which appear in the low-energy tail region have been smoothed out to simplify the data analysis.

$P(k)$ can be determined from a measured pulse-height distribution by numerical inversion, depends on the detailed shape of the photon spectrum. In the present case, the measurements indicate that the bremsstrahlung photons have a well-behaved continuous distribution, which falls off rapidly with energy, and which cuts off at a maximum photon energy. The pulse-height distribution data (Fig. 2) have statistical errors that increase up to 30% as the background level is approached in the region of the cut-off point. It is therefore not reliable to carry through the numerical inversion by a simple peeling-off process where the value of the photon flux at a given energy would be critically dependent on the corresponding pulse height value. A more accurate treatment is obtained if it is assumed that the photon spectrum is linear in a small region: then the inversion procedure can be initiated at a pulse-height corresponding to the maximum photon energy, and with the aid of a simple perturbation type calculation, a line by line solution of the simultaneous equations is permissible. Such inversion computations were made for the pulse-height distributions measured with 500- and 1000-kev electrons and with different target materials and photon angles. The resulting correction factor,

[23] *Nuclear Data*, National Bureau of Standards Circular No. 499 (U. S. Government Printing Office, Washington, D. C., 1950).
[24] M. J. Berger and J. Doggett, Rev. Sci. Instr. (to be published).
[25] Gladys R. White, National Bureau of Standards Report NBS-1003, 1952 (unpublished).

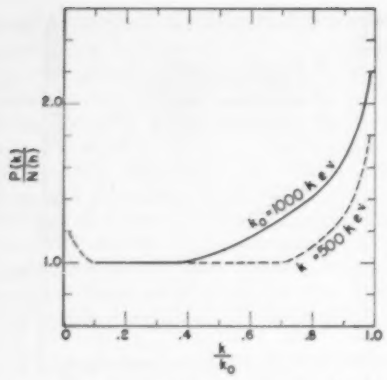

FIG. 4. Spectrometer response correction factor for the bremsstrahlung spectra. Below 100 kev, the correction factor included the effect of absorption by materials (0.24 g/cm² Al and 1.2 g/cm² MgO) in the path of the photon beam before it strikes the NaI crystal.

$P(k)/N(k)$, is plotted in Fig. 4 as a function of the ratio k/k_0, where k_0 is the maximum photon energy. For a given k_0, a single correction curve is obtained for the different cases, probably because all of the spectra have the common property that the flux density $P(k)$ drops sharply with increasing photon energy. Except in the cut-off region of the spectrum, the correction factor is inversely proportional to the photo-fraction (defined above) of the response curve. Because the photo-fraction increases as the photon energy decreases,[24] it is not surprising that the correction factors are smaller for the 500-kev curve. In the region below 100 kev, these curves include a correction which accounts for the photon absorption in the windows of the target chamber and NaI(Tl) crystal, and in the MgO powder that is used as a reflector around the crystal.

G. Calibration Measurements

The photon energies measured by the spectrometer were calibrated with the gamma rays from the radioactive sources listed in Sec. F. Frequent checks on the pulse height stability of the spectrometer were made with the gamma rays from the Co^{60}, Cs^{137}, and Hg^{203} sources, and it was found that the pulse-height corresponding to a given photon energy showed less than a 2 percent variation during a days run. No effects on the energy calibration due to the earth's magnetic field were observed as the spectrometer was rotated into the various positions used in the measurements.

The accuracy with which photon intensities were determined was checked by measurements made with a calibrated Co^{60} source and with cavity ionization chambers. A Co^{60} source was calibrated by the method of gamma-gamma coincidences and the absolute disintegration rate was found to be $(2.03\pm0.01)\times10^7$

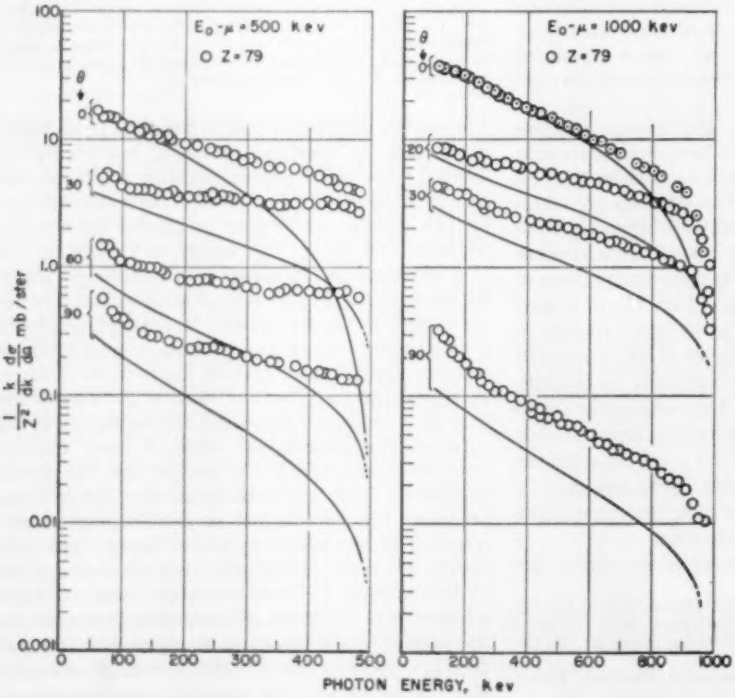

FIG. 5. Differential cross sections for 0.5- and 1.0-Mev bremsstrahlung at photon energies k and angles θ. The experimental values (open circles) were obtained with a gold target. The fractional standard deviations due to statistical counting errors are less than 5% for points below $0.8k_0$, less than 20% for points below $0.9k_0$, and less than 30% for points below k_0, where k_0 is equal to $(E_0-\mu)$. The theoretical cross sections (without screening) are shown by the solid curves which were computed from Sauter's results [see expression (1)].

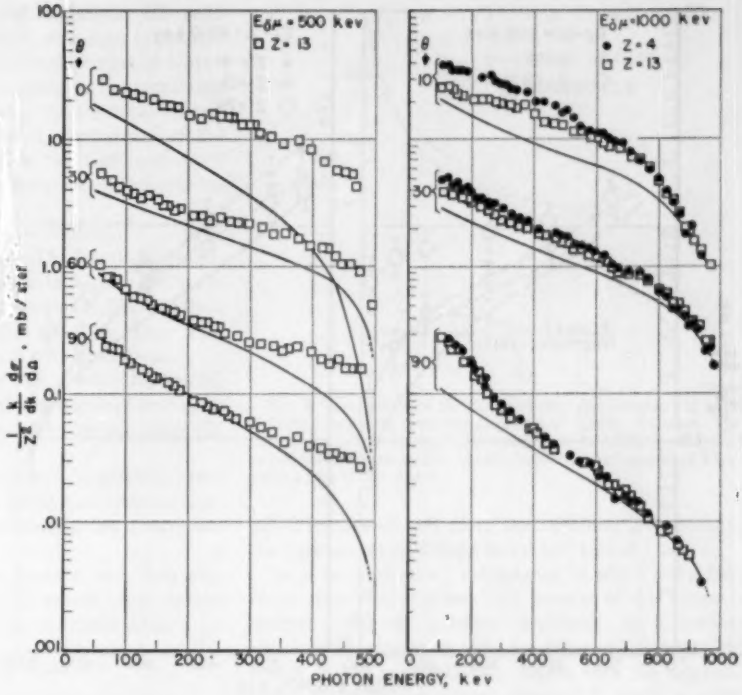

FIG. 6. Differential cross sections for 0.5- and 1.0-Mev bremsstrahlung at photon energies k and angles θ. The experimental values were obtained with beryllium (closed circles) and aluminum (squares) targets, and have the same statistical error limits as discussed in Fig. 5. The Sauter theoretical cross sections (without screening) are shown by the solid curves [see expression (1)].

disintegrations per second.[26] In comparison, the disintegration rate of this source as measured by the spectrometer with the source at the target position was found to be 2.23 ± 0.05 disintegrations per second. This latter result was obtained from the product of the area under the pulse-height distribution curve produced by the Co^{60} gamma-rays, the detection efficiency of the NaI crystal (the absorption coefficient was selected from White's Tables[25] for an average photon energy of 1.25 Mev), and the solid angle correction factor (where the collimator diameter was used to determine the area subtended at the crystal). The 10% excess rate measured by the spectrometer was used as a solid angle correction factor for 1-Mev photons, which arises because of photon penetration through the collimator (see Sec. E).

III. EXPERIMENTAL RESULTS

The experimental values of the differential cross section are divided by Z^2 in order to eliminate the expected Z^2 dependence of the bremsstrahlung radiation. The results are summarized in Figs. 5 and 6, which show the high-Z and low-Z measurements respectively for the initial electron kinetic energies of 0.5 and 1.0 Mev. (Additional results for other values of θ (see Part II-B) are omitted to avoid crowding of the data.) The solid lines in these graphs represent the Sauter theoretical values which are obtained from expression (1) and do not include the effect of screening.

The experimental values of the cross section integrated over the direction of the photon emission are obtained by graphical integration of the results given in Figs. 5 and 6, and are shown in Fig. 7. The theoretical values computed from expression (2) are given by the solid lines.

Finally, the total integrated cross section ϕ_{rad}, which is equal to the quantity $(1/E_0)\int_0^{E_0-\mu}k(d\sigma_k/dk)dk$, was found by integrating the data given in Fig. 7, and is presented in Fig. 8. The theoretical values for ϕ_{rad} are shown by the solid line in Fig. 8, and were obtained from the results given in reference 2. The screening effect which becomes important at the higher energies is shown by the dashed line for $Z=82$. In order to account for the contribution of electron-electron bremsstrahlung, Fig. 8 indicates the shift in the low-Z results that is produced by the factor $Z^2/Z(Z+1)$.

As a final check on the accuracy of the photon flux $P(k,\theta)$ that is determined from the spectrometer measurements, a Landsverk 200-milliroentgen ionization chamber was used to measure the dose produced by the bremsstrahlung radiation at a point on the collimator axis at the front face of the crystal 80 cm from the target. These measurements were made for three different targets, with θ equal to 10 degrees, $(E_0-\mu)$ equal

[26] This calibration was made by Dr. George Minton who is preparing a description of his measurements for publication.

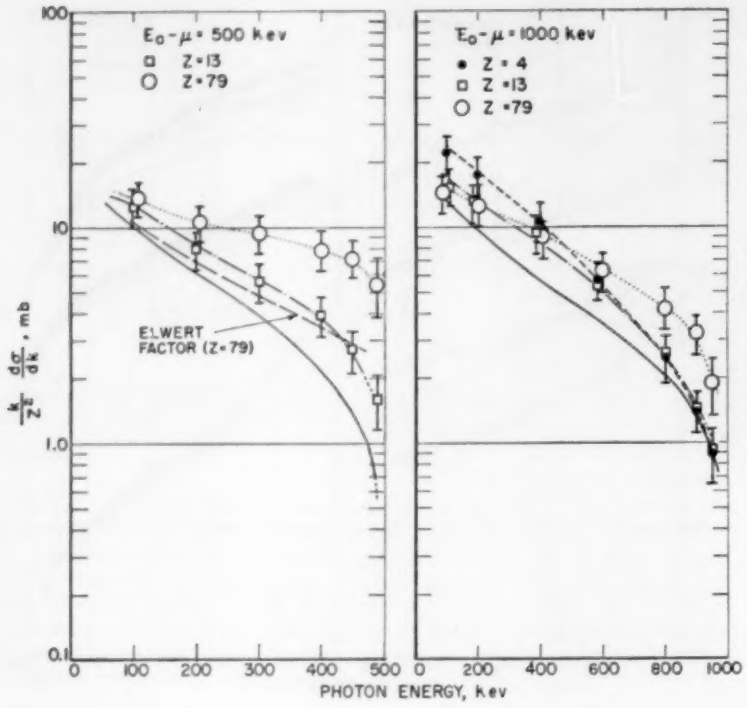

FIG. 7. Cross sections for 0.5- and 1.0-Mev bremsstrahlung integrated over the direction of photon emission. The experimental values were obtained with a gold (open circles), aluminum (squares), and beryllium (closed circles) target, and are shown with the total error limits. The Bethe-Heitler theoretical cross section [see Expression (2)] is shown by the solid lines. The 500-kev Bethe-Heitler curve corrected by the Elwert factor[29] with Z equal to 79 is shown by the dashed curve.

to 1 Mev, and the total electron charge incident on the target equal to 1.7×10^{-3} coulomb. For comparison, the dose was computed from the spectrometer measurements made under the above conditions by integrating the photon energy flux density over photon energy. An approximate conversion factor of 2900 ergs per cm² per roentgen was used over this energy range. This value was obtained by using 0.029 cm²/g for the mass absorption coefficient of air and 33.5 ev for the energy required to produce an ion pair. Also, the dose was computed for the photon energy flux density that would be produced according to the Sauter-Bethe-Heitler theory under the same conditions. The results are shown in Table I, where the accuracy of the values measured by the chamber and spectrometer is estimated to be approximately 10% (see Part IV). The spectrometer measurements show good agreement with the chamber dose measurements compared to the considerably lower values computed from the theoretical cross sections.

TABLE I. Comparison of expected and measured dose 80 cm from target ($E_0-\mu=1000$ kev, $\theta=10°$, $Q=1.7\times10^{-3}$ coulomb).

		Milliroentgens		
Z	Foil mg/cm²	Landsverk ionization chamber	Spectrometer	Sauter-Bethe-Heitler theory
4	4.3	120	113	60
13	0.63	47	44	30
79	0.43	147	147	110

IV. SUMMARY OF ERRORS

The accuracy of the experimental values obtained for the bremsstrahlung cross sections may be estimated from a survey of the important errors and corrections involved in the measurements.

Sources of systematic error and estimates of the upper error limits are given as follows:

(1) Photon angle (Part II-E): A maximum error of one degree gives a corresponding error of approximately 10% in the value of the photon flux $P(k,\theta)$ (Part II-B).

(2) Target current (Part II-C): ±2%.

(3) Target uniformity and thickness (Part II-D): ±3%.

(4) Angle between target plane and incident electron direction (Part II-D): A maximum error of 2 degrees gives a 2% error for the effective target thickness.

(5) Photon flux $P(k,\theta)$ (Part II-F, G): ±5%.

If these errors were in the same direction, the total error would be ±22%.

The important corrections made in the measurements include:

(1) Foil impurity correction (Part II-D). The photon intensities $P(k,\theta)$ (Part II-F) measured with the low-Z beryllium and aluminum targets were reduced by 5% to account for the contribution from the high-Z impurities. The reliability of this correction is estimated to be better than 30%.

(2) Solid angle correction (Part II-E). Because of

photon penetration through the collimator, the solid angle computed with the $\frac{3}{8}$-inch diameter collimator was increased by 10 percent for the detection of 1-Mev photons. For decreasing photon energies, the correction decreases in a manner determined by the total photon absorption coefficient for brass. A comparison of the measurements (Part II-E) with the Co^{60} and Cs^{137} sources indicates that this correction is reliable to within 30%.

Other experimental errors are as follows:

(1) Statistical counting errors. The fractional standard deviations for the points given in Figs. 5 and 6 are less than 5% in the energy region below $0.8k_0$, less than 20% between $0.8k_0$ and $0.9k_0$, and less than 30% between $0.9k_0$ and k_0, where k_0 is equal to $E_0-\mu$.

(2) Variation in the window width of the differential analyzer (Part II-A). The fractional standard deviation for the window width is estimated to be less than 4% for any given bin.

(3) Error arising from graphical integration over photon energy and angle of the differential cross section. The maximum uncertainty produced by this integration is estimated to be $\pm 3\%$.

From a consideration of the above errors, it is estimated that the values for the integrated cross section ϕ_{rad} (shown in Fig. 8) are reliable to within 20%.

V. DISCUSSION OF RESULTS

A. Breakdown of the Born Approximation

The theoretical cross sections given in the above results have been formulated on the basis of certain assumptions[27] of which the most important is the Born approximation. The necessary conditions for this approximation are severe: namely that $(2\pi Z/137)(c/v_0)$ and $(2\pi Z/137)(c/v)\ll 1$, where v_0 and v are the electron

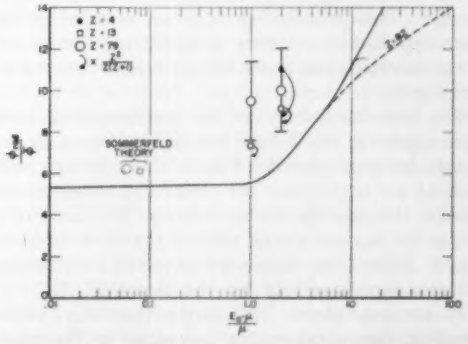

FIG. 8. Cross section for the energy lost by radiation. ϕ_{rad} is equal to $(1/E_0)\int_0^{E_0-\mu} k(d\sigma_k/dk)dk$, where $d\sigma_k$ is given by Expression (2), and $\bar{\phi}$ is $5.8\times10^{-28}Z^2$ cm². The dashed line indicates the screening effect for Z equal to 82. The low-Z experimental values are multiplied by $Z^2/Z(Z+1)$ to account for electron-electron bremsstrahlung. Theoretical values obtained from the Sommerfeld theory[1] are shown in the nonrelativistic region.

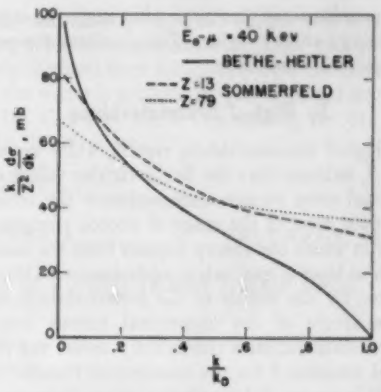

FIG. 9. Comparison of the Bethe-Heitler and Sommerfeld cross sections integrated over the direction of photon emission. The maximum photon energy, k_0, is equal to 40 kev. The Sommerfeld values for the cross section are obtained from the results of Kirkpatrick and Wiedmann.[28]

velocities before and after the collision. Accordingly, the approximation breaks down for large Z.

As v_0 becomes small, the manner in which the differential cross section is modified because of this approximation is difficult to follow intuitively. As a possible aid, it is of interest to compare the exact Sommerfeld theory in the nonrelativistic region with the approximate Bethe-Heitler-Sauter theory.[3-5] Such a comparison provides some grounds for inferring possible qualitative differences between an exact theory and the Bethe-Heitler-Sauter theory at the higher energies ($T_0\approx\mu$). The Sommerfeld and Bethe-Heitler values of the cross section integrated over the direction of photon emission are plotted in Fig. 9 for an initial electron kinetic energy of 40 kev. The Sommerfeld values for Z equal to 13 and 79 were obtained from the calculations made by Kirkpatrick and Wiedmann[28] and the Bethe-Heitler values were obtained from Eq. (18) in reference 3. A comparison of these curves gives the following information for the nonrelativistic region: (a) The approximate Bethe-Heitler bremsstrahlung theory underestimates the cross section as given by the exact Sommerfeld theory. In the exact theory, the cross section approaches a finite value at the upper limit of photon energies compared to the sharp drop to zero of the Bethe-Heitler curve. At small photon energies, the Bethe-Heitler curve which does not include screening, rises above the exact theory curves. (b) The exact cross sections are not simply proportional to Z^2. At low photon energies, the values of the low-Z curve are greater than the high-Z values, and with increasing photon energies there is a crossover where the low-Z curve drops below the high-Z curve. This crossover feature makes the cross section integrated over photon energies approximately proportional to Z^2. The above

[27] See reference 3, p. 254.

[28] P. Kirkpatrick and L. Wiedmann, Phys. Rev. 67, 321 (1945).

results provide some clue as to what might be expected in the higher energy region ($T_0 \approx \mu$) where the present measurements were made.

B. High-Z Bremsstrahlung

The high-Z bremsstrahlung results, which are shown in Fig. 5, indicate that the Bethe-Heitler values of the differential cross section underestimate the measured values over most of the range of photon energies. The manner in which the theory departs from the measurements is at least in qualitative agreement with the trend suggested by the results in the nonrelativistic region. The departure of the theoretical curves from the measurements increases consistently as (a) the photon angle of emission θ (or the momentum transfer to the nucleus) increases, (b) the photon energy increases, and (c) the initial electron kinetic energy decreases. The trends (b) and (c) hold also for the cross section integrated over the direction of photon emission, as shown by the results in Fig. 7. The error given for each experimental point in Fig. 7 is an estimated upper limit for the combined errors discussed in Part IV.

Quantitative estimates of the difference expected between the approximate Bethe-Heitler theory and an exact theory were made by Elwert.[29] His results are given as a correction factor that can be applied to the Bethe-Heitler values for the cross section.[30] The Elwert corrected Bethe-Heitler curve is plotted in Fig. 7 for the case where $(E_0-\mu)$ is 500 kev and Z is 79. The large discrepancy that remains between the Elwert curve and the corresponding experimental curve, shows that Elwert's theory does not provide an adequate correction factor for the Bethe-Heitler theory.

Figure 8 shows that the high-Z experimental cross section values for the energy lost by radiation, ϕ_{rad}, are about a factor of two larger than the corresponding Bethe-Heitler values. The high-Z experimental values for $\phi_{\text{rad}}/\tilde{\phi}$ (where $\tilde{\phi}$ is $5.8\times10^{-28}Z^2$ cm^2) are 9.5 ± 1.9 at 500 kev and 10 ± 2.0 at 1000 kev compared to the theoretical values of 5.5 and 6.5 respectively.

C. Low-Z and Electron-Electron Bremsstrahlung

Low-Z bremsstrahlung is complicated by the fact that the role of atomic electrons becomes important in the process. The cross section dependence is expected to go more like $Z(Z+1)$ rather than Z^2,[31] which means that the contribution from electron-electron bremsstrahlung would be about 10 percent for aluminum and 25 percent for beryllium. The results obtained for these two materials with 1000-kev electrons are shown in Fig. 6. Except for the effect of electron-electron bremsstrahlung, it may be expected that the cross section divided by Z^2 would be approximately the same for all low-Z materials. Therefore, it is difficult to escape the conclusion that the differences shown in Fig. 6 are indeed evidence of the electron-electron bremsstrahlung process. The fact that the differences are large at 10 degrees and practically disappear at 90 degrees carries additional weight, since the radiation intensity from electron-electron bremsstrahlung is expected to be concentrated at small angles from considerations of the dynamics involved in transforming from the center-of-mass to the laboratory system. It is also of interest to determine the maximum photon energy, K_0, for electron-electron bremsstrahlung that is available in the laboratory system at the laboratory angle θ. With the aid of the Lorentz transformation, it can be shown that

$$K_0=\mu F/(1-\cos\theta\sqrt{F}), \tag{5}$$

where F is equal to $(E_0-\mu)/(E_0+\mu)$. From this expression, the values obtained for K_0 with $(E_0-\mu)$ equal to 1000 kev are 824 kev at 10 degrees, 650 kev at 30 degrees, and 253 kev at 90 degrees. These results are not inconsistent with the measurements shown in Fig. 6, where it is seen that the differences between the two materials tend to vanish as the curves approach the above values for K_0.

The low-Z cross section measurements shown in Fig. 6 indicate that even if electron-electron bremsstrahlung is accounted for, there still appears to be some discrepancy between theory and experiment. As θ becomes smaller, the Bethe-Heitler curve underestimates the measured values. For these small values of θ, a comparison of the low- and high-Z curves reveals a cross-over in which the low-Z curve drops from above to below the high-Z curve with increasing photon energies. This behavior which is not revealed in the Born approximation theory is similar to what occurs in the nonrelativistic region for the Sommerfeld theory (see Fig. 9).

The experimental values for the integrated cross section given in Fig. 7 show the combined error for the various factors discussed in Part IV. Most of these cross sections are larger than the theoretical values by an amount that exceeds the error limits. The final low-Z values for ϕ_{rad} are shown without the error limits in Fig. 8. When these values are corrected for electron-electron bremsstrahlung by the factor $Z^2/Z(Z+1)$, they are only about 30% larger than that corresponding theoretical values, compared to the much larger differences obtained in the high-Z results. The experimental values for $\phi_{\text{rad}}/\tilde{\phi}$ with the $Z^2/Z(Z+1)$ correction factor are given as 8.8 ± 1.8 and 8.4 ± 1.7 for Be and Al respectively at 1000 kev, and 6.8 ± 1.4 for Al at 500 kev. The corresponding Bethe-Heitler values are 6.5 and 5.5. The Sommerfeld values for ϕ_{rad} are also shown in Fig. 8, and it is seen that like the experimental

[29] G. Elwert, Ann. Physik **34**, 178 (1939).
[30] See reference 3, p. 246.
[31] The $Z(Z+1)$ formula gives only an estimate of order of magnitude. A detailed theory of bremsstrahlung in collisions between free electrons has not been worked out except for limiting conditions, see J. Katzenstein, Phys. Rev. **78**, 161 (1950) and M. L. G. Redhead, Proc. Phys. Soc. (London) **A66**, 196 (1953). For the role of binding in various processes involving atomic electrons, see also J. A. Wheeler and W. E. Lamb, Phys. Rev. **55**, 858 (1939) and U. Fano, Phys. Rev. **93**, 117 (1954).

values at the higher energies, they are larger than the corresponding Bethe-Heitler cross section.

VI. ACKNOWLEDGMENTS

The writer wishes to thank Dr. William Miller for his contributions and suggestions, Dr. H. O. Wyckoff for his help and advice, Mr. Fred Frantz and Mr. George Dempsey for their assistance with the measurements, and Mr. Richard Bach for his help with the calculations. Also, the writer is grateful for the beneficial discussions with Dr. U. Fano, Dr. I. Oppenheim, Dr. M. Danos, and Dr. H. W. Koch.

PHYSICAL REVIEW VOLUME 100, NUMBER 6 DECEMBER 15, 1955

Small Oscillation Theory of the Interaction of a Particle and Scalar Field

E. P. Gross
Syracuse University, Syracuse, New York
(Received July 28, 1955)

We study the interaction of a nonrelativistic particle with a scalar field, with particular application to the theory of polarons. The approach is based on a general classical method for the integration of equations of motion. The Hamiltonian is transformed by successive canonical transformations, the first corresponding to describing the motion relative to special solutions of the equations of motion. This stage as applied to suitably ordered Heisenberg equations of motion is identical with intermediate coupling theory. The second transformation treats the coupled small oscillations of particle and field oscillators about the chosen special solution. This affords a natural extension of intermediate coupling theory for this problem. Differences between the classical and quantum theories arise in the ordering of operators; the differences play a crucial role in determining the effective cutoff in wave vector space.

I. INTRODUCTION

THE theory of the interaction of an electron with lattice vibrations has received much attention recently. Aside from the question of oversimplifications customarily made in describing the physical system, there is the problem of finding quantum theoretic methods powerful enough to analyze the structure of the typical Hamiltonians encountered. The present deficiency hampers progress in the theory of normal and super conducting metals at low temperatures, and makes uncertain, estimates of lattice mobility in polar crystals and semiconductors. The electron-lattice interaction is also interesting from the point of view of the theory of elementary particles. The Hamiltonian corresponds to a simplified nonrelativistic field theory with a *bona fide* cutoff. One is concerned with developing theories of source recoil for intermediate and strong coupling which may have implications for the general theory of fields. The studies have already given rise to a new adiabatic theory.[1]

We will here be chiefly concerned with the polaron problem—loosely speaking, the theory of the interaction of a free electron with the optical modes of a polar lattice. It possesses the simplification that a minimum energy $\hbar\omega$ is required to excite a quantum of optical vibration (ω is the common frequency of the vibrations). For the lowest states of the system, one has a pure self energy situation with no free quanta present. A range of such states is possible; they are characterized by an integral of the motion $\mathbf{P}$ with the dimensions of a momentum, where $\mathbf{P}$ satisfies $P^2/2m \lesssim \hbar\omega$. Most studies[2-6] have dealt with the properties of the above class of states as a function of coupling strength, in particular the energy of the very lowest state with $P=0$, and the nearby states for which $P^2/2m \ll \hbar\omega$. Less attention has been paid to the case where $P^2/2m \approx \hbar\omega$ and to the nature of the excited states. These regions are of interest in the theory of dielectric breakdown and in mobility calculations. The determination of the energies of the low-lying states has involved mainly variational techniques. The most successful methods are those of Hohler and Feynman. The advantages are known; the disadvantages are that it is hard to make a picture of the behavior, that the intrinsic structure of the Hamiltonian is lost sight of and that the determination of the excited states is made difficult.

In the following, we note that classical theory points to a natural attack on the problem, and we explore some of the consequences. In the theory of orbits one finds a solution of the equations of motion (stable orbit) for which the initial conditions have been chosen in a particular way. Then one studies small oscillations about the orbit. If the orbit is stable, there is a region of phase space in which the full freedom in choice of initial conditions is present. At the edges of the region of stable motion the small-oscillation assumption is not valid; however, classically the amplitude may be made arbitrarily small so that there is always a domain where anharmonic terms can be neglected. For the

[1] N. Bogoliubov, Ukr. Math. J. T II, No. 2, 3 (1950); S. Tyablikov, Zhur. Eksptl. i Teort. Fiz. 21, 377 (1951).

[2] S. I. Pekar, *Untersuchungen uber die Elektronentheorie der Kristalle* (Akademische-Verlag, Berlin, 1954).

[3] H. Fröhlich, Advances in Phys. 3, 325 (1954).

[4] G. Hohler, Z. Physik 140, 192 (1955).

[5] R. P. Feynman, Phys. Rev. 97, 660 (1955). These papers contain references to earlier work.

polaron problem there is such a stable motion; the electron moves with uniform momentum and the lattice modes undergo forced oscillations. There are then neighboring states in which electron and lattice oscillators undergo coupled small oscillation. This classical picture will be applied here to the lowest states; the intimately phased motion of electrons and ions leads to lowering of the energy, and may be of the type needed in the theory of superconductivity.

Mathematically both classical and quantum theory involve a series of canonical transformations.[6] The first introduces coordinates relative to the stable orbit, and the second is a normal mode transformation; later transformations are perturbation treatments of the anharmonic terms. However, because of the finite de Broglie wavelength of the electron and the zero-point motion of the lattice, the classical and quantum transformations differ. The differences are most significant for short-wavelength modes and provide a cutoff in the quantum theory not present classically. This advantage is offset by the fact that the concept of small oscillations is not entirely natural in quantum theory, since the minimum amplitude of zero-point vibrations may take a problem inherently anharmonic. This is reflected in the mathematical formalism in questions of ordering of creation and annihilation operators, and in approximations beyond the classical scheme.

2. CLASSICAL THEORY

For details of notation and the analysis leading to the Hamiltonian we refer to Fröhlich *et al.*[7] The Hamiltonian is

$$H=\mathbf{p}^2/2m+\tfrac{1}{2}\sum_{\mathbf{k}}\{(Y_{\mathbf{k}}^2/M)+M\omega_{\mathbf{k}}^2X_{\mathbf{k}}^2\} +\sum g_{\mathbf{k}}'\{X_{\mathbf{k}}\sin(\mathbf{k}\cdot\mathbf{q})+(Y_{\mathbf{k}}/M\omega_{\mathbf{k}})\cos(\mathbf{k}\cdot\mathbf{q})\}, \quad (1)$$

where $\mathbf{p}$ and $\mathbf{q}$ are canonical coordinates of the particle of mass m; $\omega_{\mathbf{k}}$ is the frequency of a lattice oscillator with wave vector $\mathbf{k}$; $Y_{\mathbf{k}}$ and $X_{\mathbf{k}}$ are canonical momenta and coordinates of the oscillators; M is a constant with dimensions of the square of a time; $X_{\mathbf{k}}^2$ and $Y_{\mathbf{k}}^2/M$ have dimensions of energy; $g_{\mathbf{k}}'$ has dimensions of a square root of energy. We may write $g_{\mathbf{k}}'=g_{\mathbf{k}}/L^{\frac{1}{2}}$, where L is the length of the cube enclosing the system (periodic boundary conditions). Then $\mathbf{k}$ takes on the values $\mathbf{k}=\mathbf{n}2\pi/L$, where the triplet $\mathbf{n}$ consists of negative and positive integers.

One verifies that the following is a special solution of Hamilton's equations for the system[8]:

$$\mathbf{p}=\mathbf{p}_0=\text{const}; \qquad \mathbf{q}=(\mathbf{p}_0/m)t+\mathbf{q}_0;$$

$$X_{\mathbf{k}}=\frac{g_{\mathbf{k}}'}{M\omega_{\mathbf{k}}}\frac{\sin(\mathbf{k}\cdot\mathbf{q})}{(\mathbf{k}\cdot\mathbf{p}_0/m)-\omega_{\mathbf{k}}}; \quad Y_{\mathbf{k}}=g_{\mathbf{k}}'\frac{\cos(\mathbf{k}\cdot\mathbf{q})}{(\mathbf{k}\cdot\mathbf{p}_0/m)-\omega_{\mathbf{k}}}. \quad (2)$$

[6] The approach is a special case of the general method for integration of classical equations of motion. See Whittaker, *Analytical Dynamics* (Dover Publications, New York, 1944), Chap. 16.

[7] Fröhlich, Pelzer and Zienau (hereafter denoted F.P.Z.), Phil. Mag. 41, 221 (1950).

[8] E. P. Gross, Technical Report No. 55, Laboratory for Insulation Research, Massachusetts Institute of Technology, December, 1952 (unpublished).

Since there are no terms with a time dependence at the frequency of the free oscillations of the lattice, the solution must be closely related to the quantum solution for the lowest state where no free quanta are present. The quantum eigenstate will be seen however to involve at least an additional range of classical states, in which particles and oscillators undergo coupled forced oscillations of a particular type in the vicinity of the special classical solution.

The general equations have, in addition to the energy, the integral of the motion

$$\mathbf{P}=\mathbf{p}+\sum_{\mathbf{k}}\frac{\mathbf{k}}{\omega_{\mathbf{k}}}\left(\frac{Y_{\mathbf{k}}^2}{2M}+\frac{M\omega_{\mathbf{k}}^2}{2}X_{\mathbf{k}}^2\right). \quad (3)$$

The special solution (2) yields for H and $\mathbf{P}$;

$$\mathbf{P}=\mathbf{p}_0+\sum_{\mathbf{k}}\frac{\mathbf{k}}{2M\omega_{\mathbf{k}}}\frac{g_{\mathbf{k}}'^2}{[(\mathbf{k}\cdot\mathbf{p}_0/m)-\omega_{\mathbf{k}}]^2},$$

$$H=\frac{p_0^2}{2m}+\sum\frac{g_{\mathbf{k}}'^2/M\omega_{\mathbf{k}}}{(\mathbf{k}\cdot\mathbf{p}_0/m)-\omega_{\mathbf{k}}}+\tfrac{1}{2}\sum\frac{g_{\mathbf{k}}'^2/M}{[(\mathbf{k}\cdot\mathbf{p}_0/m)-\omega_{\mathbf{k}}]^2}. \quad (4)$$

The special solution thus involves a relationship between H and $\mathbf{P}$ through the intermediary of $\mathbf{p}_0$.

Equations (2) and (4) have singularities for waves whose phase velocity $\omega\mathbf{k}/k^2$ is at the particle velocity $\mathbf{p}_0/m$. If one restricts consideration to sufficiently small values of $\mathbf{p}_0$ so that $|\mathbf{k}\cdot\mathbf{p}_0/m|<|\omega_{\mathbf{k}}|$ for all oscillators, the results depend on the cut-off value of k. For a classical electron in a crystal the maximum value of k is given by the lattice spacing, and the singularity means that excitation of natural lattice oscillations must be considered. Quantum theory provides a cutoff arising from wavelength of the particle. For weak coupling this has been discussed by F.P.Z. and is $k_{\max}\sim(2m\omega/\hbar)^{\frac{1}{2}}$ which leads to an energy proportional to g^2. One can also estimate the effective mass for small $\mathbf{p}_0$ by using (4). For strong coupling the cutoff will depend on the strength of interaction, representing a tendency to confine the particle in a potential well. The question of the behavior of the cutoff is thus vital, and is inherently quantum mechanical.

We now go further into the structure of the equations of motion by studying small oscillations. The results are simplified by making the following canonical transformation:

$$\mathbf{P}=\mathbf{p}+\sum_{\mathbf{k}}\frac{\mathbf{k}}{\omega_{\mathbf{k}}}\left(\frac{Y_{\mathbf{k}}^2}{2M}+\frac{M\omega_{\mathbf{k}}^2X_{\mathbf{k}}^2}{2}\right), \quad \mathbf{Q}=\mathbf{q}, \quad (5)$$

$$Q_{\mathbf{k}}'=X_{\mathbf{k}}\cos(\mathbf{k}\cdot\mathbf{q})-\frac{Y_{\mathbf{k}}}{M\omega_{\mathbf{k}}}\sin(\mathbf{k}\cdot\mathbf{q}),$$

$$\frac{P_{\mathbf{k}}'}{M\omega_{\mathbf{k}}}=X_{\mathbf{k}}\sin(\mathbf{k}\cdot\mathbf{q})+\frac{Y_{\mathbf{k}}}{M\omega_{\mathbf{k}}}\cos(\mathbf{k}\cdot\mathbf{q}).$$

In terms of the new variables the Hamiltonian is

$$H=\frac{P^2}{2m}+\sum g_k'\frac{P_k'}{M\omega_k}+\frac{1}{2M}\sum_k\left(1-\frac{\mathbf{k}\cdot\mathbf{P}}{m\omega_k}\right)\times(P_k'^2+M^2\omega_k^2Q_k'^2)+\frac{1}{(2M)^2}\cdot\frac{1}{2m}\times\left\{\sum_k\frac{\mathbf{k}}{\omega_k}(P_k'^2+M^2\omega_k^2Q_k'^2)\right\}^2. \quad (6)$$

The solution (2) corresponds now to a simple shift in the new momentum coordinates,

$$Q_k'=Q_k^0=0, \quad P_k'=P_k^0=\frac{g_k'}{(\mathbf{k}\cdot\mathbf{p}_0/m)-\omega_k}, \quad (7)$$

and

$$\mathbf{P}=\mathbf{p}_0+\sum_k(\mathbf{k}P_k^{0\,2}/2M\omega_k).$$

To introduce variables describing the motion relative the stable orbit, we perform the following canonical transformation:

$$P_k=P_k'-P_k^0, \quad Q_k=Q_k'. \quad (8)$$

Then $H=\sum_{i=0}^4H_i$, with $H_1=0$ and

$$H_0=\frac{p_0^2}{2m}+\sum_k g_k'\frac{P_k^0}{M\omega_k}+\frac{M}{2}\sum_k\omega_k^2\left(\frac{P_k^0}{M\omega_k}\right)^2,$$

$$H_2=\frac{1}{2m}\left(\sum_k\frac{\mathbf{k}P_k^0P_k}{M\omega_k}\right)^2+\frac{1}{2M}\sum_k\left(1-\frac{\mathbf{k}\cdot\mathbf{p}_0}{m\omega_k}\right)\times(P_k^2+M^2\omega_k^2Q_k^2). \quad (9)$$

We have not written down the cubic and quartic parts of H. The constant part H_0 is just the energy of Eq. (4). The next stage in the solution is to find the normal modes for H_2. This is always possible in principle, but here H_2 has a particularly simple form which permits explicit calculation of the normal frequencies and modes. We write

$$Q_k=\sum_\lambda R_{k\lambda}\xi_\lambda, \quad P_k=\sum_\lambda R_{k\lambda}\eta_\lambda, \quad (10)$$

where ξ_λ and η_λ are the new canonical coordinates and momenta and $R_{k\lambda}$ is a real, orthogonal matrix. The quadratic portion of the Hamiltonian is diagonal in terms of the new coordinates with Ω_λ as the normal frequencies. The $R_{k\lambda}$ and Ω_λ are determined by writing the equations of motion using only H_2, and inserting into them Eqs. (10) together with

$$\ddot{\eta}_\lambda=-\Omega_\lambda^2\eta_\lambda.$$

We find

$$(\rho_k^2-\Omega_\lambda^2)R_{k\lambda}=-\frac{\rho_k\mathbf{k}P_k^0}{m_k}\cdot\sum_l\frac{\mathbf{l}P_l^0R_{l\lambda}}{M\omega_l}, \quad (11)$$

where $\rho_k=\omega_k(1-\mathbf{k}\cdot\mathbf{p}_0/m\omega_k)$.

There are two types of solutions. In the first type,

$$\beta_\lambda\equiv\sum_l\frac{\mathbf{l}P_l^0R_{l\lambda}}{M\omega_l}=0.$$

For a given λ $R_{k\lambda}=0$ unless $\rho_k^2=\Omega_\lambda^2$. The Ω_λ are simply the original lattice frequencies, (as modified by the Doppler shift), relative to a particle moving with velocity $\mathbf{p}_0/m$. Only a small fraction of the lattice oscillators satisfy $\rho_k^2=\Omega_\lambda^2$, and these are modes built out of a small number of oscillators combined so as to form standing waves with a node at the position of the electron. This is the reason why the frequencies are unmodified by interaction.

The second type has $\beta_\lambda\neq0$ and

$$R_{k\lambda}=-\frac{\rho_kP_k^0}{m}\frac{\mathbf{k}\cdot\beta_\lambda}{(\rho_k^2-\Omega_\lambda^2)}. \quad (12)$$

The β_λ are determined by the normalization condition on $R_{k\lambda}$. The Ω_λ are determined from

$$\beta_\lambda=-\sum_k\frac{\rho_kP_k^0\,\mathbf{k}(\mathbf{k}\cdot\beta_\lambda)}{mM\omega_k(\rho_k^2-\Omega_\lambda^2)}. \quad (13)$$

These modes are built up from small contributions from all the lattice oscillators and contain the coupling constant for the electron lattice interaction. The normal frequencies are found between the poles of the right-hand side of (13).

3. QUANTUM TREATMENT

Because of the similarity of the operator equations of motion in the Heisenberg representation and the classical equations the classical theory may be taken over. The new points all involve the appropriate ordering of noncommutative factors. We introduce the creation and destruction operators

$$\left\{\begin{matrix}b_k^*\\b_k\end{matrix}\right\}=\left(\frac{M\omega_k}{2\hbar}\right)^{\frac{1}{2}}(Q_k'\mp iP_k'/M\omega_k), \quad (14)$$

satisfying $[b_k,b_l^*]=\delta_{kl}$. Introduce the purely imaginary quantity (dimensions of energy),

$$V_k=-ig_k'(\hbar/2M\omega_k)^{\frac{1}{2}}, \quad (15)$$

and rewrite Eq. (6) as

$$H=\frac{P^2}{2m}+\sum\hbar\left(\omega_k-\frac{\mathbf{k}\cdot\mathbf{P}}{m}+\frac{\hbar k^2}{2m}\right)b_k^*b_k+\sum(V_kb_k+V_k^*b_k^*)+\sum_{k,l}\frac{\hbar^{\frac{3}{2}}}{2m}(\mathbf{k}\cdot\mathbf{l})b_k^*b_l^*b_kb_l. \quad (16)$$

We have made use of the fact that the zero-point

momentum $\sum \hbar\mathbf{k}/2$ is zero and have discarded the zero-point energy $\sum \hbar\omega_k/2$. The operators have been ordered so that the creation operators stand to the left of the destruction operators; this arrangement brings out the term $\sum(\hbar^2k^2/2m)b_k^*b_k$ from the quartic part of the Hamiltonian (6). This term comes originally from the $\hat{p}^2/2m$ term, i.e., from the particle kinetic energy and represents physically the DeBroglie wavelength cutoff. Now perform the shift, Eq. (8).[9] The ordering of operators is unaltered. We have

$$a_k=b_k+f(k), \quad a_k^*=b_k^*+f^*(k), \qquad Q_k=Q_k', \quad P_k=P_k'-P_k^0. \tag{17}$$

Here $a_k=(M\omega_k/2\hbar)^{\frac{1}{2}}\{Q_k+iP_k/M\omega_k\}$, and we will later show that $f(k)$ is purely imaginary. Thus $P_k^0=-(2M\hbar\omega_k)^{\frac{1}{2}}if(k)$. We will discuss the choice of $f(k)$ in detail below. Equations (9) are replaced by $H=\sum_{n=0}^{4}\times H^{(n)}$, where

$$\begin{aligned}
H^{(0)}&=\frac{P^2(1-\eta)^2}{2m}+\sum_{\mathbf{k}}\left(\hbar\omega_k+\frac{\hbar^2k^2}{2m}\right)|f(k)|^2,\\
H^{(1)}&=\sum\{\hbar\rho_kf(\mathbf{k})+V_k^*\}a_k^*+\text{c.c.},\\
H^{(2)}&=\sum\hbar\rho_ka_k^*a_k+(\hbar/2m)\sum_{\mathbf{k},\mathbf{l}}\mathbf{k}\cdot\mathbf{l}f(k)f(l)\{a_k^*a_l^*\\
&\qquad -a_k^*a_l+a_ka_l-a_l^*a_k\},\\
H^{(3)}&=(\hbar^2/m)\{\sum\mathbf{k}a_k^*f(k)\cdot\sum\mathbf{l}a_l^*a_l\\
&\qquad +\sum\mathbf{l}a_l^*a_l\cdot\sum\mathbf{k}a_kf^*(k)\},\\
H^{(4)}&=(\hbar^2/2m)\sum\mathbf{k}\cdot\mathbf{l}a_k^*a_l^*a_ka_l,
\end{aligned} \tag{18}$$

where now

$$\rho_k=\omega_k-\frac{\mathbf{k}\cdot\mathbf{P}}{m}(1-\eta)+\frac{\hbar^2k^2}{2m}, \qquad \eta\mathbf{P}=\sum\mathbf{k}|f(\mathbf{k})|^2. \tag{19}$$

One can now choose $f(\mathbf{k})$ so that $H^{(1)}$ is zero. This ensures that there are no constant "forces" in the Heisenberg equations of motion of the operators a_k and a_k^*. Thus there are no linear increases of these operators with time and we have found the stable orbit. As in the classical case, there are contributions from the quartic terms of the original equation (6) to the determination of $f(\mathbf{k})$. A reason for adopting the above order is that the terms $H^{(2)}$, $H^{(3)}$, $H^{(4)}$ have no first-order contribution to the energy of the ground state in a perturbation calculation in a representation where $a_k^*a_k$ is diagonal. The results then agree with quantum perturbation theory in the limit of weak coupling.

This stage of the procedure is precisely the intermediate coupling theory of the polaron.[9-11] Here we have been motivated by a study of the equations of motion of the operators rather than by a variational approach. The fact that the diagonal matrix elements of $H^{(2)}$, $H^{(3)}$, $H^{(4)}$ are zero means that the true ground-state energy is below the value obtained with H_0.

Now our object is to take into account the coupled vibrations of electron and lattice oscillators. We shall therefore find the normal modes of $H^{(2)}$. If one takes f as in the intermediate coupling theory, we find that including effects of the oscillations gives a solution valid for larger coupling strengths and lowers the energy at all coupling strengths. However, one does not obtain results valid in the strong coupling limit. This is connected with an important point. The a_k will be linear combinations of new creation and annihilation operators belonging to the new normal modes. Thus, the Hamiltonian will not be appropriately ordered in terms of the new variables. In so ordering, $H^{(3)}$ contains linear terms and the process of finding the normal modes destroys the stable orbit. It is therefore more appropriate to keep f free until the normal modes have been found and to determine it by then setting the linear terms equal to zero.

Now introduce coordinates and momenta appropriate to the Doppler-shifted waves. We have

$$\begin{Bmatrix} a_k \\ a_k^* \end{Bmatrix}=\left(\frac{M\rho_k}{2\hbar}\right)^{\frac{1}{2}}(G_k\mp iF_k/M\rho_k). \tag{20}$$

Then

$$G_k=Q_k(\omega_k/\rho_k)^{\frac{1}{2}}, \quad F_k=P_k(\rho_k/\omega_k)^{\frac{1}{2}}, \qquad G_k=\sum_s T_{ks}\xi_s, \quad F_k=\sum_s T_{ks}\eta_s.$$

$H^{(2)}$ becomes

$$H^{(2)}=\sum\left(\frac{F_k^2}{2M}+\frac{M\rho_k^2}{2}G_k^2\right)-\frac{1}{M\hbar m}\left(\sum\frac{\hbar\mathbf{k}fF_k}{\rho_k^{\frac{1}{2}}}\right)^2. \tag{21}$$

The lowest states are characterized by zero quanta in each of the normal modes. There will therefore be a zero-point energy $\sum_s(\hbar\Omega_s/2)$. Thus, the contribution of $H^{(2)}$ to the energy is

$$\Delta E^{(2)}=\sum_s\frac{\hbar\Omega_s}{2}-\sum_k\frac{\hbar\rho_k}{2}-\frac{\hbar^2}{2m}\sum_k k^2|f(k)|^2. \tag{22}$$

The reordering of $H^{(4)}$ gives in general an additional contribution to the energy which can be found after the normal modes are determined.

4. ENERGY OF LOWEST STATE

In this section, we treat the lowest state of the polaron for which $\mathbf{P}=0$. For simplicity of presentation we go through the calculations for a one-dimensional case. Measure energies in units of $\hbar\omega$, momenta in units of $(2m\hbar\omega)^{\frac{1}{2}}$, and introduce

$$l_k=(\rho_k/\omega)^2; \quad s=(\Omega_s/\omega)^2.$$

[9] Lee, Low, and Pines, Phys. Rev. 90, 297 (1953).
[10] M. Gurari, Phil. Mag. 44, 329 (1953).
[11] S. Tyablikov, Zhur. Eksptl. i Teort. Fiz. 25, 688 (1953).

Consider modes of type 1, and label them with the index s_0. Then the frequencies are given by

$$s_0(k)=t_k=(1+k^2)^2. \tag{23}$$

For a given $s_0>0$, there are two values of k:

$$k_\pm(s_0)=\pm[(s_0)^{\frac{1}{2}}-1]^{\frac{1}{2}}$$

Since one must satisfy $\sum(kfT_{ks_0}/\rho_k^{\frac{1}{2}})=0$, and since $f(k)$ is an even function of k for $P=0$, we have

$$T_{k_+s_0}=T_{k_-s_0}=1/\sqrt{2}. \tag{24}$$

The last step follows from the normalization condition

$$T_{k_+s_0}^2+T_{k_-s_0}^2=1.$$

Thus, for normal modes of type (1) and $P=0$,

$$\xi_{s_0}=(1/\sqrt{2})(Q_{k_+}+Q_{k_-}). \tag{25}$$

There is no shift in zero-point energy for type-1 modes.

The frequencies of type-2 modes are determined from

$$-1=\sum_k \frac{4(t_k)^{\frac{1}{2}}k^2f^2(k)}{(s-t_k)}, \tag{26}$$

with $t_k=(1+k^2)^2$ or $k^2=t_k^{\frac{1}{2}}-1$. This type of eigenvalue equation has been treated in the literature.[12,13] The poles of the right-hand side are at $s=t_k$ with $k=2\pi n/L$ the spacing of poles is

$$\epsilon(t_n)=t_{n+1}-t_n=(2n_{+1})(2\pi/L)^2\{(2\pi/L)^2 \times(2n+1)+2+2(2\pi n/L)^2\}.$$

Inserting the value of $2\pi n/L$ as a function of t_n, we have as $L\to\infty$:

$$\epsilon(t_n)\to 4(2\pi/L)(t_n^{\frac{1}{2}}-1)^{\frac{1}{2}}t_n^{\frac{1}{2}}, \tag{27}$$

which gives the spacing as a function of frequency.

Let s_m be the root lying between t_m and t_{m+1}. Then introduce the shift σ_m

$$s_m=\{1+(2\pi m/L)^2\}^2+\sigma_m, \quad 0\le\sigma_m<\epsilon(t_m). \tag{28}$$

The ratio σ_m/ϵ_m is less than unity and tends to a non-zero value as $L\to\infty$, but $\sigma_m\to 0$ as $L\to\infty$. The total shift is zero-point energy of type-2 modes is therefore (in dimensionless units),

$$\tfrac{1}{2}\sum_{\text{all } s_m}(s_m^{\frac{1}{2}}-t_m^{\frac{1}{2}})=\tfrac{1}{4}\sum_{s_m}(\sigma_m/t_m^{\frac{1}{2}}), \tag{29}$$

where we keep only the first term in the expansion of $s_m^{\frac{1}{2}}$ since $\sigma_m\to 0$ as $L\to\infty$ and t_m is finite. The energy shift is then

$$\tfrac{1}{4}\sum_{s_m}\frac{\sigma_m(s_m)}{\epsilon_m(s_m)}\frac{\epsilon_m(s_m)}{\sqrt{t_m}}\to\tfrac{1}{4}\int_{s=1}^{\infty}\frac{\sigma(s)}{\epsilon(s)}\frac{ds}{\sqrt{s}}, \tag{30}$$

since $\Delta s\to\epsilon_m$ as $L\to\infty$. To find the ratio $\sigma(s)/\epsilon(s)$, one uses the result

$$\sum_{n=-\infty}^{+\infty}\frac{\alpha_n^2}{s-t_n}=\mathrm{P}\int\frac{\alpha^2(t)dt}{s-t}+\pi\alpha^2(s)\cot\left(\frac{\pi\sigma(s)}{\epsilon(s)}\right), \tag{31}$$

where P stands for the principal value of the integral and

$$\alpha^2(t_n)=\alpha_n^2/\epsilon(t_n). \tag{32}$$

For our problem, $\alpha_n^2=4t_n^{\frac{1}{2}}(n2\pi/L)^2f^2(2\pi n/L)$, so that

$$\alpha^2(t)=(L/2\pi)f^2[(t^{\frac{1}{2}}-1)^{\frac{1}{2}}][(t^{\frac{1}{2}}-1)]^{\frac{1}{2}}. \tag{33}$$

Inserting Eq. (31) into the eigenvalue equation, we find

$$\frac{\pi\sigma(s)}{\epsilon(s)}=\tan^{-1}\left\{-\pi\alpha^2(s)\Big/\left(1+\mathrm{P}\int_1^\infty\frac{\alpha^2(t)dt}{s-t}\right)\right\}. \tag{34}$$

The normal modes of type 2 are related to the original lattice coordinates by the transformation coefficients:

$$T_{ks}^{(2)}=-\frac{4t_k^{\frac{1}{2}}f(k)\beta_s k}{t_k-s}; \quad \beta_s=\sum_k\frac{kf(k)T_{ks}^{(2)}}{\sqrt{\rho_k}}. \tag{35}$$

The $T_{ks}^{(2)}$ satisfy the orthogonality relation:

$$\textstyle\sum_k T_{ks}^{(2)}T_{ks'}^{(2)}=\delta_{ss'}, \tag{36}$$

as may be seen by breaking the left-hand side of (36) into partial fractions and using the eigenvalue equation (26). The β_s are normalization coefficients and are determined by

$$\frac{1}{|\beta_s|^2}=\sum_k\frac{4t_k|\alpha_k|^2}{(t_k-s)^2}. \tag{37}$$

To evaluate this we need the sum[14] $\sum_n[\gamma_n^2/(t_n-s)^2]$, where $\gamma^2(t)=\gamma_n^2/\epsilon_n(t)=4t|\alpha(t)|^2$. In the limit $L\to\infty$,

$$|\beta_s|^2\to\frac{2\pi}{L}\frac{(s^{\frac{1}{2}}-1)^{\frac{1}{2}}}{\pi^2(s)^{\frac{1}{2}}|\alpha^2(s)|}\sin^2(\pi\sigma/\epsilon). \tag{38}$$

For type-two modes, we therefore have

$$\xi_s=\textstyle\sum_k T_{sk}^{(2)}Q_k. \tag{39}$$

The inverse transformation giving the Q_k and P_k in terms of the ξ_s, η_s will be needed in order to rewrite the Hamiltonian in terms of the new variables. A given Q_k involves both types of normal modes. We have

$$Q_k=(1/\sqrt{2})\xi_{s_0(k)}+\textstyle\sum_s T_{ks}^{(2)}\xi_s, \tag{40}$$

where s_0 is the single value of s for the type one mode arising from k.

The above information concerning the transformation coefficients enables us to complete the calculation of the energy. We introduce creation and annihilation

[12] Wigner, Critchfield, and Teller, Phys. Rev. **56**, 530 (1939).
[13] N. V. Kampen, Kgl. Danske Videnskab. Selskab, Mat.-fys. Medd. **26**, No. 15 (1951).

operators for the normal modes:

$$\begin{cases} d_s \\ d_s^* \end{cases} = \left(\frac{M\Omega_s}{2\hbar}\right)^{\frac{1}{2}} (\xi_s \pm i\eta_s/M\Omega_s), \tag{41}$$

and

$$\xi_s = (\hbar/2M\Omega_s)^{\frac{1}{2}}\{d_s + d_s^*\},$$
$$i\eta_s/M\Omega_s = (\hbar/2M\Omega_s)^{\frac{1}{2}}\{d_s - d_s^*\}.$$

We work in a representation where $d_s^* d_s$ is diagonal and consider the ground state Ψ_0 for which $d_s\Psi_0 = 0$. Then $H^{(1)}$ and $H^{(3)}$, have an odd number of creation and annihilation operators and thus have the property

$$\langle\Psi_0, H^{(1)}\Psi_0\rangle = \langle\Psi_0, H^{(3)}\Psi_0\rangle = 0.$$

The energy of the system by our method is therefore

$$E = \langle\Psi_0, H\Psi_0\rangle = H^{(0)} + \langle\Psi_0, H^{(2)}\Psi_0\rangle + \langle\Psi_0, H^{(4)}\Psi_0\rangle. \tag{42}$$

The true energy must always be less than this value.

We now show that the quartic contribution to the energy is zero (for $P=0$). One has

$$\langle\Psi_0, H^{(4)}\Psi_0\rangle = (\hbar/2m)\sum_{k,l}(\mathbf{k}\cdot\mathbf{l})\langle a_l a_k\Psi_0, a_l a_k\Psi_0\rangle.$$

Now

$$a_k = \frac{d_{s_0(k)}}{\sqrt{2}} + \left(\frac{M\rho_k}{2\hbar}\right)^{\frac{1}{2}} \sum_s \frac{T_{ks}^{(2)}}{2}\left(\frac{\rho_k}{\Omega_s}\right)^{\frac{1}{2}} \times\left\{d_s\left(1+\frac{\Omega_s}{\rho_k}\right) + d_s^*\left(1-\frac{\Omega_s}{\rho_k}\right)\right\}. \tag{43}$$

We have made use of the fact that $s_0(k) = t_k$ (type-1 modes). Then

$$a_k\Psi_0 = \sum_s T_{ks}^{(2)}(\rho_k/\Omega_s)^{\frac{1}{2}}(1-\Omega_s/\rho_k)d_s^*\Psi_0.$$

The term $a_l a_k\Psi_0$ involves $T_{ks}T_{ls'}$ as a factor, and the entire inner product $\langle a_l a_k\Psi_0, a_l a_k\Psi_0\rangle$ involves $T_{ks}T_{ks} \times T_{ls'}T_{ls'}$ which is an even function of both k and l. The summation over k and l involves the odd factor $k\cdot l$ so that $\langle\Psi_0, H^{(4)}\Psi_0\rangle = 0$.

The complete expression for the energy is therefore $H^{(0)} + \langle\Psi_0, H^{(2)}\Psi_0\rangle$, where $f(k)$ can still be chosen freely. From this point of view, the method contains a variational principle. It will be of interest later, however, to seek to determine $f(k)$ in a natural way in accordance with our basic physical picture. The total energy is

$$E = \sum_k (V_k f + V_k^* f^*) + \sum_k \rho_k |f(k)|^2 - \sum k^2 |f|^2 + \frac{1}{4\pi}\int_{s=1}^{\infty} \frac{ds}{\sqrt{s}} \times\tan^{-1}\left\{-\pi\alpha^2(s)\Big/\left(1+\mathrm{P}\int_1^\infty \frac{\alpha^2(t)dt}{s-t}\right)\right\}. \tag{44}$$

In the one-dimensional problem, $V_k = V$ (a constant). Introduce the pure number

$$U^2 = [V^2/(\hbar\omega)^2]L(\hbar/2m\omega)^{-\frac{1}{2}}. \tag{45}$$

A simple choice for $f(k)$ is

$$f(k) = \frac{V}{1+k^2/b^2}. \tag{46}$$

For weak and intermediate coupling $b=1$, but for stronger coupling it depends on the interaction strength, i.e., the DeBroglie cutoff for a free particle is no longer appropriate. We have

$$\alpha^2(t) = \frac{U^2 b^4}{2\pi}\frac{(t^{\frac{1}{2}}-1)^{\frac{1}{2}}}{(b^2+(t)^{\frac{1}{2}}-1)^2}, \tag{47}$$

$$\mathrm{P}\int_1^\infty \frac{\alpha^2(t)dt}{s-t} = \frac{U^2 b^4}{2\pi s}\{K(s,b)+J(s,b)\}, \tag{48}$$

where

$$K(s,b) = \int_1^\infty \frac{(x-1)^{\frac{1}{2}}xdx}{(s+x)(x+b^2-1)^2} = -J(-s,b) + 2\pi\cdot\frac{2s(1+s)^{\frac{1}{2}}}{(b^2-s)^2} = \frac{2\pi}{b}\frac{2b(1+s)^{\frac{1}{2}}+1+b^2}{[b^2+(1+s)^{\frac{1}{2}}]^2},$$
$$J(s,b) = \mathrm{P}\int_1^\infty \frac{(x-1)^{\frac{1}{2}}xdx}{(s-x)(x+b^2-1)^2} = \frac{2\pi}{b} \times\frac{s(1-3b^2)-(b^2-1)^2}{(s-1+b^2)^2}. \tag{49}$$

The integrals have been evaluated by the method of residues. Examine first the case $b=1$ (intermediate coupling theory). Then the total energy of the system is

$$E = -\tfrac{3}{4}|U|^2 + \frac{1}{2\pi}\int_{r=1}^{\infty} \times\tan^{-1}\left\{\frac{(r-1)^{\frac{1}{2}}}{(r^2/|U|^2)-[(1+r)^{\frac{1}{2}}-2]}\right\}dr. \tag{50}$$

Now $\tan^{-1}x$ has the expansion

$$\tan^{-1}x = x - x^3/3 + x^5/5 \quad \text{for} \quad x^2 < 1.$$

For this expansion to be suitable for all r, we must have

$$|U|^2 < \min\frac{r^2}{|(r-1)^{\frac{1}{2}}-2+(1+r)^{\frac{1}{2}}|} \lesssim 1.6.$$

In addition, for

$$|U|^2 < \min\frac{r^2}{|(1+r)^{\frac{1}{2}}-2|} \lesssim 1.6,$$

one can expand the denominator in powers of $|U|^2$. The result is

$$E = -\tfrac{3}{4}|U|^2 - |U|^4(1/6\pi - 1/16) + \cdots. \tag{51}$$

This result is probably accurate for $|U|^2$ somewhat

>1.6 since the region of r where convergence fails is small. The additional energy is always lower than $-\frac{1}{2}|U|^2$, representing an improvement over the intermediate coupling theory. However, for very large coupling strengths the term containing the $\tan^{-1}$ saturates, and gives a dependence which is slower than $|U|^2$. The energy is then roughly $-\frac{3}{4}|U|^2$ rather than the weak coupling value of $-\frac{1}{2}|U|^2$.

Thus with the choice of f suggested by intermediate coupling theory we do not get the correct strong coupling energy given by the adiabatic approximation ($E\sim-0.1|U|^4$). From the present point of view this arises because the intermediate coupling choice of f has implicit a cutoff related to the DeBroglie wavelength of the free particle. The cutoff in reality must depend on the coupling strength, so as to represent the "binding" of the particle in the potential well created when it polarizes the lattice.

We have checked numerically that letting $b^2=1+\varphi(U)$ improves the energy in the region $|U|^2\approx10$, but have not discovered whether b^2 can be chosen as a function of coupling strength so as to obtain the strong coupling limit. In the next section, a 'natural' way to specify f is discussed.

The energy for the three-dimensional situation is easily expressed in terms of the one-dimensional results. The eigenvalue equation is a vector relation:

$$\beta_s=4\sum_k \frac{(t_k)^{\frac{1}{2}}f^2(\mathbf{k})}{(t_k-s)}\mathbf{k}(\mathbf{k}\cdot\beta_s). \tag{52}$$

There are three independent modes of type 2 for a given frequency s. We take these to have β_s along the x, y, z axes respectively. To find the frequency shift of these modes, consider, for example, the mode with β_s along the z axis. Then

$$-1=4\sum_k \frac{(t_k)^{\frac{1}{2}}k_z^2f^2(\mathbf{k})}{s-t_k}. \tag{53}$$

For the $P=0$ case $f(\mathbf{k})$ and t_k depend only on the absolute value of k. We may therefore perform the angle integrations and find

$$1\to4\cdot\frac{4\pi}{3}\left(\frac{L}{2\pi}\right)^3\int_0^\infty\left\{\frac{k^2(t_k)^{\frac{1}{2}}f^2(k)}{t_k-s}\right\}k^2dk. \tag{54}$$

The eigenvalue equation is of the same form as the one-dimensional one. Here we take

$$\alpha_n^2=\frac{8\pi}{3}\left(\frac{2\pi n}{L}\right)^4t_n^{\frac{1}{2}}f^2\left(\frac{2\pi n}{L}\right)\left(\frac{L}{2\pi}\right)^3 \tag{55}$$

or

$$\alpha^2(l)=(l^{\frac{1}{2}}-1)^{\frac{1}{2}}f^2[(l^{\frac{1}{2}}-1)^{\frac{1}{2}}]\left(\frac{L}{2\pi}\right)^3\cdot\tfrac{1}{3}\pi.$$

With this expression for $\alpha^2(l)$, the energy shift of the type-2 modes is then 3 times the value given by Eq. (35). Corresponding to the one-dimensional choice (46), in three dimensions we may take

$$f(k)=V_k/(1+k^2/b^2).$$

In dimensionless units,[7,9]

$$V_k=-(i/k)(4\pi\alpha'/L^3)^{\frac{1}{2}}.$$

Insert in Eq. (55) for $\alpha^2(l)$ and compare with Eq. (33) for one dimension. With $|U|^2=\frac{3}{4}\alpha'$ and with the factor 3, the arc-tangent term in Eq. (44) is correct for the three-dimensional case. The total energy is then

$$E=\sum(V_kf+V_k^*f^*)+\sum|f(\mathbf{k})|^2+\frac{3}{4\pi}\int_{m^2}^\infty\frac{ds}{\sqrt{s}}$$
$$\times\tan^{-1}\left\{-\pi\alpha^2(s)\Big/\left(1+\mathrm{P}\int_1^\infty\frac{\alpha^2(l)dl}{s-l}\right)\right\}. \tag{56}$$

Again, as in one dimension, the three independent type-1 normal modes of a given frequency are standing waves with modes at the particle.

5. REORDERING OF $H^{(3)}$

We return to the question of the systematic determination of f. The diagonalization of $H^{(2)}$ destroys the ordering of the cubic term. We investigate the process of determining f by the requirement that the linear terms in the Hamiltonian vanish when it is expressed in terms of ordered operators for the new normal modes. We order $H^{(3)}$, as given in Eq. (19), so that the d_s stand to the right of the d_s^* and select the linear portion.

Examine first $\sum kfa_k$ (for $P=0$). From (43), noting that $d_{s0(k)}=d_{s0(-k)}$ one sees that there is no contribution from type-1 modes. Then for the one-dimensional case,

$$\sum kfa_k=\sum_{k,s}kf(k)\frac{T_{ks}^{(2)}}{\sqrt{2}}\left(\frac{\rho_k}{\Omega_s}\right)^{\frac{1}{2}}$$
$$\times\left\{d_s\left(1+\frac{\Omega_s}{\rho_k}\right)+d_s^*\left(1-\frac{\Omega_s}{\rho_k}\right)\right\}. \tag{57}$$

Next consider $\sum ka_k^*a_k$. Since $T_{ks}^{(2)}$ is an odd function of k, only the terms consisting of products of one operator of type 1 and one of type 2 will survive the summation over k.

$$\sum ka_k^*a_k=\sum_{k,s}\frac{kT_{ks}^{(2)}}{2}\left(\frac{\rho_k}{\Omega_s}\right)^{\frac{1}{2}}\left[\left|d_s\left(1+\frac{\Omega_s}{\rho_k}\right)\right.\right.$$
$$\left.\left.+d_s^*\left(1-\frac{\Omega_s}{\rho_k}\right)\right|\frac{d_{s0(k)}^*}{\sqrt{2}}+\text{c.c.}\right]. \tag{58}$$

The linear portion of $H^{(3)}$ is then [using $f^*(k)$

$=-f(k)]$,

$$H_{11n}^{(3)}=\frac{\hbar^2}{m}\sum_{k,l,s}(\mathbf{k}\cdot\mathbf{l})f(l)\frac{Tl_s^{(2)}T_{ks}^{(2)}}{\sqrt{2}}\left(\frac{\rho_l}{\rho_k}\right)^{\frac{1}{2}}$$
$$\times(1-\Omega_s/\rho_l)\{d_{s0(k)}-d_{s0(k)}^*\}. \quad (59)$$

Since $d_{s0(k)}=d_{s0(-k)}$ and $d_{s0(k)}=(1/\sqrt{2})(a_k+a_{-k})$, one can express $H_{11n}^{(3)}$ in terms of the a_k, a_k^*.

$$H_{11n}^{(3)}=\frac{\hbar^2}{m}\sum_{k,l,s}(\mathbf{k}\cdot\mathbf{l})f(l)T_{ks}^{(2)}T_{ls}^{(2)}\left(\frac{\rho_l}{\rho_k}\right)^{\frac{1}{2}}$$
$$\times\left(1-\frac{\Omega_s}{\rho_k}\right)\{a_k-a_k^*\}. \quad (60)$$

Combining this with $H^{(1)}$, we determine $f(k)$ by setting the coefficients of a_k, a_k^* equal to zero. The condition is

$$\rho_k f^*(k)+V_k+k\sum_{l,s}lf(l)T_{ls}^{(2)}T_{ks}^{(2)}\left(\frac{\rho_l}{\rho_k}\right)^{\frac{1}{2}}\left(1-\frac{\Omega_s}{\rho_l}\right)=0.$$

Now insert expressions (35) and (36). We find

$$f(k)=V_k\Big/\left(1+4k^2\sum_s\frac{\Omega_s\rho_k\beta_s^2}{(\rho_k^2-\Omega_s^2)}\right).$$

The $\sum_s$ term is positive since $\beta_s^2<0$, and the root Ω_s is larger than the corresponding root for zero coupling. The effect of ordering of the cubic term is thus a modification of the cutoff of $f(k)$, in a way that depends on coupling strength; the change is more complicated than that of Eq. (46).

With the help of Eqs. (27), (31), (35), and (38), one finds

$$4\sum_s\frac{\Omega_s\rho_k\beta_s^2}{\rho_k^2-\Omega_s^2}=\frac{1+\mathrm{P}\int\frac{\alpha^2(l)dl}{\rho_k^2-l}}{(\pi\alpha^2)^2+\left(1+\mathrm{P}\int\frac{\alpha^2dl}{\rho_k^2l}\right)^2}$$
$$+\mathrm{P}\int\frac{\rho_k ds\,\sin^2[\pi\sigma(s)/\epsilon]}{\pi^2s^{\frac{1}{2}}\alpha^2(s)(\rho_k^2-s)}. \quad (62)$$

As the coupling strength $\to 0$ the sum tends to 1. In principle $f(k)$ can be obtained from this nonlinear integral equation with a degenerate kernel. By direct variation of the energy of Eq. (56), it can be shown that f satisfying Eq. (61) yields the lowest energy attainable by the present method. We have not succeeded in using the results of this section to find the proper explicit form of $f(k)$ for large coupling strengths.

CONCLUSIONS

Our results underscore the value of analysis of the structure of the classical equations of motion. If this can be done by canonical methods, so that a portion of the transformed Hamiltonian describes a set of classical states accurately, there is the basis for an attack on the properties of some quantum eigenstates. In the present problem one is led to a natural extension of intermediate coupling theory. It is interesting that the quantum modifications arising from the ordering of operators affect mainly the proper cutoff. The first step, leading to intermediate coupling theory, replaces a classical theory sensitive to the maximum value of k by a quantum theory with a cutoff arising from the electron wavelength; the effect comes from ordering of nonlinear terms in the equations of motion. The second step of treating the quadratic terms modifies the cutoff as discussed in Sec. 5. The approach is readily applied to the states $P=0$; this will be done elsewhere.

The important question whether the best $f(k)$ yields correct results for strong coupling has not been resolved.[14] If not, one would like to know whether anharmonic classical motions contribute, or whether classically forbidden 'motions' are needed. One should keep in mind that $H^{(4)}$ may contain quadratic terms, if reordered in terms of creation and annihilation operators for the normal modes. It appears formidable to simultaneously remove linear terms, and have quadratic terms diagonal and anharmonic terms "properly" ordered; this may be an unwarranted extension of the small-oscillation concept to the quantum theory.

[14] *Note added in proof.*—Investigations of T. Schultz show that results inferior to the adiabatic approximation are obtained in the limit of strong coupling.

Electron Correlation

JOSEPH E. MAYER
Institute for Nuclear Studies, University of Chicago, Chicago, Illinois and The Rand Corporation, Santa Monica, California
(Received May 16, 1955)

The state of a real gas of electrons of uniform density is examined. An equation for the coordinate representation of the density matrix for two particles is found which satisfies the various necessary conditions and which gives a lower energy than the antisymmetrized Single Slater Determinant. The additional negative correlation energy found is proportional to the one-sixth power of the density at high densities.

1. INTRODUCTION

WE wish to discuss the electron correlation energy in a system of electrons of uniform density and infinite extent. Start with a finite system of N electrons in a volume, V, and of density:

$$\rho_0=N/V. \tag{1.1}$$

In order that the density of electrons be kept constant, assume that there is a uniform density of positive charge, $e\rho_0$. If the unit of length is chosen to be one Bohr radius,

$$a_0=h^2/4\pi^2me^2, \tag{1.2}$$

and the unit of energy is the atomic unit,

$$e^2/a_0=27.21 \text{ ev}, \tag{1.3}$$

then the Hamiltonian of the system is

$$H=\tfrac{1}{2}\sum_{i=1}^{i=N}-\nabla_i\cdot\nabla_i+\sum_{N\geq i>j\geq 1}\sum(1/r_{ij})-a_0^3\rho_0\sum_{i=1}^{i=N}\int\int\int_V(1/r_{i0})d\tau_0+\tfrac{1}{2}a_0^6\rho_0^2\int\cdots\int_V(1/r_{01})d\tau_1d\tau_0. \tag{1.4}$$

The last constant term is the self-energy of the continuous positive charge which is added to the Hamiltonian for convenience. This term depends upon the shape of the system, and diverges at infinite volume, but cancels with the major terms in the potential of the electrons.

It is convenient to change to the equally dimensionless coordinates, x, which are $\rho_0^{\frac{1}{3}}$ times the metric length,

$$\mathbf{x}=a_0\rho_0^{\frac{1}{3}}\boldsymbol{\tau}=c^{\frac{1}{3}}\boldsymbol{\tau}, \tag{1.5}$$

where $\mathbf{r}$ is the dimensionless coordinate used in Eq. (1.4), and

$$c=\rho_0a_0^3, \tag{1.6}$$

so that c is the concentration of electrons per cubic Bohr radius. In these units the Hamiltonian is

$$H=\tfrac{1}{2}c^{\frac{1}{3}}\sum_{i=1}^{i=N}-\nabla_i\cdot\nabla_i+c^{\frac{1}{3}}\Big\{\sum_{N\geq i>j\geq 1}\sum(1/x_{ij})-\sum_{i=1}^{i=N}\int\int\int_N(1/x_{i0})d\mathbf{x}_0+\frac{1}{2}\int\cdots\int_N(1/x_{01})d\mathbf{x}_0d\mathbf{x}_1\Big\}. \tag{1.7}$$

The usual zeroth-order solution is to assume a Single Slater Determinant of plane waves with a minimum kinetic energy. With this zeroth-order solution, the kinetic energy per electron is known to be,

$$\epsilon_{0k}=(9\pi/10)(\pi/3)^{\frac{1}{3}}c^{\frac{1}{3}}, \tag{1.8}$$

and the total potential energy per electron to be,

$$\epsilon_{0p}=-(3/4)(3/\pi)^{\frac{1}{3}}c^{\frac{1}{3}}. \tag{1.9}$$

The major terms in potential energy have been made to cancel to zero by the inclusion of the self-energy of the uniform positive charge. The term, ϵ_{0p}, of Eq. (1.9) is due to the fact that the Single Slater Determinant implies a certain correlation in the position of electrons with equal spin, namely that no two electrons of the same spin approach each other infinitely closely. The term ϵ_{0p} is usually called the exchange energy. We shall attempt in this paper to derive an expression describing a state of the system which is no longer a Single Slater Determinant, and which gives a lower energy, namely one in which the energy is

$$\epsilon=\epsilon_{0k}+\epsilon_{0p}+\Delta\epsilon_c, \tag{1.10}$$

where $\Delta\epsilon_c$ will be called the correlation energy and will be given in units of double Rydbergs, e^2/a_0, Eq. (1.3).

The electron correlation energy, $\Delta\epsilon_c$, is made up of two terms, one of them positive, namely an increase in the kinetic energy, and the second term negative, due to an increased correlation between the electrons such that they are on the average less close together than given by the Single Slater Determinant solution. The units of length, $\rho_0^{-\frac{1}{3}}$, which we are using are now such that the density is unity. Let us define conceptually a function, $F_2(\mathbf{x}_1,\mathbf{x}_2)$, by the statement that F_2 shall

represent the probability density that one will simultaneously have an electron at the position $\mathbf{x}_1$ and another electron at the position $\mathbf{x}_2$. For large distances, x_{12}, between the electrons, F_2 should approach unity in value. We therefore write

$$F_2(\mathbf{x}_1,\mathbf{x}_2)=1-g(x_{12}). \tag{1.11}$$

Since the integral of F_2 over $d\mathbf{x}_1 d\mathbf{x}_2$ over the volume of the system, which in these units is N, must be equal to $N(N-1)$, we have that

$$\int_0^\infty 4\pi x^2 g(x)dx=1. \tag{1.12}$$

Due to the cancellation of the major terms, the potential energy of the system is

$$\epsilon_p=-\tfrac{1}{2}c^{\frac{1}{3}}\int_0^\infty 4\pi x g(x)dx. \tag{1.13}$$

The value of ϵ_{0p} given by Eq. (1.9), is obtained by putting into Eq. (1.13) the value

$$g_0(x)=\tfrac{1}{2}f_0^2(x), \tag{1.14}$$

where f_0 is the expression for the single particle density matrix element in coordinate representation appropriate to a Single Slater Determinant of plane waves of minimum energy, namely

$$f_0(x)=3\left\{\frac{\sin[(3\pi^2)^{\frac{1}{3}}x]}{[(3\pi^2)^{\frac{1}{3}}x]^3}-\frac{\cos[(3\pi^2)^{\frac{1}{3}}x]}{[(3\pi^2)^{\frac{1}{3}}x]^2}\right\}$$
$$\cong 1-(1/10)(3\pi^2)^{\frac{1}{3}}x^2+\cdots. \tag{1.15}$$

The kinetic energy is also determined by f and is

$$\epsilon_k=\tfrac{1}{2}c^{\frac{1}{3}}[-(\partial^2/\partial x^2)f(x)]_{x=0}, \tag{1.16}$$

which leads to the numerical value of Eq. (1.8) with Eq. (1.15) for f. The derivation of these relationships is given in Sec. 2 of this paper.

The method which we propose to use is as follows: we introduce the coordinate representation, $\rho_2(\mathbf{x}_1',\mathbf{x}_1''; \mathbf{x}_2',\mathbf{x}_2'')$, of the density matrix of two particles.[1] The diagonal element, namely that obtained when $\mathbf{x}_i'=\mathbf{x}_i''=\mathbf{x}_i$ in ρ_2, is the function F_2 of Eq. (1.11), and hence by that equation determines g and the total potential energy by Eq. (1.13). If $\mathbf{x}_2'=\mathbf{x}_2''=\mathbf{x}_2$, is set in F_2 and the function is integrated over dx_2, one obtains a function $f(x)$, where $x=|\mathbf{x}_1'-\mathbf{x}_1''|$. This function, $f(x)$ is the coordinate representation of the density matrix for single particles, and determines the kinetic energy by Eq. (1.16).

Now there are a number of necessary conditions which must be satisfied by ρ_2. Some of these are symmetry conditions and others are conditions which must be satisfied by the function $f(x)$. The most significant of the latter is imposed by the demand that the original eigenfunction, ψ, be antisymmetric in all particle exchanges. This requires that if $f(x)$ is regarded as a function of two coordinates and brought into diagonal form, the coefficients of any of the diagonal terms must lie between zero and two, expressing the condition that only two electrons with opposite spin can occupy one single-particle quantum state. In this case of uniform density, the diagonal form of $f(x)$ is given by a transformation to plane waves, and the condition simplifies to the statement that the Fourier transform of $f(x)$ in three dimensions is limited to lie between 0 and 2 in value.

We then set up a simple form for ρ_2 which satisfies the necessary conditions and try to determine, subject to this simple form, the function which minimizes the total energy. Actually, even subject to the simple form assumed, only an approximation to the best analytical function to minimize the energy is found.

One may easily see what the minimum possible potential energy is. The minimum value of ϵ_p given by Eq. (1.13) in view of (1.12) is satisfied if

$$g_m(x)=1, \quad 0\le x\le(3/4\pi)^{\frac{1}{3}},$$
$$g_m(x)=0, \quad (3/4\pi)^{\frac{1}{3}}<x\le\infty, \tag{1.17}$$

namely, when no two electrons can get within a distance $(3/4\pi)^{\frac{1}{3}}$ of each other. With this $g(x)$ in Eq. (1.13) for the potential energy, one finds

$$\epsilon_{p\min}=-(3/2)(\pi/6)^{\frac{1}{3}}c^{\frac{1}{3}}$$
$$=(2\pi/3)^{\frac{1}{3}}\epsilon_{0p}=1.637\epsilon_{0p}. \tag{1.18}$$

The correct expressions for $\Delta\epsilon_c$, Eq. (1.10), must lie between zero and this value. The Single Slater Determinant solution gives $g(x)=\frac{1}{2}$ at $x=0$ since there is correlation only between electrons of the same spin. It is interesting to look at the numbers obtained if one sets $g_0(x)=\frac{1}{2}$ for x between 0 and $(3/2\pi)^{\frac{1}{3}}$. This would be the optimum form if there were correlation only between electrons of equal spin. One then satisfies Eq. (1.12) and finds

$$\epsilon_{p\min}(\text{correlation same spin only})$$
$$=2^{-\frac{1}{3}}\epsilon_{p\min}=1.299\epsilon_{0p}. \tag{1.18'}$$

2. DENSITY MATRIX ELEMENTS

In this section we propose to define the density matrix element for paired particles, to discuss its properties, and incidentally to derive some of the equations introduced in the last section. The three dimensional space coordinates that we use are $\mathbf{x}_i=\rho_0^{\frac{1}{3}}$ times the metric coordinate of electron i, so that the volume of the system containing N particles is N. The symbol $q_i=\mathbf{x}_i,\sigma_i$ is used for the three-dimensional space coordinate and the spin coordinate, σ_i. The state of the system is given by the normalized eigenfunction $\psi(q_1,q_2,\cdots,q_n)$. The Hamiltonian of the system is given

[1] Since preparation of this manuscript a paper has appeared by Per O. Löwdin, Phys. Rev. **97**, 1474 (1955), describing the properties of this and similarly defined density matrices.

by the Eq. (1.7), in which the self-energy of the uniform positive charge has been included. Now define the element of the density matrix including spin for two particles by the equation,

$$\rho_{2s}(q_1',q_1''\,;\,q_2',q_2'')$$
$$=N(N-1)\int\int\cdots\int\psi^*(q_1',q_2',q_3,\cdots,q_N)$$
$$\times\psi(q_1'',q_2'',q_3,\cdots,q_N)dq_3\cdots dq_N, \quad (2.1)$$

and the element of the coordinates of position alone by

$$\rho_2(\mathbf{x}_1',\mathbf{x}_1''\,;\,\mathbf{x}_2',\mathbf{x}_2'')$$
$$=\int\int\rho_{2s}(\mathbf{x}_1',\sigma_1,\mathbf{x}_1'',\sigma_1\,;\,\mathbf{x}_2',\sigma_2,\mathbf{x}_2'',\sigma_2)d\sigma_1 d\sigma_2, \quad (2.2)$$

in which the integration is carried over the diagonal elements of both spins. The density matrix element ρ_1 in the coordinates of a single particle is defined by

$$\rho_1(\mathbf{x}_1',\mathbf{x}_2'')$$
$$=[1/(N-1)]\int\int\int\rho_2(\mathbf{x}_1',\mathbf{x}_1''\,;\,\mathbf{x}_2,\mathbf{x}_2)d\mathbf{x}_2. \quad (2.3)$$

The energy of the system is given by

$$E=\int\psi^*H\psi dq_1\cdots dq_N, \quad (2.4)$$

and the result is seen to be expressible as

$$E=-\tfrac{1}{2}c^1\int\int\int[\nabla''\cdot\nabla''\rho_1(\mathbf{x}',\mathbf{x}'')]_{\mathbf{x}'=\mathbf{x}''=\mathbf{x}}d\mathbf{x}$$
$$+\tfrac{1}{2}c^1\int\int\cdots\int[\rho_2(\mathbf{x}_1,\mathbf{x}_1\,;\,\mathbf{x}_2,\mathbf{x}_2)-1]d\mathbf{x}_1 d\mathbf{x}_2, \quad (2.5)$$

where the operator ∇'' operates only on x'' in ρ_1. The diagonal elements of ρ_2 are equal to the probability density function F_2 defined conceptually in the last section, and we write

$$\rho_2(\mathbf{x}_1,\mathbf{x}_1\,;\,\mathbf{x}_2,\mathbf{x}_2)=F_2(\mathbf{x}_1,\mathbf{x}_2)=1-g(x_{12}),$$
$$x_{12}=|\,\mathbf{x}_1-\mathbf{x}_2\,|, \quad (2.6)$$

in which the fact that the number density is independent of position and equal to unity has been used. The density matrix for single particles is written as

$$\rho_1(\mathbf{x}',\mathbf{x}'')=f(x), \quad x=|\,\mathbf{x}'-\mathbf{x}''\,|, \quad f(0)=1. \quad (2.7)$$

Since both expressions in (2.5) are independent of the diagonal coordinate, one may divide by the total number of particles to obtain the energy per particle by omitting one integration. The operation $(\nabla''\cdot\nabla'')_{x'=x''}=[(2/x)d/dx+d^2/dx^2]_{x=0}=3[d^2/dx^2]_{x=0}$, since f is regular and even at $x=0$. One has

$$E/N=\epsilon=\tfrac{3}{4}c^1[-(d^2/dx^2)f(x)]_{x=0}$$
$$-\tfrac{1}{2}c^1\int_0^\infty 4\pi x g(x)dx. \quad (2.8)$$

The first term on the right is the kinetic energy of Eq. (1.16) and the second term is the potential energy of Eq. (1.13).

Even in the more general case the energy of the system is completely determined by the density matrix element, ρ_{2s} of Eq. (2.1) provided none of the terms in the Hamiltonian contain the coordinates of three particles explicitly. As long as the Hamiltonian does not depend upon spin, the energy is determined completely by the elements integrated over the spin given by Eq. (2.2). Instead of seeking the eigenfunction ψ which gives the lowest energy, one may seek the density matrix element which leads to the lowest energy of the system. However the function ρ_{2s} must obey certain symmetry conditions. If P' is an operator that commutes the two primed indices, P'' an operator that commutes the two double primed indices, and P^* an operator that commutes the primes with the double primes, then

$$P'\rho_{2s}=-\rho_{2s}, \quad P''\rho_{2s}=-\rho_{2s}, \quad P^*\rho_{2s}=\rho_{2s}^*. \quad (2.9)$$

Since the Hamiltonian is real, we can choose a real solution, and write the third condition as $P^*\rho_{2s}=\rho_{2s}$. In addition to this an integral relationship on the diagonal element must be satisfied, namely

$$\int\int\int\rho_2(\mathbf{x}_1,\mathbf{x}_1\,;\,\mathbf{x}_2,\mathbf{x}_2)d\mathbf{x}_2$$
$$=(N-1)\rho_1(\mathbf{x}_1,\mathbf{x}_1)=N-1, \quad (2.10)$$

as well as the condition that the density matrix element for a single particle is given by the integral of Eq. (2.3). The application of Eq. (2.10) leads to the limitation of Eq. (1.12) on $g(x)$, namely that its integral over three dimensional space be unity.

The element ρ_1 for a single particle must be Hermitian, and therefore, if real, $f(x)$ must be even in x, and if brought into diagonal form, ρ_1 must contain elements which lie between 0 and 2 in value, since only two electrons of opposite spin can occupy one state. Since ρ_1 depends only on the distance between the coordinates, its diagonal form is obtained by the coefficients of plane waves, or is just the three dimensional Fourier transform of $f(x)$. This transform is the function:

$$\phi(l)=\int 4\pi x^2 f(x)\frac{\sin 2\pi xl}{2\pi xl}dx,$$
$$f(x)=\int 4\pi l^2\phi(l)\frac{\sin 2\pi xl}{2\pi xl}dl, \quad (2.11)$$

where t has the physical significance,

$$t=|\mathbf{P}|/h\rho_0^{\frac{1}{3}}, \tag{2.12}$$

and $\mathbf{p}$ = momentum. The condition,

$$0\leq\phi(t)\leq 2, \tag{2.13}$$

must be satisfied. The physical significance of $\phi(t)$ is that it represents the total square amplitude of the single particle plane-wave function of momentum $\mathbf{p}$ in the total eigenfunction of the system. The condition that $f(x)$ at $x=0$ should be unity imposes the limitation that

$$\int 4\pi t^2\phi(t)dt=1, \tag{2.14}$$

which can be readily seen by putting $x=0$ into the second part of Eq. (2.11). The conditions of Eqs. (2.9), (2.10), (2.13), and (2.14) with ϕ connected to ρ_2 by the sequence of Eqs. (2.2), (2.3), and (2.11), must be imposed on ρ_{2s}.

We now propose to suggest a very simple form for ρ_2 which satisfies the symmetry conditions for Eq. (2.9). This form will not be that which gives the minimum energy of the system, which in turn would be the exact solution of the problem, but we will limit ourselves to solutions which follow the form suggested. With this form we shall then attempt to approximately minimize the total energy subject to the other conditions.

Any additive term in ρ_{2s} may be written as the product of the function of the coordinates times the function of spin. For two electrons one can write one antisymmetric spin function and three symmetric functions. We will write, therefore, for the spatial part

$$\rho_2=\tfrac{3}{4}\rho_{2A}+\tfrac{1}{4}\rho_{2S}, \tag{2.15}$$

where the function ρ_{2A} which is to be multiplied by the three symmetric spin functions must obey the same symmetry conditions as Eq. (2.9), whereas ρ_{2S}, which is multiplied by the antisymmetric spin function obeys the conditions Eq. (2.9) with plus signs for the first two operators. A function of the form

$$\begin{aligned}\rho_{2A,S}=&[f(|\mathbf{x}_1'-\mathbf{x}_1''|)f(|\mathbf{x}_2'-\mathbf{x}_2''|)\\&\mp f(|\mathbf{x}_1'-\mathbf{x}_2''|)f(|\mathbf{x}_2'-\mathbf{x}_1''|)]\\&\times[1-k(|\mathbf{x}_1'-\mathbf{x}_2'|)][1-k(|\mathbf{x}_1''-\mathbf{x}_2''|)],\end{aligned} \tag{2.16}$$

satisfies the symmetry condition for ρ_{2A} with the minus sign, and for ρ_{2S} with the plus sign. The correct function ρ_2 could always be written as a sum of functions of this form. We will assume that there is only one function of the antisymmetric kind with triple weight, and one of the symmetric with single weight, and that they occur with the same function f and the same function k, where both f and k are real even functions of their variables. If the expression obtained is inserted in Eq. (2.3) for ρ_1, one finds indeed that in the limit $N\rightarrow\infty$, the function f is equal to ρ_1, namely Eq. (2.7). We thus obtain for the diagonal element of the pair density matrix,

$$F_2(\mathbf{x}_1,\mathbf{x}_2)=[1-\tfrac{1}{2}f^2(x_{12})][1-k(x_{12})]^2, \tag{2.17}$$

and for g, from Eq. (2.6):

$$g(x)=\tfrac{1}{2}f^2(x)+[1-\tfrac{1}{2}f^2(x)][2k(x)-k^2(x)]. \tag{2.18}$$

We now wish to find k and f such that

$$\int 4\pi x^2g(x)dx=1, \tag{2.19}$$

that ϕ defined by Eq. (2.11), satisfies the conditions (2.13) and (2.14), and that the total energy be a minimum.

The Single Slater Determinant solution of lowest energy has f equal to f_0 given by Eq. (1.15) for which the Fourier transform is $\phi_0(t)$,

$$\begin{aligned}&\phi_0(t)=2 \quad 0\leq t\leq(3/8\pi)^{\frac{1}{3}},\\&\phi_0(t)=0 \quad (3/8\pi)^{\frac{1}{3}}<t\leq\infty.\end{aligned} \tag{2.20}$$

This solution satisfies Eq. (2.14) as well as the condition of Eq. (2.13). It corresponds to full use of every plane wave of minimum energy up to $t=(3/8\pi)^{\frac{1}{3}}$, or from Eq. (2.12), the momentum, p, having all values less than $p_{\max}=\rho_0^{\frac{1}{3}}h(3/8\pi)^{\frac{1}{3}}$. With this solution for f the condition (2.19) demands that k be zero everywhere since the integral over the three dimensional space of $\frac{1}{2}f_0^2(x)$ is unity.

3. ANALYTICAL FORM OF THE FUNCTIONS

The next step is to find the analytical form of k and f that minimizes the total energy, subject to the conditions to be imposed on these functions. We first determine the form of k for fixed f, and secondly find a form for f that minimizes an approximation to the energy. We thus obtain a simple, but approximate, form for $f(x)$ containing one parameter to be adjusted so as to minimize the energy.

Since $k(x)$ does not directly enter into the expression (1.16) for the kinetic energy the best form for k, with $f(x)$ fixed, is that which minimizes the potential energy, Eq. (1.13), subject to the condition (1.12) that the integral of $g(x)$ over three dimensional space be unity. This is best satisfied by having $F_2=1-g$ as small as possible near the origin, or from (2.17) having $k\equiv 1$ for $0\leq x\leq x_0$, and zero for greater x. The value of x_0 up to which k be unity is to be determined from the condition (1.12) on the integral of g.

Define k by

$$\begin{aligned}k(x)&=1 \quad 0\leq x\leq x_0,\\&=0 \quad x_0<x\leq\infty,\end{aligned} \tag{3.1}$$

and since $k^2=k$ everywhere, from (2.18)

$$g(x)=\tfrac{1}{2}f^2(x)+[1-\tfrac{1}{2}f^2(x)]k(x), \tag{3.2}$$

$$\begin{aligned}g(x)&=1 \qquad 0\leq x\leq x_0,\\&=\tfrac{1}{2}f^2(x) \qquad x_0<x\leq\infty.\end{aligned} \tag{3.2'}$$

Now define four integrals of f,

$$I_2=1-\frac{1}{2}\int 4\pi x^2 f^2(x)dx,$$

$$I_1=\tfrac{3}{4}(3/\pi)^{\frac{1}{3}}-\frac{1}{2}\int 4\pi x f^2(x)dx,$$

$$J_2(x_0)=\tfrac{3}{4}\pi x_0^3-\frac{1}{2}\int_0^{x_0} 4\pi x^2 f^2(x)dx, \tag{3.3}$$

$$J_1(x_0)=\pi x_0^3-\frac{1}{2}\int_0^{x_0} 4\pi x f^2(x)dx.$$

The limit x_0 beyond which $k(x)$ is zero is determined by (1.12) as

$$\begin{aligned}(2\pi/3)x_0^3+1-I_2+J_2(x_0)&=1,\\ x_0&=(3/2\pi)^{\frac{1}{3}}[I_2-J_2(x_0)]^{\frac{1}{3}}.\end{aligned} \tag{3.4}$$

Since $f(x=0)$ is unity, f is even, and hence $f'(x=0)=0$; we may then assume that for small x_0 the function J_2 is negligible. Hence, approximately,

$$x_0\cong(3/2\pi)^{\frac{1}{3}}I_2^{\frac{1}{3}}. \tag{3.4'}$$

The potential energy, ϵ_p, is given by (1.13) as

$$\begin{aligned}\epsilon_p&=-\tfrac{1}{2}c^{\frac{1}{3}}\int 4\pi x g(x)dx\\ &=-\tfrac{1}{2}c^{\frac{1}{3}}[\tfrac{3}{4}(3/\pi)^{\frac{1}{3}}+\pi x_0^3-I_1+J_1(x_0)].\end{aligned} \tag{3.5}$$

Use the value of ϵ_{0p} given by (1.9) to write this as

$$\epsilon_p=\epsilon_{0p}-\tfrac{1}{2}c^{\frac{1}{3}}[\pi x_0^3-[I_1-J(x_0)]]. \tag{3.6}$$

In this expression assume I_1-J_1 to be negligible, and use the approximation of (3.4') for x_0. One finds

$$\epsilon_p\cong\epsilon_{0p}-(3/4)(2\pi/3)^{\frac{1}{3}}c^{\frac{1}{3}}I_2^{\frac{1}{3}}. \tag{3.6'}$$

We use this approximation to determine the analytical form of $f(x)$.

Actually it is easier to discuss the form of the three-dimensional Fourier transform, $\phi(t)$, related to f by (2.11). The Fourier transform has the property that

$$\int 4\pi t^2\phi^2(t)dt=\int 4\pi x^2 f^2(x)dx=2(1-I_2). \tag{3.7}$$

The kinetic energy is given in terms of $\phi(t)$ by the relation,

$$\epsilon_k=2\pi^2 c^{\frac{1}{3}}\int 4\pi t^4\phi(t)dt, \tag{3.8}$$

and of course ϕ must be restricted to obey the condition (2.14) on its integral over three-dimensional space.

Now find ϕ that minimizes

$$\epsilon_k+\epsilon_p-\lambda\int 4\pi t^2\phi(t)dt,$$

with λ an undetermined multiplier of the condition (2.14). Using the approximate form (3.6') for ϵ_p and (3.7) to determine I_2 by an integral over ϕ^2, one finds

$$\phi=a-bt^2,$$

with a and b rather complicated constants, independent of t. However, condition (2.13) limits ϕ to lie between zero and two. Hence we set $\phi(t)=2$ for $0\le t\le t_1$, $\phi(t)=2-b(1-t^2/t_1^2)$ from $t_1\le t\le t_1(2b^{-1}-1)^{\frac{1}{2}}$, and $\phi(t)=0$ for greater values of t. We leave b arbitrary, but use the condition (2.14) on the integral to eliminate one of the parameters, t_1 or t_2. Finally it is simpler to convert to a new variable,

$$\tau=\tau_0^{-1}(8\pi/3)^{\frac{1}{3}}t=\tau_0^{-1}(8\pi/3)^{\frac{1}{3}}|\mathbf{p}|/h\rho_0^{\frac{1}{3}}, \tag{3.9}$$

where τ_0 is related to the single parameter, γ, by the equation,

$$\begin{aligned}\tau_0&=\{[1/10\gamma][(1+\gamma)^5-(1-\gamma)^5]\}^{-\frac{1}{3}}\\ &=[1+2\gamma^2+\tfrac{1}{5}\gamma^4]^{-\frac{1}{3}},\end{aligned} \tag{3.10}$$

and write,

$$\begin{aligned}\phi(t)=\Phi(\tau)&=2 && 0\le\tau\le 1-\gamma,\\ &=2[1/4\gamma][(1+\gamma)^2-\tau^2] && 1-\gamma\le\tau\le 1+\gamma,\\ &=0 && 1+\gamma\le\tau\le\infty.\end{aligned} \tag{3.11}$$

The expression (3.10) for τ_0 is so chosen that

$$\int 4\pi t^2\phi(t)dt=\tfrac{3}{2}\tau_0^3\int\tau^2\Phi(\tau)d\tau=1. \tag{3.12}$$

We now have $\Phi(\tau)$ that satisfies the necessary conditions on the density matrix for single particles: namely from (3.12) it follows that $f(0)=1$ and hence the diagonal element does give the correct number density, and secondly, since Φ lies between zero and two there are only two or fewer electrons in every plane wave single-particle function. In the limit, $\gamma=0$, the function is that for the Single Slater Determinant of minimum energy.

The kinetic energy is now, from (3.8), (3.9), (3.10) and (3.11),

$$\begin{aligned}\epsilon_k&=(9\pi/10)(\pi/3)^{\frac{1}{3}}c^{\frac{1}{3}}(5/2)\tau_0^5\int\tau^4\Phi(\tau)d\tau\\ &=(9\pi/10)(\pi/3)^{\frac{1}{3}}c^{\frac{1}{3}}+(3\pi/2)(\pi/3)^{\frac{1}{3}}c^{\frac{1}{3}}\gamma^3\\ &\times[1+2\gamma^2+\tfrac{1}{5}\gamma^4]^{-5/3}[1+(4/15)\gamma^2+(109/945)\gamma^4\\ &\quad-(1411/6075)\gamma^6+\cdots].\end{aligned} \tag{3.13}$$

which becomes ϵ_{0k}, Eq. (1.8) for $\gamma\to 0$.

The function $f(x)$ is the Fourier transform of $\phi(t)$. Introduce

$$z=(3\pi^2)^{\frac{1}{3}}\tau_0 x,\quad z_T=2\pi t x, \tag{3.14}$$

and

$$f(x)=F(z), \tag{3.15}$$

where

$$F(z)=\tfrac{3}{2}\tau_0^3 z^{-1}\int \tau\Phi(\tau)\sin\tau z d\tau. \tag{3.16}$$

After some rather painful manipulation one obtains

$$F(z)=\tau_0^3(1/2\gamma)\int_{1-\gamma}^{1+\gamma} y^4 F_0(zy)dy, \tag{3.17}$$

$$F_0(zy)=3(zy)^{-3}[\sin zy - zy\cos zy]. \tag{3.18}$$

Obviously in the limit $\gamma\to 0$ we have $F(z)=F_0(z)$, which is necessary since in this limit one has the Single Slater Determinant solution, $F_0(z)=f_0(x)$, of Eq. (1.15).

4. POTENTIAL ENERGY

In order to compute the potential energy one must evaluate the four integrals, I_2, I_1, $J_2(x_0)$, $J_1(x_0)$, of Eq. (3.3), use I_2 and J_2 to find x_0 from Eq. (3.4), and with x_0, I_1, J_1 use (3.5) for ϵ_p. The operations are reasonably straightforward, but tedious. One ends with Eq. (4.15) expressing ϵ_p as proportional to $c^{\frac{1}{2}}\gamma^{\frac{1}{2}}$ times unity plus a power series of $\gamma^{\frac{1}{2}}$ with numerical coefficients computed for the first two members.

The first integral, I_2, is most simply computed from the Fourier transform Φ, by the use of Eq. (3.7). One finds

$$\begin{aligned} I_2&=1-\frac{1}{2}\int 4\pi t^2\phi^2(t)dt=1-\tfrac{3}{4}\tau_0^3\int \tau^2\Phi^2(\tau)d\tau \\ &=1-\tau_0^3[1/70\gamma^2][(1+\gamma)^7-(1-\gamma)^7-14\gamma(1-\gamma)^5] \\ &=1-[1-\gamma+2\gamma^2-\tfrac{2}{3}\gamma^3+\tfrac{1}{3}\gamma^4+(1/35)\gamma^5] \\ &\qquad\times[1+2\gamma^2+\tfrac{1}{3}\gamma^4]^{-1} \\ &=\gamma[1+\tfrac{2}{3}\gamma^2+(1/35)\gamma^4][1+2\gamma^2+\tfrac{1}{3}\gamma^4]^{-1}, \end{aligned} \tag{4.1}$$

which is zero, as it must be, when $\gamma\to 0$.

To compute I_1, use

$$\begin{aligned} I_1&=\tfrac{3}{2}(3/\pi)^{\frac{1}{2}}-\frac{1}{2}\int 4\pi x f^2(x)dx \\ &=\tfrac{3}{2}(3/\pi)^{\frac{1}{2}}\left[1-(4/9)\tau_0^{-2}\int zF^2(z)dz\right], \end{aligned} \tag{4.2}$$

and substitute (3.17) for $F(z)$, to find

$$I_1=\frac{3}{2}\left(\frac{3}{\pi}\right)^{\frac{1}{2}}\left\{1-\left(\frac{\tau_0^4}{9\gamma^2}\right)\int_{1-\gamma}^{1+\gamma} y^4dy\int_{1-\gamma}^{1+\gamma} x^4dx \times\int_0^\infty dz\, zF_0(xz)F_0(yz)\right\}. \tag{4.3}$$

It is convenient to take double the integral with limits $x\le y$, namely

$$I_1=\frac{3}{2}\left(\frac{3}{\pi}\right)^{\frac{1}{2}}\left\{1-\left(\frac{\tau_0^4}{2\gamma^2}\right)\int_{1-\gamma}^{1+\gamma} y^4dy\int_{1-\gamma}^{y} x^4dx \times\int_0^\infty dz(4/9)zF_0(xz)F_0(yz)\right\}. \tag{4.3'}$$

We now make various coordinate transformations. First set $yz=\xi$, $zdz=y^{-2}\xi d\xi$, then use $\zeta=x/y\le 1$, $x^4dx=y^5\zeta^4 d\zeta$. The limits on ζ are $y^{-1}(1-\gamma)$ and unity. Finally replace y by $\eta=y^{-1}(1-\gamma)$, $y^7dy=-(1-\gamma)^8\eta^{-9}d\eta$, with limits unity and $(1-\gamma)/(1+\gamma)=1-2\gamma/(1+\gamma)$. The limits on ζ are now η and unity. The expression is

$$I_1=\frac{3}{2}\left(\frac{3}{\pi}\right)^{\frac{1}{2}}\left\{1-\frac{\tau_0^4}{2\gamma^2}(1-\gamma)^8\int_{1-\epsilon}^1 d\eta\,\eta^{-9}\int_\eta^1 d\zeta\zeta^4 \times\int_0^\infty d\xi\left[\frac{4}{9}\xi F_0(\xi)F_0(\zeta\xi)\right]\right\}, \tag{4.3''}$$

with $\epsilon=2\gamma(1+\gamma)^{-1}$. The integral,

$$\theta(\zeta)=\zeta^4\int_0^\infty d\xi\left[\frac{4}{9}\xi F_0(\xi)F_0(\zeta\xi)\right], \tag{4.4}$$

is found by direct integration to be

$$\begin{aligned} \theta(\zeta)&=\tfrac{1}{2}\zeta^4+\tfrac{1}{4}\zeta^2-\tfrac{1}{4}\zeta(1-\zeta^2)^2\ln[(1+\zeta)/(1-\zeta)] \\ &=-\sum_{\nu\ge 0}[4/(2\nu-1)(2\nu+1)(2\nu+3)]\zeta^{2\nu+4}. \end{aligned} \tag{4.5}$$

This can be integrated to give

$$\begin{aligned} &\int_\eta^1 \theta(\zeta)d\zeta=\Theta(\eta) \\ &=(1/36)\left\{8+3\eta-8\eta^3-3\eta^5-\tfrac{3}{2}(1-\eta^2)^3\ln\frac{1+\eta}{1-\eta}\right\}. \end{aligned} \tag{4.6}$$

Setting $\epsilon=2\gamma(1+\gamma)^{-1}$, $1-\epsilon=(1-\gamma)(1+\gamma)^{-1}$, one finds

$$J(x)=\int_x^1 d\eta\eta^{-9}\Theta(\eta),$$

$$J[(1-\gamma)(1+\gamma)^{-1}]=2\gamma^9(1-\gamma)^{-8}\{1+(\gamma^2/18) \times[35+10\gamma^2+91\gamma^4-12\ln(\gamma^{-1})]\}. \tag{4.7}$$

Finally, with Eq. (3.9) for τ_0, one finds that

$$I_1=(3/\pi)^{\frac{1}{2}}\gamma^2[\ln(\gamma^{-1})+1.0833]+O(\gamma^4). \tag{4.8}$$

To compute $J_2(x_0)$ and $J_1(x_0)$ of Eq. (3.3) we assume x_0 to be small and find the asymptotic expansion of $F(z)$, Eq. (3.17) for small z to be

$$F(z)=1-(1/10)[1+3\gamma^2-\cdots]z^2+(1/280)z^4 -(1/15\,120)z^6+\cdots, \tag{4.9}$$

and with (3.14), (3.15),

$$f^2(x)=1-(1/5)(3\pi^2)^{\frac{1}{3}}[1+(5/3)\gamma^2+\cdots]x^2 +(3/175)(3\pi^2)^{4/3}x^4-(4/4725)(3\pi^2)^2x^6+\cdots. \quad (4.10)$$

Using this in (3.3) one has

$$J_2=(6\pi^2/25)(\pi/3)^{\frac{1}{3}}[1+(5/3)\gamma^2+\cdots]x_0^5 -(18\pi^4/1225)(3/\pi)^{\frac{1}{3}}x_0^7+(8\pi^5/4725)x_0^9-\cdots, \quad (4.11)$$

$$J_1=(3\pi^2/10)(\pi/3)^{\frac{1}{3}}[1+(5/3)\gamma^2+\cdots]x_0^4 -(3\pi^4/175)(3/\pi)^{\frac{1}{3}}x_0^6. \quad (4.12)$$

In these employ the zeroth-order expression, Eq. (3.4′), $(2\pi x_0^3/3)=I_2$, with I_2 from (4.1), to obtain a zeroth-order approximation for J_2, and continue to iterate. One finds

$$x_0^3=(3/2\pi)\gamma(1+2\gamma^2+\tfrac{1}{2}\gamma^4)^{-1}[1-0.70160\gamma^{\frac{1}{3}} +1.0715\gamma^{4/3}-1.512\gamma^{6/3}+\cdots]. \quad (4.13)$$

With this, in (4.12) for J_1 one has

$$J_1=(9\pi/20)2^{-\frac{1}{3}}\gamma^{4/3}[1-1.20063\gamma^{\frac{1}{3}}+\cdots]. \quad (4.14)$$

One now has the necessary quantities, x_0 from (4.13), J_1 of (4.14), and I_1 of (4.8) to compute $\Delta\epsilon_p$ from (3.5). The leading term is seen to be that due to x_0^3, proportional to $\gamma^{\frac{1}{3}}$, which alone was used in Sec. 3 to obtain the "best" analytical form for $f(x)$. We find

$$\epsilon_p=\epsilon_{0p}-\tfrac{3}{4}(2\pi/3)^{\frac{1}{3}}c^{\frac{1}{3}}\gamma^{\frac{1}{3}}[1+2\gamma^2+\tfrac{1}{2}\gamma^4]^{-\frac{1}{3}}F(\gamma), \quad (4.15)$$

where

$$F(\gamma)=\gamma^{-\frac{1}{3}}[1+2\gamma^2+\tfrac{1}{2}\gamma^4]^{\frac{1}{3}} \times[(2\pi x_0^3/3)^{\frac{1}{3}}+\pi^{-1}(2\pi/3)^{\frac{1}{3}}(J_1-I_1)] =1+0.11693\gamma^{\frac{1}{3}}-0.5982\gamma^{4/3} -0.51311\gamma^{4/3}\ln(\gamma^{-1}). \quad (4.15')$$

5. ENERGY MINIMIZATION

Set

$$\gamma^{\frac{1}{3}}=\beta \quad (5.1)$$

and the kinetic energy, ϵ_k, Eq. (3.13) is

$$\epsilon_k=\epsilon_{0k}+4.78539c^{\frac{1}{3}}\beta^5[1+2\beta^3+0.2\beta^6]^{-5/3}K(\beta), \quad (5.2)$$

$$K(\beta)=1+0.26667\beta^3+0.11534\beta^6 -0.23226\beta^9+\cdots. \quad (5.2')$$

The potential energy from Eq. (4.15) is

$$\epsilon_p=\epsilon_{0p}-0.959579c^{\frac{1}{3}}\beta[1+2\beta^3+0.2\beta^6]^{-1}P(\beta), \quad (5.3)$$

$$P(\beta)=1+0.1169\beta-0.5982 -0.7696\beta^2\ln(\beta^{-1})+\cdots. \quad (5.3')$$

Differentiation of the sum with respect to β gives zero when

$$\beta=0.25854c^{-1/6}[P+dP/d\ln\beta]^{\frac{1}{3}}, \quad (5.4)$$

plus terms of order β^9. From the zeroth-order approximation, $\beta=0.258c^{-1/6}$, one sees that with $c\cong 1/27$, or one electron per three Bohr radii cubed, one has β equal to about one-half. The correction terms are significant at these low densities. Using (5.3′) for $P(\beta)$, and replacing $\ln(\beta^{-1})$ by the zeroth-order approximation, $\ln(\beta^{-1})=\frac{1}{6}\ln c+1.35274$, one finds

$$\beta=0.25854c^{-1/6}\{1+0.1169 -[2.0805+0.19241\ln c]\beta^3+\cdots\} =0.25854c^{-1/6}\{1+0.0302c^{-1/6} -[0.1381+0.01286\ln c]c^{-\frac{1}{3}}+\cdots\}. \quad (5.5)$$

6. RESULTS

Enter (5.2) for the kinetic energy and (5.3) for the potential energy with (5.5) for β. One obtains

$$\epsilon_{0k}=2.87123c^{\frac{1}{3}}\text{ atomic units}, \quad =78.134\quad c^{\frac{1}{3}}\text{ ev}, \quad (6.1)$$

$$\Delta\epsilon_k=0.08269c^{1/6}k(c)\text{ atomic units} \quad =2.250\quad c^{1/6}k(c)\text{ ev}, \quad (6.2)$$

$$k(c)=[1+0.0346c^{-\frac{1}{3}}]^{-5/3}\{1+0.0907c^{-1/6} -[0.4117+0.0386\ln c]c^{-\frac{1}{3}}\} \times[1+0.0046c^{-\frac{1}{3}}+\cdots], \quad (6.2')$$

$$\epsilon_{0p}=-0.73856c^{\frac{1}{3}}\text{ atomic units} \quad =-20.098\quad c^{\frac{1}{3}}\text{ ev}, \quad (6.3)$$

$$\Delta\epsilon_p=-0.24890c^{1/6}p(c)\text{ atomic units} \quad =-6.751\quad c^{1/6}p(c)\text{ ev}, \quad (6.4)$$

$$p(c)=[1+0.03456c^{-\frac{1}{3}}]^{-1}[1+0.0604c^{-1/6} -(0.2459+0.0214\ln c)c^{-\frac{1}{3}}+\cdots]. \quad (6.4')$$

The total correlation energy is

$$\Delta\epsilon_c=-0.16540c^{1/6}[\tfrac{1}{2}k(c)+\tfrac{1}{2}p(c)]\text{ atomic units}, \quad =-4.500\quad c^{1/6}[\tfrac{1}{2}k(c)+\tfrac{1}{2}p(c)]\text{ ev}. \quad (6.5)$$

In these equations c, of Eq. (1.6) is the concentration of electrons per cubic Bohr radius,

$$c=0.1481\times\text{number of electrons per (angstrom)}^3. \quad (6.6)$$

The distance, x_0, out to which $k(x)$ is unity is given by (4.11) as

$$x_0=0.39742c^{-\frac{1}{3}}[1-0.1502c^{-1/6}+\cdots], \quad (6.7)$$

which is measured in such units that the number density is unity. The volume, v_0, occupied by this "hole" around each electron is then

$$v_0=(4\pi/3)x_0^3=0.26283c^{-\frac{1}{3}}[1-0.4506c^{-1/6}+\cdots], \quad (6.7'')$$

measured in units of the volume per electron in the gas.

The momentum distribution of the electrons is determined by $\Phi(\tau)$ of Eq. (3.11), with τ related to momentum by (3.9) and $\gamma^{\frac{1}{3}}=\beta$. For the Single Slater Determinant all momentum states up to

$$|\mathbf{p}|=p_0=(3/8\pi)^{\frac{1}{3}}h\rho_0^{\frac{1}{3}} \quad (6.8)$$

are filled with two electrons each. For the "correlated"

system the momentum states up to

$$|\mathbf{p}|_l = p_0(1-\beta^1)(1+2\beta^3+0.2\beta^6)^{-\frac{1}{3}} \cong p_0(1-0.1314c^{-\frac{1}{3}}) \quad (6.9)$$

are filled with two electrons each, and all above

$$|\mathbf{p}|_u \cong p_0(1+0.1314c^{-\frac{1}{3}}) \quad (6.9')$$

are empty. The number per state decreases monotonically from 2 to 0 with a term proportional to $|\mathbf{p}|^2$ between $|\mathbf{p}|_l$ and $|\mathbf{p}|_u$.

To obtain some idea of the range of applicability of the equations we may try them with the alkalis. If one considers the valence electron alone, so that one treats only one electron per atom, the concentration c is lowest for cesium than for any other metal, and is generally low in the alkalis.

For cesium one has

$$c=0.001256, \quad \text{Cs, one electron,}$$
$$\beta=0.7870[1+0.092-0.483+\cdots].$$

The convergence of the series approximation (5.5) for β is obviously nonexistent at these low concentrations. For $k(c)$ and $p(c)$ the convergence is equally bad, and direct calculation with the equations given leads to an expression for $\Delta\epsilon_p$ which is greater in magnitude than the value $0.637\epsilon_{0p}$ found from Eq. (1.18) as the lowest possible reduction in potential energy due to electron correlation.

However for lithium, with

$$c=0.00686, \quad \text{Li, one electron,}$$
$$\beta=0.5931[1+0.069-0.390+\cdots],$$

there is some sign of nearing convergence.

The general integrations given in Sec. 4 are actually adequate even for the low-density examples quoted. Equation (4.1) for I_2 is exact. Even with the maximum possible value of x_0, $x_0^3=3/4\pi$, the quantity J_2 is given by (4.11) adequately. The evaluation of x_0 is then awkward, but possible, and the other integrals are satisfactorily given.

PHYSICAL REVIEW VOLUME 100, NUMBER 6 DECEMBER 15, 1955

Cadmium Sulfide with Silver Activator

JOHN LAMBE
United States Naval Research Laboratory, Washington, D. C.
(Received July 20, 1955)

Further experimental evidence is presented in connection with a model which has been proposed by Lambe and Klick for CdS(Ag). In this model, the silver activator is assumed to give rise to a level which is approximately 0.4 ev below the conduction band, and that luminescence occurs when an electron in such an activator level recombines with a free hole. It is shown that irradiation in the 1μ infrared region stimulates luminescence by generating free holes, while also causing well known quenching effects in photocurrent. It is also shown that 3μ irradiation gives rise to photoconduction by exciting electrons from the activator levels into the conduction band. The proposed model indicates that irradiation in the 3μ region should quench luminescence by removing electrons from activator levels, and this is found experimentally. These experiments further substantiate the proposed model for CdS(Ag).

I. INTRODUCTION

IN a recent paper[1] (referred to as LK), a model for CdS(Ag) was discussed based on observations of infrared stimulation of photocurrent and luminescence and on relationships observed between photoconductivity and luminescence. The essential point of this model was that silver activation in CdS gave rise to an activator level about 0.4 ev below the conduction band (see Fig. 1). It was assumed that luminescence occurs when an electron in this level recombines with a free hole. This model differs from earlier models[2,3] for sulfide phosphors in the position of this activator level. It had previously been assumed that the activator level was just above the valence band, and that luminescence occurred when a free electron returned to this level from the conduction band. The purpose of this paper is to report further experimental evidence which relates to the model proposed in LK for CdS(Ag).

The cadmium sulfide crystals used in these experiments were activated by first immersing them in a 0.5N solution of $AgNO_3$ for approximately 30 seconds and then, after washing with distilled water and drying, firing at 800°C for one hour in a helium atmosphere. All experiments here were done at 77°K and temperature control was obtained by direct immersion of the crystals in liquid nitrogen.

II. EFFECTS OF 1μ IRRADIATION ON PHOTOCONDUCTION AND LUMINESCENCE

In LK, experimental evidence was presented showing separately the effects of 1μ irradiation on luminescence and photoconduction. The 1μ irradiation produced a

[1] J. Lambe and C. C. Klick, Phys. Rev. **98**, 909 (1955). This paper will be referred to as LK.
[2] M. Schön, Z. Physik **119**, 463 (1942).
[3] H. A. Klasens, Nature **158**, 306 (1946).

stimulation of luminescence, and an over-all quenching of photoconduction. These effects were attributed to the freezing of holes by 1μ irradiation.[1] This conclusion has been questioned by several workers on the basis that 1μ irradiation has actually two effects on photoconduction; an initial stimulation and then a quenching.[4] Thus 1μ irradiation might generate free electrons as well as holes and perhaps the free electrons are responsible for the luminescence stimulation. Unfortunately, the observations previously reported did not show the effect of 1μ irradiation on photocurrent and luminescence simultaneously. In order to clarify this point, such simultaneous observations have been made.

In order to do this, measurements of luminescence and photocurrent were made under the following conditions. CdS(Ag) crystals are cooled to 77°K and then excited by ultraviolet light. The ultraviolet light is removed, and then photocurrent and luminescence are observed. The luminescence drops rapidly to zero, and

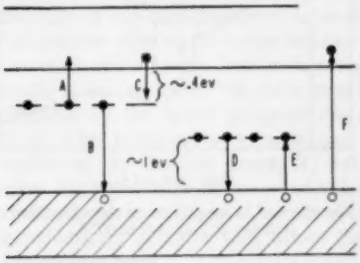

FIG. 1. Proposed model for CdS(Ag).[1] The level 0.4 ev below the conduction band arises from silver activation. The levels 1 ev above the valence band are normally present in CdS. Processes occurring are (*A*) excitation of electrons from activator level, (*B*) luminescence, (*C*) capture of electrons by activator levels, (*D*) trapping of holes, (*E*) release of trapped holes by infrared excitation, and (*F*) excitation of phosphor by irradiation in fundamental band.

the photocurrent decays slowly. After approximately a minute, light in the 1μ region is applied to the sample. The result of this is shown in Fig. 2. In the photocurrent one observes a slight increase and then a steady quenching effect while the luminescence is stimulated and then slowly decreases as irradiation continues and the stored energy is exhausted. This experiment shows clearly that the stimulating action of 1μ light is not due to the production of free electrons because before this stimulating light was applied, a substantial photocurrent was flowing and very little transient increase in photocurrent is observed due to the action of the light. Thus the change in the number of free electrons is not significant. The fact that photocurrent is subsequently quenched while the luminescence is stimulated is in accord with the conclusion that the 1μ irradiation generates free holes, and these are responsible for luminescence stimulation and photocurrent quenching.

[4] R. Frerichs, Phys. Rev. 72, 594 (1947).

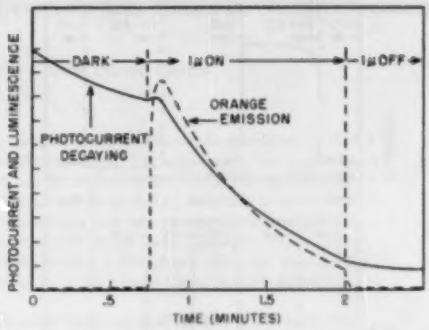

FIG. 2. Simultaneous observation of the effect of 1μ irradiation on luminescence and photocurrent. $T=77°K$.

A further point in favor of the above conclusion is the following. In Sec. III it will be shown that 3μ irradiation excites free electrons, but it is found that 3μ irradiation does not stimulate luminescence. Thus the stimulation of luminescence could not be due simply to the exciting of electrons into the conduction band, followed by a subsequent recombination at a luminescent center.

III. SIGN OF CARRIER DURING 3μ IRRADIATION

In LK, it was reported that silver activation of CdS introduced an infrared photoconduction band in the 3μ to 6μ region. It was believed that this photoconduction was due to free electrons, and some indirect evidence was presented to support this. It was felt that more direct proof of this could be obtained by observing the type of rectification present with a point contact rectifier.

In the experiment which was performed, a CdS(Ag) crystal was mounted with a large indium base electrode and a tungsten point electrode. This assembly was immersed in liquid nitrogen, and the forward and back resistance was measured under various conditions of illumination.

In the first measurement the crystal was illuminated with light at 4400 A at 77°K. A potential of 50 volts ($E\cong 100$ v/cm) was applied to the crystal first with one polarity and then with the polarity reversed. The resultant current flow is shown in Fig. 3(a). It is seen that a much larger current flows when the point contact is positive in voltage with respect to the base electrode than when it is negative. This indicates free-electron-type conduction which is in agreement with Hall effect measurements[5] for this type of excitation.

The next step was to remove the 4400 A excitation and to excite the crystal in the 3μ region. This was done by means of a rocksalt prism monochromator and a glowbar. Again the current was measured under different polarities. This result is shown in Fig. 3(b). It is seen that the direction of rectification indicates free-

[5] R. W. Smith, R.C.A. Rev. 12, 350 (1951).

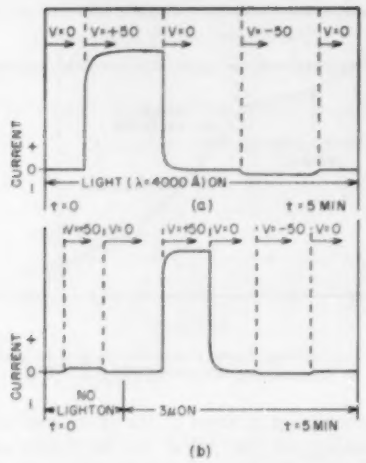

FIG. 3. Point contact rectifier experiments on CdS(Ag) at 77°K. The voltage V refers to the voltage applied to the tungsten point contact with respect to the indium base electrode. $T=77°K$.

electron-type conductivity and this is produced by irradiation in the 3μ region. It is possible, therefore, to conclude that the 3μ excitation excites electrons from a level below the conduction band into this band. This is in agreement with the conclusion reached in LK based on a different experimental approach.

When the above experiment was attempted with 1μ irradiation little or no conduction could be observed, and no conclusion could be made with regard to the sign of the carrier under this irradiation. One should expect perhaps to observe conduction due to free holes and thus a reversal in the rectification. In general, however, attempts to observe hole conductivity in CdS have not been successful.[8] This may be due to a very short lifetime or a low mobility for free holes.

IV. RELATION BETWEEN THE 3μ BAND AND LUMINESCENCE

It was shown in LK that if CdS(Ag) is first excited with ultraviolet light at 77°K and then the ultraviolet is removed, the characteristic orange luminescence can be stimulated by irradiation with light at about 1μ. The results of Sec. II indicate that this stimulation should be attributed to the freeing of holes by 1μ light.

The purpose of this section is to demonstrate the relationship between 3μ irradiation and luminescence. We consider a CdS(Ag) crystal in which luminescence is being stimulated by 1μ irradiation. On the model proposed in LK, the holes which are freed migrate and recombine with electrons in the activator levels and give rise to emission. Suppose that during this stimulation process, the crystal is irradiated with 3μ light. This should raise electrons from the activator levels into the conduction band and thus the emission should decrease.

This experiment was carried out as follows. CdS(Ag) crystals were placed on a plaque and immersed in liquid nitrogen. The crystals were illuminated with light from a mercury discharge lamp for one minute and then kept in darkness for 5 minutes. The sample was then illuminated with a tungsten light through a Corning 7-85 filter, which passes a narrow band of infrared at about 1μ, and the stimulated emission was observed with a photomultiplier. While this was occurring, the crystals were irradiated with 3μ light from a glowbar in conjunction with a rocksalt prism monochromator. In Fig. 4 the result is shown. The 3μ light produces a definite decrease in the stimulated emission as predicted on the basis of the proposed model.

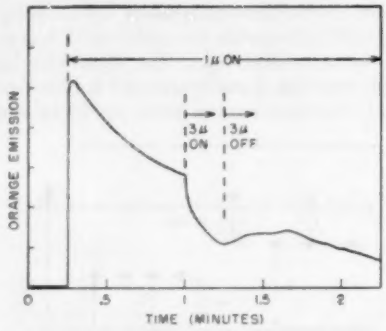

FIG. 4. The effect of 3μ irradiation on the stimulated orange emission of CdS(Ag) at 77°K.

In order to check this experiment, the monochromator was run from 3μ down to 1μ. In the 1μ region, additional stimulation is observed and thus there is a transition from quenching of luminescence to stimulation as should be expected.

CONCLUSION

The significant results of these experiments may be summarized as follows. Irradiation of CdS(Ag) in the 3μ region gives rise to photoconductivity at 77°K by exciting free electrons; and also this irradiation has a quenching effect on luminescence. Irradiation in the 1μ region gives rise to a quenching of photocurrent and a stimulation of luminescence, and it has been shown that the stimulating action on luminescence arises from free holes. These observations lend further support to the model which has been proposed for CdS(Ag), wherein silver introduces a level about 0.4 ev below the conduction band and luminescence is the result of a recombination between an electron in this level and a free hole.

ACKNOWLEDGMENTS

The author is indebted to Dr. C. C. Klick for many valuable discussions and suggestions in the course of this work.

Magnetic Susceptibility of Impurity-Trapped Electrons and Holes in Semiconductors

E. MOOSER*
Division of Pure Physics, National Research Council, Ottawa, Canada
(Received August 3, 1955)

The magnetic susceptibility of charge carriers in impurity sites of a semiconductor is calculated in this paper. According to the impurity content two cases can be distinguished. For sufficiently low impurity concentration, the interaction between the impurity centers can be neglected and the paramagnetic contribution of the trapped carriers to the susceptibility is of the Langevin type, i.e., inversely proportional to the temperature. The onset of interaction at higher concentrations, however, causes the impurity level associated with isolated impurities to broaden into a quasi-continuous energy band. The electrons or holes in such a band are free to move through the crystal and thus, forming a Fermi gas, give rise to a Pauli paramagnetism which at low temperatures is practically constant. In both cases the orbital diamagnetism is essentially the same and independent of temperature.

The susceptibilities corresponding to the two cases are compared with one another and it is found that low-temperature susceptibility data should give valuable information on impurity bands. Measurements on Si are interpreted according to the present theory.

INTRODUCTION

IF some atoms in the otherwise perfect lattice of a semiconductor are replaced by foreign atoms, the band structure of the semiconductor is modified. A number of electron sites equal to the number of substituted atoms is shifted away from each energy band into normally forbidden zones.[1,2] If, to be more specific, a semiconductor of the fourth group of the periodic table (Si, Ge, α-Sn) contains N_d atoms per unit volume of an element of say the fifth group, N_d donor sites occur below the lower edge of the conduction band. Correspondingly, the presence of N_a atoms of the third group introduces N_a acceptor sites above the upper edge of the valence band.

As long as the concentration of impurity atoms is sufficiently small, the wave functions of the electrons or holes in the impurity sites may be found in much the same way as the wave function of the electron in an isolated hydrogen atom. However, with increasing concentration the wave functions of the trapped charge carriers start to overlap. As a result of this overlap, the discrete energy level associated with isolated impurities broadens into a narrow impurity band.

While various attempts[3-6] have been made to calculate the wave functions of the charge carriers in impurity bands, there exists as yet no solution of this problem which is free of all ambiguity. Nevertheless, it is at present generally accepted that the impurity band wave functions extend through the whole crystal, i.e., the trapped carriers are free to move from one impurity to another, thus contributing to the over-all conductivity of the semiconductor.

Impurity band conduction has first been reported by Busch and Labhart[7] in SiC and was recently discovered in Ge by Hung and Gliessman[8] and by Fritzsche and Lark-Horovitz.[9]

Unfortunately it is not possible to determine all the parameters characterizing an impurity band, namely its width and shape, its position in the band scheme, and the mobility of its charge carriers, from the electrical properties of a semiconductor. However, according to Busch and Mooser,[10] additional information on the band structure of a semiconductor can be gained from susceptibility measurements. It is with this possibility in mind that we study in the present paper the magnetism of impurity-trapped charge carriers.

Restricting the discussion to donors (a similar reasoning holds for acceptors), we first calculate the susceptibility for noninteracting, hydrogen-like impurity centers. Next, assuming the electrons in a donor band to form a Fermi gas, we evaluate their susceptibility and compare it with that of the noninteracting centers. It will be found from this comparison that at low temperatures an appreciable difference exists between the two susceptibilities, and this difference should make it possible to detect the presence of an impurity band in a semiconductor from magnetic measurements.

Finally, susceptibility measurements on silicon reported by Portis, Kip, Kittel, and Brattain[11] are interpreted in terms of the present theory. In agreement with Baltensperger's[6] predictions, a narrow donor band is found in silicon containing 1.5×10^{18} phosphorus atoms per cm^3.

* National Research Laboratories Postdoctorate Fellow.
[1] J. C. Slater, Phys. Rev. 76, 1592 (1949).
[2] H. M. James, Phys. Rev. 76, 1602 (1949).
[3] H. M. James and A. S. Ginzbarg, Phys. Rev. 77, 749 (1950); J. Phys. Chem. 57, 840 (1953).
[4] C. Erginsoy, Phys. Rev. 80, 1104 (1950); 88, 893 (1952).
[5] G. W. Castellan and F. Seitz, *Semiconducting Materials* (Butterworth Scientific Publications, London, 1951), p. 8.
[6] W. Baltensperger, Phil. Mag. 44, 1355 (1953).
[7] G. Busch and H. Labhart, Helv. Phys. Acta 19, 463 (1946).
[8] C. S. Hung and J. R. Gliessman, Phys. Rev. 79, 726 (1950); 96, 1226 (1954).
[9] H. Fritzsche and K. Lark-Horovitz, Physica 20, 834 (1954).
[10] G. Busch and E. Mooser, Helv. Phys. Acta 24, 329 (1951); 26, 611 (1953); Z. physik. Chem. 198, 23 (1951).
[11] Portis, Kip, Kittel, and Brattain, Phys. Rev. 90, 988 (1953).

SUSCEPTIBILITY OF ELECTRONS IN NONINTERACTING DONORS

Calculating first the paramagnetic susceptibility of the electrons in isolated, hydrogen-like donors, we note that their wave functions are s-like (we only consider the ground state of the donors), having zero orbital moment. Apart from a small diamagnetic susceptibility due to their orbital motion, the trapped electrons therefore give rise to a spin susceptibility only. The latter is readily calculated from the difference between the concentration n_+ of electrons with positive spin and the concentration n_- of electrons with negative spin.

Denoting the total number of donors per unit volume by N_d and the concentration of nonoccupied donors by n_0, we have:

$$n_0+n_++n_-=N_d. \tag{1}$$

If then E_+ and E_- are the energies of the trapped electrons with positive and negative spins, respectively, it can be shown that

$$n_0:n_+:n_-=1:\exp\left(\frac{\zeta-E_+}{kT}\right):\exp\left(\frac{\zeta-E_-}{kT}\right), \tag{2}$$

where ζ is the Fermi energy, k the Boltzmann constant, and T the absolute temperature.

In the absence of a magnetic field E_+ and E_- are equal, and with $E_+=E_-=E_d$ the concentration $n_d=n_+ +n_-$ of occupied donors becomes

$$n_d=\frac{N_d}{1+\frac{1}{2}\exp[(E_d-\zeta)/kT]}. \tag{3}$$

In the presence of a magnetic field H the energy of an electron with its spin pointing along H is lowered by μH (μ = Bohr magneton), while the energy of an electron with opposite spin is raised by the same amount. Therefore

$$E_+=E_d-\mu H, \quad E_-=E_d+\mu H,$$

and it follows from (1) and (2) that a number of spins, namely

$$n_+-n_-=\frac{N_d\sinh(\mu H/kT)}{\frac{1}{2}\exp[(E_d-\zeta)/kT]+\cosh(\mu H/kT)},$$

are then not compensated, giving rise to a magnetic moment per unit volume of

$$M=\mu(n_+-n_-).$$

Dividing M by H, we find the paramagnetic susceptibility of the trapped electrons:

$$\kappa_{\text{para}}=\frac{\mu}{H}\frac{N_d\sinh(\mu H/kT)}{\frac{1}{2}\exp[(E_d-\zeta)/kT]+\cosh(\mu H/kT)}. \tag{4}$$

As long as $\mu H \ll kT$, (4) can be approximated by

$$\kappa_{\text{para}}=n_d\mu^2/kT, \tag{4a}$$

n_d being the total number of trapped electrons as given by (3).

Equation (4) shows that the paramagnetism of the electrons in isolated donors is of the Langevin type. This is what one might expect, assuming the trapped electrons to be independent of one another, because only thermal motion opposes the spin alignment. It then follows immediately that complete spin saturation can be achieved by reducing the temperature. Indeed, putting $\mu H \gg kT$, Eq. (4) becomes

$$\kappa_{\text{para}}=\frac{N_d\mu}{H}\frac{1}{1+\exp[(E_d-\zeta-\mu H)/kT]}=\frac{n_+\mu}{H}. \tag{4b}$$

This expression represents a state in which the N_d donors are occupied with n_+ electrons whose spins all point along the field H. Noting that with the highest fields available at present the condition $\mu H \gg kT$ is satisfied only at temperatures near or below 1°K, we can further simplify (4b). At these low temperatures, ζ lies about half-way between the donor level and the lower edge of the conduction band. With $\zeta > E_d$ and $\mu H \gg kT$ it follows that $\exp[(E_d-\zeta-\mu H)/kT] \ll 1$. Hence, (4b) immediately takes the form

$$\kappa_{\text{para}}=N_d\mu/H. \tag{4c}$$

So far we have considered only the spin susceptibility of the trapped electrons, and there remains to be evaluated the susceptibility arising from their orbital motion. Since according to our assumptions the donors contain only s electrons with zero orbital moment, we are left with an induced diamagnetism. The corresponding susceptibility is given by the Larmor-Langevin formula

$$\kappa_{\text{dia}}=-(n_de^2/6m^*c^2)r^2, \tag{5}$$

where r is the radius of the electron orbit, e the electronic charge, m^* the effective mass of an electron near the bottom of the conduction band, and c the velocity of light. The total susceptibility κ of electrons in noninteracting donors, being the sum of the two terms κ_{para} and κ_{dia}, therefore is

$$\kappa=n_d\left(\frac{\mu^2}{kT}-\frac{e^2r^2}{6m^*c^2}\right) \tag{6}$$

except at the very lowest temperatures, where the temperature-dependent term has to be replaced by (4c).

A similar expression holds for the susceptibility of holes in noninteracting acceptors.

SUSCEPTIBILITY OF ELECTRONS IN A DONOR BAND

The electrons in a donor band, being free to move through the whole crystal, form a Fermi gas. The alignment of their spins by a magnetic field is therefore no longer opposed only by thermal motion, as in the case of isolated impurities, but is also governed by the Pauli exclusion principle. This results in an appreciable

change of the paramagnetism of the trapped electrons. Moreover, we expect the diamagnetism of a donor band to be somewhat larger than that of a donor level, since, in addition to the Larmor-Langevin susceptibility (5) associated with the movement of the electrons around the impurities, a second negative term now enters the susceptibility. Corresponding to the Landau diamagnetism of free electrons, this second term arises from the movement of the electrons from one impurity to another. It will, however, be found that at low temperatures the Landau diamagnetism of donor band electrons is very small.

The spin susceptibility of a Fermi gas consisting of n_d particles is given by

$$\kappa_{\text{para}}=\mu^2\partial n_d/\partial\zeta \tag{7}$$

(see, e.g., reference 10). The main task in evaluating κ_{para} is therefore to find n_d as a function of the Fermi energy ζ. Thinking of the trapped electrons as described by an appropriate set of Bloch waves (see reference 6), we assume that the number N_s of available sites in the donor band is equal to twice the number N_d of donors.[12] If then $D(E)$ denotes the density of states in the donor band, we have

$$N_s=2N_d=2\int_{E_{d_1}}^{E_{d_2}}D(E)dE, \tag{8}$$

where E_{d_1} and E_{d_2} are the energies of the two band edges.

With our notation the number n_d of occupied sites becomes

$$n_d=2\int_{E_{d_1}}^{E_{d_2}}D(E)\frac{1}{1+\exp[(E-\zeta)/kT]}dE, \tag{9}$$

and we see that without explicit knowledge of $D(E)$, n_d can only be evaluated at high temperatures, where

$$E_{d_2}-E_{d_1}\ll kT.$$

In this case it is possible to replace the Fermi function under the integral sign by its value at $\bar{E}_d=(E_{d_1}+E_{d_2})/2$, and therefore

$$n_d=\frac{1}{1+\exp[(\bar{E}_d-\zeta)/kT]}2\int_{E_{d_1}}^{E_{d_2}}D(E)dE$$

$$=\frac{2N_d}{1+\exp[(\bar{E}_d-\zeta)/kT]}. \tag{10}$$

κ_{para} is now readily found to be

$$\kappa_{\text{para}}=\frac{n_d\mu^2}{kT}\frac{\exp(\bar{E}_d-\zeta/kT)}{1+\exp[(\bar{E}_d-\zeta)/kT]}. \tag{11}$$

[12] As James and Ginzbarg[9] pointed out, this assumption is an oversimplification. Because of the random distribution of the impurities, N_s is somewhat smaller than $2N_d$.

Next, consider low temperatures for which

$$kT\ll E_{d_2}-E_{d_1}.$$

Here the Fermi function

$$F(E)=\frac{1}{1+\exp[(E-\zeta)/kT]}$$

can be approximated by an idealized step function,

$$F(E)=\begin{cases}0 & \text{for } E>\zeta\\ 1 & \text{for } E\leq\zeta\end{cases},$$

and the number of trapped electrons becomes

$$n_d=2\int_{E_{d_1}}^{\zeta}D(E)dE. \tag{12}$$

Introducing (12) in (7), we find

$$\kappa_{\text{para}}=2\mu^2D(\zeta). \tag{13}$$

The expressions (11) and (13) for the paramagnetic susceptibility of donor band electrons both differ from the simple Langevin susceptibility found for the electrons in isolated donors. Before discussing these differences in detail, however, we want to add a few words concerning the diamagnetic susceptibility κ_{dia} of the donor band electrons. As mentioned above, κ_{dia} may be written as the sum of two terms, a "bound electron" term

$$\kappa_{\text{dia}}'=-\frac{n_d e^2}{6m^*c^2}r^2,$$

and a "free electron" term κ_{dia}''. Busch and Mooser[10] pointed out that κ_{dia}'' can in general not be evaluated. However, at temperatures $kT\ll E_{d_2}-E_{d_1}$ the drop of the Fermi function from one to zero extends only over a very narrow region of the impurity band. It is then possible to define an appropriate effective mass m^+ so that the relation between the energy E and the wave vector k of an electron in this region is approximately

$$E=(\hbar^2/2m^+)k^2.$$

With this approximation κ_{dia}'' becomes

$$\kappa_{\text{dia}}''=-\frac{\mu^2}{3}\frac{\partial n_d}{\partial\zeta}\left(\frac{m}{m^+}\right)^2. \tag{14}$$

Baltensperger[6] has shown that normally $m^+\gg m$. At low temperatures κ_{dia}'' therefore is very small, and the diamagnetism of the electrons in a donor band is essentially the same as that of electrons in isolated donors.

DISCUSSION

In the preceding two sections expressions have been derived for the susceptibility of isolated donors and for

that of a donor band. It remains here to discuss what information can be gained, according to these formulas, from susceptibility measurements.

At low temperatures, where $kT \ll E_{d_2} - E_{d_1}$, the paramagnetic susceptibility of a donor band is given by

$$\kappa_{\text{para}} = 2\mu^2 D(\zeta). \tag{13}$$

This expression deviates markedly from the Langevin value (4a) found for isolated donors, and it should therefore be possible to detect the presence of a donor band in a semiconductor from low-temperature susceptibility measurements.

At high temperatures, where $kT \ll E_{d_2} - E_{d_1}$, the situation is somewhat more involved. Here the donor band susceptibility is

$$\kappa_{\text{para}} = \frac{n_d \mu^2}{kT} \frac{\exp[(\bar{E}_d - \zeta)/kT]}{1+\exp[(\bar{E}_d - \zeta)/kT]} \tag{11}$$

differing by the factor

$$\exp[(\bar{E}_d - \zeta)/kT] / \{1+\exp[(E_d - \zeta)/kT]\}$$

from the susceptibility of isolated donors. With $\zeta \ll \bar{E}_d$ this factor is approximately 1, becomes $\frac{1}{2}$ for $\zeta = \bar{E}_d$ and finally goes to zero like $\exp[(\bar{E}_d - \zeta)/kT]$ as ζ increases further. An appreciable difference between (11) and (4a), which should allow a donor band to be detected, therefore exists only if the Fermi level ζ lies close to or above the donor states. When this condition is satisfied, the paramagnetic susceptibility of a donor band stays below the Langevin value even when $kT \sim E_{d_2} - E_{d_1}$ and the approximation (11) breaks down. As is readily seen from an argument similar to the one leading to (11), κ_{para} then satisfied the following inequality:

$$\kappa_{\text{para}} < \frac{n_d \mu^2}{kT} \frac{\exp[(E_{d_2} - \zeta)/kT]}{1+\exp[(E_{d_2} - \zeta)/kT]}.$$

Now in the intrinsic range of a semiconductor, that is at high temperatures, ζ normally lies near the middle of the forbidden energy zone.[13] As the temperature is lowered, the semiconductor enters the extrinsic range and ζ gradually moves closer towards the donor states. Here, then, one expects to find the first measurable deviation of the donor band susceptibility from the Langevin value, and it follows from our discussion that, while one has to take measurements in the extrinsic range to detect a donor band, one need not necessarily go to the very low temperatures for which (13) holds.

[13] In semiconductors such as InSb which are degenerate in the intrinsic range, ζ lies in the conduction band, that is, well above the donor states. Nevertheless, it is not possible in this case to detect a donor band from susceptibility measurements, because in the intrinsic range the number of free charge carriers is so large that their susceptibility completely masks the difference between (11) and (4a).

At present the only susceptibility data known to exhibit an appreciable departure from the Langevin value are those reported by Portis, Kip, Kittel, and Brattain.[11] These authors measured the paramagnetic susceptibility of a silicon sample containing 1.5×10^{18} donors per cm^3. If we try to interpret these results according to the present theory we must remember that they do not simply represent κ_{para} as calculated above, but rather the sum of κ_{para} and a second term κ_{para}' which arises from the spin of the free electrons. If n_f denotes the concentration of free electrons, then, according to reference 10, κ_{para}' is

$$\kappa_{\text{para}}' = n_f \mu^2 / kT.$$

In the extrinsic range, $n_d + n_f = N_d$, and if the concentration of donors were not high enough to lead to the formation of a donor band the sum of κ_{para} and κ_{para}' would simply be given by

$$\kappa = \kappa_{\text{para}} + \kappa_{\text{para}}' = N_d \mu^2 / kT.$$

The experimental results clearly deviate from this $1/T$ law below about 40°K, indicating the presence of a donor band in the silicon sample. Since, at the lowest temperatures at which measurements were taken, the number of free electrons is negligible, we have $\kappa \approx \kappa_{\text{para}}$ at these temperatures. Introducing the experimental value of κ at 4°K in (13) therefore yields the density of states near the middle of the donor band:

$$D(\zeta) = 3.2\times10^{20} \text{ cm}^{-3} \text{ ev}^{-1}.$$

Finally, putting $D(\zeta) = N_d/(E_{d_2} - E_{d_1})$, we find the width of this donor band to be approximately

$$E_{d_2} - E_{d_1} \approx 5\times10^{-3} \text{ ev}.$$

This rather small width corresponding to 1.5×10^{18} donors per cm^3 agrees quite well with Baltensperger's[6] prediction that in silicon a donor band does not form until an impurity concentration of 10^{18} cm^{-3} is reached.

It is worthwhile adding here that expression (13) allows the density of states to be measured at any point of the donor band, if it is possible to displace the Fermi level without altering the temperature. Fortunately, this can readily be done by introducing a small number of acceptors in a semiconductor. Some electrons will then fall down from the donor band to fill up the acceptors, and accordingly ζ will shift downwards. Measurements on a sample in which the number of acceptors is gradually increased by successive exposures to neutron radiation should yield very interesting results.

ACKNOWLEDGMENTS

The author wishes to thank Dr. D. K. C. MacDonald and Dr. W. Kohn for many helpful discussions.

Pressure Dependence of the Resistivity, Hall Coefficient, and Energy Gap for InAs†

JULIUS H. TAYLOR
Morgan State College, Baltimore, Maryland
(Received August 31, 1955)

The effect of hydrostatic pressure on the resistivity of intrinsic *n*-type InAs has been measured in the range from 1 to 2000 atmospheres. The resistivity and Hall constant were found to increase exponentially with increasing pressure. Measurements of the resistivity and Hall effect yield an increase of 19 and 12 percent respectively for a change in pressure of 2000 atmospheres. If it is assumed the increase in resistivity is produced by an increase in the energy gap our measurements indicate a shift of 8.8×10^{-6} ev/atmosphere. The increase in Hall constant represents a shift of 5.5×10^{-6} ev/atmosphere.

THIS paper presents the experimental results of hydrostatic pressure on the resistivity, Hall coefficient, and energy gap for *n*-type polycrystalline indium arsenide. Unfortunately, the purity of sample used in this investigation was such that measurements had to be taken at temperatures of the order of 200 degrees centigrade in order to work in the intrinsic range. This presents experimental difficulties because of the temperature dependence of the constants being measured. Our results show the resistivity and Hall coefficient increase exponentially with increasing hydrostatic pressure.

Indium arsenide is a semiconducting compound by uniting elements of the III and V columns of the periodic table. It has a zincblende structure thereby exhibiting cubic symmetry. The forbidden band width is about 0.47 electron volt[1] at absolute zero and becomes smaller with increasing temperature at a rate of 4×10^{-4} ev/°K.

A commercial high-pressure bomb was used to make measurements of changes of resistivity with pressure. An adaptor unit of nonmagnetic stainless steel was provided for Hall coefficient measurements. The bomb was immersed in a Prestone motor oil bath which was electronically thermostated at constant temperatures to the order of 1/100 of a degree centigrade. Samples were cut into rectangular parallelepipeds, copper spots were electroplated on the sample, and pressure contacts were made by using phosphorus bronze spring clips. In all measurements, the current and magnetic field were reversed and an average effect was computed. It is assumed in all measurements that changes in sample dimensions accompanying changes in pressure produce a negligible effect. The magnetic field used was 2000 gauss.

Figure 1 shows curves of the resistivity and Hall coefficient as a function of inverse absolute temperature. These curves are typical of these quantities for the intermetallic group.

In Fig. 2 the experimental data for log resistivity and log Hall coefficient are plotted against pressure at different temperatures. Both increase exponentially with pressure, the resistivity at a rate larger than the Hall coefficient at each temperature. Measurements on other samples of different purity show these curves to be typical of the behavior of *n*-type InAs. These curves represent data taken on a sample of highest purity available at the time the experiment was performed. The curves taken at 201 degrees centigrade represent data taken at points on the curves of resistivity and Hall coefficient *vs* reciprocal absolute temperature that are well into the intrinsic range. These curves show a change of 19 and 12 percent, respectively, for the two constants for a change of 2000 atmospheres pressure. This 7 percent difference is explained below.

For an effective mass of 0.06, the largest value of conduction electrons consistent with the accurate use of classical statistics is 0.97×10^{17} per cubic centimeter at 201 degrees centigrade.[2] This criterion is satisfied in the samples used in this investigation.

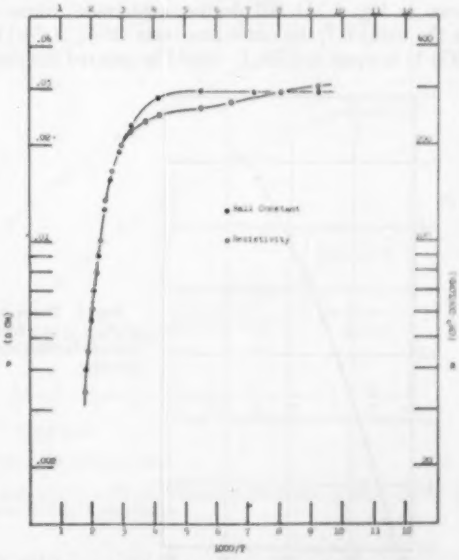

FIG. 1. The resistivity and Hall constant of InAs plotted as a function of the reciprocal absolute temperature.

† This work was supported by a grant from the Office of Ordnance Research, U. S. Army.

[1] Folberth, Madelung, and Weiss, Z. Naturforsch. **99**, 954 (1954).

[2] J. S. Blakemore, Elec. Commun. **29**, 131–133 (1952).

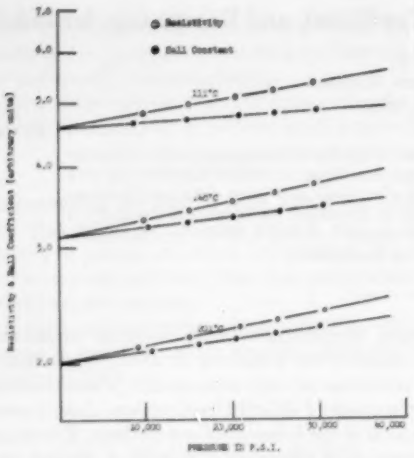

FIG. 2. Relative values of the pressure dependence of the resistivity and Hall constant plotted as a function of pressure in psi at three temperatures.

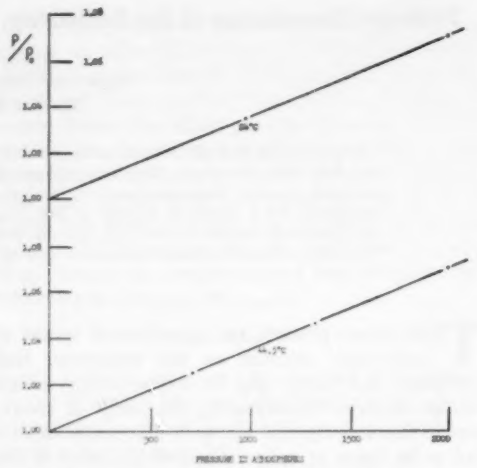

FIG. 4. The pressure dependence of the resistivity of n-type InAs for two temperatures in the extrinsic range.

It can be shown that Eq. (1) represents the relationship between the shift in energy gap and the change in $\ln\rho$ with pressure at constant temperature.[3]

$$\frac{dE_g}{dp}\Big)_T = -\frac{kT(x^2+C)(x^2+1)}{x^2(C+1)}\frac{d(\ln\rho)}{dp}, \qquad (1)$$

where $x^2=p/n$, $C=u_e/u_h=70$(InAs). The values of x^2 plotted as a function of absolute temperature calculated from Hall constant and resistivity measurements are shown in Fig. 3. At 201 degrees centigrade, where x has the value 0.7, the correction term $(x^2+C)(x^2+1)/x^2(C+1)$ is equal to 2.43. It should be pointed out that

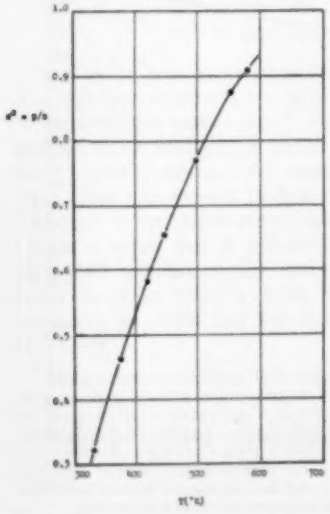

FIG. 3. The value of $x^2=p/n$ as a function of absolute temperature.

[3] J. H. Taylor, Phys. Rev. **80**, 919 (1950).

Eq. (1) represents the shift in energy gap with pressure in the absence of any change in mobility.

For semiconductors of high mobility ratio, the density of the more mobile carriers n is proportional to the reciprocal of the Hall constant, R.

$$n=1/Re. \qquad (2)$$

From Eq. (2) an expression similar to Eq. (1) for the shift in energy gap as a result of changes in Hall coefficient with pressure may be derived.

Values for the various constants investigated are shown in Table I. The results for 111°C are calculated from measurements taken in the extrinsic range thereby yielding results much lower than those taken at 148 and 201°C. From room temperature to 100°C the value of the Hall coefficient remained constant for pressure changes of 2000 atmospheres.

Figure 4 shows the results of the pressure dependence of resistivity for low temperatures. These measurements are taken at temperatures where the number of conduction electrons remain relatively constant. In this region, if a change in resistivity is effected by the application of pressure, it must be attributed to a change in the mobility of the carriers. The graph shows a 7 percent increase in resistivity for a pressure change of 2000 atmospheres. Therefore, the value of 5.5×10^{-6}

TABLE I. Values of the observed pressure coefficient of resistivity, Hall constant, and shift in energy gap for InAs at three temperatures. Columns four and five are calculated from changes in resistivity and Hall constant respectively.

°C	$\Delta\rho/\rho$	$\Delta R/R$	$dE_g/dp)_T$ (ev/atmos) (resistivity)	$dE_g/dp)_T$ (ev/atmos) (Hall coefficient)
111	6.13×10^{-6}	2.82×10^{-6}	1.87×10^{-6}	0.81×10^{-6}
148	10.0×10^{-6}	5.43×10^{-6}	8.28×10^{-6}	5.14×10^{-6}
201	10.1×10^{-6}	5.98×10^{-6}	8.83×10^{-6}	5.50×10^{-6}

ev/atmosphere calculated from changes in Hall constant is more representative of the true shift in energy gap since it is independent of changes in mobility. Since mobility equals the Hall constant divided by the resistivity, the mobility of InAs decreases with increasing hydrostatic pressure.

I am indebted to Dr. Robert Talley and Mr. Frank Stern of the U. S. Naval Ordnance Laboratory, Silver Spring, Maryland for providing me with samples and many helpful discussions. I should like to thank Donald Long of the University of Pennsylvania, Department of Physics for his informative assistance.

PHYSICAL REVIEW VOLUME 100, NUMBER 6 DECEMBER 15, 1955

Magnetic Properties of Erbium Metal*

J. F. ELLIOTT,† S. LEGVOLD, AND F. H. SPEDDING
Institute for Atomic Research, and Department of Physics, Iowa State College, Ames, Iowa

(Received August 3, 1953; revised manuscript received August 31, 1955)

Measurements of the magnetic moment of erbium metal in the temperature range from 20.4°K to 90°K are reported. The initial susceptibility shows a maximum at 78°K and the metal appears to become ferromagnetic near 20°K.

NEEL,[1] working with the magnetic data of Klemm and Bommer,[2] has predicted a Curie point for erbium at about 40°K. Barson's[3] work on the electrical resistivity of erbium has shown an anomaly at about 80°K. This type of anomaly in the electrical resistivity has been shown to be closely associated with magnetic phenomena in gadolinium[3-5] and dysprosium.[3,6,7] This paper describes the results of investigations of some of the magnetic properties of erbium metal.

The metal used in this study was prepared by methods

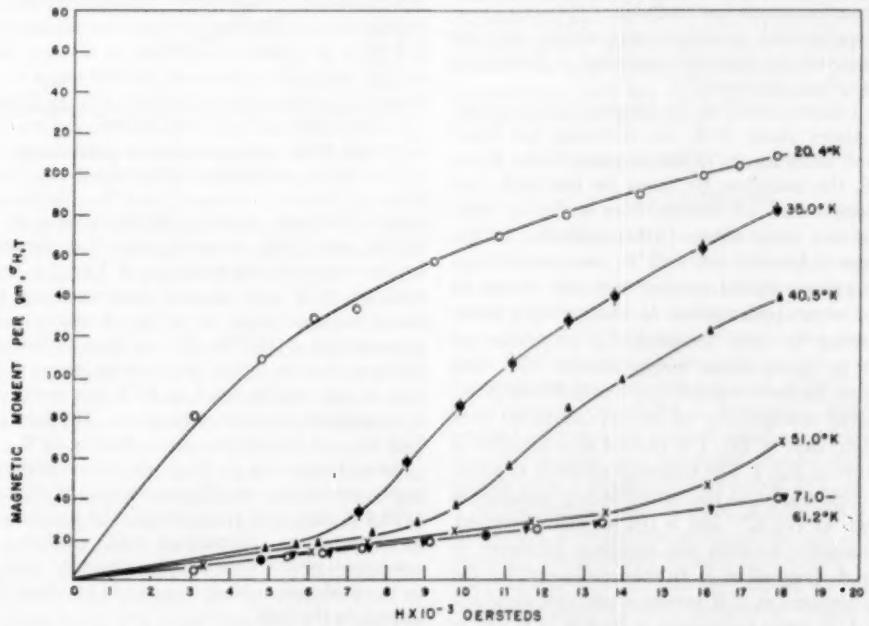

FIG. 1. Magnetization isotherms of erbium metal.

* Contribution No. 242 from the Institute for Atomic Research and Department of Physics, Iowa State College, Ames, Iowa. Work was performed in the Ames Laboratory of the U. S. Atomic Energy Commission.
† Now at General Electric, Syracuse, New York.
[1] L. Neel, Z. Electrochem. **45**, 378 (1939).
[2] W. Klemm and H. Bommer, Z. anorg. u. allgem. Chem. **231**, 138 (1937).
[3] Legvold, Spedding, Barson, and Elliott, Revs. Modern Phys. **25**, 129 (1953).
[4] Elliott, Legvold, and Spedding, Phys. Rev. **91**, 28 (1953).
[5] Urban, Weiss, and Trombe, Compt. rend. **200**, 2132 (1935).
[6] F. Trombe, Compt. rend. **221**, 19 (1945).
[7] Elliott, Legvold, and Spedding, Phys. Rev. **94**, 1143 (1954).

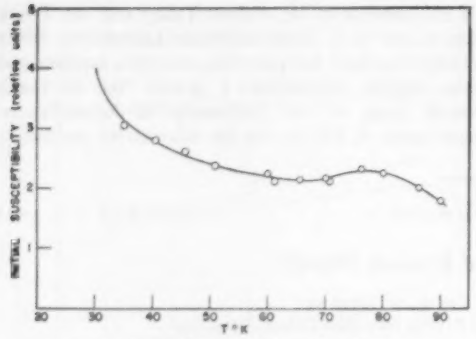

FIG. 2. The initial susceptibility of erbium as a function of temperature.

previously reported.[8,9] Spectrographic analysis showed the sample contained the following impurities: calcium, detectable but less than 100 ppm; yttrium, detectable but less than 100 ppm; iron, detectable but less than 2000 ppm; nickel, cobalt, and other rare earths not detected. These quantities of impurities are maximum upper limits as complete spectrographic standards for determining accurate quantitative amounts of impurities in erbium were not available.

The experimental procedure was similar to that used to measure the magnetic properties of gadolinium and is described elsewhere.[10,4]

Figure 1 shows several of the magnetic isotherms for erbium. Above about 75°K the isotherms are linear for applied fields up to 18 000 oersteds. From about 60°–75°K, the isotherms are linear for low fields, but show evidence that the susceptibility is slightly field-dependent for fields above 15 000 oersteds. As the temperature is lowered below 60°K, the susceptibility becomes strongly field-dependent and this occurs at lower and lower applied fields. At the hydrogen point, erbium seems to have ferromagnetic properties, as indicated by spontaneous magnetization. The data indicate that the ferromagnetic Curie point is near 20.4°.

The initial susceptibility of erbium calculated from the low-field data of Fig. 1 is plotted as a function of temperature in Fig. 2. The magnetic anomaly at about 75°K is quite similar to the corresponding anomaly in dysprosium at 176°K[6,7] but is not as well developed.

The similarity between the magnetic behaviors of erbium and dysprosium is further evidenced by the magnetic moment *vs* $1/H$ curves of the two elements. The σ *vs* $1/H$ curve for erbium at 20.4°K is shown in Fig. 3. It is to be noted that this curve seems to consist of two intersecting straight lines as do the corresponding curves of dysprosium.[7] The extrapolation of the two straight lines to $1/H=0$ yields saturation magnetizations of about 179±5 cgs units for the low-field extrapolation and 267±5 cgs units for the high-field extrapolation at 20.4°K. The spectrographic state for the erbium ion is a $^4I_{15/2}$ and one would expect an absolute saturation moment of 9 Bohr magnetons if all the spin and orbital angular momentum contributed to the ferromagnetism. For spin only the expected moment would correspond to 3 Bohr magnetons. The high-field extrapolation of the 20.4°K data of 269 cgs units corresponds to about 8.0 Bohr magnetons.

In the period since this paper was first submitted for publication, the heat capacity of erbium metal has been measured by Skochdopole *et al.*[11] and Koehler and Wollan[12] have reported neutron diffraction data on the

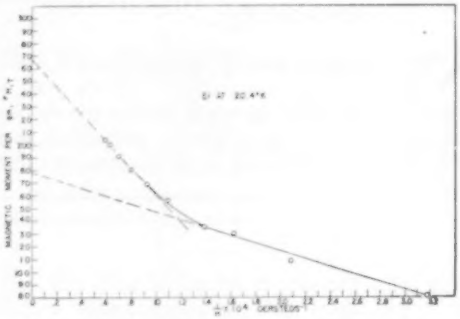

FIG. 3. The magnetic moment of erbium at 20.4°K plotted as a function of $1/H$.

metal. The heat capacity shows maxima at 19.9°K, 53.5°K, and 84°K. It would seem that the maximum in the weak-field susceptibility of Fig. 2 is associated with the 84°K heat capacity maximum and that the metal has what might be called a ferromagnetic Curie temperature at 19.9°K. The neutron diffraction data indicate that the metal is ferromagnetic at 4.2°K and that in the neighborhood of 80°K the metal could be ferromagnetic or antiferromagnetic. The data reported here rule out the ferromagnetic state at 80°K.

Several attempts to duplicate measurements of the type reported here on different samples of erbium metal at 20.4°K have been unsuccessful. The samples appeared to have large crystallites and exhibited strong anisotropy effects. One sample turned 90° with respect to the field and another was stable at about 30° with respect to the field.

The authors wish to express their thanks to J. Powell for preparing the rare earth salts and to A. H. Daane, R. Barton, and D. Dennison for preparing the metal samples.

[8] F. H. Spedding *et al.*, J. Am. Chem. Soc. **69**, 2777, 2786, 2812 (1947).
[9] F. H. Spedding and A. H. Daane, J. Am. Chem. Soc. **74**, 2783 (1952).
[10] W. S. Sucksmith, Proc. Roy. Soc. (London) **A170**, 551 (1939).
[11] Skochdopole, Griffel, and Spedding, J. Chem. Phys. (to be published).
[12] W. C. Koehler and R. O. Wollan, Phys. Rev. **97**, 1177 (1955).

Nuclear Magnetic Resonance Studies of Imperfect Ionic Crystals

F. Reif
Institute for the Study of Metals, University of Chicago, Chicago, Illinois
(Received September 2, 1955)

The method of nuclear magnetic resonance is applied to the study of ionic crystals containing point defects, i.e., vacancy, interstitial, or impurity ions. Experiments are described which show that the presence of such defects can have marked effects on the resonance line and can lead to a complicated temperature dependence of its width. A brief theoretical discussion is given of two effects important if the nucleus whose resonance is observed has a large electric quadrupole moment: (1) line width due to static second-order quadrupole interaction with defects, and (2) contribution to the nuclear relaxation time T_1 by quadrupole interaction with fluctuating electric fields caused by diffusing defects. Experimental results on the Br resonances in AgBr are analyzed in detail in terms of these effects. It is shown that the quadrupolar relaxation time due to diffusing defects in this salt can become sufficiently short to cause lifetime broadening of the resonance line, in particular that the motion of Ag vacancies seems to lead to a characteristic minimum of T_1 at about 0°C. The data also give some evidence for the association of defects in AgBr below 200°K. Cases of motional narrowing of the resonance line caused by the diffusion of defects are illustrated by experimental results on NaCl and LiBr. The existence of the various effects discussed in connection with these experiments indicates that nuclear resonance techniques can provide a means of studying the behavior of point defects in solids, their motion and in some cases their association, from a rather microscopic point of view. The desirability of careful relaxation time measurements is pointed out.

I. INTRODUCTION

THE method of nuclear magnetic resonance permits one to use the nucleus as a probe to explore the internal electromagnetic fields existing in solids and has thus proven itself useful in extending our knowledge of several aspects of solid-state physics. It seems of interest to apply nuclear resonance techniques also to the study of imperfect solids, in particular to the study of ionic crystals containing point imperfections, i.e., vacancy, interstitial, or impurity ions.[1] The defects in these relatively simple solids play an important role in the understanding of their properties. Accordingly such defects have been investigated extensively by more conventional methods, and some simple theoretical models are available to explain their behavior.[2]

The presence of point imperfections in a solid can affect the nuclear resonance in several ways, three of which will be of particular concern to us in the following pages. The first effect is specifically dependent on nuclei in the crystal lattice possessing electric quadrupole moments. Point imperfections in the lattice then destroy locally the cubic symmetry of the electrostatic field gradients at the positions of the nuclei and thus bring into play quadrupolar interactions which would not exist in a perfect crystal. Since the magnitude of the field gradient will vary from nucleus to nucleus one can expect a resultant broadening of the nuclear magnetic resonance line that depends on the configuration of defects in the solid. The other two effects we shall be interested in are connected with the diffusion of point defects through the lattice. First, the motion of defects may result in a rather short spin-lattice relaxation time for the nuclei, particularly if quadrupole interaction is involved. Second, the diffusion of defects may bring about a narrowing of the static width of the resonance line. In the present paper we give a simple theoretical discussion of some of these effects and present a number of experimental results which serve to illustrate them. Some of the more specifically theoretical points arising in connection with this work will form the subject of a subsequent paper by Cohen.[3]

II. EXPERIMENTAL ASPECTS

(a) Techniques

The radio-frequency spectrometer used in these experiments was of the Pound-Watkins type[4,5] and resonance lines were plotted on a recording meter by varying the frequency. A permanent magnet provided a magnetic field of about 5750 gauss in a gap 2 inches wide. The sample could be kept at any temperature between that of liquid nitrogen and +100°C by means of a cryostat containing a refrigerant reservoir and heater.[6] Alternatively a small water-cooled oven fitting into the magnet gap permitted one to maintain the sample at any temperature between 20°C and 500°C.

All the samples used in these experiments were polycrystalline. Introduction of impurities into the samples (doping) was achieved by melting a known amount of the pure salt to which had been added a known quantity of the impurity salt. Samples of smaller impurity ion concentration were then prepared by successive dilution with the pure salt of portions of the more highly

[1] For a preliminary report on this work see: M. H. Cohen and F. Reif, Proceedings of the Conference on Defects in Crystalline Solids, Bristol, 1954 (Physical Society, London, 1955), p. 44.
[2] N. F. Mott and R. W. Gurney, *Electronic Processes in Ionic Crystals* (Oxford University Press, New York, 1950).
[3] M. H. Cohen (to be published).
[4] R. V. Pound and W. D. Knight, Rev. Sci. Instr. **21**, 219 (1950).
[5] G. D. Watkins, thesis, Harvard University, 1952 (unpublished).
[6] The design of the cryostat was similar in conception to that described by Gutowsky, Meyer, and McClure, Rev. Sci. Instr. **24**, 644 (1953).

TABLE I. Nuclear properties of the Br isotopes: spin I, magnetic moment μ in units of the nuclear magneton, electric quardupole moment[a] Q in units of 10^{-24} cm².

Isotope	I	μ	Q	Abundance
Br^{79}	3/2	2.1058	0.335	50.6%
Br^{81}	3/2	2.2696	0.280	49.4%

[a] See reference 9.

doped specimens. Most samples were given the desired shape by compressing them in a hydraulic press into compact cylinders; they were then annealed at temperatures close to their melting point. Some care was taken to use as starting material salts of moderately high purity. For example, the reaction of $AgNO_3$ with HBr was the source of the AgBr used in the experiments; spectroscopic analysis showed this to contain a concentration less than 2.10^{-6} of metallic impurities.

(b) Experimental Results: AgBr

The substance most extensively studied in these experiments was AgBr. This salt is readily doped with $CdBr_2$, and the properties of the defects in its lattice have been thoroughly investigated by electrical conductivity measurements.[7,8] Furthermore the temperature range of interest is not excessively high for nuclear resonance experiments, even near the melting point of 434°C. The nuclear moments of the two bromine isotopes are shown in Table I.[9] Since the isotope with the larger magnetic moment has the smaller quadrupole moment, it should be experimentally possible to distinguish the effects of magnetic or electric interactions by comparison of the resonance lines of the two isotopes.

A few representative data on AgBr will serve to show that the presence of point imperfections in the lattice may have marked effects on the nuclear resonance line and may result in a rather complicated temperature dependence of this line. Doping of AgBr with $CdBr_2$ results in divalent Cd^{++} ions entering the lattice substitutionally.[7] To preserve the electrical neutrality of the crystal, an equal number of vacancies are formed on the Ag sublattice. Figure 1 shows the effect on the Br resonance line at room temperature of increasing the Cd^{++} ion concentration in AgBr. There is a rapid increase in width and consequent reduction in intensity of the line, the effect being more pronounced for the isotope with the larger quadrupole moment. The second moment of the resonance line[10] is in these experiments a poor and inaccurate measure of the line width since the line has extensive wings, partially submerged in noise, which contribute heavily to the value of the second moment. The most sensitive indication of the effects observed is D, the peak-to-peak intensity of the derivative of the resonance line. It is this derivative which is experimentally plotted directly on the recording meter, and use of the calibrating circuit[5] in the rf spectrometer makes reproducible measurements of D readily possible. D is a rough measure of the reciprocal of the square of the line width; if T denotes the absolute

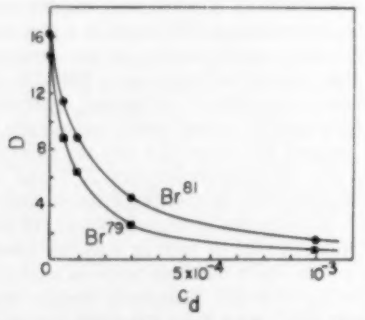

FIG. 1. Dependence of Br resonance line intensity D on the molar concentration c_d of Cd^{++} ions in AgBr at room temperature. (Note: for the same line shape, the small differences in magnetic moment and abundance should hake the Br^{79} line about 20% less intense than the Br^{81} line.)

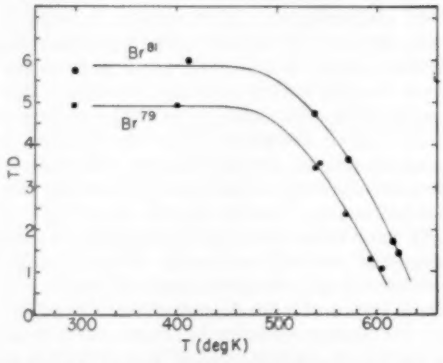

FIG. 2. Behavior of the Br resonance line intensity D in a pure sample of AgBr at high temperatures.

temperature, the quantity TD should be a constant independent of T if there is no change in line shape.

A second way of introducing point defects in a crystal is by raising its temperature sufficiently to create such defects in thermal equilibrium with the crystal lattice. In AgBr the imperfections thus produced are Frenkel defects,[7] i.e., Ag^+ vacancies and Ag^+ interstitial ions. The effect on the nuclear resonance line of heating a sample of pure AgBr is shown in Fig. 2. It is seen that beyond about 500°K there is a rapid decrease in intensity of the line suggestive of an exponential increase of the number of defects in the salt. Doped samples exhibit similar behavior at high temperatures. Finally, Fig. 3 shows the complicated temperature dependence of the intensity of the resonance line in some repre-

[7] J. Teltow, Ann. Physik 5, 63–88 (1950).
[8] S. W. Kurnick, J. Chem. Phys. 20, 218 (1952).
[9] The quadrupole moments are those given by J. G. King and V. Jaccarino, Phys. Rev. 94, 1610 (1954).
[10] J. H. Van Vleck, Phys. Rev. 74, 1168 (1948).

sentative samples of AgBr containing Cd^{++} impurity ions. Below 200°K the product TD remains constant for each sample and there is only a slight dependence of the intensity on the impurity concentration, amounting to less than 20% in going from the pure sample to one containing 10^{-3} atomic fraction of $CdBr_2$. There is a rapid decrease in intensity beginning at the same temperature of about 200°K for the resonance lines of both isotopes in all the doped samples. The intensity then reaches a minimum (and correspondingly the line width a maximum) the magnitude of which depends on the Cd^{++} ion concentration, but the position of which occurs at the well-defined temperature of 273

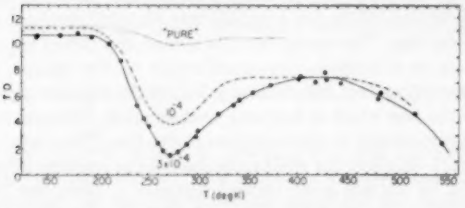

FIG. 3. Behavior of the Br^{81} resonance line intensity D as a function of temperature in samples of AgBr doped with $CdBr_2$. Dotted line: "pure" sample (less than 2×10^{-5} concentration of metallic impurities). Dashed line: molar concentration of $Cd^{++}=10^{-4}$. Solid line with experimental points: Cd^{++} concentration $=3\times10^{-4}$.

±2°K irrespective of Br isotopes or impurity concentration. We shall postpone until later the discussion of these results.

III. STATIC QUADRUPOLE INTERACTION

The interaction of a nucleus of spin I and electric quadrupole moment Q with an electrostatic potential V due to charges external to it is given by the Hamiltonian[11]:

$$\mathcal{H}=[eQ/4I(2I-1)]\{(3I_z^2-\mathbf{I}^2)V_0+(I_+I_z+I_zI_+)V_{-1}+(I_-I_z+I_zI_-)V_1+I_+^2V_{-2}+I_-^2V_2\}, \quad (1)$$

where $I_\pm=I_x\pm iI_y$, $V_0=V_{zz}$, $V_{\pm1}=V_{xz}\pm iV_{yz}$, $V_{\pm2}=\frac{1}{2}(V_{xx}-V_{yy})\pm iV_{xy}$, and where $V_{xy}=\partial^2V/\partial x\partial y$, etc. The z-axis can be taken along the direction of the external magnetic field H. We consider the specific case of interest, $I=\frac{3}{2}$. If V at the position of a nucleus has cubic symmetry (perfect ionic crystal), then the quadrupole interaction vanishes; the resonance line consists of three superposed lines at the nuclear Larmor frequency ω_0 and of a width determined solely by magnetic dipole-dipole interactions between all the nuclei. (See Fig. 4.) If V does not have cubic symmetry at the position of a nucleus, then to first-order perturbation theory the central line ($\frac{1}{2}\leftrightarrow-\frac{1}{2}$ transition) is not affected, while the $\frac{1}{2}\leftrightarrow\frac{3}{2}$ and $-\frac{1}{2}\leftrightarrow-\frac{3}{2}$ transitions give rise to two satellite lines at frequencies $\omega_0\pm\frac{1}{2}eQV_0\hbar^{-1}$, each of which has an intensity $\frac{3}{4}$ that of the central line.

[11] R. V. Pound, Phys. Rev. **79**, 685 (1950).

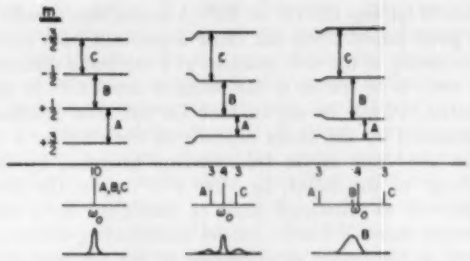

FIG. 4. Static electric quadrupole effects for a nucleus of spin 3/2. Top: energy levels. Middle: spectrum for a single nucleus. Bottom: resulting resonance in a crystal containing defects. Left: vanishing quadrupole interaction. Center: first-order effects of quadrupole interaction. Right: second-order effects of quadrupole interaction. ω_0 = Larmor frequency.

In an imperfect crystal where field gradients vary from nucleus to nucleus this will lead to a resonance line which consists of a central component at frequency ω_0 and of width determined by magnetic interactions only, and of two smeared out satellite lines. The latter will in general tend to broaden the observed resonance line. If, however, the quadrupolar interaction is sufficiently large, the satellite lines become smeared out to the extent that they become unobservable and one then sees only the remnant central line. This last situation is one which seems to prevail in the case of nuclei with large quadrupole moments even in pure well-annealed crystals because of the inevitable presence of a sufficient number of dislocations in the lattice.[12] Finally, if the quadrupole interaction effects are large enough, one has to go to second-order perturbation theory. One then finds that the central line too becomes affected by quadrupole interaction so that in an imperfect crystal, where the field gradients vary, one can expect a broadening of the central line.

A divalent impurity like Cd^{++} or an interstitial Ag^+ ion may be looked upon as an extra positive charge, an Ag^+ vacancy as an extra negative charge in the lattice. The field gradient due to such a defect may then be computed from its electrostatic potential $V=\pm e/r$, provided one multiplies the result by a correction factor $\beta=\beta_s\beta_0$. Here β_s is a factor taking into account the electric polarization of the ions in the solid; for defects sufficiently far away, a Lorentz type internal field argument based on a continuum model of the crystal of dielectric constant ϵ gives $\beta_s=(\epsilon+2)/3\epsilon$. Of much greater importance is the factor β_0 due to the distortion of the ion core surrounding the nucleus, since even a slight departure from spherical symmetry of the core can produce a large field gradient at this nucleus. In particular β_0 includes an "antishielding" factor β_∞ due to such a distortion of the core by the field gradient of the external charge; theoretical estimates[13] show that

[12] G. D. Watkins and R. V. Pound, Phys. Rev. **89**, 658 (1953); R. V. Pound, J. Phys. Chem. **57**, 743 (1953).

[13] Foley, Sternheimer, and Tycko, Phys. Rev. **93**, 734 (1954).

$\beta_\infty \approx 50$ for ions like Cl^- or Rb^+. A second way in which a point imperfection can cause departures from cubic symmetry in the field gradient at a nucleus a distance r away is by virtue of the strain it introduces in the lattice. It can be shown that the net field gradient produced by the strain depends on the distance r in the same way as the field gradient produced by the charge of the defect, i.e., like r^{-3}.[14] Again the field gradient so calculated must be multiplied by a correction factor β which includes antishielding effects as well as the result of distortion of the ion core surrounding the nucleus by direct interaction with neighboring ion cores through polarization and covalent effects.[15,16]

For the discussion of the experimental results it is of interest to consider in slightly greater detail the second-order quadrupolar broadening of the central line. The frequency deviation ω' of the $\frac{1}{2}\leftrightarrow-\frac{1}{2}$ transition from the Larmor frequency ω_0 is given by:

$$\omega' = -(2I+3)[8I^2(2I-1)]^{-1} \times (eQ/\hbar)^2\omega_0^{-1}[|V_1|^2-\tfrac{1}{2}|V_2|^2]. \quad (2)$$

Considering V_1 and V_2 as due to the electrostatic charges $\pm e$ of the defects labeled by n, one gets:

$$V_1 = 3\beta\sum_n e_n r_n^{-3}\cos\theta_n \sin\theta_n e^{i\varphi_n},$$
$$V_2 = \tfrac{3}{2}\beta\sum_n e_n r_n^{-3}\sin^2\theta_n e^{2i\varphi_n}, \quad (3)$$

where $\mathbf{r}_n$ denotes the position of the defect with respect to the nucleus under consideration, θ_n and φ_n being the polar and azimuthal angles of $\mathbf{r}_n$ with respect to the z-axis. Equation (2) then yields:

$$\omega' = -B\sum_{m,n}\rho_m^{-3}\rho_n^{-3}\Psi_{mn}, \quad (4)$$

where

$$\Psi_{mn} = \{2\sin2\theta_m\sin2\theta_n\cos(\varphi_m-\varphi_n) - \sin^2\theta_m\sin^2\theta_n\cos2(\varphi_m-\varphi_n)\},$$

and where $\rho_n = r_n/R$, R being the nearest neighbor distance in the crystal lattice. B is a characteristic frequency given by

$$B = \frac{9}{64}\frac{2I+3}{I^2(2I-1)}\left(\beta\frac{e^2Q}{\hbar R^3}\right)^2\omega_0^{-1}. \quad (5)$$

Equation (4) includes explicitly only charge effects; to the extent that strains caused by defects are important, their effect may be imagined as effectively increasing the value of β in (5).

The line shape will depend on the statistical properties of the sum in (4), but its calculation is rather difficult.[3,17]

On the other hand assuming a completely random distrubution of N defects in the solid, a calculation of the moments of the resonance line[10] from Eq. (4) involves only simple algebra. In particular the second moment $\langle(\Delta\omega)^2\rangle_Q = \langle\omega'^2\rangle - \langle\omega'\rangle^2$ is found by suitable averaging over the angular factors in (4) to be:

$$\langle(\Delta\omega)^2\rangle_Q = \frac{64}{45}B^2\left\{(\sum_n \rho_n^{-6})^2 + \frac{6}{7}\sum_n \rho_n^{-12} - \frac{6}{5N}(\sum \rho_n^{-6})^2\right\}. \quad (6)$$

Unfortunately, as we already pointed out, the moments of the line fail to give a satisfactory physical description of the line. The reason for this is that, if a defect is too close to a nucleus, the contribution to the resonance absorption from this nucleus will lie in the extreme wings of the line where it becomes unobservable, yet contributes markedly to the moments of the line. Thus defects which do affect the observable part of the resonance line will lie outside some critical distance ρ_c from the Br nuclei under consideration such that the approximate frequency shift $\Omega = B\rho_c^{-6}$ due to an impurity a distance ρ_c away is not too large. On a simple continuum model, denoting by vR^3 the volume occupied per defect, the sums in (6) can be replaced by integrals to give the second moment due to defects at distances $\rho > \rho_c$ as

$$\langle(\Delta\omega)^2\rangle_Q = 1.70B^2xv^{-1}\rho_c^{-9}[1+14.7xv^{-1}\rho_c^3],$$
$$\rho_c^{-3} = (\Omega/B)^{\frac{1}{2}}, \quad (7)$$

where x is the atomic fraction of defects in the solid. It must be emphasized that, in the absence of a knowledge of the line shape, (7) can only give a very crude estimate of the line width and its concentration dependence.

IV. QUADRUPOLAR RELAXATION EFFECTS

In a salt like AgBr the motion of point imperfections in the lattice creates fluctuating electric fields at the position of a Br nucleus and thus may constitute an important relaxation mechanism for this nucleus through interaction with its electric quadrupole moment. We should like to obtain a simple expression for the relaxation time T_1 due to this process for a nucleus of spin $I=\frac{3}{2}$ for the particular case that only the central line is observed.

This situation is slightly unusual since one only observes the absorption of rf power in the $\frac{1}{2}\leftrightarrow-\frac{1}{2}$ transition, while the quadrupolar Hamiltonian $\mathcal{H}_Q$ responsible for the relaxation induces transitions between all energy levels and, to first order, $\langle\frac{1}{2}|\mathcal{H}_Q|-\frac{1}{2}\rangle = 0$. To examine the precise meaning of T_1 under these conditions, we first establish the behavior of the absorption line when saturation effects are included. Let w denote the transition probability per unit time for $\frac{1}{2}\leftrightarrow-\frac{1}{2}$ transitions induced by the applied rf field. Since

[14] See, for example, reference 3. It is there also shown that the magnitude of the strain effect is about 10% that of the charge effect if one assumes the same ion core distortion in both cases.

[15] N. Bloembergen, Proceedings of the Conference on Defects in Crystalline Solids, Bristol, 1954 (Physical Society, London, 1955), p. 1.

[16] J. van Kranendonk, Physica 20, 781 (1954).

[17] A diagram showing the shape to be expected for the simplest case of a single defect at a fixed distance r from the nucleus can be found in reference 15.

the spectral densities of the fluctuating fields are slowly varying functions of frequency, we shall as a first approximation in computing transition probabilities due to $3\mathcal{C}_Q$ consider the four energy levels of a Br nucleus as essentially equally spaced by amounts $\hbar\omega_0$. Then, by (1), the matrix elements of $3\mathcal{C}_Q$ are such that we can write for the upward transition probabilities per unit time due to $3\mathcal{C}_Q$: $W_{\frac{1}{2},-\frac{1}{2}}=0$, $W_{\frac{1}{2},\frac{1}{2}}=W_{-\frac{1}{2},-\frac{1}{2}}\equiv W_1$, $W_{\frac{1}{2},-\frac{1}{2}}=W_{\frac{1}{2},-\frac{1}{2}}\equiv W_2$, where the quantities W_1 and W_2 thus defined represent transition probabilities between levels separated by amounts $\hbar\omega_0$ and $2\hbar\omega_0$ respectively. One can then write the downward transition probabilities in the form: $W_{-\frac{1}{2},\frac{1}{2}}=0$, $W_{\frac{1}{2},\frac{1}{2}}=W_{-\frac{1}{2},-\frac{1}{2}}=W_1(1+\Delta)$, $W_{-\frac{1}{2},\frac{1}{2}}=W_{-\frac{1}{2},\frac{1}{2}}=W_2(1+2\Delta)$, where $\Delta=\hbar\omega_0/kT\ll 1$. The four equations determining the number of nuclei in each of the four energy levels, denoted by index m (or n), are then:

$$\dot{N}_m=\sum_{n\neq m}\{-N_m(W_{mn}+w_{mn})+N_n(W_{nm}+w_{nm})\}, \quad (8)$$

where $w_{mn}=0$, except $w_{\frac{1}{2},-\frac{1}{2}}=w_{-\frac{1}{2},\frac{1}{2}}=w$. For a steady state the left sides of these equations are put equal to zero and the resulting algebraic equations are readily solved. One thus obtains for the power absorbed from the rf field $H_x=H'\cos\omega t$:

$$\mathcal{P}=\hbar\omega w(N_{\frac{1}{2}}-N_{-\frac{1}{2}})=\tfrac{1}{2}N\Delta\hbar\omega w \times[1+\tfrac{1}{2}w(W_1+W_2)/W_1W_2]^{-1}. \quad (9)$$

Here $w=\frac{1}{2}\pi\gamma^2H'^2g(\omega)$, where $g(\omega)$ is the normalized line shape function. Hence the saturation term in (9) assumes the customary form[18] $(1+\frac{1}{4}\gamma^2H'^2T_1T_2)$ if one makes the usual definition $T_2=\pi g(\omega)_{\max}$ and the identification:

$$T_1=(W_1+W_2)/W_1W_2. \quad (10)$$

This somewhat unusual form of composition of W_1 and W_2 to yield T_1 implies that it is the smaller of the two quantities W_1 and W_2 which mainly determines T_1. This is physically plausible since, in order to restore the thermal equilibrium between the levels $\frac{1}{2}$ and $-\frac{1}{2}$, $3\mathcal{C}_Q$ must give rise to transitions involving both W_1 and W_2 in succession.

It remains to determine W_1 and W_2 due to the motion of point imperfections. V_1 and V_2 in the expression (1) for $3\mathcal{C}_Q$ are now random functions of time and we can evaluate the pertinent matrix elements for spin $I=\frac{3}{2}$ to write the general result[19]:

$$W_1=W_{\frac{1}{2},\frac{1}{2}}=(\pi/6\hbar^2)e^2Q^2J_1(\omega_0),$$
$$W_2=W_{\frac{1}{2},-\frac{1}{2}}=(\pi/6\hbar^2)e^2Q^2J_2(2\omega_0), \quad (11)$$

where J_1 and J_2 are the spectral densities of the functions V_1 and V_2 respectively. In particular, if we consider V_1 and V_2 as due to the electrostatic effects of charged point defects, then Eqs. (3) apply where now r_n, θ_n, φ_n are random functions of time. The form of Eqs. (3) makes it clear, however, that mathematically the calculation of the correlation functions and spectral densities of V_1 and V_2 is very similar to the corresponding computations occurring in the theory of nuclear relaxation via magnetic dipole-dipole interaction between diffusing nuclei.[20] Torrey's results can therefore be carried over to the present problem with practically no modification. Specifically we wish to consider the situation in which the Br nuclei are fixed in position while singly charged point defects (vacancies or interstitials) diffuse independently through the lattice with a mean jump frequency ν per second. We further assume a quasi-continuum model in which the defect moves a distance b in arbitrary direction in each jump, its distance of closest approach to a Br nucleus being denoted by a. If c is the atomic concentration of defects in the solid, $4c/(2R)^3$ will give the number of defects per cm^3 in the AgBr lattice. W_1 and W_2 can then be written in the form:

$$W_1=(32\pi/15)(R/a)^3Bc(\omega_0/\nu)G(k,\omega_0/\nu),$$
$$W_2=(32\pi/15)(R/a)^3Bc(\omega_0/\nu)G(k,2\omega_0/\nu), \quad (12)$$

where B is the characteristic frequency already defined in (5) and where G is an integral involving a spherical Bessel function and defined by Torrey as:

$$G(k,y)=\frac{2k}{\pi}\int_0^\infty\frac{1-x^{-1}\sin x}{(1-x^{-1}\sin x)^2+y^2}j_1^2(kx)dx,\ k\equiv a/b. \quad (13)$$

An approximate evaluation of G can be obtained by considering $x^{-1}\sin x\ll 1$ everywhere in the integrand and expanding the latter accordingly. After integration one then obtains for $k>\frac{1}{2}$:

$$G(k,y)=\tfrac{1}{4}(1+y^2)^{-1}[1+k'(1-y^2)(1+y^2)^{-1}],$$
$$k'=\tfrac{3}{16}k^{-3}-\tfrac{3}{4}k^{-1}+1. \quad (14)$$

This approximation is very good for $y>1$, it determines quite well the value of y for which $yG(y)$ is a maximum, and it gives results about 35% too low for $y\ll 1$. By (10) one then gets an approximate expression for the relaxation time T_1 due to a particular kind of defect:

$$1/T_1=(16\pi/45)(1+k')(a/R)^{-3}Bc\nu\omega_0^{-1} \times[(\nu\omega_0^{-1})^2+(5/2)(1+k')^2]^{-1}. \quad (15)$$

For vacancies $a=R$, $b=\sqrt{2}R$, so that $1+k'=1.116$. The temperature dependence of ν is given by $\nu=\nu^0\exp(-U/kT)$, while at the lower temperatures c is a constant determined by the concentration of divalent impurity atoms added to the lattice. Hence, with increasing temperature T_1^{-1} will increase to a characteristic maximum reached when $\nu\approx(5/2)^{\frac{1}{2}}(1+k')\omega_0$, after which T_1^{-1} will decrease again. At sufficiently high temperatures, however, c will increase exponentially because of the generation of intrinsic defects in themal equilibrium, and as a result T_1^{-1} will tend to increase again. The

[18] Bloembergen, Purcell, and Pound, Phys. Rev. **73**, 679 (1948).
[19] A. Abragam and R. V. Pound, Phys. Rev. **92**, 954 (1953).
[20] H. C. Torrey, Phys. Rev. **92**, 962 (1953).

general behavior is shown in Fig. 6. Note also that the magnitude of T_1^{-1} at its maximum is determined by the parameter Bc. Hence, when quadrupolar interactions are large enough so that a static configuration of defects gives rise to second-order quadrupolar broadening of the resonance line, one can expect that these defects in motion will also give rise to appreciable relaxation effects.

V. DISCUSSION OF AgBr RESULTS

The experimental data on AgBr seem to indicate that, in agreement with the findings of Pound and Watkins,[12] the number of imperfections, such as dislocations, in any crystal is large enough so that, even in our purest sample of AgBr, we observe essentially only the $\frac{1}{2}\leftrightarrow-\frac{1}{2}$ transition of the Br resonance line. There are two kinds of evidence in support of this conclusion. First, an absolute intensity measurement shows that the integrated intensity of the line, neglecting contributions far out in the wings, is closer to 40% than to 100% of the combined intensity to be expected from all three transitions.[1] Second, the width of the line in the pure sample is *smaller* than one would compute even from magnetic interactions only by naively using Van Vleck's formula.[10] Specifically the line shape, except far out in the wings, is approximately Gaussian with a width $\Delta\nu'$, measured between points of maximum slope, $\Delta\nu_{79}'=0.925$ kc/sec and $\Delta\nu_{81}'=1.030$ kc/sec for the two isotopes respectively.[21] Now, the width of the central line caused by magnetic interactions should indeed be somewhat smaller than the width for all three transitions superimposed, the case to which Van Vleck's formula[10] is applicable. The physical reason for this is that, as the quadrupolar interaction causes the energy levels of a Br nucleus to be unequally spaced, some of the flip-flop processes between pairs of Br nuclei are no longer possible with conservation of energy, and thus such processes no longer contribute to the magnetic line width. If the field gradient varies from nucleus to nucleus in the crystal, then the second moment of the central line due to magnetic interactions can be computed to yield a result identical with Van Vleck's formula,[10] except that the factor $\frac{3}{4}I(I+1)$ in the term for "like" nuclei must be replaced by: $[\frac{1}{3}I(I+1)+\frac{1}{3.2}(2I+1)+\frac{1}{4}]$.[22] The resulting formula yields the calculated line widths $\Delta\nu_{79}'=0.945$ kc and $\Delta\nu_{81}'=1.025$ kc/sec,[23] values about 0.84 as large as those given by Van Vleck's unmodified expression. These values are in good agreement with the experimental ones, and indicate incidentally that the central line in the pure sample is not appreciably broadened by second-order quadrupole interactions.

[21] These measurements were checked at 150°K to eliminate any possible misleading effects due to residual impurities in the pure sample.

[22] We wish to thank Professor N. Bloembergen for communicating this result to us.

[23] Since the magnetic moments of the Ag isotopes are very small, they contribute only slightly to the calculated widths.

In order to discuss the specifically quadrupolar effects caused by the point defects, we need to estimate the characteristic (angular) frequency B. In our magnetic field the Br^{81} resonance frequency lies at 6630 kc, so that $\omega_0=4.16\times10^7$ radians/sec. Taking the lattice constant R as 2.88×10^{-8} cm Eq. (5) gives for Br^{81}:

$$B=2.95\times10^4\beta^2 \text{ rad/sec.} \tag{16}$$

As for the correction factor β, the discussion in Sec. III shows that only exceedingly crude estimates are possible. β includes an antishielding factor which is expected to be larger for the negative Br^- ion than that calculated for Rb^+,[13] i.e., larger than 50. The dielectric constant correction, only meaningful for defects sufficiently far from the nuclei they effect, amounts to about 0.4. Strain and covalent effects will tend to increase β, but as a conservative order of magnitude estimate let us assume $\beta\approx20$. Then $B=1.2\times10^7$ sec^{-1}. It is therefore clear that quadrupolar effects can be very important both for line-broadening and relaxation effects.

In interpreting the experimental results it is essential to keep in mind the fact that point imperfections in the lattice can be highly mobile. Careful conductivity measurements[7,8] on single crystals of AgBr allow (subject to certain assumptions about the association of the defects[7]) the determination of the mobilities μ_v and μ_i of Ag vacancy and interstitial ions respectively, in addition to the determination of c_{i0}, the atomic concentration of thermally produced Frenkel defects existing in the pure crystal. Using the Einstein relation $D=(kT/e)\mu$, one can compute the diffusion coefficients of the defects and thence the jump frequencies $\nu_v=3R^{-2}D_v$ for vacancies and $\nu_i=6R^{-2}D$ for interstitial ions. The results, using Kurnick's data,[8] are shown in

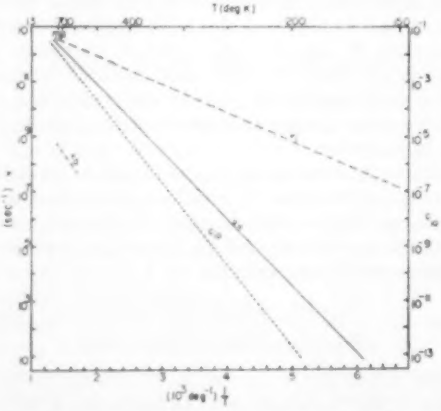

FIG. 5. Jump frequencies and concentration of interstitial defects calculated from Kurnick's[8] data. Solid line: jump frequency of Ag vacancies, $\nu_v=5.9\times10^{13}\exp(-5620/T)$. Dashed line: jump frequency of Ag interstitial ions, $\nu_i=9.4\times10^{13}\exp(-2360/T)$. Dotted line: fractional concentration of Ag interstitial ions in a pure sample of AgBr, $c_{i0}=1.9\times10^{-4}\exp(-6900/T)$. Dash-dotted line: Cd^{++} jump frequency ν_d estimated from data in reference 24.

Fig. 5. It should be pointed out that, since the conductivity measurements were all made at temperatures above 200°C, the jump frequencies computed for low temperatures represent somewhat of an extrapolation. Conductivity measurements also indicate that the Br^- ions remain relatively immobile up to very high temperatures[8] and that Cd^{++} impurity ions diffuse only very slowly.[24]

One can expect that, when the motion of a defect is sufficiently rapid, its contribution to the static quadrupolar line width of a nucleus will average to zero. The problem of the "line narrowing" of the second-order quadrupolar interaction is a rather complex one.[25] But, crudely speaking, one would expect the customary criterion,[18] i.e., that the contribution to the static quadrupolar line width due to a defect disappears when the jump frequency of the defect is large compared to the magnitude of the quadrupolar width produced by this defect. Hence purely static quadrupolar effects of the kind discussed in Sec. III should only come into play at sufficiently low temperatures where the point defects are not too mobile, i.e., below about 200°K for Ag vacancies and below about 350°K for Cd^{++} ions.

On the other hand, the rapid motion of defects should have marked effects on the relaxation time T_1 of the Br nuclei. At temperatures below about 450°K Fig. 5 shows that the mobile defects in the lattice[26] are predominantly the Ag^+ vacancies whose concentration is equal to c_d, the concentration of divalent Cd^{++} ions in the lattice. By Eq. (15), $1/T_1$ will be a maximum when the vacancy jump frequency ν_v reaches a critical value ν_v^* given by $\nu_v^* = 1.83\omega_0 = 7.6\times10^7$ sec^{-1} for Br^{81} in our magnetic field. Also, since B is so large, it is possible that $(1/T_1)_{max}$ becomes comparable to or larger than 6×10^3 sec^{-1}, the magnetic line width in angular frequency units. In that event, the short relaxation time should lead to a lifetime broadening of the nuclear resonance line in the solid. We believe that the maximum in width (or minimum in intensity) observed at about 273°K (see Fig. 3) is due to this effect. Note that Eq. (15) predicts that the temperature at which the maximum of $1/T_1$ occurs depends only on the magnitude of the jump frequency ν_v and is thus independent of c_d, while the magnitude of $(1/T_1)_{max}$ is a function of c_d. The experimental results discussed in Sec. II and shown in Fig. 3 appear in agreement with this conclusion. The conductivity data allow one to estimate the temperature T^* for which ν_v reaches its

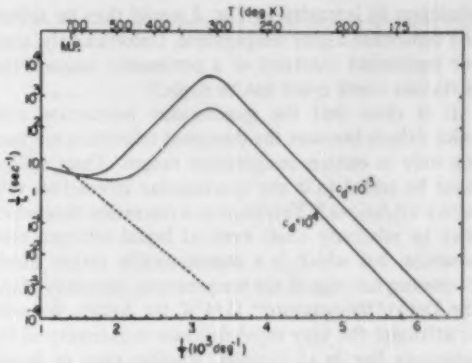

FIG. 6. Behavior of the Br^{81} relaxation time T_1 as a function of temperature calculated from Eq. (15), using the conservative estimate $\beta = 20$ and the results of Fig. 5 as obtained from Kurnick's data for AgBr. Solid line: $1/T_1$ due to quadrupolar interaction with vacancies in AgBr samples containing Cd^{++} ion concentrations of 10^{-3} and 10^{-4} respectively. Dotted line: $1/T_1$ due to interstitial ions in a pure sample.

critical value ν_v^*. Kurnick's data[7] give $T^* = 308$°K, Teltow's[8] give $T^* = 287$°K; these are in fair agreement with the observed minimum in intensity at 273°K. Figure 6 shows a plot of $1/T_1$ due to vacancies obtained if Kurnick's data are used in Eq. (15) with our conservative estimate $\beta \approx 20$. It is seen that $1/T_1$ at its maximum is indeed of the right order of magnitude to cause lifetime broadening of the resonance line. E.g., in Fig. 3, the quantity TD at the temperature T^* of its minimum is, in the sample with $c_d = 10^{-4}$, about 3.4 times less than at low temperatures; i.e., the width of the line at temperature T^* is, crudely speaking, about $\sqrt{3.4}$ times the magnetic width of 6.5×10^3 radians/sec. The extra width, when attributed to relaxation time broadening, should be of order $2/T_1$; hence one arrives at the order of magnitude estimate $1/T_1 \approx 2.3\times10^3$ sec^{-1}. Comparison with Fig. 6 shows then that a value of β about 2.5 times larger than was assumed, i.e., $\beta \approx 50$, would lead to better agreement with the observed broadening. Finally, an attempt was made to check the relaxation time more directly by investigating the saturation behavior of the resonance line as the rf magnetic field is increased. It was found that, while a pure sample of AgBr at room temperature (which is fairly close to T^*, the temperature of the maximum in $1/T_1$) or a doped sample ($c_d = 10^{-4}$) at 185°K could be made to show some saturation effects, this doped sample at room temperature showed no trace of saturation of its resonance line at the highest rf power level available in our equipment. From this one can make the rough estimate that T_1 in this sample at room temperature is shorter than 5 millisec, a result which is consistent with the possibility of lifetime broadening effects. There is one more experiment which suggests itself as a check of the interpretation of the data, namely to increase the Larmor frequency ω_0 by, say, doubling the value of the external magnetic field. Equation (15) would predict that the

[24] Schöne, Stasiw, and Teltow, Z. physik. Chem. **197**, 145 (1951).

[25] For further discussion see reference 3. For example, the first moment $\langle\Delta\omega'\rangle$ of a line does not average to zero in second order.

[26] It should be remembered that the jump frequencies shown in Fig. 5 are based on the assumption of negligible association of the defects. Note also that the concentration of interstitial ions is negligible (i.e., less than $2\cdot10^{-5}$, the concentration of defects in a "pure" sample) below 450°K, especially since, by virtue of the law of mass action, the presence of the deliberately introduced vacancies in a doped sample tends to decrease the number of Frenkel defects at a given temperature compared to that existing in a pure sample.

minimum in intensity in Fig. 3 would then be shifted to a somewhat higher temperature. Unfortunately, since our equipment consisted of a permanent magnet, this particular check could not be made.[27]

It is clear that the quadrupolar interaction with point defects becomes the dominant relaxation mechanism only in certain temperature ranges. There always must be added to it the quadrupolar interaction with lattice vibrations.[16] This leads to a relaxation time which may be relatively short even at liquid nitrogen temperature, but which is a monotonically rather slowly decreasing function of the temperature, especially above the Debye temperature[16] (144°K for AgBr). We wish to attribute the very rapid decrease in intensity of the resonance line in all samples, whether pure or doped, at high temperatures to lifetime broadening of the line by virtue of interaction of the Br nuclei with the moving point defects created in thermal equilibrium with the lattice. Incidentally an experimental check showed that the resonance line is not observable in liquid AgBr, presumably because of too short a relaxation time[28]; i.e., at high temperatures the line becomes too weak to observe in the solid and does not reappear at the melting point. Equation (15), with $a=(\sqrt{3}/2)R$, should allow one to estimate T_1 due to Ag^+ interstitial ions. It must be pointed out, however, that the effective correction factor β for interstitials may well be different from that for vacancies. The reason for this is that point defects closest to a nucleus make the largest contribution to the transition probability of the nucleus and hence to $1/T_1$,[29] and that an interstitial ion next to a Br^- ion can be expected to give rise to large strains and to distortion of the Br^- ion core by covalent effects tending to make the net field gradient at the Br nucleus exceptionally large, i.e., effectively enhancing the value of β contained in Eq. (15). Returning to Eq. (15) we note further that the contribution of defects to the relaxation time T_1 and to the electrical conductivity σ is quite different. Putting $c_i=c_i^0\exp(-W/kT)$ and $\nu_i=\nu_i^0\exp(-U/kT)$, we have in the temperature range where $\nu_i\gg\omega_0$:

$$1/T_1\sim c_i/\nu_i\sim\exp[(W-U)/kT],$$
$$\sigma\sim c_i\nu_i\sim\exp[(W+U)/kT]. \tag{17}$$

The large jump frequencies ν_i make $1/T_1$ due to interstitial Ag ions rather small unless B is large; computed values for $1/T_1$ are shown in Fig. 6. It is seen that, in order to account for the line broadening at high temperatures by a sufficiently short T_1 due to Ag interstitials, one would need an effective value of β about 20 times as large as that assumed for vacancies, i.e., $\beta\approx1000$. Such a value seems rather large, though it cannot be considered entirely impossible; e.g., values of the correction factor β between 100 and 1000 have been invoked to account for nuclear relaxation times due to quadrupolar interaction with lattice vibrations.[16] Figure 6 also shows that Ag^+ vacancies at high temperatures are not responsible for a very short T_1. There is, however, another mechanism which may determine T_1 at high temperatures. Kurnick[8] has some evidence for the formation of Br^- vacancies (Schottky defects) in the lattice above 570°K, their concentration being about equal to that of the Ag vacancies at 680°K. These Br^- vacancies contribute negligibly to the conductivity at this temperature. Some diffusion measurements[30] show, however, that such Br^- vacancies are by no means completely immobile, though their jump frequency at 680°K may be somewhat more than 1000 times less than that of the Ag^+ interstitials in the lattice. By Eq. (17), the small jump frequency of the Br^- vacancies will make their contribution to the electrical conductivity correspondingly small, but their contribution to $1/T_1$ correspondingly large. Very careful measurements of T_1 might decide whether such Br^- vacancies constitute indeed the main relaxation mechanism in the high-temperature range and could help to clarify some of the still unsettled questions of the behavior of Schottky defects in AgBr.

Finally we turn our attention to the low temperatures where the line shape is determined by static effects only. We note at the very outset that the defects in the solid at these low temperatures would not be expected to be randomly distributed. The reason for this is that the electrostatic attraction existing between Ag^+ vacancies and Cd^{++} impurities leads to correlation between their positions; in particular, it makes the state of lowest energy of the crystal one in which Ag^+ vacancies and Cd^{++} impurities lie on adjacent positions of the Ag sublattice, thus forming associated pairs ("complexes").[31] When the association process is complete, the field gradients due to $2N$ charges are replaced by field gradients approximately like those of N point dipoles. Hence association of defects at low temperatures should lead to smaller field gradients at the Br nuclei and hence to smaller quadrupolar broadening.

Following the discussion of Sec. III, one can try to estimate the order of magnitude of the static quadrupolar line width, assuming all defects to be randomly distributed. The concentration of defects $x=2c_d$, since the number of vacancies is equal to that of the impurity ions; also the volume vR^3 available to a defect is $2R^3$, since there are four Ag lattice sites in a cube of volume $(2R)^3$. We can say that, roughly speaking, contributions to the line more than 10 kc/sec from its center can be considered unobservable, i.e., we chose the cut-off

[27] Variation of the external magnetic field would also constitute a useful check in the study of lines broadened by *static* second-order quadrupole interaction since the line width should then be field-dependent.

[28] There are several cases known where the Br nuclear resonance is not observable in a liquid because of too short a relaxation time caused by quadrupole interaction. See R. V. Pound, Phys. Rev. **72**, 1273 (1947).

[29] This is in contrast to the static line width where defects which are close to a nucleus contribute only to the unobservable wings of the resonance line.

[30] A. Murin, Doklady Akad. Nauk. S.S.S.R. **99**, 529 (1954).

[31] For a recent discussion of association, see A. B. Lidiard, Phys. Rev. **94**, 29 (1954).

frequency in Eq. (7) as $\Omega = 2\pi \times 10^4$ sec^{-1}. We shall take the correction factor $\beta \approx 50$, as suggested by the discussion of relaxation effects connected with vacancies. For $c_d = 10^{-3}$, Eq. (7) then yields $\langle(\Delta\omega)^2\rangle_Q = 3.5 \times 10^8$ sec^{-2} as compared to the second moment due to magnetic interactions only, $\langle(\Delta\omega)^2\rangle_m = 10^7$ sec^{-2}. Since $\langle(\Delta\omega)^2\rangle_Q \sim B^{\frac{1}{2}}\Omega^{\frac{1}{2}}$, the result would not be greatly changed if a somewhat different cut-off frequency had been chosen. One thus sees that the assumption of a completely random distribution of defects at temperatures below 200°K would seem to lead to more pronounced effects on the line width in going from a pure sample to our most highly doped one than were actually observed. This conclusion is in agreement with the expectation that the defects are associated at these low temperatures. Finally, it seems possible that the *initial* broadening of the lines at about 200°K is connected with the onset of dissociation of the defects. Comparison with Lidiard's curves[31] and the fact that, unlike what one would expect from simple lifetime broadening due to vacancies, this initial broadening occurs at essentially the same temperature irrespective of impurity concentration, would suggest such an interpretation.[1] But both Fig. 6, which is based on a somewhat uncertain extrapolation of the conductivity data to these low temperatures, and some very crude experimental estimates of T_1 show that one cannot completely exclude the possibility of lifetime broadening effects already making some contribution to the line width around this temperature. Only careful relaxation time measurements might help to separate unambiguously the various effects. Such measurements in the low-temperature region would also be of interest since they might show an influence on T_1 due to the possibility of reorientation of complexes.

VI. FURTHER EXPERIMENTS

We want to mention briefly some experiments which illustrate the narrowing of resonance lines produced by the motion of defects. As a first example we consider NaCl doped with $CdCl_2$. Na has a small nuclear electric quadrupole moment (approximately 0.1×10^{-24} cm^2)[32] and, since the Na^+ ion is small, the effects of ion core distortion are correspondingly less important. As a result the parameter B for Na^+ is probably about 200 times smaller than that for Br^-. One thus expects Na quadrupolar interaction effects in NaCl to be much less significant than they are for Br in AgBr. Figure 7 shows the effect on the Na resonance line width $\Delta\nu'$ (measured between points of maximum slope) of increasing the temperature of a doped sample of NaCl.[33] The resulting curve is of the form characteristic of the motional

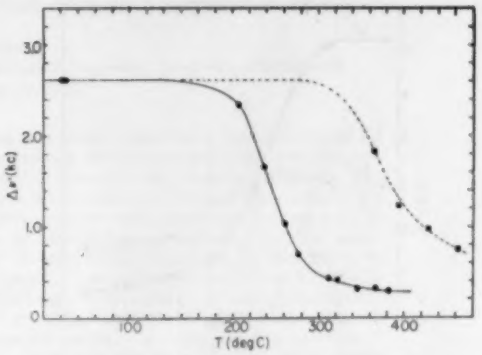

FIG. 7. Behavior of Na line width $\Delta\nu'$ (measured between points of maximum slope) as a function of temperature in NaCl. Solid curve: NaCl sample doped with a molar concentration 6×10^{-4} of $CdCl_2$. Dotted curve: "pure" NaCl sample.

narrowing of resonance lines.[34,35] One would expect that the width of the Na line would begin to decrease appreciably when the jump frequency ν_{Na} of the Na^+ ions, which determines the rate of fluctuation of the internal magnetic fields at the position of a Na nucleus, becomes comparable to the static Na line width $\Delta\omega$ at low temperatures.[36] But $\nu_{Na} \approx c_v \nu_v$, where c_v is the atomic concentration of Na^+ vacancies ($\ll 1$), or probability of a vacancy being next to a Na^+ ion, and ν_v is the vacancy jump frequency. Below 500°C the thermal production of defects is negligible[37] and $c_v = c_d$, the concentration of divalent impurity ions. Thus one expects the line width to show appreciable narrowing when the temperature becomes high enough so that:

$$\nu_{Na} = c_v \nu_v \approx \Delta\omega. \tag{18}$$

In agreement with Fig. 7, the Na line in samples of higher impurity concentration should therefore begin to narrow at a lower temperature. The conductivity data[37] give information as to the mobility of the Na^+ vacancies and hence allow the calculation of ν_v. Using these data one predicts that in a sample containing 6×10^{-4} atomic fraction of $CdCl_2$, the narrowing criterion (18) should be satisfied at 230°C, in fair agreement with Fig. 7. The simplified theory of motional narrowing[18,34] permits one to construct from Fig. 7 a curve of ν_v vs $1/T$. From the slope of the resulting straight line one can estimate the activation energy for the diffusion of Na^+ ions to be 0.66 ev. This compares with a value of 0.77 ev obtained from diffusion[38] and 0.83 ev from conductivity measurements.

[32] Perl, Rabi, and Senitzky, Phys. Rev. **98**, 611 (1955).

[33] $\Delta\nu'$ at room temperature is about 1 kc/sec larger than one would compute from magnetic interactions alone, but independent of impurity concentration. Though we did not investigate in detail the source of the extra width, it is likely to be due to first-order quadrupole interaction with dislocations in the crystal.

[34] H. S. Gutowsky and G. E. Pake, J. Chem. Phys. **18**, 162 (1950).

[35] H. S. Gutowsky, Phys. Rev. **83**, 1073 (1951).

[36] Note that motional narrowing will be caused by *any* type of jumping of Na ions in the lattice, e.g., even by a localized jumping which only causes reorientation of an impurity complex without contributing to diffusion or electrical conductivity in the crystal.

[37] H. W. Etzel and R. J. Maurer, J. Chem. Phys. **18**, 1003 (1950).

[38] Mapother, Crooks, and Maurer, J. Chem. Phys. **18**, 1231 (1950).

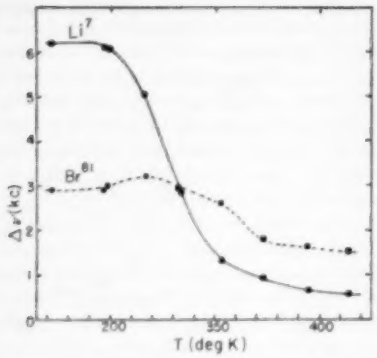

FIG. 8. Behavior of the resonance line widths $\Delta\nu'$ (measured between points of maximum slope) in a LiBr sample containing a molar concentration 2×10^{-3} of $MgBr_2$. Solid curve: Li^7 line width. Dotted curve: Br^{81} line width.

As a final illustration we want to mention the case of LiBr, which is also of some interest in connection with our interpretation of the AgBr results. Both Li and Br have magnetic moments large enough to make their resonance lines readily observable; on the other hand, Li has a very small quadrupole moment, unlike the Br nuclei already discussed in connection with AgBr. The electrical conductivity of LiBr has been studied by Haven[39]; Li vacancies are readily introduced into the salt by doping with $MgBr_2$. We want to consider what one would expect about the behavior of the line widths in a sample of LiBr containing, say, a concentration $c_d=2\times10^{-3}$ of $MgBr_2$. Turning our attention first to the Li line, it should begin to narrow when the jump frequency of Li ions is equal to the static Li line width $(\Delta\omega)_{Li}$, i.e., at about 310°K estimated from the conductivity measurements. At higher temperatures the line width should approach essentially zero since the internal fields at a Li^+ ion, whether due to Li^+ or Br^- ions, will average to zero when the Li^+ ion jumps fast enough. The situation here is analogous to that of Na^+ ions in NaCl. Now consider the Br line, neglecting at first the Br quadrupole moment. This line will begin to narrow when $\nu_{Li}\approx(\Delta\omega)_{Br}$, i.e., at about the same temperature where the Li line narrows, since then the magnetic width due to the Li nuclei begins to disappear. But, since the Br^- ions remain stationary, the line width at higher temperatures should not go to zero, but should approach a width due to magnetic interactions among the Br nuclei only. (From magnetic interactions one would calculate, for Br^{81}, $\Delta\nu'=3.2$ kc/sec in the limit of low, and $\Delta\nu'=1.2$ kc/sec in the limit of high temperatures.) Now, remembering the large Br electric quadrupole moment, one would expect, in analogy to our interpretation of the AgBr results, a line *broadening* due to the short relaxation time produced by quadrupole interaction with moving vacancies to occur when $\nu_s\approx1.8\omega_0$ (ω_0=Larmor frequency of Br ion), i.e., at about 335°K for Br^{81}. Thus the Br line width should be a rather complicated function of temperature, a maximum in width due to lifetime broadening being superposed in the same temperature range where the line would otherwise tend to narrow. Figure 8 shows the experimental results obtained for one such doped sample of LiBr prepared to check these general predictions.[40] The maximum in the Br line width is confirmed by a corresponding decrease in its intensity, and the temperature dependence of the curves is seen to be essentially as expected.

[39] Y. Haven, Rec. trav. chim. **69**, 1471 (1950).

VII. CONCLUDING REMARKS

We have seen that nuclear magnetic resonance techniques provide a means of studying point defects in ionic crystals from a rather microscopic point of view. Measurements can be made on polycrystalline samples to yield values of the defect jump frequencies and their approximate activation energies by line narrowing or relaxation time observations; in some cases information may be obtained as to the association of defects in the solid. Our general discussion shows that variation of the external magnetic field and, most particularly, careful measurements of nuclear relaxation times as affected by the presence of point defects would certainly be of physical interest, as well as being desirable as a check on the interpretation of some of our results.

ACKNOWLEDGMENTS

We wish to thank Professor M. H. Cohen for his continuing interest in this work and for many discussions. Professor A. W. Lawson kindly lent us some specimens of AgBr for use in preliminary measurements. Finally, we are very grateful to Professor N. H. Nachtrieb for his generous help with the chemical preparation of the samples.

[40] Note that experimental line width curves of the type shown in Fig. 8 allow an immediate determination as to which ion in the crystal is the mobile one.

Properties of Indium and Thallium at Low Temperatures*

C. A. SWENSON†
Cryogenic Engineering Laboratory, Massachusetts Institute of Technology, Cambridge, Massachusetts
(Received August 18, 1955)

The pressure-volume relationships for superconductors near absolute zero are of potential interest for comparison with theories which attempt to explain the variation of the superconducting transition temperature with pressure. Such data for thallium are of special interest since the variation of transition temperature with pressure is different for thallium than for any other known pure metal. In these experiments, measurements on indium of the total compression to 10 000 atmos for various temperatures down to 4.2°K served as a check of similar measurements on thallium. No unusual behavior was found for either metal. These results were combined with the measurement of the total thermal expansions for both metals to give isobars at both zero pressure and at 10 000 atmos pressure over the range from 4.2° to 300°K. The results of some low-temperature compressive testing experiments on both metals are also given, together with some indirect evidence as to the vanishing of work hardening effects at low temperature and moderate hydrostatic pressures. Finally, measurements on the electrical resistance of indium show an unexplained kink in the R *vs* T curve at about 210°K. The effect on the electrical resistance of indium due to tensile (plastic) deformation at 4.2°K was also measured.

INTRODUCTION

THE measurement of the effects of high hydrostatic pressures on superconducting transition points has currently become a fairly important branch of low-temperature research.[1] While the general field has been surveyed and data exist for various substances, probably the only generalization which can be made is that the superconducting transition point *usually* decreases as the applied pressure is increased. Little is known about the basic theory behind this effect, and as yet there exist no bases for correlating these pressure effects and others, such as the changes in volume or electrical resistance with pressure. If the superconducting transition is very sensitive to volume changes, as it seems to be, then measurements of $P-V$ isotherms at low temperature for superconducting elements can be of considerable interest. The measurement of these is not too difficult, since a number of the superconductors (indium and thallium in particular, and probably pure tin, lead, mercury, and cadmium)[2] retain sufficient plasticity at their transition points so that variations of volume with pressure can be obtained at liquid helium temperatures by using a method which has been described elsewhere.[3-5]

The work on indium and thallium which is given below was undertaken to provide such $P-V$ data for these substances. There are two considerations which govern the choice of materials; first, and foremost, they must be plastic, and, secondly, they must be of specific interest. Indium was chosen initially because of its plasticity, and the original work done on it was an attempt to discover the relationship between the extrusion experiments performed by Stewart[2] and the shear yield strength and work hardening of a substance. Both extrusion pressures and compressive stress-strain curves were measured, and very unusual results were obtained which indicated a shear sensitive transition at very low temperatures. As a result of this, several different low-temperature properties of indium were measured in the hope that they would shed some light on this suspected transition. These experiments included: (a) the electrical resistance as a function of temperature from 300° to 4.2°K; (b) the electrical resistance of a wire as a function of strain (plastic) at 4.2°K; (c) an x-ray Laue pattern taken before and after deformation at 4.2°K; (d) the total volume change at 10 000 atmos pressure between 300° and 4.2°K.

Outside of a kink in the electrical resistance about 210°K (a discontinuity in the temperature coefficient of resistance), no unusual effects were found. Attempts to reproduce the yield strength and extrusion phenomena a year later were not successful, and as the original effects remain unexplained, only the second set of stress-strain curves (of normal behavior) are given below. The total linear thermal expansion of indium was also roughly measured to 4.2°K so that it would be possible to convert the compressibility measurements into actual molar volumes at 10 000 atmos pressure from 4.2°K to room temperature.

Thallium also satisfies the plasticity criterion at low temperature, and, whereas there was no reason to suspect abnormal behavior for indium, thallium represents an exception among pure metallic superconductors in that it initially shows an increase of superconducting

* This work was performed under a contract with the U. S. Army Office of Ordnance Research.
† Present address: Physics Department, Iowa State College, Ames, Iowa.
[1] See the article by C. F. Squire in *Progress in Low-Temperature Physics*, edited by C. J. Gorter (Interscience Publishers, Inc., New York, 1955), p. 151.
[2] J. W. Stewart, doctoral thesis, Harvard University, submitted May, 1954 (unpublished).
[3] C. A. Swenson, "The application of high hydrostatic pressures at liquid helium temperatures," Paper No. 54-33-3, delivered before the Instrument Society of America Meeting, Philadelphia, 1954 (to be published in the Proceedings); also reported in slightly revised and corrected form under the same title as U. S. Army Office of Ordnance Research Technical Memorandum, TM-55-1 (unpublished).
[4] J. W. Stewart, Phys. Rev. **97**, 578 (1955).
[5] C. A. Swenson, Phys. Rev. **99**, 423 (1955).

transition point with pressure, although for quite high pressures (several thousand atmospheres) the effect is normal.[6] Chester has suggested the possibility of a phase transition in thallium to explain this result,[7] and it was with the object of testing this hypothesis that the work on the $P-V$ curves of thallium was undertaken. Indium, presumably having a normal behavior, was useful as a comparison sample, to verify that any unusual effects observed were solely a function of the sample being tested, and not due to the apparatus. Thermal expansion data also were taken for thallium, so that, again, it would be possible to have two isobars, one at zero pressure and one at 10 000 atmos. As was the case for the similar measurements on indium, no unexpected behavior was found.

Neither indium nor thallium are "nice" substances to work with from a physical viewpoint, since they both have anisotropic crystal structures. Indium has a slightly distorted face-centered cubic lattice (face-centered tetragonal with $c/a=1.07$ at room temperature),[8] while thallium is hexagonal with an axial ratio of 1.598.[9] Thus, every effort was made to assure that the abovementioned thermal expansion and electrical resistance data were taken on finely polycrystalline samples with no preferred orientation, so that the true average effects were being observed. The object, fortunately, was to look for anomalous behavior or transitions, and not to try to present data of theoretical interest.

No anomalies were expected in the zero-pressure range, since the heat capacities of both indium and thallium have been measured, the former between 2°K and room temperature,[10,11] and the latter from 1.5° to 4.2°K, and from 15° to 300°K.[12,13] The gap existing for thallium is very tantalizing, since the data obtained on the two sides of it seem inconsistent. Both metals have rather low melting points, as is characterized by their low Debye θ's, about 130° for indium and 94° for thallium.

Finally, thallium has the disadvantage that it oxidizes very rapidly at room temperature, so that detailed electrical resistance measurements were not attempted.

MATERIALS USED

The indium and thallium used were both obtained from A. D. Mackay, Inc., and were specified as 99.9% pure. Fortunately, the actual purity should not be too important for either the compression or the rather qualitative thermal expansion data which were taken. The purities were probably much better, since the residual resistances were about $10^{-3}R_{273}$ for indium and $3\times10^{-3}R_{273}$ for thallium. Both wires were extruded and not annealed. The indium was cast under vacuum from ingots into rods from which samples were machined or formed by pressure at room temperature. The thallium was furnished in the form of a rod from which the samples were machined on a lathe and then stored under water which had been boiled. It was never possible to keep all traces of the oxide from the surface of the thallium samples. The residual resistances quoted above refer to samples taken from the metals after processing.

TEMPERATURE MEASUREMENT

All temperatures recorded in these experiments were measured with Leeds-Northrup copper-constantan thermocouple wire (No. 30 B. and S. gauge, enamel and glass insulation), which had been calibrated in this laboratory between 4.2° and 300°K, using a constant volume gas thermometer. The accuracy is estimated to be of the order of 0.1 degree down to 50°K, and about 0.5° from 50° to 15°K. This was not a limiting factor in any of the measurements.

COMPRESSION MEASUREMENTS

The apparatus and techniques used in measuring the total compressions of indium and thallium to 10 000 atmos are identical with those described elsewhere,[3,5,14] and will not be given here in detail. The sample (0.375 in. long by 0.253 in. diam) was placed in a cylinder of hardened tool steel of the same diameter, and was compressed in an elongated press by two hardened steel pistons. The low-temperature end of this press could be placed in a Dewar, or in a special cryostat where it could be kept at any desired temperature between 4.2°K and room temperature to a constancy of about 0.1°. As will be described later, both indium and thallium are quite plastic at the lowest temperatures, so the resulting pressure (force applied/area) is hydrostatic to a good approximation, and the motion of the pistons is a measure of the volume change of the sample. Several cycles were necessary to season the sample initially at each temperature so as to obtain reproducible data.

Basically, three corrections must be applied to any data taken; these are concerned with friction (both in the sample and in the hydraulic press), background stretch of the apparatus with no sample present, and expansion of the sample holder cylinder due to the internal hydrostatic pressures up to 10 000 atmos. The first correction is obtained by taking data at both increasing and decreasing pressure and the second by doing blank runs at all temperatures in both the cryostats used. The third correction is determined by comparing the room temperature compression of a

[6] M. D. Fiske, Phys. Rev. **94**, 495 (1954).
[7] P. F. Chester (private communication).
[8] W. A. Betteridge, Proc. Phys. Soc. (London) **A50**, 519 (1938).
[9] H. Lipson and A. R. Stokes, Nature **148**, 437 (1941).
[10] K. Clusius and L. Schachinger, Z. angew. Physik **4**, 442 (1952).
[11] J. R. Clement and E. H. Quinnell, Phys. Rev. **92**, 258 (1953).
[12] W. H. Keesom and J. A. Kok, Physica **1**, 175, 503, 595 (1933–1934); Leiden Comm. 230c, 230e, and 232a.
[13] J. F. Hicks, Jr., J. Am. Chem. Soc. **60**, 1000 (1938).
[14] C. A. Swenson and R. H. Stahl, Rev. Sci. Instr. **25**, 608 (1954).

substance, obtained using the two above corrections, with the true value which is known quite accurately from other measurements. This correction must be extrapolated to low temperature by the assumption that it is inversely proportional to the elastic (or Young's) modulus of the steel used in making the sample holder cylinder.[15]

The last two corrections are quite large, and introduce a basic uncertainty of about five percent into any volume change obtained in the present experiments. However, the correction data, while showing considerable scatter, could be represented by smoothed curves which were taken as being correct and which were used consistently. The philosophy was that if the sample holder and sample were placed in the press, and then in the cryostat, the relative accuracies would be much better if the setup were not disturbed during a series of runs at various temperatures. Thus, for any series the data should be consistent (and were) to about one percent, while if the sample holder were removed and then replaced in the press, the answer could vary by about 5%.

In practice, the cylinder expansion correction was determined for each sample and for each loading of the sample holder in the press by doing a room-temperature run, since Bridgman's work gives fairly accurate room temperature compression data for both indium and thallium.[16] The series of experiments on thallium shown in Fig. 1 lasted over a period of a week, with the sample holder remaining undisturbed in the press during this time, and the scatter of four room-temperature runs made at different times is shown about an average correction figure. There is an added advantage to making a final correction in this way since it automatically takes into account any small effects which might have been otherwise overlooked. It does, of course, make any results relative to those of Bridgman, and subject to any correction which may be later made in his data.

The actual procedure which was used to calculate the results shown in Fig. 1 is given below, and was necessitated by the small total compressions observed. The change in length of the sample was measured for small pressure increments from 1500 to 10 000 atmos for both increasing and decreasing pressures, and the total apparent change in volume (measured as a change in length, δl) between 1500 and 10 000 atmos was obtained by applying the friction and background stretch corrections. The curves showed no signs of abrupt volume changes, so only the total ΔV was measured. The lower limit of 1500 atmos was due to apparatus

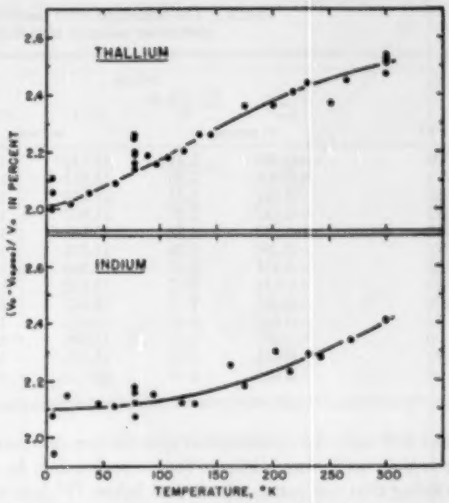

FIG. 1. The total hydrostatic compressions in 10 000 atmos of indium and thallium as a function of temperature. V_0 refers to the volume of the sample at zero pressure and the temperature of the test.

limitations,[8] and also uneven friction. The total compression was assumed to be linear (the deviations are small), and this change in length was converted into a total change in length in 10 000 atmos. The same experiment gave a measurement of the length, l_0, and the final $\delta l/l_0$ obtained in this way was corrected to a true $\Delta V/V_0$ in 10 000 atmos by subtracting the cylinder expansion correction. V_0 here is the volume at zero pressure at the temperature of the experiment. The cylinder expansion correction was calculated using the linear assumption also, so unless the small curvature which is observed by Bridgman changes radically with temperature, it should result in fairly accurate values for the true $\Delta V/V_0$ in 10 000 atmos, even though the curvature has presumably been ignored.

The final results for indium and thallium are given in Fig. 1, with the smooth curve being drawn through the points (not indicated) which were most consistent. The smoothed curves are summarized in Table I. There is some arbitrariness about drawing the indium curve, but since occasional points do seem to lie off the smooth curve for no known reason, little weight was given to the two points which lie high at about 160° and 200°K. The scatter at 77°K is common to both metals, and although it is presumably an apparatus effect, it is not understood. The 77°K points shown represent a variety of cooling rates in both the Dewar and cryostat, ranging from six to eight hours to ten minutes, done with both zero pressure on the sample and also with a pressure of 10 000 atmos. No consistent trend could be observed, although the calibration runs, done under similar conditions, showed no such scatter. The slowest cooling rate gave the lowest point for thallium, and this

[15] The elastic modulus of a piece of the same steel as used in the cylinder (Omega, Rockwell "C", 656) was measured directly as a function of temperature in this laboratory, using the same press and cryostat. These measurements showed a linear variation of the Young's modulus from 24.5×10^6 psi at room temperature to 27.6×10^6 psi at 60°K, with a rapid leveling off from this value to 28.0×10^6 psi at 4.2°K.

[16] P. W. Bridgman, Proc. Am. Acad. Arts Sci. **76**, 1 (1945).

TABLE I. The smoothed total thermal expansions, compressions in 10 000 atmos, and molar volumes of indium and thallium at low temperature.

	Indium				Thallium			
	$\frac{l-l_{373}}{l_{373}}$	$\frac{V_0-V_{10\,000}}{V_0}$			$\frac{l-l_{373}}{l_{373}}$	$\frac{V_0-V_{10\,000}}{V_0}$		
T(°K)	in percent		$V_{p=0}$	$V_{p=10\,000}$	in percent		$V_{p=0}$	$V_{p=10\,000}$
			cc/mole				cc/mole	
300	+0.085	2.41	15.712	15.333	+0.061	2.51	17.124	16.694
275	+0.006	2.36	15.673	15.305	+0.003	2.48	17.094	16.670
250	−0.072	2.31	15.638	15.276	−0.055	2.45	17.065	16.647
225	−0.147	2.27	15.602	15.250	−0.113	2.42	17.036	16.624
200	−0.220	2.23	15.568	15.222	−0.168	2.38	17.007	16.603
175	−0.290	2.20	15.534	15.196	−0.222	2.33	16.980	16.585
150	−0.357	2.17	15.503	15.169	−0.274	2.28	16.954	16.568
125	−0.424	2.15	15.472	15.143	−0.324	2.23	16.929	16.551
100	−0.485	2.13	15.442	15.117	−0.373	2.17	16.904	16.536
75	−0.543	2.12	15.413	15.092	−0.420	2.12	16.880	16.522
50	−0.596	2.11	15.390	15.067	−0.461	2.08	16.858	16.508
25	−0.634	2.10	15.375	15.051	−0.494	2.04	16.842	16.498
0	−0.643	2.10	15.370	15.048	−0.507	2.02	16.836	16.496

agreed well with the continuation into the low-temperature region, so it was taken as the correct value. It is gratifying that the curves above and below 77° join up so well, since the background stretch correction is discontinuous at this point, with the temperature gradients along the press supports changing as the refrigerating fluid is changed from liquid nitrogen to liquid helium, and liquid nitrogen is added to the outer jacket. The scatter at 4.2° is due to, roughly, the same reasons. In all cases, the scatter is about the five percent which was expected.

The curves of Fig. 1 show no sign of discontinuities in the total compression to 10 000 atmos, at least none greater than $5\times10^{-4}V_0$. Thus, one must conclude that the possibility of a first-order transition in the region from room temperature to liquid helium temperatures, and from zero to 10 000 atmos, is quite small for either substance.

THERMAL EXPANSIONS OF INDIUM AND THALLIUM

The total compression measurements are more useful when expressed as a change in molar volume at a pressure of 10 000 atmos, since the data of Fig. 1 come out in terms of the volume at zero pressure at the temperature of the experiment. In order to make these calculations, the change in molar volume at zero pressure must be measured as a function of temperature for each substance. In principle, it would be possible to obtain this from the observed changes in length of the samples in the press, but any answer so obtained would be with respect to stainless steel. Unfortunately, these figures showed considerable scatter, so that it was thought worth while to check them with an independent setup. The accuracy required is not high, and it was quite sufficient to know the ratio $V_{4.2}/V_{273}$ to 0.01%.

A simple setup was built which used a specimen three inches long and 0.25 in. in diameter, held freely in a copper jacket at low temperature, and with fixed quartz feeler rods connected to its top and bottom and also to a dial gauge at room temperature. The dial gauge was calibrated against a micrometer screw, so that changes in length could be measured reliably to better than 10^{-4} inch. The whole setup was placed with its low temperature section in the cryostat, and changes in length were measured as a function of temperature over the temperature region from room temperature to 4.2°K. In order to check the accuracy of the setup, and to allow a correction to be made for the thermal expansion of the quartz and any temperature inhomogeneities, a piece of very pure (99.999%) copper was also run, and the results compared with the more accurate ones of Bijl and Pullan. The correction so determined amounted to about one percent of the values for $\delta l/l_{273}$ shown in Fig. 2 and also listed in Table I.

These data were then used to calculate the total volume changes, and finally the variation of molar volume with temperature at both zero pressure and, by using the compression measurements, at 10 000 atmos. The volumes at zero pressure were taken as 15.71 cc for indium, at 25°C, based on a density of 7.303,[17] and 17.114 cc at 18°C for thallium, based on x-ray data.[9] The number of significant figures carried in the tables does not reflect the inaccuracies in these starting points, but they are used only as a convenience to show the variations of molar volume. These molar volumes are also listed in Table I for both indium and thallium.

The heat capacity results can be used in conjunction with these data to obtain a value for the Grueneisen constant, γ, which is defined in the equation,

$$dV/dT=\gamma K_0 C_v,$$

where V is the molar volume, K_0 is the initial compressibility, and C_v is the specific heat at constant volume. While the thermal expansions are not accurate enough to give a reliable value for γ in the region below 77°, above this temperature the data can be represented quite closely by a γ of 2.35 for indium and 1.80 for

[17] D. D. Williams and R. R. Miller, J. Am. Chem. Soc. 72, 3821 (1950).

thallium. One must not take these results too seriously, since there is no assurance that the thermal expansion measured is for a genuinely polycrystalline sample of either substance.

The volume expansion coefficient calculated for indium for the region near the ice point (95×10^{-6}/degree) agrees well, however, with the figure of Williams and Miller (97.5×10^{-6}/degree),[17] which is an average for the region from 25°C to the melting point. Since they measured a volume expansion directly, this gives some confidence that the assumption that this sample was a true polycrystal of random orientation is justified.

MECHANICAL PROPERTIES OF INDIUM AND THALLIUM AT LOW TEMPERATURE

One of the limiting factors in the use of these techniques for compression measurements at low temperatures is that the substances used must remain quite plastic at the lowest temperatures reached—that is, they must have a low shear yield strength and very small work-hardening so that pressure differences cannot be set up between the sides and ends of the samples. Earlier extrusion measurements by Stewart[2] listed both of these substances as of doubtful plasticity, but the criterion used was very rigid, and the extrusion pressures which he measured were of the order of hundreds of times the yield strengths as found in these experiments. The extrusion experiments were also repeated in this work, but are not of sufficient interest to be described in detail.[18]

In order to investigate these mechanical properties, the same hydraulic press which was used for the compression measurements was used to measure the stress-strain curves, in compression, for cylinders of both materials (0.40 in. long and 0.353 in. in diameter). The samples were annealed in boiling water for two hours after machining or forming. This annealing seemed to be quite important for reproducible results at 77°K (the stress-strain curve for indium at 77°K actually resembled the 4.2°K curve if the only annealing given was to leave it at room temperature for a week), but had little or no effect on the 20°K or 4.2°K curves. These measurements, typical results of which are shown in Figs. 3(a) and (b), were made with the sides of the cylinders unsupported, and the departure from linearity shown corresponds to plastic deformation of the samples.

In another identical experiment, the results of which are not illustrated, the stress-strain curve for indium at 4.2°K was found to increase linearly to a strength

[18] The extrusion experiments at 4.2°K (see reference 3 for experimental details) usually behaved as follows: As the pressure on the sample was increased, the material began to flow through the hole at about the yield strength, tending to form a button, but, due to work hardening effects, the button merely increased slightly in length with each pressure application until at about 400 times the yield strength an explosive, irreproducible, extrusion was found. This was quite different from the case at 77°K where, at slightly smaller pressures, free flow was observed, the rate of flow depending very markedly on the applied pressure.

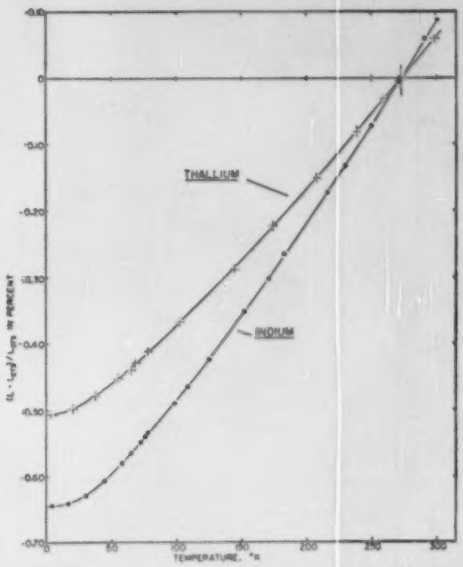

FIG. 2. The total linear thermal expansions of indium and thallium at zero pressure, after apparatus corrections have been applied.

of about 15 kg/mm² (or 1500 atmos) when the length of the sample was decreased by 15%. This represents an increase by work-hardening of a factor of thirty in yield strength, and should be compared with room temperature where a maximum increase of about two or three is possible before free flow sets in. It must be emphasized that these experiments give a compressive yield strength, which is roughly twice the shear yield strength which applies above.

This work-hardening can be quite serious, since because of the geometry of the experiments on total compression, the samples undergo considerable plastic deformation during the course of a single cycle of the pressure from zero to 10 000 atmos, and then back to zero. The sources of this plastic deformation are twofold. First, the area of the sample holder increases elastically by about one percent because of the hydrostatic pressure exerted by the sample, and the sample must first flow outwards to fill this extra volume, and then flow back as the pressure is relieved. This results in a two percent plastic deformation. The second effect is more basic, and is due to the fact that the sample material must flow even in the absence of any change in area of the holder in order for the one-sided compression to be transformed into a uniform change in density.

This latter effect can be estimated by considering an "equivalent" path through which the sample must pass to get from zero pressure and volume, V_0, to 10 000 atmos pressure and the volume $V_0-\Delta V$. One first applies a pure hydrostatic pressure of 10 000 atmos

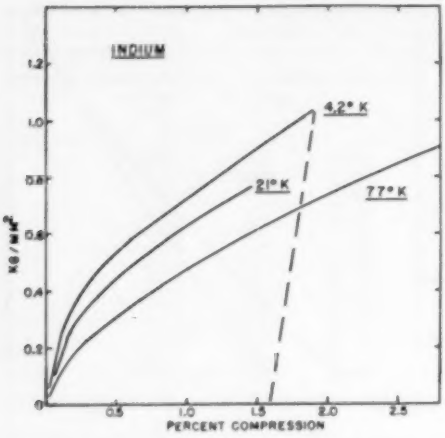

FIG. 3. The stress-strain curves for (a) indium and (b) thallium cylinders (0.4 in. long by 0.353 in. diam) under a compressive load with the sides of the cylinder unsupported. The dashed lines represent the elastic deformation of the cylinder and hydraulic press. The pressures given are not true stress, but are total loads expressed in terms of the initial areas of the samples.

and notes the change in dimensions of the sample ($\Delta V/3V_0$ in length and diameter). Effectively, the sample shrinks in from the walls of the holder during this stage. Next, a pure one-side compression is applied to the sample until it has deformed plastically enough so that is just fills the cylinder. The change in length required to do this, $2\Delta V/3V_0$, is a measure of the total plastic deformation which a sample undergoes upon the increase of pressure from zero to 10 000 atmos. An exactly equivalent argument holds when the pressure is released, and as the sample flows upwards. Thus the plastic deformation per cycle can be estimated at about 3.2%, or, considering the change in area, at about 5% total. This should be roughly independent of temperature, but should only be serious at low temperature where tremendous increases in strength by work-hardening are possible. If this full effect were to apply, an increase in shear yield strength of about 250 atmos would be expected on each cycle.

This effect would show up as an increase in friction during an experiment, since the sample would behave elastically with its behavior governed by both the shear modulus and the compressibility,[18] until the shear yield strength was exceeded, while after this point its change in length would be governed solely by the compressibility and the average pressure. The same would apply in reverse as the pressure was decreased. This would result in a widening of the hysteresis loop from cycle to cycle, or a seeming irreproducibility of the data, something which was never observed. The friction was usually of the order of 250 atmos for both indium and thallium, and about 50 atmos of this was inherent in the hydraulic press, while some was undoubtedly surface friction at the walls. It showed no variation from cycle to cycle on a given sample. This was demonstrated by a special run at 4.2°K, in which the hysteresis loop taken for an indium sample after one seasoning cycle was compared with the loop taken after fifteen subsequent cycles. The two loops coincided exactly. This is very strange, and certainly not what one would expect from the reasoning given in the previous paragraph. The indications are that the mechanism which causes work-hardening ceases to become operative at low temperature when moderate (a few hundred atmos) hydrostatic pressures are present. Bridgman has found many unusual changes in mechanical properties at room temperature and very high pressures and in general finds an increase in ductility with pressure.[20] However, the general trend seems (as is usual) that high-pressure phenomena correspond to low temperature, and in contrast the lack of work-hardening found here would resemble, basically, a high-temperature effect.

Naturally, more work is necessary to verify this effect, since the present conclusions are arrived at rather indirectly. But, this hypothesis does offer an explanation for two previously contradictory phenomena found, respectively, by Fiske[21] at the General Electric Laboratories and Hatton at Harvard.[22] Both of these workers have used solid hydrogen as a "bath" with which to apply hydrostatic pressures to metals for electrical measurements. Fiske finds that the solid hydrogen, supposedly of low shear strength, can deform tin single crystals, while Hatton finds that the strength of solid hydrogen is so low that very fragile arsenic single

[18] See the modulus, χ, defined by F. H. Newman and V. H. L. Searle, *The General Properties of Matter* (Edward Arnold and Company, London, 1948), fourth edition, pp. 94, 116.
[20] P. W. Bridgman, *Studies in Large Plastic Flow and Fracture* (McGraw-Hill Book Company, Inc., New York, 1952).
[21] M. D. Fiske, invited paper read before the American Physical Society Chicago Meeting, 1954 [Phys. Rev. 98, 244(A) (1955)].
[22] J. Hatton, Phys. Rev. 100, 681 (1955)

crystals are not injured by repeated pressure applications. The two observations can be reconciled if one postulates that most substances become more plastic under hydrostatic pressures.

A series of rather strange stress-strain curves found for indium in some initial work indicated a shear-sensitive transition at very low temperatures. W. B. Pearson at the National Research Council, Canada, kindly investigated this possibility by taking a Laue x-ray diffraction pattern of an indium wire before and after deformation in liquid helium, with no sign of a change from the room temperature structure.[23] Similar experiments performed by I. Simon at Arthur D. Little, Inc. in conjunction with the author, also gave negative results. The earlier mechanical deformation experiments were quite consistent at the time, and cannot be explained on the basis of any known quirks of the setup. Unfortunately, they could not be reproduced, and are mentioned here solely because of a reference which was made to them by Pearson in his report.

ELECTRICAL RESISTANCE OF INDIUM

This was measured initially to look for the above-mentioned shear sensitive transition, but the work was continued because of an apparent discontinuity in the slope of the resistance-temperature curve at about 210°K. This was found originally in the same indium as was used for the compressibility and mechanical properties work, using wire (0.015 in. diam) which had been extruded in our laboratory. The low-temperature behavior was normal, with a residual resistance of about 0.1% of the ice-point value, and a temperature variation of the resistance after the residual resistance had been subtracted of about T^3 below 20°K. The resistance was linear with temperature above 210°K, and also linear from 160° to 210°K, but with a change in slope of about 10%. In order to verify that this was a true effect, a second lot of indium wire (0.020 in. in diam) was ordered from A. D. Mackay, and a second experiment in a different sample holder, with a different thermocouple attached, was run, with the object being to obtain more precision. Requisite stability was obtained by using the cryostat again for these measurements.

The results of the two sets of experiments were indistinguishable, and the actual experimental points obtained in the second, more accurate, experiment (above 77°K) are listed in Table II, along with smoothed values for the resistance below 77°K. The effect is real, although small, and is unexplained. It is in the opposite direction from what would be expected from the normal change in density with temperature.

Another set of experiments, also inspired by the elusive shear sensitive transition, measured the change in resistance of an indium wire, 0.015 in. in diameter and six inches long, as it was extended in liquid helium. These results were about what would be expected, with no change in resistance noted until the elastic region was passed, and after this, a change of about 2.5% (or 2×10^{-10} ohm-cm) in resistance for every one percent change in length. In giving this result, the geometrical effect due to the change in diameter of the wire on extension has been subtracted. The agreement between two runs on wire from the same source was within 10%, in spite of a great deal of scatter on the first run. The total deformation in each case was of the order of 6 to 8%.

TABLE II. The electrical resistances of indium as a function of temperature. The data above and including 77.7° are actual experimental points, while below 77.7° the values given are smoothed.

T(°K)	$R/R_{273.2}$	
272.2	0.9942	
257.3	0.9286	
242.0	0.8603	$\frac{1}{R_{273}}\frac{dR}{dT}=0.00443$
227.0	0.7929	
210.8	0.7224	
194.7	0.6576	
180.7	0.6023	$\frac{1}{R_{273}}\frac{dR}{dT}=0.00400$
160.5	0.5214	
143.0	0.4549	
117.6	0.3607	
77.7	0.2189	
60	0.152	
40	0.082	Below 20°K,
20	0.020	$\frac{R}{R_{273}}-\frac{R_{4.2}}{273}\propto T^3$
4.2°	0.0010	

CONCLUSIONS

The results of the compression and thermal expansion experiments, given in Table I in terms of molar volumes at constant pressure, show that neither indium nor thallium exhibit any signs of a phase transformation under pressure in the low temperature region. This means that the anomalous behavior with pressure of the superconducting transition in thallium must be a characteristic of the metal as it normally exists at very low temperatures. No consistent effects on the total compression were observed for various rates of cooling, although it would be interesting to verify that this has no effect on the pressure coefficient of the transition temperature. No unusual effects were found in either the low-temperature stress-strain curves, or their temperature dependence, when the variation of compressive yield strength with temperature was measured.

The only anomalous effect which was found was in the electrical resistance of indium, and this showed up as a kink in the resistance *vs* temperature curve at 210°K. This effect is unexplained, and resembles a similar result which has been found for rubidium,[24] although the corresponding effect found in the thermal expansion

[23] W. B. Pearson, Can. J. Phys. 33, 473 (1955).

[24] D. K. C. MacDonald, Phil. Mag., Ser. 7, 43, 479 (1952).

by Pearson is lacking.[35] The specific heat, in contrast with the specific heat of rubidium, is also normal in this region.

The author is indebted to numerous people for assistance and discussion during these experiments which extended over a period of years, and wishes to express his appreciation especially to Dr. R. Berman, Dr. Z. S. Basinski, Dr. I. Simon, Dr. W. B. Pearson, and Dr. J. J. M. Beenakker.

[35] F. M. Kelley and W. B. Pearson, Can. J. Phys. 33, 17 (1955).

PHYSICAL REVIEW VOLUME 100, NUMBER 6 DECEMBER 15, 1955

Fast-Neutron Bombardment of GaSb

J. W. Cleland and J. H. Crawford, Jr.
Oak Ridge National Laboratory, Oak Ridge, Tennessee

(Received August 19, 1955)

Fast-neutron irradiation decreases the carrier concentration of polycrystalline samples of *n*- and *p*-type GaSb, indicating the production of low-lying traps. Vacuum heat treatment evidently removes such traps but also introduces additional acceptors, indicating a different rate of annealing for bombardment produced interstitial and vacancy atoms. Irradiation and heat treatment of *n*-type GaSb therefore results in the production of material of lower carrier concentration and reirradiation results in the conversion to *p*-type material. Repeated irradiations followed by heat treatments, however, do not reduce the net effective concentration of electrons in *n*-type material below $\sim 5\times 10^{17}$ cm^{-3}. The mobility of all samples is decreased by bombardment. Heat treatment subsequent to irradiation increases the mobility of *n*-type material but decreases the mobility of *p*-type samples still further below the decrease produced by bombardment. Low-temperature (−125°C) irradiation and subsequent warm-up and cool-down curves indicate the presence of defects of low thermal stability. No evidence was obtained for regions of low resistivity resulting from superlattice disordering as a result of quenching as might be expected from the thermal spike picture. The type and position of fast-neutron-introduced lattice defects is discussed with relation to previous models for Ge and InSb.

INTRODUCTION

THE effect of fast-neutron bombardment on the electrical properties of InSb has recently been reported.[1] This paper reports the results of similar studies carried out on polycrystalline GaSb.[2] This material, like InSb, is one of a series of semiconducting intermetallic compounds composed of elements of the third and fifth columns of the periodic table. Its electrical and optical properties have been studied by a number of workers.[3–7] It is characterized by a zinc-blende structure, a forbidden energy gap of ~0.7 ev at room temperature, and electron and hole mobilities of ~2000 and ~800 cm^2 volt^{-1} sec^{-1}, respectively.

Prior to this work Moyer[8] exposed several *p*-type GaSb specimens in the Brookhaven reactor and observed a decrease in hole concentration. Behavior other than expected was observed on annealing, consistent with the observations to be reported here.

[1] J. W. Cleland and J. H. Crawford, Jr., Phys. Rev. 93, 894 (1954); 95, 1177 (1954).
[2] We are indebted to Dr. Raymond L. Smith of the Franklin Institute for the *p*-type samples and to Dr. H. P. R. Frederikse of the National Bureau of Standards for the *n*-type samples used in these experiments.
[3] H. Welker, Z. Naturforsch. 7a, 744 (1952); 8a, 248 (1953).
[4] D. P. Detwiler, Phys. Rev. 94, 1431 (1954).
[5] H. N. Liefer and W. C. Dunlap, Jr., Phys. Rev. 95, 51 (1954).
[6] Blunt, Hosler, and Frederikse, Phys. Rev. 96, 576 (1954).
[7] Briggs, Cummings, Hrostowski, and Tanenbaum, Phys. Rev. 93, 912 (1954).
[8] J. W. Moyer (private communication).

EXPERIMENTAL PROCEDURES

All room-temperature fast-neutron exposures were carried out in the Oak Ridge graphite reactor in a fission chamber with a fast-neutron flux comparable to or greater than the thermal-neutron flux, and two specimens were irradiated at −125°C in a low-temperature facility of comparable flux distribution. Specimens were cut in the form of rectangular plates and were characterized by measurements of Hall coefficient R and resistivity ρ as a function of temperature (77 to 300°K) before and after bombardment. The conductivity was recorded during exposure. In order to reduce effects of nuclear doping (both Ga and Sb transmute to donor impurities giving Ge and Te, respectively), several of the specimens were shielded against thermal and resonance neutrons by wrapping with layers of Cd and In foil. After exposure and measurement, the specimens were subjected to various annealing treatments and recharacterized. Some of the specimens were reirradiated after extensive annealing periods.

RESULTS

The effect of reactor irradiation on the conductivity of representative samples of shielded and unshielded *n*- and *p*-type GaSb is indicated in Fig. 1 and the initial carrier concentration, temperature of exposure, and the initial rate of removal of current carriers calculated under the assumption that the mobility is initially

unaffected are listed in Table I. These data indicate that the conductivity of both n- and p-type samples, shielded or unshielded, decreases monotonically during irradiation. The removal rate of current carriers appears to be temperature dependent, but is approximately equal for all samples of high carrier concentration. The initial removal rate of holes for p-type material is less for a sample of low initial carrier concentration, whereas the initial rate of removal of electrons for n-type material is not markedly dependent upon initial carrier concentration and does not appear to approach a saturation condition. Slow-neutron-produced donor atoms would not be expected to affect appreciably the initial removal rate of carriers, since the principal transmutations appear with a finite half-life.

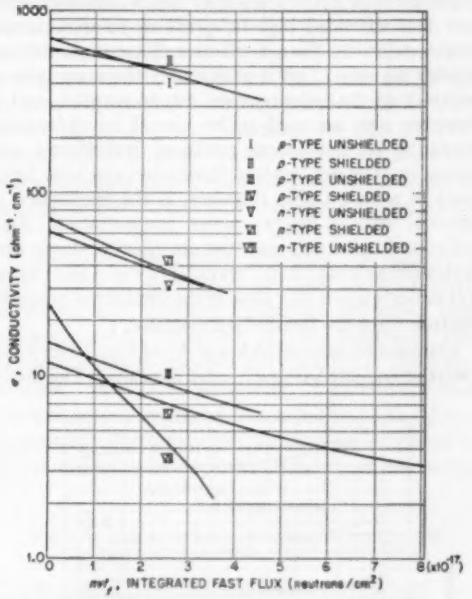

FIG. 1. The effect of reactor irradiation on the conductivity of polycrystalline samples of n- and p-type GaSb. Some samples were shielded with In and Cd foil against thermal and resonance neutrons.

The Hall coefficient and resistivity data for a typical p-type sample are shown in Figs. 2 and 3. Prolonged irradiation apparently introduces a sizeable number of hole traps with an apparent depth of ~0.14 ev. That some of these hole traps are thermally annealable is indicated by the fact that a relatively short (~1 hour) low-temperature (~140°C) heat treatment increased the hole concentration and conductivity considerably and decreased the slope of the Hall coefficient curve to a value corresponding to ~0.12 ev.

It has been previously shown that vacuum heat treatment at ~500°C for Ge[9] and ~350°C for InSb[1]

[9] Cleland, Lark-Horovitz, and Pigg, Phys. Rev. 78, 814 (1950).

TABLE I. Initial behavior of carrier concentration in irradiated GaSb.

Sample	Type	Shielded	Original carrier concentration n_0 cm^{-3}	Temperature of exposure T, °C	Removal rate $-[dn/d(nvt)]_{t=0}$
I	p	No	14.25×10^{17}	37	2.57
II	p	Yes	12.95×10^{17}	46	1.40
III	p	No	2.59×10^{17}	42	0.68
IV	p	Yes	1.36×10^{17}	47	0.41
V	n	No	18.50×10^{17}	24	4.90
VI	n	Yes	12.30×10^{17}	41	2.97
VII	n	No	5.80×10^{17}	29	4.40
VIII	n	Yes	6.36×10^{17}	34	3.06
IX	n	No	6.71×10^{17}	−125	10.35
X	p	No	8.20×10^{18}	−128	1.26

removes essentially all fast-neutron-introduced donors and acceptors, leaving only those donor or acceptor atoms resulting from nuclear transmutations. The behavior of GaSb under similar treatment is more complicated. Curves IV of Fig. 2 might be interpreted as an indication that extended high-temperature vacuum anneal removes most of the irradiation-produced acceptors but all of the curves of Fig. 3, obtained after successive periods of vacuum anneal at increasing temperatures, indicate that a large number of additional holes are being introduced by some mechanism.

The purest GaSb currently available is p-type, with an initial carrier concentration of 10^{17} cm^{-3}, doping with Te being necessary to produce n-type material. A

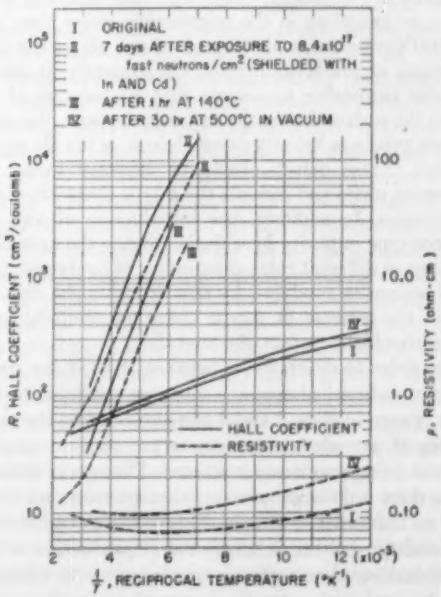
I ORIGINAL
II 7 days AFTER EXPOSURE TO 8.4x10¹⁷ fast neutrons/cm² (SHIELDED WITH In AND Cd)
III AFTER 1 hr AT 140°C
IV AFTER 30 hr AT 500°C IN VACUUM
HALL COEFFICIENT
RESISTIVITY
R, HALL COEFFICIENT (cm³/coulomb)
ρ, RESISTIVITY (ohm-cm)
1/T, RECIPROCAL TEMPERATURE (°K⁻¹)

FIG. 2. Hall coefficient and resistivity of p-type GaSb as a function of temperature. (I) Prior to irradiation, (II) after irradiation, (III) after 1 hour at 140°C, (IV) after 30 hr at 500°C in vacuum.

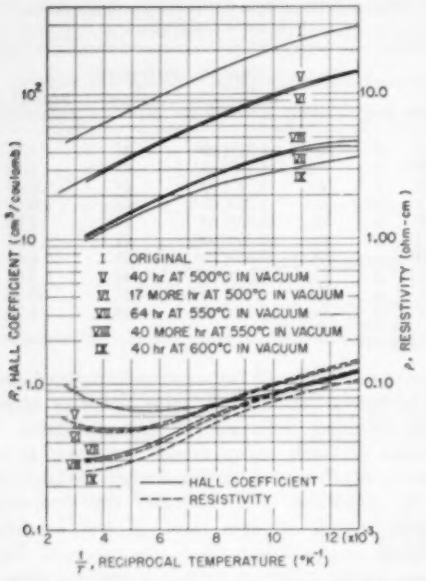
R, HALL COEFFICIENT (cm³/coulomb)
ρ, RESISTIVITY (ohm-cm)
I ORIGINAL
V 40 hr AT 500°C IN VACUUM
VI 17 MORE hr AT 500°C IN VACUUM
VII 64 hr AT 550°C IN VACUUM
VIII 40 MORE hr AT 550°C IN VACUUM
IX 40 hr AT 600°C IN VACUUM
HALL COEFFICIENT
RESISTIVITY
1/T, RECIPROCAL TEMPERATURE (°K⁻¹)

FIG. 3. Hall coefficient and resistivity of p-type GaSb as a function of temperature. (I) Prior to irradiation, (V–IX) after various heat treatments.

slight departure from true stoichiometry in the original melt, amounting to 1 part in 10^5 of Sb vacancies, has been suggested as the cause of this initial p-type character.[10] Moreover, Detwiler[11] has reported that vacuum annealing in the temperature range from 700 to 900°C resulted in the deposit of free Sb on the cool portions of the furnace tube. Consequently, it would appear reasonable to assume that evaporation of Sb from the surface during the successive anneals discussed above produces Schottky-type defects in the Sb superlattice. These defects would be expected to act as acceptor states and increase the p-type character of the specimens. In addition, the introduction of any acceptor-type impurity by diffusion during the annealing process or different rates of annealing of the interstitials and vacancies produced by irradiation might also explain the increase in p-type character resulting from extensive high-temperature annealing.

In order to differentiate between the various possibilities outlined above, a companion specimen to the one shown in Figs. 2 and 3 was subjected to the same series of extended high-temperature vacuum anneals wihout being previously irradiated. The results indicate that there is no large increase in acceptor concentration for an unirradiated sample. This seems to exclude the possibility of either Schottky defect production or the introduction of an acceptor-type impurity by diffusion as the explanation for the increased acceptor concentration, since these two processes should also be operative in unirradiated material as well. We therefore postulate that different annealing rates of the various irradiation produced interstitials and vacancies are responsible for the experimental results obtained here. This point will be examined in greater detail below.

The Hall coefficient and resistivity data for a typical n-type sample are shown in Fig. 4. The decrease in carrier concentration and conductivity as a result of irradiation indicates that electron traps are produced. That some of these electron traps are also thermally annealable is indicated by the fact that a 1.5-hour anneal at 110°C increased the carrier concentration and conductivity slightly. Curves IV and V, however, indicate that extended high-temperature vacuum anneal decreases greatly the net effective donor concentration of such material. This is presumably the same type of behavior as that observed on p-type samples, and is therefore also assumed to be caused by differential annealing of irradiation produced interstitials and vacancies. The net result of irradiation and heat treatment of n-type GaSb, therefore, is the production of material with a lower carrier concentration. Reirradiation further decreases the net effective donor concentration as is shown in Curves VI of Fig. 4 and Curves VII indicate again that some of the irradiation produced electron traps are thermally annealable.

The samples numbered V and VI of Fig. 1 and Table I were reirradiated after extended annealing. The results

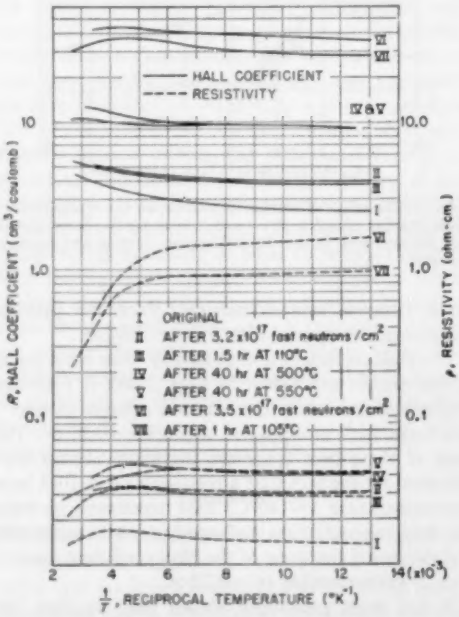
HALL COEFFICIENT
RESISTIVITY
R, HALL COEFFICIENT (cm³/coulomb)
ρ, RESISTIVITY (ohm-cm)
I ORIGINAL
II AFTER 3.2 x10¹⁷ fast neutrons/cm²
III AFTER 1.5 hr AT 110°C
IV AFTER 40 hr AT 500°C
V AFTER 40 hr AT 550°C
VI AFTER 3.5 x10¹⁷ fast neutrons/cm²
VII AFTER 1 hr AT 105°C
1/T, RECIPROCAL TEMPERATURE (°K⁻¹)

FIG. 4. Hall coefficient and resistivity of n-type GaSb as a function of temperature after various reactor irradiations and vacuum heat treatments.

[10] H. J. Hrostowski (private communication).
[11] D. P. Detwiler, Phys. Rev. 97, 1575 (1955).

are listed as samples VII and VIII of Table I. Figure 5 indicates that the conductivity of sample VIII passes through a minimum at an exposure of $\sim 1\times10^{18}$ fast neutrons cm^{-2}. Hall coefficient measurements after a total exposure of 1.6×10^{18} fast neutrons cm^{-2} reveal that conversion to p-type material has occurred. Moreover, the slope of the log ρ *vs* $1/T$ curve measured after exposure is quite steep in the room-temperature range, indicating a large ionization energy for the bombardment-produced acceptors (>0.2 ev), but is much decreased toward low temperature, revealing a wide range of acceptor energies.

Continued reirradiation and heat treatment, however, does not reduce the net effective concentration of electrons in n-type GaSb below $\sim 5\times10^{17}$ cm^{-3}, at least in the polycrystalline material used here. The original irradiation of Sample VIII of Fig. 5 was 4×10^{17} fast neutrons cm^{-2} and the decrease in net effective electron concentration after heat treatment was 6.2×10^{17} cm^{-3}. The second irradiation of 1.6×10^{18} fast neutrons cm^{-2} and subsequent heat treatment, however, reduced the net effective electron concentration by only 1.5×10^{17} cm^{-3}.

Fast-neutron irradiation decreases the mobility of both n- and p-type samples of GaSb, an effect that is similar to that previously observed for other semiconductors.[1,12,13] The effect of heat treatment after irradiation was to improve the mobility of the n-type samples, but each succeeding higher-temperature vacuum anneal decreased the mobility of the p-type samples still further below the decrease produced by bombardment. The apparent mobility of the n-type sample of Fig. 5 after conversion to p-type was only ~ 1 cm^2 volt^{-1} sec^{-1} at 300°K.

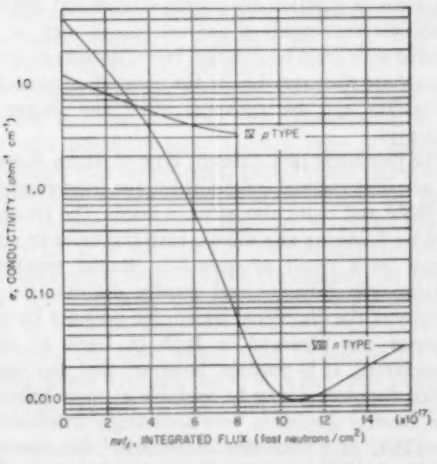

FIG. 5. The effect of reactor irradiation on the conductivity of an irradiated and heat-treated n-type sample of GaSb. The effect of reactor irradiation on the conductivity of a p-type specimen is also indicated.

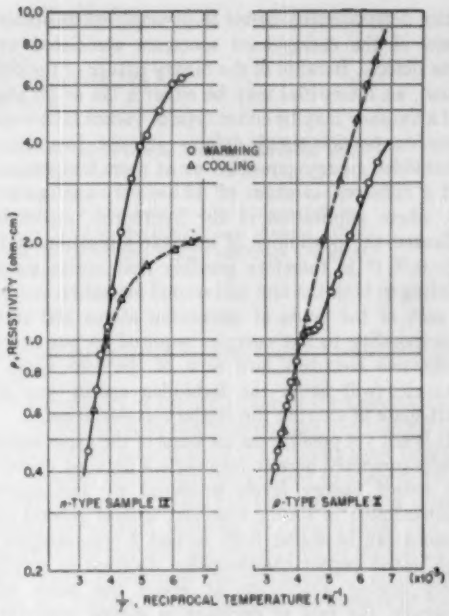

FIG. 6. Warming and cooling resistivity curves as a function of temperature of n- and p-type samples of GaSb after exposure to 3.5×10^{17} fast neutrons cm^{-2} at −125°C.

Two GaSb samples, one n- and one p-type, were irradiated at −125°C. The initial rate of carrier removal was increased at this temperature (samples IX and X of Table I) over the values observed for room-temperature exposure, indicating more efficient carrier-trapping. The behavior of resistivity as a function of temperature, obtained by warming and cooling in the reactor subsequent to the low-temperature exposure, is shown in Fig. 6. The resistivity at −125°C is increased by a factor of three for the p-type specimen and decreased by about the same factor for the n-type specimen as a result of thermal cycling. Furthermore, the resistivity of the p-type sample shows an interesting, almost discontinuous change in the range −60 to −40°C during the initial warm up which is absent in the cooling curve. These results indicate strongly that a group of electron traps which decrease the electron concentration in n-type material and which enhance the hole concentration in p-type material (by minority carrier trapping) are introduced by the low-temperature irradiation and that warming anneals the defects responsible for these traps well below room temperature. Similar indications of defects of low thermal stability have been obtained on n- and p-type Ge after low-temperature exposure.[12,13]

DISCUSSION

If it is assumed that the defects produced in GaSb by bombardment can be described in terms of simple

[12] Cleland, Crawford, and Pigg, Phys. Rev. **98**, 1742 (1955).
[13] Cleland, Crawford, and Pigg, Phys. Rev. **99**, 1170 (1955).

lattice defects, it is possible in principle to construct a model of the energy-level spectrum associated with these defects. Because of the binary nature of the compound, an interstitial may be either a Ga or Sb atom and a vacancy may be either type of vacant lattice site. Thus four possible simple defects can exist. In addition, a forbidden energy gap of 0.7 ev at room temperature[5] and a dielectric constant of[7] 14 are very analogous to Ge, where application of the hydrogenic model has indicated the possibility of multiple ionization of the defects.[14] It is therefore possible that states corresponding to both the first and second ionization energies of each of the types of interstitial atoms and states corresponding to the energies required to put successively two electrons into each of the two types of vacancies will lie in the forbidden energy gap and participate in altering the carrier concentration.

It is not yet possible on the basis of the experimental results presented here to formulate a detailed model of the defect energy levels produced by fast-neutron bombardment of GaSb; however, several general conclusions can be made. Both *n*- and *p*-type samples of high initial carrier concentration decrease in conductivity during irradiation at about the same rate. However, the rate of decrease in *p*-type material is strongly dependent on initial hole concentration whereas the rate of decrease in *n*-type material is not dependent on initial electron concentration. Moreover, one of the reirradiated *n*-type samples was converted to *p*-type by sufficient exposure. In view of these results, it appears that the electron traps are deep-lying and, if several such traps are present, at least one of them lies below the middle of the forbidden band and hence is capable of acting as an acceptor. In *p*-type material, on the other hand, the hole traps are apparently shallow, since the rate of hole removal is strongly dependent on the initial position of the Fermi level. The apparent depth of one of these hole traps is ~ 0.14 ev. In general, the behavior of GaSb is quite similar to that of Ge.

The complex annealing behavior of irradiated GaSb is not well understood. If it is assumed that the presence of interstitial atoms is indirectly responsible for the hole traps,[14] their removal or partial removal relative to vacancies would have the effect of increasing the net acceptor concentration in *p*-type and of decreasing the net donor concentration in *n*-type material. The mechanism of such a process is not very clear. However, clustering of interstitials, migration to dislocations, or grain boundaries are possible processes which might account for this behavior. Such effects have been observed to accompany low-temperature annealing (0 to 120°C) in bombarded Ge[15] and Mayburg[16] finds similar indications at higher temperatures (500 to 600°C) in quenched material.

There is a second possible mechanism for the increase in acceptor concentration resulting from exposure and subsequent heat treatment which requires the assumption that the Ga interstitial is much the more mobile defect. Hence, the Ga interstitials could recombine with either Ga or Sb vacancies with near equal probability. Although the Ga atom in the Sb site would increase the energy of the crystal and hence be a metastable configuration, the binding energy in such a position would be considerable. Such a process would have the result of increasing the total acceptor concentration by virtue of the two incomplete orbitals localized at that site. This explanation would not be valid if the Sb interstitials also had an appreciable mobility, since they would tend to distribute themselves indiscriminantly over the remaining vacancies and the donors produced by misplaced Sb atoms would be equal in concentration and cancel the effect of acceptors produced by misplaced Ge atoms.

Although it is possible to explain the annealing behavior of irradiated GaSb by either of these mechanisms, the saturation of the acceptor concentration increase, as evidenced by results obtained on annealing the reirradiated *n*-type specimens, remains puzzling. This can be understood only in terms of the first mechanism and then only if the interstitial sinks become nearly saturated by the first exposure and anneal. Such an explanation would probably rule out the possibility of interstitial clustering, since it is difficult to see how this process could be readily saturated. It should be remembered, however, that the specimens in question are polycrystalline and hence it is possible that much of the complexity may be associated with grain boundaries. Investigations on single crystals are necessary before the question of annealing mechanism can be answered with any degree of certainty.

The possibility of a different type of lattice damage, the so-called thermal-spike picture, has been suggested for InSb[1] and could also occur in GaSb. The resultant disorder following any atomic rearrangement or interchange as a result of quenching should provide a metallic-type behavior and greatly decrease the resistivity of the disordered region. No evidence for such behavior was observed in InSb or GaSb at room temperature. It is possible, however, that any superlattice disordering may be unstable at room temperature. Several specimens were accordingly irradiated at ~ -125°C to a total flux of $\sim 5 \times 10^{17}$ fast neutrons cm^{-2}, and again no electrical evidence for such an effect was observed for this length of exposure and temperature.

[14] H. M. James and K. Lark-Horovitz, Z. physik. Chem. **198**, 107 (1951).
[15] Cleland, Crawford, and Pigg (unpublished).
[16] S. Mayburg, Phys. Rev. **95**, 38 (1954).

Field Emission Microscopy of an Allotropic Transformation: α–β Titanium

ERNEST G. BROCK
General Electric Research Laboratory, Schenectady, New York
(Received July 26, 1955)

The field emission microscope has been applied to a study of the allotropic transformation in single microcrystals of titanium. Patterns with symmetry characteristic of the high and low temperature phases are presented. Techniques for analyzing the patterns are outlined. Data derived from the pattern analyses give an orientation relation between patterns of the two phases that is consistent with the Burgers relation. The field emission microscope thus constitutes a new method for direct observation of phase changes. At the same time, it offers to the study of allotropic transformations the advantages of high resolution and great magnification that are not available with conventional methods.

INTRODUCTION

THE field emission microscope is uniquely suited to the study of fundamental physical properties of solid materials.[1,2] Its high resolving power, 20 A, and great magnification, 10^6, permit single microcrystal samples less than 10^{-4} cm in diameter to be examined. Its patterns can be used to determine crystal orientation. It is sensitive to surface contaminants in concentrations equivalent to very small fractions of a monomolecular layer.[3] It offers relatively contaminant-free environment: total pressures of chemically active residual gases usually are less than 10^{-11} mm Hg and often as low as 10^{-14} mm Hg.[4] The entire temperature range from the sample melting point down to liquid helium temperatures is readily available for study.[5]

Application of the field emission microscope to a wide variety of problems and materials has been made.[1] Investigations include surface adsorption, desorption, diffusion, and catalysis; crystal structure and growth; and electron emission properties as influenced by crystal plane and contaminant. Materials include W, Mo, Ta, Nb, Pt, V, Ni, Fe, Cu, and Re.[6]

A problem that has not been studied with the field emission microscope is the direct observation of an allotropic transformation. Another type of emission microscopy that uses thermal electrons has had success in detecting phase transformation effects on grain growth in zirconium sheet.[7] However, magnified images of only 100 or so are possible. Observations are limited to a temperature range in which the sample gives thermionic emission. And the orientation of the crystals must be obtained from auxiliary experiments. Other less direct but more widely used techniques for observing phase changes, such as x-ray and electron diffraction, cannot offer the potentially high spatial resolution and magnification of the field emission microscope.[8]

The possibility of studying allotropic transformations in microcrystals with the field emission microscope was explored in the present work. The results show how the field emission microscope can be used to observe phase transformations in crystals of titanium; how a unique orientation relation between the two phases can be demonstrated and how the crystal can be studied in its intermediate forms as it changes phase.[9] A subsequent paper will discuss the crystallographic aspects of these observations in more detail.

EXPERIMENTAL APPARATUS

The field emission microscope used in these experiments is shown schematically in Fig. 1. It is a five-inch

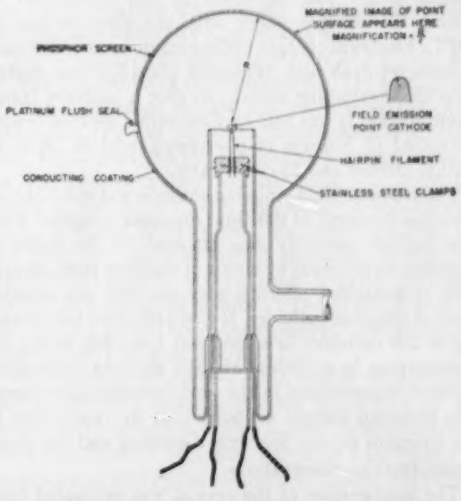

FIG. 1. Experimental field emission microscope in which the effect of phase transformations on the field emission patterns from titanium microcrystals is observed.

[1] E. W. Müller, Ergeb. exakt. Naturwiss. **27**, 290 (1953).
[2] F. Ashworth, Advances in Electronics **3**, 1 (1951).
[3] E. W. Müller, Naturwiss. **37**, 333 (1950).
[4] J. A. Becker, Bell System Tech. J. **30**, 907 (1951).
[5] R. Gomer and J. K. Hulm, J. Am. Chem. Soc. **75**, 4114 (1953).
[6] G. Barnes, Phys. Rev. **97**, 1579 (1955).
[7] W. G. Burgers, *Handbuch der Metallphysik* (Akademische Verlagagesellschaft, Leipzig, 1935), Vol. III, p. 280.
[8] C. S. Barrett, *Phase Transformations in Solids* (John Wiley and Sons, Inc., New York, 1951), p. 343.
[9] Preliminary discussion of this work has been given. See E. G. Brock and J. E. Taylor, Phys. Rev. **98**, 1169(A) (1955); E. G. Brock, Phys. Rev. **99**, 1651(A) (1955).

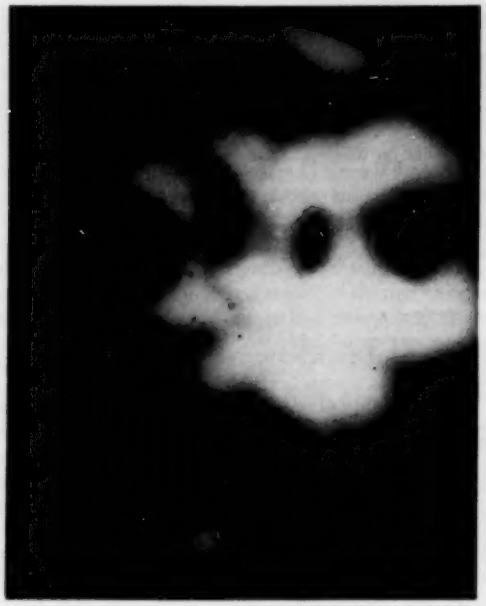

FIG. 2. Typical field emission pattern from titanium crystal that has not been heated above its transformation temperature. Pattern shows no long-range symmetry.

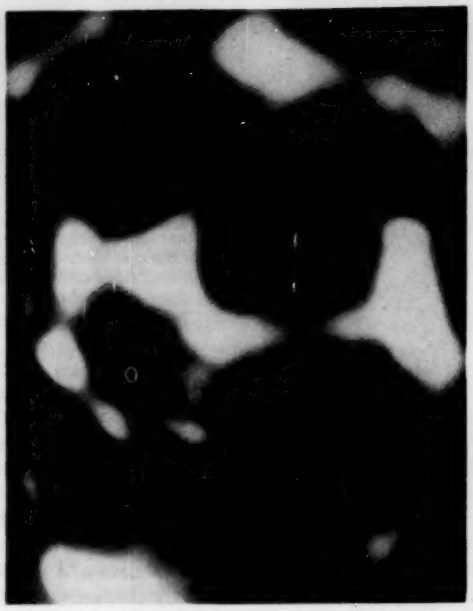

FIG. 3. Field emission pattern from titanium crystal that has been heated above its transformation temperature. Long-range hexagonal symmetry is discernible but imperfect.

diameter spherical Pyrex vacuum tube with a four-lead press. The inner wall of the sphere has a conducting coating which was deposited by the interaction of fuming tin chloride vapor with the glass surface at 500°C. Electrical contact to the outside is made through a platinum flush seal. Willemite phosphor was dusted onto the conducting surface to give a uniform translucent screen. It was held in place with a sprayed binder consisting of 5 drops of phosphoric acid in 75 cc of methyl alcohol and 25 cc of water.

The titanium field emission cathode was mounted on a hairpin filament of 0.010-in. diameter tungsten wire. The hairpin assembly was fastened to the 0.080-in. diameter nickel leads by a pair of stainless steel clamps. This arrangement afforded easy removal and replacement of titanium cathodes. It also permitted the mounting of the cathodes in a modified specimen holder for examination in a Philips® Metalix electron microscope between observations in the field emission microscope. The tungsten hairpin supplied heat by conduction to the titanium crystal for both degassing and for phase transformation observations.

The temperature of the crystal was estimated from the temperature-resistance tables of Jones and Langmuir,[10] corrected for lead losses.[11]

Centered about the titanium crystal and mounted on two other nickel leads was a one-turn ½-in. diameter spiral of 0.015-in. diameter tungsten wire. This spiral had two uses. During processing the wire supplied thermal electrons for electron bombardment degassing of the phosphor screens. During operation, the wire could be run at cathode or anode potential or at some intermediate value, so that magnification of the field emission pattern for constant electric field could be varied.

Titanium field emission cathodes were fabricated from an arc-melted ingot of commercially pure sponge titanium.[12] Small bars about 0.060-in. on a side were first cut from the ingot. These were turned uniformly round in a jeweler's lathe and then reduced to 0.010-in. diameter wires by chemical etching in 1 part concentrated hydrofluoric acid and 3 parts concentrated nitric acid by volume. The wires were spot welded to the apex of the tungsten hairpin loop in an atmosphere of helium. After clamping the hairpin filament to the stem leads, the titanium wire was sharpened to form a field emission cathode point of the order of 10^{-5}-cm diameter. This was done by electrochemical etching at 2 to 3 volts ac applied between the titanium wire and a platinum wire in the same reagents used for the chemical etching.

Standard high vacuum procedure[13] was followed in preparing the vacuum tubes for field emission observa-

[10] H. A. Jones and I. Langmuir, Gen. Elec. Rev. **30**, 310 (1927).
[11] Langmuir, MacLane, and Blodgett, Phys. Rev. **35**, 478 (1930).

[12] The titanium was generously supplied by J. B. Newkirk from samples on which measurements reported in reference 17 were made.
[13] S. Dushman, *Scientific Foundations of Vacuum Technique* (John Wiley and Sons, Inc., New York, 1949).

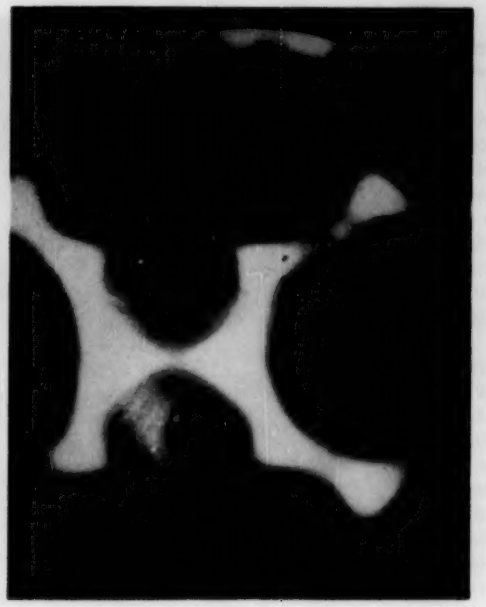

FIG. 4. High-temperature field emission pattern from titanium showing cubic symmetry.

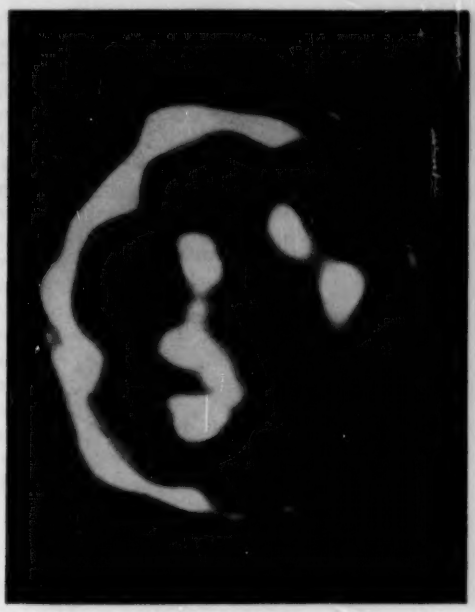

FIG. 5. Low-temperature field emission pattern from a titanium crystal that has been cooled in the presence of an electric field.

tions. The glass parts were baked at 425°C for several hours initially, and rebaked following degassing of all metal parts except for the tungsten filament and titanium cathode. When the residual pressure in the vacuum system had been reduced to 5×10^{-9} mm Hg or less, the hairpin filament was heated gradually to near but not above the transformation temperature of the titanium crystal mounted on it. The pressure was not permitted to exceed 5×10^{-9} mm Hg during this heating process or at any later time when the titanium crystal was hot. Field emission currents were then drawn from the crystal, and most field emission observations were conducted at pressures below 10^{-10} mm Hg on the continuously pumped system.

OBSERVATIONS

Field emission patterns from titanium crystals which have not been heated above the transformation temperature usually show some short-range symmetry. Figure 2 is a pattern typical of this early stage of treatment. However, prolonged heating below 850°C for as long as 200 hours in vacuum less than 1×10^{-9} mm Hg produces no improvement in symmetry. Only after a brief heat treatment at 1200°C or above do room-temperature patterns show improved symmetry. Even then the symmetry is imperfect (see Fig. 3).

If the electric field is applied when the crystal is at a temperature above 900°C, a pattern with long range cubic symmetry is observed, Fig. 4. A slow cooling of the crystal through its transformation temperature with the electric field applied often yields patterns such as Fig. 5, where one or more large areas having hexagonal symmetry are discernible. Further annealing, near the transformation temperature in an electric field, improves the symmetry of the pattern.

The hexagonal field emission pattern of Fig. 6(a) was obtained by following these procedures. The photograph of the field emission pattern was taken when the titanium crystal was just below the transformation temperature. Light from the hot supporting filament accounts for the asymmetrically located extra spot near the center of the pattern. The crystal axis coincides very nearly with the (00·1) pole. This is deduced from the fact that the center of sixfold symmetry is near the center of the pattern. Poles of other principal crystallographic planes may be obtained by comparison with an orthographic projection of these poles for the hexagonal-close-packed structure (see Fig. 7).

Upon heating this crystal to a higher temperature, part of the field emission pattern transforms by expansion and contraction of high current density emitting areas. Figures 6(b), 6(c), and 6(d) show a succession of these changes. Finally, at sufficiently high temperatures, patterns like that of Fig. 6(e) appear. This pattern has cubic instead of hexagonal symmetry. Comparison with an orthographic projection of the poles for a body-centered-cubic lattice establishes that the center of the pattern is a {110} pole (see Fig. 8). The other poles of this pattern may be found from their symmetry relations.

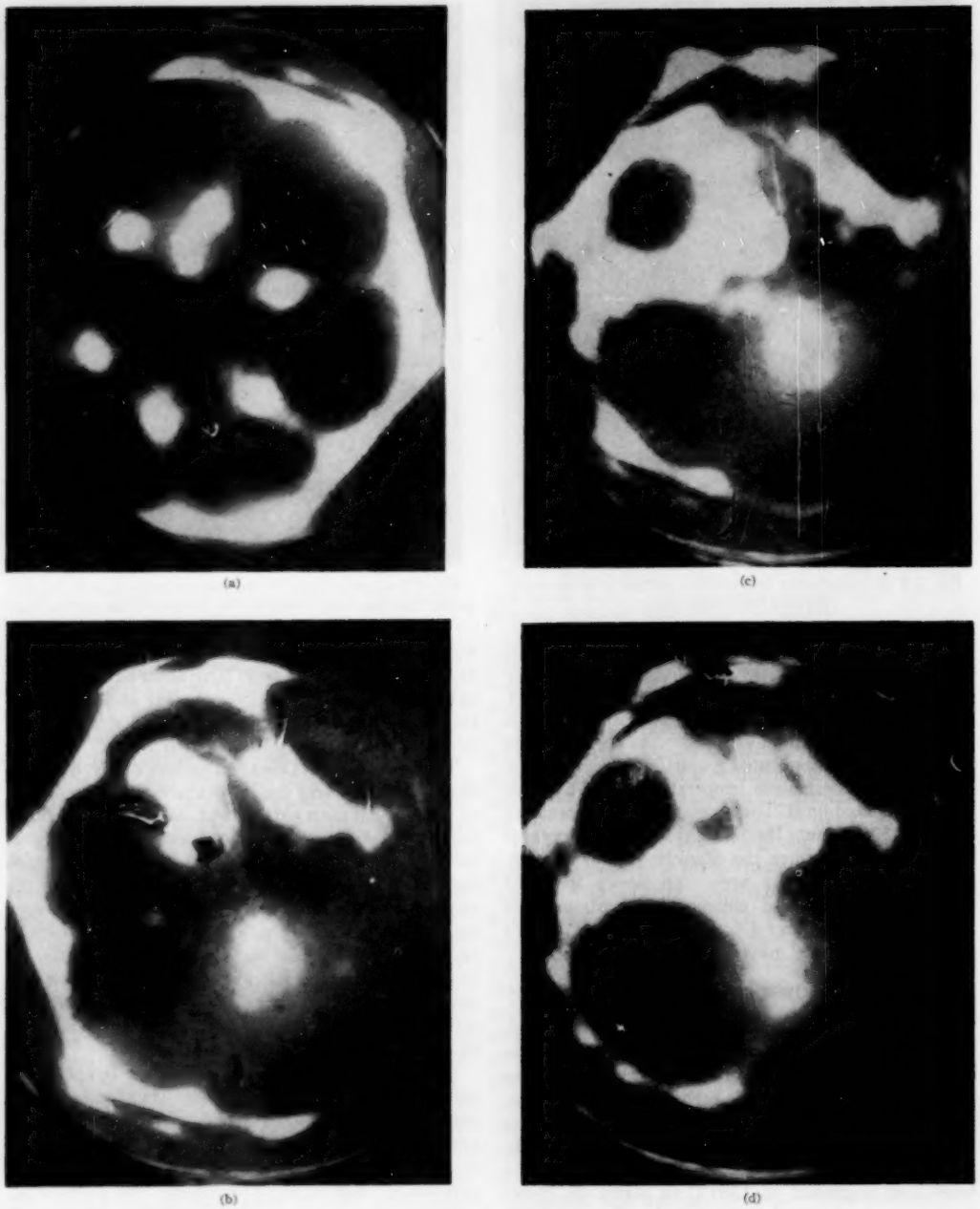

FIG. 6. Series of patterns for a titanium crystal that was heated through its transformation temperature with electric field applied. (a) Hexagonal pattern from crystal at temperature below 800°C. (b), (c), and (d) Patterns from crystal heated to successively higher temperatures. (e—on opposite page) Cubic pattern from crystal at termperature *circa* 1000°C.

ANALYSIS OF THE FIELD EMISSION PATTERNS

The poles of the field emission patterns were identified with the help of orthographic projections of the poles of the major crystallographic planes of titanium, Figs. 7 and 8. In the case of the hexagonal projection a ratio $c/a=1.587$[14] was used. It was found that the orthographic projection approximated more closely the field electron projection than the stereographic projection. This is so because the electrons, although emitted in a direction normal to the crystal, are accelerated subsequently in the forward direction by the electric field. However, the orthographic projection does not fit the patterns sufficiently well to be used to measure angular distances directly on the patterns.

A field emission pattern is analyzed by projecting its photographic negative with an enlarger onto a sheet of plain paper and drawing the boundaries of the high-intensity-emission areas. The size of the enlarged image is chosen to match the orthographic projections as closely as possible. Lines of symmetry, which correspond to zone lines in the crystal, are then sketched on the reproductions of the patterns. By using these zone lines and the orthographic projections the poles of Figs. 6(a) and 6(e) were located on their corresponding reproductions, Figs. 9 and 10.

Since each point on a field emission cathode surface corresponds uniquely to a point on its field emission pattern, the field emission patterns of Figs. 6(a) and 6(e), for example, may be used to map the poles of one phase onto the poles of the second phase. To make such a map, the crystal and the camera must remain fixed relative to the field emission vacuum tube. Frequently, however, transforming titanium crystals have been observed to move through large angles. In the case of the patterns of Figs. 6(a) and 6(e), the outline of the vacuum tube exactly matched when the two photographic negatives were placed one on top of the other, showing that the camera did not change position. Also, the boundaries of the field emission patterns matched when the two negatives were placed one on top of the other, showing that the crystal did not move.

To obtain the orientation relation between the two crystal phases from the field emission patterns, the tracings of the patterns, Figs. 9 and 10, with poles and zone lines drawn in, may be superimposed; or, the angular separations of the various poles may be estimated from the two reproductions and plotted on a single orthographic projection. This has been done in Fig. 11.

FIG. 6(e). Figs. 6(a)-(d) on opposite page.

[14] H. T. Clark, J. Metals 185, 588 (1949).

DISCUSSION

Results of the analysis of the titanium field emission patterns are interpretable in terms of the crystal properties of titanium. Titanium is a hexagonal-close-packed metal at room temperature. This alpha phase changes to a body-centered-cubic beta phase at 882°C.[15] Crystallographically, titanium is similar to zirconium. Generally, the relative orientation of the two crystal forms has been assumed to be the same as reported for zirconium.[16] Recent x-ray diffraction analyses of single-crystal hexagonal grains descended from a parent cubic crystal[17–19] have demonstrated that titanium obeys the zirconium orientation relation, namely:

- a $\{00\cdot1\}_\alpha$ hexagonal plane parallel to a $\{110\}_\beta$ cubic plane
- a $\langle11\cdot0\rangle_\alpha$ hexagonal direction parallel to a $\{111\}_\beta$ cubic direction.

Accordingly, a transformation scheme proposed originally by Burgers[16] for zirconium may apply to titanium.

This transformation scheme is illustrated by Fig. 12. In the upper left is a unit cell of the high-temperature body-centered-cubic beta form of titanium. The horizontal plane is a {110} plane. Four more unit cells may be combined to give a body-centered-tetragonal cell outlined with heavy lines. This cell is bounded laterally by {211} planes and on the ends by {110} planes. As the titanium crystal cools, the atoms move to new locations. The rearrangement process can be represented as a shear between {211} planes in a ⟨111⟩ direction. When

[15] C. J. Smithells, *Metals Reference Handbook* (Interscience Publishers, Inc., New York, 1949).
[16] W. G. Burgers, Physica 1, 561 (1933–34).
[17] J. B. Newkirk, Acta Met. 1, 370 (1953).
[18] Williams, Cahn, and Barrett, Acta Met. 2, 117 (1954).
[19] C. J. McHargue, Acta Cryst. 6, 529 (1953).

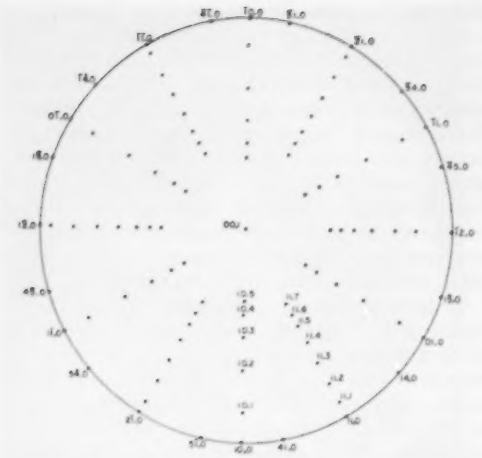

FIG. 7. (00·1) orthographic projection of poles of some major crystallographic planes of the hexagonal-close-packed phase in titanium. $c/a = 1.587$.

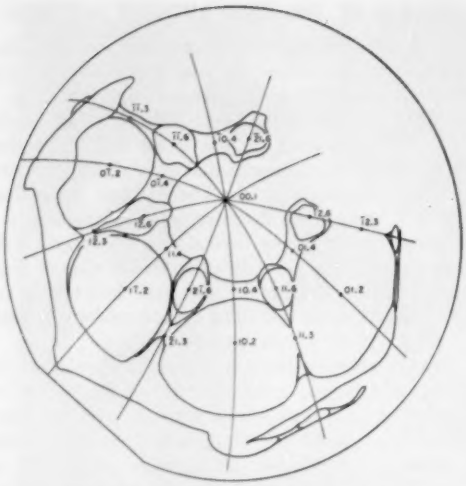

FIG. 9. Location of major crystallographic planes and zones of Fig. 6(a).

the transformation is complete, a unit hexagonal-close-packed alpha cell of the low-temperature phase of titanium results. Two modes of shear are illustrated in Fig. 12. The six-sided lattice cylinder in the lower left may be formed from three of these unit cells. If the crystal structure of titanium determines the symmetry of its field emission patterns, then the patterns from a transforming crystal should be consistent with the Burgers transformation scheme.

A discussion of field emission patterns, however, must recognize the influence of crystal structure and also the effects of surface contaminants and surface morphology on the appearance of the patterns. The generally accepted criterion for a clean metal field emission pattern is that the emission current density should vary gradually with crystal direction. The titanium patterns reported here do not have this characteristic.

Possibly the titanium surface was contaminated. Contaminated surfaces of other metal emitters frequently give patterns with sharply defined light and dark areas. The gas contaminants in the present experiments were those that constitute the residual pressure of 10^{-9} mm Hg or less in the field emission tube. Ion-

FIG. 8. (110) orthographic projection of poles of some major crystallographic planes of the body-centered-cubic phase in titanium.

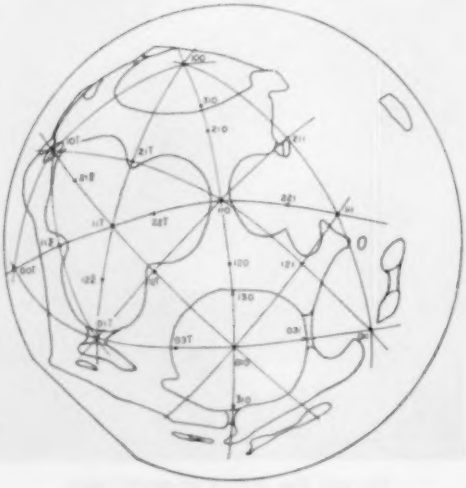

FIG. 10. Location of major crystallographic planes and zones of Fig. 6(c).

resonance mass spectrometer[20] measurements showed that N_2 was the main constituent. At the temperatures where the field emission patterns were photographed, nitrogen diffuses into the metal lattice.[21] Volume sorption together with the low partial pressures of contaminants make a contaminated titanium surface unlikely.[22]

An alternate possibility is that the titanium surface was not smooth but faceted. Tungsten field emission cathodes, when heated in the presence of an electric field to a temperature sufficient for surface migration to occur, give patterns which are attributed to the formation of edges and facets on the cathode. The intersecting boundaries of such facets are regions of smaller radii of curvature than the radius of the emitter tip. The resulting local field enhancement causes increased emission current density from those regions. In the limit, an emitter surface bounded by a few well-developed flat crystal planes would give a field emission pattern consisting of areas of low current density outlined sharply with boundaries of high current density. Since the titanium cathodes were heated while field emission current was being drawn, it is quite likely that they developed facets. Thus, facets could account for the abrupt variation of current density over the field emission pattern. They could account also for the hexagonal-shaped border which persists from the low temperature to the high temperature patterns [see Figs. 6(a) and 6(e)].

The assignment of poles to the high-temperature pattern of Fig. 6(e) or Fig. 10 could be made unambiguously. The symmetry was sufficient to determine the crystal orientation. However, the low-temperature pattern, Fig. 6(a) or Fig. 9, cannot be identified so easily. By using the argument that low-index planes generally are planes of low electron emission,[23] two sets of lines can be found each of which passes through centers of large nonemitting regions on the pattern. Their common point of intersection, of course, is a (00·1) pole. One set corresponds to the trigonal axes in the basal plane and the other set is rotated from it by 30° about the (00·1) pole. A choice between the two sets arrived at by correlating low emission planes with low index planes cannot be made conclusively. One set does meet the requirements of Burgers' orientation relation. This set was chosen as a basis for the assignment of poles to the hexagonal pattern.

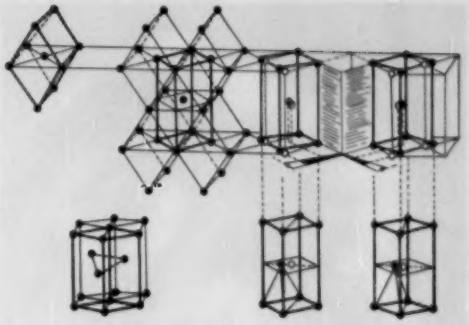

FIG. 12. Burgers' transformation scheme for titanium produces the required orientation relation between high-temperature body-centered-cubic beta phase and low-temperature hexagonal-close-packed alpha phase.

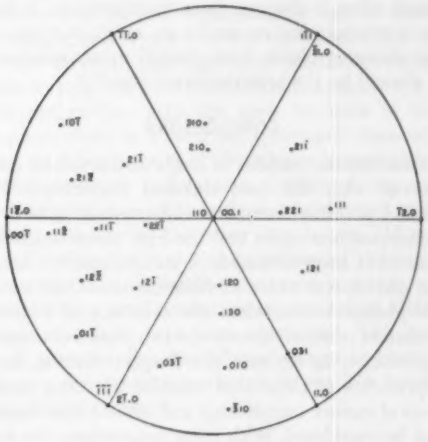

FIG. 11. Composite plot of the poles of the major crystallographic planes of the body-centered-cubic pattern identified in Fig. 10 with the trigonal axes found for the hexagonal-close-packed pattern of Fig. 9. The Burgers orientation relation is obeyed.

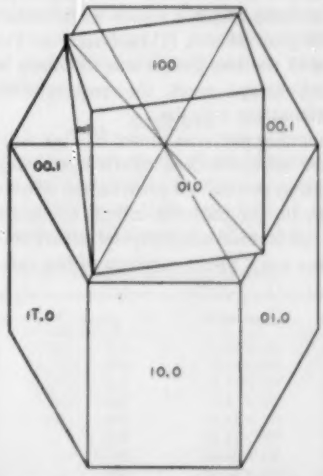

FIG. 13. Illustration of the orientation relation shown in Fig. 11 between the cubic and hexagonal phases of the titanium crystal that gave the series of field emission patterns Figs. 6(a) through 6(e).

[20] D. Alpert and R. S. Buritz, J. Appl. Phys. 25, 202 (1954).
[21] E. A. Gulbransen and K. Andrew, J. Metals 185, 741 (1949).
[22] See reference 1, p. 310.
[23] M. K. Wilkinson, J. Appl. Phys. 24, 1203 (1953).

FIG. 14. Field emission pattern from crystal that gave the patterns in Figs. 6(a) through 6(e) taken after crystal was returned from high temperature to room temperature. The original orientation and single crystal are preserved.

Within the accuracy to which the poles could be assigned, the analysis of the patterns shows that the $(00\cdot1)_\alpha$ pole became a $\{110\}_\beta$ pole when the crystal transformed. Furthermore, the positions of the 110 and 100 zone lines in the beta phase relative to the hexagonal axes in the alpha phase are such as to make a $\langle 11\cdot0\rangle_\alpha$ direction lie parallel to a $\langle 111\rangle_\beta$ direction. The relative orientation of the two phases was as shown in Fig. 13. These relationships meet the requirements of the Burgers orientation relation.

The remaining patterns shown in Figs. 6(b) through 6(d) can be interpreted as intermediate stages in the transformation process. At present, the effect of surface morphology on the patterns cannot be separated from the effect of transforming crystal structure. Possibly the patterns are a direct measure of the rate of transformation of the crystal. On the other hand, because of the influence of the electric field, the changes in the patterns may measure only the rate of change in physical shape of the surface. These latter changes could lag considerably the actual transformation of the bulk crystal. That the surface morphology can assume ultimately a symmetry consistent with the symmetry of the underlying crystal may be concluded from the initial and final patterns of this sequence, Figs. 6(a) and 6(e).

It is interesting to note that these patterns show one alpha crystal of titanium can transform to one beta crystal. Subsequently, the crystal was returned to room temperature, and the pattern in Fig. 14 was photographed. This pattern has the identical orientation of the initial hexagonal pattern. The transformation sequence illustrated by Figs. 6(a), 6(e), and 14 demonstrates that a crystal need not break up into several crystals when it changes phase. Furthermore, it shows that a crystal may return to its original orientation after changing pnase, even though other orientations are allowed by the orientation relation.[17,18]

CONCLUSIONS

Phase transformations in single microcrystals can be observed with the field emission microscope. Field emission patterns from titanium crystals in both the low temperature alpha and the high temperature beta phase have been obtained. A comparison of patterns from one crystal which at different times had been in both phases demonstrates the existence of a definite orientation relation between the two phases of titanium. This relation agrees with the Burgers relation. In the intepretation of these field emission patterns, possible effects of surface morphology and surface contaminants must be considered. With these precautions, the study of phase transformations in solids appears to be a feasible extension of field emission microscopy.

ACKNOWLEDGMENTS

The author would like to acknowledge several valuable discussions held with Dr. D. Turnbull, Dr. J. B. Newkirk, and Dr. J. E. Taylor. The work was initiated with Dr. J. E. Taylor.

Diffusion of Zinc in Single Crystals of Silver*

A. Sawatzky and F. E. Jaumot, Jr.
The Franklin Institute Laboratories for Research and Development, Philadelphia, Pennsylvania
(Received September 15, 1955)

The diffusion of Zn in Ag has been measured in the temperature range from 640°C to 925°C, using high-specific-activity Zn^{65} as a tracer. The data indicate that the diffusion coefficient is given to within 2% by the equation, $D=0.54\exp(-41\,700/RT)$ cm²/sec.

INTRODUCTION

In order to understand the basic mechanism involved in diffusion in metals, or alternately, in order to decide among the various theoretical explanations for the differences in diffusion rates in alloys containing the same base metal, it has become necessary to obtain data of considerably higher accuracy than much of that presently in the literature. It has been demonstrated recently[1] that data of high accuracy can be obtained by using single crystals of a monovalent cubic metal for the solvent, and high-specific-activity tracer as solute to keep the solute concentration small.

In conjunction with the need for data of higher accuracy, there is a need for systematic data on the effect on diffusion rates of the valence, atomic size, and crystal structure (interatomic forces) of the solute. The recent work cited[1] investigated the effect of valence, without considering the other two factors. Thus, the logical choice as a first step in increasing the accurate systematic data in the literature was a solute of the same valence and crystal structure but of different atomic size than that used previously. The present report gives the data for diffusion of zinc in silver, and supports the contention that it is possible to obtain data of high accuracy.

EXPERIMENT

Single crystals of silver (99.99% pure, obtained from Handy and Harman) were grown by using a modified Bridgeman technique. Particular attention was paid to obtaining crystals free from excessive substructure. Experience has indicated that it requires considerable care to obtain single crystals essentially free from dislocation boundaries; and it has been observed[2] that these boundaries materially affect diffusion rates, particularly at lower temperatures. Acceptable single crystals were cut into short cylinders, etched, formed accurately in the lathe on which they were to be sectioned later, lightly polished, etched, and annealed at 850°C for one hour to remove residual strains. After a final etch to check monocrystallinity, the ends of the specimens were plated on one end with high-specific-activity Zn^{65}, obtained from the Oak Ridge National Laboratory. The estimated thickness of the plated layer ranged from 20 to 200 A.

The specimens were then placed in pairs, with active faces together, in evacuated Vycor tubes. The specimens were held accurately in place in the tubes by Vycor rods welded to the tube walls, and thermocouples affixed to the tubes in positions corresponding to the diffusion interfaces. During the diffusion anneals, the temperatures of the furnaces were controlled by Celectrays with the variation at any sample not exceeding ±1°C.

After diffusion, 30 to 60 mils were removed from the sides of the cylindrical samples in order to eliminate edge effects. Uniform sections, 0.001 cm thick, were then removed using a precision jeweler's lathe, and the activity of each section determined with a thin mica end-window Geiger tube in a standard scaling circuit. The cuts were then weighed to check their thickness and finally, the total weight of all sections was compared with the known total amount removed from the sample. In the rare cases where these values did not agree, the weights were used as proportional thickness measurements and the activity determined as (counts/minute) per milligram, so that the specific activity is not affected by small losses of material during transfer. The entire counting geometry was, of course, accurately reproduced for each count and each section was "counted" at least twice.

RESULTS

Diffusion runs were made at six temperatures in the range from 640°C to 925°C, for times ranging from eight hours to slightly more than ten days. A linear curve was obtained, for all samples, when the logarithm of

Table I. Summary of data.

Sample	Temp. (°C)	Time (sec)	D (cm²/sec)
1	924	2.88×10^{4}	1.32×10^{-8}
2	924	2.88×10^{4}	1.28×10^{-8}
3	847	6.57×10^{4}	3.86×10^{-9}
4	847	6.57×10^{4}	3.84×10^{-9}
5	801	6.12×10^{4}	1.77×10^{-9}
6	801	6.12×10^{4}	1.73×10^{-9}
7	748	10.44×10^{4}	6.33×10^{-10}
8	748	10.44×10^{4}	6.44×10^{-10}
9	702	29.52×10^{4}	2.36×10^{-10}
10	702	29.52×10^{4}	2.43×10^{-10}
11	643	86.76×10^{4}	6.09×10^{-11}
12	643	86.76×10^{4}	5.88×10^{-11}

* This work was supported by the U. S. Atomic Energy Commission, Division of Research.
[1] See, for example, C. T. Tomizuka and L. Slifkin, Phys. Rev. 96, 610 (1954).
[2] F. E. Jaumot, Jr., and R. L. Smith, J. Metals (to be published).

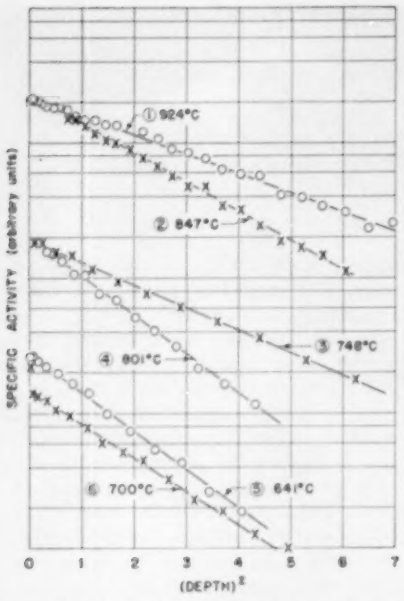

FIG. 1. Penetration-depth curves for diffusion of Zn in Ag. Scale factors: Curves 1 and 2—5×10^{-4} cm²; Curve 4—2.5×10^{-4} cm²; Curve 6—2×10^{-4} cm²; Curves 3 and 5—10^{-4} cm². In all cases, only every other section has been plotted, and in curves 2 and 4 the initial points have been omitted to avoid confusion.

the concentration was plotted against the square of the penetration distance, indicating little effect of any imperfections in the crystals. Typical concentration-depth curves are shown in Fig. 1. A "least-squares fit" of these data allowed the diffusion coefficient to be calculated directly. Table I summarizes the results for individual samples and Fig. 2 gives a plot of the logarithm of the diffusion coefficients as a function of the reciprocal of the absolute temperature.

DISCUSSION OF RESULTS

Inasmuch as the effects of any imprefections in the sample are magnified at low temperatures, the data at the higher temperatures should yield more accurate values of the activation energy, Q, and the frequency factor, D_0. On this basis, Q and D_0 were obtained from a least-squares fit of the data for the four highest temperatures (samples one through eight) and values of 41 690 cal/mole and 0.538 cm²/sec, respectively, were obtained. A least-squares fit of all the data gives $Q=41\,660$ cal/mole and $D_0=0.528$ cm²/sec. With an estimated probable error of $\pm2\%$ in D, $+0.5\%$ in Q, and $\pm10\%$ in D_0, the data can be represented, well within these errors, by

$$D=0.54\exp(-41\,700/RT)\ \text{cm}^2/\text{sec}.$$

The mean deviation of the individual points from the value given by this equation is 1.3%, with a maximum deviation of 2% (sample No. 11). The deviations are markedly reduced by using the more detailed values given above, but these are not warranted in view of the estimated accuracy of the measurements.

Since one of the primary motivations of the present diffusion program is to determine the effect of the atomic size of the solute on diffusion parameters, it is interesting to compare the results for Zn with those previously reported for Cd,[1] even though it is obviously impossible to draw conclusions from one comparison. Zinc is smaller in both atomic radius (based on distance of closest approach of atoms in the pure solid) and ionic radii than Cd, but has the same valence and the same

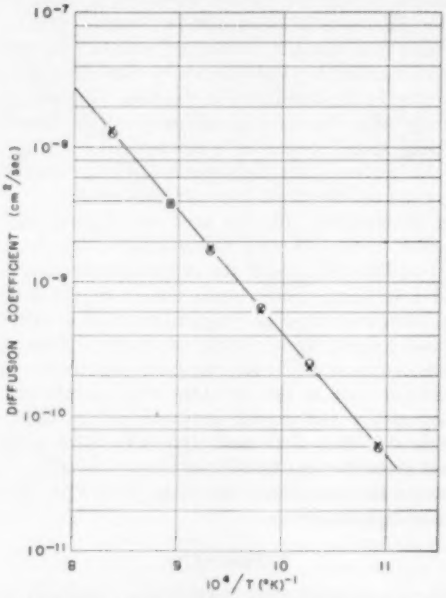

FIG. 2. The diffusion data plotted as log D *versus* $1/T$.

crystal structure. Tomizuka and Slifkin[1] give for diffusion of Cd in Ag

$$D=0.454\exp(-41\,700/RT)\ \text{cm}^2/\text{sec},$$

with the same estimated error as given for the present work. The indication, although far from conclusive, is that the atomic size has little effect on the activation energy, and certainly its effect is less than the effect of valence. On the other hand, it would seem that the frequency factor is affected, since it would require that the maximum error in both determinations be called into play in order to bring the two values of D_0 into coincidence. More work is needed to substantiate these very tentative conclusions.

The present work agrees with that of Tomizuka and Slifkin in that the values of D_0 and Q for solute diffusion are much nearer those for self-diffusion than has

generally been reported in the literature. Since these authors discussed this point in detail, there is no need to do so here.

Finally, calculating D_0 from Zener's theory[3] and using the value of the vibration frequency, ν, obtained from the Debye temperature for zinc, one obtains 0.537 cm²/sec. Similarly, using Nowick's method[4] for calculating Q from the highest-temperature data, one obtains 41 690 cal/mole. These values are in obviously fortuitous agreement with the experimental data.

[3] C. Zener, J. Appl. Phys. 22, 372 (1951).

[4] A. Nowick, J. Appl. Phys. 22, 1182 (1951).

PHYSICAL REVIEW VOLUME 100, NUMBER 6 DECEMBER 15, 1955

Amphoteric Impurity Action in Germanium*

W. Crawford Dunlap, Jr.
Electronics Laboratory, General Electric Company, Syracuse, New York

(Received May 31, 1955)

A new type of impurity action in germanium is described. This is "amphoteric" impurity action, to be contrasted with "donor" and "acceptor" action of the usual impurities in germanium. An amphoteric impurity, of which gold is shown to be an example, is an element that may either donate or accept electrons in the semiconductor, depending upon the nature and amount of other impurities present, that is, upon the position of the Fermi level as determined by these impurities. Previously the acceptor action of gold in germanium had been described, and it was shown there were two acceptor levels, 0.15 and 0.55 ev above the valence band. Morton, Hahn, and Schultz have found evidence of a third state which they interpret as the first acceptor level. In the present investigation, the existence of a third state is confirmed, and it is shown, with rather high degree of certainty, to be a donor level 0.05 ev above the valence band. This appears to be the first nonhydrogenic donor state yet observed in germanium. When gold is added to germanium containing third column elements in amounts less than the gold content, the carrier density remains constant, but the carriers acquire an ionization energy of 0.05 ev. Good agreement was obtained with several sources of gold. This behavior, it appears, can be explained most simply by assuming that neutral gold atoms may give up electrons to low-lying empty states to form Au^+. The upper gold states when filled are still interpreted as Au^- and Au^{--}.

INTRODUCTION

THE acceptor action of gold in germanium has been described in several papers.[1] In this work it was shown that gold was capable of taking up electrons at two energy levels, situated about 0.15 and 0.55 ev above the valence band. It was suggested that these levels were probably due to the formation of, first Au^- and then Au^{--}. These states were shown to be highly different in ionization energy from the states due to ordinary donor and acceptor impurities in germanium. Because of the great depth of these levels, a wide variety of new applications were opened up, including studies of trapping and secondary photoconductivity, and studies utilizing the high resistivity available at 77°K.

Morton, Hahn, and Schultz[2] have recently investigated the action of gold in germanium, and, in addition to confirming the existence of the above acceptor levels, have found evidence for a third state. They interpret their results as indicating an acceptor level 0.05 ev above the valence band, which takes up electrons to form Au^-. The upper two levels when filled with electrons would then be Au^{--} and Au^{---}.

There are several difficulties in accepting this interpretation of these results. In the first place, the original investigations[1] had indicated, with an accuracy somewhat better than 25%, that there were only two acceptors per gold atom, these levels being present in approximately equal numbers. Secondly, there is an intrinsic difficulty in assuming an Au^{---} center only 0.5 ev above the valence band. The electrostatic repulsion of the two electrons toward a third electron should be rather large.

Because of these difficulties, an investigation was made of the third gold level. This work confirmed the existence of such a level, but indicated that it was a donor level 0.05 ev above the valence band. With this change of interpretation, all the results were found to be consistent with previous studies on gold-doped germanium. Besides fitting in well with the finding of two acceptor states per gold atom, the new hypothesis agreed with previous results that when gold was added to pure germanium, the product was always p-type. This follows from the great depth of the donor level, and its inability to contribute directly to the number of conducting electrons. The state shows up only in p-type material, where it furnishes a supply of electrons for trapping holes, and for furnishing acceptor levels associated with re-excitation of holes back to the valence band.

* Work performed at General Electric Research Laboratory, Schenectady, New York.

[1] W. C. Dunlap, Jr., Phys. Rev. 91, 1282 (1953); 97, 614 (1955).

[2] Morton, Hahn, and Schultz, Atlantic City Photoconductivity Conference, November, 1954 (John Wiley and Sons, Inc., New York, 1956).

TABLE I. Segregation coefficients for gold and ordinary donor elements, showing concentrations of each donor required exactly to balance out possible acceptor levels of the gold. PPM refers to the required content of each element in the gold used for doping, in parts per million, that will give an electron concentration in the solid crystal, just equal to the gold content.

	Approximate segregation coefficient	PPM by wt to balance gold content in Ge
Gold	1.5×10^{-5}	...
Phosphorus	0.1	2.4
Arsenic	0.01	56
Antimony	0.001	860

In the previous studies of Morton, Hahn, and Schultz, the apparent presence of electrons was ascribed by them to accidental donor impurities in the added gold. In the present work, this hypothesis is ruled out by careful counting of states, and by the demonstration that different sources of high-purity gold lead to almost identically the same results. The effects observed in the present work could be accounted for by assuming the existence in the added gold of a donor impurity capable of furnishing in the germanium an electron density exactly equal (within a few percent) to the gold content. The probability of this occurring is so small that it can be ruled out.

EXPERIMENTAL METHODS

The methods used in the investigation were similar to those used in previous studies on gold. Single crystals were grown containing various quantities of gold and other impurities, and wafers for Hall and resistivity measurements were cut from selected portions of these ingots. Since the donor levels show up only in p-type material, the added impurity was usually gallium, added in various quantities up to and equal to the gold content in the crystal. An important assumption is made that the gallium content did not vary rapidly over a distance of about one-fourth inch, the distance required to obtain two wafers of, respectively, zero gold content, and known gold content.

The gold used came from two sources. The first, Johnson-Matthey spectrographically assayed gold, was the same as that used by Morton and his collaborators in their studies.[3] This gold was assayed as 99.999% pure, the analysis showing mostly traces of silver and copper. The second type of gold came from Sigmund Cohn, and was the gold mainly used by the author in his previous studies on gold-doped germanium. This material was assayed in the General Electric Research Laboratory and found to be comparable in purity with the Johnson-Matthey gold-again, silver and copper were found to be the important impurities. Because of the low sensitivity of the spectrograph for detection of phosphorus, arsenic, and antimony, no independent evaluation of the gold with respect to these impurities could be made. To give an electron density in the crystal just equal to the gold content, a donor element must be present in the gold exactly in the amount indicated in Table I.

[3] The author is indebted to Dr. G. A. Morton for a sample of this gold.

RESULTS

Figure 1 shows the properties of a sample of p-type gold-doped germanium grown as shown in the inset. After initial doping with gallium, the crystal was grown about one-half inch, when 100 mg Johnson-Matthey gold was added. Two Hall wafers were cut close to the point of doping, one before and the other after. The Hall curve of the wafer taken prior to the gold-doping shows little of interest below 77°K—there is a slow rise of Hall coefficient corresponding to the well-known ionization energy for gallium, 0.01 ev. The Hall curve for the gold-doped specimen, on the other hand, shows several interesting features:

(1) At the lowest temperatures, in the range of 30°K, the resistivity and Hall coefficient are very high, and drop with temperature at a rate indicating an ionization energy of about 0.05 ev.

(2) At saturation, (77°K) the Hall curve drops to almost exactly the level it had before the gold doping.

(3) Above 77°K, the Hall curve drops by an amount to be expected from previous results, as a result of the action of the lower acceptor level.

From (1) we confirm the existence of a third state of gold, as suggested by Morton, Hahn, and Schulz. It remains to be determined whether or not these apparent acceptor levels are due to an acceptor state of the gold, or are due to re-excitation of electrons (to the empty donor gold levels) that were trapped out by the gallium present. Item (2) is particularly pertinent in this res-

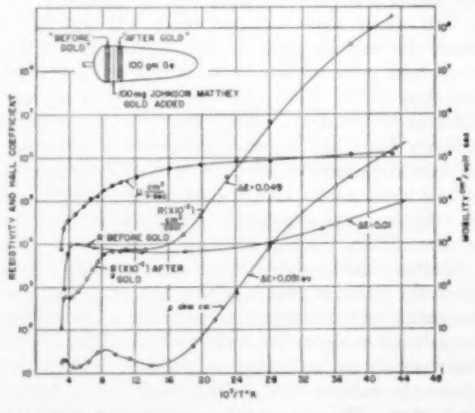

FIG. 1. Hall coefficient, resistivity, and Hall mobility of a sample of germanium doped with gallium and gold during growth of the single crystal. The large slope at lower temperatures indicates the presence of a state of energy about 0.05 ev. Also, the coincidence of the two Hall curves at 77°K is evidence for the donor level hypothesis, barring the occurrence of an extremely unlikely coincidence in which the gold would carry just exactly the required impurity donor content to balance out each and every gold center.

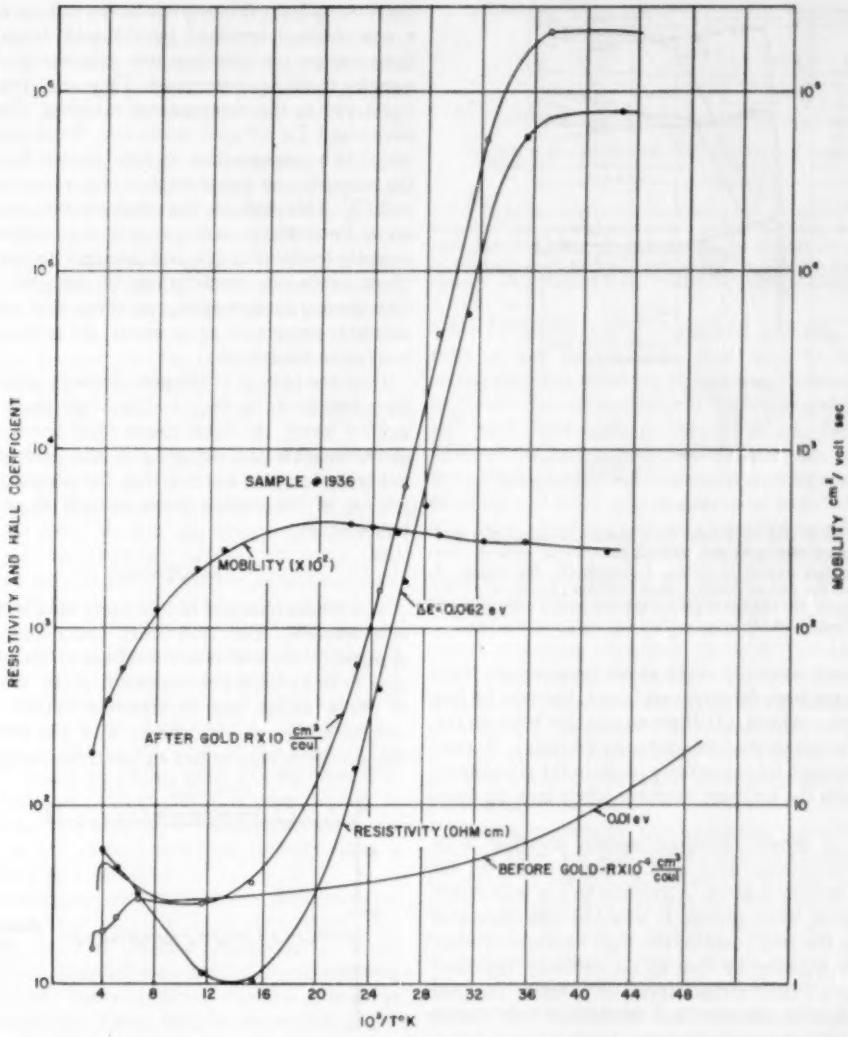

FIG. 2. Similar results to those of Fig. 1, on another sample, and with another source of gold. The conclusions to be drawn are the same as those of Fig. 1. The good agreement is added evidence against the occurrence of accidental donors in the gold.

pect. It shows that if each gold atom were contributing an acceptor level at 0.05 ev, there must be present exactly as many impurity electrons as gold atoms, in order to maintain the carrier content at 77°K equal to the original carrier content due to gallium.

Figure 2 shows results on a similar sample, made with another source of gold. The conclusions obtained from the study of this sample agree with those from Fig. 1. Because of the unlikelihood of the impurity content in gold from two independent sources being accidentally in the very narrow range required to produce the observed effects on the "gold-acceptor+impurity-electron" picture, the necessity of assuming that the gold states are donor levels becomes even more strongly apparent.

The samples of Figs. 1 and 2 show characteristics similar to those of copper- and zinc-doped germanium specimens. The mobility, for example, rises as the temperature is lowered, until a maximum is reached at about 50°K. Below this temperature, because of increased scattering by impurities and lattice imperfections, the Hall mobility tends to fall off slightly, or remain nearly constant. Another effect noticed in these as in other high-resistivity samples, is the leveling off

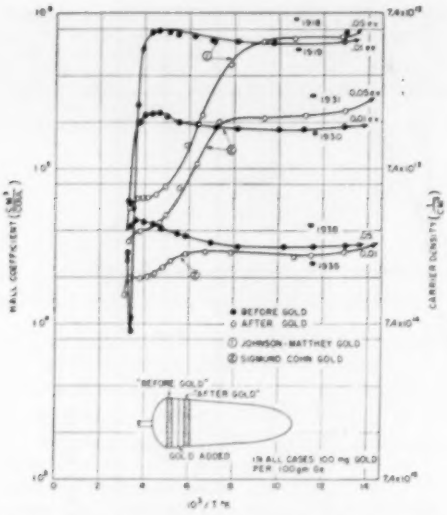

FIG. 3. Plot of Hall coefficient for a number of samples of germanium doped with gold and various amounts of gallium. The high-temperature region is shown, to emphasize the degree of constancy of the carrier density upon addition of gold, at 77°K. In several cases, the change of carrier density is only a few percent of the gold content added.

the Hall and resistivity curve at low temperature. This effect has not been definitely explained, but may be due to (1) surface effects, (2) direct conduction between the impurity levels themselves (impurity banding), (3) conduction through inhomogeneity paths in the germanium along which the ordinary acceptor levels may be dominant.

Figure 3 shows additional results obtained with samples containing fixed gold content, and with increasing gallium content. According to the gold donor level scheme, when gallium is added in concentrations exceeding the gold content, the high ionization energy should be replaced by that of the ordinary (gallium) states. At all intermediate levels of gallium, the gold levels should be effective, and the 0.05-ev level should be seen.

Figure 3 shows the high-temperature portion of the Hall curves of Figs. 1 and 2, with one additional curve for high gallium content. Because of the increased scale sensitivity, the changes in carrier density accompanying the addition of gold can be seen more easily than in the other figures. In the case of curves (1), the addition of gold changed the carrier density by only 3% of the gold content while in the other two cases the differences were less than 10%. In view of the uncertainties in doping experiments of this kind, and the possibilities of accidental addition of donors, the agreement with the donor model is good, as previously indicated.

The gold acceptor level density is determined from the high-temperature portions of these curves—between 77°K and room temperature. There the Hall curves drop from values given by the gallium density to a new value determined by the gold density. From these values the gold-acceptor densities in all three samples could be determined. They were found to be equal within the experimental accuracy. The values were about 2×10^{14} gold atoms/cm³. When gallium was added to a concentration slightly greater than 2×10^{14}, the resistivity no longer reached high values on cooling to 20°K. This confirms the rough equality in the number of lower states (0.05 ev) with the number of gold acceptor levels (0.15 ev), and indicates further that the donor levels are characteristic of the gold atoms in their normal configuration, not atoms that might have different properties as a result of some abnormal location in the lattice.

Thus the picture of the gold levels in germanium is that indicated in Fig. 4. The half-circles indicate unfilled levels, the filled circles filled levels. The diagrams indicate the emptying of the gold levels into low-lying acceptor states at low temperature, and the refilling of the various levels at each stage of rising temperature.

DISCUSSION

The results obtained in this study have a number of new features. The gold level under discussion is, apparently, the first donor level not of the hydrogenic type to be found in germanium. It is also the first case of donor action due to elements outside the fifth column of the periodic table, with the exception of lithium. Since lithium has an ionization energy of 0.01

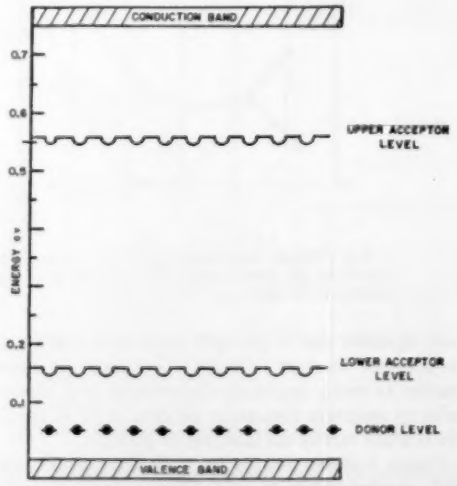

FIG. 4. Model of the gold center in germanium. These levels represent the energy of an electron added to a state containing −1, 0, and 1 electron, respectively, starting at the bottom. Thus the gold ion has the charge 0, −1, and −2, when the respective states are filled with electrons. When the lowest state is empty, the gold ion has the charge +1, so that the gold occurs in four ionic states in germanium.

ev, this case falls under the label "hydrogenic." The donor action of the gold may, as in the case of lithium, be ascribed to the single valence electron, in this case a 6s electron. It appears probable that gold can give up this electron to low-lying empty levels and thereby become Au^+.

Because of the low level of the donor state, it is not possible to see donor action directly due to gold in germanium, and the effects are seen only through the trapping action upon p-type germanium. When gold is added to pure germanium, the product is always p-type.

A second significant feature of the present result is that gold appears to be the first element in germanium that is capable of both donor and acceptor action in the same sample. Because gold has both an electropositive and electronegative character in Ge, the term "amphoteric" impurity element appears to describe it accurately.

When the sample, of say, Fig. 1 is heated from 0°K to room temperature, the gold levels initially possess the charge Au^+. As the temperature reaches 77°K, practically all the electrons that had been trapped by the gallium states are re-excited to the gold levels, and these become Au^0. On going to still higher temperatures, the electrons in the valence band have enough energy to be excited directly to the lower acceptor level and the gold becomes Au^-. An interesting feature of the model is that these electrons cannot come from the gold donor level, since the states have to be filled before the lower acceptor level exists, that is before the gold atoms are in a position to take up electrons at this energy. The sequence of events on adding gold, heating from 0°K to 77°K, and from 77°K to 298°K is shown in Fig. 5. Once again we see that at higher temperature the donor levels add no free carriers, and their primary effect is that of a trapping state.

The upper acceptor level, 0.2 ev below the conduction band, does not enter into any of the present data. Because of the onset of intrinsic conduction, it is not possible for an appreciable number of electrons to be excited into these levels—intrinsic conduction, in other words, restrains the Fermi level to the middle of the forbidden region.

The question remains as to the importance of the donor level in the statistical analysis of the p-type gold-doped specimens. It appears that no major extension of the work described in the previous paper is needed to account for the presence of this level. Nor is the closeness of the donor level to the valence band and to the lower acceptor level a problem, since for concentrations usually used in experiments of the present type, the excitation in the various regions is confined to separate temperature ranges—the ordinary donors are excited from 1°–20°K, the 0.05 level between 20° and 77°K and, the lower acceptor level between 77°K and 298°K. All that needs to be kept in mind is the availability of a supply of electrons at an energy level 0.05 ev above the valence band, and equal to the number of gold atoms.

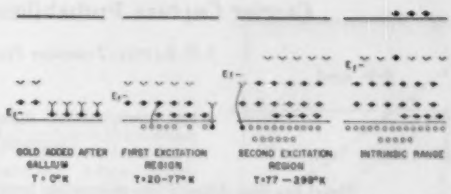

FIG. 5. Diagram showing the sequence of events in the various stages of the experiments shown in Fig. 1. Note that at any particular stage, only the level above that highest one containing an electron exists. As each level in turn is filled the next highest appears. This diagram is not to scale, in terms of energy.

We have seen that in germanium gold may take on, even at low temperatures, four different ionization states, and that there are three energies corresponding to the addition of electrons to the single positive, neutral, and single negative charged states. Besides the different ionization energies, these states are characterized by highly different capture cross sections for electrons and holes—the empty donor level being more selective in capturing electrons, the filled acceptor levels more selective in capturing holes, because of their Coulomb forces. Further studies on the properties of the various states are now in progress.

The results obtained on germanium now appear consistent with those on silicon, in which Taft and Horn[4] found a donor level 0.35 ev above the valence band. This level is probably similar in nature to the donor level in gold-doped germanium. The present work on germanium also makes it appear likely that a search will reveal acceptor levels in gold-doped silicon analogous to those found for germanium.

There also remains the interesting question as to whether there are such donor states of elements other than gold in germanium. Low-lying donors are rather difficult to show up, since they produce no direct effects as donors, but only as trapping centers for holes. It appears quite possible that a search among the transition elements, which have been shown to produce acceptor levels like gold in germanium, may also show up one or more donor levels for these elements.

Also of interest are the other elements of the gold group, particularly copper, platinum, and the other noble metals, such as rhodium and iridium. Previous work on platinum indicated the presence of an acceptor level at 0.04 ev above the valence band, and 0.2 ev below the conduction band. There seems some question as to whether or not the lower of these states might be, in actuality, a donor level as in the case of gold.

ACKNOWLEDGMENTS

The author wishes to acknowledge with thanks the help of Dr. W. W. Tyler in obtaining the low-temperature data.

[4] E. A. Taft and F. H. Horn, Phys. Rev. 93, 64 (1954).

Carrier Capture Probabilities in Nickel Doped Germanium*

J. F. BATTEY, *Transistor Products, Inc., Waltham, Massachusetts*

AND

R. M. BAUM, *Sylvania Electric Products, Woburn, Massachusetts*

(Received August 22, 1955)

Nickel has been diffused into germanium in order to study the carrier capture probabilities of the two nickel acceptor levels. Measurements of minority carrier lifetime as a function of temperature show that the electron capture probability of low-resistivity p-type samples is temperature-independent. The electron capture probability of high-resistivity p-type samples increases exponentially with increasing temperature, as does the hole capture probability of high-resistivity n-type samples. Possible interpretations of the results are discussed.

I. INTRODUCTION

IN a previous publication[1] we have discussed the recombination of minority carriers in germanium through the agency of recombination levels. The levels were introduced into the forbidden energy gap by copper atoms in the germanium lattice. The expression for the electron lifetime that is pertinent to this work has been given as[2]

$$\tau_n=\frac{(1/C_p)(n_0+n_1)+(1/C_n)[p_0+p_1+N_t(1+p_0/p_1)^{-1}]}{n_0+p_0+N_t(1+p_0/p_1)^{-1}(1+p_1/p_0)^{-1}}, \quad (1)$$

where N_t is the density of recombination levels; C_p is the product of the trap density and the probability per unit time of an individual trap capturing a hole, averaged over the holes in the valence band; C_n is the product of the trap density and the probability per unit time of an individual trap capturing an electron, averaged over the electrons in the conduction band; n_0 and p_0 are the equilibrium electron and hole densities; and n_1 and p_1 are the values the equilibrium electron and hole densities would have if the Fermi level were located at the same position in energy as the recombination traps.

In a copper-doped sample, the recombination proceeds through the upper acceptor level located 0.30 ev above the top of the valence band. In this instance C_p is known to be much larger than C_n. If the sample is doped in such a fashion that the upper copper level is partially populated, then the term in the numerator of (1) involving $1/C_p$ is negligible compared to the one involving $1/C_n$. Since n_0 in the denominator is small compared with p_0, $\tau_n \simeq 1/C_n f_{p1}$, where f_{p1} is the probability that the upper copper level is empty. When the carrier concentration is small compared to N_t, then f_{p1} is virtually constant, and the temperature dependence of C_n is given by the reciprocal of the lifetime. A study of τ_n vs temperature showed that the principal temperature dependence of C_n is $\exp(-E/kT)$, where $E=0.22$ ev. The proposed interpretation of this result was that only electrons of energy greater than 0.22 ev above the bottom of the conduction band can get into the traps.

In this paper, we wish to present evidence that similar phenomena occur in nickel-doped germanium. The selectivity in the electron capture process may be due to a Coulombic repulsion between the negatively charged acceptor sites and the incoming electrons. Evidence is also obtained for qualitatively similar selectivity in the hole capture process by nickel atoms. The explanation in this instance cannot be due to Coulombic repulsion.

It has been shown that nickel introduces two acceptor levels in germanium, one at 0.22 ev above the top of the valence band,[3-5] the other at 0.30 ev below the bottom of the conduction band.[3] It is not clear whether the upper level exists at its observed energy before the lower level is filled, or whether the lower level exists at

TABLE I. Sample properties before and after nickel diffusion. The nickel atom concentration was calculated by locating the Fermi level, F, from the experimental carrier concentration determined at a suitable temperature. The carrier concentration was equated to $2(2\pi mkT/h^2)^{\frac{3}{2}}\exp[-(E_c-F)/kT]$ for n-type samples, and $2(2\pi mkT/h^2)^{\frac{3}{2}}\exp[-(F-E_v)/kT]$ for p-type samples, where E_c is the bottom edge of the conduction band and E_v is the top edge of the valence band. The population of the nickel levels was next calculated. The nickel atom concentration was then obtained from the carrier concentration before and after nickel diffusion.

	Before nickel diffusion		After nickel diffusion		
Sample	N_D-N_A (cm^{-3})	τ_{hi} (μsec) at room temperature	τ_{hi} (μsec) at room temperature	Nickel atom concentration (cm^{-3})	Diffusion temperature (°K)
BB-10	8.0×10^{14}	10	0.20	4.4×10^{16}	1010
BB- 8	5.4×10^{14}	150	0.25	3.0×10^{16}	990
BB-12	7.9×10^{13}	45	2.0	3.7×10^{15}	920
BB- 6	1.0×10^{13}	180	0.60	1.1×10^{15}	1033
BB- 3	9.3×10^{14}	140	0.20	9.8×10^{16}	1005
BB- 7	N_A-N_D 4.5×10^{16}	20	0.60	1.8×10^{16} [a]	962

[a] Obtained from reference 5.

* This work was begun at Sylvania Electric Products, Ipswich, Massachusetts.

[1] R. M. Baum and J. F. Battey, Phys. Rev. **98**, 923 (1955).

[2] W. Shockley and W. T. Read, Jr., Phys. Rev. **87**, 835 (1952).

[3] Tyler, Newman, and Woodbury, Phys. Rev. **98**, 461 (1955).

[4] Burton, Hull, Morins, and Severiens, J. Phys. Chem. **57**, 853 (1953).

[5] F. van der Maessen and J. A. Brenkman, Philips Research Repts. **9**, 225 (1954).

its observed energy after the upper level is filled. It is not presently known for a given resistivity and temperature whether the recombination goes predominantly through the upper or lower nickel level. However, if the recombination goes through a negatively charged atom, C_n should vary exponentially with temperature. If the recombination goes through an uncharged atom, no temperature dependence of C_n would be expected.

II. SAMPLE PREPARATION

It has been shown that nickel diffuses very rapidly in germanium at elevated temperatures.[3-6] 99.99% pure nickel was electroplated on the germanium samples, which were then sealed in evacuated vycor capsules. The nickel was diffused into the germanium by holding the samples at an appropriate temperature for such a time as to closely approximate the solubility limit of nickel in germanium[3] throughout the sample. Thereafter the samples were quenched. The concentration of nickel introduced into the various samples referred to in this paper is shown in Table I.

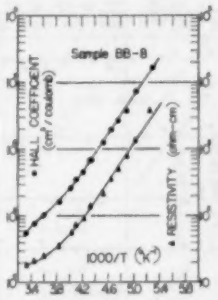

FIG. 1. Resistivity and Hall coefficient as a function of temperature for a high-resistivity n-type nickel-doped germanium sample.

In samples that were strongly p-type before diffusion due to group III acceptor doping, the introduction of nickel leads to no perceptible change in carrier concentration, as indicated by Hall coefficient and resistivity measurements. In samples that were originally n-type due to group V donor doping, the carrier concentration decreased and in some instances converted to p-type with the introduction of nickel.

Samples that were changed to high-resistivity n-type showed the existence of an acceptor level approximately 0.30 ev below the bottom of the conduction band, as is evident from Fig. 1. This is in agreement with the results of Tyler *et al.*[3] The concentration of nickel was calculated for such samples from the carrier concentration before and after diffusion under the presumption that each nickel atom introduces two acceptor levels, one or both of which are filled.

For samples that were converted to high-resistivity p-type, Hall coefficient and resistivity data showed the existence of an acceptor level approximately 0.22 ev above the top of the valence band in agreement with previous measurements.[3-6] This is shown in Fig. 2. In these samples the concentration of nickel was

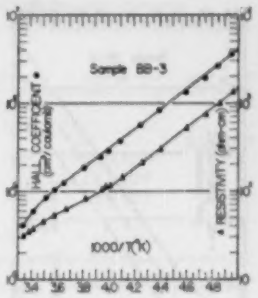

FIG. 2. Resistivity and Hall coefficient as a function of temperature for a high-resistivity p-type nickel-doped germanium sample.

calculated from the carrier concentration before and after nickel diffusion by assuming that each nickel atom accepts either one or no electrons. The solubilities calculated in this fashion agree within better than a factor of two with the data published by van der Maessen and Brenkman.[5] The small discrepancies are probably due to the lack of precise knowledge of sample temperature during diffusion.

The acceptor concentrations introduced were small compared to the solubility of copper. Also, the lifetime of the material following the heat treatment was much too short to be attributed to copper atoms in concentrations that are consistent with the observed resistivity changes, or even with the solubility limit of copper at the diffusion temperatures in question. For all samples that are discussed in this paper, the room temperature lifetime was reduced by more than an order of magnitude by the nickel doping.

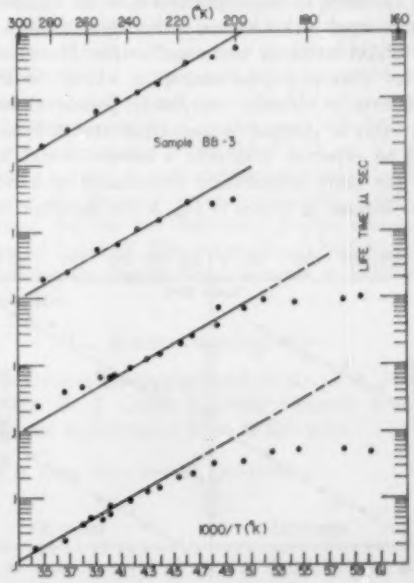

FIG. 3. Electron lifetime as a function of temperature for the high-resistivity p-type nickel-doped germanium sample for which Hall coefficient and resistivity data are shown in Fig. 2.

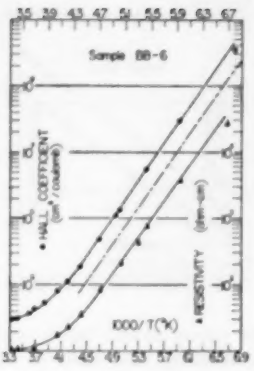

FIG. 4. Resistivity and Hall coefficient as a function of temperature for a high-resistivity p-type nickel-doped germanium sample which presumably also contains a small amount of copper. The broken line indicates the theoretically calculated slope of the carrier concentration for a sample that contains 1.0×10^{13} group V donors, 1.1×10^{13} nickel atoms, and 1.1×10^{14} copper atoms per cm^3.

III. RECOMBINATION PROCESSES

A. p-Type Samples

Figure 3 shows plots of electron lifetime *vs* reciprocal temperature for the p-type sample for which Hall coefficient and resistivity data are shown in Fig. 2. The method of lifetime measurement has been previously described.[1] If it is again presumed that the first term in the numerator of Eq. (1) is small compared to the second term, then, as in the copper case, C_n has the temperature dependence of $1/\tau_n$. It will be seen that again C_n varies as $\exp(-E/kT)$, with E approximately 0.23 ev. If Coulombic repulsion is to provide the explanation for the exponential temperature dependence of C_n, then it must be presumed that the electrons are being captured in the upper nickel levels by already singly charged nickel atoms, rather than through the lower nickel levels by uncharged atoms. It would be expected that a p-type sample in which the lower nickel level is virtually completely populated has a larger ratio of charged to uncharged atoms. Hence it would be expected that such a sample would again show the same temperature dependence of minority carrier lifetime as is seen in Fig. 3. On the other hand, for very p-type samples the lower nickel level is virtually empty, and the nickel atoms are uncharged. In this case, one would not expect any temperature dependence of C_n due to Coulombic repulsion between the nickel atoms and electrons about to be captured. For sufficiently p-type samples, the lifetime is equal to $1/C_n$, as can be seen from Eq. (1). However it may be that the C_n in this instance is to be associated with the lower nickel level.

In Fig. 4, Hall coefficient and resistivity curves are shown for a sample which approximately fulfills the requirement of having the lower nickel level completely populated. The Hall coefficient curve shows an activation energy of about 0.26 ev. All other high-resistivity p-type samples showed an activation energy of 0.22 $\pm$0.01 ev. The higher activation energy of 0.26 ev is what would be expected if a small amount of copper were introduced into the sample in addition to the relatively large amount of nickel, and further, if the group V donor concentration was sufficient to partially populate the upper copper level and nearly completely populate the lower nickel level. Figure 5 shows plots of electron lifetime *vs* reciprocal temperature for this sample. The anticipated exponential dependence of lifetime on reciprocal temperature is observed.

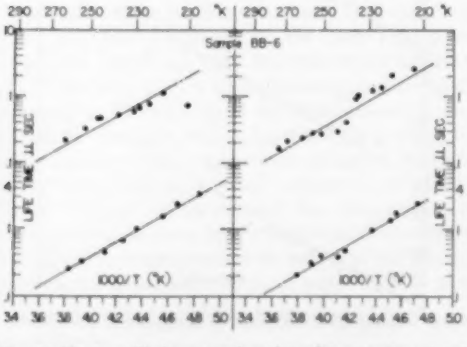

FIG. 5. Electron lifetime as a function of temperature for the high-resistivity p-type nickel-doped germanium sample for which resistivity and Hall coefficient data are shown in Fig. 4.

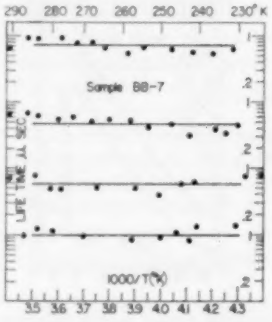

FIG. 6. Electron lifetime as a function of temperature for a low-resistivity p-type nickel-doped germanium sample.

For sufficiently p-type samples in which the lifetime is equal to $1/C_n$, the lifetime becomes independent of carrier concentration. It can be seen from the work of Burton *et al.*[4] that a sample with a room temperature hole concentration of 4.5×10^{15} cm^{-3} is sufficiently p-type for this to be true. Consequently, for such a sample τ_n equals $1/C_n$. Plots of lifetime *vs* reciprocal temperature after nickel doping are shown for a sample of this carrier concentration in Fig. 6. It will be seen that within the accuracy of the data, C_n, is temperature-independent. Inasmuch as there is no Coulombic repulsion between the uncharged nickel atoms and the recombining electrons, this is the result to be expected in the absence of other effects which would selectively favor the recombination of electrons of certain energies. Presumably, in this instance, the recombination is going through the lower nickel level.

B. *n*-Type Samples

Some additional measurements of lifetime *vs* temperature have been made on *n*-type samples similar to the one for which Hall coefficient and resistivity data are shown in Fig. 1. Representative lifetime data on a number of samples are shown in Fig. 7. It will be noticed that the lifetime decreases exponentially as the temperature increases. The hole lifetime in a *n*-type sample whose recombination is dominated by a single energy level is given by[2]

$$\tau_p=\frac{(1/C_n)(p_0+p_1)+(1/C_p)[n_0+n_1+N_t(1+n_0/n_1)^{-1}]}{n_0+p_0+N_t(1+n_0/n_1)^{-1}(1+n_1/n_0)^{-1}}. \quad (2)$$

Hall coefficient and resistivity measurements taken as a function of temperature show that the dominant term in the denominator, over the temperature range of interest, is $N_t(1+n_0/n_1)^{-1}(1+n_1/n_0)^{-1}$. If it is assumed that the first term dominates the numerator of (2) and the known temperature dependences of the various factors are used, it would be expected that τ_p would show a strong exponential increase with increasing temperature. This is the behavior exhibited by most germanium samples.[6] Since this is not what is observed in this instance, it must be assumed that the second term in the numerator is dominant. Then, it is expected that $\tau_p \simeq (1/C_p)(1+n_1/n_0)$. In the temperature range of interest, $(1+n_1/n_0)$ is only weakly temperature-dependent. Consequently, the temperature dependence of τ_p gives the temperature dependence of $1/C_p$. The suggestion is again advanced that C_p increases exponentially with increasing temperature because only holes of energy less than a certain critical value can enter the recombination traps. The critical energy as obtained from the slopes of the lifetime *vs* reciprocal temperature curves shows appreciable differences on samples which are presumed to be similar and even on different regions of the same sample. The values range from 0.18 to 0.28 ev with a probable error of about 0.03 ev. The source of these discrepancies is not understood. It is clear that no Coulombic barrier will exist for holes approaching negatively charged nickel atoms. It is possible that only holes from the branch in the valence band derived from atomic p^1 states are entering the nickel levels. From the analysis of infrared absorption data in *p*-type samples, Kahn[7] concludes that this branch lies a minimum distance of approximately 0.30 ev below the top of the valence band.

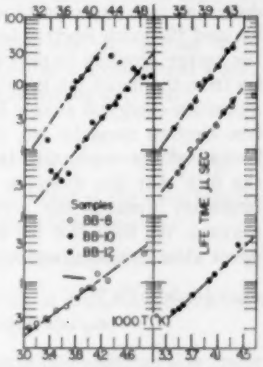

FIG. 7. Hole lifetime as a function of temperature for high-resistivity *n*-type nickel-doped germanium samples similar to the sample for which resistivity and Hall coefficient data are shown in Fig. 1.

TABLE II. Electron and hole capture constants.

Sample	Nickel atom concentration (cm^{-3})	c_{n0} ($cm^3 sec^{-1}$)	c_{p0} ($cm^3 sec^{-1}$)	c_n ($cm^3 sec^{-1}$)
BB– 3	9.8×10^{14}	4.2×10^{-6}		
BB– 6	1.1×10^{15}	6.5×10^{-6}		
BB– 7	1.8×10^{14} [a]			9.2×10^{-9}
BB– 8	3.0×10^{14}		2.6×10^{-8}	
BB–10	4.4×10^{14}		2.4×10^{-8}	
BB–12	3.7×10^{15}		1.7×10^{-8}	
Copper-doped[b]		6.4×10^{-6}		

[a] Obtained from reference 5.
[b] See reference 1.

The experimental data indicates that the temperature dependence of the electron capture probability for high-resistivity *p*-type samples can be approximately represented by $C_n=N_t c_{n0}\exp(-E_1/kT)$, with $E_1=0.23$ ev. Similarly, the temperature dependence of the hole capture probability for high-resistivity *n*-type samples can be represented by $C_p=N_t c_{p0}\exp(-E_2/kT)$, with E_2 usually appearing to be about 0.28 ev. Values of c_{n0} and c_{p0} together with the temperature-independent value of the electron capture probability, $c_n=C_n/N_t$, obtained for the low resistivity *p*-type sample, are shown in Table II. The value of c_{n0} obtained for the high-resistivity copper-doped sample[1] is included for comparison.

ACKNOWLEDGMENTS

The authors are very grateful to Mr. G. A. Servente and Mr. R. J. Carye for their valuable assistance during the experimental phase of this work.

[6] See, for instance, Fig. 1 of reference 1; also R. N. Hall, Phys. Rev. **87**, 387 (1952), and P. Ransom and F. W. G. Rose, Proc. Phys. Soc. (London) **B67**, 646 (1954).

[7] A. H. Kahn, Phys. Rev. **97**, 1647 (1955).

Impurity Band in Semiconductors with Small Effective Mass*

FRANK STERN AND ROBERT M. TALLEY
United States Naval Ordnance Laboratory, White Oak, Maryland
(Received August 19, 1955)

The energy levels of ordered impurities in semiconductors are formally equivalent to the energy levels of metallic hydrogen if a number of simplifying approximations are made. An approximate calculation of the energy states for the 1*s* band of metallic hydrogen is carried out for smaller lattice constants than those considered by Wigner and Huntington, or by Baltensperger. A simple transformation of the distance and energy scales converts the calculation for metallic hydrogen to one applying to impurities in a semiconductor, if values for the effective mass and the dielectric constant are given. Experimental results for the optical energy gap in InAs are reported as a function of impurity concentration. The effective mass required to fit the optical data for InSb published by other workers is about $0.03m$, as compared to the value $0.013m$ found by cyclotron resonance measurements.

1. INTRODUCTION

A STRIKING phenomenon observed in intermetallic semiconductors with small effective mass is the shift of the optical absorption edge to shorter wavelengths with increasing impurity concentration. This effect was first observed in indium antimonide by Tanenbaum and Briggs;[1] additional data for InSb have been reported by Hrostowski *et al.*[2] and by Breckenridge *et al.*[3] Data on the shift of the optical edge in indium arsenide are given in Sec. 3 of the present paper.

Burstein[4] proposed that the shift of the optical absorption edge is not related to a change in the band separation caused by the impurities, but rather to the fact that in impure samples the Fermi level lies well above the bottom of the conduction band. Thus, transitions to the filled levels near the bottom of the conduction band are improbable, and the absorption edge moves to higher energies.

One feature of Burstein's explanation which requires closer study is the distribution of energy levels in impure material which causes the Fermi level to rise as impurities are added. If all the impurity levels were below the bottom of the conduction band, the Fermi level could not rise sufficiently far to account quantitatively for the observed effect. In this paper, we will extend the ordinary hydrogenic model of impurities into the range of large impurity concentration, thus extending to smaller lattice constants the treatment of metallic hydrogen first carried out by Wigner and Huntington[5] and applied to semiconductors by Baltensperger.[6]

2. 1*s* BAND OF METALLIC HYDROGEN

The simple picture for explaining the ionization energy of dilute donor impurities in a semiconductor assumes that all but one of the electrons of the donor atom participates in the binding (or bonding) of the crystal, and that the remaining electron then sees the donor ion as a single positive charge. Thus, the donor ion and the extra electron look like a hydrogen atom; the energy required to remove the electron to a point far from the donor ion is given by the formula for the ionization energy of atomic hydrogen if we replace the free electron mass by m_e, the effective mass at the bottom of the conduction band, and take account of the fact that the dielectric constant κ of the semiconductor weakens the attraction between ion and electron. We then find for the ionization energy of a donor atom in a semiconductor:

$$E_D=\tfrac{1}{2}m_e(e^2/\kappa)^2\hbar^{-2}$$
$$=(m_e/m)\kappa^{-2}\,\mathrm{ry}=13.60(m_e/m)\kappa^{-2}\,\mathrm{ev}, \quad (1)$$

where m is the free electron mass and m_e is the effective mass at the bottom of the conduction band.[7] This formula gives qualitative agreement with observed activation energies for impurities in semiconductors.

A direct extension of the picture which identifies isolated impurities with free hydrogen atoms is one which relates interacting impurities to solid hydrogen. The form of solid hydrogen which we consider is the metallic form first studied by Wigner and Huntington;[5] the restraining effect of the semiconductor lattice will keep the impurity atoms from clustering in the molecular phase, which is more stable than the metallic phase of hydrogen for large lattice constants. Our calculation is similar to the work of Baltensperger,[6] who applied the results to a discussion of impurity band conduction. Because of the very small effective mass of InAs and InSb, the overlap between donor electron orbits is much greater than in other known

* This work was supported in part by the Office of Naval Research. Preliminary accounts were presented by Robert Talley at the Symposium on Intermetallic Semiconductors, held April 26–27, 1955, at Baldock, England, and by Frank Stern at the Symposium on Physics of Semiconducting Materials, held June 6–8, 1955, at Ann Arbor, Michigan.

[1] M. Tanenbaum and H. B. Briggs, Phys. Rev. **91**, 1561 (1953).

[2] Hrostowski, Wheatley, and Flood, Phys. Rev. **95**, 1683 (1954).

[3] Breckenridge, Blunt, Hosler, Frederikse, Becker, and Oshinsky, Phys. Rev. **96**, 571 (1954).

[4] E. Burstein, Phys. Rev. **93**, 632 (1954).

[5] E. Wigner and H. B. Huntington, J. Chem. Phys. **3**, 764 (1935).

[6] W. Baltensperger, Phil. Mag. **44**, 1355 (1953); see also G. W. Castellan and F. Seitz, *Semiconducting Materials*, edited by H. K. Henisch (Academic Press, Inc., New York, 1951), p. 8; C. Erginsoy, Phys. Rev. **88**, 893 (1952).

[7] A Rydberg (ry) is the ionization energy of atomic hydrogen for a nucleus of infinite mass. One ry equals 13.60 ev.

semiconductors; thus, the usual picture of impurity levels well separated from a conduction band will not hold here except for very low impurity concentrations. Our calculation extends the work of Baltensperger into this region of larger overlap between donor electrons.

Let us first list some of the approximations underlying this calculation:

(a) The electron sees the donor ion as a single positive charge; the interaction between electron and ion is $-e^2/\kappa r$ for all values of r.

(b) The interaction of the electron with the periodic potential of the semiconductor lattice is taken into account by assigning to the electron an effective mass m_c.

(c) This effective mass is isotropic.

(d) The impurity ions form an ordered array of high symmetry.

(e) The zero level of energy is identified with the energy of the bottom of the conduction band in pure material.

(f) No electrons are thermally excited from the highest filled band to the lowest empty band, and the impurities are uncompensated.

The Schrödinger equation for the motion of an electron in the neighborhood of a donor ion in a semiconductor is, on the basis of our assumptions:

$$(\hbar^2/2m_c)(d^2P_l/dr^2) - [(\hbar^2/2m_c)l(l+1)r^{-2} - (e^2/\kappa r) - E]P_l = 0, \quad (2)$$

where P_l is r times the radial part of the wave function belonging to angular momentum l. We put:

$$r = (\kappa m/m_c)x, \quad E = (m_c/m\kappa^2)\epsilon. \quad (3)$$

If we use Bohr radii as units of distance and Rydbergs as energy units we can write:

$$(d^2P_l/dx^2) + [(2/x) + \epsilon - l(l+1)x^{-2}]P_l(x) = 0. \quad (4)$$

The energy ϵ_B for the $1s$ wave function with propagation vector $k=0$ is found from the usual Wigner-Seitz boundary condition that the radial derivative of the wave function vanish at the surface of the unit sphere surrounding each ion. Our boundary condition is:

$$\{d[x^{-1}P_0(x)]/dx\}_{x_s} = 0 \quad \text{for} \quad \epsilon = \epsilon_B, \quad (5)$$

where x_s is the radius of the unit sphere; see Eqs. (18) and (19) for expressions relating x_s to the impurity concentration.

The solution of Eq. (4) with the boundary condition given by Eq. (5) will give us ϵ_B, the energy of the bottom of the $1s$ band, as a function of x_s. To find the energy levels for electrons with propagation vectors different from zero, we use a method developed by Bardeen. We assume that in the lower part of the band the energy is given approximately by

$$\epsilon(k) = \epsilon_B + \alpha k^2. \quad (6)$$

In other words, the $1s$ band of metallic hydrogen is assumed to be parabolic in shape, with an effective mass α^{-1}. Then the density of states (including a factor two for spin) is given by:

$$\rho(\epsilon) = \alpha^{-\frac{1}{2}}(\epsilon - \epsilon_B)^{\frac{1}{2}}/2\pi^2 \text{ Bohr radii}^{-3} \text{ ry}^{-1}. \quad (7)$$

There is one orbital state in the $1s$ band for each atom; each of these states may be occupied by two electrons with oppositely directed spin orientation. We find for the width of the filled portion of the $1s$ band:

$$w = (9\pi/4)^{\frac{1}{2}}\alpha x_s^{-2} = 3.6832\alpha x_s^{-2}. \quad (8)$$

Bardeen's formula[8] for α is:

$$\alpha = \frac{x_s^3[P_0(x_s)]^2\{d[x^{-1}P_1(x)]/dx\}_{x_s}}{3P_1(x_s)\int_0^{x_s}[P_0(x)]^2dx}. \quad (9)$$

This method of finding α is different from the one used by Baltensperger.[6] He found the energy of the top of the band from the boundary condition $P_1(x)=0$, and used the band width to find the effective mass. Bardeen's method is likely to be more accurate since it is valid for the region near the bottom of the band where the parabolic approximation holds best. A perturbation theory expression for α developed by Wigner and Seitz[9] shows that α will be less than or equal to one if all the perturbing levels lie above the level in question. Thus $\alpha \leq 1$ for the $1s$ band, while Baltensperger finds values between 1 and 1.7 for $x_s < 2$. On the other hand, Baltensperger's method gives a quick estimate for the width of a band, and can give such an estimate even for p bands and bands of higher angular momentum, where the parabolic approximation of Eq. (6) is no longer applicable.

The solution of the reduced Schrödinger equation, Eq. (4), which vanishes at the origin is given for negative values of ϵ by Whittaker and Watson[10] in the form:

$$P_l(x) \sim M_{n,\,l+\frac{1}{2}}(2x/n) \sim x^{l+1}e^{-x/n} \times \left\{1 + \sum_{i=1}^{\infty} \frac{(1+l-n)(2+l-n)\cdots(i+l-n)}{i!(2l+2)(2l+3)\cdots(2l+i+1)}(2x/n)^i\right\}, \quad (10)$$

where

$$n = (-\epsilon)^{-\frac{1}{2}}. \quad (11)$$

It is most convenient to choose a value for ϵ, say $\epsilon = \epsilon_B$, evaluate $P_0(x)$ by using this value, and then find the value of x for which the boundary condition of Eq. (5) is satisfied. Using this value of x_s, we then calculate α using Eq. (9). A separate power series is

[8] J. Bardeen, J. Chem. Phys. 6, 367 (1938).

[9] E. Wigner and F. Seitz, Phys. Rev. 46, 509 (1934); see F. Seitz, *Modern Theory of Solids* (McGraw-Hill Book Company, Inc., New York, 1940), pp. 352–3.

[10] E. T. Whittaker and G. N. Watson, *Modern Analysis* (Cambridge University Press, Cambridge, 1950), fourth edition, Sec. 16.1.

TABLE I. Calculated points for metallic hydrogen.[a]

x_s	ϵ_B(ry)	α	$\psi(x_s)/\psi(0)$
0.03003	−100	1.0000	0.985
0.06765	−44.44	1.0000	0.967
0.12049	−25	0.9999	0.941
0.27258	−11.11	0.9995	0.870
0.7726	−4	0.995_4	0.665
1.580	−2.041	0.963	0.410

[a] x_s is the radius of a sphere whose volume is the reciprocal of the concentration; it is given in units of the Bohr radius. ϵ_B is the energy of the bottom of the 1s band relative to the energy of an electron at rest far from the crystal. α^{-1} is the effective mass near the bottom of the 1s band. The last column gives the ratio of the value of the 1s wave function at the edge of the cell to its value at the center.

derived, using Eq. (10), for each of the factors needed to evaluate Eq. (9). For the values of ϵ_B which we consider, i.e., $\epsilon_B<-2$, the power series converge quite rapidly and an accuracy of 0.1% is attained if ten terms in the power series are used.

The power series solution of Eq. (4) given above is useful for finding the wave function for the bottom of the 1s band. We will list here a number of solutions valid for other ranges of ϵ. When $-1<\epsilon<0$, the expansion given by Kuhn[11] is convenient. For $\epsilon=0$, Eq. (4) has the solution:

$$P_l(x)\sim(8x)^{\frac{1}{2}}J_{2l+1}((8x)^{\frac{1}{2}}), \tag{12}$$

where J_{2l+1} is a Bessel function of order $2l+1$. When $\epsilon>0$, we can use tables of Coulomb wave functions[12] which cover the range $0\leq x\leq 5$. Finally, if $\epsilon^{-1}\sim 0$, we have:

$$P_l(x)\sim(x\sqrt{\epsilon})^{\frac{1}{2}}J_{l+\frac{1}{2}}(x\sqrt{\epsilon}). \tag{13}$$

We list in Table I the results of our calculation for ϵ_B and for α as functions of x_s. We used empirical fits for ϵ_B and α as functions of x_s to draw up the more complete list of values given in Table II. The entries in this table are given as functions of x_s^{-3}, since this quantity is proportional to the density of metallic hydrogen—and to the concentration of impurities in a semiconductor. The proportionality factor is given in Eq. (19). In Table II, we list ϵ_B, α, and f, where f is the position of the Fermi level at absolute zero and is given by:

$$f=\epsilon_B+w. \tag{14}$$

The approximate empirical expressions we used in calculating the entries for Table II are:

$$x_s=-(3/\epsilon_B)[1-(1/10\epsilon_B)+(1/15\epsilon_B^2)-(1/20\epsilon_B^3)+\cdots], \tag{15}$$

$$\alpha^{-1}=1+0.006x_s^2+0.001x_s^3+0.002x_s^6. \tag{16}$$

These expressions are good to within about 0.1% for x_s in the range covered by our calculations, i.e., $0.03<x_s<1.58$.

[11] T. S. Kuhn, Quart. Appl. Math. 9, 1 (1951).

[12] *Tables of Coulomb Wave Functions*, U. S. National Bureau of Standards Applied Mathematics Series (U. S. Government Printing Office, Washington, D. C., 1952), Vol. 17.

We can qualitatively characterize our results for the 1s band of metallic hydrogen by saying that for the range of lattice constants covered in our calculation the effective mass is slightly larger than the free electron mass. For small lattice constants, the energy of the bottom of the band is given approximately by $-3/x_s$, and the width of the band by $3.68/x_s^2$. As the lattice constant decreases, the Fermi level rises much more rapidly than the bottom of the band falls. It is this fact which is responsible for the shift of the absorption edge to shorter wavelengths with increasing impurity concentration in semiconductors with small effective mass.

We have calculated the energy of the bottom of the 2s and 2p bands, with the boundary condition used by Baltensperger,[6] i.e., vanishing derivative at the edge of the cell. (Note that the bottom of the 2p band will not be at $k=0$, but at the edge of the Brillouin zone along the cubic axes.) Baltensperger found that in the range of lattice constants covered in his calculation the 2s band was always well above the top of the 1s band, while the bottom of the 2p band crossed the top of the 1s band for $x_s\sim 2$. We have verified that for smaller lattice constants the 2s band remains well separated from the 1s band; the bottom of the 2p band remains below the top of the 1s band for lattice constants smaller than the crossover value. However, the bottom of the 2p band never falls below the energy level at which the 1s band is half-filled. In other words, the density of states below the Fermi level at absolute zero is the density of states in the 1s band alone, with no other band contributing.

Application to Semiconductors

Our calculation to this point, as summarized in Table II, refers directly only to metallic hydrogen. We can easily convert the results so that they apply to impurities in semiconductors. The conversion factor for the energy scale, as in Eq. (3) is:

$$E_B/\epsilon_B=F/f=13.60(m_c/m)\kappa^{-2}. \tag{17}$$

TABLE II. 1s band in metallic hydrogen.[a]

x_s^{-3}	f(ry)	α	ϵ_B(ry)
36 930	3984	1.0000	−100
15 940	2257	1.0000	−75.6
7630	1369	1.0000	−59.2
3230	761	1.0000	−44.4
1521	452.5	1.0000	−34.6
571.6	228.7	0.9999	−25
246.1	125.8	0.9998	−18.9
117.4	73.5	0.9997	−14.79
49.38	38.44	0.9995	−11.11
16.31	15.95	0.9990	−7.72
6.36	6.94	0.998_0	−5.67
2.168	2.14	0.995_4	−4.00
0.690	0.06	0.987	−2.78
0.253	−0.62	0.963	−2.041

[a] f is the Fermi level at absolute zero, i.e. the energy at which the 1s band is half filled. The other quantities are defined as in Table I. See Eqs. (17) and (19) to apply these numbers to impurities in semiconductors.

Here the units are electron volts for the quantities referring to the semiconductor (E_B,F) and Rydbergs for the quantities referring to metallic hydrogen (ϵ_B,f). E_B and F give the energy of the bottom of the 1s impurity band and the energy of the Fermi level at absolute zero, respectively, relative to the energy of the bottom of the conduction band in pure material.

To relate x_s to the impurity concentration we note that the radius r_s of the cell surrounding each impurity atom is given by:

$$4\pi r_s^3/3 = N_D^{-1}, \tag{18}$$

where N_D is the donor concentration. If we use Eq. (3), we find

$$x_s^{-3} = 6.2064\times10^{-25}(\kappa m/m_c)^3 N_D, \tag{19}$$

where x_s is given in Bohr radii and N_D in cm^{-3}. Using Eqs. (17) and (19), with suitable values for the dielectric constant and the effective mass, we can convert the entries of Table II into graphs showing the dependence of the Fermi level on impurity concentration.

3. COMPARISON WITH EXPERIMENT

The experiment to which the foregoing calculations most closely apply is the dependence of the optical energy gap on impurity concentration. The experiments give ΔE, the difference between the optical energy gap in an impure sample and the gap in a pure sample. From the theory one can determine the position of the Fermi level, given κ and m_c. The shift of the edge is related to the Fermi level by the equation,

$$\Delta E = [1+(m_c/m_v)](F-\gamma kT), \tag{20}$$

where m_v is the effective mass near the top of the valence band. Equation (20) is similar to an equation given by Burstein,[4] who used $\gamma=4$. In general, γ will depend both on the value of F and on α_E, the value of absorption constant used to define the edge. For sufficiently low values of α_E, γ will increase continuously from zero as the Fermi level rises. Also, γ will decrease as α_E increases. This explains why the National Bureau of Standards[3] points ($\alpha_E\sim10^2$) in Fig. 2 lie below the Bell Telephone Laboratory[2] points ($\alpha_E\sim10^3$).

TABLE III. Experimental results for indium arsenide.*

Sample	N_D-N_A (cm^{-3})	Optical gap (ev)	Doping agent
9	5×10^{16}	0.30_7	none
8	2×10^{17}	0.32_5	none
15	1×10^{18}	0.35	Se
25	3×10^{18}	0.36_5	Se
27a	3.3×10^{18}	0.40	Se
12	6×10^{18}	0.44_4	Se
28a	7.7×10^{18}	0.46	Se
24	1.8×10^{19}	0.47_4	Se
29	2.1×10^{19}	0.57	Se
11	-7×10^{17}	0.29_4	Cd

* N_D-N_A was determined from the saturation value of the Hall constant at low temperatures. The optical gap given here is the room temperature value, for an absorption constant of 30 cm^{-1}.

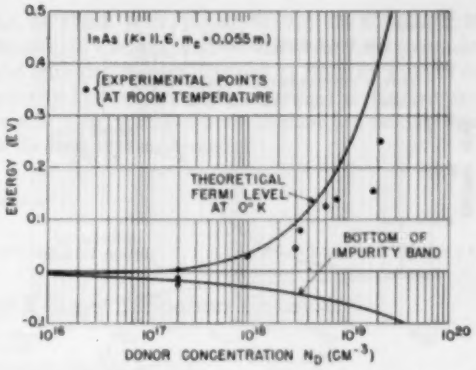

FIG. 1. The top curve shows the theoretical Fermi level at absolute zero for InAs as a function of donor impurity concentration; the bottom curve shows the energy of the bottom of the 1s impurity band. Both are given relative to the energy of the bottom of the conduction band in pure InAs. κ is the dielectric constant, m_c is the effective mass at the bottom of the conduction band, and m is the free electron mass. The points are our experimental results for the shift of the optical energy gap with impurity concentration.

In comparing ΔE and F for InAs and InSb, we have neglected the term (m_c/m_v) in Eq. (20), since no data for m_v are available. Thus our value for m_c will be too low by perhaps 10%, which is within the uncertainty in m_c. For a different method of analyzing the optical data, see the paper of Kaiser and Fan.[13]

Experimental Results for InAs

The results of our determination of the optical energy gap as a function of impurity concentration in indium arsenide are summarized in Table III. The samples were prepared in evacuated sealed Vycor containers, as described previously.[14] The optical samples were about 1 mm thick, with ground and polished surfaces. Large cleavage faces are not obtained with this material. The transmission samples are polycrystalline, but in most cases they contain only a few crystals. Two transmission curves have been previously published.[14]

In order to make our determination of the optical absorption edge independent of sample thickness, we calculated the absorption constant as a function of energy, assuming 50% reflection loss. The absorption gap, or edge, was defined as the energy for which the absorption constant is 30 cm^{-1}. This was a convenient value because of the thickness of our samples, but has no other special significance. Lacking data for a very pure sample, we estimate that the absorption edge (at 30 cm^{-1}) for pure InAs at room temperature would be 0.32 ev.

Our results for the shift of the absorption edge with impurity concentration are given by the points of Fig. 1. For comparison we draw a curve for the Fermi

[13] W. Kaiser and H. Y. Fan, Phys. Rev. **98**, 966 (1955).
[14] R. M. Talley and D. P. Enright, Phys. Rev. **95**, 1092 (1954).

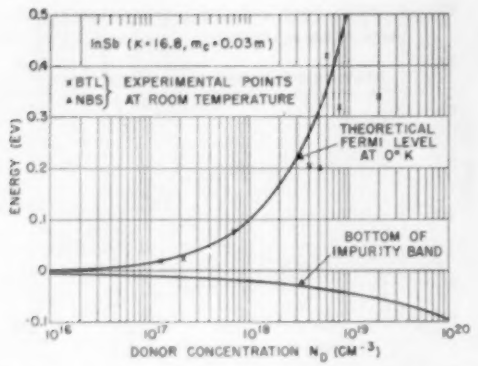

FIG. 2. Comparison of theory and experiment for InSb. The curves and symbols are defined as in Fig. 1. The points marked BTL and NBS come from references 2 and 3, respectively.

level at absolute zero based on Table II, using[15] 11.6 as the value of the dielectric constant. We have used $m_c=0.055m$ for the conduction band effective mass; a smaller value would raise the curve showing the position of the Fermi level, while a larger value would lower it. In view of the considerations mentioned above, the optical edge will lie somewhat below the Fermi level; the theoretical curve for $m_c=0.055m$, therefore, agrees approximately with the experimental points. We have also drawn the curve for E_B, the energy of the bottom of the 1*s* band; this curve is quite insensitive to the value of effective mass used.

An interesting effect is observed in the three samples in Fig. 1 drawn for a donor concentration of 2×10^{17}. These samples were prepared from arsenic of about the same purity, and are assumed to have about the same donor concentration. They correspond to samples 8, 9, and 11 of Table III, with sample 8, which is assumed to be nearly uncompensated, having the biggest optical gap. Sample 9, which we assume to be partially compensated although no impurities were purposely added, has a smaller gap. Sample 11 was purposely doped with Cd, and was *p*-type; it has the smallest gap of the three. We can explain this behavior by saying that the three samples represent different stages of the emptying of the 1*s* impurity band, with the electrons being drained off to acceptor atoms. This could account for the observations, but a theoretical study of the dependence of impurity band energy levels on degree of compensation is needed, as well as further experimental study of compensated samples.

InSb

In Fig. 2, we show a theoretical curve for the Fermi level at absolute zero and experimental points for the shift of the optical energy gap as a function of impurity concentration for InSb. The experimental points are taken from data of Hrostowski *et al.*[2] and Breckenridge *et al.*,[3] marked BTL and NBS, respectively. The BTL points correspond to various absorption constants of the order of 10^3 cm^{-1}; the NBS points are in the 10^2 cm^{-1} range. The theoretical curve is calculated using a dielectric constant of[15] 16.8 and an effective mass for the conduction band of 0.03*m*.

4. DISCUSSION

A quantitative check of the value of effective mass required to fit the experimental results for the shift of the optical absorption edge as a function of impurity concentration is possible for InSb, where the effective mass in the conduction band has been measured by cyclotron resonance. The value found by Dresselhaus *et al.*[16] is $(0.013\pm0.001)m$. This is to be compared with the value 0.03*m*, which gives approximate agreement between the theoretical Fermi level and the optical points. One way to explain the discrepancy would be to assume that there is more than one minimum in the conduction band. There would then be a *g*-fold multiplicity in the impurity band, where *g* is the number of minima in the conduction band. This has been discussed in connection with impurity states in silicon and germanium by Kittel and Mitchell[17] and by Kohn and Luttinger.[18] The approximate effect on our results would be to decrease the effective mass required to explain the optical data by a factor $g^{\frac{1}{3}}$, since the optical effective mass is essentially a density-of-states mass. The cyclotron resonance mass would still refer only to a single minimum.

A second effect which acts to improve the agreement between the cyclotron resonance effective mass and the optical data as interpreted by our theory is the lowering of the energy levels which results from the fact that in the neighborhood of the donor ion the dielectric constant of the lattice is no longer effective in reducing the Coulomb attraction between ion and electron. This effect is, in part, responsible for the differences between the ionization energies of different impurities in germanium, and in silicon. A quantitative treatment would require a calculation similar to the one described by Kohn and Luttinger.[18] If this effect were appreciable one would expect the shift of the optical absorption edge to be measurably different for different impurities in the same column of the periodic table, e.g., for S and Se or Te in InAs.

The most serious objection to a calculation like ours is its neglect of randomness. The work of James and Ginzbarg[19] and of Aigrain and Jancovici[20] has shown that when impurities are randomly distributed, there will be a tail in the density of states at both edges of

[15] F. Oswald and R. Schade, Z. Naturforsch. **9a**, 611 (1954).

[16] Dresselhaus, Kip, Kittel, and Wagoner, Phys. Rev. **98**, 556 (1955).

[17] C. Kittel and A. H. Mitchell, Phys. Rev. **96**, 1488 (1954).

[18] W. Kohn and J. M. Luttinger, Phys. Rev. **97**, 883 (1955); **98**, 915 (1955).

[19] H. M. James and A. S. Ginzbarg, J. Phys. Chem. **57**, 840 (1953).

[20] P. Aigrain, Physica **20**, 978 (1954).

the band. What influence this will have on our results remains to be determined.

5. ACKNOWLEDGMENTS

The authors have benefited from the opportunity to give informal presentations of this material.* In particular, we thank J. M. Ziman, R. Petritz, E. Adams, H. Brooks, E. Conwell, and W. Kohn for their comments and criticism. We are indebted to Dorothy Enright for growing the crystals and preparing the samples used in this work, and to Frank Matossi for making some of the optical measurements.

PHYSICAL REVIEW VOLUME 100, NUMBER 6 DECEMBER 15, 1955

Detection of Vacancies Created by X-Rays in Sodium Chloride

H. W. ETZEL
United States Naval Research Laboratory, Washington, D. C.
(Received September 2, 1955)

The creation of vacancies in sodium chloride by x-rays is detected using optical techniques. The *F*-band absorption produced by ultraviolet irradiation is measured and the band is then optically bleached. The crystal is then x-rayed and optically bleached. The crystal is again subjected to the same ultraviolet radiation as it received prior to x-raying, and the optical absorption of the *F*-band is remeasured. It is found that the sensitivity of a single crystal of NaCl to ultraviolet radiation is enhanced by a factor of 100 after it has been exposed to 40-kvp x-rays at 13 milliamperes for 30 minutes. Experiments are also performed to determine the stability at room temperature of the excess vacancies under visible and ultraviolet radiation.

INTRODUCTION

THE generally accepted model for the *F*-center in the alkali halides is that it consists of an electron trapped at a negative-ion vacancy in the lattice. This model of the *F*-center was tested experimentally by Estermann, Leivo, and Stern.[1] It had been determined[1] that the *F*-band which is observed in various alkali halides is greater than that which would be expected on the basis of the number of vacancies in the crystal before prolonged x-ray irradiation. If this model is valid then the dimensions of the crystal should change under or after such irradiation. This change was detected by Estermann, Leivo, and Stern who measured the decrease in density of single crystals of KCl after x-ray irradiation. More recently the increase in the dimensions of alkali halide crystals under irradiation has been measured by Sakaguchi and Suita[2] using an electrical technique. Their experiment had been carried out in air and it has since been repeated by Lin and Russell[3] in an inert atmosphere, thereby ruling out any surface effects due to atmospheric contamination. The work of Estermann, Leivo, and Stern did not show definitely that the decrease in density observed was not in part due to a change in the lattice parameter. Recently, Berry,[4] using an x-ray diffraction technique, has shown that the contribution to the increase in volume due to an increase in lattice parameter is negligible. The present work is not intended to substantiate the *F*-center model further, but to show that the creation of vacancies by x-rays can be detected by using simple optical measurements.

EXPERIMENTAL DETAILS

The crystals used in this experiment were grown by the Kyropoulos technique using sodium chloride which had been treated with dithizone to remove any heavy metal impurities. The $\frac{1}{4}$ in.$\times\frac{1}{4}$ in. plates were cleaved to 0.008 in.$\pm$0.001 in. in thickness to insure the usefulness of the data on a comparative basis even if the *F*-band produced by the x-rays was not uniform throughout the crystal.

The ultraviolet source was an Allen hydrogen-arc lamp with a lithium fluoride window. The x-ray machine used was operated at 40 kvp and 13 milliamperes and

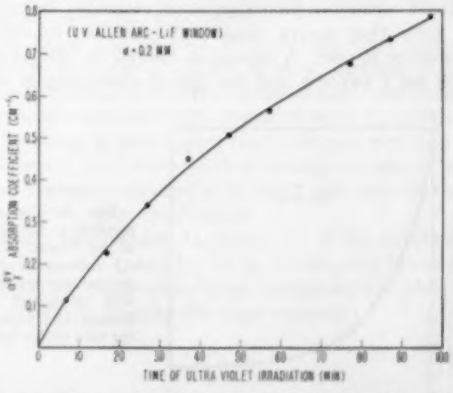

FIG. 1. The growth of the *F*-band in NaCl during ultraviolet irradiation at room temperature. Measured at $\lambda = 4650$ A.

[1] Estermann, Leivo, and Stern, Phys. Rev. **75**, 627 (1949).
[2] K. Sakaguchi and T. Suita, Technol. Repts. Osaka Univ. **2**, 177 (1952).
[3] L. Lin and B. R. Russell, Phys. Rev. **99**, 657 (1955).
[4] C. R. Berry, Phys. Rev. **98**, 934 (1955).

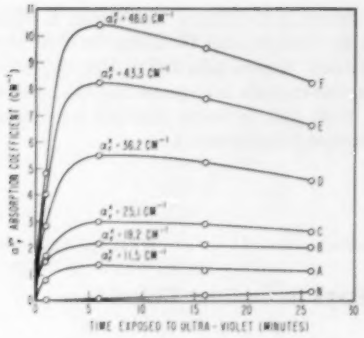

FIG. 2. The growth of the F-band in NaCl during ultraviolet irradiation in crystals having had the following x-ray exposures: A—15 seconds/side, B—30 seconds/side, C—1 minute/side, D—2½ minutes/side, E—5 minutes/side, F—15 minutes/side, N—not x-rayed.

was equipped with a Machlett *OEG-60* tungsten target. The crystals were placed 5 centimeters from the target and were exposed on both faces to insure maximum uniformity of coloration. A Beckman Model-DU Spectrophotometer was used to measure the optical density of the crystals in the 2100 A to 7000 A region of the spectrum and a Baird Associates vacuum spectrophotometer was used below 2150 A.

The bleaching experiments were carried out using a microscope illuminator unit containing a glass-envelope 100w tungsten lamp with a water filter. In all the crystals used the F-band produced by x-raying was completely bleached in 30 minutes. The crystals were placed about 15 centimeters from the lamp.

RESULTS

The F-band absorption produced in a single NaCl crystal by irradiating with ultraviolet light prior to x-raying is shown in Fig. 1. If this crystal is optically bleached and recolored the rate of coloration is now somewhat greater, indicating that the ultraviolet light is itself capable of producing some vacancies. In order to show that x-rays create vacancies the following procedure is used. A crystal is colored by ultraviolet light for 6 minutes and the optical absorption at the peak of the F-band, α_F^{uv}, is measured. The band is then optically bleached. The crystal is then x-rayed and the optical absorption of the F-band is measured. After the x-ray-induced F-band is optically bleached, the crystal is again exposed to ultraviolet light for 6 minutes and the F-band absorption measured. The increase in the F-band produced by ultraviolet radiation after x-raying over that observed before x-raying can be seen by comparing curves A,B,C,D,E,F to curve N in Fig. 2. The crystal represented by curve N has not been x-rayed and is the curve is Fig. 1 replotted. It appears that more than a 6-minute exposure to ultraviolet light begins to bleach the F-band in the crystals which have been x-rayed. The shape of the curves in Fig. 2 suggest that two processes are active simultaneously, namely: The ultraviolet light creates F-centers in the crystals and also destroys some F-centers. The destruction of these centers can be shown to be due to the destruction of the excess vacancies introduced by x-raying by the following experiment. A crystal which has been x-rayed and optically bleached is recolored with 15 minutes of ultraviolet light. The resulting F-band absorption, $\alpha_F^{uv}=9.6$ cm^{-1}, is plotted in Fig. 3. The crystal is then optically bleached for 30 minutes and α_F^{uv} then is zero. When the crystal is again exposed to ultraviolet light for 15 minutes, α_F^{uv} is found to be 5.8 cm^{-1}. This cycle of bleaching and recoloring is repeated until there is no longer a decrease in α_F^{uv}.

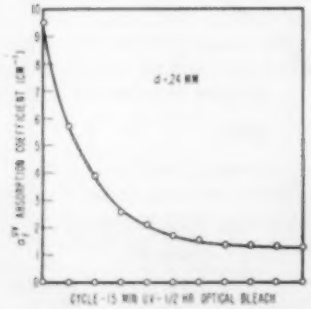

FIG. 3. The absorption at the peak of the F-band (4650 A) measured after successively coloring with ultraviolet radiation and bleaching with visible light.

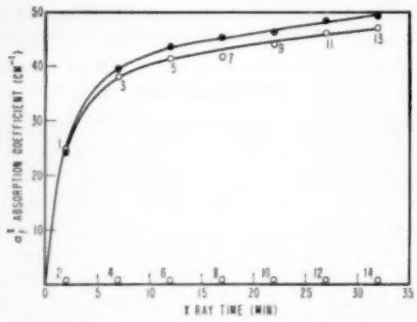

FIG. 4. Growth curves of the x-ray-produced F-band in NaCl: ●—measured after each x-ray exposure; ○—measured after each x-ray exposure but with the F-band optically bleached before successive x-ray exposures.

Since the cycle just described involves the use of visible light for bleaching, the question arises whether any part of the destruction of the x-ray produced vacancies is due to it. In order to determine this, two new crystals were x-rayed simultaneously and then the F-band absorption was measured. The upper curve in Fig. 4 shows the growth of the F-band in the crystal which was never optically bleached. The lower curve in Fig. 4 shows a crystal which has been optically bleached after each x-ray exposure and the sequence of the absorption measurements is numbered. It can

be seen that the two curves differ by less than 5%, which indicates that the act of optically bleaching a crystal has little effect in destroying vacancies. If x-raying had produced no vacancies, or if the bleaching light destroyed all the vacancies created by x-raying, then $\alpha_F{}^x$ would have always been about 25 cm^{-1} for subsequent exposures.

In order to ascertain that the enhanced F-band absorption, observed in those crystals which are colored by ultraviolet light after being x-rayed, is not due to an increased absorption of ultraviolet quanta, the absorption spectrum of the crystals was measured in the ultraviolet region. Figure 5 shows the ultraviolet absorption of a crystal before being x-rayed and after being x-rayed 30 minutes and optically bleached. This x-ray exposure is the same as that given the crystal denoted by F in Fig. 2. The ultraviolet absorption shown in Fig. 4 does increase after 30 minutes of

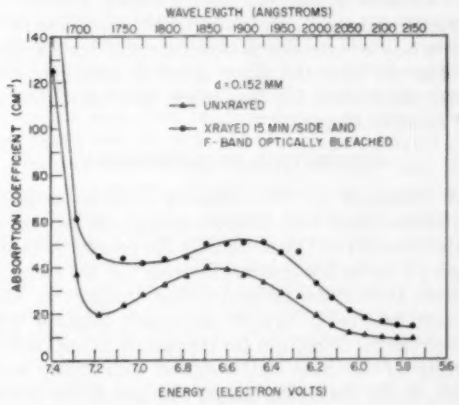
WAVELENGTH (ANGSTROMS)
1700 1750 1800 1850 1900 1950 2000 2050 2100 2150
ABSORPTION COEFFICIENT (CM⁻¹)
d = 0.152 MM
UNXRAYED
XRAYED 15 MIN/SIDE AND F-BAND OPTICALLY BLEACHED
ENERGY (ELECTRON VOLTS)

FIG. 5. The ultraviolet absorption spectrum of NaCl: ▲—before exposure to x-rays; ●—after 30 minutes of x-rays and optical bleach of the F-band.

x-raying by a factor of 2 but the $\alpha_F{}^{uv}$ for crystal F in Fig. 2 has increased a factor of 100 over $\alpha_F{}^{uv}$ for crystal N. This indicates that the increase in the ultraviolet absorption is not significant. It is interesting to note that there is an absorption band in the unirradiated NaCl at 1870 A. The nature of this band is not yet understood.

The stability at room temperature of the vacancies introduced by x-raying was determined in the following way. Three crystals were x-rayed simultaneously and then optically bleached. One of the three was colored with ultraviolet light immediately after the completion of the bleach, the second was colored 2 hours later, and the third was colored 18 hours later. All three crystals

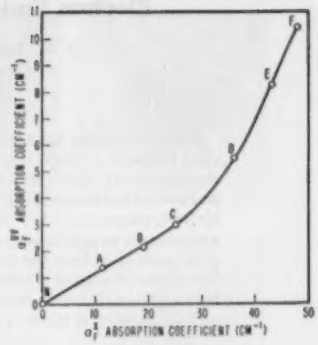

FIG. 6. The F-band produced by x-rays *versus* the F-band produced by ultraviolet light in crystals in which the x-ray created F-band has been bleached.

were found to have the same $\alpha_F{}^{uv}$, indicating no detectable loss of vacancies from the crystal.

Figure 6 shows the data of Fig. 2 plotted in such a way is to indicate the relationship between $\alpha_F{}^x$ and $\alpha_F{}^{uv}$. The F-band absorption, $\alpha_F{}^x$, is measured after x-raying but before bleaching the crystal. After optically bleaching the F-band produced by x-rays, the crystal is exposed to 6 minutes of ultraviolet light and the F-band absorption, $\alpha_F{}^{uv}$, is measured. The absorption coefficient of the x-ray-created F-band does not grow as rapidly as that produced by the ultraviolet radiation, indicating that prolonged x-raying anneals out some of the F-centers.

The same increased sensitivity to ultraviolet radiation after x-raying to before x-raying, as observed in NaCl, has been found to exist in KCl and KBr. It would have been desirable to have used monochromatic ultraviolet radiation for coloring the crystals, but a measureable F-band could not be produced with available sources in a reasonable time. It is interesting to note that even for very short x-ray exposures (30 seconds, crystal A of Fig. 2) a marked increase in the sensitivity of the crystal to ultraviolet light is observed. If there is an induction period for production of vacancies by x-rays it must be less than the 30-second exposure used in this experiment.

Although the crystals after having been x-rayed contain vacancies in excess of those inherent in the lattice, there is no observable diffusion of these vacancies to the surface of the crystal at room temperature in 18 hours. It does appear that prolonged exposure to ultraviolet light destroys these x-ray-produced vacancies, whereas irradiation with visible light only removes the electron from the F-center.

The author wishes to thank Dr. J. H. Schulman, Dr. C. C. Klick, and Dr. D. L. Dexter, and Mr. R. J. Ginther for many stimulating discussions, and Mrs. E. W. Claffy for growing the single crystals.

Electron Emission from a Lattice Step on Clean Tungsten*

J. K. Trolan, J. P. Barbour, E. E. Martin, and W. P. Dyke
Physics Department, Linfield College, McMinnville, Oregon

(Received June 27, 1955)

Electron emission has been observed from the edges of the outermost atom layer of a (110) crystal face of clean tungsten. A bright ring appears in the (110) area of the emission pattern on a pulsed T-F emission electron microscope when current densities exceeding 10^7 amp/cm^2 are drawn. When the emitter is maintained at an elevated temperature, $T \geqq 1700°K$, the ring decreases in radius and eventually disappears. This is followed by the appearance of a new ring at the periphery of the dark (110) region, making possible the observation of a sequence of such collapsing rings. An experiment is reported which associates the ring collapse with the loss of an atom layer from the cathode tip, causing a change in its length, which is equal on the average to the interplanar spacing of the (110) crystal direction. This association proves that electron emission is observed from a lattice step and provides a convenient means for the study of the corresponding processes by which cathode material is transported.

INTRODUCTION

THE techniques of pulsed T-F emission microscopy[1] have been employed in the present work to observe effects of atom transport processes active on the clean tungsten cathode surface at elevated temperatures. These processes have long been known to dull and shorten field emitters.[2,3]

An emission pattern detail is shown to originate in electron emission from the edge atoms of a lattice plane of atomic thickness. Further, the transport processes which dull the emitter are shown to remove such planes from its tip in a manner which is detectable through the pattern detail.

The ability to identify and trace the progress of a lattice edge of atomic thickness may find a number of uses. For example, an accurate measurement of length change may provide means for calibrating the magnification and resolution of commercial electron microscopes. Also, the ability to resolve an atomic lattice step may prove useful for crystal surface studies where present optical interferometric methods[4] have been limited to 15 A step-height resolution. It is also clear that the methods herein discussed may be used in quantitative studies of the transport mechanisms occurring on small, heated metal objects. Subsequent studies, to be reported later, indicate that the observed process is surface migration, and provide a measure of the constants involved in that process.

Similar emission pattern effects have been observed by others[5,6]; however, direct proof of the resolution of electron emission from the edge of an atomic plane has not been found in the literature.

This paper offers the first conclusive proof that electron emission is observed from a surface irregularity of atomic dimensions. It would appear that these techniques may be extended to determine whether emission is observed from the single atom or molecular site, about which there has been much speculation, but as yet no adequate proof.[7–9]

DESCRIPTION OF PHENOMENA

A discussion of the difference between emission patterns obtained from tungsten during pulse and steady state operation will help to clarify the present methods. Figure 1 shows the contrast between (a) the emission pattern from clean monocrystalline tungsten at high current density ($J = 5 \times 10^7$ amp/cm^2) obtained with pulsed electric fields, and (b) the pattern at low current density ($J = 25$ amp/cm^2) obtained with steady state fields. In (b) the crystal planes with low Miller indices can be correlated with the large dark regions of the pattern in a well-known manner,[10] and correspond to the regions of high effective work function and hence of low electron emission. Recent measurements[6] show

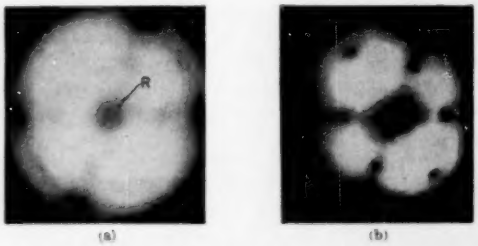

FIG. 1. Photographs of electron projection patterns from a clean, monocrystalline tungsten emitter under the conditions of (a) high current density, $J = 5 \times 10^7$ amp/cm^2, during pulse T-F operation (note the ring at R in the central dark area); and (b) low current density, $J = 25$ amp/cm^2, typical steady-state field emission.

* This work was sponsored by the Office of Naval Research. For preliminary reports of this work see: Abstracts of the Field Emission Symposium, November 10–12, 1954, Mellon Institute, Pittsburgh, Pennsylvania; Trolan, Barbour, Martin, and Dyke, Phys. Rev. 98, 262(A) (1955).

[1] W. P. Dyke and J. P. Barbour, J. Appl. Phys. (to be published).

[2] E. W. Müller, Z. Physik 126, 642 (1949).

[3] C. Herring, in *Structure and Properties of Solid Surfaces*, edited by R. Gomer and C. S. Smith (University of Chicago Press, Chicago, 1953), pp. 50, 63.

[4] Ajit Ram Verma, *Crystal Growth and Dislocations* (Academic Press, Inc., New York, 1953).

[5] E. W. Müller, 16-mm Film, Tagesztg. Deut. Physik. Gesell. September 1951, in Karlsruhe (unpublished).

[6] E. W. Müller, J. Appl. Phys. 26, 732 (1955).

[7] E. W. Müller, Z. Naturforsch. 59, 473 (1950).

[8] R. Gomer and D. A. Speer, J. Chem. Phys. 21, 73 (1953).

[9] J. A. Becker, J. Chem. Phys. (to be published).

[10] E. W. Müller, Z. Physik 106, 541 (1937).

the ratio of current density in the brightest regions of the clean tungsten pattern to that in the dark central (110) plane to be greater than 16 000/1 at the relatively low fields ($2.5\times10^7<F<3.5\times10^7$ v/cm) generally employed in steady state emission. It becomes apparent that observation of emission in the (110) crystal direction under such low fields is difficult and requires shielding the phosphor from scattered light and other excitation sources including x-rays, secondary electrons, and negative ions. Müller[6] reports this accomplishment in a tube where a metal anode shielded the phosphor from all electron emission except that originating in the central (110) region.

The pattern of Fig. 1(a) differs from that of 1(b) in several respects. First, the emission occurs over an increased area as evidenced by the spreading of the emission to crystal planes further from the central (110) region and by the decrease in the area of the dark "holes." Second, the current density becomes more uniform over the pattern as evidenced by the decrease in contrast between the highest and the lowest current density regions.[11] This can be attributed to two causes: (1) a decrease in the ratio of current densities between the low and high work function regions at high fields, as compared with the ratio at low fields as predicted by the Fowler-Nordheim field emission theory,[12] and (2) electron space-charge effects[13] which tend to prevent further current density increase in "bright" regions while permitting such increase where current density is still relatively low. These two effects decrease the pattern contrast and make it possible to observe detail that may occur in the low-index planes such as at *R* of Fig. 1(a), where a bright ring[14] of emission is apparent near the periphery of the central (110) dark region. When patterns such as Fig. 1(a) are observed by the methods of pulsed *T-F* emission microscopy as described in reference 1, and when a cathode temperature in the range 1700° to 3000°K is used for tungsten, the ring *R* in the figure is seen to decrease in diameter and eventually to disappear; later another ring will appear and the process of ring collapse can be repeated. Such a sequence is illustrated in Fig. 2. The ring initially becomes apparent at the periphery of the dark (110) area as illustrated at *R* in Fig. 2(a), and as the emitter temperature is kept constant the ring continuously decreases in diameter as shown in Figs. 2(b) and (c) until it finally vanishes as at (d). Following the disappearance of the ring, the 110 region remains devoid of detail for a short period of time, after which another ring can be resolved at the periphery, to be followed by

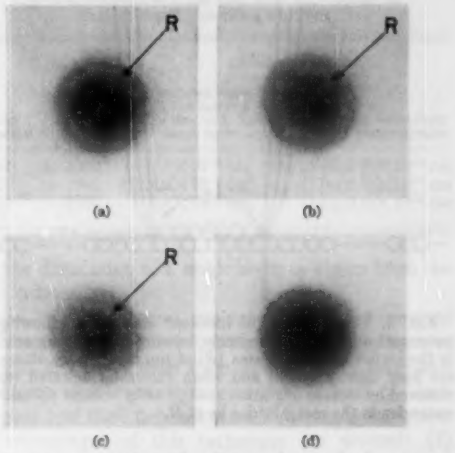

FIG. 2. Photographs of the central 110 plane on the emission pattern showing successive stages of ring collapse [(a) through (d)] corresponding to the dissolution of the outermost atom layer from the 110 crystal plane of the heated tungsten tip, viewed by pulsed *T-F* emission electron projection microscopy.

the shrinking sequence described in the foregoing. If a constant, high emitter-tip temperature is maintained, the sequence will recur at nearly uniformly spaced intervals of time. The repetitive pulsing technique is used only for purposes of viewing the pattern; at the pulse lengths and repetition rates used herein, i.e., 1 μsec and 30 to 1000 pps (pulses per second) respectively, the average value of the electric field is negligible.

The number of such collapsing rings per unit of time, herein referred to as "ring rate," increases rapidly with increasing tip temperature, decreases with increasing radius of curvature of the tip, and decreases with increasing polar angle for a given type of crystal plane. It is also strongly dependent on the state of cleanliness of the tip surface; for example, less than a monolayer of carbon will impede the rate of ring collapse on tungsten. A ring may be "frozen-in" or held at any diameter by reducing the tip temperature below 1000°K.

PROPOSED ORIGIN OF EMISSION IN THE RING AND THE MECHANISM OF RING DISSOLUTION

The existence of the ring can be explained on the basis that the corresponding electron emission originates at the edge atoms of the top atom layer of the (110) face as illustrated in Fig. 3. Geometrical considerations show the electric field at the edge atoms to be greater than that existing at the smooth, tightly packed surface of the plane; these edge atoms may also present a lower effective work function due to increased surface roughness.[15] Both effects result in increased field emission as compared with that of their surface neighbors. Thus a ring of emission would be expected to

[11] Dyke, Trolan, Dolan, and Grundhauser, J. Appl. Phys. **25**, 106 (1954).
[12] R. H. Fowler and L. W. Nordheim, Proc. Roy. Soc. (London) **A119**, 173 (1928).
[13] Barbour, Dolan, Trolan, Martin, and Dyke, Phys. Rev. **92**, 45 (1953).
[14] Not to be confused with the "ring and tilt" associated with vacuum arc initiation. [Dyke, Trolan, Martin, and Barbour, Phys. Rev. **91**, 1043 (1953).]
[15] R. Smoluchowski, Phys. Rev. **60**, 661 (1941).

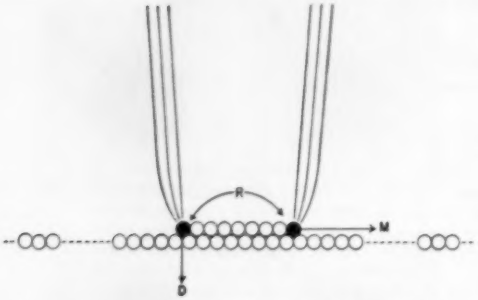

FIG. 3. Cross section of idealized emitter tip showing two outermost atom layers. Emission forming pattern ring originates in the vicinity of edge atoms (R) of top layer. Edge atoms at R are least tightly bound and when thermally agitated may be removed by surface migration as at M or by volume diffusion into vacancies in the metal lattice as at D.

occur and also to be resolved in the emission pattern detail, provided the diameter of the top lattice step was sufficiently smaller than that of the underlying step to be resolved by the field emission microscope. The resolving power of the device is calculated to be about 40 A for the smooth cathode[16] and 3 A in the presence of surface roughness.[17] If an emitter tip having a radius of about 1000 atoms, a size appropriate for this study, is idealized as a hemisphere, several single lattice steps should be individually resolvable with the field emission microscope; however, the shape assumed by the cathode at elevated temperatures is such that the low-index planes are extended in size and lattice steps become bunched in the region between the simple planes. A resolvable separation between the edge of the top atom layer and underlying layers occurs occasionally following flash heating of the tip, or periodically on a continuously heated emitter.

If the emitter tip is maintained at an elevated temperature, the thermal energy of the atoms may become sufficient to break some of the bonds of the less tightly bound edge atoms, as at R of Fig. 3. These atoms may then proceed across the plane by surface migration, as represented by the arrow at M, or they may, by the process of volume diffusion, follow a path D into the interior of the metal. The rates of these transport processes have been discussed by Herring.[3] At high temperatures evaporation can also remove atoms; however, at the temperatures employed in this work, the latter process can be neglected. The removal of atoms from the lattice step results in a decrease in the diameter of both the top atom layer and its associated emission ring.

The proposed explanation of the ring formation and removal assumes that electron emission from the edge of a single atom layer is resolved. The following experiment establishes that assumption and gives assurance that rings, under the conditions of the present experiment, do not correspond to multiple atom layers.

[16] E. W. Müller, Z. Physik **120**, 270 (1943).
[17] D. J. Rose, Phys. Rev. **98**, 1169 (1955).

EXPERIMENTAL PROCEDURE AND RESULTS

The purpose of the experiment was to observe a sufficient number of successive collapsing rings on the emission pattern from a single tip that, if one assumes each ring to be associated with the removal of one or more atom layers, the resulting change in emitter tip length would be large enough to be accurately measured by other means. A convenient method of such measurement is by use of electron micrographs where a resolution of 100 A requires a total of about 400 rings for a reasonably accurate measurement of emitter length change.

In order to have a reference point from which to measure the emitter-tip length, it is necessary to have some identifying mark or characteristic in the vicinity of the tip, which will remain fixed relative to the bulk of the emitter during heat treatment. Desirable reference markings were produced when emitters were fabricated from tungsten wire composed of small crystals about 10^{-3} to 10^{-4} cm in length. Emitters etched from this stock were smooth and uniform following the etching process. They were then heated in good vacuum at a temperature of 2000°C from two to ten minutes for the dual purposes of forming indentations at crystal boundaries as at point P of the tip shadowgraph of Fig. 4(a), and to smooth and round the tip to the extent indicated in the same figure. Further heating to clean and outgas during the final evacuation process was held to a minimum to reduce

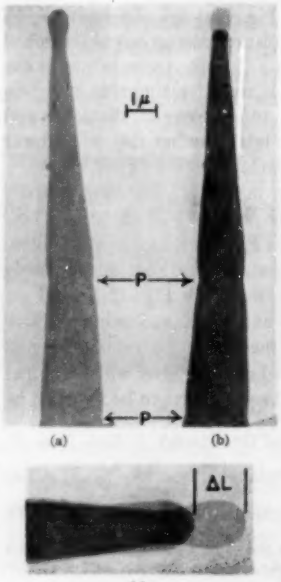

FIG. 4. Electron microscope shadowgraphs of the profile of emitter X160. A, before operation, with length-reference point indicated at P. B, superposition of shadowgraphs obtained before and after operation with matched reference indentations at P. C shows an expanded view of the superimposed tips; ΔL is the decrease in emitter length resulting from the collapse of 3000 rings.

undesired changes in the emitter length. The double indentations in the shank of the emitter shown in Fig. 4(a) serve as double reference points and permit detection of possible reference point shift through grain growth. No change in grain size or movement of grain boundaries was noted during the experiment. In other cases, curved emitter blanks afforded an independent reference for the measurement of length change.

After fabrication, electron micrographs were obtained and each emitter was mounted in an electron projection tube,[11] evacuated as previously described[18] and sealed off at a pressure of about 10^{-8} mm of Hg. After seal-off and prior to operation, tantalum gettering decreased the static, chemically active gas pressure to about 10^{-12} mm of Hg.

During *T-F* emission, the total number of collapsing rings was determined either by direct count, as was done in the case of emitter No. X127 of Table I, or by observing the rate at known intervals of time and adding the individual rate-time products. After the collapse of some 2000 to 3000 rings had been observed, the emitters were removed from their envelopes and again micrographed at a known magnification. The shadowgraphs of each emitter obtained before and after the ring count were then adjusted to the same magnification and carefully superimposed at the reference notches as at *P* in Fig. 4(b) and the change in emitter length measured. Table I shows a column of values of the measured change in length for three emitters with an uncertainty estimated at $\pm 10\%$ which includes errors due to microscope calibration and matching the micrographs as the principal sources. Table I also shows for comparison purposes the predicted change in length for each emitter, assuming that each collapsing ring is associated with the removal of a single atom layer from the (110) plane of the tip. The interplanar spacing in the (110) crystal direction for tungsten is 2.23×10^{-8} cm; thus, for example, the removal of 2500 atom layers from the tip amounts to a length change of 5.6×10^{-5} cm. Good agreement is noted between the measured and predicted columns of the table.

TABLE I. Number of collapsing rings and change in emitter length, for three emitters.

Emitter designation	Number of rings	Change in emitter length: Predicted value on the basis: 1 ring to 1 atom layer	Change in emitter length: Measured value from emitter shadowgraphs
X160	3000	6.7×10^{-4} cm	$(6.4\pm0.6)\times10^{-4}$ cm
X127	1960	4.4×10^{-4} cm	$(5.0\pm0.5)\times10^{-4}$ cm
Q218	2500	5.6×10^{-4} cm	$(5.7\pm0.6)\times10^{-4}$ cm

CONCLUSION

The foregoing describes conditions under which the emission from the edge atoms of an atomic plane on the (110) face of clean tungsten is resolved in the field emission microscope. The results show that the collapse of an emission ring of the type described is associated with the dissolution of a single layer of atoms from the plane in question.

Since, by these means, one can identify the removal of such minute quantities of material as a single layer or a portion of a single layer from an emitter tip, one has a convenient tool for studying the mechanisms of atom transport and their dependence on various parameters. The advantages of this technique are several: (1) transport measurements can be made on an emitter while its gross geometry, which through mean surface curvature mainly determines the transport rate,[3] is essentially constant; (2) the transport process is made continuously visible through electron emission resulting from a high electric field, yet undesired effects due to the field can be avoided by use of pulsed operation at a very low duty-cycle[1]; (3) the temperature necessary for the transport of detectable amounts of tungsten cathode material also causes evaporation of most surface contaminants, so that the surface is maintained in a relatively clean condition.

Direct observation of a virtually instantaneous transport rate may be useful in several related problems. By measuring the dependence of the ring rate on temperature one may deduce the activation energy of the process involved; such a result should be readily accessible for several metals. Rates of transport may be expected to depend not only on temperature but on temperature gradient, surface curvature and its gradient, applied field, state of cleanliness or contamination, and perhaps other factors. Conversely, study of the rate during controlled variation of these parameters may clarify some of the present obscurity concerning the mutual relationship of the corresponding mechanisms.

ACKNOWLEDGMENTS

The authors are grateful to L. M. Perry, D. M. Barney, J. L. Boling, and F. M. Collins for valuable assistance extended during this work.

[18] W. P. Dyke and J. K. Trolan, Phys. Rev. 89, 799 (1953).

Statistics and Galvanomagnetic Effects in Germanium and Silicon with Warped Energy Surfaces*

BENJAMIN LAX AND J. G. MAVROIDES
Lincoln Laboratory, Massachusetts Institute of Technology, Lexington, Massachusetts

(Received September 15, 1955)

A method is developed for calculating the statistical properties and galvanomagnetic effects of p-type Ge and Si for weak magnetic fields. The calculations involving the use of the Boltzmann transport theory are applied to the warped energy surfaces which have been determined by the cyclotron resonance experiments. Expressions are developed for the hole densities, conductivity, effective masses, intrinsic carrier concentration, and Hall coefficient as a series expansion in terms of the anisotropy parameters of the warped surfaces. Results have been obtained for the assumption that the relaxation time $\tau=l\epsilon^{-\lambda}$, where l is a constant, ϵ is the energy of the carriers and λ is a parameter whose numerical value depends on the scattering processes. By using the results of the calculations and existing experimental data, a speculation is made concerning the possible change with temperature of the combined effective mass of holes in germanium and the corresponding change in the band structure.

I. INTRODUCTION

SINCE the energy surfaces for the bottom of the conduction band and the top of the valence band are now reasonably well known for germanium and silicon, it is desirable to carry out the statistical and galvanomagnetic calculations for these materials taking into account the nature of the energy surfaces. For the ellipsoidal models these calculations have been clearly outlined by Abeles and Meiboom[1] and Shibuya.[2] However, the comparable task for holes, where the energy surfaces consist of two sets of degenerate warped spheres,[3,4] has not yet been done. Calculations for p-type germanium based on appropriate approximations in terms of spherical energy surfaces but taking both types of holes into account[5] have been very effective for describing the Hall effect and magnetoresistance effects as a function of the magnetic field. However, this treatment cannot account for directional effects of either the magnetoresistance or the Hall effect.

We shall describe a method for carrying out calculations of the statistical properties and the galvanomagnetic effects of germanium and silicon which is valid for weak magnetic fields and takes the anisotropy into account. The results are directly applicable to materials which have a structure similar to that of the valence band of these two semiconductors. This paper deals specifically with problems related to the hole densities, conductivity, effective masses, intrinsic carrier concentration, and Hall coefficient. A later publication will apply the techniques discussed here to the interpretation of directional effects of the magnetoresistance in p-type germanium and silicon.

* The research in this document was supported jointly by the Army, Navy, and Air Force under contract with the Massachusetts Institute of Technology.

[1] B. Abeles and S. Meiboom, Phys. Rev. **95**, 31 (1954).
[2] M. Shibuya, Phys. Rev. **95**, 1385 (1954).
[3] Dexter, Zeiger, and Lax, Phys. Rev. **95**, 557 (1954).
[4] R. N. Dexter and B. Lax, Phys. Rev. **96**, 223 (1954).
[5] Willardson, Harman, and Beer, Phys. Rev. **96**, 1512 (1954); this reference will be referred to hereafter as WHB.

II. THEORY

By using results of the Boltzmann transport theory[6] an expression for the current density in the presence of electric and magnetic fields can be obtained as a power series in terms of the magnetic field H. The contribution to the current density j_i from a constant energy surface may be expressed as

$$j_i=\sigma_{ij}E_j+\sigma_{ijl}E_jH_l+\sigma_{ijlm}E_jH_lH_m+\sigma_{ijlmn}E_jH_lH_mH_n+\cdots, \quad (1)$$

where E_j, H_l, H_m, and H_n are the electric field and magnetic field components respectively. Since the surfaces that we are discussing possess cubic symmetry, the conductivity coefficients also must have cubic symmetry as can be seen from the expressions in Appendices A and B which are given in terms of the parameters of the energy surfaces. Thus the first coefficient in Eq. (1) is the usual zero-magnetic-field electrical conductivity, the second coefficient is associated with the nondirectional Hall effect, the third is associated with the magnetoresistance which may be directional, and the fourth term gives the directional properties of the Hall effect. Since in practice the coefficients become increasingly complex to evaluate, we shall restrict our calculations to the first three coefficients. These are defined in Appendix A, in the manner of Abeles and Meiboom.[1]

From the definitions of the coefficients it is seen that in order to carry out specific calculations, it is necessary to specify (a) the shape of the energy surfaces at the top of the valence band and (b) the dependence of the relaxation time on the wave vector **k**.

A. Shape of the Energy Surfaces

Observation of cyclotron resonance in p-type germanium[3] and silicon[4] indicate that near the top of the valence band the energy surfaces in both of these semiconductors consist of warped spheres. There are two

[6] A. H. Wilson, *The Theory of Metals* (Cambridge University Press, London, 1953), second edition, p. 224.

sets of such surfaces with their maxima at the center of the first Brillouin zone and corresponding to two kinds of holes. Using this model, Dresselhaus, Kip, and Kittel[7] have shown by means of a perturbation calculation that the energy ϵ, as a function of the wave vector $\mathbf{k}$, can be expressed in the following form:

$$\epsilon=-\frac{\hbar^2}{2m_0}\{Ak^2\pm[B^2k^4+C^2(k_x^2k_y^2+k_x^2k_z^2+k_y^2k_z^2)]^{\frac{1}{2}}\}. \tag{2}$$

Here the plus sign is associated with the holes of the small effective mass and the minus sign, with holes of the larger effective mass. The $\mathbf{k}$ coordinate system is coincident with the cubic axes, m_0 is the mass of the free electrons and A, B, and C are constants determined experimentally[3,4] to have the following values[8]:

For germanium: $A=13$, $B=8.7$, and $C=11.4$;

For silicon: $A=4.1$, $B=1.4$, and $C=3.7$.

B. Relaxation Time

The relaxation time τ will be assumed to be dependent on the energy, ϵ, as follows:

$$\tau=l\epsilon^{-\lambda}, \tag{3}$$

where l is a constant and λ is a parameter whose numerical value may be chosen to best approximate the principal scattering mechanism. The relaxation time τ should actually be taken as a combination of terms of the type in Eq. (3). For example, if lattice and impurity scattering are both to be considered, λ is chosen as $\frac{1}{2}$ and $-\frac{3}{2}$ respectively; hence the total relaxation time τ is given by

$$1/\tau=(1/\tau_l)+(1/\tau_i), \tag{4}$$

where τ_l and τ_i are the lattice and impurity scattering relaxation times respectively. For our purposes in the cases we are considering it will be sufficient to describe the situation by a single process. This simplifies the calculations considerably. We shall ignore interband scattering as such except perhaps in that a suitable dependence of τ on energy may describe such a process. Hence in these approximations the contributions to the conductivity from the two degenerate surfaces will be assumed as simply additive.

As can be seen from Eq. (2) the dependence of the energy on the components of the wave vector $\mathbf{k}$ is quite involved. For purposes of computation it is convenient to expand the expressions under the radical in increasing powers of the anisotropy term such that the series converges fairly rapidly. This is accomplished by suitably adding and subtracting a term $\frac{1}{4}C^2k^4$ under the radical. Thus Eq. (2) becomes, to the first order,

$$\epsilon=-\frac{\hbar^2k^2}{2m_0}(A\pm B')\times\left\{1-\gamma\left[\frac{(k_x^2k_y^2+k_x^2k_z^2+k_y^2k_z^2)}{k^4}-\frac{1}{6}\right]+\cdots\right\}$$

$$=-g(\theta,\phi)k^2KT, \tag{5}$$

where $B'=(B^2+\frac{1}{6}C^2)^{\frac{1}{2}}$, $\gamma\equiv\mp\frac{1}{2}C^2/B'(A\pm B')$, K is Boltzmann's constant, T is the temperature, θ and ϕ are the usual spherical coordinates, and

$$g(\theta,\phi)\equiv\frac{\hbar^2}{2m_0}\frac{(A\pm B')}{KT}\times\{1+\tfrac{1}{2}\gamma[\sin^4\theta(\cos^4\phi+\sin^4\phi)+\cos^4\theta-\tfrac{3}{4}]\}. \tag{6}$$

In this approximation, neglecting the next higher order term represents an error of about one percent for germanium and five percent for silicon under the worst conditions, namely in the high-mass energy surface with $\mathbf{k}$ along the [111] direction. The total error is probably less since the quantities to be evaluated have to be averaged over all angles.

The choice of spherical coordinates, as we shall see, is essential for performing the integrations necessary to obtain the conductivity components. The integrals are computed by integrating first with respect to k and then with respect to θ and ϕ. The general method may be illustrated by considering the simplest of the calculations, namely the density of holes. Assuming a Maxwellian distribution, the number of holes per unit volume, p, is given by[9]

$$p=\int_{\epsilon_1}^{\epsilon_2}e^{(\epsilon_F+\epsilon-\epsilon_F)/KT}N(\epsilon)d\epsilon\approx\frac{e^{(\epsilon_F-\epsilon_F)/KT}}{4\pi^3}\int e^{\epsilon/KT}dV_k$$

$$=\frac{e^{(\epsilon_F-\epsilon_F)/KT}}{4\pi^3}\int_0^{2\pi}\int_0^{\pi}\int_0^{\infty}\times\exp[-g(\theta,\phi)k^2]k^2dk\sin\theta d\theta d\phi, \tag{7}$$

where ϵ_v is the energy at the top of the valence band and ϵ_F is the Fermi energy level. After integrating over k, Eq. (7) becomes

$$p=\frac{1}{16\pi^{5/2}}e^{(\epsilon_v-\epsilon_F)/KT}\int_0^{2\pi}\int_0^{\pi}[g(\theta,\phi)]^{-\frac{3}{2}}\sin\theta d\theta d\phi. \tag{8}$$

The angular integrations are performed by first expanding $[g(\theta,\phi)]^{-\frac{3}{2}}$ in the following series in γ which is then integrated term by term over θ and ϕ.

$$[g(\theta,\phi)]^{-\frac{3}{2}}=\left[\frac{\hbar^2(A\pm B')}{2m_0KT}\right]^{-\frac{3}{2}}\times\{1-\tfrac{3}{2}\gamma q+(15/8)\gamma^2q^2-(35/16)\gamma^3q^3+\cdots\}, \tag{9}$$

[7] Dresselhaus, Kip, and Kittel, Phys. Rev. **95**, 568 (1954).

[8] The values for Ge have been revised from more recent data obtained by the Lincoln Group.

[9] W. Shockley, *Electrons and Holes in Semiconductors* (D. Van Nostrand Company, Inc., New York, 1950), p. 240.

where $q=\frac{1}{2}[\sin^4\theta(\cos^4\phi+\sin^4\phi)+\cos^4\theta-\frac{3}{5}]$. For the p calculation, the first three terms in the series give an accuracy better than one percent for the holes of the larger mass in germanium. In any case, the expression for p is

$$p=\left[2\frac{(2\pi m_0KT)^{\frac{3}{2}}}{h^3}e^{(\epsilon_F-\epsilon_P)/KT}\right][(A\pm B')^{-\frac{1}{2}}$$
$$\times(1+0.05\gamma+0.01635\gamma^2+0.000908\gamma^3+\cdots)]. \quad (10)$$

The galvanomagnetic coefficients given in Eq. (1) can be evaluated using the same general procedure as was illustrated for the carrier density calculation. In this manner one obtains

$$\sigma_{ij}=\left[\frac{8}{3\sqrt{\pi}}\left(\frac{2\pi m_0KT}{h^2}\right)^{\frac{3}{2}}e^{(\epsilon_F-\epsilon_P)/KT}\frac{e^2l}{m_0}\Gamma(5/2-\lambda)(KT)^{-\lambda}\right]$$
$$\times[(A\pm B')^{-\frac{1}{2}}(1+0.01667\gamma+0.041369\gamma^2$$
$$+0.00090679\gamma^3+0.00091959\gamma^4$$
$$+0.00002106\gamma^5+\cdots)]\delta_{ij}, \quad (11)$$

$$\sigma_{ijl}=\left[\frac{32\pi}{3}\frac{e^3l^2}{h^3c(2m_0)^{\frac{1}{2}}}e^{(\epsilon_F-\epsilon_P)/KT}(KT)^{\frac{1}{2}-2\lambda}\Gamma(5/2-2\lambda)\right]$$
$$\times[(A\pm B')^{\frac{1}{2}}(1-0.01667\gamma+0.017956\gamma^2$$
$$-0.0069857\gamma^3+0.0012610\gamma^4+\cdots)]\epsilon_{ijl}. \quad (12)$$

Here $\Gamma(n)$ represents the gamma function, δ_{ij} the Kronecker symbol, ϵ_{ijl} is the permutation tensor, and it is assumed that $\tau=l\epsilon^{-\lambda}$. Furthermore, it can be shown from symmetry considerations that only the components given above in Eqs. (11) and (12) are different from zero.

The current density due both to holes of large effective mass and of small effective mass can be obtained by modifying Eq. (1) to read

$$J_i=\Sigma_{ij}E_j+\Sigma_{ijl}E_jH_l+\Sigma_{ijlm}E_jH_lH_m+\cdots, \quad (13)$$

where the Σ coefficients represent the sum of the individual σ coefficients for the two kinds of holes.

By inverting Eq. (13), the usual Hall and magnetoresistance constants may be found as follows:

$$E_i=\Lambda_{ij}J_j+\Lambda_{ijl}J_jH_l+\Lambda_{ijlm}J_jH_lH_m+\cdots. \quad (14)$$

Following Abeles and Meiboom, Eq. (14) is substituted into Eq. (13) and the Λ coefficients are evaluated by equating terms of same order in H and neglecting terms of higher order than H^2. Since these coefficients have already been published,[1] they are given in Appendix B.

III. APPLICATIONS OF THE THEORY

A. Effective Masses

In the case of spherically symmetrical energy surfaces, the mass is a scalar and hence has the same value for the conductivity and the density of states. For nonspherical energy surfaces, on the other hand, this is not the case and one has to deal with two kinds of effective masses, the density-of-states effective mass m_d which we shall define from the relationship

$$p=\frac{2(2\pi m_dKT)^{\frac{3}{2}}}{h^3}e^{(\epsilon_F-\epsilon_P)/KT},$$

and a conductivity mass, m_σ, which is found from the expression

$$\sigma=pe^2\bar{\tau}_\sigma/m_\sigma,$$

where $\bar{\tau}_\sigma$ is an appropriate mean free time as defined by Shockley.[10] Expressions for the various masses have been worked out by using the results of Eqs. (10) and (11) and are given here:

$$m_{di}=\frac{m_0}{(a\pm b')}[1+0.03333\gamma_i+0.01057\gamma_i^2$$
$$-0.00018\gamma_i^3-0.00003\gamma_i^4+\cdots], \quad (15)$$
$$m_{\sigma i}=\frac{m_0}{(a\pm b')}[1+0.03333\gamma_i-0.02566\gamma_i^2$$
$$-0.00095\gamma_i^3+0.00111\gamma_i^4+\cdots],$$

where the second subscript i refers to the hole in question.

In problems such as those associated with the Haynes mobility experiment and transistor phenomena, it is customary to consider only one type of hole or electron. This implies that the total number of holes or electrons are equal to the sum of those moving on the separate energy surfaces and that these equivalent particles move on a single spherical energy surface. In our definition of equivalent conductivity masses, we shall assume that the average scattering time is the same for the individual particles and their single equivalent. This assumption of equal average $\bar{\tau}_\sigma$ is fairly reasonable in view of WHB results[5] and also from cyclotron resonance measurements where the $\bar{\tau}_\sigma$ are determined from the half-widths. Then in accordance with these restrictions we can say

$$\sigma=\sigma_L+\sigma_H=\frac{pe\bar{\tau}_\sigma p}{m_\sigma}=\frac{p_Le\bar{\tau}_{\sigma L}}{m_{\sigma L}}+\frac{p_He\bar{\tau}_{\sigma H}}{m_{\sigma H}},$$

or

$$\frac{1}{m_\sigma}=\frac{1}{p}\left[\frac{p_L}{m_{\sigma L}}+\frac{p_H}{m_{\sigma H}}\right], \quad (16)$$

where the subscript L refers to the light holes and the subscript H, to the heavier holes. The mass with no second subscript is the appropriate effective mass of the equivalent single hole which is the combination of the light and heavy holes.

[10] See reference 9, p. 276. Shockley uses τ_a for this mean free time; we are using $\bar{\tau}_\sigma$ to emphasize that this mean free-time is associated with the conductivity mobility and not the Hall mobility.

Since $p=p_L+p_H$,

$$m_d^{\frac{1}{2}}=m_{dL}^{\frac{1}{2}}+m_{dH}^{\frac{1}{2}}. \quad (17)$$

From Eqs. (16) and (17) one obtains the following expression for an equivalent conductivity mass:

$$m_c=m_{cH}\left[1-\left(\frac{m_{dL}}{m_{dH}}\right)^{\frac{1}{2}}\left(\frac{m_{cH}}{m_{cL}}\right)\right]\left[1+\left(\frac{m_{dL}}{m_{dH}}\right)^{\frac{1}{2}}\right]. \quad (18)$$

Since the small hole may be quite light compared to the heavy hole, it is convenient to expand the above expressions to

$$m_d\approx m_{dH}\left[1-\frac{2}{3}\left(\frac{m_{dL}}{m_{dH}}\right)^{\frac{1}{2}}\right], \quad (19)$$

$$m_c\approx m_{cH}\left[1-\left(\frac{m_{dL}}{m_{dH}}\right)^{\frac{1}{2}}\left(\frac{m_{cH}}{m_{cL}}-1\right)\right]. \quad (20)$$

Assuming the ellipsoidal model for the conduction band, it can be shown, as was done in Eq. (7) for the hole density in the valence band, that the electronic density is

$$n=2\left(\frac{2\pi m_e KT}{h^2}\right)^{\frac{3}{2}}N_c e^{(\epsilon_F-\epsilon_c)/KT}, \quad (21)$$

where m_e is the effective density of states mass for electrons (equal to 0.22 m_0 for germanium and 0.33 m_0 for silicon), ϵ_c is the energy at the bottom of the conduction band, and N_c is the number of ellipsoids in the conduction band (equal either to four or eight for germanium and either to three or six for silicon). The density of states mass, m_e, is given by[1]

$$m_e=m_t^{\frac{2}{3}}m_l^{\frac{1}{3}}, \quad (22)$$

where m_t and m_l are the transverse and longitudinal electron masses respectively. Multiplying together the expressions for p and n from Eqs. (10) and (21) respectively we obtain, after taking the square root, the following expression for the intrinsic carrier concentration[11] n_i:

$$n_i=(pn)^{\frac{1}{2}}=2N_c^{\frac{1}{2}}\left(\frac{2\pi m_a KT}{h^2}\right)^{\frac{3}{2}}e^{-\epsilon_G/2KT}$$

$$=NT^{\frac{3}{2}}e^{-\epsilon_G/2KT}, \quad (23)$$

where ϵ_G is the energy gap, equal to $(\epsilon_c-\epsilon_v)$, see Fig. 4, and m_a is a combined density effective mass defined by Eq. (23), associated with both holes and electrons and equal to $(m_c m_e)^{\frac{1}{2}}$. These various effective masses have been calculated and are given in Table I.

Another quantity of interest is the ratio of the number of small holes to heavy holes; using the results of Eq. (10) and the appropriate numerical values, this ratio becomes 0.0423 for germanium and 0.165 for silicon. It should be noted that the value for germanium is about twice that determined by WHB from Hall coefficient data near room temperature.

[11] See reference 9, p. 304.

TABLE I. Effective masses in germanium and silicon.

Material	Density of states masses for holes m_{dH}/m_0	m_{dL}/m_0	m_d/m_0	Conductivity masses for holes m_{cH}/m_0	m_{cL}/m_0	m_c/m_0	Combined density of states mass, m_a (includes both holes and electrons)
Germanium	0.36	0.043	0.37	0.31	0.044	0.25	0.29
Silicon	0.53	0.14	0.59	0.49	0.16	0.38	0.44

Values for the quantity N which is defined in Eq. (23) are 1.48×10^{15} or 2.1×10^{15} cgs units (for N_c equal to four or eight respectively) for germanium and 2.45×10^{15} or 3.46×10^{15} cgs units (for N_c equal to three or six respectively) for silicon. These values which are calculated from the cyclotron resonance data may be compared with those determined from the measurements of Morin and Maita. The latter give, for N, 1.76×10^{15} cgs units for germanium[12] and 3.87×10^{15} cgs units for silicon.[13] Assuming that the discrepancy between the theoretical and measured values of N is due to a linear variation of the energy gap with temperature one can solve for this variation, by equating the theoretical and experimental intrinsic carrier expressions, thus obtaining[14]

$$\epsilon_G(T)=\epsilon_G(0)-\beta T, \quad (24)$$

where for germanium[12] $\epsilon_G(0)=0.785$ ev and $\beta=4.3\times10^{-4}$ or 3.7×10^{-4} ev/°K, depending on whether 4 or 8 ellipsoids are taken for the conduction band and for silicon[13] $\epsilon_G(0)=1.21$ ev and $\beta=4.8\times10^{-4}$ or 4.2×10^{-4} ev/°K, depending on whether 3 or 6 ellipsoids are chosen. The above calculations are based upon the assumption that the effective masses which are measured at 4.2°K do not change at the higher temperatures. This is probably not true since with increasing temperature the curvature of the energy surface is likely to change. It is of interest to compare the calculated temperature coefficient of the energy with that obtained experimentally from infrared absorption edge measurements. In the temperature range 100°K to 700°K the temperature coefficient is reported[15] as 5.4×10^{-4} ev/°K for germanium and 5×10^{-4} ev/°K for silicon.

More recently, Macfarlane and Roberts have made similar measurements in germanium[16] and silicon.[17] Their results are shown in Figs. 1 and 2 by the solid lines. Plotted on the same figures is the variation of ϵ_G with temperature, calculated from Morin and Maita's data by using the cyclotron resonance effective masses for 4.2°K. It is seen that the four-ellipsoid model seems

[12] F. J. Morin and J. P. Maita, Phys. Rev. **94**, 1525 (1954).
[13] F. J. Morin and J. P. Maita, Phys. Rev. **96**, 28 (1954).
[14] G. L. Pearson and J. Bardeen, Phys. Rev. **75**, 865 (1949).
[15] Purdue University Semiconductor Research Final Report PRF-489 dated September 1, 1948 to November 30, 1951 (unpublished), p. 147.
[16] G. G. Macfarlane and V. Roberts, Phys. Rev. **97**, 1714 (1955).
[17] G. G. Macfarlane and V. Roberts, Phys. Rev. **98**, 1865 (1955).

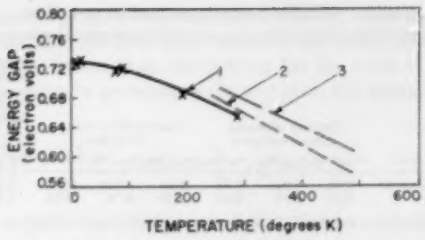

FIG. 1. Variation of the energy gap in germanium with temperature. Curves are labeled (1), (2), and (3). (1): data of Macfarlane and Roberts; (2): Lincoln Laboratory calculations for the 4-ellipsoid model; and (3): Lincoln Laboratory calculations for the 8-ellipsoid model.

to give best agreement for germanium and the six-ellipsoid, for silicon. However, it must be remembered that the combined effective mass has been assumed constant with temperature. Macfarlane and Roberts claim that for both germanium and silicon the conduction band minima do not lie at the band edges and hence the number of ellipsoids are 8 and 6 for germanium and silicon respectively. From this information an estimate of the temperature variation of the effective mass can be made by fitting the calculated values from Morin and Maita's experiments to the optically determined values of ϵ_G. From this the combined effective mass of germanium appears to decrease from $0.29\,m_0$ to $0.20\,m_0$ in going from 4.2°K to room temperature whereas the combined effective mass of silicon seems to increase from $0.44\,m_0$ to $0.46\,m_0$ in the same temperature range. The variation in germanium is of the same direction and order of magnitude as estimated for electrons in germanium by Kahn[18] from the infrared absorption coefficient.

B. Ratio of Hall Mobility to Conductivity Mobility at Zero Magnetic Field

The Hall mobility μ_H can be defined as $R\sigma_0$, where R is the Hall coefficient and σ_0 is the conductivity at zero magnetic field; the conductivity mobility μ_σ, on the other hand, is simply σ_0/pe. Thus the ratio of these two mobilities is

$$\mu_H/\mu_\sigma = Rpe. \tag{25}$$

Since R_∞, the Hall coefficient in the limit of infinite magnetic field, equals $1/pe$,[19] it is evident that

$$\mu_H/\mu_\sigma = R/R_\infty. \tag{26}$$

Making use of Eqs. (10), (11), and (12) and Appendix B and assuming that $\tau_H = \tau_L = l\epsilon^{-\lambda}$, it can be shown that R_0, the Hall coefficient in the limit of zero magnetic field, equals

$$R_0 = \frac{1}{pec}\,\frac{DF}{E^2}\,\frac{\Gamma(5/2)\Gamma(5/2-2\lambda)}{\Gamma^2(5/2-\lambda)}, \tag{27}$$

where D, E, and F are the second brackets in Eqs. (10), (11), and (12) respectively, but with each of these quantities summed over both types of holes.

Substituting the appropriate constants and assuming that τ is constant ($\lambda=0$) gives the zero-field value of the mobility ratio of Eq. (25) as 1.76 for germanium and 1.24 for silicon, whereas assuming lattice scattering ($\lambda=\frac{1}{2}$) gives this ratio as 2.07 for germanium and 1.45 for silicon. Experimentally Morin finds that for germanium this ratio for holes varies from 1.13 at 50°K to 1.73 at 275°K, and he suggests that this temperature variation is connected with shape and number of surfaces of minimum energy in the Brillouin zone.[20] Morin does not, however, give the magnitude of the magnetic field which he used in these measurements. WHB, on the other hand, show that by assuming a constant magnetic field (for example 4000 gauss) that the large-field approximation is fairly good in the low-temperature region whereas near room temperature one is approaching the low-field limit and can account for the variation of the mobility ratio in this manner if both types of holes are included. Since our calculations are based on the low-field approximation, our results should be compared with the measurements near room temperature. Morin and Maita have also measured the mobility ratio for silicon;[12] they find $\mu_H/\mu_\sigma < 1$.

The theoretical calculation of μ_H/μ_σ for germanium using the warped surfaces also may be compared to the ratio R_0/R_∞ for a p-type sample as shown in Fig. 1 of reference 5. In the extrinsic region for a temperature of 205°K where we assume with WHB that lattice scattering is the dominant process,[21] $R_0/R_\infty = 1.9$ which is in reasonable agreement with the calculated value of 2.07.

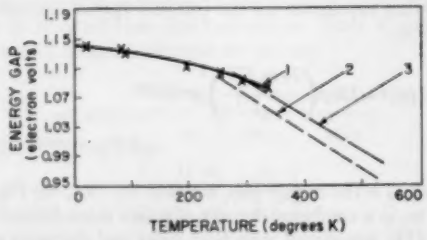

FIG. 2. Variation of the energy gap in silicon with temperature. Curves are labeled (1), (2), and (3). (1): data of Macfarlane and Roberts; (2): Lincoln Laboratory calculations for the 3-ellipsoid model; and (3): Lincoln Laboratory calculations for the 6-ellipsoid model.

[18] A. H. Kahn, Phys. Rev. 97, 1647 (1955).

[19] This relationship has been pointed out by M. Shibuya for ellipsoidal surfaces, C. Herring for the simple "many-valley" model and E. N. Adams, L. Roth, and H. Zeiger for warped surfaces.

[20] F. J. Morin, Phys. Rev. 93, 62 (1954).

[21] We are defining lattice scattering as corresponding to $\lambda=\frac{1}{2}$. It must be noted, however, that this is only an approximation since $\lambda=\frac{1}{2}$ does not correspond to the experimental determination of hole mobility variation with temperature.

C. Hall Constant in the Transition Region

In the transition region, that is in the neighborhood of the temperature at which the Hall coefficient goes to zero, it is necessary to consider electrons as well as the two kinds of holes. The Hall constant then becomes, by use of Appendices A and B,

$$R=\frac{\Sigma_{xyz(\text{electrons})}+\Sigma_{xyz(\text{holes})}}{\{\sigma_{0(\text{electrons})}+\sigma_{0(\text{holes})}\}^2}, \tag{28}$$

where $\Sigma_{xyz(\text{electrons})}$ and $\sigma_{0(\text{electrons})}$ have been calculated by Abeles and Meiboom for low magnetic fields using ellipsoidal surfaces.

If one assumes that the relaxation time τ_ϵ is independent of energy for all three carriers,[22] then there remains but one unknown in Eq. (28), namely the ratio $\tau_{\epsilon n}/\tau_{\epsilon p}$, where $\tau_{\epsilon n}$ is the relaxation time for the electrons.

Calculations corresponding to the p-type sample of WHB have been made. First, the experimental temperature at which the Hall constant goes to zero has been used to find $\tau_{\epsilon n}/\tau_{\epsilon p}$ and then, with this ratio known, the Hall constant has been computed for the temperatures given in Fig. 3 of WHB.[23] The results are plotted in Fig. 3 and it is seen that the agreement with experiment is fairly good.

IV. DISCUSSION

In our treatment of galvanomagnetic effects we have carried out the calculations for low magnetic fields using warped energy surfaces and, to a limited extent, taking into account the energy dependence of the scattering time. In principle what is desired is a general theory which can be used for all values of magnetic field. This, however, is very difficult to achieve in this case. The low-field limit which we have treated has been very useful for evaluating expressions for the hole density, conductivity, and Hall constant. These results have been used to analyze existing data. In particular the evaluation of effective masses can be useful in speculating about the changes of the band structure as a function of temperature. For germanium the percent change for the combined effective mass of both types of carriers

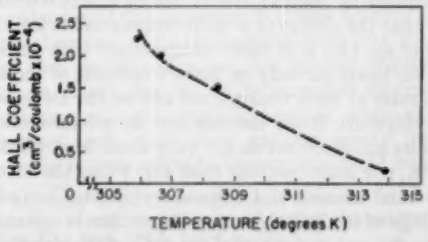

FIG. 3. Variation of the zero-field Hall coefficient with temperature. Points are taken from data of Willardson, Harman, and Beer. The curve is obtained from our calculations.

[22] As before $\tau_{\epsilon H}=\tau_{\epsilon L}=\tau_{\epsilon S}$.

[23] Details of the method of calculation are given in Appendix C.

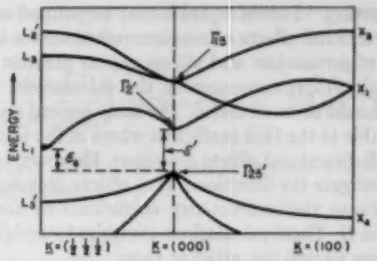

FIG. 4. Energy band contours in pure germanium (according to Herman, reference 25).

in going from 4.2°K to room temperature as estimated from our calculations, assuming the eight ellipsoid model for electrons to be correct at room temperature, is of the order of 30 percent. Kahn's estimate for the electrons alone is also about 30 percent; hence it follows from the definition of m_a, i.e., $m_a=(m_d m_c)^{\frac{1}{2}}$, that the change in the combined mass of holes must be of this order of magnitude. This percent change can be reconciled with the model of the band structure which has been constructed from theoretical work and known experimental data. From his theoretical work, Herman[24,25] estimates that the $\Gamma_{2'}$ minimum of the conduction band at $K=(000)$ moves in the same direction, as a function of temperature and pressure, as the L_1 minimum but at approximately two or three times the rate of the L_1 minimum (see Fig. 4). From perturbation considerations it can be shown that the curvature at the top of the valence band is affected primarily by the $\Gamma_{2'}$ minimum and that the proportional change in effective mass is $\Delta m_d/m_d \approx \Delta\epsilon'/\epsilon'$. According to Macfarlane's data of Fig. 1, the change in the energy gap ϵ_0 (Fig. 4) for this temperature range is a reduction of the order of 10 percent. The analysis of the experimental data which indicates a 30 percent change in effective mass therefore predicts a comparable percent change in ϵ'. The situation in silicon is not as complete and well established; hence such a picture cannot as yet be constructed.

As we pointed out there seems to be a discrepancy between our calculations and the WHB results. We find a value for the ratio of the number of light to heavy holes which is about twice that determined by WHB from low-field Hall data at room temperatures. This discrepancy seems unexplainable since according to WHB the ratio p_L/p_H appears to decrease with decreasing temperature whereas our value which is determined from data taken at 4.2°K is always greater.

The techniques described in this paper are being used to evaluate the magnetoresistance coefficients in order to investigate the directional effects of p-type germanium and silicon. The results will be compared with the experimental data of Pearson and Suhl[26] and Pearson

[24] F. Herman (private communication).

[25] F. Herman, Phys. Rev. 95, 847 (1954).

[26] G. L. Pearson and H. Suhl, Phys. Rev. 83, 768 (1951).

and Herring.[27] In this regard it may be pointed out that the directional effects of magnetoresistance for valence bands of germanium and silicon appear greatest at low magnetic fields; consequently the calculations in this limit should be most useful. The same general remark is applicable to the Hall coefficient where in the saturation limit all directional effects disappear. However, in order to investigate the directional Hall effects, it is necessary to evaluate the conductivity coefficients of the cubic terms in H. These calculations are quite formidable and therefore we will not attempt them.

The magnetoresistance and Hall effect can be evaluated in the high-field limit; however, these do not appear to be useful in investigating the directional galvanomagnetic effects in p-type germanium.

The treatment which we have presented gives the dc conductivities. For rf calculations, it can be shown by use of the Boltzmann equation that $1/\tau$ must be replaced by $(1/\tau+j\omega)$ in the integrals given in Appendix A. If the relaxation time is not a function of the energy this amounts to simply substituting $(1/\tau+j\omega)$ for $1/\tau$ in the final integrated expressions.

The results obtained in this paper and the method used are quite general and should be useful for investigating the properties of similar surfaces in materials other than germanium and silicon, provided the anisotropy is not so large as to impair the rapid convergence of the series in terms of the anisotropy parameter γ.

ACKNOWLEDGMENTS

The authors would like to thank Professor H. Brooks, Mrs. Laura Roth, and Dr. H. J. Zeiger for helpful discussions and Dr. F. Herman for information relating to the energy band of germanium. We are also indebted to Mrs. Virginia Johnson and Miss Janet Beck for carrying out the computations.

APPENDIX A

The single-energy-surface conductivity coefficients are defined as follows: The current density j_i per energy surface may be expressed as

$$j_i=\sigma_{ij}E_j+\sigma_{ijl}E_jH_l+\sigma_{ijlm}E_jH_lH_m+\cdots,$$

where

$$\sigma_{ij}=-\frac{e^3}{4\pi^3\hbar^3}\int\tau\frac{\partial f_0}{\partial\epsilon}\frac{\partial\epsilon}{\partial k_i}\frac{\partial\epsilon}{\partial k_j}dV_k,$$

$$\sigma_{ijl}=\frac{e^4}{4\pi^3\hbar^4c}\int\tau\frac{\partial f_0}{\partial\epsilon}\frac{\partial\epsilon}{\partial k_i}\frac{\partial\epsilon}{\partial k_r}\frac{\partial}{\partial k_s}\left(\tau\frac{\partial\epsilon}{\partial k_j}\right)\epsilon_{lrs}dV_k,$$

$$\sigma_{ijlm}=-\frac{e^5}{4\pi^3\hbar^6c^2}\int\tau\frac{\partial f_0}{\partial\epsilon}\frac{\partial\epsilon}{\partial k_i}\frac{\partial\epsilon}{\partial k_r}\frac{\partial}{\partial k_s}\times\left[\tau\frac{\partial\epsilon}{\partial k_t}\frac{\partial}{\partial k_u}\left(\tau\frac{\partial\epsilon}{\partial k_j}\right)\right]\epsilon_{mrs}\epsilon_{ltu}dV_k.$$

Here τ is the relaxation time, f_0 is the unperturbed distribution function, ϵ is the energy, dV_k is an element of volume in k space and the remaining symbols have their usual meaning; the Einstein summation notation is used, with ϵ_{ijl} acting as the permutation tensor.

APPENDIX B

The magnetoresistance coefficients, obtained by substituting Eq. (14) into Eq. (13) and equating terms of like orders in H, are

$$\Lambda_{ij}=\delta_{ij}/\sigma_0,$$

$$\Lambda_{ijl}=-\Sigma_{ijl}/\sigma_0^2\equiv-R_0\epsilon_{ijl},$$

$$\Lambda_{ijlm}=-\frac{1}{\sigma_0^2}\left[\Sigma_{ijlm}-\frac{1}{\sigma_0}\Sigma_{iml}\Sigma_{ajm}\right].$$

APPENDIX C. OUTLINE OF τ_{en}/τ_{ep} CALCULATION

Substituting into Eq. (28), and assuming the τ_{ei} independent of energy one obtains R, the Hall coefficient, in the form

$$R=\frac{Gn\tau_{en}^2-Hp\tau_{ep}^2}{(Ln\tau_{en}+Mp\tau_{ep})^2},\tag{C.1}$$

where G, H, L, and M are known numerical constants. For $R=0$, we obtain

$$\frac{\tau_{en}}{\tau_{ep}}=\left(\frac{H}{G}\frac{p}{n}\right)^{\frac{1}{2}}.\tag{C.2}$$

Thus what is required is the ratio p/n. This can be found by solving the following two equations simultaneously.

$$p=p_0+n,\tag{C.3}$$

and

$$np=n_i^2=N^2T_0^3e^{-\epsilon_G/KT_0},\tag{C.4}$$

where p_0 is the extrinsic hole concentration and T_0 is the temperature at which the Hall constant goes to zero.

Note added in proof.—(1) Recent information on the infrared absorption[28] and magnetic susceptibility of germanium[29] contradict some of the arguments presented to support the Macfarlane-Roberts 8-ellipsoidal model. The infrared data of Dash and Newman of absorption by indirect transitions at $K=(0\,0\,0)$ indicate that the change in ϵ' with temperature is less than that of ϵ_G. This is in direct disagreement with our contention based partially on Kahn's estimate of the electron mass at room temperature and on the assumption of 8 ellipsoids. If one assumes that the effective masses of holes and electrons do not vary much from 4.2°K to 300°K, one must conclude from Fig. 1 that the conduction band consists of 4 ellipsoids which are located at the edge of the Brillouin zone. This is then in agreement with the conclusions of Crawford, Schweinler, and Stevens, from their magnetic susceptibility measure-

[27] G. L. Pearson and C. Herring, Physica **20**, No. 11, 975 (1954).

[28] W. C. Dash and R. Newman, Phys. Rev. **99**, 1151 (1955).

[29] Crawford, Schweinler, and Stevens, Phys. Rev. **99**, 1330 (1955).

ments. (2) Using the method outlined in our paper it is a simple matter to evaluate the expressions for the diamagnetic susceptibility of holes in germanium and silicon, using Wilson's[30] equation (6.8.1):

$$\chi=\frac{e^2}{12\pi h^2c^2}\int\int\left[\frac{\partial^2\epsilon}{\partial k_z^2}\frac{\partial^2\epsilon}{\partial k_y^2}-\left(\frac{\partial^2\epsilon}{\partial k_z\partial k_y}\right)^2\right]^2\left|\frac{\partial f_0}{\partial\epsilon}\right|dV_k.$$

[30] See reference 6, p. 175.

If we apply the expansion scheme in spherical coordinates we obtain

$$\chi=\frac{1}{6}\frac{e^2}{hc^2}\left(\frac{KT}{2\pi m_0}\right)\exp[(\epsilon_v-\epsilon_F)/KT](A\pm B')^{\frac{1}{2}}\{\gamma_x\},$$

where $\{\gamma_x\}$ is the γ series which appears above in the expression for σ_{ij}, Eq. (12).

PHYSICAL REVIEW VOLUME 100, NUMBER 6 DECEMBER 15, 1955

Mechanical Strength of Thin Films of Metals*

J. W. Beams, J. B. Breazeale, and W. L. Bart
University of Virginia, Charlottesville, Virginia

(Received September 12, 1955)

The tensile strength of silver films are determined as a function of their thickness. The films are electrodeposited on the complete cylindrical surfaces of small steel rotors and the rotor speeds necessary to throw them off are determined. Both the tensile strength and the adhesion of the films are obtained by using rotors of different radii. Also, the adhesion is measured by electrodepositing the films on the rotor in circumferentially disconnected patches which eliminate the hoop stresses. In most of the measurements, the adhesion is made vanishingly small by dipping the rotors in an albumin solution before electrodepositing the film and by thermal cycling. The tensile strengths of the films thicker than about 6×10^{-6} cm are found to be independent of thickness and approximately equal to that of bulk silver at the corresponding temperature. For thickness from 6×10^{-6} cm to 2.5×10^{-6} cm the data show some scatter, but below 2.5×10^{-6} cm the tensile strength increases many-fold. The region where the tensile strength increases very rapidly is slightly dependent upon the electrodeposition current but within experimental error is independent of film temperature.

UNDER the influence of tensile or shearing forces, a metal deforms elastically at first, and then plastically. Usually, plastic flow begins with stresses at least 100 times smaller than should be required to cause whole atomic planes in a perfect metal crystal to move over one another. This discrepancy between the caculated and observed values of the stresses required to produce plastic flow is generally attributed to the movement of lattice imperfections or dislocations which are believed to exist in most ordinary metal crystals.[1] This dislocation theory has been remarkably successful, not only in accounting for the low mechanical strength of metal crystals, but also for many other observed properties of substance that otherwise would be difficult to understand.[2] Consequently, if it were possible to free a metal crystal of its dislocations or to lock them so that they could not move, the stresses required to produce plastic flow would be increased enormously. Furthermore, in polycrystalline metals, where at temperatures well below their melting points fracture generally is observed to be transcrystalline,[3,4] increased strength should also be obtained. Apparently, the above conditions are at least partially realized experimentally, by forming the material in sufficiently fine filaments or thin sheets. Griffith[5] found that under certain conditions the tensile strengths of very fine fibers of glass and of metals, were many times that of the bulk material from which they were made, while Orowan[6] observed that extremely thin sheets of mica were very strong. More recently, Herring and Galt[7] and others, have found that metal crystals (whiskers), approximately 18×10^{-6} cm in diameter, are several orders of magnitude stronger than the ordinary bulk metal. In some preliminary experiments[8] an increase in the tensile strength of thin films of silver has been observed when their thickness was reduced to between 10^{-4} cm and 10^{-6} cm. The purpose of this paper is to report, in more detail, an extension and improvement of these measurements.

In order to prevent tearing or stress concentrations in the very thin films, a centrifugal field has been used to apply the stresses. The method consists in uniformly depositing thin metal films on the cylindrical surface of a small rotor with rounded ends and then spinning the rotor in a vacuum until the film is thrown off. By this procedure, accurately known stresses may be applied

* Supported by the Office of Ordnance Research.

[1] A. H. Cottrell, *Progress in Metal Physics* (Interscience Publishers, New York, 1949), Vol. 1, p. 770.

[2] Seitz, Shockley, Read, and Mott in *Imperfections in Nearly Perfect Crystals* (John Wiley and Sons, Inc., New York, 1952).

[3] R. King and B. Chalmers, *Progress in Metal Physics* (Interscience Publishers, New York, 1949), Vol. 1, p. 127.

[4] C. S. Barrett, *Structure of Metals* (McGraw-Hill Book Company, Inc., New York, 1952), second edition.

[5] A. A. Griffith, Trans. Roy. Soc. (London) **221**, 163 (1921).

[6] E. Orowan, Z. Physik **82**, 235 (1933).

[7] C. Herring and J. K. Galt, Phys. Rev. **85**, 1060 (1952).

[8] Beams, Walker, and Morton, Phys. Rev. **87**, 524 (1952). Beams, Morton, and Turner, Science **118**, 567 (1953).

uniformly, and at almost any desired rate. By assuming that the centrifugal action is opposed by the hoop stresses, and the adhesion of the film to the rotor, it can be shown that in the case of a hollow thin-walled cylindrical rotor, unsupported at the ends,

$$4\pi^2N^2R^2d=T+AR/h, \quad (1)$$

where N is the rotor speed in rps, R is the rotor radius, d the density of the deposited film, h the thin-film thickness, T the tensile strength of the film, and A the adhesion.

It will be observed that the second term on the right contains R/h, while the first does not, so that by experimenting with rotors of different radii, both the tensile strength and the adhesion can be obtained. On the other hand, if the ratio of the rotor radius to the film thickness is large, the second term on the right of Eq. (1) overshadows the first, and, unless the adhesion is small, minute variations in the adhesion make it difficult to get reliable values for the tensile strength. Although experiments are underway in which it is hoped that this ratio can be greatly reduced, in the present experiments this ratio is several hundred for the thinnest films. Consequently, the films have been deposited and treated in such a way that the adhesion is small.

If the adhesion of the film is vanishingly small, $4\pi^2N^2R^2d=T$, which shows that the tensile strength is independent of the film thickness. This neglects the small effect of the circumferential strain or stretching of the film, and assumes that the film is thin and behaves plastically in a homogeneous way. On the other hand, if the hoop stress vanishes, as in the case when the material is deposited on the rotor surface in circumferentially disconnected patches, then the adhesion is given by $A=4\pi^2N^2Rhd$.

DESCRIPTION OF EXPERIMENTAL ARRANGEMENT

The rotors are suspended magnetically in a vacuum and are spun around a vertical axis by a rotating magnetic field. The method is a modification of one previously described.[9] Figure 1 shows a schematic diagram of a magnetic suspension apparatus for spinning rotors at various temperatures. The steel rotor is freely suspended inside of a glass vacuum chamber by the axially-symmetric diverging magnetic field of the solenoid. The vacuum chamber is surrounded by two concentric glass Dewar vessels, and the solenoid which is outside the outer Dewar vessel. They all have a common axis, as shown in Fig. 1. A small pickup coil, mounted inside the inner Dewar, and just below the vacuum chamber, serves as a sensing element of a servo-circuit, which regulates the current through the solenoid in such a way that the rotor is maintained at the desired vertical position. The rotor automatically seeks the strongest part of the field which is on the axis of the solenoid. However, if disturbed, it swings around the axis. In order to prevent these horizontal oscillations, a steel damping needle (1 cm long and 0.1 cm diameter) is placed just below the sensing coil, and fastened to a weight in the inner Dewar with a fine gold chain 3.5 cm long. In order to spin the rotor at reduced temperatures, the two Dewars are filled with various liquids, i.e., when liquid nitrogen temperature is desired, they are filled with liquid nitrogen, etc. If the rotor starts to swing, the magnetic field follows it, and hence pulls the needle along with it. The viscous drag produced by the liquid on the damper is sufficient to stop the horizontal motion of the rotor. A cone-shaped plastic shield around the damper keeps bubbles formed near the bottom of the inner Dewar from disturbing the damper. The support solenoid consists of 21 110 turns of No. 23 *AGW* enamel copper wire wound on a plastic form. It has a resistance of 710 ohms, an inductance of 37 henries, and a disturbed capacity of 380 $\mu\mu$f. The support circuit is shown in Fig. 2. The pick up coil L_1 is the inductive element in the grid circuit of a partially neutralized tuned-grid, tuned-plate oscillator which operates at about 6 Mc/sec. A change in the vertical

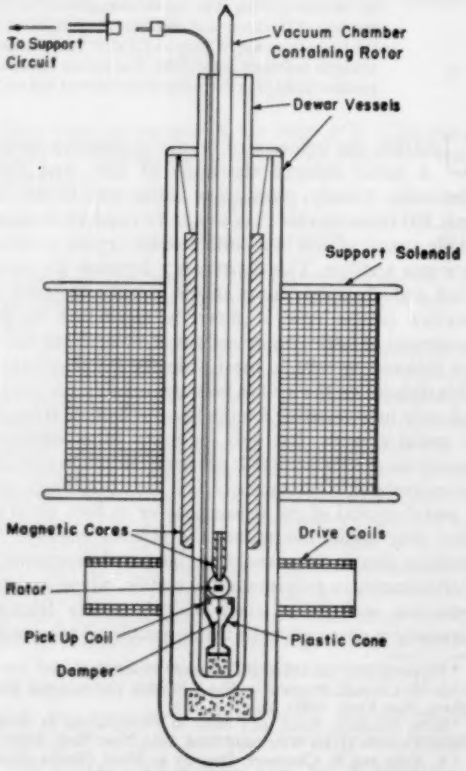

FIG. 1. Diagram of appratus for spinning rotors at various temperatures.

[9] Beams, Young, and Moore, J. Appl. Phys. 17, 886 (1946).

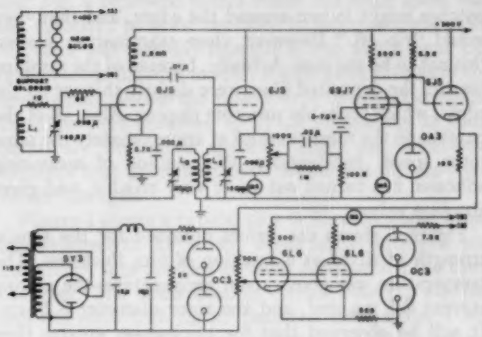

FIG. 2. Magnetic suspension circuit.

position of the rotor with respect to the pickup coil changes the Q of the oscillator circuit, and hence the amplitude of the oscillations. The output of the oscillator is applied to the grid of a 6J5 in an infinite-impedance detector stage which does not load the oscillator. The dc voltage appearing across the cathode resistor is proportional to the amplitude of the oscillations, and therefore is an electrical measure of the rotor height above the pickup coil. This output of the detector is amplified and used to control the grid voltage, and thus the plate current of the power amplifier, which is also the current through the support solenoid. The result is that any change in the position of the rotor produces a change in the support solenoid current which tends to correct the original change in position. In order to prevent vertical hunting of the rotor, a phase lead, together with effective damping is introduced into the amplifier stage, which prevents all observable vertical hunting. If desired, the current in the solenoid required to support the rotor may be reduced by placing a soft iron core inside the vacuum chamber, together with a soft iron sleeve inside the outer Dewar as shown in Fig. 1.

Two shapes of rotors were used. The first consisted of a solid cylinder 0.55 cm in diameter, and 0.20 cm high, on top of which was an inverted cone 0.318 cm high, and with half-angle of 30°. The second type was a solid cylinder 0.276 cm in diameter, and 0.234 cm high (the length of the cylinder is less than $\sqrt{3}$ times its radius). The rotors were made from 0.95/1.10 carbon tool steel, which was heated to 1450°F and quenched in water. They were tempered by heating to 425°F and quenching in water. They were then polished with emory paper, starting with No. 0 and progressing down to No. 0000. Some of the rotors were polished further with jewelers' rouge. In some of the low-temperature experiments, a special steel was used for the rotors, with coefficients of expansion somewhat closer to that of silver. The silver films were deposited on the rotors by electro-deposition. Contrary to most commercial electroplating problems, where good film adherence is of importance, the film adherence was purposely reduced to a minimum. The silver was deposited from a fresh cyanide solution containing 31 gm/l of silver cyanide, 45 g/l of potassium cyanide and 55 gm/l of potassium carbonate, maintained at 32.4±0.1°C. The rotors to be plated were carefully cleaned in acetone, then in warm water containing a commercial detergent (Surf), rinsed thoroughly, and dried. They were then dipped in a solution of 0.2 g/l of purified human albumin in water, as recommended by Jacquet[10] for eliminating adhesion. The thin layer of albumin which remains on the rotor is conducting, and hence allows the electrodeposition of excellent films, but reduces their adhesion to a negligible value. In addition, some of the rotors were thermally cycled by dipping in liquid nitrogen, to further reduce adhesion. The rotor was spun at 2 rpm in the center of the anode which consisted of a helix of 1 mm pure silver wire during the electrodeposition. When patches were plated on the rotor, thin sections of plastic were fitted over portions of the rotor which were to be left bare. The rotor is spun inside the vacuum chamber by a rotating magnetic field in a manner similar to that of the armature of an induction motor. The method has been described in detail previously.[9] During the accelerating period, the rotor is, of course, heated by the eddy currents induced by the rotating magnetic field, but by using very slow acceleration rates, especially at speeds near where the film ruptures, the heating was made comparatively small. However, especially at temperatures below that of liquid nitrogen, this heating is greater than can be tolerated, so we are developing a method in which the rotor accelerates as a synchronous motor in which the frequency of the rotating magnetic field increases at the same rate as the rotor speed. This reduces the eddy currents and the heating to a negligible value. The rotor friction due to the mangetic suspension, is extremely small, and can be accounted for entirely as due to gaseous friction on the spinning rotor. By maintaining the gas pressure in the chamber surrounding the rotor below 10^{-6} mm of Hg this friction is very minute, and hence produces no appreciable heating. In order to stop the rotor in a reasonable time, the direction of rotation of the magnetic field must be reversed and the rotor driven to rest. The rotor speed is determined by reflecting light off the rotor into a photomultiplier tube. A mark on the top (or upper cone) of the rotor causes the output of the photomultiplier tube to be periodic, with a repetition rate equal to the speed of the rotor. This output signal is amplified and compared with that from a variable-frequency oscillator on a cathode-ray oscilloscope screen. From the resulting Lissajous pattern, the speed may be determined. When the film comes off, the rotor always is slightly disturbed, and this is easily observed by the change in pattern on the screen. Also this rotor disturbance varies the Q of the pickup circuit, which in turn changes the frequency of oscillation of

[10] P. Jacquet, Compt. rend., 118, 921 (1933).

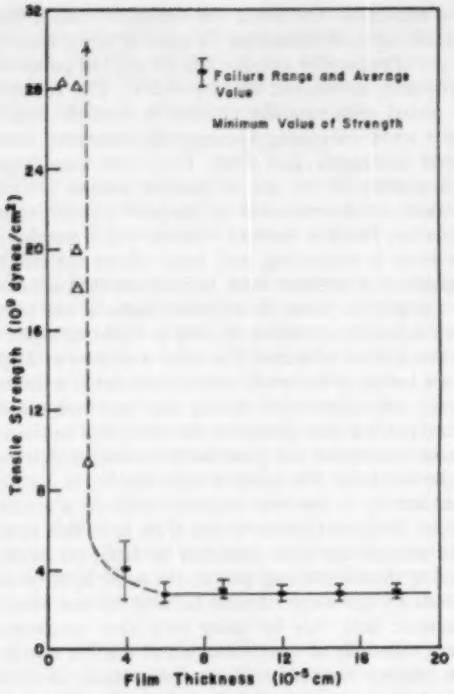

FIG. 3. Curve of tensile strength *versus* film thickness for silver at maximum temperature of 170°K.

the support circuit. Since this frequency is radiated, it may be picked up by a radio receiver in its vicinity. A highly selective RCA type CRV-46131 receiver has been used in this work. With the receiver beat-frequency oscillator in operation, the receiver is tuned to the support-circuit frequency and then detuned to give a low audio-frequency note in the loudspeaker. This note changes pitch abruptly when the film is thrown off the rotor. Also, such a system is useful in monitoring the support circuit.

The film thicknesses were measured by the usual weighing technique, and by light interference methods. In most of the experiments, curves of film thickness *versus* charge transferred in the electroplating process were made. The film thicknesses could then be determined from the amount of charge transferred, with an over-all precision of about one percent.

As pointed out above, the measurement of tensile strength is greatly simplified if the adhesion can be reduced to a negligible value. Consequently, silver films of different thicknesses were deposited on the rotors in patches, and the absolute value of the adhesion A determined by the relation $A=4\pi^2N^2Rhd$. By this procedure the technique of electroplating, described above, for effectively eliminating adhesion was developed and tested. At first sight, it may appear that the patches might loosen around the edges, and that they would "rip off." However, close examination showed this not to be the case. Actually, because of the masking plastic, the deposited films were slightly thinner on the edges, which probably prevents ripping. Also, all of the patches on the rotor came off at approximately the same rotor speed. Incidentally, this method of measuring adhesion has turned out to be very reliable, and gives absolute values.

Figure 3 shows the values obtained for the tensile strength of silver as a function of film thickness. The temperature was above room temperature, the plating current 8.5 ma/cm^2, and the rotor diameter 0.28 cm. It will be observed that for thicknesses greater then 6×10^{-5} cm the tensile stre.ngth is about 1.2×10^9 dynes/cm^2, and is independent of the thickness. This is approximately equal to the bulk strength of the silver at the operating temperature. Data not plotted in the figure showed the tensile strength to be independent of film thickness up to at least 10^{-4} cm. For thicknesses between 6×10^{-5} cm and 2.7×10^{-5} cm the data are more erratic, but there is some indication of a small increase in tensile strength. However, for thicknesses less than 2.5×10^{-5} cm, there is a many-fold increase in tensile strength. In fact, the tensile strengths of the thin silver films are so great that the solid steel rotors explode before the films burst. The triangles in Fig. 3

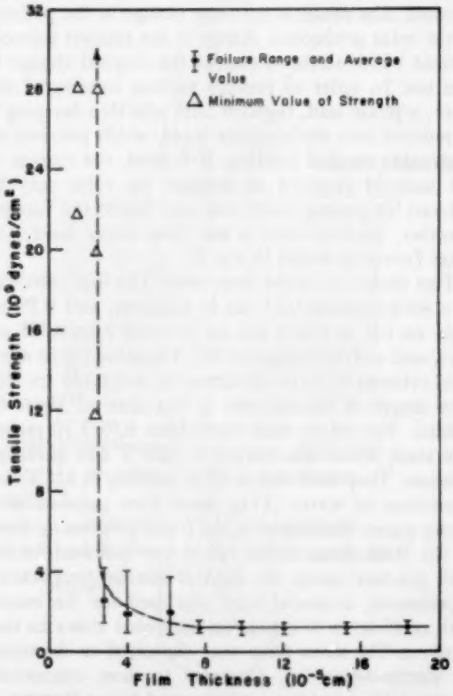

FIG. 4. Curve of tensile strength *versus* film thickness for silver at approximately 330°K.

and Fig. 4 represent points where the rotor speed was not sufficient to burst the film. In some of these cases the rotor was carefully brought to rest and a small cut made across the film in such a way as to eliminate the hoop stress. When the rotors were accelerated again, the films were observed to fly off completely at comparatively low rotor speeds, which was additional evidence that adhesion played no part in the observed tensile strength.

Figure 4 shows a typical plot of film thickness *versus* tensile strength for silver, when liquid nitrogen was introduced into the Dewar flasks surrounding the rotor chamber. The electroplating current was 8.5 ma/cm² and the rotor 0.28 cm in diameter. Here again it will be observed that the tensile strength is within experimental error, independent of the film thickness for thicknesses greater than about 6×10^{-4} cm. However, the strengths of these films are somewhat larger (about 2.9×10^{9} dynes/cm²). It is believed that this is the bulk strength of the silver at the temperature of the rotor. Also, as in Fig. 3, the tensile strength increases many times for thicknesses less than 2.5×10^{-4} cm. Because of the rotor heating discussed above, produced by the eddy currents induced in the rotor by the acceleration, the exact temperatures of the rotors used in obtaining the data for both Fig. 3 and Fig. 4 can only be roughly estimated. However, the temperature of the rotor in Fig. 3 was probably around 330°K and that of Fig. 4 at least 160°K lower or a maximum of 170°K. In view of this, the data indicate that the thickness below which the tensile strength shows the very rapid increase is within experimental error, independent of temperature.

First it should be emphasized that the observed strength of the thick films (1.2×10^{9} dynes/cm²) is of the order of 200 times the yield stress of 5.9×10^{6} dynes/cm² ($3\times10^{-3}\mu$, where μ is the minimum shear modulus) of an annealed single crystal of silver.[4] This may be due to the fact that every grain deforms and hardens by ordinary multiple slip. However, it is possible that the high strength results from the fact that only a fraction of the grains (the larger ones) contain Frank-Read sources[11,12] of length smaller than the grain size (say 10^{-4} or smaller). The piling up of dislocations produced by these sources at the grain boundaries, necessary to nucleate dislocations in the neighboring grains, would then provide the high strength. This interpretation implies, of course, a further increase of strength if the grain size is further decreased. If this interpretation is correct, then it is probable that when the films consist of a monolayer of grains, none of them should be able to stabilize Frank-Read sources in their interior,[12] and therefore the films should quite suddenly increase their strength to the theoretical shear strength. In fact, if an orientation factor of the order of 2 is taken into consideration, the maximum shear strength observed with our thinner films approach within roughly an order of magnitude of the theoretical value.[11,12]

If the greatly increased tensile strength at small film thicknesses is due to the absence of dislocations, the difficulty of generating new dislocations, etc., then one should observe no appreciable slip in the stretched films. However, it is difficult to decide this point, even by the electron microscope, because of the small thickness of the films, but we have in progress special experiments which should not only determine the slip, but also the Young's modulus in films formed both by electrodeposition and by evaporation. Recently, Mr. W. K. Ford and one of us, have found an increase in the tensile strength of evaporated films when the films are very thin, by measuring the bulge of the films through a support, produced by air pressure. However, the results so far, are preliminary, and much less precise than the data of Figs. 3 and 4.

ACKNOWLEDGMENTS

We are much indebted to Dr. H. S. Morton, Jr., and Dr. E. F. Turner, Jr., who carried through a large amount of the preliminary work of this problem. Also, we wish to gratefully acknowledge the help of Professor Nicolas Cabrera for assistance with the theoretical interpretation of the results.

[11] F. C. Frank and W. T. Read, Jr., Phys. Rev. **79**, 722 (1950).
[12] A. H. Cottrell, *Dislocations and Plastic Flow in Crystals* (Oxford University Press, New York, 1953).
[13] W. T. Read, Jr., *Dislocation in Crystals* (McGraw-Hill Book Company, Inc., New York, 1953).

Effect of Antimony Impurity on Self-Diffusion of Silver*†

E. SONDER‡
Department of Physics, University of Illinois, Urbana, Illinois
(Received August 3, 1955)

Coefficients for diffusion of Ag^{110} into single crystals of alpha silver antimony were measured as a function of temperature and concentration, over the range 550–900°C and 0–1½% antimony concentration. In addition, a number of measurements were made of the diffusion of Sb^{124} into similar alloys. The activation energy for silver self-diffusion was found to decrease by 1½ kcal per percent added antimony. Effects of impurity were appreciably less for solute diffusion than for solvent diffusion. The results are in qualitative agreement with theories of Overhauser and Lazarus, and indicate that effects due to changes in vacancy concentration are smaller than those resulting from changes in mobility energy.

INTRODUCTION

COMPARISON of pre- and postwar data for the diffusion of antimony into silver[1] demonstrated considerable differences in results, probably due in part to the large gradients and solute concentrations necessitated by the earlier techniques. The existence of these large discrepancies indicated the desirability of a fundamental investigation of both impurity and gradient effects, using modern tracer methods.

It had been proposed by Seitz[2] that the role of vacancies in diffusion processes might be studied by enhancing the density of vacancies in the lattice. Small amounts of dissolved impurity, it was suggested, might cause such an enhancement.

Previous studies of the effects of impurities on diffusion had been made[3,4] and increases of diffusivity noted. Within the past few months, Hoffman, Turnbull, and Hart[5] have reported additional measurements on polycrystalline samples of AgPb and other silver alloys over a range of 700–900°C. The present investigation was designed to make measurements on alloy single crystals over a larger temperature range, in order to determine the existence and magnitude of changes, due to impurities, of the activation energy Q and frequency factor D_0, both defined by the equation

$$D_{Ag}=D_0 \exp(-Q/RT), \qquad (1)$$

where D_{Ag} is the self-diffusion coefficient of silver in the alloy, R is the universal gas constant, and T is the absolute temperature.

EXPERIMENTAL

In order to preclude grain boundary diffusion in low-temperature measurements, single crystals were used for all specimens diffused below 850°C. These were prepared from 99.99% pure vacuum-cast silver and 99.9% pure antimony. The metals were placed in a National Carbon Co. A.U.C. grade graphite crucible, which had previously been cleaned by boiling in aqua regia, leaching in hot distilled water, and baking in vacuum at 1000°C. The filled crucible was sealed in Vycor at a pressure of 10^{-5} mm Hg, and the contents mixed by repeated tipping at a temperature above the melting point of silver. Following this, the sealed container was removed to a Bridgeman-type furnace, where the single crystal was grown. A gradient of 100°C per inch was maintained in the furnace by water cooling the lower end. It was possible to obtain crystals with an antimony concentration up to 1½% by lowering the charge through the gradient at a rate of about one inch per hour.

Methods of preparation and diffusion of the individual specimens have been described previously.[6,7] Most of the diffusion coefficients were determined by standard sectioning techniques, using a precision lathe to obtain cuts of ¾ to 3 mils thickness.

An attempt was made to extend the temperature range down to 450°C by use of a precision grinding machine which permitted removal of sections 3 microns in thickness.[8] These latter data were unfortunately less reliable due to macroscopic voids in the alloy crystals used. Metallographic examination showed these voids to be roughly spherical, 5–20 microns in diameter, and of varying sizes in different specimens. Thus the apparent diffusion coefficients in grinder samples, where the total penetration, $4(Dt)^{\frac{1}{2}}$, was less than 2 mils (50) microns), could easily have been 10–20% high, as the results indicated.[9] For this reason, low-temperature results are not included here. However, the data reported, in the range above 550°C, do not suffer from this source of error, since penetration depths were invariably greater than 10 mils. It should be noted that such voids have not been observed in pure silver or

* Supported in part by the U. S. Atomic Energy Commission.
† Based on a thesis submitted by E. Sonder to the University of Illinois in partial fulfillment of requirements for the degree of Doctor of Philosophy in Physics.
‡ Present address: Department of Physics, Iowa State College, Ames, Iowa.
[1] Slifkin, Lazarus, and Tomizuka, J. Appl. Phys. 23, 1405 (1952).
[2] F. Seitz, Acta Cryst. 3, 355 (1950).
[3] W. Seith and A. Keil, Z. physik. Chem. B22, 350 (1933).
[4] R. E. Hoffman and D. Turnbull, J. Appl. Phys. 23, 1409 (1952).
[5] Hoffman, Turnbull, and Hart, Acta Met. (to be published).
[6] Sonder, Slifkin, and Tomizuka, Phys. Rev. 93, 970 (1954).
[7] Slifkin, Lazarus, and Tomizuka, J. Appl. Phys. 23, 1032 (1952).
[8] Letaw, Slifkin, Portnoy, Rev. Sci. Instr. 25, 865 (1954).
[9] E. Sonder, Ph.D. thesis, University of Illinois, 1955 (unpublished).

copper crystals which are grown more slowly and in a continuously pumped rather than sealed vacuum.

The chemical composition of the alloy specimens was determined, after the diffusion measurements had been completed, by the Detroit Testing Laboratory. The method used consisted essentially of separation of the silver and antimony by precipitation and filtration and subsequent volumetric titration of the antimony against potassium bromate to a methyl orange end point. The analyses showed that specimens originating from the same ingot differed less than 15% in composition, indicating that segregation in the grown crystal ingots was small, and that the maximum variation in composition in any particular diffusion sample was less than 2%, since none of the samples were longer than $\frac{1}{8}$ the length of the original ingot.

A summary of the results of 21 measurements between 500 and 900°C appears in Table I. The coefficients given were calculated by a least squares method from the raw data, shown plotted in Figs. 1–4. To permit consideration of these results in terms of activation energy, the diffusion coefficients for each concentration range have been normalized to the same concentration and are shown plotted logarithmically as a function of $1000/T$ in Fig. 5. Also included in Fig. 5 and shown dotted are curves for the diffusion of antimony into pure silver as well as for self-diffusion of silver. The antimony line is from reference 6, while the silver self-diffusion line has been obtained from preliminary results of a re-evaluation of the activation energy for this process.[10]

TABLE I. Experimental data.

Tracer	Atom% Sb in alloy	Diffn. coeff. (cm²/sec)	Temperature (deg C)
Ag	0.54	1.17×10^{-11}	629.2
Ag	0.56	9.66×10^{-11}	716.9
Ag	0.67	2.27×10^{-9}	882.3
Ag	0.67	3.20×10^{-9}	899.8
Ag	0.92	2.71×10^{-12}	568.6
Ag	0.92	2.67×10^{-12}	568.6
Ag	0.90	1.06×10^{-10}	716.3
Ag	0.88	2.46×10^{-9}	875.7
Ag	0.85	2.84×10^{-9}	890.4
Ag	1.36	3.50×10^{-12}	567.8
Ag	1.43	1.74×10^{-11}	629.3
Ag	1.33	1.38×10^{-10}	716.5
Ag	1.38	6.23×10^{-10}	792.7
Ag	1.42	2.94×10^{-9}	875.3
Ag	1.45	3.80×10^{-9}	890.6
Sb	0.72	2.09×10^{-11}	567.7
Sb	0.72	1.96×10^{-11}	567.7
Sb	0.73	5.54×10^{-10}	714.7
Sb	0.73	5.89×10^{-10}	714.7
Sb	2.73	7.15×10^{-10}	709.9
Sb	2.73	7.07×10^{-10}	709.9

[10] Upon connecting diffusion coefficients at the same temperature but different composition by smooth curves, it was found that extrapolation to zero Sb concentration indicated appreciable difference from published values (reference 7) for self-diffusion of pure silver. Since one of the purposes of the present investigation was to determine the change of activation energy with impurity concentration, it was deemed of critical importance to have a very accurate value of Q for the slef-diffusion of silver. A redetermination of the temperature dependence of self-diffusivity was thus begun. Partially completed results are given by $D=0.4\exp(-44.1/RT)$ cm²/sec.

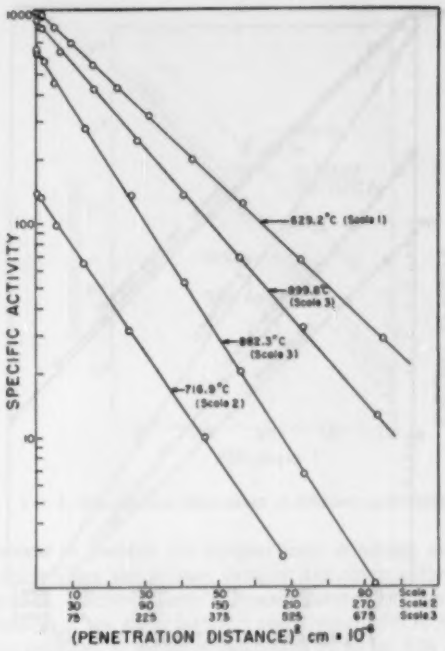

FIG. 1. Penetration curves, 0.53% Sb alloy, silver tracer.

The diffusion coefficients determine, within experimental error, straight lines. The activation energies obtained from these by a least squares method are listed in Table II, together with the frequency factors, D_0. The results may be summarized by the relations: $Q(c)-Q(c=0)=1.5c$, and $D_0(c)/D_0(c=0)=0.25c$, where c is the antimony concentration in atom percent and Q is in kilocalories.

Exploratory results indicate that, for diffusion of antimony in the same alloy system, impurity effects are appreciably smaller. Four measurements on 0.7% antimony samples, indicated by filled triangles in Fig. 5, show no difference from diffusion in pure silver. However, in a 2.8 atomic percent antimony polycrystalline sample, a small but significant increase (20% above the value for pure silver) was noted. That point is shown by a filled circle. It might be observed that the total amount of antimony soluble in silver, 7%, is only slightly more than twice the 2.8% in the sample showing increased diffusion.

An estimate of the accuracy of the data was made from the reproducibility of repeat measurements and from the standard deviation of the data from the Arrhenius plots, both being approximately 6%. In-

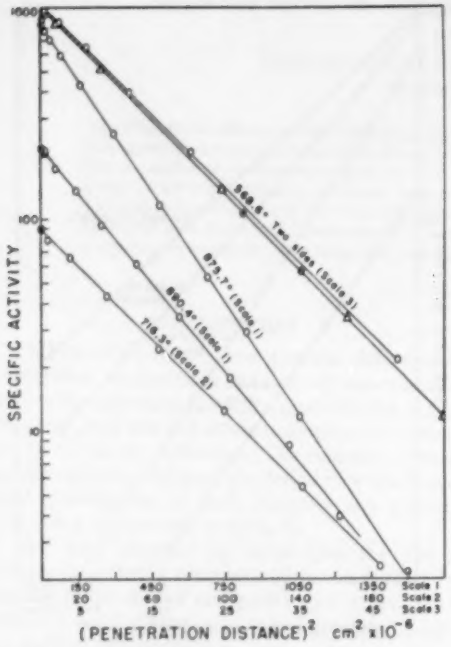
SPECIFIC ACTIVITY
(PENETRATION DISTANCE)² cm² x10⁻⁶
569.6° - Two slices (Scale 3)
878.7° (Scale 1)
890.4° (Scale 1)
718.3° (Scale 2)
150 450 750 1050 1350 Scale 1
20 60 100 140 180 Scale 2
5 15 25 35 45 Scale 3

FIG. 2. Penetration curves, 0.89% Sb alloy, silver tracer.

cluding a possible 2° error in temperature calibration, one would estimate the probable error in D_0 and Q to be 15–20% and about 0.8% respectively.

DISCUSSION

A. Comparison with Prewar Data

As mentioned previously, pre- and postwar measurements of the diffusion of antimony into silver yielded inconsistent results.[1] Diffusion coefficients differed by as much as a factor of ten; the activation energies differed by 100%. The present experiment shows that these discrepancies are not due to the higher antimony concentrations in the prewar measurements. The diffusion couples of these early experiments consisted of pure silver and a 3% antimony alloy. According to the present results, the maximum change in diffusion coefficient ascribable to a 3% antimony concentration is about 50%; changes in activation energy should not exceed 10%. It therefore seems that the inconsistencies are caused by gradients in concentration or by the poor sensitivity of the prewar techniques.

TABLE II. Experimental results showing change of activation energy, Q, and frequency factor, D_0, due to added antimony.

	Pure silver	0.53% Sb	0.89% Sb	1.42% Sb
Q	44.05	43.5	42.6	42.0
D_0	0.403	0.382	0.302	0.275
ΔQ		0.55	1.45	2.05

B. Possibility of Large Changes in the Number of Vacancies

The fact that reasonably constant slopes were obtained from plots of log D as a function of $1/T$ indicates that the impurity atoms cause little increase, if any, in the concentration of vacancies in the lattice. A large number of impurity-created vacancies would probably evidence itself by a diminished activation energy at low temperatures, where the number of thermally activated vacant sites would become smaller than the more or less constant number accompanying the impurity atoms.

C. Possible Changes in Mobility Energy

It is well known that solution of an impurity may change the lattice spacing of a metal.[11] Since the mobility energy of diffusion seems to be quite sensitive to interatomic spacing, it has been proposed by Overhauser[12] and later by Lazarus[13] that impurity effects

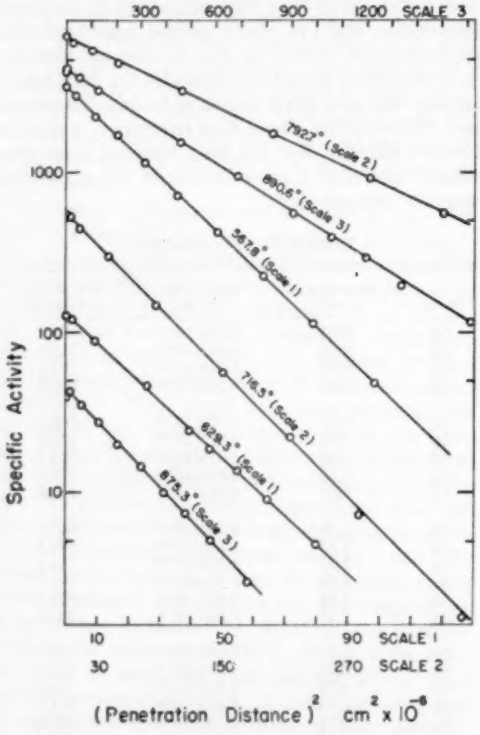

FIG. 3. Penetration curves, 1.4% Sb alloy, silver tracer.

[11] See, for instance, Hume-Rothery, Lewin, and Reynolds, Proc. Roy. Soc. (London) **A157**, 167 (1936).
[12] A. Overhauser, Phys. Rev. **90**, 393 (1953); **91**, 246(A) (1953).
[13] D. Lazarus, "*Impurities and Imperfections in Metallic Diffusion*," American Society of Metals, Chicago Meeting, 1954 (unpublished).

may be viewed in terms of changes of the mobility energy.

Overhauser considered the impurity atoms as sources of strain in a continuous medium. Assuming a Born-Mayer repulsive potential between atoms, $W=K\times\exp(-r/\rho)$, where r is the nearest neighbor distance and K and ρ are constants, Overhauser calculated the change in diffusion barrier height as a function of strain at any point. Subsequent averaging over the strain field permitted derivation of an expression for the change in mobility energy,

$$\Delta E=RTX\left[\frac{128\pi}{45}\left(\frac{b}{r_0}\right)^3\left(\frac{gk}{RT}\right)^2+\frac{32\pi\gamma}{3}(1-3\lambda)\left(\frac{gk}{RT}\right)\right],$$

where

$$k=\frac{Kb\sqrt{\frac{3}{2}}}{\rho}\exp\left(-\frac{b}{\rho}\sqrt{\frac{3}{8}}\right),$$

$$\lambda=\exp\left[-\left(\frac{2-\sqrt{3}}{2\sqrt{2}}\frac{b}{\rho}\right)\right],$$

$$\gamma=2(1-2\mu)/(1+\mu).$$

μ is Poisson's ratio, b is the lattice constant, X is the fraction of impurity atoms, g is a numerical constant proportional to the strain discontinuity introduced by the impurity atom, and r_0 is a cut-off parameter of the order of the lattice spacing, introduced in the averaging process to prevent the integral from diverging at the origin. Using the present data for the silver antimony system, Hume-Rothery's measurements for the expansion of the silver lattice,[11] and a value of 0.20 A for the constant ρ, we have calculated r_0 to be 4.04 A, a value which differs little from the lattice constant of the silver lattice, 4.08 A. The fact that the r_0 calculated from these data does approximate the lattice constant would indicate that an approach like Overhauser's can very well account for the small changes observed, i.e., that the changes in Q may very well be due to changes in mobility energy for vacancies.

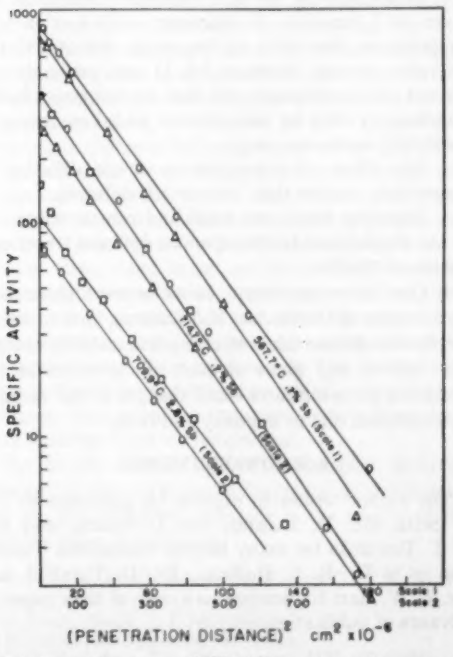

FIG. 4. Penetration curves, 0.7% 2.8% Sb alloy, antimony tracer.

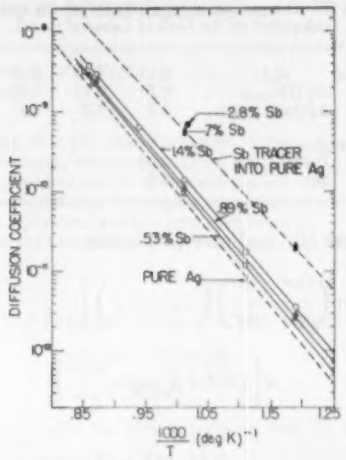

FIG. 5. Temperature dependence of diffusion coefficients.

A more quantitative calculation has been presented presented by Lazarus, who based his calculation on a model in which a diffusion jump is viewed as a unit shear of the lattice cell containing the diffusing atom and a vacancy. The change in mobility energy is thus equal to one-half the change in the atomic 110 shear modulus, which can be calculated for a uniform expansion of the lattice by the method of Fuchs.[14] Localized effects were taken into account separately by assuming that a solvent atom that is adjacent to both members of an impurity vacancy pair will be able to shear into the vacancy with no higher mobility energy than the impurity atom. The resulting expression for the ratio of jump probabilities in the impure (p^i) to that in the pure (p^0) lattice is given by

$$p^i/p^0=1-4X+4X\exp(-\Delta E_{mi}/RT), \qquad (3)$$

where ΔE_{mi} is the difference in mobility energy between the solvent and solute atoms diffusing in the pure lattice.

Including also a small effect due to a slight increase in the vacancy concentration, Lazarus arrived at the following expression for the ratio of self-diffusivities in

[14] K. Fuchs, Proc. Roy. Soc. (London) 153, 622 (1936).

TABLE III. Comparison of experimental results and values calculated on the basis of Lazarus' model.

Theoretical	$\rho(A)$	0.15	0.20	0.25
	$D_0/(D_0)_{pure}$	0.50	0.72	1.02
	ΔQ(kcal/mole)	1.3	1.2	1.1
Experimental				
	$D_0/(D_0)_{pure}$	0.73		
	ΔQ	1.5		

an impure (D^i) and pure (D^p) lattice,

$$\frac{D^i}{D^p}=\left[\exp\left(\frac{C\alpha r}{R}-\frac{1}{RT}\right)\left(E_m{}^i-E_m{}^0\right)\right]\times\left[1-X+X\exp-\frac{\Delta E_{vi}}{RT}\right]\times\left[1-4X+4X\exp-\frac{\Delta E_{mi}}{RT}\right], \quad (4)$$

where α is the linear coefficient of thermal expansion, r is the nearest neighbor distance, $E_m{}^0$ and $E_m{}^i$ are the mobility energies in the pure and impure lattice calculated on the basis of uniform expansion, C is a constant of the order of 3, and ΔE_{mi} and ΔE_{vi} are the differences of mobility and vacancy creation energies between diffusion of the solvent and solute. The sum of these last two, $\Delta Q=\Delta E_{mi}+\Delta E_{vi}$, can be obtained from diffusion measurements of solvent and solute in the pure lattice.

Since the Born-Mayer exponent, ρ, which appears as a parameter in the theory, is not accurately known, effective activation energies, Q, and intercepts, D_0, have been calculated for three values of ρ, 0.15, 0.20, and 0.25. These effective values were obtained by calculating diffusion coefficients for temperatures of 700, 800, 900, and 1000 deg K and then fitting them to an Arrhenius equation, as had been done for the experimentally determined diffusion coefficients. Ratios of values of D_0 for a 1% alloy and pure silver as well as differences in activation energy, Q pure $-Q1\%$ impurity, are compared with the experimental results in Table III. It might be pointed out that the theory does not wholly account for the observed changes, although qualitative agreement is excellent.

D. Jump Frequency Formalism

In connection with their data on Pb, Cu, Ge, and Al impurities in silver, Hoffman, Turnbull, and Hart[6] have presented a formalism in which diffusion coefficients for solvents and solutes in pure and impure material are written in terms of three jump frequencies, those of the solute, pure solvent, and a solvent atom in a zone around an impurity. They have neglected effects due to the overall expansion of the lattice, but have derived an expression that takes into account short-range effects from all sources, i.e., changes in mobility as well as in vacancy concentration. The self-diffusivity, in an impure solvent in which the impurity diffuses faster than the solvent, is given by

$$D_1=(1-aX)D_1{}^0+aXD_2, \quad (5)$$

where $D_1{}^0$ is the self-diffusivity of the pure solvent, D_2 is the diffusion coefficient for the solute in the solvent, and a is the number of effective solvent vacancy exchanges during the time the solute exchanges once with the vacancy. This number cannot be greater than the total number of solvent atoms in the region strained by the impurity, since additional jumps could not be classed "effective."

It is interesting to compare this result with the expression derived by Lazarus [Eq. (3)] under much more restrictive assumptions. He assumed that the mobility of only those four atoms that can be nearest neighbors to both the impurity and the vacancy will be enhanced, hence the four in Eq. (3). It might seem reasonable to assume as did Hoffman, Turnbull, and Hart that other atoms in the region may also diffuse more easily; hence substitution of a number greater than four would seem justified. The present data suggest that a value in the range of six or seven is needed for agreement.

SUMMARY

1. Measurements of self-diffusion coefficients of silver as a function of antimony concentration and temperature show that in the range 550–900°C the activation energy decreases by 1½ kcal per mole per percent added antimony, and that the frequency factor decreases by 25% for each percent added antimony in the 0–1½% antimony range.

2. The effect of impurities on solute diffusion is appreciably smaller than that on self-diffusion.

3. Impurity effects are small and can therefore not be the major cause of discrepancies between tracer and nontracer results.

4. Qualitative agreement exists between these data and theories of Overhauser and Lazarus, both of which ascribe the effects mainly to changes in mobility energy. The lack of any great amount of curvature in the Arrhenius plots indicates small changes in the vacancy concentration due to impurity additions.

ACKNOWLEDGMENTS

The author wishes to express his gratitude to Dr. F. Seitz, Dr. D. Lazarus, Dr. L. Slifkin, and Dr. C. T. Tomizuka for many helpful discussions. Thanks also go to Dr. R. E. Hoffman, Dr. D. Turnbull, and Dr. E. W. Hart for sending us a copy of their paper in advance of publication.

Interpretation of the Optical Properties of Metal Surfaces

S. ROBERTS
General Electric Research Laboratory, Schenectady, New York
(Received September 6, 1955)

The surface optical properties of the metals Ag, Au, Cu, Pt, Ir, and Ni in the infrared are shown to obey a simple generalized form of the Drude formula for the free electron theory, but involving two types of free electrons. If the surface optical constants are not anomalous, this procedure may be interpreted as a source of information on the density and relaxation times of free electrons in different overlapping energy bands. The evidence for and against anomalous surface optical constants is reviewed and it is concluded that the optical constants in the interior are the same as those measured on the surface.

I. INTRODUCTION AND MATHEMATICAL FORMULATION

IN 1900 Drude[1] proposed a formula for the optical properties of metals based on the postulated existence of two kinds of free charge carriers. In 1904 Drude[2] abandoned this formulation since it seemed inconsistent with the electron theory which was being developed at that time. He then restricted the charge carriers to one kind. Since that time it has become evident that Drude's restricted formula may be used with only limited success and does not bring optical data into harmony with data for dc conductivity unless the optical properties of the interior are assumed to be different from those derived from reflection experiments on the surface.

It will be shown that Drude's more general formula does apply without limit to the free electron contribution to optical properties in all metals which have been studied, and that there need be no essential difference between the optical properties of the surface and those of the interior to be consistent with the dc conductivity.

Since quantum mechanics and the exclusion principle were then unknown, Drude could not have guessed that electrons in different Brillouin zones can behave differently, nor could he have suspected the existence and important function of "holes." Nevertheless, the properties which he ascribed in his earlier paper to positive and negative "ions" show a remarkable resemblance to modern ideas about holes and electrons. The parallel modern interpretation of conductivity of transition metals was proposed by Mott.[3] Mott recognized that both *s*-electrons and *d*-electrons are of importance for the conductivity of transition metals. The present work extends Mott's interpretation to optical properties and indicates that even nontransition metals may have more than one type of free electron.

The Drude formula gives the complex dielectric constant, K, as a function of frequency or wavelength. The complex dielectric constant is the square of the complex index of refraction.

$$K=[n(1-i\kappa)]^2=K'-iK''. \tag{1}$$

The real and imaginary parts of K are, respectively,

$$K'=n^2(1-\kappa^2),$$
$$K''=2n^2\kappa. \tag{2}$$

In our notation the Drude formula may be written

$$K=K_\infty-i\frac{\sigma_\infty\lambda}{2\pi c\epsilon_0}-\frac{\lambda^2}{2\pi c\epsilon_0}\left(\frac{\sigma_1}{\lambda_1-i\lambda}+\frac{\sigma_2}{\lambda_2-i\lambda}\right). \tag{3}$$

In Eq. (3), λ is the wavelength in meters, σ_1 and σ_2 are components of conductivity in ohms^{-1} m^{-1} due to the two different kinds of charge carriers, and λ_1 and λ_2 are the corresponding wavelengths of relaxation. With these units, the value of $2\pi c\epsilon_0$ is 0.01668. K_∞ represents the contribution of "bound" electrons at long wavelengths compared to their wavelengths of resonance. σ_∞ has no theoretical foundation, but is inserted in the equation because it is useful in describing certain deviations from theory in imperfect metal films.

The dc conductivity, σ_0, may be derived from Eq. (3) by the relation

$$\sigma_0=\lim_{\lambda\to\infty}(i2\pi c\epsilon_0K/\lambda)=\sigma_1+\sigma_2+\sigma_\infty. \tag{4}$$

It is found not only that Eq. (3) gives an adequate description of the optical properties of all metals which do not have resonance frequencies for bound electrons in the visible or infrared region, but also that it may be reduced to even simpler approximate forms. In some metals both λ_1 and λ_2 are substantially greater than the wavelengths at which data are reported. In other metals only λ_2 is large. These conditions correspond to the two special cases summarized below.

Case I: $\lambda_1^2, \lambda_2^2 \gg \lambda^2$

$$K\cong K_\infty-i\frac{\sigma_\infty\lambda}{2\pi c\epsilon_0}-\frac{\lambda^2}{\lambda_a\lambda_b}\frac{\sigma_1+\sigma_2}{2\pi c\epsilon_0}(\lambda_b+i\lambda), \tag{5}$$

where

$$\lambda_a=\frac{(\sigma_1/\lambda_1)+(\sigma_2/\lambda_2)}{(\sigma_1/\lambda_1^2)+(\sigma_2/\lambda_2^2)};\quad \lambda_b=\frac{\sigma_1+\sigma_2}{(\sigma_1/\lambda_1)+(\sigma_2/\lambda_2)}.$$

Note that $\lambda_1<\lambda_a<\lambda_b<\lambda_2$.

Case II: $\lambda_2^2 \gg \lambda^2$

$$K\cong K_\infty-i\frac{\sigma_\infty\lambda}{2\pi c\epsilon_0}-\frac{\lambda^2}{2\pi c\epsilon_0}\left[\frac{\sigma_1}{\lambda_1-i\lambda}+\frac{\sigma_2(\lambda_2+i\lambda)}{\lambda_2^2}\right]. \tag{6}$$

[1] P. Drude, Physik. Z. **1**, 161 (1900).
[2] P. Drude, Ann. Physik **14**, 936 (1904).
[3] N. F. Mott, Proc. Roy. Soc. (London) **A153**, 699 (1936).

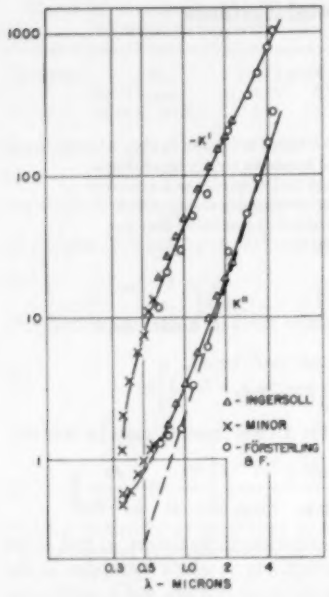

FIG. 1. Surface dielectric constant of silver.

II. COMPARISON WITH EXPERIMENT

Years ago, Meier[4] determined the resonance frequencies of the so-called "bound" electrons in several metals. In silver he found the longest wavelength of resonance at about 0.27μ. In gold a resonance was found at about 0.37μ and in copper at about 0.50μ. Equation (5) may be used successfully at wavelengths greater than roughly twice these values.

Of these three metals, silver has the widest range of wavelength free of resonances and is probably the metal most frequently studied. Figure 1 shows data for the complex components of the optical dielectric constant of silver. The smooth curves are calculated from Eq. (5) using the parameters listed in Table I, with the exception of σ_∞ which is 0.019×10^6 ohm^{-1} m^{-1}. The data in the infrared are from Foersterling and Freedericksz[5] and Ingersoll.[6] The data of Minor[7] are used in the visible range. Figure 1 is plotted on logarithmic coordinates, according to which $(-K')$ and K'' should follow straight lines with slopes of two and three respectively, if in Eq. (5) the parameters K_∞ and σ_∞ are omitted. The deviations from straight lines are attributable to the nonvanishing values of K_∞ and σ_∞. The straight line asymptote for K'' is shown dashed in the figure.

More recent data for silver obtained by Schulz[8] and Schulz and Tangherlini,[9] which had not been published when Fig. 1 was drawn, indicate values of $(-K')$ which coincide with the curve in Fig. 1 in agreement with the older data. The new data for K'' are different, however, in that they coincide with the dashed straight line instead of the curve in the wavelength range 0.5 to 0.95 micron. Schulz and Tangherlini stressed the importance of careful annealing of their metal films and they measured the reflectivity from the glass-metal interface which was presumably free of contamination by the atmosphere. Our conclusion from these data is that σ_∞ does vanish, as it should, on a suitably prepared surface. Conversely, a nonvanishing σ_∞ may be taken as a possible indication of surface defects. σ_∞ appears to be more sensitive to surface defects than are the other parameters in the equation.

The situation in gold and copper is somewhat similar to that observed in silver except that there is more scatter in the classical data. It should be noted that all three metals are very difficult to measure in the important infrared range because of their high reflectivities. The values of λ_a, λ_b, and K_∞ for gold and copper shown in Table I were calculated from the data of Schulz and Tangherlini which also indicate that σ_∞ vanishes for these metals. This table also lists representative values of the dc conductivity, σ_0, of these metals at room temperature taken from the Landolt-Bornstein[10] tables.

In the Drude formula for one type of free electron [obtained from Eq. (3) by putting $\sigma_2=\sigma_\infty=0$] one finds that $K''>(-K')$ when $\lambda>\lambda_1$, neglecting the effect of K_∞. In this range of wavelength $(-K')$ increases only very slightly with increasing wavelength. In the metals platinum, iridium, and nickel, $K''>(-K')$ while $(-K')$ changes much more than could be explained by the simple formula. The data for these metals can be accounted for only under the assumption that there are two relaxation wavelengths, in this case as given by Eq. (6). In Eq. (6), σ_1 and σ_2 appear in different terms so that these parameters may be determined independently On the contrary, Eq. (5) contains only the sum of these parameters. By fitting experimental data to Eq. (6), one can find actual values of σ_1 and σ_2 as well as λ_1 and λ_2.

A graphical method has been found most satisfactory in the evaluation of numerical values of parameters in Eq. (6). The graphical analysis is based on a family of standard curves which show at a glance how a change in any one of the parameters would affect the shape of the resulting curves. Figures 2, 3, and 4 show the ex-

TABLE I. Parameters derived from optical data.

Metal	$\lambda_a(\mu)$	$\lambda_b(\mu)$	K_∞	$\sigma_0\times10^{-6}$ (ohm^{-1} m^{-1})
Ag	23.0	84.	4.6	60.7
Au	16.7	59.	~5	43.2
Cu	22.4	74.	~6	58.0

[4] W. Meier, Ann. Physik **31**, 1017 (1910).
[5] K. Foersterling and V. Freedericksz, Ann. Physik **40**, 201 (1913).
[6] L. R. Ingersoll, Astrophys. J. **32**, 282 (1910).
[7] R. S. Minor, Ann. Physik **10**, 581 (1903).
[8] L. G. Schulz, J. Opt. Soc. Am. **44**, 357 (1954).
[9] L. G. Schulz and F. R. Tangherlini, J. Opt. Soc. Am. **44**, 362 (1954).
[10] Landolt-Bornstein, *Physikalisch-Chemische Tabellen* (Springer-Verlag, Berlin, Germany, 1923-36), Vol. 2 and Suppl.

perimental data for platinum, iridium, and nickel. These data include the work of Lauch,[11] von Wartenburg,[12] Quincke,[13] and Tool[14] in addition to those sources already mentioned. The parameters used in calculation of the curves in these figures are listed in Table II along with the dc conductivity. Some of the parameters which could not be determined uniquely by the graphical method are either omitted or enclosed in parentheses.

Iron is an exception to the above formulas since it has a resonance frequency in the visible range. The data for iron are shown in Fig. 5 along with a smooth curve calculated according to Eq. (6). The deviations from the smooth curve centered at about 0.57μ are characteristic of a resonance such as is usually attributed to bound electrons. In this case it is possible that the resonance may be magnetic in origin. A similar resonance is observed in cobalt at around 1.35μ.

III. INTERPRETATION OF RESULTS

If one considers the electronic energy diagram for copper as calculated by Krutter,[15] it is clear that in the solid metal there is an overlapping of the $4s$ and $4p$ bands and that the Fermi level falls in this overlapping range. According to this model both $4s$ and $4p$ electrons will contribute to the conductivity. Free electrons in these different bands would be expected to have different effective masses and scattering probabilities or relaxation wavelengths. Silver and gold are known to have similar electronic properties as compared with copper; therefore, one might expect a similar energy band model to apply to these metals. In silver the expected overlapping bands would be $5s$ and $5p$ and in gold, $6s$ and $6p$. The fact that the two-electron model appears to give a better interpretation of the experimental data than the one-electron model tends to support the conclusion that both s- and p-electrons contribute to the conductivity in these metals. The existing data do not allow separate determination of λ_1, λ_2, σ_1, and σ_2; however, it is evident that these can be determined by conducting experiments at longer wavelengths.

In platinum and iridium the situation should be, and is, quite different, since these metals have unfilled d-orbits; the overlapping occurring between the $5d$- and $6s$-bands. In nickel $3d$- and $4s$-states would be involved. The values obtained for λ_1 and σ_1 in these metals are attributed to d-states, while the values for λ_2 and σ_2 are attributed to s-states. The small values of λ_1 are interpreted to indicate that the charge carriers in d-states have a much greater probability of scattering

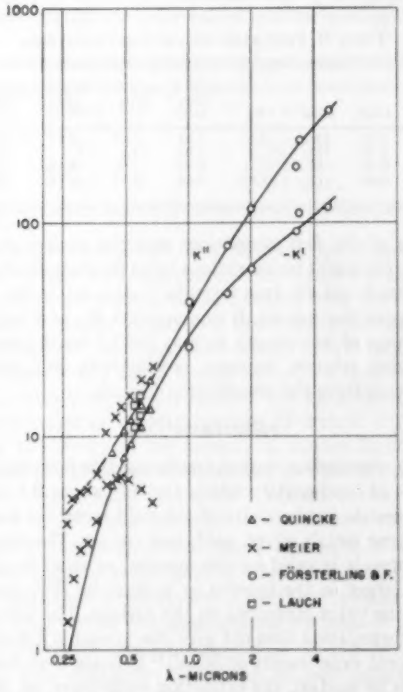

FIG. 2. Surface dielectric constant of platinum.

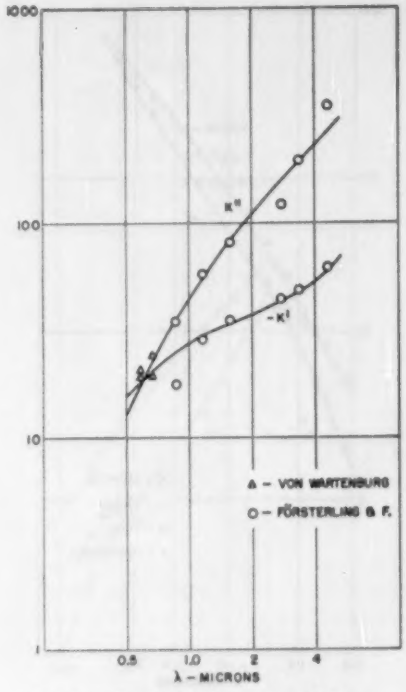

FIG. 3. Surface dielectric constant of iridium.

[11] K. Lauch, Ann. Physik (4), **74**, 55 (1924).
[12] H. von Wartenburg, Verhandl deut physik Ges. **12**, 105 (1910).
[13] G. Quincke, Poggend. Ann. Jubelband 336 (1874).
[14] A. Q. Tool, Phys. Rev. **31**, 1 (1910).
[15] H. M. Krutter, Phys. Rev. **48**, 664 (1935).

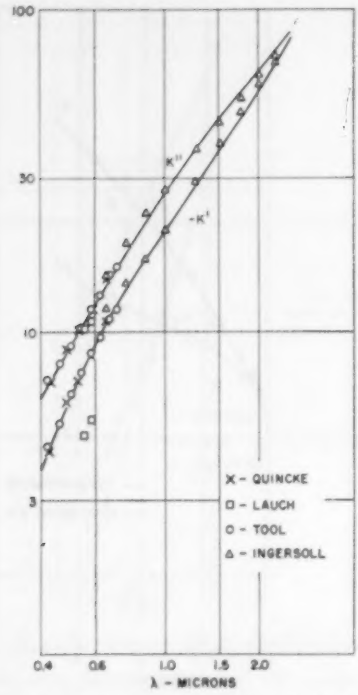

FIG. 4. Surface dielectric constant of nickel.

than do those for either *s*- or *p*-states. For these transition metals, one may use the experimentally derived values of λ_1 and σ_1 in a calculation of the effective number, n_1, of electrons or other charge carriers in the *d*-state. This calculation is based on the classical relation

$$n_1/n_a = 2\pi c m_1 \sigma_1/n_a e^2 \lambda_1, \tag{7}$$

where n_a is the number of atoms per unit volume, c is the velocity of light, e is the electronic charge, and m_1 is the effective electronic mass. This equation is not capable of determining both n_1 and m_1, but if one assumes that m_1 is the rest mass of an electron in free space, then one obtains a representative value for n_1. The values of n_1/n_a for platinum, iridium, and nickel calculated according to this convention are shown in Table III.

Platinum and iridium have similar electronic configurations except that iridium has one less electron. In view of this, it is interesting that iridium has a noticeably greater number of charge carriers in the *d*-state. Since the metal with fewer electrons has the greater number of charge carriers, the latter may be identified as holes. This is reasonable since the *d*-band has room for ten electrons and is nearly filled. The charge carriers associated with the *s*-states are believed to be electrons. Most of the conductivity is due to these *s*-electrons since they have so much greater lifetime than the *d*-holes.

IV. ANOMALOUS SURFACE LAYER

Until now it has been generally believed that the optical properties of metals are influenced by an anomalous surface layer. This layer has been discussed at length by several authors.[16] The analysis presented here appears to cast some doubt as to whether such a surface layer does have any significant effect on the optical properties of metals in the infrared at ordinary temperatures. Accordingly, it is relevant to review the evidence for and against the anomalous surface optical constants resulting from such a layer.

The point in dispute is whether the optical constants determined from surface measurements are valid for points in the interior of the metal. To settle this point properly, one should compare experimental data for the optical constants in question. The surface constants are well known for a number of metals, but data for the interior as reported in the literature are relatively meager. However, these data do definitely support the view that the optical constants of the interior are the same as those of the surface.

TABLE II. Parameters derived from optical data.

Metal	$\lambda_1(\mu)$	$\lambda_2(\mu)$	K_∞	$\sigma_1\times10^{-6}$ (ohm^{-1} m^{-1})	$\sigma_2\times10^{-6}$ (ohm^{-1} m^{-1})	$\sigma_\infty\times10^{-6}$ (ohm^{-1} m^{-1})	$\sigma_0\times10^{-6}$ (ohm^{-1} m^{-1})
Pt	1.27	205.	2.4	1.03	8.22	0.25	9.5
Ir	0.58	724.	...	1.02	15.4	...	16.4
Ni	0.70	44.	(2.7)	0.45	7.90	(0.15)	8.5
Fe	0.39	75.	(1.15)	0.24	9.52	(0.24)	10.0

One of the first suggestions that the surface optical constants might be anomalous came from application of the Drude one-electron formula [$\sigma_2=\sigma_\infty=0$ in Eq. (3)] to copper-like metals. If one neglects K_∞ and restricts the range of wavelength so that $\lambda^2 \ll \lambda_1^2$ one obtains the following relation between conductivity and optical constants from the one-electron formula

$$\sigma \cong \pi c \epsilon_0 (n\kappa)^2/\lambda n. \tag{8}$$

If one uses surface optical constants, this formula gives values of conductivity which are only about 0.3 of the observed dc conductivity of the solid metal for each of the three metals silver, gold, and copper. Therefore, if the formula is valid for the interior, $n\kappa$ must be about 49% larger in the interior or n must be 70% smaller than the value measured on the surface. The two-electron formulation does not give rise to such a difference.

Recent experiments of Schulz[17] indicate that, for the metals he studied, the extinction coefficients, $n\kappa$, of the

[16] A. B. Pippard, Proc. Roy. Soc. (London) **A191**, 385 (1947); **A203**, 98 (1950); R. G. Chambers, Nature **165**, 239 (1950); Ph.D. dissertation Cambridge, 1951 (unpublished); Physica **19**, 365 (1953); E. H. Sondheimer, Advances in Phys. **1**, 1 (1952); R. B. Dingle, Physica **19**, 311, 729–36 (1953).

[17] L. G. Schulz, J. Opt. Soc. Am. **44**, 540 (1954).

interior were not much, if any, different from those of the surface. Schulz observed the transmission through films of varying thickness and from these data calculated separate values of $n\kappa$ for the surface and for the interior. He also determined $n\kappa$ for the surface independently by reflection. Observed differences up to about 15 percent between surface and interior values of $n\kappa$ were much too small to reconcile the simple Drude formula with the dc conductivity. These differences are not regarded as significant in the present discussion, and on this basis Schulz's experiments may be interpreted to signify that the interior and surface values of the extinction coefficient are substantially the same.

Schulz did not determine the real component, n, of the index of refraction of the interior. However, this property was measured many years ago by Kundt[18] using metal wedges. With the exception of silver, Kundt's interior results for "white" light are in very good agreement with the surface indices reported by others. Kundt's interior value of n for Ag is several times higher than the latest surface value of Schulz and Tangherlini.[9] Kundt's value for Ag is probably in error since the discrepancy in the one-electron formulation is even greater using his value. There is better agreement between Kundt's interior values and the surface values

TABLE III. Analysis of charge carriers.

Metal	n_1/n_e
Pt	0.79(5*d*)
Ir	1.64(5*d*)
Ni	0.47(3*d*)

of n for the metals Pt and Ni than for copper-like metals. This would be expected since Kundt did not use monochromatic light, and the values of n for the metals Pt and Ni are not such critical functions of wavelength.

The evidence for anomalous surface optical constants is not based on a direct comparison of the surface constants with those of the interior but on a theoretical interpretation of other properties of metals. Furthermore, the theory of the anomalous surface layer is in internal disagreement when applied to different experiments. For example, Andrew[19] obtained the value $\sigma_0/l = 4.5\times10^{22}$ Gaussian units for the ratio of the conductivity to the electronic mean free path in tin as derived from measurements of the dc conductivity of thin foils at low temperatures. Chambers[16] obtained the value 8.6×10^{22} for the same ratio on the basis of microwave resistance measurements, also at low temperatures. This difference appears to be well outside the

[18] A. Kundt, Ann. Physik **34**, 469 (1888).
[19] E. R. Andrew, Proc. Phys. Soc. (London) **A62**, 77 (1949).

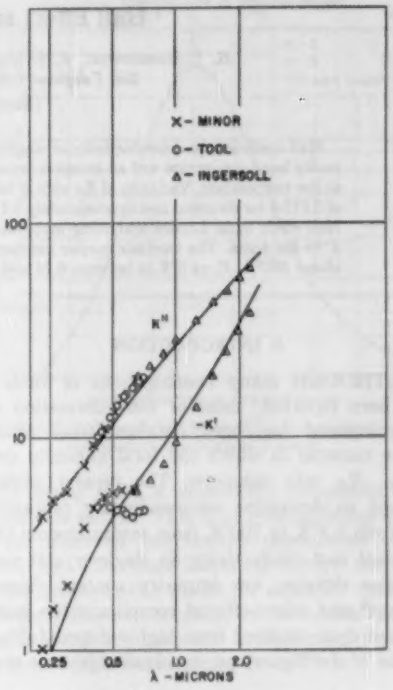

FIG. 5. Surface dielectric constant of iron (steel).

limits of experimental error; therefore, one may conclude either that the theory is deficient, or that the anomalous surface layer is less deep for microwave frequencies than for direct current—and perhaps of quite negligible depth at infrared wavelengths.

Sondheimer[16] gives a method for calculating the effective conductivity of a surface layer of any given depth. Sondheimer's theory has been subjected to an extreme degree of refinement by Dingle.[16] Notwithstanding these efforts, there does not seem to be any satisfactory way, analogous to Eq. (8), to calculate the dc conductivity from the surface optical constants or vice versa as long as the one-electron model is used. Nor do these theories offer any help in explaining the observed wavelength dependence of the surface optical properties of transition metals. In addition to these shortcomings it must be reckoned that the anomalous surface layer is just a theory, insofar as optical properties of metals are concerned, whereas direct experiments indicate that anomalies in the surface optical constants are either small or nonexistent at room temperature.

The author acknowledges with thanks the comments of R. E. Scott which were helpful in the revision of this paper.

Hall Effect and Conductivity of InSb

H. J. Hrostowski, F. J. Morin, T. H. Geballe, and G. H. Wheatley
Bell Telephone Laboratories, Murray Hill, New Jersey

(Received August 19, 1955)

Hall coefficient and conductivity of single-crystal InSb have been measured from 1.3°K to 700°K. Impurity band conduction and an acceptor ionization energy of 7×10^{-3} ev have been observed in p-type InSb at low temperature. Variation of R_H with H indicates a complicated valence band structure. Effective masses of $0.015m$ for electrons and approximately $0.17m$ for holes are consistent with mobility and low temperature Hall effect data. Lattice scattering mobilities are proportional to $T^{-1.65}$ for electrons and approximately $T^{-2.1}$ for holes. The intrinsic carrier concentration product is given by $np=3.6\times10^{33}T^3\exp(-0.26/kT)$ above 200°K. E_g at 0°K is between 0.26 and 0.29 ev.

1. INTRODUCTION

ALTHOUGH many investigations of InSb have been reported,[1] most of the information about this compound has been obtained from relatively impure material in which the total impurity concentration, N_I, was unknown. The present work was designed to determine semiconducting properties of InSb from 1.3°K to 700°K from measurements of Hall coefficient and conductivity on single-crystal samples of rather definite, low impurity content. Since degeneracy[2] and other effects[3] complicate the interpretation of data obtained from highly doped InSb, only samples of the highest purity obtainable were studied.

2. EXPERIMENTAL

Samples were cut from single crystals pulled[4] from melts of InSb purified by extensive zone refining.[5] Measurements were made on oriented bridge shape[6] samples using indium alloyed contacts below 300°K and platinum 10 percent rhodium wire pressure contacts above this temperature. For high-temperature measurements the samples were heated in an atmosphere of N_2.

TABLE I. Electrical properties of InSb samples at 78°K.

	Sample	N_d-N_a (cm^{-3})[a]	$R_H\sigma$ (cm^2/volt sec)
n-type	1	7.7×10^{14}	3.75×10^5
	2	9.8×10^{14}	3.70×10^5
	3	1.2×10^{15}	2.30×10^5
	4	8.8×10^{14}	3.80×10^5
p-type	A	2.9×10^{14}	9.5×10^3
	B	4.4×10^{14}	1.0×10^4
	C	1.8×10^{14}	8.1×10^3
	D	1.1×10^{15}	9.3×10^3

[a] Obtained from $n=(3\pi/8)(1/eR_H)$; $H=3080$ gauss for all cases except Samples 3 and C where $H=750$ gauss.

Table I gives the extrinsic electrical properties of the samples used.

Above 500°K acceptors were introduced during the measurements. The effects were small and generally did not change the extrinsic properties by more than 10 percent. At 300°K the changes were not detectable unless the sample had been heated above 650°K. Different samples of comparable carrier concentration were used for the high- and low-temperature regions because of this and the low melting point of indium in the alloyed contacts.

3. VARIATION OF HALL COEFFICIENT WITH MAGNETIC FIELD

The Hall coefficient, R_H, was measured as a function of magnetic filed strength, H, for a number of samples using fields ranging from 250 to 4300 gauss. In n-type InSb, R_H is independent of H up to 4300 gauss at 300°K. At 78°K, R_H decreases linearly with increasing H. The decrease of R_H over this range of H is dependent on electron concentration and varies from sample to sample. It amounted to less than 5 percent for the samples investigated.

For p-type InSb, R_H varies with H in a manner somewhat similar to that observed for p-type germanium.[7] Figure 1, which shows the behavior of samples A and B at several temperatures, indicates that the variation of R_H with H depends on acceptor concentration as well as temperature.[8]

The field dependence of R_H in p-type germanium has been successfully interpreted[7] by assuming the presence of a small percentage of high-mobility holes in addition to the usual positive charge carriers. Recent cyclotron resonance experiments[9] on InSb show the existence of two anisotropic holes with effective masses of approximately $0.18m$ and $1.2m$. Analysis of low-temperature Hall effect data (see Sec. 4) gives an average effective mass of $0.17m$ which is very close to the lower cyclotron

[1] O. Madelung and H. Weiss, Z. Naturforsch. **9a**, 527 (1954), give a comprehensive review of the literature.
[2] Harman, Willardson, and Beer, Phys. Rev. **93**, 912 (1954).
[3] Hrostowski, Wheatley, and Flood, Phys. Rev. **95**, 1683 (1954).
[4] G. K. Teal and J. B. Little, Phys. Rev. **78**, 647 (1950).
[5] W. G. Pfann, Trans. Am. Inst. Mining Met. Engrs. **194**, 747 (1952).
[6] P. P. Debye and E. M. Conwell, Phys. Rev. **93**, 693 (1954).
[7] Willardson, Harman, and Beer, Phys. Rev. **96**, 1512 (1954) and references cited there.
[8] Harman, Willardson, and Beer, Phys. Rev. **95**, 699 (1954), find little field dependence of R_H in the extrinsic range for samples with 2×10^{14} acceptors per cm^3.
[9] Dresselhaus, Kip, Kittel, and Wagoner, Phys. Rev. **98**, 556 (1955).

resonance value. This result indicates that the heavy holes are considerably less abundant. Since these would be expected to influence R_H only at relatively high fields it appears that the observed behavior of R_H below 4300 gauss results primarily from a complicated valence band structure.

The Hall coefficient is given by the relation $R_H = (\mu_H/\mu)(1/ep)$, where μ_H/μ, the ratio of Hall to conductivity mobility, is strongly dependent on magnetic field. Although μ_H/μ cannot be determined exactly without independent measurements of drift mobility,[10] approximate values ranging from 1.5 to 1.8 can be obtained from the ratio of the low- and high-field values of R_H since $(\mu_H/\mu)_{H\to\infty}=1$. Thus,

$$R_{H=0}/R_{H=\infty}=\mu_H/\mu. \quad (1)$$

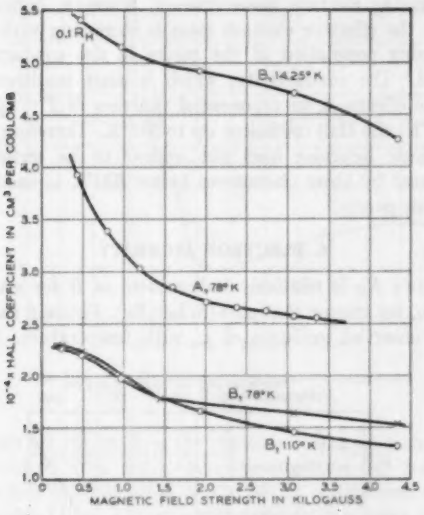

FIG. 1. Variation of Hall coefficient with magnetic field for p-type InSb.

These values are much greater than $3\pi/8$, the value for spherical energy surfaces. They are also somewhat approximate because of the onset of impurity scattering, which influences μ_H/μ at liquid nitrogen temperatures.

4. LOW-TEMPERATURE RESULTS

Figures 2 and 3 show, respectively, the temperature dependence of the Hall coefficient (for $H=3080$ gauss) and conductivity, σ, for two samples of low extrinsic carrier concentration. Measurements were taken to 1.3°K in both cases.

There is no evidence of donor ionization in Sample 2 in the temperature range studied. An effective electron mass, m_n, of $0.015m$ (see Sec. 6), where m is the free

[10] The lifetime of holes in InSb is apparently too low to measure drift mobilities by existing techniques.

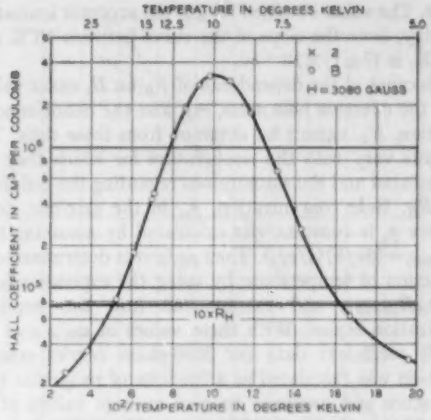

FIG. 2. Hall coefficient below 50°K vs reciprocal temperature for Samples 2 and B.

electron mass, gives a degeneracy temperature[11] of 28°K for this sample. This is in reasonable agreement with the observed temperature dependence of the conductivity. The donor ionization energy calculated from the hydrogen-like model for impurity centers is 10^{-3} ev for a dielectric constant[12] of 16. Ionization from this level would be observable in Hall effect measurements on nondegenerate samples ($n\approx 10^{13}$ cm^{-3}) around 2°K.

The data for p-type sample B show ionization of acceptors with increasing temperatures above 10°K and impurity band conduction[13,14] below this tempera-

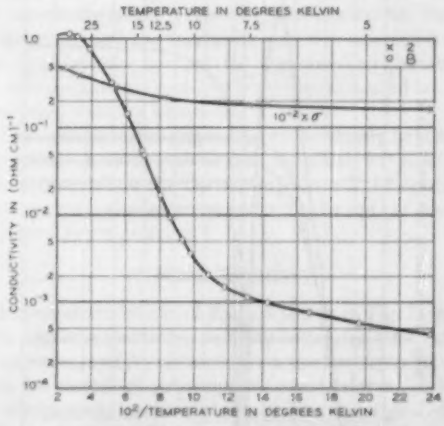

FIG. 3. Conductivity below 50°K vs reciprocal temperature for Samples 2 and B.

[11] W. Shockley, *Electrons and Holes in Semiconductors* (D. Van Nostrand and Company, Inc., New York, 1950).
[12] Briggs, Cummings, Hrostowski, and Tanenbaum, Phys. Rev. 93, 912 (1954).
[13] C. S. Hung and J. R. Gliessman, Phys. Rev. 96, 1226 (1954).
[14] Impurity band conduction in p-type InSb has also been observed recently by H. Fritzsche and K. Lark-Horovitz, Phys. Rev. 98, 1532(A) (1955).

ture. The value obtained for E_a, the acceptor ionization energy, from the slope of the curve between 10°K and 20°K, is $(7\pm1)\times10^{-4}$ ev.

Because of the dependence of R_H on H, exact values for the effective hole mass, m_p, and the donor concentration, N_d, cannot be obtained from these data. The results vary with the temperature for which they are calculated and the assumptions regarding the definition of R_H. Hole concentration, p_e, in the extrinsic range where p_e is constant was calculated by assuming that $R_{(H=0)}=(3\pi/8)(1/ep_e)$. Then μ_H/μ was determined as a function of temperature by using the expression $\mu_H/\mu=p_eeR_{(H=3080)}$ and extrapolated into the impurity ionization region. With these values of μ_H/μ and the Hall coefficient data for 3080-gauss carrier concentration was calculated as a function of reciprocal temperature and analyzed to give average values of $m_p=0.17m$ and $N_d=8\times10^{14}$ cm^{-3}. The estimated uncertainty of the values is less than 50 percent.

Below 10°K, impurity band conduction is observed in p-type InSb. A Hall coefficient maximum similar to that reported for germanium by Hung and Gliessman[13] is observed. This maximum occurs at a higher temperature and impurity band conduction occurs at lower impurity concentrations than for germanium because of the smaller effective hole mass in InSb. Although the mobility of the acceptor band carriers can be estimated to be 1 cm^2/volt sec, analysis of these results is not justified without a clearly defined R_H. Furthermore, the acceptor centers are residual impurities and were not introduced in a controlled manner. Thus, it is possible that there are several chemically different acceptor centers with different ionization energies.

5. HALL EFFECT AND CONDUCTIVITY ABOVE 78°K

Hall effect and conductivity as functions of T^{-1} are shown in Figs. 4(a), 4(b), 5(a), and 5(b), respectively, for temperatures from 78°K to 700°K. The data for n- and p-type samples merge into common intrinsic curves around 300°K. The curvature in the conductivity and Hall effect curves at high temperature has been attributed to degeneracy by several investigators.[1,2] The shift in the optical absorption edge with increasing electron concentration, however, indicates that the effective electron mass is increasing with increasing population of the states in the conduction band.[3] The conductivity, which is most sensitive to these effects, is an exponential function of T^{-1} up to 465°K, the Hall coefficient up to 535°K. Therefore the intrinsic behavior does not appear to be seriously affected by these phenomena below 500°K in samples of this purity.

6. ELECTRON MOBILITY

Since R_H is relatively independent of H for n-type InSb, we assume that $\mu_n=(8/3\pi)(R\sigma)$. Figure 6 shows the observed variation of μ_n with temperature. Also

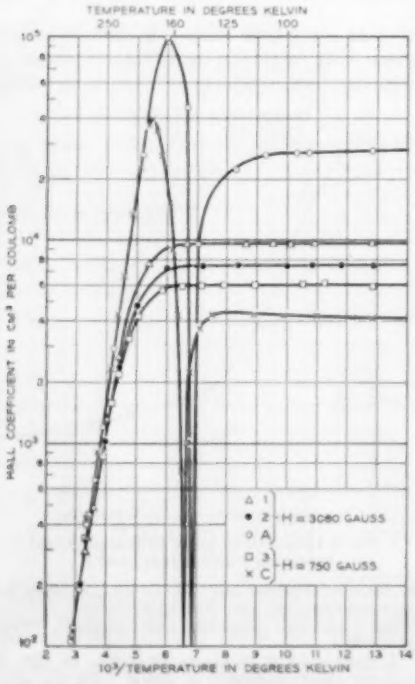

FIG. 4(a). Hall coefficient vs reciprocal temperature from 78°K to room temperature.

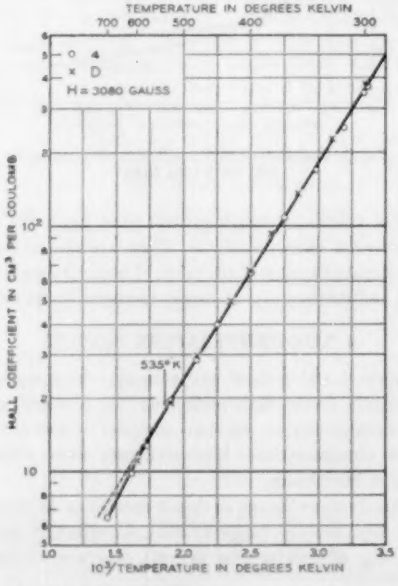

FIG. 4(b). Hall coefficient vs reciprocal temperature in the intrinsic range.

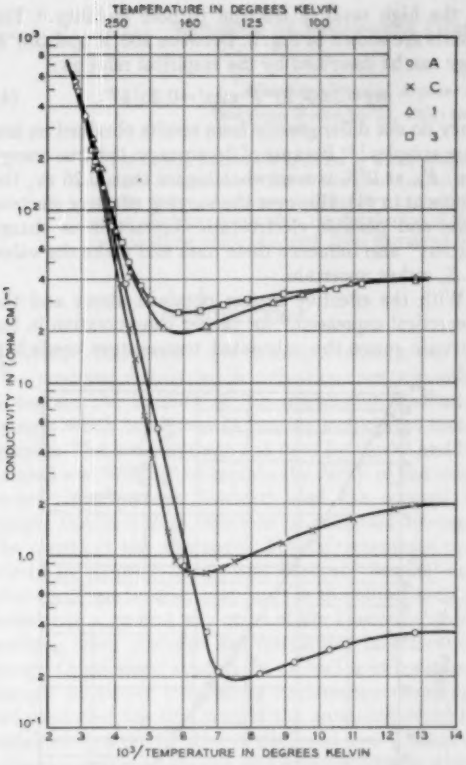

FIG. 5(a). Conductivity *vs* reciprocal temperature from 78°K to room temperature.

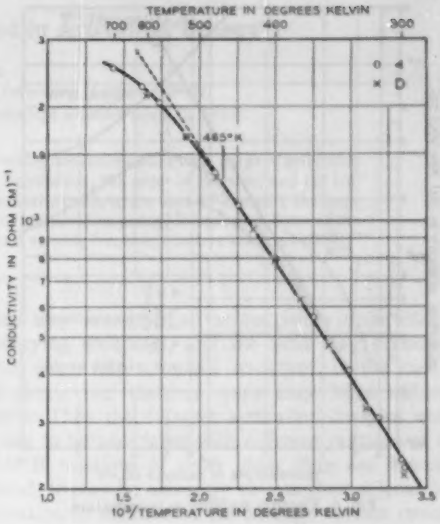

FIG. 5(b). Conductivity *vs* reciprocal temperature in the intrinsic range.

shown are values of μ_I, the impurity scattering mobility calculated from the Brooks-Herring formula[15] for an effective electron mass of $0.015m$. It is apparent that samples 1 and 2 have approximately the same total impurity concentration. Assuming $N_I \cong N_d - N_a = 9.8 \times 10^{14}$ cm^{-3} for sample 2, the electron lattice scattering mobility, μ_{Ln}, was calculated by the method of Conwell[16] by adjusting m_n to give the best straight line over the temperature range from 50°K to 400°K. A value of $m_n = 0.015m$ gives a significantly better result than $0.01m$ or $0.02m$. This value of m_n is very close to that determined from cyclotron resonance experiments.[9] The calculated lattice scattering mobility shown in Fig. 6 can be described by the equation

$$\mu_{Ln} = 1.09 \times 10^9 \ T^{-1.68}. \qquad (2)$$

The experimental results for sample 3 give good agreement with this equation for $N_I = 3.6 \times 10^{15}$ cm^{-3}.

The curvature of μ_n above 465°K is somewhat similar to that observed in germanium[17] at comparable intrinsic carrier density and attributed to electron-hole scattering. The dashed curve in Fig. 6 shows the calculated temperature dependence of μ_{Ln} including μ_{np}, the electron-hole scattering mobility, obtained by using the intrinsic carrier concentration determined in Sec. 8 and the effective masses given above. Since the inclusion of electron-hole scattering gives a result which is not in accord with the experimental data, it is concluded to be an unimportant scattering mechanism in InSb. Degeneracy and the increasing effective electron mass can qualitatively account for the observed deviation of the experimental mobility from the calculated lattice scattering mobility above 465°K.

The temperature dependence of electron lattice scattering mobility is almost identical to that of germanium where the deviation from a $T^{-1.6}$ dependence has been attributed to scattering by optical modes or intervalley scattering.[17]

7. HOLE MOBILITY

Experimental values of $R_H\sigma$ are shown in Fig. 7 along with impurity scattering mobility calculated for a range of values m_p and N_I obtained from the low-temperature data for sample B. Although the exact relation of $R_H\sigma$ to conductivity mobility is not clear, these probably differ by less than 20 percent above 50°K for $H = 3080$ gauss. The temperature dependence of lattice scattering mobility, μ_{Lp}, can be estimated from impurity scattering mobility and the conductivity data using hole densities obtained from the Hall coefficients. Results of these calculations indicate that the temperature dependence of μ_{Lp} is approximately $T^{-2.3}$. Impurity scattering, low temperature effects and the variation of R_H with H

[15] This is discussed in reference 6.
[16] E. Conwell, Proc. Inst. Radio Engrs. **40**, 1331 (1952).
[17] F. J. Morin and J. P. Maita, Phys. Rev. **94**, 1529 (1954).

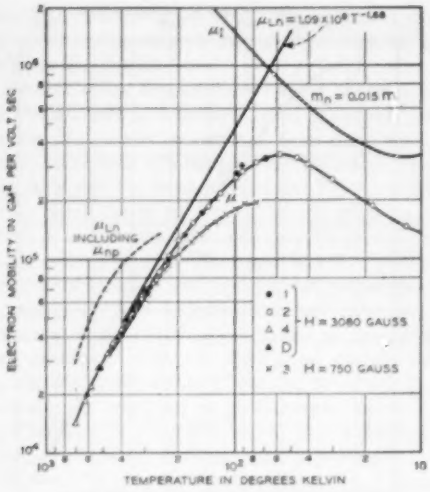

FIG. 6. Electron mobility *vs* temperature.

make it difficult to draw more quantitative conclusions.

8. CARRIER CONCENTRATION

Intrinsic carrier concentration has been determined from conductivity using measured electron mobility and extrinsic carrier concentration obtained from the Hall coefficient in the saturation range. The method is similar to that used by Morin and Maita[17] except that the contribution of holes has been neglected because of the high ratio of electron to hole mobility.[18] The results are shown in Fig. 8. Between 200°K and 600°K they can be described by the empirical relation:

$$np = 3.6\times10^{29}T^3\exp(-0.26/kT). \qquad (4)$$

They do not differ greatly from results obtained on less pure samples.[1,18] Because of degeneracy[1] the true energy gap, E_g, at 0°K is somewhat higher than 0.26 ev, the exponent in (4). However the varying effective electron mass and possible electrostatic interaction of charge carriers[17] also influence these data and make the value of E_g rather uncertain.

With the effective masses obtained above and the theoretical expression[11] for carrier concentration in the intrinsic range the calculated temperature coefficient of E_g is $(-3.9\pm0.3)\times10^{-4}$ ev/°K if a linear temperature dependence is assumed. Combining this with $E_g=0.17$ at 300°K, a value obtained from optical measurement[19] on "pure" InSb, E_g at 0°K is 0.29 ± 0.005 ev. Although this is probably an upper limit to the true value, it indicates the over-all consistency of these results.

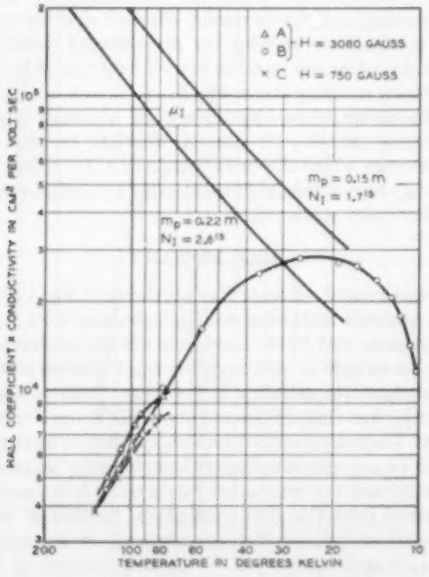

FIG. 7. Hole "mobility" *vs* temperature.

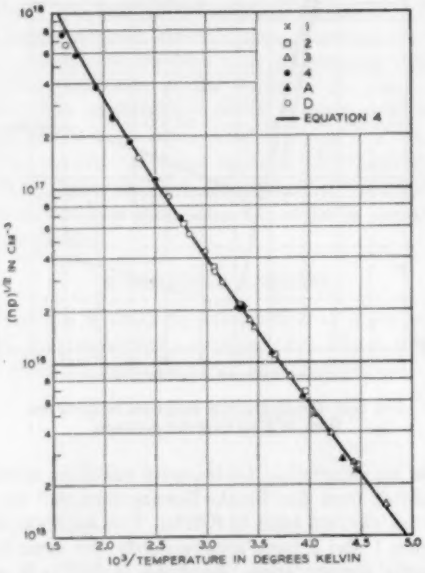

FIG. 8. Square root of the product of electron and hole concentration *vs* reciprocal temperature in the intrinsic range.

ACKNOWLEDGMENTS

We are indebted to J. P. Maita and W. L. Feldman for assistance with some of the measurements. We wish to thank Professor C. Kittel for informing us of the results of the cyclotron resonance experiments before publication and Dr. M. Tanenbaum for assistance and encouragement during the early phases of this work.

[18] M. Tanenbaum and J. P. Maita, Phys. Rev. **91**, 1009 (1953).
[19] L. N. Hand and H. J. Hrostowski (to be published).

Kinetics of Processes Distributed in Activation Energy*†

W. PRIMAK
Chemistry Division, Argonne National Laboratory, Lemont, Illinois
(Received November 18, 1954; revised manuscript received April 22, 1955)

The kinetic behavior of systems in which processes occur which are distributed over a range of activation energies is considered. The effects produced by the initial distribution, the order of reaction, and the frequency factor are discussed. Imaginary and actual experimental situations are used to illustrate the large errors which can result when the distribution of the processes in activation energy is neglected. Some of the complications which can result from successive reactions and varying frequency factors are mentioned.

INTRODUCTION

VAND[1] introduced the concept of a group of processes distributed in activation energy in order to explain the kinetics of the irreversible resistance changes which take place in heating evaporated metal deposits. The same concept was used by Curie[2] and by Randall and Wilkins[3] to explain the decay of the long-period phosphorence. Neubert[4] used the concept to explain the annealing behavior of radiation damage. The merits of the alternative kinetic treatments considered by Brown,[5] Dienes and Parkins,[6] Bowen,[7] and others will not be discussed for it is the object here to consider in a general way some of the kinetic behavior resulting when processes are distributed in activation energy. Overhauser[8] studied the annealing of resistance changes in copper induced by high-energy deuterons and concluded the first part of the annealing could be explained by a distribution of processes over a range of activation energies followed by a single process in which the annealing proceeded by kinetics of order 2.5. Honig[9] considered the integral transformation of one of the equations arising in the kinetics of processes distributed in activation energy. These references furnished the background for the present paper and are not intended to represent an exhaustive survey.

The above investigations all involved solids which may be considered to be molecularly inhomogeneous in some sense. In the case of evaporated metal films, the crystal structure consists of random mosaic deposits; in the case of radiation damage by energetic particles, the stopping process is itself localized, the displaced atoms may be trapped at various points in the solid, or in varying groupings, and the solid may eventually break down into a mosaic structure; in the case of phosphors, the electron traps may have different depths. Thus the different activation energies would appear to be associated with different portions of the solid. If reactions of order other than one are considered, it may be necessary to introduce a local concentration in addition to the average volume concentration.

* Based on work performed under the auspices of the U. S. Atomic Energy Commission.
† Enlarged from a manuscript submitted as a letter November 18, 1954.
[1] V. Vand, Proc. Phys. Soc. (London) **A55**, 222 (1943).
[2] M. Curie, Trans. Faraday Soc. **35**, 114 (1939).
[3] J. T. Randall and M. H. F. Wilkins, Proc. Roy. Soc. (London) **A184**, 390 (1945).
[4] T. J. Neubert was probably the first to apply Vand's method to the annealing of radiation damage [work done at the Metallurgical Laboratory, 1944 (to be published)].
[5] F. W. Brown, North American Aviation Report NAA-SR-16, 1950 (unpublished).
[6] G. J. Dienes and W. E. Parkins, North American Aviation Report NAA-SR-60, 1950 (unpublished).
[7] D. Bowen, North American Aviation Report NAA-SR-41, 1950 (unpublished).
[8] A. W. Overhauser, Phys. Rev. **90**, 393 (1953).
[9] J. M. Honig, J. Chem. Phys. **22**, 1689 (1954).

1. FORMAL THEORY OF THE KINETICS OF PROCESSES DISTRIBUTED IN ACTIVATION ENERGY; ISOTHERMAL ANNEALING AND TEMPERING

1.1. It has been customary to consider that in analogy with the kinetic processes in gases and in solution, the annealing processes obey a differential equation of the kind

$$-(dq/dt)=kq^n, \tag{1}$$

where q is the concentration of possible kinetic processes, t is the time, k is a constant, and n is the order of reaction (not restricted to integer values). In general, q cannot be measured directly. If a property is measured which is proportional to the number of processes which can occur, then for the processes which proceed at a particular value of the activation energy,

$$-(dp/dt)=kf(p/f)^n, \tag{2}$$

where f is the change in property accompanying the occurrence of a kinetic process (termed the importance factor) and p is a property or property change which can be used to measure the concentration of kinetic processes which can yet occur. It is usually assumed that the rate constant, k, can be equated to the Arrhenius expression for the activation energy. Then

$$-(dp/dt)=Afe^{-\epsilon/\tau}(p/f)^n, \tag{3}$$

where ϵ is the activation energy (units of ev will be used here), τ is the product of Boltzmann's constant and the temperature, and A is a constant having the dimensions of frequency when n is unity. In the case of isothermal annealing, this equation can be integrated to give

$$p=p_0[1-(1-n)At(f/p_0)^{(1-n)}e^{-\epsilon/\tau}]^{1/(1-n)} \tag{4}$$

$$=p_0[1-(1-n)Bte^{-\epsilon/\tau}]^{1/(1-n)}, \tag{5}$$

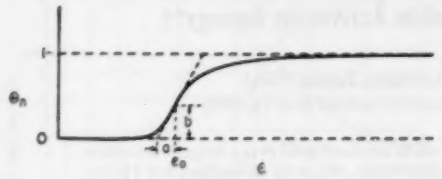

FIG. 1. The characteristic annealing function for isothermal annealing, $\Theta_n=[1-(1-n)Bte^{-\epsilon/\tau}]^{1/(1-n)}$, $a=n\tau$, $b=n^{1/(1-n)}$, $\epsilon_0=\tau\ln(Bt)$.

where p_0 is the value of p at $t=0$. The quantity B which is defined by Eqs. (4) and (5) has the dimensions of frequency for all orders of reaction. If the processes are distributed in activation energy, p and p_0 are distribution functions (the dependence of B and f on the activation energy will be disregarded in this section) and the measured value of the property is[10]

$$P=\int_0^\infty p_0[1-(1-n)Bte^{-\epsilon/\tau}]^{1/(1-n)}d\epsilon, \tag{6}$$

or

$$P(t)=\int_0^\infty p_0(\epsilon)\Theta_n(\epsilon,t)d\epsilon, \tag{7}$$

where P is the observed value of a suitable property. The function Θ defined by Eqs. (6) and (7) is termed the characteristic isothermal-annealing function. The distribution of processes over a range of activation energies is termed a spectrum.[11]

1.2. In dealing with a broad activation-energy spectrum, the annealing behavior is dominated by the exponential dependence on ϵ appearing in Θ_n, and the modifications introduced by p_0, the initial activation-energy spectrum, and the dependence of B and f on ϵ may be treated as perturbations of the gross behavior. The characteristic annealing function for isothermal annealing is shown schematically in Fig. 1. Solving for ϵ,

$$\epsilon=\tau\{\ln[(1-n)B]+\ln t-\ln[1-\theta^{(1-n)}]\}, \tag{8}$$

it is seen that as the isothermal annealing progresses, the curve is displaced along ϵ, but does not alter in shape. The point of inflection is termed here the characteristic activation energy and is designated ϵ_0. It is seen that

$$\epsilon_0=\tau\ln(Bt). \tag{9}$$

[10] In applying limits to integrals involving the characteristic annealing functions it is necessary to exercise some care when the order is not unity. If the order is less than unity the characteristic annealing function is zero from $\epsilon=0$ to $\epsilon=\tau\ln[(1-n)Bt]$ while the functional form given is negative in this region, and thus integrals involving $\Theta_{n<1}$ or $d\Theta_{n<1}/dt$ should be taken from $\tau\ln[(1-n)Bt]$ as a lower limit when the functional form given is used. If the order is greater than 2, $-\int_0^\infty(d\Theta_n/dt)d\epsilon$ diverges and hence a finite upper limit must be employed with this integral.

[11] This term was introduced in the course of studies by Neubert (reference 4) in 1944 and has been in common use in the subject since then.

The rate of annealing is[10]

$$-\frac{dP}{dt}=-\frac{d}{dt}\int_0^\infty p\,d\epsilon$$
$$=\int_0^\infty\left(-\frac{dp}{dt}\right)d\epsilon \tag{10}$$
$$=\int_0^\infty p_0\left(-\frac{d\Theta_n}{dt}\right)d\epsilon.$$

Thus neglecting, for the moment, the effect of the initial activation energy spectrum, of the processes occurring simultaneously, those at the maximum of $d\Theta_n/dt$ make the maximum contribution. Since in isothermal annealing $d\Theta_n/dt$ and $d\Theta_n/d\epsilon$ (regarded as functions of ϵ) are proportional to each other (again neglecting any dependence of B and f on ϵ), they possess a maximum at the same value of ϵ, and hence the processes possessing the characteristic activation energy make the maximum contribution to those occurring simultaneously. However, because $(dp/dt)(\epsilon)$ is usually unsymmetrical about ϵ_0, the average activation energy of the processes undergoing simultaneous annealing is slightly displaced from ϵ_0, an effect which is small and which will be considered later. From the value and the slope of the characteristic annealing function at the characteristic activation energy

$$\Theta_n(\epsilon_0)=n^{1/(1-n)}, \tag{11}$$

$$\frac{d\Theta_n}{d\epsilon}(\epsilon_0)=\frac{n^{n/(1-n)}}{\tau}, \tag{12}$$

it is seen that for reasonable values of n, most of the processes occurring simultaneously lie in a narrow band of activation energies of the magnitude several times $n\tau$ (Fig. 1).

1.3. The presentation of the activation-energy spectrum as a function of time is a complete representation of the formal kinetic behavior of a suitable property for any kind of annealing program. Experimentally all that is observed is the integral of the activation-energy spectrum as a function of time. The customary kinetic interpretation of the data would consist of finding the initial activation-energy spectrum; and then through a proper choice of order and frequency factor (B), the activation-energy spectrum as a function of time would be given by the equations. If this could not be done, complications of kinetic behavior would be assumed. This matter is discussed later.

1.4. The kinetic behavior for isothermal annealing in the case of a broad activation-energy spectrum is easily visualized and is drawn schematically in Fig. 2. As time proceeds, the initial activation-energy spectrum is swept out as the characteristic annealing function advances in activation energy. If the initial activation-energy spectrum is very broad, many times $n\tau$, the

characteristic annealing function may be approximated by a step function. Then Eq. (7) becomes

$$P(t)\cong\int_{\epsilon_0}^{\infty}p_0(\epsilon)d\epsilon, \tag{13}$$

and

$$dP/dt\cong-p_0(\epsilon_0)(d\epsilon_0/dt). \tag{14}$$

From Eq. (9),

$$p_0[\tau\ln(Bt)]\cong-(t/\tau)(dP/dt). \tag{15}$$

1.5. The result Eq. (15) which gives the initial-activation-energy spectrum from the isothermal annealing data, was derived by Vand[1] for first-order processes, but is seen here to be quite general and applies to processes of any order. The order does not affect the initial activation energy spectrum (for it was present before annealing was started) but rather the shape of the changing portion of the activation-energy spectrum as the annealing proceeds. This shape was ignored when a step function was used to approximate the characteristic-annealing function, and hence the result applies to all orders. It is seen from Eq. (15) that the effect of the frequency factor in isothermal annealing is to cause a simple displacement along the activation energy axis. Thus the result gives the correct approximate shape for the initial activation-energy spectrum, but does not fix its location. For the usual range of times which can be realized in careful isothermal annealing, about three decades, it can be seen from Eq. (15) that the portion of the activation energy spectrum which is revealed is but several tenths of an electron volt, only a small portion of the several electron-volt wide activation energy spectra observed in disordered solids. If the whole spectrum is to be found by isothermal annealing, it is necessary to conduct isothermal annealings at a number of different temperatures. However, in this case the parts of the spectrum revealed at the different temperatures will not fit togther unless the frequency factor is correctly chosen (however, see paragraph 4.3) since the displacement along the activation energy axis involves a product of temperature and (logarithm of) frequency factor. If this is used as a method to obtain the frequency factor, it is important to fit the parts of the activation energy spectrum together rather than the observed property changes as is shown in paragraph 2.3.

1.6. The treatment given here may be extended to the case of tempering, i.e., an annealing conducted by raising the temperature in a gradual manner. For a case in which the temperature of *the sample* is raised according to the law

$$t=c\tau, \tag{16}$$

when annealing a group of processes characterized by a discrete activation energy, the differential equations are

$$-(dq/cd\tau)=Ae^{-\epsilon/\tau}q^n, \tag{17}$$

$$-(dp/fcd\tau)=Ae^{-\epsilon/\tau}(p/f)^n, \tag{18}$$

for which the solution is

$$p=p_0[1-(1-n)Bc\tau E_2(\epsilon/\tau)]^{1/(1-n)}. \tag{19}$$

If the processes are distributed in activation energy, p and p_0 are distribution functions, and the measured value of the property is

$$P=\int_0^{\infty}p_0[1-(1-n)Bc\tau E_2(\epsilon/\tau)]^{1/(1-n)}d\epsilon, \tag{20}$$

or

$$P(\tau)=\int_0^{\infty}p_0(\epsilon)\Phi(\epsilon,\tau)d\epsilon, \tag{21}$$

where Φ is the characteristic annealing function in tempering.

The functions $E_m(x)$ are defined as

$$E_m(x)=x^{m-1}\int_x^{\infty}u^{-m}e^{-u}du, \tag{22}$$

and have been tabulated.[13] A property of interest is

$$dE_m(x)/dx=-E_{m-1}(x). \tag{23}$$

For the range of x of interest here (20–50), the first term of Blanch's asymptotic expansion,[13]

$$E_m(x)\cong(x+m)^{-1}e^{-x}, \tag{24}$$

is a satisfactory approximation, and when used with the approximation

$$(x+a)(x+b)\simeq(x+j)(x+k), \tag{25}$$

where a, b, j, and k are small integers and

$$a+b=j+k, \tag{26}$$

the algebraic operations with these exponential integrals are greatly simplified while their identification is preserved. Often different expressions result from introducing the approximation at different stages of the algebraic operations; but because the values of x of interest here are so large, they do not differ significantly from each other numerically. Where alternative expressions were obtained, one convenient for the purpose at hand was chosen.

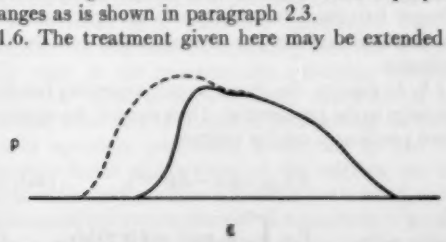

FIG. 2. An activation energy spectrum in isothermal annealing. The portion of the initial activation energy spectrum which has been annealed is shown as a dashed curve.

[13] G. Placzek, National Research Council of Canada Report NRC-1547, 1946.

1.7. As in the case of isothermal annealing, the annealing behavior in tempering is dominated by the exponential dependence on ϵ appearing in Φ_n which is here termed the characteristic annealing function for tempering. It is sigmoid-shaped, somewhat like the curve drawn in Fig. 1, and varies from zero to one. Upon solving for ϵ using the approximation, Eq. (24),

$$\epsilon+\tau\ln[(\epsilon/\tau)+2] \cong\tau\{\ln[(1-n)B]+\ln(c\tau)-\ln(1-\Phi_n^{1-n})\}, \quad (27)$$

it is thus seen that as the annealing proceeds (whether plotted in temperature as is customary, or in time), the sigmoid form of the characteristic annealing function advances in activation energy, and it also reclines instead of retaining its original form as it does in an isothermal annealing.

Using Eqs. (23)–(26), it is found that the point of inflection of the characteristic annealing function for linear tempering occurs at

$$\epsilon_0\cong\tau\{\ln(Bc\tau)-\ln[(\epsilon_0/\tau)+2]\}. \quad (28)$$

The rate of annealing is

$$-dP/d\tau=\int_0^\infty p_0(-d\Phi_n/d\tau)d\epsilon. \quad (29)$$

Neglecting, for the present, the effect of the initial activation-energy spectrum, the maximum contribution to the annealing at any moment is made by the processes occurring at the maximum of $-d\Phi_n/d\tau$ which does not occur at ϵ_0 but at ϵ_τ given by

$$\epsilon_\tau=\tau\{\ln Bc\tau-\ln[(\epsilon_\tau/\tau)+2] +\ln[(\epsilon_\tau/\tau)+n](\epsilon_\tau/\tau)^{-1}\}, \quad (30)$$

which is at a slightly higher activation energy than the characteristic activation energy. Because $d\Phi_n/d\tau$ is unsymmetrical about its maximum, the average activation energy of the processes undergoing simultaneous annealing is even farther removed from the characteristic activation energy. However these displacements are usually small in comparison with the effects which the initial activation-energy spectrum can exert. At the characteristic activation energy, the characteristic function has the value

$$\Phi_n(\epsilon_0)=n^{1/(1-n)}. \quad (31)$$

The slope of the characteristic annealing function is

$$\frac{d\Phi_n}{d\epsilon}(\epsilon_0)=\frac{1}{\tau}n^{n/(1-n)}\left(1+\frac{\tau}{\epsilon_0}\right), \quad (32)$$

which in a typical case would be a few percent greater than in isothermal annealing. Thus, for reasonable values of n most of the processes occurring simultaneously in tempering also lie in a narrow band of activation energies, several times $n\tau$. Hence, the mathematical artifice used here, that of starting the tempering at $\tau=0$, does not introduce a serious restriction.

1.8. An approximate solution for the initial activation-energy spectrum can be obtained in the manner used previously. From Eq. (21),

$$P(\tau)\cong\int_{\epsilon_0}^\infty p_0 d\epsilon, \quad (33)$$

and taking the derivative with respect to τ,

$$p_0(\epsilon_0)=-\frac{1}{d\epsilon_0/d\tau}\frac{dP}{d\tau}. \quad (34)$$

Writing y_0 for ϵ_0/τ, Eq. (28) becomes

$$y_0+\ln(y_0+2)=\ln(Bc\tau). \quad (35)$$

Since the annealing takes place in a small range of y and since $y_0+\ln(y_0+2)$ is a very slowly varying function, it is quite permissible to take

$$y_0+\ln(y_0+2)\cong a+by_0, \quad (36)$$

where a and b are constants appropriate to the range of y under consideration. Then writing ξ for $-a+\ln(Bc\tau)$,

$$\epsilon_0\cong\tau\xi/b, \quad (37)$$

$$d\epsilon_0/d\tau\cong(\xi+1)/b\cong1+\xi/b \quad (38)$$

(for b is close to unity), and

$$p_0\left(\tau\frac{\xi}{b}\right)\cong-\frac{dP}{d\tau}\frac{1}{(\xi/b)+1}. \quad (39)$$

Since ξ/b varies only slowly with temperature, the initial activation energy spectrum is nearly proportional to the tempering curve which plots $(-dP/d\tau)$ against τ when the heating rate of the sample, $(1/c)$, has been constant. The resolution is several times $n\tau$ (see Vand[1]) and the method applies when the activation-energy spectrum is broad compared to $n\tau$ and to reasonable orders of reaction. Changing the frequency factor causes a displacement of the derived initial activation-energy spectrum along the activation energy axis as described for isothermal annealing in paragraph (1.5). However, since in tempering the temperature is continuously changing, a change in choice of frequency factor also causes a distortion of the derived spectrum. Choosing a larger frequency factor expands the spectrum along its abscissas (activation energy) and contracts its ordinates.

1.9. At n unity, the characteristic annealing functions converge to the exponential. Then some of the equations given previously can be written

$$p=p_0\exp(-At\epsilon^{-\epsilon/\tau}), \quad (4a), (5a)$$

$$P=\int_0^\infty p_0\exp(-At\epsilon^{-\epsilon/\tau})d\epsilon, \quad (6a)$$

$$\epsilon=\tau[\ln(At)-\ln_2(1/\Theta)], \quad (8a)$$

$$\epsilon_0=\tau\ln(At), \tag{9a}$$

$$\Theta(\epsilon_0)=e^{-1}, \tag{11a}$$

$$(d\Theta/d\epsilon)(\epsilon_0)=(\tau e)^{-1}, \tag{12a}$$

$$p_0(\tau\ln(At))\cong-(t/\tau)(dP/dt), \tag{15a}$$

$$p=p_0\exp[-Ac\tau\mathbf{E}_2(\epsilon/\tau)], \tag{19a}$$

$$P=\int_0^\infty p_0\exp[-Ac\tau\mathbf{E}_2(\epsilon/\tau)]d\epsilon, \tag{20a}$$

$$\epsilon+\tau\ln[(\epsilon/\tau)+2]\cong\tau[\ln(Ac\tau)-\ln_2(1/\Phi)], \tag{27a}$$

$$\Phi(\epsilon_0)=e^{-1}, \tag{31a}$$

and

$$\frac{d\Phi}{d\epsilon}(\epsilon_0)=\frac{1+(\tau/\epsilon_0)}{\tau\epsilon}, \tag{32a}$$

where $\ln_2(x)\equiv\ln(\ln x)$.

1.10. In tempering, if the heating rate is given by the equation

$$t=c\tau^m, \tag{40}$$

where m is integral and greater than unity, the equations may be integrated by the methods given here, and it is found that the characteristic-annealing function involves the exponential integral $\mathbf{E}_{m+2}(\epsilon/\tau)$.

2. SOME EFFECTS PRODUCED BY THE INITIAL ACTIVATION ENERGY SPECTRUM

2.1. The exact mathematical inversion of the isothermal annealing data $P(t)$ to obtain $p_0(\epsilon)$ by means of a Laplace transform has been given by Honig.[9] In order to do this, it is necessary to know the function dP/dt sufficiently well analytically to determine its behavior over the whole of the complex plane. From the discussion in paragraph (1.5) it is obvious that this is impossible in practice. Honig's conclusion that a constant initial activation-energy spectrum cannot exist, while entirely correct, has no practical significance. Since, effectively, only the processes over a small range of activation energies occur simultaneously, and since only a small portion of the possible range of activation energies can be observed in an isothermal annealing, the portion of the initial activation-energy spectrum which for practical purposes can be considered to be involved in a particular experiment can be constant.[10] In this case the annealing behavior is essentially that of the characteristic annealing function. When the initial activation-energy spectrum is not constant, some care is needed in interpreting the data. This is especially true when attempting to find the frequency factor or the order of the reaction, for the effects which they produce and which are studied, occur in a range of activation energies of magnitude $\sim n\tau$, the range over which the processes are occurring simultaneously, and any variation of the initial activation-energy spectrum in this region will weight the processes occurring in some parts of this range with respect to those occurring in other parts of this range. Some of the effects which are observed are treated by giving two illustrations, one treating the analysis of isothermal data, and the other treating the analysis of step-annealing data.

2.2. It is useful here to introduce a comparison between the shape S_0 of the rapidly rising portion of the characteristic annealing function and the shape S_p of the portion of the activation-energy spectrum existing at that time in the same range of activation energies. The qualitative effect of a rising initial activation-energy spectrum is that S_p is steeper than S_0. Thus if it is not realized that p_0 is rising, it may be considered that the frequency factor is greater than its correct value. It may also be considered that the order is less than its correct value. However the point of inflection in S_p may not correspond to this latter interpretation for, in general, it will be higher than for S_0 corresponding to a greater order of reaction and would be lower than in S_0 only if p_0 although increasing possessed a negative radius of curvature, small compared to $n\tau$.

It is also readily seen by sketching some of the possible forms of initial activation-energy spectra and the S_p they yield that the maximum displacements of S_p with respect to S_0 can be of the magnitude $\sim n\tau$ for the most steeply rising initial activation-energy spectra. The reverse displacements will occur with falling initial activation-energy spectra. Accordingly, with the use of Eq. (14) or (39), processes occurring at a discrete activation energy will yield an approximate spectrum of width several times $n\tau$, and a smaller distortion will be found when the actual initial activation energy spectrum is less steep than a delta function.

2.3. In isothermal annealing, it is convenient, to plot the measured value of the property (P) against

$$\ln t\equiv x. \tag{41}$$

Then Eq. (15) may be written

$$p_0(\tau\ln B+\tau x)\cong-\tau^{-1}(dP/dx). \tag{42}$$

Over the small portion of the activation energy spectrum which is revealed, the distribution may change very little. Thus dP/dx will change very little, perhaps within the experimental error of the data. It is tempting to draw $P(x)$ as a straight line and thus miss the variations in the initial activation energy spectrum, p_0. It is necessary to be extremely cautious in interpreting isothermal annealing data extending from several minutes to several hours, but two decades in time.

If the data $P(x)$ for a number of independent isothermal annealings conducted at different temperatures are plotted, they will form a family of curves which are nearly straight lines, the higher temperature curves lying below the lower temperature ones. These curves are nearly parallel as can be shown by taking $\partial(dp/dx)/\partial\tau$ which is seen to be small when the relation $Bte^{-\epsilon/\tau}\sim1$ [Eq. (9)] is inserted. If the temperatures are

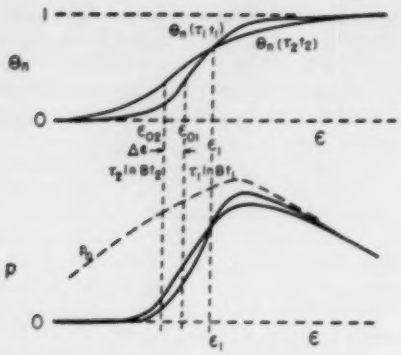

FIG. 3. The appearance of the characteristic annealing functions and the activation-energy spectra for two isothermal annealings conducted at different temperatures when the measured value of the property is the same.

sufficiently close together, the first measured values of the property at the beginning of one annealing will be greater than the last measured values at the end of the annealing performed at a lower temperature. Respective points on the two curves having the same measured values of the property are related kinetically as follows:

$$P=\int_0^\infty p_0\Theta_n(\tau_1,t_1,\epsilon)d\epsilon=\int_0^\infty p_0\Theta_n(\tau_2,t_2,\epsilon)d\epsilon. \quad (43)$$

The approximation introduced in deriving Eq. (15) would lead to the result

$$\epsilon_0(\tau_1,t_1)\equiv\epsilon_{01}\cong\epsilon_{02}\equiv\epsilon_0(\tau_2,t_2), \quad (44)$$

where ϵ_{01}, ϵ_{02} are the characteristic activation energies at the respective temperatures, and hence the approximate value of $\ln B$ is $\ln B'$, where

$$\ln(B')=(\tau_1x_1-\tau_2x_2)/(\tau_2-\tau_1). \quad (45)$$

The behavior of $\ln(B')$ can be visualized with the aid of Fig. 3. The characteristic annealing functions for the two annealings will intersect at some activation energy, ϵ_1, and hence the activation energy spectra will also intersect at this activation energy. The condition Eq. (43) requires that when the measured value of the property is the same for the two annealings, the area between the activation-energy spectra to the left of ϵ_1 must be equal to the area between the two spectra to the right of ϵ_1. In general, the characteristic activation energies, ϵ_{01} and ϵ_{02} respectively, will not be at ϵ_1, and hence defining $\Delta\epsilon$ as

$$\Delta\epsilon=\epsilon_{01}-\epsilon_{02}, \quad (46)$$

$$\ln B=\ln(B')-\Delta\epsilon/(\tau_2-\tau_1). \quad (47)$$

For a rising initial activation-energy spectrum it is seen that ϵ_1 is advanced relative to ϵ_{01} and ϵ_{02} and hence $\Delta\epsilon$ is increased, and the reverse is true for a falling initial activation-energy spectrum. These variations in $\Delta\epsilon$ can be of the magnitude ($\sim n\tau$) since it is reasonable for the intersection of the characteristic annealing functions to occur over any part of their steep regions. Thus if τ_1 is about 0.05 and τ_2 is 0.055, B can differ from B' by factors ranging from $\sim10^{-4n}$ to $\sim10^{4n}$.

Even if the initial activation-energy spectrum is constant in the region of activation energies which are annealing, B must, in general, differ from B'. It is readily seen that with a constant initial spectrum, if the region of the initial spectrum undergoing annealing is not too close to the end of the initial spectrum, the condition of equality of areas between the activation-energy spectra on either side of their intersection requires the ordinate of the intersection decrease for pairs of points at greater times; accordingly $\Delta\epsilon$ decreases and from Eq. (47), $\ln B'$ also decreases. The same reasoning requires that $\ln B'$ increase when the region of the initial spectrum undergoing annealing is close to its end. These effects are several orders of magnitude smaller than the possible effects of the rising and falling regions of the initial spectrum.

2.4. For two successive stages of step-annealing, if the processes occur at a discrete activation energy, then

$$-(dp/dt)_1=Af\epsilon^{-\epsilon/\tau_1}(p/f)^n, \quad (48)$$

$$-(dp/dt)_2=Af\epsilon^{-\epsilon/\tau_2}(p/f)^n. \quad (49)$$

At the beginning of the second stage, the value of the property is the same as at the end of the first stage. Designating the ratio of the rates at the two temperatures at this point as R and $\tau_1\tau_2/(\tau_1-\tau_2)$ as ζ, it is seen that

$$\epsilon=\zeta\ln R, \quad (50)$$

a relation pointed out by Overhauser.[8] When the processes are distributed in activation energy, it is obvious that this relation can at best hold only approximately since different distributions of processes are taking place at the two temperatures. The number which is obtained in this case upon introducing the experimentally determined rates and temperatures into Eq. (50) will be designated E and its meaning is investigated here.

If the first of the two particular stages of step-annealing considered has been conducted for a time t_1 sufficiently long to advance the characteristic annealing function at least several $n\tau_1$, the activation-energy spectrum will have become

$$p_1=p_0[1-(1-n)Bt_1\epsilon^{-\epsilon/\tau_1}]^{1/(1-n)}, \quad (51)$$

or, for $n=1$,

$$p_1=p_0\exp(-At_1\epsilon^{-\epsilon/\tau_1}). \quad (51a)$$

If at this point another annealing is started, the rate at which the property changes is

$$-\frac{dP}{dt}=\int_0^\infty p_0[1-(1-n)Bt_1\epsilon^{-\epsilon/\tau_1}]^{1/(1-n)} \times[1-(1-n)Bt\epsilon^{-\epsilon/\tau_2}]^{n/(1-n)}B\epsilon^{-\epsilon/\tau_2}d\epsilon.$$

At the beginning of the second annealing $t=0$, and hence[10]

$$-\left(\frac{dP}{dt}\right)_0=\int_0^\infty p_0[1-(1-n)Bt_1e^{-\epsilon/\tau_1}]^{1/(1-n)}Be^{-\epsilon/\tau_2}d\epsilon, \tag{52}$$

and for first-order processes

$$-\left(\frac{dP}{dt}\right)_0=\int_0^\infty p_0\exp(-At_1e^{-\epsilon/\tau_1})Ae^{-\epsilon/\tau_2}d\epsilon. \tag{52a}$$

The integrals, Eqs. (52) and (52a), are various forms of the Euler integrals. If the initial activation-energy spectrum is constant, then for first-order processes, upon setting $z=At_1e^{-\epsilon/\tau_1}$ and $\sigma=\tau_1/\tau_2$, Eq. (52a) becomes

$$-\left(\frac{dP}{dt}\right)_0=p_0\frac{\tau_1}{t_1}(At_1)^{(1-\sigma)}\int_0^{At_1}e^{-z}z^{(\sigma-1)}dz. \tag{53}$$

Since At_1 is a very large number, the upper limit may be taken to be infinite. Hence,

$$-\left(\frac{dP}{dt}\right)_0=p_0\frac{\tau_1}{t_1}(At_1)^{(1-\sigma)}\Gamma(\sigma), \tag{54}$$

where Γ is the gamma function. The rate at the end of the first annealing stage is obtained by setting $\sigma=1$. As before, designating the ratio of the rate at the beginning of the second stage to that at the end of the first stage as R,

$$R=(At_1)^{1-\sigma}\Gamma(\sigma), \tag{55}$$

and

$$(1-\sigma)\ln(At_1)=\ln[R/\Gamma(\sigma)]. \tag{56}$$

If it is assumed that the processes which are annealing simultaneously may be characterized by the characteristic activation energy at the end of the annealing at the lower temperature, from Eq. (9a),

$$\epsilon_0=\zeta\ln[R/\Gamma(\sigma)]. \tag{57}$$

Usually $0.9<\sigma<1$, hence $\Gamma(\sigma)$ is near unity, and the result may seem to be insignificantly different from Eq. (50). However, this small correction is but one of a number which it will be seen are quite important in interpreting the kinetic significance of the annealing data. If the order is less than unity, and the initial activation-energy spectrum is constant, by setting $Bt_1e^{-\epsilon/\tau_1}=y$, Eq. (52) may be written[10]

$$-\left(\frac{dP}{dt}\right)_0=p_0\frac{\tau_1}{t_1}(Bt_1)^{1-\sigma}\times\int_0^{1/(1-n)}[1-(1-n)y]^{1/(1-n)}y^{\sigma-1}dy \tag{58}$$

$$=p_0\frac{\tau_1}{t_1}(Bt_1)^{1-\sigma}(1-n)^{-\sigma}\beta\left(\sigma,\frac{2-n}{1-n}\right), \tag{59}$$

where β is the beta function; and hence

$$R=(1+\alpha_2)(Bt_1)^{1-\sigma}\Gamma(\sigma), \tag{60}$$

where

$$1+\alpha_2\equiv(1-n)^{1-\sigma}\times\Gamma[1+(2-n)/(1-n)]/\Gamma[\sigma+(2-n)/(1-n)]. \tag{61}$$

The respective values of α_2 for $n=\frac{1}{2}$, $\frac{2}{3}$, $\frac{3}{4}$, are 0.056, 0.040, and 0.032. The same treatment can be employed for orders $1<n<2$, and then Eq. (52) becomes

$$-\left(\frac{dP}{dt}\right)_0=p_0\frac{\tau}{t_1}(Bt_1)^{1-\sigma}\int_0^{Bt_1}\frac{y^{\sigma-1}dy}{[1+(n-1)y]^{1/(n-1)}},$$

and since Bt_1 is a large number, upon marking the upper limit infinite, this becomes

$$-\left(\frac{dP}{dt}\right)_0=p_0\frac{\tau}{t_1}(Bt_1)^{1-\sigma}(n-1)^{-\sigma}\beta\left(\sigma,\frac{1}{n-1}-\sigma\right), \tag{63}$$

and hence

$$R=(1-\alpha_3)(Bt_1)^{1-\sigma}\Gamma(\sigma), \tag{64}$$

where

$$1-\alpha_3\equiv(n-1)^{1-\sigma}\Gamma\left(\frac{1}{n-1}-\sigma\right)\Big/\Gamma\left(\frac{1}{n-1}-1\right). \tag{65}$$

The respective values of α_3 for orders $n=1.5$, 1.9, and 1.99 are about 0.133, 0.497, and 0.9142. Part of the large correction α_3 for large values of the order arises in the region of large values of ϵ which in practice would not exist, while part of the smaller correction in the region of ϵ of significance would be partially compensated for by the displacement of the average activation energy of the processes undergoing simultaneous annealing from the characteristic activation energy. If the order is 2 or greater, it is necessary to limit the extent of the initial activation-energy spectrum in order to perform the integrations. However, it is seen that the deviations of the behavior of processes distributed in activation energy from Eq. (50) can all be cast into the same form. The deviations will be estimated here for several kinds of initial activation-energy spectra for processes following first-order kinetics. The same kind of corrections would apply when the order differs from unity, but the magnitudes of the corrections would, in general, differ somewhat. The corrections to be considered are those arising from the first of two consecutive stages of step-annealing being insufficiently protracted and from rising and falling regions in the initial activation-energy spectrum. To indicate the magnitude of the corrections, the results will be applied to the step-annealing data published by Overhauser.[8]

(*a*) *Length of the steps in step-annealing.*—It was shown (Fig. 1) that most of the rising part of the first-order-characteristic-annealing function lies in a range of activation energies $\sim 3\tau$. Hence for first-order processes, if one of the stages of a step-annealing is conducted for a time sufficient to advance the charac-

teristic-annealing function about 3τ, practically none of the activation-energy spectrum lies under portions formed in previous stages of annealing, and hence the spectrum is practically that which would have arisen if the final annealing were the only annealing which had been performed. Since in isothermal annealing, the characteristic-annealing function moves to higher activation energies without altering its shape, its motion may be followed by choosing any point on it; and in the present case the characteristic-activation energy is a convenient point. Then the length of successive stages of step annealing should be determined from

$$\epsilon_{02}=\epsilon_{01}+3\tau_1, \tag{66}$$

or

$$\tau_2\ln(At_2)=\tau_1\ln(At_1)+3\tau_1, \tag{67}$$

and hence

$$t_2=t_1e^{3\sigma}(At_1)^{\sigma-1}\equiv\lambda t_1. \tag{68}$$

If At_1 were about 10^{13}, a number which seems reasonable for Overhauser's data (V.I.), and if it were desired to conduct each stage of step-annealing for the same length of time, σ should be about 0.91. Actually for most of his annealings $\sigma\cong 0.94$ and Eq. (68) suggests each stage should have been three times as long as the previous one; i.e., $\lambda=3$. Since it has not been, a residue of the spectrum of the previous annealing remains and hence Eq. (52a) is altered to

$$-\left(\frac{dP}{dt}\right)_{02}=\int_0^\infty p_0\exp(-At_1e^{-\epsilon/\tau_1}-At_2e^{-\epsilon/\tau_2})Ae^{-\epsilon/\tau_2}d\epsilon. \tag{69}$$

Letting $\sigma_1=\tau_2/\tau_1$, $\sigma=\tau_1/\tau_2$, $r=At_1/At_2$, $z=At_2e^{-\epsilon/\tau_2}$, and $\beta=r(At_1)^{1-\sigma}z^{\sigma-1}$,

$$-\left(\frac{dP}{dt}\right)_{02}=\frac{\tau_2}{t_2}(At_2)^{1-\sigma}\int_0^{At_2}p_0e^{-z(1+\beta)}z^{\sigma-1}dz. \tag{70}$$

Now β is small, and regarding it as constant gives a somewhat greater effect than it actually exerts. For a constant activation-energy spectrum it is approximately true that

$$-\left(\frac{dP}{dt}\right)_{02}=p_0\frac{\tau_2}{t_2}(At_2)^{1-\sigma}\Gamma(\sigma)(1+\beta)^{-\sigma}, \tag{71}$$

and hence, upon altering the subscript on t to correspond to the nomenclature of Eq. (55),

$$R=(At_1)^{1-\sigma}\Gamma(\sigma)(1+\beta)^{1-\sigma}. \tag{72}$$

Since $\Gamma(\sigma)$ is nearly unity, this can be written

$$R=(At_1)^{1-\sigma}[1+\alpha+(1-\sigma)\beta], \tag{73}$$

where α is a small number.

For Overhauser's conditions, $(1-\sigma)\beta$ is about 0.002 to 0.010 which, it will be seen, is small compared to the value of α.

(*b*) *The effect of rising regions in the initial activation energy spectrum.*—These can be easily investigated by setting p_0 proportional to powers of ϵ or to negative powers of $\epsilon^{-\epsilon/\tau_1}$. Two effects are produced: a correction factor equivalent to increasing α is obtained, and the average activation energy of the processes undergoing simultaneous annealing is altered relative to the characteristic-activation energy.

If the initial activation-energy spectrum in the region is rising proportionately to an integral power (μ) of ϵ,

$$p_0=k\epsilon^\mu, \tag{74}$$

and hence

$$-\left(\frac{dP}{dt}\right)_0=k\frac{\tau_1^{\mu+1}}{t_1}(At_1)^{1-\sigma}\int_0^{At_1}e^{-z}z^{\sigma-1}\times[\ln(At_1)-\ln z]^\mu dz, \tag{75}$$

which is seen to consist of a sum of products of gamma and polygamma functions.[13] The result can be cast into the form of Eq. (73) but α is now greater. Typically, when approaching a peak in the initial activation-energy spectrum, the spectrum rises so rapidly that it is best expressed by an exponential as

$$p_0=ke^{\nu\epsilon/\tau_1}, \tag{76}$$

where k and ν are constants. Hence

$$-\left(\frac{dP}{dt}\right)_0=k\frac{\tau_1}{t_1}(At_1)^{1-\sigma}\int_0^{At_1}e^{-z}z^{\sigma-\nu-1}dz, \tag{77}$$

and therefore

$$R=(At_1)^{1-\sigma}\Gamma(\sigma-\nu)/\Gamma(\nu). \tag{78}$$

Since $\Gamma(\sigma-\nu)/\Gamma(\nu)$ is nearly unity but is greater than $\Gamma(\sigma)$, Eq. (78) can be written in the form of Eq. (73) and hence the effect of the exponentially rising distribution is to increase α. The average activation energy $\bar{\epsilon}$ of the processes annealing simultaneously is

$$\bar{\epsilon}=\int(dp/d\bar{t})\epsilon d\epsilon\Big/\int(dp/d\bar{t})d\epsilon. \tag{79}$$

For spectra rising as powers of ϵ [Eq. (74)], the integrals in Eq. (79) are like those of Eq. (75) and are easily evaluated with the aid of tables of gamma and polygamma functions.[13] It is found that while the activation energy at which the processes annealing simultaneously possess the maximum rate of annealing is about

$$(1+10^{-3}\mu)\tau_1\ln(At_1), \tag{80}$$

the average activation energy of the processes annealing simultaneously is about

$$(1.017+2\mu\ 10^{-3})\tau_1\ln(At_1) \tag{81}$$

for small integral values of μ. For exponentially rising

[13] H. T. Davis, *Tables of Higher Mathematical Functions* (Principia Press, Bloomington, 1933), Vol. 2.

spectra, Eq. (76), Eq. (79) becomes

$$\bar{\epsilon}=\frac{(\tau_1^{\nu}/l_1)(At_1)^{\nu-1}\int_0^{At_1} e^{-z}z^{1-\nu-1}[\ln(At_1)-\ln z]dz}{(\tau_1/l_1)(At_1)^{\nu-1}\int_0^{At_1} e^{-z}z^{1-\nu-1}dz} \tag{82}$$

$$=[1-\Psi(1-\nu)/\ln(At_1)]\tau_1\ln(At_1). \tag{83}$$

where Ψ is the logarithmic derivation of the gamma function. The quantity $\Psi(1-\nu)/\ln(At_1)$ is a small negative number; and hence, as found for spectra rising as powers of ϵ, $\bar{\epsilon}$ can be expressed as

$$\bar{\epsilon}=\epsilon_0(1+\delta), \tag{84}$$

and for a constant activation-energy spectrum ($\nu=0$), $\delta\cong 0.02$ as before. For a falling initial activation-energy spectrum δ and α will assume values less than their values with a constant initial activation-energy spectrum in about the same proportion as for rising initial spectra. Thus, taking into account the effects of the lengths of the annealing stages, Eq. (72), the effects of the initial activation-energy spectrum Eqs. (75) and (78), and the nomenclature of Eqs. (73) and (84), Eq. (57) may be written

$$\epsilon_0=\zeta\ln\{R/[1+\alpha+(1-\sigma)\beta]\}, \tag{85}$$

and the average activation energy of the processes undergoing annealing simultaneously is therefore

$$\bar{\epsilon}=(1+\delta)\ln\{R/[1+\alpha+(1-\sigma)\beta]\}, \tag{86}$$

and hence

$$E\cong(1-\delta)\bar{\epsilon}+[\alpha+(1-\sigma)\beta]\zeta. \tag{87}$$

The corrections α, β, δ are to be considered approximate and maximal since the finite character of each type of behavior has not been taken into consideration. From Eqs. (84) and (9a), it is seen that the average activation energy of the processes occurring simultaneously $\bar{\epsilon}$ at equal values of At_1 in a region in which the initial activation-energy spectrum is constant is proportional to the absolute temperature at which the annealing is conducted. When the initial activation-energy spectrum is rising, this average activation energy is above this line; and when the initial activation-energy spectrum is falling, this average activation energy is below this line. Since α increases nearly proportionately to δ, the effect of the initial activation-energy spectrum on E is less than its effect on this average activation energy. In Overhauser's case, ζ was about $\bar{\epsilon}/2$ and hence in this case the deviations of E from a linear dependence on τ would be about half as great as the deviations of $\bar{\epsilon}$ from a linear dependence on τ and opposite in sign.

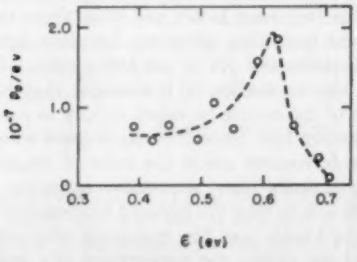

FIG. 4. The approximate activation energy spectrum from Overhauser's isothermal annealing data assuming first-order kinetics and a frequency factor 10^9.

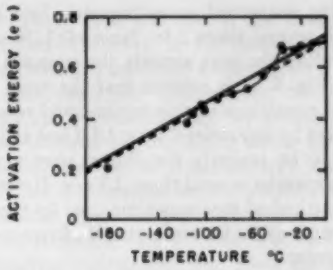

FIG. 5. The behavior of E (plotted points) and $1.02\epsilon_0$ (solid line) as a function of temperature.

The results published by Overhauser[8] illustrate the effects shown here. An approximate value of A may be obtained from the slope of the curve E as a function of temperature given in Fig. 5, taken from Overhauser's Fig. 4, and is about 10^9. The approximate initial activation-energy spectrum obtained by introducing the slopes at the end of his stages of step-annealing (his Fig. 3) into Eq. (14), no correction being made for previous stages of annealing, is shown in Fig. 4. The sharp peak is readily apparent; and from the discussion in paragraph (2.2), the actual peak must be somewhat sharper. The peak in Fig. 4 rises about as $\tau^{10\epsilon}$ (or $e^{0.3\epsilon/\tau_1}$), changing α and δ by *ca* 0.02; and falls about as $e^{-20\epsilon}$, changing α and δ by *ca* -0.04. Now ζ can be written

$$\zeta=\tau_1/(1-\sigma), \tag{88}$$

and since for these experiments $\sigma\cong 0.94$, $\zeta\cong 1/5$. Thus, since $\bar{\epsilon}\cong 0.6$, the deviation of E from a straight line should be about -0.01 ev just before the peak and should be about $+0.02$ ev just following the peak. This expected deviation is readily apparent in Fig. 5 when the straight line (solid line) is drawn at slightly greater slope than was done by Overhauser (dashed line). Thus the data shown in Fig. 5 cannot be taken as proof of a 2.5 order; they can be as easily explained by first-order kinetics. Within the precision of the data and of the approximations of the theory, the results could be explained by any order of reaction over quite a range of orders. The data given by Overhauser are affected mainly by the initial activation-energy spectrum, and as was shown in Sec. 1, such data is rather insensitive to order or frequency factor. That short isothermal annealings in the region of the peak can be fitted by kinetics of order 2.3 using a discrete activation energy is but an expression of the fact that the peak obtained

by inserting isothermal annealing rates into Eq. (14) is of width several times 2.3τ. Since $\tau \cong 1/30$ ev in the region in which the peak anneals, the expected width is shown in Fig. 4. It is evident that the rates in short isothermal annealings in this region could equally well be explained by any order $0<n<2.3$ if one assumes the processes to be properly distributed over a range of activation energies several times $2.3\ \tau/n$. It would seem that the method of step-annealing used by Overhauser might be more useful for evaluating the frequency factor than the order.

3. DETERMINATION OF THE ORDER BY A COMBINATION OF ISOTHERMAL ANNEALING AND TEMPERING

3.1. A possible method for determining the order of a group of processes which occur over a range of activation energies is suggested by the physical picture presented in paragraphs 1.3 and 1.4. The method is best applied when it is found that the initial activation-energy spectrum is quite constant over a sufficient range of activation energies. This fact can be easily ascertained, for then the approximation, Eq. (39), is quite good. If a sample of a substance possessing such an initial activation-energy spectrum is subjected to an isothermal annealing at a suitable temperature for a sufficient length of time, the rising portion of the resultant activation-energy spectrum has the form of the corresponding portion of the characteristic annealing function. If a tempering experiment is now conducted on the isothermally annealed sample, the nature of the characteristic isothermal annealing function is revealed. The portion of the tempering curve of interest is that resulting from the steeply rising portion of the isothermal annealing curve. Here the approximation of Eq. (39) is useless. However, since the original initial activation-energy spectrum was constant (here designated p_0), the equations can be integrated directly. The tempering rate if the processes are first order is

$$-\frac{dP}{dt}=p_0\int_0^\infty Ac \times\exp[-At_1e^{-\epsilon/\tau_1}-Ac\tau\mathbf{E}_2(\epsilon/\tau)-\epsilon/\tau]d\epsilon, \quad (89)$$

where the isothermal annealing has been conducted for a time t_1 at a temperature τ_1. When the isothermal annealing has been conducted for a long time, at the initial part of the tempering curve the condition $t_1\gg c\tau/(y+2)$ where $y=\epsilon/\tau$ maintains. Letting $\rho=\tau_1/\tau$, Eq. (89) becomes

$$-\frac{dP}{d\tau}\cong p_0\int_0^\infty Ac\tau\exp[-At_1e^{-y/\rho}-y]dy, \quad (90)$$

which is seen to be

$$-\frac{dP}{d\tau}\cong p_0\left(\frac{c\tau}{t_1}\right)^\rho(Ac\tau)^{1-\rho}\rho\Gamma(\rho). \quad (91)$$

Equation (91) is useful for values of Θ up to $\sim\frac{1}{2}$ in practice.

Similarly, when the order is not unity,

$$-\frac{dP}{d\tau}=p_0\int_0^\infty[1-(1-n)Bt_1e^{-y/\rho}]^{1/(1-n)} \times[1-(1-n)Bc\tau\mathbf{E}_2(y)]^{n/(1-n)}Bc\tau e^{-y}dy, \quad (92)$$

and when $t_1\gg c\tau/(y+2)$,

$$-\frac{dP}{d\tau}\cong p_0\int_0^\infty[1-(1-n)Bt_1e^{-y/\rho}]^{1/(1-n)}Bc\tau e^{-y}dy, \quad (93)$$

which, for the particular case of orders between 1 and 2, is

$$-\frac{dP}{d\tau}\cong p_0\left(\frac{c\tau}{t_1}\right)^\rho(Bc\tau)^{1-\rho}\rho\Gamma(\rho) \times\left[(n-1)^{-\rho}\Gamma\left(\frac{1}{n-1}-\rho\right)\Big/\Gamma\left(\frac{1}{n-1}\right)\right]. \quad (94)$$

The quantity in the brackets approaches unity when n approaches unity and increases when n increases over the range 1–2. Since the expression refers to the beginning of the rising portion of the tempering curve, that on the low-temperature side of the inflection point, it is in accord with the physical picture that the tempering curve is nearly proportional to the initial activation-energy spectrum, and that the slope of the rising portion of the isothermal annealing curve decreases with increasing order. Because the frequency factor affects the characteristic annealing function and the characteristic tempering function differently, it is necessary to choose a correct frequency factor (and indeed is a useful method of determining the frequency factor). If the frequency factor has been established, a comparison of the actual tempering curve with the results which are expected for first-order processes can be a method for investigating the actual order of the processes. The method is not necessarily confined to the initial portion of the tempering curve or to the simple experimental conditions chosen here if graphical integration is resorted to. It may then be possible to determine both frequency factor and order from the same experiment since they affect the functions differently.

3.2. *Experimental use of tempering rates.*—For significant kinetic studies, it is essential that the temperature of the sample be raised strictly in accordance with a known law. Since thermal changes whose temperature derivatives are of the order of magnitude of the heat capacity often accompany annealing, it may be insufficient to raise the ambient temperature according to the known law, the customary procedure. The effects of not raising the temperature of a sample according to a known law are qualitatively the same for the kinetic systems considered here; they are easily

demonstrated for processes obeying first-order kinetics and possessing a constant initial activation-energy spectrum. Then

$$-\frac{dP}{d\tau}=p_0 Ac\tau\int_0^\infty \exp[-y-Ac\tau E_2(y)]dy, \quad (95)$$

where $y=\epsilon/\tau$. From Eq. (24):

$$-\frac{dP}{d\tau}\cong p_0 Ac\tau\int_0^\infty \exp[-y-Ac\tau e^{-y}/(y+2)]dy. \quad (96)$$

Let $v=\exp[-Ac\tau e^{-y}/(y+2)]$; then, using the approximation Eq. (36),

$$y+\ln(y+2)=\ln(Ac\tau)-\ln_2(1/v)\cong a+by, \quad (97)$$

and hence

$$y=(1/b)[\ln(Ac\tau)-\ln_2(1/v)-a]. \quad (98)$$

Over the effective range of y, the variable v ranges from nearly zero to nearly one; hence

$$\begin{aligned}-\frac{dP}{d\tau}&\cong p_0 Ac\tau\int_0^1 e^{-y}dv/bv\ln(1/v)\\&=p_0 Ac\tau\int_0^1 \exp[-\ln(Ac\tau)+\ln_2(1/v)\\&\qquad+\ln(y+2)]dv/b\ln(1/v)\\&=(p_0/b)\int_0^1 (y+2)dv\\&=(p_0/b^2)\int_0^1[\ln(Ac\tau)-\ln_2(1/b)-a+2b]dv\\&=(p_0/b^2)[\ln(Ac\tau)+\gamma-a+2b], \quad (99)\end{aligned}$$

where $\gamma=0.577\cdots$.

The quantity $-dP/d\tau$, which will be called the annealing rate, is greater the lower the tempering rate, for c is the inverse tempering rate. This is to be expected, for the lower the tempering rate, the longer the sample remains at any temperature. If the tempering rate is not constant, but starts changing, an exaggerated effect is observed. The qualitative nature of the effect is easily shown for an increasing tempering rate such as that governed by the law of Eq. (40). The annealing rate corresponding to Eq. (99) is then

$$-(dP/d\tau)=(p_0/s^2)[\ln(Amc\tau^m)+\gamma-r+(m+1)s], \quad (100)$$

where $\ln(y+m+1)\cong r+sy$ [see Eq. (36)]. Since r and s have nearly the same values as a and b, the major effect is due to the power of the temperature appearing in the logarithm term. For a typical case at a temperature several hundred degrees centigrade, if the tempering rate were parabolic ($m=2$), the annealing rate would be about 10% less than if the tempering rate were constant. However, if the tempering rate were originally constant, and were to change to a parabolic one at some particular temperature, the decline in annealing rate would obviously be greater than the difference between the annealing rates for the two powers m because the activation-energy spectrum at the particular temperature for the constant tempering rate is smaller than for the parabolic one. Such an increase in tempering rate is common at the beginning of a tempering experiment, and since the tempering curve is usually interpreted as if the tempering rate were constant, it may be said that the initial portion of the tempering curve is depressed. As the constant tempering rate is approached, the tempering rate is declining, and here the tempering curve is elevated. The same effect frequently occurs at the end of the tempering range where a declining tempering rate is common. The result of these variations in tempering rate is the introduction of "false peaks" into the tempering curve. When thermal changes accompany annealing even more severe effects can occur.[14]

4. COMPLICATIONS

4.1. The treatment given here has considered the behavior of processes distributed in activation energy when the frequency factor and order are constant. The physical justification of this treatment is that the experimentally observed range of activation energies affects the gross kinetic behavior more severely than the range of expected orders and frequency factors. Despite the lack of any detailed kinetic investigations, it is worth noting some of the effects which may be treated as variations of order and frequency factor.

4.2. *Variations in order due to the property chosen for investigation.*—It was pointed out by Brown[5] that if a property is proportional to a power of the number of processes which can occur,

$$p=fq^n, \quad (102)$$

then the property will obey kinetics of order n/ν.

4.3. *Variations in frequency factor.*—The results which were derived here were based upon a slow variation of frequency factor with activation energy. This may seem a rather severe restriction, especially when the order is not unity and the frequency factor contains a concentration. However, this concentration is the original concentration, that given by the initial activation-energy spectrum. Since the annealing which is observed is due mainly to processes for which

$$[\tau\ln(B\tau)-\epsilon]\sim 0, \quad (103)$$

the variations in B needed to affect the results are variations orders of magnitude larger than the ranges of ϵ being considered. Such variations in concentration have already been excluded in many of the results given

[14] W. Primak (to be published).

here by the requirement that the initial activation-energy spectrum be broad compared to several times $n\tau$. However some physical circumstances might give rise to large variations in frequency factor and perhaps diffusion controlled processes might be so treated.

From Eq. (103) it is seen that if B changed greatly enough to affect $\ln B$ to an extent comparable to the ranges of ϵ under study, the processes with the changed B would be attributed to some other activation energy, despite the fact that they occur with the same activation energy. Then when an isothermal annealing is performed at another temperature, the processes would be attributed to still another activation energy. Thus when the frequency factor shows marked variations and it is assumed constant, the initial activation-energy spectrum seems to be different at different temperatures. The effect is easily seen by considering a case in which the activation energy is constant but there is a distribution of frequency factors and is illustrated here for processes obeying first-order kinetics.

In an isothermal annealing of processes of one activation energy distributed in frequency factor and obeying first-order kinetics, the annealing rate is

$$-\frac{dP}{dt}=\int_0^\infty p_0(A)\exp(-At\epsilon^{-\epsilon/\tau})dA, \qquad (104)$$

and taking as a specific example one in which the distribution $p_0(A)$ is a constant p_a over a range A_1 to A_2 and zero elsewhere,

$$-\frac{dP}{dt}=p_a\int_{A_1}^{A_2}\exp(-At\epsilon^{-\epsilon/\tau})dA, \qquad (105)$$

$$-\frac{dP}{dt}=\frac{p_a\tau}{t\epsilon^{-\epsilon/\tau}}[(1+A_1t\epsilon^{-\epsilon/\tau})\exp(-A_1t\epsilon^{-\epsilon/\tau}) - (1-A_2t\epsilon^{-\epsilon/\tau})\exp(-A_2t\epsilon^{-\epsilon/\tau})]. \qquad (106)$$

From Eq. (105), it is seen that at the instant the annealing starts, the rate is $p_a(A_2-A_1)$. However, after any appreciable time, since A_1 will be greater than A_2 by orders of magnitude, the annealing rate becomes

$$-\frac{dP}{dt}=\frac{p_a\tau}{t\epsilon^{-\epsilon/\tau}}(1+A_1t\epsilon^{-\epsilon/\tau})\exp(-A_1t\epsilon^{-\epsilon/\tau}). \qquad (107)$$

If it is erroneously assumed that the system consists of processes possessing a single frequency factor A_1, but distributed in activation energy, then $A_1t=\epsilon^{-\epsilon_0/\tau}$ and inserting Eq. (107) into Eq. (15a) there is obtained

$$p_0(\epsilon_0)=p_aA_1(1+\epsilon^{-(\epsilon-\epsilon_0)/\tau})\exp(-\epsilon^{-(\epsilon-\epsilon_0)/\tau}). \qquad (108)$$

In Eq. (108), ϵ is fixed and ϵ_0 is the variable. The fictitious activation-energy spectrum given by this equation resembles the form of a characteristic-annealing function because both are dominated by the negative exponential of a negative exponential. For the fictitious activation-energy spectrum: the point of inflection occurs at $\epsilon_0=\epsilon+\tau\ln 2$ where the slope is $p_0A_1 4\epsilon^{-2}/\tau$; most of the rise occurs over a small range of ϵ_0 several times τ; no change takes place in time since it is an initial spectrum; and the ordinate $2p_0A_1/e$ remains fixed at $\epsilon_0=\epsilon$ for all temperatures. Thus the segments of the fictitious activation-energy spectrum obtained by isothermal annealings at different temperatures do not join. For a series of segments obtained with successively higher temperatures, points obtained at higher temperatures will lie above points having the same value of ϵ_0 obtained at lower temperatures when $\epsilon_0<2p_0A_1/e$. When $\epsilon_0>2p_0A_1/e$, the higher temperature points will lie below the lower temperature points of the same ϵ_0. It should be noted that the lower values of the frequency factor dominate the kinetic behavior.

The effect of using a higher frequency factor in Eqs. (15) and (15a) is to displace the derived initial-activation-energy spectrum to higher energies, and in Eq. (39) to displace the spectrum, to reduce its height, and to spread it over a greater range of activation energies. A twofold distribution of processes in frequency factor and activation energy could be represented in Cartesian space, and its projection on a vertical plane parallel to the activation energy axis would be a band. If the experimental rates of isothermal annealing at various temperatures are inserted into Eqs. (15) and (15a), there results an effect similar to that obtained in considering a distribution in frequency factor alone: the segments of the fictitious initial activation-energy spectrum obtained at various temperatures do not form a continuous curve; and for an appropriate mean frequency factor fall within the band.

4.4. *Successive reactions.*[15]—Successive reactions are possible for the systems considered here. The effect is the occurrence of a process which involves a property change and which thereby generates another process which will occur at a higher activation energy. The appearance of such additional property change at activation energies close to those at which the original process occurred would steepen the activation-energy spectra in these regions; and if the data were analyzed by the methods given here, an apparent order lower than the actual order and/or a frequency factor higher than the actual frequency factor would be derived.

4.5. *Experimental elucidation of the kinetics.*—It is seen that once the kinetics of annealing is admitted to have complexities as great as a distribution of activation energies, other complexities of behavior can be excluded only by experimental evidence. It is necessary (1) to ascertain that the property measured is a suitable one, (2) to exclude or ascertain successive reactions, (3) to ascertain the frequency factor, and (4) to ascertain the

[15] This possibility was suggested by others in the course of radiation damage studies at the Metallurgical Laboratory and the Argonne National Laboratory, among whom are Simpson, Neubert, and Hennig.

order of reaction. Each of these requirements must be met by suitably planned sets of annealings or combinations of annealings over the whole of the temperature range to be investigated. The writer is not familiar with any investigation sufficiently detailed to meet these requirements. Since much of the complexity commonly results from the fact that the properties which are studied do not identify particular chemical species in particular environments (an analogy which could be taken in chemical kinetics would be the measurement of pressure in the pyrolysis of a gaseous mixture of organic compounds which was not simultaneously subjected to chemical analysis), it may be hoped that when suitable properties or combination of properties are studied much of the complexity of a particular system can be removed.

PHYSICAL REVIEW VOLUME 100, NUMBER 6 DECEMBER 15, 1955

Exciton Absorption in Cuprous Oxide

J. H. APPEL, *Department of Physics, University of California, Berkeley, California*

AND

L. N. HADLEY,* *Wilder Laboratory of Physics, Dartmouth College, Hanover, New Hampshire, and Department of Physics, University of California, Berkeley, California*

(Received August 24, 1955)

The exciton absorption spectrum of Cu_2O has been measured at low temperatures. As reported by Gross, the observed lines fit a hydrogen-like series formula. The wavelength shift of the position of the optical absorption band edge has also been measured as a function of temperature. The dependence is approximately quadratic.

INTRODUCTION

IN a series of papers, Gross and his collaborators[1] have reported on the exciton absorption in crystals of Cu_2O. This absorption appears as a series of lines near the main optical absorption edge which occurs in the red end of the visible region. The observation is made at low temperatures (77°K or lower) and with thin crystal slabs (of the order of 10 to 50 microns thickness). The observed lines may be empirically fitted to a hydrogen-like series formula with astonishing accuracy.

Wannier,[2] in 1937, postulated the existence of the corresponding energy levels, and proposed the following as a model. When an electron in an otherwise perfect dielectric crystal is raised to an excited state, it may be thought of as belonging to the crystal as a whole rather than to any particular atom. If its energy is insufficient to raise it to the conduction band, then it will remain within the Coulomb influence of the positive hole which it has left behind in the lattice. This electron-hole system may exist in stationary states, and will behave with respect to the remainder of the crystal as if embedded in a dielectric medium. The system is, however, free to migrate within the crystal.

The expected energy levels, measured from the ionization continuum (the conduction band), will be given by the Bohr expression:

$$W_k = -\mu e^4/4\pi\epsilon^2 k^2 c\hbar^3,$$

where $\mu = m_h^* m_e^*/(m_h^* + m_e^*)$, the reduced mass of the electron-hole system; ϵ is the dielectric constant of the dielectric material; k is the ordinal number of the level and takes on integral values. The other symbols have their usual meaning. The radii of the Bohr orbits will be given by

$$a = k^2\epsilon\hbar/\mu e^2.$$

These expressions for the energy and the radius differ from those obtained in the Bohr theory for atomic hydrogen only in that the value for the reduced mass is much different, and that a dielectric constant has been introduced into the force equation. It should be noted also that the "ground state" for this system is the recombined state in which the electron has collapsed into its hole. This occurs at an energy W_g (the width of the forbidden energy gap) below the conduction band. Consequently the series formula for the expected lines will be given by

$$\nu = W_g - W_k/k^2, \quad k = 1, 2, 3, \cdots.$$

EXPERIMENTAL

We have repeated the earlier measurements of Gross *et al.*, using the apparatus shown diagrammatically in Fig. 1. The spectrograph was a three-meter concave grating machine having a dispersion of roughly five angstroms per millimeter. The source was a tungsten filament. A water cell was placed between source and

* Now at Department of Physics, Colorado Agricultural and Mechanical College, Ft. Collins, Colorado.

[1] Ye. F. Gross and N. A. Karryev, Doklady Akad. Nauk S.S.S.R. **84**, 261 (1952); **84**, 471 (1952); Ye. F. Gross and B. P. Zakharchenya Doklady Akad. Nauk S.S.S.R. **90**, 745 (1953); Gross, Zakharchenya, and Reinov, Doklady Akad Nauk S.S.S.R. **92**, 265 (1953).

[2] G. Wannier, Phys. Rev. **52**, 191 (1937).

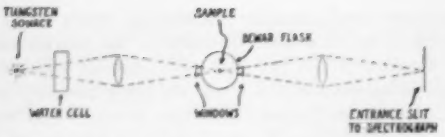

FIG. 1. Optical arrangement used to observe exciton absorption.

sample to remove extraneous heat radiation. The light passing through the sample was focused onto the slit of the spectrograph. The sample was placed within a metal Dewar flask with quartz windows. The cuprous oxide samples were prepared either by grinding or etching to a thickness of 10 to 50 microns from slabs which were originally approximately one millimeter thick.

Figure 2 shows a typical spectrum. The sample was etched in this case to a thickness of about 25 microns. The two mercury yellow lines ($\lambda=5769.60$ and $\lambda=5790.66$) are also shown for wavelength calibration and to give some notion of line widths of the exciton lines as compared to instrumental line widths. The lines of ordinal number $k=2$, 3, 4, and 5 are clearly shown above the background noise. For wavelength measurements in this particular case, the mercury source was turned off while sweeping through the line $k=2$, in order to avoid distortion of the line.

Several observations were made at temperatures of 4°K and 77°K. In addition, one run was made at a temperature of 2°K and one at 195°K. The position of the absorption edge at room temperature was observed in a small constant deviation spectroscope. For the 2°K run, both the positions and the line widths were not appreciably changed from their values at 4°K within the limit of our observations. At the temperature of 195°K, the only lines seen were those of ordinal number $k=2$ and $k=3$ which were barely distinguishable above noise. At room temperature, no structure which could be interpreted as line structure was observed.

Table I shows the results obtained at 77°K. Column (1) gives the ordinal number of the lines. Column (2) gives the average value of the measured wavelengths. Column (3) shows the corresponding wave numbers. Column (4) shows the wave numbers obtained from the formula

$$\nu=17460-843/k^2,$$

in which the two constants have been adjusted to give the best fit for the lines $k=3$, 4, and 5. The measured position of the line $k=2$ thus deviates by about three angstroms from its computed value. Column (5) shows the corresponding wavelengths measured by the Russian group. It will be noticed that at this temperature our values are somewhat higher than theirs, while at 4°K (see Table II) our values are lower than theirs.

Table II shows the corresponding values at liquid helium temperature. These are best expressed by the following formula:

$$\nu=17521-786/k^2.$$

TABLE I. $T=77$°K. Ordinal number, wavelength, and frequency of the exciton absorption lines in Cu_2O. The last column quotes values obtained by Gross.

k	λ_{exp}	ν_{exp}	ν_{theor}	$\lambda_{Russ.}$
2	5794.4	17258	17249	5792.7
3	5758.3	17366	17366	5756.6
4	5744.9	17407	17407	5743.8
5	5738.7	17426	17426	5738.1

TABLE II. $T=4$°K. Otherwise same as Table I.

k	λ_{exp}	ν_{exp}	ν_{theor}	$\lambda_{Russ.}$
2	5771.6	17326	17325	5775.8
3	5736.2	17433	17434	5740.3
4	5723.4	17472	17472	5727.4
5	5717.2	17491	17490	5721.7

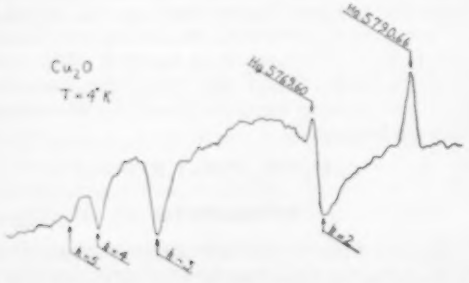

FIG. 2. Spectrometer record of exciton series in Cu_2O at a temperature of 4°K. The lines whose ordinal numbers are $k=2$, 3, 4, and 5 are shown. The two mercury yellow lines are shown in emission for the purposes of calibration and to indicate instrumental band width.

Table III shows a further series of values obtained from a ground crystal whose thickness was not determined but was probably close to 10 microns. The temperature was not accurately determined in this case but was intermediate between the temperatures of liquid helium and nitrogen. This series is shown only to indicate the greater number of lines observed in this case. These are fitted by the formula:

$$\nu=17508-800/k^2.$$

The position of the band edge (interpreted as the series limit of the above series) shifts approximately quadratically with absolute temperature as it does with germanium and silicon.[3] Figure 3 shows the experimental values obtained at the various temperatures. The solid curve is the empirical equation,

$$\lambda=0.00347^2+5707.4 \text{ (in angstrom units)}.$$

DISCUSSION

While the energy W_g is essentially a property of the crystal, the energy W_k may be thought of as a property

[3] G. G. Macfarlane and V. Roberts, Phys. Rev. 98, 1865 (1955).

of the exciton within the crystal environment. The actual values of the reduced mass and of the dielectric constant are not well known, but if reasonable values are taken for them, the constant W_k may be evaluated. Choosing the value for the reduced mass as half the free-electron mass, and taking the dielectric constant to be 10, the computed value of W_k is about 550 cm^{-1}. This is in fair agreement with the observed values at the various temperatures. The value is, of course, quite sensitive to the value of the index of refraction, and hence of dielectric constant, of the Cu_2O crystal.

The observed line widths do not seem to be particularly sensitive to temperature, at least in the range from 2°K to 77°K. The observed widths are of the order of a few angstroms, leading to lifetimes of the order of 10^{-12} second. An attempt was made to observe the lines in fluorescence emission at a temperature of 77°K with no success. Evidently other recombination processes compete too strongly to observe such radiation.

The line $k=1$ was not observed by us. Gross reports that it is somewhat weaker than the other lines, and that there is a considerably discrepancy between its observed position and that calculated from the series formula.

TABLE III. Same as Table I except that the temperature is intermediate between 4° and 77°K. (A different crystal sample was used than that of Tables I and II.)

k	λ_{exp}	ν_{exp}	ν_{theor}
2	5777.7	17308	17308
3	5741.2	17418	17419
4	5728.2	17457	17458
5	5722.1	17476	17476
6	5718.9	17486	17486
7	5716.5	17493	17492

It is of some interest to calculate the size of the Bohr orbits for the exciton. Using the values given above for the reduced mass and for the dielectric constant, the first orbit has a radius of 10 angstroms, while that associated with the line $k=7$ in Table III would have a radius of approximately 500 angstroms. Thus,

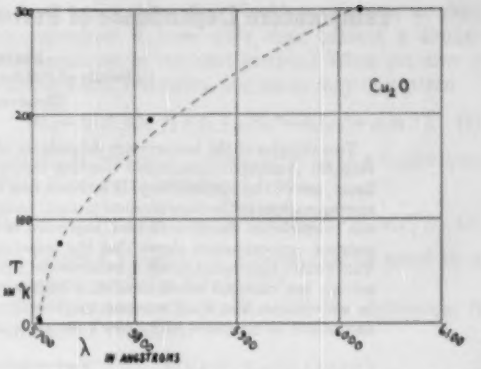

FIG. 3. Shift of the position of the absorption edge (series limit of the exciton series) as a function of absolute temperature.

from this picture, the electron is still able to feel the Coulomb influence of its hole at a distance of several hundred atomic spacings. It is conceivable that the reported misfit of the line $k=1$ by Gross, and our misfit for the line $k=2$ (Table I) may be due to the inability of the exciton to see the average value of the dielectric constant when so few atoms of the crystal lattice are contained within the orbit.

ACKNOWLEDGMENTS

We wish to express our thanks to Professor Charles Kittel for suggesting this problem, and to Professor Kittel, Professor A. F. Kip, and Mr. Gene Dresselhaus for many helpful and stimulating discussions. One of us (L. N. H.) is indebted to the Fund for the Advanced ment of Education for a Fellowship which made it possible to carry on this work.

The Cu_2O crystals were furnished us by Dr. Walter Brattain of the Bell Telephone Laboratory and have been described by him.[4] These crystals have a specific resistivity at room temperature of the order of 50 to 100 ohm-cm; they were prepared by the oxidation of high-purity copper.

[4] W. H. Brattain, Revs. Modern Phys. 23, 203 (1951).

Temperature Dependence of Ferromagnetic Anisotropy in Cubic Crystals*

FREDERIC KEFFER
University of Pittsburgh, Pittsburgh, Pennsylvania
(Received July 11, 1955)

Two theories of the temperature dependence of ferromagnetic anisotropy in cubic crystals, the nearest-neighbor quadrupole-quadrupole coupling theory of Van Vleck, and the more recent classical theory of Zener, seem to be contradictory. It is shown that these theories are, respectively, high- and low-temperature approximations to the same physical picture: namely, an anisotropy which decreases with rising temperature due to statistical fluctuations from alignment of anisotropically-coupled neighbor spins. Zener's low-temperature approximation shows that the anisotropy decreases as the tenth power of the magnetization, Van Vleck's high-temperature approximation yields a lower power law. It is argued that most of the anisotropy has vanished before sufficiently high temperatures are reached for Van Vleck's approximation to be appropriate. Van Vleck's nearest-neighbor dipole-dipole coupling theory, which has no classical analog and cannot be compared with Zener's theory, is discussed from a spin-wave picture.

I. INTRODUCTION

THE standard theoretical study of the temperature dependence of ferromagnetic anisotropy in cubic crystals has been given by Van Vleck.[1] Recently Zener[2] has proposed a very simple classical theory which, at first sight, seems to be at variance with Van Vleck, both as to method and as to results. It is the purpose of this paper to show that the methods of Van Vleck and of Zener are different limiting approximations of the same physical picture. We shall attempt to arrive at the true state of affairs by taking a judicious middle path between these two limiting approximations.

Van Vleck considers the anisotropy to originate from an indirect coupling between nearest-neighbor spins i and j produced by the series of interactions: spin i—orbit i—crystalline field—orbit j—spin j. The effective coupling energy is then expanded into a dipole-dipole term

$$\mathcal{H}_D=\sum_{(i,j)} C_{ij}[\mathbf{S}_i\cdot\mathbf{S}_j-3r_{ij}^{-2}(\mathbf{S}_i\cdot\mathbf{r}_{ij})(\mathbf{S}_j\cdot\mathbf{r}_{ij})], \quad (1)$$

plus a quadrupole-quadrupole term

$$\mathcal{H}_Q=\sum_{(i,j)} \gamma_{ij}r_{ij}^{-4}(\mathbf{S}_i\cdot\mathbf{r}_{ij})^2(\mathbf{S}_j\cdot\mathbf{r}_{ij})^2. \quad (2)$$

Here r_{ij} connects nearest neighbors, and C_{ij} and γ_{ij} are coupling constants, considered temperature-independent and acting only between nearest neighbors. The temperature dependence of the resultant anisotropy is caused by statistical deviations of $\mathbf{S}_i$ and $\mathbf{S}_j$ from maximum alignment.

In a cubic crystal whose bulk magnetization vector makes direction cosines α_1, α_2, α_3 with the three cubic axes, symmetry restrictions require the anisotropy to be an expression of the form

$$E_A=K_1(\alpha_1^2\alpha_2^2+\alpha_2^2\alpha_3^2+\alpha_3^2\alpha_1^2)+K_2\alpha_1^2\alpha_2^2\alpha_3^2+\cdots. \quad (3)$$

Van Vleck's calculations are numerical, and he gives his results in tabular form. For convenience we express the temperature dependence of the anisotropy as a power of the temperature dependence of the magnetization:

$$K_1(T)/K_1(0)=[M(T)/M(0)]^n. \quad (4)$$

In Fig. 1 we present Van Vleck's results in terms of the exponent n.

The anisotropy coming from $\mathcal{H}_Q$, as evaluated in the molecular-field approximation, behaves with an exponent n dropping slowly from 6 to 5 as the temperature decreases. Van Vleck also gives an improved calculation, in which part of the exchange energy is taken explicitly into account; in this calculation the exponent n drops from 10 to 5. For the anisotropy from $\mathcal{H}_D$ the exponent rises slowly from 2 to 4 as the temperature increases. In Fig. 1 the values of the magnetization are determined in the same theoretical approximation as are the values of K_1.

Van Vleck makes no attempt to evaluate the temperature dependence of K_2.

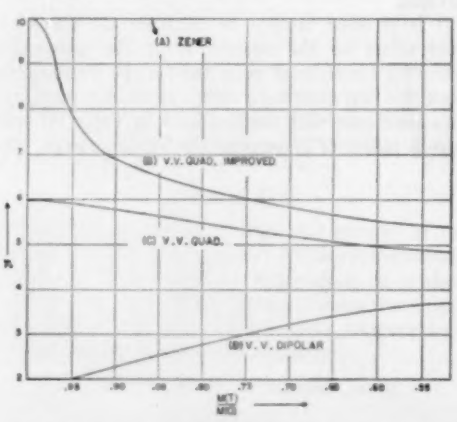

FIG. 1. The exponent n in Eq. (4) plotted against $M(T)/M(0)$. Curve (A), Zener's tenth-power law; curves (B) and (C), Van Vleck's quadrupolar results; and curve (D), Van Vleck's dipolar result. In all cases $M(T)/M(0)$ is evaluated in the same theory as is the anisotropy.

* Work was done in the Sarah Mellon Scaife Radiation Laboratory and research was supported by the United States Air Force, through the Office of Scientific Research of the Air Research and Development Command.

[1] J. H. Van Vleck, Phys. Rev. **52**, 1178 (1937).

[2] C. Zener, Phys. Rev. **96**, 1335 (1954).

Zener's method, on the other hand, is both classical and macroscopic. He considers the crystal to be composed of many small regions of unspecified dimensions, and in each region the magnetization vector is taken as constant in length but subject to random fluctuations in direction. The anisotropy energy of each region is a function of the direction of magnetization in that region, the functional form being taken as Eq. (3). Local fluctuations in the directions of magnetization then give rise to a temperature dependence of the total anisotropy energy of the crystal. Zener then evaluates the net effect of the fluctuations by a random-walk calculation. He finds the exponent in Eq. (4) to be 10 for K_1 and 21 for K_2, independent of temperature.

Both Van Vleck and Zener obtain their temperature effects from statistical deviations from maximum alignment. Van Vleck's calculation is somewhat cumbersome, but his interactions are quite explicit and his approach, except for the use of the molecular field, is quantum-mechanical. Zener's approach, although giving a classical fuzz to the nature of the interactions, is very direct and simple, and his mathematical methods are extremely powerful. For example, he is able to evaluate the temperature dependence of K_2 [and indeed of all the other constants in the expansion (3)] in a quite general manner.

As pointed out by Van Vleck, an interaction of the form $\mathcal{H}_D$ is incapable of yielding the anisotropy of Eq. (3) in a classical approximation. This is because in $\mathcal{H}_D$ the direction cosines of $\mathbf{r}_{ij}$ appear at most in the square, whereas Eq. (3) is at least quartic in the direction cosines of the resultant bulk magnetization. Quantum-mechanically, however, because of terms nondiagonal in $\sum_j S_i^x$, the dipole-dipole interaction in a cubic crystal does give rise to anisotropy. This anisotropy is calculated by Van Vleck by means of second-order perturbation theory, and the temperature dependence is evaluated in the molecular-field approximation. In Sec. VII of this paper we discuss this temperature dependence and conclude that Van Vleck's molecular-field method gives too high a value of the exponent in Eq. (4).

However, we are concerned here principally with the interaction $\mathcal{H}_Q$, which classically is capable of yielding an anisotropy of quartic form. Only for this interaction can the Van Vleck and Zener theories be compared, since only for this interaction do the two theories represent the same physical reality.

II. VAN VLECK'S APPROACH TO $\mathcal{H}_Q$

In the quadrupole-quadrupole Hamiltonian (2), the spins are quantized with respect to the axis of magnetization. To exhibit the anisotropy it is necessary to transform Eq. (2) into an expression involving α_{ij}, β_{ij}, γ_{ij} (the direction cosines of $\mathbf{r}_{ij}$ with respect to the crystal axes) times an expression involving α_1, α_2, α_3 (the direction cosines of the crystal axes with respect to the axis of magnetization). This transformation is given in detail in Sec. 11 of Van Vleck's paper,[1] and we shall not reproduce it here. (We shall present a similar transformation in the next section.) When account is taken of cubic symmetry, the result may be written

$$\mathcal{H}_Q = H_0 + \tfrac{1}{2}\Omega_5[f_1+f_2][\alpha_1^2\alpha_2^2+\alpha_2^2\alpha_3^2+\alpha_3^2\alpha_1^2]. \quad (5)$$

Here H_0 is isotropic. The quantity Ω_5 is a lattice sum which is temperature independent:

$$\Omega_5 = -N\textstyle\sum_j \gamma_{ij}[1-5(\alpha_{ij}^2\beta_{ij}^2+\beta_{ij}^2\gamma_{ij}^2+\gamma_{ij}^2\alpha_{ij}^2)]. \quad (6)$$

The factor $\frac{1}{2}$ before Ω_5 is a correction as noted in a subsequent paper by Van Vleck.[2]

The temperature dependence of the anisotropy is contained in the factor

$$[f_1+f_2] = \textstyle\sum_{i,\,x\neq y\neq z}\{(S_i^x)^2[(S_j^x)^2-\frac{1}{2}(S_j^y)^2] - \frac{1}{2}S_i^xS_i^y(S_j^xS_j^y+S_j^yS_j^x)\}. \quad (7)$$

Since $\mathcal{H}_Q$ is small compared to the exchange part of the ferromagnetic Hamiltonian, we may evaluate the anisotropy energy by taking the expectation value of (7) with respect to the exchange (first-order perturbation). To facilitate calculation we now introduce the operators $S^{\pm}=S^x\pm iS^y$. Dropping all terms in (7) nondiagonal in S^+S^-, we then obtain

$$\begin{aligned}\langle f_1+f_2\rangle = \langle &[\tfrac{3}{2}(S_i^z)^2-\tfrac{1}{2}S(S+1)][\tfrac{3}{2}(S_j^z)^2-\tfrac{1}{2}S(S+1)] \\ &+\tfrac{1}{16}[(S_i^+)^2(S_j^-)^2+(S_i^-)^2(S_j^+)^2] \\ &-\tfrac{1}{4}(2S_i^z-1)S_i^+S_j^-(2S_j^z-1) \\ &-\tfrac{1}{4}S_i^-(2S_i^z-1)(2S_j^z-1)S_j^+\rangle. \quad (8)\end{aligned}$$

The problem of the temperature dependence of the anisotropy constant K_1 is now reduced to the evaluation of (8). The rapidity with which (8) goes to zero as the temperature increases will depend upon the correlation assumed between the directions of neighbor spins, $\mathbf{S}_i$ and $\mathbf{S}_j$. Unfortunately, we have no exact way of taking into account this correlation. However, the several approximations considered below put well-defined limits on the temperature dependence.

III. LIMIT OF NO CORRELATION—THE SIXTH POWER LAW FOR $\mathcal{H}_Q$

The limit of no correlation between neighbor spins has been considered in detail by Van Vleck.[1] Each spin is independently quantized in a molecular field, and Eq. (8) reduces to

$$\langle f_1+f_2\rangle = [\tfrac{3}{2}\langle m^2\rangle-\tfrac{1}{2}S(S+1)]^2. \quad (9)$$

Here $\langle m^2\rangle$ is the expectation value of $(S_i^z)^2$ in the molecular field. Van Vleck evaluates (9) as a function of temperature for $S=1$. His numerical results indicate a temperature dependence going as $\langle m\rangle^6$ for $T/T_c \lesssim 0.5$ and dropping to approximately $\langle m\rangle^3$ at higher temperatures. Here $\langle m\rangle$ is the calculated Brillouin function for $S=1$, and not the experimental ratio $M(T)/M(0)$. We show Van Vleck's numerical results in Fig. 1.

[2] J. H. Van Vleck, Phys. Rev. 78, 266 (1950), footnote 13.

A simple physical picture of the effect of temperature on the anisotropy energy may be achieved as follows: We apply the molecular-field approximation directly to the Hamiltonian (2). Since $\mathbf{S}_i$ and $\mathbf{S}_j$ are independently quantized, we may expand $\langle r_{ij}^{-3}(\mathbf{S}_i\cdot\mathbf{r}_{ij})^2\rangle$ in a series of Legèndre polynomials $P_n(\Theta_{ij})$ where Θ_{ij} is the angle between $\mathbf{r}_{ij}$ and the axis of quantization. Reversing the direction of $\mathbf{r}_{ij}$ cannot change the sign of $(\mathbf{S}_i\cdot\mathbf{r}_{ij})^2$; hence the odd Legendre polynomials cannot appear in the expansion. Furthermore, since the direction cosine between $\mathbf{S}_i$ and $\mathbf{r}_{ij}$ is present only in the square, no polynomials beyond $P_2(\Theta_{ij})$ can appear. Thus

$$\langle r_{ij}^{-3}(\mathbf{S}_i\cdot\mathbf{r}_{ij})^2\rangle = aP_0(\Theta_{ij})+bP_2(\Theta_{ij}). \tag{10}$$

The coefficient a is determined by averaging over all directions Θ_{ij}. In this average $P_2(\Theta_{ij})\to 0$ and the left side of (10), regardless of the "direction" of S_i, goes to the unweighted average of all possible values of m^2. Hence

$$a=\frac{1}{2S+1}\sum_{m=-S}^{S} m^2=\tfrac{1}{3}S(S+1). \tag{11}$$

To determine the coefficient b we let $\Theta_{ij}=0$. Then (10) reduces to

$$\langle m^2\rangle = a+b. \tag{12}$$

When (11) and (12) are inserted into (10), we have

$$\langle r_{ij}^{-3}(\mathbf{S}_i\cdot\mathbf{r}_{ij})^2\rangle=\tfrac{1}{3}S(S+1)+[\langle m^2\rangle-\tfrac{1}{3}S(S+1)]P_2(\Theta_{ij}),$$

and hence,

$$\langle\mathcal{H}_Q\rangle = E_1+[\langle m^2\rangle-\tfrac{1}{3}S(S+1)]^2\textstyle\sum_{(i,j)}\gamma_{ij} \times[\frac{3}{2}\cos^2(\Theta_{ij})]^2. \tag{13}$$

In the above equation we have lumped some of the isotropic terms into E_1. As we have noted, the angles Θ_{ij} are defined with respect to the axis of quantization. We now let this axis make the direction cosines $\alpha_1, \alpha_2, \alpha_3$ with the crystal axes. On taking account of the cubic symmetry we find

$$\textstyle\sum_{(i,j)}\gamma_{ij}[\frac{3}{2}\cos^2(\Theta_{ij})]^2 = E_2+\frac{3}{4}\Omega_3(\alpha_1^2\alpha_2^2+\alpha_2^2\alpha_3^2+\alpha_3^2\alpha_1^2), \tag{14}$$

where E_2 is isotropic and Ω_3 is given by Eq. (6). We are thus led to Van Vleck's expression Eq. (5) above, with $\langle f_1+f_2\rangle$ as given by Eq. (9).

In the classical limit (large values of S), we note from Eq. (9):

$$\langle f_1+f_2\rangle=[P_2(\Theta)]^2, \tag{15}$$

where Θ is the angle between the direction of the classical spin and the axis of magnetization. We could have obtained this temperature dependence of the anisotropy of a classical spin directly from the Hamiltonian (2) on using the addition theorem for Legendre polynomials. Thus we see in a very direct way how the temperature effect arises from statistical fluctuations.

It is interesting to calculate the temperature dependence in the classical limit. We have

$$\langle P_n(x)\rangle=\int_{-1}^{1}P_n(x)e^{\epsilon x}dx\Big/\int_{-1}^{1}P_0(x)e^{\epsilon x}dx, \tag{16}$$

where

$$\epsilon=g\beta H/kT.$$

Here H is the molecular field. In terms of the Bessel functions of imaginary argument,[4]

$$\langle P_n(x)\rangle=I_{n+\frac{1}{2}}(\epsilon)/I_{\frac{1}{2}}(\epsilon). \tag{17}$$

For $n=1$, the right-hand side of (17) reduces to the familiar Langevin function.

In the limit of large ϵ (low T), Eq. (17) yields

$$\langle P_n(x)\rangle\sim\langle P_1(x)\rangle^{\frac{1}{2}n(n+1)}. \tag{18}$$

Thus the classical limit, as well as Van Vleck's case $S=1$, starts out with a sixth-power law. In fact, for the entire temperature range there seems to be no significant difference between the classical and quantum-mechanical averages when expressed as functions of $\langle m\rangle$.

IV. LIMIT OF COMPLETE CORRELATION—THE TENTH-POWER LAW FOR $\mathcal{H}_Q$

The limit of complete correlation has been considered by Zener.[3] In this limit a region of spins may be thought of as pointing in the same direction and moving together as a unit. Zener considers the total spin of this region to behave in a classical way. The anisotropy energy of the region depends on the direction cosines of the total spin in a manner described by Eq. (3). As the temperature rises the various correlated regions of spins will point in different directions, and the total anisotropy will be a statistical average of expressions of the form of Eq. (3).

We may derive Zener's result from Van Vleck's approach. We let the direction of S_i coincide with the direction of its neighbor S_j. From Eq. (8) we then obtain

$$\langle f_1+f_2\rangle=\tfrac{1}{8}\{35\langle m^4\rangle-5[6S(S+1)-5]\langle m^2\rangle +3S(S+1)[S(S+1)-2]\}, \tag{19}$$

where S is now the quantum number of the system of two spins. We note that (19) yields zero for any value of S less than 2. This is because we are considering spins $\mathbf{S}_i$ and $\mathbf{S}_j$ "locked" together as a unit, and in order for this unit to exhibit anisotropy in a cubic field it must behave as a 2^4 pole.

We have obtained (19) from Van Vleck's calculation, but it may also be obtained from the quantum-mechanical analog of Zener's method. As in the steps leading to Eq. (10), we now assume

$$\langle r_{ij}^{-4}(\mathbf{S}_i\cdot\mathbf{r}_{ij})^4\rangle=cP_0(\Theta_{ij})+dP_2(\Theta_{ij})+eP_4(\Theta_{ij}).$$

[4] Numerical values are given in C. W. Jones, *A Short Table for the Bessel Functions* $I_{n+\frac{1}{2}}(x)$, $(2/\pi)K_{n+\frac{1}{2}}(x)$ (Cambridge University Press, Cambridge, 1952).

The constant c is evaluated by averaging over all directions Θ_{ij}:

$$c=\frac{1}{2S+1}\sum_{m=-S}^{S} m^4=\frac{1}{15}S(S+1)(3S^2+3S-1).$$

We may determine d and e from the equations obtained when $\Theta_{ij}=0$:

$$\langle m^4\rangle=c+d+e,$$

and when $\Theta_{ij}=\pi/2$:

$$\langle(S_i^x)^4\rangle=c-\tfrac{1}{2}d+\tfrac{3}{8}e.$$

Equation (19) then follows when we invoke cubic symmetry, and when we use the general relation

$$\langle(S_i^x)^4\rangle=\tfrac{3}{8}\langle(S^2+S-m^2)\rangle+\tfrac{3}{8}\langle m^2\rangle-\tfrac{1}{4}(S^2+S).$$

We have derived (19) by this alternate method because it is now clear that if an entire region R of spins may be thought of as correlated, and not just the neighbors $\mathbf{S}_i$ and $\mathbf{S}_j$, we may expand

$$\langle\textstyle\sum_R r_{ij}^{-4}(\mathbf{S}_i\cdot\mathbf{r}_{ij})^2(\mathbf{S}_j\cdot\mathbf{r}_{ij})^2\rangle = cP_0(\Theta_{ij})+dP_2(\Theta_{ij})+eP_4(\Theta_{ij}).$$

Again we are led to Eq. (19), with S now the quantum number of the total spin of the region. If this spin is large enough we may make a classical approximation, and Eq. (19) becomes

$$\langle f_1+f_2\rangle=\langle P_4(\Theta)\rangle. \tag{20}$$

This is precisely Zener's result. We note that in the limit of complete correlation it makes no difference whether we use a Hamiltonian involving the interaction between neighbor spins, such as Eq. (2), or a Hamiltonian involving single spins in some sort of an anisotropic crystalline field. In either case the temperature dependence of K_1 will go as $\langle P_4(\Theta)\rangle$.

It now remains to evaluate $\langle P_4(\Theta)\rangle$ in terms of the magnetization. Zener does this by imagining the directions of magnetization of the various regions as points on the surface of a unit sphere. At 0°K all these points are at the pole of the sphere, and as the temperature is increased the points are to be envisioned as undergoing a random walk (diffusing) on the surface of the sphere. On solving the resultant diffusion equation, Zener finds

$$\langle P_n(\Theta)\rangle_{RW}=\langle P_1(\Theta)\rangle_{RW}^{\frac{1}{2}n(n+1)}. \tag{21}$$

This is the same as Eq. (18), except that it holds for all temperatures, and not just in the low-temperature limit. The reason for the high-temperature disagreement between (17) and (21) may be traced to the omission of any molecular field in Zener's random walk. That is, Zener assumes it just as probable that a point on the sphere of diffusion moves away from the pole as it is that the point moves towards the pole; on the other hand a Boltzmann average in a molecular field may be thought of as a random walk in which the probability of returning to the pole is greater (random walk in a field of force).

Now if nearest neighbors are to be thought of as correlated, the ordering effect generally thought to take place in ferromagnetism has been completely taken into account. Thus, in the limit of complete correlation, we believe Zener's method of averaging to be correct. It will break down at temperatures at which neighbor spins move appreciably out of alignment, that is, at the same temperatures at which the general method of this section also breaks down.

V. VAN VLECK'S APPROXIMATION OF PARTIAL CORRELATION IN $\mathfrak{IC}_Q$

The two approximations of complete correlation and of no correlation are extremes, representing respectively low- and high-temperature limits. We now examine a calculation also given by Van Vleck[1] in which the correlation is partially taken into account.

Van Vleck focuses attention on the spins $\mathbf{S}_i$ and $\mathbf{S}_j$ for which he is calculating the interaction energy of Eq. (2). He takes the exchange interaction between these two spins rigorously into account, representing only the interaction between these spins and the rest of the neighbors by the molecular field. The justification for this method is that the quadrupole-quadrupole interaction energy between two spins is most sensitive to the relative alignment of those two spins. However, since all neighbor spins are coupled together, the form of the total quadrupole-quadrupole energy will not be identical to the sum of Van Vleck's partially-correlated terms. Nevertheless, we should expect the results of this calculation to lie between those of Secs. III and IV, i.e., between the sixth- and tenth-power laws.

The results are given in Fig. 1 under the label "Van Vleck Improved." It can be shown that in the low-temperature limit the anisotropy goes as $\langle m\rangle^{10}$. It drops very quickly to approximately $\langle m\rangle^6$.

VI. THE SPIN-WAVE APPROXIMATION TO $\mathfrak{IC}_Q$

By means of the spin-wave approximation we gain some appreciation of the manner in which the limit of complete correlation fades into the limit of no correlation as the temperature rises.

Following Holstein and Primakoff[3] we define:

$$\begin{aligned} S_i^z&=S-n_i,\\ S_i^+&=(2S)^{\frac{1}{2}}f_i a_i,\\ S_i^-&=(2S)^{\frac{1}{2}}a_i^* f_i,\\ f_i^2&=1-(n_i/2S). \end{aligned} \tag{22}$$

Here n_i is the "spin-deviation" and equals $a_i^* a_i$ where a_i^* and a_i are creation and destruction operators. We insert the operators (22) into Eq. (8) and make the following low-temperature approximations:

[3] T. Holstein and H. Primakoff, Phys. Rev. 58, 1098 (1940).

(1) We drop all terms involving two creation or two destruction operators on the same spin;
(2) We assume n_i is 0 or 1. Thus we set $n_i^2=n_i$;
(3) We assume $f_i=1$.
The result is

$$\langle f_1+f_2\rangle=(S-\tfrac{1}{2})^2S[S-6\langle n_i\rangle-4\langle a_i^*a_j\rangle]. \quad (23)$$

Introducing spin-wave operators a_k^* and a_k:

$$\begin{aligned} a_i&=N^{-\frac{1}{2}}\textstyle\sum_k \exp(-i\mathbf{k}\cdot\mathbf{r}_i)a_k;\\ a_i^*&=N^{-\frac{1}{2}}\textstyle\sum_k \exp(i\mathbf{k}\cdot\mathbf{r}_i)a_k^*; \end{aligned} \quad (24)$$

we obtain:

$$\langle f_1+f_2\rangle=(S-\tfrac{1}{2})^2S[S-N^{-1}\textstyle\sum_k n_k(6+4\gamma_k)]. \quad (25)$$

Here

$$\gamma_k=z^{-1}\textstyle\sum_\delta \exp(i\mathbf{k}\cdot\mathbf{r}_\delta), \quad (26)$$

where $\mathbf{r}_\delta=\mathbf{r}_i-\mathbf{r}_j$, and the sum is over the z nearest neighbors j to any spin i.

We have obtained (25) with the aid of Van Vleck's transformation (Sec. II); the same result can be obtained, but with more trouble, directly from the Hamiltonian (2).

Equation (25) points out the correlation problem in a very illuminating way. If we assume the power law (4) and introduce

$$\begin{aligned} \Delta K_1&=K_1(0)-K_1(T),\\ \Delta M&=M(0)-M(T), \end{aligned}$$

then, at low temperatures,

$$1-\frac{\Delta K_1}{K_1(0)}\approx 1-n\frac{\Delta M}{M(0)},$$

or

$$\frac{\Delta K_1}{K_1(0)}\approx n\frac{\Delta M}{M(0)}. \quad (27)$$

Now according to the spin-wave picture,

$$\Delta M/M(0)=N^{-1}\textstyle\sum_k n_k. \quad (28)$$

Comparison of (25), (27), and (28) shows that:

(1) In the approximation of no correlation, since $\langle a_i^*a_j\rangle=0$, we have only the term in (25) with the multiplicative factor 6. Thus we get a sixth-power law in agreement with Sec. III.

(2) In the approximation of complete correlation, only spin waves of very long wavelength are excited. Thus, in effect, $\mathbf{k}=0$, and we have the tenth-power law of Sec. IV.

Now standard spin-wave theory[5] gives as the energy of a spin wave of wave number $\mathbf{k}$:

$$E_k=2SJz(1-\gamma_k),$$

where J is the exchange integral. Hence

$$\begin{aligned} \textstyle\sum_k n_k\gamma_k&=\textstyle\sum_k n_k[1-(E_k/2SJz)]\\ &=N\left(\frac{\Delta M}{M(0)}-\frac{E}{2SJz}\right), \end{aligned} \quad (29)$$

where E is the density of spin-wave energy. We may now write (25) in the form

$$\langle f_1+f_2\rangle=(S-\tfrac{1}{2})^2S\left\{S-\frac{10\Delta M}{M(0)}+\frac{2E}{SJz}\right\}. \quad (30)$$

To relate E to ΔM, we note that for spin waves of small k,

$$\begin{aligned} \frac{\Delta M}{M(0)}&\approx\text{const}\int_0^\infty\frac{E^{\frac{1}{2}}dE}{\exp(E/kT)-1};\\ E&\approx\text{const}\int_0^\infty\frac{E^{\frac{1}{2}}dE}{\exp(E/kT)-1}; \end{aligned}$$

where the constants are the same. Carrying out the integration, we have

$$E\approx\frac{\Delta M}{M(0)}\frac{1.782}{2.315}kT.$$

Thus,

$$\langle f_1+f_2\rangle\approx(S-\tfrac{1}{2})^2S\left\{S-\left(10-\frac{(S+1)T}{ST_c}\right)\frac{\Delta M}{M(0)}\right\}. \quad (31)$$

We have approximated $2Jz$ by $[3kT_c/(S^2+S)]$, where T_c is the Curie temperature.

From Eq. (31) we note that the "tenth-power" gradually drops with increasing temperature. Long before the drop is important, however, Eq. (27) has ceased to hold, and furthermore the spin-wave approximation itself has broken down.

Nevertheless, the general picture of the way the anisotropy energy behaves with temperature is now clear.

VII. SOME REMARKS ABOUT $\mathcal{H}_D$

As we have seen in Sec. I, since the anisotropy arising from $\mathcal{H}_D$, for cubic crystals, appears only in second-order perturbation theory, it has no classical analog and cannot be approximated by Zener's theory.

In addition to the second-order perturbation approach of Van Vleck, this anisotropy may be evaluated in the spin-wave approximation. Holstein and Primakoff[5] have indicated the general spin-wave method of handling dipole-dipole interactions. The resultant anisotropy at 0°K has been calculated (a) in the presence of a strong applied field (or in a molecular field)[6]; and (b) in the absence of exchange interaction (dipolar ferromagnetism).[7]

It is clear from the above-mentioned calculations that the anisotropy at 0°K arises from the zero-point spin-wave energy. Furthermore, it is clear that the overwhelming part of this anisotropy comes from short-wave (high-energy) spin waves. This is readily seen

[6] J. R. Tessman, Phys. Rev. 96, 1192 (1954).
[7] M. H. Cohen and F. Keffer, Phys. Rev. 99, 1135 (1955).

when one recalls that the long-wave spin waves merely cause changes in the direction of magnetization of large regions of spins; and the energy cannot be sensitive to these changes of direction, since there is no classical analog to dipolar anisotropy in cubic crystals. Anisotropy can only appear in a cubic array of dipoles when the dipoles near one another become significantly misaligned, and this misalignment can only be caused by short-wave spin waves.

Let us picture our cubic ferromagnetic crystal at 0°K with its zero-point anisotropy energy. As the temperature is raised, $\sum_{\mathbf{k}} n_{\mathbf{k}}$ spin waves will be excited, and their energy will add to the zero-point energy, so that

$$E=\sum_{\mathbf{k}} (n_{\mathbf{k}}+\tfrac{1}{2})E_{\mathbf{k}}. \tag{32}$$

To a first approximation, $E_{\mathbf{k}}$ will be given by the exchange energy alone, and will be proportional to k^2. Thus the majority of excited spin waves are of low $\mathbf{k}$ and, in accordance with our above remarks, add a negligible amount to the anisotropy. A detailed calculation of the temperature dependence of the anisotropy would present a formidable numerical task, but it is clear that this temperature dependence cannot be very strong—at least not until quite high temperatures are reached and the occupation number of high-energy spin waves is significant compared to $\frac{1}{2}$.

It is seen from Fig. 1 that Van Vleck's results show that the dipolar anisotropy disappears much more slowly than does the quadrupolar. Furthermore, the value of the exponent n for the dipolar case *increases* as $M(T)$ drops. This general trend bears out what we have said above about high-temperature effects. Nevertheless, we think that the difference between the dipolar and quadrupolar must be even more pronounced than obtained by Van Vleck. His molecular-field method allows too many neighbor spins to take angles with respect to each other at low temperatures. In all likelihood the dipolar anisotropy energy does not change very much at all up to a large fraction of T_c.

VIII. CONCLUSIONS

In attempting any comparison of theory and experiment we must first bear in mind the following two points which have been emphasized by Van Vleck:

(1) Depending upon the sign of the coupling constant γ_{ij}, the interaction $\mathcal{H}_Q$ can lead to a positive or negative sign of K_1. On the other hand, since the coupling constant C_{ij} is squared in the second-order calculation, the interaction $\mathcal{H}_D$ can lead only to a negative sign of K_1.

(2) Unless the spin quantum-number of the individual atom is larger than $\frac{1}{2}$, the interaction $\mathcal{H}_Q$ is zero.

Since the average nickel atom has a spin of even less than $\frac{1}{2}$, it is probable that the only interaction present in nickel is of the type $\mathcal{H}_D$. This leads to the correct (negative) sign of K_1, but the temperature dependence is completely off. The anisotropy in nickel disappears with temperature as something like the twentieth power of the magnetization. We can only conclude that this anisotropy is of an entirely different nature than dealt with here.

On the other hand, there are both theoretical[8] and experimental[9] indications that the spin quantum-number of an iron atom is very nearly 1. The positive sign of K_1 in iron indicates an interaction $\mathcal{H}_Q$. As Zener has pointed out, experimentally the constant K_1 falls with temperature as the tenth power of the magnetization *at all temperatures*.

We have shown that this tenth-power law is to be expected only if the spins of neighbor atoms are very highly correlated. Now, as the spin directions of neighbors begin to misalign, the tenth-power law will give way to a law of lower power, eventually to a sixth- or fifth-power law. However, we make the following point: if at the temperature where the misalignment has become appreciable, the anisotropy has essentially disappeared, or has become so small as to defy accurate measurement, it may well appear that the tenth-power law is holding, as Zener maintains, at all temperatures. We believe this is the situation in iron.

There are several experimental confirmations of strong correlation in iron:

(1) The magnetization curve falls well above the Brillouin curve for $S=1$ at high temperatures.

(2) Neutron diffraction experiments[10] indicate that small but coherent domains are present in iron even through the Curie point.

(3) A sizeable fraction of the area of the curve of the specific-heat anomaly is above the Curie point.

These facts indicate considerable correlation even at temperatures above the point of "zero" anisotropy, $\sim 0.8T_c$. Thus it is quite reasonable that at $0.8T_c$, at which temperature $M(T)/M(0)\approx 0.8$, the correlation is nearly complete, or at least sufficient to maintain the tenth-power law.

The same arguments should hold, but with even more force, for Zener's twenty-first power law for K_2.

In this entire discussion we have been using the atomic model of ferromagnetism. A band model has been used by Brooks,[11] and more recently by Fletcher,[12] to yield in a very rough way the anisotropy of nickel at 0°K. Neither author attempts to explain the temperature dependence. We are well aware of the limitations of our atomic model. Still, we believe there is

[8] P. Argyres and C. Kittel, Acta Metallurgica **1**, 241 (1953). These authors conclude from the value of the ferromagnetic resonance g-factor that, of the 2.2 Bohr magnetons per iron atom, approximately 0.2 magneton comes from orbital magnetization.

[9] S. B. Gunst and L. A. Page, Phys. Rev. **92**, 970 (1953). These authors, using 2.62-Mev gamma rays, measured directly the spin (as contrasted with orbit) magnetization of an iron atom.

[10] C. G. Shull and M. K. Wilkinson, Phys. Rev. **94**, 1439 (1954).

[11] H. Brooks, Phys. Rev. **58**, 909 (1940).

[12] G. C. Fletcher, Proc. Phys. Soc. (London) **A67**, 505 (1954).

much truth in the picture of a change in anisotropy with statistical fluctuations, and we feel that any further synthesis of the band and atomic methods must take this picture into account.

ACKNOWLEDGMENTS

I wish to thank Dr. C. Zener of Westinghouse Research Laboratories and my colleagues E. Gerjuoy and A. M. Portis for a number of stimulating discussions.

PHYSICAL REVIEW VOLUME 100, NUMBER 6 DECEMBER 15, 1955

Interaction of Impurities and Mobile Carriers in Semiconductors*

GUY W. LEHMAN† AND HUBERT M. JAMES
Purdue University, West Lafayette, Indiana

(Received July 29, 1955)

The interaction of mobile carriers in semiconductors with impurity atoms and ions tends to reduce the impurity activation energy. This effect is studied using the familiar model of the semiconductor as a uniform medium of dielectric constant K in which randomly distributed impurity ions appear as fixed unit charges and the mobile carriers as charges with opposite sign and effective mass m^*. The treatment is based on the solution of Hartree equations for nonlocalized orbitals ψ_i describing mobile carriers and localized orbitals φ_i describing electrons trapped in the neighborhood of impurity ions. Determination of the individual nonlocalized orbitals is made unnecessary by a method that expresses the fluctuation in mobile carrier density approximately as a linear functional of the fluctuations in electronic potential due to impurity atoms and ions. On use of this relation, Poisson's equation becomes a linear integro-differential equation for the electronic potential energy, which can be solved in terms of integrals involving the localized orbitals φ_i. All localized orbitals are taken to have the same form φ, satisfying an integro-differential equation obtained by averaging the potential energy for a trapped electron over all configurations of the other impurities; this is solved by a variational procedure. All orbitals in the theory depend on temperature T, the Fermi level ζ, and the impurity density N/V, since the distribution of qauntum numbers of the occupied orbitals depends on these quantities. The free energy F of the system, first expressed in terms of the orbitals, T, and ζ, is then reduced to a function of ζ, T, and N/V. For given T and N/V, the physically significant ζ is determined as that which minimizes F; the carrier density and the effective impurity activation energy are then computed as functions of T and N/V. The theory differs from all others in predicting a marked T-dependence of the activation energy, especially for high impurity concentrations. This appears because the polarizability of the mobile carrier distribution, which has an important effect on the interaction of impurities and mobile carriers, is temperature dependent in the present theory, and is completely ignored in earlier theories. For moderately high T the reduction in impurity activation energy predicted by the present theory is of the order of that predicted by Shifrin, and by Pearson and Bardeen; at low temperatures it is much less. Existing data on germanium and silicon suggest that the theory underestimates the reduction in activation energy at high impurity concentrations.

1. INTRODUCTION

THE first theoretical attempt to compute the ionization energy of impurity atoms in a semiconductor as a function of concentration was made by Shifrin.[1] Shifrin used the hydrogenic model of the impurities, which pictures the neutral atom as consisting of a single potential carrier (hole or electron) with appropriate effective mass m^*, moving about a fixed point charge (the atom core) in a medium of dielectric constant K. The ionization energy of an isolated impurity is then

$$E_0 = E_H m^*/mK^2, \tag{1.1}$$

where m is the true electronic mass and E_H the ionization energy of a hydrogen atom; the "radius" of the atom in the ground state is

$$a_0 = a_H K m/m^*, \tag{1.2}$$

where a_H is the Bohr radius. Shifrin assumes that in the impure semiconductor the impurity states with principal quantum number n merge with the continuum, and form its lower bound, when the "radius" n^2a_0 of the corresponding orbitals is the radius of a sphere of volume V/N, where N/V is the density of impurity atoms. He thus concludes that the activation energy of the impurity is given as a function of impurity density by

$$\Delta E_S = E_0\left[1-\left(\frac{4\pi}{3}a_0^3\right)^{\frac{1}{3}}\left(\frac{N}{V}\right)^{\frac{1}{3}}\right]. \tag{1.3}$$

A less schematic calculation has been made by Pearson and Bardeen[2] who note that the energy required to remove an electron from an impurity atom is reduced by the interaction of the resulting ion with the free carriers in the system. Treating the free carrier distribution as unaffected by the presence of the ions, and assuming that almost all impurities are ionized, they arrive at a formula resembling that of Shifrin:

$$\Delta E_{PB} = E_0\left[1-3.29\left(\frac{4\pi}{3}a_0^3\right)^{\frac{1}{3}}\left(\frac{N}{V}\right)^{\frac{1}{3}}\right]. \tag{1.4}$$

Like Shifrin, they thus conclude that the decrease in

* Based in part on a thesis presented by G. W. Lehman in partial fulfillment of the requirements for the degree of Doctor of Philosophy at Purdue University, January, 1954.
† Now at North American Aviation, Inc., Downey, California.
[1] K. S. Shifrin, J. Theoret. Phys. (U.S.S.R.) 14, 43 (1944).
[2] G. L. Pearson and J. Bardeen, Phys. Rev. 75, 865 (1949).

the activation energy is proportional to $(N/V)^{\frac{1}{3}}$. Castellan and Seitz[3] point out that it is usually not sufficiently accurate to equate the density of free carriers to the impurity density, and suggest other changes in the theory. They conclude, consequently, that the factors considered by Pearson and Bardeen will not reduce the activation energy simply proportionally to $(N/V)^{\frac{1}{3}}$, and cannot account for the experimental results of Pearson and Bardeen. They examine a number of other possible mechanisms, but do not succeed in fully explaining the observed effects.

The present theory again uses as the model of the semiconductor a uniform medium of dielectric constant K, in which randomly distributed impurity ions appear as fixed unit charges, and the mobile carriers as charges of opposite sign and effective mass m^*. (For simplicity in terminology, the carriers will henceforth be thought of as electrons, and the ions as positively charged donor ions.) It attempts to go beyond earlier theories in giving a more systematic and consistent treatment of what appears to be the dominant factor in reducing the activation energy: the interactions of impurity ions with trapped and with mobile carriers. This treatment is based on the determination of one-electron orbitals by solution of Hartree equations. It is unusual, however, in that the electronic orbitals depend on the temperature and carrier density as parameters. In treating conduction electrons as free, one describes a given state of electronic motion by the same orbital, regardless of what other orbitals are occupied. When the electrons are subject to external forces, such as interactions with ions or atoms, this is no longer a satisfactory approximation. One must expect solutions of the Fock or Hartree equations to yield orbitals depending on the quantum numbers of all orbitals involved in describing the system—as is the case, for example, in atomic and molecular problems. In the present problem a change in the quantum numbers of any single occupied orbital would have an insignificant effect on any single other orbital; all that matters in determining the form of an orbital is the distribution of the quantum numbers of the other occupied orbitals. This distribution is essentially the same for almost all ψ's that might describe the crystal at any given T, and is sufficiently defined when one gives the energy level distribution in the conduction band, the density n_e of free carriers, and the temperature. Thus the form of the orbitals comes to depend on the parameters n_e and T.[4]

Determination of this dependence adds another element of complexity to the problem. The determination of the quantum numbers to be used in solving the Hartree equations for the orbitals involves statistical considerations; these considerations, in turn, involve energies that have to be determined by solution of the Hartree equations. Thus the statistical and wave-mechanical aspects of the problem must be developed in a self-consistent way.

A characteristic feature of the present theory is the predicted temperature dependence of the impurity activation energy. The formal basis of this temperature dependence will be clear from the preceding paragraphs; the physical basis can be pictured as follows. The mobile carriers form a polarizable charge distribution, made nonuniform by its interaction with the impurity ions and atoms. The polarizability of this charge distribution depends on the distribution of electrons over the continuum states—on the electron density, and on the temperature as well. Around each positive ion is an induced average charge distribution of total amount $-e$, which tends to shield the positive ion. In the neighborhood of each neutral impurity atom there is also an induced average charge distribution of total amount zero, which modifies the effective potential acting on the trapped electron, and thus the activation energy, in a temperature dependent way. Further, each mobile carrier is regarded as moving in the field of the fixed charges plus the associated temperature-dependent induced electronic distributions. These interactions modify the energy levels in the conduction band, changing the position of the band edge and the distribution of the levels within the band in temperature-dependent ways. This again affects the activation energy, in a way that appears to be much more important than the change of energy of the trapping states. The two effects are not, however, treated separately in the theory, but appear as interdependent factors in a self-consistent formalism.

The complexity of the calculation makes it desirable to give a preliminary survey of the procedure used here. Solution of the Hartree equations is based on the assumption that the system can be properly described by use of two types of orbitals: orbitals ψ_i that extend throughout the very large volume of the crystal and describe conduction electrons, and $1s$ orbitals φ_j that describe electrons trapped in localized states about the impurity atoms (Sec. II). Each conduction electron moves in a potential field due to the trapped electrons, the impurity centers, and rest of the conduction electrons. For very large systems this differs negligibly from the potential energy $V_e(\mathbf{r})$ of an electron interacting with the total average charge distribution of the system; thus one can assume that all conduction orbitals obey the same Hartree equation with potential energy $V_e(\mathbf{r})$. On the other hand, it would involve a large error to proceed as if the electron in the localized orbital φ_j interacted with its own average charge distribution, as would be the case if the effective potential energy for this electron were taken to be V_e. Hence one must use a different effective potential energy for computing each trapped orbital,

[3] G. W. Castellan and F. Seitz, *Semiconducting Materials* (Butterworth Publications, London, 1950), p. 8.

[4] Formal treatments of such problems have been given by several authors; e.g., K. Husimi, Phys.-Math. Soc. Japan **22**, 264 (1940); W. M. MacDonald III and J. M. Richardson, Phys. Rev. **96**, 18 (1954).

that required for the calculation of φ_j being

$$V_{tj}(\mathbf{r})=V_c(\mathbf{r})-\frac{e^2}{K}\int d\mathbf{r}'\frac{|\varphi_j(\mathbf{r}')|^2}{|\mathbf{r}-\mathbf{r}'|}. \tag{1.5}$$

For any given form of $V_c(\mathbf{r})$, one could in principle compute the corresponding nonlocalized orbitals; given the distribution of electrons over these orbitals, one could then compute the total average density $n_e(\mathbf{r})$ of untrapped electrons in the system. In practice, such a procedure is out of the question. An approximation method, developed in Sec. III, gives $n_e(\mathbf{r})$ directly in terms of $V_c(\mathbf{r})$, the Fermi level ζ, and T, it being assumed that the distribution of electrons over the levels of the conduction band is of the Boltzmann form.

One could determine $V_c(\mathbf{r})$ by solving Poisson's equation, if one were given the positions of the impurity ions, the forms of the occupied localized orbitals φ_j, and the density $n_e(\mathbf{r})$ of the conduction electrons. Substitution of the form of $n_e(\mathbf{r})$ mentioned above converts Poisson's equation into an integro-differential equation for V_c, which also involves the position of the impurity ions and atoms, the orbitals φ_j, ζ, and T. Section IV shows how this determines $V_c(\mathbf{r})$ and $n_e(\mathbf{r})$ as a sum of contributions associated with the individual impurity atoms and ions, and expresses these contributions in terms of ζ, T, and the localized orbitals φ_j.

The form of the localized orbitals would, ideally, depend somewhat on the positions of nearby atoms and ions. To simplify the problem, the effective potential $V_{tj}(\mathbf{r})$ for the orbital φ_j is averaged over all configurations of the impurities (Sec. V). There results an integro-differential equation for φ_j, the same for all j, which is later (Sec. IX) solved approximately by a variational method. In Secs. VI and VII the total energy, free energy, and carrier density are expressed in terms of T, ζ, and the averaged form φ of the localized orbitals. Simplifying approximations, discussed in Secs. VIII and IX, then lead to complicated, but usable, expressions for the free energy F and for n_e in terms of T, ζ, and the impurity density (Sec. X). For given T and impurity density, the significant value of ζ is that which minimizes F; when this is known, the carrier density can be computed immediately.

2. FORMULATION OF THE HARTREE EQUATIONS

In formulating the wave mechanical treatment of our model, we start from the standard form of the Hartree equations for N carriers of charge $-e$, effective mass m^*, interacting with N fixed charges $+e$, in a medium of dielectric constant K:

$$\left\{-\frac{\hbar^2}{2m^*}\nabla^2-\frac{e^2}{K}\sum_{j=1}^{N}\frac{1}{|\mathbf{R}_j-\mathbf{r}|}+\frac{e^2}{K}\int\frac{d\mathbf{r}'}{|\mathbf{r}-\mathbf{r}'|}\sum_{i'\neq i}^{N}|\psi_{i'}(\mathbf{r}')|^2\right\}\psi_i(\mathbf{r})=E_i\psi_i(\mathbf{r}). \tag{2.1}$$

Here $\mathbf{R}_j$ and $\mathbf{r}$ are vectors giving the positions of positive and negative charges, respectively; ψ_i is the normalized orbital to which the ith electron is assigned, and E_i is the corresponding energy paramcter. The total energy of the system is, in the Hartree approximation,

$$E=\sum_{i=1}^{N}\int d\mathbf{r}\psi_i^*(\mathbf{r})\left[-\frac{\hbar^2}{2m^*}\nabla^2-\frac{e^2}{K}\sum_{j=1}^{N}\frac{1}{|\mathbf{R}_j-\mathbf{r}|}\right]\psi_i(\mathbf{r})+\sum_{i\neq i'}^{N}\sum^{N}\frac{e^2}{2K}\int\int\frac{d\mathbf{r}d\mathbf{r}'}{|\mathbf{r}-\mathbf{r}'|}|\psi_i(\mathbf{r})|^2|\psi_{i'}(\mathbf{r}')|^2+\sum_{j\neq j'}^{N}\sum^{N}\frac{e^2}{2K}\frac{1}{|\mathbf{R}_j-\mathbf{R}_{j'}|}, \tag{2.2}$$

or

$$E=\sum_{i}^{N}E_i-\sum_{i\neq i'}^{N}\sum^{N}\frac{e^2}{2K}\int\int\frac{d\mathbf{r}d\mathbf{r}'}{|\mathbf{r}-\mathbf{r}'|}|\psi_i(\mathbf{r})|^2|\psi_{i'}(\mathbf{r}')|^2+\sum_{j\neq j'}^{N}\sum^{N}\frac{e^2}{2K}\frac{1}{|\mathbf{R}_j-\mathbf{R}_{j'}|}. \tag{2.3}$$

The quantity on the right of Eq. (2.2) is stationary to variations of the ψ_i that maintain normalization.

It is well known that the Hartree equations may possess solutions that are without physical significance: for example, Pekar[5] has pointed this out in connection with the treatment of an assemblage of hydrogen atoms. We shall assume that in the system under consideration the physically significant solutions of the Hartree equation involve orbitals of two types:

(a) orbitals localized about individual impurity ions, representing electrons trapped by these ions. We shall denote a 1s-orbital localized about the jth impurity ion by $\varphi_j(\mathbf{r})$. We shall neglect the possibilities that electrons might be trapped in excited localized states of other types, or that two electrons might be trapped by a single impurity atom.

(b) orbitals extending through the whole system, representing mobile carriers in the conduction band. Henceforth the symbol $\psi_i(\mathbf{r})$ will be reserved for orbitals of this type.

We shall write the particle density due to trapped electrons as

$$n_t(\mathbf{r})=\sum_{j=1}^{N}a_j|\varphi_j(\mathbf{r})|^2, \tag{2.4}$$

where

$$a_j=\begin{cases}0 \text{ if orbital } \varphi_j \text{ is empty,}\\ 1 \text{ if orbital } \varphi_j \text{ is occupied.}\end{cases} \tag{2.5}$$

The particle density due to conduction electrons is, of course, $\sum|\psi_j(\mathbf{r})|^2$, where the sum is over all orbitals occupied by the conduction electrons. Because of the nonlocalized character of the ψ orbitals, no single term makes an appreciable contribution to this sum. We

[5] S. I. Pekar, *Abhandlungen aus der Sowjetischen Physik, Folge II* (Verlag Kultur, und Fortschritt, Berlin, 1951), pp. 61–72.

shall therefore take as the particle density due to conduction electrons

$$n_e(\mathbf{r})=\sum_i f(E_i)|\psi_i(\mathbf{r})|^2, \tag{2.6}$$

where $f(E_i)$ is the fraction of occupied orbitals ψ_i in a small energy range about E_i, and the sum is over all nonlocalized orbitals of both spins. The error involved in using Eq. (2.6), with $f(E_i)$ a smoothly varying function, will be negligible for all statistically important distributions of conduction electrons over the nonlocalized states. The average potential energy of interaction of an electron with the total electronic distribution and the fixed positive charges is then

$$V_e(\mathbf{r})=-\frac{e^2}{K}\sum_{j=1}^{N}\frac{1}{|\mathbf{R}_j-\mathbf{r}|}+\frac{e^2}{K}\int d\mathbf{r}'\frac{[n_i(\mathbf{r}')+n_e(\mathbf{r}')]}{|\mathbf{r}-\mathbf{r}'|}. \tag{2.7}$$

The potential energy term in Eq. (2.1) differs from this primarily in the restriction $i'\neq i$ in the sum over electronic states.

In using Eq. (2.1) to determine a conduction orbital ψ_i, one will make only an error of relative magnitude $1/N$ if one includes the term $i'=i$ in the electronic potential energy, thereby including a spurious interaction of the conduction electron with its own averaged charge density. To this approximation, all conduction orbitals satisfy the same wave equation, which we write as

$$\left[-\frac{\hbar^2}{2m^*}\nabla^2+v_e(\mathbf{r})\right]\psi_i(\mathbf{r})=\epsilon_i\psi_i(\mathbf{r}), \tag{2.8}$$

where

$$v_e(\mathbf{r})=V_e(\mathbf{r})-\langle V_e(\mathbf{r})\rangle, \tag{2.9}$$

$$\epsilon_i=E_i-\langle V_e(\mathbf{r})\rangle. \tag{2.10}$$

Thus $v_e(\mathbf{r})$ and E_i are the electronic potential energy and the energy parameter of the orbital, measured from $\langle V_e\rangle$, the average value of V_e in the crystal, which will henceforth be taken as the zero of energy. Important use will later be made of the obvious relation

$$\langle v_e(\mathbf{r})\rangle=0. \tag{2.11}$$

Since the potential due to an electron trapped by an ion is large just where the localized orbital is large, it would be a serious error to include in Eq. (2.1) the interaction of a trapped electron with itself. The effective potential energy for an electron in the localized orbital $\varphi_j(\mathbf{r})$ must therefore be obtained by subtracting from V_e the potential energy due to an electron in the orbital φ_j, to obtain $V_{1j}(\mathbf{r})$, as given in Eq. (1.5). We write the corresponding wave equation as

$$\left[-\frac{\hbar^2}{2m^*}\nabla^2+v_e(\mathbf{r})-\frac{e^2}{K}\int\frac{d\mathbf{r}'}{|\mathbf{r}-\mathbf{r}'|}|\varphi_j(\mathbf{r}')|^2\right]\varphi_j(\mathbf{r})=\mu_j\varphi_j(\mathbf{r}), \tag{2.12}$$

where μ_j denotes the energy parameter of the jth localized orbital, as distinguished from the energy parameters ϵ_i of the conduction orbitals.

Equation (2.12), taken for each impurity j with a trapped electron, and Eq. (2.8) for the conduction orbitals, constitute the Hartree equations used in this theory. Since $V_e(\mathbf{r})$ involves implicitly the parameters a_j and the function $f(\epsilon)$, as well as the orbitals themselves, the solution of this system of equations will depend on which ions are assumed to have trapped electrons, and on the energy distribution of the untrapped electrons.

In terms of the quantities thus far introduced, Eq. (2.3) for the total energy of the system can be written as

$$E=\sum_i f(\epsilon_i)\epsilon_i+\sum_{j=1}^{N}a_j\mu_j+N\langle V_e\rangle+\sum_{j\neq j'}^{N}\sum^{N}\frac{e^2}{2K}\frac{1}{|\mathbf{R}_j-\mathbf{R}_{j'}|}-\frac{e^2}{2K}\int\int\frac{d\mathbf{r}d\mathbf{r}'}{|\mathbf{r}-\mathbf{r}'|}\times[n_e(\mathbf{r})n_e(\mathbf{r}')+\sum_{j\neq j'}^{N}\sum^{N}a_ja_{j'}|\varphi_j(\mathbf{r})|^2|\varphi_{j'}(\mathbf{r}')|^2+2n_e(\mathbf{r})n_i(\mathbf{r}')]. \tag{2.13}$$

In the first term, the sum over occupied conduction orbitals has been replaced by a sum over all conduction orbitals, just as this was done in formulating Eq. (2.6). The first term in the double integral includes one half the interaction of every electron with its own average charge distribution. This corrects only in part for the inclusion of such self-interaction terms in Eq. (2.8), used in calculating the ϵ_i, but the fractional error is negligibly small in any case, being of the order of $1/N$.

In using the Hartree equations and the energy expression of Eq. (2.13), we shall be neglecting the exchange and correlation energies that play an important role in the theory of metals. The reasonableness of this, as concerns the exchange energy in nondegenerate semiconductors, is easily checked. Wigner and Seitz[6] have shown that in the case of a completely degenerate free-electron gas the exchange energy per electron is

$$E_{ex}=-0.458e^2/r_s, \tag{2.14}$$

where r_s is defined in terms of the electron density N/V by

$$(4\pi/3)r_s^3=V/N. \tag{2.15}$$

If one regards the electrons as moving in a medium of dielectric constant K, as in the present model, an extra factor of $1/K$ will appear on the right in Eq. (2.14). By similar methods it can be shown that for a nondegenerate gas of electrons with effective mass m^*, in a medium with dielectric constant K, having a Boltzmann distribution of energies corresponding to tempera-

[6] E. Wigner and F. Seitz, Phys. Rev. 46, 509 (1934).

ture T, the exchange energy per electron is

$$E_{ex}=-\frac{3}{4}\frac{e^2}{r_s}\frac{1}{K}\frac{m}{m^*}\frac{E_H}{kT}\left(\frac{a_H}{r_s}\right)^2, \tag{2.16}$$

where a_H is the Bohr radius. $E_H=e^2/2a_H$ is the ionization energy of the hydrogen atom, and m is the true electronic mass. As an example we take $N/V=10^{18}/\text{cm}^3$, $K=13$, $T=187°\text{K}$, $m^*=0.45m$. Then Eq. (2.16) yields $E_{ex}=-0.0018$ ev, compared with the impurity activation energy -0.036 ev found by use of the hydrogenic model.

3. CALCULATION OF SUMS OVER STATES

In solving our problem, it will be necessary to evaluate certain sums over the conduction orbitals, such as $n_e(\mathbf{r})$ [Eq. (2.6)]. Even if $v_c(\mathbf{r})$ were known to begin with, it would obviously be impracticable to do this by solving Eq. (2.8) explicitly for the individual ψ_i and ϵ_i, and then summing. Fortunately, when the distribution of electrons in the conduction band is of the Boltzmann form,

$$f(\epsilon_i)=\exp[-(\epsilon_i-\zeta)/kT], \tag{3.1}$$

such sums are easily expressed directly in terms of integrals involving the electronic potential energy $v_e(\mathbf{r})$.

We shall assume that Eq. (2.8) is to be solved within the very large volume V of the crystal, surrounded by an infinite potential barrier. (Our theory will, however, neglect surface effects due to the bounding barrier.) Let

$$Z(\mathbf{r}',\mathbf{r};t)=\sum_i\psi_i^*(\mathbf{r}')\psi_i(\mathbf{r})\exp(-\epsilon_i t), \tag{3.2}$$

where the sum is over all *spin-free* solutions of Eq. (2.8) normalized to 1 in the volume V. We shall assume that Eq. (2.8) has only nonlocalized solutions,[7] and can then write

$$n_e(\mathbf{r})=2e^{\zeta/kT}Z(\mathbf{r},\mathbf{r};1/kT). \tag{3.3}$$

The factor 2 enters because Eq. (2.6) involves a sums over spins, whereas Eq. (3.2) does not

In principle, $Z(\mathbf{r}',\mathbf{r};t)$ can be determined by solving a diffusion problem. It follows from Eqs. (2.8) and (3.2) that, for $t>0$,

$$-D\nabla_r^2Z(\mathbf{r}',\mathbf{r};t)+v_e(\mathbf{r})Z(\mathbf{r}',\mathbf{r};t)=-\partial Z/\partial t, \tag{3.4}$$

where

$$D=\hbar^2/2m^*. \tag{3.5}$$

From the closure property[8] of the ψ's, it follows that

$$Z(\mathbf{r}',\mathbf{r};0)=\delta(\mathbf{r}'-\mathbf{r}), \tag{3.6}$$

where δ is the Dirac delta function. The presence of the infinite potential barrier at the surface S of the crystal requires $\psi_i(\mathbf{r})=0$ and

$$Z(\mathbf{r}',\mathbf{r};t)=0, \text{ for } \mathbf{r} \text{ on } S. \tag{3.7}$$

For each $\mathbf{r}'$, $Z(\mathbf{r}',\mathbf{r};t)$ could be obtained by solving Eq. (3.4), subject to the initial condition of Eq. (3.6) and the boundary condition of Eq. (3.7). If the parameter t is interpreted as time, $Z(\mathbf{r}',\mathbf{r};t)$ can be interpreted as the density of a system of diffusing particles at point $\mathbf{r}$, at time t, per particle released at point $\mathbf{r}'$ at time $t=0$, when the following conditions are satisfied: (a) the diffusion constant is D; (b) a particle at point $\mathbf{r}''$ may disappear with probability $v_e(\mathbf{r}')$ per unit time if $v_e(\mathbf{r}'')>0$, or give rise to another particle with probability $-v_e(\mathbf{r}'')$ per unit time if $v_e(\mathbf{r}'')<0$; (c) any particle reaching the surface S is withdrawn from the system.

An alternative interpretation of these equations makes it easy to write down an equivalent integral formulation of the problem. One can regard $Z(\mathbf{r}',\mathbf{r};t)$ as the average density of particles at point $\mathbf{r}$ at time t, due to release of one particle at point $\mathbf{r}'$ at time $t=0$, plus the release of $-v_e(\mathbf{r}'')Z(\mathbf{r}',\mathbf{r}'';t')$ particles per unit volume and per unit time, for all $\mathbf{r}''$ in V and all $t'>0$; as before, any particle reaching the surface S is withdrawn from the system. Let $Z_0(\mathbf{r}',\mathbf{r};\Delta t)$ denote the average density at $\mathbf{r}$ at time t per particle released at $\mathbf{r}'$ at time $t-\Delta t$. Then the total particle density due to the system of sources described above is obviously

$$Z(\mathbf{r}',\mathbf{r};t)=Z_0(\mathbf{r}',\mathbf{r};t)-\int_0^t dt'\int_V d\mathbf{r}''v_e(\mathbf{r}'')\times Z(\mathbf{r}',\mathbf{r}'';t')Z_0(\mathbf{r}'',\mathbf{r};t-t'). \tag{3.8}$$

From the character of the diffusion problem, it is evident that for $|\mathbf{r}-\mathbf{r}'|$ small compared to the distance of $\mathbf{r}$ and $\mathbf{r}'$ from the surface S of the crystal, and for not too large t, the nature of the solution will be negligibly changed by ignoring the boundary condition on S, Eq. (3.7). Then $Z_0(\mathbf{r}',\mathbf{r};t)$ can be taken as the solution of Eq. (3.4), with $v_e(\mathbf{r})\equiv 0$, subject to the initial condition of Eq. (3.6): that is, it can be replaced by the familiar diffusion function

$$Z_0(|\mathbf{r}-\mathbf{r}'|;t)=[4\pi Dt]^{-\frac{1}{2}}\exp[-|\mathbf{r}-\mathbf{r}'|^2/4Dt]. \tag{3.9}$$

Making this approximation, we write

$$Z(\mathbf{r}',\mathbf{r};t)=Z_0(|\mathbf{r}-\mathbf{r}'|;t)-\int_0^t dt'\int_\infty d\mathbf{r}''v_e(\mathbf{r}'')\times Z(\mathbf{r}',\mathbf{r}'';t')Z_0(\mathbf{r}-\mathbf{r}'';t-t'). \tag{3.10}$$

This equation can be solved by a familiar iterative method. Writing

$$Z(\mathbf{r}',\mathbf{r};t)=\sum_\tau Z_\tau(\mathbf{r}',\mathbf{r};t), \tag{3.11}$$

[7] In principle, Eq. (2.8) might possess localized solutions, which would be without physical significance [since any localized orbital should satisfy an equation of the type of Eq. (2.12)] and should therefore be excluded from the sum over conduction orbitals. In the practical cases under consideration here K is large and the binding energy of localized solutions of Eq. (2.12) is small. Localized solutions of Eq. (2.8) will have even smaller binding energy, and their contribution to the sums seems safely negligible compared to that of the numerous nonlocalized solutions.

[8] D. Bohm, *Quantum Theory* (Prentice-Hall, Inc., New York, 1951), p. 221.

where Z_τ is of the τth order in $v_e(\mathbf{r})$, substituting this into Eq. (3.10), and equating terms on the two sides that are of the same order in v_e, one finds

$$Z_{\tau+1}(\mathbf{r}',\mathbf{r};t)=-\int_0^t dt'\int_\infty d\mathbf{r}''v_e(\mathbf{r}'')\times Z_\tau(\mathbf{r}',\mathbf{r}'';t')Z_0(\mathbf{r}-\mathbf{r}'';t-t'). \quad (3.12)$$

The successive integrations over t' can be carried out without difficulty. One finds

$$Z_1(\mathbf{r}',\mathbf{r};t)=-\frac{1}{4\pi D}\int d\mathbf{r}_1 v_e(\mathbf{r}_1)\left[\frac{|\mathbf{r}-\mathbf{r}_1|+|\mathbf{r}_1-\mathbf{r}'|}{|\mathbf{r}-\mathbf{r}_1|\,|\mathbf{r}_1-\mathbf{r}'|}\right]\times Z_0(|\mathbf{r}-\mathbf{r}_1|+|\mathbf{r}_1-\mathbf{r}'|;t), \quad (3.13)$$

$$Z_2(\mathbf{r}',\mathbf{r};t)=\frac{1}{(4\pi D)^2}\int d\mathbf{r}_1\int d\mathbf{r}_2 v_e(\mathbf{r}_1)\times v_e(\mathbf{r}_2)\left[\frac{|\mathbf{r}-\mathbf{r}_1|+|\mathbf{r}_1-\mathbf{r}_2|+|\mathbf{r}_2-\mathbf{r}'|}{|\mathbf{r}-\mathbf{r}_1|\,|\mathbf{r}_1-\mathbf{r}_2|\,|\mathbf{r}_2-\mathbf{r}'|}\right]\times Z_0(|\mathbf{r}-\mathbf{r}_1|+|\mathbf{r}_1-\mathbf{r}_2|+|\mathbf{r}_2-\mathbf{r}'|;t); \quad (3.14)$$

the generalization is obvious.

If $v_e\equiv 0$, one has $Z_\tau=0$, for $\tau>0$. If $v_e(\mathbf{r})$ is constant, it follows easily from the definition in Eq. (3.2), together with the fact that introduction of a constant potential v_e changes every ϵ_i by this same amount, that

$$Z(\mathbf{r}',\mathbf{r};t)=Z_0(|\mathbf{r}-\mathbf{r}'|;t)\exp[-v_e t]. \quad (3.15)$$

On the other hand, Eqs. (3.11) to (3.14) yield

$$Z(\mathbf{r}',\mathbf{r};t)=Z_0(|\mathbf{r}-\mathbf{r}'|;t)[1-v_e t+\tfrac{1}{2}(v_e t)^2-\cdots]. \quad (3.16)$$

Roughly speaking, then, Eq. (3.11) gives an expansion of Z in terms of increasing order in $v_e(\mathbf{r})t$. It is easily shown that, for bounded $v_e(\mathbf{r})$ and for $t>\epsilon>0$, the series in Eq. (3.11) is uniformly convergent in t; it will not, however, be rapidly convergent if $v_e(\mathbf{r})t$ is large at many points. As applied in the present work, Eq. (3.11) will yield expansions in powers of $v_e(\mathbf{r})/kT$; the practical necessity for dealing with only the first few terms of the expansions will then limit the accuracy of the results more severely the lower the value of T.

It follows from these results, together with Eq. (3.3), that

$$n_e(\mathbf{r})=2e^{\xi/kT}\left\{\left(\frac{2\pi m^* kT}{h^2}\right)^{\frac{1}{2}}-\frac{4\pi m^*}{h^2}\int d\mathbf{r}_1\frac{v_e(\mathbf{r}_1)}{|\mathbf{r}-\mathbf{r}_1|}\times Z_0(2|\mathbf{r}-\mathbf{r}_1|;1/kT)+\left(\frac{2\pi m^*}{h^2}\right)^2\int d\mathbf{r}_1\int d\mathbf{r}_2\times\frac{v_e(\mathbf{r}_1)v_e(\mathbf{r}_2)}{|\mathbf{r}-\mathbf{r}_1|\,|\mathbf{r}_1-\mathbf{r}_2|\,|\mathbf{r}_2-\mathbf{r}|}RZ_0(R;1/kT)-\cdots\right\}, \quad (3.17)$$

where

$$R=|\mathbf{r}-\mathbf{r}_1|+|\mathbf{r}_1-\mathbf{r}_2|+|\mathbf{r}_2-\mathbf{r}|. \quad (3.18)$$

In the present theory it is impractical to use terms beyond those explicitly written out in Eq. (3.17). In fact, this expression will be further simplified by replacing the last term by its average over $\mathbf{r}$, thus retaining only the first-order fluctuations in $n_e(\mathbf{r})$, given by the first integral on the right. Since the average value of $v_e(\mathbf{r})$ is zero by definition [Eq. (2.9)], the average value of the first integral in Eq. (3.17) is zero. The average value of the second integral is easily obtained by integrating in elliptic coordinates with $\mathbf{r}_1$ and $\mathbf{r}_2$ as foci. One finds, to our approximation,

$$\langle n_e\rangle=2e^{\xi/kT}\left\{\left(\frac{2\pi m^* kT}{h^2}\right)^{\frac{1}{2}}+\frac{2\pi m^*}{h^2 kT}\frac{1}{V}\int_V d\mathbf{r}_1\int_\infty d\mathbf{r}_2\times\frac{v_e(\mathbf{r}_1)v_e(\mathbf{r}_2)}{|\mathbf{r}_1-\mathbf{r}_2|}Z_0(2|\mathbf{r}_1-\mathbf{r}_2|;1/kT)\right\}, \quad (3.19)$$

$$n_e(\mathbf{r})-\langle n_e\rangle=-\frac{8\pi m^*}{h^2}e^{\xi/kT}\int d\mathbf{r}_1\frac{v_e(\mathbf{r}_1)}{|\mathbf{r}-\mathbf{r}_1|}\times Z_0(2|\mathbf{r}-\mathbf{r}_1|;1/kT). \quad (3.20)$$

Important simplifications and some characteristic features of the present theory arise from the linearized relation of $n_e(\mathbf{r})$ to $v_e(\mathbf{r})$, as given in Eq. (3.20).

4. CALCULATION OF THE ELECTRONIC POTENTIAL ENERGY

The potential energy $v_e(\mathbf{r})$ of an electron in the crystal is related to the total charge density by Poisson's equation, which can here be written as

$$\nabla^2 v_e(\mathbf{r})=\frac{4\pi e^2}{K}[\sum_i\delta(\mathbf{r}-\mathbf{R}_i)-n_e(\mathbf{r})-n_i(\mathbf{r})]. \quad (4.1)$$

Using Eqs. (2.4) and (3.20), one can reduce this to the form

$$\nabla^2 v_e(\mathbf{r})-\kappa e^{\xi/kT}\int_\infty d\mathbf{r}_1\frac{v_e(\mathbf{r}_1)}{|\mathbf{r}-\mathbf{r}_1|}Z_0(2|\mathbf{r}-\mathbf{r}_1|;1/kT)=\frac{4\pi e^2}{K}\{-\langle n_e\rangle+\sum_i(1-a_j)\delta(\mathbf{r}-\mathbf{R}_j)+\sum_i a_j[\delta(\mathbf{r}-\mathbf{R}_j)-|\varphi_j(\mathbf{r}-\mathbf{R}_j)|^2]\}, \quad (4.2)$$

where

$$\kappa=32\pi^3 m^{*3}e^3/Kh^3. \quad (4.3)$$

This constitutes a linear integro-differential equation for $v_e(\mathbf{r})$, which is to be solved subject to the condition that $\langle v_e(\mathbf{r})\rangle=0$.

The bracket on the right of Eq. (4.2) describes what may be regarded, at this stage of the problem, as the fixed charges in the crystal: the average electronic charge density, the charges of impurity ions without trapped electrons, and the charge distributions of the

impurity "atoms"—ions plus trapped electrons. The total fixed charge is zero.

Because of the linear character of Eq. (4.2), its solution is easily expressed in terms of the solution of a similar equation with a single fixed point charge. We write

$$\nabla^2 V_i(\mathbf{r}) - \kappa e^{\zeta/kT} \int_\infty d\mathbf{r}_1 \frac{V_i(\mathbf{r}_1)}{|\mathbf{r}-\mathbf{r}_1|} Z_0(2|\mathbf{r}-\mathbf{r}_1|\,; 1/kT) = \frac{4\pi e^2}{K}\delta(\mathbf{r}), \quad (4.4)$$

to be solved for V_i subject to the boundary condition that $V_i(\mathbf{r}) \to 0$ as $r \to \infty$. $V_i(\mathbf{r})$ can be regarded as the electronic potential energy that would be produced in the crystal by a single impurity ion placed at the origin; it is the potential energy of interaction of an electron with the ion itself, plus its energy of interaction with the distribution of mobile electrons, of density $P_i(\mathbf{r})$, induced by presence of the ion. V_i and P_i must obviously satisfy the relations

$$\nabla^2 V_i(\mathbf{r}) = \frac{4\pi e^2}{K}\{\delta(\mathbf{r}) - P_i(\mathbf{r})\}, \quad (4.5)$$

$$V_i(\mathbf{r}) = \frac{e^2}{K}\left[-\frac{1}{r} + \int d\mathbf{r}_1 \frac{P_i(\mathbf{r}_1)}{|\mathbf{r}-\mathbf{r}_1|}\right]. \quad (4.6)$$

Comparison of Eqs. (4.4) and (4.5), with use of Eqs. (4.3) and (3.5), shows also that

$$P_i(\mathbf{r}) = -\frac{1}{\pi D} e^{\zeta/kT} \int d\mathbf{r}_1 \frac{V_i(\mathbf{r}_1)}{|\mathbf{r}-\mathbf{r}_1|} \times Z_0(2|\mathbf{r}-\mathbf{r}_1|\,; 1/kT). \quad (4.7)$$

From Eq. (4.5), and the boundary condition on $V_i(\mathbf{r})$, it follows that

$$\int d\mathbf{r} P_i(\mathbf{r}) = 1; \quad (4.8)$$

the total charge of the ion and the induced electronic distribution that surrounds it is zero.

Equation (4.4) is easily solved by Fourier transform methods. One finds

$$V_i(\mathbf{r}) = -\frac{e^2}{2\pi^2 K}\int_\infty d\mathbf{p} \frac{e^{i(\mathbf{p}\cdot\mathbf{r})}}{p^2 + H(\mathbf{p})}, \quad (4.9)$$

where

$$H(\mathbf{p}) = \kappa e^{\zeta/kT} \int_\infty d\mathbf{r}_1 \frac{e^{-i(\mathbf{p}\cdot\mathbf{r}_1)}}{r_1} Z_0(2r_1; 1/kT). \quad (4.10)$$

On substituting Eq. (4.9) into Eq. (4.7), one finds

$$P_i(\mathbf{r}) = \frac{1}{(2\pi)^3}\int_\infty d\mathbf{p} e^{i(\mathbf{p}\cdot\mathbf{r})} \frac{H(\mathbf{p})}{p^2 + H(\mathbf{p})}. \quad (4.11)$$

Calculation of V_i and P_i for given ζ and T is thus reduced to a matter of quadratures. These functions will be discussed in Sec. VIII.

It will also be convenient to define the electronic potential energy $V_a(\mathbf{r})$ produced in the crystal by an atom—ion plus trapped electron—at the origin. This satisfies the relation

$$\nabla^2 V_a(\mathbf{r}) - \kappa e^{\zeta/kT} \int_\infty d\mathbf{r}_1 \frac{V_a(\mathbf{r}_1)}{|\mathbf{r}-\mathbf{r}_1|} Z_0(2|\mathbf{r}-\mathbf{r}_1|\,; 1/kT) = \frac{4\pi e^2}{K}\{\delta(\mathbf{r}) - |\varphi(\mathbf{r})|^2\}, \quad (4.12)$$

where φ is the orbital of the trapped electron. $V_a(\mathbf{r})$ consists of terms representing the interaction of an electron with the ion, with the trapped electron, and the distribution of mobile electrons, of density $P_a(\mathbf{r})$, induced by presence of the atom:

$$V_a(\mathbf{r}) = \frac{e^2}{K}\left[-\frac{1}{r} + \int d\mathbf{r}_1 \frac{|\varphi(\mathbf{r}_1)|^2}{|\mathbf{r}-\mathbf{r}_1|} + \int d\mathbf{r}_1 \frac{P_a(\mathbf{r}_1)}{|\mathbf{r}-\mathbf{r}_1|}\right]. \quad (4.13)$$

Comparison of Eq. (4.12) with the obvious analog of Eq. (4.5) shows that

$$P_a(\mathbf{r}) = -\frac{1}{\pi D} e^{\zeta/kT} \int d\mathbf{r}_1 \frac{V_a(\mathbf{r}_1)}{|\mathbf{r}-\mathbf{r}_1|} \times Z_0(2|\mathbf{r}-\mathbf{r}_1|\,; 1/kT). \quad (4.14)$$

Comparison of Eqs. (4.4) and (4.12) shows that

$$V_a(\mathbf{r}) = V_i(\mathbf{r}) - \int d\mathbf{r}_1 |\varphi(\mathbf{r}_1)|^2 V_i(\mathbf{r}-\mathbf{r}_1), \quad (4.15)$$

while comparison of Eqs. (4.7) and (4.14) yields

$$P_a(\mathbf{r}) = P_i(\mathbf{r}) - \int d\mathbf{r}_1 |\varphi(\mathbf{r}_1)|^2 P_i(\mathbf{r}-\mathbf{r}_1). \quad (4.16)$$

From Eqs. (4.15) and (4.16) it follows that

$$\int d\mathbf{r} P_a(\mathbf{r}) = \int d\mathbf{r} V_a(\mathbf{r}) = 0; \quad (4.17)$$

both the net charge in the mobile electron distribution induced by a neutral impurity atom and the average potential due to the whole set of charges will vanish.

We shall assume that all the localized orbitals φ have the same form. Then from Eqs. (4.4) and (4.12), and the linear character of Eq. (4.2), it follows that

$$v_e(\mathbf{r}) = \sum_{\substack{j \\ \text{atoms}}} V_a(\mathbf{r}-\mathbf{R}_j) + \sum_{\substack{j \\ \text{ions}}} V_i(\mathbf{r}-\mathbf{R}_j) - \langle n_e \rangle \int d\mathbf{r} V_i(\mathbf{r}). \quad (4.18)$$

Similarly, the mobile electron density is

$$n_e(\mathbf{r})=\sum_{\text{atoms}}{}_j\, P_a(\mathbf{r}-\mathbf{R}_j)+\sum_{\text{ions}}{}_j\, P_i(\mathbf{r}-\mathbf{R}_j). \quad (4.19)$$

Thus the mobile electron density is expressed as the sum of contributions associated with each atom and ion; the potential energy fluctuation $v_e(\mathbf{r})$ is similarly expressed as a sum of contributions from the atoms and ions, minus the average value of these contributions. The possibility of expressing $v_e(\mathbf{r})$ and $n_e(\mathbf{r})$ in this way depends entirely on the linearization of the theory resulting from the assumption, expressed in Eq. (3.20), that the mobile carrier density is a linear functional of the potential energy fluctuation. It is this linearization of the theory that gives it a relatively simple form, but restricts its applicability to sufficiently small $v_e(\mathbf{r})$.

5. HARTREE EQUATION FOR LOCALIZED ORBITALS

In the preceding section we have seen how to determine the form of $v_e(\mathbf{r})$ for any specified ζ, T, and any distribution of trapped electrons in localized orbitals φ_j, by a series of quadratures. Physically, one would expect the localized orbitals to have slightly different forms and energy parameters μ_j, because of the different relative positions of the other impurity ions and atoms with which the trapped electron interacts. To make the problem more tractable, we shall replace the interaction of each trapped electron with the neighboring impurities by an average interaction—the average taken over all trapped electrons in a fixed random arrangement of impurity atoms and ions, or, what is equivalent, an average taken over all configurations of the impurities surrounding a given trapped electron. We shall accordingly write

$$\varphi_j(\mathbf{r})=\varphi(\mathbf{r}-\mathbf{R}_j). \quad (5.1)$$

Combining Eqs. (2.12) and (4.18), one can express the Hartree equation for an electron trapped by an impurity ion at the origin as

$$\left\{-\frac{\hbar^2}{2m^*}\nabla^2+\sum_{\text{atoms}} V_a(\mathbf{r}-\mathbf{R}_j)+\sum_{\text{ions}} V_i(\mathbf{r}-\mathbf{R}_j) -\langle n_e\rangle\int d\mathbf{r}V_i(\mathbf{r})-\frac{e^2}{K}\int d\mathbf{r}_1\frac{|\varphi(\mathbf{r}_1)|^2}{|\mathbf{r}-\mathbf{r}_1|}\right\}\varphi(\mathbf{r}) =\mu\varphi(\mathbf{r}). \quad (5.2)$$

Averaging over all configurations of the neighboring impurities, or over all $\mathbf{R}_j$ (except that of the ion under consideration), one obtains

$$\langle\langle V_a(\mathbf{r}-\mathbf{R}_j)\rangle\rangle=0, \quad (5.3)$$

by Eq. (4.17), and

$$\langle\langle V_i(\mathbf{r}-\mathbf{R}_j)\rangle\rangle=\frac{1}{V}\int d\mathbf{r}V_i(\mathbf{r}), \quad (5.4)$$

where V is the volume of the crystal, and the configuration average is indicated by double angular brackets. This averaging removes from Eq. (5.2) all terms representing interactions with neighboring atoms, while the average value of the interaction with the N_i ions in the crystal cancels out against the fourth term. Thus one obtains

$$\left\{-\frac{\hbar^2}{2m^*}\nabla^2+V_a(\mathbf{r})-\frac{e^2}{K}\int d\mathbf{r}_1\frac{|\varphi(\mathbf{r}_1)|^2}{|\mathbf{r}-\mathbf{r}_1|}\right\}\varphi(\mathbf{r}) =\mu\varphi(\mathbf{r}). \quad (5.5)$$

The dependence of this equation on φ can be made completely explicit by use of Eq. (4.15) for V_a:

$$\left\{-\frac{\hbar^2}{2m^*}\nabla^2+V_i(\mathbf{r})-\int d\mathbf{r}_1|\varphi(\mathbf{r}_1)|^2 \times\left[V_i(\mathbf{r}-\mathbf{r}_1)+\frac{e^2}{K}\frac{1}{(\mathbf{r}-\mathbf{r}_1)}\right]\right\}\varphi(\mathbf{r})=\mu\varphi(\mathbf{r}). \quad (5.6)$$

Use of Eq. (4.13) instead yields

$$\left\{-\frac{\hbar^2}{2m^*}\nabla^2-\frac{e^2}{Kr}+\frac{e^2}{K}\int d\mathbf{r}_1\frac{P_a(\mathbf{r}_1)}{|\mathbf{r}-\mathbf{r}_1|}\right\}\varphi(\mathbf{r})=\mu\varphi(\mathbf{r}), \quad (5.7)$$

which expresses the effective potential energy for the trapped electron as the sum of contributions from its interaction with the nucleus and with the mobile carrier distribution P_a induced by presence of the nucleus plus trapped electron.

In connection with Eq. (5.7), it may be well to emphasize the significance of the present application of the Hartree approximation. The induced distribution of mobile carriers is here treated as determined by the time-average distribution $|\varphi(\mathbf{r})|^2$ of positions of the trapped electron, rather than its instantaneous position. In effect, the trapped electron is treated as moving rapidly as compared with the conduction electrons. In consequence of this approximation, the induced distribution of mobile carriers, $P_a(\mathbf{r})$, is treated as static, and like the inducing atom, has zero net charge. The electronic potential energy due to $P_a(\mathbf{r})$ falls off exponentially as r increases; thus the effective potential energy for the trapped electron assumes the Coulomb form $-e^2/Kr$ at large r. This is in contradiction to another natural picture of the situation (inconsistent with the Hartree approximation) which would have the trapped electron moving slowly at large r in the field of an ion effectively screened by the conduction electron distribution induced by the ion alone. At least for large r, the present theory appears to underestimate the effect of shielding by the conduction electrons, by overestimating the effectiveness of the trapped electron in keeping the conduction electrons away from the nucleus.

6. TOTAL ENERGY OF THE SYSTEM

An expression for the total energy of the system has been given in Eq. (2.13). By use of Eqs. (2.4) and (4.19)

this can be expressed in terms of the localized orbitals φ and the distributions of mobile carriers P_e and P_i induced about impurity atoms and ions, respectively. To this expression we apply the process of configuration averaging, as discussed in the preceding section. The calculation is elementary, but requires a little care. Let N_a and N_i denote the number of impurity atoms and ions, respectively. Then one finds

$$\langle\langle E\rangle\rangle=\langle\langle\textstyle\sum_i f(\epsilon_i)\epsilon_i\rangle\rangle+N_a\mu - N_i\frac{e^2}{2K}\int\int\frac{d\mathbf{r}d\mathbf{r}'}{|\mathbf{r}-\mathbf{r}'|}P_i(\mathbf{r})P_i(\mathbf{r}') - N_a\left[\frac{e^2}{2K}\int\int\frac{d\mathbf{r}d\mathbf{r}'}{|\mathbf{r}-\mathbf{r}'|}P_a(\mathbf{r})P_a(\mathbf{r}') + \frac{e^2}{K}\int\int\frac{d\mathbf{r}d\mathbf{r}'}{|\mathbf{r}-\mathbf{r}'|}|\varphi(\mathbf{r})|^2P_a(\mathbf{r}')\right]. \quad (6.1)$$

As usual, the total energy appears as the sum of the Hartree parameters of the occupied orbitals, corrected by subtraction of the interaction terms that are duplicated when one considers each electron in turn. Here the configuration average of these subtracted terms is expressed as the sum of the self energies of the mobile carrier distributions induced by each ion and atom, plus the energy of interaction of each trapped electron with the carrier distribution induced about the same center.

Configuration averaging has removed from Eq. (6.1) all terms that refer explicitly to interactions of charge distributions associated with different impurities. The interaction of impurities is now entirely implicit in the dependence of $P_i(\mathbf{r})$ and $P_a(\mathbf{r})$ on ζ, which depends on N_i and T, and is ultimately determined by T and the total impurity concentration.

The relation between the number N_i of mobile electrons and the parameter ζ is implicit in Eq. (3.19). To average this equation over all configurations of the impurities, one can use Eqs. (4.18), (5.3), and (5.4) to find

$$\langle\langle v_e(\mathbf{r}_1)v_e(\mathbf{r}_2)\rangle\rangle=N_a\langle\langle V_a(\mathbf{r}_1)V_a(\mathbf{r}_2)\rangle\rangle + N_i\langle\langle V_i(\mathbf{r}_1)V_i(\mathbf{r}_2)\rangle\rangle, \quad (6.2)$$

after neglect of the quantity $-N_i\langle\langle V_i\rangle\rangle^2$, which is of higher order in $1/V$. Insertion of Eq. (6.2) into Eq. (3.19), and application of Eqs. (4.7) and (4.14) yields

$$N_i/V=\langle\langle n_e\rangle\rangle=n_0(\zeta,T)-\frac{1}{2kT}\left[\frac{N_a}{V}\int d\mathbf{r}P_a(\mathbf{r})V_a(\mathbf{r}) + \frac{N_i}{V}\int d\mathbf{r}P_i(\mathbf{r})V_i(\mathbf{r})\right], \quad (6.3)$$

where

$$n_0(\zeta,T)=2\left(\frac{2\pi m^*kT}{h^2}\right)^{\frac{3}{2}}e^{\zeta/kT} \quad (6.4)$$

is the electron density in an ideal unperturbed semiconductor with the given ζ and T. For a fixed number of impurity atoms,

$$N=N_a+N_i, \quad (6.5)$$

Eq. (6.3) provides an implicit relation between N_i and ζ that depends on the values of N and T. (The dependence of the integrals on ζ must not be forgotten.) The complexity of this relation, as compared with the usual Eq. (6.4), arises from the fact that the theory takes some account of the change in the energy distribution of the conduction levels caused by interaction of the conduction electrons with the impurity atoms and ions.

A quantity of fundamental interest in the theory is the average energy change per electron removed from a localized level:

$$\left.\frac{\partial\langle\langle E\rangle\rangle}{\partial N_i}\right|_{N,T}=\left.\frac{\partial\langle\langle E\rangle\rangle}{\partial N_i}\right|_{N,\zeta,T}+\left.\frac{\partial\zeta}{\partial N_i}\right|_{N,T}\left.\frac{\partial\langle\langle E\rangle\rangle}{\partial\zeta}\right|_{N,N_i,T}. \quad (6.6)$$

The first term on the right could be computed from Eq. (6.1), after properly expressing $\langle\langle f(\epsilon_i)\epsilon_i\rangle\rangle$ as a function of N, N_i, ζ, and T; it represents the average energy required to bring into the conduction band an electron trapped by an isolated impurity, ζ being held constant. The second term could be computed by use of Eqs. (6.1) and (6.3); it represents the additional energy required, on the average, because of the change in the interaction of the ionized impurity with the other impurities, and the associated changes in the self-energies of the charge distributions around those other impurities. It would be complicated and unnecessary to disengage these terms from each other before completing the calculation.

7. CALCULATION OF THE FREE ENERGY

In preceding Sections we have seen how to calculate $\langle\langle E\rangle\rangle$, the contribution of mobile and trapped carriers to the internal energy of the system, as a function of N, T, and ζ or N_i. It remains to determine the physically occurring values of ζ or $\langle N_i\rangle$ as a function of N and T. These are the values that minimize the free energy

$$F(N,T,\zeta)=\langle\langle E\rangle\rangle-TS(N,T,\zeta). \quad (7.1)$$

The entropy S is given by

$$S=k\ln W=k\ln W_e+k\ln W_i, \quad (7.2)$$

where W is the number of ways of choosing occupied orbitals, localized and unlocalized, consistent with the specified values of N, T, and ζ, and W_e and W_i are the number of ways of choosing conduction and trapping orbitals, respectively.

The number of ways of distributing $N_e=N-N_i$ electrons over N impurities is

$$W_i=\frac{N!}{N_i!(N-N_i)!}2^{N-N_i}, \quad (7.3)$$

the last factor taking account of the two spin possibilities for each electron. The corresponding term in the entropy can be written, using Sterling's approximation, as

$$S_i = k \ln W_i = k\{(N-N_i)[\ln 2 - \ln(1-N_i/N)] - N_i \ln(N_i/N)\}. \quad (7.4)$$

The other entropy term, S_e, can be expressed in terms of the distribution function $f(\epsilon)$ [Eq. (3.1)] by familiar methods.[9] Let $\rho(\epsilon)$ be the density of conduction band levels, both spins included. Then W_e is the number of ways of distributing $Z_i = f(\epsilon_i)\rho(\epsilon_i)\Delta\epsilon_i$ electrons over $N_i = \rho(\epsilon_i)\Delta\epsilon_i$ levels in each of the energy ranges $\Delta\epsilon_i$, and

$$S_e = k \ln W_e = -k \int d\epsilon \rho(\epsilon) \times \{f(\epsilon) \ln f(\epsilon) + [1-f(\epsilon)] \ln[1-f(\epsilon)]\}. \quad (7.5)$$

Separate calculation of this quantity is unnecessary: it is more convenient to associate it with the corresponding term in $\langle\langle E \rangle\rangle$,

$$\langle\langle \textstyle\sum_i f(\epsilon_i)\epsilon_i \rangle\rangle = \int d\epsilon \rho(\epsilon) f(\epsilon) \epsilon, \quad (7.6)$$

and to compute

$$F_e = \langle\langle \textstyle\sum_i f(\epsilon_i)\epsilon_i \rangle\rangle - TS_e. \quad (7.7)$$

With the assumed Boltzmann form of $f(\epsilon_i)$, this becomes

$$F_e = \int d\epsilon \rho(\epsilon)\{\zeta f(\epsilon) + kT[1-f(\epsilon)] \ln[1-f(\epsilon)]\}. \quad (7.8)$$

Treating f as small throughout the conduction band, one can replace $(1-f)\ln(1-f)$ by f; the integration then yields

$$F_e \cong N_i(\zeta - kT). \quad (7.9)$$

With this approximation we have

$$F = N_i \Big\{ \zeta - kT[1 - \ln(N_i/N)] - \frac{e^2}{2K} \int\int \frac{d\mathbf{r}d\mathbf{r}'}{|\mathbf{r}-\mathbf{r}'|} P_i(\mathbf{r}) P_i(\mathbf{r}') \Big\} + (N-N_i) \Big\{ \mu - kT[\ln 2 - \ln(1-N_i/N)] - \frac{e^2}{2K} \int\int \frac{d\mathbf{r}d\mathbf{r}'}{|\mathbf{r}-\mathbf{r}'|} P_a(\mathbf{r})[P_a(\mathbf{r}') + 2|\varphi(\mathbf{r}')|^2] \Big\}, \quad (7.10)$$

where μ, P_i, P_a, and φ all depend implicitly on ζ, and ζ and N_i are related by Eq. (6.3).

[9] H. A. Bethe and A. Sommerfeld, *Handbuch der Physik* (Verlag Julius Springer, Berlin, 1933), Vol. 24, Part 2, p. 34.

8. THE MOBILE CARRIER DISTRIBUTION $P_i(\mathbf{r})$ INDUCED BY AN IMPURITY ION

The calculations in the present work have been based on use of a simple analytical approximation to the distribution function $P_i(\mathbf{r})$, which must now be discussed.

The exact form of $P_i(\mathbf{r})$ is given by Eqs. (4.10) and (4.11). On substituting into Eq. (4.10) the form of Z given in Eq. (3.9), and carrying out the integration over directions of $\mathbf{r}$, one obtains

$$H(\mathbf{p}) = \frac{2\pi x n_0(\zeta,T)}{p} \int_0^\infty dr \sin(pr) \exp(-kTr^2/D). \quad (8.1)$$

Let

$$q = \tfrac{1}{2}p(D/kT)^{\frac{1}{2}}, \quad (8.2)$$

and define[10]

$$q\Theta(q) = \int_0^\infty dx \sin(2qx) \exp(-x^2) = \exp(-q^2) \int_0^q dx \exp(x^2). \quad (8.3)$$

One can then write

$$H(\mathbf{p}) = n_0(\zeta,T) \cdot \frac{4\pi e^2}{KkT} \cdot \Theta(q). \quad (8.4)$$

The function $q\Theta(q)$ has been tabulated and discussed by Rosser.[11] Here it is sufficient to note that

$$\Theta(0) = 1, \quad (8.5)$$

$$\Theta(q) \cong 1/2q^2, \quad \text{for} \quad q > 10. \quad (8.6)$$

In the classical limit, $h \to 0$, $D \to 0$, and $q \to 0$. In this limit one can replace $H(\mathbf{p})$ in Eqs. (4.9) and (4.11) by

$$\frac{1}{r_f^2} = \frac{4\pi e^2}{KkT} n_0(\zeta,T), \quad (8.7)$$

and carry out the integrations without difficulty, to obtain

$$V_{ie}(\mathbf{r}) = -(e^2/Kr) \exp(-r/r_f), \quad (8.8)$$

$$P_{ie}(\mathbf{r}) = (1/4\pi r_f^2 r) \exp(-r/r_f). \quad (8.9)$$

The potential V_{ie} due to an ion in the crystal thus appears as a shielded Coulomb potential, with range of the order of the distance r_f. The length r_f is identical with the characteristic length that appears in the classical theory of potential fluctuations in semiconductors.[12] The infinity in $P_{ie}(\mathbf{r})$ at the origin is a

[10] The equivalence of the two forms for $I = q\Theta(q)$ can be established by noting that both satisfy the first-order equation $dI/dq = 1 - 2qI$ and assume the value 0 when $q = 0$.

[11] J. B. Rosser, Office of Scientific Research and Development Report OSRD No. 5861 (unpublished).

[12] G. W. Lehman, M.S. thesis, Purdue University, 1950 (unpublished); also available as a Signal Corps Report.

peculiarity of the classical limiting form, and appears neither in the exact quantum-mechanical result, nor in the approximate one next to be derived.

Convenient analytical approximations to $P_i(\mathbf{r})$ and $V_i(\mathbf{r})$ can be obtained by introducing a simple approximation to $\Theta(q)$. Equations (8.5) and (8.6) suggest that one may be able to approximate $\Theta(q)$, with sufficient accuracy for present purposes, by an expression of the form $1/(1+dq^2)$. Here it is desirable to choose d so that the approximation has its first and second derivatives correct at the origin.

$$\Theta_a(q)=1/(1+\tfrac{3}{4}q^2). \tag{8.10}$$

This is a good approximation for small q, but it is in error by a factor of 3 when q is large. For large q, however, $\Theta(q)$ is small, and contributes little to the denominator in Eq. (4.9). We write this denominator as

$$p^2+H(\mathbf{p})=\frac{4kT}{D}\left\{q^2+\frac{3}{2}\frac{\xi^2}{(\xi^2+1)^2}\Theta(q)\right\}, \tag{8.11}$$

where ξ is a parameter defined by

$$\frac{6kT}{D}\frac{\xi^2}{(\xi^2+1)^2}=\frac{4\pi e^2}{KkT}n_0(\zeta,T)=\frac{1}{r_f^2},\quad 0\leq\xi\leq 1. \tag{8.12}$$

Numerical checks show that replacement of Θ in Eq. (8.11) by Θ_a will introduce an error of no more than $1\frac{1}{2}$ percent for any q, so long as $\xi\leq\frac{1}{4}$, as is the case in most of our calculations; the corresponding approximate forms of $V_i(\mathbf{r})$, and $P_i(\mathbf{r})$ should be correspondingly accurate. With this approximation, the integrations in Eqs. (4.9) and (4.11) are easily performed by contour integration. One finds

$$V_i(\mathbf{r})=-\frac{e^2}{K(1-\xi^2)}\frac{1}{r}\times[\exp(-r/r_s)-\xi^2\exp(-r/\xi r_s)], \tag{8.13}$$

$$P_i(\mathbf{r})=\frac{1}{4\pi(1-\xi^2)r_s^2}\frac{1}{r}\times[\exp(-r/r_s)-\exp(-r/\xi r_s)], \tag{8.14}$$

where

$$r_s=r_f/(1+\xi^2)^{\frac{1}{2}}. \tag{8.15}$$

These approximations will be used henceforth. Elementary integration yields

$$\int d\mathbf{r}V_i(\mathbf{r})P_i(\mathbf{r})=-\frac{e^2}{2Kr_s}\frac{1+\xi+\xi^2}{(1+\xi)^3}. \tag{8.16}$$

The approximate forms in Eqs. (8.13) and (8.14) satisfy Eq. (4.5), and hence Eq. (4.6); applying the latter equation and integrating, one finds

$$\frac{e^2}{K}\int\int\frac{d\mathbf{r}d\mathbf{r}'}{|\mathbf{r}-\mathbf{r}'|}P_i(\mathbf{r})P_i(\mathbf{r}')=\int d\mathbf{r}\left\{V_i(\mathbf{r})+\frac{e^2}{Kr}\right\}P_i(\mathbf{r})=\frac{e^2}{2Kr_s}\frac{1+3\xi+\xi^2}{(1+\xi)^3}. \tag{8.17}$$

9. APPROXIMATE FORM OF THE LOCALIZED ORBITALS

Having determined the form of $V_i(\mathbf{r})$, one can turn to the solution of Eq. (5.6) for the localized orbital $\varphi(\mathbf{r})$. A variational method will be used here to determine a simple approximate form for this orbital.

Solution of Eq. (5.6) is equivalent to finding functions $\varphi(\mathbf{r})$ that make

$$H(\varphi)=\int d\mathbf{r}\varphi^*(\mathbf{r})\left[-\frac{\hbar^2}{2m^*}\nabla^2+V_i(\mathbf{r})\right]\varphi(\mathbf{r})-\frac{1}{2}\int d\mathbf{r}\int d\mathbf{r}'|\varphi(\mathbf{r})|^2|\varphi(\mathbf{r}')|^2\times\left\{V_i(\mathbf{r}-\mathbf{r}')+\frac{e^2}{K}\frac{1}{|\mathbf{r}-\mathbf{r}'|}\right\} \tag{9.1}$$

stationary to variations of $\varphi(r)$ that maintain its normalization. The corresponding value of μ can be written in terms of integrals involving $V_i(\mathbf{r})$, or, as is most quickly evident from Eq. (5.7), as

$$\mu(\varphi)=\int d\mathbf{r}\varphi^*(\mathbf{r})\left[-\frac{\hbar^2}{2m^*}\nabla^2-\frac{e^2}{Kr}\right]\varphi(\mathbf{r})+\frac{e^2}{K}\int\int\frac{d\mathbf{r}d\mathbf{r}'}{|\mathbf{r}-\mathbf{r}'|}P_a(\mathbf{r})|\varphi(\mathbf{r}')|^2. \tag{9.2}$$

We are interested in the form of φ that makes $H(\varphi)$ an absolute minimum. The functional $\mu(\varphi)$ is not stationary with respect to deviations of φ from this form, but, as in any Hartree calculation, the total energy of the system is stationary with respect to variations of the orbitals φ, if the other orbitals ψ (and thus P_i and P_a) are held constant.

Equation (5.7) expresses the effective potential energy for a trapped electron as the sum of a Coulomb term and a contribution due to the presence of an induced distribution of carriers about the impurity atom. Since the inducing charge distribution has total charge zero, the induced distribution $P_a(\mathbf{r})$ of carriers will have total charge zero, and, moreover, will tend to be small in magnitude everywhere. Thus the potential energy term due to the induced carrier distribution can

be expected to be very small; the total effective potential will be nearly of Coulomb form, and $\varphi(\mathbf{r})$ will be approximately of hydrogenic form. For simplicity, we shall base our calculation on the use of an approximate orbital of hydrogenic form,

$$\varphi(\alpha;\mathbf{r})=\left[\frac{\alpha^3}{8\pi r_s^3}\right]^{\frac{1}{2}}\exp(-\alpha r/2r_s), \tag{9.3}$$

where α is an adjustable parameter so chosen as to extremalize $H(\varphi)$. The adequacy of this approximation will appear later.

On using this form of φ, together with our approximations for V_i and P_i, one can compute the free carrier distribution about a neutral impurity by use of Eq. (4.16). One finds

$$P_a(\mathbf{r})=\frac{1}{4\pi(1-\xi^2)r_s^3}\cdot\frac{1}{x}\cdot[-A_1\exp(-x)+A_2\exp(-x/\xi)$$
$$+(A_1-A_2-A_3\alpha x/2)\exp(-\alpha x)], \tag{9.4}$$

where

$$x=r/r_s, \tag{9.5}$$

$$A_1=\frac{\alpha^4}{(\alpha^2-1)^2}-1,$$
$$A_2=\frac{\alpha^4\xi^4}{(\alpha^2\xi^2-1)^2}-1, \tag{9.6}$$
$$A_3=\alpha^2\left[\frac{\xi^2}{\alpha^2\xi^2-1}-\frac{1}{\alpha^2-1}\right].$$

The contribution of this induced carrier distribution to the electronic potential energy is

$$V_{ia}(\mathbf{r})=\frac{e^2}{2Kr}[B_1\exp(-x)-B_2\exp(-x/\xi)$$
$$+(B_2-B_1+B_3\alpha x)\exp(-\alpha\xi)], \tag{9.7}$$

where

$$B_1=2A_1/(1-\xi^2),$$
$$B_2=2\xi^2A_2/(1-\xi^2), \tag{9.8}$$
$$B_3=A_3/\alpha^2(1-\xi^2).$$

A tedious calculation based on Eq. (9.1) yields

$$H(\varphi)=E_0\left[\left(\frac{\alpha}{\alpha_0}\right)^2-\frac{5}{8}\frac{\alpha}{\alpha_0}-\frac{1}{8(1-\xi^2)}\frac{\alpha}{\alpha_0}\right.$$
$$\left.\times\{f(\alpha)-\xi^2f(\xi\alpha)\}\right], \tag{9.9}$$

where E_0 is, as previously defined, the ionization energy of an isolated impurity, α_0 is defined by the relation

$$\frac{\alpha_0}{2r_s}=\frac{1}{a_0}=\frac{E_0}{e^2/2K}, \tag{9.10}$$

and

$$f(\alpha)=\frac{11\alpha^4+28\alpha^3+15\alpha^2}{(1+\alpha)^4}. \tag{9.11}$$

To minimize $H(\varphi)$, one must have

$$\frac{\alpha}{\alpha_0}=1+\frac{1}{16}\frac{\alpha^{-3}}{1-\xi^2}\{g(\alpha)-\xi^5g(\xi\alpha)\}, \tag{9.12}$$

where

$$g(\alpha)=\frac{75\alpha^3+119\alpha^2+65\alpha+13}{(1+\alpha)^5}. \tag{9.13}$$

For $\xi\leq\frac{1}{4}$ and $a_0\geq4$, the cases in which we shall be particularly interested, Eq. (9.12) shows that α/α_0 is very nearly equal to 1; at worst, for $\xi=\frac{1}{4}$, $\alpha_0=4$, one has $\alpha/\alpha_0=1.007$. We shall therefore take $\alpha=\alpha_0$ in all the calculations that follow. Equations (9.3) and (9.10) show that this amounts to neglecting the change in form of the trapped electron orbital due to the free carrier distribution induced about the neutral impurity. The small deviation of α from α_0 suggests that the use of hydrogenic orbitals is an adequate approximation, and this is confirmed by test calculations of V_{ia}, which show that this quantity is small and roughly constant in the region where φ is large.

The total electronic potential due to an impurity atom is V_{ia} plus the potential due to the unshielded impurity atom:

$$V_a(\mathbf{r})=V_{ia}(\mathbf{r})-\frac{e^2}{Kr}\left(1+\frac{\alpha r}{2r_s}\right)\exp(-\alpha r/r_s). \tag{9.14}$$

In calculating N_i/V by Eq. (6.3) and F by Eq. (7.10) we shall neglect the very small integral

$$\int\int\frac{d\mathbf{r}d\mathbf{r}'}{|\mathbf{r}-\mathbf{r}'|}P_a(\mathbf{r})P_a(\mathbf{r}')=\int d\mathbf{r}V_{ia}(\mathbf{r})P_a(\mathbf{r}). \tag{9.15}$$

To this approximation one finds

$$\int d\mathbf{r}V_a(\mathbf{r})P_a(\mathbf{r})\cong\frac{e^2}{2Kr_s}\cdot\frac{1}{8\alpha(1-\xi^2)}$$
$$\times[h(\alpha)-h(\xi\alpha)], \tag{9.16}$$

where

$$h(\alpha)=\frac{25\alpha^3+36\alpha+13}{(1+\alpha)^4}. \tag{9.17}$$

With our choice of $\varphi(\mathbf{r})$, Eq. (9.2) for μ becomes

$$\mu=-E_0+\frac{e^2}{K}\int\int\frac{d\mathbf{r}d\mathbf{r}'}{|\mathbf{r}-\mathbf{r}'|}P_a(\mathbf{r})|\varphi(\mathbf{r}')|^2. \tag{9.18}$$

The last integral in this expression also appears explicitly in Eq. (7.10) for F, but cancels out when this value for μ is introduced. Evaluation of this integral is therefore unnecessary unless it is desired to determine μ as a function of N_i and T.

10. PARAMETRIC EXPRESSIONS FOR THE FINAL RESULTS

The calculations and approximations described in previous sections bring the problem into the following form. The conduction electron density is related to T, ζ, and the impurity density N/V by Eq. (6.3). By use of Eqs. (8.16) and (9.16), this can be written as

$$\langle\langle n_e\rangle\rangle\left\{1-\frac{e^2}{4KkTr_s}\left[\frac{1+\xi+\xi^2}{(1+\xi)^3}+\frac{1}{8\alpha_0(1-\xi^2)}\times(h(\alpha_0)-h(\xi\alpha_0))\right]\right\}=n_0(\zeta,T)-\frac{N}{V}\frac{e^2}{4KkTr_s}\frac{1}{8\alpha_0(1-\xi^2)}(h(\alpha_0)-h(\xi\alpha_0)), \quad (10.1)$$

where $h(\alpha)$ is defined by Eq. (9.17), and n_0, ξ, r_s, and α_0 are defined as functions by T and ζ by Eqs. (6.4), (8.12), (8.15), and (9.10), respectively. The electronic free energy per unit volume, as given by Eq. (7.10), becomes, on use of Eqs. (8.17) and (9.18) and neglect of the smallest integral,

$$\frac{F}{V}=\langle\langle n_e\rangle\rangle\left\{\zeta-kT[1-\ln(V\langle\langle n_e\rangle\rangle/N)]-\frac{e^2}{4Kr_s}\frac{1+3\xi+\xi^2}{(1+\xi)^3}\right\}+\left\{\frac{N}{V}-\langle\langle n_e\rangle\rangle\right\}\times\{-E_0+kT\ln[(N-V\langle\langle n_e\rangle\rangle)/2N]\}. \quad (10.2)$$

The physically significant value of ζ is that which minimizes F, for fixed T and N/V. Given this, all other quantities of interest can be calculated.

The carrier density depends on T, N/V, and the two constants that characterize our model of the pure semiconductor: K and m^*, or the binding energy E_0 and radius a_0 of the impurity orbitals at zero impurity concentration, as defined by Eqs. (1.1) and (1.2). The present theory establishes a relation between just three dimensionless parameters:

$$\tau=\tfrac{3}{2}kT/E_0, \quad (10.3)$$

which characterizes the temperature of the system, and

$$\eta_i=(N/V)\cdot 3\pi a_0^3, \quad (10.4)$$

$$\eta_e=\langle\langle n_e\rangle\rangle\cdot 3\pi a_0^3, \quad (10.5)$$

which characterize the impurity and carrier densities, respectively. Except for a numerical factor of the order of 1, introduced to simplify numerical calculations, η_i and η_e are the average number of impurities and free carriers in the volume occupied by a trapped electron orbital.

For practical calculations it is convenient to replace ζ as the adjustable parameter by ξ [see Eq. (8.12)]:

$$(6\pi\tau)^{\frac{1}{2}}\xi^3/(1+\xi^2)^3=\exp(\zeta/kT), \quad 0<\xi<1. \quad (10.6)$$

In terms of ξ, one has

$$\alpha_0^2=(1+\xi^2)/\xi^2\tau, \quad (10.7)$$

$$n_0(\zeta,T)=\tau^2\xi^6/3\pi a_0^3(1+\xi^2)^3, \quad (10.8)$$

$$r_s^2=a_0^2(1+\xi^2)/4\tau\xi^2. \quad (10.9)$$

Equation (10.1) assumes the form

$$\eta_e\left\{1-\frac{3}{2\alpha_0\tau}\left[\frac{1+\xi+\xi^2}{(1+\xi)^3}+\frac{1}{8\alpha_0(1-\xi^2)}(h(\alpha_0)-h(\xi\alpha_0))\right]\right\}=\frac{\xi^3\tau^3}{(1+\xi^2)^2}-\frac{3\eta_i}{16\alpha_0^2\tau(1-\xi^2)}(h(\alpha_0)-h(\xi\alpha_0)), \quad (10.10)$$

and Eq. (10.2) the form

$$\frac{F}{V}=\frac{kT}{3\pi a_0^3}\left[\eta_e\left\{\ln[(6\pi\tau)^{\frac{1}{2}}\xi^3/(1+\xi^2)^2]-1+\ln(\eta_e/\eta_i)-\frac{3}{2\alpha_0\tau}\frac{1+3\xi+\xi^2}{(1+\xi)^3}\right\}+(\eta_i-\eta_e)\left\{-\frac{3}{2\tau}+\ln((\eta_i-\eta_e)/2\eta_i)\right\}\right]. \quad (10.11)$$

The last two equations define $3\pi a_0^3F/VkT$ as a function of τ, η_i, and ξ only. Solution of

$$(\partial F/\partial\xi)_{\tau,\eta_i}=0 \quad (10.12)$$

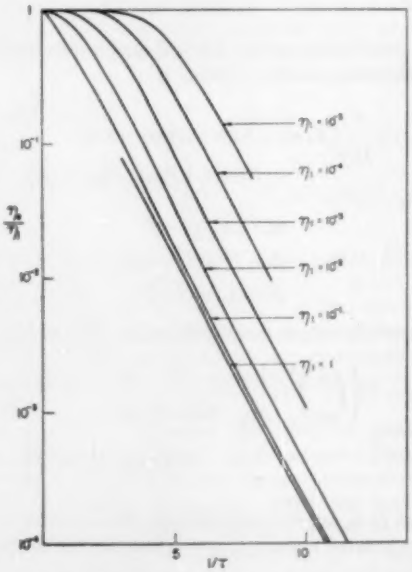

FIG. 1. Ratio of carrier concentration to impurity concentration, plotted against reciprocal temperature for various impurity concentrations η_i [see Eqs. (10.3), (10.4)].

fixes ξ as a function of τ and η_i, whereupon Eq. (10.10) gives η_e as a function of these quantities.

11. RESULTS AND CONCLUSIONS

The calculations described in the preceding paragraph have been carried out on the punched card digital computer of the Purdue Statistical Laboratory, using a method of successive approximations. They have been limited to ranges of the parameters for which $\xi \gtrsim \frac{1}{4}$, to assure the accuracy of the approximations for V_i and P_i [Eqs. (8.13) and (8.14)], and for which $\zeta < -2kT$, to assure reasonable accuracy for the assumption of classical statistics for the electrons in the conduction band. The basic results of the calculations are presented graphically in Fig. 1, where the ratio of carrier to impurity concentration is plotted as a function of $1/\tau$ for various impurity concentrations. Curves for $\eta_i = 10$ and $\eta_i = 100$ would be scarcely distinguishable from that for $\eta_i = 1$.

The difference between the present theory and earlier ones appears more clearly in Fig. 2. The relation between the densities of carriers and impurities at a given T can be expressed in terms of an effective ionization energy:

$$\Delta E = -kT \ln\left[\left(\frac{h^2}{2\pi m^* kT}\right)^{\frac{3}{2}} \frac{n_e^2}{N/V - n_e}\right]. \quad (11.1)$$

As thus defined, ΔE is the ionization energy required in the usual model of noninteracting impurities if a concentration N/V of impurities is to give rise to a concentration n_e of carriers at temperature T. The ratio of ΔE to the ionization energy at zero impurity concentration, expressed in terms of our dimensionless parameters, is

$$w = -\frac{2\tau}{3} \ln\left[\left(\frac{24\pi}{\tau^3}\right)^{\frac{3}{2}} \frac{\eta_e^2}{\eta_i - \eta_e}\right]. \quad (11.2)$$

Figure 2 shows w as a function of impurity concentration, for a series of values of temperature; it shows also

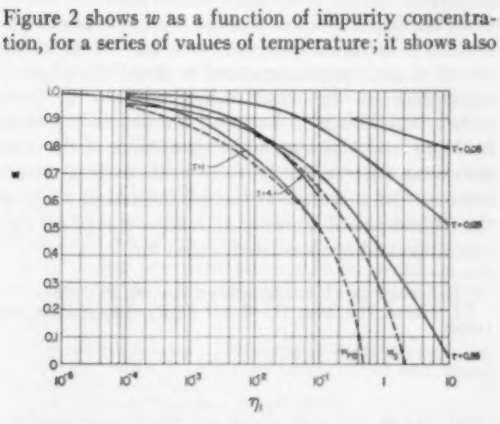

FIG. 2. Solid lines give $\Delta E/E_0$ as a function of impurity concentration, for several temperatures τ, according to the present theory. Dashed lines indicate the temperature-independent results of the theories of Shifrin and of Bardeen and Pearson.

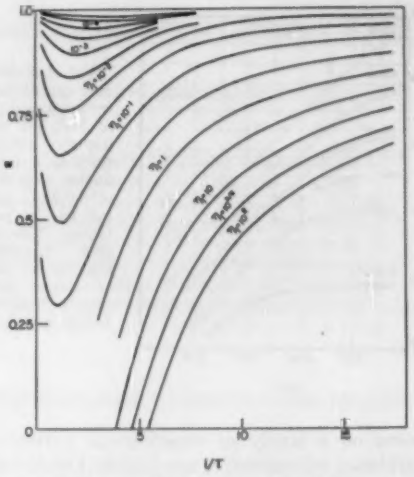

FIG. 3. Dependence of $\Delta E/E_0$ on reciprocal temperature, for various impurity concentrations.

the temperature-independent values given by the theories of Shifrin and of Pearson and Bardeen. The present theory gives about the same reduction in activation energy by impurity interaction as do the other theories when the temperature is relatively high, but a much smaller reduction at low temperatures, where the carrier concentration is low.

The most striking result of the present theory is the strong predicted dependence of effective activation energy on temperature, when the impurity concentration is high. This is shown most clearly in Fig. 3, where w is plotted against reciprocal temperature for various impurity concentrations. The existence of a minimum in the curves, for not-too-high impurity concentrations, is easily understood. When τ is reduced from its value at the minimum, w tends to increase because the carrier concentration is decreasing, and with it the shielding effects that tend to reduce the activation energy. On the other hand, w increases when τ is raised, because the relatively smaller increase in carrier concentration is overbalanced by the decrease in polarizability of the electron distribution, which also tends to diminish the shielding effects. The curves for the larger values of η_i presumably approach 1 as $1/\tau$ goes to zero, but no attempt has been made to compute this part of the curves.

The theory predicts that the family of plots of $\ln n_e$ against $1/T$, for different impurity concentrations, will always have the same form for all semiconductors with the simple band structure discussed here, and for all impurities describable by the hydrogenic model. More precisely, the plots will differ only by a vertical displacement determined by the value of a_0 or Km/m^*, and by a horizontal scale factor determined by the value of E_0 or m^*/mK^2. If K and m^* are known from other sources, a family of theoretical curves can be super-

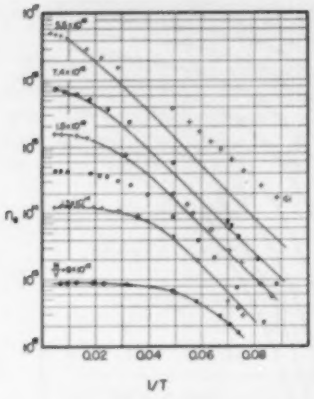

FIG. 4. Solid lines give carrier concentration as a function of $1/T$, for various impurity concentrations in a semiconductor with $K=16$, $m^*=0.25m$, according to the present theory. The points give experimental data on six samples of n-type germanium, as obtained by Debye and Conwell.

imposed on a family of experimental curves without arbitrary adjustment of any factors. Figure 4 shows such a family of curves, drawn for $K=16$, $m^*/m=\frac{1}{4}$.

Even though the band structure of germanium and silicon is more complex than that assumed in the present model,[13] it is tempting to compare experimental data for these materials with the theory, anticipating that the tensor effective mass may be replacable by some mean m^*. As an example, we take the carefully analyzed data of Debye and Conwell[14] for n-type germanium. Figure 4 shows experimental data taken from their work (Fig. 10), in comparison with theoretical curves calculated for the observed value of K and a generally appropriate value of m^*—actually that used in the theoretical analysis of Debye and Conwell. In the case of the purer samples the fit is generally satisfactory, except that the observed carrier densities begin to fall more rapidly than is indicated by theory as $1/T$ becomes large. That this effect is due to the presence of acceptor impurities is already indicated by both the mobility and the concentration data of Debye and Conwell. On the other hand, the experimental data on the less pure sample 61 of Debye and Conwell deviates from the experimental curves in a way that cannot be attributed to the presence of acceptor impurities. Debye and Conwell fit a theoretical curve to this data by assuming a decidedly lower activation energy (0.007 ev) than is predicted by the present theory. It seems clear that the present theory, at least as applied to germanium, underestimates the decrease in activation energy at high impurity concentrations.

The observations of Morin and Maita[15] on n-type silicon deviate from the theory in a somewhat similar way; for instance, the behavior of their sample 126 of silicon doped with arsenic suggests that the impurity activation energy is temperature dependent and considerably lower than would be predicted by the present theory. (The larger value of E_0 and the smaller value of a_0 make the continuous dielectric model of the semiconductor less reliable here than in the case of germanium.)

Replacement of the scalar m^* by a tensor effective mass would make it easier to compare the theory with observations on germanium and silicon. It is probable, however, that the most serious approximation in the present theory is the use of a linearized relation between the carrier density fluctuation and the potential fluctuation [Eqs. (3.19) and (3.20)], and that this is responsible for the underestimate of the decrease in activation at high impurity concentrations. It appears that this approximation can be removed by use of the methods of Friedel,[16] together with other simplifications suggested by the outcome of the present work. In principle, the theory can also easily be extended to materials containing both donor and acceptor impurities—an extension that is certainly required if careful quantitative comparison is to be made with existing experimental results.

Morin and Maita have shown that it is often, though not invariably, possible to obtain impressive agreement between experimental data on carrier concentration and a theory based on the assumption of constant activation energy, if one uses as parameters adjustable separately for each sample the concentration of majority and minority impurities, the activation energy of the majority impurity and, independently, the effective mass of the carriers. However, in view of the strong indication given by the present theory that the effective activation energy is strongly temperature dependent when the impurity concentration is high, it seems reasonable to attribute their success in part to the multiplicity of their parameters, and to doubt the physical significance of the exact values assigned to these parameters. This is in line with the doubts expressed by Morin and Maita as to the significance of the mass parameter determined by their method. It therefore seems to the authors that further theoretical study of the dependence of impurity activation energy on concentration and temperature is called for.

[13] The present calculation can be extended to band structures such as those of n-type Ge and Si without appreciable difficulty.
[14] P. P. Debye and E. M. Conwell, Phys. Rev. **93**, 693 (1954).
[15] F. J. Morin and J. P. Maita, Phys. Rev. **96**, 28 (1954).
[16] J. Friedel, Phil. Mag. (7) **43**, 153 (1952); Ann. phys. **9**, 158 (1954).

Ferromagnetic Resonance in Manganese Ferrite Single Crystals*

P. E. TANNENWALD
Lincoln Laboratory, Massachusetts Institute of Technology, Lexington, Massachusetts
(Received June 23, 1955)

The microwave properties of two types of manganese ferrite single crystals have been investigated by means of the ferromagnetic resonance phenomenon from 300°K to 4.2°K and at 24 000, 9100, 5600, and 2800 Mc/sec. The low resistivity of one of the crystals, believed to be related to the presence of divalent iron, led to significantly different microwave behavior. Resonance lines as narrow as 47 oe have been obtained; however the width depends markedly on crystal direction, temperature and microwave frequency. The g-values are close to 2.00 under all conditions. The anisotropy, although frequency insensitive, increases rapidly at low temperatures. The Kramers-Krönig relations between absorption and dispersion are satisfied, and the line shape is roughly Lorentzian. Double resonances have been observed, and it is speculated that this may be a general phenomenon in single-crystal ferrites under suitable conditions.

I. INTRODUCTION

THE ferromagnetic resonance phenomenon in ferrites can be described satisfactorily in terms of the solution of the equation of motion for the precessing magnetization vector. The phenomenological description requires use of the appropriate effective magnetic field acting on the magnetization and of relaxation parameters which determine the line width. The sources contributing to the effective field can be accounted for theoretically, but the origin of the relaxation is not understood at the present time. To this end, it would be of value to have information on the frequency, crystal direction, and temperature dependence of the line width, as well as dependence on ferrite composition.

It is the purpose of this paper to furnish a comprehensive set of data on two types of manganese ferrite single crystals, including magnetic anisotropy, g-value, line width, and their frequency and temperature variations, and to point out new features in the microwave behavior. Earlier a number of microwave experiments on ferrite single crystals have been reported[1–5]; in general the objectives and results were of more limited scope or different emphasis.

In the following sections we describe methods and results of measurements made from room temperature down to 4.2°K and at frequencies from 24 000 Mc/sec to 2800 Mc/sec. Two types of single crystals were used, whose essential difference depended on their respective resistivities. This will be shown to have an important consequence on the line width and its temperature dependence. Finally, an additional resonance, which we believe occurs when the magnetization vector is not lined up with the applied magnetic field, was observed at low temperatures.

* The research reported in this document was jointly supported by the Army, Navy, and Air Force under contract with Massachusetts Institute of Technology.

[1] L. R. Bickford, Phys. Rev. 78, 449 (1950).
[2] Yager, Galt, Merritt, and Woods, Phys. Rev. 80, 744 (1950).
[3] D. Healy, Phys. Rev. 86, 1009 (1952).
[4] Okamura, Kojima, and Torizuka, Science Repts. Research Inst. Tohoku Univ. Ser. A, 4, No. 1 (1952).
[5] T. Okamura and Y. Kojima, Phys. Rev. 86, 1040 (1952).

II. EXPERIMENTAL APPARATUS AND TECHNIQUES

The essential components of the basic microwave setup are shown in Fig. 1. Power from a frequency-modulated klystron is sent into a cavity which is placed between the poles of an electromagnet. Both the incident and reflected signals from the cavity are monitored by a pair of directional couplers and crystals. The direct and reflected signals are alternately selected by an electric switch and are viewed simultaneously on an oscilloscope. This permits Q-measurements to be made by comparing incident and reflected powers from the cavity. Sufficient attenuation is inserted into the direct signal arm to balance the reflected power from the cavity. This attenuation is a measure of the reflection coefficient which, in turn, is related to the VSWR and Q's of the cavity.[6] Standard microwave techniques were employed for measuring band widths of cavity resonances and frequency shifts of cavity resonances due to ferrite dispersion. With a stabilized microwave source providing a heterodyning signal, frequency changes of 0.02 Mc/sec could be detected. The power reflected from the cavity could also be recorded automatically. In this scheme the klystron is frequency-stabilized on the cavity, and the magnetic field is swept through its total range.

All X-band measurements were made in a cavity oscillating in the rectangular TE_{101} mode. The sample can be rotated on a dielectric post inserted through the end wall of the cavity. The K-band measurements were taken in a cylindrical cavity oscillating in the circular TE_{111} mode (the degeneracy was removed by a small loop of wire placed over the coupling iris in the E plane of the undesired mode), while the C- and S-band measurements were made with TE_{103} rectangular cavities.

Low-temperature measurements were carried out with the wave guide and cavity surrounded by a double Dewar system. The desired temperatures were obtained by filling the outer Dewar with dry ice and acetone, or

[6] For details see J. O. Artman and P. E. Tannenwald, Technical Report No. 70, Lincoln Laboratory, Massachusetts Institute of Technology, 1954 (unpublished).

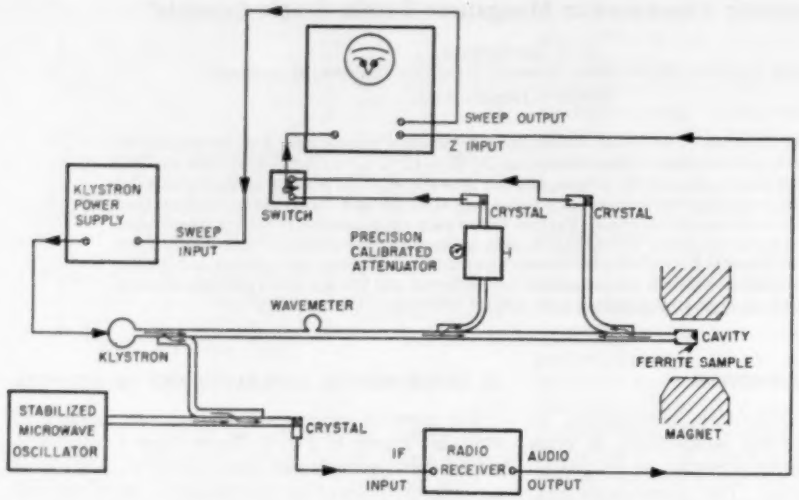

FIG. 1. Experimental setup used at room temperature.

with liquid nitrogen; for the 4.2°K work the cavity and sample were immersed in liquid helium.

The samples employed in this experiment were cut from single crystals of nominal manganese ferrite.[7] One crystal (Mn-Fe ferrite) contained a small (but unknown) amount of ferrous ion as evidenced by the resistivity of the order of 10 ohm-cm;[8] the second contained a small quantity of zinc and had a resistivity of about 10^4 ohm-cm; the third was manganese ferrite of 10^5 ohm-cm resistivity. By tumbling small pieces in an air stream against abrasive material, spheres were ground which ranged in diameter from 0.2 to 0.8 mm. These spheres were oriented and mounted[9] on the sample post by an x-ray back reflection technique in such a way that a crystal [110] axis was parallel to the axis of the post.

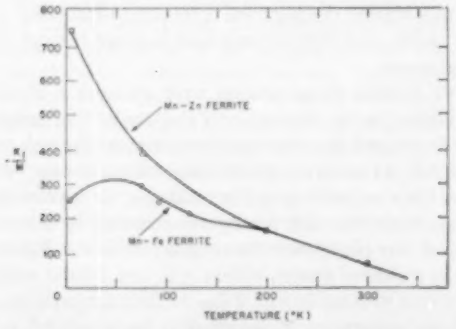

FIG. 2. Temperature variation of first-order anisotropy constant in two ferrites.

[7] Grown by G. W. Clark at Linde Air Products Company.

[8] J. H. Rowen, Bell Sys. 32, 1333 (1953) has demonstrated the extreme sensitivity of the dc conductivity to iron excess or deficiency from stoichiometry.

[9] Kindly performed by D. Tuomi and E. P. Warekois of Lincoln Laboratory.

With this arrangement, the dc magnetic field (which was always perpendicular to the rf magnetic field) could be pointed along all crystallographic directions in the (110) plane.

III. RESULTS

Reduction of Data

The general resonance condition for a ferromagnetic material subject to an effective magnetic field H_{eff} and a microwave field of frequency ω is[10]

$$\omega=\gamma H_{eff}.$$

γ, the gyromagnetic ratio, is equal to $g(e/2mc)$. H_{eff} includes effects due to magnetic anisotropy and sample shape demagnetization and is given by

$$H_{eff}^2=\left[H_a+(N_x-N_z)M+\frac{K_1}{M}f_x(\theta)+\frac{K_2}{M}g_x(\theta)\right]\times\left[H_a+(N_y-N_z)M+\frac{K_1}{M}f_y(\theta)+\frac{K_2}{M}g_y(\theta)\right],$$

where H_a is the externally applied field, M is the saturation magnetization, $N_{x,y,z}$ are the geometrical demagnetizing factors, and $K_{1,2}$ are the first- and second-order anisotropy constants; $f_{x,y}$ and $g_{x,y}$ are functions of θ, the angle between the [100] axis and H_a, calculated by Bickford.[11]

If H_{eff} is eliminated between the two equations above, three unknown quantities will appear: γ (or g), K_1/M, and K_2/M. ω is the fixed operating frequency, and for spheres $N_x=N_y=N_z$. Experimentally, H_a necessary for

[10] C. Kittel, Phys. Rev. 73, 155 (1948).

[11] L. R. Bickford, Technical Report No. 23, Laboratory for Insulation Research, Massachusetts Institute of Technology, 1949 (unpublished).

resonance is found for different θ's in the (110) plane. Three pairs of experimental quantities are substituted for θ and H_a, and the three equations are solved simultaneously. The three points chosen are the principal crystal axes $\theta=0°$, 55°, and 90° respectively. Experimental location of these points is facilitated because the applied field goes through an extremum at each.

At low microwave frequencies, resonance would occur before spherical samples could be magnetized; consequently at 2800 Mc/sec disk-shaped samples had to be employed. The arrangement in which the magnetic field is parallel to the plane of the disk is undesirable for two reasons. First, slight deviations from parallel surfaces seriously affect the resonance condition and half-width. Second, the internal dc field at which resonance occurs may not be large enough compared to the anisotropy to assure that the magnetization vector is lined up with the applied field.

The arrangement in which H_a is perpendicular to the plane of the disk is more satisfactory for line-width measurements. Clearly this precludes determination of K_1/M, K_2/M, and g; however, values for these parameters may be assumed from C-band results. If M is not known from independent measurements, it can

TABLE I. Ratio of first-order anisotropy constant to the saturation magnetization for Mn-Zn ferrite.

Frequency (Mc/sec)	K_1/M
5600	-73 ± 2
9100	-71 ± 1
24 000	-69 ± 1

be calculated on the basis of these assumptions. Subsequently then, all quantities are known to make the conversion from external to effective internal magnetic field.

Anisotropy

It must be kept in mind that even if K_2/M were as large as K_1/M, its contribution to the anisotropy energy would only be one-ninth that of K_1/M because of the usual normalization of anisotropy energy. Consequently we have attempted to calculate a second-order anisotropy from the data only when the anisotropy is large; even then K_2/M is not of much significance in the manganese ferrites. However, it should be stated that no combination of K_1/M, K_2/M, and g, gave a good fit to the angular variation of H_a. Furthermore, the frequency dependence of the anisotropy is very slight (or absent), and there is essentially no difference between Mn-Zn and Mn-ferrite. So if we are willing to limit ourselves to 10% accuracy, we can make the following simple statement: K_1/M, which is shown as a function of temperature for Mn-Fe ferrite and Mn-Zn ferrite in Fig. 2, is the same at all frequencies, and K_2/M is not significant.

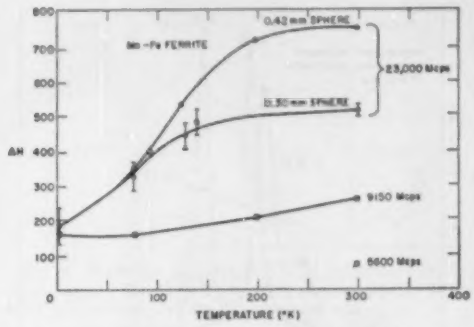

FIG. 3. Temperature dependence of the line width in Mn-Fe ferrite. No size-effect was apparent at 9150 Mc/sec.

Table I gives an example of the small variation of K_1/M with frequency. The largest second-order anisotropy encountered was of the order of $|K_2/M| \cong 2\times10^2$ oe.

g-Values

The value of g is constant at a value of 2.00 at all frequencies and temperatures measured in all three samples. Although occasional minor variations occurred, there was no consistent departure from 2.00. In most cases, g could be measured to an accuracy of ±0.01.

Line Width

The full widths at half-maximum susceptibility (ΔH) are shown plotted in Figs. 3 and 4 for Mn-Fe ferrite and Mn-Zn ferrite respectively. The graphs indicate both the temperature and frequency dependence of the line widths. Furthermore, for the Mn-Fe ferrite, which had the low resistivity, a size effect is apparent at 23 000 Mc/sec. However at 9150 Mc/sec the 0.30- and 0.42-mm spheres gave the same results. In the other samples, spheres ranging in diameter from 0.22 to 0.41 mm were used, where no size effect could be observed.

The Mn-Zn ferrite exhibits remarkably narrow lines at room temperature. The frequency dependence of ΔH is such that the narrowest lines occur at 5600 Mc/sec.

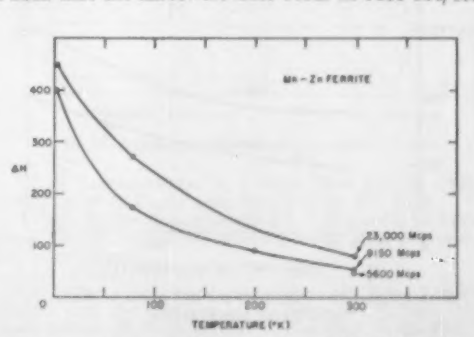

FIG. 4. Temperature dependence of the line width in Mn-Zn ferrite.

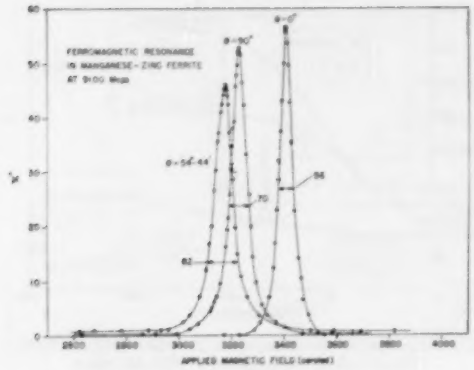

FIG. 5. Resonance absorption in the (110) plane, showing variations in line width.

With decreasing temperature, ΔH slowly increases and near 4.2°K shows a rapid broadening.

Another noteworthy feature is the directional dependence of the line width. The narrowest ΔH's occur in the [100] crystal directions and these are the ones that have been plotted in the graph. However, Fig. 5 shows the three resonance curves measured with the magnetic field applied in the three principal crystal axes. At other temperatures and frequencies the relative difference in line widths is approximately the same. Occasionally the [110] line width has been observed to fluctuate between the [100] and [111] extremes, but we attribute this to experimental uncertainties. Quite generally, the Mn-Zn and Mn ferrites gave identical results. Furthermore, data taken on Mn ferrite by Geschwind[12,13] at the Bell Telephone Laboratories give excellent agreement with the present results.

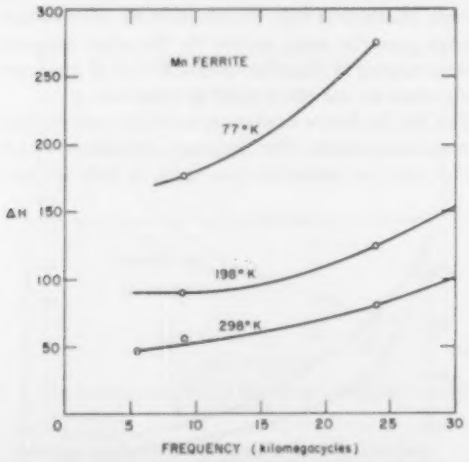

FIG. 6. Frequency variation of the line width in Mn-ferrite at different temperatures.

[12] S. Geschwind (private communication).
[13] Dillon, Geschwind, and Jaccarino, Phys. Rev. (to be published).

The frequency dependence of the Mn ferrite line width at three different temperatures is shown in Fig. 6. The qualitative behavior of ΔH seems to be approximately the same at the three temperatures. Data at 2800 Mc/sec have not been included as yet in the frequency dependence. We have made measurements on an 1/8-inch disk on Mn ferrite 6 mils thick with the magnetic field applied both parallel and perpendicular to the plane of the disk. The results indicate strongly that the line width tends to become broader than at 5600 Mc/sec. However, probably due to nonuniformities or cracks in the disk, the results are not consistent as yet. We hope to clarify this point by further measurements on other samples.

The behavior of Mn-Fe ferrite is completely different, as can be seen in Fig. 3. The lines are broad at room temperature and decrease in width with decreasing temperature. It appears to be a general rule that whenever a ferrite contains Fe^{++}, the temperature dependence of the line width is obscured, or even reversed, by the superposition of an additional loss mechanism.[14]

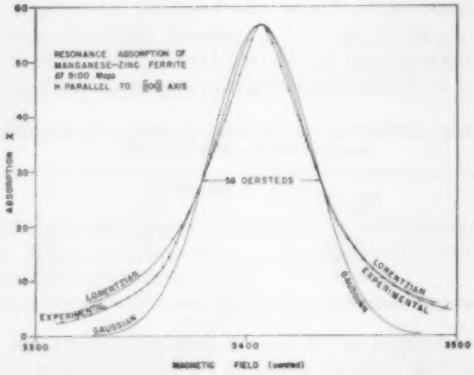

FIG. 7. Comparison of line shapes.

Line Shape

We have tried to fit a theoretical line shape expression to the experimental points measured on Mn-Zn ferrite at 9100 Mc/sec in the [100] direction. It can be seen from Fig. 7 that a Gaussian curve does not fit the data. However, a Lorentzian line gives closer agreement. The Lorentzian curve was expressed through a modification of the Bloch-Bloembergen relations[15] and gives for the absorptive component of the susceptibility:

$$\chi'' = 4\pi M H H_0 \Delta H / [(H^2 - H_0^2)^2 + H_0^2 (\Delta H)^2].$$

We have replaced the damping parameter $1/\gamma T_2$ by $\Delta H/2$, which is accurate to approximately 1% in

[14] Galt, Yager, and Merritt, Phys. Rev. 93, 1119 (1954) believe that there exist losses in ferrites near the magnetite transition temperature due to a relaxation in short-range order among the divalent and trivalent iron ions. Our data do not show a maximum in the temperature dependence of ΔH.
[15] N. Bloembergen, Phys. Rev. 78, 572 (1950).

the present case. The resonance field H_0 and the full width ΔH at half-maximum susceptibility were taken from the experimental data, namely $H_0=3407$ oe and $\Delta H=56$ oe. Furthermore, since the saturation magnetization is actually not known for this particular sample, the curves were also matched at their peaks.

Kramers-Krönig Relations

In one particular case, at 9100 Mc/sec on the Mn-Fe ferrite sample, we have made a precise measurement of the ferrite dispersion as well as absorption. According to the Bloch-Bloembergen expressions, the absorptive and dispersive components of the susceptibility are related by

$$\chi'=\chi''(H^2-H_0^2)/H_0\Delta H.$$

However, partly due to the Fe^{++} line broadening in Mn-Fe ferrite, the Bloch-Bloembergen expressions do not describe the data accurately. Therefore we have

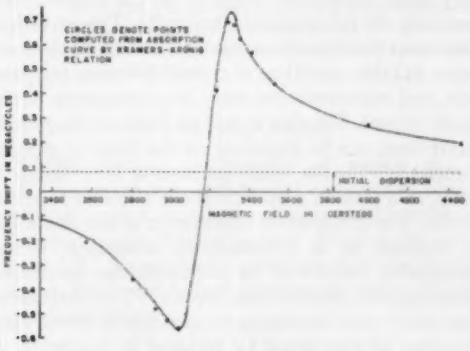
CIRCLES DENOTE POINTS COMPUTED FROM ABSORPTION CURVE BY KRAMERS-KRONIG RELATION
INITIAL DISPERSION
MAGNETIC FIELD IN OERSTEDS
FREQUENCY SHIFT IN MEGACYCLES

FIG. 8. Frequency shift of microwave cavity due to ferrite dispersion.

made a theoretical comparison between the absorption and dispersion data by way of the more general Kramers-Krönig relations.[16] The solid line in Fig. 8 is drawn through the solid points, which were measured from the frequency shift of the cavity. The heavy dots were computed from the corresponding absorption data. The absolute magnitude of the points has been adjusted arbitrarily. The fit can be regarded as satisfying the Kramers-Krönig relations.

Double Peaks

The behavior of all samples turned out to be rather remarkable at very low temperatures. At 4.2°K the samples of Mn-Zn ferrite and Mn ferrite showed double resonances in and near the hard crystal axes. In the case

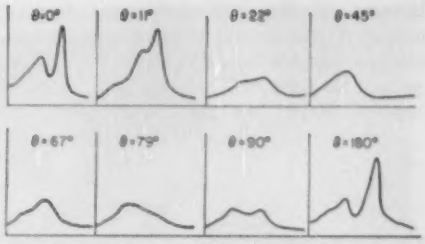

FIG. 9. Absorption as a function of magnetic field applied in various crystal directions in the (110) plane in Mn-Zn ferrite at 4.2°K and 9100 Mc/sec. $\theta=55°$ is the easy axis.

of the Mn-Fe ferrite, double peaks already occurred somewhere below 200°K.

Figure 9 shows the absorption as a function of magnetic field applied in various crystal directions. From measurements at 23 900 Mc/sec, where the usual single resonance is observed in all crystal directions, the anisotropy was found to be $K_1/M=-750$. It has been pointed out previously[17] that whenever the anisotropy becomes of the order of the applied magnetic field necessary for resonance, an additional resonance is possible in the nonaligned state of the magnetization vector. For spherical samples used here, the applied field necessary for resonance is the same as the resonance field in an infinite medium without anisotropy. In a thin disk, however, with the magnetic field applied along the plane of the disk, the external field need only be very small for gyromagnetic resonance and hence resonance in a nonaligned state becomes possible with relatively low anisotropy.[18] For the case of the magnetic field applied perpendicular to the plane of the disk, the situation is somewhat different.[19] In the present case the anisotropy is not sufficiently large to account for the double peaks directly. However, if we admit the possibility that some domain walls still exist, then the dynamic surface charges induced on the walls[20] may

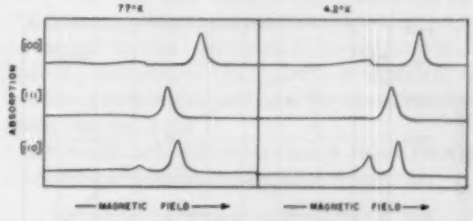

FIG. 10. Appearance of secondary peak at X-band.

[16] For a general discussion, see, e.g., J. H. Van Vleck, in *Propagation of Short Radio Waves*, edited by D. E. Kerr, *Radiation Laboratory Series* (McGraw-Hill Book Company, Inc., New York, 1951), Massachusetts Institute of Technology Radiation Laboratory Series, Vol. 13, Chap. 8.

[17] P. E. Tannenwald and H. J. Zeiger, Phys. Rev. **98**, 1562(A) (1955) and P. E. Tannenwald, Phys. Rev. **99**, 463 (1955).

[18] This is the condition under which A. F. Kip and R. D. Arnold, Phys. Rev. **75**, 1556 (1949), observed double peaks in a sheet of iron single crystal.

[19] See H. Suhl, Phys. Rev. **97**, 555 (1955).

[20] The effect of dynamic demagnetizing fields induced on 180° domain walls was proposed by D. Polder and J. Smit, Revs. Modern Phys. **25**, 89 (1953) and T. Nagamiya, Progr. Theoret. Phys. (Japan) **10**, 72 (1953). The latter used this model to explain Bickford's double peaks in magnetite at low temperatures.

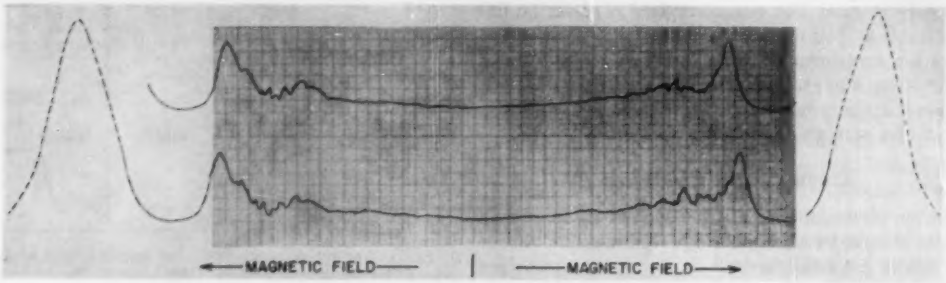

FIG. 11. Fine structure of secondary peak, showing extent to which it is reproducible upon field reversal and upon repetition. Sample is Mn-Fe ferrite single crystal, at 83°K, with field parallel to the [110] axis.

cause a sufficient modification of the simple double resonance condition. We plan to make the appropriate calculations for this type of situation.

The appearance of double peaks is somewhat different in Mn-Fe ferrite. Figure 10 shows the absorption at 77°K and 4.2°K in the three principal crystal axes. The second peak is absent at 23 000 Mc/sec.

Double peaks in ferromagnetic resonance absorption experiments have been reported as early as 1948 when Kip and Arnold showed that a second resonance peak in a sheet of iron single crystal was the result of incomplete alignment of the magnetization vector with the direction of the applied field.[21] Bickford[11] observed rather complex absorption spectra, including double peaks, in magnetite at low temperatures. It appears that double resonances are a quite general phenomenon in ferrites. The evidence from the present experiment suggesting failure of M to line up with H_a plus some remnant domain walls, is as follows:

(1) Double peaks do not occur in the easy crystal direction. (See Figs. 9 and 10.)

(2) Barkhausen-type jumps are observed on the initial rise of the low-field resonance. (See Fig. 11.)

(3) The location of the low-field peak in Mn-Fe ferrite varies with temperature in a similar fashion as the saturation magnetization. (See Fig. 12.)

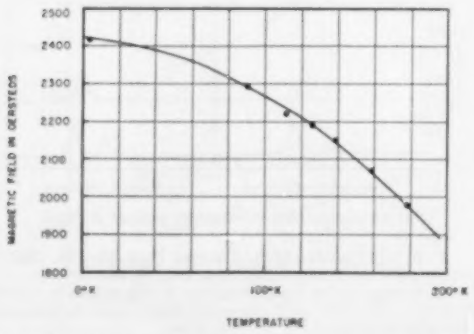

FIG. 12. Location of secondary peak with temperature in the [110] direction at X-band in Mn-Fe ferrite.

CONCLUSION

The most remarkable and at the same time theoretically least understood property of the single-crystal ferrites is the ferromagnetic line width. This investigation shows that lines as narrow as 47 oe can be obtained under suitable conditions of crystal direction, temperature, and microwave frequency in a manganese ferrite single crystal. Yet this is still an order of magnitude larger than can be explained on the basis of existing theories.[22,23] The line width increases at lower temperatures, in a fashion similar to Healy's results on nickel ferrite. The temperature dependence of the line width is reversed for a low-resistivity manganese ferrite, presumably because of an additional loss mechanism involving the divalent iron impurity. This decrease in line width with decreasing temperature is in the same direction as that found by Bickford in magnetite. In general the line width increases with frequency, but there is possibly a minimum in the vicinity of 5600 Mc/sec.

The g-values are close to 2.00 under all conditions. The anisotropy is insensitive to external magnetic field magnitude, but, as expected, increases sharply at lower temperatures. No change in sign was found in the first-order anisotropy constant, and the second-order constant is of relatively small significance. It is true on the other hand that a theoretical anisotropy fit to the experimental data using experimentally determined K_1/M, K_2/M, and g is less than satisfactory.

The Kramers-Krönig relations between absorption and dispersion are satisfied, and the line shape is roughly Lorentzian. It is interesting to note, however, that the areas under the resonance curves in the three principal crystal directions are not equal. (See Fig. 5.)

An increase in anisotropy as well as remnant domain walls are believed to be the basis of a mechanism resulting in secondary resonances, which can occur when

[21] A. F. Kip and R. D. Arnold, Technical Report No. 91, Research Laboratory of Electronics, Massachusetts Institute of Technology, 1948 (unpublished).

[22] C. Kittel and E. Abrahams, Revs. Modern Phys. **25**, 233 (1953).

[23] N. Bloembergen and S. Wang, Phys. Rev. **93**, 72 (1954).

the magnetization vector is not aligned with the applied magnetic field.

ACKNOWLEDGMENTS

The author takes pleasure in acknowledging the generous assistance of many persons in the completion of this work; particularly B. Lax for his constant encouragement and helpful criticism and J. O. Artman and R. N. Dexter for technical aid and suggestions; N. Bloembergen of Harvard University for reading and criticizing the manuscript, and W. H. Kleiner for helpful discussions.

PHYSICAL REVIEW VOLUME 100, NUMBER 6 DECEMBER 15, 1955

Thermal Conductivity of Indium-Thallium Alloys in the Normal and Superconducting States*†

NORMAN E. PHILLIPS‡
Department of Chemistry, The University of Chicago, Chicago, Illinois

(Received August 29, 1955)

Thermal conductivity measurements have been made on three indium-thallium alloys between 0.15° and 0.8°K. Temperature gradients were measured using carbon resistance thermometers. The alloys were of the type which show an increase in thermal conductivity on entering the superconducting state. At temperatures below 1°K the superconducting state thermal conductivity decreases rapidly with decreasing temperature, becoming roughly proportional to T^3 and to the grain size in the specimens at the lowest temperatures. The data are interpreted as meaning that phonon conductivity limited by boundary scattering is important in this region.

I. INTRODUCTION

THE thermal conductivity of metals can be separated into two terms—an electron conductivity K_e and a lattice or phonon conductivity K_g. The total conductivity K is then given by the sum of K_e and K_g. Experimental and theoretical results show that in the liquid helium temperature region K_e may be represented by[1]

$$1/K_e=\rho_0/L_0T+\alpha T^2, \tag{1}$$

where ρ_0 is the residual electrical resistance, L_0 is the Lorenz number $\frac{1}{3}(\pi k/e)^2$, α is a constant which depends on the strength of the phonon-electron interaction, and T is the temperature. The first term on the right-hand side of Eq. (2) represents the contribution to the thermal resistance of scattering of electrons by impurities, and the second term is the resistance due to scattering of electrons by phonons. At a given temperature the relative importance of the two terms depends on the impurity content and on the Debye temperature. For impure metals and alloys at low temperatures impurity scattering is always dominant, but for pure metals with a low Debye temperature phonon scattering may be important. For pure metals, K_e is the order of a few watt units at 1 or 2°K, but this value is reduced by the presence of strains or impurity atoms, and is two or three orders of magnitude smaller for alloys.

In the same temperature region K_g is usually limited by scattering of the phonons by conduction electrons and is proportional to T^3. At lower temperatures the mean free path of the phonons would be comparable to the crystal dimensions and presumably would be determined by the scattering of phonons at crystal boundaries. In this case K_g should have the same temperature dependence as the lattice specific heat and should be given by Casimir's formula.[2] A dependence of K_g on T^3 has been found in superconductors below 1°K [3,4] and in dielectric crystals over a wider temperature range.[5] In most pure metals K_g is very much smaller than K_e, and phonon conductivity is important only in alloys and in metals having a very small number of conduction electrons.

If the additional subscripts s and n denote the superconducting and normal states, then

$$K_s=K_{es}+K_{gs}, \tag{2a}$$

$$K_n=K_{en}+K_{gn}, \tag{2b}$$

where K_s and K_n are the total thermal conductivities of the same specimen in the two different states. K_n will be determined by the same factors considered above

* Based on a dissertation submitted in partial fulfillment of the requirements for the Ph.D. degree at the University of Chicago; the work was performed in the Low Temperature Laboratory of the Institute for the Study of Metals.

† Supported in part by a grant from the National Science Foundation.

‡ Present address: Department of Chemistry, University of California, Berkeley, California.

[1] For a review of thermal conductivities of metals at low temperature see: J. L. Olsen and H. M. Rosenberg, Advances in Phys. 2, 28 (1953).

[2] H. B. G. Casimir, Physica 5, 595 (1938).

[3] J. L. Olsen and C. A. Renton, Phil. Mag. 43, 946 (1952).

[4] K. Mendelssohn and C. A. Renton, Phil. Mag. 44, 776 (1953).

[5] R. Berman, Advances in Phys. 2, 103 (1953).

for normal metals, and the behavior of K_s will depend on which combination of heat transport mechanism and scattering process is important. For pure metals, in which $K_{en} \gg K_{gn}$, K_s/K_n decreases rapidly as T is decreased below T_c, the temperature of the superconducting transition in zero magnetic field. The experimental ratios are in reasonable agreement with Heisenberg's calculations for the case in which the electron mean free path is limited by impurity scattering. For impure metals the ratio K_s/K_n does not decrease as rapidly with decreasing T as it does for pure metals, and for several alloys values of $K_s/K_n > 1$ have been reported. Mendelssohn and Olsen[6] have suggested that K_s/K_n may be greater than unity in alloys because of the presence of a circulation heat flow, analogous to that in liquid helium, when the alloy is in the superconducting state. However, Klemens[7] has pointed out that this mechanism for heat transport would be present even in pure metals and would in any case be too small to explain the observed values of K_s. An alternative explanation suggested by Hulm[8] is that the superconducting electrons do not interact with the lattice and make no contribution to scattering of the phonons. On the basis of this suggestion K_{gs} would be greater than K_{gn}, and when the specimen enters the superconducting state the increase in K_g might more than compensate for the decrease in K_e. This could happen only in alloys for which K_{gn} is comparable in magnitude with K_{en}.

Sladek[9] has measured K_s and K_n for a series of single-crystal indium-thallium alloys ranging in composition from pure indium to 20 atom percent thallium. For pure indium $K_s/K_n < 1$ for all temperatures; for the 5% thallium specimen K_s falls below K_n as T decreases from T_c, but at about 2°K the curve for K_s bends toward that for K_n and apparently crosses it at 1.3°K—the lowest temperature at which measurements were made; for the 15% and 20% specimens, K_s/K_n is greater than unity for all temperatures from T_c down to 1.3°K, and there is some indication of a minimum in K_s at about 1.4°K.

The present paper describes thermal conductivity measurements at temperatures below 1°K on some of these alloy specimens. The experiments were undertaken in the hope that a study of the dependence of K_s on temperature and crystal size would give some indication of the mechanism by which K_s becomes greater than K_n.

II. EXPERIMENTAL

The Apparatus

Figure 1 shows the essential features of the apparatus. Temperatures below 1°K were produced by adiabatic demagnetization of the salt pill N from a starting temperature of about 1.3°K. The salt was cylindrical in shape, 10 cm in length, and 2.5 cm in diameter. Thermal contact between the salt and the thermal conductivity specimen was made by a method described by Mendoza[10]; the powdered salt was pressed onto a system of thin copper vanes under a pressure of about 20 tons/sq in. The tops of the vanes were connected through a thin copper disk M to a copper wire J using an alloy of copper, silver, and phosphorus as solder. The top of the copper wire was soldered to the lower end of the thermal conductivity specimen F. Two carbon resistance thermometers E and a resistance heater D were attached to the specimen as shown. The thermometers were prepared by painting a thin layer of colloidal graphite onto a Formex insulated copper wire, stripping the Formex from one end of the wire, and soldering that end to the specimen. The heater was similar to the thermometers except that the layer of carbon was replaced with a 2000-ohm coil of manganin wire held in place with varnish. Electrical leads to the heater and thermometers consisted of 20-cm lengths of number 40 manganin wire tinned with soft solder and therefore superconducting at the temperatures of measurement; they were taken out into the helium bath through Kovar seals B. The salt pill was supported by threads inside a fiber tube (not shown), and the specimen was supported from the salt by stiffening the copper wire J with a Plexiglas tube. The salt pill and specimen were contained in a glass tube R which was connected by the copper-glass seal C to a pumping

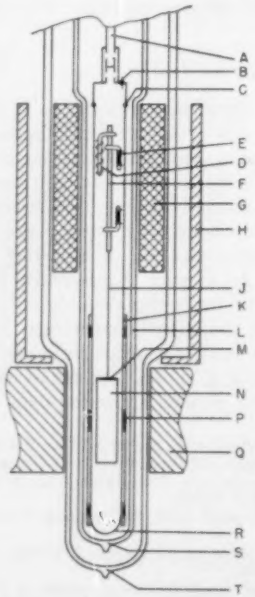

FIG. 1. The apparatus.

[6] K. Mendelssohn and J. L. Olsen, Proc. Phys. Soc. (London) **A63**, 2 (1950).
[7] P. K. G. Klemens, Proc. Phys. Soc. (London) **A66**, 576 (1953).
[8] J. K. Hulm, Proc. Roy. Soc. (London) **A204**, 98 (1950).
[9] R. J. Sladek, Phys. Rev. **97**, 902 (1955).
[10] E. M. Mendoza, Ceremonies Langevin-Perrin, Paris, 1948.

tube A. The pumping tube led to the usual system for introducing and pumping out exchange gas. The helium and nitrogen Dewars are shown at S and T, and the magnet pole pieces at Q. A solenoid G was capable of producing magnetic fields of 1000 gauss in the region of the specimen.

The data of Sladek on the same alloy specimens used in the present investigation have shown that it is essential not to expose the specimen to magnetic fields greater than the critical field H_c (or $\frac{1}{2}H_c$ if the field is transverse) at any time after it has become superconducting. Otherwise, it would be left with "frozen-in flux" in the superconducting state and the observed thermal conductivity would differ from the correct value. For this reason a cylindrical iron shield H was placed around the outside of the cryostat in the neighborhood of the specimen. The shield reduced the fringing field of the magnet at the lower end of the specimen to about 80 gauss.

Since the salt, and also the specimen, warmed up during the magnetization, it was necessary to prevent them from warming to a temperature at which the transverse field of 80 gauss would exceed $\frac{1}{2}H_c$. The temperature of the lower thermometer was followed continuously during the magnetization of the salt, and the field was increased slowly, allowing the exchange gas to conduct away the heat of magnetization so that the temperature never rose above 1.4°K. The H_c-T relation for indium-thallium alloys is approximately parabolic,[11] with $H_c(T=0)$ about 280 and a zero-field transition temperature of about 3.3°K. Therefore, at 1.4°K the critical field is about 230 gauss, and the presence of a transverse field of 80 gauss during the magnetization should have no effect on subsequent measurements of thermal conductivity. The shield was removed whenever magnetic measurements were made on the salt.

A mutual inductance was wound on a plastic coil former K (Fig. 1) fastened to the outside of the glass vacuum container. The secondary consisted of a main coil P of 3000 turns connected in series-opposition with two compensating coils L of 1500 turns each. The primary was a uniform solenoid wound over the whole length of the coil former, but with extra turns added at the ends. The number of extra turns was adjusted so that in the absence of the salt the total mutual inductance was almost zero. This arrangement also provided a uniform primary field over the length of the salt pill.

Calibration of the Salt

Susceptibility measurements on the salt were made by observing the deflection θ in a ballistic galvanometer connected to the secondary coils, when a current i was made or broken in the primary. A fixed mutual inductance in the secondary circuit was used to check the sensitivity of the galvanometer. Below 1°K the magnetic temperature T^* was defined by the usual relation[12]:

$$(\theta-\theta_0)(T^*-\Delta)=Ai,$$
$$\Delta=\delta'+c(4\pi/3-n)=\delta'+\delta. \quad (3)$$

The constants A and θ_0 were determined by measurements of θ in the helium region, where T^* was set equal to the thermodynamic temperature T; c is the Curie constant/cm^3, and n is the demagnetizing factor for the salt. δ' corrects for deviations from Curie's law for a salt pill of spherical shape.

Chromium potassium alum and copper potassium Tutton salt were both used as cooling agents. By taking for n the value it would have for an ellipsoid of the same length and diameter, the values of Δ were as follows: for the chromium salt $\delta'=0$ and $\delta=0.022°$; for the copper salt $\delta'=0.035°$ [13] and $\delta=0.006°$. Strictly speaking, the above treatment is valid only for ellipsoids; for cylinders, the demagnetizing field is not uniform and cannot be defined. However, since the length of the salt was four times its diameter and the measuring coils were well removed from the ends, the nonuniform demagnetizing field should not have introduced an error of more than a few thousandths of a degree.

Calibration of the Thermometers

Following a demagnetization to the lowest attainable temperature, the salt was allowed to warm with no power input to the heater. The residual heat leak produced a temperature rise of the order of 0.001 deg/min or less. During the warm-up period successive measurements of the thermometer resistances and ballistic galvanometer deflections were made. From the ballistic measurements a graph of temperature *versus* time was constructed, and the temperature of the salt at the time corresponding to each resistance measurement was obtained by interpolation. On the assumption that the thermometers and the salt were at the same temperature, it was then possible to make a calibration curve for each thermometer.

Thermal Conductivity Measurements

Thermal conductivities were measured by demagnetizing the salt and then making resistance measurements on the two thermometers with a heat current flowing through the specimen. Values of the temperature difference and mean temperature were read from graphs of temperature *versus* time and were combined with the heater power to give the thermal conductivity as a function of temperature. Whenever possible, the heater current was chosen to give tem-

[11] J. W. Stout and L. Guttman, Phys. Rev. **88**, 703 (1952).

[12] N. Kurti and F. Simon, Phil. Mag. **26**, 849 (1938).

[13] R. J. Benzie and A. H. Cooke, Proc. Phys. Soc. (London) **63**, 213 (1950).

perature differences of about 10% of the absolute temperature. At temperatures above 0.5°K this was not usually practical because of the combined effect of the high thermal conductivity of the specimen and the low heat capacity of the salt.

Errors

The total heat leak to the salt-specimen system was almost constant at about 1 microwatt. Because the heat capacity of the salt was so much larger than that of the specimen, any part of the residual heat leak which was directed to the specimen would have to flow to the salt. The resulting heat current would produce a temperature gradient in the specimen and copper wire and would therefore introduce an error into the thermometer calibration.

The temperature difference between the two thermometers during the calibration run can easily be shown to produce no error in the thermal conductivity measurements, if it is assumed that the distribution of the residual heat leak over the length of the specimen is the same in the thermal conductivity run as in the calibration run. This assumption seems to be justified by the fact that when the heater is turned on the temperature difference between the upper end of the specimen and the bath changes by no more than a few percent and the heat leak (exclusive of heater current) is unchanged.

The thermal resistance between the lower thermometer and the salt was measured and was found to be in rough agreement with that found for salt-metal interfaces by Mendoza[13] and Goodman.[14] By assuming that the fraction of the residual heat leak which goes to the specimen is proportional to its area, the temperature difference between the lower thermometer and the salt during the calibration was estimated to be about 0.002° at 0.15°K and to be negligible above 0.25°K. Even at the lowest temperatures this will not introduce an error of more than a few percent into the thermal conductivities, because the error in both thermometers is in the same direction and partially cancels in measuring temperature differences.

The ballistic galvanometer could be read to better than 1 mm, and below 1°K the primary current was adjusted to give a deflection of 60 to 80 cm. Equation (3) then shows that T^* is measured to approximately 1 part in 1000. This also represents the precision of the thermometer calibration. Therefore, when temperature differences of $0.1T^*$ were used, ΔT^* could be measured to about 2%, but as was pointed out above this was not always possible. If we neglect for the moment differences between T^* and T, the measured thermal conductivity points should be accurate to about 3% below 0.4°K but at higher temperatures the low resistance specimens may be as much as 10% in error.

[14] B. B. Goodman, Proc. Phys. Soc. (London) A46, 217 (1953).

III. RESULTS

Copper Specimen

With the magnetic fields available it was not possible to cool chrome alum below 0.25°K, and measurements at lower temperatures had to be made by using copper potassium Tutton salt as the cooling agent. Unfortunately, the heat capacity of the copper salt was so small at the higher temperatures that it could not be used above 0.25°K. It will be seen from the results for indium-thallium alloys that measurements made with the two salts do not join smoothly at 0.25°K and that values of K_n obtained with the chromium salt deviate from a straight line below 0.4 or 0.5°K. The results of some measurements on a copper specimen are shown in Fig. 2 and are introduced at this point to illustrate more clearly the nature of the discrepancy. The thermal conductivity is proportional to the temperature, at least at the higher temperatures, and the value of the proportionality constant is approximately the same as that found for another copper specimen by Nicol and Tseng.[15]

It seems clear that the difference in the results obtained with the two salts must be a consequence of different relations between T^* and T. For copper potassium Tutton salt the difference between T^* and T is probably small above 0.1°K [16]; this is in agreement with the observation that the values of K obtained with this salt fall on the same straight line through the origin as the points obtained above 0.5°K with chrome

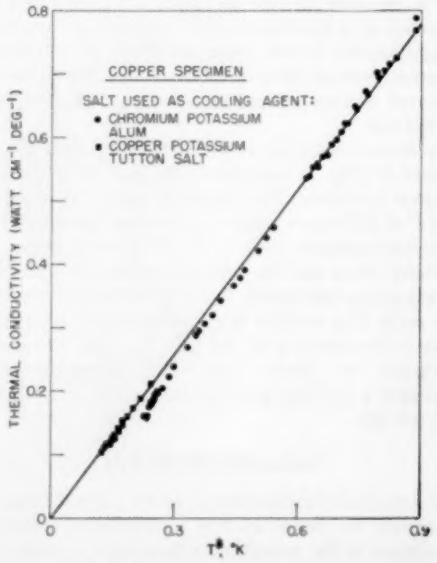

FIG. 2. Thermal conductivity of the copper specimen.

[15] James Nicol and T. P. Tseng, Phys. Rev. 92, 1062 (1953).
[16] C. G. B. Garrett, Ceremonies Langevin-Perrin, Paris, 1948.

alum and leads to the conclusion that this line represents K as a function of T. The difference between T^* and T for chrome alum would then have to be about twice as great at 0.25°K as measured by Bleaney using the γ-ray heating method.[17] There is a considerable amount of conflicting data on the low-temperature properties of chrome alum which is sometimes thought to indicate the possibility that these properties depend on the previous treatment of the salt, and while there has been no such evidence bearing directly on the present question it is possible that this provides an explanation for the unexpectedly large deviations from a straight line of the chrome alum points.

Indium-Thallium Alloys

Measurements of the thermal conductivity in the normal and superconducting states have been made on three indium-thallium alloys—a 15% thallium polycrystalline specimen with a grain size of 1 or 2 mm, a 15% single crystal, and a 20% thallium single crystal. The measurements of K_s extend from about 0.15°K to about 0.8°K but K_n was measured only down to 0.25°K. The specimens were 6 mm in diameter and were originally prepared by Stout and Guttman,[11] who have reported on their magnetic and electric properties. Sladek has made thermal conductivity measurements on the two single crystals above 1°K, but, since it was not clear from his work with higher thallium content polycrystals whether or not grain size had any effect on K_s above 1°K, measurements on the 15% polycrystal in the helium region are included in the work reported here. The measurements above 1°K were carried out by placing the copper wire attached to the specimen in thermal contact with the helium bath instead of with the salt.

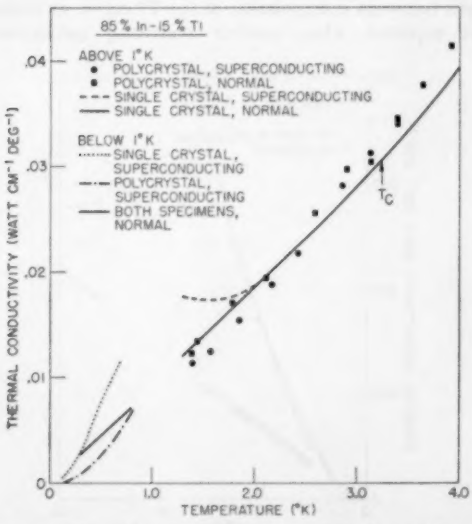

FIG. 3. Thermal conductivity of the 15% thallium single and polycrystal specimens. The curves for the single crystal above 1°K are from Sladek's measurements.

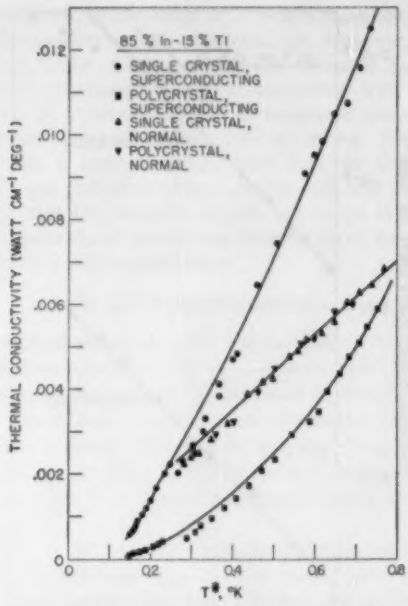

FIG. 4. Thermal conductivity of the 15% thallium specimens below 1°K.

Figure 3 shows the smoothed values of K_s and K_n for the two 15% specimens below 1°K, Sladek's smoothed curves for the 15% single crystal above 1°K, and the experimental points for the 15% polycrystal above 1°K. The experimental points for the same specimens below 1°K are shown in Fig. 4. In all figures the curves are drawn to fit the low temperature points obtained using the copper Tutton salt as the cooling agent. Figure 5 is a log-log plot of K_s *versus* T for the same specimens; the low-temperature points obtained with chrome alum are omitted in the belief that they do not represent the correct temperature dependence of K_s. Data for the 20% specimen are plotted in Fig. 6.

IV. DISCUSSION

It is evident from Figs. 3–5 that, although the presence of grain boundaries has no effect on K_n, it has a marked effect on K_s. The absence of an effect on K_n is easily understood in terms of the concept of thermal conductivity as a product of the heat capacity, velocity, and mean free path of the heat carriers. Sladek has analyzed the data for the 15% single crystal to give the separate contributions of the electrons and phonons to the thermal conductivity. The mean free paths of both phonons and electrons—estimated by equating Sladek's values of K_{gs} and K_{es} to the product

[17] B. Bleaney, Proc. Roy. Soc. (London) **A204**, 216 (1951).

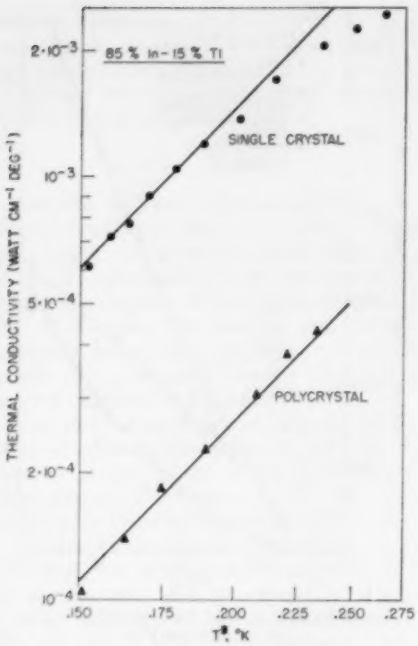

FIG. 5. Plot of $\log K_s$ *versus* $\log T$ for the 15% thallium specimens showing only points obtained with copper potassium Tutton salt. The straight lines are drawn with a slope of three.

of the heat capacity, velocity, and mean free path of the phonons and electrons respectively—are several orders of magnitude smaller than the grain size in the polycrystal. Therefore, it is to be expected that the presence of grain boundaries should not influence K_n. The difference in K_s between the two 15% specimens can be explained if it is supposed that the mean free path of one of the heat carriers is much longer in the superconducting state than in the normal state. Qualitatively, the experimental results agree with Hulm's suggestion that the mean free path of phonons becomes longer in the superconducting state and that it is this effect which makes $K_s > K_n$ in the neighborhood of 1°K.

On the basis of this explanation the maximum observed in K_s for the single crystals is similar in origin to the one occurring in dielectric crystals at temperatures in the helium region and above. On the high-temperature side the mean free path of the phonons decreases more rapidly with increasing temperature than their heat capacity increases (the decrease is caused by electron scattering in the present case and by Umklapp processes in the dielectric crystals). On the low-temperature side the mean free path is constant, limited only by crystal dimensions, and the temperature dependence of the conductivity is determined by the lattice heat capacity. (In the present case there is also the complication of a second heat transport mechanism being important on the high-temperature side.)

The above interpretation is very similar to that given by Laredo[18] in connection with his measurements on a series of tin specimens. He concluded that at temperatures well below 1°K the contribution of electron conductivity to K_s became negligible and that the phonon mean free path was determined by boundary scattering.

A quantitative comparison with theory is possible only at the lowest temperatures. No theory has been developed for phonon conductivity under the conditions that would exist in the present case near 1°K. At lower temperatures, however, the contribution to K_s from electron conductivity probably decreases exponentially, becoming negligible at a few tenths of a degree, and if scattering of phonons by electrons decreases until only grain boundary scattering is important K_s should be given by the theory developed by Casimir for dielectric crystals.[2] Casimir's formula predicts a conductivity proportional to T^3 and to the diameter of the crystal (for long single crystals of uniform cross section). Figure 5 shows that for the polycrystal K_s is proportional to T^3 between 0.15 and 0.25°K and that for the single crystal the slope of $\log K_s$ *versus* $\log T$ increases with decreasing T but becomes equal to three below 0.2°K. Furthermore, in the region in which K_s is proportional to T^3 for both 15% specimens it is greater for the single crystal by a factor of about five, which is approximately the ratio of the diameter of the single crystal to the grain size of the polycrystal. This suggests that at the lowest temperatures K_s is entirely a lattice conductivity limited by the grain-boundary scattering of phonons. At temperatures above the T^3 region K_s falls below an extrapolation of the T^3 curve, as would be expected when another scattering mechanism

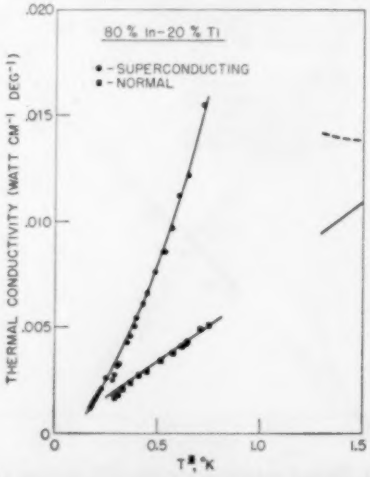

FIG. 6. Thermal conductivity of the 20% thallium specimen. The curves above 1°K are from Sladek's measurements.

[18] S. J. Laredo, Proc. Roy. Soc. (London) **A229**, 473 (1955).

(electron scattering) becomes important. For the 20% single crystal the slope of a $\log K_s$ *versus* $\log T$ plot (not shown) is increasing with decreasing T but is still only 2.5 at 0.15°K.

Although K_s becomes proportional to T^3 and to grain size, the magnitude of the conductivity is about ten times smaller than the value calculated from Casimir's formula using a Debye temperature of 100. Experiments on dielectric crystals show that Casimir's formula gives values of the conductivity which are in some cases an order of magnitude too high (in some cases the agreement is good). These discrepancies are probably connected with the presence of some type of lattice imperfection and their existence shows that the lack of quantitative agreement need not exclude the interpretation of K_s given above. In addition to the usual types of imperfections there is, in the indium-thallium alloys, the additional possibility that there were small normal-state regions "frozen in" when the specimen first became superconducting (the earth's field was not compensated). There would undoubtedly be some normal regions formed at the ends of the specimen during the magnetization of the salt even though the field did not exceed $\frac{1}{2}H_c$ but it is unlikely that these extended into the part of the specimen between the thermometers to any appreciable extent. Any resistance due to these effects cannot be too large or it would mask the observed dependence of K_s on crystal size. However, the observed factor of five between the values of K_s for the 15% specimens is not incompatible with the presence of a certain amount of resistance due to a mechanism other than boundary scattering. In this connection it must be remembered that the Casimir formula was derived for long cylinders and that in the present case the irregular shapes and range of sizes of the grains make the relation between grain size and conductivity very approximate.

V. ACKNOWLEDGMENTS

The writer wishes to thank the members of the low temperature laboratory for their interest and advice. In particular, Professor E. A. Long and Professor J. K. Hulm contributed much helpful discussion of the problems involved. The indium-thallium alloys were provided by Professor J. W. Stout and Professor L. Guttman; Dr. J. A. Rayne helped with many of the experiments.

The E. I. du Pont de Nemours Company and the Union Carbide and Carbon Company have very generously provided fellowships during the period in which the experiments were carried out.

Theory of the Hyperfine Structure of the NO Molecule. II. Errata and Some Additional Discussion*

CHUN C. LIN,† *Harvard University, Cambridge, Massachusetts*

AND

MASATAKA MIZUSHIMA,‡ *Department of Physics, Duke University, Durham, North Carolina*

(Received August 4, 1955)

A theoretical formula for the magnetic hfs of diatomic molecules previously given by one of us (M.M.) is revised by including the Fermi term and correcting an error in the choice of phase. The new formula gives $eQq=-1.7$ Mc/sec and $eQq'=22$ Mc/sec for the $^2\Pi$ state of the NO molecule. It was found that these constants together with the values $a=23.14$ Mc/sec, $b=14.056$ Mc/sec, for the parameters of the magnetic hfs, defined in the first paper give theoretical frequencies which explain not only $1/2\rightarrow3/2$ spectra but also the $3/2\rightarrow5/2$ transitions of the $^2\Pi_{\frac{3}{2}}$ state. A discussion on the theory of the magnetic resonance spectrum of the $^2\Pi_{\frac{3}{2}}$ state is also given.

NOTE ON MAGNETIC HFS

ALTHOUGH the first-order theory of the magnetic interaction of NO has been given by several authors,[1-3] the second-order effects remain to be examined. The Hamiltonian for NO, exclusive of nuclear quadrupole and Λ-doubling effect, can be written as[4]

$$\begin{aligned}H&=H_0+H_1,\\ H_0&=D\Lambda S_z+B[(J_x-S_x)^2+(J_y-S_y)^2]\\ &\qquad+2B(J_xS_x+J_yS_y),\\ H_1&=-2B(J_xS_x+J_yS_y)\\ &\quad+\frac{2g_n\beta_n\beta}{r^3}\left[\mathbf{I}\cdot\mathbf{L}+\frac{3(\mathbf{I}\cdot\mathbf{r})(\mathbf{S}\cdot\mathbf{r})}{r^2}-\mathbf{I}\cdot\mathbf{S}\right]\\ &\quad+\frac{16\pi}{3}g_n\beta_n\beta|\psi(0)|^2(\mathbf{I}\cdot\mathbf{S}).\end{aligned}\tag{1}$$

Here D and B represent the spin-orbit coupling constant and the rotational constant, respectively, of NO. The other symbols have a fairly standard significance. We shall construct the Hamiltonian matrix in a Hund's case (a) representation, i.e., a representation where Ω, Σ, Λ, J, I, and F are diagonal. H_0 is completely diagonal in this scheme and will be taken as the unperturbed Hamiltonian. If we introduce the symbols a, b, c, and d as defined by Dousmanis[5] (also by Frosch and Foley[1]), the matrix elements of H_1 can be expressed as

$$(\Sigma,\Omega,J|H_1|\Sigma,\Omega,J)=-\tfrac{1}{2}\Omega[a\Lambda+(b+c)\Sigma]R(J)[J(J+1)]^{-1},\tag{2}$$

$$(\Sigma,\Omega,J|H_1|\Sigma,\Omega,J-1)=-\tfrac{1}{2}[a\Lambda+(b+c)\Sigma](J^2-\Omega^2)^{\frac{1}{2}}\times f(J)[J(4J^2-1)^{\frac{1}{2}}]^{-1},\tag{3}$$

$$(\Sigma,\Omega,J|H_1|\Sigma\pm1,\Omega\pm1,J-1)=\mp\tfrac{1}{2}b[(J\mp\Omega)(J\mp\Omega-1)]^{\frac{1}{2}}[S(S+1)-\Sigma(\Sigma\pm1)]^{\frac{1}{2}}\times f(J)[J(4J^2-1)^{\frac{1}{2}}]^{-1},\tag{4}$$

$$(\Sigma,\Omega,J|H_1|\Sigma+1,\Omega+1,J)=\tfrac{1}{2}b[J(J+1)-\Omega(\Omega+1)]^{\frac{1}{2}}[S(S+1)-\Sigma(\Sigma+1)]^{\frac{1}{2}}\times R(J)[J(J+1)]^{-1}+B[J(J+1)-\Omega(\Omega+1)]^{\frac{1}{2}}\times[S(S+1)-\Sigma(\Sigma+1)]^{\frac{1}{2}},\tag{5}$$

$$(\Sigma=-\tfrac{1}{2},\Omega=\tfrac{1}{2},J|H_1|\Sigma=\tfrac{1}{2},\Omega=-\tfrac{1}{2},J)=\tfrac{1}{4}d(J+\tfrac{1}{2})R(J)[J(J+1)]^{-1},\tag{6}$$

$$(\Sigma=\mp\tfrac{1}{2},\Omega=\pm\tfrac{1}{2},J|H_1|\Sigma=\pm\tfrac{1}{2},\Omega=\mp\tfrac{1}{2},J-1)=\pm\tfrac{1}{8}df(J)/J,\tag{7}$$

where

$$f(J)=[(F+J-I)(F+I-J+1)\times(F+I+J+1)(J+I-F)]^{\frac{1}{2}},\tag{8}$$

$$R(J)=J(J+1)+I(I+1)-F(F+1).$$

We have omitted the "high-frequency" matrix elements connecting Λ and Λ±1. The first-order magnetic interaction energy arises from the matrix elements (2) and (6). To obtain the second-order correction we apply a Van Vleck transformation[6] to remove the nondiagonality in J and Ω. It is then found that all the second-order terms are negligibly small except the one arising from the matrix elements of the type (5), where $\Sigma=-1/2$, $\Omega=1/2$. This is the one which comes from the mixture of $\Pi_{\frac{1}{2}}$ state and $\Pi_{\frac{3}{2}}$ state. Although the effect of this mixing was already taken into account in the formula (36) of Part I, the Fermi-type hfs effect was neglected there. The following formula is the

* This research was supported in part by the United States Air Force through the Office of Scientific Research of the Air Research and Development Command.

† duPont Company predoctoral fellow (Chemistry), 1954–1955. Present address: Department of Physics, University of Oklahoma, Norman, Oklahoma.

‡ Present address: Department of Physics, University of Colorado, Boulder, Colorado.

[1] R. A. Frosch and H. M. Foley, Phys. Rev. **88**, 1337 (1952).

[2] M. Mizushima, Phys. Rev. **94**, 569 (1954). It is called Part I or I in this paper.

[3] G. C. Dousmanis, Phys. Rev. **97**, 967 (1955).

[4] J. H. Van Vleck, Revs. Modern Phys. **23**, 213 (1951).

[5] See, for example, E. C. Kemble, *The Fundamental Principles of Quantum Mechanics* (McGraw-Hill Book Company, Inc., New York, 1937), p. 394.

generalization of the formula (36) of I:

$$\Delta W_{c,d}=-(b\nu/8)[(2J+3)(2J-1)]^{\frac{1}{2}}[J(J+1)]^{-1}\times[F(F+1)-I(I+1)-J(J+1)] \quad (9)$$

where

$$b=-g_n\beta_n\beta\left\langle\frac{3\cos^2\theta-1}{r^3}\right\rangle_{av}+(16\pi/3)g_n\beta_n\beta|\psi(0)|^2.$$

This formula gives

$$\Delta P_{c,d}(J=3/2)=+0.20 \text{ Mc/sec} \quad (10)$$

as a contribution to the value of P (formula (39) of Part I) of the $J=3/2$ state, instead of the former value +0.18 Mc/sec, and is closer to +0.23 Mc/sec required from the experimental result.

ERRATA ABOUT ELECTRIC QUADRUPOLE HFS

There was an error in the calculation published by one of the present authors[2] on the same title, and the formula for the electric quadrupole hfs obtained there was wrong. The error came from the formula (A6) of Part I:

$$(^2\Pi_{\frac{1}{2}}Jm|=(4J+2)^{-\frac{1}{2}}[(2J-1)^{\frac{1}{2}}(KSJm|+(2J+3)^{\frac{1}{2}}(K+1SJm|]$$

In that paper the same formula for $(J_+m|$ and $(J_-m|$ states, where J_+ and J_- mean states where the component of J along the molecular axis is positive and negative, respectively, was used. The correct wave function should be

$$(^2\Pi_{\frac{1}{2}}J_+m|=(4J+2)^{-\frac{1}{2}}[(2J-1)^{\frac{1}{2}}(K_+SJm|+(2J+3)^{\frac{1}{2}}(K+1_+SJm|], \quad (11a)$$

and

$$(^2\Pi_{\frac{1}{2}}J_-m|=(4J+2)^{-\frac{1}{2}}[(2J-1)^{\frac{1}{2}}(K_-SJm|-(2J+3)^{\frac{1}{2}}(K+1_-SJm|]. \quad (11b)$$

These wave functions give the following result for the nuclear electric quadrupole effect:

$$W_{c,d}'=eQqY(F)[3(\tfrac{1}{2})^2(J^2+J)^{-1}-1], \quad (12)$$

where

$$Y(F)=[\tfrac{3}{4}C(C+1)-J(J+1)I(I+1)]\times[2(2J-1)(2J+3)I(2I-1)]^{-1},$$

instead of the formulas (30) of Part I.

Formula (12) is nothing but the usual formula for a symmetric top molecule and the anomaly reported in I was fallacious. Accordingly, the formulas (42) and (43) in I which gave the value of the coupling constant of the electric hfs should be changed. The correct value for them will be given below. The formulas (44) and (46) should be revised also.

NEW FORMULA FOR ELECTRIC QUADRUPOLE HFS

It was emphasized in Part I that a rotational state of the ground electronic state is not a pure $^2\Pi_{\frac{1}{2}}$ state, but a small amount of $^2\Pi_{\frac{1}{2}}$ state is mixed because of the end-over-end rotation (Zeeman effect showed $^2\Sigma$ is also mixed to a still smaller extent[6]). Thus, the wave functions $(J_+m|$ and $(J_-m|$ should be

$$(J_\pm m|=\mu(^2\Pi_{\frac{1}{2}}J_\pm m|+\nu(^2\Pi_{\frac{1}{2}}J_\pm m|, \quad (13)$$

where one should take upper or lower signs together. Each rotational state splits into two, because of the Λ-type doubling, and their wave functions are

$$(cJm|=2^{-\frac{1}{2}}\{(J_+m|+(J_-m|\}, \quad (14a)$$

$$(dJm|=2^{-\frac{1}{2}}\{(J_+m|-(J_-m|\}, \quad (14b)$$

where c designates the lower component and d the higher.

If we express the interaction between electrons and the nuclear electric quadrupole moment as

$$H_2=\mathbf{Q}\cdot\nabla E, \quad (15)$$

it is evident that H_2 is diagonal in Σ (component of spin along the molecular axis) since H_2 does not contain any spin coordinates. Thus, only

$$(^2\Pi_{\frac{1}{2}}J_\pm m|H_2|^2\Pi_{\frac{1}{2}}J_\pm m), \quad (^2\Pi_{\frac{1}{2}}J_\pm m|H_2|^2\Pi_{\frac{1}{2}}J_\mp m)$$

and

$$(^2\Pi_{\frac{1}{2}}J_\pm m|H_2|^2\Pi_{\frac{1}{2}}J_\pm m)$$

are finite while all the other matrix elements are zero. We obtain from the formulas (14a), (14b), and (15):

$$(cJm|H_2|cJm)=A'+B', \quad (16a)$$

$$(dJm|H_2|dJm)=A'-B', \quad (16b)$$

where

$$A'=\{(^2\Pi_{\frac{1}{2}}J_+m|H_2|^2\Pi_{\frac{1}{2}}J_+m)+(^2\Pi_{\frac{1}{2}}J_-m|H_2|^2\Pi_{\frac{1}{2}}J_-m)\}/2, \quad (16c)$$

$$B'=\nu\{(^2\Pi_{\frac{1}{2}}J_+m|H_2|^2\Pi_{\frac{1}{2}}J_-m)+(^2\Pi_{\frac{1}{2}}J_-m|H_2|^2\Pi_{\frac{1}{2}}J_+m)\}/2. \quad (16d)$$

We assumed $|\mu|\gg|\nu|$, $\mu\simeq 1$.

It can be shown that (16c) reduces to the conventional formula,

$$A'=eQqY(F)[3(\tfrac{1}{2})^2(J^2+J)^{-1}-1]\sim W_{c,d}', \quad (17)$$

while the B' term will give something new. The calculation of this term can be performed by using Racah's method and the formulas obtained in I.[7] The wave functions one should use are shown in the formulas (11a) and (11b) and the similar formulas for $(^2\Pi_{\frac{1}{2}}J_\pm m|$ can be obtained from the formula (A7) of I.

The same results can be obtained by another pro-

[6] Mizushima, Cox, and Gordy, Phys. Rev. 98, 1034 (1955).

[7] There were some misprints in those formulas in Sec. 4 of I: in (15b), $I(2I-1)$ should be $\sqrt{I(2I-1)}$; in (18), the right-hand side should be $(-1)^{-K-J+\frac{1}{2}}\{A(A+1)-(4/3)J(J+1)K(K+1)\cdots$; in (19) the last factor in the right-hand side should be $[4K(K+1)\cdots]^{-\frac{1}{2}}$; in (20), the right-hand side $\cdots K(K+1)\times(2K+3)(2K-1)]^{-\frac{1}{2}}\cdots$; in (23), the right-hand side should start as $-\frac{1}{4}\{K(K+1)\cdots$; in (24), $\frac{1}{4}$ should be taken off. Formula (A7) should be $-(\Pi_{\frac{1}{2}}J|=\cdots$.

TABLE I. Observed and calculated frequencies (Mc/sec).

J	F	ν(obs.)	ν(calc.)
	$3/2\rightarrow 5/2$	150 176.54	150 176.29
	$1/2\rightarrow 3/2$	150 198.85	150 198.86
	c $3/2\rightarrow 3/2$	150 218.89	150 218.84
	$1/2\rightarrow 1/2$	150 225.75	150 225.83
	$3/2\rightarrow 1/2$	150 245.69	150 245.81
$1/2\rightarrow 3/2$			
	$3/2\rightarrow 1/2$	150 375.48	150 375.62
	$3/2\rightarrow 3/2$	150 439.22	150 439.19
	d $3/2\rightarrow 5/2$	150 546.50	150 546.34
	$1/2\rightarrow 1/2$	150 580.70	150 580.73
	$1/2\rightarrow 3/2$	150 644.37	150 644.40
	$5/2\rightarrow 7/2$	250 435.60	250 435.26
	$3/2\rightarrow 5/2$	250 439.20	250 439.19
	c $1/2\rightarrow 3/2$	250 447.16	250 447.41
	$3/2\rightarrow 3/2$	250 474.42	250 474.24
	$5/2\rightarrow 5/2$	250 481.52	250 481.82
$3/2\rightarrow 5/2$			
	$5/2\rightarrow 7/2$	250 794.98	250 795.47
	$3/2\rightarrow 5/2$	250 814.64	250 814.81
	d $1/2\rightarrow 3/2$	250 816.24	250 816.02
	$3/2\rightarrow 3/2$	250 752.61	250 752.45
	$5/2\rightarrow 5/2$	250 707.92	250 707.66

cedure, namely, using Van Vleck's method.[4] The result of them is

$$(^2\Pi_{\frac{1}{2}}J_+IF|H_2|^2\Pi_{\frac{1}{2}}J_-IF)=-\tfrac{1}{4}eQq'(2J+1)\times[(2J-1)(2J+3)]^{\frac{1}{2}}(J^2+J)^{-1}Y(F), \quad (18)$$

where

$$q'=-\left(e_+\left|\frac{\partial^2V}{\partial x^2}+2i\frac{\partial^2V}{\partial x\partial y}-\frac{\partial^2V}{\partial y^2}\right|e_-\right)=3e\left\langle\frac{x^2+y^2}{r^5}\right\rangle_{\pi\ \text{odd}}n. \quad (19)$$

The symbol $\langle\ \rangle_{\pi\ \text{odd}}$ means the average value over the odd π electron and n is the effective number of such electrons. From the above formula, we obtain

$$B'=-\tfrac{1}{4}\nu eQq'(2J+1)[(2J-1)(2J+3)]^{\frac{1}{2}}\times(J^2+J)^{-1}Y(F), \quad (20)$$

$$R=eQ\{-q\mp\nu q'(2J+1)[(2J+3)(2J-1)]^{-\frac{1}{2}}\}/8J(J+1)I(2I-1), \quad (21)$$

where the double sign means $-$ for c and $+$ for d states, respectively. Since we know that $\nu=-0.0247$ in the $J=3/2$ state, we can obtain the value of the coupling constants by comparing the formulas (16a), (16b), (18), and (21) with the value of R shown in Table I of I as follows:

$$eQq=-1.7\ \text{Mc/sec}, \quad (22)$$

$$eQq'=\ 22\ \ \text{Mc/sec}. \quad (23)$$

eQq' is a quantity which has never been observed for any molecule previously. At first sight it appears rather surprising that q' be so large compared to q. The following rough theoretical estimates, however, make the magnitude found for q' appear reasonable. As is shown in the definition (19), only the odd $p\pi$ electron contributes to this quantity. If we assume that there is exactly one odd electron which is in the pure $p\pi$-orbital, we can estimate q'. Using the Slater wave function $(\alpha^5/2\pi)^{\frac{1}{2}}r\sin\theta e^{i\varphi}e^{-\alpha r}$, one can easily obtain

$$q'=(8/5)e\alpha^3=3.82\times10^{16}\ \text{cgs esu}, \quad (24)$$

where the numerical value is obtained with $\alpha=1.95$ a.u. (atomic units). Somewhat more accurate value can be obtained by using the Hartree wave function. Dousmanis[5] calculated $\langle(x^2+y^2)/r^5\rangle_\pi$ by employing the Hartree wave function and modifying the result. From his result, we obtain

$$q'=2.58\times10^{16}\ \text{cgs esu}. \quad (25)$$

Using the observed value shown in (23), we obtain

$$Q=0.008\times10^{-24}\ \text{cm}^2\ \text{from (24)},\qquad Q=0.012\times10^{-24}\ \text{cm}^2\ \text{from (25)}. \quad (26)$$

Both of these estimates agree with the value 0.01×10^{-24} cm^2 obtained by Sheridan and Gordy,[6] but is smaller than the value 0.02×10^{-24} cm^2 obtained by Townes and Dailey.[9] This value, however, is based on the assumption that exactly one electron contributes to eQq', which is not necessarily true as will be shown in the third paper of this series.[10] The more detailed discussion on this point and accordingly a more reliable value of Q will be given there.

ANALYSIS OF $J=3/2\rightarrow5/2$ TRANSITIONS

Johnson and Gallagher[11] observed the next rotational transition $J=3/2\rightarrow J=5/2$ of the NO molecule at $^2\Pi_{\frac{1}{2}}$ state. Their experimental data are cited in Table I.

The hfs of $J=5/2$ state must be expressed by formula (39) of Part I:

$$W=P\{F(F+1)-I(I+1)-J(J+1)\}+R[\tfrac{3}{4}C(C+1)-J(J+1)I(I+1)].$$

The theoretical formula with the values of the parameters given by formula (40) of I yields

$$P_c=-7.00\ \text{Mc/sec},\quad P_d=12.29\ \text{Mc/sec}. \quad (27)$$

The contribution due to the mixing of the $^2\Pi_{\frac{1}{2}}$ state is by formula (9)

$$\Delta P_{c,d}=-\frac{\sqrt{8}}{35}b\nu, \quad (28)$$

and ν, the parameter which gives the extent of mixing of the $^2\Pi_{\frac{1}{2}}$ state, is calculated in the same way as was done in the appendix of I, to be

$$\nu(J=5/2)=-0.0404; \quad (29)$$

[8] J. Sheridan and W. Gordy, Phys. Rev. **79**, 513 (1950).
[9] C. H. Townes and B. P. Dailey, J. Chem. Phys. **17**, 782 (1949).
[10] M. Mizushima, Phys. Rev. (to be published).
[11] C. M. Johnson and J. J. Gallagher, post-deadline paper, American Physical Society meeting, Columbia University, New York, New York (January, 1954).

thus

$$\Delta P_{c,d} = +0.23 \text{ Mc/sec.} \tag{30}$$

The theoretical values of R can be calculated by the formulas (21), (22) and (23). The results are given in Table II.

Although in Part I one of the authors tried to adjust the numerical values of the parameters P and R so as to reproduce the observed frequencies of $J=1/2\rightarrow J=3/2$ transition[12] as far as possible, we were not concerned about the theoretically predicted relations between them. In this paper, we have tried to reduce everything into eight parameters, whose numerical values are shown in Table III. In Table III, the ν_0's are the frequencies which are obtained by subtracting the effect of hfs, while a and b are quantities which were defined in the formulas (11a) and (11b) of Part I and which are related to Dousmanis' parameters[3] as follows:

$$\begin{aligned} 4a &= a-(b+c)/2 \text{ of Dousmanis,} \\ 8b &= d \text{ of Dousmanis.} \end{aligned} \tag{31}$$

As the correction in P due to the mixing of $^2\Pi_{\frac{1}{2}}$ state, the theoretical values cited in (10) and (30) are used. The calculated frequencies agree with the observed values with the average deviation of 0.08 Mc/sec for the $J=1/2\rightarrow 3/2$ transition, and 0.24 Mc/sec for the $J=3/2\rightarrow 5/2$ transition. See Table I. Most of the deviations are within the experimental error which is assumed to be about 0.10 Mc/sec for $J=1/2\rightarrow 3/2$ and 0.25 Mc/sec for $J=3/2\rightarrow 5/2$.

TABLE II. The values of hfs parameters derived by the values cited in Table I (Mc/sec).

J	$^{1/2}$		$^{3/2}$		$^{5/2}$	
	c	d	c	d	c	d
P	−6.66	68.37	−8.63	21.37	−6.77	12.52
R	0	0	0.08	0.04	0.04	0.008

TABLE III. The adjusted values of hfs parameters (Mc/sec).

$a=$ 23.14	$\nu_{0,0}(J=1/2\rightarrow 3/2)=150\,195.40$
$b=$ 14.065	$\nu_{0,0}(J=1/2\rightarrow 3/2)=150\,550.54$
$eQq=-1.7$	$\nu_{0,0}(J=3/2\rightarrow 5/2)=250\,443.13$
$eQq'=$ 22	$\nu_{0,0}(J=3/2\rightarrow 5/2)=250\,797.00$

THEORY OF THE MAGNETIC RESONANCE SPECTRUM OF NO IN $^2\Pi_{\frac{1}{2}}$ STATE

The magnetic resonance spectrum of NO in $^2\Pi_{\frac{1}{2}}$ state has been observed by Beringer and Castle,[13] and a theoretical account has been given by Margenau and Henry[14] and also by Henry.[15] Recently Beringer, Rawson, and Henry[16] have made more accurate measurements on the spectrum. With the new data it is seen that the Margenau and Henry treatment, in which the secular equation is set up in the Hund's case (b) representation, does not provide very good agreement between the calculated and experimental results. Since NO is a good Hund's case (a) molecule, it should be more natural to solve this problem by starting from a case (a) representation and treating the Zeeman effect, rotational distortion terms, etc., as perturbations.

The Hamiltonian of NO in a magnetic field exclusive of the interactions due to the nuclear spin, can be written as

$$H = H_0 + H',$$

where

$$H' = -2B(J_x S_x + J_y S_y) + \mu_0(\Lambda+2S)\cdot\mathfrak{H} \tag{32}$$

and H_0 is given in (1). In a representation where Σ, Λ, Ω, J, and M_J are diagonal, the matrix elements of the first term in (32) are well-known, and the second term can be expressed as

$$(\Lambda+2S)_{z'} = 2\lambda_{z'x}S_x + 2\lambda_{z'y}S_y + \lambda_{z'z}(\Lambda+2\Sigma),$$

where x', y', z' and x, y, z represent coordinate axes systems fixed in space and in the molecule respectively, and the λ's are the directional cosines. The matrix elements of $(\Lambda+2S)_{z'}$ can therefore be calculated by taking the direct products of $\lambda_{z'z}$ and S_z, etc. We thus find

$$\begin{aligned}
&(J,\Omega,\Sigma,M_J|H'|J+1,\Omega-1,\Sigma-1,M_J) \\
&\quad = -(J+1)^{-1}[(2J+1)(2J+3)]^{-\frac{1}{2}}Q(J+1,M_J) \\
&\qquad \times[(J-\Omega+1)(J-\Omega+2)]^{\frac{1}{2}}P(S,\Sigma)\mu_0\mathfrak{H}, \\
&(J,\Omega,\Sigma,M_J|H'|J,\Omega-1,\Sigma-1,M_J) \\
&\quad = B[J(J+1)-\Omega(\Omega-1)]^{\frac{1}{2}}P(S,\Sigma) \\
&\qquad -[J(J+1)]^{-1}[(J+\Omega)(J-\Omega+1)]^{\frac{1}{2}} \\
&\qquad \times P(S,\Sigma)M_J\mu_0\mathfrak{H}, \\
&(J,\Omega,\Sigma,M_J|H'|J-1,\Omega-1,\Sigma-1,M_J) \\
&\quad = [J^2(4J^2-1)]^{-\frac{1}{2}}[(J+\Omega)(J+\Omega-1)]^{\frac{1}{2}} \\
&\qquad \times Q(J,M_J)P(S,\Sigma)\mu_0\mathfrak{H}, \\
&(J,\Omega,\Sigma,M_J|H'|J+1,\Omega,\Sigma,M_J) \\
&\quad = (J+1)^{-1}[(2J+1)(2J+3)]^{-\frac{1}{2}} \\
&\qquad \times[(J+\Omega+1)(J-\Omega+1)]^{\frac{1}{2}} \\
&\qquad \times Q(J+1,M_J)(\Lambda+2\Sigma)\mu_0\mathfrak{H}, \\
&(J,\Omega,\Sigma,M_J|H'|J,\Omega,\Sigma,M_J) \\
&\qquad = [J(J+1)]^{-1}\Omega(\Lambda+2\Sigma)M_J\mu_0\mathfrak{H},
\end{aligned} \tag{33}$$

where

$$P(S,\Sigma)=[S(S+1)-\Sigma(\Sigma-1)]^{\frac{1}{2}}, \quad Q(x,y)=[x^2-y^2]^{\frac{1}{2}}.$$

To calculate the energy levels in a magnetic field, we apply the perturbation method to the third order. Taking 124.2 cm^{-1} as the value[17] of D and neglecting the uninteresting terms independent of M_J, we obtain

[12] C. A. Burrus and W. Gordy, Phys. Rev. **92**, 1437 (1953).
[13] R. Beringer and J. G. Castle, Jr., Phys. Rev. **78**, 581 (1950).
[14] H. Margenau and A. Henry, Phys. Rev. **78**, 587 (1950).
[15] A. Henry, Phys. Rev. **80**, 549 (1950).
[16] Beringer, Rawson, and Henry, Phys. Rev. **94**, 343 (1954).
[17] M. Guillery, Z. Physik **42**, 121 (1927); Jenkins, Barton, and Mulliken, Phys. Rev. **30**, 150 (1927).

TABLE IV. Experimental and calculated values of the microwave frequency for NO spectrum.

Line	Transitions $M_J, M_I \quad M_J-1, M_I$	Resonance field (in gauss)	Microwave frequency observed (in Mc/sec)	Frequency calculated (neglecting Schwinger's spin-moment anomaly) (in Mc/sec)	Frequency calculated (including Schwinger's spin-moment anomaly) (in Mc/sec)
H_1	$3/2, \quad 1 \rightarrow \quad 1/2, \quad 1$	8398.61	9269.94	9270.5	9275.6
H_2	$3/2, \quad 0 \rightarrow \quad 1/2, \quad 0$	8425.71	9270.65	9270.7	9276.0
H_3	$3/2, -1 \rightarrow \quad 1/2, -1$	8453.44	9270.65	9270.7	9275.8
H_4	$1/2, \quad 1 \rightarrow -1/2, \quad 1$	8501.49	9270.65	9269.6	9274.7
H_5	$1/2, \quad 0 \rightarrow -1/2, \quad 0$	8528.28	9270.65	9269.2	9274.3
H_6	$1/2, -1 \rightarrow -1/2, -1$	8555.84	9270.65	9269.5	9274.7
H_7	$-1/2, \quad 1 \rightarrow -3/2, \quad 1$	8600.97	9269.81	9267.4	9272.5
H_8	$-1/2, \quad 0 \rightarrow -3/2, \quad 0$	8629.71	9270.65	9268.5	9273.7
H_9	$-1/2, -1 \rightarrow -3/2, -1$	8656.46	9270.65	9268.6	9274.2

for the energy levels:

$$E \text{ (in Mc/sec)} = 0.77713 M_J \mu_0 3\mathcal{C} + 3.917 \times 10^{-7} M_J^2 \mu_0^2 3\mathcal{C}^2 - 4.4699 \times 10^{-12} M_J \mu_0^3 3\mathcal{C}^3 + 7.221 \times 10^{-12} M_J^3 \mu_0^3 3\mathcal{C}^3. \quad (34)$$

The interaction arising from the nuclear spin in nitrogen consists of the nuclear spin-orbit, dipole-dipole, and Fermi $|\psi(0)|^2$ couplings as given in Eq. (1) and the nuclear quadrupole coupling. If we denote the operator for these interactions by H_N, it follows that[18]

$$\begin{aligned}(J,\Omega,M_J,M_I|H_N|J,\Omega,M_J,M_I) &= [J(J+1)]^{-1}[a\Lambda+(b+c)\Sigma]\Omega M_J M_I \\ &\quad - eQq[J(J+1)-3\Omega^2] \\ &\quad \times [4I(2I-1)(2J-1)(2J+3)J(J+1)]^{-1} \\ &\quad \times [J(J+1)-3M_J^2][I(I+1)-3M_I^2].\end{aligned}$$

The nuclear quadrupole effect is small enough that a first-order perturbation treatment is sufficient. The off-diagonal matrix elements for the magnetic interaction terms in H_N can be calculated by the method described for H_1. Calculations show that the only second-order terms which amount to more than 0.1 Mc/sec are those from the cross-term between H' and H_N in

$$\frac{|(J,\Omega,\Sigma,M_J,M_I|H'+H_N|J,\Omega-1,\Sigma-1,M_J,M_I)|^2}{E_{J,\Omega,\Sigma}-E_{J,\Omega-1,\Sigma-1}}$$

and

$$\frac{|(J,\Omega,\Sigma,M_J,M_I|H'+H_N|J+1,\Omega,\Sigma,M_J,M_I)|^2}{E_{J,\Omega,\Sigma}-E_{J+1,\Omega,\Sigma}}.$$

For $J=3/2$ and $\Omega=3/2$, these two second-order terms become

$$\begin{aligned}&-0.0120bM_IM_J+4.197 \\ &\quad \times 10^{-7}[a+(b+c)/2]M_IM_J^2\mu_0 3\mathcal{C}.\end{aligned}$$

The total energy including the nuclear effect is therefore

$$\begin{aligned}E = 0.77713 M_J \mu_0 3\mathcal{C} &+ 3.915 \times 10^{-7} M_J^2 \mu_0^2 3\mathcal{C}^2 - 4.4699 \\ &\times 10^{-12} M_J \mu_0^3 3\mathcal{C}^3 + 7.221 \times 10^{-12} M_J^3 \mu_0^3 3\mathcal{C}^3 \\ &+ \{\tfrac{2}{3}[a+(b+c)/2]-0.0120b\} M_I M_J \\ &+ 4.197 \times 10^{-7}[a+(b+c)/2] M_I M_J^2 \mu_0 3\mathcal{C} \\ &+ eQq(20-4M_J^2)(2-3M_I^2)/80. \quad (35)\end{aligned}$$

If one takes the Schwinger spin moment anomaly[19] into consideration, the term $\mu_0(\Lambda+2S)\cdot 3\mathcal{C}$ in Eq. (32) should be replaced by $\mu_0(\Lambda+2.002290S)\cdot 3\mathcal{C}$ and the matrix elements in Eqs. (33) should be modified accordingly. The equation corresponding to Eq. (35) in this case is

$$\begin{aligned}E = 0.77756 M_J \mu_0 3\mathcal{C} &+ 3.9020 \times 10^{-7} M_J^2 \mu_0^2 3\mathcal{C}^2 - 4.4699 \\ &\times 10^{-12} M_J \mu_0^3 3\mathcal{C}^3 + 7.221 \times 10^{-12} M_J^3 \mu_0^3 3\mathcal{C}^3 \\ &+ \{\tfrac{2}{3}[a+\tfrac{1}{2}(b+c)]-0.0120b\} M_I M_J \\ &+ 4.197 \times 10^{-7}[a+\tfrac{1}{2}(b+c)] M_I M_J^2 \mu_0 3\mathcal{C} \\ &+ eQq(20-4M_J^2)(2-3M_I^2)/80.\end{aligned}$$

Table IV shows a comparison between the experimental and calculated values of the frequencies corresponding to the transitions $\Delta M_J=1$ and $\Delta M_I=0$ at various magnetic field strengths. It is readily seen that when the Schwinger correction to the gyromagnetic ratio of the electronic spin is considered, all the theoretical frequencies are invariably higher than the experimental values. As an error of 1 cm^{-1} in the spin-orbit interaction constant would cause a difference of 2 Mc/sec in the microwave frequency, the uncertainty in D may be responsible for the discrepancies in Table IV.

One of us (C.C.L.) wishes to thank Professor J. H. Van Vleck for his constant help and encouragement during the course of this work.

[18] C. K. Jen, Phys. Rev. **76**, 1494 (1949).

[19] J. Schwinger, Phys. Rev. **73**, 416 (1947).

Quadrupole Spectrum of $BiCl_3$†

HUGH G. ROBINSON
Department of Physics, Duke University, Durham, North Carolina

(Received July 18, 1955)

Pure nuclear quadrupole resonance absorptions were observed for Bi^{209}, Cl^{35}, and Cl^{37} nuclei in polycrystalline $BiCl_3$ at both room and liquid air temperatures. Line assignments and the evaluation of the electric field gradient asymmetry parameter η allow the following coupling constants to be calculated: $|eQq|_{Bi}=318.76$ Mc/sec for $\eta=0.555$; $|eQq|_{Cl^{35}}=30.196$ Mc/sec, 38.310 Mc/sec. Two "forbidden" $|\Delta m'|=2$ transitions were observed. A brief discussion of the data in connection with chemical bonding in the solid is given.

INTRODUCTION

As a continuation in the study of the nuclear quadrupole resonance[1] of Bi^{209}, solid $BiCl_3$ was investigated. Both Cl and Bi resonances were observed in the quadrupole spectrum of this molecule. Even though the couplings of both constituents of the molecule are known, a description of the chemical bonding is made difficult because the solid state structure is evidently unknown. Therefore, the data presented may perhaps become more meaningful when the crystal structure is determined.

EXPERIMENTAL

A 30-cc polycrystalline sample of $BiCl_3$ was dried in vacuum and sealed in a glass tube at atmospheric pressure. Due to the deliquescent nature of $BiCl_3$, a dry sealed sample is necessary to maintain a high Q in the oscillator tank circuit.

The resonance absorption lines were observed by means of super-regenerative detection. At room temperature, all but the Cl^{37} lines were observable by frequency modulating the oscillator and oscilloscopic display. The temperature was maintained relatively constant by water-cooling the copper radio-frequency shield surrounding the sample. During runs at liquid air temperature a forty-cycle off-on square-wave Zeeman-modulation magnetic field together with conventional narrow-band phase-sensitive detection techniques were used.

The majority of the resonances observed were so broad that side-bands due to super-regenerative detection were not resolved when using the spectrometer with a normal high-Q tank circuit. In order to be able to use sufficiently high quench frequencies for side-band resolution, the Q of the tank circuit was lowered to approximately one-half its original value by shunting the tank with an appropriate resistor. With this modification, observations of the relative motion of the line, side-bands, and marker lattice over a relatively wide range of quench frequencies were possible. Hence, one is able to eliminate errors due to guessing the center of an unresolved line-side-band combination.

It was possible to apply 10-mw peak power to the sample without causing noticeable saturation broadening.

ASSIGNMENTS

Assignments for the Cl resonances were made by using the known[2] ratio of the quadrupole moments for the Cl^{35} and Cl^{37} isotopes. A $Cl^{35,37}$ spin of 3/2 allows only one line per lattice site per isotope. The set of four lines observed may thus be interpreted as indicating two nonequivalent lattice sites in the unit cell. Since no value of the asymmetry parameter η was determined for the field gradient of the Cl nucleus, the coupling constant $|eQq|$ was calculated by doubling the observed frequency, i.e., assuming $\eta=0$.

The identification of the four $|\Delta m|=1$ transitions and the calculation of the asymmetry parameter for the Bi^{209} nucleus follows a method proposed by Cohen.[3] One plots calculated frequency ratios as a function of η. Because a given value of η implies a unique set of frequency ratios, the measured frequency ratios should intersect the calculated ratios in a verticle line over the η appropriate for a fit of the data. In addition to the evaluation of η, the identifications of the transitions are

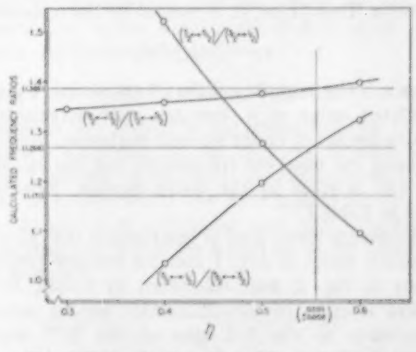

FIG. 1. Determination of η and line assignments.

† This research was supported by The United States Air Force through the Office of Scientific Research of the Air Research and Development Command.

[1] Robinson, Dehmelt, and Gordy, Phys. Rev. 89, 1305 (1953).

[2] R. Livinston, Phys. Rev. 82, 289 (1951).

[3] M. H. Cohen, Phys. Rev. 96, 1278 (1954).

TABLE I. Allowed transitions in $BiCl_3$: measured frequencies all accurate to at least ±11 kc/sec at 299°K, ±20 kc/sec at 83°K.

Lattice site	Temp. (°K)	Observed frequency (Mc/sec)	Observed frequency ratios	Calculated relative frequency factors r_i	Calculated frequency ratios	Assignments	$\lvert eQq\rvert$ (Mc/sec)
I		15.955	1.2688			Cl^{35}	38.310
		12.573				Cl^{37}	
II		19.155	1.2690			Cl^{35}	30.196
		15.0976				Cl^{37}	
	299±1°				$\eta=0.555$ ±0.002	Bi^{209}	$24\nu_i/r_i$
		51.740	1.386	3.898	1.387	(9/2↔7/2)	318.56
		37.340		2.810		(7/2↔5/2)	318.92
		31.876	1.171	2.400	1.1708	(3/2↔1/2)	318.76
		25.131	1.268	1.892	1.2685	(5/2↔3/2)	318.79
							Average 318.76±0.20
I		15.849	1.268				
		12.498					
II		19.531	1.269				
		15.387					
	83°				$\eta=0.583$ ±0.008	Bi^{209}	$24\nu_i/r_i$
		52.704	1.391	3.889	1.393	(9/2↔7/2)	325.25
		37.900		2.792		(7/2↔5/2)	325.79
		33.726	1.124	2.486	1.123	(3/2↔1/2)	325.59
		25.905	1.302	1.911	1.301	(5/2↔3/2)	325.34
							Average 325.5±0.3

determined. Figure 1 shows this solution on an expanded scale; in this case, the value of η is determined to an accuracy limited by the graphical solution.

The magnitude of the coupling constant $|eQq|$ can now be found by plotting the relative frequency factors against η. This factor, r_i, is defined by the equation

$$\nu_i = r_i|eQq|/24,$$

where ν_i is the frequency of the ith transition. Using the calculated value of η, one can now determine the relative frequency factor for each transition. See Fig. 2. By using the observed frequencies and the calculated r_i, $|eQq|$ is given by the above formula. Results are listed in Table I.

The energy levels used in determining the calculated frequency ratios in Fig. 1 and the relative frequency factors in Fig. 2, were calculated by Cohen[3] by numerical solution of the fifth-order secular equation appropriate to the 9/2 spin of the Bi^{209} nucleus. Bersohn's fourth-order formulas[4] obtained by perturbation methods cannot be used for so large a value of the asymmetry parameter, 0.555. In fact, with a 9/2 spin and asymmetry greater than 0.1, the perturbation formulas produce a significant error in the value of the (3/2↔1/2) transition for $|eQq| \geq 300$ Mc/sec. In contrast to this the (9/2↔7/2) transition is relatively insensitive to the asymmetry parameter and the value

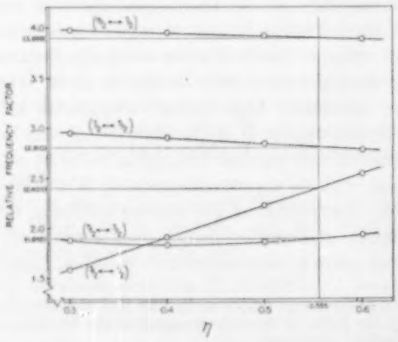

FIG. 2. Determination of the relative frequency factors, r_i.

[4] R. Bersohn, J. Chem. Phys. 20, 1505 (1952).

of $|eQq|$ calculated from the perturbation formula,

$$|eQq| = 6\nu(9/2 \leftrightarrow 7/2)/(1-0.08095\eta^2-0.0043\eta^4),$$

agrees with that determined graphically.

FORBIDDEN TRANSITIONS

Heretofore, only allowed magnetic dipole transitions $|\Delta m|=1$ have been reported for pure nuclear quadrupole resonance.[5] In the case of $BiCl_3$, as a result of the large asymmetry in the field gradient, the magnetic sub-states for which $|\Delta m'|=2$ are connected providing an observable transition probability. The $(1/2 \leftrightarrow 5/2)$ and $(3/2 \leftrightarrow 7/2)$ transitions were observed to within the experimental error at frequencies corresponding to the sum of the two appropriate $|\Delta m|=1$ transitions; i.e., the sum of $(1/2 \leftrightarrow 3/2)$ and $(3/2 \leftrightarrow 5/2) = (1/2 \leftrightarrow 5/2)$. See Table II. Although no careful measurement of the relative intensities of the allowed and forbidden transitions was attempted, the order-of-magnitude agreement with Cohen's calculations was experimentally confirmed. See Fig. 3 for a recording of the $(1/2 \leftrightarrow 5/2)$ transition.

The possibility of d-admixture in the orbitals of the Bi^{209} together with the 9/2 spin of this nucleus allow a magnetic octuple interaction. One effect of such interaction should be the mixing of the $|m|=3/2$ levels, thereby removing the $\pm m$ degeneracy. However, the energy difference involved here should be several orders of magnitude smaller than that of the electric quadrupole interaction so that no observable effect should be noticed with the resolution attainable in this type of experiment. A recording of the $(3/2 \leftrightarrow 5/2)$ line with the spectrometer operating in the regenerative mode revealed no broadening attributable to the above effect.

DISCUSSION

The structure of $BiCl_3$ in the solid state was not found in the literature. Nevertheless, from the observed Cl resonances two nonequivalent positions in the unit cell may be inferred for this nucleus. In addition, the line widths and intensities indicate approximately equal numbers, 1:1 or 1:2, of Cl nuclei in each of these positions at both room and liquid air temperatures. Variation in spectrometer sonativity and possible distortion of the line shape due to super-regenerative detection prevents one from making more definite conclusions.

TABLE II. "Forbidden" transitions in $BiCl_3$.

Observed frequency (Mc/sec)	Assignments	Sum of $\|\Delta m\|=1$ transitions (Mc/sec)
56.98	$(5/2 \leftrightarrow 1/2)$	$(5/2 \leftrightarrow 3/2)+(3/2 \leftrightarrow 1/2)$ 57.01
62.49	$(7/2 \leftrightarrow 3/2)$	$(7/2 \leftrightarrow 5/2)+(5/2 \leftrightarrow 3/2)$ 62.47

[5] G. Lamarche and G. M. Volkoff, Can. J. Phys. 31, 1010 (1953), suggested the possibility of observing forbidden transitions in $LiAl(SiO_3)_2$. R. M. Cotts and W. D. Knight, Phys. Rev. 96, 1285 (1954), attempted without success to observe such transitions in $KNbO_3$.

FIG. 3. The $(1/2 \leftrightarrow 5/2)$ pure quadrupole transition (forbidden transition) of Bi^{209} in $BiCl_3$.

The low value of the Cl coupling indicates an ionic character of the order of 65% for the BiCl bonds. The effect of asymmetry in the field gradient at the Cl nucleus may be seen from the formula for 3/2 spin[6]:

$$|eQq| = 2\nu(3/2 \leftrightarrow 1/2)/(1+\tfrac{1}{3}\eta^2)^{\frac{1}{2}}.$$

Thus, if $\eta=0$, the coupling is lower, and larger amounts of hybridization and/or ionic character are necessary than indicated above. However, for an asymmetry of 0.6 the coupling is reduced only by 5 percent from that for zero asymmetry so that effects of the asymmetry on the coupling may be neglected in this approximate treatment.

In discussing crystal structure in connection with the coupling, it must be remembered that the principle contributor to the field gradient will be p-electrons—the direct contribution of d-electrons will be negligible. However, d-electrons will play a significant role in determining the crystal structure. This also applies to p-d hybridized orbitals which contain at least one electron. Therefore, for heavy atoms in which d-hybridization is likely, s-p hybridization alone may not be sufficient to describe the resulting bond angles and coupling. In cases where s-p hybridization alone is thought to be sufficient, one can relate the percent s-character, α, to the bond angle B-A-B, γ, in AB_3 molecules by the formula

$$\alpha = -\cos\gamma/(1-\cos\gamma),\ 0 \leq \gamma \leq \tfrac{1}{2}.$$

This formula was derived by the assumption that bonds are formed according to the principle of maximum overlap. Thus one can calculate[7] the molecular coupling $(eQq_{zz})_A$ as a function of the bond angle, the percent ionic character β of each bond, and $(eQq_0)_A$ which is the coupling due to a single p-electron in the magnetic substate $m_l=0$:

$$(eQq_{zz})_A = \frac{-3\cos\gamma}{(1-\cos\gamma)}(1+2\beta)(eQq_0)_A.$$

[6] R. V. Pound, Phys. Rev. 79, 685 (1950).

[7] Compare Gordy, Smith, and Trambarulo, *Microwave Spectroscopy* (John Wiley and Sons, Inc., New York, 1953), p. 281.

This assumes a positive charge on A resulting from the ionic character of the bond. An alternate expression[8] using the coupling $(eQq')_A$ along the bond direction due to one electron in the hybridized bonding orbital is

$$(eQq_{zz})_A = -3\cos\gamma(1+2\beta)(eQq')_A.$$

Making the simplifying assumption that the AB_3 structure applies for crystalline $BiCl_3$, 3% s-character in the Bi bonding orbital or a Cl-Bi-Cl angle of 91.2° is given by the formulas for α and $(eQq_{zz})_A$. A value[1] of 1500 Mc/sec was used for $(eQq_0)_{Bi}$ in this calculation. An s-character of zero would indicate pure orbitals of Bi, i.e., a Cl-Bi-Cl angle of 90°, and the coupling due to p-electrons would vanish.

If one assumes that individual $BiCl_3$ molecules exist in the solid, Gordy's formulas[9] may be applied. These are:

$$\beta_\sigma = 1-\rho_q-\gamma_\pi/2 = |x_{Cl}-x_{Bi}|/2,$$

$$x = 0.31\left[\frac{n+1+c}{r}\right]+0.5,$$

where $\rho_q = |\text{molecular } eQq/2\times\text{atomic } eQq|$ for halogen, β_σ = ionic character of the σ component of the bond, $\gamma_\pi = \pi$ character of the bond, x = electronegativity, n = number of electrons in the unfilled shell of the neutral atom, c = positive charge in electron units on the atom, $=3(\beta_\sigma-\gamma_\pi)$ for AB_3 molecule, and r = covalent radius. Solving the above equations simultaneously, with $x_{Cl}=3.0$, $\rho_q = 35.1/109.74 = 0.32$, $n=5$, $r=1.46$, we have $\beta_\sigma = 0.53$ and $\gamma_\pi = 0.29$.

Gordy has demonstrated the applicability of the above formulas to several molecules in the solid state where each molecule essentially retains its identity. That so large a value of π character is indicated by the formulas may be taken as evidence that a significant amount of cross-bonding occurs in the solid $BiCl_3$. Only 9% π character is found for $SnCl_4$ and only 14% for $GeCl_4$. If one assumes 14% normal π bonding in the BiCl bonds, there would be roughly 15% cross bonding. Such cross bonding should be expected for polar molecules in the solid state. The tetrahedral structure observed for gaseous[10] $BiCl_3$ would require an asymmetry parameter of zero; the large value of η observed is an indication of distortion from the C_{3v} symmetry and again points to cross bonding. The cross bonding would probably involve p-d hybridized orbitals as in I_2.

The effects of change in temperature may also indicate cross-bonding. That η decreases with increasing temperature is consistent with the view that intermolecular bonds are weakened with rising temperature. However, one might expect that such loosening of the intermolecular bonds would cause the field gradient q_{zz} to increase with temperature. This effect is in opposition to the averaging of q_{zz} due to the thermal motion of the crystal lattice which results in a negative temperature coefficient for q_{zz}. If one corrects for the change in frequency at liquid air temperature due to the change in η, there remains a difference in frequency compared with room temperature which implies for $(q_{zz})_{Bi}$ a net negative temperature coefficient whose magnitude agrees with that expected for such an averaging process[11]; i.e., a temperature coefficient of $\approx -10^{-4}$/°C.

A structure of the BiI_3 type, in which the Bi is surrounded octahedrally by six I, can be rejected for $BiCl_3$ on the basis that a perfect octahedral surrounding the Bi would produce a zero field gradient. Even if the octahedra were distorted, if C_{3v} symmetry remained, there would result zero symmetry.

A dimeric molecular structure, Bi_2Cl_6, similar to that of Al_2Cl_6 is evidently not possible because an unshared pair of electrons occupies an orbital in the plane containing the bonds which would be supposed to resonate.

ACKNOWLEDGMENTS

Grateful acknowledgment is given for discussions with Professor Walter Gordy and Dr. Masataka Mizushima.

[8] This expression, with a change in sign, has been given by S. Kojima *et al.*, J. Phys. Soc. Japan **9**, 805 (1954).
[9] Walter Gordy, Discussions Faraday Soc. (to be published).
[10] H. A. Skinner and L. E. Sutton, Trans. Faraday Soc. **36**, 681 (1940).
[11] H. G. Dehmelt and H. Kruger, Z. Physik **129**, 401 (1951).

Microwave Spectra of the Free Radicals OH and OD*

G. C. Dousmanis, T. M. Sanders, Jr.,† and C. H. Townes
Physics Department, Columbia University, New York, New York

(Received August 18, 1955)

Experiments are reported on the microwave spectra of the free OH radical. The radicals are produced by an electric discharge in concentrations near 10% at pressures of approximately 0.1 mm Hg. The spectra are detected by Zeeman modulation. They are due to direct transitions between the Λ-doublet levels of each rotational state in the ground vibrational level of the molecule. Spectra due to $O^{16}H$, $O^{18}H$, and $O^{16}D$ in $^2\Pi_{\frac{1}{2}}$ and $^2\Pi_{\frac{3}{2}}$ states have been observed in the 7.7 to 37 kMc/sec region. Intensity of the lines ranges from about 5×10^{-4} cm^{-1} to 5×10^{-3} cm^{-1}.

Van Vleck's theory of molecular energies in $^2\Pi$ and $^2\Sigma$ states is extended to include terms of order $(E_{rot}$ or $E_{el})^3/E_{el}^2$. The experimental results are in agreement with theoretical expectations to about one part in 2000 which is the order of accuracy of the theory. An improved agreement (to one part in 3500) is obtained if one allows a small variation (one part in 1400) of the electronic wave function from one rotational state to the next. The values of the molecular constants determined from the Λ-type doubling data are

$$4\sum_{\Sigma\text{-states}}(-1)^s\langle\Pi|AL_y+2BL_y|\Sigma\rangle\langle\Sigma|BL_y|\Pi\rangle/(E_\Sigma-E_\Pi)$$
$$=-2361.37\pm2.95 \text{ Mc/sec in } O^{16}H$$
and -1548.99 ± 2.10 Mc/sec in $O^{16}D$;

$$4\sum_{\Sigma\text{-states}}(-1)^s|\langle\Pi|BL_y|\Sigma\rangle|^2/(E_\Sigma-E_\Pi)=576.18\pm1.64 \text{ Mc/sec}$$
in $O^{16}H$ and 161.94 ± 1.61 Mc/sec in $O^{16}D$;

$A/B=-7.444\pm0.017$ in $O^{16}H$ and -13.954 ± 0.032 in $O^{16}D$. The spectra include magnetic hyperfine structure from which the following values are obtained for parameters that describe the unpaired electron distribution in the molecule:

$$(1/r^3)_{Av}=(0.75\pm0.25)\times10^{24} \text{ cm}^{-3}$$

and

$$(\sin^2\chi/r^3)_{Av}=(0.49\pm0.01)\times10^{24} \text{ cm}^{-3}.$$

The hyperfine structure, the molecular magnetic moment and the line intensities are strongly dependent on the extent of intermediate coupling in agreement with theoretical expectations. The microwave spectrum can be used in studying chemical properties of the radical. Its lifetime was determined to be near $\frac{1}{4}$ sec, and the effects of certain substances on radical concentration were examined.

1. INTRODUCTION

FREE radicals are unstable molecules or molecular fragments which usually possess one or more unpaired electrons. They are chemically very reactive substances with short lifetimes in most cases much less than one second. Many have been detected, or postulated to be present, in electrical discharges, flames, detonations, and in the gas of comets.

The ground electronic state of many free radicals, in contrast to the vast majority of stable molecules, is not a $^1\Sigma$ state. In addition to the rotational terms, their energy levels show prominent fine structure and effects of coupling between rotation and electronic motion such as Λ-type doubling, ρ-type doubling etc.

Study of free radicals by microwave spectroscopy should yield detailed information on their energy level structure and, in addition, one might use the microwave spectrum to obtain information on their lifetimes, and the kinetics of chemical processes.

Unstable molecules have been produced in a variety of ways, e.g., by electric discharges, photolysis, and pyrolysis. In the experiments to be described, electric discharges were used, largely because this seemed the simplest method for our purposes.

Since the plasma of an electric discharge will attenuate microwaves strongly, the radicals must be examined either in a different location or at a different time from that at which they are produced. In either case the radicals must, of course, not be permitted to recombine before they are observed. The choice of materials for the surfaces with which radicals come in contact, in view of their high degree of reactivity, is of paramount importance. In addition, charged particles produced in the discharge should not be present to any large extent when the gas is examined by microwaves. In the present experiments, the discharge tube and the absorption cell were separated in space, the radicals flowing into the absorption cell through a glass tube. The alternative method of examining the radicals in the place they are produced but at a slightly later time could be particularly useful in the study of very short-lived substances. This advantage however would probably be accompanied by considerable complication of the apparatus.

For the detection of the spectra a rather conventional modulation spectrometer[1] with associated narrow-band amplifier and phase sensitive detector was constructed. However, advantage was taken of the large magnetic moment exhibited by many free radicals. Modulation was accomplished by radio-frequency variation of a magnetic field rather than the usual electric field. Such a modulation scheme simplifies the searching problem since the spectra of stable molecules, which may be used as the source of radicals, are not detectable with the Zeeman spectrometer. The method also makes it unnecessary to obstruct the wave guide with a metal

* Work supported jointly by the Department of the Army (Signal Corps), the Department of the Navy (Office of Naval Research), and the Department of the Air Force (Air Research and Development Command).

† RCA Fellow, now at Physics Department, University of Minnesota, Minneapolis, Minnesota.

[1] A. H. Sharbaugh, Rev. Sci. Instr. **21**, 120 (1950).

septum which would reduce the pumping speed and produce a disastrous amount of recombination of radicals.

Precise information on free radicals, obtained from optical or near-optical spectroscopic work, is very scarce. One is therefore confronted with a searching problem, since in most cases the microwave spectra cannot be predicted with much accuracy. Although the situation is much worse than in the case of stable molecules, this searching problem is certainly not as formidable as the ones connected with their instability.

The OH radical was selected for study because it had been the subject of a considerable amount of quantitative work. The lifetime of the radical was known to be relatively long[2] and the absorption frequencies to be expected[3] in the microwave region, could be predicted with sufficient accuracy to render the search problem not too prohibitive. It was further believed possible to establish the presence of the radicals by other than spectroscopic means.[4,5] This last would provide a check on the operation of the production and transport phase of the experiment.

The ground electronic state of OH is a $^2\Pi$. The particular lines that have been observed in this work are due to transitions between the two members of the Λ-type doublet into which each J level is split. Spectra have been observed in both the Π_1 and Π_4 states of the ground vibrational level. The OH radical is so light that its rotational spectrum lies in the far infrared. It is only because the electronic angular momenta are not zero that transitions appear in the microwave region.

2. EXPERIMENTAL TECHNIQUES

(a) Production of OH–Vacuum System

The OH is produced by a discharge through water vapor. The all-glass vacuum system (Fig. 1) consists of a water source, a discharge tube of 28 mm Pyrex, the absorption cell, a pair of connecting tubes of 18 mm Pyrex and a liquid nitrogen trap located near the output end of the absorption cell. The cell itself consists of a Corning 707 glass tube, 150 cm long and 30 mm in diameter. Type 707 glass was used because of its low dielectric loss at microwave frequencies. In the early part of this work[6] a much shorter (75 cm) absorption cell was in use. The glass tube in the absorption cell is sealed at both ends and these ends are blown to minimum thickness (to facilitate microwave transmission) consistent with adequate strength. The system is pumped by a Welch type 1397B mechanical pump and, if needed, a DPI MB-100 oil diffusion pump. In the experiments described here use of the diffusion pump was not necessary.

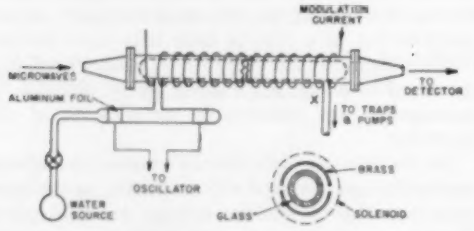

FIG. 1. Vacuum system and absorption cell.

Under the operating conditions of continuous flow about 3 g of water leave the source per hour. The water vapor enters the discharge tube and the discharge products flow into the absorption cell and from there to the liquid nitrogen trap and pumps. A thermocouple gauge located at point X (Fig. 1) indicates a pressure near 0.1 mm Hg. This figure must be taken with some reservations since (1) recombination of radicals occurs on the thermocouple wires, giving rise to spurious temperature readings; (2) the gauge reading is dependent on the composition of the gas which is not known and which varies with discharge conditions.

The discharge is maintained either with a dc supply and aluminum electrodes, or as shown in Fig. 1, with external aluminum foil electrodes and power supplied by a 300-watt oscillator operating in the vicinity of two megacycles. The high-pressure limit on the stable operation of the discharge is set by its tendency, at high pressures, to pass from one electrode into the absorption cell rather than between the two electrodes. This tendency of the discharge to "jump" inside the absorption cell can be appreciably reduced by a horseshoe magnet placed around the glass tube connecting the discharge tube with the absorption cell.

The abundance of radicals in the absorption cell, as measured by the intensity of the microwave lines, is strongly dependent on pressure and discharge current.[7] In the present apparatus it is not simple to distinguish between changes in the rate of production of the radicals and in the rate of their subsequent disappearance through recombination. It may be noted that maximum intensity is produced with only moderate excitation. Under conditions of optimum line intensity, the dc power input to the oscillator is in the neighborhood of 100 watts. To obtain comparable radical abundance with the dc discharge, more than 500 watts must be supplied. The discharge is normally powered by the two-megacycle oscillator.

[2] O. Oldenberg, J. Chem. Phys. **3**, 266 (1935).
[3] G. H. Dicke and R. M. Crosswhite, Bumblebee Report No. 87, Johns Hopkins University, November, 1948 (unpublished); Hicks, Ostofsky and Jones, Technical Note No. 130, Ballistic Research Laboratories, Aberdeen Proving Ground, Maryland, November, 1949 (unpublished).
[4] W. H. Rodebush and M. H. Wahl, J. Chem. Phys. **1**, 696 (1933); R. W. Campbell and W. H. Rodebush, J. Chem. Phys. **4**, 293 (1936).
[5] H. S. Taylor and G. I. Lavin, J. Am. Chem. Soc. **52**, 1910 (1930). W. V. Smith, J. Chem. Phys. **11**, 110 (1943).
[6] Sanders, Schawlow, Dousmanis, and Townes, Phys. Rev. **89**, 1158 (1953); G. C. Dousmanis, Phys. Rev. **94**, 789 (A) (1954).
[7] Sanders, Schawlow, Dousmanis, and Townes, J. Chem. Phys. **22**, 245 (1954).

(b) Microwave Spectrometer

We confine the description of the microwave spectrometer to the wave guide enclosing the absorption cell and the apparatus for Zeeman modulation. The other components and detection circuits are those of a conventional Stark modulation spectrometer[1] and need not be described here.

A brass pipe, split in half (Fig. 1) and with holes for input and output tubes is mounted around the glass tubing. It operates as a cylindrical wave guide in the dominant (TE_{11}) mode. Microwave power enters and leaves the absorption cell through tapered sections which establish connection with standard sizes of rectangular wave guide. The microwave properties of this system are inferior to those of a Stark modulation cell. The presence of the glass cell inside the wave-guide results in an attenuation of the transmitted power by a factor of about 30. In addition, as the microwave frequency is varied the transmission varies as a result of reflections due to the glass, the tapered sections and the large holes cut in the wave guide. Despite these shortcomings sufficient power can be transmitted through the system for spectroscopic work in the region from 7000 to about 45 000 Mc/sec.

Magnetic fields of a few gauss are produced by a close-wound single layer coil of No. 14 wire wound over the wave guide. Since this magnetic field is axial, and the wave guide is operated in a TE mode only $\Delta M=\pm 1$ Zeeman components of electric dipole transitions are observed. During the greater part of these experiments a modulation frequency near 227 kc/sec was used. Modulation at a frequency of 100 kc/sec, which was used in the earlier part of this work,[6] is equally effective.

The best sensitivity with such a system may be obtained by use of a square current wave form. However, production of this type of wave in the coil (whose self-resonance frequency is approximately one megacycle) appeared so formidable a problem that a sine wave plus an appropriate amount of dc bias were used instead.

The sentivity of the instrument was determined by comparison with a Stark spectrometer of known sensitivity. Microwave absorption lines of NO_2 and ClO_2 were examined with both instruments, and the sensitivity (minimum detectable absorption) was found to be near 10^{-8} cm^{-1}. A somewhat low sensitivity is to be expected, because of the inefficient modulation system.

(c) Intensity Considerations

The intensity to be expected for one Λ-type doubling transition in OH could not be calculated accurately before any measurements were made, because of several uncertainties. First, the abundance of radicals which may be expected to be present in the absorption cell was not known. Second, the permanent electric dipole moment of OH is unknown. Third, one could not predict with precision the width of the OH lines at any particular pressure.

An expression for the peak absorption coefficient of a microwave line is[8,9]

$$\gamma_{\max}=\frac{8\pi^2 Nf|\mu_{ij}|^2\nu^2}{3ckT\Delta\nu}, \tag{1}$$

where Nf is the number of molecules per cm^3 in the lower state of transition, $|\mu_{ij}|^2$=square of matrix element of the dipole moment (electric in our case) for the transition, ν=frequency of transition, and $\Delta\nu$=half-width of the line at one half maximum intensity.

Assuming thermal equilibrium, the fraction of OH molecules in any state may be evaluated, since the energy level structure is well known. The form of the dipole moment matrix element is well known[9] in the approximation of pure Hund's case (b) coupling:

$$|\mu_{ij}|^2=\mu^2\Lambda^2/(J+1)(2J+1). \tag{2}$$

[The effect of intermediate coupling on the matrix element will be discussed in Sec. 4(f).]

Inserting numerical values in (1) for the $J=9/2$ Λ-type doubling transition in the $^2\Pi_{\frac{1}{2}}$ state of OH at $\nu\sim 23\,800$ Mc/sec, one obtains for a single hyperfine component

$$\gamma_{\max}=2\times 10^{-6}(\beta\mu^2/\Delta\nu)\ \text{cm}^{-1},$$

where β is the percentage of all molecules which are OH radicals. μ is the dipole moment in Debye units and $\Delta\nu$ the line breadth parameter in (Mc/sec) per mm. Inserting the tentative values[10] $\mu=1.5$ and $\Delta\nu=5$, we obtain

$$\gamma_{\max}=0.9\beta\times 10^{-6}\ \text{cm}^{-1}.$$

Two previous determinations of the abundance of OH radicals were available. The first, obtained from measurements on the ultraviolet spectrum of OH produced by thermal dissociation of water, and in dc discharges yields an abundance in the latter case[11–13] of about 0.1%. With abundance of this order we would have in the present work $\gamma_{\max}\sim 9\times 10^{-8}$ cm^{-1}, which is detectable, but with some difficulty.

The second method is less direct, and consists in inferring the radical abundance in the vapor from the concentration of H_2O_2 in the condensate produced on the liquid nitrogen trap exposed to this vapor.[6] This method rests on a belief that the mechanism responsible for the production of H_2O_2 is $OH+OH+M\rightarrow H_2O_2$,[14]

[8] J. H. Van Vleck and V. Weisskoff, Revs. Modern Phys. **17**, 228 (1945).
[9] C. H. Townes and A. L. Schawlow, *Microwave Spectroscopy* (McGraw-Hill Book Company, Inc., New York, 1955).
[10] R. P. Madden and W. S. Benedict, J. Chem. Phys. **23**, 408 (1955).
[11] A. A. Frost and O. Oldenberg, J. Chem. Phys. **4**, 642 (1936).
[12] O. Oldenberg and F. F. Rieke, J. Chem. Phys. **6**, 439 (1938); **7**, 485 (1939).
[13] R. J. Dwyer and O. Oldenberg, J. Chem. Phys. **12**, 351 (1944).
[14] See K. H. Geib, J. Chem. Phys. **4**, 391 (1938) for objections to such a mechanism of H_2O_2 production.

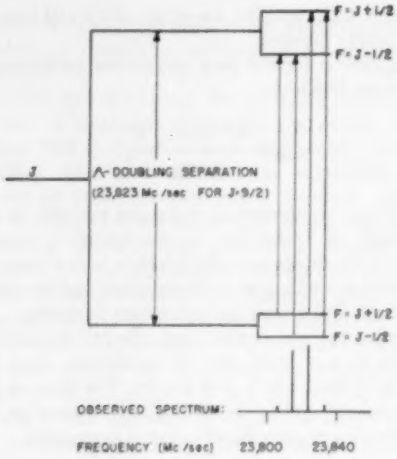

FIG. 2. Diagram indicating the Λ-type doubling and hyperfine structure in one rotational level of the $\Pi_{\frac{1}{2}}$ state of $O^{16}H$. The spectrum shown is that of the $J=9/2$ level.

where M is a third body in or on the trap walls. H_2O_2 concentrations as high as 50% have been obtained both by the original experimenters and the present workers, leading to the conclusion that the dissociation of H_2O is nearly complete. From the above expression, $\beta=50\%$ gives $\gamma_{max}=4.5\times10^{-5}$ cm^{-1}, or a signal-to-noise ratio of about 4000 or more. However, these tests for OH were found to need re-evaluation when the microwave spectrum was detected.

3. OBSERVED SPECTRA OF OH AND OD

Each rotational level of OH, in both the $\Pi_{\frac{1}{2}}$ and the $\Pi_{\frac{3}{2}}$ states, is split into a Λ-type doublet. Each component of the doublet is further split by magnetic hyperfine structure, due to hydrogen or deuterium, into components characterized by the total angular momentum $\mathbf{F}(=\mathbf{J}+\mathbf{I})$. F, of course, takes on the values $J+\frac{1}{2}$ and $J-\frac{1}{2}$ in OH, and $J+1$, J and $J-1$ in OD. Figure 2 shows the energy level arrangement for $J=9/2$ in the $\Pi_{\frac{1}{2}}$ state of OH.

From the selection rule $\Delta F=0, \pm1$, every Λ-type doubling transition is expected to be split into four hyperfine components in OH and seven in OD. In transitions of the type $\Delta J=0$, the hyperfine lines arising from the $\Delta F=0$ transitions will be the strongest. There are two such components in OH and three in OD. The $\Delta F=\pm1$ transitions ("satellite" lines) are much weaker[15] than the main ($\Delta F=0$) lines. These satellites have been observed in the strongest of the Λ-doubling transitions ($J=9/2$ $\Pi_{\frac{1}{2}}$ state) in OH that are reported here.

Transitions due to several rotational states of $O^{16}H$, $O^{18}H$, and $O^{16}D$, in both the $\Pi_{\frac{1}{2}}$ and $\Pi_{\frac{3}{2}}$ states have been observed. The observed signal to noise ratio ranges from 10/1 ($\Pi_{\frac{1}{2}}$ state, $J=11/2$ of OD) to about 1000/1 ($\Pi_{\frac{3}{2}}$ state, $J=9/2$ of OH). The $O^{18}H$ spectrum was obtained with a water sample enriched to 1.4% in O^{18}. A representative value of the line half-width at one-half maximum intensity is about 800 kc/sec. This rather large width is due to a somewhat higher (0.1 mm Hg) pressure than is usual for microwave spectroscopy and to the sine wave modulation.

The measured frequencies and their quantum assignments are given in Table I. The quantum number N designates the sum of the electron orbital (**A**) and the rotational angular momentum. **J** is **N**+**S** and equals $N+\frac{1}{2}$ in the $\Pi_{\frac{3}{2}}$ state and $N-\frac{1}{2}$ in the $\Pi_{\frac{1}{2}}$ state. It is

TABLE I. Frequencies of the observed Λ-type doubling transitions in OH and OD.

Molecule	Electronic state	N	J	Hyperfine transition	Experimental frequency (Mc/sec)
$O^{16}H$	$\Pi_{\frac{1}{2}}$	2	3/2	$F=1\rightarrow F=1$	7 760.36±0.15
				$F=2\rightarrow F=2$	7 819.92±0.10
		3	5/2	$F=2\rightarrow F=2$	8 135.51±0.15
				$F=3\rightarrow F=3$	8 188.94±0.10
	$\Pi_{\frac{3}{2}}$	3	7/2	$F=3\rightarrow F=3$	13 434.62±0.05
				$F=4\rightarrow F=4$	13 441.36±0.05
		4	9/2	$F=5\rightarrow F=4$	23 806.5 ±0.5
				$F=4\rightarrow F=4$	23 818.18±0.05
				$F=5\rightarrow F=5$	23 826.90±0.05
				$F=4\rightarrow F=5$	23 837.8 ±0.3
		5	11/2	$F=5\rightarrow F=5$	36 983.47±0.15
				$F=6\rightarrow F=6$	36 994.43±0.15
$O^{18}H$	$\Pi_{\frac{3}{2}}$	4	9/2	$F=4\rightarrow F=4$	23 469.5 ±0.5
				$F=5\rightarrow F=5$	23 479.1 ±0.5
$O^{16}D$	$\Pi_{\frac{1}{2}}$	3	5/2	$F=3/2\rightarrow F=3/2$	8 110.20±0.10
				$F=5/2\rightarrow F=5/2$	8 117.69±0.10
				$F=7/2\rightarrow F=7/2$	8 127.64±0.15
		4	7/2	$F=5/2\rightarrow F=5/2$	9 578.51±0.15
				$F=7/2\rightarrow F=7/2$	9 586.03±0.10
				$F=9/2\rightarrow F=9/2$	9 595.26±0.10
		5	9/2	$F=7/2\rightarrow F=7/2$	10 191.64±0.10
				$F=9/2\rightarrow F=9/2$	10 199.10±0.10
				$F=11/2\rightarrow F=11/2$	10 208.14±0.10
		6	11/2	$F=9/2\rightarrow F=9/2$	9 914.39±0.10
				$F=11/2\rightarrow F=11/2$	9 921.53±0.10
				$F=13/2\rightarrow F=13/2$	9 929.88±0.10
$O^{16}D$	$\Pi_{\frac{3}{2}}$	5	11/2	$F=9/2\rightarrow F=9/2$ $F=11/2\rightarrow F=11/2$ $F=13/2\rightarrow F=13/2$	8 672.36±0.10
		6	13/2	$F=11/2\rightarrow F=11/2$ $F=13/2\rightarrow F=13/2$ $F=15/2\rightarrow F=15/2$	12 918.01±0.10
		7	15/2	$F=13/2\rightarrow F=13/2$ $F=15/2\rightarrow F=15/2$ $F=17/2\rightarrow F=17/2$	18 009.60±0.10
		8	17/2	$F=15/2\rightarrow F=15/2$ $F=17/2\rightarrow F=17/2$ $F=19/2\rightarrow F=19/2$	23 907.12±0.10

[15] Relative intensities for the hyperfine components are given in reference 9 and elsewhere.

noted that the quantum number N is well defined only for the higher rotational states.

The initial assignment[6] N,J for the $^2\Pi_{\frac{1}{2}}$ state of OH was based on ultraviolet data.[3] However, these quantum numbers can be assigned from the fact that the frequencies of any two of the observed transitions of OD or of the $^2\Pi_{\frac{1}{2}}$ state of OH allow, with the proper assignment, accurate prediction of all the other frequencies. The assignment is furthermore confirmed by relative intensity measurements and the observed hfs patterns.

Assignment of the quantum number F is based on the observed relative intensities of the strongest ($\Delta F=0$) hyperfine components for a given J, which should be approximately proportional to the respective values of F.

One might be surprised that transitions due to the $^2\Pi_{\frac{1}{2}}$ state have been detected with a magnetic spectrometer. The magnetic moment in this state, in a pure Hund's case (a) quantization would be expected to be close to zero as a result of cancellation of the contributions from the electron orbital motion and the electron spin. However, the rotational energy will gradually decouple the spin from the orbital angular momentum [intermediate coupling between Hund's cases (a) and (b)]. This spin uncoupling effect introduces a substantial magnetic moment into the $^2\Pi_{\frac{1}{2}}$ state even for as low a value of J as $\frac{3}{2}$, and makes possible the Zeeman modulation of the spectra by magnetic fields of about 5 gauss. A more detailed discussion of the molecular magnetic moment appears in Sec. 4(d).

4. THEORY

(a) The Hamiltonian, Wave Functions in the Intermediate Coupling State, and Approximate Energies

The molecular Hamiltonian involves (a) the rotational terms and the fine structure interaction $\mathbf{L}\cdot\mathbf{S}$ (designated hereafter as H_1), (b) magnetic hyperfine structure (H_2), and (c) the interaction with an external magnetic field (H_3). The interaction due to the quadrupole moment of the deuteron is expected to be small and will not be discussed since the observed hyperfine structure in OD can be accounted for within the present experimental error by the magnetic hyperfine interaction alone.

H_{total} is then taken as $H_1+H_2+H_3$, where

$$\begin{aligned} H_1 &= B[(J_x-S_x-L_x)^2+(J_y-S_y-L_y)^2] \\ &\quad +AL_zS_z+A(L_xS_x+L_yS_y) \\ &= B[J(J+1)-\Lambda^2]+BS(S+1)+AL_zS_z-2B\mathbf{J}\cdot\mathbf{S} \\ &\quad +B(L_x^2+L_y^2)+(2B+A)(L_xS_x+L_yS_y) \\ &\quad -2B(J_xL_x+J_yL_y). \end{aligned} \tag{3}$$

The z direction is along the internuclear axis. As usual, A and B designate the fine structure interaction and rotational constants respectively, $\mathbf{L}$ and $\mathbf{S}$ the electron orbital and spin angular momenta, and $\mathbf{J}$ the total molecular angular momentum exclusive of nuclear spin. Λ is the quantum number associated with L_z. Definitions of the various symbols used and values of the constants in OH and OD are given in Appendix I.

The first two lines in (3) give rise to the rotational and spin-orbit interaction energies; these terms are diagonal in Λ. The term $B(L_x^2+L_y^2)$ is diagonal in Λ and, to a high order of approximation, independent of J. Hence it adds to the energy a constant that will be ignored for the moment. The terms $(2B+A)(L_xS_x+L_yS_y)$ and $-2B(J_xL_x+J_yL_y)$ are off-diagonal in Λ and give rise to the Λ-type doubling. Note that A and B are the fine structure and rotational constants with their usual meaning only in those terms of (3) that are diagonal in Λ.

The magnetic hyperfine and Zeeman parts of the Hamiltonian (H_2 and H_3) are discussed in Secs. 4(c) and 4(d), respectively. In the present section the eigenvalues arising from H_1 will be given and wave functions constructed for $^2\Pi$ states in the general coupling scheme, intermediate between Hund's cases (a) and (b). These wave functions are necessary for the calculation of the molecular magnetic moment, the hyperfine structure and the electric dipole moment matrix element, since the experimental data indicate a strong dependence of these quantities on the extent of intermediate coupling.

The matrix elements of H_1 have been given by Van Vleck[16] on the basis of wave functions that correspond to a Hund's case (a) coupling scheme. In this representation both the electron orbital and spin angular momenta are quantized along the internuclear axis with eigenvalues Λ and Σ, respectively. The total angular momentum along the axis is designated by $\Omega(=\Lambda+\Sigma)$. The angular momentum due to the end over end rotation of the nuclei is added to Ω to form J.

There are six states to be considered: $\Pi_{\frac{1}{2}}$, $\Pi_{-\frac{1}{2}}$, $\Pi_{\frac{1}{2}}$, $\Pi_{-\frac{1}{2}}$, $\Sigma_{\frac{1}{2}}$, $\Sigma_{-\frac{1}{2}}$. The interactions between all pairs of states form a six-by-six determinant which can be factored[16] into two cubics by introducing wave functions of the symmetric and antisymmetric type rather than those that represent angular momentum of constant sign about the internuclear axis. In terms of the previous set ($\Pi_{\frac{1}{2}}$, $\Pi_{-\frac{1}{2}}$, etc.) the new wave functions are

$$\psi_{\text{sym, ant.}}=[\psi(\Lambda,\Sigma,\Omega)\pm\psi(-\Lambda,-\Sigma,-\Omega)]/\sqrt{2}. \tag{4}$$

One of the two 3-by-3 determinants into which the secular equation factors is

$$\begin{array}{c|ccc} & \Sigma_{\frac{1}{2}} & \Pi_{\frac{1}{2}} & \Pi_{\frac{1}{2}} \\ \Sigma_{\frac{1}{2}} & \kappa-\lambda & \mu & \eta \\ \Pi_{\frac{1}{2}} & \mu^* & \beta-\lambda & \epsilon \\ \Pi_{\frac{1}{2}} & \eta^* & \epsilon^* & \gamma-\lambda \end{array}. \tag{5}$$

The matrix elements, as given by Van Vleck,[16] along with the phase conventions to be observed, are reproduced in Appendix II. In (5), $\kappa=\alpha+\delta$ and $\mu=\theta+\zeta$,

[16] J. H. Van Vleck, Phys. Rev. 33, 467 (1929).

where

$$\alpha=E_\Sigma-E_\Pi+B_v(J+\tfrac{1}{2})^2,\quad \delta=(-1)^J B_v(J+\tfrac{1}{2}),$$
$$\theta=\langle\Pi|AL_y+2BL_y|\Sigma\rangle$$

and

$$\zeta=(-1)^J 2\langle\Pi|BL_y|\Sigma\rangle(J+\tfrac{1}{2}).$$

The other cubic determinant is identical with (5) except that $\kappa=\alpha-\delta$ and $\mu=\theta-\zeta$.

Our procedure in this paper is to diagonalize (5) to successively higher orders of approximation. The energies can be written (order of magnitude) as

$$E\sim[(1+A/B+(B \text{ or } A)/E_{\text{elec}} +((B \text{ or } A)/E_{\text{elec}}))^2+\cdots]B. \quad (6)$$

The expansion parameters, then are $(E_{\text{rotational}}/E_{\text{electronic}})$, and $(E_{\text{fine structure}}/E_{\text{electronic}})$.[17] $E_{\text{elec}}=E_\Sigma-E_\Pi$. With the constants[18] $A=-139.7$ cm^{-1}, $B=18.52$ cm^{-1}, and $E=32\,682.5$ cm^{-1}, the numerical values of the expansion parameters in OH are $(B/E)=1/1765$ and $(A/E)=1/234$. (In other molecules the values are of the same general order of magnitude and in all cases the expansion converges rather rapidly.) A representative figure for our experimental accuracy is one part in 150 000. Hence the expansion should include terms of at least second order in the expansion parameters. Even the third order term $[(B \text{ or } A)^3/E_{el}^3]B$ is actually somewhat larger than the experimental error. There are, however, several other small effects of the same order of magnitude (see Sec. 5a) that are neglected; hence inclusion of this term alone would not be justified. The terms of (6) will be corrected, to the appropriate order, for effects of coupling of rotation to vibrational motion, i.e., B is to be taken as $B_v[=B_e-(v+\tfrac{1}{2})\alpha_e]$, where α_e is the vibration-rotation interaction constant and also is to be corrected for centrifugal distortion.

The two Π states are only 140 cm^{-1} apart, whereas the Σ state lies 32 683 cm^{-1} above them. Hence the rotational and spin-orbit energies [zero-order term in (6)] can be obtained by diagonalizing the submatrix

$$\begin{pmatrix}\beta-\lambda & \epsilon\\ \epsilon^* & \gamma-\lambda\end{pmatrix}. \quad (7)$$

The result is[18]

$$\lambda=\tfrac{1}{2}(\beta+\gamma)\pm\tfrac{1}{2}[(\beta-\gamma)^2+4|\epsilon|^2]^{\frac{1}{2}} =\tfrac{1}{2}(\beta+\gamma)\pm\tfrac{1}{2}B_pX, \quad (8)$$

where

$$X\equiv+[4(J+\tfrac{1}{2})^2+\lambda(\lambda-4)]^{\frac{1}{2}},\quad \lambda\equiv A/B_p. \quad (9)$$

The diagonalization of (7) yields in addition the needed wave functions:

$$\psi_{\text{Int. }1}=\left(\frac{X-2+\lambda}{2X}\right)^{\frac{1}{2}}\psi(\Pi_{\frac{1}{2}})\mp\left(\frac{X+2-\lambda}{2X}\right)^{\frac{1}{2}}\psi(\Pi_{\frac{1}{2}}),$$
$$\psi_{\text{Int. }2}=\pm\left(\frac{X-2+\lambda}{2X}\right)^{\frac{1}{2}}\psi(\Pi_{\frac{1}{2}})+\left(\frac{X+2-\lambda}{2X}\right)^{\frac{1}{2}}\psi(\Pi_{\frac{1}{2}}). \quad (10)$$

$\psi(\Pi_{\frac{1}{2}})$ and $\psi(\Pi_{\frac{1}{2}})$ represent pure Hund's case (a) wave functions. In the double signs of (10) the upper ones apply to regular fine structure doublets (λ positive) and the lower to inverted doublets (λ negative). By letting $\lambda\to+\infty$ one sees from (10) that $\psi_{\text{Int. }1}$ and $\psi_{\text{Int. }2}$ denote those wave functions in the intermediate state that represent the pure $\Pi_{\frac{1}{2}}$ and $\Pi_{\frac{3}{2}}$ states respectively in the limit of Hund's case (a) of regular doublets. For inverted doublets this connection is reversed, i.e., for negative values of λ,

$$\psi_{\text{Int. }1}\to\psi(\Pi_{\frac{3}{2}}),\quad \psi_{\text{Int. }2}\to\psi(\Pi_{\frac{1}{2}}).$$

In the limit, Hund's case (b) ($2BJ\gg|A|$), the wave functions (10) will represent the two components of the spin doublet. In particular $\psi_{\text{Int. }1}$ and $\psi_{\text{Int. }2}$ go over to the states with $J=N+\frac{1}{2}$ and $J=N-\frac{1}{2}$ respectively. Expression (10) applies also to the lowest rotational level and properly expresses the fact that this state ($|J|=\frac{1}{2}$) is a pure $\psi(\Pi_{\frac{1}{2}})$ level. For $J=\frac{1}{2}$ $\psi_{\text{Int. }1}$ and $\psi_{\text{Int. }2}$ equal $\psi(\Pi_{\frac{1}{2}})$ for λ positive and negative respectively. As mentioned above, wave functions (10) will be used in evaluating the magnetic moment, hfs and line intensities. The effect of the Σ state which has been neglected in constructing (10) can be taken into account, when required in the calculation of these quantities, by second-order perturbation theory.

(b) Molecular Energies to Order $[(E_{\text{rot}} \text{ or } E_{\text{fs}})/E_{el}]^2$. Λ-Doubling in $^2\Pi$ and ρ-Doubling in $^2\Sigma$ States

The terms in first and second order in the expansion parameters that are to be considered arise from the interactions between the $^2\Pi$ and $^2\Sigma$ states. The most important effects of these interactions are the Λ-type doubling in the $^2\Pi$ states and the ρ-type doubling in the $^2\Sigma$ state.

These higher order terms are derived as follows: The determinant (5) is expanded and written in the form

$$\kappa\beta\gamma+\mu\epsilon\eta^*+\eta\mu^*\epsilon^*-\beta\eta\eta^*-\gamma\mu\mu^*-\kappa\epsilon\epsilon^* -(\kappa\beta+\kappa\gamma+\beta\gamma-\epsilon\epsilon^*-\mu\mu^*-\eta\eta^*)\lambda+(\kappa+\beta+\gamma)\lambda^2-\lambda^3 =(\lambda-\lambda_1)(\lambda-\lambda_2)(\lambda-\lambda_3), \quad (11)$$

where

$$\lambda_i=\lambda_i^{(0)}+\lambda_i^{(1)},\quad i=1,2,3. \quad (12)$$

In (12) $\lambda_1^{(0)}$, $\lambda_2^{(0)}$, $\lambda_3^{(0)}$ are the zero-order solutions of (5):

$$\lambda_1^{(0)}=\kappa,\quad \lambda_{2,3}^{(0)}=\tfrac{1}{2}(\beta+\gamma\pm B_pX). \quad (13)$$

If the λ_i from (12) are introduced into (11) and terms higher than first-order in $\lambda_1^{(1)}$ or $1/E$ are omitted, three

[17] One may note that in expansion (6) the terms $(B/E)^n$, $(B/E)^1$, $(B/E)^2$ correspond to terms $(m/M)^1$, $(m/M)^2$, $(m/M)^3$, in Born-Oppenheimer approximation.

[18] G. Herzberg, *Molecular Spectra and Molecular Structure*. (D. Van Nostrand Company, Inc., New York, 1950), vol. 1.

linear equations for the unknowns $\lambda_i^{(1)}$ are obtained.

$$\lambda_1^{(1)}=(\mu\mu^*+\eta\eta^*)/E,$$

$$\lambda_{2,3}^{(1)}=-\frac{(\mu\mu^*+\eta\eta^*)}{2E}\mp\frac{1}{EB_pX}\Big[\frac{(\beta-\gamma)(\mu\mu^*-\eta\eta^*)}{2}+\mu\epsilon\eta^*+\mu^*\epsilon^*\eta\Big]. \quad (14)$$

The energies to this order had already been given[16] in terms of these matrix elements.

We carry out this procedure once more to obtain the next order terms. The derivation will be only briefly outlined here since it is rather straightforward, although tedious and lengthy. We write

$$\lambda_i=\lambda_i^{(0)}+\lambda_i^{(1)}+\lambda_i^{(2)}, \quad i=1, 2, 3 \quad (15)$$

$\lambda_i^{(0)}+\lambda_i^{(1)}$ is the sum of the zero and first order terms given by (13) and (14). Inserting (15) in (11) and equating coefficients of the same powers of λ on both sides, one obtains three cubics in the new unknowns $\lambda_i^{(2)}$. These become the following three linear equations when terms in powers of $\lambda_i^{(2)}$ higher than the first and those in $1/E$ higher than the second are omitted.

$$\lambda_1^{(2)}=\frac{1}{E^2}[\mu\mu^*\beta+\eta\eta^*\gamma+\mu\epsilon\eta^*+\eta\mu^*\epsilon^*-(\eta\eta^*+\mu\mu^*)(\alpha'+\delta)], \quad (16)$$

$$\begin{aligned}\lambda_{2,3}^{(2)}=\frac{\pm1}{E^2B_pX}\Big[&(\mu\mu^*+\eta\eta^*)\Big(\frac{(\beta+\gamma)^2-B_p^2X^2}{4}\Big)\\&-(\mu\mu^*\beta+\eta\eta^*\gamma+\mu\epsilon\eta^*+\eta\mu^*\epsilon^*)\Big(\frac{\beta+\gamma\pm B_pX}{2}\Big)\\&-(\alpha'+\delta)(\beta\eta\eta^*+\gamma\mu\mu^*-\mu\epsilon\eta^*-\mu^*\epsilon^*\eta)\\&+(\alpha'+\delta)(\eta\eta^*+\mu\mu^*)\Big(\frac{\beta+\gamma\pm B_pX}{2}\Big)\\&+\frac{1}{B_p^2X^2}[(\beta-\gamma)^2\mu\mu^*\eta\eta^*+\epsilon\epsilon^*(\mu^2\mu^{*2}+\eta^2\eta^{*2})\\&-2\mu\mu^*\eta\eta^*\epsilon\epsilon^*-(\beta-\gamma)(\mu\mu^*-\eta\eta^*)\\&\times(\mu\epsilon\eta^*+\eta\mu^*\epsilon^*)]\Big]. \quad (17)\end{aligned}$$

In Eqs. (13)–(17) where double signs occur the upper ones are to be taken for the $\Pi_{\frac{1}{2}}$ state and the lower for the $\Pi_{\frac{3}{2}}$ state in inverted doublets. In regular doublets the upper signs apply to the $\Pi_{\frac{3}{2}}$ state and the lower to the $\Pi_{\frac{1}{2}}$ state.

The energies then, to second order, are the sum

$$\lambda_i^{(0)}+\lambda_i^{(1)}+\lambda_i^{(2)}.$$

The λ_i given above represents only one component of the Λ-type doublet in each Π state and given J. The energy of the other is given by the same expressions except that δ is replaced by $-\delta$ and ζ by $-\zeta$.

The energy expressions involve the molecular constants $E(\equiv E_\Sigma-E_\Pi)$, B_p, B_s, $\lambda(\equiv A/B_p)$ and the following two products of specific matrix elements connecting the $^2\Pi$ with the $^2\Sigma$ state:

$$\langle\Pi|AL_y+2BL_y|\Sigma\rangle\langle\Sigma|BL_y|\Pi\rangle$$

and

$$|\langle\Pi|BL_y|\Sigma\rangle|^2.$$

One considers the quantities

$$\alpha_p\equiv4\sum_{\Sigma\text{-states}}(-1)^s\frac{\langle\Pi|AL_y+2BL_y|\Sigma\rangle\langle\Sigma|BL_y|\Pi\rangle}{E_\Sigma-E_\Pi},$$

$$\beta_p\equiv4\sum_{\Sigma\text{-states}}(-1)^s\frac{|\langle\Pi|BL_y|\Sigma\rangle|^2}{E_\Sigma-E_\Pi} \quad (18)$$

as additional molecular parameters that measure the effects of $^2\Sigma$ states on the $^2\Pi$ state. The summation over Σ states in (18) is to indicate that the interactions of all Σ states with the $^2\Pi$ are taken into account.

The interaction with the $^2\Sigma$ state produces a shift in the energy of each J level in the $^2\Pi$ states and in addition splits it into the Λ-type doublet. We write then for the energy of a level with given J:

$$W=W_1\pm\tfrac{1}{2}W_2, \quad (19)$$

where W_2 represents the splitting of the Λ-type doublet.

Explicit expressions for W in terms of J and the molecular constants can be obtained from Eqs. (13), (14), and (17) using the matrix elements listed in Appendix II. They are

$$\begin{aligned}W_1=&B_p'(J-\tfrac12)(J+\tfrac32)\pm\frac{B_p''X}{2}+C_1\\&\mp\frac{\alpha_p}{X}\Big[(J-\tfrac12)(J+\tfrac32)\Big(1+\frac{B_p}{E}(J-\tfrac12)(J+\tfrac32)\\&-\frac{B_s}{E}(J+\tfrac12)^2\Big)-\Big(\frac{2-\lambda}{2}\Big)\frac{B_s}{E}(J+\tfrac12)^2\Big]\\&\mp\frac{\beta_p}{2X}\Big[(2-\lambda)\Big(1+\frac{B_p}{E}(J-\tfrac12)(J+\tfrac32)-\frac{B_s}{E}(J+\tfrac12)^2\Big)\\&+\frac{B_pX^2}{E}J(J+1)-\frac{4B_s}{E}(J+\tfrac12)^2(J-\tfrac12)(J+\tfrac32)\Big]\\&\mp\frac{\alpha_p^2}{8\beta_p}\Big(\frac{2-\lambda}{X}\Big)\Big[1+\frac{B_p}{E}(J-\tfrac12)(J+\tfrac32)-\frac{B_s}{E}(J+\tfrac12)^2\Big]\\&\pm\frac{(J-\tfrac12)(J+\tfrac32)}{B_pX^2}\Big[\alpha_p^2\Big(\Big(\frac{2-\lambda}{2}\Big)^2+J(J+1)+\tfrac34\Big)\\&+\beta_p^2(J+\tfrac12)^2[(2-\lambda)^2+1]-2\alpha_p\beta_p(2-\lambda)\\&\times[J(J+1)+\tfrac34]+\frac{\alpha_p^4}{16\beta_p^2}-\frac{\alpha_p^2(2-\lambda)}{4\beta_p}\Big]\\&-\frac{\beta_p(B_p-B_s)}{E}J^2(J+1)^2, \quad (20)\end{aligned}$$

where

$$B_p'=B_p-\beta_p\left(1-\frac{B_p}{E}\right)-\alpha_p\left(1+\frac{\alpha_p}{4\beta_p}\right)\left(\frac{B_p-B_s}{2E}\right),$$

$$B_p''=B_p\left(1-\frac{\alpha_p^2-2\beta_p^2}{8\beta_pE}\right),$$

$$C_1=-\frac{\alpha_p^2}{8\beta_p}\left(1-\frac{\lambda B_p}{2E}+\frac{B_p-B_s}{E}\right)-\frac{1}{2}\beta_p\left(1+\frac{\lambda B_p}{2E}-\frac{B_p-B_s}{8E}\right)+\frac{\alpha_pB_s}{2E}.$$

(One may add to C_1 the term $B_p(L_z^2+L_y^2)$ that was neglected earlier.) Denoting the first- and second-order contributions to W_2 as $\nu_\Lambda^{(1)}$ and $\nu_\Lambda^{(2)}$ one obtains

$$W_2=\nu_\Lambda^{(1)}+\nu_\Lambda^{(2)}, \tag{21}$$

$$\nu_\Lambda^{(1)}=-\alpha_p(J+\tfrac{1}{2})\left(\frac{\pm X+2-\lambda}{\pm X}\right)\mp\frac{4\beta_p}{X}(J-\tfrac{1}{2})\times(J+\tfrac{1}{2})(J+\tfrac{3}{2}), \tag{22}$$

$$\nu_\Lambda^{(2)}=\pm\frac{(J+\frac{1}{2})}{EX}\alpha_p\Big[(2(J-\tfrac{1}{2})(J+\tfrac{3}{2})\pm X)\Big((B_s-B_p)(J+\tfrac{1}{2})^2+B_p\Big(\frac{\lambda\mp X}{2}+(J-\tfrac{1}{2})(J+\tfrac{3}{2})\Big)\Big)$$
$$-2B_s((J+\tfrac{1}{2})^2(J(J+1)-7/4+\lambda/2)-(J-\tfrac{1}{2})(J+\tfrac{3}{2}))\Big]\pm\frac{(J+\frac{1}{2})}{EX}\beta_p[(2(J-\tfrac{1}{2})(J+\tfrac{3}{2})\pm X)$$
$$\times(2B_s(J(J+1)-\tfrac{1}{4})-2B_p(J-\tfrac{1}{2})(J+\tfrac{3}{2}))+B_s(2(J+\tfrac{1}{2})^2-\lambda)]$$
$$\mp\frac{(J+\frac{1}{2})}{EX}\frac{\alpha_p^2}{4\beta_p}B_s(\lambda-2\mp X)\mp\frac{C_2(J-\frac{1}{2})(J+\frac{1}{2})(J+\frac{3}{2})}{B_pX^3}, \tag{23}$$

where

$$C_2=-2\alpha_p\beta_p(\lambda^2-4\lambda+6)+(3\alpha_p^2+4\beta_p^2)(2-\lambda)-\alpha_p^3/\beta_p.$$

In (20), (22), and (23) the upper signs apply to the $\Pi_{\frac{1}{2}}$ states of regular doublets and the $\Pi_{\frac{1}{2}}$ states of inverted ones. The lower signs are to be taken for the $\Pi_{\frac{1}{2}}$ state of regular and the $\Pi_{\frac{1}{2}}$ state of inverted doublets. For molecules close to Hund's case (*b*) the upper and lower signs apply to states with $N=J+\frac{1}{2}$ and $N=J-\frac{1}{2}$, respectively.

The terms in first and second order in expansion parameters appear above in a somewhat disguised form. First order terms are directly proportional to α_p, β_p or α_p^2/β_p, whereas the ones in second order have denominators E or B_pX^3.

The energy expressions given above do not contain terms due to the interaction between the electron magnetic moment and magnetic fields generated directly by the rotation of the nuclei. Such terms have the form $\gamma\mathbf{N}\cdot\mathbf{S}$. These small effects are not easily separated from the ones due to the $^2\Pi-{}^2\Sigma$ interaction. The $\gamma\mathbf{N}\cdot\mathbf{S}$ interaction may be explicitly introduced in the Hamiltonian. One then should add the constant term $-\gamma/2$ to the energies of $\Pi_{\frac{1}{2}}$ and $\Pi_{\frac{1}{2}}$ states and replace in the intermediate coupling formulas λ by $\lambda+\gamma/B_p$ and X approximately by

$$X'\equiv[4(J+\tfrac{1}{2})^2(1-\gamma/2B_p)^2+\lambda(\lambda-4)+2\lambda\gamma/B_p]^{\frac{1}{2}}.$$

γ is of order $(m/M)A$, and hence much smaller than either A or B. In the $^2\Sigma$ state this interaction will, in addition, contribute directly to the ρ-type doubling as will be discussed below.

We will discuss here the Λ-type doubling in some detail. The energy expressions given above apply in the general coupling scheme intermediate between Hund's cases (*a*) and (*b*). Simplified forms of the first order term $\nu_\Lambda^{(1)}$ for the pure cases (*a*) or (*b*) can be obtained. However, if one uses the second order term $\nu_{\Lambda 1}^{(2)}$, the general formula (22) should be used for $\nu_\Lambda^{(1)}$ rather than any limiting case form since the effects of intermediate coupling are almost always larger than the correction $\nu_\Lambda^{(2)}$.

On the other hand, along with the general formula (22) for $\nu_\Lambda^{(1)}$ one can use, for molecules extremely close to pure coupling scheme, simplified forms of $\nu_\Lambda^{(2)}$. From (23), letting $\lambda\to\pm\infty$, one derives for pure Hund's case (*a*) ($|A|\gg 2BJ$) for $\Pi_{\frac{1}{2}}$ states:

$$\nu_\Lambda^{(2)}=\mp\left(\frac{\alpha_p-2\beta_p}{2E}\right)\left(|A|-\frac{B_s(\alpha_p-2\beta_p)}{\beta_p}\right)(J+\tfrac{1}{2}), \tag{24}$$

and for $\Pi_{\frac{1}{2}}$ states

$$\nu_\Lambda^{(2)}=\pm\left(\frac{\alpha_p-2\beta_p}{2E}\right)(|A|)(J+\tfrac{1}{2}). \tag{25}$$

In (24) and (25) the upper and lower signs apply to inverted and regular doublets respectively. In deriving these formulas terms of the form AB^2/E^2 and B^3/E^2 have been neglected as small compared to A^2B/E^2.

For the limiting case (*b*) ($2BJ\gg|A|$) from (23)

letting $\lambda \to 0$

$$\nu_\Lambda^{(2)} = \pm \frac{2(B_s - B_p)}{E} \beta_p \left[J^2(J+1)^2 \pm J(J+1)(2J+1) + \tfrac{1}{2}J(J+1) + \tfrac{3}{16} \right] \pm \frac{B_s + B_p}{E} \beta_p \left[2J(J+1) + \tfrac{1}{4} \pm 1 \right]. \quad (26)$$

The upper and lower signs apply to states with $N = J + \frac{1}{2}$ and $N = J - \frac{1}{2}$ respectively. Again in deriving (26) only terms of the form B^3/E^2 have been retained, the terms A^2B/E^2 and AB^2/E^2 being neglected. Hence (26) and also (24), (25) should hold only for cases very close to the pure coupling schemes. For cases such as the OH where $|A| \sim 2BJ$ the general formula (23) has to be applied.

In the $^2\Sigma$ state for each rotational level with rotational angular momentum quantum number N there are two states that correspond to the two orientations of $\mathbf{S}$ relative to $\mathbf{N}$. The energies are the sum $\lambda_1^{(0)} + \lambda_1^{(1)} + \lambda_1^{(2)}$ given by (13), (14), and (16). Corresponding to $J = N \mp \frac{1}{2}$, one takes in these expressions $\kappa = \alpha \pm (-1)^S \delta$ and $\mu = \theta \pm (-1)^S \zeta$. Thus for levels of the same N:

$$W_\Sigma = C_s + B_s' N(N+1) \pm \left[\alpha_s \left(1 - \frac{\lambda B_p}{2E} \right) - 2\beta_s \left(1 - \frac{B_p}{2E} \right) - \frac{\alpha_s^2 B_p}{4\beta_s E} \right] (N + \tfrac{1}{2}) \pm (\alpha_s - 2\beta_s) \left(\frac{B_p - B_s}{E} \right) N(N+1)(N+\tfrac{1}{2}) + 2\beta_s \left(\frac{B_p - B_s}{E} \right) N^2(N+1)^2, \quad (27)$$

where

$$C_s = E - \frac{\alpha_s}{2} \left[1 + \left(\frac{4-\lambda}{2} \right) \frac{B_p}{E} \right] + \frac{\beta_s B_p}{2E} (3 - \lambda) + \frac{\alpha_s^2}{4\beta_s} \left(1 + \left(\frac{1-\lambda}{2} \right) \frac{B_p}{E} \right),$$

and

$$B_s' = B_s + 2\beta_s \left(1 - \frac{B_p}{E} \right) - \alpha_s \left(\frac{B_p - B_s}{2E} \right) + \frac{\alpha_s^2}{4\beta_s} \left(\frac{B_p + B_s}{E} \right).$$

The constants α_s, β_s are defined as

$$\alpha_s \equiv 4 \sum_{\Pi\text{-states}} (-1)^\epsilon \frac{\langle \Pi | AL_y + 2BL_y | \Sigma \rangle \langle \Sigma | BL_y | \Pi \rangle}{E_\Sigma - E_\Pi},$$
$$\beta_s \equiv 4 \sum_{\Pi\text{-states}} (-1)^\epsilon \frac{|\langle \Pi | BL_y | \Sigma \rangle|^2}{E_\Sigma - E_\Pi}, \quad (28)$$

and differ from α_p and β_p only in that the summation is over all Π instead of over all Σ states. If only one Π state interacts with one Σ state then $\alpha_p = \alpha_s$, $\beta_p = \beta_s$. The upper and lower signs in (27) apply to the states with $J = N - \frac{1}{2}$ and $J = N + \frac{1}{2}$ respectively.

The energy difference between these two states gives the ρ-type doubling:

$$\nu_\rho = 2 \left[\alpha \left(1 - \frac{\lambda B_p}{2E} \right) - 2\beta_s \left(1 - \frac{B_p}{2E} \right) - \frac{\alpha_s^2 B_p}{4\beta_s E} \right] (N + \tfrac{1}{2}) + (\alpha_s - 2\beta_s) \left(\frac{B_p - B_s}{E} \right) N(N+1)(2N+1). \quad (29)$$

One sees from (29) that when the magnetic interaction constant A is zero, $\alpha_s = 2\beta_s$ and both first- and second-order contributions to ν_ρ vanish. Hence in this case the interaction with the $^2\Pi$ state (L-uncoupling) does not remove the degeneracy of the levels with $J = N \pm \frac{1}{2}$ in $^2\Sigma$ state. The degeneracy however can be removed directly by magnetic fields generated by the rotation of the nuclei themselves rather than the transfer of rotational angular momentum to the electrons. The direct interaction ($\mathbf{N} \cdot \mathbf{S}$) produces a splitting

$$\nu_\rho' = \text{const}\,(N + \tfrac{1}{2}),$$

which is of the same form as the first term of (29).

Certain points concerning the form of the energy expressions for the $^2\Pi$ and $^2\Sigma$ states should be noted. The inclusion of effects in second order does not introduce any new parameters. α_p, β_p and the similar quantities α_s and β_s suffice to describe the $^2\Pi - ^2\Sigma$ interactions to both first and second order in expansion parameters.[19] Part, but not all, of the first and second order terms (aside from the ones that contribute to doubling) have the J or N dependence of the usual rotational energy terms. The effect of these terms appears as a contribution to that due to the "bona fide" moment of inertia. However, only a part of the higher order terms can be accounted for by expressions like $B_{\text{effective}} J(J+1)$. There are also terms of the form $J^2(J+1)^2$ or $N^2(N+1)^2$ which will add to the usual centrifugal distortion term.

The relative order of magnitude of the first and second order terms can be readily established by comparing, for instance, the two contributions $\nu_\Lambda^{(1)}$ and $\nu_\Lambda^{(2)}$ to the Λ-type doubling. Inserting approximate numerical values in (22) and (23) above for OH, one sees that

$$\nu_\Lambda^{(2)} \sim (1/350) \nu_\Lambda^{(1)},$$

which is of the order to be expected from the values (1/234) and (1/1726) of our expansion parameters.

From this result one might surmise that the energy

[19] *Note added in proof.*—The constants α^2, β^2 that appear in some of the second-order terms are strictly the squares of the first-order constants α and β only in the approximation of one Π state interacting with one or several closely spaced Σ states.

expressions given above should account for the $^2\Pi-^2\Sigma$ interactions to about one part in 100 000 which is comparable to the experimental accuracy. There are, however, substantial corrections to be applied to these formulas. The most important one, which also can be readily taken into account, is the effect of centrifugal distortion on the moment of inertia. In addition to B this would affect λ and also α_p, β_p, α_s, β_s.

The rotational constant may be written

$$B=B_0\left[1-\frac{D_0}{B_0}f(N \text{ or } J)\right],$$

where D_0 is the centrifugal distortion constant $(=4B^3/\omega_{\text{vib}}{}^2)$. In $^2\Sigma$ states and also in the limiting Hund's case (b) for $^2\Pi$ states, $f(N)$ is $N(N+1)$. We will use here a more elaborate form, derived in Sec. 4f, which applies to intermediate coupling states. λ then has the form

$$\lambda=\lambda_0\left(1+\frac{D_0}{B_0}f\right),$$

and in quantities such as α_p,

$$\langle \Pi|BL_y|\Sigma\rangle = (\langle \Pi|BL_y|\Sigma\rangle)_0\left(1-\frac{D_0}{B_0}f\right). \quad (30)$$

Expression (30) implies the separation of B from the rest of the matrix element (pure precession hypothesis, only approximately correct), but only for the centrifugal correction on B. For the main contribution to the energies the constants to be determined from the data, defined in (18) and (28) above, are quite independent of this restriction.

When one strives for theoretical accuracy comparable to that of the data, the question arises whether the constants α_p, β_p, α_s, β_s are independent of small changes in internuclear distance (aside from the direct effect on B) that result from centrifugal stretching. A small change of the wave function from one rotational state to the next, affecting the matrix $\langle \Pi|L_y|\Sigma\rangle$ is not unexpected in extremely light molecules such as the OH. Such a variation is indicated by the experimental data and is discussed, along with some other small contributions to the energies, in Sec. 5(a).

(c) Magnetic Hyperfine Structure

The magnetic hyperfine structure may be considered to arise from (a) the interaction $(\mathbf{I}\cdot\mathbf{L})$ of the nuclear magnetic moment with the orbital motion of the unpaired electron or electrons (b) the dipole-dipole interaction $\mathbf{I}\cdot\mathbf{S}/r^3-3(\mathbf{I}\cdot\mathbf{r})(\mathbf{S}\cdot\mathbf{r})/r^5$ and (c) the relativistic part of the spin-spin interaction that is characteristic of atomic s-states.

The theory of magnetic hyperfine structure in diatomic molecules has been given by Frosch and Foley,[20] who derived the Hamiltonian from the Dirac equation for the electron. An alternative and simplified derivation of the hyperfine interaction, along the lines indicated in the preceding paragraph, has also been given.[21] This recent re-examination of the theory has revealed that two constants (denoted below by d and e) in the Hamiltonian of Frosch and Foley need be corrected by numerical factors of two. Aside from this the Hamiltonian is that of Frosch and Foley. Thus

$$H_2=a\mathbf{I}\cdot\mathbf{L}+(b+c)I_zS_z+\tfrac{1}{2}b(I^+S^-+I^-S^+) +\tfrac{1}{2}d(e^{2i\varphi}I^-S^-+e^{-2i\varphi}I^+S^+) +e[e^{i\varphi}(S^-I_z+I^-S_z)+e^{-i\varphi}(S^+I_z+I^+S_z)], \quad (31)$$

where

$$I^+=I_x+iI_y, \quad I^-=I_x-iI_y, \quad \text{etc.},$$

$$a=2\mu_0\frac{\mu_I}{I}(1/r^3)_{\text{av}},$$

$$b=-\mu_0\frac{\mu_I}{I}[(3\cos^2\chi-1)/r^3]_{\text{av}}+\frac{16\pi}{3}\mu_0\frac{\mu_I}{I}\psi^2(0),$$

$$c=3\mu_0\frac{\mu_I}{I}[(3\cos^2\chi-1)/r^3]_{\text{av}},$$

$$d=3\mu_0\frac{\mu_I}{I}(\sin^2\chi/r^3)_{\text{av}},$$

$$e=3\mu_0\frac{\mu_I}{I}(\sin\chi\cos\chi/r^3)_{\text{av}}.$$

μ_0 is the Bohr magneton (taken as positive) and μ_I and I are the nuclear magnetic moment and spin respectively. $\mathbf{r}$ denotes the radius vector from the nucleus to the interacting electron and χ the angle between $\mathbf{r}$ and the internuclear axis. The angle φ is defined through the relations $x=r\sin\chi\cos\varphi$, $y=r\sin\chi\sin\varphi$, hence the φ dependence of the wave function is $e^{\pm i\Lambda\varphi}$. $\psi^2(0)$ is the probability density of electron spin at the nucleus whose hyperfine interaction is being considered.

The averages are to be taken only over the electron or electrons that contribute to the hyperfine interaction. In particular, the average involved in the constant a is to be taken over the electron(s) possessing unpaired orbital angular momentum, whereas the constants b, c, d, and e are associated with electron(s) carrying unpaired spins. The terms aI_zL_z and $(b+c)I_zS_z$ in (31) have matrix elements diagonal in Λ and Σ and give the same energy contributions to each member of the Λ-type doublet. The operator

$$d(e^{2i\varphi}I^-S^-+e^{-2i\varphi}I^+S^+)/2$$

[20] R. A. Frosch and H. M. Foley, Phys. Rev. **88**, 1347 (1952).
[21] G. C. Dousmanis, Phys. Rev. **97**, 967 (1955).

has matrix elements of the form $\Delta\Lambda=\pm 2$ and for specific values of Λ and Σ gives equal and opposite contributions to each member of the Λ doublet.[22]

The matrix elements of H_2 are written down in a pure Hund's case (a) representation, using the relation[23]:

$$\langle \alpha J|I^z|\alpha' J\rangle=\langle \alpha J|J^z|\alpha' J\rangle \mathbf{I}\cdot\mathbf{J}/J(J+1)$$

for matrix elements diagonal in J.

Thus

$$\begin{aligned}\langle \Pi_{\frac{1}{2}}|H_2|\Pi_{\frac{1}{2}}\rangle&=\tfrac{1}{2}[a-\tfrac{1}{2}(b+c)]\mathbf{I}\cdot\mathbf{J}/J(J+1)\\&\quad\pm\tfrac{1}{2}d(J+\tfrac{1}{2})\mathbf{I}\cdot\mathbf{J}/J(J+1),\\\langle \Pi_{\frac{1}{2}}|H_2|\Pi_{\frac{3}{2}}\rangle&=\tfrac{3}{2}[a+\tfrac{1}{2}(b+c)]\mathbf{I}\cdot\mathbf{J}/J(J+1),\\\langle \Pi_{\frac{3}{2}}|H_2|\Pi_{\frac{3}{2}}\rangle&=-\tfrac{1}{2}b[(J-\tfrac{1}{2})(J+\tfrac{3}{2})]^{\frac{1}{2}}\mathbf{I}\cdot\mathbf{J}/J(J+1).\end{aligned}\tag{32}$$

The hyperfine energies are evaluated from these matrix elements and the wave functions given in (10) above. For the general coupling case intermediate between (a) and (b)

$$\begin{aligned}W_{\rm hfs}=\frac{1}{\pm 4X}\Big[&2a(\pm 2X+2-\lambda)\\&+b(4(J-\tfrac{1}{2})(J+\tfrac{3}{2})\pm X+4-2\lambda)\\&+c(\pm X+4-2\lambda)\Big]\frac{\mathbf{I}\cdot\mathbf{J}}{J(J+1)}\\&\pm\frac{d}{2}\left(\frac{\pm X-2+\lambda}{\pm 2X}\right)\left(\frac{(J+\tfrac{1}{2})\mathbf{I}\cdot\mathbf{J}}{J(J+1)}\right).\end{aligned}\tag{33}$$

The double signs in (33) need elaborate explanation. The positive sign in front of X applies to states that go over to the pure $\Pi_{\frac{1}{2}}$ state of Hund's case (a) for regular fine structure doublets or the $\Pi_{\frac{3}{2}}$ state in inverted doublets. For states close to case (b), the positive sign applies to that state that goes over to the $J=N+\frac{1}{2}$ member of the spin doublet. The negative sign in front of X is to be taken with states that are connected in case (a) with the $\Pi_{\frac{3}{2}}$ state for regular doublets or the $\Pi_{\frac{1}{2}}$ state for inverted ones, and in Hund's case (b) with the state $J=N-\frac{1}{2}$.

The terms of (33) proportional to a, b and c give identical hyperfine structure for each member of the Λ doublet. Superimposed on this structure appears the "hyperfine doubling" term in d which gives equal and opposite contributions to each member of the Λ doublet. The positive sign in front of d applies to the upper and the negative to the lower Λ-doublet level in $\Pi_{\frac{1}{2}}$ states in case (a) and the state with $J=N+\frac{1}{2}$ case (b). The signs are the reverse in case (b) for the state $J=N-\frac{1}{2}$. The term in d vanishes for $\Pi_{\frac{1}{2}}$ states in case (a).

[22] For a detailed description of this "hyperfine doubling" see reference 9.

[23] E. U. Condon and G. H. Shortley, *The Theory of Atomic Spectra* (Cambridge University Press, Cambridge, 1953), p. 61.

Simplified expressions for $W_{\rm hfs}$ that apply in the limiting cases can be derived from (33) by letting $\lambda\to\pm\infty$ or $\lambda\to 0$. These special formulas have been given elsewhere.[9]

Certain second-order effects have been neglected in deriving (33). These are due to cross terms between molecular (H_1) and hyperfine operators (H_2) with matrix elements of the form $\Delta\Lambda=\pm 1$, which connect $^2\Pi$ and $^2\Sigma$ states. These effects are very similar to the $C\mathbf{I}\cdot\mathbf{J}$ interactions in $^1\Sigma$ molecules. Their approximate magnitude is

$$\frac{A}{E_\Sigma-E_\Pi}\cdot W_{\rm hfs}\quad\text{or}\quad\frac{BJ}{E_\Sigma-E_\Pi}\cdot W_{\rm hfs}$$

or for OH about 0.4 Mc/sec. These effects then would give contributions somewhat larger than our experimental error, but not substantial enough to warrant quantitative determination from the present data. Terms of the form $W_{\rm hfs}^2/(E_\Sigma-E_\Pi)$, $W_{\rm hfs}^2/(E_{\Pi_{\frac{1}{2}}}-E_{\Pi_{\frac{3}{2}}})$ and $W_{\rm hfs}^2/E_{\rm rot}$ are smaller than the experimental error by an order of magnitude.

(d) Molecular Magnetic Moment and Zeeman Effect

The effects of intermediate coupling manifest themselves rather prominently in the molecular magnetic moment. In a Hund's case (a) coupling scheme both $\mathbf{L}$ and $\mathbf{S}$ are quantized along the internuclear axis. The magnetic moment in the $\Pi_{\frac{1}{2}}$ state would be rather large (about two Bohr magnetons) whereas it would be close to zero in the $\Pi_{\frac{3}{2}}$ state. An increasing amount of end-over-end rotation of the nuclei gradually decouples the spin from the axis and the $\Pi_{\frac{3}{2}}$ state gains thereby magnetic moment at the expense of the $\Pi_{\frac{1}{2}}$ state. The extent of spin uncoupling for given J depends exclusively on the relative values of the spin-orbit coupling constant A and the rotational constant B.

Quantitatively, the magnetic moment operator $(-\mu_0)(\mathbf{L}+2\mathbf{S})$ is evaluated in the appropriate intermediate coupling eigenstate represented by the wave functions (10) above. We assume that the applied magnetic fields are too small (as is our case) to influence the molecular coupling. The matrix elements are

$$\begin{aligned}&\langle \Pi_{\frac{1}{2}}|\mu_J|\Pi_{\frac{1}{2}}\rangle=0,\\&\langle \Pi_{\frac{1}{2}}|\mu_J|\Pi_{\frac{3}{2}}\rangle=-3\mu_0/[J(J+1)]^{\frac{1}{2}},\\&\langle \Pi_{\frac{3}{2}}|\mu_J|\Pi_{\frac{3}{2}}\rangle=\mu_0[(J-\tfrac{1}{2})(J+\tfrac{3}{2})/J(J+1)]^{\frac{1}{2}}.\end{aligned}$$

From above and (10) the magnetic moment is obtained as

$$\mu_J=-\frac{\mu_0}{[J(J+1)]^{\frac{1}{2}}}\left(\frac{3}{2}\pm\frac{2(J-\frac{1}{2})(J+\frac{3}{2})-\frac{3}{2}\lambda+3}{[4(J+\frac{1}{2})^2+\lambda(\lambda-4)]^{\frac{1}{2}}}\right).\tag{34}$$

In the double sign of (34), the positive one applies to $\Pi_{\frac{1}{2}}$ states of regular and $\Pi_{\frac{3}{2}}$ states of inverted doublets in Hund's case (a) and to the state with $J=N+\frac{1}{2}$ in

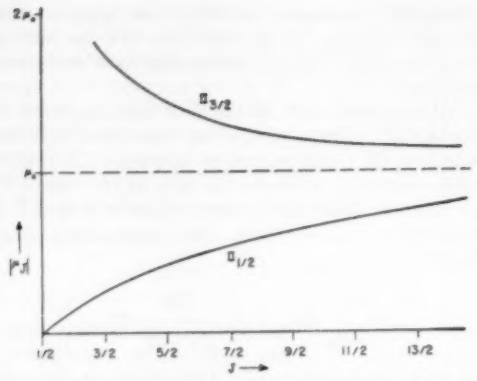

FIG. 3. The magnetic moment of OH as a function of J (from theory). Intermediate coupling introduces increasing amounts of magnetic moment into the $^2\Pi_{\frac{1}{2}}$ state. Neglected effects of the $^2\Sigma$ state and the anomalous moment of the electron would give small contributions (of order 0.001 μ_0) to all rotational states.

case (*b*). The negative sign applies to all other cases. μ_0 is taken as positive. This result can also be obtained by expanding, in the zero-field limit, the general formulas for the Zeeman effect given by Hill.[24]

The effects of the $^2\Sigma$ state are neglected. To this approximation both members of the Λ-type doublet have identical magnetic moments given by (34). A more detailed calculation should take into account the anomalous moment of the electron and the influence of the $^2\Sigma$ state. Both of these effects are of the same order of magnitude ($\sim 0.001\mu_0$) and much smaller than the contributions from intermediate coupling, except for the lowest rotational level $J=\frac{1}{2}$ in $^2\Pi_{\frac{1}{2}}$ states where the intermediate coupling effect vanishes. In pure case (a), for $^2\Pi_{\frac{1}{2}}$ states, (34) becomes

$$\mu_J=\frac{-3\mu_0}{[J(J+1)]^{\frac{1}{2}}}; \tag{35}$$

and in case (*b*),

$$\mu_J=\frac{-\mu_0}{[J(J+1)]^{\frac{1}{2}}}\left(\tfrac{3}{2}\pm(J+\tfrac{1}{2})\pm\frac{1}{2J+1}\right); \tag{36}$$

and for extremely high rotational states $\mu_J\rightarrow\pm\mu_0$ as one would expect, since $\mathbf{\Lambda}$ is perpendicular and $\mathbf{S}$ parallel or antiparallel to $\mathbf{J}$.

The behavior of μ_J in OH ($\lambda=-7.44$) as a function of J as given by (34) is shown in Fig. 3. The rise of the magnetic moment with J in the $^2\Pi_{\frac{1}{2}}$ state, and a value already of $0.3\mu_0$ for $J=\frac{3}{2}$, demonstrates that substantial Zeeman splittings can be obtained with fields of only a few gauss, which allows convenient detection of the spectra by Zeeman modulation.

At low fields that do not disturb the coupling scheme, and if nuclear spin is neglected for the moment, the Zeeman energies are

$$W_3=-\boldsymbol{\mu}\cdot\mathbf{H}=g_J\mu_0HM_J. \tag{37}$$

The molecular g-factor g_J is given by dividing the expressions for μ_J by $(-\mu_0)[J(J+1)]^{\frac{1}{2}}$.

When the hyperfine structure is much larger than the Zeeman energy, Zeeman effects in the presence of hyperfine structure can easily be calculated. Approximate numerical comparison of (33) with (37) ($H\sim 5$ gauss) shows that this is the case in the $^2\Pi_{\frac{1}{2}}$ state of both OH and OD and the $^2\Pi_{\frac{3}{2}}$ state of OH. In these states

$$W_3'=g_F\mu_0HM_F,$$
$$g_F=g_J\frac{F(F+1)+J(J+1)-I(I+1)}{2F(F+1)}. \tag{38}$$

The small term $\boldsymbol{\mu}_I\cdot\mathbf{H}$ is neglected in (38). For the $^2\Pi_{\frac{3}{2}}$ state in OD, (33) and (37) show that the hyperfine structure and the Zeeman effect are of the same order. This case requires more detailed treatment.[9] In the present work the Zeeman effect was used exclusively for detection purposes and precise measurements of it were not attempted.

(e) Matrix Element for Λ-Type Doubling Transitions in Intermediate Coupling

We are interested in the matrix element for electric dipole transitions of the type $\Delta J=0$ between the two members of the Λ doublet. The quantity that need be evaluated is

$$\langle\alpha J|\mu\mathbf{k}|\alpha' J\rangle,$$

where α and α' stand for the two states of the symmetric and antisymmetric type given by (4) above, μ is the electric dipole moment and $\mathbf{k}$ a unit vector along the internuclear axis.

In pure case (*a*) the matrix element is[9]

$$|\mu_{ij}|=\mu\Omega/[(J+1)(2J+1)]^{\frac{1}{2}}.$$

We use wave functions (10) to evaluate this in intermediate coupling. Since the electric dipole moment operator has no matrix elements connecting the $^2\Pi_{\frac{1}{2}}$ and $^2\Pi_{\frac{3}{2}}$ states, μ_{ij} is simply the sum of the contributions from the two pure components in each of the wave functions (10). Hence

$$|\mu_{ij}|^2=\frac{\mu^2}{(J+1)(2J+1)4X^2}[\Omega_1^2(\pm X-2+\lambda)^2$$
$$+\Omega_2^2(\pm X+2-\lambda)^2+2\Omega_1\Omega_2(X^2-(2-\lambda)^2)]. \tag{39}$$

With $\Omega_1=\frac{1}{2}$ and $\Omega_2=\frac{3}{2}$ in (39), the upper signs in front of X are to be taken for the state $J=N+\frac{1}{2}$ in case (*b*) or in case (*a*) for the $^2\Pi_{\frac{3}{2}}$ state when λ is positive and for the $^2\Pi_{\frac{1}{2}}$ state when λ is negative. The lower signs apply to the state which gives $J=N-\frac{1}{2}$ in case (*b*), or to the

[24] E. L. Hill, Phys. Rev. **34**, 1507 (1929).

$\Pi_{\frac{1}{2}}$ or $\Pi_{\frac{3}{2}}$ state in case (*a*) if λ is positive or negative respectively.

In the limit of pure case (*b*), we can neglect $(2-\lambda)$ compared to X and (39) becomes

$$|\mu_{ij}|^2=\frac{\mu^2}{(J+1)(2J+1)}\left(\frac{\Omega_1+\Omega_2}{2}\right)^2=\frac{\mu^2\Lambda^2}{(J+1)(2J+1)}. \tag{40}$$

This expression applies to both components of the spin doublet, and is identical with the one for *l*-type doublet transitions in linear triatomic molecules.[9]

The main feature of the intermediate coupling formula (39) is that $|\mu_{ij}|^2$ in case (*a*) is 9 times stronger (for the same J) for the $\Pi_{\frac{1}{2}}$ state than for the $\Pi_{\frac{3}{2}}$ state. During the transition from case (*a*) to (*b*) the ratio $|\mu_{ij}|^2$ in $\Pi_{\frac{1}{2}}$ to that in $\Pi_{\frac{3}{2}}$ state gradually decreases until it becomes unity in case (*b*).

Expression (39) is the appropriate one to be substituted into (1) for the calculation of line intensities.

(f) Centrifugal Distortion in Intermediate Coupling

Effects of centrifugal distortion for a light molecule such as the OH represent substantial corrections that have to be applied to all expressions involving the rotational constant B. One uses

$$B=B_0\left(1-\frac{D_0}{B_0}f\right), \tag{41}$$

where D_0 is the centrifugal constant and f has the form $N(N+1)$ in pure case (*b*).

We need the form of f that applies in the intermediate coupling state. One can see that the distortion will depend on the extent of intermediate coupling from the following simple consideration. In pure case (*b*) the distortion depends exclusively on N, which fails to be a good quantum number when the perturbation $A\mathbf{L}\cdot\mathbf{S}$, with matrix elements $\Delta N=\pm1$, introduces intermediate coupling.

One can calculate f in the general case starting with basic wave functions of case (*a*) [(10) above] or case (*b*). It is probably more appropriate to use for this correction basic wave functions of Hund's case (*b*), since in OH the value of D_0 has been obtained from ultraviolet measurements[3] involving higher rotational states and using the form $N(N+1)$. We will then calculate this distortion starting with the case (*b*) representation, where the fine structure rather than the rotational energy is considered as a perturbation. To obtain the required intermediate wave functions the matrix

$$\begin{array}{c} \\ N=J+\frac{1}{2} \\ N=J-\frac{1}{2} \end{array}\begin{array}{c} \begin{array}{cc} N=J+\frac{1}{2} & N=J-\frac{1}{2} \end{array} \\ \begin{pmatrix} H_{11} & H_{12} \\ H_{21} & H_{22} \end{pmatrix} \end{array} \tag{42}$$

need to be diagonalized. The matrix elements are[10]

$$H_{11}=B[(J+\tfrac{1}{2})^2+J-\tfrac{1}{2}]-A/(2J+1),$$
$$H_{22}=B[(J^2-\tfrac{1}{4})-1]+A/(2J+1),$$
$$H_{12}=A[(J+\tfrac{1}{2})^2-1]^{\frac{1}{2}}/(2J+1).$$

(42) of course yields the same energies (8) that were obtained on the basis of the case (*a*) representation. The intermediate wave functions, in terms now of those in pure case (*b*), that are derived from the diagonalization of (42) are

$$\psi_{\text{Int. I, II}}=\left(\frac{\pm X+2(J+\frac{1}{2})-\lambda/(J+\frac{1}{2})}{\pm 2X}\right)^{\frac{1}{2}}\psi(N=J-\tfrac{1}{2})$$
$$\pm\left(\frac{\mp X+2(J+\frac{1}{2})-\lambda/(J+\frac{1}{2})}{\mp 2X}\right)^{\frac{1}{2}}\psi(N=J+\tfrac{1}{2}). \tag{43}$$

The upper signs apply to the states $N=J-\frac{1}{2}$ in pure case (*b*), and to the $\Pi_{\frac{1}{2}}$ and $\Pi_{\frac{3}{2}}$ state in case (*a*) for λ positive and negative respectively. The lower signs apply to states that connect with $N=J+\frac{1}{2}$ in case (*b*), and to $\Pi_{\frac{1}{2}}$ and $\Pi_{\frac{3}{2}}$ states in case (*a*) for positive and negative values of λ respectively.

In the pure state $N=J-\frac{1}{2}$, $f=N(N+1)=J^2-\frac{1}{4}$ and in state $N=J+\frac{1}{2}$, $f=N(N+1)=(J+1)^2-\frac{1}{4}$. Since this correction term for B has the form N^2 and no matrix elements of the type $\Delta N=\pm1$, for intermediate coupling

$$f_{\text{Int.}}=a^2J^2+(1-a^2)(J+1)^2-\tfrac{1}{4}.$$

Here a and $(1-a^2)^{\frac{1}{2}}$ are the amplitudes of the pure case (*b*) states in the intermediate wave function as given by (43). This becomes, if the constant term is neglected.

$$f_{\text{Int. I, II}}=J^2+\left(\frac{\mp X+2(J+\frac{1}{2})-\lambda/(J+\frac{1}{2})}{\mp X}\right)(J+\tfrac{1}{2}),$$
$$B=B_0\left(1-\frac{D_0}{B_0}f_{\text{Int.}}\right). \tag{44}$$

The states to which the upper or lower signs apply are as explained for (43). Expression (44) reduces to the appropriate forms $N(N+1)+\text{cnost}$ for both members of the spin doublet in case (*b*) and to $J(J+1)+\text{const}$ for $\Pi_{\frac{1}{2}}$ and $\Pi_{\frac{3}{2}}$ states in case (*a*).

In all formulas where B appears, including λ and $\langle\Pi|BL_y|\Sigma\rangle$, it will be corrected according to (44).

5. INTERPRETATION OF EXPERIMENTAL RESULTS—COMPARISON WITH THEORY

(a) Λ-Type Doubling Variation of the Matrix $\langle\Pi|L_y|\Sigma\rangle$ with Rotation

One obtains the separations of the two Λ-type doublet levels (ν_Λ) by subtracting the hyperfine structure (using

[10] E. Hill and J. H. Van Vleck, Phys. Rev. **32**, 250 (1928).

TABLE II. Comparison of experimental and calculated values of the Λ-type doubling separations (ν_Λ) in OH and OD. The experimental values are obtained by subtracting the hyperfine structure from the data of Table I. Calculation *A* shows a fit with the theory that includes terms in both first and second order in $[(E_{rot}$ or $E_{el})/E_{el}]$. In calculation *B*, in addition, a small variation of $|\langle\Pi|L_y|\Sigma\rangle|^2$ ($\sim$ one part in 1400) from one rotational state to the next is allowed. Centrifugal distortion has been taken into account in *A* and *B* (see text).

Molecule	Electronic state	N	J	ν_Λ experimental (Mc/sec)	*A* ν_Λ(cal.) − ν_Λ(exp.)	*B* ν_Λ(cal.) ν_Λ(exp.)
$O^{16}H$	$^2\Pi_1$	2	3/2	7 797.59±0.15	−1.29	+1.35
		3	5/2	8 166.08±0.15	+3.86	−2.81
	$^2\Pi_1$	3	7/2	13 438.41±0.05	−15.14	−6.65
		4	9/2	23 822.98±0.05	−11.19	−6.54
		5	11/2	36 989.41±0.15	+33.11	+11.40
$O^{18}H$	$^2\Pi_1$	4	9/2	23 474.8 ±0.5	−13.8	−9.7
$O^{16}D$	$^2\Pi_1$	3	5/2	8 120.37±0.15	−7.56	+2.46
		4	7/2	9 587.93±0.15	−7.64	−1.49
		5	9/2	10 200.71±0.10	−0.25	−3.02
		6	11/2	9 922.78±0.10	+12.39	−4.17
	$^2\Pi_1$	5	11/2	8 672.36±0.10	−11.60	−1.62
		6	13/2	12 918.01±0.10	−11.16	−1.59
		7	15/2	18 009.60±0.10	−2.24	+1.54
		8	17/2	23 907.12±0.10	+24 29	+12.79

the Interval Rule) from the measured frequencies listed in Table I.

These undisplaced frequencies are compared with the theory that includes both first and second order terms in expansion parameters as given by (22) and (23) above. Centrifugal distortion is taken into account according to (44) which is applied to B, λ and $\langle\Pi|BL_y|\Sigma\rangle$. Of the seven molecular constants (λ, α_p, β_p, B_p, B_e, D_0, $E\equiv E_\Sigma - E_\Pi$) that enter the theoretical expressions the ones that appear in the main term $[\nu_\Lambda^{(1)}]$, aside from D_0, are λ, α_p, and β_p. These three constants will be determined from the present data. The others, including D_0, appear only in the second order term $\nu_\Lambda^{(2)}$ or in the small centrifugal correction to $\nu_\Lambda^{(1)}$ and are known from earlier work[3,18] to an accuracy sufficient for present purposes. The values which were used are listed in Appendix I.

There are hence three parameters to be evaluated from the data for each molecule. For OH these three must satisfy five equations, and the three constants for OD must fit eight equations. One such fit that can be considered as best is compared with the experimental results in Table II (Column A). The values of the constants are, in OH: $\lambda=-7.410$, $\alpha_p=-2358.95$ Mc/sec, $\beta_p=572.99$ Mc/sec; and in OD: $\lambda=-13.890$, $\alpha_p=-1545.99$ Mc/sec, $\beta_p=160.72$ Mc/sec. The deviations appear as systematic functions of J. The average deviation is about 13 Mc/sec in OH and 9.6 Mc/sec in OD or about one part in 2000. One can fit the experimental data with an average deviation of about 15 Mc/sec even when terms in second order ($\nu_\Lambda^{(2)}$) are neglected. Such fits, however, and the constants thereby determined, do not have much meaning since the term $\nu_\Lambda^{(2)}$ is as large as 120 Mc/sec.

For the above calculation (results in Table II, Column *A*) the matrix $\langle\Pi|L_y|\Sigma\rangle$ involved in the constants α_p, β_p is assumed to be independent of J. We may allow for some variation in the electronic wave function with the change of internuclear distance that results from centrifugal stretching. The order of magnitude of such a variation can be established from the following consideration. A change of the internuclear distance by 100%, for example, would produce a change roughly of the same order in the molecular wave function (and the Λ-type doubling). Hence for infinitesimal displacements

$$\Delta\psi/\psi\sim\Delta r/r=-D_0N(N+1)/2B,$$

where D_0 is the centrifugal distortion constant. We write then approximately

$$(|\langle\Pi|L_y|\Sigma\rangle|^2)_N=(|\langle\Pi|L_y|\Sigma\rangle|^2)_0[1-CN(N+1)], \quad (45)$$

where C is of order D_0/B_0, and one may use the intermediate coupling formula (44) instead of $N(N+1)$.

Introducing this variation in the parameters α_p and β_p and using again (22), (23), and (44) we obtain the fit shown in Column *B* of Table II. The agreement between calculated and experimental values is considerably better here than above when no variation in the wave function was allowed. The average deviation is reduced to 5.8 Mc/sec in OH and 3.6 Mc/sec in OD or about one part in 3500. The better agreement with theory, in all cases, of the OD data is not surprising in view of the faster convergence of the energy expansion (6) in this molecule $[B(\mathrm{OD})/E\sim\frac{1}{2}B(\mathrm{OH})/E]$. The value of the parameters obtained from this calculation, which we take as the values of the molecular constants are for OH as follows:

$$\lambda^0=-7.444\pm0.017,$$
$$\alpha_p{}^0=-2361.37\pm2.95 \text{ Mc/sec},$$
$$\beta_p{}^0=576.18\pm1.64 \text{ Mc/sec},$$
$$C \text{ in } (45)=(1.2\pm0.5)D_0/B_0;$$

and for OD:

$$\lambda^0 = -13.954 \pm 0.032,$$
$$\alpha_p^0 = -1548.99 \pm 2.10 \text{ Mc/sec},$$
$$\beta_p^0 = 161.94 \pm 0.61 \text{ Mc/sec},$$
$$C = (1.2 \pm 0.5) D_0/B_0.$$

The superscript 0 indicates that these values apply to the lowest vibrational and rotational levels. For higher rotational states the parameters are to be evaluated from the values given above and (44), (45). With the above value for C, expression (45) represents a variation of about one part in 1400 in the electronic wave function from one rotational state to the next.

The uncertainties quoted in the molecular constants are mostly due to neglected effects in the theory rather than the experimental error. These are

(*a*) The interaction $\gamma \mathbf{N}\cdot\mathbf{S}$, where γ is of order $(m/M)A$. The Λ-type doubling will be affected to the extent that this interaction will influence the intermediate coupling as discussed above. The order of magnitude of the effect is $(m/M)\nu_\Lambda^{(1)}$ or about 2.5 Mc/sec for the $J=13/2$ state of $O^{16}D$. Inclusion of this effect would bring the calculated frequencies in somewhat better agreement with the experimental results.

(*b*) The effect of the $^2\Sigma$ state in third order in expansion parameters, contributing terms of the form

$$\left(\frac{A \text{ or } BJ}{E_\Sigma - E_\Pi}\right)^2 \nu_\Lambda^{(1)}.$$

This would be about 0.3 Mc/sec for $J=13/2$ in $O^{16}D$.

(*c*) The influence of the $^2\Delta$ state. The Λ-type doubling in the $^2\Delta$ state is[16]

$$\frac{48B^6(J-1)J(J+1)(J+2)}{(E_\Sigma - E_\Pi)^2(E_\Sigma - E_\Delta)}.$$

The corresponding terms in $^2\Pi$ states would be of order

$$\left(\frac{A \text{ or } BJ}{E_\Sigma - E_\Pi}\right)\left(\frac{BJ}{E_\Sigma - E_\Delta}\right)\nu_\Lambda^{(1)}.$$

The value of $E_\Sigma - E_\Delta$ is not known. If one assumes it to be comparable to $E_\Sigma - E_\Pi$, this contribution would be of the same magnitude as the one due to the $^2\Sigma$ state in third order [(*b*) above].

(*d*) Centrifugal distortion to order $(B/\omega_{vib})^4$. The rotational constant B has been corrected to order $(B/\omega_{vib})^2$ by (44). The next correction term in the rotational energy has the form $HJ^3(J+1)^3$, where

$$H = \frac{2B^3}{3\omega_{vib}^4}(2B^2 - \alpha_e\omega_{vib}).$$

The effect on the Λ-type doubling is

$$\frac{2H}{B}J^3(J+1)^3\nu_\Lambda^{(1)},$$

or about 0.1 Mc/sec in $J=13/2$ of $O^{16}D$.

TABLE III. Effects that contribute to or affect the Λ-type doubling. The numerical values apply to the $J=13/2$ state in the Π_1 level of $O^{16}D$. By taking into account (1)–(4) and using the experimentally determined constants one calculates a frequency $\nu_\Lambda = 12\,916.42$ Mc/sec. The observed value is 1.59 ± 0.10 Mc/sec higher. One sees that the estimated contribution from the neglected effects (5), (6), (7), and (8) is comparable to 1.59 Mc/sec.

Description	Order of magnitude	Numerical value (Mc/sec)
(1) Effect of $^2\Sigma$ state to first order in expansion parameters	$\left(\frac{A \text{ or } BJ}{E_\Sigma - E_\Pi}\right) BJ \equiv \nu_\Lambda^{(1)}$	12 957.00
(2) Centrifugal distortion on B to order $(B/\omega)^2$	$\frac{8B^3J^3}{\omega_{vib}^2}\nu_\Lambda^{(1)}$	−71.49
(3) Effects of $^2\Sigma$ state state to second order	$\left(\frac{A \text{ or } BJ}{E_\Sigma - E_\Pi}\right)\nu_\Lambda^{(1)}$	+66.73
(4) Variation of electronic wave function with rotation	$\frac{4B^3J^3}{\omega_{vib}^2}\nu_\Lambda^{(1)}$	−35.82
(5) Effect of the interaction $\gamma \mathbf{N}\cdot\mathbf{S}$	$\frac{m}{M}\nu_\Lambda^{(1)}$	~2.5
(6) Effect of $^2\Sigma$ state to third order	$\left(\frac{A \text{ or } BJ}{E_\Sigma - E_\Pi}\right)^2 \nu_\Lambda^{(1)}$	~0.3
(7) Effect of $^2\Delta$ state	$\left(\frac{A \text{ or } BJ}{E_\Sigma - E_\Pi}\right)\left(\frac{BJ}{E_\Sigma - E_\Delta}\right)\nu_\Lambda^{(1)}$	~0.3
(8) Centrifugal distortion on B to order $(B/\omega)^3$	$\frac{4B^3J^4}{3\omega_{vib}^2}\left(\frac{12B^2}{\omega_{vib}} - \alpha_e\right)\nu_\Lambda^{(1)}$	~0.1

The numerical estimates of the contributions (*a*), (*b*), (*c*) and (*d*), based on the above approximate expressions, are comparable with the deviations between calculated and experimental frequencies (see Table II). We note also that the deviations are seen from Table II to be monotonic functions of J, which is the behavior to be expected from the higher order terms. One may then ascribe the discrepancies (about one part in 3500) to the neglected effects (*a*), (*b*), (*c*), and (*d*). A small part of the deviations may also be due to use of the pure precession hypothesis in calculating centrifugal effects on B. From what follows, the hypothesis would appear to be somewhat inadequate for evaluating the centrifugal effects with accuracy commensurate to that of the data. The various contributions to the Λ-type doubling, with numerical values for a particular value of J, are summarized in Table III.

We compare the present values for the molecular constants in $O^{16}H$ with those previously obtained from ultraviolet work. Our value for λ (-7.444 ± 0.017) is 1.3% lower than the previous value of Dicke and Crosswhite, who reported[3] −7.547. Inspection of their data indicates that the uncertainty may be as large as

TABLE IV. Parameters that describe the Λ-type doubling and values calculated from the pure precession hypothesis. α_p and β_p are in Mc/sec.

Parameter	$O^{16}H$ Experimental	$O^{16}H$ Calculated	$O^{16}D$ Experimental	$O^{16}D$ Calculated
$\lambda(=A/B)$	-7.444 ± 0.017		-13.954 ± 0.032	
α_p	-2361.37 ± 2.95	-3491	-1548.99 ± 2.10	-2172
β_p	576.18 ± 1.64	629	161.94 ± 0.61	179
$\left(\frac{\alpha_p-2\beta_p}{\beta_p}\right)$	-6.098 ± 0.013	$-7.444(=\lambda)$	-11.558 ± 0.025	$-13.954(=\lambda)$

0.8% which may be increased to one percent if one considers uncertainties due to centrifugal distortion, not taken into account in the earlier work. Consideration of the centrifugal effects on λ would actually bring the earlier value somewhat closer to the present one. In that case the two experimental values would be in marginal agreement. We note that the present value of λ is also favored by the magnetic hyperfine results in that the hfs constants determined from the $^2\Pi_{\frac{1}{2}}$ data are more consistent with those in the $^2\Pi_{\frac{1}{2}}$ state if one uses it rather than the earlier value in (33). Only crude values exist in previous literature[3,26] for the specific Λ-doubling constants α_p and β_p. They are -2.3×10^3 Mc/sec and 5.7×10^2 Mc/sec respectively and are in good agreement with the present values -2361.37 ± 2.94 and 576.18 ± 1.65 in $O^{16}H$. The Λ-type doubling in OD is also of the magnitude indicated by ultraviolet work.[27]

It is of interest to compare the experimentally determined constants in the different isotopic species. The constant $(\alpha_p-2\beta_p)$ is directly proportional to B whereas β_p is proportional to B^2. The constant B is not known in $O^{18}H$ but, if one assumes a structure identical with that of $O^{16}H$, the constants $(\alpha_p-2\beta_p)$ and β_p can be derived from those of $O^{16}H$ and the reduced molecular masses. The $O^{18}H$ frequency in Table II has been calculated in this way and agrees very well with the experimental value. One sees that this line is predicted from the theory and the $O^{16}H$ data with an accuracy comparable to that for the $O^{16}H$ lines themselves. The agreement, to one part in 8000, depends on the close similarity of the electronic structure in the two isotopic species.

The experimental value for the ratio

$$[(\alpha_p-2\beta_p)_{OH}/\alpha_p-2\beta_p)_{OD}]$$

is 1.8761 ± 0.0030 compared with 1.8763 for the ratio $(B)_{OH}/(B)_{OD}$. And $(\beta_p)_{OH}/(\beta_p)_{OD}=3.5585\pm0.0035$ compared to 3.5204 for the ratio $[(B)_{OH}/(B)_{OD}]^2$. The agreement is quite good in view of the fact that the constants α_p and β_p depend explicitly on the electronic wave function (through $\langle\Pi|L_y|\Sigma\rangle$) in addition to B. The electron wave function is assumed in this comparison to be identical in OH and OD, and $E_\Sigma-E_\Pi$ in OD is taken to be identical with that in OH (32682.5 cm^{-1}). The result above indicates that a value reported[28,18] for $E_\Sigma-E_\Pi$ in OD, about 10 percent different from that in OH, must be in error. It is also implicitly assumed in the above comparison that the inverse moment of inertia B can be taken as a constant multiplying the matrix $\langle\Pi|L_y|\Sigma\rangle$ in α_p and β_p. This is part of the pure precession hypothesis.[16]

The pure precession hypothesis makes the assumption that the orbital electronic angular momentum is of constant magnitude and precesses at a constant rate about the internuclear axis. Under these conditions the constant α_p becomes

$$\frac{4(A+2B)|\langle\Pi|L_y|\Sigma\rangle|^2}{E_\Sigma-E_\Pi}=\frac{(2A+4B)B}{E_\Sigma-E_\Pi},$$

and

$$\beta_p=\frac{2B^2}{E_\Sigma-E_\Pi}.$$

The values of the constants so obtained are compared in Table IV with the experimental results. One sees that the agreement is only to within 35%. Despite this, the pure precession hypothesis is quite useful since one can estimate from it the magnitude of these higher order effects in the absence of precise experimental work.

(b) Relative Line Intensities

The observed relative line intensities confirm the prediction of the intermediate coupling formula (39) as to the behavior of the electric dipole matrix element in the transition from Hund's case (*a*) to (*b*). The observed intensities in the $^2\Pi_{\frac{1}{2}}$ lines relative to those in $^2\Pi_{\frac{3}{2}}$ state are larger than one would predict from Hund's case (*a*) quantization [or smaller than predicted from case (*b*)] and appear to vary from one rotational state to next in accordance with (39).

(c) Magnetic Hyperfine Structure and Coupling Constants

The magnetic hyperfine structure results are fitted with (33) above. The hyperfine doubling term in d is a measure of the difference in the hyperfine structures of the two Λ-doublet levels, which equals the frequency difference of the two main ($\Delta F=0$) lines in OH or the

[26] R. S. Mulliken and A. Christy, Phys. Rev. **35**, 87 (1931).
[27] M. Ishaq, Proc. Roy. Soc. (London) **159**, 110 (1937); additional references are given in reference 18.

difference between the two extreme members of the main hyperfine triplet in OD (see Fig. 2). Denoting this frequency difference by $\Delta\nu_1$, we have from (33), in OH:

$$\Delta\nu_1 = d\left(\frac{\pm X-2+\lambda}{\pm 2X}\right)\frac{(J+\frac{1}{2})^2}{J(J+1)}, \tag{46}$$

and in OD:

$$\Delta\nu_1 = d\left(\frac{\pm X-2+\lambda}{\pm 2X}\right)\frac{2(J+\frac{1}{2})^2}{J(J+1)}, \tag{47}$$

where the upper and lower signs apply to the $^2\Pi_{\frac{1}{2}}$ and $^2\Pi_{\frac{3}{2}}$ states respectively. The hyperfine results (Table I) for the main lines are fitted with the single parameters d in each of the two isotopic species. The values obtained are, in Mc/sec,

$$d(\mathrm{OH}) = 57.0 \pm 1.5 \quad \text{and} \quad d(\mathrm{OD}) = 8.69 \pm 0.16.$$

The calculated and experimental values of $\Delta\nu_1$, are compared in Table V. The agreement is to about 2% and quite satisfactory in view of the approximations used in deriving (33).

The hyperfine structure in $O^{18}H$ should according to theory be equal, within the present experimental error, to that in $O^{16}H$. Our measured value for $\Delta\nu_1$ in $O^{18}H$ for $J=9/2$ is 9.6 ± 0.5 Mc/sec compared to 8.72 ± 0.10 in $O^{16}H$. The indicated discrepancy is so marginal that more precise measurements are required to establish any real difference in the hfs of the two species. Such a difference would be rather surprising.

The other experimental information, besides the hyperfine doubling, is the frequency separation of the two satellite lines ($\Delta F=\pm1$). This frequency separation is equal to the sum of the hyperfine structures in the two Λ-doublet levels (see Fig. 2). From (33) we have, in OH

$$\Delta\nu_s \equiv \Delta(\nu_{F=J+\frac{1}{2}} - \nu_{F=J-\frac{1}{2}})$$
$$= \frac{2J+1}{\pm 4J(J+1)X}\left[2a(\pm 2X+2-\lambda)\right.$$
$$\left.+4b(J-\tfrac{1}{2})(J+\tfrac{3}{2})+(b+c)(\pm X+4-2\lambda)\right], \tag{48}$$

where the upper and lower signs in front of X apply to the $^2\Pi_{\frac{1}{2}}$ and $^2\Pi_{\frac{3}{2}}$ states respectively. Because of their low intensity, we have been able to observe these satellites only in the strong $J=9/2$ spectrum of $O^{16}H$ in the $^2\Pi_{\frac{3}{2}}$ state. In this state $\Delta\nu_s=31.3\pm0.8$ Mc/sec. From this information alone the three constants a, b, and c involved in (48) cannot be determined. If one assumes that the electron with the orbital angular momentum is also the one that carries the free spin, then the relation $c=3(a-d)$ holds and one is left in (48) with the two constants a and b. In a pure p state $\psi^2(0)=0$ and the constant b is from (31) simply $-c/3$. However, a small admixture of s state (about 2.5%) has been found in the similar cases of the $O^{16}O^{17}$ and NO molecules[31,32] to contribute to the hyperfine structure an amount comparable to the classical dipole-dipole part of the interaction. Calculations based on atomic orbital approximations and on the NO results[30] indicate that only a crude value of a (accurate to about 40 percent) can be obtained if one assumes $\psi^2(0)=0$ and solves (48) for a using the experimental result for $\Delta\nu_s$. The value so derived is

$$a = 58 \pm 20 \text{ Mc/sec},$$

where the correct value is probably closer to the lower rather than the upper limit. Measurements of these satellites are needed in additional rotational states to determine the constants b and c and reduce the uncertainty in a. This would require a spectrometer of somewhat higher sensitivity.

Expression (33) predicts that the satellites must be symmetrically spaced with respect to the main lines. The observed satellite frequencies in the $^2\Pi_{\frac{1}{2}}$ state (Table I) are, within experimental error, in agreement with this requirement. It is interesting to note that the theory, with the values for the constants given above, indicates that in the $^2\Pi_{\frac{1}{2}}$ state the satellites should be inside the main lines rather than outside as observed in $^2\Pi_{\frac{3}{2}}$ state. This is due to the preponderance of the hyperfine doubling term over the rest of the hyperfine structure in the $^2\Pi_{\frac{1}{2}}$ state, which inverts the hyperfine components in the lower Λ-doublet level. Such behavior has been observed in the spectrum of NO.[29,30]

TABLE V. Magnetic hyperfine structure in OH and OD. $\Delta\nu_1$ designates the frequency difference between the two main ($\Delta F=0$) lines in OH or the difference between the two extreme members of the main hyperfine triplet in OD. $\Delta\nu_s$ denotes the frequency separation between the two satellite ($\Delta F=\pm1$) lines in OH (see Fig. 2). All values are in Mc/sec.

Molecule	Electronic state	N	J	$\Delta\nu_1$ exp.	$\Delta\nu_1$ calc.
$O^{16}H$	$^2\Pi_{\frac{1}{2}}$	2	3/2	59.56±0.25	58.94
		3	5/2	53.43±0.25	54.47
	$^2\Pi_{\frac{3}{2}}$	3	7/2	6.74±0.10	6.56
		4	9/2	8.72±0.10	8.79
		5	11/2	10.96±0.30	10.77
$O^{18}H$	$^2\Pi_{\frac{3}{2}}$	4	9/2	9.6±0.5	8.74
$O^{16}D$	$^2\Pi_{\frac{1}{2}}$	3	5/2	17.44±0.25	17.36
		4	7/2	16.75±0.25	16.77
		5	9/2	16.50±0.20	16.25
		6	11/2	15.49±0.20	15.78
	$^2\Pi_{\frac{3}{2}}$	5	11/2	<2.1	1.70
		6	13/2	<3.0	2.14
		7	15/2	<3.0	2.53
		8	17/2	<3.0	2.90
Also $O^{16}H$	$^2\Pi_{\frac{3}{2}}$	4	9/2	$\Delta\nu_s=31.3\pm0.8$	$\Delta\nu_s=31.31$

[30] Miller, Townes, and Kotani, Phys. Rev. 90, 452 (1953).
[31] C. A. Burrus and W. Gordy, Phys. Rev. 92, 1437 (1953).
[32] Gallagher, Bedard, and Johnson, Phys. Rev. 93, 729 (1954).

(d) Molecular Electronic Structure

Parameters that depend on the electronic wave functions are involved in the present results on the Λ-type doubling and the hyperfine structure and can be used as tests of proposed schemes for the electronic structure of the molecule.

The most important structure for OH is expected to be[26]

$$(1s\sigma)^2(2s\sigma)^2(2p\sigma)^2(2p\pi)^3.$$

In Λ doubling, the experimentally determined parameters a_p and β_p depend on the electronic wave function through the quantity $|\langle\Pi|L_y|\Sigma\rangle|^2$. The above structure for OH with the pure precession hypothesis gives values for the Λ-type doubling which agree, at least qualitatively, with the experimental results (Sec. 5a above).

More definite information on the distribution of the unpaired electron orbital and spin angular momenta in the molecule is provided by the hyperfine structure parameters a and d. From the experimetal values of these quantities and using the definitions (31), one derives, in OH:

$$(1/r^3)_{Av}=(0.75\pm0.25)\times10^{24}\ \text{cm}^{-3},$$
$$(\sin^2\chi/r^3)_{Av}=(0.490\pm0.013)\times10^{24}\ \text{cm}^{-3}.$$

For OD,

$$(\sin^2\chi/r^3)_{Av}=(0.486\pm0.009)\times10^{24}\ \text{cm}^{-3},$$

in excellent agreement with the value for OH. The uncertainty in the value of $(1/r^3)_{Av}$ is due to the assumption that $\psi^2(0)=0$. As already mentioned, the correct value may be closer to the lower limit than to the upper limit.

Similar experimental results in the $O^{16}O^{17}$ and NO molecules have been used in studying the electronic structure.[21,30,31] In these cases one finds the appropriate combination of atomic wave functions (which is taken as the electronic structure) that yields the observed values of the hyperfine parameters. Effects of overlapping can be neglected since for atoms like N and O the parts of the electron distribution which contribute substantially to the hyperfine interaction are, by comparison with the internuclear distance, quite close to the nuclei.

In OH the observed constants are of the order of magnitude one would expect from such a scheme. One cannot, however, use a similar simple analysis to determine the electronic structure since in this case the oxygen nucleus is well within the $2p$ electron orbit of the hydrogen and a $2p$ atomic orbital would hence be a very poor approximation. The experimental results, given also in Table VI, can be used as definite tests of molecular wave functions that may be constructed, but rather careful calculations must be made to evaluate the expected hyperfine structure from the chosen wave functions.

[31] Townes, Dousmanis, White, and Schwarz, Trans. Faraday Soc. (to be published).

TABLE VI. Parameters, derived from the magnetic hyperfine structure data, that describe the unpaired electron distribution in OH and OD. The vector $\mathbf{r}$ is the radius vector from the proton or deuteron to the unpaired electron and χ the angle between $\mathbf{r}$ and the internuclear axis. These values are in units of 10^{24} cm^{-3}.

Parameter	Experimental value $O^{16}H$	$O^{16}D$
$(1/r^3)_{Av}$	0.75±0.25	
$(\sin^2\chi/r^3)_{Av}$	0.490±0.013	0.486±0.009

The present results yield information on the unpaired electron distribution about the proton or deuteron. Experimental results on $O^{17}H$ would be interesting since they would involve the hyperfine interaction of O^{17} and hence would measure the electron distribution about the oxygen. For O^{17}, simple calculations could give approximate values of the hyperfine constants to be expected from a given electronic structure.

6. LINE INTENSITIES AND RADICAL ABUNDANCE—SURFACE TESTS AND THE LIFE TIME OF OH IN GLASS

The strongest of the observed OH spectra is that due to the $J=9/2$ state in the $^2\Pi_1$ level. Under the best conditions these lines were detected by the spectrometer with a signal to noise ratio of approximately 1000:1. The signal to noise ratio was about 10:1 for the $J=11/2$ spectrum of $O^{16}D$ in the $^2\Pi_1$ state, which is the weakest of the observed Λ-type doubling transitions. From these values, using the figure of 0.5×10^{-8} cm^{-1} for the minimum detectable absorption with this instrument, one sees that the intensity of the observed lines of OH and OD ranges approximately from 5×10^{-6} cm^{-1} to 5×10^{-8} cm^{-1}. From the line intensity, combined with the line breadth (~1 Mc/sec) one may derive an approximate value for the radical abundance in the absorption cell. The following conditions however must be noted:

(1) It is necessary to assume that the radicals are in thermal equilibrium with the walls. This assumption is on rather safe ground since a radical makes approximately 10^5 collisions between the time it leaves the discharge tube and enters the absorption cell.

(2) One has to assume a reasonable line breadth at the operating total pressures.

(3) The electric dipole moment of the molecule is not well known. We have used the tentative value[10] of 1.5 Debye units.

The value obtained for the maximum percentage of radicals present in the gas is between 3% and 30%. The large uncertainty quoted comes from estimates of the errors which may be produced by the uncertainties listed above. A previous spectroscopic measurement of OH radical abundance in the products of a water discharge is available.[32] In this method the intensities of ultraviolet absorption due to OH produced by thermally dissociated water and by discharge were

compared. A partial pressure of OH of approximately 1×10^{-3} mm Hg was found at a total pressure near 1 mm Hg. The present work indicates the presence of very much higher radical concentrations.

Since different conditions were used in the two measurements, the two values are not necessarily inconsistent. In the earlier work a pulsed dc discharge was used with a total current of 180 ma and a current density of 9.5 ma/cm². In the present apparatus measurements on a dc discharge indicate that at 0.1 mm Hg optimum intensity is produced with a total current of 400 ma and a density of 80 ma/cm². Maximum line intensity is produced by higher discharge currents as the pressure is increased and one would expect that higher currents are needed at 1 mm Hg. In addition, the radical abundance may be expected to be lowered by the use of a pulsed discharge.

No quantitative explanation of the variation of the line intensity with discharge current and pressure will be attempted here. In the present experiments the effects of changing radical production and of varying recombination are not easily separated. It seems qualitatively that at different pressures the discharge conditions producing a relative maximum in line intensity all correspond to approximately the same average electron energies in the discharge tube. That the absolute maximum occurs at the high-pressure end of the available range suggests that wall rather than volume recombination is the dominant effect in removing the radicals.

In order to determine the effect of recombination on destroying the radicals during their transit through the absorption cell, measurements of radical abundance at different points in the cell were made. By passing the modulating current through only a portion of the solenoid one may detect absorption due to radicals in the corresponding part of the cell. Measurements were made by applying the modulation to two 10 cm lengths of the coil one at each end of the cell, which in this case was 75 cm long. The measured intensity difference was approximately 10%. The actual difference in radical abundance at the two ends is somewhat greater because of the finite length of the test intervals including the effect of fringing fields. From this figure we infer that the radical lifetime is approximately equal to the time required by a molecule to traverse the cell. This figure is approximately $\frac{1}{3}$ sec and is in good agreement with spectroscopic measurements in the ultraviolet region.[3]

In addition to spectroscopic techniques, two other methods for detecting OH and studying its properties have been reported in previous literature. These involve (*a*) measurements of the temperature rise of a probe coated with KCl on which the OH radicals are presumed to recombine,[5] and (*b*) the H_2O_2 concentration measurement[4] described in Sec. 2b above. These tests were used in the earlier part of this work to make sure that OH radicals were in the absorption cell. Once the microwave spectrum was found, however, it became apparent that these tests (at least to the extent that we have been able to reproduce and apply them) give results that are not correlated with the OH concentration as measured by the intensity of the microwave lines. The evidence for this has already been published elsewhere.[7]

Some tests have been made to determine whether the presence of certain surfaces in the path of gas flow would affect the concentration of the OH radicals. The OH concentration would decrease if a particular substance either directly combines with OH or simply provides a convenient surface for radical recombination.

A side tube was blown in the tube connecting the discharge to the absorption cell. In this side tube a glass rod was introduced, bearing on one end the substance to be tested and on the other a magnetic core (glass-covered) so that the rod could be moved from outside with a small magnet. Thus line intensities could be measured with the sample in and out of the path of radical flow, all other conditions being the same. The following surfaces decreased greatly the OH concentration: Copper, graphite, nickel, and kovar. Substances that do not appreciably affect the OH are apiezon wax, Teflon, glyptal, potassium chloride, and aluminum. Mica is found to decrease the OH but not as effectively as members of the first group.

These results, especially the ones that indicate that a substance does not affect the OH, are to be taken with some reservations. These are (*a*) the surface exposed to the discharge products is rather limited in size ($\sim\frac{1}{4}$ cm², tube cross section ~1 cm²); (*b*) the time of exposure also was rather short. We have carried out more elaborate tests with extended aluminum surfaces which indicate that, despite the result of the test described above, the OH does not live long in aluminum environment. Thus if an aluminum tube is substituted for a large (5 inches) section of the glass tube that connects the discharge to the absorption cell the line intensity decreases steadily to zero in a matter of a few minutes. This indicates an alteration of the aluminum oxide surface which increases its ability to destroy OH.

7. CONCLUSION

The experiments on the microwave spectrum of the free OH radical provide detailed information on finer effects in the energy level structure such as the Λ-type doubling and magnetic hyperfine structure. The experimental accuracy for effects of the former kind is for the first time high enough to provide an adequate check on the theory. The results are in agreement with theory to the expected accuracy of the latter. The magnetic hyperfine structure yields parameters that describe the distribution of electronic angular momentum in the molecule and are directly connected to the electronic structure. In addition, the microwave spectrum can be used in determining the lifetime of the radical and in studying its reactivity with various substances. Results

obtained so far give rise to substantial hope that microwave techniques can be quite useful in this direction for other radicals as well as for OH.

8. ACKNOWLEDGMENTS

This work has benefited greatly from the aid of the personnel of the Columbia Radiation Laboratory, to whom we wish to express our appreciation. In particular we wish to acknowledge substantial contributions from Dr. W. A. Hardy and from Dr. A. L. Schawlow, who initiated experimental work on the OH radical.

APPENDIX I. NOTATION

$\mathbf{S}, \mathbf{I}, \mathbf{L}(\mathbf{A})$	Electron spin, nuclear spin, electronic orbital angular momentum.
$\mathbf{N}$	Angular momentum of molecule exclusive of electron and nuclear spin.
$\mathbf{J}$	Angular momentum exclusive of nuclear spin.
$\mathbf{F}$	Total angular momentum.
Λ, Σ, Ω	Quantum numbers associated with L_z, S_z, J_z.
A	Fine structure interaction constant (energy $=A\mathbf{L}\cdot\mathbf{S}$).
B_p	Rotational constant in $^2\Pi$ state (18.515 cm^{-1} in OH, 9.868 cm^{-1} in OD).
B_s	Rotational constant in $^2\Sigma$ state (16.961 cm^{-1} in OH, 9.03 cm^{-1} in OD).
λ	A/B_p.
X	$[4(J+\frac{1}{2})^2+\lambda(\lambda-4)]^{\frac{1}{2}}$.
D_0	Centrifugal distortion constant (0.00187 cm^{-1} in OH, 0.00052 cm^{-1} in OD).
E	$E_\Sigma - E_\Pi$ (32 682.5 cm^{-1} in OH, we use the same value in OD).
α_p	$4\sum_{\Sigma\text{-states}}(-1)^s\dfrac{\langle\Pi\vert AL_y+2BL_y\vert\Sigma\rangle\langle\Sigma\vert BL_y\vert\Pi\rangle}{E_\Sigma-E_\Pi}$
β_p	$4\sum_{\Sigma\text{-states}}(-1)^s\vert\langle\Pi\vert BL_y\vert\Sigma\rangle\vert^2/(E_\Sigma-E_\Pi)$.
α_s, β_s	same as α_p, β_p except that the summation is over all Π rather than Σ states.

The values of the constants B, D_0, and E are from references 3, 18. The values of D_0 and E for OD quoted in 18 must be in error (see text). The value for D_0 given above has been calculated from B and ω_{vib}. Presently determined values for λ, α_p, and β_p are given in Table IV.

APPENDIX II. MATRIX ELEMENTS OF H_1 (AFTER VAN VLECK[16])

$$(\Sigma_{\frac{1}{2}}|H_1|\Sigma_{\frac{1}{2}})=(\Sigma_{-\frac{1}{2}}|H_1|\Sigma_{-\frac{1}{2}})=B_s[J(J+1)+\tfrac{1}{4}]+E\equiv E+\alpha'\equiv\alpha,$$

$$(\Pi_{\frac{1}{2}}|H_1|\Pi_{\frac{1}{2}})=(\Pi_{-\frac{1}{2}}|H_1|\Pi_{-\frac{1}{2}})=B_p[J(J+1)+\tfrac{1}{4}]-\tfrac{1}{2}A\equiv\beta,$$

$$(\Pi_{\frac{1}{2}}|H_1|\Pi_{\frac{1}{2}})=(\Pi_{-\frac{1}{2}}|H_1|\Pi_{-\frac{1}{2}})=B_p[J(J+1)-7/4]+\tfrac{1}{2}A\equiv\gamma,$$

$$(\Sigma_{\frac{1}{2}}|H_1|\Sigma_{-\frac{1}{2}})=(\Sigma_{-\frac{1}{2}}|H_1|\Sigma_{\frac{1}{2}})=B_s(J+\tfrac{1}{2})\equiv(-1)^s\delta,$$

$$(\Pi_{\frac{1}{2}}|H_1|\Pi_{\frac{1}{2}})=(\Pi_{-\frac{1}{2}}|H_1|\Pi_{-\frac{1}{2}})=B_p[(J-\tfrac{1}{2})(J+\tfrac{3}{2})]^{\frac{1}{2}}\equiv\epsilon,$$

$$(\Pi_{\frac{1}{2}}|H_1|\Sigma_{-\frac{1}{2}})=(-1)^s(\Pi_{-\frac{1}{2}}|H_1|\Sigma_{\frac{1}{2}})=2\langle\Pi|BL_y|\Sigma\rangle(J+\tfrac{1}{2})\equiv(-1)^s\zeta,$$

$$(\Pi_{\frac{1}{2}}|H_1|\Sigma_{\frac{1}{2}})=(-1)^s(\Pi_{-\frac{1}{2}}|H_1|\Sigma_{-\frac{1}{2}})=2\langle\Pi|BL_y|\Sigma\rangle[(J-\tfrac{1}{2})(J+\tfrac{3}{2})]^{\frac{1}{2}}\equiv\eta,$$

$$(\Pi_{\frac{1}{2}}|H_1|\Sigma_{\frac{1}{2}})=(-1)^s(\Pi_{-\frac{1}{2}}|H_1|\Sigma_{-\frac{1}{2}})=\langle\Pi|AL_y+2BL_y|\Sigma\rangle\equiv\theta.$$

The following phase conventions are observed:

$$\pm i\langle\Sigma|S_x|\Sigma\pm1\rangle=\langle\Sigma|S_y|\Sigma\pm1\rangle=\tfrac{1}{2}[S(S+1)-\Sigma(\Sigma\pm1)]^{\frac{1}{2}},$$

$$\langle\Sigma|S_z|\Sigma\rangle=\Sigma,\quad\langle\Omega|J_z|\Omega\rangle=\Omega,$$

$$\pm i\langle\Omega|J_x|\Omega\pm1\rangle=-\langle\Omega|J_y|\Omega\pm1\rangle=\tfrac{1}{2}[J(J+1)-\Omega(\Omega\pm1)]^{\frac{1}{2}}.$$

Because of the cylindrical symmetry of the molecular field about the internuclear axis (z-direction):

$$\pm i\langle\Lambda|L_x|\Lambda\pm1\rangle=\langle\Lambda|L_y|\Lambda\pm1\rangle.$$

Ionization by Alpha Particles in Mixtures of Gases*

WILLIAM P. JESSE AND JOHN SADAUSKIS
Argonne National Laboratory, Lemont, Illinois
(Received August 17, 1955)

The presence of minute impurities greatly increase the ionization produced by Po alpha particles in helium. Systematic studies of this effect show an increase in ionization up to 40 percent for approximately 0.1 percent of argon. Similar results have been obtained with CO_2, Kr, Xe, H_2, N_2, and C_2H_4 as the contaminant. Preliminary experiments with mercury vapor in helium confirm the large effect already reported by others. A similar increase in ionization in pure argon is obtained by the addition of C_2H_2 or C_2H_4. These increases in ionization seem to be caused by the production of ions, when metastable atoms in the parent gas undergo collisions with molecules of the impurity. In mixtures of H_2, N_2, or A with helium, the excess in ionization is observed to decrease by a few percent as the pressure of the gas mixture is increased from 48 to 110 cm of mercury. For no other contaminant gases tested thus far in helium is such a pressure change in ionization observed.

FOR some time experiments have been in progress in this laboratory to study the rather striking changes in alpha-particle ionization in the noble gases produced by the introduction of minute quantities of other gases. Although a complete explanation of all the effects observed cannot be given at the moment, it seems worthwhile at this time to give a more extended description of the phenomena observed than has as yet been published.[1,2]

APPARATUS AND METHOD

Two methods were employed to measure the ionization produced by alpha particles in gaseous mixtures. In the first method[1,3] the ionization produced by single polonium alpha particles was measured by collimating these alpha particles along the axis of a long brass cylindrical ionization chamber (Fig. 1). The effective path was about 20 cm. The ions produced by each alpha particle were collected and fed into a vibrating-reed electrometer connected to a Brown strip chart recorder. The length of jump on the chart produced by each alpha particle was measured and the total of a large number of these averaged. With a knowledge of the voltage sensitivity and electrical capacity of the system one can determine the average number of ion pairs produced per polonium alpha particle. A very small correction for the ions lost within the collimating system was made.

In later determinations of the effect of the pressure of the gas mixture upon the ionization, a more robust chamber was used, in which the energy of alpha particles from Am^{241} was reduced to about 1 Mev by passage through a thin sheet of mica as they entered the chamber. A diagram of the arrangement used has already been given as Fig. 3 in a previous paper.[4] In this arrangement the total integrated current was measured.

Both types of measurement could be compared for any given gas mixture by computing the ratio of the ionization observed for any given impurity concentration to that observed in pure helium.

Elaborate precautions were taken to insure the purity of the gases used. The chamber shown in Fig. 1 was constructed with quartz insulators, to permit baking and pumping for a period of twelve hours at a temperature above 200°C. The gases used were taken from breaker-flasks and were known to be of very high purity. However, variable results in ionization were always obtained with helium and neon unless these gases were further purified by continuous circulation through a purification system consisting of a cocoanut charcoal tube immersed in liquid nitrogen. Such a positive continuous circulation was obtained through the use of a simple metal bellows pump.

When the chamber was filled with presumably pure helium and the circulation started over the purification system, a marked decrease in alpha-particle ionization was always observed within a few minutes after the pump was started. The ionization continued to decrease until a minimum value was reached, beyond which further circulation of the gas produced no effect. This minimum ionization was taken to be characteristic of pure helium, and the attainment of such a minimum was indeed used as a practical measure of the purity of the helium before contaminants were introduced.

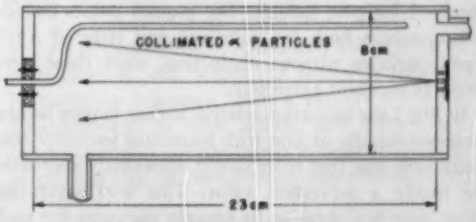

FIG. 1. Schematic diagram of ionization chamber used.

* Work performed under the auspices of the U. S. Atomic Energy Commission
[1] W. P. Jesse and J. Sadauskis, Phy. Rev. 88, 417 (1952); Phy. Rev. 94, 764(A) (1954).
[2] W. P. Jesse, Argonne National Laboratory Report No. 4944, 1952 (unpublished).
[3] Jesse, Forstat, and Sadauskis, Phy. Rev. 77, 782 (1950).
[4] W. P. Jesse and J. Sadauskis, Phy. Rev. 97, 1668 (1955).

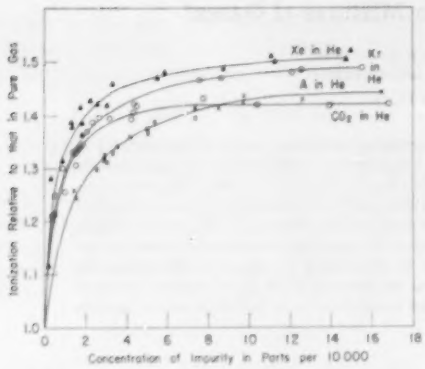

FIG. 2. Relative ionization measured as a function of the impurity concentration in helium.

It may of course be that more effective methods of purification could be devised which would produce a minimum ionization below that observed here. The minimum observed, however, seemed very stable under a wide variety of experimental conditions, and every effort to diminish it by such methods as prolonged gas circulation and periodic rebaking of the charcoal tube proved unavailing. The use of hot calcium as a purifying agent did not seem as effective as the charcoal tube.

The gaseous impurities were introduced into the pure noble gases in accurately measured quantities by means of a system resembling an inverse McLeod gauge. The impurity gas, in general from a breaker flask, was introduced into a small calibrated volume between two stopcocks and its pressure measured. It was then expanded into the accurately calibrated volume associated with the ion chamber and there mixed with a known volume of the noble gas. The composition of the mixture could thus be determined with an error of less than one percent.

EXPERIMENTAL RESULTS

Some of the data on alpha-particle ionization in helium mixtures are shown in Fig. 2. As abscissas are plotted the concentrations of the various impurity gases in parts per 10 000 by volume. As ordinates are plotted the ionization values observed for each impurity concentration relative to the ionization values observed for pure helium. The plotted points include measurements both for polonium and reduced Am^{241} alpha particles without distinction, since these were found in excellent agreement.

In Fig. 2 the ionization relative to that in pure helium increases rapidly at first with increasing impurity concentration, and then more slowly, apparently approaching finally a saturation value. This final saturation value does not seem to be exactly the same for each of the impurities in helium.

The effect of the various impurities can be seen with more exactness from the data in Table I. Here for convenience the ionization data are tabulated as a function of the concentration of the impurity and of the total pressure of the gaseous mixture. Where no pressures are indicated in Table I the ionization values have been shown to be independent of pressure, and those recorded represent a composite of readings taken at several pressures.

The effect of contaminants on the ionization observed in helium is not confined solely to the ionization produced by alpha particles of 5.3 and 1 Mev. Similar experiments for argon in helium mixtures, subjected to radiation from gamma rays from a radium source and also to beta particles from a Ni^{63} source, gave curves very similar to those shown in Fig. 2.

In order to observe the role of the pressure of the gas mixture, extensive measurements were made with the alpha particles of reduced ranges already mentioned. With hydrogen, nitrogen, and argon as contaminants in helium, a change in the ionization relative to that for pure helium was observed as the pressure of the gas mixture was altered between the limits of 45 and 110 cm of mercury. Typical results may be seen in the plotted curves for nitrogen in helium (Fig. 3) at the two pressures indicated, as well as in Table I. At lower pressures the relative ionization was found to be always higher than at the higher pressures. At lower impurity concentrations this change with pressure seems larger and diminishes with increasing concentration until, within the limits of accuracy of measurement, it seems to disappear at the highest concentrations used. Extensive measurements for argon in helium for pressures intermediate between 45 and 100 cm of mercury show an almost linear relation between the change in ionization and pressure. From the discussion which follows, it would seem that this could possibly be represented by an hyperbola of very small curvature, which deviates but little from a straight line within the small range of pressures investigated.

This change in relative ionization with pressure was observed only for the gases hydrogen, argon, and

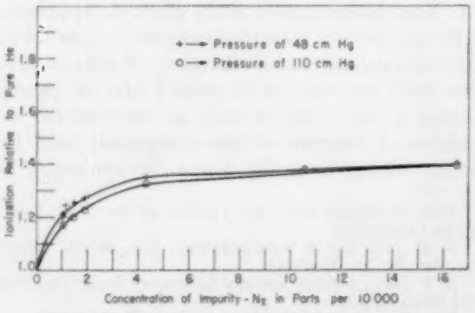
Pressure of 48 cm Hg
Pressure of 110 cm Hg
Ionization Relative to that in Pure He
Concentration of Impurity - N_2 in Parts per 10 000

FIG. 3. Ionization curves for N_2 in He, showing the effect of pressure of the gas mixture.

TABLE I. Experimental results for relative ionization as a function of impurity concentration.

Gas mixture	Gas press. cm	Impurity concentration in parts per 10 000 by volume 0.25	0.50	1.00	1.50	2.0	3.0	4.0	5.0	6.0	8.0	10.0	12.0	14.0	16.0	18.0	25.0	30.0
A in He	87.5	1.068	1.122	1.195	1.246	1.280	1.323	1.353	1.374	1.390	1.414	1.429	1.435	1.439	1.440			
Kr in He	···	1.169	1.236	1.296	1.337	1.365	1.401	1.422	1.439	1.451	1.466	1.473	1.480	1.484	1.484			
CO_2 in He	···	1.114	1.190	1.277	1.320	1.347	1.379	1.398	1.408	1.414	1.418	1.418	1.418	1.419	1.419			
Xe in He	···	1.170	1.252	1.331	1.369	1.398	1.436	1.455	1.468	1.477	1.488	1.495	1.502	1.503	1.504			
N_2 in He	48	1.080	1.13	1.206	1.246	1.273	1.317	1.347	1.357	1.360	1.370	1.390	1.390	1.400	1.402			
N_2 in He	110	1.049	1.097	1.166	1.207	1.236	1.283	1.316	1.330	1.338	1.350	1.364	1.375	1.390	1.400			
C_2H_4 in He	···	1.105	1.173	1.250	1.302	1.330	1.357	1.360	1.366	1.370	1.376	1.380	1.382	1.385	1.388	1.391		
H_2 in He	87.5	1.036	1.066	1.110	1.141	1.162	1.208	1.237	1.254	1.268	1.290	1.316	1.342	1.370	1.390	1.393	1.420	
H_2 in Ne	87.5	1.035	1.065	1.109	1.143	1.167	1.201	1.223	1.234	1.243	1.258	1.274	1.290	1.306	1.322	1.338		1.355
A in Ne	87.5	1.040	1.073	1.130	1.173	1.207	1.266	1.308	1.339	1.362	1.389	1.402	1.416	1.429				
Xe in Ne	87.5	1.170	1.240	1.303	1.343	1.371	1.407	1.430	1.444	1.453	1.460	1.460	1.460	1.461	1.462			
C_2H_2 in A	22.0	1.023	1.047	1.086	1.118	1.143	1.181	1.205	1.221	1.232	1.239	1.242	1.247	1.251	1.254	1.258		
C_2H_4 in A	22.0	1.012	1.023	1.041	1.055	1.067	1.084	1.093	1.099	1.102	1.107	1.110						

nitrogen as contaminants in helium. For no other gases was this change with pressure found, although similar measurements were made with CO_2, Kr, Xe, and C_2H_4. For the last four gases the ionization change between the limits of pressure indicated, if it exists at all, cannot be more than ten percent of that found for hydrogen, nitrogen, and argon. This represents the estimated limit of accuracy of the measurements.

COLLISION CROSS SECTIONS FOR METASTABLE ATOMS

A plausible explanation of the increase in alpha-particle ionization described in the last section is that this increase results from a transfer of energy from the metastable states in helium,[5] when an excited atom of helium encounters an impurity atom—let us say an argon atom. In the process the argon is ionized and a pair of ions collected in the chamber. Thus for argon in helium we have

$$He^* + A \rightarrow He + A^+ + e^-. \quad (1)$$

Any additional energy imparted by the metastable helium atom He^* to the argon atom A above that energy to produce an ion pair is carried off as kinetic energy in the ejected electron e^-. The above reaction has already been studied under quite different experimental conditions in connection with metastable atoms.[6,7]

According to this explanation the two metastable states, 2^1S and 2^3S occurring in helium, of energy respectively 20.6 and 19.8 ev, should be able to ionize any impurity gas whose ionization potential is lower than these energies. However, neon, whose ionization potential is 21.6 ev, should not be ionized when added as an impurity. This is in accord with experiment, where no significant increase in ionization is observed when neon is added to helium.

With argon it is not easy to find a contaminant ionizable by its metastable states, since the energy available is low—about 11.6 ev. However, benzene vapor (ionization potential 9.2 ev) was found to give a marked effect. Similar effects were found for acetylene and ethylene as impurities in argon (Table I). The ionization potentials of these two gases are 11.4 and 10.5 ev, respectively.

The maximum increase in ionization produced by the various contaminants seemed to vary much more in the case where argon was the parent gas than for either helium or neon. Thus, the increase in ionization produced by acetylene in argon is almost double that produced by ethylene, Table I. Furthermore, an increase in ionization of about one percent was found when five percent of CO_2 or CH_4 were added to pure argon. Such an effect has already been noted.[8,9] Since the ionization potentials of both these gases are well above the energy available in the metastable states of argon, it would seem possible that the discharge of higher excited states in argon accounts for this ionization increase. Thus, in general, our own results confirm those already cited[9] to indicate that in argon mixtures the metastable states may not play as dominant a role in ionizing the impurity atoms as do the metastable states in helium and neon.

Methods of Calculation of Cross Sections

It is possible from the experimental results given in Fig. 1 and Table I to make an estimate of the relative cross sections for the reactions of metastable helium atoms with the various impurity atoms, as indicated by Eq. (1). In very pure helium this reaction does not take place at all, whereas for high impurity concentrations, we shall assume that almost all of the metastable helium atoms are destroyed by this process.

It is evident that in addition to the process above, where metastable helium atoms are destroyed with the production of ions, there must also be another process of destruction of metastable atoms without the production of ions, where the energy is lost perhaps by radiative processes. Such a process would be the dominant one in pure helium and would continue to compete with the ionization process in the presence of an impurity. In the present experiment these two

[5] The writers are indebted to Dr. Roland Meyerott who first suggested to them this explanation of the above phenomena.
[6] M. A. Biondi, Phy. Rev. **88**, 660 (1952).
[7] A. V. Phelps and J. P. Molnar, Phy. Rev. **89**, 1202 (1953).
[8] J. Sharpe, Proc. Phys. Soc. (London) **A65**, 859 (1952).
[9] Melton, Hurst, and Bortner, Phy. Rev. **96**, 643 (1954).

TABLE II. Calculation of cross sections for metastable atoms.

Gas	Direct method conc.	K_i/K_d-reciprocal of last column	K_i/K_d Stern-Volmer	Mean K_i/K_d	σ_i/σ_d	σ_i cm²
A in He	1.23×10^{-4}	8.1×10^{3}	5.7×10^{3}	6.9×10^{3}	9.3×10^{3}	Biondi (9.7×10^{-17})
H_2 in He	3.4×10^{-4}	2.9×10^{3}	3.0×10^{3}	3.0×10^{3}	2.4×10^{3}	2.5×10^{-17}
N_2 in He			6.5×10^{3}	6.5×10^{3}	8.6×10^{3}	9×10^{-17}
CO_2 in He	0.58×10^{-4}	17.2×10^{3}	13.0×10^{3}	15.1×10^{3}	20.4×10^{3}	21.3×10^{-17}
Kr in He	0.60×10^{-4}	16.7×10^{3}	17.1×10^{3}	16.9×10^{3}	23.3×10^{3}	24.4×10^{-17}
Xe in He	0.30×10^{-4}	20×10^{3}	20.9×10^{3}	20.5×10^{3}	28.5×10^{3}	29.7×10^{-17}
C_2H_4 in He	0.63×10^{-4}	15.9×10^{3}	12.2×10^{3}	14.0×10^{3}	18.5×10^{3}	19.4×10^{-17}
Hg in He	0.015×10^{-4}	670×10^{3}		670×10^{3}	950×10^{3}	1×10^{-14}
A in Ne	2.3×10^{-4}	4.4×10^{3}	4.0×10^{3}	4.2×10^{3}	4.8×10^{3}	Biondi (2.6×10^{-16})
Xe in Ne	0.45×10^{-4}	22.2×10^{3}	23.7×10^{3}	23.0×10^{3}	30.4×10^{3}	16.4×10^{-16}
H_2 in Ne	2.3×10^{-4}	4.4×10^{3}	4.6×10^{3}	4.5×10^{3}	1.9×10^{3}	1.0×10^{-16}

competing processes would be the major sources of destruction of metastable helium atoms. The discharge of such atoms by diffusion to the walls of the chamber, while very important in small chambers at a few millimeters gas pressure, is negligible for the large chamber volume and gas pressures used here. Likewise the interaction of one metastable atom upon another with the production of an ion pair and a neutral atom must be assumed negligible here because of the relatively low density of metastable atoms.

In the two competing processes we may assume that the probability of a collision producing an ion pair is given by $\sigma_i N_i V_i$ and the probability of a collision producing the destruction of a metastable atom without ion formation by $\sigma_d N_{\mathrm{He}} V_d$. Here N_{He} and N_i are the number of atoms per cc of helium and of the impurity gas respectively, and σ_i and σ_d are the cross sections for the two reactions. V_i and V_d are the relative velocities of approach of the particles in the two cases.

At the impurity concentration where the probabilities of the two reactions are equal, we have the relation

$$\frac{\sigma_i V_i}{\sigma_d V_d} \equiv \frac{K_i}{K_d} = \frac{N_{\mathrm{He}}}{N_i} = \frac{1}{C},$$

where C is the concentration of the impurity in helium for this particular set of conditions. For convenience we shall henceforth represent the product terms $\sigma_i V_i$ and $\sigma_d V_d$ by the symbols K_i and K_d.

The impurity concentration corresponding to equal probabilities for the two methods of destruction of metastable atoms is easily determined from the corresponding plot of Fig. 1. At zero impurity concentration, that is, for pure helium, no metastables produce ions, while at the estimated maximum of the curve all the metastables produce ion pairs. The difference in these two ordinate values is proportional to the total number of metastables produced and one half the difference represents the case where half the metastables produce ions. The corresponding impurity concentration may easily be read from the curve for this particular set of conditions.

Thus for argon in helium the maximum ordinate of the curve is estimated to be 1.44, and the value for pure helium is unity by definition. The concentration corresponding to the mean of the two values is read on the curve to be 1.23×10^{-4}. Hence, $K_i/K_d = 1/C = 8100$. The K_i value for collisions producing ionization is hence some 8100 times larger than the K_d value for de-excitation without ionization. The ratios K_i/K_d thus determined are shown in column 3 of Table II.

It should be pointed out that in this somewhat naive method of determining K_i/K_d, no attempt has been made to correct the results for the ionization produced by "subexcitation electrons," which have been postulated by Platzman[10] to account for the differences in maximum value attained by the curves for the various impurity gases in helium. According to such a postulate, from each of these maximum values there should be subtracted a correction corresponding to the ionization produced by subexcitation electrons, and this adjusted maximum should be used in the calculations above. Since no precise estimates of the corrections involved are at present available, no such correction has been made here.

A more precise mathematical method for the computation of the ratio K_i/K_d may be employed.[11] It follows in general a relation first formulated by Stern and Volmer[12] in experiments dealing with the decay of fluorescent radiation.

Here virtually the same assumptions are made as were made above. Thus the metastable helium atom may be destroyed either by impact with an impurity atom resulting in an ion pair or by impact with one or more helium atoms resulting in de-excitation with ionization.

A simple mathematical derivation[2] results in the equation

$$\frac{1}{N_p - N_0} = \left(\frac{K_d}{K_i}\frac{1}{\alpha_0}\right)\frac{1}{C} + \frac{1}{\alpha_0}. \qquad (2)$$

[10] R. L. Platzman, Radiation Research 2, 1 (1955).

[11] The authors are indebted to Professor Robert Platzman who first called this useful method of representation of the data to their attention.

[12] O. Stern and M. Volmer, Physik Z. 20, 183 (1919).

Here N_0 is the total number of ion pairs collected per alpha particle in pure helium, and N_p is the total number of ion pairs collected in helium in the presence of an impurity at a partial pressure p. α_0 is the initial number of metastable helium atoms produced by one alpha particle. This equals the maximum value of $(N_p - N_0)$ for high-impurity concentrations, if we ignore the correction for subexcitation electrons; C is the concentration of the impurity in helium; K_i and K_d are the constants as previously defined.

If, following the equation above, one plots on the ordinate axis the variable $1/(N_p - N_0)$ from the experimental data against $1/C$ on the abscissa axis, one should get a linear relation. The slope of the resulting straight line is equal to $(K_d/K_i)(1/\alpha_0)$ and the intercept on the ordinate axis is equal to $1/\alpha_0$, the reciprocal of the initial number of metastable atoms produced per alpha particle.

The Stern-Volmer plots derived from the data of Table I are shown in Fig. 4. For the data for H_2 and A as impurities, where some variation of ionization with the pressure of the gas mixture has been found, the data corresponding to a pressure of 87.5 cm of mercury were used in the plots. The implications of the variation with pressure will be discussed later.

It will be seen in Fig. 4 that the plotted points derived from the He data of Table I lie reasonably well on straight lines as is predicted by the Stern-Volmer equation. The heavier gas impurities have smaller slopes for their straight lines, corresponding to smaller values of $(K_d/K_i)(1/\alpha_0)$, and hydrogen has a much larger value for the slope. All the lines, with the possible exception of that for H_2, seem to meet at a common ordinate intercept indicating a constant value of $1/\alpha_0$. This is what would be expected if the effect of ionization by subexcitation electrons is assumed negligible, i.e., that the maximum ordinate of all the curves in Fig. 1 is the same. The data in Table I, however, show small but definite differences in these values at high-impurity concentrations. These small differences are apparently not readily distinguishable in the relatively small value of the reciprocal $1/\alpha_0$. Perhaps, on the whole, the chief deficiency of the Stern-Volmer relation is the difficulty in determining from the plots an accurate value of the ordinate intercept $1/\alpha_0$, since this intercept value is at times very sensitive to the exact manner in which the straight line is drawn through the plotted points—as in the plot for H_2 above.

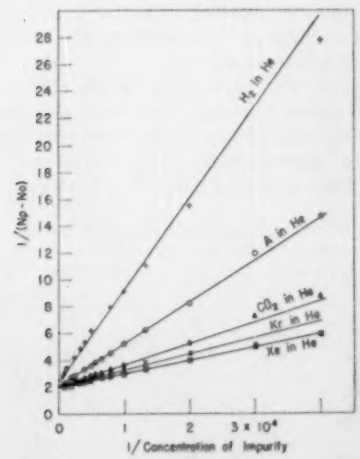

FIG. 4. Stern-Volmer plots for contaminants in helium.

Since the slopes of the Stern-Volmer lines are equal to $(K_d/K_i)(1/\alpha_0)$, one can determine values of the cross-section ratios K_i/K_d from values of the slopes and intercepts $1/\alpha_0$ in Fig. 4. These values are given in column 4 of Table II for comparison with the ratios obtained by the simpler method. The agreement between the two methods is satisfactory.

EFFECT OF PRESSURE OF THE GASEOUS MIXTURE

In order to interpret the observed change in ionization with the pressure of the gas mixture in the cases of H_2, N_2, and A, it is necessary to consider the mechanism by which a metastable atom may be de-excited in pure helium (see references 6 and 11). Such a de-excitation may occur through the following mechanisms:

(1) A two-body collision with a neutral helium atom. The possibility of raising by collision the electron from the metastable state to a higher state from which it can radiate would seem ruled out in helium because of the large energy required. It is possible, however, by a suspension of the selection rules for the electron to fall to a lower state during the collision and thus radiate energy. The probability for collision in any such two-body problem would increase directly with the number of helium atoms per unit volume and hence with the pressure of the mixture.

(2) A second possibility of de-excitation is a three-body collision of the metastable atom with two neutral helium atoms. An excited helium molecule is formed, which radiates energy and then immediately dissociates. Such a possibility has already been suggested by Burhop[15] from a consideration of preliminary data from our experiment. Thus

$$\mathrm{He^*+He+He\rightarrow He_2^{excited}+He}$$
$$\mathrm{\rightarrow He_2^{ground}+He+h\nu\rightarrow He+He+He+}h\nu.$$

The probability of such a three-body collision, being a compound probability, would be proportional to the square of the gas pressure. Thus,

$$\text{Collision probability}=Kp^2=(Kp)p.$$

For convenience the collision cross section may be considered to be (Kp), which is itself a function of pressure, and this quantity identified with the K_d

[15] E. H. S. Burhop, Proc. Phys. Soc. (London) A67, 276 (1954).

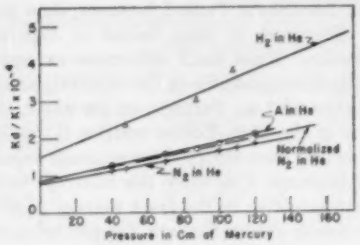

FIG. 5. Dependence of K_d/K_i upon pressure for H_2, N_2, and A in He.

above, with the understanding that K_d is now itself a function of pressure wherever this three-body collision is involved.

In Fig. 5 we have plotted for H_2, N_2, and A mixtures the values of K_d/K_i, the reciprocal of the quantity previously computed, against the corresponding pressure of the gas mixture. The plotted values of K_d/K_i are obtained by the following process. From a series of measurements at different impurity concentrations the approximate straight line relation between relative ionization and pressure is established for each value of impurity concentration. Ionization values for a series of interpolated pressures are then read from each plot. A Stern-Volmer plot for each interpolated pressure may then be constructed, relating the reciprocals of ionization values to those of impurity concentrations. From these straight lines the values of K_d/K_i may be computed by the method above. These values are plotted in Fig. 5 against the corresponding interpolated pressures. In the case of hydrogen, values of K_d/K_i, taken directly from three curves similar to those of Fig. 3, at 87.5, 108, and 48 cm pressure, were used in the plot.

All three plots in Fig. 5 for mixtures of helium with A, N_2, and H_2 show a linear increase of K_d/K_i with pressure, but each line has a definite intercept on the ordinate axis instead of passing through the origin. The latter might be expected if the three-body interaction is the only reaction involved. It would thus seem that $K_d/K_i = Kp + \text{constant}$, indicating a cross section directly proportional to pressure combined with a cross section which is independent of pressure—the latter probably a two-body interaction. For each of the mixtures the two component cross sections become equal when the pressure is approximately 80 to 90 cm of mercury.

If the hypothesis of Burhop is correct, the variation of K_d/K_i with pressure is caused by a variation in K_d rather than the alternative variation in K_i with pressure. In this case, since the variation in K_d is common to the three mixtures, the three plots in Fig. 5 should be identical except for the ordinate scale.

In Fig. 5 the dotted lines represent the plots for N_2 and H_2 after they are normalized to agree in intercept value with the argon value. This is done by multiplying each ordinate value by an appropriate constant. The normalized line for N_2 falls just below the argon line. The normalized H_2 line falls almost exactly on the argon plot—so close in fact that no additional line has been drawn. It should be noted, however, that the almost exact agreement between A and H_2 is somewhat subject to question, since the three experimental points in the original H_2 plot do not uniquely determine any straight line drawn through them.

The reasonably good agreement found here would seem to indicate the general correctness of the hypothesis of Burhop, that de-excitation of the metastable helium atoms takes place at least in part by a process of formation of excited molecules. There is, however, in addition another process of de-excitation of the metastable helium atoms the cross section for which is independent of pressure, probably representing an additional two-body interaction.

Perhaps the most puzzling part of the present experiment is the fact that for mixtures of helium with H_2, N_2, and A the pressure effect described above is observed, while mixtures with Xe, Kr, CO_2, and C_2H_4 give no detectable pressure change. A clue to the situation, however, seems to be furnished by a grouping of these gases in the order of their ionization potentials as in Table III. Here it seems that the pressure effect is observed with gaseous impurities whose ionization potential exceeds about 15 ev, while it is not observed in gases whose ionization potential falls below this approximate value. The widely diverse physical and chemical properties of the gases comprised in each group would serve to argue against any other criterion for classification than the value of the ionization potential.

No entirely satisfactory explanation of these facts is at once apparent. Perhaps the most plausible is that which assumes that the net energy available for transfer in the excited state of the helium molecule is about 15 ev. This net energy is the energy in the first vibrational level of the excited molecular state minus the energy of repulsion of two normal helium atoms at the same internuclear separation.

To explain the presence or absence of pressure effects let us first consider an idealized case, where the helium metastable atoms in pure helium are assumed to be de-excited solely by two-body collisions. When an impurity is added, one has then a competition be-

TABLE III. The presence or absence of a pressure effect in helium as it depends upon the gaseous contaminant.

Contaminant	Pressure effect	Ionization potential of contaminant gas (ev)
A	+	15.76
N_2	+	15.51
H_2	+	15.43
Kr	0	14.0
CO_2	0	13.73
Xe	0	12.127
C_2H_4	0	10.5

tween two processes the cross section of each of which is independent of pressure. Hence, K_d/K_i is not pressure-dependent.

Now let us assume that in the mixture helium metastable atoms may also in part be de-excited by the formation of helium molecules as described above. Provided the ionization potential of the impurity molecules is above the energy available in the excited molecule, a helium excited molecule cannot produce ions directly and must lose its energy only by radiative processes. Thus the competitive balance between the two processes is altered and K_d/K_i, following the law of formation of helium molecules, becomes pressure-dependent.

If, on the other hand, the ionization potential of the impurity molecules is below the energy available in the helium molecule, it might be expected that a direct energy transfer would take place on collision, resulting in the production of an ion pair. Thus the competition between the processes of radiation and direct ionization is again restored and the pressure effect would tend to be diminished.

In favor of the tentative hypothesis advanced above is the fact that independent measurements would seem to give a value for the available energy in the excited helium molecule in the neighborhood of 15 ev. Meyerott,[14] from optical spectra measurements, has argued for a potential energy curve for the helium molecule somewhat above that of Slater, and has established two points on the new curve. In Fig. 1 of Meyerott's paper the energy difference from the extreme limit of vibrational energy to his potential energy curve, somewhat extrapolated, is consistent with the value of 15 ev indicated by the results above.

Perhaps at present the most serious objection to the above hypothesis rests in the fact that we make the tacit assumption that for impurities of lower ionization potential the excited molecule may either produce directly a pair of ions on collision with an impurity, or radiate its energy on collision with a neutral helium atom. This assumes essentially that the excited helium molecule is in a metastable state.

Platzman has made calculations[15] to show that for the ionization by alpha particles in the present experiment more than 90 percent of the helium metastable atoms formed are in the singlet rather than the triplet state. Such singlet metastable atoms produce singlet helium molecules, while triplet metastable atoms produce triplet helium molecules. Only the latter molecules are metastable. The singlet molecules are in excited states and radiate with a comparatively short half-life. If the hypothesis above really depends on the assumption that the reacting helium molecules are metastable, it is difficult to see how one can obtain them in sufficient quantity by alpha-particle ionization processes which result, according to Platzman, mainly in singlet metastable atoms.

[14] R. Meyerott, Phy. Rev. **70**, 671 (1946).

[15] The authors are indebted to Professor Platzman for a private communication giving them the results of such calculations.

COMPARISON WITH OTHER EXPERIMENTS

Any valid comparison of the above results with the work of others is extremely difficult in that in the above work one determines only a ratio of cross sections σ_i/σ_d. Any absolute determination of either depends upon an assumed absolute value of the other. To obtain such an absolute value from the work of others is again difficult, since it is not at all certain that the same cross sections are being measured in the various experiments.

Absolute measurements of σ_d and σ_i for pure helium and for argon in helium have been made both by Biondi[6] and by Phelps and Molnar.[7] The former used a microwave technique to measure the ionization produced by metastable atoms in the afterglow of a pulsed discharge, while the latter made similar measurements using an optical absorption method. The measurements of both were made at gas pressures of a few millimeters of mercury. It seems apparent[16] that both of the above experiments dealt with interactions of metastable helium atoms mainly in the triplet state, while in our own case, according to the calculations of Platzman, the singlet state greatly predominated. Thus the expected cross sections in our own experiment should differ somewhat from the other two.

Although no exact agreement can be expected, it is possible to compare the three experiments solely as to order of magnitude of the results. If, so far as order of magnitude is concerned, Biondi's absolute measured value of 9.7×10^{-17} cm^2 for σ_i for argon in helium is identified with our own σ_i, then from our corrected ratio one can solve and obtain a value of $\sigma_d=9.8\times10^{-21}$ cm^2, which is in excellent agreement with Biondi's direct measurement of 9.6×10^{-21} cm^2. The exact agreement is somewhat illusory, since at least part of our cross section σ_d is a variable with pressure. Since the total cross section at 87.5 cm pressure is made up of almost equal parts of pressure dependent and pressure independent quantities, to correspond with the pressures of a few millimeters used by Biondi our own σ_d value should be reduced to about half the above value, or 4.9×10^{-21} cm^2.

Phelps and Molnar have found for the interaction of triplet state metastable atoms with neutral helium atoms a variation of the cross section σ_d with pressure according to the relation $\sigma_d=0.3\times10^{-23}p$ cm^2. Here p is the pressure in millimeters of mercury in experiments ranging from 20 to 100 millimeters. They apparently found no pressure independent cross section term as in the present experiment. For a pressure of 875 mm, corresponding to our own experiment, the Phelps and Molnar relation gives an extrapolated value for σ_d of 26×10^{-21} cm^2. This should correspond to the variable portion of our own cross section of σ_d, which at 875 mm

[16] A. V. Phelps, Phy. Rev. **91**, 436(A) (1953).

is about half the total of 9.8×10^{-21} cm^2 or 4.9×10^{21} cm^2. This is about five times smaller than that computed from the Phelps and Molnar relation.

While it may be possible that the fivefold discrepancy in cross section results from a difference in behavior between triplet and singlet metastable atoms, this divergence would seem somewhat excessive. It may also be that the large extrapolation with pressure in the calculation from the Phelps and Molnar relation is not justified.

For the sake of completeness, estimated values of σ_i for the various impurity gases are assembled in the last column of Table II. It should be pointed out again that at best these can only indicate order of magnitude. The values of σ_i were obtained by the following procedure.

The values of the cross section ratios σ_i/σ_d in column 6 were obtained from the K_i/K_d ratios in the preceding column by correcting for the relative velocities of approach of the particles in the two cases. This involves multiplying by

$$V_d/V_i=\left[\left(\frac{1}{m}+\frac{1}{m}\right)\Big/\left(\frac{1}{M}+\frac{1}{m}\right)\right]^{\frac{1}{2}}.$$

Here V_d and V_i represent, respectively, the relative velocities of approach for the interaction of a helium metastable atom with a neutral helium atom and for a helium metastable atom in its interaction with an impurity atom. The quantities M and m represent the mass numbers for the impurity atom and the helium atom respectively.

The relative velocity correction for a two-body interaction has been used here throughout, although for great accuracy the more complicated relation for a three-body interaction should in part probably be used. The final accuracy of the results, however, would hardly seem to warrant this added refinement.

The values of σ_i listed in the last column of Table II are obtained by again assuming σ_i for argon in He to be equal in order of magnitude to the Biondi value of 9.7×10^{-17} cm^2. The values of σ_i for the other gaseous impurities are computed on this basis from the relative ratios of σ_i/σ_d in the preceding column. This essentially assumes the constancy of σ_d in column 6. Similarly for the values where neon is the parent gas, the Biondi value of 2.6×10^{-16} cm^2 was adopted and other values calculated from this.

The values of σ_i in the last column are, as might be expected, of the same order of molecular cross sections as are computed by kinetic theory considerations. The variation in collision cross section does not seem very large with the exception of that for mercury, which is of the order of a hundred times greater than the others. This is in agreement with the findings of Biondi.

ACKNOWLEDGMENTS

It is a pleasure to express our thanks to a large number of friends and colleagues for the many stimulating discussions of this subject. Among these are Professor Robert L. Platzman, Dr. Roland Meyerott, Dr. Francis R. Shonka, Mr. John E. Rose, and Mr. L. D. Marinelli. We also acknowledge our indebtedness to Dr. Manfred A. Biondi and Dr. E. H. S. Burhop for correspondence discussing details of their work before formal publication. Finally, we wish to express our thanks to Mr. L. C. Ellsworth for his skillful construction of the ionization chambers used.

Tc *K* X-Ray Spectrum

GEORGE L. ROGOSA* AND WILLIAM F. PEED
Oak Ridge National Laboratory, Oak Ridge, Tennessee
(Received August 12, 1955)

Fluorescent x-ray radiation from 100 mg of $KTc^{99}O_4$ was analyzed with a Cauchois-type curved-crystal spectrometer and four *K*-series x-ray lines of Tc were recorded. The wavelengths accurate to within 0.1 xu are: $K\alpha_2$, 677.90; $K\alpha_1$, 673.57; $K\beta_{1,3}$, 600.20; $K\beta_{2,4}$, 588.99; all wavelengths in xu.

TECHNETIUM, element 43, was first isolated in milligram quantities from uranium fission by Parker, Reed, and Ruch.[1] Convincing evidence of its existence and isolation was obtained through the recording of its *K* x-ray spectrum by Burkhart, Peed, and Saunders.[2] Using a 25-cm Bragg spectrometer, they observed four *K*-series lines. Later, Marmier, Blaser, Preiswerk, and Scherrer,[3] using a Cauchois curved-crystal spectrometer, observed three *K*-series Tc lines resulting from the radioactive decay of a Tc isomer.

We have remeasured the *K* x-ray spectrum of Tc for the purpose of establishing the wavelength values with higher accuracy. One-hundred milligrams of $KTc^{99}O_4$ were irradiated using a tungsten-target x-ray tube operating at 48 kv and 20 ma, the high voltage and tube current both being regulated. The fluorescent radiation from the $KTc^{99}O_4$ was analyzed with a 5.73-inch Cauchois-type curved-crystal spectrometer employing the (331) planes of mica and a detector slit of 0.01° resolving width. The dispersion of the instrument at the Tc settings is close to 2.55xu/0.1°. X-ray intensities were detected with a Kr-filled proportional counter. The goniometer had an accuracy of 0.002° and was calibrated using the $K\alpha$ lines from Sr through Ag. The wavelength values given by Inglestam[4] were assumed.

TABLE I. Measured wavelengths of Tc *K* x-ray lines, in xu.

	Values of Burkhardt *et al.*[a]	Values of Marmier *et al.*[b]	New values
Tc $K\alpha_2$	677.8	677.9	677.90
Tc $K\alpha_1$	673.5	673.4	673.57
Tc $K\beta_{1,3}$	601.4	600	600.20
Tc $K\beta_{2,4}$	589.9		588.99

[a] See reference 2.
[b] See reference 3.

The x-ray lines were recorded by manual setting, in steps of 0.005° through the main part of the line and 0.01° at the sides of the line. Counts for a one-minute time interval were recorded. Numerous runs were taken for each line. The Tc wavelengths given here are accurate to within 0.1 xu. Comparison with the previous measurements[2,3] shows agreement on the $K\alpha$ lines, but disagreement on the weaker $K\beta$ lines. Table I gives the wavelength values previously reported and those obtained here. Figures 1 and 2 show the recorded spectrum.

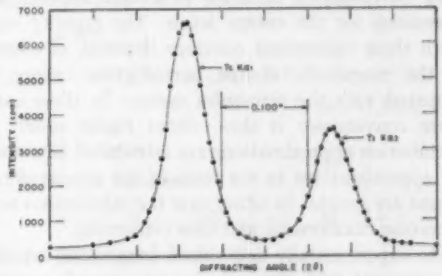

FIG. 1. Tc $K\alpha$ x-ray lines.

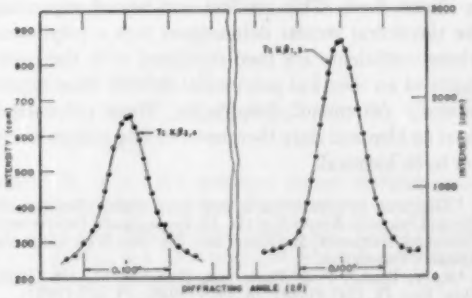

FIG. 2. Tc $K\beta$ x-ray lines.

ACKNOWLEDGMENTS

We thank George W. Parker and William J. Martin of the Oak Ridge National Laboratory for the loan of the Tc compound.

* Permanent address: Department of Physics, Florida State University, Tallahassee, Florida.

[1] Parker, Reed, and Ruch, U. S. Atomic Energy Commission Report AECD-2043, 1948 (unpublished).
[2] Burkhart, Peed, and Saunders, Phys. Rev. **73**, 347 (1948).
[3] Marmier, Blaser, Preiswerk, and Scherrer, Helv. Phys. Acta. **22**, 155 (1949).
[4] E. Inglestam, Nova. Acta. Regiae Soc. Sci. Upsaliensis **4**, No. 5 (1936).

Nuclear Magnetic Dipole and Electric Quadrupole Energy Relations*

L. Carlton Brown and Paul M. Parker
Department of Physics, The Ohio State University, Columbus, Ohio
(Received August 31, 1955)

Calculations based on existing theory of nuclear magnetic dipole and electric quadrupole transitions provide general expressions in closed form relating I, μH_0, e^2Qq, η, θ, and ϕ to experimentally determined frequencies ν_{ij}. The angles θ and ϕ determine the orientation of $\mathbf{H}_0$ in the principal axis system of $\nabla\mathbf{E}$. Methods of applying the expressions in specific situations are discussed. Application of the procedure to similar systems, such as the asymmetric rotator, is pointed out.

I. INTRODUCTION

THE original work of Pound[1] on the quadrupolar splitting of nuclear magnetic resonances and of Dehmelt and Kruger[2] on pure quadrupole transitions has been followed by a number of papers[3–11] in which the calculation of theoretical expressions for the dipolar-quadrupolar energy levels has been treated. Except for certain restricted cases in which exact expressions are available, the usual procedure is to apply perturbation methods to obtain approximate expressions for the energy levels. The rapidity with which these expressions converge depends, of course, on the magnitude of the perturbation energy as compared with the zero-order energy. In those cases where convergence is slow, either higher orders of perturbation approximations are introduced or numerical approximations to the roots of the secular determinant are sought. In either case the calculations tend to become cumbersome and time consuming.

The experimentally determined frequencies can also be compared with theoretical expressions in another way which permits the development of general relations in closed form. This method consists of expanding the theoretical secular determinant into a polynomial whose coefficients are then compared with the coefficients of an identical polynomial derived from experimentally determined frequencies. These polynomials must be identical since their roots F_i (the energy levels) are to be identical.

* This work was supported in part by a contract between the Office of Scientific Research of the Air Research and Development Command, Baltimore, Maryland, and The Ohio State University Research Foundation.

[1] R. V. Pound, Proc. Phys. Soc. (London) **61**, 576 (1948); Phys. Rev. **73**, 1247 (1948); **76**, 1410 (1949); **79**, 685 (1950).
[2] H. G. Dehmelt and H. Kruger, Naturwiss. **37**, 111 (1950); **37**, 398 (1950); Z. Physik **129**, 401 (1950).
[3] H. Kruger, Z. Physik **130**, 371 (1951).
[4] R. Bersohn, J. Chem. Phys. **20**, 1505 (1952).
[5] E. F. Carr and C. Kikuchi, Phys. Rev. **78**, 470 (1950).
[6] Volkoff, Petch, and Smellie, Can. J. Phys. **30**, 270 (1952).
[7] G. M. Volkoff, Can. J. Phys. **31**, 820 (1953).
[8] P. M. Parker, J. Chem. Phys. (to be published).
[9] C. Dean, doctoral dissertation, Harvard University, 1952 (unpublished).
[10] L. C. Brown and D. Williams, Phys. Rev. **95**, 1110 (1954); J. Chem. Phys. (to be published).
[11] L. Carlton Brown, doctoral dissertation, The Ohio State University, 1955 (unpublished).

II. PROCEDURE

It is convenient to express the F_i in units of frequency and to fix the reference level from which they are measured by requiring that the sum of the energies be zero, i.e.,

$$\sum_i F_i=0, \quad i=1, 2, 3, \cdots, 2I+1. \tag{1}$$

It is necessary in this procedure to have sufficient experimental frequency data to construct an energy level diagram and to compute the term values with the help of Eq. (1). In the system under consideration this requirement is not particularly demanding. For example, with $I=5/2$, $\nu_i=F_{i+1}-F_i$, and F_1, F_2, $\cdots$, F_6 labeled in order of increasing (or decreasing) magnitude, the expressions

$$\begin{aligned}
F_6&=\tfrac{1}{6}(\nu_1+2\nu_2+3\nu_3+4\nu_4+5\nu_5),\\
F_5&=\tfrac{1}{6}(\nu_1+2\nu_2+3\nu_3+4\nu_4-\nu_5),\\
F_4&=\tfrac{1}{6}(\nu_1+2\nu_2+3\nu_3-2\nu_4-\nu_5),\\
F_3&=\tfrac{1}{6}(\nu_1+2\nu_2-3\nu_3-2\nu_4-\nu_5),\\
F_2&=\tfrac{1}{6}(\nu_1-4\nu_2-3\nu_3-2\nu_4-\nu_5),\\
F_1&=\tfrac{1}{6}(-5\nu_1-4\nu_2-3\nu_3-2\nu_4-\nu_5),
\end{aligned} \tag{2}$$

satisfy both

$$\nu_i=F_{i+1}-F_i \quad \text{and} \quad \sum_i F_i=0. \tag{3}$$

If the sign of each F_i is changed and the order of labeling is reversed, i.e., if the energy diagram is inverted, the relations in Eq. (3) are still satisfied, thus the absolute signs of the F_i are ambiguous unless additional information is available regarding the signs of μH_0 and e^2Qq.

In the case of pure quadrupole transitions the above example reduces to

$$\begin{aligned}
F_6&=F_5=\tfrac{1}{3}(\nu_2+2\nu_4),\\
F_4&=F_3=\tfrac{1}{3}(\nu_2-\nu_4),\\
F_2&=F_1=\tfrac{1}{3}(-2\nu_2-\nu_4),
\end{aligned} \tag{4}$$

since $\nu_1=\nu_3=\nu_5=0$ and the observable frequencies are ν_2 and ν_4.

There are situations in which transitions between adjacent levels are not directly observable; however, in many of these cases transitions between nonadjacent levels are present and provide the necessary data for

constructing the energy diagram. In any case the problem of correctly assigning labels to the observed frequencies is of fundamental importance.

With the F_i determined from experimental data, the secular polynomial can be formed as follows:

$$(F-F_1)(F-F_2)(F-F_3)\cdots(F-F_n)=0, \quad (5)$$

where $n=2I+1$ is the multiplicity. Equation (5) can be written as

$$F^n+a_1F^{n-1}+a_2F^{n-2}+a_3F^{n-3}+\cdots+a_n=0, \quad (6)$$

with

$$\begin{aligned} a_1&=-\textstyle\sum_i F_i=0, && \text{from Eq. (3)},\\ a_2&=\textstyle\sum_i\sum_j F_iF_j, && i<j,\\ a_3&=-\textstyle\sum_i\sum_j\sum_k F_iF_jF_k, && i<j<k,\\ &\text{etc.} \end{aligned} \quad (7)$$

The a_r are the well-known symmetric functions of the roots of a polynomial equation. The restrictions $i<j$, etc., are introduced to avoid duplications in the sums. It is more convenient to work with sums of powers of the roots which become (with $a_1=0$),

$$\begin{aligned} S_1&=\textstyle\sum_i F_i=-a_1=0,\\ S_2&=\textstyle\sum_i (F_i)^2=-2a_2,\\ S_3&=\textstyle\sum_i (F_i)^3=-3a_3. \end{aligned} \quad (8)$$

Terms involving higher powers of the F_i are omitted from this discussion since the experimental quantities S_1, S_2, and S_3 provide sufficient information in most situations.

The Hamiltonian for the system can be written as

$$\mathfrak{H}=-\boldsymbol{\mu}\cdot\mathbf{H}_0-\tfrac{1}{2}\mathbf{Q}\cdot\boldsymbol{\nabla}\mathbf{E}+\mathfrak{H}' \quad (9)$$

where $\boldsymbol{\mu}$ is the magnetic dipole moment of the nucleus in question, $\mathbf{H}_0$ is the external magnetic field, $\mathbf{Q}$ is the nuclear electric quadrupole moment tensor, and $\boldsymbol{\nabla}\mathbf{E}$ is the electric field gradient tensor (dyadic form). $\mathfrak{H}'$ represents interactions involving higher order moments (if present) and neighboring systems. This term is considered to be sufficiently small to be omitted in the present work.

In the xyz coordinate system which diagonalizes $-(\boldsymbol{\nabla}\mathbf{E})_{ij}=\phi_{ij}$, such that

$$|\phi_{zz}|\leq|\phi_{yy}|\leq|\phi_{xx}|, \quad (10)$$

Eq. (9) with the omission of $\mathfrak{H}'$ can be written in units of frequency as

$$\begin{aligned} W=&-\nu_0(\sin\theta\cos\phi I_x+\sin\theta\sin\phi I_y+\cos\theta I_z)/h\\ &+(c_3/6)[3I_z^2-I^2+\eta(I_x^2-I_y^2)]/h^2, \end{aligned} \quad (11)$$

where I_x, I_y, I_z, and I^2 are angular momentum operators, I is the nuclear spin,

$$W=\mathfrak{H}/h, \quad (12)$$

$$\nu_0=\mu H_0/Ih, \quad (13)$$

$$c_1=3eQ\phi_{zz}/2I(2I-1)h=-\tfrac{1}{2}(1-\eta)c_3, \quad (14)$$

$$c_2=3eQ\phi_{yy}/2I(2I-1)h=-\tfrac{1}{2}(1+\eta)c_3, \quad (15)$$

$$c_3=3eQ\phi_{xx}/2I(2I-1)h=3e^2Qq/2I(2I-1)h, \quad (16)$$

$$\eta=(\phi_{xx}-\phi_{yy})/\phi_{zz}=(c_1-c_2)/c_3, \quad (17)$$

and the angles θ and ϕ are the polar and azimuthal angles respectively of the vector $\mathbf{H}_0$ in the xyz system. The quantity ν_0 is the Larmor frequency and c_3 is the frequency interval between pure quadrupole transition frequencies with $\eta=0$. The quantities c_1 and c_2 are defined in analogy with c_3 and satisfy the relation

$$c_1+c_2+c_3=0. \quad (18)$$

The nonzero matrix elements of W in a representation such that

$$I^2\psi_m=I(I+1)\hbar^2\psi_m \quad (19)$$

and

$$I_z\psi_m=m\hbar\psi_m \quad (20)$$

are

$$W_{m,m}=-m\nu_0\cos\theta+\tfrac{1}{6}[3m^2-I(I+1)]c_3, \quad (21)$$

$$W_{m,m+1}=-\tfrac{1}{2}[(I-m)(I+m+1)]^{\frac{1}{2}}\nu_0\sin\theta e^{i\phi}, \quad (22)$$

$$W_{m+1,m}=W^*_{m,m+1}, \quad (23)$$

$$\begin{aligned} W_{m,m+2}=&(1/12)[(I-m)(I+m+1)\\ &\times(I-m-1)(I+m+2)]^{\frac{1}{2}}\eta c_3, \end{aligned} \quad (24)$$

$$W_{m+2,m}=W_{m,m+2}. \quad (25)$$

The secular equation

$$(-1)^n|W_{mm'}-F\delta_{mm'}|=0, \quad n=2I+1 \quad (26)$$

reduces to the polynomial form

$$F^n+a_1F^{n-1}+a_2F^{n-2}+a_3F^{n-3}+\cdots+a_n=0 \quad (27)$$

upon expansion. The coefficients have the form

$$\begin{aligned} a_1&=-\textstyle\sum_i M_i,\\ a_2&=\textstyle\sum_i\sum_j M_{ij}, && i<j\\ a_3&=-\textstyle\sum_i\sum_j\sum_k M_{ijk}, && i<j<k\\ &\text{etc.}, \end{aligned} \quad (28)$$

where M_i is a 1×1 principal minor determinant of $(W_{mm'})$, M_{ij} is a 2×2 principal minor determinant of $(W_{mm'})$, i.e., formed from rows i and j and columns i and j, M_{ijk} is a 3×3 principal minor determinant of $(W_{mm'})$, etc. By summing Eq. (21) over m from I to $-I$, it follows that

$$a_1=-\textstyle\sum_i M_i=-\sum_m W_{m,m}=0, \quad (29)$$

i.e., the trace T of the W matrix is zero, thus satisfying the arbitrary requirement imposed by Eq. (1).

In other systems, such as the asymmetric rotator energies for a fixed value of J, the trace may not vanish. In this case Eq. (26) can be modified to read

$$\begin{aligned} (-1)^n|W_{mm'}-(T/n)\delta_{mm'}&\\ +(T/n)\delta_{mm'}-F\delta_{mm'}|=0& \end{aligned} \quad (30)$$

or

$$(-1)^n|W_{mm'}-F'\delta_{mm'}|=0, \tag{31}$$

where

$$W_{mm'}=W_{mm'}-(T/n)\delta_{mm'} \tag{32}$$

and

$$F'=F-T/n. \tag{33}$$

In this form the trace of W' vanishes and Eq. (1) becomes $\sum_i F_i'=0$.

Upon equating the coefficients of the polynomials in Eqs. (6) and (27), the expressions in (8) become

$$\begin{aligned} S_1&=\textstyle\sum_i M_i=0,\\ S_2&=-2\textstyle\sum_i\sum_j M_{ij}, \quad i<j\\ S_3&=3\textstyle\sum_i\sum_j\sum_k M_{ijk}, \quad i<j<k. \end{aligned} \tag{34}$$

The details[11] of calculating the indicated sums in Eqs. (34) are omitted. The procedure involves expanding the minor determinants, introducing the matrix elements given in Eqs. (21)–(25), and arranging the resulting expressions so that the following finite sums over m from I to $-I$ may be introduced:

$$\begin{aligned} &\textstyle\sum m^r=0 \text{ with } r \text{ an odd integer},\\ &\textstyle\sum m^0=2I+1,\\ &\textstyle\sum m^2=(1/3)I(I+1)(2I+1),\\ &\textstyle\sum m^4=(1/15)I(I+1)(2I+1)(3I^2+3I-1),\\ &\textstyle\sum m^6=(1/21)I(I+1)(2I+1)(3I^4+6I^3-3I+1). \end{aligned} \tag{35}$$

The resulting expressions, which must be satisfied in the general case, are

$$S_1=0, \tag{36}$$

$$S_2=p_2c_2^2(1+\eta^2/3)+p_1\nu_0^2, \tag{37}$$

$$S_3=p_3c_2^3(1-\eta^2)+3p_2c_3\nu_0^2(3\cos^2\theta-1+\eta\sin^2\theta\cos 2\phi), \tag{38}$$

where p_1, p_2, and p_3 depend only on I as follows:

$$\begin{aligned} p_1&=2I(I+1)(2I+1)/3!,\\ p_2&=2I(I+1)(2I-1)(2I+1)(2I+3)/3(5!),\\ p_3&=2I(I+1)(2I-3)(2I-1)(2I+1)\\ &\quad\times(2I+3)(2I+5)/3(7!). \end{aligned} \tag{39}$$

It should be noted from Eqs. (36) and (37) that the sum of the squares of the energy levels as well as the sum of the first powers is independent of the orientation of the crystal in the magnetic field. This remarkable fact provides an immediate check on the problem of assignments since in general S_2 can be expected to remain constant for different crystal orientations only when assignments are correctly made.

Equations (37) and (38) can be written in a more symmetric form by introducing c_1 and c_2 as follows:

$$S_2=(2/3)p_2(c_1^2+c_2^2+c_3^2)+p_1\nu_0^2, \tag{40}$$

$$S_3=(4/3)p_3(c_1^3+c_2^3+c_3^3)+6p_2(c_1\nu_x^2+c_2\nu_y^2+c_3\nu_z^2), \tag{41}$$

where the vector $\boldsymbol{\nu}$ is defined as

$$\boldsymbol{\nu}=\mu\mathbf{H}_0/Ih \tag{42}$$

and has the magnitude ν_0.

It can be shown that terms involving ν_0 to an odd power do not appear in any of the polynomial coefficients and that odd powers of c_3 appear only in relations involving F_i to odd powers. It follows that a change in sign of μ does not affect any of the S_r and a change in sign of e^2Qq changes the sign of S_r with r odd.

Three special cases of Eqs. (36)–(38) are of interest. The first case considered will be that of the pure quadrupole interaction ($\nu_0=0$). Equations (37) and (38) reduce to

$$S_2=p_2c_2^2(1+\eta^2/3) \tag{43}$$

$$S_3=p_3c_2^3(1-\eta^2). \tag{44}$$

Except for the isolated case of $I=3/2$ in which $p_3=0$, Eqs. (43) and (44) can be used to determine η and the magnitude of e^2Qq for arbitrary I. Thus with

$$(1-\eta^2)^3/(1+\eta^2/3)^3=1-\alpha=p_3^3S_2^3/p_2^3S_3^3, \tag{45}$$

a single tabulation of $\eta=\eta(\alpha)$, $0\leq\eta\leq 1$, $0\leq\alpha\leq 1$, is sufficient to determine η and, with η known,

$$e^2Qq/h=[2I(2I-1)/3][S_2/p_2(1+\eta^2/3)]. \tag{46}$$

For $\eta=0$, Eq. (46) reduces to a form which can be calculated directly from

$$F_m=[e^2Qq/4I(2I-1)h][3m^2-I(I+1)],$$

which is valid in this case.

The well-known fact that it is not possible to determine both e^2Qq and η ($\eta\neq 0$) from pure quadrupole spectra alone in the case of $I=\frac{3}{2}$ appears in the form $p_3=0$ in this development. The remaining polynomial coefficient a_4 is proportional to a_2^2 in this case and thus gives no additional information.

The second special case concerns selected orientations of the crystal in the external field. It is possible experimentally to orient $\mathbf{H}_0$ parallel to each of the principal axes of $\nabla\mathbf{E}$ in succession by observing changes in the frequency patterns with changes in crystal orientations. The experimental procedure depends on the symmetry properties of the frequency patterns with respect to the principal axis orientations of $\mathbf{H}_0$. If S_3^x, S_3^y, and S_3^z are the experimental quantities determined in these three orientations then

$$\begin{aligned} S_3^x&=p_3c_2^3(1-\eta^2)+3p_2c_3\nu_0^2(-1+\eta),\\ S_3^y&=p_3c_2^3(1-\eta^2)+3p_2c_3\nu_0^2(-1-\eta),\\ S_3^z&=p_3c_2^3(1-\eta^2)+3p_2c_3\nu_0^2(2). \end{aligned} \tag{47}$$

Elimination between these equations results in the relations

$$\eta=3(S_3^x-S_3^y)/(2S_3^z-S_3^x-S_3^y), \tag{48}$$

which is independent of I,

$$c_3=[(S_3^x+S_3^y+S_3^z)/3p_3(1-\eta^2)], \quad I\neq\tfrac{3}{2}, \quad \eta\neq 1, \tag{49}$$

and

$$\nu_0=[(2S_3^{\,a}-S_3^{\,\sigma}-S_3^{\,\gamma})/18p_2c_3]^{\frac{1}{3}}. \quad (50)$$

For $I=\frac{3}{2}$, Eq. (49) is indeterminate but c_3 can be determined by eliminating ν_0 between Eqs. (37) and (47).

Experimental data recently obtained from Al^{27} and Be^9 resonances in beryl[10] have been reviewed in terms of the above procedure. The resulting coupling constants were found to be essentially identical with those calculated previously on the basis of expressions for individual energy levels.

The third special case involves determining S_2 and S_3 at two different magnitudes of the magnetic field, say H and λH. From the resulting two sets of equations for $S_2(H)$, $S_2(\lambda H)$, $S_3(H)$, $S_3(\lambda H)$ it follows that

$$\nu_0=\{[S_2(\lambda H)-S_2(H)]/p_1(\lambda^2-1)\}^{\frac{1}{3}} \quad (51)$$

$$c_3^2(1+\eta^2/3)=[\lambda^2S_2(H)-S_2(\lambda H)]/p_2(\lambda^2-1) \quad (52)$$

$$c_3^3(1-\eta^2)=[\lambda^2S_3(H)-S_3(\lambda H)]/p_3(\lambda^2-1), \quad I\neq\tfrac{3}{2}. \quad (53)$$

The values of η and c_3 follow from Eqs. (52) and (53) in a manner similar to that given by Eqs. (45) and (46).

It should be noted that, for $\eta=0$, the quantities S_2 and S_3 determined at two values of H_0 are sufficient to determine the angle θ between the field and the unique axis of $\nabla\mathbf{E}$.

III. CONCLUSIONS

The procedure of relating experimental data to theory through the coefficients of secular polynomials can be used advantageously in those cases in which the mathematically equivalent method of relating their roots, the individual energy levels, presents computational difficulties.

Application of the procedure to nuclear resonances in crystals results in relatively simple general expressions for the coupling constants in terms of the resonant frequencies.

Energy relations for the asymmetric rotator, similar to those for the pure quadrupole case, can be developed by a corresponding procedure.

ACKNOWLEDGMENTS

The authors wish to express their appreciation to Professor Dudley Williams and Professor Jan Korringa for their helpful suggestions with regard to the problem.

PHYSICAL REVIEW VOLUME 100, NUMBER 6 DECEMBER 15, 1955

"Contact Interaction" in the Relativistic Energy of Two-Electron Atoms

TA-YOU WU AND G. E. TAUBER
Division of Pure Physics, National Research Council, Ottawa, Canada

(Received September 30, 1954; revised manuscript received July 18, 1955)

It is shown that the "contact interaction" recently pointed out by Sessler, Sucher, and Foley for the relativistic two-electron atoms can be very simply and unambiguously obtained from the field-theoretical form of the theory of Breit and Møller, whereas the original "reduction" procedure (reducing the equation for the 16-component wave function to one for the four big components by successive approximation) does *not* lead to this contact term. The effect of the singular behavior of relativistic wave function at the origin gives rise to a correction of order α^4 in the energy.

I. INTRODUCTION[1]

THE problem of finding the relativistic energy of a two-electron atom (He-like atoms) was first treated by Breit.[2] Many calculations have been made subsequently. Recently, Sessler and Foley[3] gave on classical arguments an additional term of order $(v/c)^2$ in the energy of the ground state of helium, and in a more recent paper, Sucher and Foley[4] obtained this additional term from the original method of Breit. This term, of the nature of a contact potential and previously found also by Berestetskii and Landau[5] in connection with the positronium problem, has in fact been found much earlier and included in their work by Breit and his co-workers,[6] although not explicitly in connection with the ground state of helium. The purpose of the present work is to point out that by

[1] After the above work was finished, our attention has been called by Dr. S. Shanmugadhasan, to whom we wish to express our thanks, to a paper by A. I. Andreev, Vestnik Moskov. Univ. Ser. Fiz.-Mat. i Estestven. Nauk **3**, No. 5, 65–9 (1954), in which the author employs simultaneously the reduction procedure to the big components and the matrix element of H in (1) with respect to the 16-component wave function, thereby obtaining the contact term H_c of (12), but also the B'^2 term in (10) [or the $H^{(7)}$ in (11)] as well. The procedure given in Sec. III in the present note gives H_c but not $H^{(7)}$.

Our result is essentially the same as that of Berestetskii and Landau, reference 5. Our method differs from theirs in that we use the wave functions in (15) thereby obtaining the relativistic correction very simply by one simple integration in (18), whereas the other authors express the small components in terms of the big components and obtain the various operators in (11) and (12) in separate forms in a longer calculation.

[2] G. Breit, Phys. Rev. **34**, 553 (1929); **39**, 616 (1932).

[3] A. M. Sessler and H. M. Foley, Phys. Rev. **92**, 1321 (1953).

[4] J. Sucher and H. M. Foley, Phys. Rev. **95**, 966 (1954).

[5] V. Berestetskii and L. Landau, J. Exptl. Theoret. Phys. (U.S.S.R.) **19**, 673 (1949).

[6] G. Breit, Phys. Rev. **72**, 1023 (1947); G. Breit and G. E. Brown, Phys. Rev. **74**, 1278 (1948); Breit, Brown, and Arfken, Phys. Rev. **76**, 1299 (1949).

following the original procedure (reduction of 16-component wave equation to one for the 4 big components), one does *not* obtain the contact term, whereas a calculation of the interaction between the two electrons in the manner of Breit and of Møller[7] does lead very simply and unambiguously to this contact term.

II. "REDUCTION" PROCEDURE

The theory of Breit[2] in the earlier form is as follows. The Hamiltonian of a two-electron atom is taken to be

$$H(1,2)=H_0(1)+H_0(2)+e^2/r_{12}+B, \tag{1}$$

where H_0 is the Dirac Hamiltonian for one electron:

$$H_0(1)=-c(\boldsymbol{\alpha}_1\cdot\boldsymbol{\Pi}_1)-\beta_1mc^2-Ze^2/r_1, \tag{2}$$

$$B=-\frac{e^2}{2r_{12}}\left[(\boldsymbol{\alpha}_1\cdot\boldsymbol{\alpha}_{II})+\frac{1}{r_{12}^2}(\boldsymbol{\alpha}_1\cdot\mathbf{r}_{12})(\boldsymbol{\alpha}_{II}\cdot\mathbf{r}_{12})\right], \tag{3}$$

$$\boldsymbol{\Pi}_{1s}=\mathbf{p}_{1s}+(e/c)\mathbf{A}_{1s}.$$

Here and in the following, the subscripts I, II refer to electron 1 and 2 respectively. On writing

$$\Pi_0=-\frac{\hbar}{i}\frac{\partial}{\partial t}+\frac{Ze^2}{c}\left(\frac{1}{r_1}+\frac{1}{r_2}\right)-\frac{e^2}{cr_{12}}, \tag{4}$$

and on denoting the 16-component wave function ψ by four 4-component wave functions

$$\psi=\begin{pmatrix}\phi & u\\ v & \Psi\end{pmatrix}, \tag{5}$$

and writing

$$B'=\frac{e^2}{2r_{12}}\left[(\boldsymbol{\sigma}_1\cdot\boldsymbol{\sigma}_{II})+\frac{1}{r_{12}^2}(\boldsymbol{\sigma}_1\cdot\mathbf{r}_{12})(\boldsymbol{\sigma}_{II}\cdot\mathbf{r}_{12})\right], \tag{6}$$

where $\boldsymbol{\sigma}_1$, $\boldsymbol{\sigma}_{II}$ are the Pauli matrices for the two electrons, the wave equation can be put in the form

$$(\Pi_0-2mc)\Psi+(\boldsymbol{\sigma}_1\cdot\boldsymbol{\Pi}_1)u+(\boldsymbol{\sigma}_{II}\cdot\boldsymbol{\Pi}_{II})v+(B'/c)\phi=0, \tag{7a}$$

$$(\boldsymbol{\sigma}_1\cdot\boldsymbol{\Pi}_1)\Psi+\Pi_0u+(B'/c)v+(\boldsymbol{\sigma}_{II}\cdot\boldsymbol{\Pi}_{II})\phi=0, \tag{7b}$$

$$(\boldsymbol{\sigma}_{II}\cdot\boldsymbol{\Pi}_{II})\Psi+(B'/c)u+\Pi_0v+(\boldsymbol{\sigma}_1\cdot\boldsymbol{\Pi}_1)\phi=0, \tag{7c}$$

$$(B'/c)\Psi+(\boldsymbol{\sigma}_{II}\cdot\boldsymbol{\Pi}_{II})u+(\boldsymbol{\sigma}_1\cdot\boldsymbol{\Pi}_1)v+(\Pi_0+2mc)\phi=0. \tag{7d}$$

The 12 small components ϕ, u, v are expressed in terms of the 4 big components Ψ by solving (7b), (7c), (7d) by successive approximation,[8]

$$\phi\cong\frac{1}{4m^2c^2}(\boldsymbol{\sigma}_1\cdot\boldsymbol{\Pi}_1)(\boldsymbol{\sigma}_{II}\cdot\boldsymbol{\Pi}_{II})\Psi-\frac{B'}{4mc^2}\Psi, \tag{8}$$

$$u\cong-\Pi_0^{-1}(\boldsymbol{\sigma}_1\cdot\boldsymbol{\Pi}_1)\Psi+\frac{1}{2mc^2}B'\Pi_0^{-1}(\boldsymbol{\sigma}_{II}\cdot\boldsymbol{\Pi}_{II})\Psi-\Pi_0^{-1}(\boldsymbol{\sigma}_{II}\cdot\boldsymbol{\Pi}_{II})\phi, \tag{9}$$

$$v\cong-\Pi_0^{-1}(\boldsymbol{\sigma}_{II}\cdot\boldsymbol{\Pi}_{II})\Psi+\frac{1}{2mc^2}B'\Pi_0^{-1}(\boldsymbol{\sigma}_1\cdot\boldsymbol{\Pi}_1)\Psi-\Pi_0^{-1}(\boldsymbol{\sigma}_1\cdot\boldsymbol{\Pi}_1)\phi,$$

such that when they are substituted in Eq. (7a), all quantities of order $(v/c)^4$ are included. On using (8) and (9), Eq. (7a) gives the original equation of Breit for the 4 big components

$$\left[\frac{\Pi_0}{2mc}-1-\frac{1}{2mc}\{(\boldsymbol{\sigma}_1\cdot\boldsymbol{\Pi}_1)\Pi_0^{-1}(\boldsymbol{\sigma}_1\cdot\boldsymbol{\Pi}_1)+(\boldsymbol{\sigma}_{II}\cdot\boldsymbol{\Pi}_{II})\Pi_0^{-1}(\boldsymbol{\sigma}_{II}\cdot\boldsymbol{\Pi}_{II})\}-\frac{1}{8m^4c^4}(\boldsymbol{\sigma}_1\cdot\boldsymbol{\Pi}_1)^2(\boldsymbol{\sigma}_{II}\cdot\boldsymbol{\Pi}_{II})^2+\frac{1}{8m^3c^4}\{(\boldsymbol{\sigma}_1\cdot\boldsymbol{\Pi}_1)B'(\boldsymbol{\sigma}_{II}\cdot\boldsymbol{\Pi}_{II})+(\boldsymbol{\sigma}_{II}\cdot\boldsymbol{\Pi}_{II})B'(\boldsymbol{\sigma}_1\cdot\boldsymbol{\Pi}_1)+B'(\boldsymbol{\sigma}_1\cdot\boldsymbol{\Pi}_1)(\boldsymbol{\sigma}_{II}\cdot\boldsymbol{\Pi}_{II})+(\boldsymbol{\sigma}_1\cdot\boldsymbol{\Pi}_1)(\boldsymbol{\sigma}_{II}\cdot\boldsymbol{\Pi}_{II})B'\}-\frac{1}{8m^2c^4}B'^2\right]\Psi=0. \tag{10}$$

This equation can be put in the form[9]

[7] C. Møller, Z. Physik **70**, 786 (1931).

[8] From (7b) and (7c), one obtains u, v up to (v/c). Putting these into (7d), one obtains ϕ up to $(v/c)^2$ in (8). Putting this back in (7b) and (7c) one obtains u, v in (9).

[9] The various operators are given in reference 2 and in the notation of (11) by H. A. Bethe, *Handbuch der Physik* (J. Springer, Berlin, 1933), Vol. 24, Part 1. Concerning the operators $H^{(1)}$, $H^{(3a)}$, $H^{(4)}$ [see H. A. S. Erickson, Z. Physik **109**, 762 (1938), and reference 3], the following remarks may be useful. The above operators come from the terms

$$(\boldsymbol{\sigma}_1\cdot\boldsymbol{\Pi}_1)\Pi_0^{-1}(\boldsymbol{\sigma}_1\cdot\boldsymbol{\Pi}_1)+(\boldsymbol{\sigma}_{II}\cdot\boldsymbol{\Pi}_{II})\Pi_0^{-1}(\boldsymbol{\sigma}_{II}\cdot\boldsymbol{\Pi}_{II})$$

in (10). In the following it is sufficient to refer to the first of these two terms and to consider the case with no external field ($\boldsymbol{\Pi}=\mathbf{p}$). On omitting the subscript I, one has

$$c(\boldsymbol{\sigma}\cdot\mathbf{p})\Pi_0^{-1}(\boldsymbol{\sigma}\cdot\mathbf{p})=\frac{1}{2m}(\boldsymbol{\sigma}\cdot\mathbf{p})\frac{1}{U}(\boldsymbol{\sigma}\cdot\mathbf{p})=\frac{1}{2mU}(\boldsymbol{\sigma}\cdot\mathbf{p})^2+\frac{1}{2m}(\boldsymbol{\sigma}\cdot\mathbf{p})U^{-1}\cdot(\boldsymbol{\sigma}\cdot\mathbf{p}), \tag{A}$$

where

$$U=1+\frac{1}{2mc^2}(E-2mc^2+eV)=1+\mathfrak{v}$$
$$\cong1+O(v^2/c^2),\ \text{except at } r_1,\ r_2,\ r_{12}=0,$$
$$\to\infty \text{ as } \frac{1}{r_1},\ \frac{1}{r_2},\ \frac{1}{r_{12}} \text{ as } r_1,\ r_2,\ r_{12}\to0 \text{ respectively.} \tag{B}$$

The dot behind U^{-1} indicates that the operator in the front does not extend beyond U^{-1}. On carrying out the calculation, one obtains

$$c(\boldsymbol{\sigma}\cdot\mathbf{p})\Pi_0^{-1}(\boldsymbol{\sigma}\cdot\mathbf{p})=\frac{1}{2mU}p^2+\frac{1}{U^2}(H^{(3a)}+H^{(4)}), \tag{C}$$

where

$$H^{(3a)}=\frac{e\hbar}{4m^2c^2}([\mathcal{E}\times\mathbf{p}]\cdot\boldsymbol{\sigma}),$$

$$H^{(4)}=-i\frac{e\hbar}{4m^2c^2}(\mathcal{E}\cdot\mathbf{p}).$$

$$\mathcal{E}=-\boldsymbol{\nabla}V=-(2mc^2/e)\boldsymbol{\nabla}U.$$

The usual procedure is to expand $1/U\cong1-\mathfrak{v}$ in the first term in (C) and replace U^2 by 1 in the second and third term in (C). This procedure is not correct, it leading to the indeterminate value $\infty\cdot0$ for the matrix element of $H^{(3a)}$. Only working with the exact operator $(1/U^2)H^{(3a)}$ gives the value 0 to the spin-orbit interaction for the S-state. [See E. U. Condon and G. Shortley, *Theory of Atomic Spectra* (Cambridge University Press, London, 1935), p. 130.]

On forming the matrix element of

$$\frac{1}{2mU}p^2+\frac{1}{U^2}H^{(4)}=\frac{\hbar^2}{2m}\left[-\frac{1}{U}\nabla^2+\frac{1}{U^2}(\boldsymbol{\nabla}U\cdot\boldsymbol{\nabla})\right], \tag{D}$$

$$[H_{NR}+H_r+H^{(4)}+H_B]\Psi=E\Psi,$$
$$H_r=H^{(1)}+H^{(3a)}+H^{(4)},\qquad (11)$$
$$H_B=H^{(2)}+H^{(3b)}+H^{(5)}+H^{(7)}.$$

H_{NR} is the nonrelativistic Hamiltonian, $H^{(1)}$ the quantum mechanical analog of the classical Sommerfeld correction, $H^{(3a)}$ the spin-orbit interaction, $H^{(4)}$ the "S-state" correction, $H^{(6)}$ the interaction with external fields. The term $H^{(3b)}$ representing some sort of "spin-other orbit" interaction and the term $H^{(5)}$ representing the spin-spin interaction, arise from the magnetic interaction $(\boldsymbol{\alpha}_I\cdot\boldsymbol{\alpha}_{II})$ in the operator B, the term $H^{(2)}$ arises from the retardation term in B, and the term $H^{(7)}$ from both in B. (10) and (11) are the original result of Breit. It is to be emphasized here that according to this procedure of reduction, the additional contact term,[3-6]

$$H_c=-\frac{8\pi}{3}\left(\frac{e\hbar}{2mc}\right)^2(\boldsymbol{\sigma}_I\cdot\boldsymbol{\sigma}_{II})\delta(r_{12}),\qquad (12)$$

does *not* appear.[10]

This "reduction" procedure leads to the term B'^2 in (10), or $H^{(7)}$ in (11), which Breit[2] has immediately given some arguments for discarding and which has later been shown by Bethe[9] to come from the second order perturbation when the Breit operator B is taken to be a perturbation. Even before the development of the field theory, Breit[2] already cautioned against treating (1) as the exact Hamiltonian. In the later developments, it became clear that there is ground for treating separately the interactions between two electrons through the longitudinal fields which give rise to the Coulomb term e^2/r_{12}, and the interactions through the transverse fields of which the first term in the series in powers of $e^2/\hbar c=\alpha$ is the Breit operator B. In the field-theoretical form of the theory of Breit and of Møller, one does not regard H in (1) as the exact Hamiltonian, but treats B as a perturbation. In the following, we shall show that a simple calculation of the diagonal matrix element of B with respect to the 16-component wave function gives unambiguously H_c in the case of the ground state of two-electron atoms (for which $H^{(2)}$, $H^{(3b)}$, $H^{(5)}$ vanish).

III. CONTACT TERM IN THE THEORY OF BREIT AND MØLLER

Let us consider the case of two electrons in the central field of a charge Ze and let us assume that Z

---

and integrating the first term by parts, one obtains

$$\int\psi^*\left(\frac{p^2}{2mU}+\frac{1}{U^2}H^{(4)}\right)\psi d\tau=\frac{\hbar^2}{2m}\int\frac{1}{U}(\nabla\psi)^2d\tau.\qquad (E)$$

On expanding $1/U\cong 1-v$ and integrating the above integral by parts, one has

$$\frac{\hbar^2}{2m}\int'(1-v)(\nabla\psi)^2d\tau=\frac{\hbar^2}{2m}(\psi\nabla\psi)_S+\frac{1}{2m}\int'\psi p^2\psi d\tau-\frac{\hbar^2}{2m}(v\psi\nabla\psi)_S$$
$$-\frac{1}{2m}\int'v\psi p^2\psi d\tau-\frac{\hbar}{2mi}\int'\psi(\nabla v\cdot\mathbf{p}\psi)d\tau,$$

where the prime on the integrals indicate that a small spherical volume of radius R around each of the poles r_1, r_2, $r_{12}=0$ of U in (B) is to be excluded so that the expansion $1/U=1-v$ does not introduce any singularity at these points at which $1/U=0$. The two surface integrals denoted by the subscript S vanish in the limit $R\to 0$. One finally obtains for (E) the usual result

$$\int\psi^*\left[\frac{1}{2m}p^2+H^{(1)}+H^{(4)}\right]\psi d\tau$$
$$=\frac{1}{2m}\int\psi^*p^2\psi d\tau-\frac{1}{8m^3c^2}\int(p^2\psi^*)(p^2\psi)d\tau+\int\psi^*H^{(4)}\psi d\tau$$

in which the prime has been removed by allowing R to approach zero.

[10] In the second paper in reference 2, Breit employed a different procedure from the "reduction" procedure outlined in (8), (9), (10) and treated the operator B' as a perturbation in Eqs. (7). From (7) and the approximation

$$u=-\Pi_0^{-1}(\boldsymbol{\sigma}_I\cdot\boldsymbol{\Pi}_I)\Psi,\quad v=-\Pi_0^{-1}(\boldsymbol{\sigma}_{II}\cdot\boldsymbol{\Pi}_{II})\Psi,$$
$$\phi=\frac{1}{(2mc)^2}(\boldsymbol{\sigma}_I\cdot\boldsymbol{\Pi}_I)(\boldsymbol{\sigma}_{II}\cdot\boldsymbol{\Pi}_{II})\Psi,\qquad (F)$$

the perturbation energy due to B' comes out to be

$$-\frac{1}{4m^2c^2}\int\{[(\boldsymbol{\sigma}_I\cdot\boldsymbol{\Pi}_I)\Psi]^\dagger B'(\boldsymbol{\sigma}_{II}\cdot\boldsymbol{\Pi}_{II})+[(\boldsymbol{\sigma}_{II}\cdot\boldsymbol{\Pi}_{II})\Psi]^\dagger B'(\boldsymbol{\sigma}_I\cdot\boldsymbol{\Pi}_I)$$
$$+\Psi^\dagger B'(\boldsymbol{\sigma}_I\cdot\boldsymbol{\Pi}_I)(\boldsymbol{\sigma}_{II}\cdot\boldsymbol{\Pi}_{II})+[(\boldsymbol{\sigma}_I\cdot\boldsymbol{\Pi}_I)(\boldsymbol{\sigma}_{II}\cdot\boldsymbol{\Pi}_{II})\Psi]^\dagger B'\}\Psi d\tau.\qquad (G)$$

A correct evaluation of the last term by Sucher and Foley[4] yields the contact term (12).

The procedure employed in the foregoing in arriving at (G), while in agreement with the field-theoretical point of view in treating the Breit operator B' as a perturbation, seems to have involved the multiplication of (7a), (7b), (7c), (7d) by $\phi^\dagger$, $u^\dagger$, $v^\dagger$, $\phi^\dagger$, respectively, the use of (F), and the addition of the four resulting equations. On writing out these four equations separately before them, one finds

$$\Psi^\dagger\left[\frac{\Pi_0}{2mc}-1-\frac{1}{2mc}\{(\boldsymbol{\sigma}_I\cdot\boldsymbol{\Pi}_I)\Pi_0^{-1}(\boldsymbol{\sigma}_I\cdot\boldsymbol{\Pi}_I)\right.$$
$$+(\boldsymbol{\sigma}_{II}\cdot\boldsymbol{\Pi}_{II})\Pi_0^{-1}(\boldsymbol{\sigma}_{II}\cdot\boldsymbol{\Pi}_{II})\}$$
$$\left.+\frac{B'}{8m^3c^4}(\boldsymbol{\sigma}_I\cdot\boldsymbol{\Pi}_I)(\boldsymbol{\sigma}_{II}\cdot\boldsymbol{\Pi}_{II})\right]\Psi=0,\quad (Ha)$$

$$-[\Pi_0^{-1}(\boldsymbol{\sigma}_I\cdot\boldsymbol{\Pi}_I)\Psi]^\dagger\left[\frac{1}{(2mc)^2}(\boldsymbol{\sigma}_I\cdot\boldsymbol{\Pi}_I)(\boldsymbol{\sigma}_{II}\cdot\boldsymbol{\Pi}_{II})^2\right.$$
$$\left.-\frac{1}{2mc^2}B'\Pi_0^{-1}(\boldsymbol{\sigma}_{II}\cdot\boldsymbol{\Pi}_{II})\right]\Psi=0,\quad (Hb)$$

$$-[\Pi_0^{-1}(\boldsymbol{\sigma}_{II}\cdot\boldsymbol{\Pi}_{II})\Psi]^\dagger\left[\frac{1}{(2mc)^2}(\boldsymbol{\sigma}_I\cdot\boldsymbol{\Pi}_I)^2(\boldsymbol{\sigma}_{II}\cdot\boldsymbol{\Pi}_{II})\right.$$
$$\left.-\frac{1}{2mc^2}B'\Pi_0^{-1}(\boldsymbol{\sigma}_I\cdot\boldsymbol{\Pi}_I)\right]\Psi=0,\quad (Hc)$$

$$[(\boldsymbol{\sigma}_I\cdot\boldsymbol{\Pi}_I)(\boldsymbol{\sigma}_{II}\cdot\boldsymbol{\Pi}_{II})\Psi]^\dagger\frac{B'}{8m^3c^4}\Psi=0.\quad (Hd)$$

While adding these equations leads to

$$\Psi^\dagger\left[\frac{\Pi_0}{2mc}-1-\frac{1}{2mc}\{(\boldsymbol{\sigma}_I\cdot\boldsymbol{\Pi}_I)\Pi_0^{-1}(\boldsymbol{\sigma}_I\cdot\boldsymbol{\Pi}_I)\right.$$
$$\left.+(\boldsymbol{\sigma}_{II}\cdot\boldsymbol{\Pi}_{II})\Pi_0^{-1}(\boldsymbol{\sigma}_{II}\cdot\boldsymbol{\Pi}_{II})\}-\frac{1}{8m^3c^4}(\boldsymbol{\sigma}_I\cdot\boldsymbol{\Pi}_I)^2(\boldsymbol{\sigma}_{II}\cdot\boldsymbol{\Pi}_{II})^2\right]\Psi$$
$$+\frac{1}{8m^3c^4}\{[(\boldsymbol{\sigma}_I\cdot\boldsymbol{\Pi}_I)\Psi]^\dagger B'(\boldsymbol{\sigma}_{II}\cdot\boldsymbol{\Pi}_{II})+[(\boldsymbol{\sigma}_{II}\cdot\boldsymbol{\Pi}_{II})\Psi]^\dagger B'(\boldsymbol{\sigma}_I\cdot\boldsymbol{\Pi}_I)$$
$$+\Psi^\dagger B'(\boldsymbol{\sigma}_I\cdot\boldsymbol{\Pi}_I)(\boldsymbol{\sigma}_{II}\cdot\boldsymbol{\Pi}_{II})+[(\boldsymbol{\sigma}_I\cdot\boldsymbol{\Pi}_I)(\boldsymbol{\sigma}_{II}\cdot\boldsymbol{\Pi}_{II})\Psi]^\dagger B'\}\Psi=0,\ (I)$$

adding and hence to (G) with the contact term, the four equations (H) are obviously incorrect. There is thus an ambiguity in the result depending on whether one first adds up the four equations $\Psi^\dagger\times(7a)$, $u^\dagger\times(7b)$, etc., and then puts in (F), or whether one first uses (F) as above to get the equations (H) and then adds them. That the equations (H) are incorrect arises from the fact that the approximation (F) does not satisfy Eqs. (7) up to $(v/c)^4$ [the lowest order term being $(v/c)^3$ in (7a)].

is large so that the electron-electron interactions, up to α^2,

$$\frac{e^2}{r_{12}}-\frac{e^2}{2r_{12}}\left\{(\boldsymbol{\alpha}_{\mathrm{I}}\cdot\boldsymbol{\alpha}_{\mathrm{II}})+\frac{1}{r_{12}^2}(\boldsymbol{\alpha}_{\mathrm{I}}\cdot\mathbf{r}_{12})(\boldsymbol{\alpha}_{\mathrm{II}}\cdot\mathbf{r}_{12})\right\}, \quad (13)$$

are small compared with the electron-nucleus interactions. In this case one may calculate the interaction energy between the electrons through their fields by calculating the diagonal matrix element of (13) with respect to the 16-component wave function of the two hydrogenic electrons. The work of Breit,[3] Møller[7] and Bethe and Fermi[11] shows that taking the diagonal matrix element of (13) is equivalent to calculating the integral

$$\int\int\frac{1}{r_{12}}\exp\left(\frac{2\pi i\nu_{if}r_{12}}{c}\right)\times[\rho(1)\rho'(2)-\mathbf{j}(1)\cdot\mathbf{j}'(2)]d\tau_1 d\tau_2. \quad (14)$$

For the ground state of He-like atoms,

$$\nu_{if}=0.$$

To take account of the Pauli principle, one has

$$\rho(1)\rho'(2)=\frac{e^2}{2}\begin{vmatrix}\psi_{\frac{1}{2}}^{\dagger}(1) & \psi_{-\frac{1}{2}}^{\dagger}(1)\\ \psi_{\frac{1}{2}}^{\dagger}(2) & \psi_{-\frac{1}{2}}^{\dagger}(2)\end{vmatrix}\begin{vmatrix}\psi_{\frac{1}{2}}(1) & \psi_{\frac{1}{2}}(2)\\ \psi_{-\frac{1}{2}}(1) & \psi_{-\frac{1}{2}}(2)\end{vmatrix}$$

$$=\tfrac{1}{2}[\rho_{\frac{1}{2}\frac{1}{2}}(1)\rho_{-\frac{1}{2}-\frac{1}{2}}(2)+\rho_{-\frac{1}{2}-\frac{1}{2}}(1)\rho_{\frac{1}{2}\frac{1}{2}}(2)-\rho_{\frac{1}{2}-\frac{1}{2}}(1)\rho_{-\frac{1}{2}\frac{1}{2}}(2)-\rho_{-\frac{1}{2}\frac{1}{2}}(1)\rho_{\frac{1}{2}-\frac{1}{2}}(2)],$$

$$\rho_{\frac{1}{2}-\frac{1}{2}}(1)=-e\psi_{\frac{1}{2}}^{\dagger}(1)\psi_{-\frac{1}{2}}(1), \quad \text{etc.},$$

$\psi_{\frac{1}{2}}$ being a four-component column matrix corresponding to $M=\frac{1}{2}$, $\psi_{\frac{1}{2}}^{\dagger}$ a row matrix, etc. Similarly,

$$\mathbf{j}(1)\cdot\mathbf{j}'(2)=\tfrac{1}{2}[\mathbf{j}_{\frac{1}{2}\frac{1}{2}}(1)\cdot\mathbf{j}_{-\frac{1}{2}-\frac{1}{2}}(2)+\mathbf{j}_{-\frac{1}{2}-\frac{1}{2}}(1)\cdot\mathbf{j}_{\frac{1}{2}\frac{1}{2}}(2)-\mathbf{j}_{\frac{1}{2}-\frac{1}{2}}(1)\cdot\mathbf{j}_{-\frac{1}{2}\frac{1}{2}}(2)-\mathbf{j}_{-\frac{1}{2}\frac{1}{2}}(1)\cdot\mathbf{j}_{\frac{1}{2}-\frac{1}{2}}(2)],$$

where

$$\mathbf{j}_{\frac{1}{2}-\frac{1}{2}}(1)=e\psi_{\frac{1}{2}}^{\dagger}\boldsymbol{\alpha}_1\psi_{-\frac{1}{2}}, \quad \text{etc.}$$

For the hydrogenic electron, we have[12]

$$M=\tfrac{1}{2}, \qquad \psi_{\frac{1}{2}}^{\dagger}=N(if\cos\vartheta,\ if\sin\vartheta e^{-i\varphi},\ g,\ 0),$$

$$M=-\tfrac{1}{2}, \quad \psi_{-\frac{1}{2}}^{\dagger}=N(-if\sin\vartheta e^{i\varphi},\ if\cos\vartheta,\ 0,\ -g),$$

$$g=e^{-Zr/a_0\gamma}r^{\gamma},\ \gamma=[1-(Z\alpha)^2]^{\frac{1}{2}}-1, \quad (15)$$

$$f=\frac{Z\alpha}{1+[1-(Z\alpha)^2]^{\frac{1}{2}}}g,\ \cdot\ \alpha=\frac{e^2}{\hbar c},$$

so that

$$(\rho\rho'-\mathbf{j}\cdot\mathbf{j}')=N^4e^2\{[f^2(1)+g^2(1)][f^2(2)+g^2(2)]+8f(1)g(1)f(2)g(2)\cos\vartheta_{12}\}. \quad (16)$$

Evaluation of (14) leads to

$$\int\int\frac{1}{r_{12}}\rho\rho'd\tau_1 d\tau_2=\frac{5}{4}Z+0.46Z^3\alpha^2 \quad \text{in Rydberg units,} \quad (17)$$

$$-\int\int\frac{1}{r_{12}}\mathbf{j}\cdot\mathbf{j}'d\tau_1 d\tau_2=\frac{1}{2}Z^3\alpha^2 \quad \text{in Rydberg units.} \quad (18)$$

The matrix element (18) of the Breit operator B is to be compared with the terms $H^{(2)}$, $H^{(3b)}$, $H^{(5)}$ in (11) that arise from the operator B. The matrix elements of $H^{(2)}$, $H^{(3b)}$, $H^{(5)}$ with respect to hydrogenic wave functions are all zero for the ground state of He-like atoms, but the matrix element of the contact interaction H_c in the same approximation is exactly $\frac{1}{2}Z^3\alpha^2$ Rydberg. Thus the matrix element of B with respect to the 16-component wave function *does* lead to the contact term H_c for the relativistic energy of the ground state of two-electron atoms. It is, however, not yet clear why H_c does not appear if one follows the "reduction" procedure, as shown in Sec. II. This might again be traced to a cause related to that mentioned at the end of Sec. II.

Expressions (17) and (18) give the energy from the electron-electron interaction (13); the total relativistic energy of the two-electron atom of course is the sum of (17), (18), and the relativistic energy of the two hydrogenic electrons containing the Sommerfeld, the spin-orbit and the S-state corrections for the two electrons. The first term in (17) is the nonrelativistic energy arising from e^2/r_{12}. The second term, which in this approximation of unscreened relativistic hydrogenic wave function is $0.46Z^3\alpha^2$ Rydberg, has no corresponding term in (10)–(12). It arises from the singular behavior of the wave function (15) at the origin, and is the consequence of treating (13) by the perturbation procedure. A rigorous treatment of the relativistic system

$$\left[H_0(1)+H_0(2)+\frac{e^2}{r_{12}}\right]\psi=E\psi \quad (19)$$

is not known; but on plausible considerations, the effect of the singular behavior of the relativistic wave function in (19) at the origin can be expected to contribute a correction of the order α^4, and must be treated together with the higher order interactions in the field theory.

The authors wish to thank Dr. H. M. Foley and Dr. G. Breit for helpful discussions.

[11] H. A. Bethe and E. Fermi, Z. Physik **77**, 296 (1932).
[12] C. G. Darwin, Proc. Roy. Soc. (London) **A118**, 654 (1928).

Tensor Scattering Matrix for the Electromagnetic Field*

DAVID S. SAXON
University of California, Los Angeles, California
(Received August 8, 1955)

The scattering of an arbitrary incoming electromagnetic wave by an unrestricted scattering object is described in terms of a tensor scattering matrix. General reciprocity relations and the cross-section theorem, including an interesting extension, are established using this representation. The results are related to the special case of plane-wave scattering and the scattering matrix is explicitly exhibited in terms of the plane-wave scattering amplitude for two mutually perpendicular directions of polarization.

GENERAL FORMULATION

IN the following note, we delineate those general features of the scattering of electromagnetic waves which are consequences of the asymptotic properties of Maxwell's equations but are independent of the nature of the scatterer.[1] For this purpose, it is convenient to describe the scattering by introducing a tensor scattering matrix. Using this representation, reciprocity and the cross-section theorem, including an interesting extension, are easily established as we now proceed to show.[2]

Outside the scattering region, and in particular as $r\to\infty$, the fields satisfy the free-space Maxwell's equations, which we write (in Gaussian units) in the form

$$\nabla\times\mathbf{E}=ik\mathbf{H},\quad \nabla\times\mathbf{H}=-ik\mathbf{E}, \tag{1}$$

where we have assumed harmonic time dependence $e^{-i\omega t}$ and where k is the free-space wave number. We now decompose the asymptotic field $\mathbf{E}(\mathbf{n}r)$, $r\to\infty$ into incoming and outgoing waves along $\mathbf{n}$; that is, we write

$$\mathbf{E}(\mathbf{n}r)=\mathbf{F}_1(\mathbf{n})\frac{e^{-ikr}}{r}+\mathbf{F}_2(\mathbf{n})\frac{e^{ikr}}{r}, \tag{2}$$

where, as a consequence of the divergence condition,

$$\mathbf{F}_1(\mathbf{n})\cdot\mathbf{n}=\mathbf{F}_2(\mathbf{n})\cdot\mathbf{n}=0. \tag{3}$$

In the above and throughout, we neglect terms of higher order than the first in reciprocal powers of r; we deal only with pure radiation fields.

As a consequence of the linearity of Maxwell's equations, the outgoing fields must be linearly related to the incoming fields which we assume to be arbitrary. Thus, we introduce a linear connective $\mathcal{S}(\mathbf{n},\mathbf{n}')$, called the tensor scattering matrix, by writing

$$\mathbf{F}_2(\mathbf{n})=-\int d\Omega'\,\mathcal{S}(\mathbf{n},\mathbf{n}')\cdot\mathbf{F}_1(-\mathbf{n}'), \tag{4}$$

where the choice of signs is such that $\mathcal{S}$ reduces to the unit operator when there is no scattering. As a consequence of Eq. (3)

$$\mathbf{n}\cdot\mathcal{S}(\mathbf{n},\mathbf{n}')=\mathcal{S}(\mathbf{n},\mathbf{n}')\cdot\mathbf{n}'=0 \tag{5}$$

so that $\mathcal{S}$ has only four independent components.[3]

We first establish reciprocity relations for the electromagnetic field starting from the fact that if $\mathbf{E}$ and $\mathbf{E}'$ are any two solutions of the source-free Maxwell's equations (but with the same harmonic time-dependence), then

$$\int_{r\to\infty}d\Omega r^2\mathbf{n}\cdot\{\mathbf{E}'(\mathbf{n}r)\times[\nabla\times\mathbf{E}(\mathbf{n}r)]-\mathbf{E}(\mathbf{n}r)\times[\nabla\times\mathbf{E}'(\mathbf{n}r)]\}=0, \tag{6}$$

provided that the dielectric, permeability, and conductivity tensors are symmetric. The proof of this relation is straightforward. Under the stated conditions it is easily established from Maxwell's equations that $\nabla\cdot(\mathbf{E}'\times\mathbf{H}-\mathbf{E}\times\mathbf{H}')$ vanishes identically. Integration over all space, followed by an application of Gauss's theorem, then yields Eq. (6) for there are no sources except at infinity and asymptotically the fields satisfy Eq. (1). (It is of interest to remark that the symmetry of the constitutive tensors seems to be a necessary condition for reciprocity.)

Decomposing $\mathbf{E}'$ as well as $\mathbf{E}$ in Eq. (6) into incoming and outgoing waves along $\mathbf{n}$, we obtain the following after some algebra:

$$\int d\Omega[\mathbf{F}_1'(\mathbf{n})\cdot\mathbf{F}_2(\mathbf{n})-\mathbf{F}_1(\mathbf{n})\cdot\mathbf{F}_2'(\mathbf{n})]=0,$$

where the prime denotes the amplitudes associated with $\mathbf{E}'$. Expressing the outgoing fields in terms of the

* This work was supported in part by the Geophysics Research Directorate of the Air Force Cambridge Research Center. Some of the results were presented at the URSI symposium on Electromagnetic Wave Theory, University of Michigan, 1955 (unpublished), and a more detailed discussion of some aspects is given in "Lectures on the Scattering of Light" by D. S. Saxon (notes by R. S. Fraser), University of California at Los Angeles, Department of Meteorology, Scientific Report No. 9, May, 1955 (unpublished).

[1] We assume, however, that the scattering region consists of a linear medium which contains no sources and does not extend to infinity. We do not assume that the scatterer is homogeneous or isotropic or lossless.

[2] See E. Gerjuoy and D. S. Saxon, Phys. Rev. **94**, 1445 (1954), for a similar discussion of scattering without absorption for scalar fields. In the present paper, the development is generalized to the vector field, including absorption.

[3] Since $\mathbf{F}_1$ is transverse, strictly speaking $\mathcal{S}(\mathbf{n},\mathbf{n}')\cdot\mathbf{n}'$ is undefined according to Eq. (4). However, we complete the definition by taking it to be zero.

incoming by Eq. (4), we then have

$$\int d\Omega \int d\Omega' [\mathbf{F}_1'(\mathbf{n}) \cdot \mathcal{S}(\mathbf{n},\mathbf{n}') \cdot \mathbf{F}_1(-\mathbf{n}') - \mathbf{F}_1(\mathbf{n}) \cdot \mathcal{S}(\mathbf{n},\mathbf{n}') \cdot \mathbf{F}_1'(-\mathbf{n}')] = 0.$$

Replacing $\mathbf{n}$ by $-\mathbf{n}'$ and $\mathbf{n}'$ by $-\mathbf{n}$ in the last term and transposing the product, this becomes

$$\int d\Omega \int d\Omega' \{\mathbf{F}_1'(\mathbf{n}) \cdot [\mathcal{S}(\mathbf{n},\mathbf{n}') - \mathcal{S}^T(-\mathbf{n}', -\mathbf{n})] \cdot \mathbf{F}_1(-\mathbf{n}')\} = 0,$$

where the superscript T signifies the transposed tensor:

$$(\mathcal{S}^T)_{ij} = \mathcal{S}_{ji}.$$

Since $\mathbf{F}_1$ and $\mathbf{F}_1'$ are arbitrary, we thus have

$$\mathcal{S}(\mathbf{n},\mathbf{n}') = \mathcal{S}^T(-\mathbf{n}', -\mathbf{n}), \tag{7}$$

and this is the reciprocity condition in its general form. Later we exhibit it in more familiar form when we apply our results to plane wave scattering.

Next consider the energy relations which hold for the field. The time-average energy flux inward through the sphere at infinity must of course be equal to the average power P absorbed by the scatterer, and hence

$$-\frac{c}{8\pi} \operatorname{Re}\left[\int_{r\to\infty} (\mathbf{E}\times\mathbf{H}^*) \cdot \mathbf{n} r^2 d\Omega\right] = P.$$

Expressing $\mathbf{H}$ in terms of $\mathbf{E}$ by the first Maxwell equation, we then find using Eq. (2) and Eq. (3)

$$\frac{c}{8\pi} \int [\mathbf{F}_2^*(\mathbf{n}) \cdot \mathbf{F}_2(\mathbf{n}) - \mathbf{F}_1^*(\mathbf{n}) \cdot \mathbf{F}_1(\mathbf{n})] d\Omega + P = 0.$$

Upon substitution of Eq. (4), we obtain, after appropriate transpositions and relabeling of the integration variables,

$$\frac{c}{8\pi} \int d\Omega' \mathbf{F}_1^*(-\mathbf{n}') \cdot \left[\int \mathcal{Q}(\mathbf{n}',\mathbf{n}'') \cdot \mathbf{F}_1(-\mathbf{n}'') d\Omega'' - \mathbf{F}_1(-\mathbf{n}')\right] + P = 0, \tag{8}$$

where

$$\mathcal{Q}(\mathbf{n}',\mathbf{n}'') = \int d\Omega \mathcal{S}^{*T}(\mathbf{n},\mathbf{n}') \cdot \mathcal{S}(\mathbf{n},\mathbf{n}''). \tag{9}$$

From Eq. (8) we see that the energy loss is determined in terms of the incoming field alone and can itself be characterized by a tensor $\mathcal{K}(\mathbf{n}',\mathbf{n}'')$ defined by the relation

$$P \equiv \frac{c}{8\pi} \int \int d\Omega d\Omega' \mathbf{F}_1^*(-\mathbf{n}') \cdot \mathcal{K}(\mathbf{n}',\mathbf{n}'') \cdot \mathbf{F}_1(-\mathbf{n}''). \tag{10}$$

Actually, only the transverse parts of $\mathcal{K}$ are defined by this relation, and we complete the definition by the additional conditions:

$$\mathbf{n}' \cdot \mathcal{K}(\mathbf{n}',\mathbf{n}'') = \mathcal{K}(\mathbf{n}',\mathbf{n}'') \cdot \mathbf{n}'' = 0. \tag{11}$$

From the fact that P is real, it follows at once from Eq. (10) that $\mathcal{K}$ is Hermitian, $\mathcal{K}^{*T}(\mathbf{n}'',\mathbf{n}') = \mathcal{K}(\mathbf{n}',\mathbf{n}'')$. If we regard $\mathcal{K}$ as a continuous supermatrix, this can be written in matrix notation as $\mathcal{K}^\dagger = \mathcal{K}$, where the adjoint symbol means to take the complex conjugate and to transpose all indices, continuous and discrete.

Equation (8) can now be rewritten in the form

$$\int \int d\Omega' d\Omega'' \mathbf{F}_1^*(-\mathbf{n}') \cdot [\mathcal{Q}(\mathbf{n}',\mathbf{n}'') - \epsilon\delta(\mathbf{n}'-\mathbf{n}'') + \mathcal{K}(\mathbf{n}',\mathbf{n}'')] \cdot \mathbf{F}_1(-\mathbf{n}'') = 0.$$

Now $\mathbf{F}_1$ is arbitrary, except that it must remain transverse, and hence we infer that the transverse part of the bracketed expression vanishes. Of course $\mathcal{Q}$ and $\mathcal{K}$ are already transverse and we need only extract the transverse part of the unit tensor. Denoting this by $\epsilon_T(\mathbf{n})$, we evidently have

$$\epsilon_T(\mathbf{n}) = \epsilon - \mathbf{nn}, \tag{12}$$

since $\mathbf{n} \cdot \epsilon_T(\mathbf{n}) = \epsilon_T(\mathbf{n}) \cdot \mathbf{n} = 0$. On the other hand, if $\mathbf{B}$ is any vector perpendicular to $\mathbf{n}$, then $\mathbf{B} \cdot \epsilon_T(\mathbf{n}) = \epsilon_T(\mathbf{n}) \cdot \mathbf{B} = \mathbf{B}$ so that ϵ_T maintains its character as a unit tensor with respect to such vectors. In any case, using Eq. (9), we have

$$\int d\Omega \mathcal{S}^{*T}(\mathbf{n},\mathbf{n}') \cdot \mathcal{S}(\mathbf{n},\mathbf{n}'') = \epsilon_T(\mathbf{n}')\delta(\mathbf{n}'-\mathbf{n}'') - \mathcal{K}(\mathbf{n}',\mathbf{n}''). \tag{13}$$

Finally, introducing the reciprocity relation in this last result, we find after a little manipulation

$$\int d\Omega \mathcal{S}(\mathbf{n}',\mathbf{n}) \cdot \mathcal{S}^{*T}(\mathbf{n}'',\mathbf{n}) = \epsilon_T(\mathbf{n}')\delta(\mathbf{n}'-\mathbf{n}'') - \mathcal{K}'(\mathbf{n}',\mathbf{n}''), \tag{14}$$

where $\mathcal{K}'(\mathbf{n}',\mathbf{n}'') = \mathcal{K}^*(-\mathbf{n}', -\mathbf{n}'') = \mathcal{K}^T(-\mathbf{n}', -\mathbf{n}'')$. In matrix notation, these relations have the form

$$\mathcal{S}^\dagger \mathcal{S} = 1 - \mathcal{K}, \quad \mathcal{S}\mathcal{S}^\dagger = 1 - \mathcal{K}'$$

and $\mathcal{S}$ is seen to be properly unitary in the lossless case when $\mathcal{K}$ and $\mathcal{K}'$ are zero.

APPLICATION TO PLANE WAVE SCATTERING

We now specialize to the case in which a plane wave is incident along the direction $\mathbf{n}_0$, so that the field at large distances from the scattering region has the form

$$E(\underset{r\to\infty}{\mathbf{n}r}) = \mathbf{q}e^{ikr\mathbf{n}_0\cdot\mathbf{n}} + \mathbf{A}_\mathbf{q}(\mathbf{n},\mathbf{n}_0)\frac{e^{ikr}}{r}. \tag{15}$$

Here $\mathbf{q}$ is a unit vector in the direction of polarization of the incident wave and $\mathbf{A}_\mathbf{q}(\mathbf{n},\mathbf{n}_0)$ is the amplitude of

the wave scattered in the direction $\mathbf{n}$, the notation serving to indicate explicitly the direction of the incident wave and its polarization as well as the direction of the scattered wave. Of course $\mathbf{q}\cdot\mathbf{n}_0$ and $\mathbf{n}\cdot\mathbf{A}_q(\mathbf{n},\mathbf{n}_0)$ are both zero. The decomposition of this field into its incoming and outgoing parts leads in a straightforward way[3] to the result

$$\mathbf{E}(\underset{r\to\infty}{\mathbf{n}r})=\frac{2\pi i}{k}\mathbf{q}\delta(\mathbf{n}_0+\mathbf{n})\frac{e^{-ikr}}{r}+\left[\mathbf{A}_q(\mathbf{n},\mathbf{n}_0)-\frac{2\pi i}{k}\mathbf{q}\delta(\mathbf{n}_0-\mathbf{n})\right]\frac{e^{ikr}}{r}. \quad (16)$$

Hence, regarding this as a special form of Eq. (12), we have at once from the definition of the scattering matrix,

$$\mathbf{A}_q(\mathbf{n},\mathbf{n}_0)=\frac{2\pi i}{k}\delta(\mathbf{n}_0-\mathbf{n})\mathbf{q}-\frac{2\pi i}{k}\mathcal{S}(\mathbf{n},\mathbf{n}_0)\cdot\mathbf{q}. \quad (17)$$

Equivalently, we can write

$$\mathbf{A}_q(\mathbf{n},\mathbf{n}_0)=\mathcal{A}(\mathbf{n},\mathbf{n}_0)\cdot\mathbf{q}, \quad (18)$$

where $\mathcal{A}(\mathbf{n},\mathbf{n}_0)$, which we shall call the tensor scattering amplitude,[4] is given by

$$\mathcal{A}(\mathbf{n},\mathbf{n}_0)=\frac{2\pi i}{k}[\epsilon_T(\mathbf{n}_0)\delta(\mathbf{n}_0-\mathbf{n})-\mathcal{S}(\mathbf{n},\mathbf{n}_0)]. \quad (19)$$

Regarding (18) as the definition of $\mathcal{A}$, and supposing that $\mathbf{q}_1$ and $\mathbf{q}_2$ are two mutually perpendicular polarization directions and $\mathbf{A}_{q_1}$ and $\mathbf{A}_{q_2}$ are the corresponding scattering amplitudes, we have simply

$$\mathcal{A}(\mathbf{n},\mathbf{n}_0)=\mathbf{A}_{q_1}(\mathbf{n},\mathbf{n}_0)\mathbf{q}_1+\mathbf{A}_{q_2}(\mathbf{n},\mathbf{n}_0)\mathbf{q}_2. \quad (20)$$

Accordingly, by (19),

$$\mathcal{S}(\mathbf{n},\mathbf{n}_0)=\epsilon_T(\mathbf{n}_0)\delta(\mathbf{n}_0-\mathbf{n})-\frac{k}{2\pi i}\mathcal{A}(\mathbf{n},\mathbf{n}_0)$$

$$=\epsilon_T(\mathbf{n}_0)\delta(\mathbf{n}_0-\mathbf{n})-\frac{k}{2\pi i}[\mathbf{A}_{q_1}(\mathbf{n},\mathbf{n}_0)\mathbf{q}_1+\mathbf{A}_{q_2}(\mathbf{n},\mathbf{n}_0)\mathbf{q}_2], \quad (21)$$

which is thus an explicit construction of $\mathcal{S}$ in terms of the plane wave scattering amplitude for two mutually perpendicular direction of polarization.

We are more interested however in examining the properties of $\mathcal{A}$ corresponding to the previously derived general features of $\mathcal{S}$. Thus the reciprocity relation Eq. (7) yields at once, with the aid of the first form of Eq. (21)

$$\mathcal{A}(\mathbf{n},\mathbf{n}_0)=\mathcal{A}^T(-\mathbf{n}_0,-\mathbf{n}), \quad (22)$$

or equivalently, using Eq. (18)

$$\mathbf{q}'\cdot\mathbf{A}_q(\mathbf{n},\mathbf{n}_0)=\mathbf{q}\cdot\mathbf{A}_{q'}(-\mathbf{n}_0,-\mathbf{n}). \quad (23)$$

For the special case in which $\mathbf{q}=\mathbf{q}'$, this last relation states that if we interchange the direction of the incident wave and the direction of observation, the component of the scattered wave in the direction of polarization is unchanged; and this is the more customary (and more restricted) statement of reciprocity.

Next we examine the consequences of energy conservation as expressed by Eq. (13). Upon substitution of the first form of Eq. (21), we obtain

$$\int d\Omega\left[\epsilon_T(\mathbf{n}_0)\delta(\mathbf{n}_0-\mathbf{n})+\frac{k}{2\pi i}\mathcal{A}^{T*}(\mathbf{n},\mathbf{n}_0)\right]\cdot\left[\epsilon_T(\mathbf{n}_0')\delta(\mathbf{n}_0'-\mathbf{n})-\frac{k}{2\pi i}\mathcal{A}(\mathbf{n},\mathbf{n}_0')\right]=\epsilon_T(\mathbf{n}_0')\delta(\mathbf{n}_0'-\mathbf{n}_0'')-\mathcal{K}(\mathbf{n}_0',\mathbf{n}_0''). \quad (24)$$

Noting that $\epsilon_T(\mathbf{n}_0)\cdot\mathcal{A}(\mathbf{n}_0,\mathbf{n}_0')=\mathcal{A}(\mathbf{n}_0,\mathbf{n}_0')$, since $\mathcal{A}$ is transverse, we then find, after the δ function terms are integrated,

$$\int\mathcal{A}^{T*}(\mathbf{n},\mathbf{n}_0)\cdot\mathcal{A}(\mathbf{n},\mathbf{n}_0')d\Omega+\frac{4\pi^2}{k^2}\mathcal{K}(\mathbf{n}_0,\mathbf{n}_0')=\frac{2\pi}{ik}[\mathcal{A}(\mathbf{n}_0,\mathbf{n}_0')-\mathcal{A}^{T*}(\mathbf{n}_0',\mathbf{n}_0)]; \quad (25)$$

and this is a rather interesting extension of the cross-section theorem. It reduces to its conventional form upon setting $\mathbf{n}_0'=\mathbf{n}_0$ and taking scalar products from left and right with $\mathbf{q}$, for we then have, using Eq. (18),

$$\int\mathbf{A}_q^*(\mathbf{n},\mathbf{n}_0)\cdot\mathbf{A}_q(\mathbf{n},\mathbf{n}_0)d\Omega+\frac{4\pi^2}{k^2}\mathbf{q}\cdot\mathcal{K}(\mathbf{n}_0,\mathbf{n}_0)\cdot\mathbf{q}=(4\pi/k)\,\mathrm{Im}[\mathbf{q}\cdot\mathbf{A}_q(\mathbf{n}_0,\mathbf{n}_0)]. \quad (26)$$

Now from Eq. (10), and recalling that $\mathbf{F}_1(\mathbf{n})=(2\pi i/k)\mathbf{q}\delta(\mathbf{n}_0+\mathbf{n})$ for a plane wave incident along $\mathbf{n}_0$, the rate of energy absorption P is

$$P=\frac{c}{8\pi}\cdot\frac{4\pi^2}{k^2}\mathbf{q}\cdot\mathcal{K}(\mathbf{n}_0,\mathbf{n}_0)\cdot\mathbf{q},$$

while the energy flux in the incident plane wave is $c/8\pi$. Hence the second term on the left of Eq. (26) is simply the absorption cross section σ_a while the first term is, of course, the total scattering cross section σ_s and thus, as expected,

$$\sigma_s+\sigma_a=(4\pi/k)\,\mathrm{Im}[\mathbf{q}\cdot\mathbf{A}_q(\mathbf{n}_0,\mathbf{n}_0)]. \quad (27)$$

It is worth emphasizing that this result, as well as the more general relation Eq. (25), both of which are statements of conservation of energy, involve inter-

[4] *Note added in proof.*—Morse and Feshbach, *Methods of Theoretical Physics* (McGraw-Hill Book Company, Inc., 1953). See pp. 1897–1898 where a tensor scattering amplitude is introduced to describe scattering from a sphere.

ference between the scattered and incident fields. To make this more explicit, recall that in our treatment the incident wave is represented by δ functions. Thus the left side of Eq. (24), representing the total outgoing energy, contains the scattered energy, the outgoing energy in the incident wave and interference terms between the scattered and incident fields. The right side represents the incoming energy (arising only from the incident wave, of course) from which is subtracted the energy absorbed in the scatterer. The purely incident wave terms cancel, as they must, and the scattered plus absorbed energy is accounted for by destructive interference between the incident wave and the forward scattered wave. This is the physical content of Eq. (27).

The structure of these relations perhaps becomes more transparent if we repeat our derivation using matrix notation. Thus, corresponding to Eq. (21) we have

$$\mathcal{S}=1-k\mathcal{A}/2\pi i,$$

and hence

$$\mathcal{S}^\dagger\mathcal{S}=1-k(\mathcal{A}-\mathcal{A}^\dagger)/2\pi i+k^2\mathcal{A}^\dagger\mathcal{A}/4\pi.$$

Recalling that from energy conservation $\mathcal{S}^\dagger\mathcal{S}=1-\mathcal{K}$, we thus obtain, corresponding to Eq. (25)

$$\mathcal{A}^\dagger\mathcal{A}+4\pi\mathcal{K}/k^2=2\pi(\mathcal{A}-\mathcal{A}^\dagger)/ik. \tag{28}$$

The diagonal elements of this result give directly the cross-section theorem (for specific directions of incidence and polarization), the usefulness of which is so well known. However, perhaps because of their complexity, little consideration appears to have been given to the off-diagonal elements.[5] It is our belief, as we now attempt to demonstrate, that extension of the cross-section theorem to off-diagonal elements also has its utility.

One obvious application is simply as an algebraic check on specific calculations of scattering amplitudes. As an example of the kind of relations which can be derived, consider a lossless scatterer, $\mathcal{K}=0$, which is axially symmetric and has a symmetry plane perpendicular to its symmetry axis; e.g., a spheroid or a dumbell shaped scatterer. Consider now plane waves incident along the axis of symmetry in both directions; i.e., in Eq. (25) take $\mathbf{n}_0$ along the axis of symmetry and take $\mathbf{n}_0'=-\mathbf{n}_0$. Further, let each incident wave have the same polarization $\mathbf{q}$. Using Eq. (18), we then obtain

$$\int \mathbf{A}_q^*(\mathbf{n},\mathbf{n}_0)\cdot\mathbf{A}_q(\mathbf{n},-\mathbf{n}_0)d\Omega = \frac{2\pi}{ik}\mathbf{q}\cdot[\mathbf{A}_q(\mathbf{n}_0,-\mathbf{n}_0)-\mathbf{A}_q^*(-\mathbf{n}_0,\mathbf{n}_0)].$$

Because of the symmetry, $\mathbf{A}_q(\mathbf{n},-\mathbf{n}_0)=\mathbf{A}_q(-\mathbf{n},\mathbf{n}_0)$ while the two backward waves are equal and have the same polarization as the incident waves and can thus be written as $\mathbf{q}A_b$. Referring $\mathbf{n}$ to $\mathbf{n}_0$ as polar axis, we thus obtain the simple result

$$\int \mathbf{A}_q^*(\theta,\varphi)\cdot\mathbf{A}_q(\pi-\theta,\pi+\varphi)d\Omega=\frac{4\pi}{k}\,\mathrm{Im}[A_b].$$

This relation is easily verified for a spherically symmetric scatterer directly from the (vector) spherical harmonic expansions. Evidently similar but more complicated relations can be derived for other symmetries.

Finally we mention a rather different kind of application in which one uses off-diagonal elements to learn something about the large-angle scattering. For this purpose, consider a lossless, rather soft, spherically symmetrical scatterer in the short-wave limit. Here, the scattering is predominantly in the forward direction and the integral in Eq. (25) can be approximately evaluated as follows. Assuming the effective radius of the scatterer to be a, the angular width $\delta\theta$ of the main diffraction peak is roughly $(1/ka)$ and the main contributions to the integral evidently occur when $\mathbf{n}$ is near $\mathbf{n}_0$ and when it is near $\mathbf{n}_0'$, i.e., when one of the factors in the integrand is the forward scattering amplitude. For simplicity, let us take both incident waves to have the same polarization $\mathbf{q}$ (which means that we restrict our attention to the situation in which $\mathbf{n}$ and $\mathbf{n}_0$ lie in the plane perpendicular to $\mathbf{q}$) and let us assume that the large-angle scattering amplitude does not fluctuate violently over $\delta\theta$. We then obtain,

$$\frac{\pi}{(ka)^2}\{\mathbf{A}_q^*(\mathbf{n}_0,\mathbf{n}_0)\cdot\mathbf{A}_q(\mathbf{n}_0,\mathbf{n}_0')+\mathbf{A}_q^*(\mathbf{n}_0,\mathbf{n}_0')\cdot\mathbf{A}_q(\mathbf{n}_0',\mathbf{n}_0')\} \simeq\frac{2\pi}{ik}\mathbf{q}\cdot[\mathbf{A}_q(\mathbf{n}_0,\mathbf{n}_0')-\mathbf{A}_q^*(\mathbf{n}_0',\mathbf{n}_0)].$$

Using the obvious relations between the scattering amplitudes which follow from the spherical symmetry, this can be reduced to the relation

$$\sin\gamma\simeq\frac{1}{2ka^2}|A_f|\cos(\gamma_0-\gamma), \tag{29}$$

where we have written

$$\mathbf{A}_q(\mathbf{n}_0,\mathbf{n}_0)=\mathbf{q}|A_f|e^{i\gamma_0},$$

and

$$\mathbf{q}\cdot\mathbf{A}_q(\mathbf{n}_0,\mathbf{n}_0')=|\mathbf{q}\cdot\mathbf{A}|e^{i\gamma},$$

so that γ is the phase angle of the component of the complex scattering amplitude along $\mathbf{q}$ and γ_0 denotes this phase angle for forward scattering. Using similar evaluation techniques for the total cross section,[6] we have

$$\sigma_{\text{scatt}}\simeq\pi|A_f|^2/(ka)^2, \tag{30}$$

[5] *Note added in proof.*—However, see Glauber and Schomaker [Phys. Rev. **89**, 667 (1953)] for a discussion in the scalar field case without dissipation.

[6] E. Gerjuoy and D. S. Saxon, Phys. Rev. **94**, 478 (1954), Eq. (70) ff.

and hence, according to the cross-section theorem for lossless scatterers,

$$\sin\gamma_0 \simeq |A_f|/4k\sigma^{\frac{1}{2}}. \tag{31}$$

Eliminating $|A_f|$ between Eq. (29) and Eq. (31), we see that $\gamma=2\gamma_0$ to the accuracy of these relations. In words, under the stated assumptions, the phase of the complex scattering amplitude (more precisely, of its component along the direction of polarization of the incident wave) increases from its value γ_0 for forward scattering to roughly twice this value outside the main diffraction peak and, surprisingly, then becomes independent of scattering angle. Further, using Eq. (30), we note that in the usual electromagnetic scattering problem, where the total cross section tends to a constant value in the short-wave limit, the phasee γ_0 and γ also tend to definite limiting values. On ths other hand, if the total cross section tends to zero, as for example in the scattering by a free electron cloud, then the phases tend to zero as $\sigma^{\frac{1}{2}}$. This latter case, which is infrequently encountered in electromagnetic scattering, is the usual situation in quantum mechanics. In this connection see reference 6, in which some discussion of the Born and variational approximations is given on this basis. Presumably, relations such as those above can be generally useful in evaluating the consistency and convergence of approximation methods, but we shall not elaborate further.

PHYSICAL REVIEW VOLUME 100, NUMBER 6 DECEMBER 15, 1955

Scattering by a Symmetric Potential

R. J. FINKELSTEIN AND M. MOE
University of California, Los Angeles, California
(Received July 20, 1955)

Scattering by a symmetric structure, such as a regular molecule or crystal, is discussed in terms of a variational principle. The appropriate partial waves are labelled by the irreducible representations of the crystallographic groups and may be generated by a set of projection operators, one for each irreducible representation. The trial functions are chosen to lie in a space spanned by the crystallographic partial waves. Methods are indicated for generating either the infinite set of partial waves needed for an exact solution or a finite set more useful in an approximate calculation.

INTRODUCTION

THE analysis of term splitting in symmetric potentials[1] is one of the well-known physical applications of group theory, but no systematic remarks on the corresponding scattering problem appear to have been published. In this connection, one might consider the scattering of particles by regular molecules or crystals, or macroscopically the scattering of sound by regular polyhedra. As long as these problems are done in Born approximation they are sufficiently simple so that there is no appreciable advantage in discussing further simplifications associated with the symmetry. But there are, of course, situations in which the Born approximation may not be adequate, such as electron diffraction by molecules containing potentials of very different strengths.[2] In this case more refined methods are needed, and then it may be helpful to handle the symmetry conditions in a systematic way. In the following, this will be done in connection with a variational principle proposed by Schwinger.[3,4]

[1] H. A. Bethe, Ann. Physik **3**, 133 (1929).
[2] The example of uranium hexafluoride has been discussed by R. Glauber and V. Schomaker, Phys. Rev. **89**, 667 (1953).
[3] J. Schwinger, *Lectures on Nuclear Physics*, Harvard University, 1947 (unpublished).
[4] E. Gerjuoy and D. Saxon, Phys. Rev. **94**, 478 (1954). Gerjuoy and Saxon have used this principle to discuss scattering from a spherically symmetric potential and have shown that even in this case it is convenient to utilize a cyclic group. The present note was suggested by their work.

PARTIAL WAVES

Consider scattering by a potential u having the symmetry of a rotation group G. Let the incoming wave be ψ_c and the outgoing wave be ψ_d. They are connected by S, the scattering operator:

$$\psi_d = S\psi_c = e^{i\eta}\psi_c, \tag{1}$$

where S and η commute with all the elements R of G:

$$(S,R)=(\eta,R)=0. \tag{2}$$

Equation (2) implies that η and S are multiples of the unit matrix, when the representation of G is irreducible, and that they have no elements connecting different irreducible representations. When G is the complete rotation group, one obtains the irreducible representations by choosing the basis functions to be the spherical harmonics Y_{lm}, and then

$$\eta(i,j)=\eta(lm;l'm')=\eta_l\delta(lm,l'm'). \tag{3}$$

The eigenvalues η_l determine the phase shifts and there is one for each irreducible representation.

In the case of the crystallographic groups, G contains only a finite number of elements and has only a small number of irreducible representations (Γ_γ). Every representation of the complete rotation group D_l may be decomposed into the Γ_γ:

$$D_l=\sum a_{l\gamma}\Gamma_\gamma.$$

In terms of basis functions:

$$Y_{lm}=\sum \chi_{l\gamma\mu}U(l\gamma\mu;lm), \tag{4}$$

where the $\chi_{l\gamma\mu}$ are an irreducible basis of the crystallographic group. Corresponding to (3) one has

$$\eta(l\gamma\mu;l'\gamma'\mu')=\eta(l\gamma;l'\gamma)\delta(\gamma\mu;\gamma'\mu'). \tag{5}$$

Consider the submatrix for which $l=l'$. The corresponding phase shift η_l is split by the lower symmetry into the set $\eta(l,\gamma)$ where γ labels the irreducible representations of which D_l is composed. These relations are entirely analogous to equations which describe the splitting of energy levels and the introduction of matrix elements between different angular momentum states by crystalline fields. According to (5) the usual constants of the motion, l and m, are no longer conserved in the scattering, but γ and μ are.

VARIATIONAL PRINCIPLE

Let the incident plane wave in the direction $\mathbf{k}$ be $\psi_{\mathbf{k}}{}^0$ and let $\psi_{\mathbf{k}}{}^\pm$ be solutions of the time-independent integral equations:

$$\psi_{\mathbf{k}}{}^\pm=\psi_{\mathbf{k}}{}^0+G_\pm u\psi_{\mathbf{k}}{}^\pm, \tag{6}$$

where $G_\pm$ are the outgoing and incoming Green's functions. The variational principle then states that the solutions of (6) may be obtained by finding the stationary value of a certain functional (J) with respect to variations of the unknown functions $\psi_{\mathbf{k}}{}^+$ and $\psi_{\mathbf{k}'}{}^-$ about their correct forms. J may be written as the following matrix element:

$$4\pi(\mathbf{k}'|J|\mathbf{k})=(\mathbf{k}'|A|\mathbf{k})(\mathbf{k}'|B|\mathbf{k})/(\mathbf{k}'|C|\mathbf{k}), \tag{7}$$

where

$$(\mathbf{k}'|A|\mathbf{k})=(\psi_{\mathbf{k}'}{}^0,u\psi_{\mathbf{k}}{}^+), \tag{8a}$$

$$(\mathbf{k}'|B|\mathbf{k})=(\psi_{\mathbf{k}'}{}^-,u\psi_{\mathbf{k}}{}^0), \tag{8b}$$

$$(\mathbf{k}'|C|\mathbf{k})=(\psi_{\mathbf{k}'}{}^-,\mathbf{u}\psi_{\mathbf{k}}{}^+), \tag{8c}$$

$$\mathbf{u}=u-uG_+u \tag{8d}$$

and (,) means Hermitian scalar product. When ψ^+ and ψ^- are actually solutions of (6), these matrix elements are equal to each other and to the scattering amplitude.

TRIAL FUNCTIONS AND SOLUTIONS

Choose the comparison functions $\psi^\pm$ to lie in a space spanned by the sets $\varphi_\alpha{}^\pm$:

$$\psi_{\mathbf{k}}{}^+(\mathbf{x})=\sum \varphi_\alpha{}^+(\mathbf{x})S_{\alpha\mathbf{k}}, \tag{9a}$$

$$[\psi_{\mathbf{k}'}{}^-(\mathbf{x})]^*=\sum[\varphi_\alpha{}^-(\mathbf{x})]^*S_{\alpha\mathbf{k}'}{}^*, \tag{9b}$$

where the $\varphi_\alpha{}^+$ and $\varphi_\alpha{}^-$ may be different. In obtaining the stationary value of J, the $S_{\alpha\mathbf{k}}$ and $S_{\alpha\mathbf{k}'}{}^*$ are to be varied independently. The φ_α are to be regarded as a fixed basis which will be defined in terms of G in the next paragraph. For the present we mention only the following property:

$$(\varphi_\alpha{}^-,F\varphi_\beta{}^+)=0, \quad \alpha\neq\beta, \tag{10}$$

where F is any function invariant under the rotations of G.

Substituting now (9) in (7), performing the variation, and using (10) one obtains

$$S_{\alpha\mathbf{k}}=[(\mathbf{k}'|C|\mathbf{k})/(\mathbf{k}'|B|\mathbf{k})]\times[(\alpha|\bar{B}|\mathbf{k})/(\alpha|\bar{C}|\alpha)], \tag{11a}$$

$$S_{\alpha\mathbf{k}'}{}^*=[(\mathbf{k}'|C|\mathbf{k})/(\mathbf{k}'|A|\mathbf{k})]\times[(\mathbf{k}'|\bar{A}|\alpha)/(\alpha|\bar{C}|\alpha)], \tag{11b}$$

where

$$(\mathbf{k}|\bar{A}|\alpha)=(\psi_{\mathbf{k}}{}^0,u\varphi_\alpha{}^+), \tag{11c}$$

$$(\alpha|\bar{B}|\mathbf{k})=(\varphi_\alpha{}^-,u\psi_{\mathbf{k}}{}^0), \tag{11d}$$

$$(\alpha|\bar{C}|\beta)=(\varphi_\alpha{}^-,\mathbf{u}\varphi_\alpha{}^+)\delta_{\alpha\beta}. \tag{11e}$$

By (7) the best choice of the scattering amplitude itself is

$$4\pi(\mathbf{k}'|J|\mathbf{k})=\sum_\alpha(\mathbf{k}'|\bar{A}|\alpha)(\alpha|\bar{B}|\mathbf{k})/(\alpha|\bar{C}|\alpha). \tag{11f}$$

Equations (11) solve the variational problem for a basis with the orthogonality property (10). The next step is to give a specific definition of this basis in terms of G.

PROJECTION OPERATORS

Following the usual nomenclature the group is divided into sets of conjugate elements, called *classes*. Adopting a matrix representation, one defines a class average as

$$\Lambda_s=(1/n_s)\sum R_i, \tag{12}$$

where the sum extends over all members of the sth class (which contains n_s elements). The Λ_s commute with all members of G and therefore with each other. They therefore form a mutually commuting set, every member of which also commutes with the scattering potential.

$$(\Lambda_s,\Lambda_{s'})=0, \quad (\Lambda_s,u)=0. \tag{13}$$

From the set $\{\Lambda_s\}$ one may construct other mutually commuting sets. In particular the projection operators e_γ may be formed as follows[5]:

$$e_\gamma=(n_\gamma/g)\sum_s n_s\chi_\gamma{}^*(s)\Lambda_s. \tag{14}$$

Here g is the order of G, n_γ is the dimensionality of the irreducible representation Γ_γ, and $\chi_\gamma(s)$ is the trace of Λ_s in this irreducible representation. There is one e_γ for each Γ_γ. In the irreducible representation $\Gamma_{\gamma'}$,

$$e_\gamma=(n_\gamma/g)\sum n_s\chi_\gamma{}^*(s)[\chi_{\gamma'}(s)/n_{\gamma'}]=\delta_{\gamma\gamma'}. \tag{15}$$

Hence e_γ is the unit matrix in Γ_γ, but vanishes in every other irreducible representation. By considering a completely reduced representation, one verifies the

[5] B. L. v. d. Waerden, *Moderne Algebra* (Verlag Julius Springer, Berlin, 1940), second edition, Sec. 117.

invariant relations:

$$e_\gamma e_{\gamma'} = e_\gamma \delta_{\gamma\gamma'}, \tag{16a}$$

$$\sum e_\gamma = E. \tag{16b}$$

The projection operators also satisfy the equations

$$\Lambda_\epsilon e_\gamma = \lambda_{\epsilon\gamma} e_\gamma, \tag{17a}$$

where the $\lambda_{\epsilon\gamma}$ are numbers. Hence the common eigenvectors of the $\{\Lambda_\epsilon\}$ are $e_\gamma\varphi$, where φ is an arbitrary vector. Finally we remark that, by multiplication by e_γ, any basis $\{\varphi_i\}$ may be converted into the irreducible one $\{e_\gamma\varphi_i\}$. For example:

$$e_\gamma Y_{lm} = \chi_{l\gamma\mu}, \tag{17b}$$

where the Y_{lm} are the spherical harmonics and the $\chi_{l\gamma\mu}$ are the crystallographic partial waves referred to earlier.

CONSTRUCTION OF BASIS

If the $\chi_{l\gamma\mu}$ just obtained in (17b) are substituted for the $\varphi_\alpha^\pm$ in the variational principle through Eq. (9), then one may obtain an exact solution to the scattering problem. In the method to be described next, however, only a small number of partial waves are employed. They are

$$\varphi_\alpha^\pm = e_\alpha(\mathbf{n}^\pm)\varphi^0(\mathbf{n}^\pm\mathbf{x}), \tag{18a}$$

where φ^0 is some unspecified function of argument $\mathbf{nx}$ and $\mathbf{n}$ is a constant vector which orients φ^0; for example $\varphi^0 = \exp(i\mathbf{nx})$. The operator $e_\alpha(\mathbf{n})$ may be expressed as follows:

$$e_\alpha(\mathbf{n}) = \sum_i R_i(\mathbf{n}) U_{i\alpha}, \tag{18b}$$

and the argument $\mathbf{n}$ means that the indicated rotations work on $\mathbf{n}$ rather than on $\mathbf{x}$. As pointed out in connection with (17a) the φ_α as so defined are common eigenfunctions of the commuting set $\{\Lambda_\epsilon, u\}$. It will now be shown that they also satisfy the basic orthogonality relation (10). Written out more explicitly, (10) is

$$(\varphi_\alpha^-(\mathbf{x}'), F(\mathbf{x}',\mathbf{x})\varphi_\beta^+(\mathbf{x})) = \int\int d\mathbf{x}d\mathbf{x}'\,\varphi_\alpha^-(\mathbf{x}')F(\mathbf{x}',\mathbf{x})\varphi_\beta^+(\mathbf{x}) = 0,$$

where F is invariant under G:

$$R_\epsilon^{-1}(\mathbf{x}')R_\epsilon^{-1}(\mathbf{x})F(\mathbf{x}',\mathbf{x})R_\epsilon(\mathbf{x})R_\epsilon(\mathbf{x}') = F(\mathbf{x}',\mathbf{x}).$$

It may be proved as follows:

$$\begin{aligned}(\varphi_\alpha^-, F\varphi_\beta^+) &= (e_\alpha(\mathbf{n}^-)\varphi^0(\mathbf{n}^-\mathbf{x}'), F(\mathbf{x}',\mathbf{x})e_\beta(\mathbf{n}^+)\varphi^0(\mathbf{n}^+\mathbf{x})) \\ &= \sum_i (e_\alpha(\mathbf{n}^-)\varphi^0(\mathbf{n}^-\mathbf{x}'), F(\mathbf{x}',\mathbf{x})R_i(\mathbf{n}^+)\varphi^0(\mathbf{n}^+\mathbf{x}))U_{i\beta} \\ &= \sum_i (e_\alpha(\mathbf{n}^-)\varphi^0(\mathbf{n}^-\mathbf{x}'), F(\mathbf{x}',\mathbf{x})R_i^{-1}(\mathbf{x})\varphi^0(\mathbf{n}^+\mathbf{x}))U_{i\beta}\end{aligned}$$

since $R_i(\mathbf{n}^+)\varphi^0(\mathbf{n}^+\mathbf{x}) = R_i^{-1}(\mathbf{x})\varphi^0(\mathbf{n}^+\mathbf{x})$. Then, since

$$\begin{aligned}\sum R_i(\mathbf{x}')U_{i\beta}^* &= \sum R_i^{-1}(\mathbf{n}^-)U_{i\beta}^* \\ &= \sum R_i^\dagger(\mathbf{n}^-)U_{i\beta}^* = e_\beta^\dagger(\mathbf{n}^-),\end{aligned}$$

we obtain

$$\begin{aligned}&(\varphi_\alpha^-, F\varphi_\beta^+) \\ &= \sum_i (e_\alpha(\mathbf{n}^-)\varphi^0(\mathbf{n}^-\mathbf{x}'), R_i^{-1}(\mathbf{x}')R_i^{-1}(\mathbf{x})F(\mathbf{x}',\mathbf{x})\varphi^0(\mathbf{n}^+\mathbf{x}))U_{i\beta} \\ &= \sum (R_i(\mathbf{x})R_i(\mathbf{x}')e_\alpha(\mathbf{n}^-)\varphi^0(\mathbf{n}^-\mathbf{x}'), F(\mathbf{x}',\mathbf{x})\varphi^0(\mathbf{n}^+\mathbf{x}))U_{i\beta} \\ &= (e_\beta^\dagger(\mathbf{n}^-)e_\alpha(\mathbf{n}^-)\varphi^0(\mathbf{n}^-\mathbf{x}'), F(\mathbf{x}',\mathbf{x})\varphi^0(\mathbf{n}^+\mathbf{x})).\end{aligned}$$

Since the projection operators have real eigenvalues, they are Hermitian: $e_\beta^\dagger(\mathbf{n}^-) = e_\beta(\mathbf{n}^-)$. In addition, $e_\alpha(\mathbf{n}^-)e_\beta(\mathbf{n}^-) = 0$, $\alpha \neq \beta$. Therefore,

$$(\varphi_\alpha^-, F\varphi_\beta^+) = 0, \quad \alpha \neq \beta.$$

The φ_α defined by Eq. (18a) are consequently satisfactory basis functions, and Eqs. (11) are correct in terms of them.

Finally,

$$(\varphi_\alpha^-, F\varphi_\alpha^+) = e_\alpha(\mathbf{n}^+)(\varphi^0(\mathbf{n}^-\mathbf{x}'), F(\mathbf{x}',\mathbf{x})\varphi^0(\mathbf{n}^+\mathbf{x})). \tag{10a}$$

EVALUATION OF THE SCATTERING AMPLITUDE

Choose $\mathbf{n}^+ = \mathbf{k}$ and $\mathbf{n}^- = \mathbf{k}'$. Then

$$\begin{aligned}\varphi_\alpha^+ &= \sum R_i(\mathbf{k})\varphi^0(\mathbf{kx})U_{i\alpha} \\ &= \sum \varphi_i(\mathbf{kx})U_{i\alpha}, \\ \varphi_\alpha^- &= \sum \varphi_i(\mathbf{k}'\mathbf{x})U_{i\alpha},\end{aligned}$$

where

$$U_{i\alpha} = (n_\alpha/g)\chi_\alpha^*(i), \quad \varphi_i = R_i\varphi^0.$$

In terms of the functions φ_i and the numbers $U_{i\alpha}$, characteristic of the group, the results of the variational procedure, expressed by (11) take the form

$$\begin{aligned}(\mathbf{k}|\bar{A}|\alpha) &= \sum (\psi_{\mathbf{k}}^0, u\varphi_i(\mathbf{kx}))U_{i\alpha} \\ &= \sum (\mathbf{k}|u|i)U_{i\alpha} = (\mathbf{k}|uU|\alpha),\end{aligned} \tag{20a}$$

$$\begin{aligned}(\alpha|\bar{B}|\mathbf{k}) &= \sum (\varphi_i(\mathbf{k}'\mathbf{x}), u\psi_{\mathbf{k}}^0)U_{i\alpha}^* \\ &= \sum U^\dagger(\alpha,i)(i|u|\mathbf{k}) = (\alpha|U^\dagger u|\mathbf{k}),\end{aligned} \tag{20b}$$

$$\begin{aligned}(\alpha|\bar{C}|\alpha) &= \sum (\varphi_i(\mathbf{k}'\mathbf{x}'), \mathbf{u}(\mathbf{x}',\mathbf{x})\varphi_j(\mathbf{kx}))U_{i\alpha}^* U_{j\alpha} \\ &= \sum U^\dagger(\alpha,i)(i|\mathbf{u}|j)U(j,\alpha) \\ &= (\alpha|U^\dagger \mathbf{u} U|\alpha).\end{aligned} \tag{20c}$$

Therefore, the final result may be written

$$(\mathbf{k}'|J|\mathbf{k}) = \sum_\alpha (\mathbf{k}'|J^{(\alpha)}|\mathbf{k}), \tag{21}$$

where the partial amplitudes $J^{(\alpha)}$ are summed over all irreducible representations, and

$$\begin{aligned}&4\pi(\mathbf{k}'|J^{(\alpha)}|\mathbf{k}) \\ &\quad = (\mathbf{k}'|uU|\alpha)(\alpha|U^\dagger u|\mathbf{k})/(\alpha|U^\dagger \mathbf{u} U|\alpha).\end{aligned} \tag{22}$$

An alternative form is

$$\begin{aligned}4\pi(\mathbf{k}'|J^{(\alpha)}|\mathbf{k}) &= \sum (\mathbf{k}'|u|i)w_\alpha(i,j)(j|u|\mathbf{k})/ \\ &\qquad \sum (i|\mathbf{u}|j)w_\alpha(j,i),\end{aligned} \tag{23a}$$

where

$$\begin{aligned}w_\alpha(i,j) &= U(i,\alpha)U^\dagger(\alpha,j) \\ &= (n_\alpha/g)^2 \chi_\alpha^*(i)\chi_\alpha(j).\end{aligned} \tag{23b}$$

Because of the character orthogonality relations, the

$w_\alpha(i,j)$ are not independent, but satisfy

$$\sum_\alpha w_\alpha(i,j)/n_\alpha^2=(1/gn_i)\delta(i,j),$$
$$\sum_\alpha w_\alpha(i,j)/n_\alpha^2=1/g, \tag{24}$$

where n_i is the number of elements in class i and n_α is the dimensionality of the representation α.

The symmetry of the potential enters (23a) to determine the matrix $w_\alpha(i,j)$ as well as the basis in which u and $\mathbf{u}$ are calculated. The weight to be assigned to each irreducible representation α is determined by $w_\alpha(i,j)$.

A final very convenient expression for $J^{(\alpha)}$ is

$$4\pi(\mathbf{k}'|J^{(\alpha)}|\mathbf{k})=\frac{[e_\alpha(\mathbf{k})(\psi_{\mathbf{k}'}{}^0,u\varphi^0(\mathbf{kx}))][e_\alpha(\mathbf{k})(\varphi^0(\mathbf{k}'\mathbf{x}'),u\psi_{\mathbf{k}}{}^0)]}{[e_\alpha(\mathbf{k})(\varphi^0(\mathbf{k}'\mathbf{x}'),\mathbf{u}(\mathbf{x}',\mathbf{x})\varphi^0(\mathbf{kx}))]}. \tag{25}$$

This form follows from (10a) and the argument leading to that equation. It is entirely analogous to Eq. (43) of reference 4.

All of these equations take their simplest forms when $\varphi^0(\mathbf{kx})=e^{i\mathbf{kx}}$. Then (25) becomes

$$4\pi(\mathbf{k}'|J^{(\alpha)}|\mathbf{k})=[e_\alpha(\mathbf{k})A(\mathbf{k},\mathbf{k}')]^2/[e_\alpha(\mathbf{k})C(\mathbf{k},\mathbf{k}')], \tag{26a}$$

where

$$A(\mathbf{k},\mathbf{k}')=(e^{i\mathbf{k}'\mathbf{x}},ue^{i\mathbf{kx}}), \tag{26b}$$

$$C(\mathbf{k},\mathbf{k}')=(e^{i\mathbf{k}'\mathbf{x}'},\mathbf{u}(\mathbf{x}',\mathbf{x})e^{i\mathbf{kx}}). \tag{26c}$$

EXAMPLES OF PROJECTION OPERATORS

(a) If G is a dihedral group, it is Abelian, each element is a class by itself, and there are altogether g irreducible representations all one-dimensional. In this case, according to (14), and in agreement with reference 4, Eq. (25)

$$e_\gamma=g^{-1}\sum_{s=0}^{g-1}\omega^{-\gamma s}R^s,$$

where $\omega^g=1$.

(b) Let G be the group of the regular tetrahedron (which is the shape of the methane molecule, for example). This has twelve members and four classes; it has, therefore, four irreducible representations, three of which are one-dimensional, and one of which is three-dimensional. It may be generated by the cyclic permutations (123) and (124), where the indices $1\cdots4$ refer to the four vertices. Let $A=(123)$ and $B=(124)$. Then

$$\Lambda_1=E,$$
$$\Lambda_2=(AB+BA+BA^{-1}B)/3,$$
$$\Lambda_3=(A+B^{-1}+A^{-1}B+BA^{-1})/4,$$
$$\Lambda_4=(A^{-1}+B+B^{-1}A+AB^{-1})/4.$$

The character table and the projection operators follow.

	χ^1	χ^2	χ^3	χ^4	
C_1	1	3	1	1	$e_1=[\Lambda_1+3\Lambda_2+4\Lambda_3+4\Lambda_4]/12,$
C_2	1	−1	1	1	$e_2=[3\Lambda_1-3\Lambda_2](3/12),$
C_3	1	0	ω	ω^2	$e_3=[\Lambda_1+3\Lambda_2+4\omega\Lambda_3+4\omega^2\Lambda_4]/12,$
C_4	1	0	ω^2	ω	$e_4=[\Lambda_1+3\Lambda_2+4\omega^2\Lambda_3+4\omega\Lambda_4]/12.$

The e_γ for other crystallographic groups are given by Meijer.[6]

As already mentioned one may start with the Y_{lm} and generate from them by means of the e_γ an infinite set of crystallographic partial waves; in this way one may arrive at an exact solution of the scattering problem. By working with a less extensive class of basis functions, one may obtain approximations which are more tractable. One such class has just been discussed.

SCATTERING BY A TETRAHEDRAL MOLECULE

Pursuing the last example further, let us consider the scattering of electrons by a molecule with the chemical formula X_4, and let us assume that the potential seen by the electron is

$$u=\sum_1^4 u_i,$$

where

$$u_i=u_0\exp(-|\mathbf{x}-\mathbf{X}_i|)/|\mathbf{x}-\mathbf{X}_i|,$$
$$u_0=-2mV_0a^2/\hbar^2,$$
$$\mathbf{x}=\mathbf{r}/a,$$
$$\mathbf{X}_i=\mathbf{R}_i/a.$$

Here $\mathbf{R}_i$ is the distance of the ith nucleus from the center of the molecule, a is the range of the screened Coulomb potential, and u_0 is the dimensionless potential corresponding to V_0.

The functions $A(\mathbf{k},\mathbf{k}')$ and $C(\mathbf{k},\mathbf{k}')$ appearing in (26) are

$$A(\theta)=u_0g(k,\theta)F,\quad C(\theta)=u_0[g(k,\theta)-u_0G(k,\theta)]F,$$

where F is the familiar form factor:

$$F=\sum\exp[i(\mathbf{k}-\mathbf{k}')\cdot\mathbf{X}_i]$$

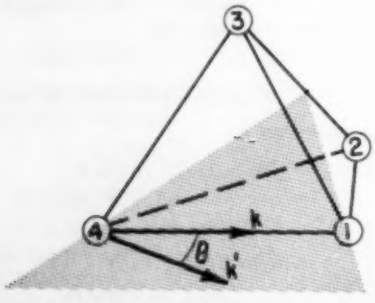

FIG. 1. The plane of $\mathbf{k}$ and $\mathbf{k}'$ in relation to the tetrahedral molecule.

[6] The usefulness of these operators for the problem of term splitting in crystalline fields was pointed out by P. Meijer, Phys. Rev. 95, 1443 (1954). They are referred to by this author as the idempotent elements of the ring associated to the group.

TABLE I. Results of the Born and variational calculations.

	Scattering amplitude					
	$u_0=19$, $k=25$		$u_0=19$, $k=10$		$u_0=1.25$, $k=10$	
θ	Born	Variational	Born	Variational	Born	Variational
0	76.0	$73.6+13.9i$	76.0	$63.0+30.5i$	5.0000	$5.0029+0.156i$
$\pi/2$	$0.0228+0.00001i$	$0.0024+0.0073i$	$-0.113-0.115i$	$+0.02-0.02i$	$-0.0074-0.0075i$	$-0.0045-0.0091i$
π	0.030	$0.039-0.036i$	0.0195	$-0.06-0.02i$	0.0013	$0.0012+0.0005i$
	Differential cross sections					
θ	Born	Variational	Born	Variational	Born	Variational
0	5776	5619	5776	4898	25.000	25.053
$\pi/2$	0.00052	0.000059	0.026	0.00095	0.00011	0.00010
π	0.0009	0.0028	0.00038	0.0041	1.7×10^{-6}	1.7×10^{-6}

and

$$k^2=2mEa^2/\hbar^2,$$

$$\cos\theta=\mathbf{k}\cdot\mathbf{k}'/k^2,$$

$$g(k,\theta)=[1+4k^2\sin^2(\theta/2)]^{-1},$$

$$G(k,\theta)=\frac{1}{(2k\sqrt{s})\sin(\theta/2)}\left[\tan^{-1}\left(\frac{k\sin(\tfrac{1}{2}\theta)}{\sqrt{s}}\right)+\frac{1}{2}\,i\ln\frac{\sqrt{s}+2k^2\sin(\tfrac{1}{2}\theta)}{\sqrt{s}-2k^2\sin(\tfrac{1}{2}\theta)}\right],$$

$$s=(1+2k^2)^2-4k^4\cos^2(\theta/2).$$

The expression for A is exact. In the evaluation of C, however, we have dropped interference terms between different atoms; i.e., double scatterings on the same atom are taken into account but double scatterings involving two atoms are neglected, for reasons of simplicity.

A simple illustration is provided by letting the incident wave $\mathbf{k}$ lie along the edge of the tetrahedron joining vertices 4 and 1, and letting the scattered wave $\mathbf{k}'$ lie in the plane passing through $\mathbf{k}$ and the midpoint of the opposite edge, as shown in Fig. 1.

In Eq. (26), we must evaluate expressions of the form

$$e_\alpha(\mathbf{k})f(\theta)=\sum R_i(\mathbf{k})U_{i\alpha}f(\theta)=\sum U_{i\alpha}f(\theta_i),$$

where $f(\theta)$ stands for either $A(\theta)$ or $C(\theta)$ and θ_i is the new angle between $\mathbf{k}$ and $\mathbf{k}'$ produced by the rotation $R_i(\mathbf{k})$. In the present example, the values of θ_i are

R_i	E	AB	BA	$BA^{-1}B$	A	B^{-1}	$A^{-1}B$	BA^{-1}	A^{-1}	B	$B^{-1}A$	AB^{-1}
θ_i	θ	$\pi-\theta$	$\pi/2$	$\pi/2$	a	$\pi-a$	$\pi-b$	b	a	$\pi-b$	$\pi-a$	b

where

$$a=\cos^{-1}[\tfrac{1}{3}\cos\theta-\tfrac{1}{3}\sqrt{2}\cos(\tfrac{1}{4}\pi-\theta)],$$

$$b=\cos^{-1}[\tfrac{1}{3}\cos\theta+\tfrac{1}{3}\sqrt{2}\cos(\tfrac{1}{4}\pi-\theta)].$$

The scattering amplitude has been calculated at $\theta=0$, $\pi/2$, and π for $u_0=19$, $a=\frac{1}{3}\times10^{-8}$ cm, and $X=4$. These are approximately the parameters appropriate to the phosphorus molecule P_4. In Table I, the results of calculations for $k=10$ and 25 ($E=3.4$ and 21 kev, respectively) are tabulated along with the Born approximation for comparison. A third case with $k=10$ and $u_0=1.25$ is also given as an example in which the conditions for the validity of the Born approximation are very well satisfied. These conditions are $u_0/k^2\ll1$ and $u_0/k<1$.

We conclude that, where the Born approximation is valid and the second Born correction is small, the variational method necessarily gives a good estimate of the phase as well as the magnitude of the forward scattering. In fact, it gives essentially the second Born approximation. When the Born method is not valid, the variational procedure still gives a reasonable estimate of the forward scattering. This is indicated in reference 4 where the variational results are compared with exact values.

Even when the conditions for the Born approximation are satisfied and the second Born effectively corrects the forward scattering, the larger-angle scattering need not be given correctly in either magnitude or phase by the Born approximations. The fact that the variational method can handle this region is important if details about the shape of the electronic charge distribution are of interest.

Finally, it ought to be emphasized that the preceding very sketchy numerical calculations are meant only to be illustrative of the general method. In systematic calculations designed to determine the electron distribution, it would be natural to expand the molecular potential itself in irreducible representations of the group of the molecule.

ACKNOWLEDGMENTS

We wish to thank Professor David S. Saxon for having discussed this problem with us and in particular for those preceding comments, which are based on the experience of reference 4, concerning the relative usefulness of the Born and Schwinger methods.

Relativistic Theory of Discrete Momentum Space and Discrete Space-Time

E. L. Hill
University of Minnesota, Minneapolis, Minnesota
(Received August 25, 1955)

An examination is made of the result of restricting translations and Lorentz transformations in space-time to those with rational coefficients. This removes the major defect of Schild's model of discrete space-time by elimination of the lower bound on the relative velocities of reference systems. The theory is formulated in two stages. In the first the energy and momentum components of a particle are restricted to a countable set satisfying the relativistic energy-momentum relation while the space-time variables are continuous. This gives a theory of discrete energy-momentum space in which wave functions are almost periodic functions. In the second stage the space-time variables are restricted to rational values. This leads to the theory of discrete space-time.

1. INTRODUCTION

IT has been conjectured frequently that a treatment of space and time as having a discrete structure would be of interest as a test of the character of physical theories.[1] Heisenberg's suggestion of the existence of a minimal space length has aroused particular interest among physicists.[2] A number of trials have been made at the reformulation of quantum mechanical theory by assumptions depending on the nature of the space and time variables considered as operators.[3]

One of the major difficulties encountered arises from the supposed necessity of preserving invariance of the theory under the full continuous group of Lorentz transformations, L. Some years ago Schild examined the consequences of assuming a lattice structure of space-time, requiring only the discrete group of Lorentz transformations under which the lattice as a whole was invariant.[4] For the case of a cubic lattice he found the smallest permissible velocity parameter to be $v/c=\frac{1}{2}\sqrt{3}$, which is impossibly large to make the model of use for physical purposes. There is little doubt that other space-time lattices suffer from the same defect.

We assume the character of a space to be determined by its allowed group of symmetry transformations in the same sense as was used in Schild's model. The property of discreteness can be achieved by other methods of selecting sets of transformations from L. The principal requirements which it seems necessary to impose in order to make any such set a reasonable starting point for a physical theory of space-time are the following: (a) the set must form a group in order to have closure under successive transformations and symmetry with respect to the senses of backward and forward, and (b) it must be dense in the full group L. To form a discrete subgroup of L is easy. One has only to take any finite or countably infinite complex K from L which contains the inverse of every element in it, and then form all possible products from the elements in K. The resulting extended complex will be a subgroup of L which will be at most countably infinite. However, when the complex K is chosen in an arbitrary manner it will be generally quite difficult to test whether its extension will be dense in L.

The present work starts with the selection of transformations from L which have *rational* coefficients. In this case the necessary analysis reduces to certain problems in the theory of numbers. The general properties of the resulting infinite discrete group, to which we shall refer as the rational proper Lorentz group, L_r, are developed briefly in the Appendix. The group L_r is dense in L and so is sufficiently extensive to remove doubt that it can be made the basis of a physical theory. It thus avoids the principal weakness of Schild's model in preserving the property of discreteness without setting lower bounds on the parameters of its transformations.

The theory is developed along two lines. In the first the space-time variables are allowed to be continuous but the energy and momentum variables of a particle are restricted to a certain countable set which is described later (Sec. 2). We refer to this as the theory of discrete energy-momentum space. The major result of quantum mechanical interest is that wave functions here become a special case of almost periodic functions. This interpretation provides an approach to the handling of continuous spectrum problems which, in principle at least, is more in consonance with current quantum mechanical theory in which strict normalization of the wave functions is not required than is the Hilbert space theory of von Neumann.[5] However, it does not appear that it will lead to any great improvement in the handling of convergence problems in perturbation theory without a revision in the nature of interaction operators.

[1] An interesting discussion is given by B. Russell, *The Analysis of Matter* (Dover Publications, New York, 1954), especially Chaps. 11 and 29.

[2] W. Heisenberg, Z. Physik **120**, 513 (1943); W. Heisenberg, *Festschrift der Akad. Wissen. Göttingen* (Springer-Verlag, Berlin, 1951), p. 30.

[3] H. S. Snyder, Phys. Rev. **71**, 38 (1947); **72**, 68 (1947); V. Rojansky, Phys. Rev. **97**, 507 (1955).

[4] A. Schild, Can. J. Math. **1**, 29 (1949). The problem was under independent investigation in this Laboratory by C. N. Kelber at the time of the appearance of Schild's paper. The writer is indebted to Dr. Kelber for discussions of his work.

[5] J. von Neumann, *Mathematical Foundations of Quantum Mechanics* (Princeton University Press, Princeton, 1955).

In the second form of the theory the property of discreteness is extended to space-time. One has the choice of treating the energy-momentum variables as discrete or continuous. This leads to alternative interpretations of wave functions of which the implications have not been analyzed fully.

The major part of the discussion will be devoted to the formulation of the models of discrete energy-momentum space and discrete space-time. The treatment of wave functions will be incomplete owing to the fact that a suitable reformulation of the quantum mechanical operator theory has not yet been carried through.

2. MODEL OF DISCRETE ENERGY-MOMENTUM SPACE

The energy and momentum of a particle are invariant under all translations of the reference system in space-time. The translations are therefore equivalent to the identity for the discussion of this section and so can be omitted.

We take as the coordinates of the energy-momentum space of a particle the four quantities

$$\pi_0 = E/m_0c^2, \quad \pi_i = p_i/m_0c. \quad (i=1, 2, 3) \qquad (1)$$

Under all transformations of the full continuous group of proper Lorentz transformations, L, these quantities transform like the components of a real four-vector with the invariant (energy-momentum equation of the particle)

$$\pi_0^2-\pi_1^2-\pi_2^2-\pi_3^2=1. \qquad (2)$$

More particularly, under the discrete group of rational Lorentz transformations, L_r, the set of points in energy-momentum space having *rational* coordinates which satisfy Eq. (2) will be invariant. These points constitute our discrete energy-momentum space.

The possible values of the energy and momentum of a particle which satisfy these restrictions can be characterized in the following manner. We consider only positive values of the energy for definiteness. Let

$$\pi_0 = m/n, \quad \pi_i = m_i/n_i. \quad (i=1, 2, 3) \qquad (3)$$

These rational fractions are supposed to be reduced to their lowest terms so that[6]

$$(m,n)=1, \quad (m_i,n_i)=1. \qquad (4)$$

It is clear that $m \geqslant n$. Since the choice $m=n$ leads to the obviously acceptable energy value $E=m_0c^2$, it will be convenient in the following discussion to make the restriction $m>n$.

Equation (2) hence takes the form

$$(m/n)^2-(m_1/n_1)^2-(m_2/n_2)^2-(m_3/n_3)^2=1. \qquad (5)$$

[6] We use the notation given in the text by G. H. Hardy and E. M. Wright, *An Introduction to the Theory of Numbers* (Oxford University Press, Oxford, 1945), second edition. The greatest common divisor of two integers m and n is indicated by (m,n) and the least common multiple by $\{m,n\}$.

If $\{n, n_1, n_2, n_3\}=sn=s_1n_1=s_2n_2=s_3n_3$ is the least common multiple of the n's, we can write (5) in the form

$$s^2(m^2-n^2)=(s_1m_1)^2+(s_2m_2)^2+(s_3m_3)^2. \qquad (6)$$

Every solution of this Diophantine equation in integers leads to a solution of Eq. (2) in rationals, and conversely.

Equation (6) shows that the positive integer $s^2(m^2-n^2)$ is expressible as the sum of three squares of integers. It is known that an integer is expressible in this manner if and only if it is not of the form $4^a(8b+7)$, where a and b are non-negative integers.[7] To make use of this result in connection with Eq. (6) we employ the following lemma.[8]

Lemma.—The positive integer $s^2(m^2-n^2)$ with $(m,n)=1$ will be of the form $4^a(8b+7)$ if and only if $(m^2-n^2)\equiv 7 \pmod 8$.

It follows immediately that the rational values $E/m_0c^2=m/n$, with $(m,n)=1$, will be allowed energy values if and only if $(m^2-n^2)\not\equiv 7 \pmod 8$; that is, if and only if (m^2-n^2) is not an integer of the form $8b+7$. For example, the value $4/3$ is not allowed since $4^2-3^2=7$.

One can show easily that the allowed values of energy are dense in the range $E/m_0c^2 \geqslant 1$. For since the rational numbers are dense in this range we have only to show that the allowed values of E/m_0c^2, all of which are rational, are dense among the rationals. Let x/y be any positive rational number such that $x>y$ and $(x,y)=1$. Then if r is any positive integral multiple of 8, so that $r\equiv 0 \pmod 8$, the rational number $(rx+3)/(ry+2)$ will be an allowed value of E/m_0c^2, since $[(rx+3)^2-(ry+2)^2]\equiv 5 \pmod 8$.[9] By taking a sufficiently large value of r this number can be made to approximate x/y with arbitrary accuracy. Similarly, the numbers $(rx+4)/(ry+3)$ will be unallowed values, from which we can conclude that the rational numbers which are unallowed for E/m_0c^2 are also dense in the open interval $(1, \infty)$.

For any allowed value of E/m_0c^2 other than unity there will be infinitely many rational solutions of Eq. (2) for the components of the momentum vector, $\mathbf{p}/m_0c$.[10] The allowed momentum vectors will form an infinite countable set which is dense in direction and magnitude in space. No convenient parametrization has been found for this set. In the following discussion the allowed energy values will be designated as E_α and the allowed momentum vectors by $\mathbf{p}_{\alpha\beta}$ with $\alpha, \beta = 1, 2, 3 \cdots$.

[7] See reference 6, Sec. 20.10.

[8] Write s in the form $s=2^ar$, where r is odd. Since the square of any odd integer is of the form $8l+1$, one has $s^2=4^a(8l+1)$. Since $(m,n)=1$, m^2-n^2 can at most be of the form $8q+7$. Suppose $m^2-n^2=8q+7$, then it is apparent at once that $s^2(m^2-n^2)=4^a(8b+7)$ with $b=8lq+7l+q$, which proves the first part of the lemma. Conversely, if $s^2(m^2-n^2)=4^a(8l+1)(m^2-n^2)=4^a(8b+7)$ then we must have $a=p$, so that $(8l+1)(m^2-n^2)=8b+7$. But in any event $(m^2-n^2)=8r+g$, where $0\leqslant g\leqslant 7$. It is apparent by inspection that the only possible choice is $g=7$, which proves the second part of the lemma.

[9] No integer of the form $4^a(8b+7)$ is congruent to 5 (mod 8).

[10] These solutions are to be obtained from Eq. (6) by specifying the integers m and n, with $(m,n)=1$, and then taking all cases $s=1, 2, 3, \cdots$. Almost all of the solutions will arise from very large values of s.

The usual representation of the wave function of a particle in terms of a Fourier integral must now be replaced by a sum over the allowed states.

$$\psi(x,y,z,t)=\sum_\alpha\sum_\beta A_{\alpha\beta}\exp[i(\mathbf{p}_{\alpha\beta}\cdot\mathbf{r}-E_\alpha t)/\hbar]$$
$$=\sum_\alpha\sum_\beta A_{\alpha\beta}\exp[i(m_0c/\hbar)(\boldsymbol{\pi}\cdot\mathbf{r}-\pi_0ct)]. \quad (7)$$

The space-time coordinates will be considered to be continuous variables and no restriction will be placed on the numerical value of the Compton wavelength.

Functions of the form (7), with appropriate convergence requirements, belong to the special class of almost periodic functions known as limit periodic functions.[11] They are the natural generalization of the very special periodic functions which appear in the method of "quantization in a box," or that of periodic boundary conditions. They are very different from the functions which are representable by Fourier integrals. This is shown by the fact that no almost periodic function can vanish at infinity without being identically zero. The sums in (7) are free from the measure restrictions associated with Fourier integrals, but of course they are not normalizable in the usual sense.

The coefficients in the expansion (7) can be evaluated by the method of mean values, in the sense of an initial value problem. If $M\{F(x,y,z)\}$ is the mean value of the function F taken over all space, and if $u(x,y,z)$ is the form of the wave function at $t=0$, then[12]

$$A_{\alpha\beta}=M\{u(x,y,z)\exp[-i(\mathbf{p}_{\alpha\beta}\cdot\mathbf{r})/\hbar]\}. \quad (8)$$

The wave functions (7) will be solutions of the Klein-Gordon equation, of course, but an exactly similar procedure can be used for the construction of free particle solutions of the Dirac equation and the other equations of quantum mechanics.

The manner in which these wave functions are to be used for the calculation of interactions between particles and fields presents some questions of principle which have not been solved. It does not appear likely that convergence difficulties will be lessened appreciably so long as the usual differential interaction operators are allowed. The situation may be improved if it is found possible to revise the operators in such a manner that they are given, or at least are approximated, by matrices having nonvanishing elements only connecting the allowed states in the momentum representation. The results which have been obtained to date are too scanty to justify their further discussion here.

3. MODEL OF DISCRETE SPACE-TIME

Under the group L_r the set of points of space-time (coordinates $x^0=ct$, $x^1=x$, $x^2=y$, $x^3=z$) having rational coordinates will be invariant. This property will be preserved under translations provided the components of the translation vectors are restricted to rational values; these will be referred to as rational translations. This allows us to define the rational translation group T_r in space-time as the family of all rational translations. Clearly there is in it no smallest step in any of the variables.

The group combination laws for successive applications of transformations of L_r and T_r will be valid and any transformation generated in this manner will leave the set of points in space-time having rational coordinates invariant. This provides our model of discrete space-time.

The construction of wave functions in this case depends on the interpretation assigned to energy-momentum space. If the energy-momentum variables are allowed to be continuous then Fourier integrals can be formed in the usual manner, but the symmetry between energy-momentum and space-time wave functions will be lost. If both spaces are taken to be discrete the situation becomes more extreme. The mathematical implications of these methods have not been examined in sufficient detail to permit their application to physical problems.

4. CONCLUSION

The foregoing theory has been designed mainly to show the possibility of constructing a self-consistent theory of discrete energy-momentum space and discrete space-time without doing utter violence to the invariance under Lorentz transformations. The extensiveness of the group of allowed transformations is so great as to leave no room for direct experimental disproof of the theory. However, this does not mean that there may not be some consequences which will be subject to experimental verification.

Since the group L_r is embedded in the full continuous group L and is dense in it, L_r will have most of the properties of L which are used in physical theory. In particular, the matrix representations of L which are now used will still be applicable. However, the discrete group L_r may well allow the existence of representations which cannot be extended to the full group. This suggests the following point which might ultimately become of some importance as a possible means of experimental test. The restriction of the quantized values of angular momentum to those employed in the usual vector model is dependent on the assumption of continuity of the matrix representations of the 3-dimensional rotation group. These representations will still be available for L_r, with a slight reinterpretation to take account of the discreteness of L_r. But if L_r admits of other representations for its subgroup of rational rotations then the vector coupling model may no longer be applicable. This seems to be a very delicate question which the writer has not succeeded in working out as yet.

APPENDIX A. RATIONAL HOMOGENEOUS PROPER LORENTZ GROUP, L_r

The continuous group of proper homogeneous Lorentz transformations, L, is given by the set of real 4×4 matrices $l=[l_\mu^\nu]$

[11] A. S. Besicovitch, *Almost Periodic Functions* (Dover Publications, New York, 1954), p. 32. The theory can be extended to functions of any number of variables.

[12] See reference 11, p. 12.

$(i,j=0,1,2,3)$ subject to the conditions[13]

$$l_0^0 \geq 1, \quad \det(l) = +1, \quad l^{-1} = \eta l^T \eta, \tag{A-1}$$

where l^T is the transpose of l and

$$\eta = \begin{bmatrix} -1 & 0 & 0 & 0 \\ 0 & 1 & 0 & 0 \\ 0 & 0 & 1 & 0 \\ 0 & 0 & 0 & 1 \end{bmatrix}. \tag{A-2}$$

It is evident from an inspection of these conditions that they will all be satisfied, as will the law of group multiplication, if we restrict the matrices to those having rational numbers as elements. This set of matrices forms a subgroup of L to which we shall refer as the *rotational Lorentz group*, L_r, as stated in the text, and which forms the basis of the theory given in this paper. The separation of the transformations of L into rotations and special Lorentz transformations holds as it does for L simply because L_r is embedded in L.

The writer has been unable to give a direct algebraic proof that L_r is dense in L. To avoid this we show in the next three parts of the Appendix that L_r contains a subgroup which is dense in L. While this is sufficient to show that L_r itself is dense in L, it leaves open the question whether the Euler factorization process is valid for L_r.

APPENDIX B. RATIONAL ROTATION SUBGROUP OF L_r

If $R(\mathbf{n};\lambda)$ is a rotation through an angle λ about an axis in space specified by the unit vector $\mathbf{n}$, the associated coordinate transformations on the space-time variables are

$$\mathbf{r}' = \mathbf{r}\cos\lambda + \mathbf{n}(\mathbf{n}\cdot\mathbf{r})2\sin^2\lambda/2 + (\mathbf{n}\times\mathbf{r})\sin\lambda, \quad t' = t. \tag{B-1}$$

Examination of the coefficients in these equations shows that a necessary and sufficient condition that they be rational is that the quantities $\cos\lambda$ and $n_i\sin\lambda$ $(i=1,2,3)$ be rational. The search for the set of rational rotations can be reduced to the solution of Eq. (6). For, if we set

$$\cos\lambda = p/q, \quad n_i\sin\lambda = p_i/q_i, \tag{B-2}$$

where these rational fractions are reduced to their lowest terms, we must have

$$(p/q)^2 + (p_1/q_1)^2 + (p_2/q_2)^2 + (p_3/q_3)^2 = 1. \tag{B-3}$$

With $\{qq_1q_2q_3\} = rq = r_1q_1 = r_2q_2 = r_3q_3$ as the least common multiple of the q's, we can write

$$r^2(q^2 - p^2) = (r_1p_1)^2 + (r_2p_2)^2 + (r_3p_3)^2, \tag{B-4}$$

which is equivalent to Eq. (6) of the text. There is thus a simple one-to-one correspondence between the allowed points of the discrete energy-momentum space and the rational rotation subgroup of L_r.

For the special case of a rotation through an angle θ about one of the coordinate axes $\cos\theta$ and $\sin\theta$ must be rational. In this case the allowed rotation angles are easily determined. Since $\cos^2\theta + \sin^2\theta = 1$, we must solve this Diophantine equation in rational numbers. The general solution is[14]

$$|\cos\theta(t)| = \frac{1-t^2}{1+t^2}, \quad |\sin\theta(t)| = \frac{2t}{1+t^2}, \tag{B-5}$$

where t is an arbitrary rational number such that $0 \leqslant t \leqslant 1$. An alternative formulation is $|\tan(\theta/2)| = t$.

Since the values of t are dense in $[0,1]$ and since relations $(B-5)$ are continuous in this interval, the allowed rotation angles will be dense in the interval $[0,2\pi]$. We can make the usual identification $R(\mathbf{n};\pi+\theta) = R(-\mathbf{n};\pi-\theta)$.

APPENDIX C. RATIONAL SPECIAL LORENTZ TRANSFORMATIONS OF L_r

The special Lorentz transformations to moving reference systems, the direction and speed of the relative motion being arbitrary, can be written in the form

$$\mathbf{r}' = \mathbf{r} - \frac{\mathbf{v}}{c}\left\{\frac{\mathbf{r}\cdot\mathbf{v}/c}{v^2/c^2}\left[1 - \frac{1}{(1-v^2/c^2)^{\frac{1}{2}}}\right] + \frac{ct}{(1-v^2/c^2)^{\frac{1}{2}}}\right\}$$
$$ct' = \frac{ct - \mathbf{r}\cdot\mathbf{v}/c}{(1-v^2/c^2)^{\frac{1}{2}}}. \tag{C-1}$$

These transformations do not form a group by themselves, of course, but by combination with the three-dimensional rotations the full group L can be generated.

Inspection of the coefficients shows that a necessary and sufficient condition that they be rational is that $(1-v^2/c^2)^{\frac{1}{2}}$ and v_i/c $(i=1,2,3)$ be rational. From this one can reduce the analysis of the rational transformations of type (C-1) to that of Eq. (6).

Again restricting attention to motion along one of the coordinate axes it is easy to find the allowed values of the relative velocity. With the notation

$$a = \frac{1}{(1-v^2/c^2)^{\frac{1}{2}}}, \quad b = \frac{v/c}{(1-v^2/c^2)^{\frac{1}{2}}}, \tag{C-2}$$

these quantities must be rational. Since $a^2 - b^2 = 1$ we need the general solution in rationals of this Diophantine equation. It is[14]

$$a = (r^2+1)/2r, \quad |b| = (r^2-1)/2r, \tag{C-3}$$

where r is any rational number $r \geqslant 1$. Alternatively, the allowed values of v/c are given by $|v/c| = (r^2-1)/(r^2+1)$. These values are dense in the open interval $(-1, 1)$.

APPENDIX D. DENSENESS OF L_r IN L

Let L_x', L_y', L_z' represent special Lorentz transformations of type (C-1) along the coordinate axes, and R_x', R_y', R_z' be rotations about the same axes. The Euler factorization process for the full group L shows that any transformation in it can be factorized as a product of the form $R_x'R_y'R_z'L_x'L_y'L_z'$.[15] Furthermore, the resultant transformation is a continuous function of each of the transformations in the product.

It is not known to the writer whether the group of rational transformations L_r admits this same type of factorization. In any event, starting with the allowed rational transformations of the indicated special forms as a complex of L_r we can form all possible products. In this way we obtain a countably infinite subgroup of L_r, which may or may not be a proper subgroup but which we argue is dense in L. For taking any transformation of L and writing it as this type of product we can approximate each of the separate transformations by a corresponding rational transformation to any desired degree of accuracy. The continuity of the product in each of the multiplicands assures us that the final product transformation (which is in L) can be approximated arbitrarily closely by a product of transformations from L_r. Hence L_r must be dense in L.

[13] F. D. Murnaghan, *The Theory of Group Representations* (Johns Hopkins University Press, Baltimore, 1938), Chap. 12.

[14] Hardy and Wright (reference 6, Sec. 13.2) give the solution of the equation $a^2+b^2=c^2$ in integers from which our result can be found. The solution in rationals is given directly by O. Ore, *Number Theory and its History* (McGraw-Hill Book Company, Inc., New York, 1948), p. 169.

[15] See reference 13, p. 357.

Letters to the Editor

PUBLICATION of brief reports of important discoveries in physics may be secured by addressing them to this department. The closing date for this department is five weeks prior to the date of issue. No proof will be sent to the authors. The Board of Editors does not hold itself responsible for the opinions expressed by the correspondents. Communications should not exceed 600 words in length and should be submitted in duplicate.

Effect of Pressure on the Superconducting Transition Temperature of Thallium

J. HATTON
Department of Physics, Harvard University, Cambridge, Massachusetts
(Received November 2, 1955)

THE effect of pressure on the superconducting transition temperature of thallium has been investigated at pressures up to nearly 5000 kg/cm². Pressure was applied to the thallium by a piston and cylinder arrangement, using solid hydrogen as the pressure-transmitting medium, and the electrical resistance of the thallium was measured as a function of temperature. The experimental arrangement has been described in an earlier publication.[1]

The results of this preliminary study are shown in Fig. 1. The sharpness of the transitions, even at maximum pressure, suggests that the stress transmitted to the specimen is rather uniform. In Fig. 2 is shown the transition temperature *vs* pressure as derived from the curves of Fig. 1. At low pressures, we find $\partial T_c/\partial P \sim +1.2\times10^{-5}$ deg/(kg/cm²), whereas for pressures greater than about 2500 kg/cm² we get $\partial T_c/\partial P \sim -0.43\times10^{-5}$ deg/(kg/cm²). The transition temperature has a maximum at a pressure in the neighborhood of 1500 kg/cm². The values given for the pressure are calculated from the thrust on the piston and should be corrected for friction; this correction is not serious.

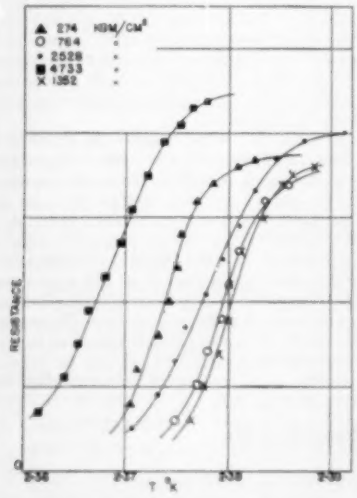

FIG. 1. Electrical resistance *vs* temperature for thallium at different pressures.

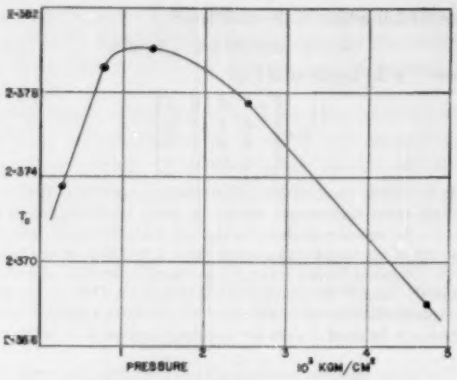

FIG. 2. Superconducting transition temperature of thallium *vs* pressure.

These results account for some of the wide disagreement between hitherto published values of $\partial T_c/\partial P$ for thallium.[2]

In the experiments reported here, the pressure-transmitting medium actually used was solid HD. The results obtained when solid H_2 was used showed a significant difference which we ascribe to the effect of pressure on the *ortho-para* conversion rate in solid H_2. It seems that this conversion rate increases appreciably with pressure, at least up to 2000 kg/cm², but no reliable quantitative data can yet be given.

Similar investigations have been made on a number of other superconductors and a more detailed report will be submitted for publication later.

Thanks are due Mr. Ray Sawyer for his assistance with the measurements.

[1] J. Hatton, Phys. Rev. **100**, 681 (1955).
[2] N. L. Muench, Phys. Rev. **99**, 1814 (1955) gives a convenient summary of published results for thallium.

Exchange Effects in Spin Resonance of Impurity Atoms in Silicon

G. FEHER, R. C. FLETCHER, AND E. A. GERE
Bell Telephone Laboratories, Murray Hill, New Jersey
(Received October 31, 1955)

FLETCHER *et al.*[1] observed in the microwave resonance of donors in silicon weak satellite lines located halfway between pairs of the $2I+1$ main lines. The main lines arise from the hyperfine interaction of the electron with the magnetic moment of the donor atom, while the satellites originally were believed to

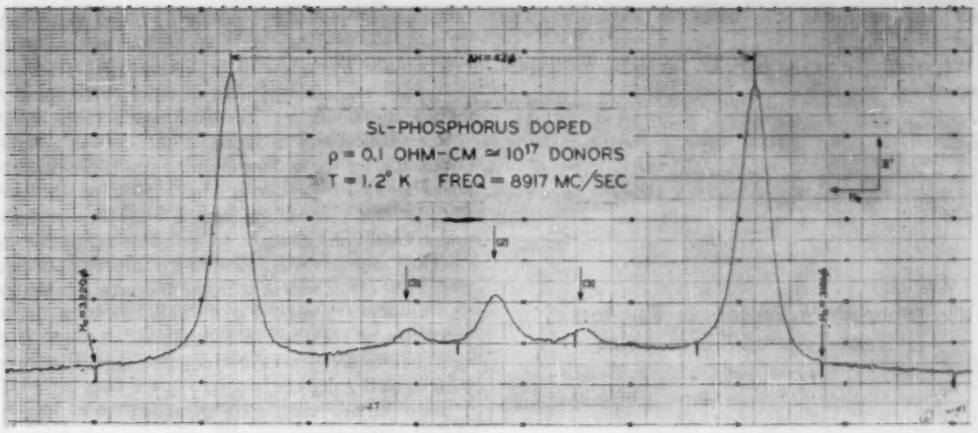

FIG. 1. Electron spin resonance lines in phosphorus-doped silicon under fast-passage conditions. Resistivity of sample 0.1 ohm cm. Small vertical lines are magnetic field markers.

arise from a forbidden transition associated with the simultaneous flip of the electron and nucleus. Slichter[2] suggested that the satellite lines arise from the exchange coupling between two electrons which, acting as a unit, see the average field of the nuclei. The purpose of the present note is to confirm Slichter's theory by reporting the observation of additional lines attributable to an exchange between 2, 3, and 4 electrons.

The samples used were phosphorus-doped silicon with resistivities of 0.1 ohm cm and 0.04 ohm cm, respectively, cut from different crystals. Measurements were made at ~9000 Mc/sec at a temperature of 1.2°K. By the phase unbalance of a microwave bridge, the equipment was made sensitive to the real part of the magnetic susceptibility. Magnetic field modulation, heterodyne microwave detection, and lock-in amplifier were used to record the resonance lines. The results obtained are shown in Fig. 1 and Fig. 2. The 0.1 ohm cm sample clearly shows the lines arising from the exchange between 2 and 3 electrons and the heavier doped 0.04 ohm cm sample between 2, 3, and 4 electrons. The places at which the lines should appear are indicated by the arrows, the numbers in parentheses referring to the number of donors in the cluster. The large background signal may arise from clusters which are larger in size or whose exchange interaction is comparable with the hyperfine interaction.

The electronic relaxation time of the 0.1 ohm cm sample is of the order of seconds and hence the shape is as expected for Bloch's fast-passage case.[3] The 0.04 ohm cm sample had a relaxation time of less than 10^{-5} second and shows the regular slow-passage line shape. The origin of the wide range of relaxation time is now being investigated.

A study of the amplitudes of the various satellites should shed light on the clustering of the atoms and

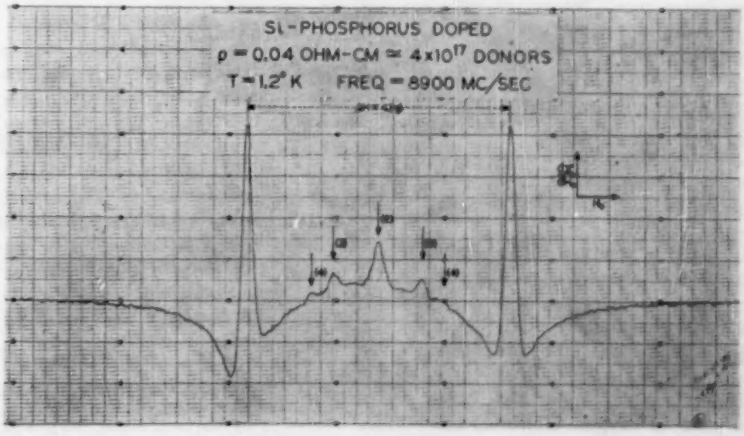

FIG. 2. Electron spin resonance line in phosphorus-doped silicon under slow-passage conditions. Resistivity of sample 0.04 ohm cm.

may help elucidate the onset of impurity band conduction.

We would like to thank P. W. Anderson for helpful discussions.

[1] Fletcher, Yager, Pearson, Holden, Read, and Merritt, Phys. Rev. **94**, 1392 (1954); Fletcher, Yager, Pearson, and Merritt, Phys. Rev. **95**, 844 (1954).
[2] C. P. Slichter, Phys. Rev. **99**, 479 (1955).
[3] F. Bloch, Phys. Rev. **70**, 460 (1946); A. M. Portis, Phys. Rev. **99** (1955).

Thermal Acceptors in Vacuum Heat-Treated Germanium

ROBERT L. HOPKINS AND EDWARD N. CLARKE
Physics Laboratory, Sylvania Electric Products, Inc., Bayside, New York
(Received September 14, 1955)

WE wish to describe an experiment in which it is found that very few acceptor centers are introduced into copper-free germanium by quenching from high temperatures. The result is of interest because the number of acceptor centers found in the present quenched specimens is far smaller than that reported previously for germanium.[1,2] We believe that these new results are obtained because greater care has been taken in maintaining the germanium surface free of impurities.

The bar of single-crystal germanium is heated in vacuum by passing a large alternating current through it, the temperature attained being measured by means of an optical pyrometer. The current leads are tantalum spot-welded to the germanium. Voltage probes are germanium side arms (continuous parts of the crystal) formed during the initial sample shaping procedure. The germanium is quenched from high temperature by shutting off the current and allowing the crystal to cool by radiation. The initial quenching rate of about 170°/sec (from 900°C) is comparable to (but somewhat faster than) Mayburg's radiation quench[2] and probably slower than Logan's oil bath quench.[1] The concentration of quenched-in acceptors is calculated from measured values of conductivity (at 195°K) combined with the mobility data of Prince.[3]

Some typical results are shown in Fig. 1 in which we plot the concentration of quenched-in acceptors as a function of temperature from which the germanium is quenched. Earlier results on copper-free germanium are also indicated.

It should be mentioned that because of the relatively small conductance changes measured in the present experiment, the increase in surface conductance with heating in vacuum as reported by Clarke[4,5] becomes an appreciable fraction of the total conductance change (about 25% for a crystal 0.07 cm in thickness). The increased surface conductance arises, in part, from desorption of oxygen. However, this surface conductance can be reduced to nearly its initial value either by means of readsorption of oxygen or by producing a new surface by means of brief etching.[4,5] This latter procedure was adopted here in order to estimate the surface contribution to the total conductance change.

The smallest concentration of quenched-in acceptors obtained after the surface cleaning procedure described below is 1×10^{13} centers/cm^3 at 894°C as shown on Fig. 1. The germanium sample was then recleaned under conditions thought to be identical to the first cleaning, and this was followed by further heat treatment. The result was an increase in acceptor concentration as shown also on Fig. 1. This lack of reproducibility can be regarded as a strong indication that the quenched-in acceptors correspond to impurities rather than to lattice defects.

Since the new results are thought to arise from the use of germanium samples with less contaminated surfaces, it is desirable to list the detailed handling procedure. After shaping and attachment of the current and voltage leads, the germanium is (1) etched in a solution consisting of 10 parts of HNO_3 conc. ACS and 1 part of HF 48% ACS, (2) rinsed three times in double demineralized water, (3) immersed for 1 hour in 10% KCN (ACS) aqueous solution (double demineralized water) to help remove copper and possibly other metallic ions,[1] (4) rinsed five times in double demineralized water, and finally (5) enclosed and under vacuum within two minutes after the final rinsing. The ger-

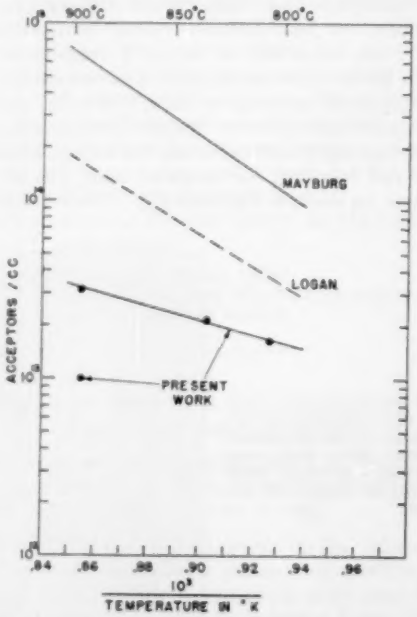

FIG. 1. Concentration of acceptors quenched into germanium after vacuum heat treatment at various temperatures as found by Mayburg, Logan, and present work.

manium is placed into the vacuum system by using a demountable arrangement with a ground glass joint. This avoids glass-blowing procedures which might result in impurities being deposited onto the germanium surface from the hot glass prior to heat treatment studies. The direct Joule heating of the germanium is then carried out in a vacuum of 5×10^{-7} mm Hg with cool walls surrounding the germanium. This provides a method for removing copper[5,6] and possibly other volatile surface impurities.

Since the concentration of quenched-in acceptors appears to be somewhat different after "identical" surface cleaning procedures, we do not feel justified in claiming that the acceptors quenched into germanium in the present experiment are the result of lattice defects. Rather, it is thought that even the acceptor centers here observed may arise from surface impurities which diffuse into the crystal during heating and which might conceivably have been removed with even more refined surface processing and handling. We are therefore led to question the earlier interpretation based upon lattice defects.[2] In view of the present experiment it appears likely that the earlier results may correspond to some unknown impurity not removed from the surface prior to heat treatment.

[1] R. A. Logan, Phys. Rev. **91**, 757 (1953).
[2] S. Mayburg, Phys. Rev. **95**, 38 (1954).
[3] M. B. Prince, Phys. Rev. **92**, 681 (1953).
[4] E. N. Clarke, Sylvania Technologist **7**, 102 (1954).
[5] E. N. Clarke, Phys. Rev. **95**, 284 (1954).
[6] G. Finn, Phys. Rev. **91**, 754 (1953).

Atomic Distribution in Liquid Helium-3*

R. M. Mazo and J. G. Kirkwood
Sterling Chemistry Laboratory, Yale University, New Haven, Connecticut
(Received September 26, 1955)

In a previous paper,[1] the authors have shown how the radial distribution function of a fluid obeying quantum mechanical laws, at a temperature T and molar volume v, can be approximated by the radial distribution function of a classical liquid with the same molar volume, and at a temperature $\tau(T,v)$. $3k\tau/2$ is the mean kinetic energy per molecule of the quantum fluid. We have recently applied this theory to liquid He^3.

The value of τ appropriate to 0°K and the experimental molar volume of He^3 was determined by calculating E, the internal energy as a function of τ, and equating this to the negative of the heat of evaporation at 0°K.[2] τ turned out to be 12.5°K. The radial distribution function, $g(R)$, was calculated from the tables of Kirkwood, Lewinsohn, and Alder.[3] $g(R)$ was Fourier-transformed numerically to give the coherent x-ray scattering factor. The resulting normalized intensity distribution is shown in Fig. 1 together with the corresponding calculated factor for He^4. We do not exhibit $g(R)$ since the scale used for reproduction would not show the difference between He^3 and He^4.

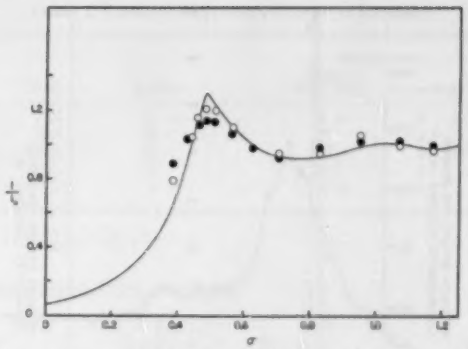

FIG. 1. $I(\theta)/I_0$ *versus* $\sigma=(a/\lambda)\sin\frac{1}{2}\theta$. ○—$He^4$ (calc); ●—He^3 (calc); — He^4 experiment [Gordon, Daunt, and Shaw, Phys. Rev. **96**, 1444 (1954)].

We hope that this communication will stimulate experimental work on the structure of He^3.

We should like to thank Miss Elaine C. Smith for carrying out the numerical integrations for He^3.

* This research was supported by the Office of Naval Research under contract with Yale University.
[1] R. M. Mazo and J. G. Kirkwood, Proc. Natl. Acad. Sci. (U. S.) **41**, 204 (1955).
[2] Abraham, Osborne, and Weinstock, Phys. Rev. **80**, 366 (1950).
[3] Kirkwood, Lewinsohn, and Alder, J. Chem. Phys. **20**, 929 (1955).

Radiation-Induced Amorphism in Diamond*

Paul W. Levy and Otto F. Kammerer
Brookhaven National Laboratory, Upton, New York
(Received October 26, 1955)

DIAMOND may be considered the least stable form of carbon, with graphite and amorphous carbon (lampblack), in this order, more stable. When one irradiates diamond with energetic particles such as are available in a reactor, the radiation damage may occur in several steps. The initial step is the creation of vacancies and interstitials, causing the lattice to be strained which results in an increased lattice parameter. Damage in this stage has been observed by Primak[1] and Wittels.[2] When the damage is more severe, or is concentrated, e.g., along the path of a charged damaging particle or recoil atom, the carbon atoms may rearrange by forming double or even triple bonds. This latter possibility has been dealt with by Dienes and Kleinman,[3] who considered the effects on the elastic constants of bombarded diamond containing regions of damage consisting of double-bonded carbon. In very severely

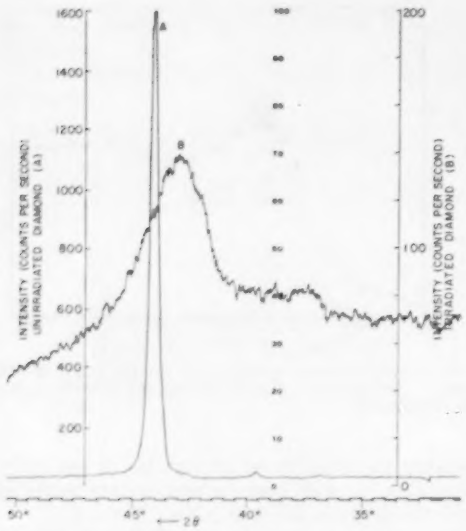

FIG 1. The (111) reflections of (A) normal and (B) severely damaged diamond.

damaged diamond, one may expect to find evidence for amorphous carbon, or perhaps, even graphite.

To search for these possibilities, 270-mesh diamond powder was first annealed at 500°C for two hours, to remove strain, and then irradiated in the Arco materials testing reactor. The total exposure was 2.4×10^{21} *nvt* "thermal" and about 3.8×10^{20} *nvt* "fast." It is estimated that the maximum temperature the sample reached was 65°C. Before irradiation the powder appeared perfectly white, and after irradiation it was shiny black, reminiscent of hardcoal dust. After irradiation, x-ray diffraction patterns of both irradiated and control material were run on a Norelco spectrometer using filtered Cu$-K_\alpha$ radiations. The pattern obtained from the unirradiated material was typical of normal diamond in every respect. In the irradiated sample, the normal reflections no longer appeared. Instead, we found the continuous almost structureless pattern of an amorphous material. Figure 1 shows the spectrometer tracings of the (111) reflection of both samples, and similarly, Fig. 2 is the tracings of the (220) reflections. Only these two reflections appear to be somewhat retained by the damaged material. From the data shown in Fig. 1, one can obtain a rough estimate of the lattice expansion, which is 2.4%. In addition, the damaged crystals contain a fairly definite but broad peak at $2\theta\approx18.5°$ and a much weaker broad peak at $2\theta=20.3°$. At the moment, we do not have a definite explanation for these reflections but they are probably due to hydrated aluminum oxide from the container in which the sample was irradiated. In summary, it can be said that this diamond sample has been damaged to the extent that it is now amorphous. A detailed x-ray study of this material is being made by D. T. Keating and will be published shortly.

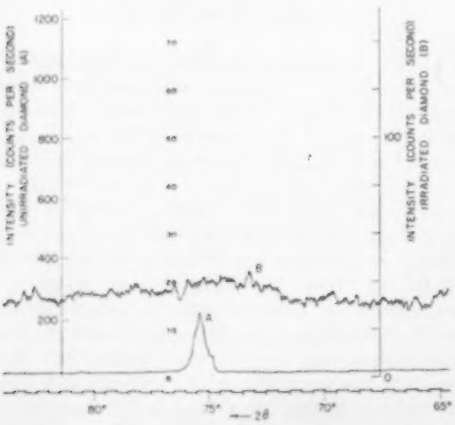

FIG. 2. The (220) reflection of (A) normal and (B) severely damaged diamond.

* Under the auspices of the U. S. Atomic Energy Commission.
[1] Primak, Fuchs, and Day, Phys. Rev. **92**, 1064 (1953).
[2] As described by J. H. Crawford and M. C. Wittels in paper No. 753, presented at the *International Conference for the Peaceful Uses of Atomic Energy* (1955).
[3] G. J. Dienes and D. F. Kleinman, Phys. Rev. **91**, 238 (1953).

Instability in the Motion of Ferromagnets at High Microwave Power Levels

P. W. ANDERSON AND H. SUHL
Bell Telephone Laboratories, Murray Hill, New Jersey
(Received September 22, 1955)

DAMON, Bloembergen, and Wang[1,2] were the first to measure ferromagnetic resonance at high power. Among other phenomena they found a marked broadening and lowering of the resonance line at powers rather low compared to those thought to be necessary for saturation.

We have found that the equations of motion of ferromagnetism lead to a physical instability which probably accounts for this result. Because of the nonlinear effect of the demagnetizing field certain spatially inhomogeneous perturbations tend to grow rather than decay at high enough powers. The simplest case which shows the physical origin of the effect occurs in the disk-shaped sample perpendicular to the dc magnetic field. Suppose there is a small perturbation in the precession angle of a horizontal stratum in this sample. (Figure 1 illustrates the quantities involved in the following.) Then the average moment of the stratum in the z-direction changes by $-\delta M_z$, and because of the demagnetizing effect the effective dc field changes by

$4\pi\delta M_z$. This may bring the stratum closer to resonance than before, increasing thereby the rf permeability, and thus, by the relationship $M_x^2+M_y^2+M_z^2=M_s^2$,[3] causing δM_z to take on a new value $\delta M_z'$. If $\delta M_z'/\delta M_z > 1$, the perturbation will grow indefinitely.

Using for convenience circular polarization and Landau-Lifshitz damping, the equation for M_z' is

$$(M_z')^2 = M_z^2\left(1-\frac{H_{rf}^2}{(H_z^{eff}-\omega/\gamma)^2+(\Delta H)^2}\right)^4. \quad (1)$$

The instability condition $\delta M_z'/\delta M_z > 1$ is equivalent to

$$4\pi M H_{rf}^2\cdot\frac{H_z^{eff}-\omega/\gamma}{[(H_z^{eff}-\omega/\gamma)^2+(\Delta H)^2]^2}\leq -1. \quad (2)$$

This may finally be optimized with respect to $H_z^{eff}-\omega/\gamma$, the deviation from resonance, and we get

$$H_{rf}^2 \geq 3.08(\Delta H)^3/4\pi M \quad (3)$$

at $H_z^{eff}-\omega/\gamma=-\Delta H/\sqrt{3}$. Note that (3) predicts, for a typical 40-oersted half-breadth, that the power required for instability is only of the order 1/30 of saturation power ($H_{rf\ sat}^2=\Delta H^2$). This justifies our use of small-signal theory in (1).

While it is conceptually simple, the horizontal stratum of the disk is unfortunately a poor example, since the disk moving as a whole is itself unstable under the same conditions. However, we have found similar striations to be unstable under similar conditions in all sample shapes we have considered (e.g., the sphere, which moving as a whole is perfectly stable at all times). The most unstable striations even in the disk are not of macroscopic size but so small that the exchange field must be included in their equations of motion. The appropriate wavelength depends on the demagnetizing fields of the sample. These short-wave striations are most unstable at resonance, where instead of (3) we have

$$H_{rf}^2 \geq 2(\Delta H)^3/4\pi M. \quad (3a)$$

Perturbations of various other geometries than striations perpendicular to H_{dc} (e.g., striations in spheres parallel to H_{dc}) are also unstable, but the above is the best case. We have also calculated the growth rate of

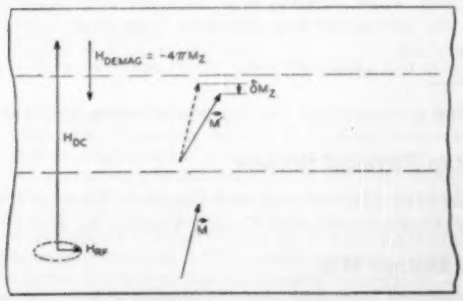

FIG. 1. Perturbed stratum in a disk-shaped sample.

TABLE I. Calculated and observed onset of instability.

		H_{rf} for onset	
T °K	$1/\gamma T_1$[a]	Theory [Eq. (3a)]	Experiment[b]
725	51 oe	8 oe	9
580	46	7	5.5
400	36	5	4
300	23	2.5	1
77	7	0.45	0.55

[a] Reference 2, Fig. 11.
[b] Reference 2, Fig. 8.

these instabilities, which is

$$\lambda=\left[\left(\frac{2P}{P_{crit}}-1\right)^{\frac{1}{4}}-1\right]\frac{1}{T_1}, \quad (4)$$

where P_{crit} is the critical rf power from (3a) and T_1 the relaxation time. Calculations on the new steady state which is established are under way and will be published later.

We have compared (3a) with experiment in the following way. The instability will almost certainly broaden the resonance. We thus compare the minimum rf field from (3a) with the point of onset of broadening from Bloembergen and Wang's figure 8,[2] for their sphere of $NiFe_2O_4$. For ΔH, we use $1/\gamma T_1$ as measured in reference 2 rather than the observed line breadth $1/\gamma T_2$, because $T_1 \neq T_2$ cannot hold for fine-scale phenomena in ferromagnets, so that there must be contributions to $1/T_2$ from inhomogeneities of larger scale than those we consider here. We can only hope that the present phenomenon does not spoil the principle behind the T_1 measurement. Of course, above room temperature the line breadth and T_1 agree, giving us greater confidence in the comparison. The results are shown in Table I. The agreement in both trend and absolute value is gratifying in view of the possible experimental error. (we estimate one-figure accuracy in H_{rf}).[5] One obtains similar results for the Supermalloy data of reference 2; on the other hand, the polycrystalline ferrites seem to be more stable than (3a) predicts.

We have no explanation for the subsidiary low-field absorption peaks observed by Bloembergen *et al.*,[1,2] which may well be an entirely distinct phenomenon. We do feel we have probably explained the early onset of nonlinearity of the main peak.

We should like to acknowledge helpful discussions with A. M. Clogston, L. R. Walker, and H. W. Lewis.

[1] R. W. Damon, Revs. Modern Phys. **25**, 239 (1953).
[2] N. Bloembergen and S. Wang, Phys. Rev. **93**, 72 (1954).
[3] This relationship, while not always satisfied by the Bloch equations used by Bloembergen *et al.* to describe their data, nonetheless is required for the small-scale motions we shall discuss later; otherwise excessive amounts of exchange energy must be supplied.
[4] We have checked our use of small-signal theory to describe nonlinear behavior against the full nonlinear theory in the range of interest.
[5] Further errors of a factor of about $\sqrt{2}$ may enter because the experiments use linear polarization. The difference can hardly be important at this stage.

Errata

Pressure-Volume Isotherms of He^4 below 4.2° K, WILLIAM E. KELLER [Phys. Rev. **97**, 1 (1955)]. During the course of calculations performed in attempting to adjust the reported values of $T_{48}-T_{\text{isotherm}}$ (Table II) in accordance with a "smoothed" table of T_{48} *vs* He^4 vapor pressure,[1] discrepancies appeared which were considerably larger than expected from the "roughness" of the original table used for T_{48}.[2] The source of these discrepancies was traced to the manner in which the measured vapor pressures were reduced to obtain the corresponding temperatures. Originally, all vapor pressures were reduced to mm Hg at 0°C; just before publication, the author became aware that T_{48} is given in terms of mm Hg at 20°C, and attempted to correct for this by adding an amount to $(PV/N)_{\text{corr}}$ (Table I) corresponding to the difference in density of the Hg at the two reference temperatures. It is now clear that this correction should not have been added, since the relation between the raw data of each point and the temperature to which it is normalized has not been changed by the change of reference.

As a consequence of this error, the numerical values for $A=RT$, $T_{48}-T_{\text{isotherm}}$, and $(PV/N)_{\text{corr}}$ require revision. For a given isotherm, a constant quantity, q, is to be added to each $(PV/N)_{\text{corr}}$. Table I lists the correction

TABLE I. Corrections for isotherm measurements.

Isotherm	A	B	C	D	E
$A=RT$, cc-mm/mole	246 693	208 154	178 160	144 595	133 872
$T_{48}-T_{\text{isotherm}}$, °K	0.0052	0.0103	0.0052	0.0054	0.0073
q, cc-mm/mole	−249	−187	−125	−125	−62

quantities. No other data, either raw or derived, are affected by these changes; nor was the type of error mentioned here made in the data for the He^3 isotherms.[3]

The author is indebted to J. R. Clement who initiated the recalculations based on the smoothed T_{48} scale and who has pointed out two typographical errors: (1) for point A-11-2, "$P=116.58$ mm Hg" should read "$P=166.58$ mm Hg" and (2) for point $\alpha-3-1$ in reference 3, "$(PV/N)_{\text{corr}}=129\,979$" should read "$(PV/N)_{\text{corr}}=128\,979$."

[1] Clement, Logan, and Gaffney, Naval Research Laboratory Report NRL-4542, 1955 (unpublished).
[2] H. van Dijk and D. Shoenberg, Nature **164**, 151 (1949).
[3] W. E. Keller, Phys. Rev. **98**, 1571 (1955).

Soluble Problem in the Theory of Coulomb Excitation, L. C. BIEDENHARN AND C. M. CLASS [Phys. Rev. **98**, 691 (1955)]. The sign of the last two terms in Eq. (6) (that is, the two terms involving the cosine of the Coulomb phase shifts) was given incorrectly. The sign of these terms should be *negative*. Figure 2 as presented is therefore also incorrect, and a corrected version of this figure is given below.

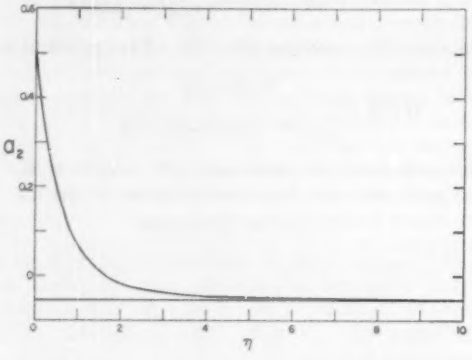

FIG. 2. The particle parameter a_2 *versus* η for no energy loss. The classical limit (solid line) is -0.05425. The intercept at $\eta=0$ is $+0.5002$.

None of the qualitative conclusions of the paper are affected by this change, since the corrected values of the particle parameter a_2 deviate even more markedly from the (corrected) classical limit, as shown in the accompanying figure.

Intermediate Coupling in Odd-Odd Nuclei, R. ADKINS AND J. G. BRENNAN [Phys. Rev. **99**, 706 (1955)]. The last term of Eq. (3) should read "$-\zeta\sum_i \mathbf{l}_i\cdot\mathbf{s}_i$," instead of "$-V_0\zeta\sum_i \mathbf{l}_i\cdot\mathbf{s}_i$." The factor ζ is an energy constant showing the strength of the spin-orbit coupling, and V_0 does not belong.

Electroluminescence of Zinc Sulfide Single Crystals, D. R. FRANKL [Phys. Rev. **100**, 1105 (1955)]. In Fig. 2 the abscissa scale markers are displaced to the left about two divisions from their correct positions.

PHYSICAL REVIEW VOLUME 100, NUMBER 6 DECEMBER 15, 1955

Proceedings of the American Physical Society

ABSTRACTS OF PAPERS TO BE PRESENTED AT THE 1955 WINTER MEETING ON THE PACIFIC COAST AT LOS ANGELES, CALIFORNIA (Corresponding to *Bulletin of the American Physical Society*, Volume 30, No. 8)*

Erratum Pertaining to Abstract M10

M10, by David O. Caldwell and Yash Pal. Line 10 should read "mass. Such mass measurements on a 'negative proton' will be reported."

* The usual preamble to these abstracts and additional errata will be published in the Bulletin early in 1956. Abstracts of meetings in 1956 and subsequent years will not be published in *The Physical Review*.

PROGRAMME

WEDNESDAY MORNING AT 10:00

133 Founders Hall

(J. R. RICHARDSON, presiding)

Invited Papers on High-Energy Physics

A1. Nuclear Reactions and Element Synthesis in Stars. W. A. FOWLER, *California Institute of Technology.* (30 min.)

A2. Pion Production by the Inelastic Scattering of Electrons in Hydrogen. G. B. YODH, *Stanford University.* (30 min.)

A3. π-p, p-p, and n-p Collisions at Bevatron Energies. W. M. POWELL, *University of California.* (30 min.)

A4. Nucleon-Nucleon Interactions. A. M. THORNDIKE, *Brookhaven National Laboratory.* (30 min.)

WEDNESDAY MORNING AT 10:30

129 Founders Hall

(W. D. HERSHBERGER, presiding)

Solid State I

B1. The Significance of Nuclear Spin Echo Experiments for the Foundation of Statistical Mechanics. JEROME ROTHSTEIN, *Signal Corps Engineering Laboratories.*—We have shown the essential identity of the entropy of information theory and statistical[1] or thermodynamical[2] entropy, and characterized reversible processes as those in which information is conserved, irreversible as those in which information is lost.[2] The Wieder- or Umkehreinwand is then valid if information storage (memory) is possible, invalid otherwise. Boltzmann's statistical argument, replacing the kinetic H-theorem proof criticized by Loschmidt and Zermelo, implicitly admits information loss. Spin echo experiments[3] demonstrate that memory permits reversibility, with irreversibility following loss of stored information. More generally, a kind of "phase coherence" (classical or quantal) corresponds to reversibility, incoherence to irreversibility. For spin echoes, phase memory is carried in Larmor precession of the spins; for inhomogeneous magnetic field Brownian motion is the chief memory destroyer, masking others like spin-spin and spin-lattice interactions. With latter negligible and perfectly homogeneous field, or with memory and retracing of complete dynamical trajectories, entropy increase of spin system would be prevented with resulting reversibility.

[1] J. Rothstein, Science **114**, 171 (1951).
[2] J. Rothstein, Phys. Rev. **85**, 135 (1952).
[3] E. L. Hahn, Phys. Rev. **80**, 580 (1950), Phys. Today **6**, 4 (Nov. 1953).

B2. Ferrimagnetic Interaction and Remanence in Cobalt Carbonate. WARREN E. HENRY, *U. S. Naval Research Laboratory.*—Magnetization studies have been carried out for $CoCO_3$ in strong magnetic fields and at low temperatures to investigate the nature of interactions therein. A ballistic, sample motion method[1] has been used to perform the magnetic measurements in magnetic fields up to 60 000 gauss and at temperatures down to 1.3°K. Cobalt carbonate exhibits ferrimagnetic interaction, has a transition temperature at about 10°K and a moment at 60 000 gauss and 1.3°K of about 0.05 Bohr magneton per atom of cobalt. When the remanence is plotted against the temperature, there seems to be a change in the sign of $(\partial^2 M/\partial T^2)$ at about 3°K. An analysis of the interaction is made in terms of departures[2] from the Brillouin function and in terms of theories[3] of Van Vleck, of Néel, of Gorter, and of Yaffet and Kittel. The observation of ferrimagnetism is also interpreted on the basis of predictions that could be made from recent high-temperature susceptibility measurements of Bizette.[4]

[1] W. E. Henry, Phys. Rev. **88**, 559 (1952).
[2] E. Henry Phys. Rev. **94**, 1146 (1954).
[3] J. H. Van Vleck, J. phys. radium **12**, 262 (1951); Revs. Modern Phys. **25**, 220 (1953); L. Néel, Proc. Roy. Soc. (London) **A65**, 869 (1952); C. J. Gorter, Physica **18**, 861 (1952); Y. Yaffet and C. Kittel, Phys. Rev. **87**, 290 (1952).
[4] H. Bizette, Compt. rend. **241**, 546 (1955).

B3. Frequency Doubling in Ferrites. W. P. AYRES, P. H. VARTANIAN, AND J. L. MELCHOR, *Electronic Defense Laboratory of Sylvania Electric Products Inc.**—The torque equation for the motion of the magnetization in a magnetized ferrite yields a component along the direction of the applied dc magnetic field. The time dependent part of this component is of second order in rf quantities and has previously been neglected. With high incident powers an observable double-frequency output is predicted. A high intensity microwave magnetic field and an orthogonal dc magnetic field were applied to a ferrite body. Double frequency magnetic fields were generated in the same direction as the dc magnetizing field. A primary frequency of 3175 mc was used with peak powers up to 200 watts. The peak output power at 6350 mc was found to increase linearly with the square of the peak input power over a range of 50 db. Reasonable agreement was found between theory and experiment.

* This work was performed under a Signal Corps Contract.

B4. Energy Band Calculations in f.c.c. Thorium.* G. W. LEHMAN, *North American Aviation, Inc.*—The lowest energy bands of face-centered cubic thorium have been worked out along the (001), (011), and (111) directions in

the Brillouin zone using a simplified variational approach originally developed by Kohn.[1] Using the Thomas-Fermi model, it was found that the 5*f* and 6*d* bands form the low-lying states corresponding to the observed lattice spacing. From this model, the 7*s* and 7*p* states lie several electron volts above the Fermi level and have been neglected. The trial wave functions used in the variational calculation were taken as linear combinations of Cubic Harmonics and radial wave functions computed for an energy lying between the two- and threefold degenerate *d* states at the center of the Brillouin zone. (A more general procedure has been used by Jenkins and Pincherle.[2]) This approximation has the general formal character of Slater's LCAO method where all but nearest neighbor interactions are neglected. The 12 x 12 secular determinant, resulting from the variational approximation, factors along symmetry lines according to the group theoretical results of Bouchaert, Smoluchowski, and Wigner. The energy contours are being used to calculate a density of states curve in f.c.c. thorium.

[1] W. Kohn, Phys. Rev. **87**, 472 (1952).
[2] D. P. Jenkins and L. Pincherle, Phil. Mag. **45**, 93 (1954).
* This work performed under Contract for the U. S. Atomic Energy Commission.

B5. Quadrupole Broadening of NMR Lines by Reversible Axial Stress. R. G. SHULMAN, B. J. WYLUDA, AND H. J. HROSTOWSKI, *Bell Telephone Laboratories.*—Nuclear electric quadrupole moments interact with electric field gradients at the nucleus. In a perfect cubic crystal $\nabla \cdot \mathcal{E} = 0$, and there are no quadrupolar interactions. Watkins and Pound[1] have shown that in alkali halides internal strains destroy the spherical symmetry of the electric field. Nuclear magnetic resonance[2] studies of the semiconductors InSb and GaSb have revealed no quadrupolar interactions in our samples indicating a high degree of crystalline perfection. By applying axial stresses to these crystals, we have been able to destroy the crystalline symmetry reversibly, thereby producing quadrupole broadening of the nuclear magnetic resonance lines. In InSb the application of 500 lb/in.[2] along the <110> axis reduced the intensity of the In^{115} resonance by 11% and increased the second moment by 30%. This corresponds to $e^2qQ \sim 45$ kc under these conditions.

[1] G. D. Watkins and R. V. Pound, Phys. Rev. **89** 658 (1953).
[2] Shulman, Mays, and McCall, Phys. Rev. **98**, 1182 (1955).

B6. Quadrupole Polarization of Charge-Clouds in Ions.* T. P. DAS AND R. BERSOHN, *Department of Chemistry, Cornell University.*—A variational method has been developed for calculating the quadrupole polarization of charge clouds of ions. This method obviates the step by step numerical integration of the relevant Schrödinger equation as adopted by Foley, Sternheimer, and Tycko.[1] The form of the variation function for the perturbation of the electronic wave function by an external charge at distance r is taken as

$$u_1 = u_0 r^2 (3\cos^2\theta -) P(r),$$

where $P(r)$ is a polynomial in r containing adjustable parameters. Preliminary calculations for the radial $2p \rightarrow p$ excitations in Na^+ and Al^{+++} give values of γ_∞ of -5.2 and -3.1, respectively. The value -5.2 for Na^+ is reasonably close to Sternheimer's[2] value of -4.56. A brief discussion of the method will be given and the complete values of γ_∞ for Na^+ and Al^{+++} will be reported.

* This work was supported by the U. S. Atomic Energy Commission.
[1] Foley, Sternheimer, and Tycko, Phys. Rev. **93**, 734 (1954).
[2] R. M. Sternheimer (private communication).

B7. Magnetic Resonance Demonstration of Charge Transfer in Iron Group Fluorides. M. TINKHAM,* *Clarendon Laboratory, Oxford.*—The paramagnetic resonance spectra of iron group fluorides highly diluted with ZnF_2 have been studied. In the cases of Mn^{++}, Co^{++}, and Fe^{++}, viewed along principal axes, each line of the normal spectrum is found to be split into 15 "super-hyperfine structure" components by the interaction of the magnetic electrons with the nuclei of the surrounding F ions. The coupling constants are 10–20 gauss, depending on the cation, the neighbor involved, and the angle. The large magnitude of the effect requires that the orbitals of the magnetic electrons be modified by attaching orbitals centered about the F nuclei. It is then deduced that the dominant interaction occurs through attached *s*-orbitals about the F ions. The anisotropy comes from the direct dipolar interaction with the central magnetic ion and from attached p-orbitals. In terms of admixtures, their seems to be roughly equal amounts of fluorine s, p_σ, and p_π orbitals, the admixtures being of the order of 1% of each type on each center. This picture receives striking support from the *absence* of resolvable structure in the case of Cr^{+++}, which has no magnetic electrons in σ-bonding orbitals and hence can not attach the *s*-functions needed to give the dominant interaction.

* National Science Foundation Postdoctoral Fellow; now at University of California, Berkeley.

B8. Electron Spin Resonance of Defect Centers in Magnesium Oxide.* JOHN E. WERTZ AND JUANA L. VIVO, *University of Minnesota.*—Attempts to find electron spin resonance (ESR) absorption by imperfection centers in MgO were complicated by the multiplet spectra of impurities. After a detailed study, we found one line which disappears on heating in vacuum. The splitting factor g is 2.003 along a principal axis, and the corresponding line width is 4.2 gauss, twelve-fold narrower than for KCl. This line and an absorption band at 2600 A which disappears on heating in vacuum, are presumably the result of excess oxygen. Heating in air at 600°C increases the intensity of the ESR line. Tentatively it is assumed that the ESR centers are O^- ions, although experiments[1] on oxygen uptake at higher temperatures would indicate that at 600° the process would be very slow. Exposure to x-rays after annealing gives an ESR line of similar g-value and width, which decays slowly.

* Supported in part by the Air Force Office of Scientific Research.
[1] B. V. Haxby (unpublished results).

WEDNESDAY MORNING AT 10:30

226 Founders Hall

(C. C. LAURITSEN, presiding)

Nuclear Physics

C1. Isotope Shift in the Spectra of Hg^{198}–Hg^{200}. FRED MCCLUNG AND JOHN R. HOLMES, *University of Southern California.*—By using separated isotopes, direct measurements of the shift have been made on several lines. A direct recording system using electronic detection, photomultiplier tube or PbS cell, and recording on a strip chart recorder,

is used. High resolution is obtained from a Fabry-Perot interferometer, which is scanned by varying the air pressure between the plates, and is crossed with a grating. The light from each discharge tube is alternately directed into the interferometer while scanning, providing a direct measurement of the shift without overlapping of the lines of the two sources. Because of the type of recording, probable errors are small. Preliminary results are

Wavelength (A)	$\nu^{198}-\nu^{198}$ cm^{-1}
5769.6	−0.0052
5460.7	0.0594±0.0005
4916.0	0.013 ±0.001
4358.3	0.0576±0.0004
4046.5	0.0557

The spacers used were 4.60, 4.59, and 13.50 cm. Other lines are under study.

C2. Obtaining High Temperatures for Nuclear Fusion. R. E. Vollrath and J. A. R. Samson, *University of Southern California.*—The possibility of reaching extremely high temperatures in a limited amount of a gas is being explored. The so-called "pinch effect" first noted by Northrup in 1907 in connection with liquid conductors may make it possible to heat a volumn of gas by means of an electrical discharge and at the same time confine it to a thin column out of contact with any walls. Such a contraction occurs as the result of the interaction of the current in the discharge with its own magnetic field. We have noted the beginning of such a contraction in a toroidal discharge tube containing hydrogen and excited by pulsed discharges. The tube encircles one leg of a closed Hypersil transformer core. The other leg of the core is encircled by a single turn of copper ribbon through which a 150-μf capacitor at 5000 v is discharged. Currents of 5000 amp are obtained through hydrogen at 1-mm pressure and lower. The discharge was initiated with ease at these low pressures by aid of photoelectric emission from a thin film of caesium deposited inside the tube.

C3. A Neutron Dosimeter with Uniform Sensitivity from 0.1 to 3.0 Mev.* J. De Pangher and W. C. Roesch, *General Electric Company.*—The dose rate sensitivity of a moderated BF_3 counter was investigated as a function of moderator thickness and neutron energy. Neutrons were obtained with a 2.0-Mev Van de Graaff accelerator and from a PoB source. The dose rate was calculated by the first-collision theory of neutron dose from flux measurements made with a long counter. For cylindrical moderators with axes perpendicular to the neutron beam and for a given neutron energy, the dose rate sensitivity increased with moderator thickness, reached a maximum, and decreased. These sensitivity curves, for three energies investigated, intersected in the region beyond the maximum at 4.5 in. of paraffin. A cylindrical paraffin moderator 12 in. long and with a 4.5-in. wall was constructed to enclose a brass BF_3 counter 1 in. in diameter with a sensitive region 7 in. long. This dosimeter showed a sensitivity constant to within 10% from 0.1 to 3.0 Mev.

* This paper describes in part, work conducted under Contract between the General Electric Company and the U. S. Atomic Energy Commission.

C4. Nonelastic Cross Sections at 14 Mev.* M. H. MacGregor, William P. Ball, and Rex Booth, *University of California, Livermore.*—The 14-Mev neutron beam from the Livermore Cockcroft-Walton Accelerator was used to measure nonelastic cross sections by means of the sphere transmission technique. Automatic equipment was built which removes and replaces the sphere and records data at four detector biases simultaneously. Table I gives uncorrected cross-section data in barns.

Table I.

Neutron bias (Mev)				
Be	0.79	0.66	0.56	0.44
C	0.77	0.68	0.59	0.47
Mg	1.12	1.01	0.94	0.85
Al	1.12	1.03	0.96	0.88
Fe	1.43	1.38	1.33	1.25
Ni	1.45	1.40	1.36	1.31
Cu	1.59	1.52	1.48	1.41
Sn	1.96	1.92	1.87	1.80
Sb	2.03	1.96	1.89	1.82
Pb	2.65	2.59	2.52	2.45

Approximate corrections for multiple scattering and elastic energy loss will be discussed.

* This work was performed under the auspices of the U. S. Atomic Energy Commission.

C5. Neutron Yields from 32-Mev Protons on Thick Targets.* George P. Millburn, Burton J. Moyer, Yuin-Kwei Tai, and Selig N. Kaplan, *University of California, Berkeley.*—The yield of neutrons from 32-Mev protons bombarding thick targets (greater than a range) have been measured for 59 elements and compounds. The neutrons were detected by capturing them in a $MnSO_4$ solution surrounding the target and counting the resulting Mn^{56} activity with immersion Geiger counters. The detection system was calibrated against a standard Ra-α-Be source. The yields for light elements varied from 18.1×10^{10} for Be to 0.60×10^{10} for C (in neutrons per μcoulomb). The yield increased abruptly by a factor of 2 at two places, near $Z=20$ and $Z=30$. A sharp dip was found at Ni; yields were Co, 7.7×10^{10}; Ni, 3.1×10^{10}; Cu, 8.5×10^{10}. The yield from neighboring odd-even and even-even nuclei for $Z<30$ fluctuated by about 20%. U gave the highest yield measured, 22×10^{10}, but elements near Pb had a lower yield (10×10^{10}) than elements for $Z=46$ to 74 (13×10^{10}). The yields were analyzed in terms of the average number of neutrons emitted per nuclear interaction, averaged over energy from 0 to 32 Mev.

* This work was performed under the auspices of the U. S. Atomic Energy Commission.

C6. Double-Channel Magnetic Beta-Ray Spectrometer for Short-Lived Activities.* C. R. Sun and Byron T. Wright, *University of California, Los Angeles.*—A semicircular beta-ray spectrometer has been developed for studying proton-induced activities with half-lives as short as tenths of seconds and end-point energies to 12 Mev. At a given magnetic field, beta particles of different momenta are focused at distances of twelve and eight inches from the source. This double channel arrangement provides a means of normalization which is superior to that of using a monitor counter near the source in those cases in which there are gamma rays from secondary activities. The choice of the detector positions has been optimized. The slit system is adjustable. At the present setting, the resolution for each channel is 1.7% and the transmissions for the 12-in. and 8-in. channels are 0.052% and 0.076%. Targets, after being irradiated in the cyclotron beam, can be transferred to the source position within 0.2 second through a 16-foot pneumatic tube.

* This work was partially supported by the joint program of the Office of Naval Research and the U. S. Atomic Energy Commission.

C7. Preparation of Thin N^{14} Targets.* F. B. Hagedorn, *California Institute of Technology.*—Difficulties in preparing thin nitrogen targets, both stable and sufficiently free from carbon and oxygen contamination, has delayed a detailed investigation of the elastic scattering of protons from nitrogen. At least a partial solution to this problem has been found. A 20-kev mass-28 nitrogen ion beam was collected in

beryllium. The targets thus prepared were bombarded with the proton beam from an electrostatic accelerator. Magnetic analysis of the elastically scattered protons indicates that the nitrogen layer is about 2 kev thick for 1.7-Mev protons and that the ratio of nitrogen to carbon and oxygen is about 5:1. Reducing the carbon and oxygen contamination to the present level has involved using freshly evaporated beryllium as a collector and keeping the collection chamber at a pressure of 10^{-6} mm. Further reduction of this contamination appears extremely difficult. This type of target has not decomposed either under bombardment or from exposure to the atmosphere for as long as a month. Nitrogen ions driven into tantalum have also proven to be exceptionally stable targets. This technique is now being investigated for other nuclei. Preliminary work in preparing 90% enriched N^{15} targets has been successful.

* Assisted by the joint program of the Office of Naval Research and the U. S. Atomic Energy Commission.

C8. Half-Life of Sn^{110}.* S. W. MEAD, M. D. PETROFF, AND W. O. DOGGETT, *University of California, Berkeley* (introduced by A. C. Helmholz).—A half-life of 4.0±0.2 hours has been tentatively assigned to Sn^{110}. A target containing enriched Cd^{110} was bombarded with 32-Mev alphas in the 60-inch cyclotron. After separation of indium, sources were prepared from the tin fraction and were observed with a crystal spectrometer and a magnetic lens spectrometer. The 670-kev γ ray in the decay of In^{110} was observed to grow with a half-life of approximately 1 hour followed by a 4-hour decay. A γ ray of 285 kev, identified with the decay of In^{108} by McGinnis,[1] was also followed in the spectrometer. Readings were begun half an hour after chemical separation. Since no growth was observed and the decay half-life was, within experimental error, the same as that of the 670-kev line, it appears that the 285-kev line might be properly identified with an excited state of In^{110} formed in the Sn^{110} decay. Further investigations are in progress in an attempt to clarify this situation.

* This work was done under the auspices of the U. S. Atomic Energy Commission.
[1] C. L. McGinnis, Phys. Rev. **81**, 734 (1951).

C9. Inelastic Scattering of Protons from Li^7, C^{13}, Mg^{24}, and Si^{28}.* HOMER E. CONZETT, *University of California, Berkeley*.—Thin targets of Li, polystyrene, Mg, and SiO were bombarded with 12-Mev protons, and differential cross sections were measured on proton groups identified with the 4.65-Mev level in Li^7, the 4.43 in C^{12}, the 1.368 in Mg^{24}, and the 1.78 in Si^{28}. The Li distribution shows a maximum near 12° (c.m.), a minimum at 106°, and a secondary maximum at 125°, with approximate relative cross sections of 2.7, 1.0, and 1.1, respectively. The C and Mg data are significantly different from those found at 10 Mev.[1] At 12 Mev, on C a maximum appears near 10°, a minimum at 95°, and a maximum at 160°, with relative cross sections of approximately 6.1, 1.0, and 3.1. The Mg distribution shows a sharp rise forward of 20°, continuing to 8°, the smallest angle at which a measurement was possible. Minima appear at 50° and 115°, maxima at 85° and 140°. The Si distribution has maxima at 20° and 165°, a minimum at 120°. These angular distributions will be compared with those predicted by theory.

* This work was done under the auspices of the U. S. Atomic Energy Commission.
[1] G. E. Fischer, Phys. Rev. **96**, 704 (1954).

C10. Internal Conversion Coefficients of Low Excited States of F^{19}.† W. R. MILLS, JR.,* H. H. HILTON, III, AND C. A. BARNES,‡ *California Institute of Technology*.—A magnetic lens spectrometer has been used to measure the internal conversion electron yield of the first and second excited states of F^{19} produced by $F^{19}(p,p')F^{19*}$. A NaI(Tl) crystal was used to obtain the γ-ray yields. Correcting for the theoretical K to L ratio, and the anisotropy of the 197-kev state, we obtained $\alpha_K(109)=(2.10\pm0.45)\times10^{-3}$, $\alpha_K(.197)=(1.91\pm0.60)\times10^{-3}$. These compare with the theoretical values as follows:

	α_K(experimental)/α_K(theoretical)			
	E1	*M1*	*E2*	*M2*
109	1.14±0.24	2.89±0.62	0.089±0.019	0.282±0.060
197	6.84±2.1	10.8 ±3.4	0.888±0.28	1.79 ±0.56

Hence the assignment of *E*1 to the 109-kev state and *E*2 to the 197-kev state is consistent with $J=1/2^-$ for the 109-kev state and $J=5/2^+$ for the 197-kev state.

* Now at General Electric Company, Schenectady, New York.
† Assisted by the joint program of the Office of Naval Research and the U. S. Atomic Energy Commission.
‡ Now at University of British Columbia, Vancouver, B. C., Canada.

C11. Elastic Scattering of Protons at 9.9 Mev.* NORTON M. HINTZ, *University of Minnesota*.—Using 9.89-Mev protons from the first stage of the Minnesota linear accelerator, a program of elastic scattering has been initiated. The proton beam is deflected into a 24-in. diameter scattering chamber with a rotatable lid to support the detector assembly. Either solid or gas targets may be used. A NaI detector (~3% energy resolution) with conventional electronics is used. The angular resolution is approximately ±1.5°. Points were taken at 5° intervals; generally from 15° to 165°. Data will be presented for Be,[1] N, A, Al, Ni,[2] Sn, and Au. The general features of the angular distributions are similar to the data at 22 Mev[3] in that the light element cross sections oscillate above coulomb at the back angles and the heavy elements oscillate below. The cross section for gold is Coulombic out to 170°.

* Supported in part by the U. S. Atomic Energy Commission.
[1] Unpublished data of S. W. Rasmussen.
[2] Unpublished data of M. K. Brussel.
[3] B. L. Cohen and R. V. Neidigh, Phys. Rev. **93**, 282 (1954).

WEDNESDAY AFTERNOON AT 2:00

133 Founders Hall

(J. W. M. DUMOND, presiding)

Invited Papers Sponsored by the Division of Electron Physics

D1. Modern Trends in the Interaction of Electron Beams with High-Frequency Fields. L. M. FIELD, *Hughes Aircraft*. (30 min.)

D2. Some Experiments in Field and Ion Emission. R. GOMER, *University of Chicago*. (30 min.)

D3. The Dissociation of Solid Compounds by Electron Impact. G. E. MOORE, *Bell Telephone Laboratories*. (30 min.)

D4. Some Electronic Effects of Germanium Containing Double Acceptor Impurities. H. H. WOODBURY, *General Electric Research Laboratory*. (30 min.)

WEDNESDAY AFTERNOON AT 2:00

129 Founders Hall

(R. F. CHRISTY, presiding)

Invited Papers in Theoretical Physics

E1. The Optical Model of the Nucleus. D. S. SAXON, *University of California, Los Angeles.* (25 min.)

E2. Causality and Scattering. M. GELL-MANN, *California Institute of Technology.* (25 min.)

E3. The Interactions of Electrons and Nucleons. D. R. YENNIE, *Stanford University.* (25 min.)

E4. Numerical Calculations of Stellar Evolution. L. G. HENYEY, *Radiation Laboratory, Livermore Site, University of California.* (25 min.)

E5. Velocity Dependence of the Nuclear Potential. E. TELLER, *University of California, Berkeley.* (20 min.)

THURSDAY MORNING AT 9:30

133 Founders Hall

(W. A. FOWLER, presiding)

Shell Structure and Nuclear Physics

Invited Papers

F1. Some Current Problems in Collective Nuclear Models. B. A. JACOBSOHN, *University of Washington.* (30 min.)

F2. Origin of Nuclear Moments of Inertia. D. R. INGLIS, *Argonne National Laboratory.* (30 min.)

Nuclear Structure

F3. Low-Lying Level Structure of the Zn^{65} Nucleus.* J. B. MARION† AND R. A. CHAPMAN, *The Rice Institute.*—Sulfur and beryllium samples have been used as energy-selective neutron absorbers to investigate the low-lying level structure of the Zn^{65} nucleus. The transmission through the samples of the neutrons from the $Cu^{65}(p,n)Zn^{65}$ reaction was measured as a function of the proton energy and the known resonances in the neutron total cross sections of S and Be were observed for both the neutron group leaving Zn^{65} in the ground state and for a group leaving Zn^{65} in an excited state at 118±8 kev. This excited state is probably identical with that from which γ radiation has been observed[1] in the Ga^{65} decay. At a proton energy of 2.9 Mev, the two neutron groups are of approximately the same intensity. The Q-value for the $Cu^{65}(p,n)Zn^{65}$ reaction was found to be -2.131 ± 0.005 Mev. The 585-kev resonance in S was observed with neutrons from the $V^{51}(p,n)Cr^{51}$ reaction and the threshold energy of 1.566 Mev for this reaction was confirmed.

* Supported in part by the U. S. Atomic Energy Commission.
† Now at Kellogg Radiation Laboratory, California Institute of Technology, Pasadena, California.
[1] B. Crasemann, Phys. Rev. **98**, 1034 (1954).

F4. Excited States of Ge^{72}.* E. BRUN, W. E. MEYERHOF, AND J. J. KRAUSHAAR, *Stanford University.*—The decay of 14-hour Ga^{72} has been studied[1] and more recently also that of 26-hour As^{72} in order to obtain information on the excited states of Ge^{72}. The 0.3-μsec isomeric state[2] has been found to be the first excited state at 0.69 Mev, with spin zero and even parity. The second and third excited states are at 0.84 and 1.46 Mev and have been assigned spin two and even parity. The gamma rays feeding the isomeric state have been determined by delayed coincidence experiments, and originate primarily at a new level at 2.39 Mev. Decay schemes of both Ga^{72} and As^{72} will be presented. Possible reasons for the exceptional spin of the first excited state of Ge^{72} will be discussed.

* Supported in part by the joint program of the Office of Naval Research and U. S. Atomic Energy Commission.
[1] Kraushaar, Brun, and Meyerhof (to be published in Phys. Rev.)
[2] Bowe, Goldhaber, Hill, Meyerhof, and Sala, Phys. Rev. **73**, 1219 (1948).

F5. Differential Cross Sections for the Scattering of Charged Particles by Beryllium.* R. G. SUMMERS-GILL,† *University of California, Berkeley.*—A beryllium target has been bombarded with 12-Mev protons, 24-Mev deuterons, and 48-Mev alpha particles. With the three projectiles the differential cross sections for inelastic scattering leading to the formation of the 2.43-Mev state have been measured. Their magnitude and forward peaking indicate that compound nucleus formation plays a minor role. Application of inelastic scattering theory[1] leads to the assignment 1/2, 3/2, or 5/2 and even parity for this level. A very weak inelastic proton group has been found confirming the recently reported level in Be^9 at ~1.8 Mev. The cross section for the formation of this state is about 1/100 that for the formation of the 2.43-Mev state. The differential cross section for the pickup reaction $Be^9(p,d)Be^8$ has also been measured. This angular distribution agrees favorably with that obtained from the Butler theory of stripping and the known ground states involved.

* This work was performed under the auspices of the U. S. Atomic Energy Commission.
† National Research Council of Canada Special Scholar.
[1] Huby and Newns, Phil. Mag. **42**, 1442 (1951); Austern, Butler, and McManus, Phys. Rev. **92**, 350 (1953).

F6. Nuclear Spin and Magnetic Moment of 54-min In^{116m}.* L. S. GOODMAN AND S. WEXLER, *Argonne National Laboratory.*—The nuclear spin, magnetic moment, and the sign of the magnetic moment of 54-min In^{116m} have been determined by the atomic beam magnetic resonance method.[1,2] The values found are $I=5\hbar$ and $\mu=4.4$n.m. Multiple quantum transitions[3] were observed in resonances of the inactive In^{115} used for the calibration of the magnetic fields. Some properties of these transitions and the limitation in accuracy of the determination of the nuclear magnetic moment of In^{116m} introduced by their presence will be discussed.

* Work performed under the auspices of the U. S. Atomic Energy Commission.
[1] J. R. Zacharias, Phys. Rev. **61**, 270 (1942).
[2] L. Goodman and S. Wexler, Phys. Rev. **99**, 192 (1955).
[3] P. Kusch, Phys. Rev. **93**, 1022 (1954).

F7. 15-Mev Gamma Radiation from B^{11}+d.† C. A. BARNES* AND R. W. KAVANAGH, *California Institute of Technology.*—Several investigators have reported observation of 15.1-Mev γ radiation in C^{13} via $Be^9(\alpha,n)$, $B^{10}(He^3,p)$, $B^{11}(d,n)$, $C^{13}(p,p')$, and $C^{12}(n,n')$. Using a 4 in. x 4 in. NaI(Tl) crystal, we have measured the cross section for the reaction $B^{11}(d,n)C^{12*}(\gamma)C^{12}$ from threshold at $E_d=1.633$ ±0.003 Mev to 3.26 Mev. The thin target yield curve exhibits a sharp decrease in slope at $E_d=2.18\pm0.01$ Mev, thereafter remaining fairly constant except for a weak resonance ($\gamma\sim175$ kev) at 3.07 Mev. The cross section at $E_d=2.18$ Mev is 17±5 mb. Using magnetic analysis at 60°, attempts to detect α particles from C^{12*} to Be^8 and Be^{8*} gave negative results; assuming isotropy, we estimate $\Gamma_\alpha/\Gamma_\gamma<5$. The 15.1-Mev state in C^{13} presumably being the analog of the B^{13} ground state, the branching of the B^{13} β decay was examined. γ rays of 4.4 Mev were found in coincidence with 1.3±0.4% of the β transitions, indicating $J=1^+$ for B^{13}. β coincidences with 3.2-Mev γ rays were not present for more than 0.2% of total decays, nor for more than 0.2% with 7.6-Mev γ rays.

* Present address: University of British Columbia, Vancouver, B. C., Canada.
† Assisted by the Office of Naval Research and the U. S. Atomic Energy Commission.

F8. Nuclear Compressibility and the O^+ States of Oxygen-Sixteen and Carbon-Twelve.* R. A. FERRELL AND W. M. VISSCHER, *University of Maryland.*—The anomalously large β-decay ft-value of C^{14} can be accounted for by an accidental cancellation in the matrix element.[1] O^{14} is a member of the same isotopic spin triplet as C^{14} and its β-decay ft-value should be the same, except for Coulomb effects. Actually, the O^{14} ft-value is fifty times smaller,[2] which can be naturally accounted for by a 6% greater size due to the repulsive effect of the two additional protons. This changes the ground-state wave function so that the cancellation is no longer nearly complete. Employing harmonic oscillator wave functions, we have evaluated the Coulomb force producing the size increase and thus have determined the nuclear compressibility. A straightforward calculation of the radial modes of oscillation of the O^{16} and C^{12} nuclei then yields O^+ excited levels at 6.97 Mev and 8.20 Mev, as compared experimentally with 6.06 Mev and 7.65 Mev, respectively. Considering the limitations of the model, the agreement is satisfactory.

* Research supported by the Office of Naval Research.
[1] B. Jancovici and I. Talmi, Phys. Rev. **95**, 289 (1954), and a paper by the present authors (submitted to *The Physical Review*).
[2] J. B. Gerhart, Phys. Rev. **95**, 288 (1954).

F9. An Anomaly in Nuclear Energy Level Density Measurements.* G. IGO AND H. E. WEGNER, *Brookhaven National Laboratory.*—An analysis has been made of nuclear reactions which proceed through a compound nucleus mechanism and in which the nuclei are excited into the continuum. In the interpretation of these reactions, which determine the dependence of the level density on excitation energy and upon atomic number, one uses the level density of a degenerate Fermi gas, const $\exp[2(aE)^{\frac{1}{2}}]$, where E is the energy of excitation. When inelastic scattering and reaction experiments are corrected for contributions from noncompound nucleus processes, the quantity a determined from the corrected spectrum increases monotonically with atomic number. This is in agreement with the predictions of the Fermi gas model[1] and is compatible with the dependence on atomic weight of the neutron spectroscopy level density measurements at approximately 8 Mev. On the other hand, the value of a determined from excitation function experiments and from (α,p) reactions at 40 Mev, corrected for noncompound nucleus processes, shows an anomalous behavior. The quantity a is constant, independent of atomic number, and an order of magnitude smaller than in the former group.

* Work performed under the auspices of the U. S. Atomic Energy Commission.
[1] Lang and LeCouteur, Proc. Phys. Soc. (London) **A67**, 586 (1954).

THURSDAY MORNING AT 10:30

229 Founders Hall

(C. H. ECKART, presiding)

Invited Papers on Physical Oceanography

G1. Heat Flow through the Ocean Bottom. R. REVELLE, *Scripps Institution of Oceanography.* (30 min.)

G2. General Circulation of the Ocean. C. O'D. ISELIN, *Woods Hole Oceanographical Institution.* (30 min.)

G3. Earthquake Waves as a Tool for Exploring Ocean Basins. M. EWING, *Lamont Geological Observatory, Columbia University.* (30 min.)

THURSDAY MORNING AT 10:30

129 Founders Hall

(E. W. COWAN, presiding)

High-Energy Physics

H1. Analysis of Nuclear Emulsion Tracks by Scattering Measurements. JOHN S. URBAN AND JOHN J. MCCLURE, *University of Oklahoma.*—A technique will be described for analyzing tracks in nuclear emulsions which makes use of only an arbitrary section of track. Such a technique is particularly useful when the particle has left the emulsion or decayed in its flight. From scattering measurements only, the mass of a particle and its residual range may be found. The equation for the second difference due to scattering as a function of residual range is well known. A graphical method of obtaining approximate values of two constants which appear in the equation leads to an evaluation of these constants by method of successive approximations involving least squares. One of these constants yields the mass of the particle and the other its residual range.

H2. High-Velocity Particle Ranges in Emulsion.* WALTER H. BARKAS, PAUL H. BARRETT, PIERRE CUER, HARRY H. HECKMAN, FRANCES M. SMITH, AND HAROLD K. TICHO, *University of California, Berkeley.*—The range-velocity relations for all stopping materials are at present considered unreliable at high particle velocities because of recent evidence[1] that the mean ionization potentials are seriously in error. The situation is particularly intolerable for nuclear track emulsion, because important questions regarding the masses and decay schemes of K particles and hyperons depend on accurate energy determinations from the measured ranges of secondaries. A complication in emulsion is that for this material the density must be determined before the material is specified adequately. We have exposed emulsion blocks of accurately measured density to pions and protons for which the momentum is known to about 1 part in 1000. The momentum is measured by 180-degree bending in a magnetic field. Several points on the range curve at equivalent proton energies of up to 800 Mev have been measured to a precision of better than one percent. More ranges are being measured in an effort to reduce the statistical error.

* This work was performed under the auspices of the U. S. Atomic Energy Commission.
[1] D. O. Caldwell, Nuovo cimento **2**, 183 (1955); L. Vigneron, J. phys. radium **14**, 145 (1953).

H3. A Strange Cosmic-Ray Event. C. H. SKEEN AND W. Z. OSBORNE, *University of Oklahoma.*—A strange event has been found in a small stack of Ilford G-5, 400 micron pellicles that was exposed to the cosmic radiation at 93 000 ft.* This event consists of a track which emanates from a star and subsequently "splits" into two tracks. Measurements reveal that the three tracks are coplanar in the neighborhood of their intersection. Mass and energy estimates have been made for the various particles involved. Various interpretations of the event consistent with the above measurements are considered, the most plausible of which seems to be that a doubly charged, heavy, unstable particle or fragment was emitted from the star and then decayed in flight into two singly charged particles. Further measurements are now being made.

* Exposed at San Angelo, Texas (41° N geomagnetic latitude) on January 18, 1955 by courtesy of the Office of Naval Research Project "Skyhook."

H4. Cloud-Chamber Observations of μ-Meson Induced Electron Showers.* C. A. ROUSE, *California Institute of Technology.*—During 1476 hours of operation of a magnet-cloud chamber with proportional counter control, 31 pictures were obtained in which electron showers of 40 or more particles were produced in a 5 cm lead absorber by cosmic-ray μ mesons at Pasadena. Of the 31 events, 7 had 100 or more electrons. The cross section per lead nucleus for the production of showers of 40 or more electrons emerging from 5 cm of lead is 3.8×10^{-28} cm^2 and for showers of more than 100 electrons is 2.6×10^{-29} cm^2. These values are in agreement with theoretical cross sections obtained by numerical integration of the knock-on and bremsstrahlung cross sections[1] for μ mesons of spin 1/2 together with the use of cascade shower curves.[2] These cross sections were obtained from direct observations of the showers and have the advantage over previous ionization chamber measurements that no effects of stars and air showers are included.

* Assisted by the joint program of the Office of Naval Research and U. S. Atomic Energy Commission. Reproduction in whole or in part is permitted for any purpose of the United States Government.
[1] R. F. Christy and S. Kusaka, Phys. Rev. **59**, 405, 414 (1941).
[2] B. Rossi and K. Greisen, Revs. Modern Phys. **13**, 240 (1941).

H5. Elastic Scattering of Electrons by Li^6 and Li^7.* J. F. STREIB,† *Stanford University.*—Using techniques developed in this laboratory,[1] the elastic scattering of electrons by Li^6 and Li^7 has been studied,[2] with emphasis on the comparison of their cross sections. With high resolution, the inelastic scattering by the 0.477-Mev state of Li^7 appears as a broadening of the main scattering peak, and its small contribution (~10%) is determined by comparison with the Li^6 peak. At 187 Mev, $\sigma_1/\sigma_0=\rho$ varies smoothly from 1.00 (35°) to 1.17 (80°). The magnetic contribution to ρ is estimated from the values $\rho(187\text{ Mev}, 65°)=1.07$ and $\rho(117\text{ Mev}, 118°)=1.12$; the two conditions involve equal momentum transfers; a crude interpretation of Rosenbluth's formula[3] indicates that the effect adds 2% at 80° and less at smaller angles. For both isotopes the angular distribution at 187 Mev indicates a charge distribution between the uniform and the Gaussian, with a rms radius $(2.38\pm0.05)\times10^{-13}$ cm, the ratio of rms radii being $r_7/r_6=0.99\pm0.01$.

* Supported by the Office of Naval Research and the U. S. Atomic Energy Commission, and by the U. S. Air Force through the Office of Scientific Research.
† On leave of absence from the University of Washington. Appointment supported by the National Science Foundation.
[1] Hofstadter, Fechter, and McIntyre, Phys. Rev. **91**, 422 (1953); Phys. Rev. **92**, 978 (1953); Hofstadter, Hahn, Knudsen, and McIntyre, Phys. Rev. **95**, 512 (1954); J. H. Fregeau and R. Hofstadter, Phys. Rev. **99**, 1503 (1955).
[2] Li^6 target courtesy of Oak Ridge National Laboratory.
[3] M. N. Rosenbluth, Phys. Rev. **79**, 615 (1950).

H6. Inelastic Electron Scattering by Carbon.* D. G. RAVENHALL, *Stanford University.*—The experimental results of Fregeau and Hofstadter on the scattering of 187-Mev electrons by Carbon[1] contain differential cross sections for both elastic and inelastic processes. The former can be related to the charge distribution of the nucleus in its ground state, and the latter are associated with nuclear excitation, in this case to each of the first three levels, at 4.43, 7.68, and 9.61 Mev. The spins and parities of the first two levels are known to be 2^+ and 0^+ respectively, and the experimental

results relating to these levels and to the ground state are in qualitative agreement with the predictions of the shell model. In this paper a discussion will be given of the excitation to the 9.61-Mev level, and of the information it gives concerning the spin and parity of this level. Further experiments which could assist in giving an unambiguous assignment will also be discussed.

* Supported by the Air Force through the Office of Scientific Research.
[1] J. H. Fregeau and R. Hofstadter, Phys. Rev. **99**, 1503 (1955).

H7. Z-Dependence of Bremsstrahlung in the Case of Complete Screening.* K. L. Brown, *Stanford University.*—The relative yield of bremsstrahlung produced by Cu, Ta, and U for incident electrons of energy 500 Mev is being measured using the reaction $\gamma+p\rightarrow\pi^{+}+n$ as the photon detector. The π^{+} mesons are detected by observing the positrons from the $\pi\rightarrow\mu\rightarrow e$ decay as used by Crowe and others in previous experiments.[1] The π^{+} mesons are selected in both energy and angle. Therefore, from the kinematics of the reaction, only photons in the energy range 235±12 Mev are detected. The tentative results to date are consistent with a deviation from the Bethe-Heitler bremsstrahlung theory of $-(2.0\pm0.6)\times10^{-4}$ Z^2 percent. This result is in good qualitative agreement with the previously observed experimental deviations from the Bethe-Heitler pair-production theory at high energies.[2]

* Supported by the joint program of the Office of Naval Research and the U. S. Atomic Energy Commission.
[1] Crowe, Friedman, and Motz (in preparation).
[2] For a summary of these results, see Davies, Bethe, and Maximon, Phys. Rev. **93**, 788 (1954).

Thursday Afternoon at 1:00

129 Founders Hall

(R. L. Walker, presiding)

π Mesons

I1. π^{+} Photomeson Production from Various Nuclei at 135°.* William Imhof, V. Perez-Mendez, and H. Easterday,† *University of California, Berkeley, and Livermore.*—Cross sections for the photoproduction of positive pions by the 335-Mev bremsstrahlung of the Berkeley synchrotron from various elements were measured at an angle of 135° to the beam. The elements bombarded were polyethylene, lithium, beryllium, boron, carbon, aluminum, copper, silver, and lead. The pions were identified in a telescope consisting of four plastic scintillators by the π-μ decay method.[1] The relative π^{+} yields for these elements were measured at five different pion energies, ranging from 21 Mev to 65 Mev. At 65 Mev the relative yield per proton in the target nucleus showed an approximate $A^{-1/3}$ dependence agreeing within statistics with the work of Littauer and Walker.[2] Little variation in the relative cross sections at different pion energies was seen except for a drop-off in the relative yield from the high-Z elements at the lower energies (probably resulting from effects of the nuclear Coulomb potential).

* This work was done under the auspices of the U. S. Atomic Energy Commission.
† Now at the University of Oregon.
[1] Jakobson, Schuls, and Steinberger, Phys. Rev. **81**, 894 (1951).
[2] Littauer and Walker, Phys. Rev. **86**, 838 (1952).

I2. Neutral Pion Production in Proton-Proton Collisions.* Robert K. Squire and Burton J. Moyer, *University of California, Berkeley.*—The characteristics of the production of neutral mesons in proton-proton collisions near threshold has been studied. The external beam of the Berkeley synchrocyclotron was allowed to bombard a liquid-hydrogen target and the high-energy gamma rays arising from the creation and decay of π^{0} mesons were detected with a counter telescope. Four independent experiments, consisting of three bombarding energies at one angle, and one energy at two angles, allowed a separation of the production contributions from the various angular-momentum states that can occur. The excitation function is composed of two terms: σ (millibarns)$=(0.02\pm0.01)\eta_0^2+(0.57\pm0.11)\eta_0^5$, where η_0 is the maximum meson momentum in units of μc. The angular distribution is

$$\frac{d\sigma}{d\Omega}=\frac{1}{4\pi}(0.02\pm0.01)\eta_0^2+\frac{3}{4\pi}(0.57\pm0.11)\eta_0^5\cos^2\theta.$$

It appears from this work that the production of π^{0} mesons occurs principally in the P-state, accompanied by two nucleons in a P-state relative to each other, down to energies about 15 Mev above threshold, at which energy this production equals the production in S-states.

* This work was performed under the auspices of the U. S. Atomic Energy Commission.

I3. High-Energy Pion-Proton Cross Sections.* Baxter H. Armstrong, *University of California, Berkeley.*—The pion-proton cross sections have been analyzed phenomenologically into a superposition of hard-sphere elastic scattering, and resonance reaction and scattering contributions. The analysis was made in terms of the isotopic spin 1/2 and 3/2 cross sections, a fit to current experimental data being obtained for the $\pi^{+}p$ (or $T=3/2$) case to about 1900 Mev, and for the $\pi^{-}p$ case of 1100 Mev. The superposition obtained was, for the $T=1/2$ cross section, the sum of elastic hard-sphere scattering in the $j=3/2$, $L=2$ state and a pure elastic resonance (reduced width 5 Mev) interfering with elastic hard-sphere scattering in the $j=5/2$, $L=2$ state. The $T=3/2$ cross section was the sum of the well-known $j=3/2$, $L=1$ resonance, hard-sphere scattering in the $j=5/2$, $L=3$ state, and a pure resonance (no hard-sphere scattering) with both reaction and elastic contributions in the $j=7/2$, $L=3$ state. The positions of these resonances were 1180 Mev (incident pion lab energy) for the $T=1/2$ and 1200 Mev for the $T=3/2$ state. The total reduced width in the latter case was 7 Mev. The same hard-sphere radius of 1.22×10^{-13}cm was used throughout.

* This work was done under the auspices of the U. S. Atomic Energy Commission.

I4. Yield of π^{0} Photomesons as a Function of Atomic Number.* J. D. Anderson, R. W. Kenney, and C. A.

McDONALD, *University of California, Berkeley.*—With a single gamma counter[1] at 135° to the incident photon beam, the relative yields of π^0 mesons per nucleon were observed for Be, C, Al, Ti, Fe, Cu, Ag, and Pb. The yields were observed as a function of the maximum energy of the bremsstrahlung beam from the 340-Mev Berkeley Synchrotron. The beam was monitored with a Cornell-type thick-walled ionization chamber. The root-mean-square counting errors at 340 Mev were less than 3% on all targets. The targets were designed to have the same absorption for 100-Mev gamma rays. The full energy curve is within the counting statistics of Panofsky's[2] data normalized to carbon. For $A \gtrsim 27$ the yield per nucleon goes as $A^{-1/3}$. For $A \lesssim 27$ the production was approximately constant and is not within statistics of an $A^{-1/3}$ dependence. The data at other energies (E_{max}=270, 200, and 170 Mev) are within statistics (~20%) of the 340-Mev data and are compatible with a mean free path for reabsorption of 1 to 3 r_0.

* This work was done under the auspices of the U. S. Atomic Energy Commission.

[1] Cocconi and Silverman, Phys. Rev. **88**, 1230 (1952).
[2] Steinberger, Panofsky, and Steller, Phys. Rev. **86**, 180 (1952).

I5. Inelastic Cross Sections for 5-Bev π^- Bevatron Beam in Lead and Aluminum.* JOHN ISE, JR., ANDRE LAGARRIGUE (*Ecole Polytechnique, Paris*), AND ROBERT V. PYLE, *University of California, Berkeley.*—A multiplate expansion cloud chamber, 20 by 16 by 5 inches has been used to obtain the inelastic or absorption cross section for the high-energy π^- beam from the bevatron, in lead and aluminum. Neglecting scattering angles less than 1° the cross sections for lead and aluminum are 1.71±0.13 and 0.40±0.04 barn, respectively. Comparison of these results with cosmic-ray and other measurements will be made.

* This work was done under the auspices of the U. S. Atomic Energy Commission.

I6. Pi Meson Production in Lead and Carbon.* M. ABRAHAM AND S. J. GOLDSACK, *University of California, Berkeley* (introduced by R. B. Brode).—Nuclear emulsion pellicles were flown at about 93 000 feet for eight hours.† Semicircular bands of lead and carbon of approximately equal mass were arranged so that π mesons coming from the right were identified as originating in the carbon, while π's from the left originated in the lead. Assuming that the production of π's is proportional to the geometrical cross sections and that the multiplicity is the same, the ratio of π's from the carbon to π's from lead was calculated to be 2.6. Of the 46 stopping π's observed in the scanning now in progress, the directions of 25 are from the carbon and 21 from the lead. This data indicates that the assumption of equal multiplicity of production in lead and carbon is not valid.

* Assisted by the joint program of the Office of Naval Research and the U. S. Atomic Energy Commission.
† We are indebted to the Office of Naval Research "Operation Skyhook" for their assistance.

I7. Photoproduction of Neutral Pions from Protons at Forward Pion Angles.* W. S. McDONALD AND VINCENT PETERSON, *California Institute of Technology*, AND DALE R. CORSON, *Cornell University.*—Low-energy recoil protons from the process $\gamma+p \rightarrow p+\pi^0$, detected by nuclear emulsions placed within the hydrogen gas target container, have been used to measure the differential cross section. The entering angle and range of protons stopping in a tilted C-2 600-micron emulsion are measured, and from these data the incident photon energy and pion angle can be determined. In this manner protons of energies as low as 5 Mev can be detected at laboratory angles corresponding to emission of a pion at center-of-mass angles as low as 26°. This experiment thus supplements that of Walker and Oakley which covers the same range of photon energies (200-500 Mev), but is restricted to pion angles greater than about 70° resulting from higher minimum detectable proton energy. Common experimental points provide intercomparison of absolute values. The data at lower photon energies may also be compared to the results of the M.I.T. and Illinois groups. The effect of the present results upon the angular distributions and total cross sections deduced from previous data will be presented and discussed. In particular, the measurement in the forward hemisphere provides a sensitive check on the value of B in the angular distribution $A+B\cos\theta+C\cos^2\theta$.

* Research supported by the U. S. Atomic Energy Commission.

I8. Pion Pair Photoproduction.* R. M. FRIEDMAN AND K. M. CROWE, *Stanford University.*—A π^- signal has been observed by bombarding liquid hydrogen with the bremsstrahlung spectrum from 575-Mev electrons with a 2:1 signal:noise ratio. The π^-/π^+ ratio of H relative to C was measured at a 60° laboratory angle for various pion energies by delayed coincidences described elsewhere.[1] Using π^+ photoproduction data,[2] the π^- differential cross section was (in units of millimicrobarn/sterad/Mev/equivalent quantum): 4.6±0.9, 4.4±0.8, 3.2±0.5, 2.1±0.4 at pion energies of 20±10, 34±10, 50±10, and 68±10 Mev, respectively. In addition to statistics, the errors quoted include uncertainties in the C ratio, π^+ cross section, and increase in π^+ yield due to pairs. Uncertainties in energy and subtracted background could alter the absolute cross section by an additional 20%. Checks made at 68±10 Mev pion energy are: (1) signal with meson-deflecting magnet off was ≤16% of the π^- signal; (2) cross sections measured at 400, 495, and 575-Mev primary electron beam energies were 0.3±0.3, 0.3±0.3, and 2.1±0.4, respectively, in the above units.

* Supported by the joint program of the Office of Naval Research and the U. S. Atomic Energy Commission.
[1] Crowe, Friedman, and Motz, Bull. Am. Phys. Soc. **29**, No. 8, L3 (1954).
[2] Walker, Teasdale, Peterson, and Vette, Phys. Rev. **99**, 210 (1955).

I9. π^+ Photoproduction Ratio of Deuterium to Hydrogen.* K. M. CROWE, R. M. FRIEDMAN, AND D. C. HAGERMAN,† *Stanford University.*—The ratio of the π^+ photoproduction cross section for D to H has been measured at five laboratory angles for (60±10) Mev pions. C, CH_2, and CD_2 targets were irradiated with the bremsstrahlung spectrum produced by 350-Mev electrons from the Stanford linear accelerator. The counting arrangement has been described elsewhere.[1] The measured ratios are 0.92±0.04, 0.88±0.05, 0.86±0.07, 0.85±0.04, and 0.89±0.07 at laboratory angles of 30°, 45°, 60°, 75°, and 90°, respectively. On the basis of calculations[2] of meson production from deuterons using an impulse approximation and splitting the interaction Hamiltonian into spin-flip and non-spin-flip terms, the results would indicate a predominantly spin-flip interaction. Attempts are being made to compare the results to the phenomenological theory of π^+ photoproduction of Gell-Mann and Watson.[3]

* Supported by the joint program of the Office of Naval Research and the U. S. Atomic Energy Commission.
† Now at the Los Alamos Scientific Laboratory.
[1] Crowe, Friedman, and Motz, Bull. Am. Phys. Soc. **29**, No. 8, Abstract L3 (1954).
[2] G. F. Chew and H. W. Lewis, Phys. Rev. **84**, 779 (1951); M. Lax and H. Feshbach, Phys. Rev. **88**, 509 (1952).
[3] M. Gell-Mann and K. M. Watson, Ann. Revs. Nuclear Sci. **4**, 219 (1954).

THURSDAY AFTERNOON AT 1:00

226 Founders Hall

(A. BAÑOS, presiding)

General Physics

J1. Townsend's First Ionization Coefficient in Nitrogen.* MELVIN A. HARRISON, *Seattle Pacific College.*—Measurements of Townsend's first ionization coefficient have been made in nitrogen for values of E/p from 24 to 82. Sodium azide was used as a nitrogen source in an effort to obtain pure nitrogen. Data were also taken in tank nitrogen and mass spectrographic analysis of gas from both sources was made. No impurities were detectable in the sodium azide produced gas, while the tank nitrogen was found to contain some contamination even after a purification process. Results at low values of E/p differ considerably from previously reported data,[1] while at high values the results agree very well with data obtained by Bowls.[1] Values of α/p in tank nitrogen were found to be considerably lower at low E/p than those found in gas produced from sodium azide, although at high values the difference was small. The effect of wall potential on α/p was investigated and was found to be unimportant over a range from 50% to 100% of anode potential.

* Supported by a grant from the Research Corporation.
[1] For references see L. B. Loeb, *Basic Processes of Gaseous Electronics* (University of California Press, Berkeley).

J2. Absorption of Vacuum Ultraviolet Radiation by Thin Plastic Films. G. L. WEISSLER AND L. Z. MAUDLIN, *University of Southern California.*—The absorption coefficients of thin Formvar and collodion films have been determined photometrically between 600 A and 1600 A. Both materials exhibited continuous absorption which rose to a flat maximum at about 1050 A and then decreased towards shorter wavelengths. Collodion showed about twice the value of the absorption coefficient, k, at this maximum than Formvar, with $k_c=6.4\times10^{-6}$ cm^{-1} and $k_F=3.9\times10^{-6}$ cm^{-1} respectively. In nylon and polystyrene, qualitatively only, the absorption was still greater.

J3. Temperature Anomalies in the Properties of Liquid Water. W. DROST-HANSEN AND H. W. NEILL, *New Mexico Institute of Mining and Technology.*—The temperature dependence of a number of properties of aqueous solutions and pure water has been studied using data from the literature. Solubilities of approximately 200 substances have been plotted as a function of temperature. Avoiding unnecessary smoothing it has been found that more or less abrupt changes in solubility occur at one or more of the following temperatures: 15°, 30°, 45°, and 60°C, all within a few degrees. A number of properties of dilute and concentrated aqueous solutions (activity coefficients, transference numbers, ionization constants, and reaction rates) seem to possess similar anomalies, and pure water appears also to exhibit these characteristics (index of refraction, viscosity, vapor pressure, specific heat, ultrasonic absorption). The existence of these anomalies reveal an intrinsic property of liquid water, and a discussion of this will be given in the light of Eucken's polymer model for water and Bjerrum's dipole-dipole structures. The relation between the "two states" model, suggested by Hall to explain the ultrasonic absorption in liquid water, and the ideas presented above will be discussed.

J4. Dependence of the Discrete Acoustic Frequencies Emitted by a Jet on Vortex-Ring Coalescence at Reynolds Numbers up to 7000. A. B. C. ANDERSON (introduced by G. J. Plain).—Visualization of the vortex flow pattern in typical jets emitting jet-tones was made by means of shadowgraph techniques to show the nature of the ever-present process of vortex coalescence in the jet and how this determines the values of the eigentone sound frequencies radiated by the jet. These frequencies are superimposed on the noise background radiated by the jet. The dependence of (a) vortex shedding frequency from the orifice, (b) jet-tone frequencies, and (c) translational velocity of the vortices on Reynolds (Re) number is shown. These studies were carried out with carbon dioxide jets discharging into the atmosphere. The flow channel geometry consisted of an orific plate containing a sharp-edged, circular orifice, 0.250 in. in diameter and 0.093 in. thick attached to a large stilling tank partly filled with sound-absorbing material to eliminate any effects of cavity resonances on the jet. The studies were carried out over the range from Re zero to Re 7000 where $\mathrm{Re}=v\rho t/\mu$ where v is mean velocity of discharge of jet; ρ, gas density; t, orifice plate thickness, and μ, gas viscosity.

J5. Projectile Penetration into Sand. EARLE B. MAYFIELD, HARVEY L. MORRISON, AND WILLIAM A. ALLEN, *U. S. Naval Ordnance Test Station.*—When a projectile penetrates with velocity v into granular material such as sand, its negative acceleration is predicted by Poncelet's[1] equation, $-dv/dt=\alpha v^2+\beta$, where the parameters α and β are constants. Prior theoretical[2] effort has been based solely upon knowledge of experimental determination of maximum depth of penetration. A new approach has been made in which projectile arrival times have been measured at several spatial stations in sand. When the projectile breaks a fine grid wire embedded in the medium, the bias is removed from a thyratron and a condenser discharges through a neon bulb to produce a light pulse which is photographed with a sweeping-film camera. Several rounds of a cylindrical steel 0.50-cal projectile 1½-in. in length have been fired from a rifled barrel at about 2800 ft/sec into quartz sand of 1-mm grain size and specific gravity 1.64. Poncelet's equation with the value $\alpha=0.0564\pm0.0015$ represents, within experimental uncertainty, the dynamical behavior of the projectile during the first 40 cm of penetration. Penetration subsequent to this depth is anomalous.

[1] J. V. Poncelet, Mém. acad. sci. **15**, 55 (1829).
[2] Marguerite M. Rogers, Phys. Rev. **99**, 1632 (1955).

J6. Phase Transformations in the Microstructure of Explosively Loaded Iron and Steel. E. W. LAROCCA (introduced by G. J. Plain).—By subjecting annealed low carbon steel and commercially pure iron to explosive loadings, structures resembling martensite are induced in the materials. The structure, which is of a Widmanstatten form, is most noticeable in Armco iron. X-ray diffraction studies show no residual phases other than alpha iron present after impulsive loading, but the microstructure indicates a phase change has occurred (locally) with alpha iron reforming along the octahedral planes of the gamma phase.

J7. Deformation Zones Produced by Explosive Shocks in Ferrous Metals. SAMUEL KATZ, *Stanford Research In-*

stitute.—Collision of explosive-induced shocks in ferrous metals produces characteristic deformation zones. In low and medium carbon steels these zones are narrow regions of intense twinning, with sharp boundaries outside of which less than 10% of the grains are twinned, and with a narrow central strip (0.1 mm) of decreased twin density. These observations suggest the existence of a minimum stress and impulse required for this twinning transformation. For collision at normal incidence a preferred twin orientation parallel to the collision plane is observed. Twin-free regions symmetrically oriented with respect to the collision zone may be explained by an untwinning mechanism. The shock velocity of 5 mm/μsec determined from these experiments[1] is independent of the heat treatment and carbon content (0.01–0.4% C), and suggests that these collision zones are associated with the phase transformation in iron at 131 kb reported by Minshall.[2] This and the observed dependence of collision zone width on explosive and specimen thickness lead to attenuation estimates. Comparable loading of stainless steel specimens (Types 304 and 310) transforms the collision region to martensite, as indicated by a marked increase in permeability.

[1] S. Katz, Phys. Rev. **98**, 256(A) (1955).
[2] S. Minshall, Phys. Rev. **98**, 271(A) (1955).

J8. Free Surface Motion Due to Obliquely Incident Shock Waves. J. O. Erkman, *Stanford Research Institute.*—The problem is considered of a uniform shock obliquely incident on the free surface of a solid or a liquid for which an isentropic equation of state is known. As the shock progresses along the surface, the pressure is relieved by a rarefaction fan which is centered at the intersection of the shock and the surface. The velocity and direction of the resulting flow may be calculated on the basis of the hydrodynamic theory as a function of the angle of incidence of the shock and the shock strength. Results of such calculations for iron, aluminum, and water will be presented. Failure of this simple flow pattern occurs when the velocity behind the incident shock becomes sonic. If the angle of incidence and the flow can be observed by using high speed photography techniques, the calculations may be compared directly with experiments. Such observations for water are discussed.

J9. Normal Modes Characterizing Magneto-Elastic Plane Waves. Alfredo Baños, Jr., *University of California, Los Angeles.*—In an earlier paper we presented the general theory of Alfvén waves in an ideal, unbounded, homogeneous and isotropic, conducting fluid embedded in a constant and uniform field of magnetic induction. The techniques employed there have now been extended to the study of homogeneous magneto-elastic plane waves in an unbounded conducting solid, which is fully characterized by its Lame moduli and by the rigorously constant macroscopic parameters μ, ϵ, and σ. It is found that, in the presence of the magnetic field, the medium sustains five distinct modes of propagation as already pointed out by Knopoff. The first two are *pure shear* waves, one of which is a slightly attenuated shear mode with phase velocity modified anisotropically by the presence of Alfvén's phase velocity, and the other is a highly attenuated modified electromagnetic wave (modified by the presence of the phase velocity of shear waves). The remaining three are *shear-compression* waves, except in certain preferred directions which are discussed. The three modes in question can be characterized by saying that one mode exhibits a phase velocity intermediate between the phase velocities of shear waves and compressional waves, the second mode has a phase velocity which exceeds that of compressional waves, and the last mode is again a modified electromagnetic wave.

Thursday Afternoon at 2:45

133 Founders Hall

(E. M. McMillan, presiding)

Invited Papers on the Anti-Proton

K1. Properties of the Anti-Proton. E. Segrè, *University of California, Berkeley.* (20 min.)
K2. Mass Determination of the Anti-Proton. C. Wiegand, *Radiation Laboratory, University of California.* (30 min.)
K3. The Velocity-Selecting Čerenkov Counter. O. Chamberlain, *University of California, Berkeley.* (20 min.)
K4. Observations on Negative Particles of Protonic-Mass Stopping in a Čerenkov Counter. J. J. Murray, *Radiation Laboratory, University of California.* (10 min.)
K5. Theoretical Background of the Anti-Proton. R. Serber, *Columbia University.* (30 min.)

Thursday Evening at 8:00

Roger Young Auditorium

(R. T. Birge, presiding)

Banquet of the American Physical Society

Address of Welcome: F. D. Fagg, Jr.
After-Dinner Speech: L. A. DuBridge, "Physicists Wanted"

FRIDAY MORNING AT 9:30

133 Founders Hall

(S. SIEGEL, presiding)

Invited Papers Sponsored by the Division of Solid-State Physics

L1. Electronic Structure of the Heaviest Metals. D. B. BOWEN, *North American Aviation.* (30 min.)

L2. Developments in Crystal Growth (with movies). J. C. FISHER, *General Electric Research Laboratory.* (30 min.)

L3. Recent Developments in Transistor Physics. W. SHOCKLEY, *Beckman Instruments, Inc.* (30 min.)

L4. Normal Fluid Excitation in Liquid He ii. J. R. PELLAM, *California Institute of Technology.* (30 min.)

L5. Remarks on the Problem of Superconductivity. R. P. FEYNMAN, *California Institute of Technology.* (30 min.)

FRIDAY MORNING AT 10:00

129 Founders Hall

(H. K. TICHO, presiding)

K-Mesons, etc.

M1. Proton-Proton Interactions at 5.3 Bev.* ROBERT W. WRIGHT, GEORGE SAPHIR,† WILSON M. POWELL, GEORGE MAENCHEN, AND WILLIAM B. FOWLER, *University of California, Berkeley.*—The cloud-chamber study of the interaction with protons of negative pions[1] and neutrons[2] at Bevatron energies has been extended to include proton-proton interactions. A 36-atmosphere hydrogen-filled diffusion cloud chamber operating in a pulsed magnetic field of 21 500 gauss is being exposed to a 5.3-Bev scattered proton beam from the Bevatron. Thirty-nine events have been obtained to date. Of these, six are elastic scatters, fourteen are inelastic scatters with two charged outgoing prongs, 16 have four charged outgoing prongs, two have six charged outgoing prongs, and one event has two charged outgoing prongs and an associated Λ^0. Thirty-one of these events, which occurred in a well-defined projected area in the cloud chamber, give 29.5±5.5 mb for the proton-proton total cross section at 5.3 Bev. The standard error is nearly all from statistical uncertainty.

* This work was done under the auspices of the U. S. Atomic Energy Commission.

† Also at the University of San Francisco.

[1] Maenchen, Powell, Saphir, and Wright, Phys. Rev. **99**, 1619 (1955).

[2] Fowler, Maenchen, Powell, Saphir, and Wright, Phys. Rev. (to be published).

M2. Production of Unstable Particles in 4.5-Bev π^--p Collisions.* GEORGE MAENCHEN, WILLIAM B. FOWLER, WILSON M. POWELL, GEORGE SAPHIR,† AND ROBERT W. WRIGHT, *University of California, Berkeley.*—A 36-atmosphere hydrogen-filled diffusion cloud chamber was exposed to the 4.5-Bev negative pion beam from the Bevatron. Three events involving the production and subsequent decay of heavy unstable particles have been observed. In two of these events only one decay was seen. One of these is a Λ^0 which is produced together with a positive particle that appears, from its momentum and relative ionization, to be a K-meson. Another event contains two charged outgoing particles and a θ^0. The pions from the θ^0 can be measured quite well and yield a Q-value of 222.2±7.0 Mev. The third event is interpreted as the associated production of a θ^0 and a positive unstable particle, both of which decay before leaving the chamber. Visual estimates of the relative ionization of the positive particle and its proper time of flight of 1 to 2×10^{-10} sec favor its interpretation as a Σ^+ rather than a K^+. The decay product of this particle cannot be identified.

* This work was done under the auspices of the U. S. Atomic Energy Commission.

† Also at the University of San Francisco.

M3. Masses of Positive K-Particles. I. Identification of K-Particles and Analysis of Secondaries. FRANCES M. SMITH, HARRY H. HECKMAN, AND WALTER H. BARKAS, *University of California, Berkeley.*—Our program on the measurement of meson masses has now been extended to include several types of K^+-mesons produced by the Bevatron and detected in emulsion. In order to identify the types of K's involved, the secondaries were analyzed in terms of grain density, range, and multiple scattering. The τ mesons are easily identified from the three charged pion daughters. The ranges in the emulsion of these secondaries are being measured to obtain an energy spectrum of the secondaries and a Q-value for the decay process. This is of particular value as we have carefully determined the density of the emulsion used in this study. We are also completing an experimental determination of the range-momentum relation in the emulsion as a part of the program. The τ'-mesons and $K_{\mu 2}$-particles included in the study were identified by following the secondary to the end of its range. These secondaries have grain densities substantially above minimum and thus have a high probability of stoping in the emulsion stack. Measurement of their ranges enables one to obtain the energy spectra of the secondaries from the τ' and $K_{\mu 2}$. The grain density at the beginning of the track of the $K_{\mu 2}$ daughter is about 1.05 minimum while that of the $K_{\tau 2}$ is about 1.20 minimum. A reasonable separation was obtained by grain-counting those secondary tracks whose "dip" angles were less than 15°.

M4. Masses of Positive K-Particles. II. Method, Analysis, and Results.* HARRY H. HECKMAN, FRANCES M. SMITH, AND WALTER H. BARKAS, *University of California, Berkeley.*—K-particle masses were measured by comparing ranges of $K_{\mu 3}$, $K_{\pi 3}$, $K_{\mu 2}$, and τ' mesons with the ranges of τ mesons and protons of the same momentum. For the momentum analysis we have used the Kerth-Stork arrangment, introducing several modifications that enabled us to obtain a mass resolution of 1.6% for an individual particle. The mesons were produced by bombarding a Ta target with 4.8-Bev protons. They had a flight time of about 1.2×10^{-8} sec before entering the detector, a stack of nuclear track emulsions. The scanning procedure was to traverse the emulsion 1.5 cm from the calculated depth of penetration for τ mesons, and to follow particles that fulfilled criteria of grain density and direction to the ends of their ranges. The data recorded for each K-particle included the mode of decay, the range (measured along the track), and the position of entrance into the stack. The mass differences of the K-mesons were calculated from the differences in the mean ranges of each type of particle. We have obtained the following masses, in units of the electron mass, when the mean of the τ mass is taken to be 966: $\tau(966\pm3.1)$, $K_{\mu 2}(962.5\pm3.2)$, $K_{\pi 2}(972.2\pm4.7)$, $K_{\mu 3}(951.2\pm10.6)$, $\tau'(951.5\pm10.9)$. If the particles are compared directly with protons of the same momentum, the masses are in close agreement with those measured relative to the τ mass.

* This work was performed under the auspices of the U. S. Atomic Energy Commission.

M5. Negative K-Particle Interactions in Nuclear Emulsion. I.* CHARLES E. VIOLET, F. C. GILBERT, AND R. STEPHEN WHITE, *University of California, Berkeley and Livermore.*—An emulsion stack, composed of 112 Ilford G. 5 emulsions 6 by 6 in. by 600 microns, has been exposed to a beam of magnetically analyzed negative K-particles produced at the Berkeley Bevatron. The momentum interval subtended by the stack extended from 280 to 400 Mev/c. The methods of exposure, processing, and labeling the stack will be described. Emulsions were systematically scanned for tracks fulfilling certain selection criteria which will be discussed. The observed negative K-particle interactions will be summarized.

* This work was done under the auspices of the U. S. Atomic Energy Commission.

M6. Negative K-Particle Interactions in Nuclear Emulsion. II.* F. C. GILBERT, CHARLES E. VIOLET, AND R. STEPHEN WHITE, *University of California, Berkeley and Livermore.*—Interactions of about 75 negative K-particles that came to rest in the emulsion stack described in the preceding abstract have been analyzed. Prong distributions, π-meson ratios, Σ-particle ratios, unstable heavy particles, energy distributions, and other related properties will be given. The results will be compared with those of other groups working on this problem.

* This work was done under the auspices of the U. S. Atomic Energy Commission.

M7. Negative K-Particle Interactions in Nuclear Emulsion. III.* R. STEPHEN WHITE, F. C. GILBERT, AND CHARLES E. VIOLET, *University of California, Berkeley and Livermore.*—Data concerning the interactions in flight of the negative K-particles listed in the two preceding papers will be discussed. From a measurement of the negative K-particle time of flight an estimate of the lifetime will be given. Individual negative K-meson interactions and Σ-hyperon decays and interactions of interest will be discussed. A value of the positive Σ mass which is based on the range of the decay secondary will be given. The results will be compared with those of other groups investigating the properties of negative K-particles.

* This work was done under the auspices of the U. S. Atomic Energy Commission.

M8. One Hundred Bevatron τ''s.* ROY HADDOCK, *University of California, Berkeley* (introduced by D. H. Stork).—The decays of 100 τ''s found during systematic scanning of 3 emulsion stacks exposed to a magnetically separated K^+-beam at the Bevatron have been analyzed. The ranges of the π's were measured along the track. On the basis of Barkas's[1] range-energy relation the average Q was 75.20 ±0.12 Mev. The distributions in the π^- energy and the angle θ (angle between the relative momentum of the two $\pi^{\pm}$s and the momentum of the π^-) have been compared by an χ^2 test with the theoretical relativistic distributions given by Fabri.[2] The cases for which a τ and a χ could be the same are excluded for spin less than 4. Of the remaining cases 1^+ is excluded and 0^-, 2^-, 3^+ can be fit satisfactorily. The decay plane normals were computed and the distributions appeared to be isotropic.

* This work was done under the auspices of the U. S. Atomic Energy Commission.

[1] W. H. Barkas and D. M. Young, "Emulsion tables. I. Heavy-particle functions," University of California Radiation Laboratory Report No. UCRL-2579 (rev).

[2] E. Fabri, Nuovo cimento **11**, 479 (1954).

M9. Mass Values of Identified K-Mesons.* JAMES R. PETERSON, *University of California, Berkeley.*—The charged decay products of positive K-mesons have been identified, and the masses of the primaries measured by the momentum-range method.[1] The K-mesons were found in two nuclear emulsion stacks (meson energies of 170 and 114 Mev) after exposure behind the strong-focusing magnetic spectrometer at the Bevatron with incident proton energies of 5.7 and 6.2 Bev. Decay modes of mesons other than τ's were established by either (a) following the secondary to the end of its range (20 $K_{\mu 2}$'s and 20 $K_{\pi 2}$'s), (b) estimating the relative ionization by blob count at a considerable distance from the point of decay, or (c) measuring the relative ionization at the decay point. Reliable ratios of the frequencies of occurrence of various modes of decay have been obtained and are $K_{\mu 2}:K_{\pi 2}:\tau=100:56:12$ (τ includes alternate modes of decay), while the $K_{\mu 3}$ and K_{e3} each account for several percent of the total. Masses of the mesons are all consistent with that of the tau within a few electron masses. The data were obtained from about 200 events systematically selected from a total of some 1600 K-mesons.

* This work was done under the auspices of the U. S. Atomic Energy Commission.

[1] Birge *et al.*, Proceedings of the International Conference on Elementary Particles held in Pisa, Italy, in June, 1955 (to be published in *Il Nuovo Cimento*).

M10. Photometric Mass Determinations in a Multiplate Cloud Chamber.* DAVID O. CALDWELL AND YASH PAL, *M.I.T.*—A projection-type photometer has been adapted for measuring the opacity of multiplate cloud-chamber tracks. The ionization of a track may be determined by comparing its opacity with that of a track of known ionization in the same part of the chamber and in the same picture, or one taken under similar conditions. The ionization may be used to find the particle's range, or if the range is known, its mass measurements on a "negative proton" will be reported. For range measurements on identified particles, one needs to determine only the change in track opacity occurring when a plate is traversed. A nomogram then gives the residual range from the amount of material traversed and the ratio of ionizations on each side of the plate. Ranges of $K_{\mu 2}$ and $K_{\pi 2}$ secondaries have been found to be about 78 and

44 g/cm² of copper, respectively; more precise ranges and masses will be given. By combining the ionization ratio and ionization comparison methods, both the range and mass of a particle may be measured.

* This work has been supported in part by the joint program of the Office of Naval Research and the U. S. Atomic Energy Commission.

M11. Anomalous V^0-Particles.* W. H. ARNOLD,† J. BALLAM, M. GRISARU, C. MCGREW, AND W. H. WYLD, *Princeton University.*—From photographs obtained with the Princeton dual cloud chamber[1] 82 neutral V-events have been found for which Q-values could be calculated. Out of these there were 30 Λ^0 and 31 θ^0 and 21 which could be either. In addition there were 5 events which are considered as anomalous in the sense that the Q-value calculated on the basis of either $\Lambda^0 \rightarrow p+\pi^-+37$ Mev[2] or $\theta^0 \rightarrow \pi^++\pi^-+214$ Mev[3] actually deviates from either of these two values by three or more standard deviations. The data on these individual events will be presented. The Q-value for our Λ^0-events is 36±1 Mev and for the θ^0-events it is 212±4 Mev. If we assume that the anomalous events can be described by the decay $K^0 \rightarrow \mu^\pm+\pi^\mp+\nu$ then from the measured data the energy of the neutrino in the rest system of the K^0 can be calculated. This has been done for our and other published anomalous events. Results will be presented and compared with the "phase volume" distribution for this process.

* Supported by the joint program of the Office of Naval Research and the U. S. Atomic Energy Commission.
† Now with Westinghouse Electric Company, Pittsburgh, Pennsylvania.
[1] Hodson, Ballam, Arnold, Harris, Reynolds, and Treiman, Phys. Rev. **96**, 1089 (1954).
[2] Friedlander, Keefe, Menon, and Merlin, Phil. Mag. **45**, 333 (1954).
[3] Thompson, Burwell, Cohn, Hugget, Karzmark, and Kim, *Proceedings of the Rochester Conference* (Interscience Publishers, Inc., New York, 1954).

FRIDAY MORNING AT 10:30

226 Founders Hall

(K. R. MACKENZIE, presiding)

Cyclotrons and Scattering

N1. Theoretical Study of Relativistic Constant Frequency Cyclotrons.* DAVID L. JUDD, *University of California, Berkeley.*—A principle for circumventing relativistic effects limiting maximum energy of cyclotrons was discovered by L. H. Thomas and independently rediscovered by E. M. McMillan in 1949. On this was based an extensive program of theoretical investigation and calculation carried out by the author during 1950–1952. Greatest attention was paid to magnetic fields of the form $\mathbf{H}_z(\epsilon=0)=(m_0\omega c/e)[1+A(\omega r/c)\cos N\theta+B(\omega r/c)^2+C(\omega r/c)^3\cos N\theta+D(\omega r/c)^4+\cdots]$, forming an extension of Thomas's work. The work was keyed to the model program described in the following abstract, for which $N=3$ was chosen to avoid resonances and simplify pole-tip shaping. An exact analytical scalar potential for the field above was obtained and found useful. Calculations included orbit shapes, "resonance condition" for equal periods, frequencies of radial and vertical betatron oscillations, energy limits, effects of a variety of field errors, and a "regenerative peeler"-type beam extraction scheme. Elctric field calculations were made for electrode systems of threefold symmetry driven by 3-phase rf power, including effects of electrical and mechanical misalignments, focusing effects, and details of pickup from arc sources at the center. The relationship of this work to more recent developments will be discussed, as will its application in modifying existing cyclotrons.

* The work was performed under the auspices of the U. S. Atomic Energy Commission.

N2. Electron Models of Relativistic Constant Frequency Cyclotrons.* ROBERT V. PYLE, ELMER L. KELLY, J. REGINALD RICHARDSON (*U.C.L.A.*), AND ROBERT L. THORNTON, *University of California, Berkeley.*—Two model c-w cyclotrons based on the principle of L. H. Thomas will be described. (The theory as extended by David L. Judd is discussed in the preceding abstract.) Both accelerated electrons to speeds about half that of light, in magnetic fields of threefold azimuthal periodicity. The first was used to test a number of accelerating electrode structures and methods of extracting the beam by means of modifications in the magnetic field. Nearly all of the circulating current could be collected outside of the machine and some progress was made toward focusing it into a single external beam. The second, a one-eighth scale model of a possible 300-Mev deuteron cyclotron, has a pole diameter of 40.5 inches, a central magnetic field of 19.3 gauss, and a minimum beam aperture of 1.3 inches. Three 60-degree wide, wedge shaped "triants" driven 120 degrees out of phase at 54.1 megacycles give a maximum energy gain per turn of 3 eV where V is the peak triant to ground voltage. Electrons have been accelerated without axial loss to v/c=0.50 (75 kilovolts) with V=23 volts. This "threshold" voltage corresponds to a triant voltage of less than 100 kv for the 300-Mev accelerator and is set by the geometry of the source structure rather than by the magnetic field.

* This work was done under the auspices of the U. S. Atomic Energy Commission.

N3. Studies with a Three-Dee Three-Phase Proton Cyclotron.* MYRON HEUSINKVELD,† MARK JAKOBSON,‡ LAWRENCE RUBY, BOB H. SMITH, AND BYRON T. WRIGHT,§ *University of California, Berkeley.*—As part of the program to investigate the properties of the cloverleaf cyclotron (see N1 and N2), a 20-in. diameter proton cyclotron was constructed. In such a three-dee three-phase system it is possible to accelerate protons, deuterons, and tritons at the same setting of frequency and magnetic field but on different modes of the rf. Three-phase rf was established on the 60° dees by a driven rf system. The signal originated at a crystal oscillator and the three phases were produced by a phase generator. It was necessary to employ servomechanisms in order to maintain the dees and final amplifier grids in tune. Interaction between the servos required neutralization of the inter dee capacitance by means of suitable transmission lines connected from dee stem to dee stem. The rf system maintained the phase of the dee voltages to within 1° of the desired 120° values. Under such conditions it was possible to attain steadily 6.0 ma of protons at 1.0 Mev in the forward mode and 6.5 ma of deuterons at 0.5 Mev in the reverse mode.

* This work was performed under the auspices of the U. S. Atomic Energy Commission.
† Now at the University of California Radiation Laboratory.
‡ Now at Montana State University.
§ Now at the University of California at Los Angeles.

N4. Elastic Scattering of 48-Mev Alpha Particles.* LARRY SCHECTER† AND R. E. ELLIS, *University of California, Berkeley.*—The angular distributions of 48-Mev alpha particles scattered elastically from Ag, Au, and Pb targets have been measured, using a proportional counter telescope as a detector inside a large evacuated scattering chamber. Deviations by three to four orders of magnitude from pure Coulomb scattering have been observed beyond the forward angles. In addition, some regular structure appears in these distributions, whose main features can be described by an exponential fall-off between 25° and 90°. By fitting the data with a simple modification of Blair's scattering theory, it has been possible to determine interaction radii. Nuclear radii have been derived which are in agreement with those found from medium-energy nucleon scattering.

* This work was done under the auspices of the U. S. Atomic Energy Commission.
† Now at Oregon State College.

N5. Proton-Proton Scatterings at 19.6 Mev.* J. W. BURKIG, GLEN E. SCHRANK, AND J. REGINALD RICHARDSON, *University of California, Los Angeles.*—The differential scattering cross section for 19.8-Mev protons scattered from hydrogen has been measured at a number of angles ranging from 7° to 45° in the laboratory system of coordinates. The statistical accuracy of counting is ±1% for each point. The relative accuracy between points is ±1.5% as determined from the variation of a number of measurements at fixed angle. The absolute accuracy is estimated to be ±2.5%, this larger value being due to the presence of counts in the energy region below the scattering peak and to a low energy component of the beam of about 0.5%. The experiment was performed in a 30-in. scattering chamber filled with hydrogen, and using a scintillation counter and photomultiplier as a detector. Counting was done on either side of zero angle and the average used. Repeated measurements were made at several lower angles to check the accuracy of angular setting and for contamination of the hydrogen. In a second experiment (due to J.W.B. alone), using the same equipment, the $p-\alpha$ cross section was measured with a decreased statistical accuracy. These results will also be reported.

* This work was supported in part by the joint program of the Office of Naval Research and the U. S. Atomic Energy Commission.

N6. Relative Stopping Power of Some Metallic Elements for 20-Mev Protons.* V. C. BURKIG AND K. R. MACKENZIE, *University of California, Los Angeles.*—The stopping power per electron relative to Al has been measured for 23 metallic elements from Be to Th with a probable error of 0.2% in most cases. The 20-Mev proton beam of the UCLA cyclotron was used with a differential ionization chamber as an energy-sensitive detecting device. An approximate straight line relationship was found as a function of ln Z with some deviations noted from Ta to Th and in the region of the filling of the 3*d* shell (Ca to Ni). Results are as follows: Be −1.169; Ca −0.982; Ti −0.936; V −0.918; Fe −0.886; Ni −0.872; Cu −0.867; Zn −0.866; Nb −0.816; Mo −0.809; Rh −0.800; Pd −0.793; Ag −0.791; Cd −0.789; In −0.782; Sn −0.782; Ta −0.715; W −0.706; Ir −0.703; Pt −0.695; Au −0.692; Pb −0.677; Th −0.691.

* This work was supported in part by the joint program of the Office of Naval Research and the U. S. Atomic Energy Commission.

N7. Analysis of Elastic Scattering of 31.5-Mev Protons.* MICHEL A. MELKANOFF, JOHN NODVIK, AND DAVID S. SAXON, *University of California, Los Angeles.*—Recent experiments performed on the Berkeley linear accelerator have yielded differential cross sections for the elastic scattering of 31.5-Mev protons from about 20 elements throughout the periodic table.[1] We have analyzed this data[2] on the basis of the diffuse surface optical model of the nucleus.[3] The best fit with experiment is obtained with a complex potential depth of about 36+15*i* Mev for all elements heavier than say Fe (lighter elements show some fluctuations). This result may be compared with the value 45+8*i* Mev which has been found to give the best fit at 17 Mev.[4] The space dependence of the potential, however, is not significantly altered. Detailed comparisons between calculated and observed cross sections will be presented.

* Supported in part by the National Science Foundation, the Office of Naval Research, and the Office of Ordnance Research.
[1] We are indebted to B. T. Wright, B. B. Kinsey and J. Leahy, each of whom has furnished his results prior to publication.
[2] The calculations were performed on the SWAC, Numerical Analysis Research Project, Dept. of Mathematics, UCLA using the code prepared by R. D. Woods.
[3] R. D. Woods and D. S. Saxon, Phys. Rev. **95**, 577 (1954).
[4] To be published. See also UCLA Physics Dept. Technical Report 7-12-55.

N8. Small-Angle Proton-Proton Scattering at 20 Mev.* HERBERT N. ROYDEN AND BYRON T. WRIGHT, *University of California, Los Angeles.*—The differential cross section for the scattering of 19.8-Mev protons by protons has been measured for angles between 18° and 36° in the center-of-mass system, using photographic emulsions as detectors. The angular resolution was 0.6°. Cross sections were measured simultaneously at all angles and azimuths, one run with analyzing slits closed serving to evaluate the small slit-edge correction. The scattering chamber used was a modification of that described by Faris and Wright.[1] The external proton beam of the U.C.L.A. 20-Mev synchrocyclotron passed through a collimator and the scattering chamber, filled with hydrogen gas at one atmosphere, and was collected in a Faraday cup. The charge collected by the Faraday cup was measured with a 100% feedback electrometer which had been calibrated to 0.3%, using a current-time method.[2] A scintillation counter was used to monitor contaminants in the hydrogen gas. Results will be presented.

* Supported in part by the joint program of the Office of Naval Research and the U. S. Atomic Energy Commission.
[1] F. E. Faris and B. T. Wright, Phys. Rev. **79**, 577 (1950).
[2] H. N. Royden and D. O. Caldwell, Rev. Sci. Instr. (to be published).

N9. Energy Loss of Protons in Metals.* R. E. PIXLEY, M. BADER, AND WARD WHALING, *California Institute of Technology.*—The rate at which protons lose energy in passing through thin evaporated layers of metal has been measured for protons in the energy range between 50 and 600 kev. The materials studied are Li, Be, Al, Cr, Mn, Fe, Co, Ni, Cu, Zn, Au, and Pb. Together with earlier measurements in this laboratory of the rate of energy loss in several gases, these results provide information about the variation of energy loss with the atomic number of the stopping material. For high energy protons, the energy loss per stopping atom increases smoothly with Z; the scattered results that are available are consistent with the theoretical $Z^{1/3}$ dependence. The influence of molecular binding on the stopping cross section of compounds becomes noticeable below 150 kev. For protons of 500 kev, a fairly uniform Z-dependence is apparent over most of the periodic table, but two types of deviation are still observed. First, the stopping cross sections of the noble gases are relatively lower than that of their neighbors. This effect can be understood in terms of the reduced energy loss to the more tightly bound electrons of closed shells. Second, in the region from Z=23–29, the stopping cross section decreases with increasing Z. With the exception of a high value at Cr, the decrease is fairly uniform from V through Cu.

* Assisted by the joint program of the Office of Naval Research and the U. S. Atomic Energy Commission.

FRIDAY AFTERNOON AT 1:30

133 Founders Hall

(C. D. ANDERSON, presiding)

Invited Papers on Cosmic Rays and K-Mesons

O1. The Interaction of K-Particles from the Bevatron. G. GOLDHABER, *University of California, Berkeley.* (25 min.)

O2. Properties of Positive K-Mesons. D. H. STORK, *Radiation Laboratory, University of California.* (25 min.)

O3. K-Meson Counter Experiments. M. L. GOOD, *Radiation Laboratory, University of California.* (25 min.)

O4. Orgin of Cosmic Rays. L. DAVIS, JR., *California Institute of Technology.* (25 min.)

O5. Recent Experiments on Primary Cosmic Rays. E. P. NEY, *University of Minnesota.* (30 min.)

FRIDAY AFTERNOON AT 1:30

129 Founders Hall

(E. L. KINSEY, presiding)

Solid State II

P1. Compound Formation between Lithium and Boron Dissolved in Single Crystal Silicon. C. S. FULLER AND H. REISS, *Bell Telephone Laboratories.*—At high temperatures (above 800°C) the solubility of lithium in silicon doped with boron is considerably higher than in undoped silicon. The detection of this phenomenon is based on measurements of the resistivities of crystals saturated with lithium by diffusion. The increased solubility is not explicable in terms of the hole-electron mechanism developed previously.[1] A theory which fits the data quantitatively can be developed by assuming that lithium, boron, and a vacancy which has accepted an electron combine to form LiB^- complexes in which the lithium occupies an sp^3 position relative to the boron and is bound to it by a covalent bond. The reaction in favor of the complex is aided by the high concentrations of vacancies and conduction electrons available at higher temperatures.

[1] H. Reiss and C. S. Fuller, Phys. Rev. **97**, 559 (1955); also to be published in the *Journal of Metals.*

P2. Ionization of Hydrogen in Germanium and Silicon. HOWARD REISS, *Bell Telephone Laboratories.*—Considerable evidence exists that grown germanium and silicon crystals contain large amounts of dissolved hydrogen which do not appear to affect the semiconducting properties of the crystals.[1] The failure of hydrogen to ionize, when dissolved, is puzzling because lithium which, like hydrogen, is presumably interstitial possesses the lowest ionization energy of all known donors in germanium and silicon. A quantum-mechanical treatment of this anomaly reveals that the situation is consistent with theory. In pictorial terms the explanation is as follows. A lattice interstice may be regarded as a spherical cavity in a dielectric. An interstitial hydrogen, being small, fits entirely into the cavity while lithium is large enough to spill over into the surrounding dielectric. As a result the dielectric medium is *inside* the lithium atom and *outside* the hydrogen, reducing the ionization energy of the former and having a much less profound effect on the latter.

[1] O. H. Johnson, Chem. Revs. **51**, 431 (1952).

P3. Thermal Conductivity of Neutron-Damaged Graphite. NED S. RASOR AND JOHN E. HOVE, *North American Aviation, Inc.*—Graphite conducts heat by lattice waves and the thermal conductivity of the artificial pitch-bonded graphites exhibits an anomalous temperature dependence in that it is stronger than the temperature variation of the specific heat at low temperatures. This has been explained in terms of the two-medium nature of such graphites.[1,2] The present paper shows the effect of pile neutron exposure on the thermal conductivity of three types of artificial graphite with crystallite sizes of about 6000 A, 3000 A, and 300 A. In all cases, the values have been measured as a function of temperature from 15°K to 300°K. There is a large decrease in the magnitude of the conductivity (e.g., by a factor of five for the large crystallite graphite after being exposed to a fast flux of about 2×10^{18} nvt) while the temperature dependence of the thermal conductivity also changes with damage, but less strongly. These data have been analyzed on the basis of the two medium theory[2] by which the relative number of internal defects has been obtained as a function of neutron exposure and found to vary in an inverse manner with the crystallite size. The general behavior of the thermal conductivity with damage supports the basic theory very well.

[1] A. W. Smith, Phys. Rev. **98**, 1563(A) (1955).
[2] J. E. Hove, Phys. Rev. **98**, 1563(A) (1955).

P4. Magnetic Susceptibility of Neutron-Damaged Graphite.* JOHN E. HOVE, *North American Aviation, Inc.*—A recent paper[1] attempts to establish a quantitative theory of the magnetic susceptibility of graphite. The experimental results obtained from bromine-graphite residue compounds are used to verify the theory. The effect of introducing bromine into the graphite in this manner is to trap some of the conduction electrons and thereby alter the value of the diamagnetism. Similarly, one of the results of irradiating graphite in a reactor is the trapping of electrons. As expected, therefore, the diamagnetic susceptibility of damaged graphite is markedly decreased. The values of the total susceptibility (i.e., the sum of the susceptibilities measured

in three mutually perpendicular directions) of AGOT-KC graphite have been measured by J. D. McClelland (unpublished) at room temperature and at liquid nitrogen temperature as a function of integrated neutron flux. The interpretation of these data in terms of the above theory[1] yields two results of interest: (1) The quantitative theory is again verified and (2) a value of $1.4+10^{-4}$ electron (per carbon atom) trapped after 1.7×10^{17} nvt of fast neutrons is obtained for the rate of electron trapping with pile exposure. This agrees very well with that determined by use of the bromine-graphite residue compounds.

* Based on studies conducted for the U. S. Atomic Energy Commission.
[1] John E. Hove, Phys. Rev. 100, 645 (1955).

P5. Stored Energy Release in Graphite Irradiated at Low Temperatures.* S. B. Austerman, *North American Aviation, Inc.*—Previous measurements of electrical and thermal resistivities and paramagnetic resonance have shown that graphite, when irradiated near liquid nitrogen temperature, retains considerable damage which anneals out below room temperature. This report deals with the release of stored energy associated with this damage. To compute stored energy release, the relative specific heat of an irradiated specimen is compared with that of the specimen after annealing. Various types of artificial and natural graphite were irradiated in the liquid nitrogen facility of the Brookhaven reactor. The stored energy release spectrum during steady temperature rise shows a peak at 215°K for graphite having large crystallites (3000 A length) and about 185°K for fine-crystallite graphite (300 A length). If the defects are assumed to diffuse out of the crystallites on heating, the dependence of the annealing behavior on crystallite size can be accounted for with an activation energy of about 0.4 ev. The total stored energy releasable below 275°K accumulates linearly with neutron exposure at a rate of 1.4 cal/g per 10^{18} nvt. By estimating the number of responsible defects from neutron scattering data, the stored energy per atomic displacement is found to be of the order of 2 ev. An apparent increase in specific heat appears at low temperatures and can be qualitatively accounted for on the basis of isolated interstitial atoms behaving as Einstein oscillators.

* This work supported by the U. S. Atomic Energy Commission.

P6. Ion Pairing Involving Lithium in Germanium and Silicon. F. J. Morin, Howard Reiss, and C. S. Fuller, *Bell Telephone Laboratories.*—The formation of ion pairs involving the donor lithium and the acceptors boron and gallium, has been observed experimentally in the semiconductors silicon and germanium. Several methods of observation have shown the effect. Measurements of the diffusion coefficient of lithium revealed a reduction in diffusivity as pairing occurred. Measurements of the mobilities of carriers in the ionized impurity scattering region showed large changes as pairing removed scatterers. Observation, by Hall effect, of energy diagrams showed alterations of the impurity levels in the presence of pairing. In germanium it is found that the pair distributions relax towards equilibrium at temperatures as low as 100°K. At such temperatures very complete pairing occurs even when the impurities are present in traces, e.g. 10^{15} atoms per cm^3.

P7. Effect of Low-Temperature Electron Irradiation on the Electrical Resistivity of Copper.* C. J. Meechan, *North American Aviation, Inc.*—High purity copper has been irradiated at −196°C with 1.25-Mev electrons. The electrical resistivity (ρ) was measured (1) as a function of exposure (ϕ) during the irradiation and (2) as a function of annealing temperature following the irradiation. An initial curvature was observed in the ρ *vs* ϕ curve up to approximately 6×10^{17} electron/cm^2. From this point, up to at least 3×10^{18} electron/cm^2, the exposure curve is linear. The slope of this linear portion of the curve was $4.24+10^{-26}$ ohm-cm per electron/cm^2. Approximately 50% of the induced resistivity change recovers in a well-defined state centered at 25°C. About 30% of the damage recovers at lower temperatures. The remaining 20% begins to recover at 125°C and all of the damage was removed at 300°C.

* This work performed under contract for the U. S. Atomic Energy Commission.

P8. A New Method for the Determination of Activation Energies.* J. A. Brinkman, *North American Aviation, Inc.*—A new procedure for obtaining and analyzing data for the purpose of determining activation energies governing the recovery of the physical property changes of damaged solids has been developed. For situations in which the method is applicable, it generally yields greater accuracy and is frequently more convenient to use than other methods. If a general recovery equation of the form, $d\rho/dt=F(\rho)\exp(-E/kT)$, is assumed, where ρ is the measured property, two initially identical specimens are required for the determination of the activation energy, E, by this method. An isothermal annealing curve is obtained by annealing the first specimen at a constant temperature and measuring ρ as a function of time. A tempering curve is obtained by heating the second specimen to successively higher temperatures for equal time intervals and measuring ρ after each such temperature pulse. If an equation of the form, $d\rho/dt=-\nu\rho^\gamma\exp(-E/kT)$, is assumed, only the tempering curve is needed to determine E; thus one specimen is sufficient. Application of the method to the 25°C recovery state described in the preceding abstract yielded an activation energy of 0.63 ev and a value of 2.5 for γ in the above equation.

* This work performed under contract for the U. S. Atomic Energy Commission.

P9. Influence of Lattice Defects on the Young's Modulus of Copper.* H. Dieckamp, *North American Aviation, Inc.*—The Young's modulus of copper has been measured as a function of energetic electron flux. Relative measurements of the Young's modulus of 99.999% purity copper were made by observing the driven resonant frequency of a cantilever beam during bombardment with 1-Mev electrons at a temperature below −50°C. The modulus is observed to increase with the change saturating at an increase of about 1 to 2% after an exposure of about 10^{18} electrons/cm^2. A model involving the pinning of dislocations by interstitials and/or vacancies seems to be appropriate. The introduction of such a model into the result of Mott for the dislocation contribution to Young's modulus, $\Delta E/E=1/6N\beta^2$, yields a flux dependence of the modulus which fits the experimental data. The choice of an appropriate value for the probability of producing a pinning point allows the theory to yield reasonable values for the number and average length of dislocations in a sample.

* This work performed under contract for the U. S. Atomic Energy Commission.

P10. Field Dependence of the Hall Potential and Magnetoresistance of Irradiated Graphite.* J. D. McClelland, *North American Aviation, Inc.*—The magnetic field dependencies of the Hall potential and magnetoresistance have been determined for a series of irradiated artificial graphite samples. Measurements were made at room temperature at fields between 5 and 15 kilogauss. Irradiations ranged up to an integrated fast neutron flux of 2×10^{18} nvt. The Hall coefficient changes from a value of −0.66 emu for the

unirradiated sample to +0.86 for the most highly damaged sample. In all cases the absolute value of the Hall potential increased linearly with field and extrapolated to zero at zero field. Over the range of magnetic field studied the magnetoresistance can be expressed as $(\Delta R/R)=AH^{\alpha}$. At a field of 10 kilogauss the value of $\Delta R/R$ fell from a pre-irradiation value of 2×10^{-4} to 7×10^{-4} for the highly damaged specimen. At the same time the exponent of H increased with exposure from 1.77 to 1.88. Thus, with neutron damage, the magnetoresistance of graphite appears to approach the behavior typical of a good metal, both in absolute value and in field dependence. The reasons for this will also be discussed.

* This work performed under contract for the U. S. Atomic Energy Commission.

P11. Thermal Conductivity of Superconducting Lead below 1°K. B. R. Felix, L. Passell, and H. B. Silsbee, *University of California, Berkeley.*—The thermal conductivity of single crystals of high purity lead has been measured from 0.15°K to 0.8°K in the superconducting state. The electronic contribution should be negligible in this region, while the lattice conductivity is expected to follow the prediction of Casimir.[1] The experimental temperature dependence is as $T^{2.7\pm0.3}$, i.e, faster than the T^3 to be expected from the specific heat, and the magnitude of the conductivity is appreciably smaller than predicted. The results suggest a scattering mechanism for phonons for which the cross section increases with decreasing temperature. A speculative explanation of the results will be offered.

[1] Casimir, Physica **5**, 495 (1938).

P12. Thermal Conductivity of Aluminum at Low Temperatures. L. Passell, B. R. Felix, and H. B. Silsbee, *University of California, Berkeley.*—The thermal conductivity of pure polycrystalline aluminum has been measured in its normal state from 1.3°K to 3.5°K and, by adiabatic demagnetization techniques, in its superconducting state from 0.3°K to 0.8°K. The high Debye temperature of aluminum makes the lattice conduction negligible compared to the electronic contribution. If the normal results are extrapolated to the lower temperature range, the ratio of the superconducting to the normal conductivity may be plotted as a function of reduced temperature, T/T_c crit. The points thus obtained can be combined with previous results[1,2] for the electronic conductivity which may be compared with theory.

[1] Hulm, Proc. Roy. Soc. (London) **A204**, 98 (1950).
[2] Goodman, Proc. Phys. Soc. (London) **A66**, 217 (1953).

P13. Transverse Field Effects in PbS. D. E. Martz and R. S. Witte, *U. S. Naval Ordnance Test Station.*—Recent investigations on commercial lead sulfide cells have revealed that large changes in resistance, time constant, and sensitivity can occur when the cells are subjected to dc electric fields that are directed normal to the surface of the layer. A field directed from the substrate to the layer gives rise to an initial increase in layer resistance followed by a long term (days) decrease to a very low value. Typical values of the initial resistance, peak resistance, and final equilibrium value are 1.0 megohms, 100 megohms, and 1000 ohms, respectively. The rate of change in resistance is approximately proportional to the applied field and is strongly temperature dependent. In producing these changes, a metal film is either evaporated or painted onto the underside of the glass substrate and voltage is applied between this backing and the layer. The changes are not observed if a thin insulating layer is placed between the metallic back and the glass. A two-step mechanism is postulated. The field introduces ions from the glass into the layer and these ions then distribute themselves throughout the layer by means of thermal diffusion.

Friday Afternoon at 1:30

226 Founders Hall

(R. Feynman, presiding)

Theory

Q1. An Alternative Interpretation of Magnetic Forces between Moving Charges. John Backus, *University of Southern California.*—Magnetic interactions of charges are usually described in terms of a force between a charge in motion (relative to an assumed reference system) and another charge in motion. It will be shown that magnetic forces may be interpreted in terms of moving charges exerting forces on charges at rest, i.e., as forces acting on charges in relative motion. If charge q_1 is moving with a velocity $\mathbf{v}$ relative to charge q_2, and $\mathbf{r}$ is the vector from q_1 to q_2, then if a force $\mathbf{f}_2$ (in addition to the Coulomb force) is assumed to act on q_2, the usual formulas for the magnetic interactions of circuits will result if $\mathbf{f}_2=-q_2\nabla\phi$, where, in mks units, $\phi=-(\mu_0 q_1/16\pi)\{[3(\mathbf{v}\cdot\mathbf{r})^2/r^3]-(v^2/r)\}$.

Q2. Generalized Theory of Mobility. Melvin Lax, *Bell Telephone Laboratories and Syracuse University.*—In the presence of strong interaction between an electron and a scattering system it is difficult, if not impossible, to decompose the Hamiltonian of the electron plus scattering system uniquely into an unperturbed portion (describing the renormalized electron) and a perturbation. Furthermore, the time between scatterings may be short compared to the characteristic times of the scattering system, so that we no longer have a succession of independent scattering events with no phase relations between them, i.e., a Boltzmann transport equation may be meaningless. A theory has therefore been developed that omits the customary assumptions and treats only the electric field as a perturbation. The resulting mobility is $\mu=e\tau/m$ where the (tensor) relaxation time τ is given by $i\hbar\tau=\int_{-\infty}^{0}\exp(i\omega t)\ \mathrm{trace}\ [(\mathbf{r}(t),\ \mathbf{p})\rho_0]dt$, where $\mathbf{r}(t)$ is the Heisenberg position of the electron $\exp(iHt/\hbar)\cdot\mathbf{r}\exp(-iHt/\hbar)$ and ρ_0 is the thermal equilibrium density matrix $\exp(-\beta H)/\mathrm{trace}\ [\exp(-\beta H)]$, with $\beta=(kT)^{-1}$ and H is the total (undecomposed) Hamiltonian of the electron-lattice system. A generalized Nyquist theorem will be given that relates both the real and the imaginary part of the conductivity $\sigma(\omega)=ne^2\tau/m$ to the current fluctuations.

Q3. A Schrödinger-Like Equation for the Measurement Process. Richard Scalettar, *University of Southern California.*—It has been shown[1] that, if ρ_b and ρ_a are the density matrices before and after an ideal measurement and E is the measurement projection operator, then $\rho_a=E\rho_b E$. If a se-

quence of measurements, $E(t_j)$, is performed at times $t_j = j\epsilon (j=0, 1, 2, \cdots)$ and in the time intervals, ϵ, between measurements, the system propagates undisturbed with a time-independent Hamiltonian, H, then the probabilistic behavior at time t_n is given by the state vector,

$$|\psi(t_n)> = E(t_n) \exp\left(-\frac{i}{\hbar}\epsilon H\right)|\psi(t_{n-1})>.$$

It follows that, if the measurement process is continuous in a sense to be defined precisely,

$$\left\{E(t)H - \frac{\hbar}{i}\frac{dE(t)}{dt}\right\}|\psi(t)> = -\frac{\hbar}{i}\frac{d|\psi(t)}{dt}>,$$

a Schrödinger-like equation for the ideal measurement process. (It is assumed that ρ is initially pure.) The physical significance of this result, its relation to the question of reversibility, and an application to Feynman's statistical assertions[2] will be discussed.

[1] G. Ludwig, *Die Grundlagen der Quantenmechanik* (Springer-Verlag, Berlin, 1954).
[2] R. P. Feynman, Revs. Modern Phys. **20**, 367 (1948).

Q4. Variational Methods in Scattering Problems.* MILDRED M. MOE AND DAVID S. SAXON, *University of California, Los Angeles.*—The application of variational methods to scattering problems has been limited by (a) the complexity of the integration required in the use of the Schwinger formulation[1] even for the simplest trial functions, and (b) the difficulty of finding adequate trial functions in the relatively simple Kohn formulation.[2] We have slightly modified the latter by setting the trial function equal to the incident wave plus a correction term and then rewriting the variational principle in a form independent of the amplitude of the correction term. In this form, any trial function can immediately be generalized using finite sets of partial waves as previously reported in connection with the Schwinger formulation. We have also examined the relation between the Kohn formulation in terms of phase shifts and in terms of the total scattering amplitude. As a result we have been led to the view that the variational principles for scattering can be formulated in an enormous variety of ways none of which can be selected *a priori* as preferable to any other. Possible criteria for a choice are being sought.

* Supported in part by the National Science Foundation.
[1] B. P. Lippman and J. Schwinger, Phys. Rev. **79**, 469 (1950).
[2] W. Kohn, Phys. Rev. **74**, 1763 (1948).

Q5. Polarization Effects in Electron-Photon Interactions. CRAMER SCHULTZ AND ROSS D. F. THOMPSON, *University of Southern California.*—This paper discusses the means of detecting the circular polarization states of gamma rays. It is shown that an analysis of Compton scattering, using a method suggested by Halpern, offers the most effective means of determining the polarization. In addition, other experiments to detect circular polarization are discussed.

Q6. Radiative Corrections to Decay Processes.* R. E. BEHRENDS, R. J. FINKELSTEIN, AND A. SIRLIN, *University of California, Los Angeles.*—Radiative corrections associated with the electromagnetic field have been determined for the decay of a fermion of arbitrary mass into a lighter one with the emission of a single boson or of two other fermions; no special assumptions have been made about the nature of the interaction responsible for the instability. The particular example of the muon-electron decay has been worked through in detail. Sufficiently accurate experimental determination of the muon spectrum would permit the observation of a Lamb effect without vacuum polarization. Modified formulas for the Michel parameter ρ are given. The experimental results of Lederman *et al.*[1] are modified by this correction from ρ exp$=0.64\pm0.10$ to 0.68 ± 0.10. In addition the ρ values of the various proposed Fermi interactions are slightly altered. For example, the ρ of $S-T+P$ is decreased from 0.75 to 0.727.

* This work was supported in part by the National Science Foundation.
[1] L. Lederman (private communication).

Q7. Photoproduction of π-Meson Pairs in Hydrogen. F. ZACHARIASEN, *M.I.T.* (introduced by S. D. Drell).—The reaction $\gamma+p\rightarrow p+\pi^0+\pi^-$ has been studied in the Chew-Low formalism,[1] assuming a linear P-wave meson-nucleon coupling and no meson-meson interaction. It is found that in the low-energy region, where the production consists primarily of S- and P-wave mesons, the cross section for this process can be related exactly to the experimental meson-nucleon scattering phase shifts. In this region the pair production comes almost entirely from the $\boldsymbol{\sigma}\cdot\mathbf{A}\boldsymbol{\tau}\cdot\boldsymbol{\phi}$ coupling, only 10 to 15% being contributed by the meson current. The cross section obtained here seems to be consistent with existing experimental evidence.[2] Experimental information on the π-pair production in the energy region threshold to almost 500 Mev will then produce information on the size of the meson-meson interaction (of S- and P-wave mesons).

[1] G. P. Chew and F. E. Low, private communication.
[2] M. L. Sands, private communication.

Q8. Some Remarks on Strangeness. S. EPSTEIN, *University of Nebraska.*—We consider couplings of the form (baryon)(baryon)$'$(meson) between the baryons Ξ, Σ, Λ, and N, and the mesons θ, ϑ, and π, and try to determine the minimum physical requirements which must be imposed so that the resultant classification of couplings as strong or forbidden agrees with the strangeness rules.[1] Our results may be stated as follows. There are several classifications consistent with the requirements that (A) hyperons and mesons should be stable against π emission and (B) that in π-N collisions any of the hyperons can be produced in association with one or more heavy mesons, the nature of the latter being subject to the restriction (C) that it be impossible to convert two nucleons into two hyperons. The strangeness classification is then distinguished by the fact that it alone then permits Σ and Λ particles to be produced in association with but one positive heavy meson. We will also comment on the fact that with this model any reaction which conserves strangeness can be realized by a sequence of strong couplings.

[1] M. Gell-Mann, Phys. Rev. **92**, 833 (1953); T. Nakano and K. Nishijima, Progr. Theoret. Phys. Japan **10**, 581 (1953).

Q9. Difference in Lifetimes of θ^0 and θ^+ Mesons.* S. OKUBO AND R. MARSHAK, *University of Rochester.*—The lifetime of θ^0 is approximately 100 times shorter than that of θ^+. Dalitz[1] has suggested one possible explanation of this difference (assuming that θ is scalar) by remarking that the $\theta^0\rightarrow\pi^++\pi^-$ decay is compatible with the selection rule $\Delta I = \pm 1/2$ (I is the isotopic spin) whereas $\theta^+\rightarrow\pi^++\pi^0$ requires $\Delta I = \pm 3/2$ and therefore may be more strongly forbidden. We have examined an alternative explanation by postulating a strong pion-pion attraction in the appropriate $I=0$ state but not in the $I=2$ state. The parameters of the pion-pion attractive potential are determined by invoking the conjecture of Piccioni, Dyson,[2] and Takeda that it is the same interaction which is responsible for the second maximum in the negative pion-proton scattering cross section. The effect on the θ^0 lifetime is sensitive to the assumed range of the pion-pion potential. If the range is the nucleon Compton wavelength, it appears possible to reconcile the θ^0 and θ^+ lifetimes.

If the range is closer to the pion Compton wavelength, the present explanation seems insufficient.

* Supported in part by the U. S. Atomic Energy Commission.
[1] Private communication.
[2] See F. J. Dyson, Phys. Rev. 99, 1037 (1955).

Q10. Remarks on the Anti-Proton.* T. REGGE, S. OKUBO, AND R. MARSHAK, *University of Rochester.*—There is a striking resemblance between the K-meson pair production mechanism at Cosmotron energies and the proton pair production at Bevatron energies. This analogy is utilized to estimate the anti-proton yield at 6 Bev from the measured K^--yield at 3 Bev.[1] The annihilation reactions $p+p\rightarrow K^++K^-$ or $K^0+\bar{K}^0$ conserve the "strangeness" quantum number so that they should *a priori* compete favorably with the reactions $p+p\rightarrow\pi^++\pi^-$ or $2\pi^0$.[2] Estimates of the relative annihilation cross sections have been made up to 500 Mev kinetic energy for the incident antiproton, considering both scalar and pseudoscalar K-mesons. Finally, the hypothesis of a strongly bound state of the proton-antiproton system[3] (called nucleonium) has been examined for its bearing on the production and annihilation processes involving antiprotons. In particular, estimates are made of the relative production cross section for nucleonium and the relative cross section for the one pion annihilation reaction which it makes possible.

* Supported in part by the U. S. Atomic Energy Commission.
[1] E. O. Salant (private communication).
[2] Multiple pion emission is also possible, even likely; multiple K-meson emission is rather improbable.
[3] M. Lévy and R. Marshak, Nuovo cimento Supplem. No. 2, 253 (1954).

Q11. Wave Equations for Arbitrary Spin. C. FRONSDAL, *University of California, Los Angeles.*—A method is presented for deriving wave equations for particles of arbitrary spin, without subsidiary conditions. The equations obtained are equivalent to that of Dirac, for spin $\frac{1}{2}$, and to that of Fierz for spin 3/2. The equations are not all of the first order, but of orders $2s$ in the operator ∂.

SUPPLEMENTARY PROGRAMME

SP1. Electron Spin Resonance of Impurities in Magnesium Oxide.*† JOHN E. WERTZ, JUANA L. VIVO, AND BORIS MUSULIN, *University of Minnesota.*—All magnesium oxide crystals we have been able to locate show a six-line hyperfine splitting pattern found previously upon deliberate addition of manganese.[1] Technical MgO powder shows the same behavior as does also a reagent grade which has been heated to 1200°C. Their line width is as small as 1.5 gauss, very narrow for an ionic crystal, and much narrower than found previously.[1] The fourth line (counting from the low-field end) shows unusually large variations of intensity relative to the other five. Each of the principal lines has four satellites, explainable for an electronic spin of 5/2. At high spectrometer sensitivity, a number of weak lines are found in pairs. Their origin is being investigated. Heating to 200°C in the resonant cavity of the spectrometer decreases the ESR line intensity by an amount expected from Curie's law. An impurity of nuclear spin 7/2 and electronic spin 3/2 gives eight principal lines over a 560 gauss region. Each has two satellites.

* Supported in part by the Air Force Office of Scientific Research.
† To be given at the end of Session B if the chairman rules that time permits.
[1] W. D. Hershberger and H. N. Leifer, Phys. Rev. 88, 714 (1952).

Author Index to Papers Presented at the 1955 Los Angeles Meeting

Abraham, M. and S. J. Goldsack—I6
Anderson, A. B. C.—J4
Anderson, J. D., R. W. Kenney, and C. A. McDonald—I4
Armstrong, Baxter H.—I3
Arnold, W. H., J. Ballam, M. Grisaru, C. McGrew, and W. H. Wyld—M11
Austerman, S. B.—P5
Ayres, W. P., P. H. Vartanian, and J. L. Melchor—B3
Backus, John—Q1
Baños, Alfredo, Jr.—J9
Barkas, Walter H., Paul H. Barrett, Pierre Cuer, Harry H. Heckman, Frances M. Smith, and Harold K. Ticho—H2
Barnes, C. A. and R. W. Kavanagh—F7
Behrends, R. E., R. J. Finkelstein, and A. Sirlin—Q6
Bowen, D. B.—L1
Brinkman, J. A.—P8
Brown, K. L.—H7
Brun, E., W. E. Meyerhof, and J. J. Kraushaar—F4
Burkig, J. W., Glen E. Schrank, and J. Reginald Richardson—N5
Burkig, V. C. and K. R. MacKenzie—N6
Caldwell, David O. and Yash Pal—M10
Chamberlain, O.—K3
Conzett, Homer E.—C9
Crowe, K. M., R. M. Friedman, and D. C. Hagerman—I9
Das, T. P. and R. Bersohn—B6
Davis, L., Jr.—O4
De Pangher, J. and W. C. Roesch—C3
Dieckamp, H.—P9
Drost-Hansen, W. and H. W. Neill—J3
Epstein, S.—Q8
Erkman, J. O.—J8
Ewing, M.—G3
Felix, B. R., L. Passell, and H. B. Silsbee—P11
Ferrell, R. A. and W. M. Visscher—F8
Feynman, R. P.—L5
Field, L. M.—D1
Fisher, J. C.—L2
Fowler, W. A.—A1
Friedman, R. M. and K. M. Crowe—I8
Fronsdal, C.—Q11
Fuller, C. S. and H. Reiss—P1
Gell-Mann, M.—E2
Gilbert, F. C., Charles E. Violet, and R. Stephen White—M6
Goldhaber, G.—O1
Gomer, R.—D2
Good, M. L.—O3
Goodman, L. S. and S. Wexler—F6
Haddock, Roy—M8
Hagedorn, F. B.—C7
Harrison, Melvin A.—J1
Heckman, Harry H., Frances M. Smith, and Walter H. Barkas—M4
Henry, Warren E.—B2
Henyey, L. G.—E4
Heusinkveld, Myron, Mark Jakobson, Lawrence Ruby, Bob H. Smith, and Byron T. Wright—N3
Hintz, Norton M.—C11
Hove, John E.—P4
Igo, G. and H. E. Wegner—F9
Imhof, William, V. Perez-Mendez, and H. Easterday—I1
Inglis, D. R.—F2
Ise, John, Jr., Andre Lagarrigue, and Robert V. Pyle—I5
Iselin, C. O'D.—G2
Jacobsohn, B. A.—F1
Judd, David L.—N1
Katz, Samuel—J7
LaRocca, E. W.—J6
Lax, Melvin—Q2
Lehman, G. W.—B4
MacGregor, M. H., William P. Ball, and Rex Booth—C4
Maenchen, George, William B. Fowler, Wilson M. Powell, George Saphir, and Robert W. Wright—M2
Marion, J. B. and R. A. Chapman—F3
Martz, D. E. and R. S. Witte—P13
Mayfield, Earle B., Harvey L. Morrison, and William A. Allen—J5
McClelland, J. D.—P10
McClung, Fred and John R. Holmes—C1
McDonald, W. F., Vincent Peterson, and Dale R. Corson—I7
Mead, S. W., M. D. Petroff, and W. O. Doggett—C8
Meechan, C. J.—P7
Melkanoff, Michel A., John Nodvik, and David S. Saxon—N7
Millburn, George P., Burton J. Moyer, Yuin-Kwei Tai, and Selig N. Kaplan—C5
Mills, W. R., Jr., H. H. Hilton, III, and C. A. Barnes—C10
Moe, Mildred M. and David S. Saxon—Q4
Moore, G. E.—D3
Morin, F. J., Howard Reiss, and C. S. Fuller—P6
Murray, J. J.—K4
Ney, E. P.—O5
Okubo, S. and R. Marshak—Q9
Passell, L., B. R. Felix, and H. B. Silsbee—P12
Pellam, J. R.—L4
Peterson, James R.—M9
Pixley, R. E., M. Bader, and Ward Whaling—N9
Powell, W. M.—A3
Pyle, Robert V., Elmer L. Kelly, J. Reginald Richardson, and Robert L. Thornton—N2
Rasor, Ned S. and John E. Hove—P3
Ravenhall, D. G.—H6
Regge, T., S. Okubo, and R. Marshak—Q10
Reiss, Howard—P2
Revelle, R.—G1
Rothstein, Jerome—B1
Rouse, C. A.—H4
Royden, Herbert N. and Byron T. Wright—N8
Saxon, D. S.—E1
Scalettar, Richard—Q3
Schecter, Larry and R. E. Ellis—N4
Schultz, Cramer and Ross D. F. Thompson—Q5
Segrè, E.—K1
Serber, R.—K5
Shockley, W.—L3
Shulman, R. G., B. J. Wyluda, and H. J. Hrostowski—B5
Skeen, C. H. and W. Z. Osborne—H3
Smith, Frances M., Harry H. Heckman, and Walter H. Barkas—M3
Squire, Robert K. and Burton J. Moyer—I2
Stork, D. H.—O2
Streib, J. F.—H5
Summers-Gill, R. G.—F5
Sun, C. R. and Byron T. Wright—C6
Teller, E.—E5

Tinkham, M.—B7
Thorndike, A. M.—A4
Urban, John S. and John J. McClure—H1
Violet, Charles E., F. C. Gilbert, and R. Stephen White—M5
Vollrath, R. E. and J. A. R. Samson—C2
Weissler, G. L. and L. Z. Maudlin—J2
Wertz, John E. and Juana L. Vivo—B8
——, Juana L. Vivo, and Boris Musulin—SP1
White, R. Stephen, F. C. Gilbert, and Charles E. Violet—M7
Wiegand, C.—K2
Woodbury, H. H.—D4
Wright, Robert W., George Saphir, Wilson M. Powell, George Maenchen, and William B. Fowler—M1
Yennie, D. R.—E3
Yodh, G. B.—A2
Zachariasen, F.—Q7

PHYSICAL REVIEW VOLUME 100, NUMBER 6 DECEMBER 15, 1955

Author Index to Volume 97

References with (A) are to abstracts of papers presented at meetings of the American Physical Society; references with (T) designate title only. References with (L) are to Letters to the Editor. References with (E) are to Errata.

Adair, R. K. New unstable particles—254(T)
Alba, F. (see Bonner, T. W.)—985
Albrecht, O. (see Mandeville, G. E.)—347
Alers, George A. Ultrasonic attenuation in Zn single crystals while undergoing plastic deformation—863
Alger, R. S. and R. D. Jordan. *F* centers in pure and hydride-containing alkali halide crystals—277
Allen, J. S. (see Maxson, D. R.)—109
Allen, Richard B. and H. E. Farnsworth. Diode characteristics of metal point contacts on vacuum heated Ge—252(A)
Ambler, E., R. P. Hudson, and G. M. Temmer. Alignment of Ce^{141} and Nd^{147} nuclei—1212
Ament, W. S. and G. T. Rado. Electromagnetic effects of spin wave resonance in ferromagnetic metals—1558
Anderson, John H. and Clyde A. Hutchison, Jr. Paramagnetic resonance absorption in $PrCl_3$—76
Anderson, Roy S. Variation of line width with rotational state and temperature in the microwave spectrum of OCS—1654
Argyres, Petros N. Theory of Faraday and Kerr effects in ferromagnetics—334
Arnowitt, R. and S. Gasiorowicz. Renormalization of covariant approximation scheme in field theory—823
Aroeste, Henry. Theory of melting and yield strengths—1723(L)
Askey, C. M. (see Palmatier, E. D.)—486
Askowith, Joseph G. and Kurt Sitte. Penetrating showers in light and heavy elements—159
Atkins, K. R. and M. H. Edwards. Coefficient of expansion of liquid He-II—1429
Axel, Peter, John D. Fox, and Richard H. Parker. Identification of Mo^{91} and Mo^{91m}—975

Backofen, E. W. and R. H. Herber. Half-lives of Mn^{53} and Mn^{54}—743
Ballam, J., A. L. Hodson, W. Martin, R. Ronald Rau, Geo. T. Reynolds, and S. B. Treiman. Orientation of planes in double V^0 decay events—245(L)
Baños, Alfredo, Jr. Fundamental wave functions in unbounded magneto-hydrodynamic field. I. General theory—1435
Banta, H. E. (see Macklin, R. L.)—753
Barber, W. C. Specific ionization by high-energy electrons—1071
Bardeen, J. Theory of Meissner effect in superconductors—1724(L)
Barnes, C. A. γ radiation from inelastic scattering of protons by F^{19}—1226
Barnes, George. Field emission from Re: Emission pattern corresponding to hexagonal crystal structure—1579
Bashkin, S. and R. R. Carlson. γ rays from proton bombardment of Li^6—1245
Battat, M. E. and E. R. Graves. γ rays from 14-Mev neutron bombardment of C^{13}—1266
Bay, Z., V. P. Henri, and F. McLernon. Simultaneity in Compton effect—1710
——, V. P. Henri, and F. McLernon. Upper limit for lifetimes of excited states of Ni^{60}—561(L)
Bayard, Robert T. and J. L. Yntema. Scattering of 0.6-, 1.0-, and 1.7-Mev electrons from Al and Au—372
Behrends, R. E. (see Finkelstein, R. J.)—568(L)
Bender, R. S. (see Levine, S. H.)—1249
Bendt, P. J. and F. R. Scott. Short-period delayed neutrons from fission—744
Béné, Georges J. and R. C. Extermann. Paramagnetic resonance in low fields—238(L)
Benjamin, Ben (see Burrus, Charles A.)—1661
Bernstein, S. (see Wilkinson, M. K.)—889
Berry, Chester R. Physical defects in Ag halides—676
Beyster, J. R., R. L. Henkel, and R. A. Nobles. Inelastic collision cross sections at 1.0, 4.0, and 4.5-Mev neutron energies—563(L)
Bhatia, A. B. Vibration spectra and specific heats of cubic metals. I. Theory and application to sodium—363
Biedenharn, L. C., R. L. Gluckstern, M. H. Hull, Jr., and G. Breit. Coulomb functions for large charges and small velocities—542
Biot, M. A. Variational principles in irreversible thermodynamics with application to viscoelasticity—1463
Birman, Joseph. Effect of overlap on electrostatic lattice potentials in ionic crystals—897
Blevins, Gilbert S., Albert W. Jache, and Walter Gordy. Millimeter wave spectra of AsH_3 and AsD_3—684
—— (see Jache, Albert W.)—680
Block, M. M. and D. T. King. Nuclear absorption of fast charged hyperon—1415(L)
Bloembergen, N. and T. J. Rowland. Nuclear spin exchange in solids: Tl^{203} and Tl^{205} magnetic resonance in Tl and TlO—1679
Bloom, Arnold L. and James N. Shoolery. Effects of perturbing rf fields on nuclear spin coupling—1261
Bloom, M., E. L. Hahn, and B. Herzog. Free magnetic induction in nuclear quadrupole resonance—1699
—— (see Marmier, P.)—103
Boehm, F. (see Murray, J. J.)—1007
Bolsterli, Mark and Eugene Feenberg. Matrix elements in superallowed transitions—736
Bonner, T. W., F. Alba, A. Fernandez, and M. Mazari. Scattering of fast neutrons in Pb and Ag—985
Bostick, Winston H. and Morton A. Levine. Ionized gas in magnetic field—13
Boyle, W. S. and P. Kisliuk. Departure from Paschen's Law of breakdown in gases—255

Brand, Frank A. and Harold Jacobs. Energy distributions of field-dependent secondary electrons—81
Breit, G., J. B. Ehrman, and M. H. Hull, Jr. Polarization and amplitudes in nucleon-nucleon scattering—1051
—— **and M. H. Hull, Jr.** Amplitudes in nucleon-nucleon scattering—1047
—— (see Biedenharn, L. C.)—542
Brennan, J. G. and A. B. Volkov. Magnetic moments of conjugate nuclei—1380
Brown, Fielding and Charles L. Gravel. Domain rotation in Ni ferrite—55
Brown, Frederick C. Temperature dependence of electron mobility in AgCl—355
Browne, C. I. (see Jaffe, H.)—142
Brueckner, K. A. Two-body forces and nuclear saturation. III. Details of structure of nucleus—1353
—— **and C. A. Levinson.** Approximate reduction of many-body problem for strongly interacting particles to problem of self-consistent fields—1344
Buechner, William W. Recent results in magnetic analysis of nuclear reactions—252(T)
Bunker, M. E. and J. W. Starner. Decay of Ti^{51} and Gr^{51}—1272
Burns, Fred P. and S. L. Quimby. Ordering processes in Cu_3Au—1567
Burrus, Charles A., Walter Gordy, Ralph Livingston, and Ben Benjamin. One-to-two mm wave spectra of TCl and TBr—1661
Burson, S. B. (see LeBlanc, J. M.)—750
Burstein, Elias (see Lax, Melvin)—39

Callaway, Joseph. Orthogonalized plane wave method—933
Campbell, E. C. (see Stelson, P. H.)— 1222
Carlson, R. R. (see Bashkin, S.)—1245
—— Biquadratic spinor identities—810
Case, K. M. (see Mendlowitz, H.)—33
Chase, C. E. and Melvin A. Herlin. Ultrasonic propagation in magnetically cooled He—1447
Chou, C. N. and Marcel Schein. Cosmic-ray studies of penetrating showers and bremsstrahlung at 11 200 ft by using plastic scintillation counters—206
Christian, Russell H. (see Walsh, John M.)—1544
Christie, Dan E. Vectorial approach to principal equation of rigid-body kinematics—253(A)
Clark, Arnold F. (see Grandey, Raymond A.)—791
Cohen, Robert S. Hertz's abandonment of concept of force in logical clarification of classical mechanics—253(A)
Cohen, Victor W. (see Gilbert, D. A.)—243(L)
Collins, T. L., Jr. (see White, F. A.)—566(L)
Cooper, H. G., J. S. Koehler, and J. W. Marx. Irradiation effects in Cu, Ag, and Au near 10°K—599
Cooper, Leon N. and W. Tobocman. Deuteron stripping and problem of nuclear radii—243(L)
—— **and James Rainwater.** Theory of multiple Coulomb scattering from extended nuclei—492
Cork, J. M. (see LeBlanc, J. M.)—750
Cormack, A. M. Internal Rayleigh scattering—986
—— Neutrinos from sun—137
Crandall, Walter E. (see Schecter, Larry)—184
Crane, W. W. T., G. H. Higgins, and S. G. Thompson. Average number of neutrons emitted during spontaneous fission of Cf^{252}—242(L); 1727(E)
Crawford, Frank S., Jr., and M. Lynn Stevenson. Reaction $p+p\rightarrow\pi^{+}+d$—1305
Culler, Vaughn and R. W. Waniek. Total cross sections for high-energy neutrons—252(A)

Dabrowski, J. and J. Sawicki. Simple model of Li^6 nucleus and $Li^6(n,t)He^4$ reaction—1002
Dash, J. Gregory. Supercritical damping of oscillating disks in liquid He II—1038
—— (see Sommers, Henry S., Jr.)—855
Dash, W. G. Effect of crystal distortion upon change of resistivity of Si by heat treatment—354
da Silveira, Adel. Particles with spin two—1144
Davidon, William C. Proper-time electron formalism—1131
—— Proper-time quantum electrodynamics—1139
Davis, Raymond, Jr. Attempt to detect anti-neutrinos from nuclear reactor by $Cl^{37}(\bar{\nu},e^{-})A^{37}$ reaction—766
Davis, Roland W. (see Graves, Elizabeth R.)—1205
Day, Paul P. Electromagnetic spectum of Am^{241}—689
DeBenedetti, S. (see Stearns, M.)—240(L)
Debs, R. J., J. T. Eisinger, A. W. Fairhall, I. Halpern, and H. G. Richter. Yields of photonuclear reactions with 320-Mev x-rays. I. Experimental results—1325
—— (see Halpern, I.)—1327
der Mateosian, E. Neutron capture cross section of Ta^{183}—1023
Deshotels, W. J. and A. H. Weber. Effect of strong electrostatic fields on resistance of W wires in high vacua—66
Detwiler, D. P. Electrical properties of GaSb—1575
Deutsch, Robert W. Analysis of secondary particles resulting from high-energy nuclear bombardment—1110
Dicke, Robert H. Angular momentum of real field—536
—— Optically induced polarization of atoms and nuclei—252(T)
Dietz, F. T. Physics and oceanography—252(A)
Dixon, W. R. and L. E. H. Trainor. Nature of positron annihilation in liquids and solids—733
Dondes, S. (see Harteck, P.)—1727(E)
Dousmanis, George C. Magnetic hyperfine effects and electronic structure of NO—967
Doyle, W. T. and A. R. Quinton. Energy levels from some (α,n) type reactions—252(A)
Drummond, J. E. Masses of light nuclei—1004
DuMond, J. W. M. (see Murray, J. J.)—1007
Dunlap, W. C., Jr. Au-doped Ge—614

Eden, R. J. and N. C. Francis. Theory of nuclear models—1366
Edwards, M. H. (see Atkins, K. R.)—1429
Ehrman, J. B. (see Breit, G.)—1051
Eisberg, L. M., W. B. Fowler, R. M. Lea, W. D. Shephard, R. P. Shutt, A. M. Thorndike, and W. L. Whittemore. π^{-}-p interactions at 1.4 Bev—797
Eisinger, J. T. (see Debs, R. J.)—1325
—— (see Halpern, I.)—1327
Ellis, R. Hobart, Jr., H. H. Rossi, and G. Failla. Stopping power of water films—1043
Evans, J. E., E. G. Joki, and R. R. Smith. Evidence for second naturally occurring isotope in Ta—565(L)
Ewald, A. W. and E. E. Kohnke. Measurements of electrical conductivity and magnetoresistance of gray Sn filaments—607
Extermann, R. C. (see Béné, Georges J.)—238(L)

Failla, G. (see Ellis, R. Hobart, Jr.)—1043
Fairhall, A. W. (see Debs, R. J.)—1325
—— (see Halpern, I.)—1327
Famularo, K. F. (see Simmons, B. E.)—89
Farney, G. K., H. H. Givin, B. D. Kern, and T. M. Hahn. High-energy γ rays from proton bombardment of F—720
Farnsworth, H. E. (see Allen, Richard B.)—252(A)
Farringer, L. D. (see Ting, Yu)—1037
Feenberg, Eugene. (see Bolsterli, Mark)—736
Feingold, Arnold M. and Sherman Frankel. Geometrical corrections in angular correlation measurements—1025
Fernandez, A. (see Bonner, T. W.)—985
Fernbach, Sidney, Warren Heckrotte, and Joseph V. Lepore. Theory of polarization of nucleons scattered elastically by nuclei—1059
Feynman, R. P. Slow electrons in polar crystal—660
Fields, T. H. (see Sutton, R. B.)—783

Finkelstein, R. J. and R. E. Behrends. Radiative corrections to muon decay—568(L)
Fireman, E. L. Tritium production by 2.2-Bev protons on Fe and its relation to cosmic radiation—1303
—— **and F. S. Rowland.** Tritium and neutron production by 2.2-Bev protons on N and O—780
Florence, M. G. (see Hyde, E. K.)—1255
Ford, K. W. (see Wall, N. S.)—726
Fowler, E. C. (see Walker, R. M.)—1086
Fowler, W. B. (see Eisberg, L. M.)—797
Fox, J. G. (see Sutton, R. B.)—783
Fox, John D. (see Axel, Peter)—975
Francis, N. C. (see Eden, R. J.)—1366
Frankel, Sherman (see Feingold, Arnold M.)—1025
Frazer, B. C. (see Shirane, Gen)—1179(L)
Freistadt, Hans. Classical field theory in Hamilton-Jacobi formalism—1158
Friedman, M. H. Nucleon anomalous moment in cut-off meson theory—1123
Froehlich, Fritz E. and Kurt Sitte. Mean free path for shower production by high-energy π mesons—151
—— (see Sitte, Kurt)—166
Fry, W. F., J. Schneps, and M. S. Swami. K-mesonic decay of slow secondary particles—1189(L)
Fuller, C. S. (see Reiss, Howard)—559(L)
Furst, Milton and Hartmut Kallmann. Enhancement of fluorescence in solutions under high-energy irradiation—583

Gasiorowicz, S. (see Arnowitt, R.)—823
Geiger, Felix E., Jr. K band in additively colored KCl at 18°K—560 (L)
Gell-Mann, M. and A. Pais. Behavior of neutral particles under charge conjugation—1387
Gerjuoy, E. and S. Stein. Rotational excitation by slow electrons—1671
Gilbert, D. A. and Victor W. Cohen. Nuclear hfs interaction in 3.1-hr Cs^{134m}—243(L)
Gindler, J. E. (see Studier, M. H.)—88
Givens, M. Parker. (see Woodruff, Robert W.)—52
Givin, H. H. (see Farney, G. K.)—720
Glaser, Donald A. and David C. Rahm. Characteristics of bubble chambers—474
Glasoe, G. N. Physics at Brookhaven National Laboratory—254 (T)
Gluckstern, R. L. (see Biedenharn, L. C.)—542
Gold, Louis. Macroscopic aspects of neutron interaction in magnetics—79
Goldberg, A. E. (see Mitchell, G. R.)—239 (L)
Goldberger, Marvin L. Use of causality conditions in quantum theory—508
Goldschmidt-Clermont, Y., L. S. Osborne, and M. Scott. Photoproduction of π^0 mesons from protons—188
Goldstein, Louis (see Sommers, Henry S., Jr.)—855
Goodman, Clark (see McClelland, Clyde)—1191
Goodman, L. S. and S. Wexler. Hyperfine splitting and sign of magnetic moment of Cs^{134m}—242(L)
Gordy, Walter (see Blevins, Gilbert S.)—684
—— (see Burrus, Charles A.)—1661
—— (see Jache, Albert W.)—680
Gottlieb, M. B. (see Meredith, L. H.)—201
Gove, H. E. and E. B. Paul. Angular distribution of γ rays from proton capture in B^{11}—104
Grandey, Raymond A. and Arnold F. Clark. Scattering of 151-Mev positive pions by protons—791
Gravel, Charles L. (see Brown, Fielding)—55
Graves, Elizabeth R. and Roland W. Davis. Cross sections for nonelastic interactions of 14-Mev neutrons with various elements—1205
—— (see Battat, M. E.)—1266
Graves, William E. and Allan C. G. Mitchell. Disintegration of As^{71}—1033
Green, H. S. Goldstein's eigenvalue problem—540
Gross, E. P. Shape of collision-broadened spectral lines—395
Guier, William H. (see Hart, Robert W.)—841
Gummel, Hermann and Melvin Lax. Thermal ionization and capture of electrons trapped in semiconductors—1469
Gürsey, F. Connection between Dirac's electron and classical spinning particle—1712

Hahn, E. L. (see Bloom, M.)—1669
Hahn, T. M. (see Farney, G. K.)—720
Hall, L. H. Photodiffusion current Hall effect: transient behavior—1471
Halpern, I., R. J. Debs, J. T. Eisinger, A. W. Fairhall, and H. G. Richter. Yields of photonuclear reactions with 320-Mev x-rays. II. Interpretation of results—1327
—— (see Debs, R. J.)—1325
Hamilton, J. Functional analysis and strong-coupling theory—1390
Hammel, Edward F. (see Kilpatrick, John E.)—9; 1634
Hancock, D. A. (see Hunt, S. E.)—567(L)
Hans, Harnam Singh, Babulal Saraf, and C. E. Mandeville. Coincidence studies of disintegration of Pm^{151} and Nd^{147}—1267
Hart, Robert W. and William H. Guier. Statistical treatment of weakly interacting particles in Newtonian potential—841
Harteck, P. and S. Dondes. Origin of nitrous oxide in atmosphere—1727(E)
Hayden, R. J. (see Wasserburg, G. J.)—86
Haynes, J. B. (see Hornbeck, J. A.)—311
Hebb, Elizabeth. Disintegration of Te^{131}—987
Heckrotte, Warren (see Fernbach, Sidney)—1059
Heiberg, E., U. Kruse, J. Marshall, L. Marshall, and F. Solmitz. Slowing down of polarized protons—250(L)
Henkel, R. L. (see Beyster, J. R.)—563(L)
Hennig, G. R. (see Smaller, B.)—239(L)
Henri, V. P. (see Bay, Z.)—561(L); 1710
Herber, R. H. (see Backofen, E. W.)—743
Herlin, Melvin A. (see Chase, C. E.)—1447
Herzog, B. (see Bloom, M.)—1669
Hicks, Donald A., John Ise, Jr., and Robert V. Pyle. Multiplicity of neutrons from spontaneous fission of Cf^{252}—564(L)
Higgins, G. H. (see Crane, W. W. T.)—242(L); 1727(E)
Hines, K. C. Energy distribution of protons due to collision energy loss—1725(L)
Hodson, A. L. (see Ballam, J.)—245(L)
—— (see Treiman, S. B.)—244(L)
Hofstadter, R. (see Van Sciver, W.)—1181(L)
Horn, F. H. Densitometric and electrical investigation of B and Si—1521
Hornbeck, J. A. and J. B. Haynes. Trapping of minority carriers in Si. I. P-type Si—311
Hove, John E. Electronic density of states of graphite—1717(L)
Huber, Elsa L. Breakdown processes in N_2, O_2, and mixtures—267
Hudson, R. P. (see Ambler, E.)—1212
Hughes, D. J. Neutron physics at Brookhaven—254(T)
Hull, Gordon F. Some optical analogues in microwave experiments—252(T)
Hull, M. H., Jr. (see Biedenharn, L. C.)—542
—— (see Breit, G.)—1047; 1051
Humblet, J. Definition of virtual level of deuteron—1145
Hunt, S. E. and D. A. Hancock. Proton-gamma resonances in Mg—567(L)
Hunten, D. M. Excitation of Na D lines in night-glow—1178(L)
Hutchison, Clyde A., Jr. (see Anderson, John H.)—76

Hyde, E. K., M. G. Florence, and A. E. Larsh. Isomeric state of Y^{88} in decay of Zr^{88}—1255
—— (see Mathur, Hirdaya B.)—117

Inghram, Mark G., Earl Long, and Lothar Meyer. Adsorption of mixtures of He^3 and He^4—1453
Inglis, D. R. Dynamics of nuclear deformation—701
Ingram, D. J. E. and J. G. Tapley. Electron resonance in gas discharges—238(L)
Irving, J. and D. S. Schonland. Energy of ground state of Li^6—446
Ise, John, Jr. (see Hicks, Donald A.)—564(L)
—— (see Schecter, Larry)—184

Jache, Albert W., Gilbert S. Blevins, and Walter Gordy. Millimeter wave spectra of SbH_3 and SbD_3—680
—— (see Blevins, Gilbert S.)—684
Jackson, J. E. (see Seddon, J. C.)—1182(L)
Jacobs, Harold. (see Brand, Frank A.)—81
Jacobsen, E. H. Elastic spectrum of Cu from temperature-diffuse scattering of x-rays—654
Jaffe, H., T. O. Passell, C. I. Browne, and I. Perlman. γ- and x-radiation in the decay of Am^{241}—142
Jastrow, Robert. Λ^0 production in nuclei—181
Jensen, E. N. (see Jones, James T., Jr.)—1031
—— (see Pohm, A. V.)—432
Jentschke, W. K. (see Maxson, D. R.)—109
Jesse, William P. and John Sadauskis. Ionization in pure gases and average energy to make ion pair for α and β particles—1668
Johansson, Sven A. E. Experiments on direct photonuclear effect—434
—— Yield of photoprotons from some light elements—1186(L)
Joki, E. G. (see Evans, J. E.)—565(L)
Jona, F., G. Shirane, and R. Pepinsky. Optical study of $PbZrO_3$ and $NaNbO_3$ single crystals—1584
Jones, James, T., Jr., and E. N. Jensen. Radiations from Ce^{141}—1031
Jordan, R. D. (see Alger, R. S.)—277
Jossem, E. L. (see Parratt, L. G.)—916

Kahn, A. H. Theory of infrared absorption of carriers in Ge and Si—1647
Kalnajs, J. (see Smakula, A.)—253
Kallmann, Hartmut and Barnett Rosenberg. Persistent internal polarization—1596
—— (see Furst, Milton)—583
Kalos, M. H. (see Tobocman, W.)—132
Kane, J. A. (see Sutton, R. B.)—783
Känzig, Werner (see Ueta, Masayasu)—1591
Kaplon, M. F. (see Koshiba, M.)—193
—— (see Noon, J. H.)—769
Kauffman, J. W. and J. S. Koehler. Quenching-in of lattice vacancies in pure Au—555(L)
Kavanagh, R. W., W. R. Mills, and R. Sherr. Isomerism in Al^{26}—248(L)
Keating, D. T. X-ray measurements of pile-irradiated LiF—832(L)
Keister, G. L., E. B. Lee, and F. H. Schmidt. Radioactive decay of Cs^{134} and Cs^{134m}—451
Keller, William E. Pressure-volume isotherms of He^4 below 4.2°K—1
—— (see Kilpatrick, John E.)—9
Kelly, W. H. (see Lu, D. C.)—139
Kern, B. D. (see Farney, G. K.)—720
Keywell, Frank. Measurements and collision-radiation damage theory of high-vacuum sputtering—1611
Kilpatrick, John E., Edward F. Hammel, and Dillon Mapother. Superconductivity of U—1634
——, **William E. Keller, and Edward F. Hammel.** Second virial coefficients of He from exp-six potential—9
King, D. T. (see Block, M. M.)—1415(L)
Kisliuk, P. (see Boyle, W. S.)—255
Klein, Martin J. Principle of detailed balance—1446
Kleiner, Walter H. Excited donor levels in Si—1722(L)
—— Magnetic scattering of slow neutrons from O_2 gas—411
Klemens, P. G. Kinetic theory of liquid He—1181(L)
Koehler, J. S. (see Cooper, H. G.)—599
—— (see Kauffman, J. W.)—555(L)
Koehler, W. G. and E. O. Wollan. Neutron diffraction by metallic Er—1177(L)
Kofstad, Per K. (see Mathur, Hirdaya, B.)—117
Kohn, W. and J. M. Luttinger. Hyperfine splitting of donor states in Si—883
—— **and J. M. Luttinger.** Theory of donor levels in Si—1721(L)
—— (see Luttinger, J. M.)—869
Kohnke, E. E. (see Ewald, A. W.)—607
Korff, S. A. (see Neuberg, H. A. C.)—1276
Koshiba, M. and M. F. Kaplon. Analysis of high-energy cosmic-ray shower. I. Soft component and trident process—193
Kraybill, H. L. (see Walker, R. M.)—1086
Krohn, V. E. and S. Raboy. Gyromagnetic ratio of excited state and other angular correlation measurements for Pb^{204m}—1017
Kruse, U. (see Heiberg, E.)—250(L)
Kulp, J. Laurence (see Volchok, Herbert L.)—102
Kunz, W. E. $H^3(He^3,p)He^4$ reaction—456
Kurnick, S. W. (see Mitchell, G. R.)—239(L)

Lampert, Murray A. Ground state of impurity atoms in semiconductors having anisotropic energy surfaces—352
Lane, A. M. and D. H. Wilkinson. Concept of parentage of nuclear states and its importance in nuclear reaction phenomena—1199
Larsh, A. E. (see Hyde, E. K.)—1255
Lax, Melvin. Molecular field in spherical model—629
—— Relation between canonical and microcanonical ensembles—1419
—— **and Elias Burstein.** Infrared lattice absorption in ionic and homopolar crystals—39
—— (see Gummel, Hermann)—1469
Lea, R. M. (see Eisberg, L. M.)—797
LePlanc, J. M., J. M. Cork, and S. B. Burson. Radioactivities of Zn^{69} and Zn^{71}—750
LeCorbeiller, Philippe E. Servomechanisms—252(T)
Lee, E. B. (see Keister, G. L.)—451
Lee-Whiting, G. E. β spectrum of Bi^{210} (RaE) and coupling constants of scalar and tensor interactions in β decay—463
—— Thermalization of positrons in metals—1557
Leipuner, L. (see Stearns, M.)—240(L)
Lepore, Joseph V. (see Fernbach, Sidney)—1059
Levine, Charles A. (see Mathur, Hirdaya B.)—117
Levine, Morton A. (see Bostick, Winston H.)—13
Levine, S. H., R. S. Bender, and J. N. McGruer. Angular distributions of deuteron-induced reactions in Li—1249
Levinger, J. S. Independent-particle model and nuclear photoeffect. II—122
Levinson, C. A. (see Brueckner, K. A.)—1344
—— Sum-rules for photodisintegration of deuteron—970
Lidén, K. and N. Starfelt. Internal and external bremsstrahlung accompanying β rays of P^{32}—419
Linsley, John. Measurement of multiply charged cosmic rays by new technique—1292
Litz, L. M. (see Ring, S. O.)—427
Livingston, Ralph (see Burrus, Charles A.)—1661
Lockwood, J. A. and H. E. Yingst. Preliminary results with the correlation of meteorological parameters with cosmic ray neutron intensities—252(A)

Loeb, Leonard B. Corona threshold and the range of velocities of pulse spread in Geiger counters—275
Long, Earl and Lothar Meyer. Superfluidity in unsaturated He films above λ temperature—1717(L)
—— (see Inghram, Mark G.)—1453
Lönsjö, O. (see Roderick, H.)—97
Low, F. E. Boson-fermion scattering in Heisenberg representation—1392
Low, W. Fermi resonance in microwave spectrum of linear XYZ molecules—1664
Löwdin, Per-Olov. Quantum theory of many-particle systems. I. Physical interpretations by means of density matrices, natural spin-orbitals, and convergence problems in method of configurational interaction—1474
—— Quantum theory of many-particle systems. II. Study of ordinary Hartree-Fock approximation—1490
—— Quantum theory of many-particle systems. III. Extension of Hartree-Fock scheme to include degenerate systems and correlation effects—1509
Lu, D. C., W. H. Kelly, and M. L. Wiedenbeck. Summing studies of γ rays following decays of Ba^{131}, Se^{75}, and Ru^{106}—139
Luckey, David. Charged photomesons from carbon—469
Lukesh, Joseph S. Neutron damage to structure of vitreous silica—345
Lutes, O. S. and E. Maxwell. Superconducting transitions in Sn whiskers—1718(L)
Luttinger, J. M. and W. Kohn. Motion of electrons and holes in perturbed periodic fields—869
—— (see Kohn, W.)—883; 1721(L)
Lyon, W. S. Decay of V^{49}—121

MacDonald, D. K. C. and S. K. Roy. Vibrational anharmonicity and lattice thermal properties. II—673
Macfarlane, G. G. and V. Roberts. Infrared absorption of Ge near lattice edge—1714(L)
Macklin, R. L. and H. E. Banta. T production from Li by deuteron bombardment—753
Madansky, L. and F. Rasetti. Co^{57} decay—837(L)
Mandeville, C. E. and H. O. Albrecht. Photostimulated emission of some activated alkali halide phosphors—347
—— (see Hans, Harnam Singh)—1267
—— (see Varma, Jagdish)—977
Mann, A. K., W. E. Stephens, and D. H. Wilkinson. Evidence for independent-particle state of C^{12} at high excitation—1184(L)
Mapother, Dillon (see Kilpatrick, John E.)—1634
Marcou, R. J. (see Pfister, W.)—1183(L)
Mark, Hans (see McClelland, Clyde)—1191
Marmier, P. and F. Boehm. Energy levels of Hf^{177}—103
—— (see Murray, J. J.)—1007
Marshall, J. (see Heiberg, E.)—250(L)
Marshall, L. (see Heiberg, E.)—250(L)
Martin, W. (see Ballam, J.)—245(L)
Marx, J. W. (see Cooper, H. G.)—599
Mason, W. P. Ultrasonic attenuation due to lattice-electron interaction in normal conducting metals—557(L)
Mathur, Hirdaya B. Radiations of 34-day Xe^{127}—707
——, **Earl K. Hyde, Charles A. Levine, and Per K. Kofstad.** Studies on isomeric pair, Nb^{93m} and Nb^{93}—117
Matthias, B. T. Empirical relation between superconductivity and number of valence electrons per atom—74
Maxson, D. R., J. S. Allen, and W. K. Jentschke. Electron-neutrino angular correlation in β decay of Ne^{19}—109
Maxwell, E. (see Lutes, O. S.)—1718(L)
Mazari, M. (see Bonner, T. W.)—985
McCarthy, John A. Search for double β decay in Ca^{48}—1234
McClelland, Clyde, Hans Mark, and Clark Goodman. Electric excitation of heavy nuclei by protons—1191
McGinnis, Carl L. Radioactivity of In^{117} and Sb^{117}—93
McGruer, J. N. (see Levine, S. H.)—1249
McGuire, Thomas R. Observation of exchange resonance near ferrimagnetic compensation point—831(L)
McLernon, F. (see Bay, Z.)—561(L); 1710
McReynolds, A. W. (see Smith, L. W.)—1186(L)
Meers, J. T. (see Palmatier, E. D.)—486
Meggitt, J. E. Variable mass equations—1126
Meissner, Hans. Paramagnetic effect in superconductors. I. Theoretical aspects—1627
Mendlowitz, H. and K. M. Case. Double scattering of electrons with magnetic interaction—33
Meredith, L. H., M. B. Gottlieb, and J. A. Van Allen. Direct detection of soft radiation above 50 kilometers in the auroral zone—201
Metzger, Franz R. Angular distribution of resonance fluorescence radiation from 411-kev excited state of Hg^{199}—1258
Meyer, Lothar. Thickness of He film as function of height—22
—— (see Inghram, Mark G.)—1453
—— (see Long, Earl.)—1717(L)
Meyerhof, W. E. (see Roderick, H.)—97
Millburn, George P. (see Schecter, Larry)—184
Mills, W. R. (see Kavanagh, R. W.)—248(L)
Mitchell, Allan C. G. (see Graves, William E.)—1033
Mitchell, G. R., A. E. Goldberg, and S. W. Kurnick. InSb photovoltaic cell—239(L)
Miyazawa, Hironari. Sachs' theorem on magnetic moments of nucleons—1413
—— Strong-coupling theory for case of pseudoscalar coupling—1399
Mooser, E. and S. B. Woods. Thermoelectric power of Ge at low temperatures—1721(L)
Morinaga, H. Effects of isotopic spin selection rules on photonuclear yields—444
—— (γ,p) and (γ,n) yield ratios from self-conjugate nuclei—1185(L)
Morse, R. W. Ultrasonic attenuation in metals by electron relaxation—1716(L)
Mott, W. E. (see Sutton, R. B.)—783
Murray, J. J., F. Boehm, P. Marmier, and J. W. M. DuMond. Decays of Ta^{182} and Ta^{183}—1007

Nadelhaft, Irving (see Sitte, Kurt)—166
Nagle, D. E. Scattering of 119-Mev pions by deuterium—480
Nanda, V. S. Thermodynamic properties of He^3 and He^4 solutions—571
Nervik, Walter E. and Glenn T. Seaborg. Ta spallation and fission induced by 340-Mev protons—1092
Nethercot, A. H., Jr. (see Rosenblum, B.)—84
Neuberg, H. A. C., R. K. Soberman, M. J. Swetnick, and S. A. Korff. High-altitude cosmic-ray neutron density at geomagnetic pole—1276
Neufeld, Jacob (see Snyder, W. S.)—1636
Newcomb, W. A. and E. E. Salpeter. Mass corrections to hfs in H—1146
Newman, R. (see Tyler, W. W.)—669
Newton, Roger G. Radiative correction to electron scattering—1162
Nilan, T. G. and W. S. Paxton. Domains of reverse magnetization in ferromagnetic metals—834(L)
Nobles, R. A. (see Beyster, J. R.)—563(L)
Noon, J. H. and M. F. Kaplon. Interactions of heavy nuclei of cosmic radiation—769

Oakley, D. C. and R. L. Walker. Photoproduction of neutral pions in H; magnetic analysis of recoil protons—1283
—— (see Walker, R. L.)—1279
Osborne, L. S., W. D. Rankin, P. G. Stein, A. Wattenberg, and A. Winston. Search for electromagnetic interaction between μ mesons and electrons—809
—— (see Goldschmidt-Clermont, Y.)—188

Pais, A. (see Gell-Mann, M.)—1387
Palmatier, E. D., J. T. Meers, and C. M. Askey. Landau distribution and density effect at high gas pressures—486
Park, David. Faraday effect in polycrystalline ferrite—253(A)
—— Magnetic rotation phenomena in polycrystalline ferrite—60
Parker, Richard H. (see Axel, Peter)—975
Parmenter, R. H. Energy levels of disordered alloy—587
Parratt, L. G. and E. L. Jossem. X-ray spectroscopy of solid state: KCl—916
Passell, T. O. (see Jaffe, H.)—142
Paul, E. B. (see Gove, H. E.)—104
Paxton, W. S. (see Nilan, T. G.)—834(L)
Pearson, W. B. Resistance and thermoelectric measurements of cold-worked Cu and resistance minimum at low temperatures—666
Pepinsky, Ray (see Jona, F.)—1584
—— (see Shirane, Gen)—1179(L)
Percus, J. K. Supplementary conditions in quantized linear systems—1406
Perl, M. L., I. I. Rabi, and B. Senitzky. Nuclear electric quadrupole moment of Na^{22}—838(L)
Perlman, I. (see Jaffe, H.)—142
Petritz, Richard L. and Wayne W. Scanlon. Mobility of electrons and holes in polar crystal, PbS—1620
Pfister, W., J. C. Ulwick, and R. J. Marcou. Bifurcation in *E*-layer—1183(L)
Phillips, James A. Charge equilibrium ratios for hydrogen ions from solids—404
Pleasonton, Frances (see Snell, Arthur H.)—246(L)
Pohm, A. V., R. G. Waddell, J. P. Powers, and E. N. Jensen. β spectrum of C^{14}—432
Powers, J. P. (see Pohm, A. V.)—432
Pratt, George W., Jr. Antiferromagnetism—926
Pratt, William W. Angular distribution of protons from reaction $Ti^{48}(d,p)Ti^{49}$—131
Preston, R. S. (see Walker, R. M.)—1086
Price, P. J. Nuclear susceptibility of liquid and solid He^3—259
Pugh, Emerson M. Band model for Hall effect, magnetization, and resistivity of magnetic metals—647
Pyle, Robert V. (see Hicks, Donald A.)—564(L)

Quimby, S. L. (see Burns, Fred P.)—1567
Quinton, A. R. (see Doyle, W. T.)—252(A)

Rabi, I. I. (see Perl, M. L.)—838(L)
Raboy, S. (see Krohn, V. E.)—1017
Rado, G. T. (see Ament, W. S.)—1558
Rahm, David C. (see Glaser, Donald A.)—474
Rainwater, James (see Cooper, Leon N.)—492
Rankin, W. D. (see Osborne, L. S.)—809
Rasetti, F. (see Madansky, L.)—(837L)
Rasmussen, V. K., John R. Rees, and M. B. Sampson. Search for 15-Mev γ radiation from $N^{14}+d$ and $Be^9+\alpha$—1727(E)
Rau, R. Ronald (see Ballam, J.)—245(L)
Rees, John R. (see Rasmussen, V. K.)—1727(E)
—— (see Wall, N. S.)—726
Reiffel, L. and H. V. Watts. Compacted scintillators—1714(L)
Reiss, Howard and C. S. Fuller. Ionization and solubility in semiconductors—559(L)
Relf, Kenneth E. Cloud-chamber study of cosmic-ray air showers at sea level—172
Reynolds, Geo. T. (see Ballam, J.)—245(L)
—— (see Treiman, S. B.)—244(L)
Rice, O. K. Can He^3 be expected to exhibit superfluidity at sufficiently low temperatures?—558(L)
—— Energy levels in liquid He^3—1176(L)
—— Interpretation of magnetic behavior of liquid He^4—263
Richter, H. G. (see Debs, R. J.)—1325
—— (see Halpern, I.)—1327
Ring, S. O. and L. M. Litz. Excitation function for Na^{22} from deuterons on Al—427
Rivier, Dominique. Gauge invariance and renormalization in electrodynamics—505
Roberts, L. D. (see Wilkinson, M. K.)—889
Roberts, V. (see Macfarlane, G. G.)—1714(L)
Roderick, H., O. Lönsjö, and W. E. Meyerhof. Decay scheme of mirror nucleus P^{29} and related results—97
Rojansky, V. Quantum-mechanical operators—507
Rorschach, H. E., Jr. (see Swim, R. T.)—25
Rose, Albert. Recombination processes in insulators and semiconductors—322; 1727(E)
—— Space-charge-limited currents in solids—1538
—— (see Smith, R. W.)—1531
Rosenberg, Barnett (see Kallmann, Hartmut)—1596
Rosenblum, B. and A. H. Nethercot, Jr. Microwave spectra of TI and TBr—84
Rosenstock, Herbert B. Dynamics of simple lattices—290
Rossi, H. H. (see Ellis, R. Hobart, Jr.)—1043
Rourke, F. M. (see White, F. A.)—566(L)
Rowland, F. S. (see Fireman, E. L.)—780
Rowland, T. J. (see Bloembergen, N.)—1679
Roy, S. K. (see MacDonald, D. K. C.)—673
Rubenstein, R. A. and J. N. Snyder. New treatment of Auger effect and fluorescence yield in lighter elements—1653
Ruby, S. L. (see Rustad, B. M.)—991
Rustad, B. M. and S. L. Ruby. Gamow-Teller interaction in decay of He^6—991

Sadauskis, John (see Jesse, William P.)—1668
Salpeter, E. E. Nuclear reactions in stars. II. Protons on light nuclei—1237
—— (see Newcomb, W. A.)—1146
Sampson, M. B. (see Rasmussen, V. K.)—1727(E)
Sands, Matthew. Synchrotron oscillations induced by radiation fluctuations—470
Saraf, Babulal. Energy levels of Rh^{103} from decay of Pd^{103} and Ru^{103}—715
—— (see Hans, Harnam Singh)—1267
Satchler, G. R. Deuteron stripping and collective nuclear model—1416(L)
Sawicki, J. (see Dabrowski, J.)—1002
Scanlon, Wayne W. (see Petritz, Richard L.)—1620
Schecter, Larry, Walter E. Crandall, George P. Millburn, and John Ise, Jr. Cross sections for producing high-energy neutrons from C targets bombarded by protons, deuterons, and He^3 particles—184
Schein, Marcel (see Chou, C. N.)—206
Schiffer, John P. Energy levels in Ca^{43} and Ca^{44}—428
Schiller, Ralph. New transition to ray optics—1421
Schmidt, F. H. (see Keister, G. L.)—451
Schneps, J. (see Fry, W. F.)—1189(L)
Schonland, D. S. (see Irving, J.)—446
Schrieffer, J. R. Effective carrier mobility in surface space charge layers—641
Schwartz, Charles. Theory of hyperfine structure—380
Scott, F. R. (see Bendt, P. J.)—744
Scott, M. (see Goldschmidt-Clermont, Y.)—188
Seaborg, Glenn T. (see Nervick, Walter E.)—1092
Seagrave, John D. Recoil deuterons and disintegration protons from n-d interaction, and n-p scattering at $E_n = 14.1$ Mev—757
Seddon, J. C. and J. E. Jackson. Absence of bifurcation in the *E*-layer—1182(L)
Sen, Hari K. Nonlinear theory of space charge wave in moving, interacting electron beams with application to solar radio noise—849
Senitzky, B. (see Perl, M. L.)—838(L)
Shephard, W. D. (see Eisberg, L. M.)—797
Sherr, R. (see Kavanagh, R. W.)—248(L)

Shirane, Gen, Ray Pepinsky, and B. C. Frazer. X-ray and neutron diffraction study of ferroelectric $PbTiO_3$—1179(L)
—— (see Jona, F.)—1584
Shoolery, James N. (see Bloom, Arnold L.)—1261
Shull, C. G. and M. K. Wilkinson. Neutron diffraction studies of magnetic structure of alloys of transition elements—304
—— (see Wilkinson, M. K.)—889
Shutt, R. P. (see Eisberg, L. M.)—797
Siegert, Arnold J. F. Metastable states of finite lattice gas—1456
Sils, V. (see Smakula, A.)—253(A)
Simmons, B. E., D. M. Van Patter, K. F. Famularo, and R. V. Stuart. Coulomb excitation of Nd—89
Sitte, Kurt, Fritz E. Froehlich, and Irving Nadelhaft. Electron production in high-energy nuclear interactions—166
—— (see Askowith, Joseph G.)—159
—— (see Froehlich, Fritz E.)—151
Sladek, Ronald J. Thermal conductivity of In-Tl alloys at low temperatures—902
Slifkin, L. and C. T. Tomizuka. Mechanism of intermetallic diffusion—836(L)
Smakula, A., J. Kalnajs, and V. Sils. Imperfections in Ge single crystals—253(A)
Smaller, B., G. R. Hennig, and E. L. Yasaitis. Paramagnetic resonance absorption in graphite compounds—2397(L)
Smith, L. W., A. W. McReynolds, and G. Snow. Elastic p-p angular distribution from 440 to 1000 Mev—1186(L)
—— Experimental program centered around the Cosmotron—254(T)
Smith, R. R. (see Evans, J. E.)—565(L)
Smith, R. W. Properties of ohmic contacts to CdS single crystals—1525
—— **and A. Rose.** Space-charge-limited currents in single crystals of CdS—1531
Snell, Arthur H. and Frances Pleasonton. Spectrometry of recoils from neutrino emission in A^{37}—246(L)
Snow, G. (see Smith, L. W.)—1186(L)
Snyder, J. N. (see Rubenstein, R. A.)—1653
Snyder, W. S. and Jacob Neufeld. Disordering of solids by neutron radiation—1636
Soberman, R. K. (see Neuberg, H. A. C.)—1276
Solmitz, F. (see Heiberg, E.)—250(L)
Sommers, Henry S., Jr., J. Gregory Dash, and Louis Goldstein. Transmission of slow neutrons by liquid He. I. Experimental—855
Stallwood, R. A. (see Sutton, R. B.)—783
Starfelt, N. and N. L. Svantesson. Internal and external bremsstrahlung in connection with β decay of S^{35}—708
—— (see Lidén, K.)—419
Starner, J. W. (see Bunker, M. E.)—1272
Stearns, M., M. B. Stearns, S. De Benedetti, and L. Leipuner. Energies of K transitions of π^--mesonic x-rays—240(L)
Stearns, M. B. (see Stearns, M.)—240(L)
Steele, M. C. Anomalous longitudinal magnetoresistance of metal single crystals—1720(L)
Steffen, R. M. and W. Zobel. Magnetic moment of 247-kev excited state of Cd^{111} nucleus—1188(L)
Stein, P. G. (see Osborne, L. S.)—809
Stein, S. (see Gerjuoy, E.)—1671
Stelson, P. H. and E. C. Campbell. Cross section for excitation of Pb^{207m} by inelastic scattering of neutrons—1222
Stephens, W. E. (see Mann, A. K.)—1184(L)
Sternheimer, R. M. Polarization of nucleons elastically scattered from nuclei—1314
Stevens, C. M. (see Studier, M. H.)—88
Stevenson, M. Lynn (see Crawford, Frank S., Jr.)—1305
Stewart, John W. Compressibilities of some solidified gases at low temperature—578
Strandberg, M. W. P. (see Tinkham, M.)—937; 951
Stuart, R. V. (see Simmons, B. E.)—89
Studier, M. H., J. E. Gindler, and C. M. Stevens. Long-lived isomer of Np^{236}—88
Suhl, H. Ferromagnetic resonance in Ni ferrite between one and two kMc/sec—555(L)
Sutton, R. B., T. H. Fields, J. G. Fox, J. A. Kane, W. E. Mott, and R. A. Stallwood. p-p scattering at 437 Mev—783
Svantesson, N. L. (see Starfelt, N.)—708
Swami, M. S. (see Fry, W. F.)—1189(L)
Swetnick, M. J. (see Neuberg, H. A. C.)—1276
Swim, R. T. and H. E. Rorschach, Jr. Flow of He II through narrow slits—25
Szekeres, G. New formulation of general theory of relativity—212

Taconis, K. W. Bulk formation of He II in capillaries—1176(L)
Takeda, Gyo and K. M. Watson. Scattering of fast neutrons and protons by atomic nuclei—1336
Tamor, S. Polarization in scattering by complex nuclei—1077
Tapley, J. G. (see Ingram, D. J. E.)—238(L)
Temmer, G. M. (see Ambler, E)—1212
Temperley, H. N. V. Treatment of liquid He^3 based on "cell" model—835(L)
Thomas, R. G. Collision matrices for compound nucleus—224
Thompson, S. G. (see Crane, W. W. T.)—242(L); 1727(E)
Thorndike, A. M. (see Eisberg, L. M.)—797
Ting, Yu, L. D. Farringer, and Dudley Williams. Paramagnetic resonance absorption in $CrCl_3$—1037
Tinkham, M. and M. W. P. Strandberg. Interaction of molecular O_2 with magnetic field—951
—— **and M. W. P. Strandberg.** Theory of fine structure of molecular O_2 ground state—937
Tobocman, W. and M. H. Kalos. Numerical calculation of (d,p) angular distributions—132
—— (see Cooper, L. N.)—243(L)
Tollestrup, A. V. (see Walker, R. L.)—1279
Tomizuka, C. T. (see Slifkin, L.)—836(L)
Tonks, Lewi. Particle transport, electric currents, and pressure balance in magnetically immobilized plasma—1443
Trainor, L. E. H. (see Dixon, W. R.)—733
Trees, R. E. Polarization energy for $3d$ and $4p$ electrons—686
Treiman, S. B., Geo. T. Reynolds, and A. L. Hodson. Angular correlation effects in unstable particle decay—244(L)
—— (see Ballam, J.)—245(L)
Tyler, W. W., R. Newman, and H. H. Woodbury. Properties of Ge doped with Co—669

Ueta, Masayasu and Werner Känzig. Generation of electron traps by plastic flow in alkali halides—1591
Ulwick, J. C. (see Pfister W.)—1183(L)

Van Allen, J. A. (see Meredith, L. H.)—201
Van Patter, D. M. (see Simmons, B. E.)—89
Van Sciver, W. and R. Hofstadter. Scintillations and luminescence in unactivated NaI—1181(L)
Varma, Jagdish and C. E. Mandeville. Level scheme of In^{111}—977
Vasileff, H. D. Thermal ionization of impurities in polar crystals. II. Application to interstitials in cubic ZnS—891
Vineyard, G. H. Neutron diffraction experiments—254(T)
Volchok, Herbert L. and J. Laurence Kulp. Half-life of Y^{90}—102
Volkov, A. B. (see Brennan, J. G.)—1380

Waddell, R. G. (see Pohm, A. V.)—432
Walker, R. L., D. C. Oakley, and A. V. Tollestrup. Photoproduction of neutral pions in H; $p-\gamma$ coincidences—1279
—— (see Oakley, D. C.)—1283
Walker, R. M., R. S. Preston, E. C. Fowler, and H. L. Kraybill. Production of neutral V-events by Cosmotron neutrons—1086

Walker, William C. and G. L. Weissler. Energy distributions of photoelectrons from Au and Ge in far uv—1178(L)
Wall, N. S., J. R. Rees, and K. W. Ford. Elastic scattering of 22-Mev α particles—726
—— (see Rasmussen, V. K.)—1727(E)
Walsh, John M. and Russell H. Christian. Equation of state of metals from shock wave measurements—1544
Wangsness, Roald K. Possibility of observation of exchange resonance near ferromagnetic compensation point—831(L)
Waniek, R. W. (see Culler, Vaughn)—252(A)
Wasserburg, G. J. and R. J. Hayden. Age of meteorites by A^{40}-K^{40} method—86
Watson, K. M. (see Takeda, Gyo)—1336
Wattenberg, A. (see Osborne, L. S.)—809
Watts, H. V. (see Reiffel, L.)—1714(L)
Weber, A. H. (see Deshotels, W. J.)—66
Weissler, G. L. (see Walker, William C.)—1178(L)
Wexler, S. (see Goodman, L. S.)—242(L)
Wheeler, John Archibald. Geons—511
White, F. A., T. L. Collins, Jr., and F. M. Rourke. New naturally occurring isotope of Ta—566(L)
Whittemore, W. L. (see Eisberg, L. M.)—797
Wiedenbeck, M. L. (see Lu, D. C.)—139
Wilkinson, D. H. (see Lane, A. M.)—1199
—— (see Mann, A. K.)—1184(L)
Wilkinson, M. K., C. G. Shull, L. D. Roberts, and S. Bernstein. Neutron diffraction observations on superconducting state—889
—— (see Shull, C. G.)—304
Williams, C. Nuclear energy as a source of power—254(T)
Williams, Dudley (see Ting, Yu)—1037
Winston, A. (see Osborne, L. S.)—809
Wollan, E. O. (see Koehler, W. G.)—1177(L)
Woodbury, H. H. (see Tyler, W. W.)—669
Woodruff, Robert W. and M. Parker Givens. Soft x-ray absorption of evaporated thin films of Te—52
Woods, S. B. (see Mooser, E.)—1721(L)

Yasaitis, E. L. (see Smaller, B.)—239(L)
Yeivin, Yehudah. Charge and isotopic-spin conservation in multiple meson production—1084
Yingst, H. E. (see Lockwood, J. A.)—252(A)
Yntema, J. L. (see Bayard, Robert T.)—372

Zobel, W. (see Steffen, R. M.)—1188(L)
Zollweg, R. J. Structure in optical absorption of BaO films—288

Author Index to Volume 98

References with (A) are to abstracts of papers presented at meetings of the American Physical Society; references with (T) designate title only. References with (L) are to Letters to the Editor. References with (E) are to Errata.

Aamodt, L. C. and P. C. Fletcher. Magnetic moment and mass of Cl^{38}—1317

—— **and P. C. Fletcher.** Spin, quadrupole moment, and mass of Se^{75}—1224

Abragam, A. Overhauser effect in nonmetals—1729

Abraham, Bernard M., Darrell W. Osborne, and Bernard Weinstock. Heat capacity and entropy of liquid He^3 from 0.23 to 2°K: nuclear alignment in liquid He^3—551(L)

Abrahams, Elihu. Interaction between spin waves and conduction electrons in ferromagnetic metals—387

Abramowitz, Milton (see Stegun, Irene A.)—1851

Acharya, Y. V. G. Momentum transfer and heat diffusion in mixing of coaxial turbulent jets—1142(A)

Adams, E. N. Auxiliary conditions in Bohm-Pines theory of electron gas—1130(L)

—— Plasma oscillations in metals—947

Adams, N. I., Jr. (see Kovarik, A. F.)—46

Adel, Arthur. Cyclical variations in effective radiation temperature of ozone region—282(A)

Adkins, R. H. and J. G. Brennan. Intermediate coupling model of Li^8—235(A)

Ajzenberg, F. (see Rubin, A.)—1185(A)

Albrecht, H. O. and C. E. Mandeville. Storage of energy in BeO—1546(A)

—— (see Mandeville, C. E.)—1569(A)

Albritton, B. R., Jr. (see Mobley, R. C.)—232(A)

Alburger, D. E. and A. W. Sunyar. Decay of Bi^{207}—276(A)

Aldrich, L. T. (see Wetherill, G. W.)—250(A)

Alers, P. B. Thermal magnetoresistance of Zn at liquid He temperatures—1180(A)

Alexander, L. E. X-ray diffraction studies of crystallization in elastomers—1547(T)

Alexeff, Igor. (see Bina, Melvin J.)—251(A)

—— (see Jennings, B.)—582

Alexis, Lucien V., Sr. Force—Its nature, structure, and generation (creation) (as disclosed by $f \times t = m$)—1176(A)

Alger, R. S. and R. D. Jordan. Energy requirement for F-center formation—1550(A)

Allen, G., R. Webeler, and S. Barile. Multiple scattering of low-energy α-particles in gas—1168(A)

Allen, J. S. (see Maxson, D. R.)—230(A)

Allen, Leland C. Interpolation scheme for energy bands in solids—993; 1193(A)

Allen, Lew, Jr. Photodisintegration of deuteron by 95-Mev bremsstrahlung—705

Allen, R. B. and H. E. Farnsworth. Effect of ion-bombardment cleaning of Ge on point contact rectification—1179(A)

Allen, William A., Joe M. Mapes, and Earle B. Mayfield. Shock waves in air produced by waves in plate—256(A)

Allin, Elizabeth J., W. F. J. Hare, and R. E. MacDonald. Infrared absorption of liquid and solid hydrogen—554(L)

Allison, B. A. (see Faust, W. R.)—224(A)

—— (see Scherrer, V. E.)—224(A)

Alperovitch, Edward A. and J. Malcolm Miller. Occurrence of Tc^{99} in nature—262(A)

Alpert, D. H. Experiments at very low pressures—278(T)

Alter, B. E. K. and C. W. Curtis. Propagation of plastic strain along Pb bars—1151(A)

Alvarez, Luis W., Frank S. Crawford, Jr., and M. Lynn Stevenson. Elastic scattering of 1.6-Mev γ rays from C—280(A)

—— (see Paramentier, D.)—284(A)

Ambler, E., R. P. Hudson, and G. M. Temmer. Anisotropic γ radiation from aligned Nd^{147}—230(A)

Ames, I., H. S. Sack, and R. M. Wood. Dielectric dispersion in ZnS phosphors—1545(A)

Ammiraju, P., M. Rinehart, K. C. Rogers, and L. M. Lederman. Absorption of pions in C and N—1188(A)

Ancker, Betsy, Thomas H. Hazlett, and Earl R. Parker. Relationship between small angle dislocation boundaries and creep—1151(A)

Anderson, A. B. C. Growth, coalescence, and decay of vortices in jet accompanying Pfeifentone—256(A)

Anderson, A. G., R. L. Garwin, E. L. Hahn, J. W. Horton, G. L. Tucker, and R. M. Walker. Spin echo serial storage memory—283(A)

Anderson, C. D. Unstable particles—255(T)

Anderson, H. L. (see Glicksman, M.)—239(A)

—— (see Kruse, U.)—1188(A)

Anderson, John D., Robert W. Kenney, and Charles A. McDonald, Jr. Angular distribution of bremsstrahlung photons—258(A)

Anderson, John H. (see Holzman, G. R.)—542(L)

Anderson, K. A. (see Winckler, J. R.)—1411

Anderson, Paul A. Work function of Cd—1739

Anderson, P. W. (see Weiss, M. T.)—925

Anderson, T. H. Scintillation studies on activated alkali halides—281(A)

Andrews, R. D. Retraction of oriented polystyrene monofilaments—1547(A)

—— (see Gurnee, E. F.)—1547(A)

Aniansson, Gunner. New method for measuring the α-particle range and straggling in liquids—300

Antal, J. J., R. J. Weiss, and G. J. Dienes. Long wavelength neutron transmission as absolute method for determining concentration of lattice defects in crystals—1541(A)

Anthony, R. L. (see Ivory, J. E.)—1558(A)

Apker, L. Photoelectric experiments on excitation-energy transfer in crystals—1558(T)

Arams, Frank R. and Hans K. Jenny. Wide range electronic tuning of microwave cavities in gas atmospheres—562(A)

Argo, H. V. (see Hemmendinger, A.)—70

Argyres, P. N. and A. H. Kahn. Calculation of g-factor of metallic Li—226(A)

Armenteros, R., B. Gregory, P. Hendel, A. Lagarrigue, L. Leprince-Ringuet, F. Muller, and C. Peyrou. Results on heavy charged mesons—275(A)

Armstrong, A. H. (see Frye, G. M., Jr.)—241(A)

Arnold, J. S. Ultrasonic technique for nondestructive evaluation of metal to metal adhesive bonds—283(A)

Arnold, W. H. and J. Ballam. Analysis of charged V events—1204(A)

——, **J. Ballam, A. L. Hobson, R. Ronald Rau, George T. Reynolds, S. B. Treiman, and V. A. Van Lint.** Analysis of charged V events—275(A)

——, **J. Ballam, G. K. Lindeberg, and V. A. J. Van Lint.** Example of the cascade decay of a negative hyperon—838(L)

Aron, J. and D. Kahn. Effect of plastic deformation on surface resistivity of Cu wires—246(A)

Arrott, A., B. R. Coles, and J. E. Goldman. Magnetic susceptibility of α-Mn at low temperatures—1864(L)

—— **and J. E. Goldman.** Magnetic susceptibility in Zn ferrite—1201(A)
Asaro, F., F. Stephens, and I. Perlman. γ rays in the α decay of 100^{254}—260(A)
——, **Frank S. Stephens, Jr., S. G. Thompson, and I. Perlman.** γ-rays of 100^{254}—19
—— (see Hummel, John P.)—22; 261(A)
—— (see Perlman, I.)—262(A)
—— (see Stephens, F.)—261(A)
Aschenbrenner, F. A. Low-energy protons from targets bombarded by 15-Mev deuterons—657
Ashkin, J. (see Feiner, F.)—239(A)
Atkins, K. R. Slope of λ curve of liquid He—319
—— Surface tension of liquid He^4 and liquid He^3—1181(T)
Attix, F. H. (see Spencer, L. V.)—233(A)
Auer, P. L. Phenomenological theory of Townsend breakdown in dielectrics—320
Auerbach, T. and J. B. French. Angular momentum coupling in deuteron reactions—1276
Augustyniak, W. (see McReynolds, A. W.)—418
Averbach, B. L. and P. S. Rudman. Effect of cold work on local order—1554(A)
—— (see Kulin, S. A.)—1566(A)
—— (see Kurtz, A. D.)—1543(A)
—— (see Rudman, P. S.)—1554(A)
Azaroff, L. V. (see Brophy, J. J.)—228(A)

Babcock, H. D. (see Simpson, J. A.)—1402
Babcock, H. W. (see Simpson, J. A.)—1402
Babiskin, J. (see Steele, M. C.)—359
Bach, D. R., C. R. Lubitz, and P. V. C. Hough. Tensor force interaction energies for configurations important in O^{18} and F^{18}—235(A)
Bacon, Roger and Charles S. Smith. Elastic constants of Ag and Ag alloys—1553(A)
Bailey, L. Evan. Angle and energy distributions of charged particles from the cyclotron bombardment of Ni and Ag by 200-Mev protons—275(A)
Bair, Joe K. (see Willard, Harvey B.)—669; 1184(A)
Baker, E., A. Caretto, J. Cumming, G. Friedlander, J. Hudis, and R. Wolfgang. Excitation functions of radioactive products from interaction of high-energy protons with Pb—242(A)
Baker, Winslow F., R. E. Williams, and J. Rainwater. Elastic scattering of π mesons from nuclei. II—1188(A)
—— (see Williams, Ross)—1188(A)
Bakker, C. J. Plans of CERN for its laboratories—1191(T)
Baldwin, F. B. (see Ivory, J. E.)—1558(A)
Baldwin, G. C. Betatron orbit stability studies—1152(A)
Ballam, J. (see Arnold, W. H.)—275(A); 838(L); 1204(A)
Ballard, Stanley S. (see McCarthy, Kathryn A.)—271(A)
Banas, E. M. and B. A. Mrowca. Nuclear spin-spin relaxation time in polymers—1548(A)
——, **B. A. Mrowca, and E. Guth.** Nuclear magnetic relaxation in natural and synthetic rubbers—265(A)
Bandel, H. W. Measurement of current during formative time lag of sparks in uniform fields in air—560(A)
Bandtel, Kenneth C., W. J. Frank, L. Higgins, and B. J. Moyer. Reaction $H^3(p,t)\pi^0$ at 340-Mev proton energy—269(A)
—— (see Dixon, Dwight R.)—259(A)
Banet, Leo. Simple, empirical mass spectrum of fundamental particles—1176(A)
Barber, W. C. Specific ionization of high-energy electrons—276(A)
——, **W. D. George, and D. D. Reagan.** Absolute cross section for reaction $C^{12}(\gamma,n)C^{11}$—73
—— (see George, W.)—276(A)
Barbour, J. P. (see Dyke, W. P.)—263(A)
—— (see Trolan, J. K.)—262(A)
Barile, S. (see Allen, G.)—1168(A)
Barkas, Walter H., Frances M. Smith, and Wallace Birnbaum. Range straggling in nuclear track emulsion—605
Barker, W. A. and A. Mencher. Overhauser nuclear polarization effect—1868(L)
Barnes, George. Field emission from Re: emission pattern corresponding to hexagonal crystal structure—262(A)
Barnes, R. G. and P. J. Bray. Pure quadrupole resonances in Sb and Bi compounds—1182(A)
—— (see Bray, P. J.)—1182(A)
Barnett, C. F. and P. M. Stier. Electron capture cross section for protons—1537(A)
—— (see Stier, P. M.)—1149(A)
Barredo, Joseph G. Physical model of semiconductors—229(A)
—— Statistics for electrical phenomena—1542(A)
Barrett, A. H. (see Mandel, M.)—1159(A)
Barshay, S. (see Colladay, G. S.)—269(A)
Bartlett, James H. Helium wave equation—1067
Barut, A. O. Formulation of probability theory as physical theory—274(A)
Bashkin, S. and R. R. Carlson. γ rays from proton bombardment of Li^6—230(A)
——, **R. R. Carlson, and E. B. Nelson.** Radiative capture of protons by N^{14}—1184(A)
Batten, Hugh W. Plasma fluctuations in crossed electric and magnetic fields—559(A)
Battey, J. F. (see Baum, R. M.)—923
Baum, R. M. and J. F. Battey. Electron capture probability of upper Cu acceptor level in Ge—923
Beams, J. W. Effect of centrifugal field upon rate of transfer through He II film—1138(L)
Bean, C. P. (see Roberts, B. W.)—225(A)
Bearden, J. A. Latest developments in atomic constants—1530(T)
Beck, F. Stability of phase boundary inside superconductor—852
Becker, J. H. Studies of crystal growth, and electrical and optical properties of gray Sn—1192(A)
Becker, R. L. (see Darden, S. E.)—1147(A)
Becker, W. M. and K. Lark-Horovitz. Single-crystal layers of Ge semiconductors—228(A)
Bedard, F. and H. Meissner. Contact resistance between superconductors and normal conductors—1539(A)
Bedo, D. E. and D. H. Tomboulian. Intensity distribution among spectral orders in grazing incidence spectrograph—242(A)
Beer, A. C. Transport effects in p-type Ge—1542(T)
—— (see Harman, T. C.)—1532(A)
—— (see Willardson, R. K.)—227(A)
Behrends, R. E. (see Finkelstein, R. J.)—1155(A); 1870(E)
Belinfante, Frederick J. Emission of negative-energy gravitons by matter—1175(A)
—— Use of flat-space metric in Einstein's curved universe, and "Swiss-cheese" model of space—793
—— **and J. C. Swihart.** Quantized linear theory of gravitation—222(A)
Bemski, G., W. A. Nierenberg, and H. B. Silsbee. Cosine interaction in CsF and RbF—470
Benczer, N. (see Farrelly, B.)—1172(A)
—— (see Lidofsky, L.)—1186(A)
Benedek, G. B., W. Paul, and H. Brooks. Pressure dependence of resistivity, Hall effect, and magnetoresistance in Ge—1193(A)
Benedict, W. S., G. E. Moore, and S. Silverman. Collision line widths and shapes in vibration-rotation bands of HCl—1551(A)

Bennett, Arthur L. and Henry W. Wedaa. Detonation in gas at low pressure—256(A)
Bennett, C. O. (see Spitzer, W.)—228(A)
Bennett, Robert B. (see Ch'en, Shang-Yi)—281(A)
Bennett, W. (see Marder, S.)—1173(A)
Bennett, Willard H. More general theory of magnetic self-focusing—1169(A)
—— Self-focusing streams—1584
Bent, R. D., T. W. Bonner, and J. H. McCrary. Nuclear pairs from 3.4-Mev state in Ca^{40}—1325
——, **T. W. Bonner, J. H. McCrary, and R. F. Sippel.** γ radiation from deuteron bombardment of N^{14}—1198(A)
——, **T. W. Bonner, and R. F. Sippel.** Pair spectrometer measurements of radiations from excited states of light nuclei—1237
—— (see Bonner, T. W.)—1198(A)
Benzer, Seymour. Genetic fine structure and its relation to deoxyribonucleic acid molecule—1534(T)
Beretta, L., E. Clementel, and C. Villi. Phase shift analysis of 240-Mev p-p scattering—1526(L)
Berger, A. G. (see Walsh, J. L.)—265(A)
Bergmann, Peter G. Existence of Dirac generating functions—544(L)
—— **and Irwin Goldberg.** Dirac bracket transformations in phase space—531
—— **and Irwin Goldberg.** Transformations in phase space and Dirac brackets—1175(A)
—— (see Lebowitz, Joel)—1165(A)
—— (see Newman, Ezra)—1176(A)
Berlincourt, Ted G. and M. C. Steele. Oscillatory Hall effect, magnetoresistance, and magnetic susceptibility of graphite single crystal—227(A); 956
—— (see Overton, William C., Jr.)—1180(A)
Berman, A. S. (see Weissberg, H. L.)—1540(A)
Bernstein, H. and R. H. Kingston. Photomultiplication at surface of Ge—1566(A)
Bernstein, J. and Abraham Klein. Exchange current effects in two-nucleon system—1155(A)
Bernstein, S. (see Dabbs, J. W. T.)—1512(L)
Bernstein, W. (see Weiss, J.)—1828
Berry, Chester R. Change in KCl lattice dimensions by soft x-rays—934; 1540(A)
Besdin, D. J. and Joseph H. Robinson III. Magnetic moment of free electrons—272(A)
Beshers, D. N. and J. S. Koehler. Temperature dependence of internal friction in Cu—1553(A)
Betchov, R. Production of vorticity in isotropic turbulence—1142(A)
Bethe, H. A. π mesons and nucleons—1177(T)
Betts, D. D. and J. D. Jackson. Double electron capture by α particles in He—1149(A)
Beyster, J. R., R. L. Henkel, R. A. Nobles, and J. M. Kister. Inelastic collision cross sections at 1.0-, 4.0-, and 4.5-Mev neutron energies—1216
—— (see Walt, M.)—677
Bhadra, T. C. (see Chatterjee, S. D.)—1728
Bhatia, A. B. Vibration spectra and specific heats of cubic metals. I. Theory and application to Na—245(A)
—— **and G. K. Horton.** Vibration spectra and specific heats of cubic metals. II. Application to Ag—1715; 1181(A)
Biedenharn, L. C. and C. M. Class. Soluble problem in theory of Coulomb excitation—691
—— **and A. Simon.** Analysis of angular distribution data by electronic computers—1153(A)
Bina, Melvin J., Igor Alexeff, and Richard M. Sanders. Evapor-ion pump developments—251(A)
Bingham, H. H., J. C. Keck, and A. V. Tollestrup. Photoproduction of neutral mesons in H and D—1187(A)
Binnie, W. P. Crystal structure of InBi—228(A)
Biot, M. A. Deformation of viscoelastic plates derived from thermodynamics—1869(L)
Bird, George R. Microwave spectrum of NO_2—1160(A)
—— (see Mockler, Richard C.)—1837
Birkhoff, R. D. (see Rohr, R. C.)—1266
Birman, Joseph L. Average crystal potential—1863(L)
—— Bond dipoles and piezoelectricity in zincblende semiconductors—1567(A)
—— Effect of overlap on electrostatic lattice potentials in ionic crystals—1871(E)
Birnbaum, Wallace (see Barkas, Walter H.)—605
Biscoe, J. (see Brackett, T. E.)—1210(A)
Bishop, G. R. and J. P. Perez Y Jorba. Spins and parities of excited states of Ce^{140} and Sr^{89}—89
Bitter, F. and J. F. Waymouth. Analysis of plasma of fluorescent lamps. I—1148(A)
—— (see Waymouth, J. F.)—1148(A)
Blair, J. M. (see Stratton, T. F.)—629
Blakewood, C. H. (see Lane, C. T.)—1196(A)
Blaser, J. P. (see Feiner, F.)—239(A)
Blatt, F. J. Effect of vacancies and interstitials on electrical properties of Cu—245(A)
——, **M. C. Huse, and R. A. Rubenstein.** Resistivity due to point imperfections in Cu—1553(A)
Bleakney, Walker (see Griffith, Wayland)—1143(A)
Blewitt, T. H., J. K. Redman, F. A. Sherrill, and R. R. Coltman. Mechanical twinning in Cu—1555(A)
Blizard, J. L. B. Fundamental research in United States—1211(A)
Block, Martin M. Production of K mesons by protons of Cosmotron energy—1156(A)
——, **E. M. Harth, W. B. Fowler, R. P. Shutt, A. M. Thorndike, and W. L. Whittemore.** Charged V particle production in p-p collision—248(A)
—— (see King, D. T.)—1203(A)
Block, R. C. and H. W. Newson. Total neutron cross sections in kev region: separated isotopes of Ni and Ce—1162(A)
Bloembergen, N. Nuclear spin exchange in solids—1183(T)
Blois, M. S., Jr. Vacuum deposition of magnetic alloy films—281(A)
Bloom, Arnold L. Nuclear induction in inhomogeneous fields—1105
Bloom, S. (see Kivel, B.)—495
Bloom, Stewart D. New technique for observing cyclotron phase grouping—233(A)
Blosser, H. G., T. H. Handley, and M. K. Hullings. Survey of (p,n) reactions at 11.7 Mev—1198(A)
Bludman, S. A. and D. L. Judd. Aberrations and fringing effects in modified Siegbahn-type magnetic spectrometer—283(A)
Blumenfeld, H., E. T. Booth, L. M. Lederman, and W. Chinowsky. Production of unstable particles in C and Pb by 2-Bev pions—1203(A)
Blunt, R. F., H. P. R. Frederikse, and W. R. Hosler. Properties of Mg_2Sn—1533(A)
Bodansky, D. and A. M. Sachs. Interaction of 46-Mev π^+ mesons in deuterium—240(A)
Bodine, J. H. and F. B. Thiess. Optical absorption spectra of ThO—1532(A)
Boehm, F., P. Marmier, and J. W. M. DuMond. L-conversion in pure $E2$ transitions—280(A)
—— (see Marmier, P.)—280(A)
Bollinger, L. M., D. A. Dahlberg, R. E. Cote, H. E. Jackson, and G. E. Thomas. Neutron transmission measurements at the new Argonne reactor, CP-5—223(A)
—— (see Cote, R.)—1162(A)
Bond, John W., Jr. Recombination in argon shock front—285(A)
—— Shock front structure in argon—256(A)

Bondelid, R. O. (see Fagg, L. W.)—1538(A)
Bonner, T. W., R. D. Bent, and J. H. McCrary. Nuclear pairs from proton bombardment of Ca^{40}—1198(A)
—— (see Bent, R. D.)—1237; 1198(A); 1325
Boorse, Henry (see Smith, Bernard)—328
Booth, E. T. (see Blumenfeld, H.)—1203(A)
Boquet, F. L. (see Meyer, R. A.)—1531(A)
Borgnis, F. E. Specific directions of longitudinal wave propagation in anisotropic media—1000
Bowers, Raymond (see Melamed, Nathan T.)—1545(A)
Bowman, Harry R. and Lloyd G. Mann. γ rays accompanying spontaneous fission of Cf^{252}—277(A)
Boyle, W. S. and P. Kisliuk. Departure from Paschen's law of breakdown in gases—560(A)
—— (see Kisliuk, P.)—560(A)
Bracewell, Ronald N. Radio astronomy—278(T)
Brackett, T. E., R. D. Dunlap, and J. Biscoe. Small angle x-ray scattering by system iso-octane-*n*-heptforane—1210(A)
Brady, J. J., M. B. Larson, and T. A. O'Halloran. Internal friction as function of cold work of copper reeds at low frequencies—271(A)
—— (see Brick, R. O.)—282(A)
—— (see Perry, R. L.)—281(A)
Bragaw, Chester G., Jr. Biaxial creep fracture of high polymers—1559(A)
Bramley, Arthur. Properties of CdS films deposited in vacuo—246(A)
Bramson, H. J. Electron spectrum from muon decay—1187(A)
Brandt, Werner. Calculation of compressibility of polyethylene from energy of interaction between ($-CH_2-$) groups—243(A)
Braner, A. (see Halperin, A.)—1135(L)
Branscomb, Lewis M. and Stephen J. Smith. Electron affinity of atomic O—1127(L)
—— **and Stephen J. Smith.** Experimental cross section for photodetachment of electrons from H^- and D^-—1028
Braunstein, R. and J. W. Trischka. Molecular constants and nuclear-molecular interactions of Li^7F^{19} by molecular beam electric resonance method—1092
Bray, P. J. and R. G. Barnes. As^{75} pure quadrupole resonance—1182(A)
—— (see Barnes, R. G.)—1182(A)
Bray, Ralph. Minority carrier extraction in Ge—229(A)
Breen, R. J. and M. R. Hertz. γ radiation from Po neutron sources—599
Breitman, Leo. Glass transitions in polymer-plasticizer systems—1559(A)
Brennan, J. G. (see Adkins, R. H.)—235(A)
Brick, R. O., J. J. Brady, and M. D. Pearson. Penetration into rarer medium in total reflection of microwaves—282(A)
Brock, E. G. and J. E. Taylor. Field emission from Ti single crystals—1169(A)
Brockhouse, B. N. Slow neutron spectrometry—New tool for study of energy levels in condensed systems—1171(A)
—— Study of energy levels in solids, liquids, and magnetic materials by scattered slow neutrons—1171(T)
——, **L. M. Corliss, and J. M. Hastings.** Multiple scattering of slow neutrons by flat specimens and magnetic scattering by Zn ferrite—1721
Brode, Harold L. Blast from sphere of high-pressure gas—1158(A)
Brodnyan, J. (see Philippoff, W.)—1549(A)
Broersma, S. Nuclear magnetic relaxation of nonuniform systems—1182(A)
Broida, Herbert P. Afterglow of solid N_2—563(A)
Brolley, J. E., Jr., and F. L. Ribe. Energy loss by 8.86-Mev deuterons and 4.43-Mev protons—1112
Brooks, H. Properties of Ge and Si at high pressures—244(T)
—— (see Benedek, G. B.)—1193(A)
—— (see Warschauer, D. M.)—1193(A)
Brophy, J. J., N. Rostoker, and L. V. Azaroff. Semiconducting properties of FeO thermistor material—228(A)
Brown, Fielding and Charles L. Gravel. Direct observation of domain rotation in ferrites—442
Brown, Frederick C. Electron mobility in AgCl: Comparison of experiment with theory—263(A)
—— Properties of electrons and holes in AgCl—1549(T)
Brown, L. Carlton and Dudley Williams. Nuclear magnetic moment of K^{39}—1537(A)
Brown, Sanborn C. (see Champion, K. S. W.)—559(A)
—— (see Goldey, James M.)—1192(A); 1761
—— (see Rose, David J.)—310
—— (see Schulz, George J.)—1642; 559(A)
—— (see Weinstein, R.)—223(A)
Brown, W. L. Surface potential and surface charge distribution from semiconductor field effect measurements—1565(A)
—— (see Montgomery, H. C.)—1565(A)
Brown, W. W. Nuclear interactions of cosmic rays in Al—275(A)
Browne, C. I. (see Prestwood, R. J.)—1324
Broyles, Arthur. Stark fields from ions in plasma—1166(A)
Brubaker, W. M. Influence of space charge on potential distribution in mass spectrometer ion sources—563(A)
Brueckner, K. A. Energy levels of π-mesonic atoms—769
—— Nuclear saturation and independent-particle model of nucleus—244(T)
——, **R. J. Eden, and N. C. Francis.** High-energy reactions and evidence for correlations in nuclear ground state wave function—1445
Bube, Richard H. Temperature dependence of width of band gap in several photoconductors—431
Buckingham, M. J. Superfluidity in liquid He^3—1855(L)
Buckingham, R. A. (see Halpern, O.)—1626
Bugg, W. (see Stier, P. M.)—1149(A)
Burch, W. E. (see Newman, R.)—1536(A)
Burger, R. M., H. E. Farnsworth, and R. E. Schlier. Adsorption of H_2 and O_2 on Ge—1179(A)
—— (see Farnsworth, H. E.)—250(A)
Burgess, John C. Apparent limit of convergence of perturbation series solution for free undamped Duffing equation with hardening spring—257(A)
Burk, D. L. (see Friedberg, S. A.)—1200(A)
Burkhard, E. L. and J. H. Lewis. Ionization of air by γ rays—1154(A)
Burkhardt, Louis C. (see Sawyer, George A.)—1305
Burns, Laurence. Alternative explanation of Waymouth-Bitter experiments—1863(L)
Burson, S. B., W. C. Jordan, and J. M. LeBlanc. Decay of $_{22}Ti^{51}$ (5.8 min)—230(A)
—— (see LeBlanc, J. M.)—39
Burstein, Elias, G. Picus, B. Henvis, and M. Lax. Optical properties of group III elements in Si—1536(A)
—— (see Davisson, J. W.)—1544(A)
—— (see Lipson, H. G.)—1535(A)
—— (see Sclar, N.)—1178(A); 1757
—— (see Teitler, S.)—1561(A)
Burton, W. K. Canonical invariance in Lagrangian quantum mechanics—555(L)
Burwell, J. R., R. W. Huggett, and R. W. Thompson. Example of π^+-decay in flight—101
——, **R. W. Huggett, and R. W. Thompson.** New evidence concerning specific identity of θ^0 decay fragments and statistics of θ^0 particle—247(A)
—— (see Huggett, R. W.)—248(A)
—— (see Kim, Y. B.)—248(A)

Buschert, R., I. G. Geib, and K. Lark-Horovitz. Structure of liquid Te—1157(A)
Butler, J. W. γ-ray thresholds in $F^{19}(d,n\gamma)Ne^{20}$ reaction—241(A)
Butler, S. T. and M. H. Friedman. Partition function for system of interacting Bose-Einstein particles—287
—— (see Friedman, M. H.)—294
Byram, E. T., T. A. Chubb, and H. Friedman. Dissociation of O_3 in upper atmosphere—1594

Cabrera, N. and M. M. Levine. Polytypism and dislocations—1543(A)
Caldwell, David O. and J. Reginald Richardson. Elastic scattering of 20.6-Mev protons by deuterons—28
Callaway, Joseph. Electron band structure of Fe—1150(A)
Callen, H. B. (see Kriessman, C. J.)—1562(A)
Campbell, E. C., R. W. Pelle, F. C. Maienschein, and P. H. Stelson. Decay and fast neutron excitation of Zr^{89m}—1172(A)
Cantwell, Murray. Molecular excitation in β decay—235(A)
Carbone, Robert J., Gerald Stone, and Edgar Everhart. Cross section measurements for large angle collisions of He, Ne, and A ions with argon gas atoms at energies from 25–100 kev—1150(A)
—— (see Everhart, Edgar)—1045
—— (see Stone, Gerald)—1150(A)
Caretto, A. (see Baker, E.)—242(A)
Carlson, R. R. and E. B. Nelson. γ rays from low-energy proton bombardment of Be—1310
—— (see Bashkin, S.)—230(A); 1184(A)
Carr, R. J. (see Glass, R. A.)—261(A)
Carter, R. S. Resonance parameters in U^{235}—1161(A)
Case, K. M. Decomposition of generalized Duffin-Kemmer algebra—1189(A)
—— (see Moldauer, P. A.)—1190(A)
Caspari, M. E. Direction breakdown in alkali halide crystals—1170(A); 1679
Cassel, Hans M. Thermal expansion and aerodynamic stability of open flames—1143(A)
Castle, J. G., Jr. Magnetic resonance properties of raw cokes—1564(A)
Castle, J. W. (see Hamilton, J. F.)—1557(A)
Chamberlain, Owen. High-energy proton polarization studies involving triple scattering—266(T)
—— **and John D. Garrison.** p-p scattering experiments at 170 and 260 Mev—1167(A)
—— (see Tripp, R.)—266(A)
—— (see Ypsilantis, T.)—267(A); 840(L)
Champion, K. S. W. and S. C. Brown. Plasma resonance—559(A)
Chandrasekhar, S. Theory of turbulence—1158(T)
—— **and G. Herzberg.** Energies of ground states of He, Li^+, and O^{8+}—1050
Chang, W. Y. (see del Castillo, G.)—1163(A)
Chatterjee, S. D. and T. C. Bhadra. Abnormal increase in dielectric constant of electret-forming material—1728
Ch'en, Shang-Yi, Robert B. Bennett, and Oleg Jefimenko. Absorption bands of Rb in presence of foreign gases—281(A)
Cheng, L. S., Virginia C. Ridolfo, M. L. Pool, and D. N. Kundu. Radioactive Tl^{204} and Bi^{207}—231(A)
Chetham-Strode, A., Jr. (see Hummel, J. P.)—22
Chikazumi, Sōshin and Kenzō Suzuki. Domain patterns on rolled single crystal of Ni_2Fe—1130(L)
Chinowsky, W. (see Blumenfeld, H.)—1203(A)
Choppin, G. R., B. G. Harvey, S. G. Thompson, and A. Ghiorso. Nuclear properties of 100^{255}—1519(L)
—— (see Ghiorso, A.)—1518(L)
Choquard, P. F. (see Willardson, R. K.)—227(A)
Chou, C. N. and Marcel Schein. Scintillation counter study of energy spectra of cosmic-ray photons and electrons at 11 200 feet—162
Chraplyvy, Z. V. Some considerations concerning relativistic two-particle wave-equations—244(T)
Chrétien, Max. Radiative corrections to electron scattering—1515(L)
Christensen, H. Ultraviolet light induced surface channel and carrier lifetime effects in Ge—1178(A)
Christy, R. F. α decay of spheroidal nuclei—1205(A)
—— Reactions and models of light nuclei—260(T)
Chubb, T. A. (see Byram, E. T.)—1594
Chupp, W. W. (see Goldhaber, Gerson)—267(A)
Church, E. L. and J. E. Monahan. Internal conversion in L and M subshells—718
—— **and A. W. Sunyar.** Rotational states of excitation in U^{234}—1186(A)
Clark, D. (see Piccioni, O.)—275(A)
Clark, J. (see Wolff, G.)—1179(A)
Clark, M. A. (see Graham, R. L.)—1173(A)
Clarke, Edward N. Ge surface conductivity and effects of water vapor—1178(A)
Class, C. M. (see Biedenharn, L. C.)—691
—— (see Risser, J. R.)—1183(A)
Cleland, J. W., J. H. Crawford, Jr., and J. C. Pigg. Fast-neutron bombardment of n-type Ge—1742
Clementel, E. (see Beretta, L.)—1526(L)
Cobble, J. W. (see Glass, R. A.)—261(A)
Cohen, Alvin J. Impurity induced color centers in fused silica—1550(A)
Cohen, Bernard L. Angular distributions and yields of neutrons from (p,n) reactions—49; 1206(A)
——, **B. L. Ferrell-Bryan, D. J. Coombe, and M. K. Hullings.** Angular distribution of fission fragments from 22-Mev proton-induced fission of U^{238}, U^{235}, U^{233}, Th^{232}, and Th^{230}—685
—— **and E. Newman.** Anomalous dependence of F_p/F_a on bombarding energy—1198(A)
Cohen, David (see Shaw, Harlan)—259(A)
Cohen, E. Richard and J. W. M. DuMond. Comments on Straumanis' concepts regarding Avogadro's number—1128(L)
Cohen, Stanley. Effect of anomalous nucleon magnetic moment on π^0 lifetime—749
Cohen, Victor W. Spins and moments of radioactive nuclei—1174(T)
—— (see Gilbert, D. A.)—1194(A)
Coleman, C. and R. Smoluchowski. Grain boundary diffusion in Al-Cu system—1555(A)
Coles, B. R. (see Arrott, A.)—1864(L)
Colladay, G. S. and S. Barshay. Second-neighbor interaction in two-dimensional graphite lattice—270(A)
Collins, F. M. Dimensional changes during heat treatment thermal expansion of polycrystalline carbons and graphites—1564(A)
Collins, George B. (see Ridgway, S. L.)—247(A)
Collins, R. J., F. W. Reynolds, and G. R. Stilwell. Electrical and optical properties of GaSb films—227(A)
—— (see Spitzer, W.)—1536(A)
Collins, T. L. (see White, F. A.)—1174(A)
Coltman, R. R. (see Blewitt, T. H.)—1555(A)
Compton, W. Dale. Self-diffusion of Ag in AgCl—1543(A)
Conger, R. L. Magnetization reversal in thin films—1752
Conn, Willi M. Metallic deposits and shock waves due to electrically "exploded" wires—1551(A)
Conwell, E. M. Impurity band conduction in Ge and Si—1178(A)
Cook, E. J. and G. F. Pieper. Forty-channel pulse height analyzer—1154(A)

Cool, R. (see Piccioni, O.)—275(A)
Cooley, William J. (see Van Horn, David D.)—245(A)
Coombe, D. J. (see Cohen, B. L.)—685
Cooper, C. B. (see Enck, F. D.)—237(A)
Cooper, John N. (see Green, D. Wayne)—466
Cooper, Raymond D. and Dan J. Zaffarano. Photodisintegration of C, O, and N in nuclear emulsions—1199(A)
Coor, T., D. A. Hill, W. F. Hornyak, L. W. Smith, and G. Snow. Nuclear cross sections for 1.4-Bev neutrons—1369
Copeland, Paul L. and B. Pearson de Lany. Statistics of exponential distribution of exponential populations applied to distribution of arc lives—251(A)
—— (see de Lany, B. Pearson)—251(A)
Corak, William S., M. P. Garfunkel, C. B. Satterthwaite, and Aaron Wexler. Atomic heats of Cu, Ag, and Au from 1°K to 5°K—1699
Corbett, J. W. and W. W. Watson. Thermal diffusion in multiple component isotopic mixtures—1165(A)
Cork, Bruce. University of California bevatron—266(T)
Cork, J. M. (see LeBlanc, J. M.)—39
Corliss, L. M. (see Brockhouse, B. N.)—1721
Cornelius, R. (see Sargent, C. P.)—1349
Corrsin, S., A. L. Kistler, and V. O'Brien. Measurements of velocity and temperature fluctuations behind hot grid—1142(A)
—— (see Ruetenik, J. R.)—1142(A)
Cote, R. E. and L. M. Bollinger. $\bar{\Gamma}_n^0/\bar{D}$ for slow neutron resonances—1162(A)
—— (see Bollinger, L. M.)—223(A)
Cox, J. T. (see Mizushima, Masataka)—1034; 1159(A)
Crasemann, Bernd and D. L. Manley. Radioactivity of Co^{57}—66; 279(A)
Crawford, Frank S., Jr. (see Alvarez, Luis)—280(A)
—— (see Paramentier, D.)—284(A)
Crawford, J. H., Jr., and D. K. Stevens. Magnetic susceptibility in InSb—1532(A)
—— (see Cleland, J. W.)—1742
Crewe, A. V. Beam extraction of Liverpool synchrocyclotron—1191(T)
Crosbie, E. A. and M. Hamermesh. Coupling of betatron and phase oscillations in synchrotron—233(A)
Crowe, K. M., R. M. Friedman, and H. Motz. π^- counting by delayed coincidence—268(A)
—— (see Motz, H.)—268(A)
Crowe, R. W. and J. C. Devins. Sparking potential and molecular structure of hydrocarbon gases—560(A)
Crussard, J. (see Walker, W. D.)—240(A); 1416
Cuevas, J. (see Krasner, Sol)—1149(A)
Culler, G. (see Fernbach, S.)—273(A)
—— (see Sherman, N.)—273(A)
Culler, Vaughn and R. W. Waniek. Experimental evidence for optical model for neutrons between 60 and 110 Mev—1148(A)
Cumming, J. (see Baker, E.)—242(A)
Curtis, C. W. (see Alter, B. E. K.)—1151(A)
Cusano, D. A. Field enhanced solid-state luminescence—1169(A)
—— Radiation-controlled electroluminescence and light amplification in phosphor films—546(L)

Dabbs, J. W. T., L. D. Roberts, and S. Bernstein. "Brute force" polarization of In^{115} nuclei; angular momentum of 1.458-ev neutron resonance—1512(L)
Dahlberg, D. A. (see Bollinger, L. M.)—223(A)
Dallaporta, N. Investigations of Italian school—1166(T)
D'Altroy, F. and H. Y. Fan. Effective mass of carriers and relaxation time in Ge—1561(A)
Danforth, W. E. Short-time polarization in ThO—1177(A)
Daniels, W. B. (see Smith, Charles S.)—1553(A)
Darden, S. E., A. Okazaki, and R. L. Becker. Determination of nuclear level density—1147(A)
Darin, S. R. (see Taylor, G. R.)—1558(A)
Darnell, F. J. and S. A. Friedberg. Electrical breakdown in Ge at low temperatures—1178(A); 1860(L)
Das, T. P. and D. K. Roy. Spin echoes with four pulses—extension to n pulses—525
—— **and A. K. Saha.** Electric quadrupole interaction and spin echoes in crystals—516
Dash, W. C. Birefringence in Si—1536(A)
——, **R. Newman, and E. A. Taft.** Optical absorption in single crystals of Ge and Si—1192(A)
—— (see Newman, R.)—1536(A)
Daunt, J. G. and J. Korringa. Susceptibility and entropy of F-centers—1550(A)
Davidon, W. C. (see Kruse, U.)—1188(A)
Davis, G. L. (see Wetherill, G. W.)—250(A)
Davis, L., Jr. (see deMars, G. A.)—539(L); 1565(A)
—— (see Statz, H.)—540(L); 1566(A)
Davis, R. E. (see Goldberg, Colman)—1192(A)
Davisson, J. W., Elias Burstein, and P. L. Smith. Prismatic slip in crystals—1544(A)
Day, R. B., R. L. Mills, J. E. Perry, Jr., and F. Scherb. n-p scattering at 20 Mev—279(A)
DeBretteville, A., Jr. Second-order transition in $BaTiO_3$—1563(A)
Dehmelt, H. G. Paramagnetic resonance of atomic phosphorus—1181(A)
Déjardin, Georges, Joseph Janin, and Ivan Eyraud. Spectroscopic study of discharge and afterglow produced in nitrogen by pulsed microwaves—1149(A)
de Lany, B. Pearson and Paul L. Copeland. Duration of Hg arcs in evacuated bulbs coated with rare earths—251(A)
—— (see Copeland, Paul L.)—251(A)
Delbecq, Charles J., P. Pringsheim, and P. H. Yuster. Optical and electrical properties of LiF x-rayed at liquid nitrogen temperature—237(A)
—— (see Primak, W.)—237(A); 1708
—— (see Yuster, Philip)—233(A)
del Castillo, G., A. Snyder, L. Grodzins, and W. Y. Chang. Nuclear interaction of sea-level, cosmic-ray particles with C and Pb—1163(A)
—— (see Snyder, A.)—1163(A)
deMars, G., H. Statz, and L. Davis, Jr. Conductance of p-type inversion layers on n-type Ge—1565(A)
——, **H. Statz, and L. Davis, Jr.** Measurement and interpretation of conductance of p-type inversion layers on Ge—539(L)
—— (see Statz, H.)—540(L); 1565(A)
Denman, Eugene D. (see Richards, Hans Kohn)—250(A)
DeSorbo, W. and D. Turnbull. Precipitation in small spheres of Pb-Sn alloy—1554(A)
DeStaebler, Herbert, Jr., and B. V. Sreekantan. Nature of neutral secondary particle produced in decay of $K_{\pi 1}$-meson—1520(L)
Deutsch, M. (see Weinstein, R.)—223(A)
Devins, J. C. (see Crowe, R. W.)—560(A)
DeWire, J. W. (see Swartz, C. E.)—1164(A)
Dexter, D. L. Resistivity of dilute alloys—543(L)
—— Smakula's equation in insulating solids—1533(A)
Dexter, R. N. Third harmonic cyclotron resonance of holes in Ge—1560(A)
Dicke, R. H. (see Romer, R. H.)—1160(A)
Dieckamp, H. Shear modulus recovery of electron irradiated Cu—1531(A)
Dieke, G. H. Spectroscopy of solids—1558(T)
Dienes, G. J. (see Antal, J. J.)—1541(A)
Dillinger, J. R. (see Fleming, P. J.)—1196(A)

Dillon, J. A., Jr., and M. L. Dillon. Origins of papers presented at regular meetings of American Physical, Acoustical, and Optical Societies in 1954—1211(A)
Dillon, M. L. (see Dillon, J. A., Jr.)—1211(A)
Dingle, R. B. Diamagnetic resonance in electronic conductors—550(L)
Dixon, Dwight R. and Kenneth C. Bandtel. Photodisintegration of deuterons by high-energy γ rays—259(A)
Doggett, W. O. (see Petroff, M. D.)—279(A)
Domm, Ulrich and Hermann Foettinger. Stability of vortex streets with consideration of diffusion of vorticity of individual vortices—1142(A)
Donahue, T. M. and Robert Resnick. Resonance absorption of sunlight in twilight layers—1622
Donnay, J. H. Crystallographic significance of some recent results in solid-state physics—1558(T)
Doty, Paul. Size and shape of nucleic acids as revealed by physical-chemical techniques—1531(T)
Douglas, R. A. (see Galonsky, A.)—586
—— (see Jones, K. W.)—241(A)
Dousmanis, G. C. Magnetic hyperfine effects and electronic structure of NO—1160(A)
Downs, B. W. Polarization of deuteron—258(A)
—— Variation calculation of polarizability of deuteron—194
——, **D. G. Ravenhall, and D. R. Yennie.** Electric quadrupole effects in scattering of high-energy electrons by heavy nuclei—277(A)
—— (see Yennie, D. R.)—277(A)
Doyama, M. (see Kuczynski, G. C.)—270(A)
Doyle, W. T. and A. B. Robbins. Energy levels in F^{17} and Al^{29}—1185(A)
Dresden, M. Collective description of electron gas—1165(A)
Dresselhaus, G., A. F. Kip, and C. Kittel. Cyclotron resonance of electrons and holes in Si and Ge crystals—368
——, **A. F. Kip, C. Kittel, and G. Wagoner.** Cyclotron and spin resonance in InSb—556(L)
Dreyfus, Russell W. and Paul W. Levy. Heat treatment of irradiated NaN_3—1541(A)
Drougard, M. E., R. Landauer, and D. R. Young. Dielectric behavior of $BaTiO_3$ in paraelectric state—1010; 1563(A)
—— (see Huibregtse, E. J.)—1562(A)
Drummond, J. E. and L. Wilcox. Oscillations of plasma with skew velocity distribution transverse to static magnetic field—558(A)
—— (see Wilcox, L.)—263(A)
Dryden, Hugh L. Fifty years of boundary layer theory and experiment—1143(T)
Duboc, Charles A. Theory of Ag-halide photolysis—1557(A)
Dudziak, Walter, Ryokichi Sagane, and James Vedder. Photomeson production from H, D, and C—269(A)
—— (see Sagane, Ryokichi)—269(A)
Dugdale, J. S. and D. K. C. MacDonald. Lattice thermal conductivity—1751
Dumke, William P. Generalized deformation potential theory for n-type Ge—230(A)
DuMond, J. W. M. (see Boehm, F.)—280(A)
—— (see Cohen, E. Richard)—1128(L)
—— (see Marmier, P.)—280(A)
Duncan, B. J. and L. Swern. Temperature effects in ferrites at microwave frequencies—1201(A)
Dunlap, R. D. (see Brackett, T. E.)—1210(A)
Dunlap, W. C., Jr. Au, an "amphoteric" impurity element in Ge—1535(A)
Dunnam, F. E. (see Ralph, D. C.)—249(A)
Dunning, K. L. (see Fagg, L. W.)—1538(A)
Dutton, David. Localized photoconductivity in PbS films—1549(A)
Dyke, W. P., J. P. Barbour, J. K. Trolan, and E. E. Martin. Electrical stability of *T-F* emitter—263(A)
—— (see Trolan, J. K.)—262(A)
Dyson, Freeman J. Electron spin resonance absorption in metals. II. Theory of electron diffusion and skin effect—349
Dzurus, M. (see Hennig, G.)—227(A)

Eatherly, W. P. Effect of radiation damage on electrical and thermal properties of graphite—1531(T)
Eaton, V. E. Physics is an art—1177(T)
Eden, R. J. and N. C. Francis. Nuclear models—1205(A)
—— (see Brueckner, K. A.)—1445
Ehler, A. W. and G. L. Weissler. Absorption of radiation in vacuum uv by N atoms produced in discharge plasma in N_2—561(A)
Ehrenreich, H. and A. W. Overhauser. Mobility of holes in Si and Ge—1533(A)
Eisberg, R. M. (see Palevsky, H.)—492
Eisinger, J. T. (see Gossett, C. R.)—724
Ekstein, Hans and Norman Rostoker. Quantum correction to shot effect—222(A)
—— (see Gilbert, T. L.)—1200(A)
—— (see Rostoker, Norman)—222(A)
Elliot, J. O. Differential elastic scattering of 14-Mev neutrons—1147(A)
—— (see Faust, W. R.)—1147(A)
Elliott, David (see Probstein, Ronald F.)—1143(A)
Emmerich, W. S. Neutron cross sections in 4-Mev range—1148(A)
Emrich, Raymond J. and Robert L. Peterson. Pressure variation in shock tube flow—1141(A)
—— (see Williams, Albert C.)—1158(A)
Enck, F. D. and C. B. Cooper. Elastic constants and specific heat of KCl at elevated temperatures—237(A)
Engel, Olive G. Mechanism of high-speed-waterdrop erosion of methyl methacrylate plastic—236(A)
Englefield, M. J. Direct evaluation of fractional parentage coefficients using Young operators: normalization of four-particle wave functions—1213
Enns, J. H., R. L. Martin, and E. Katz. Sequence experiment for study of reciprocity law failure at low intensities—1556(A)
—— (see Martin, R. L.)—1556(A)
Epstein, Saul T. Derivation of Feynman-Dyson rules from time-independent theory—196
Eriksen, Erik (see Foldy, Leslie L.)—775; 1190(A)
Ernst, H. (see Hayward, R. W.)—231(A)
Etzel, H. W. Detection of vacancies created in NaCl by x-rays—1531(A)
Evans, Marjorie W., Frank I. Given, and William E. Richeson, Jr. Effects of attenuating materials on detonation induction distances in gases—256(A)
Everhart, Edgar, R. J. Carbone, and Gerald Stone. Differential cross-section measurements for large-angle collisions of He, Ne and A ions with A atoms at energies to 100 kev—1045
—— (see Carbone, Robert J.)—1150(A)
—— (see Stone, Gerald)—1150(A)
Evett, A. A. Theoretical evaluation of binding energy of HEH—1191(A)
Eyraud, Ivan (see Déjardin, Georges)—1149(A)

Fagg, L. W., E. A. Wolicki, R. O. Bondelid, K. L. Dunning, and S. Snyder. Coulomb excitation of energy levels in Te and Ag—1538(A)
Fairbank, Henry A. and J. Wilks. Heat transport and boundary layer resistance in He II below 1°K—1196(A)
Fairhall, A. W. Fission of Bi by 22-Mev deuterons—276(A)
Famularo, K. F. (see Stratton, T. F.)—629

Fan, H. Y. (see D'Altroy, F.)—1561(A)
—— (see Kaiser, W.)—966
—— (see Schulz-DuBois, E.)—1561(A)
—— (see Spitzer, W.)—228(A); 1536(A)
—— (see Stoeckmann, F.)—1535(A)
Farney, G. K. (see Hahn, T. M., Jr.)—1183(A)
Farnsworth, H. E., R. E. Schlier, and R. M. Burger. Low-energy electron diffraction studies of Ge crystal surface—250(A)
—— (see Allen, R. B.)—1179(A)
—— (see Burger, R. M.)—1179(A)
—— (see George, T. H.)—1179(A)
—— (see Schlier, R. E.)—250(A)
—— (see Woodcock, R. F.)—1152(A)
Farrall, George A. and Charles R. Mingins. Open screen technique in electron microscopy—1211(A)
Farrelly, B., L. Koerts, R. van Lieshout, N. Benczer, and C. S. Wu. Radiations of Sb^{120}—1172(A)
—— (see Koerts, L.)—1172(A); 1230
Faust, W. R., R. C. O'Rourke, and J. O. Elliot. Cloudy crystal ball analysis of 14-Mev elastic neutron scattering data—1147(A)
——, **V. E. Scherrer, and B. A. Allison.** γ-γ coincidences produced by inelastic scattering of 2.5-Mev neutrons—224(A)
—— (see Scherrer, V. E.)—224(A)
Feder, R. and A. S. Nowick. Anomalous behavior of Cu_3Au quenched from above 600°C—1152(A)
Feher, George and A. F. Kip. Electron spin resonance absorption in metals. I. Experimental—337
—— **and R. A. Levy.** Electron spin resonance in frozen metal-ammonia solutions—264(A)
Feiner, F., J. Ashkin, J. P. Blaser, and M. O. Stern. Differential cross sections for pion-proton scattering at 150 and 170 Mev—239(A)
Feld, Bernard T. Deuteron model for π-meson and photon capture by complex nuclei—1155(A)
—— Photomeson production from H—238(A)
Feldman, David. Nonrelativistic interaction between two nucleons—1456
Feldmann, W. L. (see Pearson, G. L.)—1567(A)
Ferentz, M. and N. Rosenzweig. Tabulation of F coefficients—222(A)
Ferguson, K. R. Optical absorption bands induced in γ irradiated glass—1542(A)
Fernbach, S., G. Culler, and N. Sherman. Optical model analysis of scattering of 14-Mev neutrons. II. Polarization effects—273(A)
—— (see Sherman, N.)—273(A)
Ferrell-Bryan, B. L. (see Cohen, B. L.)—685
Ferry, John D. (see Plazek, D. J.)—1548(A)
—— (see Williams, Malcolm L.)—1549(A)
Feshbach, Herman. Relativistic wave equations—801
—— **and S. I. Rubinow.** Equivalent two-body method for triton—188
Feuer, Paula. Electronic states in perturbed periodic lattice—1193(A)
Fine, S. (see Rittner, E. S.)—545(L)
Fink, Richard W. and Berol L. Robinson. K and L x-ray intensities in Cs^{135} decay—1293
—— (see Robinson, Berol L.)—231(A)
Finkelnburg, Wolfgang. Very high temperature arcs—562(A)
Finkelstein, David. Spin models—1175(A)
Finkelstein, R. J. and R. E. Behrends. Radiative corrections to muon decay—1155(A); 1870(E)
Firle, T. E. and H. Winston. Noise measurements in semiconductors at very low frequencies—1567(A)
Fischbach, D. B. and A. S. Nowick. Creation of potential difference across NaCl crystals by deformation—1543(A)
Fiske, M. D. Effect of hydrostatic pressure on superconducting transition—244(T)
—— (see Schmitt, R. W.)—246(A)
Fleming, John R. and J. J. Lord. Ionization loss in nuclear emulsions—268(A)
Fleming, P. J., J. H. Werntz, Jr., and J. R. Dillinger. Dependence of transfer rates of He II film on film length—1196(A)
Fletcher, P. C. (see Aamodt, L. C.)—1224; 1317
Fletcher, R. C. Hyperfine splitting in electron-spin resonances of donors in Si—252(T)
——, **F. R. Merritt, and W. A. Yager.** Cyclotron resonances in Ge at 1.4°K—1560(A)
Flom, D. G. Frictional properties of teflon—1548(T)
Foettinger, Hermann (see Domm, Ulrich)—1142(A)
Foldy, Leslie L. and Erik Eriksen. Vacuum polarization and p-p scattering—775; 1190(A)
Foley, H. M. (see Sessler, A. M.)—6
Folger, R. L., P. C. Stevenson, and G. T. Seaborg. High-energy proton spallation-fission of U—107
Foote, H. L., Jr. Slow neutron resonant scattering—1161(A)
—— (see Sailor, V. L.)—224(A)
Forbush, Scott E. World-wide variations in cosmic-ray intensity 1937–1952—1163(A)
—— (see Graham, John W.)—1348
Ford, Kenneth W. Calculations of energy-levels for intermediate nuclei—244(T)
—— Predicted 0+ level in $_{40}Zr^{90}$—1516(L)
Forrester, A. Theodore, Richard A. Gudmundsen, and Philip O. Johnson. Photoelectric mixing of incoherent light—1169(A)
Forstat, H. and C. A. Reynolds. "Closed" fountain effect and compressibility of He II—1196(A)
Forster, H. H. and A. Rosen. Decay of Ru^{106}—1172(A)
Forster, Michael J. Unilateral compression of rubber—1559(A)
Fowler, Charles A., Jr. (see Fryer, Edward M.)—270(A)
Fowler, E. C. (see Morris, T. W.)—1167(A)
—— (see Walker, R. M.)—1203(A)
Fowler, J. L. and C. H. Johnson. Differential elastic scattering cross section for neutrons on N—728
Fowler, J. M., S. S. Hanna, and G. E. Owen. $Be^9(n,2n)Be^8$ reaction—249(A)
—— **and C. E. Roos.** Response of anthracene and stilbene to low-energy protons and x-rays—996
Fowler, W. B., R. P. Shutt, A. M. Thorndike, and W. L. Whittemore. Production of heavy unstable particles by 1.37-Bev pions—121
—— (see Block, M. M.)—248(A)
—— (see Morris, T. W.)—1167(A)
Fox, R. E. Precision measurements of ionization probabilities of monoenergetic electrons—1159(T)
—— (see Hickam, W. M.)—557(A)
Fox, Raymond and R. W. Waniek. Bilateral development of thick nuclear emulsions—1153(A)
—— (see Waniek, R. W.)—1148(A)
Fox, T. G. and S. Loshaek. Viscosity-molecular weight relationship for long chain polymers in bulk or in concentrated solution—1549(A)
Francis, N. C. (see Brueckner, K. A.)—1445
—— (see Eden, R. J.)—1205(A)
Frank, R. M. and J. L. Gammel. p-He^3 interaction—1204(A)
Frank, W. J. (see Bandtel, K. C.)—269(A)
Frankl, D. R. Electroluminescence in ZnS single crystals—238(A)
Fraser, J. S. and J. C. D. Milton. γ-γ directional correlation in Er^{169}—1173(A)
—— (see Milton, J. C. D.)—1173(A)

Fred, Mark, Frank S. Tomkins, and William F. Meggers. Nuclear moments of Ac^{227}—1514(L)
Freda, A. R. and G. C. Kuczynski. Effect of external stresses upon rate of ordering of AuCu—270(A)
Frederikse, H. P. R. and W. R. Hosler. Galvano-magnetic effects in InSb—1532(A)
—— (see Blunt, R. F.)—1533(A)
Freedman, M. S. (see Porter, F. T.)—214(L)
Fregeau, J. H. and R. Hofstadter. Inelastic electron scattering from C at 188 Mev—1184(A)
Freistadt, Hans. Connection between recent theories of Bohm, De Broglie, Dirac, and Schrödinger—1176(A)
French, J. B. and B. J. Raz. Deuteron reactions and *j-j* coupling shell model—1523(L)
—— (see Auerbach, T.)—1276
Fretter, W. B., E. W. Friesen, G. E. Kepler, and A. Lagarrigue. Results on *K* particles—1202(A)
Freund, H. (see Loebner, E. E.)—1545(A)
Freund, R. E. (see Schwertz, F. A.)—1134(L)
Friedberg, S. A. and D. L. Burk. Specific heats of Zn ferrite and Zn chromite at low temperatures—1200(A)
—— (see Darnell, F. J.)—1178(A); 1860(L)
—— (see Guthrie, G.)—1181(A)
Friedlander, G. (see Baker, E.)—242(A)
—— (see Miller, J. M.)—1197(A)
—— (see Miskel, J. A.)—1197(A)
—— (see Piccioni, O.)—275(A)
—— (see Wolfgang, R. L.)—1871(E)
Friedman, Abraham, S. and Irwin Oppenheim. Statistical thermodynamics of isotope effects. II. Equation of state of H_2 istopes at intermediate densities—258(A)
Friedman, H. (see Byram, E. T.)—1594
Friedman, M. B. (see Ludloff, H. F.)—1140(A)
Friedman, M. H. and S. T. Butler. Bose-Einstein condensation of an imperfect gas—294
—— (see Butler, S. T.)—287
Friedman, R. M. (see Crowe, K. M.)—268(A)
—— (see Motz, H.)—268(A)
Friesen, E. W. (see Fretter, W. B.)—1202(A)
Fritzsche, H. and K. Lark-Horovitz. Hall effect and resistivity of InSb at low temperatures—1532(A)
—— (see Lark-Horovitz, K.)—1532(A)
Frost, L. S. and A. V. Phelps. Cumulative ionization processes in He positive column—559(A)
Fry, W. F., J. Schneps, and M. S. Swami. Delayed disintegration of nuclear fragments—247(A)
Frye, G. M., Jr., A. H. Armstrong, and L. Rosen. $B^{11}(n,\alpha)Li^8(\beta)Be^{8*}(2\alpha)$ reaction from 12 to 20 Mev—241(A)
Fryer, Edward M. and Charles A. Fowler, Jr. Magnetic domains in single crystal of Co near 275°C by longitudinal Kerr effect—270(A)
Fuller, E. G. and Evans Hayward. Self-absorption or self-indication in nuclear elastic scattering experiment—1537(A)
Fuller, J. C. and D. C. Ralph. Angular distribution of neutrons from reaction $D(d,n)He^3$ at 100 kev—248(A)
Fuller, Melvin Otis. Disintegration of O by 300-Mev neutrons—274(A)
Furlong, L. R. and C. F. Ravilious. Low-temperature luminescence and absorption of CdS—954

Gaffney, John (see Overton, W. C., Jr.)—969
Gallagher, J. J., W. C. King, and C. M. Johnson. Microwave spectrum of $N^{15}O^{16}$—1551(A)
Galonsky, A., R. A. Douglas, W. Haeberli, M. T. McEllistrem, and H. T. Richards. *d*-He differential scattering cross sections—586
—— **and J. Judish.** *n-p* scattering at 17.9 Mev—1168(A)
—— **and M. T. McEllistrem.** Energy levels of Li^9 from *d*-He differential cross sections—590
Gammel, J. L. (see Frank, R. M.)—1204(A)
Gamow, G. Transfer of information from nucleic acids to proteins—1534(T)
Gardiner, V. (see Hoffman, Joseph G.)—1195(A)
Gardner, Andrew L. Measurements of electron density in long-lived nitrogen afterglows—263(A)
—— (see Kunkel, W. B.)—558(A)
Garfunkel, M. P. (see Corak, William S.)—1699
Garrett, C. G. B. Physical properties of Ge surfaces—278(T)
Garrido, L. (see Waniek, R. W.)—1148(A)
Garrison, John D. (see Chamberlain, Owen)—1167(A)
—— (see Morris, T. W.)—1167(A)
Garwin, R. L. (see Anderson, A. G.)—283(A)
Gasiorowicz, S. Modified Holtzmark distribution—257(A)
—— (see Riddell, R., Jr.)—257(A)
Geballe, T. H. and G. W. Hull. Seebeck effect in Si—940
Gebbie, H. A. Excess noise and trapping in Ge—1567(A)
Geer, E. H., E. B. Nelson, and E. J. Wolicki. α-α angular correlation in $B^{11}(p,\alpha\alpha)He^4$—241(A)
Geib, I. G. (see Buschert, R.)—1157(A)
Gell-Mann, M. Theoretical views on new particles—255(T)
George, T. H., H. E. Farnsworth, and R. E. Schlier. Adsorption of O_2 and N_2 by Ti—1179(A)
—— (see Schlier, R. E.)—250(A)
George, W. D., W. Barber, and D. Reagan. Absolute cross section for reaction $C^{12}(\gamma,n)C^{11}$—276(A)
—— (see Barber, W. C.)—73
Gerjuoy, E. and S. Stein. Rotational excitation by slow electrons—557(A)
—— **and S. Stein.** Rotational excitation by slow electrons. II—1848
Germer, L. H. (see Kisliuk, P.)—560(A)
Ghiorso, A., B. G. Harvey, G. R. Choppin, S. G. Thompson, and G. T. Seaborg. New element mendelevium, atomic number 101—1518(L)
—— (see Choppin, G. R.)—1519(L)
Gibson, John B. Thermal scattering of electrons between bands in metal—1151(A)
Gilbert, D. A. and Victor W. Cohen. Nuclear spin and hfs interaction in 3.1-hr Cs^{134m}—1194(A)
Gilbert, F. C. Analysis of disintegration products from reactions of 125-Mev deuterons with Li nuclei—275(A)
Gilbert, T. L. Determination of polydisperse aerosol size distributions from analysis of light scattering data—242(A)
——, **J. M. Kelly, and H. Ekstein.** Rapid remagnetization of thin Mo permalloy tapes—1200(A)
Given, Frank I. (see Evans, Marjorie W.)—256(A)
Givens, M. Parker (see Koester, Charles J.)—1543(A)
Glaser, D. A. Bubble chambers for experiments in high-energy nuclear physics—1191(T)
Glaser, Vladimir. New relativistic two-body equation—840(L)
Glaser, Walter. Foundation of wave-mechanical theory of the electron—1176(A)
Glass, Neel W. and J. Reginald Richardson. Radionuclides Al^{24}, P^{30}, Cl^{38}, and Sc^{46}—1251
Glass, R. A., R. J. Carr, J. W. Cobble, and G. T. Seaborg. Fission-spallation competition in heavy elements—261(A)
Glasser, R. G. Relation between multiple Coulomb scattering and residual range in nuclear emulsion—174
Glassgold, A. E. Scattering of high-energy electrons by nuclei—1360
Glauber, R. J. Time-dependent displacement correlations and inelastic scattering by crystals—1692
Glaubman, Michael J. Radioactive decay of 65-hour Sb^{122}—645; 1172(A)

Glick, H. (see Smith, W.)—1141(A)
Glicksman, M. and H. L. Anderson. Scattering of 165-Mev pions by protons—239(A)
—— (see Kruse, U.)—1188(A)
Gluckstern, Robert L. Analysis of electron stripping data—276(A)
—— Electron capture and loss by ions in gases—1817
Goddard, Pliny E. (see Nail, Nelson R.)—1557(A)
Goebel, Charles J. Pion-nucleon s-wave phase shift from ps-ps with cutoff—273(A)
Goldberg, Colman and R. E. Davis. Hall effect in p-type Ge—1192(A)
Goldberg, Irwin (see Bergmann, Peter G.)—531; 1175(A)
Goldberg, J. N. New approximation method for gravitational field equations—1175(A)
Goldberg, Seymour. Studies of anode pre-breakdown phenomena in thyratrons—558(A)
Goldey, James M. and Sanborn C. Brown. Carrier effective masses in Ge—1192(A)
—— **and Sanborn C. Brown.** Microwave determination of average masses of electrons and holes in Ge—1761
Goldhaber, Gerson, W. W. Chupp, S. J. Goldsack, J. Lannutti, and F. Webb. Heavy meson and hyperon production at the bevatron—267(A)
—— **and Stephen J. Goldsack.** Measurements on K particles and their decay products—1203(A)
—— (see Goldhaber, S.)—1203(A)
—— (see Goldsack, Stephen J.)—284(A)
—— (see Lannutti, Joseph)—258(A)
Goldhaber, M. (see Mihelich, John W.)—1185(A)
Goldhaber, S., Gerson Goldhaber, H. H. Heckman, and F. M. Smith. Heavy mesons and hyperons from targets bombarded by 4.8- and 5.7-Bev protons—1203(A)
—— (see Heckman, Harry H.)—1202(A)
Goldman, J. E. (see Arrott, A.)—1201(A); 1864(L)
—— (see Guthrie, G.)—1181(A)
Goldsack, Stephen J. and Gerson Goldhaber. Multiple scattering microscope for "constant sagitta" measurements—284(A)
—— (see Goldhaber, Gerson)—267(A); 1203(A)
—— (see Lannutti, Joseph)—258(A)
Goldsmith, G. J. and D. E. Hill. Photoconductivity in paraterphenyl single crystals—238(A)
—— (see Hill, D. E.)—238(A)
—— (see Kleitman, D.)—1544(A)
Goldstein, Louis and James Reekie. Spatial distribution of atoms in liquid He^4—857
Goldwasser, E. L., L. J. Koester, and F. E. Mills. Elastic photoproduction of π^0 mesons for He—239(A)
——, **F. E. Mills, T. R. Robillard.** Direct measurement of effect of polarization on energy loss—1763
Goodenough, J. B. and A. L. Loeb. Theory of ionic ordering, crystal distortion, and magnetic exchange due to covalent forces in spinels—391
Goodman, Clark (see Mark, Hans)—249(A); 279(A); 1245
—— (see McClelland, Clyde)—249(A)
Gordon, J. P. Molecular amplification and generation of microwaves with applications to spectroscopy and to time standards—1159(T)
Gordon, R. B. and A. S. Nowick. Elastic modulus of x-irradiated rock salt—1540(A)
Gordon, S. (see Grossweiner, L. L.)—243(A)
Gordy, Walter (see Mizushima, Masataka)—1034; 1159(A)
Gossett, C. R., G. C. Phillips, and J. T. Eisinger. Absolute magnetic analysis of $F^{19}(p,p')F^{19*}$ reaction—724
Graetzer, H. G. and E. C. Pollard. Upper limit to lifetime of compound nucleus—1184(A)
Graham, John W. and Scott E. Forbush. Solar flare and magnetic storm effects in cosmic-ray intensity near geomagnetic N pole—1348
Graham, R. L., J. L. Wolfson, and M. A. Clark. Disintegration of 27-hr Ho^{166}—1173(A)
Grannis, F. H. (see McGuire, T. R.)—1562(A)
Gravel, Charles L. (see Brown, Fielding)—442
Green, A. E. S. and Kiuck Lee. IPM mass surface—1205(A)
Green, D. Wayne, John N. Cooper, and James C. Harris. Stopping cross sections of metals for protons of energies from 400 to 100 kev—466
Green, G. K. Brookhaven 25-Bev synchrotron—266(T)
Green, Louis C. (see Lewis, Margaret N.)—1210(A); 1020
Green, Milton. Magnistor, solid-state electronic valve—1169(A)
Green, Mino and J. A. Kafalas. Oxidation of clean surfaces of Ge below 25°C—1566(A)
Green, R. E. and A. T. Stewart. Angular correlation of photons from positron annihilation in light metals—486
—— (see Stewart, A. T.)—232(A)
Greenberg, D. H. (see van Lieshout, R.)—1171(A)
Greenberg, J. Mayo. Variational principle for total scattering amplitude—1189(A)
Gregg, E. C. (see Robson, J. W.)—233(A)
—— (see Stearns, R. L.)—232(A)
Gregory, B. (see Armenteros, R.)—275(A)
Griffith, G. L. γ radiation from neutron inelastic scattering—579
Griffith, Wayland and Walker Bleakney. Diffusion analogy for shocks interacting with thermal boundary layers—1143(A)
Grimm, G., L. J. Rainwater, and W. W. Havens, Jr. Slow neutron velocity spectrometer using Nevis synchrocyclotron—1161(A)
Grimsal, E. G. Hall coefficient in anisotropic media—229(A)
Grodzins, L. Multiple scattering of 2.5-Mev positrons by 0.1 mil Au foil—279(A)
—— (see del Castillo, G.)—1163(A)
Gross, E. P. Inertial effects and dielectric relaxation—1191(A)
—— Temperature effect of paramagnetic line shape—1561(A)
Grossweiner, L. L. and S. Gordon. Mechanism of photochemical reactions catalyzed by red-mercuric sulfide—243(A)
Gruen, Dieter M. (see Henry, Warren E.)—1200(A)
Gudmundsen, Richard A. (see Forrester, A. Theodore)—1169(A)
Guernsey, Janet B. Neutron cross sections for Zr—1210(A)
—— **and A. Wattenberg.** Neutron inelastic scattering—1147(A)
Gunther-Mohr, G. R. (see Koenig, S. H.)—228(A)
Gupta, Suraj N. Multiple photon production in electron-positron annihilation—247(T)
—— Multiple photon production in quantum electrodynamics—1502
Gupta, U. C. (see Miller, D. W.)—1184(A)
Gurnee, E. F., L. T. Patterson, and R. D. Andrews. Apparatus for making simultaneous stress and birefringence measurements on polymers—1547(A)
Gursky, Martin L. Particle motion in anisotropic harmonic oscillator well—1205(A)
Guth, Eugene. Dirac's method using complex variables in quantum mechanics—273(A)
—— (see Banas, E. M.)—265(A)
—— (see Harris, C. W.)—272(A)
—— (see Lockary, T. E.)—274(A)
—— (see Mullin, C. J.)—277(A)

—— (see Sells, R. L.)—272(A)
—— (see Wang, Ming Chen)—274(A)
Guthrie, G., S. A. Friedberg, and J. E. Goldman. Electronic specific heat of α-Mn—1181(A)

Haake, Claus H. Temperature dependence of electroluminescence—1544(A)
Haar, Lester. Ideal gas thermodynamic properties of isotopic hydrides of group of diatomic free radicals—1551(A)
Haeberli, W. (see Galonsky, A.)—586
Haffner, James W. Limitations of stripping theory in inelastic deuteron scattering—1156(A)
Hagstrum, Homer D. Ejection of electrons from contaminated metals by positive ions—561(A)
Hahn, Beat and Robert Hofstadter. High-energy electron scattering in Rh, Ta, W, and U—278(A)
Hahn, E. L. and B. Herzog. Diffusion model for nuclear precession relaxation in solids—265(A)
—— (see Anderson, A. G.)—283(A)
—— (see Herzog, B.)—226(A)
Hahn, T. M., Jr., B. D. Kern, and G. K. Farney. Excitation curve of reaction $B^{10}(p,\gamma)C^{11}$—1183(A)
—— (see Rayburn, L. A.)—701
Halford, Ralph S. (see Zwerdling, Solomon)—243(A)
Hall, R. N. (see Newman, R.)—1536(A)
Halperin, A. and A. Braner. Thermal bleaching of color centers—1135(L)
Halpern, J. (see Triebwasser, S.)—1562(A)
Halpern, O. and R. A. Buckingham. Symmetry effects in gas kinetics. I. He isotopes—1626
Hama, Francis R. Relations between one- and three-dimensional functions in isotropic turbulence and direct measurement of energy transfer function—1142(A)
Hamermesh, M. (see Crosbie, E. A.)—233(A)
Hamilton, D. R. Focusing atomic-beam apparatus—1174(T)
Hamilton, J. F., F. A. Hamm, and J. W. Castle. Displacement of latent image in photographic emulsion grains—1557(A)
Hamm, F. A. (see Hamilton, J. F.)—1557(A)
Handler, Harry E. and J. Reginald Richardson. γ-γ directional correlation in $Cl^{34}\rightarrow S^{34}$ decay—281(A)
Handley, T. H., W. S. Lyon, and E. L. Olson. Ho^{166}—688
—— (see Blosser, H. G.)—1198(A)
Hanna, S. S. Energy levels of Be^8—1530(T)
—— (see Fowler, J. M.)—249(A)
—— (see Segel, R. E.)—1538(A)
Hans, H. S., Babulal Saraf, and C. E. Mandeville. Coincidence studies of disintegration of Pm^{149} and Nd^{147}—1173(A)
Hanscome, T. D. and D. K. Willett. Magnetic analyzer for nuclear reactions—232(A)
—— (see Holmgren, H. D.)—241(A)
Hanson, A. O. Photodisintegration of deuterium—234(T)
Hare, W. F. J. (see Allin, Elizabeth J.)—554(L)
Harman, T. C., R. K. Willardson, and A. C. Beer. Effect of impurities on mobility in n-type InSb—1532(A)
—— (see Willardson, R. K.)—227(A)
Harrick, N. J. Attempt to detect high mobility holes in Ge using drift mobility technique—1131(L)
Harris, C. W. and E. Guth. Role of coordination number in Lee-Yang lattice gas—272(A)
—— (see Sells, R. L.)—272(A)
Harris, E. G. Disordering of polyatomic solids by neutrons—1151(A)
Harris, G. G. *K* mesons produced by 2.2 and 3 Bev protons—1202(A)
Harris, James C. (see Green, D. Wayne)—466
Harrison, S. E. (see Kriessman, C. J.)—1562(A)
Harrison, W. A. and Frederick Seitz. Theory of radiation damage—1530(A)
Hart, Edward W. Lattice resistance to dislocation motion at high velocity—1775
Harth, E. M. (see Block, M. M.)—248(A)
Harvey, B. G. (see Choppin, G. R.)—1519(L)
—— (see Ghiorso, A.)—1518(L)
Harvey, John A. Level spacings of heavy nuclei—1162(A)
Hastings, J. M. (see Brockhouse, B. N.)—1721
Hauver, G. (see Zernow, L.)—1551(A)
Havens, W. W., Jr. (see Grimm, G.)—1161(A)
Havill, J. R. (see Tautfest, G. W.)—280(A)
Hawkins, William Bruce. Orientation and alignment of Na atoms by means of polarized resonance radiation—478
Hayden, R. J. (see Wasserburg, G. J.)—250(A)
Hayn, C. H. and Vincent P. Jacobsmeyer. Photoconductivity of pyrolytic layers of B—237(A)
Haynes, J. R. New radiation resulting from recombination of holes and electrons in Ge—1866(L)
Hayward, Evans (see Fuller, E. G.)—1537(A)
Hayward, R. W. and D. D. Hoppes. Disintegration of Se^{75}—1172(A)
——, **D. D. Hoppes, and H. Ernst.** Disintegration of Nb^{95} and Nb^{97}—231(A)
Hazlett, Thomas H. (see Ancker, Betsy)—1151(A)
Heberle, J., H. Reich, and P. Kusch. New method for investigating hfs of metastable state—1194(A)
—— (see Reich, H.)—1194(A)
Heckman, Harry H., S. Goldhaber, and F. M. Smith. Observations of K^+ mesons—1202(A)
—— (see Goldhaber, S.)—1203(A)
Heckrotte, Warren. Production of high-energy neutrons and deuterons from stripping of He—259(A)
Heikes, R. R. Magnetic transformation in MnBi—1199(A)
—— Relation of magnetic structure to electrical conductivity in NiO and related compounds—225(A)
Heims, S. P., D. R. Yennie, and D. G. Ravenhall. W.K.B. approximation to phase shifts—278(A)
Heinberg, M. (see Page, L. A.)—206(L)
Hellens, R. L. (see Jennings, B.)—582
Hemmendinger, A. and H. V. Argo. Reaction $D(t,\alpha)n$ at 1.5 Mev—70
Hempstead, C. F. and L. G. Parratt. Localized energy states in crystalline alkali chlorides—1170(A)
Hendel, P. (see Armenteros, R.)—275(A)
Henkel, Richard L. (see Beyster, J. R.)—1216
—— (see Seagrave, John D.)—666
Hennig, G. and M. Dzurus. Donor impurities in graphite—227(A)
Henry, Warren E. Antiferromagnetism of Yb_2O_3 at liquid He temperatures—226(A)
—— Magneto-electric effects in Ge in strong magnetic fields—1534(A)
—— Quantized spin paramagnetism in free radical near magnetic saturation—252(A)
—— **and Dieter M. Gruen.** Saturation magnetization and remanence of β-UH_3—1200(A)
Henshaw, D. G. (see Hurst, D. G.)—224(A)
Henvis, B. (see Burstein, E.)—1536(A)
Herman, Robert, G. E. Moore, S. Silverman, and R. F. Wallis. Vibration-rotation line intensities in HCl and DCl—1550(A)
—— **and R. F. Wallis.** Model for room temperature bleaching of *F* centers by *F* light in x-rayed NaCl—1171(A)
Hernqvist, K. G. and E. O. Johnson. Retrograde motion in gas discharge plasmas—1576
Herring, D. F. (see Jones, K. W.)—241(A)
Hertz, M. R. (see Breen, R. J.)—599
Hertzberg, A. (see Smith, W.)—1141(A)
Herzberg, G. Lamb shift of 1*S* level of deuterium—223(A)
—— (see Chandrasekhar, S.)—1050

Herzfeld, C. M. Strong crystal field theory of magnetic resonance for d^3 configurations—226(A)
Herzog, B. and E. L. Hahn. Relaxation time modification by double nuclear resonance—226(A)
—— (see Hahn, E. L.)—265(A)
Heydenburg, N. P. and G. M. Temmer. Assignment of energy levels by Coulomb excitation with 5.7-Mev α particles—1198(A)
—— (see Temmer, G. M.)—1198(A); 1308
Hibdon, Carl T. and Alexander Langsdorf, Jr. Total neutron cross sections in kev region: Be, B, C, F, Ti, Ni, and Bi—223(A)
Hickam, W. M. and R. E. Fox. Negative ion formation using monoenergetic electrons—557(A)
Hicks, Donald A., John Ise, Jr., and Robert V. Pyle. Spontaneous-fission neutrons of Cf^{250} and Cm^{244}—1521(L)
—— (see Ise, John, Jr.)—1199(A)
Hiedemann, E. A. Ultrasonic light modulators for spectroscopy and measurement of very short time intervals—242(T)
Higgins, L. (see Bandtel, K. C.)—269(A)
Hildebrand, R. H. Use of Glaser bubble chambers in photographing nuclear events—227(T)
Hill, D. A. (see Coor, T.)—1369
Hill, D. E. and G. J. Goldsmith. Dark conduction in paraterphenyl single crystals—238(A)
—— (see Goldsmith, G. J.)—238(A)
Hill, R. D. Model for asymmetric fission—1272
——, **E. O. Salant, and M. Widgoff.** Chi meson produced by 3-Bev protons—247(A)
Hockney, R. W. and P. V. C. Hough. Coulomb effects in (d,p) reaction—234(A)
Hodson, A. L. (see Arnold, W. H.)—275(A)
Hoffman, D. C. (see Prestwood, R. J.)—1324
Hoffman, Joseph G., N. Metropolis, and V. Gardiner. Monte Carlo methods in study of cell growth—1195(A)
Hofstadter, Robert. Electron scattering and nuclear structure—277(T)
—— **and Robert W. McAllister.** Electron scattering from proton—217(L)
—— (see Fregeau, J. H.)—1184(A)
—— (see Hahn, Beat)—278(A)
—— (see McIntyre, John A.)—158
Holcomb, D. F. and R. E. Norberg. Nuclear spin relaxation in alkali metals—1074
—— (see Norberg, R. E.)—226(A)
Holden, A. N., B. T. Matthias, W. J. Merz, and J. P. Remeika. New class of ferroelectrics—546(L)
Holder, B. E. and M. P. Klein. Isotope abundance ratios by nuclear magnetic resonance—265(A)
—— (see Klein, M. P.)—265(A)
Holladay, W. G. and R. G. Sachs. Evidence for pion-pion interaction—1155(A)
Holland, D. H. Lattice space quantization of coupled meson and nucleon fields—788; 273(A)
Holland, R. E., D. R. Inglis, and F. P. Mooring. Search for excited states of Be^8—240(A)
Hollander, J. M. and M. I. Kalkstein. Radiations of Ba^{135}—Cs^{135}—260(A)
—— (see Smith, W. G.)—262(A); 1258
Holmgren, H. D., T. D. Hanscome, and D. K. Willett. Q values for $O^{17}(d,p)O^{18}$ and $O^{18}(d,p)O^{19}$ reactions—241(A)
Holt, N. Total neutron cross section of Eu in 0.001 to 0.01 ev region—1162(A)
Holtzberg, Frederic (see Triebwasser, Sol)—1201(A)
Holzman, G. R., John H. Anderson, and W. Koth. Spin-lattice relaxation time of Si^{29} nucleus in pure fused silica—542(L)
Hong, K. and S. Mrozowski. Studies of elastic modulus of carbons—1565(A)
Hooton, John A. and Walter J. Merz. Etch patterns and ferroelectric domains in $BaTiO_3$ single crystals—409
Hoover, C. W., Jr., and R. K. Smither. Secondary electron resonance discharge mechanism. II—1149(A)
—— (see Smither, R. K.)—1149(A)
Hopkins, R. L. Elastic strain energy stored in mechanically disturbed surfaces—1567(A)
Hoppes, D. D. (see Hayward, R. W.)—231(A); 1172(A)
Hornbostel, J. and E. O. Salant. Capture of negative K mesons—218(L)
—— **and E. O. Salant.** Heavy unstable particles from captured K^- mesons—1202(A)
Hornyak, W. F. (see Coor, T.)—1369
Horton, G. K. (see Bhatia, A. B.)—1181(A); 1715
Horton, J. W. (see Anderson, A. G.)—283(A)
Horwitz, Nahmin. Čerenkov counter flux measurement of cosmic-ray alphas at 41°—165
Hosler, W. R. (see Blunt, R. F.)—1533(A)
—— (see Frederikse, H. P. R.)—1533(A)
Hough, P. V. C. (see Bach, D. R.)—235(A)
—— (see Hockney, R. W.)—234(A)
Hove, John E. Two-medium theory of thermal conductivity of artificial graphite: Interpretation—1563(A)
Howard, Brian T. Theory of electroluminescence—1544(A)
Howard, Louis N. Vortices produced by shocks—1141(A)
Howard, R. A. (see Stier, P. M.)—1149(A)
Hubbard, Edward L. and Eugene J. Lauer. Charge distributions of O and Ne ions passing through gases—1814
—— **and Eugene J. Lauer.** Stripping electrons from accelerated O and Ne ions—276(A)
Huber, Elsa L. Breakdown processes in nitrogen, oxygen, and mixtures—560(A)
Hudis, J. (see Baker, E.)—242(A)
Hudson, Gilbert G. Streamers in positive point-to-plane breakdown in air—264(A)
Hudson, R. P. (see Ambler, E.)—230(A)
Huggett, R. W., J. R. Burwell, and R. W. Thompson. New examples of anomalous V^0 particles—248(A)
—— (see Burwell, J. R.)—101; 247(A)
—— (see Kim, Y. B.)—248(A)
Hughes, D. J. Neutron widths of nuclear energy levels—1161(A)
—— (see Levin, J. S.)—1161(A)
Hughes, V. W., S. Marder, and C. S. Wu. Static magnetic field quenching of orthopositronium decay: Angular distribution effect—1840
—— (see Marder, S.)—1173(A)
—— (see Teutsch, W. B.)—1174(A)
Huibregtse, E. J., M. E. Drougard, and D. R. Young. Electromechanical behavior of single crystals of $BaTiO_3$—1562(A)
Hull, G. W. (see Geballe, T. H.)—940
Hullings, M. K. (see Blosser, H. G.)—1198(A)
—— (see Cohen, B. L.)—685
Hulm, J. K. Superconducting Re alloys and compounds—1539(A)
Hummel, John P., F. Asaro, and I. Perlman. α decay of Pa^{231}—261(A)
——, **Frank S. Stephens, Jr., Frank Asaro, A. Chetham-Strode, Jr., and I. Perlman.** α and γ spectra of Cf^{246}—22
—— (see Stephens, F.)—261(A)
Hurley, J. P., S. W. Rudman, and P. S. Jastram. Angular correlation in decay of Co^{58}—1187(A)
Hurst, D. G. and D. G. Henshaw. Slow neutron scattering by liquid He—224(A)
Husain, A. and E. Pickup. Mass spectrum of shower particles from cosmic-ray interactions—136
—— (see Pickup, E.)—247(A)

Huse, M. C. (see Blatt, F. J.)—1553(A)
Hutchison, C. A., Jr. Paramagnetism of the transuranic elements—272(T)
Hutson, Andrew R. Velocity analysis of thermionic emission from single-crystal W—889
Hyde, Earl K. (see Mathur, Hirdaya B.)—79; 261(A)

Igo, G. (see Wertheim, M. S.)—1
Ihsan, M. A. Nuclear energy levels of Be^9 from $Li^7(d,n)Be^9$—689
Inchauspé, Nicolas. Photoconductivity in KI—1550(A)
—— Polarization in insulating crystals—1543(A)
Ingham, H. (see Pearlstein, E.)—1530(A)
—— (see Smoluchowski, R.)—1530(A)
Inghram, Mark G. Mass-spectrometric analysis of ions produced in field ion microscope—1159(T)
—— (see Porter, Richard F.)—242(A)
Inglis, D. R. (see Holland, R. E.)—240(A)
Ise, John, Jr., Donald A. Hicks, and Robert V. Pyle. Neutron multiplicity spectrum from spontaneous fission—1199(A)
—— (see Hicks, Donald A.)—1521(L)
Ishii, S. (see Sakamoto, M.)—552(L)
Itoh, Takashi (see Shimoda, Koichi)—1160(A)
Ivory, J. E., F. B. Baldwin, and R. L. Anthony. Experimental study of behavior of rubbers in simple shear—1558(A)
Iwersen, John E. and W. S. Koski. γ rays in decay of Na^{22}—1307

Jackson, H. E. (see Bollinger, L. M.)—223(A)
Jackson, J. David (see Betts, D. D.)—1149(A)
—— (see Sharp, R. T.)—1128(L)
Jacobsmeyer, Vincent P. (see Hayn, C. H.)—237(A)
Jahn, Robert G. Refraction of shock waves at gaseous interface—1141(A)
Jakobson, Mark J. (see Repp, Gordon W.)—268(A)
—— (see White, R. Stephen)—269(A)
Jamieson, C. P. Thermal conductivities of carbons and graphites—1564(A)
Janin, Joseph (see Déjardin, Georges)—1149(A)
Jankus, V. Z. Electrodisintegration of deuteron—278(A)
Jarmie, Nelson. Excitation function of $O^{16}(t,n)F^{18}$—41
Jastram, P. S. Angular correlation of aligned nuclei—1164(T)
—— (see Hurley, J. P.)—1187(A)
—— (see Wood, G. T.)—1187(A)
Jastrow, Robert. Many-body problem with strong forces—1479
Jauch, J. M. (see Rohrlich, F.)—222(A)
Jaumot, F. E., Jr., and R. L. Smith. Self-diffusion in Zn at low temperatures—1555(A)
—— (see Sawatzky, A.)—1555(A)
Jaynes, E. T. Matrix treatment of nuclear induction—1099
Jeffries, C. D. (see Sogo, P. B.)—265(A); 1316
Jefimenko, Oleg (see Ch'en, Shang-Yi)—281(A)
Jenkins, F. A. and D. R. Speck. Phase change on reflection from multilayer films—282(A)
—— (see Speck, D. R.)—282(A)
Jennings, B., J. Weddell, I. Alexeff, and R. L. Hellens. Scattering of 4.4-Mev neutrons by Fe and C—582
Jenny, Hans K. (see Arams, Frank R.)—562(A)
Jentschke, W. K. (see Maxson, D. R.)—230(A)
Jeppesen, Myron A. Raman and fluorescence spectra of allyl diglycol carbonate—1211(A)
Jesse, William P. and John Sadauskis. Comparison of energy to make an ion-pair in various gases for α and β particles—1150(A)
Jillson, D. C. and A. C. Sheckler. Segregation coefficient of As in Ge as function of crystal growth variables—229(A)
—— (see Sheckler, A. C.)—229(A)
Johnson, C. H. (see Fowler, J. L.)—728
—— (see Trail, C. C.)—249(A)
Johnson, C. M. (see Gallagher, J. J.)—1551(A)
Johnson, E. O. (see Hernqvist, K. G.)—1576
Johnson, M. H. and E. Teller. Classical field theory of nuclear forces—260(T); 783
Johnson, O. E., R. G. Johnson, and L. M. Langer. Evidence for 0+ first excited state in Zr^{96}—1517(L)
Johnson, Philip O. (see Forrester, A. Theodore)—1169(A)
Johnson, R. F. (see Webb, L. A.)—234(A)
Johnson, R. G. (see Johnson, O. E.)—1517(L)
Johnson, V. A. Electrical conductivity of liquid Te—1567(A)
—— (see Seidel, G. M.)—230(A)
Johnston, William G. Effect of plastic deformation on electrical conductivity of AgBr—1777
Jona, F., G. Shirane, and R. Pepinsky. Dielectric, x-ray, and optical study of ferroelectric $Cd_2Nb_2O_7$ and related compounds—903
——, **G. Shirane, and R. Pepinsky.** Optical properties and twinning of $PbZrO_3$ single crystals—1201(A)
Jones, K. W., M. T. McEllistrem, R. A. Douglas, D. F. Herring, and E. Silverstein. Angular distributions and excitation functions of $C^{13}(d,p)$ reaction—241(A)
Jones, L. W., K. R. Symon, K. M. Terwilliger, and D. W. Kerst. Synchrotron application of reverse field types of fixed field alternating gradient magnets—1153(A)
—— (see Kerst, D. W.)—1153(A)
—— (see Terwilliger, K. M.)—1153(A)
Jordan, R. D. (see Alger, R. S.)—1550(A)
Jordan, W. C. (see Burson, S. B.)—230(A)
Jossem, E. L. and L. G. Parratt. Energy levels in metallic K—1151(A)
Jost, Res. (see Newton, Roger G.)—1189(A)
Judd, D. L. (see Bludman, S. A.)—283(A)
Judish, J. (see Galonsky, A.)—1168(A)
Jurić, Mira K. Angular distribution of disintegration products from $O^{16}(d,p)O^{17}$, $Be^9(d,p)Be^{10}$, and $Be^9(d,t)Be^8$ reactions—85

Kac, Mark. Foundation of kinetic theory of gases—255(T)
Kafalas, J. A. (see Green, Mino)—1566(A)
Kahn, A. H. (see Argyres, P. N.)—226(A)
Kahn, B. and W. S. Lyon. Decay of Y^{91}—58
Kahn, D. (see Aron, J.)—246(A)
Kaiser, H. F. Synchro-microtron—233(A)
——, **W. T. Mayes, and W. J. Willis.** Electron beam extraction from X-band microtron—1538(A)
Kaiser, W. and H. Y. Fan. Infrared absorption of InSb—966
Kalkstein, M. I. (see Hollander, J. M.)—260(A)
Kane, R. P. Recurrence phenomenon in 24-hour variation of cosmic-ray intensity—130
Kanter, M. A. Self-diffusion in natural graphite crystals—1563(A)
Kantrowitz, Arthur and Harry Petscheck. Approach to equilibrium ionization following strong shock waves in A—1141(T)
Känzig, Werner. Space charge layer near surface of a ferroelectric—549(L)
—— **and Masayasu Ueta.** Generation of electron traps by plastic flow—236(A)
Kao, L. P. and E. Katz. Theory of anisotropy of magnetoresistance for single crystals—1534(A)

Kaplan, Joseph. Upper atmosphere—278(T)
—— Upper-atmospheric studies during international geophysical year—1159(T)
Kaplon, M. F. Abundance of Li, Be, and B in primary cosmic radiation—1164(T)
Karplus, Robert. Ferromagnetic Hall effect—1542(T)
—— **and Malvin A. Ruderman.** Applications of causality to scattering—771
—— **and M. A. Ruderman.** Some implications of causality for scattering—260(T)
Kassner, D. (see Piccioni, O.)—275(A)
Katz, E. Photographic "order principle"—1556(A)
—— (see Enns, J. H.)—1556(A)
—— (see Kao, L. P.)—1534(A)
—— (see Martin, R. L.)—1557(A)
Katz, Samuel. Velocity of explosively-induced shock in steel—256(A)
Kauffman, J. W. and J. S. Koehler. Formation energy of lattice vacancies in Au—245(A)
Kavanagh, R. W. (see Sherr, R.)—1185(A)
Kay, I. and H. E. Moses. Determination of scattering potential from spectral weight function—1190(A)
Keating, David T. X-ray measurements on low-temperature neutron-irradiated graphite—1859(L)
Keck, J. C. (see Bingham, H. H.)—1187(A)
Kedesdy, H. (see Matare, H. F.)—1179(A)
Keesom, P. H. and N. Pearlman. Anomaly in low-temperature atomic heat of Ag—548(L)
—— **and N. Pearlman.** Heat capacity measurements on pure and slightly reduced rutile (TiO_2) at very low temperatures—1539(A)
—— (see Pearlman, N.)—1539(A)
Keller, William E. Pressure-volume isotherms of He^3 between 1.5 and 3.8° K—1571
Kelly, J. M. (see Gilbert, T. L.)—1200(A)
Kenney, Robert W. (see Anderson, John D.)—258(A)
Kenty, Carl. Studies of active N in rare gases—563(A)
Kepler, G. E. (see Fretter, W. B.)—1202(A)
Kereiakes, J. G. X-ray analysis of compressed KCl powder crystals—553(L)
Kern, B. D. (see Hahn, T. M., Jr.)—1183(A)
Kerner, Edward H. and Joseph G. Logan. Invariant characteristics of one-dimensional binary lattices—1165(A)
Kerr, J. and C. Wert. Magnetic coercive force in alloys of Fe and N—225(A)
Kerst, D. W. Review of MURA high-energy accelerator programme—236(T)
——, **K. M. Terwilliger, K. R. Symon, and L. W. Jones.** Fixed field alternating gradient accelerator with spirally ridged poles—1153(A)
—— (see Jones, L. W.)—1153(A)
—— (see Terwilliger, K. M.)—1153(A)
Kerth, Leroy and Byron L. Youtz. Elastic and inelastic scattering of 90-Mev neutrons by deuterons—259(A)
Keywell, Frank. Measurements and collision theory of high vacuum sputtering—561(A)
Kierstead, Henry A. Expansion of Cu bombarded by 19-Mev deuterons—245(A)
—— (see McDonell, William R.)—1870(E)
Kiive, P. and H. T. Pinnick. Temperature dependence of magnetic susceptibility of carbons and polycrystalline graphites—1564(A)
Kim, Y. B., J. R. Burwell, R. W. Huggett, and R. W. Thompson. Evidence for charge asymmetry of V^0 particles—248(A)
King, D. T. and M. M. Block. Nuclear absorption of fast charged hyperon—1203(A)
King, R. W. Supermultiplet structure and spin dependent forces—235(A)
King, W. C. (see Gallagher, J. J.)—1551(A)
Kingston, R. H. Water vapor induced *n*-type surface conductivity on *p*-type Ge—1766
—— **and A. L. McWhorter.** Relaxation effects in field-induced surface conductance—1191(A)
—— (see Bernstein, H.)—1566(A)
Kington, Joe D. (see Willard, Harvey B.)—669; 1184(A)
Kip, A. F. Cyclotron resonance in solids—272(T)
—— (see Dresselhaus, G.)—368; 556(L)
—— (see Feher, George)—337
Kisliuk, P., W. S. Boyle, and L. H. Germer. Electrical breakdown in high vacuum—560(A)
—— (see Boyle, W. S.)—560(A)
Kisslinger, Leonard S. Scattering of mesons by light nuclei—761
—— Scattering of π mesons by nuclei—239(A)
Kister, J. M. (see Beyster, J. R.)—1216
Kistler, A. L. (see Corrsin, S.)—1142(A)
Kittel, C. Electron transfer mechanism for ultrasonic attenuation in metals—1181(A)
—— Theory of valence-band structure of Ge and Si—1542(T)
—— (see Dresselhaus, G.)—368; 556(L)
—— (see Mitchell, A. H.)—271(A)
Kivel, Bennett. Electron broadening and shift of spectral lines of He—1055
—— Electron impact broadening of spectral lines of He—1195(A)
——, **S. Bloom, and H. Margenau.** Electron impact broadening of spectral lines—495
—— (see Margenau, Henry)—1822
Klein, Abraham and Bruce H. McCormick. Meson pair theory—1428; 1155(A)
—— (see Bernstein, J.)—1155(A)
—— (see McCormick, Bruce H.)—1155(A)
Klein, M. P. and B. E. Holder. Magnetic susceptibility measurements by nuclear magnetic resonance—265(A)
—— (see Holder, B. E.)—265(A)
Klein, Martin J. Overhauser nuclear polarization effect and minimum entropy production—1736
Kleitman, D. and G. Goldsmith. Conduction in phthalocyanine crystals—1544(A)
Klema, E. D. (see Lazar, N. H.)—710; 1186(A)
Klick, Clifford C. (see Lambe, John)—1545(A); 909
—— (see Patterson, D. A.)—1546(A)
Klontz, E. E., R. R. Pepper, and K. Lark-Horovitz. Electrical properties of electron bombarded Ge—1535(A)
—— (see Stoeckmann, F.)—1535(A)
Kmetko, E. A. Properties of powdered Ge and effects of heat-treatment—1535(A)
Knapp, Myron W. and Wilson M. Powell. Negative pions from neutron bombardment of deuterons—1188(A)
Knight, W. D. (see Walsh, J. L.)—265(A)
Knowles, J. W. Anomalous absorption of neutrons in single crystals—224(A)
Kobayashi, S. (see Sakamoto, M.)—552(L)
Koehler, J. S. Quenching-in of vacancies in pure Ag—1562(T)
—— (see Beshers, D. N.)—1553(A)
—— (see Kauffman, J. W.)—245(A)
Koenig, S. H. and G. R. Gunther-Mohr. Low-temperature electrical conductivity of Ge—228(A)
Koerts, L., P. Macklin, B. Farrelly, R. van Lieshout, and C. S. Wu. Radiations of I^{126}—1172(A); 1230
—— (see Farrelly, B.)—1172(A)
Koester, Charles J. and M. Parker Givens. Extreme uv absorption spectrum of AgCl—1543(A)
Koester, Louis J., Jr. Low-energy photoproduction of π^0 mesons in H: Differential cross sections at 135°—211(L)
—— Photoproduction of π^0 mesons in H—239(A)
—— (see Goldwasser, E. L.)—239(A)

—— (see Mills, F. E.)—210(L)
Kofoed-Hansen, O. Coupling in nuclear β decay—1164(T)
Kohman, T. P. (see Simanton, J. R.)—260(A)
Kohn, Walter. Interpretation of donor state absorption lines in Si—1856(L)
—— Spin resonance widths of electrons in donor states in Si—1561(A)
—— Theory of hyperfine splitting of donor states in Si—252(T)
—— **and J. M. Luttinger.** Theory of donor states in Si—915
—— **and J. M. Luttinger.** Theory of energy levels of donor electrons in Si—1178(A)
Kolchin, Eleanor K. (see Lewis, Margaret N.)—1210(A); 1020
Kolin, Alexander. New method of microelectrophoresis—1195(A)
Kolsky, Harwood G. Method for numerical solution of transient hydrodynamic shock problems in two space dimensions—1158(A)
Korringa, J. Satellites in soft x-ray spectrum of Zr—1556(A)
—— (see Daunt, J. G.)—1550(A)
Koski, W. S. (see Iwersen, John E.)—1307
Koster, G. F. Density of states curve for Ni—901
—— Extension of Hund's rule—514
Koth, W. (see Holzman, G. R.)—542(L)
Kovarik, A. F. and N. I. Adams, Jr. Redetermination of disintegration constant of U^{235}—46
Kovasznay, Leslie S. G. Experimental study of shock wave turbulence interaction—1141(A)
Kraichnan, Robert H. Special-relativistic derivation of generally covariant gravitation theory—1118
Kramer, Mary J. Molecular orientation produced in polymethyl methacrylate by hot stretching—1170(A)
Krasner, Sol and J. Cuevas. Electron loss cross sections of moving He atoms—1149(A)
Kraybill, H. L. (see Walker, R. M.)—1203(A)
Kriessman, C. J., S. E. Harrison, and H. B. Callen. Ionic distribution in Mg ferrite—1562(A)
—— **and T. R. McGuire.** Magnetic susceptibility of Hf and Mn—936
Krimm, S. and C. Y. Liang. Infrared spectrum and structure of polyvinylidene chloride—1547(A)
—— (see Liang, C. Y.)—1548(A)
Krohn, Victor E., T. B. Novey, and S. Raboy. Gyromagnetic ratio of 6×10^{-6} sec Np^{237} by angular-correlation techniques—1187(A)
—— (see Raboy, Sol)—24; 231(A); 1187(A)
Kroll, Norman M. and Walter Wada. Internal pair production associated with emission of high-energy γ rays—1355
—— (see Mills, Robert L.)—1489
Krueger, G. C. Investigation of quantitative phase contrast method for examining nonhomogeneous media—1157(A)
Krumbein, A. D. (see Wiser, H. L.)—303
Kruse, U. E., H. L. Anderson, W. C. Davidon, and M. Glicksman. Positive pion scattering by H at 189 Mev—1188(A)
—— (see Teem, J. M.)—259(A)
v. Krzywoblocki, M. Z. New fundamentals of fluid dynamics—251(A)
Kuczynski, G. C. and M. Doyama. Second transition in $AuCu_3$—270(A)
—— (see Freda, A. R.)—270(A)
Kulin, S. A., A. D. Kurtz, and B. L. Averbach. Effect of dislocations on recombination of holes and electrons in Ge and Si—1566(A)
—— (see Kurtz, A. D.)—1543(A)
Kundu, D. N. (see Cheng, L. S.)—231(A)
Kunkel, W. B. and A. L. Gardner. Ionization accompanying long-lived nitrogen afterglow—558(A)
Kuper, Alan B., H. Letaw, Jr., L. Slifkin, E. Sonder, and C. T. Tomizuka. Self-diffusion in Cu—1870(E)
—— **and Carl T. Tomizuka.** Diffusion of Cu and Zn in ordered and disordered CuZn—244(A)
Kurbatov, J. D., B. B. Murray, and M. Sakai. Energy levels of Se^{76} appearing in disintegration of As^{76}—674
Kurşunoğlu, Behram. Proton bremsstrahlung—1156(A)
Kurtz, A. D., S. A. Kulin, and B. L. Averbach. Determination of dislocation densities with double crystal spectrometer—1543(A)
—— (see Kulin, S. A.)—1566(A)
Kusch, P. (see Heberle, J.)—1194(A)
—— (see Reich, H.)—1194(A)

Lafferty, D. L. (see Rayburn, L. A.)—701
Lagarrigue, A. S-particles and charged heavy particles—255(T)
—— (see Armenteros, R.)—275(A)
—— (see Fretter, W. B.)—1202(A)
Lagerstrom, P. Structure of solutions of Navier-Stokes equation for high and low Reynolds numbers—1141(T)
Lakin, W. Spin polarization of deuteron—139
Lamb, W. E., Jr. (see Maiman, T. H.)—1194(A)
Lambe, John. Recombination processes in CdS—985
—— **and Clifford C. Klick.** Model for luminescence and photoconductivity in sulfides—909; 1545(A)
Landauer, R. (see Drougard, M. E.)—1010; 1563(A)
Landel, Robert F. (see Williams, Malcolm L.)—1549(A)
Landon, H. H. and V. L. Sailor. Radiation width variations in slow neutron resonances of Eu and In—225(A); 1267
—— (see Sailor, V. L.)—224(A)
—— (see Wood, R. E.)—639
Lane, A. M., R. G. Thomas, and E. P. Wigner. Giant resonance interpretation of nucleon-nucleus interaction—693
—— **and C. F. Wandel.** Evaluation of imaginary part of nuclear complex potential—1524(L)
—— (see Wilkinson, D. H.)—235(A)
Lane, C. T., R. G. Wheeler, and C. H. Blakewood. Second sound attenuation in rotating He II—1196(A)
Langer, L. M. (see Johnson, O. E.)—1517(L)
Langsdorf, Alexander, Jr., J. E. Monahan, and F. Paul Mooring. Measurement of neutron transmission cross sections by self-indication technique—1148(A)
—— (see Hibdon, Carl T.)—223(A)
—— (see Monahan, J. E.)—1147(A)
Lannutti, Joseph, Gerson Goldhaber, and Stephen J. Goldsack. Stars formed by protons of 3.2 Bev from the Bevatron—258(A)
—— (see Goldhaber, Gerson)—267(A)
Larach, Simon and John Turkevich. Magnetic properties of ZnS and CdS phosphors—1015
Lark-Horovitz, K. and H. Fritzsche. Hall effect and resistivity of p-type Ge at low temperatures—1536(A)
—— (see Becker, W. M.)—228(A)
—— (see Buschert, R.)—1157(A)
—— (see Fritzsche, H.)—1532(A)
—— (see Klontz, E. E.)—1535(A)
—— (see Schulz-DuBois, E.)—1561(A)
—— (see Stoeckmann, F.)—1535(A)
Larson, M. B. (see Brady, J. J.)—271(A)
Lauer, Eugene J. (see Eugene, J.)—276(A)
—— (see Hubbard, Edward L.)—1814
Laurman, J. A. and S. A. Schaaf. Flow near leading edge of flat plate—1540(A)
Lawson, A. W. Recent experiments on high-pressure phenomena at Chicago—244(T)

Lax, Benjamin. Cyclotron resonance in semiconductors—1560(T)
—— **and Laura M. Roth.** Propagation and plasma oscillation in semiconductors with magnetic fields—548(L)
Lax, M. (see Burstein, E.)—1536(A)
—— (see Teitler, S.)—1561(A)
Lazar, N. H. and E. D. Klema. Decay of Bi^{207}—710; 1186(A)
LeBlanc, J. M., J. M. Cork, and S. B. Burson. Decay of 3.5-min metastable state of Sb^{122}—39
—— (see Burson, S. B.)—230(A)
Lebowitz, Joel and Peter G. Bergmann. Statistical ensemble representing stationary nonequilibrium states—1165(A)
Lederman, L. M. (see Ammiraju, P.)—1188(A)
—— (see Blumenfeld, H.)—1203(A)
—— (see Sargent, C. P.)—1349
Lee, Kiuck (see Green, A. E. S.)—1205(A)
Lee, T. D. and C. N. Yang. Conservation of heavy particles and generalized gauge transformations—1501
Lee, T. H. (see Winsor, L. P.)—562(A)
Lehman, G. W. Computation of electron density and density of states in narrow bands in crystals—1542(A)
Lehovec, Kurt, Alma Marcus, and Kurt Schoeni. Forward characteristic of point contact rectifier—1179(A)
——, **Alma Marcus, and Kurt Schoeni.** Theory of magnetic rectifier—229(A)
Leiss, J. E., C. S. Robinson, and S. Penner. Photoproduction of π^+ mesons from H near threshold—201(L); 1188(A)
Leivo, W. J. and R. Smoluchowski. Semiconducting diamond—1532(A)
Leonard, B. P., Jr. (see Little, R. N., Jr.)—634
Lepore, Joseph V. and Maurice Neuman. Statistical model for high-energy events—1484
Leprince-Ringuet, L. (see Armenteros, R.)—275(A)
Letaw, Harry, Jr. (see Kuper, A.)—1870(E)
—— (see Portnoy, William M.)—1536(A)
Levin, J. S. and D. J. Hughes. Radiation widths of nuclear energy levels—1161(A)
Levine, M. M. (see Cabrera, N.)—1543(A)
Levinger, J. S. Velocity-dependent nuclear potential—1205(A)
Levinson, Carl A. Nuclear configuration interaction with singlet two-body forces—1205(A)
Levy, A. (see Feher, G.)—264(A)
Lévy, Maurice M. Effect of renormalization on meson-nucleon S-scattering—1470
Levy, Paul W. Reactor and γ-ray induced coloring in Corning fused silica—1541(A)
—— (see Dreyfus, Russell W.)—1541(A)
—— (see Rosenwasser, Hyman)—1541(A)
Levy, R. A. Electron spin resonance in liquid alkali metals—264(A)
Lewis, J. H. (see Burkhard, E. L.)—1154(A)
Lewis, Margaret N., Louis C. Green, Marjorie M. Mulder, Paul C. Milner, and Eleanor K. Kolchin. Computed transition probabilities for x-ray continua of K—1020
——, **Louis C. Green, Marjorie M. Mulder, Paul C. Miller, and Eleanor K. Kolchin.** Computed transition probabilities for x-ray K-edge of K—1210(A)
Li, Chi Yao and A. S. Nowick. Critical temperature for self-induced ordering in Ag-Zn solid solutions—1152(A)
—— **and A. S. Nowick.** Effect of quenching and neutron irradiation on atomic mobility in Cu-Al alloy—1531(A)
—— (see Nowick, A. S.)—1556(A)
Liang, C. Y. and S. Krimm. Normal vibrations and infrared spectrum of polytetrafluoroethylene—1548(A)
—— (see Krimm, S.)—1547(A)
Lidofsky, L., N. Benczer, P. Macklin, and C. S. Wu. β decay of RaE—1186(A)
Lieshout, R. van (see Koerts, L.)—1230
Likely, J. G. $Li^6(p,d)Li^5$ reaction—1538(A)
Lin, C. C. Motion in boundary layer over flat plate with sudden change of speed—1143(A)
Lind, D. A. (see Van Loef, J. J.)—224(A)
Lindeberg, G. K. (see Arnold, W. H.)—838(L)
Lindqvist, Torsten and C. S. Wu. Inner bremsstrahlung from A^{37}—231(A)
Linhart, P. B. (see Price, P. J.)—243(A)
Lipson, H. G., E. Burstein, and P. L. Smith. Optical effects in plastically deformed Ge—1535(A)
Lipson, J. and J. H. Reynolds. Performance data for high-sensitivity mass spectrometer—283(A)
Little, Elizabeth A. Dynamic behavior of domain walls in $BaTiO_3$—978; 1201(A)
Little, R. N., Jr., B. P. Leonard, Jr., J. T. Prud'homme, and L. C. Vincent. Liquid scintillator measurements of angular elastic scattering of neutrons from C, Al, and S—634
Livingston, M. S. Design for a strong-focusing electron synchrotron—266(T)
Lockary, T. E. and E. Guth. Theory of successive orientational phase transitions in two- and three-dimensional systems—274(A)
Lockett, Andrew M. 3-body exchange magnetic moments of H^3 and He^3—1204(A)
Loeb, A. L. (see Goodenough, J. B.)—391
Loebner, E. E. and H. Freund. Stacked barriers in electroluminescent ZnS crystal—1545(A)
Loferski, J. J. and P. Rappaport. Electron voltaic study of electron bombardment damage and its thresholds in Ge and Si—1861(L)
Logan, Joseph G. (see Kerner, Edward H.)—1165(A)
Lokanathan, S. and J. Steinberger. Search for improbable meson decays—240(A)
Long, A. L. (see Simanton, J. R.)—260(A)
Long, Donald and Park H. Miller, Jr. Effect of pressure on electrical properties of InSb—1192(A)
Long, Earl and Lothar Meyer. Superfluidity and heat transport in unsaturated He-II film—1616
Long, Robert R. Internal finite gravity waves in stratified fluid—1144(A)
Longini, R. L. (see McKelvey, J. P.)—1566(A)
Lönsjö, O., O. Os, and R. Tangen. Yield of high-energy γ rays from proton capture in Be^9—727
Lord, J. J. (see Fleming, John R.)—268(A)
Loshaek, S. (see Fox, T. G.)—1549(A)
Love, William F. (see Passaglia, Elio)—1006
Lovejoy, D. R. Surface tension of He^3—1196(A)
Low, Francis E. and David Pines. Mobility of slow electrons in polar crystals—414
Low, W. Paramagnetic resonance spectrum of some doubly activated phosphors—426
—— Possibility of nuclear radiation detector by means of electroluminescent phosphors—556(L)
Lowry, Ralph A. and Glenn H. Miller. Measurement of ionization yield of low-energy ions in gas—243(A)
Lubitz, C. R. (see Bach, D. R.)—235(A)
Luckey, George W. Effect of Br on dark conductivity of AgBr and its relation to photoconductivity—1558(A)
—— Some recent studies of light absorption photoconductivity and photolysis of Ag halide crystals—1549(T)
Ludloff, H. F. and M. B. Friedman. Difference solution of shock diffraction problem—1140(A)
Lundberg, John Lauren. Molecular weight distributions of polymers: I. Speculations on polymerizations to equilibrium—1559(A)

Luttinger, J. M. Quantum theory of cyclotron resonance for degenerate bands—1560(A)
—— Recent developments in effective-mass theory for semiconductors—252(T)
—— (see Kohn, W.)—1178(A); 915
Lutz, B. C. (see Segel, S. L.)—1183(A)
Lyon, W. S. (see Handley, T. H.)—688
—— (see Kahn, B.)—58

MacDonald, A. (see Matare, H. F.)—1179(A)
MacDonald, A. D. and J. H. Matthews. High-frequency ionization coefficients in Ne-A mixtures—1070
—— (see MacLennan, I. A.)—559(A)
MacDonald, D. K. C. (see Dugdale, J. S.)—1751
MacDonald, R. E. (see Allin, Elizabeth J.)—554(L)
MacDonald, William M. Isotopic spin impurity in light nuclei—234(A)
—— Isotopic spin selection rule for electric dipole transitions—60
Macfarlane, G. G. and V. Roberts. Infrared absorption of Si near lattice edge—1865(L)
Machlup, Stefan. Relaxation of monatomic crystal lattice around vacancy—1556(A)
MacKenzie, K. R. (see Sonett, C. P.)—280(A)
Mackin, R. J., Jr., W. B. Mims, and W. R. Mills, Jr. γ-rays from deuteron bombardment of C^{13}—43
Mackinnon, L. Absorption of 10 Mc/sec sound in polycrystalline Mg rod between 1.5 and 4.2°K—1210(A)
—— Absorption of 10 Mc/sec sound pulses by superconducting polycrystalline Sn rod—1181(A)
Macklin, P. (see Koerts, L.)—1172(A); 1230
—— (see Lidofsky, L.)—1186(A)
MacLennan, I. A. and A. D. MacDonald. Effect of mean free path variation on high frequency breakdown—559(A)
Madansky, L. and F. Rasetti. Decay of Co^{60}—1870(E)
Maienschein, F. C. (see Campbell, E. C.)—1172(A)
Maiman, T. H. and W. E. Lamb, Jr. Triplet fine structure of He—1194(A)
Maitland, C. G. and A. O. McCoubrey. Effect of temperature on lifetime of metastable Hg molecules—558(A)
Major, J. K. Calibration of linear amplifiers with Hg relay pulse generator—1210(A)
Malenka, B. J. Asymmetry in deuteron pickup by high-energy polarized protons—1156(A)
—— Deuteron pickup by high-energy polarized protons—843(L)
Malmberg, Philip R. Elastic scattering of protons from Li^7—1167(A)
—— (see Sun, K. H.)—1154(A)
Mandel, M. and A. H. Barrett. Pure rotational spectra of Tl halides—1159(A)
Mandelkern, Leo (see Roberts, Donald E.)—1559(A)
Mandeville, C. E. and H. O. Albrecht. Storage of energy in BeO—1546(A)
——, **Jagdish Varma, and Babulal Saraf.** Ir^{194}—94; 1185(A)
—— (see Hans, H. S.)—1173(A)
—— (see Saraf, B.)—1206(A)
—— (see Swann, C. P.)—1183(A)
Manley, D. L. (see Crasemann, Bernd)—66; 279(A)
Mann, A. K. Elastic scattering of 0.41 and 0.66 Mev γ rays by Sn and Pb—234(A)
—— (see Stephens, W. E.)—241(A); 839(L)
Mann, Lloyd G. (see Bowman, Harry R.)—277(A)
Manning, Irwin and Laszlo Tisza. Variational principles in irreversible thermodynamics—1165(A)
Mapes, Joe M. (see Allen, William A.)—256(A)
Marcus, Alma (see Lehovec, Kurt)—229(A); 1179(A)
Marcus, Jules A. Oscillatory Hall effect and magnetoresistance of Bi—1540(A)
Marcus, Paul M. Anisotropic electronic stress and Mg alloys—1552(A)
Marder, S., W. Bennett, C. S. Wu, and V. W. Hughes. Effect of static electric field on positronium formation—1173(A)
—— (see Hughes, V. W.)—1840
Margenau, Henry. Electron effects in spectral line broadening—1195(A)
—— **and Bennett Kivel.** Effects of electron collisions on width of spectral lines—1822
—— (see Kivel, B.)—495
—— (see Meyerott, Roland E.)—1195(A)
Mark, Hans, Clyde McClelland, and Clark Goodman. Electric excitation of certain medium-weight nuclei by protons—1245
——, **Clyde McClelland, and Clark Goodman.** Electric excitation of nuclei near closed 50 proton and neutron shells—249(A)
——, **Clyde McClelland, and Clark Goodman.** Proton bremsstrahlung—279(A)
—— (see McClelland, Clyde)—249(A)
Markowitz, S. (see Miller, J. M.)—1197(A)
Marmier, P., F. Boehm, and J. W. M. DuMond. Energy levels of Hf^{177}—280(A)
—— (see Boehm, F.)—280(A)
Marshak, H. and H. W. Newson. Total neutron cross sections in kev region: Sc, V, Mn, and Co—1162(A)
Marshall, J., L. Marshall, and V. A. Nedzel. Differential p-p scattering cross sections at 419 Mev—1513(L)
—— (see Marshall, L.)—1398
Marshall, Leona. Experiments with high-energy proton beams—266(T)
—— **and J. Marshall.** Direction of proton spin polarization produced by elastic scattering—1398
—— (see Marshall, J.)—1513(L)
Martin, E. E. (see Dyke, W. P.)—263(A)
—— (see Trolan, J. K.)—262(A)
Martin, G. M., F. L. Roth, and R. D. Stiehler. Behavior of nonpigmented rubber vulcanizates in tension—1559(A)
Martin, R. L., J. E. Enns, and E. Katz. Low-intensity reciprocity law failure for pure AgBr emulsions of different grain size—1557(A)
—— (see Enns, J. H.)—1556(A)
Marton, L., J. Arol Simpson, and T. F. McCraw. Single scattering of 20-kev electrons in solids—1168(A)
—— (see Mendlowitz, H.)—1168(A)
Mason, W. P. Dislocation relaxations at low temperatures and determination of limiting shearing stress of metal—1136(L)
Matare, H. F., H. Kedesdy, A. MacDonald, and A. Petersen. Study of electrical characteristics of grain boundaries—1179(A)
Mathur, Hirdaya B. and E. K. Hyde. Isomeric states in the chain $Mo^{99} \rightarrow Nb^{99} \rightarrow Zr^{99}$—261(A)
—— **and Earl K. Hyde.** Radiations of Mo^{99} and isomeric states of Nb^{99}—79
Matossi, Frank. Polarization effects on brightness waves of electroluminescence—434; 1545(A)
—— **and S. Nudelman.** Electroluminescence excited with short field pulses—238(A)
—— (see Nudelman, S.)—238(A); 1545(A)
Matthews, David L. Vortex created by shock passing over vertical wall—1140(A)
Matthews, J. H. (see MacDonald, A. D.)—1070
Matthias, B. T. (see Holden, A. N.)—546(L)
Maunsell, C. D. Measurement of absorption coefficients for photoionizing radiations in low-pressure gases with space charge detector—1831
—— Photoionization by absorption in gas of radiations from discharge in same gas—263(A)

Maurer, R. D. Light scattering from optical glass—1544(A)
Maxson, D. R., J. S. Allen, and W. K. Jentschke. Electron-neutrino angular correlation in β decay of Ne^{19}—230(A)
Mayburg, Sumner. Lattice defects in Si—1177(A)
—— Ring diffusion as mechanism of self-diffusion in Ge—1134(L)
Mayes, W. T. (see Kaiser, H. F.)—1538(A)
Mayfield, Earle B. (see Allen, William A.)—256(A)
Mays, J. M., R. G. Shulman, and D. W. McCall. Nuclear magnetic resonance in semiconductors: GaSb and InSb—1182(A)
—— (see Shulman, R. G.)—1182(A)
—— (see Slichter, W. P.)—1559(A)
Mazenko, J. J. (see Schwertz, F. A.)—1133(L); 1169(A)
McAllister, Robert W. (see Hofstadter, Robert)—217(L)
McBride, John J. (see Westrum, Edgar F.)—270(A)
McCaffrey, F. (see Silver, M.)—270(A)
McCall, D. W. (see Mays, J. M.)—1182(A)
—— (see Shulman, R. G.)—1182(A)
McCarthy, Kathryn A. and Stanley S. Ballard. Thermal conductivity of Ge at ambient temperatures—271(A)
McClelland, Clyde, Hans Mark, and Clark Goodman. Electric excitation of heavy nuclei with protons—249(A)
—— (see Mark, Hans)—249(A); 279(A); 1245
McClure, J. W. Axial ratios in hexagonal crystals—449
McConnell, H. M. (see Reilly, C. A.)—264(A)
McCormick, Bruce H. and Abraham Klein. Meson pair theory—1155(A)
—— (see Klein, Abraham)—1428
McCoubrey, A. O. (see Maitland, C. G.)—558(A)
McCrary, J. H. (see Bent, R. D.)—1198(A); 1325
—— (see Bonner, T. W.)—1198(A)
McCraw, T. F. (see Marton, L.)—1168(A)
McDonald, A., Jr. (see Anderson, John D.)—258(A)
McDonell, William R. and Henry A. Kierstead. Expansion of Cu bombarded by 21-Mev deuterons—1870(E)
McEllistrem, M. T. (see Galonsky, A.)—586; 590
—— (see Jones, K. W.)—241(A)
McFarland, Robert H. (see Swanson, Robert E.)—1063
McGee, J. F. Long-wavelength x-ray reflection microscope—282(A)
McGinnis, Carl L. Disintegration of 5.8-day Sb^{120}—1172(A)
—— Radioactivity of In^{117} and Sb^{117}—1870(E)
McGowan, F. K. (see Stelson, P. H.)—249(A)
McGuire, T. R., E. J. Scott, and F. H. Grannis. Antiferromagnetism in Cr_2O_3 crystal—1562(A)
—— (see Kriessman, C. J.)—936
McHale, J. L. and R. M. Thaler. Variational expressions for N-channel collision parameters—1189(A)
—— **and R. M. Thaler.** Variational principle for tensor forces—273(A)
—— (see Thaler, R. M.)—1189(A)
McIntyre, John A. and Robert Hofstadter. Scattering of 192-Mev electrons from deuterium—158
McKelvey, J. P. and R. L. Longini. Recombination of injected carriers at dislocation edges in semiconductors—1566(A)
McKeown, Marilyn (see McReynolds, A. W.)—418
McReynolds, A. W. Diffuse magnetic neutron diffraction—1200(A)
——, **W. Augustyniak, Marilyn McKeown, and D. B. Rosenblatt.** Neutron irradiation effects in Cu and Al at 80°K—418
—— (see Smith, L. W.)—1167(A)
McWhorter, A. L. Surface traps and $1/f$ noise in Ge—1191(A)
—— (see Kingston, R. H.)—1191(A)
Mead, S. W. (see Petroff, M. D.)—279(A)
Meadows, J. W. (p,a) and (p,ab) reactions at 100 Mev—744
Medved, David B. Photoconductivity and photodesorption in ZnO—237(A)
Meggers, William F. (see Fred, Mark)—1514(L)
Meisenheimer, R. G. (see Reilly, C. A.)—264(A)
Meissner, Hans. Theory of paramagnetic effect in superconductors—1539(A)
—— (see Bedard, F.)—1539(A)
Melamed, Nathan T. and Raymond Bowers. Origin of luminescence in Cu activated ZnS phosphors—1545(A)
Melvin, M. A. Freundlich red-shift formula—884
Mencher, A. (see Barker, W. A.)—1868(L)
Mendlowitz, H. and L. Marton. Scattering of 20-kev electrons in thin films—1168(A)
Menes, M. Investigation of buildup processes in argon discharge—561(A)
Menon, M. G. K. Investigations of Bristol school—1166(T)
Mercure, R. (see Rense, William A.)—1195(A)
Merritt, F. R. (see Fletcher, R. C.)—1560(A)
Merz, Walter J. (see Holden, A. N.)—546(L)
—— (see Hooton, John A.)—409
Meshkov, S. and C. W. Ufford. Matrix elements of nuclear p^3 configuration—1204(A)
Metropolis, N. (see Hoffman, Joseph G.)—1195(A)
Metzger, Franz R. Angular distribution of resonance fluorescence radiation from 411-kev level in Hg^{198}—1186(A)
—— Spin and lifetime of 439-kev excited state of Hg^{200}—200(L)
Meyer, Lothar (see Long, Earl)—1616
Meyer, Peter and J. A. Simpson. Changes in amplitude of cosmic-ray 27-day intensity variation with solar activity—247(A)
Meyer, R. A. and F. L. Boquet. Conductivity of teflon and polyethylene during γ irradiation—1531(A)
Meyerott, Roland E. and Henry Margenau. Line broadening by electrons: Validity of simple theories—1195(A)
Michalik, E. R. (see Schwertz, F. A.)—1133(L)
Michel, L. Universal Fermi interaction—1164(T)
—— **and A. S. Wightman.** Covariant formalism describing polarization of spin one-half particles—1190(A)
Mihelich, John W. and M. Goldhaber. Evidence for mixed $M3+M4$ isomeric transition—1185(A)
Milford, F. J. Projection operator for Rarita-Schwinger equation—1488
Miller, D. W., U. C. Gupta, V. K. Rasmussen, and M. B. Sampson. Energy levels in N^{14} by inelastic α-scattering—1184(A)
Miller, E. E. Physical theory for capillary flow—251(A)
Miller, Glenn H. (see Lowry, Ralph A.)—243(A)
Miller, J. Malcolm. Radio chemical studies on nuclear reactions at the Cosmotron—260(T)
——, **G. Friedlander, and S. Markowitz.** Competition between (α,pn) and $(\alpha,2n)$ reactions on Cr^{50}—1197(A)
—— (see Alperovitch, Edward A.)—262(A)
—— (see Miskel, J. A.)—1197(A)
Miller, Park H., Jr. (see Long, Donald)—1192(A)
—— (see Rau, Richard)—1533(A)
Miller, Paul. Work function difference of Au and AuO from contact potentials with respect to Ge and Pt—1552(A)
Miller, Paul C. (see Lewis, Margaret N.)—1210(A)
Miller, W. C. (see Ruane, T. F.)—1166(A)
Mills, F. E. and L. J. Koester, Jr. Low-energy photoproduction of π^0 mesons from H: Total cross section—210(L)
—— (see Goldwasser, E. L.)—239(A); 1763
Mills, Robert L. Integral equations of meson-nucleon system—1156(A)
—— **and Norman M. Kroll.** Fourth-order radiative corrections to atomic energy levels. II—1489
—— (see Day, R. B.)—279(A)

Mills, W. R., Jr. (see Mackin, R. J., Jr.)—43
—— (see Sherr, R.)—1185(A)
Milner, Paul C. (see Lewis, Margaret N.)—1020
Milton, G. M. (see Milton, J. C. D.)—1173(A)
Milton, J. C. D., J. S. Fraser, and G. M. Milton. Long-lived isomer of Ho^{165}—1173(A)
—— (see Fraser, J. S.)—1173(A)
Mims, W. B. (see Mackin, R. J., Jr.)—43
Minden, Henry T. Molecular distortion caused by hindered rotation—1160(A)
Mingins, Charles R. (see Farrall, George A.)—1211(A)
Minshall, Stanley. Investigation of polymorphic transition in Fe at 130 kilobars—271(A)
Miskel, J. A., M. L. Perlman, G. Friedlander, and J. M. Miller. Excitation functions for reactions of Cu with high-energy protons—1197(A)
Mitchell, A. H. and C. Kittel. Donor and acceptor ionization energies in Si and Ge—271(A)
Mitchell, E. N. Velocity spectrum of cosmic-ray particles at twelve-grams atmospheric depth—1163(A)
—— (see Winckler, J. R.)—1411
Mitchell, J. W. Research on Ag halides—1549(T)
Mizushima, Masataka, J. T. Cox, and Walter Gordy. Zeeman effect in rotational spectrum of NO—1034; 1159(A)
Mobley, R. C. and B. R. Albritton, Jr. Amplitude and frequency stabilized adjustable high-frequency oscillator—232(A)
Mockler, Richard C. and George R. Bird. Microwave spectrum of CS—1837
Moldauer, P. A. and K. M. Case. Nonrelativistic limit of spin $k+\frac{1}{2}$ particle wave equations—1190(A)
Monahan, J. E. and A. Langsdorf, Jr. Analysis of neutron self-indication transmission cross sections—1147(A)
—— (see Church, E. L.)—718
—— (see Langsdorf, A.)—1148(A)
Montgomery, H. C. and W. L. Brown. Field effect in Ge—1565(A)
—— (see Pearson, G. L.)—1567(A)
Montroll, Elliott. Effect of dimensionality on long-range order in crystals—255(T)
Moore, G. E. (see Benedict, W. S.)—1551(A)
—— (see Herman, R.)—1550(A)
Moore, J. (see Foote, H. L.)—1161(A)
—— (see Sheer, C.)—565
Mooring, F. Paul (see Holland, R. E.)—240(A)
—— (see Langsdorf, A.)—1148(A)
Morgan, G. W. Wave propagation in elastic tubes filled with streaming, viscous liquid—1157(A)
Morris, T. W., J. D. Garrison, E. C. Fowler, W. B. Fowler, R. P. Shutt, A. M. Thorndike, and W. L. Whittemore. p-p scattering at 900 Mev—1167(A)
Morrison, P. Diffusion of cosmic rays in earth-sun region—1163(A)
Moser, Frank and Franz Urbach. Ag halide phosphors—1557(A)
—— (see Nail, Nelson R.)—1557(A)
Moses, H. E. (see Kay, I.)—1190(A)
Motz, H., K. M. Crowe, and R. M. Friedman. π^-/π^+ ratios in asymmetric nuclei—268(A)
—— (see Crowe, K. M.)—268(A)
Moyer, Burton J. (see Bandtel, K. C.)—269(A)
—— (see Shaw, Harlan)—259(A)
Mrowca, B. A. (see Banas, E. M.)—265(A); 1548(A)
Mrozowski, S. Physical properties of carbons and porosity—1564(A)
—— (see Hong, K.)—1565(A)
Mulder, Marjorie M. (see Lewis, Margaret N.)—1210(A); 1020
Muller, F. (see Armenteros, R.)—275(A)
Mullin, C. J. and E. Guth. Theory of nuclear excitation in inelastic electron scattering—277(A)
Munick, Raymond J. Electrical conduction in plastics—236(A)
Murakawa, Kiyoshi. Nuclear moments of Nb^{93}, La^{139}, Os^{187}, and Hg^{201}—1285
Murray, B. B. (see Kurbatov, J. D.)—674
Murray, R. B. and L. D. Roberts. Magnetic and thermal properties of $MnCl_3$ at liquid He temperatures—1180(A)
—— (see Roberts, L. D.)—1180(A)

Nail, Nelson R., Frank Moser, Pliny E. Goddard, and Franz Urbach. Optical absorption measurements on Ag halide crystals—1557(A)
Nakano, Yoshihiro. Scattering of high-energy neutrons and Johnson-Teller type nuclei—842(L)
Nambu, Yoichiro. Structure of scattering matrix—803
Nathans, Robert and Paul F. Yergin. (γ,n) cross sections in Zr^{90} and Zr^{91}—1197(A)
—— **and Paul F. Yergin.** Photoneutron cross sections in Mg^{24}, Mg^{25}, Zr^{90}, Zr^{91}—1296
—— (see Yergin, P. F.)—1198(A)
Nedzel, V. A. (see Marshall, J.)—1513(L)
Need, John Logan. Mechanism of reaction $C^{12}+p\rightarrow p+3\alpha$ at 32 Mev—1538(A)
Neher, H. Victor and Edward A. Stern. "Knee" of the cosmic-ray latitude curve—845(L)
Nelson, E. B. (see Bashkin, S.)—1184(A)
—— (see Carlson, R. R.)—1310
—— (see Geer, E. H.)—241(A)
Nervik, Walter E. and Glenn T. Seaborg. Ta spallation and fission induced by 340-Mev protons—261(A)
Neufeld, Jacob and R. H. Ritchie. Passage of charged particles through plasma—1632
Neuman, Maurice (see Lepore, Joseph V.)—1484
—— (see Gasiorowicz, S.)—257(A)
—— (see Riddell, R., Jr.)—257(A)
Neumark, Gertrude. Influence of electric field on thermoluminescence of ZnS crystals—1546(A)
Neuringer, L. J. Effect of pressure on absorption edges of Te—1193(A)
Newman, Ezra and Peter G. Bergmann. Lagrangians linear in "velocities"—1176(A)
—— (see Cohen, B. L.)—1198(A)
Newman, R., W. C. Dash, R. N. Hall, and W. E. Burch. Visible light from Si p-n junction—1536(A)
—— (see Dash, W. C.)—1192(A)
—— (see Tyler, W. W.)—461; 1192(A); 961
Newson, H. W. (see Block, R. C.)—1162(A)
—— (see Marshak, H.)—1162(A)
Newton, C. M. (see Panofsky, W. K. H.)—751
Newton, Roger G. Radiative corrections to electron scattering—1514(L)
—— **and Res Jost.** Construction of non-central potentials from S-matrix—1189(A)
Niday, James B. Half-Life of Rb^{86}—42
Nielsen, John P. Secondary recrystallization analogy in heterogeneous liquid system—1157(A)
Nierenberg, W. A. (see Bemski, G.)—470
Nilan, T. G. and W. S. Paxton. Domain configuration and crystallographic orientation in grain-oriented Fe-Si alloy—1200(A)
Nisenoff, M. (see Schulz-DuBois, E.)—1561(A)
Nishikawa, Tetsuji (see Shimoda, Koichi)—1160(A)
Nobles, R. A. (see Beyster, J. R.)—1216
Nolle, A. W. Nuclear magnetic resonance relaxation times for polyisobutylene in CCl_4 solution—1560(A)
Norberg, R. E. and D. F. Holcomb. Nuclear spin relaxation in alkali metals near their melting points—226(A)
—— (see Holcomb, D. F.)—1074

Novey, T. B. α-γ directional correlation in Th^{228}—232(A)
—— (see Krohn, V. E.)—1187(A)
—— (see Porter, F. T.)—214(L)
—— (see Raboy, S.)—1187(A)
Nowick, A. S. and Chi Yao Li. Mechanism of grain boundary relaxation in metals and alloys—1556(A)
—— (see Feder, R.)—1152(A)
—— (see Fischbach, D. B.)—1543(A)
—— (see Gordon, R. B.)—1540(A)
—— (see Li, Chi Yao)—1152(A); 1531(A)
Nudelman, Sol and Frank Matossi. Effects of electric fields on ultraviolet excited ZnS phosphors—1545(A)
—— **and F. Matossi.** Time-average light output from electroluminescent phosphors—238(A)
—— (see Matossi, F.)—238(A)

O'Brien, V. (see Corrsin, S.)—1142(A)
Odell, F. A. Strain propagation in nylon yarns loaded transversely at high speeds—1548(T)
Odian, A. C., W. Rankin, P. C. Stein, and A. Wattenberg. Neutrons in coincidence with photoprotons—248(A)
Oehme, Reinhard. Possible experiments to determine transition matrix for $\bar{p}$-p scattering—216(L)
—— Scattering of polarized nucleon beams—147
O'Halloran, T. A. (see Brady, J. J.)—271(A)
Okaya, Y., Y. Saito, and R. Pepinsky. New method in x-ray crystal structure determination involving use of anomalous dispersion—1857(L)
Okazaki, A. (see Darden, S. E.)—1147(A)
Oleson, N. L. Instantaneous probe measurements of travelling striations in argon glow discharge—559(A)
Olson, E. L. (see Handley, T. H.)—688
Oppenheim, Irwin. Statistical thermodynamics of isotope effects. I. Theory of equilibrium processes—258(A)
—— (see Friedman, Abraham)—258(A)
Ore, Aadne Entropy of radiation—887
Orear, Jay. *D*-wave solution to pion-proton scattering data—1155(A)
—— Scattering of 23-Mev positive pions on H—239(A)
O'Rourke, R. C. Problem in shower theory—"Approximation A"—1190(A)
—— (see Faust, W. R.)—1147(A)
—— (see Saenz, A. W.)—1166(A)
Os, O. (see Lönsjö, O.)—727
Osborne, Darrell W. (see Abraham, Bernard M.)—551(L)
Otter, F. A., Jr. Thermoelectric power and resistivity of dilute alloys of Mn, Pd, and Pt in Cu, Ag, and Au—1552(A)
Overhauser, A. W. (see Ehrenreich, H.)—1533(A)
Overton, William C., Jr., and Ted G. Berlincourt. Pressure dependence of de Haas-van Alphen parameters in Bi crystal at 4.2°K—1180(A)
—— **and John Gaffney.** Temperature variation of elastic constants of cubic elements. I. Cu—969
Owen, G. E. Neutron physics at Johns Hopkins University—1530(T)
—— (see Fowler, J. M.)—249(A)

Page, L. A., M. Heinberg, J. Wallace, and T. Trout. Angular correlation in two-photon annihilation in quartz—206(L)
Pagnia, H. and F. Stockman. Thermal formation of colloids from *F* centers in KCl crystals—236(A)
Pake, G. E. Paramagnetic resonance of free radicals—272(T)
—— **and R. H. Sands.** Hfs in paramagnetic resonance of V ions in solution—266(A)
Pal, Yash. Investigations of Indian school—1166(T)
Palevsky, H. and R. M. Eisberg. Magnetic scattering of slow neutrons by gaseous oxygen—492
—— (see Zimmerman, R. L.)—1162(A)
Panofsky, W. K. H. Progress with Stanford linear accelerator—266(T)
——, **C. M. Newton, and G. B. Yodh.** Pion production by electrons—751
Pao, Yoh-Han. Extension of Hertz theory of impact to viscoelastic case—1548(A)
Paramentier, D., A. J. Schwemin, L. W. Alvarez, F. S. Crawford, Jr., and M. L. Stevenson. Four-inch diameter liquid hydrogen bubble chamber—284(A)
Park, David. Magnetic rotation phenomena in polycrystalline ferrite. II—438
Parker, Earl R. (see Aticker, Betsy)—1151(A)
Parratt, L. G. (see Hempstead, C. F.)—1170(A)
—— (see Jossem, E. L.)—1151(A)
Parzen, Philip. Integral equation solution of space-charge wave propagation—257(A)
Passaglia, Elio and William F. Love. Electrical resistance of Cu-Au alloys at low temperatures—1006
Pasternak, J. (see Salkovitz, E. I.)—271(A)
Pattee, Howard, H., Jr. Metal vacuum joint suitable for field emitters—283(A)
Patterson, D. A. and C. C. Klick. Low-temperature luminescence in KCl:Tl—1546(A)
Patterson, L. T. (see Gurnee, E. F.)—1547(A)
Patton, B. J. (see Stephens, W. E.)—839(L)
Paul, H. and R. M. Steffen. Extranuclear effects on directional correlation of Ta^{181} γ rays—231(A)
Paul, William and G. L. Pearson. Pressure dependence of resistivity of Si—1755
—— (see Benedek, G. B.)—1193(A)
—— (see Warschauer, D. M.)—1193(A)
Paxton, W. S. (see Nilan, T. G.)—1200(A)
Pearlman, N. and P. H. Keesom. Atomic heat of graphite between 1° and 20°K—1539(A)
—— (see Keesom, P. H.)—548(L); 1539(A)
Pearlstein, E., H. Ingham, and R. Smoluchowski. Energy dependence of radiation effects in solids—1530(A)
—— (see Smoluchowski, R.)—1530(A)
Pearson, G. L., H. C. Montgomery, and W. L. Feldmann. Noise in Si $\bar{p}$-n junction photocells—1567(A)
—— (see Paul, William)—1755
Pearson, M. D. (see Brick, R. O.)—282(A)
Peaslee, D. C. Pion photoproduction ratios—239(A)
Peed, W. F. (see Rogosa, G. L.)—1173(A)
Peelle, Robert. Differential cross sections for scattering of protons by C as function of incident proton energy—1184(A)
—— (see Campbell, E. C.)—1172(A)
Peierls, R. E. (Title to be announced)—1166(T)
Pell, E. M. Reverse current and carrier lifetime as function of temperature in Ge and Si junction diodes—1536(A)
Penner, S. (see Leiss, J. E.)—201(L); 1188(A)
Pepinsky, Ray (see Jona, F.)—1201(A); 903
—— (see Okaya, Y.)—1857(L)
—— (see Shirane, Gen)—1201(A)
Pepper, R. R. (see Klontz, E. E.)—1535(A)
Percus, Jerome K. and George J. Yevick. New extension of collective coordinates for many-body problem—1164(A)
—— (see Yevick, George J.)—1164(A)
Perez Y Jorba, J. P. (see Bishop, G. R.)—89
Perl, M. L., I. I. Rabi, and B. Senitzky. Nuclear electric quadrupole moment of Na^{23} by atomic beam resonance method—611
—— (see Senitzky, B.)—1537(A)
Perlman, I., F. Stephens, and F. Asaro. γ rays of Ra^{228} and Tl^{208}—262(A)
—— (see Asaro, Frank)—19; 260(A)
—— (see Hummel, J. P.)—22; 261(A)
—— (see Stephens, F.)—261(A)

Perlman, M. L. (see Miskel, J. A.)—1197(A)
Perlow, G. J. Neutron spectrometer for 100–500 kev region —223(A)
Perring, J. K. and J. S. Story. Thermodynamic theory of fission—1525(L)
Perry, J. E., Jr. (see Day, R. B.)—279(A)
Perry, R. L. and J. J. Brady. Changes in photoelectric probability factor resulting from surface contamination of Al—281(A)
Persh, Jerome. Study of behavior of boundary layer in region of transition from laminar to turbulent flows—1144 (A)
Peshkin, M., J. H. Roberts, and V. L. Telegdi. Polarized neutrons on Li^6—1204(A)
Petersen, A. (see Matare, H. F.)—1179(A)
Peterson, L. (see Winckler, J. R.)—1411
Peterson, Robert L. (see Emrich, Raymond J.)—1141(A)
Petroff, M. D., S. W. Mead, and W. O. Doggett. Radioactivity of Sn^{128}—279(A)
Petscheck, Harry (see Kantrowitz, Arthur)—1141(T)
Pevsner, Aihud (see Ritson, D. M.)—1168(A)
—— (see Williams, Ross)—1188(A)
Peyrou, C. (see Armenteros, R.)—275(A)
Phelps, A. V. Diffusion and volume loss coefficients of He metastable atoms and molecules—558(A)
—— (see Frost, L. S.)—559(A)
Philippoff, W. and J. Brodnyan. Dynamic properties of glucose glass—1549(A)
Phillips, G. C. (see Gossett, C. R.)—724
Piccioni, O., D. Clark, R. Cool, G. Friedlander, and D. Kassner. External proton beam at Cosmotron—275(A)
Pickup, E. and A. Husain. Identity of shower particles in stars in region 1–2× minimum ionization—247(A)
—— (see Husain, A.)—136
Picus, G. (see Burstein, E.)—1536(A)
Pieper, G. F., G. S. Stanford, and P. von Herrmann. (α,p) reaction studies—1185(A)
—— (see Cook, E. J.)—1154(A)
—— (see Stanford, G. S.)—1154(A)
Pigg, J. C. (see Cleland, J. W.)—1742
Pines, David (see Low, Francis E.)—414
Pinnick, H. T. (see Kiive, P.)—1564(A)
Piotrowski, Edward A. (see Ziomek, Joseph S.)—243(A)
Piper, W. W. and F. E. Williams. Theory of electroluminescence—1809
Plazek, D. J. and John D. Ferry. Dynamic mechanical properties of concentrated cellulose trinitrate solutions—1548(A)
Pleasonton, Frances (see Snell, Arthur H.)—1174(A)
Plendl, H. S. and F. E. Steigert. Levels in Sc^{45}—1538(A)
Pollard, E. C. (see Graetzer, H. G.)—1184(A)
Pomerantz, Martin A. Latitude effect of cosmic radiation at low altitudes—105
Pool, M. L. (see Cheng, L. S.)—231(A)
Porter, F. T., M. S. Freedman, T. B. Novey, and F. Wagner, Jr. First-forbidden nonunique β spectra in Re^{186} —214(L)
Porter, Richard F., Paul Schissel, and Mark G. Inghram. Mass spectrometric study of gaseous species in Si-SiO_2 system—242(A)
Porter, W. C. (see Swann, C. P.)—1183(A)
Portis, A. M. and D. Shaltiel. Electron spin resonance in irradiated alkali halides—264(A)
Portnoy, William M., Harry Letaw, Jr., and Lawrence Slifkin. Self-diffusion in Ge—1536(A)
Powell, Wilson M. (see Knapp, Myron W.)—1188(A)
Pratt, George W., Jr. Localized states at boundary of two crystals—1543(A)
Preston, R. S. (see Walker, R. M.)—1203(A)
Prestwood, R. J. $(n,2n)$ cross section of Na^{23} at 14.1 Mev —47
——, **H. L. Smith, C. I. Browne, and D. C. Hoffman.** Positron emission from Np^{235}—1324
Price, J. (see Risser, J. R.)—1183(A)
Price, P. J. Configuration interaction and holes—1533(A)
—— **and P. B. Linhart.** Specific heat of He^3-He^4 solutions —243(A)
Price, William E. (see Rabin, Herbert)—1154(A)
Primak, W. Experimental evidence for thermal spikes in radiation damage—1854(L)
——, **C. J. Delbecq, and P. H. Yuster.** Photoelastic observations of expansion of alkali halides on irradiation—1708
——, **P. H. Yuster, and C. J. Delbecq.** Photoelastic observation of expansion of alkali halides in irradiation—237(A)
Pringsheim, P. (see Delbecq, C. J.)—237(A)
Probstein, Ronald F. and David Elliott. Transverse curvature effect in compressible axially symmetric laminar boundary layer flow—1143(A)
Proctor, W. G. and W. H. Tanttila. Saturation of nuclear electric quadrupole energy levels by ultrasonic excitation —1854(L)
Prud'homme, J. T. (see Little, R. N., Jr.)—634
Pyle, Robert V. (see Hicks, Donald A.)—1521(L)
—— (see Ise, John, Jr.)—1199(A)

Rabi, I. I. (see Perl, M. L.)—611
—— (see Senitzky, B.)—1537(A)
Rabin, Herbert and William E. Price. Co^{60} field distributions using Ag activated phosphate glass—1154(A)
Raboy, Sol and Victor E. Krohn. γ-γ correlation of Pb^{204m} —231(A)
—— **and V. E. Krohn.** Theorem on angular correlation—24
——, **T. B. Novey, and V. E. Krohn.** Attenuation of α-γ angular correlation of Am^{241} in liquid-film sources—1187 (A)
—— (see Krohn, V. E.)—1187(A)
Rainwater, James (see Baker, W. F.)—1188(A)
—— (see Williams, Ross)—1188(A)
Rainwater, L. J. (see Grimm, G.)—1161(A)
Ralph, D. C. and F. E. Dunnam. Neutron yields as function of energy in reactions $Li^7(d,n)Be^8$ and $Be^9(d,n)B^{10}$— 249(A)
—— (see Fuller, J. C.)—248(A)
Ramler, Warren (see Yuster, Philip)—233(A)
Ramsey, Norman F. Collision alignment of molecules, atoms, and nuclei—1853(L)
Rankin, W. (see Odian, A. C.)—248(A)
Rappaport, P. (see Loferski, J. J.)—1861(L)
Rasetti, F. (see Madansky, L.)—1870(E)
Rasmussen, J. O. and H. Slätis. Decay scheme of Np^{239}— 261(A)
Rasmussen, Stanley W. (see Williams, John H.)—56; 1167(A)
Rasmussen, V. K. (see Miller, D. W.)—1184(A)
Rasor, Ned S. Annealing kinetics of lattice defects in evaporated Cu films—1555(A)
Rau, R. Ronald (see Arnold, W. H.)—275(A)
Rau, Richard and P. H. Miller, Jr. Faraday effect in semiconductors at microwave frequencies—1533(A)
Ravenhall, D. G. and D. R. Yennie. Phase shift analysis of high-energy electron scattering—277(A)
—— (see Downs, B. W.)—277(A)
—— (see Heims, S. P.)—278(A)
—— (see Yennie, D. R.)—277(A)
Ravilious, C. F. (see Furlong, L. R.)—954
Rawitscher, George. Effect of extended size of nucleus on μ-meson pair photoproduction—272(A)

Rayburn, L. A., D. L. Lafferty, and T. M. Hahn. γ rays from inelastic scattering of neutrons in Al, Mg, and Ag—701
Raychaudhuri, Amalkumar. Relativistic cosmology. I—1123
Raz, B. J. (see French, J. B.)—1523(L)
Reagan, D. D. Energy dependence of photoyields of N^{17}—258(A)
—— (see Barber, W. C.)—73
—— (see George, W.)—276(A)
Redfield, Alfred G. Nuclear magnetic resonance saturation in solids—1787
—— Nuclear resonance saturation in solids—1182(A)
Redlich, Martin G. Shell theory for nuclei with mass 19—199(L)
Redman, J. K. (see Blewitt, T. H.)—1555(A)
Reed, George W. U^{235} thermal neutron fission yields at masses 90 and 91—1327
Reekie, James (see Goldstein, Louis)—857
Reich, H., J. Heberle, and P. Kusch. hfs of metastable H—1194(A)
—— (see Heberle, J.)—1194(A)
Reif, F. Nuclear magnetic resonance studies of imperfect ionic crystals—1549(T)
Reilly, C. A., H. M. McConnell, and R. G. Meisenheimer. Nuclear magnetic resonance spectra of annular samples—264(A)
Remeika, J. P. (see Holden, A. N.)—546(L)
Rennemann, Conrad, Jr. Minimum drag bodies of revolution in nonuniform supersonic flow field—1140(A)
Rense, William A. and R. Mercure. Oxygen gas continuous absorption in extreme uv—1195(A)
Repp, Gordon W., Mark J. Jakobson, and R. Stephen White. π^+ photomeson production at 180°. Experimental arrangement—268(A)
—— (see White, R. Stephen)—269(A)
Resnick, Robert (see Donahue, T. M.)—1622
Reynolds, C. A. (see Forstat, H.)—1196(A)
Reynolds, F. W. (see Collins, R. J.)—227(A)
Reynolds, George T. (see Arnold, W. H.)—275(A)
—— (see Van Lint, V. A. J.)—1203(A)
Reynolds, H. L., L. D. Wyly, and A. Zucker. Cross section for electron capture and loss by 26-Mev N ions—1825
——, **L. D. Wyly, and A. Zucker.** Equilibrium charge distribution of energetic N ions—474; 242(A)
—— (see Zucker, A.)—1150(A)
Reynolds, J. B. Energy levels in B^9 and Be^7 from reactions $C^{13}(p,\alpha)B^9$ and $B^{10}(p,\alpha)Be^7$—1289
—— (see Rubin, A.)—1185(A)
Reynolds, J. H. High-sensitivity mass spectrometer—283(A)
—— (see Lipson, J.)—283(A)
Rhein, W. J. Angular distribution of fast neutrons scattered from Pb—1300
Ribe, F. L. (see Brolley, J. E., Jr.)—1112
Rice, O. Comparison of energy excitations in liquid He^3 and He^4—847
Richards, H. T. (see Galonsky, A.)—586
Richards, Hans Kohn and Eugene D. Denman. Measurement of ionizing radiation by frequency variation using ferroelectric material—250(A)
Richardson, J. Reginald. European accelerators—266(T)
—— (see Caldwell, David O.)—28
—— (see Glass, Neel W.)—1251
—— (see Handler, Harry E.)—281(A)
Richeson, William E., Jr. (see Evans, Marjorie W.)—256(A)
Riddell, R., Jr., M. Neuman, and S. Gasiorowicz. Dynamical friction—257(A)
—— (see Gasiorowicz, S.)—257(A)
Ridgway, S. L. and George B. Collins. Evidence for γ rays from hyperons or heavy mesons produced by cosmotron protons—247(A)
Ridolfo, Virginia C. (see Cheng, L. S.)—231(A)
Rightmire, R. A. (see Simanton, J. R.)—260(A)
Rinehart, M. (see Ammiraju, P.)—1188(A)
—— (see Sargent, C. P.)—1349
Risser, J. R., J. Price, and C. M. Class. Angular distributions of resolved neutron groups from $B^{11}(d,n)C^{12}$ reaction—1183(A)
Ritchie, R. H. (see Neufeld, Jacob)—1632
Ritow, Herman. Field effect of space charge in intermittent glow in hydrogen—251(A)
Ritson, D. M., A. Pevsner, and R. L. Zimmerman. Scattering of 100-Mev γ rays from C—1168(A)
Rittner, E. S. and S. Fine. Localized photoeffect in PbS photocells—545(L)
Robbins, A. B. (see Doyle, W. T.)—1185(A)
Roberts, B. W. and C. P. Bean. Magnetic domain patterns observed by Kerr effect in BiMn alloy—225(A)
Roberts, Donald E. and Leo Mandelkern. Nature of stark rubber—1559(A)
Roberts, J. H. (see Peshkin, M.)—1204(A)
Roberts, L. D. and R. B. Murray. Magnetic and thermal properties of UI_3 at liquid He temperatures—1180(A)
—— (see Dabbs, J. W. T.)—1512(L)
—— (see Murray, R. B.)—1180(A)
Roberts, S. Interpretation of optical properties of metal surfaces—1151(A)
Roberts, Thomas R. and Stephen G. Sydoriak. Thermodynamic properties of liquid He^3. I. Specific heat and entropy—1672
Roberts, V. (see Macfarlane, G. G.)—1865(L)
Robillard, T. R. (see Goldwasser, E. L.)—1763
Robinson, Berol L. and Richard W. Fink. Electromagnetic radiations of Cs^{137}—231(A)
—— (see Fink, Richard W.)—1293
Robinson, C. S. (see Leiss, J. E.)—201(L); 1188(A)
Robinson, G. W. Emission spectra of some polyatomic molecules—1550(A)
Robinson, John E. Electronic relaxation time in graphite—227(A)
Robinson, Joseph H., III (see Besdin, D. J.)—272(A)
Robinson, W. H. and R. Smoluchowski. Small-angle scattering of x-rays by surface irregularities—1555(A)
Robson, J. W., R. L. Stearns, and E. C. Gregg. Emergent electron distribution resulting from bremsstrahlung incident on thin scatterer—233(A)
—— (see Stearns, R. L.)—232(A)
Rocklin, Sol (see Yuster, Philip)—233(A)
Rogers, J. V. (see Walsh, J. L.)—265(A)
Rogers, K. (see Sargent, C. P.)—1349
Rogers, K. C. (see Ammiraju, P.)—1188(A)
Rogosa, G. L. and W. F. Peed. U L_I x-ray transition from separated isotopes—1173(A)
Rohr, R. C. and R. D. Birkhoff. K-shell internal conversion coefficients—1266
Rohrlich, F. Infrared divergence in bound state problems—181
—— **and J. M. Jauch.** Infrared divergence—222(A)
Romer, R. H. and R. H. Dicke. Reduction of Doppler width of microwave lines—1160(A)
Roos, C. E. (see Fowler, J. M.)—996
Rose, Basil. Recent work with polarized protons at Harwell—1191(T)
Rose, David J. Magnification and resolution of field emission electron microscope—1169(A)
—— Redetermination of ionization coefficient α for H—558(A)

—— **and Sanborn C. Brown.** High-frequency gas discharge plasma in hydrogen—310
Rosen, A. (see Forster, H. H.)—1172(A)
Rosen, L. (see Frye, G. M., Jr.)—241(A)
Rosenblatt, D. B. (see McReynolds A. W.)—418
Rosenbluth, A. W. and M. N. Rosenbluth. Application of the Monte Carlo method to the theory of liquids—260(T)
Rosenbluth, M. N. (see Rosenbluth, A. W.)—260(T)
Rosenwasser, Hyman, and Paul W. Levy. Radiation induced coloring of NaN_3—1541(A)
Rosenzweig, N. (see Ferentz, M.)—222(A)
Ross, M. Theory of pion photoproduction—1156(A)
Rostoker, Norman and Hans Ekstein. Quantum theory of noise—222(A)
—— (see Brophy, J. J.)—228(A)
—— (see Ekstein, Hans)—222(A)
Roth, F. L. (see Martin, G. M.)—1559(A)
Roth, Laura M. (see Lax, Benjamin)—548(L)
Rothman, M. A. (see Swann, C. P.)—1183(A)
Rothstein, Jerome. Correlation of expansion coefficient anomaly in quenched Cu_3Au with properties of ordered Cu_3Au—1554(A)
—— Dislocation model of liquids—1157(A)
—— Order-disorder and ionic conductivity in Ag_2HgI_4—271(A)
Rott, N. Unsteady viscous flow in vicinity of stagnation point—1144(A)
Rourke, F. M. (see White, F. A.)—1174(A)
Roy, S. K. (see MacDonald, D. K. C.)—525
Ruane, T. F., B. Waldman, and W. C. Miller. Absolute cross sections for Coulomb scattering of 1.75-Mev electrons —1166(A)
Rubenstein, R. A. (see Blatt, F. J.)—1553(A)
Rubin, A., F. Ajzenberg, and J. B. Reynolds. Neutrons from proton bombardment of P^{31}—1185(A)
Rubin, Sylvan and D. C. Sachs. High-resolution magnetic spectrometer—284(A)
—— (see Tautfest, G. W.)—280(A)
Rubinow, S. I. Variational principle for scattering with tensor forces—183
—— (see Feshbach, Herman)—188
Ruderman, Malvin A. Polarization and cross section for inelastic scattering—267(A)
—— Theory of indirect nuclear-exchange interaction in metals—1183(T)
—— (see Karplus, Robert)—260(T); 771
Rudman, P. S. and B. L. Averbach. Measurements of x-ray diffuse scattering from Co-Pt disordered solid solutions and of long-range order for alloy CoPt—1554(A)
—— (see Averbach, B. L.)—1554(A)
Rudman, S. W. (see Hurley, J. P.)—1187(A)
Ruetenik, J. R. and S. Corrsin. Equilibrium turbulent flow in slightly divergent channel—1142(A)

Sachs, A. M. (see Bodansky, D.)—240(A)
Sachs, D. C. (see Rubin, Sylvan)—284(A)
Sachs, R. G. n-p mass difference and structure of nucleon—244(T)
—— (see Holladay, W. G.)—1155(A)
Sack, H. S. (see Ames, I.)—1545(A)
Sack, W. S. Decay times of luminescence and photoconductivity in AgCl—1549(T)
Sadauskis, John (see Jesse, William P.)—1150(A)
Saenz, A. W. and R. C. O'Rourke. Magnetic moment of Fermi-Dirac gas—1166(A)
Sagane, Ryokichi, Walter Dudziak, and James Vedder. Positron spectrum from the decay of the μ meson—269(A)
—— (see Dudziak, Walter)—269(A)
Saha, A. K. (see Das, T. P.)—516
Sailor, V. L., H. H. Landon, H. L. Foote, Jr., and R. E. Wood. Problems in analysis of neutron resonance data—224(A)
—— (see Landon, H. H.)—225(A); 1267
—— (see Wood, R. E.)—639
Saito, Y. (see Okaya, Y.)—1857(L)
Sakai, M. (see Kurbatov, J. D.)—674
Sakamoto, M., S. Kobayashi, and S. Ishii. Effect of O_2 gas on photoconductivity of BaO—552(L)
Salant, E. O. Heavy mesons produced in interaction of 2–3-Bev particles—1166(T)
—— (see Hill, R. D.)—247(A)
—— (see Hornbostel, J.)—218(L); 1202(A)
Salkovitz, Edward I., J. Pasternak, and A. I. Schindler. Brillouin zone studies of alloys. III. Matthiessen's rule for dilute Mg alloys—271(A)
—— **and A. I. Schindler.** Resistivity of dilute Mg alloys—543(L); 1553(A)
—— (see Schindler, A. I.)—1552(A)
Salpeter, E. E. 7.68-Mev level in C^{12} and stellar energy production—1183(A)
Sampson, M. B. (see Miller, D. W.)—1184(A)
Sanders, Richard M. (see Bina, Melvin J.)—251(A)
Sandoz, G. (see Stauss, H. E.)—271(A)
Sands, R. H. Paramagnetic resonance absorption in glass—266(A)
—— (see Pake, G. E.)—266(A)
Saphir, G. Scattering and absorption of 50-Mev π^+ mesons in Pb—269(A)
Saraf, Babulal, J. Varma, and C. E. Mandeville. Radiations from Y^{88}, Zr^{97}, Pr^{140}, and Pr^{143}—1206(A)
—— (see Hans, H. S.)—1173(A)
—— (see Mandeville, C. E.)—94; 1185(A)
Sargent, C. P., R. Cornelius, M. Rinehart, L. M. Lederman, and K. Rogers. Diffusion cloud chamber study of very slow mesons. I. Internal pair formation—1349
Satterthwaite, C. B. (see Corak, William S.)—1690
Saunders, V. I. (see West, W.)—1557(A)
Savedoff, Malcolm. Gas-dynamics effects of star formation —1158(T)
Savitt, Jacob. Method for observation of ionization profile behind explosive produced shocks in air—1158(A)
Sawatzky, A. and F. E. Jaumot, Jr. Isothermal anneal study of quenched and cold-worked Cu-Pd alloys—1555(A)
Sawyer, George A. and Louis C. Burkhardt. Search for reaction $T(d,\gamma)He^5$—1305
Schaaf, S. A. (see Laurman, J. A.)—1540(A)
Scharff-Goldhaber, Gertrude and Joseph Weneser. Higher excited states of even-even nuclei—1186(A)
—— **and J. Weneser.** The system of even-even nuclei—212(L)
Schein, Marcel (see Chou, C. N.)—162
Scherb, F. (see Day, R. B.)—279(A)
Scherrer, V. E., W. R. Faust, and B. A. Allison. Cascade γ rays from 2.5-Mev neutron bombardment of Au, I, and Cr—224(A)
—— (see Faust, W. R.)—224(A)
Schiefer, H. F. Stress-strain relationships in yarns subjected to rapid impact loading—1548(T)
Schiff, L. I. Electric monopole transitions in C^{12} and O^{16}—1281
—— Excited states of C^{12} and O^{16}—235(A)
—— Nuclear dispersion contribution to high-energy electron scattering—278(A); 756
Schiller, Ralph. New interpretation of Dirac equation—1176(A)
Schindler, Albert I. Ferromagnetic Hall effect of Ni alloys —1199(A)

—— **and E. I. Salkovitz.** Brillouin zone studies of alloys. IV. Additional Hall data of Mg alloys—1552(A)
—— (see Salkovitz, E. I.)—271(A); 543(L); 1553(A)
Schissel, Paul (see Porter, Richard F.)—242(A)
Schlier, R. E. Structure of evaporated Cu films on Ti—1555(A)
——, **H. E. Farnsworth, and T. H. George.** Low-energy electron diffraction studies of Ti crystal surface—250(A)
—— (see Burger, R. M.)—1179(A)
—— (see Farnsworth, H. E.)—250(A)
—— (see George, T. H.)—1179(A)
Schmitt, R. W. and M. D. Fiske. Low temperature resistance minimum—246(A)
Schneps, J. (see Fry, W. F.)—247(A)
Schoeni, Kurt (see Lehovec, Kurt)—229(A); 1179(A)
Schulte, H. F. (see Sicinski, H. S.)—1140(A)
Schulz, George J. and Sanborn C. Brown. Microwave study of positive ion collection by probes—559(A); 1642
Schulz-DuBois, E., M. Nisenoff, H. Y. Fan, and K. Lark-Horovitz. Spin resonance in neutron irradiated Si—1561(A)
Schwarzschild, Martin. Turbulence in stellar atmospheres—1158(T)
Schweber, S. S. (see Wightman, A. S.)—812
Schwemin, A. J. (see Paramentier, D.)—284(A)
Schwertz, F. A. and R. E. Freund. Voltage-dependence of electroluminescent brightness. II. Chemically-deposited phosphor films—1134(L)
—— **and J. J. Mazenko.** Light output from dielectric-imbedded electroluminescent phosphors—1169(A)
——, **J. J. Mazenko, and E. R. Michalik.** Voltage-dependence of electroluminescent brightness. I. Dielectric-imbedded phosphors—1133(L)
Sciama, Dennis. Formation of galaxies—1158(T)
Sclar, N. and E. Burstein. Optical and impact recombination in impurity photoconductivity in Ge and Si—1178(A); 1757
Scott, E. J. (see McGuire, T. R.)—1562(A)
Seaborg, G. T. (see Folger, R. L.)—107
—— (see Ghiorso, A.)—1518(L)
—— (see Glass, R. A.)—261(A)
—— (see Nervik, Walter E.)—261(A)
Seagrave, John D. and Richard L. Henkel. Total cross section of deuterium for neutrons from 0.2 to 22 Mev—666
Seeman, N., M. M. Shapiro, and B. Stiller. Cosmic-ray observations of K^+ mesons—1202(A)
Segel, R. E. and S. S. Hanna. Polarization measurement in $D(d,p)H^3$ reaction—1538(A)
Segel, S. L. and B. C. Lutz. Impurity effects on nuclear quadrupole spectrum of Cl^{35}—1183(A)
Segelken, W. G. and H. C. Torrey. Quadrupolar splitting of nuclear resonance lines in alums—1537(A)
Segrè, Emilio. Experiments on high-energy polarized protons—1191(T)
—— (see Tripp, R.)—266(A)
—— (see Ypsilantis, T.)—267(A); 840(L)
Seidel, G. M. and V. A. Johnson. Verification of Bridgman relation for mixed semiconductor—230(A)
Seidl, F. G. P. Recent mechanical improvements in Brookhaven fast chopper—1161(A)
Seitz, Frederick. Source of disordering of alloys during irradiation—1530(A)
—— (see Harrison, W. A.)—1530(A)
Seldin, E. J. Density-resistivity relationships in baked carbons—1565(A)
Sells, R. L., C. W. Harris, and E. Guth. Random walk methods in statistical mechanics of one-dimensional systems—272(A)
Selove, W. Angular distribution of pickup deuterons for 95-Mev protons on C, and implications as to internal interactions in C—208(L)
—— (see Teem, J. M.)—259(A)
Senio, P. (see Tucker, C. W., Jr.)—1541(A)
Senitzky, B., I. I. Rabi, and M. L. Perl. Quadrupole moments of Rb^{85} and Rb^{87}—1537(A)
—— (see Perl, M. L.)—611
Senitzky, I. R. Quantum effects in interaction between electrons and high-frequency fields. II—875
Sessler, A. M. and H. M. Foley. Hfs of He^{3+} and He^3—6
Shaltiel, D. (see Portis, A. M.)—264(A)
Shapiro, M. M. (see Seeman, N.)—1202(A)
Sharp, R. T. and J. David Jackson. Orthogonality of Furry-Sommerfeld-Maue wave functions and their use in perturbation theory—1128(L)
Shaw, Harlan, David Cohen, Burton J. Moyer, and Charles Waddell. Analysis of high-energy photons from cyclotron target—259(A)
Shaw, T. M. (see Windle, J. J.)—281(A)
Sheckler, A. C. and D. C. Jillson. Minority carrier lifetime as function of crystal growth variables—229(A)
—— (see Jillson, D. C.)—229(A)
Sheer, C. and J. Moore. Measurement of scattering cross sections for low-energy neutron resonances—565
Sheline, Raymond K. (see Wilkinson, Joseph R.)—1538(A)
Shen, K. Y. and S. F. Singer. Experiment for determining anisotropy of primaries—1546(A)
Sherman, Dora F. Interactions of 380-Mev α particles in Ilford G.5 emulsion—259(A)
Sherman, N., G. Culler, and S. Fernbach. Optical model analysis of scattering of 14-Mev neutrons—273(A)
—— (see Fernbach, S.)—273(A)
Sherr, R., R. W. Kavanagh, and W. R. Mills. Energy levels of Al^{28}—1185(A)
Sherrill, F. A. (see Blewitt, T. H.)—1555(A)
Shibuya, Yoshio and Seichi Tanuma. Paramagnetism observed at superconducting transition—938
Shimoda, Koichi, Tetsuji Nishikawa, and Takashi Itoh. Microwave spectrum of methylamine—1160(A)
Shirane, Gen and Ray Pepinsky. Anomalous optical properties of ferroelectric $PbTiO_3$—1201(A)
—— (see Jona, F.)—1201(A); 903
Shull, C. G. Magnetic structure of Fe—1562(T)
Shulman, C. I. Measurement of shot noise in CdS crystals—384
Shulman, R. G., J. M. Mays, and D. W. McCall. Nuclear magnetic resonance in semiconductors: Exchange broadening and line shapes—1182(A)
—— (see Mays, J. M.)—1182(A)
Shutt, R. P. High-energy interaction at Cosmotron—255(T)
—— (see Block, M. M.)—248(A)
—— (see Fowler, W. B.)—121
—— (see Morris, T. W.)—1167(A)
Sicinski, H. S. and H. F. Schulte. Mach number and yaw angle determination for conical flow regimes using two surface-flow angle indicators—1140(A)
Siegel, Armand (see Wiener, Norbert)—1190(A)
Silsbee, H. B. (see Bemski, G.)—470
Silver, E. G. (see Waniek, R. W.)—1148(A)
Silver, M., R. S. Witte, and F. McCaffrey. Rectification in thin films of PbS—270(A)
Silverman, S. (see Benedict, W. S.)—1551(A)
—— (see Herman, R.)—1550(A)
Silverstein, E. (see Jones, K. W.)—241(A)
Simanton, J. R., R. A. Rightmire, A. L. Long, and T. P. Kohman. Long-lived radioactive Al^{26}—260(A)
Simon, Albert. Ambipolar diffusion in magnetic field—317
—— (see Biedenharn, L. C.)—1153(A)

Simpson, J. Arol, H. W. Babcock, and H. D. Babcock. Association of "unipolar" magnetic region on sun with changes of primary cosmic-ray intensity—1402
—— (see Marton, L.)—1168(A)
—— (see Meyer, Peter)—247(A)
Sinclair, Rolf M. γ radiation from interaction of 4.4-Mev neutrons with Fe^{54} and Fe^{56}—1147(A)
Singer, S. F. New method for measuring low-energy spectrum of primary cosmic rays—1547(A)
—— Origin of charge spectrum of primaries—1163(A)
—— (see Shen, K. Y.)—1546(A)
—— (see Wentworth, R. C.)—1546(A)
Sinsheimer, R. L. Chemistry of nucleic acids—1531(T)
Sippel, R. F. (see Bent, R. D.)—1198(A); 1237
Skolnik, W. Scattering of 195-Mev pions by deuterium—240(A)
Slater, J. C. One-electron energies of atoms, molecules, and solids—1039
Slätis, H. (see Rasmussen, J. O.)—261(A)
Slichter, C. P. Nuclear resonance and study of metals—272(T)
Slichter, W. P. and J. M. Mays. Proton magnetic resonance in polyamides—1559(A)
Slifkin, Lawrence (see Kuper, A.)—1870(E)
—— (see Portnoy, William M.)—1536(A)
Smith, Alan W. Two-medium theory of thermal conductivity of artificial graphite: Experimental—1563(A)
Smith, Bernard. Role of substrate, surface-finish, film-height, and temperature in He II film transport—1196(T)
—— **and Henry A. Boorse.** He II film transport. I. Role of substrate—328
Smith, Charles G. Anchored Hg arc cathode spot—562(A)(A)
Smith, Charles S. and W. B. Daniels. Elastic constants of Fe-Si alloys—1553(A)
—— (see Bacon, Roger)—1553(A)
Smith, Frances M. (see Barkas, Walter H.)—605
—— (see Goldhaber, S.)—1203(A)
—— (see Heckman, Harry H.)—1202(A)
Smith, H. L. (see Prestwood, R. J.)—1324
Smith, J. Y. Tabulations of cosmic abundances—250(A)
Smith, Lyle W. Measurement of scattering constant in nuclear emulsion—100
——, **A. W. McReynolds, and G. A. Snow.** Elastic p-p angular distributions from 440 to 1000 Mev—1167(A)
—— (see Coor, T.)—1369
Smith, P. L. (see Davisson, J. W.)—1544(A)
—— (see Lipson, H. G.)—1535(A); 1535
Smith, R. L. (see Jaumot, F. E., Jr.)—1555(A)
Smith, R. V. Photomultiplier transit time measurements—1170(A)
Smith, R. W. Edge electroluminescence from CdS crystals at low dc fields—1169(A)
Smith, Stephen J. (see Branscomb, Lewis M.)—1028; 1127(L)
Smith, W., H. Glick, A. Hertzberg, and W. Squire. Schlieren studies of flow behind strong shocks—1141(A)
Smith, W. G. and J. M. Hollander. Neutron deficient chains of mass 187 through 191—262(A)
—— **and J. M. Hollander.** Radiochemical study of neutron-deficient chains in noble metal region—1258
Smither, R. K. and C. W. Hoover, Jr. Secondary electron resonance discharge mechanism. I—1149(A)
—— (see Hoover, C. W., Jr.)—1149(A)
Smoluchowski, R., E. Pearlstein, and H. Ingham. Radiation effects in solids produced by nuclear disintegrations—1530(A)
—— (see Coleman, C.)—1555(A)
—— (see Leivo, W. J.)—1532(A)
—— (see Pearlstein, E.)—1530(A)
—— (see Robinson, W. H.)—1555(A)
Smythe, W. R. and R. M. Worlock. π^0 photoproduction from protons and deuterium nucleons, II—269(A)
—— (see Worlock, R. M.)—269(A)
Snell, Arthur H. and Frances Pleasonton. Magnetic and electric deflection spectrometry of neutrino recoils in A^{37}—1174(A)
Snow, G. A. (see Coor, T.)—1369
—— (see Smith, Lyle W.)—1167(A)
Snyder, A. and G. del Castillo. Momentum distribution of low-energy cosmic-ray particles—1163(A)
—— (see del Castillo, G.)—1163(A)
Snyder, S. (see Fagg, L. W.)—1538(A)
Softky, Sheldon D. Millisecond γ emitter from protons on Ta—280(A); 736
—— Photodisintegration of C^{12} by 330-Mev bremsstrahlung—173
Sogo, P. B. and C. D. Jeffries. Nuclear magnetic moments of Cl^{36}, Rh^{103}, and W^{183}—1316
—— **and C. D. Jeffries.** Nuclear magnetic moments of Rh^{103} and W^{183}—265(A)
Sonder, E. Effect of low concentrations of impurity on diffusion in Ag—245(A)
—— (see Kuper, A.)—1870(E)
Sonett, C. P. and K. R. MacKenzie. Relative stopping powers for 20-Mev protons—280(A)
Sparrow, E. M. Laminar free convection from vertical surfaces for prescribed variations of (1) wall heat transfer rate, or (2) of wall temperature—1140(A)
Speck, D. R. and F. A. Jenkins. Preliminary report on the quadrupole moment of Nb—282(A)
—— (see Jenkins, F. A.)—282(A)
Spencer, L. V. Theory of electron penetration—1597
—— **and F. H. Attix.** Theory of cavity ionization—233(A)
Spencer, T. W. Reflection of acoustical pressure pulse from liquid-solid plane boundary—1540(A)
Spicer, William E. X-ray-induced luminescence from air—1061
Spinrad, B. I. Threshold values of internal conversion coefficients for K-shell—1302
Spitzer, W., C. O. Bennett, and H. Y. Fan. Pressure dependence of absorption edge in Ge and Si—228(A)
——, **R. J. Collins, and H. Y. Fan.** Infrared absorption in n-type Ge—1536(A)
Squire, W. (see Smith, W.)—1141(A)
Sreekantan, B. V. (see DeStaebler, Herbert, Jr.)—1520(L)
Stanford, G. S. and G. F. Pieper. Fast coincidence system with amplitude discrimination—1154(A)
—— (see Pieper, G. F.)—1185(A)
Stapp, Henry P. Analysis of triple scattering and correlation experiments—267(A)
Statz, H., L. Davis, Jr., and G. deMars. Nonsteady state conductance of inversion layers and structure of surface states on Ge—1566(A)
——, **L. Davis, Jr., and G. A. deMars.** Structure of surface states at Ge-Ge oxide interface—540(L)
—— (see deMars, G. A.)—539(L); 1565(A)
Stauss, H. E. and G. Sandoz. Linear magnetostriction of some ternary Co-Fe-Ni alloys—271(A)
Stearns, R. L., J. W. Robson, and E. C. Gregg. Determination of bremsstrahlung spectrum produced by 18-Mev electrons—232(A)
—— (see Robson, J. W.)—233(A)
Steele, M. C. Hall effect and magnetoresistance oscillations of Sb single crystals in magnetic fields at liquid He temperatures—1180(A)
—— **and J. Babiskin.** Oscillatory thermomagnetic properties of Bi single crystal at liquid He temperatures—359
—— (see Berlincourt, Ted G.)—227(A); 956
Steffen, R. M. (see Paul, H.)—231(A)

—— (see Zobel, W.)—1186(A)
Stegun, Irene A. and Milton Abramowitz. Generation of Coulomb wave functions by means of recurrence relations—1851
Steigert, F. E. (see Plendl, H. S.)—1538(A)
—— (see Yamamoto, S.)—1210(A)
Stein, P. C. (see Odian, A. C.)—248(A)
Stein, S. (see Gerjuoy, E.)—557(A); 1848
Steinberger, J. (see Lokanathan, S.)—240(A)
Stelson, P. H. and F. K. McGowan. Angular distribution of γ rays from Coulomb excitation—249(A)
—— (see Campbell, E. C.)—1172(A)
Stephens, Frank S., Jr., J. Hummel, F. Asaro, and I. Perlman. α groups and angular correlation of Am^{243}—261(A)
—— (see Asaro, Frank)—19; 260(A)
—— (see Hummel, J. P.)—22
—— (see Perlman, I.)—262(A)
Stephens, William E. and A. K. Mann. Energy spectrum of photoprotons from C—241(A)
——, **A. K. Mann, B. J. Patton, and E. J. Winhold.** Fine structure in the (γ,p) reaction in O—839(L)
—— (see Toms, M. Elaine)—626
Stern, Edward A. (see Neher, H. Victor)—845(L)
Stern, Frank. Valence wave functions for $3d^74s$ and $3d^8$ configurations of atomic Fe—1552(A)
Stern, M. O. (see Feiner, F.)—239(A)
Sternheimer, R. M. Angular distribution of pions from θ^0 decay—205(L)
—— Polarization of nucleons elastically scattered from nuclei—1156(A); 1871(E)
Stevens, D. K. Magnetic susceptibility of fast neutron bombarded crystalline quartz—1541(A)
—— (see Crawford, J. H.)—1532(A)
Stevenson, Donald T. Surface-recombination velocity and surface conductance of thin Ge slabs—1566(A)
Stevenson, M. Lynn (see Alvarez, Luis)—280(A)
—— (see Paramentier, D.)—284(A)
Stevenson, P. C. (see Folger, R. L.)—107
Stewart, A. T. and R. E. Green. Angular correlation of photons from positron annihilation in light metals—232(A)
—— (see Green, R. E.)—486
Stewart, Leona. Neutron spectrum and absolute yield of Pu-Be source—740
Stiehler, R. D. (see Martin, G. M.)—1559(A)
Stier, P. M., C. F. Barnett, R. A. Howard, and W. Bugg. Charge states of H ions in gases—1149(A)
—— (see Barnett, C. F.)—1537(A)
Stiller, B. (see Seeman, N.)—1202(A)
Stilwell, G. R. (see Collins, R. J.)—227(A)
St. John, Robert and J. G. Winans. Motion and spectrum of arc cathode spot in magnetic field—562(A); 1664
Stockman, F. (see Pagnia, H.)—236(A)
Stoeckmann, F., E. Klontz, H. Y. Fan, and K. Lark-Horovitz. Photoconductivity of electron-bombarded Ge—1535(A)
Stone, Gerald, Robert Carbone, and Edgar Everhart. Validity criteria for calculating differential cross section for collisions of kev ions with atoms—1150(A)
—— (see Carbone, Robert J.)—1150(A)
—— (see Everhart, Edgar)—1045
Story, J. S. (see Perring, J. K.)—1525(L)
Stratton, T. F., J. M. Blair, K. F. Famularo, and R. V. Stuart. Experimental determination of the absolute differential cross sections for $O^{18}(d,p)O^{17}$, $O^{18}(d,p)O^{17*}$ and $O^{18}(d,p)O^{19*}$ reactions—629
Strauch, Karl. Double-scattering experiment with 96-Mev protons—234(A)
—— Elastic scattering of protons—1168(T)
Stuart, R. V. (see Stratton, T. F.)—629
Stubbins, Warren Fenton. Experimental ion source for 184-inch cyclotron—274(A)
Studier, W. H. Nuclear properties of elements 98, 99, 100—227(T)
Sun, K. H., P. R. Malmberg, and P. Szydlik. Photographic amplification in α-particle autoradiography—1154(A)
Sunyar, A. W. Fast $E2$ transitions—653
—— (see Alburger, D. E.)—276(A)
—— (see Church, E. L.)—1186(A)
Sutherland, G. B. B. M. Infrared analysis of structure of proteins and nucleic acids—1534(T)
Sutton, R. B. Polarization effects on high-energy p-p reactions—266(T)
Suura, H. Radiative correction to electron scattering—278(A)
Suzuki, Kenzō (see Chikazumi, Sōshin)—1130(L)
Swami, M. S. (see Fry, W. F.)—247(A)
Swann, C. P., M. A. Rothman, W. C. Porter, and C. E. Mandeville. γ rays from proton capture in Li^7—1183(A)
Swann, W. F. G. Results of limitations on space current densities in galactic and intergalactic space—871; 1546(A)
Swanson, John A. Saturation Hall constant and magnetoresistance in semiconductors—1534(A)
Swanson, Robert E. and Robert H. McFarland. Temperature sensitivities of sensitized fluorescence spectrum of Th—1063
Swartz, C. D. Methods of fast neutron spectroscopy—1530(T)
Swartz, C. E. and J. W. DeWire. Preliminary studies with high-energy photon spectrometer—1164(A)
Swenson, C. A. P-V isotherms of 10 000 atmospheres at 4.2°K for four alkali metals and some condensed gases—244(T)
Swern, L. (see Duncan, B. J.)—1201(A)
Swiatecki, W. J. Average nuclear potentials and densities—204(L)
—— Nuclear surface energy and diffuseness of nuclear surface—203(L)
Swihart, J. C. (see Belinfante, F. J.)—222(A)
Sydoriak, Stephen G. (see Roberts, Thomas R.)—1672
Symon, Keith R. Fixed field alternating gradient accelerators—1152(A)
—— (see Jones, L. W.)—1153(A)
—— (see Kerst, D. W.)—1153(A)
—— (see Terwilliger, K. M.)—1153(A)
Szydlik, P. (see Sun, K. H.)—1154(A)

Taft, E. A. (see Dash, W. C.)—1192(A)
Tangen, R. (see Lönsjö, O.)—727
Tannenwald, P. E. and H. J. Zeiger. Multiple resonances in cobalt ferrite—1562(A)
Tanttila, W. H. (see Proctor, W. G.)—1854(L)
Tanuma, Seichi (see Shibuya, Yoshio)—938
Taub, A. H. Determination of flows behind stationary and pseudo-stationary shocks—1140(T)
Tauber, G. E. Energy levels of Pb^{208}—1204(A)
—— (see Wu, Ta-You)—222(A)
Tautfest, G. W., J. R. Havill, and Sylvan Rubin. Proton scattering from N^{14}—280(A)
Taylor, G. R. Stress-optical studies on amorphous and polycrystalline elastomers—1547(T)
—— **and S. R. Darin.** Tensile strength of elastomers—1558(A)
Taylor, J. C. Self-energy effects on meson-nucleon scattering according to Tamm-Dancoff method—201(L)
Taylor, J. E. (see Brock, E. G.)—1169(A)
Tchen, C. M. Statistical theory of shear turbulence in parallel flow—1158(A)
Teem, J. M., W. Selove, and U. E. Kruse. Interaction of 95-Mev protons with He^4—259(A)

Teitler, S., M. Lax, and E. Burstein. Absorption by free and bound holes in p-type Ge—1561(A)
Telegdi, V. L. (see Peshkin, M.)—1204(A)
Teller, E. (see Johnson, M. H.)—260(T); 783
Temmer, G. M. and N. P. Heydenburg. Multipolarity of γ transitions in F^{19} and Na^{23} by Coulomb excitation—1198(A)
—— **and N. P. Heydenburg.** Properties of excited states of Pd and Cd nuclei by Coulomb excitation—1308
—— (see Ambler, E.)—230(A)
—— (see Heydenburg, N. P.)—1198(A)
Tenny, F. H. (see Van Lint, V. A. J.)—1203(A)
Terwilliger, K. M., L. W. Jones, D. W. Kerst, and K. R. Symon. Application of fixed field alternating gradient principle to betatrons and cyclotrons—1153(A)
—— (see Jones, L. W.)—1153(A)
—— (see Kerst, D. W.)—1153(A)
Teutsch, W. B. and V. W. Hughes. Theory of effect of static electric field on positronium formation—1174(A)
Tewes, Howard A. Excitation functions for some proton-induced reactions of Th—25
Thaler, R. M. and J. L. McHale. S-matrix in terms of phenomenological collision parameters—1189(A)
—— (see McHale, J. L.)—273(A); 1189(A)
Thiess, F. B. (see Bodine, J. H.)—1532(A)
Thomas, G. E. (see Bollinger, L. M.)—223(A)
Thomas, R. G. Correction to exponential dependence of neutron transmissions—77
—— (see Lane, A. M.)—693
Thompson, R. W. (see Burwell, J. R.)—101; 247(A)
—— (see Huggett, R. W.)—248(A)
—— (see Kim, Y. B.)—248(A)
Thompson, S. G. (see Asaro, Frank)—19
—— (see Choppin, G. R.)—1519(L)
—— (see Ghiorso, A.)—1518(L)
Thomsen, John S. Statistical analog of second law of thermodynamics—1625
Thomson, Robb. Dislocation line energy and slip in NaCl and AgCl crystals—1171(A)
Thorndike, A. M. (see Block, M. M.)—248(A)
—— (see Fowler, W. B.)—121
—— (see Morris, T. W.)—1167(A)
Tisza, Laszlo (see Manning, Irwin)—1165(A)
Tobocman, W. (see Utiyama, R.)—780
Tollestrup, A. V. (see Bingham, H. H.)—1187(A)
Toman, L. (see Wolff, G.)—1179(A)
Tomboulian, D. H. (see Bedo, D. E.)—242(A)
Tomita, K. Rotational transition in solid H—1197(A)
Tomizuka, Carl T. (see Kuper, Alan B.)—244(A); 1870(E)
Tomkins, Frank S. (see Fred, Mark)—1514(L)
Toms, M. Elaine and William E. Stephens. Photoprotons from Pb^{208} and Ta—626
Torrey, H. C. (see Segelken, W. G.)—1537(A)
Trail, C. C. and C. H. Johnson. $Li^7(d,n)Be^8$ neutron spectrum and differential cross section—249(A)
Treiman, S. B. (see Arnold, W. H.)—275(A)
—— (see Van Lint, V. A. J.)—1203(A)
Triebwasser, Sol and J. Halpern. Curie constant, spontaneous polarization, and latent heat in ferroelectric—1201(A)
—— **and Frederic Holtzberg.** Ferroelectric behavior of solid solutions of $KNbO_3$ and $KTaO_3$—1201(A)
Tripp, R. Proposed method for obtaining high-energy polarized proton beam—1167(A)
——, **C. Wiegand, T. Ypsilantis, O. Chamberlain, and E. Segrè.** Experimental determination of complete scattering matrix in proton carbon collision—266(A)
—— (see Ypsilantis, T.)—267(A); 840(L)
Trischka, J. W. (see Braunstein, R.)—1092
Trolan, J. K., J. P. Barbour, E. E. Martin, and W. P. Dyke. Emission from single lattice step of clean W—262(A)
—— (see Dyke, W. P.)—263(A)
Trout, T. (see Page, L. A.)—206(L)
Truitt, Robert Wesley. Determination of transonic pressure drag on wedges by throat station method—1139(A)
Tucker, C. W., Jr., and P. Senio. X-ray scattering effects in irradiated boron carbide—1541(A)
Tucker, G. L. (see Anderson, A. G.)—283(A)
Turkevich, John (see Larach, Simon)—1015
Turnbull, D. (see DeSorbo, W.)—1554(A)
Turner, C. M. Performance characteristics of BNL research electrostatic accelerator—233(A)
Twersky, V. Scattering of electromagnetic waves by bounded lattice of parallel cylinders—257(A)
Tyler, W. W. and R. Newman. Hall mobility of optically excited carriers in Ge—961; 1192(A)
——, **R. Newman, and H. H. Woodbury.** Properties of Ge doped with Ni—461
—— (see Woodbury, H. H.)—1534(A)

Ueta, Masayasu (see Känzig, Werner)—236(A)
Ufford, C. W. (see Meshkov, S.)—1204(A)
Urbach, Franz (see Moser, Frank)—1557(A)
—— (see Nail, Nelson R.)—1557(A)
Urey, H. C. Temperature of primitive earth—236(T)
Utiyama, R. and W. Tobocman. Conservation of parity and new particles—780

Van Horn, David D. and William J. Cooley. Interpretation of dimensional changes on dezincification of α brass—245(A)
van Lieshout, R., D. H. Greenberg, and C. S. Wu. Decay of Cr^{49}—1171(A)
—— (see Farrelly, B.)—1172(A)
—— (see Koerts, L.)—1172(A)
Van Lint, V. A. J., George T. Reynolds, S. B. Treiman, and F. H. Tenny. Correlation of planes in V particle decay events—1203(A)
—— (see Arnold, W. H.)—275(A); 838(L)
Van Loef, J. J. and D. A. Lind. Inelastic scattering of neutrons by Fe, F, Mn, and I—224(A)
Van Roosbroeck, W. Theory of photomagnetoelectric effect in semiconductors—1533(A)
Van Vleck, J. H. Paramagnetism of solids—1558(T)
Varma, Jagdish (see Mandeville, C. E.)—94; 1185(A)
—— (see Saraf, B.)—1206(A)
Varney, Robert N. Diffusion of ions and electrons in electric field—558(A)
Vasileff, H. D. Thermal ionization of interstitials in cubic ZnS—237
Vedder, James (see Dudziak, Walter)—269(A)
—— (see Sagane, Ryokichi)—269(A)
Villaire, A. E. and L. F. Wouters. Fission fast counter using gas scintillation principle—280(A)
Villi, C. (see Beretta, L.)—1526(L)
Vincent, L. D. (see Little, R. N., Jr.)—634
von Herrmann, P. (see Pieper, G. F.)—1185(A)

Wada, Walter (see Kroll, Norman M.)—1355
Waddell, Charles (see Shaw, Harlan)—259(A)
Wagner, F., Jr. (see Porter, F. T.)—214(L)
Wagner, P. E. Contact charging between monocrystalline nonconductors and metals—264(A)
Wagoner, G. (see Dresselhaus, G.)—556(L)
Wainfan, N., W. C. Walker, and G. L. Weissler. Photoionization cross sections of CO_2, A, H_2, and H_2O—561(A)
—— (see Walker, W. C.)—562(A)

Waldman, B. (see Ruane, T. F.)—1166(A)
Walker, R. M., R. S. Preston, E. C. Fowler, and H. L. Kraybill. Production of neutral V events in Pb by neutrons from cosmotron—1203(A)
—— (see Anderson, A. G.)—283(A)
Walker, W. C., N. Wainfan, and G. L. Weissler. Photoelectric yields of metals in vacuum ultraviolet—562(A)
—— (see Wainfan, N.)—561(A)
Walker, W. D. $\Lambda^0 - \theta^0$ production in $\pi^- - p$ collisions at 1 Bev—1407
—— **and J. Crussard.** Interactions of 1.5-Bev π^- mesons—240(A)
—— **and J. Crussard.** π^--nucleon collisions at 1.5 Bev—1416
Wall, F. T. Statistical calculation of dimensions of coiling type macromolecules—1547(T)
Wallace, J. (see Page, L. A.)—206(L)
Wallace, P. R. Modification of one-particle model for nuclear radiative transitions—1205(A)
Wallis, R. F. (see Herman, Robert)—1171(A); 1550(A)
Walsh, Edward N. (see Ziomek, Joseph S.)—243(A)
Walsh, J. L., A. G. Berger, J. V. Rogers, and W. D. Knight. Direct measurement of nuclear spin-lattice relaxation time—265(A)
Walt, M. and J. R. Beyster. Interaction of 4.1-Mev neutrons with nuclei—279(A); 677
Wandel, C. F. (see Lane, A. M.)—1524(L)
Wang, Ming Chen and Eugene Guth. Two-dimensional Coulomb scattering in quantum mechanics—274(A)
Wangsness, Roald K. Magnetic resonance for arbitrary field strengths—927
—— Magnetic resonance in ferrimagnetic containing an arbitrary number of sublattices—1200(A)
Waniek, R. W., R. Fox, L. Garrido, and E. G. Silver. Interaction of high-energy neutrons with Mo—1148(A)
—— (see Culler, Vaughn)—1148(A)
—— (see Fox, Raymond)—1153(A)
Warren, Roger. Electric field measurements in glow discharge using refined electron beam technique—263(A)
—— Field measurements in glow discharges with refined electron beam probe and automatic recording—1650
—— Interpretation of field measurements in cathode region of glow discharges—1658
Warschauer, D. M., W. Paul, and H. Brooks. Effect of pressure on optical absorption edge in Si and Ge—1193(A)
Wasserburg, G. J. and R. J. Hayden. Branching ratio of K^{40} and age of meteorites—250(A)
Watson, J. D. Nucleic acid structure as revealed by x-ray diffraction—1531(T)
Watson, K. M. Partial-wave analysis of experimental photomeson cross sections and its interpretation—234(T)
Watson, W. W. (see Corbett, J. W.)—1165(A)
Wattenberg, A. (see Guernsey, Janet B.)—1147(A)
—— (see Odian, A. C.)—248(A)
Wayland, Harold. Quantitative fluid flow visualization with streaming birefringence—255(A)
Waymouth, J. F. and F. Bitter. Analysis of plasma of fluorescent lamps. II—1148(A)
—— (see Bitter, F.)—1148(A)
Weatherly, T. L. (see Williams, Quitman)—1159(A)
Webb, F. (see Goldhaber, Gerson)—267(A)
Webb, J. H. Ultra-short light-and-voltage pulses applied to Ag-halide crystals by turbine-driven mirror and electrical contacts—1558(A)
Webb, L. A. and R. F. Johnson. Effect of temperature upon scintillation efficiency of NaI(Tl)—234(A)
Webeler, R. (see Allen, G.)—1168(A)
Weber, J. Remarks on fluctuation dissipation theorem—1165(A)
Wechsler, Monroe S. Effect of quench on structure of Au—245(A)
Wedaa, Henry W. (see Bennett, Arthur L.)—256(A)
Weddell, J. (see Jennings, B.)—582
Weertman, J. Theory of steady-state creep based on dislocation climb—246(A)
Weinstein, R., M. Deutsch, and S. Brown. Fine structure of positronium—223(A)
Weinstock, Bernard. Nuclear alignment in liquid He^3—227(T)
—— (see Abraham, Bernard M.)—551(L)
Weiss, J. and W. Bernstein. Energy required to produce one ion pair for several gases—1828
Weiss, M. T. and P. W. Anderson. Ferromagnetic resonance in Ferroxdure—925
Weiss, R. J. (see Antal, J. J.)—1541(A)
Weissberg, H. L. and A. S. Berman. Velocity and pressure distributions in turbulent pipe flow with uniform wall suction—1540(A)
Weissler, G. L. (see Ehler, A. W.)—561(A)
—— (see Wainfan, N.)—561(A)
—— (see Walker, W. C.)—562(A)
Welber, Benjamin. Effect of superconducting transition on internal friction of Sn—1196(A)
Welton, T. A. Possible convergence of mass renormalization—1175(A)
Weneser, Joseph (see Scharff-Goldhaber, Gertrude)—212(L); 1186(A)
Wentworth, R. C. and S. F. Singer. Albedo contribution in measurement of cosmic-ray primaries—1546(A)
Werntz, J. H., Jr. (see Fleming, P. J.)—1196(A)
Wert, C. Internal friction in some Fe-Al alloys—246(A)
—— (see Kerr, J.)—225(A)
Wertheim, M. S. and G. Igo. Isotope shift in x-ray spectra of heavy elements—1
West, W. and V. I. Saunders. Photographic effects in single crystals of AgBr—1557(A)
Westrum, Edgar F., Jr., and John J. McBride. Temperature dependence of heat capacity of molybdenite—270(A)
Wetherill, G. W., L. T. Aldrich, and G. L. Davis. Potassium-argon ages of lepidolites—250(A)
Wexler, Aaron (see Corak, William S.)—1690
Wheeler, R. G. (see Lane, C. T.)—1196(A)
White, F. A., T. L. Collins, and F. M. Rourke. Mass spectrometric search for naturally occurring isotopes of low abundance—1174(A)
White, Harrison C. Quantum-mechanical calculation of interatomic force constants in Cu—1552(A)
White, L. D. g factor of electron in $2S$ state of H—1194(A)
White, R. Stephen, Mark J. Jakobson, and Gordon W. Repp. π^+ photomeson production at 180°. Experimental results—269(A)
—— (see Repp, Gordon W.)—268(A)
Whittemore, W. L. (see Block, M. M.)—248(A)
—— (see Fowler, W. B.)—121
—— (see Morris, T. W.)—1167(A)
Widgoff, M. (see Hill, R. D.)—247(A)
Wiegand, C. (see Tripp, R.)—266(A)
—— (see Ypsilantis, T.)—267(A); 840(L)
Wiener, Norbert. Hopf-Wiener equation system and matrix factorization—255(T)
—— **and Armand Siegel.** Joint probabilities and transition probabilities in differential-space quantum theory—1190(A)
Wightman, A. S. and S. S. Schweber. Configuration space methods in relativistic quantum field theory. I—812
—— (see Michel, L.)—1190(A)
Wigner, Eugene P. Development of compound-nucleus model—1177(T)
—— Lower limit for energy derivative of scattering phase shift—145
—— (see Lane, A. M.)—693

Wilcox, L. and J. E. Drummond. Plasma oscillations in static magnetic field—263(A)
—— (see Drummond, J. E.)—558(A)
Wildhack, W. A. Instrumentation research at National Bureau of Standards—282(T)
Wilkinson, D. H. Giant resonances of nuclear photodisintegration—1164(T)
—— **and A. M. Lane.** Importance of parentage of nuclear states for nuclear reaction phenomena—235(A)
Wilkinson, Joseph R. and Raymond K. Sheline. Nuclear levels in V^{49} as determined by decay of Cr^{49}—1538(A)
Wilks, J. (see Fairbank, Henry A.)—1196(A)
Willard, Harvey B., Joe K. Bair, and Joe D. Kington. Elastic scattering angular distributions of fast neutrons on light nuclei—669
——, **J. D. Kington, and J. K. Bair.** $C^{13}(p,\gamma)N^{14}$ reaction —1184(A)
Willardson, R. K., T. C. Harman, P. F. Choquard, and A. C. Beer. Usually large magnetoresistive effects in InSb for specialized boundary conditions—227(A)
—— (see Harman, T. C.)—1532(A)
Willett, D. K. (see Hanscome, T. D.)—232(A)
—— (see Holmgren, H. D.)—241(A)
Williams, Albert C. and Raymond J. Emrich. Mass flow in shock tube—1158(A)
Williams, Dudley (see Brown, L. Carlton)—1537(A)
Williams, Ferd E. Theoretical basis for light-amplifying phosphors—547(L)
—— (see Piper, W. W.)—1809
Williams, John H. and Stanley W. Rasmussen. Elastic scattering of 9.76-Mev protons by He—56
—— **and Stanley W. Rasmussen.** Scattering of 9.76-Mev protons by He^4—1167(A)
Williams, Malcolm L., Robert F. Landel, and John D. Ferry. Temperature dependence of relaxation mechanisms in amorphous polymers and other glass-forming liquids—1549(A)
Williams, Quitman and T. L. Weatherly. Microwave spectrum of NOBr—1159(A)
Williams, Robert W. High-energy cross sections. I. Size of nucleus—1387
—— High-energy cross sections. II. Nucleon-nucleon cross section at cosmic-ray energies—1393
Williams, Ross, Winslow Baker, Aihud Pevsner, and James Rainwater. Elastic scattering of π mesons from nuclei. I—1188(A)
—— (see Baker, W. F.)—1188(A)
Willis, W. J. (see Kaiser, H. F.)—1538(A)
Wilson, Allan N. μ meson ionization in argon at energies 10 to 100 Bev—268(A)
Winans, J. G. (see St. John, Robert M.)—562(A); 1664
Winckler, J. R., E. N. Mitchell, K. A. Anderson, and L. Peterson. Measurement of Čerenkov radiation from positive and negative π-mesons—1411
Windle, J. J. and T. M. Shaw. Microwave dielectric measurements on single fibers—281(A)
Winhold, E. J. (see Stephens, W. E.)—839(L)
Winsor, L. P. and T. H. Lee. Properties of dc arc in magnetic field—562(A)
Winston, H. (see Firle, T. E.)—1567(A)
Wiser, H. L. and A. D. Krumbein. Mechanism of termination of Geiger plateau region—303
Witmer, Enos E. Apparent importance of $(7/2)^4$ in representation of nuclear masses as multiples of electron mass —1174(A)
Witte, R. S. (see Silver, M.)—270(A)
Wolfenstein, L. Polarization effects in reaction $p+p\rightarrow\pi^+ + d$—766
—— Possible triple-scattering experiments—1870(E)
Wolff, G., L. Toman, and J. Clark. Relationship among hardness, energy gap, and melting point of diamond-type and related structures—1179(A)
Wolfgang, R. L. and G. Friedlander. Excitation function of $C^{12}(p,pn)C^{11}$ reaction in Bev region—1871(E)
—— (see Baker, E.)—242(A)
Wolfson, J. L. (see Graham, R. L.)—1173(A)
Wolicki, E. A. (see Fagg, L. W.)—1538(A)
Wolicki, E. J. (see Geer, E. H.)—241(A)
Wolke, R. L. Angular distribution of fragments from 450-Mev proton fission of Bi—1199(A)
Wood, G. T. and P. S. Jastram. Polarization correlation in decay of Co^{60}—1187(A)
Wood, R. E., H. H. Landon, and V. L. Sailor. Parameters for neutron resonance in Au—639
—— (see Sailor, V. L.)—224(A)
Wood, R. M. (see Ames, I.)—1545(A)
Woodbury, H. H. and W. W. Tyler. Properties of Ge doped with Mn—1534(A)
—— (see Tyler, W. W.)—461
Woodcock, R. F. and H. E. Farnsworth. Effects of heat treatment and ion-bombardment cleaning on catalytic activity of pure Ni surface—1152(A)
Woodruff, Truman O. Solution of Hartree-Fock-Slater equations for Si crystal by method of orthogonalized plane waves—1741
Woodyard, J. R. Charge-exchange accelerator—284(A)
Worlock, R. M. and W. R. Smythe. π^0 photoproduction from protons and deuterium nucleons, I—269(A)
—— (see Smythe, W. R.)—269(A)
Wouters, L. F. (see Villaire, A. E.)—280(A)
Wright, Ray H. Physical concepts relating to transonic wind tunnels—1139(T)
Wu, C. S. (see Farrelly, B.)—1172(A)
—— (see Hughes, V. W.)—1840
—— (see Koerts, L.)—1172(A); 1230
—— (see Lidofsky, L.)—1186(A)
—— (see Lindqvist, Torsten)—231(A)
—— (see Marder, S.)—1173(A)
—— (see van Lieshout, R.)—1171(A)
Wu, Ta-you and G. E. Tauber. Relativistic energy of two-electron atoms—222(A)
Wyly, L. D. (see Reynolds, H. L.)—242(A); 474; 1825
—— (see Zucker, A.)—1150(A)

Yafet, Y. Spin-orbit effects in conduction electron-spin resonance—1542(T)
Yager, W. A. (see Fletcher, R. C.)—1560(A)
Yagoda, Herman. Mesonic decay of ejected nuclear fragment—153
—— Pion-pair production in nuclear emulsion—103; 1187(A)
Yamaguchi, Yoshio and Yoriko Yamaguchi. Photodisintegration of deuteron—69
Yamaguchi, Yoriko (see Yamaguchi, Yoshio)—69
Yamamoto, S. and F. E. Steigert. Background tracks in nuclear emulsions—1210(A)
Yang, C. N. (see Lee, T. D.)—1501
Yennie, D. R., D. G. Ravenhall, and B. W. Downs. Modified Born approximation for electron scattering calculations—277(A)
—— (see Downs, B. W.)—277(A)
—— (see Heims, S. P.)—278(A)
—— (see Ravenhall, D. G.)—277(A)
Yergin, Paul F. and Robert Nathans. (γ,n) cross sections in Mg^{24} and Mg^{26}—1198(A)
—— (see Nathans, Robert)—1197(A); 1296
Yevick, George J. and Jerome K. Percus. Comments on Feynman's atomic theory of liquid He—1164(A)
—— (see Percus, Jerome K.)—1164(A)

Yilmaz, Huseyin. Wave functions and transition probabilities for light atoms—1190(A)
Yntema, G. B. Superconducting winding for electromagnet —1197(A)
Yodh, Gaurang B. Charged pion production in n-p collisions —268(A)
—— Production of charged pions in n-p collisions—1330
—— (see Panofsky, W. K. H.)—751
Young, D. R. (see Drougard, M. E.)—1010; 1563(A)
—— (see Huibregtse, E. J.)—1562(A)
Youngblood, J. F. Low-temperature dielectric measurements —1201(A)
Youtz, L. (see Kerth, Leroy)—259(A)
Ypsilantis, T., C. Wiegand, R. Tripp, E. Segrè, and O. Chamberlain. Depolarization in scattering of polarized protons by H at 310 Mev—267(A)
——, **C. Wiegand, R. Tripp, E. Segrè, and O. Chamberlain.** Rotation of polarization vector and depolarization in p-p scattering—840(L)
—— (see Tripp, R.)—266(A)
Yuster, Philip H., Sol Rocklin, Warren Ramler, and Charles Delbecq. Crystal technique for measuring cyclotron beam energies—233(A)
—— (see Delbecq, C. J.)—237(A)
—— (see Primak, W.)—237(A); 1708

Zaffarano, Dan J. (see Cooper, Raymond D.)—1199(A)
Zeiger, H. J. Boltzmann theory of cyclotron resonance for warped spherical energy surfaces—1560(A)
—— (see Tannenwald, P. E.)—1562(A)
Zener, Clarence. Classical theory of temperature dependence of magnetic crystalline energy—225(A)
Zernike, F. Problems of diffraction of light with demonstrations by Video—272(T)
Zernow, L. and G. Hauver. Cine-microscopy of sparks exploding wires, and fracture at framing rates $> 10^6$/second —1551(A)
Zimmerman, E. J. Response of anthracene to low-energy protons and He ions—1153(A)
Zimmerman, R. L. and H. Palevsky. Inelastic scattering of cold neutrons by Al—1162(A)
—— (see Ritson, D. M.)—1168(A)
Ziomek, Joseph S., Edward A. Piotrowski, and Edward N. Walsh. Normal coordinate treatments and calculated thermodynamic properties of $POCl_3$, POF_3, $PSCl_3$, and PSF_3—243(A)
Zobel, W. and R. M. Steffen. Magnetic moment of 0.247-Mev excited state of Cd^{111}—1186(A)
Zucker, A., H. L. Reynolds, and L. D. Wyly. Cross sections for electron capture and loss by 26-Mev N ions—1150(A)
—— (see Reynolds, H. L.)—242(A); 474; 1825
Zweifel, P. F. Capture-positron branching ratios—1870(E)
—— Nuclear orbital assignments for Ta^{180}—1174(A)
Zwerdling, Solomon and Ralph S. Halford. Direct production of spectroscopic specimens from single crystals by controlled growth from vapor; infrared absorption anisotropy and induced molecular motion in single crystal of benzene—243(A)

Author Index to Volume 99

References with (A) are to abstracts of papers presented at meetings of the American Physical Society; references with (T) designate title only. References with (L) are to Letters to the Editor. References with (E) are to Errata.

Aamodt, L. C. (see Fletcher, P. C.)—613(A)
Abe, Hidetaro (see Kumagai, Hiroo)—1116
Adams, E. N., R. E. Davis, and Colman Goldberg. Two-carrier model of p-type Ge at 77°K—625(A)
Adey, Albert W. Scattering of electromagnetic waves by coaxial cylinders—1639(A)
Adkins, R. and J. G. Brennan. Intermediate coupling in odd-odd nuclei—706
Adlington, R. H. (see Brannen, Eric)—1658(A)
Ajzenberg, F., A. Rubin, and J. G. Likely. Neutrons from proton bombardment of S^{32} and S^{34}—654(A)
Akers, Lawrence K. and Ernest A. Jones. Vibrational spectra, structure, force constants, and thermodynamic properties of AsF_5—1624(A)
Alburger, D. E. and A. W. Sunyar. Decay of Bi^{207}—695
—— (see Toppel, B. J.)—632(A)
Alexander, E. (see Steinberger, I. T.)—1217
Alexander, James D. and Wayne A. Bowers. Effect of inclusion of exchange in Thomas-Fermi treatment of molecules—1627(A)
Allen, F. G. (see Bills, D. G.)—646(A); 1662(A)
Allen, G., R. Webeler, and S. Barile. Multiple scattering of low-energy α particles in gas—556
Allen, K. W., E. Almqvist, and C. B. Bigham. Energy levels of isobars Li^8–He^8—631(A)
—— (see Almqvist, E.)—631(A)
—— (see Bigham, C. B.)—631(A)
Allin, Elizabeth J., W. F. J. Hare, and H. L. Welsh. Infrared absorption of liquid and solid H_2 and its dependence on ortho-para ratio—1639(A)
—— (see Hare, W. F. J.)—1887(L)
Allison, F. E. and Emerson M. Pugh. Hall and Nernst effects in ferromagnetic materials—1642(A)
—— (see Pugh, Emerson M.)—1642(A)
Almqvist, E., K. W. Allen, and C. B. Bigham. He^3 and T reactions in some light elements—631(A)
—— (see Allen, K. W.)—631(A)
—— (see Bigham, C. B.)—631(A)
—— (see Clarke, R. L.)—654(A)
Alpert, Daniel. Ultra-high vacuum technique—1623(T)
Altman, L., H. S. Bridge, and R. W. Williams. High-energy nucleonic component in atmosphere—609(A)
Ambler, Ernest. Nuclear orientation at low temperatures—639(T)
Anderson, A. (see O'Rourke, R. C.)—1484
Anderson, D. V., J. C. Ayers, D. C. Chandler, and G. H. Lauff. Currents and water masses in Lake Huron—1639(A)
Anderson, H. L. Mesons—630(T)
Anderson, James L. Constraints in covariant field theories. II—1009
—— Functional integration and S-matrix theory—674(A)
—— **and Parviz Merat.** Conservation of charge in Einstein's generalization of gravitation theory—1871
—— (see Takano, Y.)—674(A)
Anderson, P. W. Indirect exchange coupling of nuclear moments by electrons in semiconductors and insulators—623(A)
Anderson, Roy S. (see Gordy, Walter)—1905(L)
Andre, C. G. (see Carothers, J. E.)—651(A)
Antal, J. J., R. J. Weiss, and G. J. Dienes. Long-wavelength neutron transmission as absolute method for determining concentration of lattice defects in crystals—1081
Antonakos, Antonios. Simultaneous contrast effect in heterochromatic brightness comparisons—1626(A)
Apker, L. (see Taft, E.)—1831
Ard, William B., Jr., and Walter Gordy. Paramagnetic resonance of irradiated H_2S, D_2S, and $N_2H_5Cl_3$ at liquid air temperature—612(A)
Arfken, G. (see Klingensmith, R.)—340(A)
Argyres, Petros N. Effects of spin-orbit coupling in ferromagnetics—1641(A)
Arima, Akito (see Horie, Hisashi)—778
Armstrong, A. H. and J. E. Brolley, Jr. 14-Mev (n,α) and (n,p) cross sections in Zr. II—330(L)
Aron, W. A., J. S. McIntosh, G. Schrank, and J. H. Bigelow. Elastic scattering of 17-Mev protons by nuclei—629(A)
—— (see Reynolds, George T.)—1038(L)
Arrott, Anthony and J. E. Goldman. Magnetic susceptibility of UO_2 from 2°K to 300°K—1641(A)
Asaro, Frank and I. Perlman. Decay properties of U^{235}—37
Åström, Björn (see Rasmussen, John O.)—47
Aten, A. H. W. (see Mallmann, C. A.)—7
Atkins, K. R. Slope of λ curve of liquid He—670(A)
Ayers, J. C. (see Anderson, D. V.)—1639(A)
Aziz, R. A. and G. D. Scott. Electrical resistance properties and structure of thin evaporated Ag films—1636(A)

Babiskin, Julius. Ultra-low-level voltage detector using Bi and superconductors—668(A)
Bade, W. L. (see Jehle, Herbert)—1640(A)
Baez, Albert V. (see El-Sum, Hussein M. A.)—624(A)
Bahadur, Kanwar (see Müller, Erwin W.)—1651(A)
Bailey, E. C. (see Katz, L.)—98
Bailey, J. B. (see Rohrer, R. H.)—1626(A)
Baily, N. A. Electronic stopping power and radiation damage—341(T)
Bair, J. K. (see Cohn, H. O.)—644(A)
—— (see Kington, J. D.)—1393
Baird, D. C. Dependence of superconducting transition on measuring current—1660(A)
Baker, E. W. (see Knight, J. D.)—1646(A)
Balazs, N. L. Invariant relationship of energy-density and momentum-density of electromagnetic field—1659(A)
Baldock, C. R. (see Boyd, G. E.)—1030(L)
Baldwin, G. J., J. L. Shilts, and E. A. Coomes. Temperature scale for Mo—1650(A)
Ballam, J., A. L. Hodson, and George T. Reynolds. Observations on S particles—1038(L)
Ballard, Stanley S. (see McCarthy, Kathryn A.)—1104
Bame, S. J., Jr. (see Perry, J. E., Jr.)—1368
Bancroft, William Henry, Jr. (see Barringer, Howard Skelton)—1631(A)
Bandtel, K. C., H. A. Bostick, B. J. Moyer, R. W. Wallace, and N. F. Wikner. Pion-proton total cross sections near 4 Bev—673(A)
Banewicz, John J. (see Lindsay, Robert)—636(A)
Baranger, Elizabeth Urey. Analysis of elastic scattering of protons from F^{19}—145
Barber, W. C., A. I. Berman, K. L. Brown, and W. D. George. Z-dependence of bremsstrahlung—59
—— (see Brown, K. L.)—665(A)
Barbour, J. P. (see Dyke, W. P.)—1192

Bardeen, John and David Pines. Electron-phonon interaction in metals—1140
Barile, S. (see Allen, G.)—556
Barker, W. A. and F. N. Glover. Reduction of relativistic two-particle wave equations to approximate forms. III—317
Barkow, A. G. (see Cook, M. J.)—1628(A)
Barnes, R. G. (see Bray, P. J.)—613(A); 1653(A)
Barnes, S. W., D. Miller, J. Ring, G. Giacomelli, R. Summers, and H. R. Childs. Pion-proton elastic-scattering cross sections at 43 Mev and 37½°—673(A)
Barnett, C. F. (see Stier, P. M.)—1630(A)
Barr, T. A. and H. B. Jenkins. Calculation of diffusion coefficients for polystyrenes from measured values of osmotic pressure—1631(A)
Barrett, A. H. and M. Mandel. Microwave spectra of InCl and InBr—666(A)
Barringer, Howard Skelton and William Henry Bancroft, Jr. Secondary emissions from negative-ion bombardment of metal surfaces—1631(A)
Barschall, H. H. (see Becker, R. L.)—1646(A)
Bart, W. L. (see Breazeale, J. B.)—615(A)
Bartholomew, G. A., H. E. Gove, A. E. Litherland, and E. B. Paul. γ radiation from proton bombardment of Mg^{26}—1649(A)
—— (see Gove, H. E.)—1649(A)
—— (see Litherland, A. E.)—644(A)
—— (see Paul, E. B.)—644(A); 1339
Bartnoff, Shepard. Comparison of observed drop-size distributions in clouds and rain with proposed analytical expressions—624(A)
Bashkin, S., R. R. Carlson, and E. B. Nelson. Radiative capture of protons by N^{14}—107
Baskir, Emanuel, John Tinlot, and Sidney Spital. Polarization effects in p-p scattering at 210 Mev—639(A)
Battey, J. F. and R. M. Baum. Electron capture probability of upper Cu acceptor level—624(A)
—— (see Wallis, G.)—625(A)
Baum, R. M. (see Battey, J. F.)—624(A)
Baumann, N. P. (see Krone, R. W.)—1649(A)
Beams, J. W. (see Breazeale, J. B.)—615(A)
—— (see Connelly, J. J., Jr.)—1635(A)
Becker, J. A. Effect of adsorbed H_2 on field-emission current from 310 and 210 planes of W—1643(A)
Becker, R. L., R. B. Perkins, and H. H. Barschall. Total neutron cross sections of light elements—1646(A)
—— (see Walton, R. B.)—1649(A)
Becker, Stewart. Paramagnetic resonance at low fields—1681
Bedo, D. E. and D. H. Tomboulian. Dispersion electrons and refractive index in soft x-ray region—624(A)
Beeman, W. W. (see Neynaber, R. H.)—615(A)
Beiser, A. (see Soberman, R. K.)—608(A)
Belinfante, F. J. Flat picture of curved space—662(A)
Bell, R. E. (see Graham, R. L.)—1646(A)
Benczer, N. (see Farrelly, B.)—1440
—— (see Lidofsky, L. J.)—658(A)
Bendel, W. L., M. E. Toms, and R. A. Tobin. Photoproduction of Pb^{207m}—672(A)
Bender, R. S. (see McGruer, J. N.)—632(A)
Benson, C. B. and A. C. H. Hallett. Damping of oscillations of sphere by liquid He II at large amplitudes—1660(A)
Bent, R. D., T. W. Bonner, J. H. McCrary, W. A. Ranken, and R. F. Sippel. γ rays from deuteron bombardment of Be^9, B^{10}, N^{14}, and F^{19}—710
Berger, Martin J. and John A. Doggett. Monte Carlo calculation of response of NaI(Tl) scintillation spectrometers—663(A)
Bergman, Peter G. Peierls' introduction of canonical transformations into Lagrangian formalism—676(A)
—— **and Joel L. Lebowitz.** New approach to nonequilibrium processes—578
—— (see Newman, Ezra)—587
Berko, S. and A. J. Zuchelli. Quenching of long lifetime component of positron annihilation in benzene—1652(A)
Berlin, T. H. (see Ford, J.)—638(A)
Berlincourt, Ted G. de Haas-van Alphen effect in As—1716
—— (see Overton, W. C., Jr.)—1165
Berman, Arthur I. (see Barber, W. C.)—59
—— (see Brown, K. L.)—665(A)
—— (see Niestlie, John W., Jr.)—612(A)
Bernier, J. P., H. E. Johns, and D. V. Cormack. Calorimetric method for direct determination of energy locally absorbed in irradiated material—1640(A)
Bernstein, E. M. and H. W. Lewis. Internal conversion electrons from electric excitation—617(A)
Bernstein, Jeremy and Abraham Klein. Electromagnetic properties of deuteron. I. Charge density and quadrupole moment—966
Bernstein, S. (see Dabbs, J. W. T.)—1652(A)
Berry, H. W. Scattering of fast Ne atoms in Ne gas—553
Berson, Solomon A. (see Yalow, Rosalyn S.)—342(A)
Bes, D. R. (see Mallmann, C. A.)—7
Bickford, L. R., Jr., J. Pappis, and J. L. Stull. Magnetostriction and permeability of magnetite and Co-substituted magnetite—1210
Biedenharn, L. C. Quantum calculation of Coulomb excitation—629(A)
Bigeleisen, Jacob. Statistical mechanics of isotopic systems with small quantum corrections—638(A)
Bigelow, J. H. (see Aron, W.)—629(A)
Bigham, C. B., K. W. Allen, and E. Almqvist. Energy levels of B^{13}, C^{13}, C^{14}, and F^{19}—631(A)
—— (see Allen, K. W.)—631(A)
—— (see Almqvist, E.)—631(A)
Bills, D. G. and F. G. Allen. Ultra-high vacuum valve—646(A)
——, **F. G. Allen, and N. P. Carleton.** Measurement of pumping speed of ionization gauge—1662(A)
—— (see Carleton, N. P.)—1662(A)
Binder, D. and W. J. Sturm. Annealing process in neutron-irradiated LiF—603(L)
Biondi, Manfred A. Infrared absorption of Cu and Ag at 4.2°K—1647(A)
—— (see Chanin, Lorne M.)—1658(A)
—— (see Rogers, William A.)—1657(A)
Birchenall, C. E. (see Juenker, D. W.)—657(A)
Birge, Robert W. Current experimental work on Bevatron—1623(T)
——, **Roy P. Haddock, Leroy T. Kerth, James R. Peterson, Jack Sandweiss, Donald H. Stork, and Marian N. Whitehead.** Bevatron K-mesons—329(L)
—— (see Kerth, L. T.)—641(A)
Birkhoff, R. D., A. W. Blackstock, and R. H. Ritchie. Mean free path for discrete electron energy losses in metallic foils—647(A)
Birks, J. B. First-order magnetic anisotropy constants of ferrites—1821
Birnbaum, G. (see Maryott, A. A.)—1886(L)
Birnbaum, W. (see Crandall, W. E.)—631(A)
Bitler, W. R. (see Coles, B. R.)—627(A)
Blackstock, A. W. (see Birkhoff, R. D.)—647(A)
Blair, J. S. (see Kerlee, D. D.)—1652(A)
Blakewood, C. H. (see Wheeler, R. G.)—1667
Blatt, F. J. Effect of point imperfections on electrical properties of Cu. I. Conductivity—1708

—— Effect of screening on solute diffusion—600(L)
—— Influence of exchange and correlation on electron transport in metals—1735
Bleuler, E. and H. Morinaga. γ rays from P^{32}, Cl^{34}, and P^{30}—658(A)
—— **and D. J. Tendam.** Elastic scattering of 19-Mev α particles by Al and Cu—1605(L); 1652(A)
—— (see Blue, J. W.)—659(A)
—— (see Thieme, M. T.)—1646(A)
Blevins, M. E., M. M. Block, and E. M. Harth. π^+-p interactions at approximately 500 Mev—1628(A)
Blewett, J. P., N. C. Christofilos, and A. M. Vash. Four-pole permanent-magnet rings for focusing beams of charged particles—652(A)
Blewett, M. Hildred. Design studies for alternating-gradient magnets. I. Field distributions computed by relaxation method—652(A)
Bloch, Ingram. Nuclear shell structure—1623(T)
Bloch, M. (see Sands, M.)—652(A)
Block, Martin M. and Robert Jastrow. A^0–θ^0 ratio in Pb and C—619(A)
——, **E. M. Harth, W. B. Fowler, R. P. Shutt, A. M. Thorndike, and W. L. Whittemore.** Production of heavy unstable particles in p-p collision—261
—— (see Blevins, M. E.)—1628(A)
—— (see Slaughter, G. G.)—1626(A)
Bloom, S. D., C. O. Muehlhause, and H. E. Wegner. Cyclotron energy measurement by time-of-flight—654(A)
Blosser, H. G. (see Cohen, B. L.)—656(A)
Blue, J. W. and E. Bleuler. Decay of Sc^{44}—659(A)
Bockelman, C. K., C. M. Braams, W. W. Buechner, and D. B. Guthe. Angular distribution of proton groups from $Ca^{40}(d,p)Ca^{41}$ reaction—655(A)
Bolotin, Herbert H. and Roger G. Wilkinson. Excited states of Hg^{198}—671(A)
——, **Charles H. Pruett, Paul L. Roggenkamp, and Roger G. Wilkinson.** Excited states of Ce^{140}—62
—— (see Pruett, C. H.)—670(A)
Bömmel, H. E., W. P. Mason, and A. W. Warner, Jr. Experimental evidence for dislocations in crystalline quartz—1894(L)
Bonner, T. W., Alfred A. Kraus, Jr., J. T. Eisinger, and J. B. Marion. Protons from deuteron bombardment of C^{12}—631(A)
—— (see Bent, R. D.)—710
Boorse, Henry A. (see Smith, Bernard)—346; 358; 367
—— (see Worley, R. D.)—447
Bostick, H. A. (see Bandtel, K. C.)—673(A)
Bostrom, Norman A., Emmett L. Hudspeth, and Ira L. Morgan. Excitation curve for $F^{19}(n,\alpha)N^{16}$—643(A)
Bowers, R. Magnetic susceptibility of Na—1640(A)
—— **and N. T. Melamed.** Luminescent centers in ZnS:Cu:Cl phosphors—1781
Bowers, Wayne A. (see Alexander, James D.)—1627(A)
Box, H. C. and A. Russek. Flying-spot microscope and its application to study of cell sizes—341(T)
Boyd, G. E., J. R. Sites, Q. V. Larson, and C. R. Baldock. Production and identification of long-lived Tc isotopes at masses 97, 98, and 99—1030(L)
Bozorth, R. M., Beatrice B. Cetlin, J. K. Galt, F. R. Merritt, and W. A. Yager. Frequency dependence of magnetocrystalline anisotropy—1898(L)
——, **Elizabeth F. Tilden, and Albert J. Williams.** Anisotropy and magnetostriction of some ferrites—1788
Braams, C. M. (see Bockelman, C. K.)—655(A)
Bradley, Joe C. (see Haar, Lester)—638(A)
Bradner, Hugh and Robert E. Donaldson. Asymmetry in high-energy p-n-p double charge-exchange scattering—890
—— (see Donaldson, Robert E.)—892
Braid, T. H. and R. W. Detenbeck. Fast multichannel coincidence circuit—633(A)
Brammer, W. G. (see Neynaber, R. H.)—615(A)
Brannen, Eric, F. R. Hunt, R. H. Adlington, and R. W. Nicholls. Nuclear coincidence techniques applied to optical transitions—1658(A)
Branscomb, L. M. Direct measurement of negative-ion affinities—639(T)
—— (see Smith, S. J.)—1657(A)
Branson, Herman and Nasira F. Ledbetter. Electron impact studies with dimethylamine—1643(A)
Brattain, W. H. (see Garrett, C. G. B.)—376
Braunstein, R. Radiative transitions in semiconductors—1892(L)
Bray, P. J. and R. G. Barnes. Quadrupole resonances in multichlorobenzenes—1653(A)
—— **and R. G. Banes.** Quadrupole resonances of chloro- and bromobenzene derivatives—613(A)
Brazos, J. N. and R. M. Steffen. Dual decay of 50-day In^{114} isomer—1645(A)
—— (see Steffen, R. M.)—1646(A)
Breazeale, J. B., W. L. Bart, and J. W. Beams. Tensile strengths of Ag films of various thicknesses at different temperatures—615(A)
Breit, G. Relativistic corrections for high-energy p-p scattering—1581
—— Theory of nucleon transfer—629(A)
Brennan, J. G. (see Adkins, R.)—706
Brice, M. K. (see Cork, J. M.)—703
Brickwedde, F. G. New definition of Kelvin scale adopted by Tenth General Conference on Weights and Measures—656(T)
Bridge, H. S. (see Altman, L.)—609(A)
—— (see DeStaebler, H., Jr.)—642(A)
Brock, E. G. Field emission observations of phase transformations in Ti—1651(A)
Brockhouse, B. N. Energy distribution of neutrons scattered by paramagnetic substances—601(L)
Brode, Robert B. and Marvin J. Weber. Positive excess of high-energy μ mesons—610(A)
Broida, H. P. Temperature-measurement from molecular band spectra (nonequilibrium)—667(T)
Brolley, J. E., Jr., M. E. Bunker, D. R. F. Cochran, R. L. Henkel, J. P. Mize, and J. W. Starner. 14-Mev (n,α) cross sections in Zr. I.—330(L)
——, **W. C. Dickinson, and R. L. Henkel.** Angular dependence of neutron-induced fission. II—159
——, **and R. L. Henkel.** Angular distribution of fragments from neutron-induced fission of U^{238}—616(A)
—— (see Armstrong, A. H.)—329(L); 330(L)
Bromley, D. A. and N. S. Wall. Elastic scattering of 5-25-Mev protons on Ni and Cu—1029(L)
—— (see Fulbright, H. W.)—654(A)
Brophy, James J. Preliminary study of electrical properties of semiconducting diamond—1336(L)
Brown, Harry A. Calculation of Curie temperatures—1641(A)
—— Calculation of discontinuity in specific heat of Gd—627(A)
Brown, K. L., W. C. Barber, A. I. Berman, and W. D. George. Z-dependence of bremsstrahlung—665(A)
—— (see Barber, W. C.)—59
—— (see Tautfest, G. W.)—664(A)
Browne, C. I. (see Ghiorso, A.)—1048(L)
Browne, C. P. and W. C. Cobb. Energy levels of Na^{23}—644(A)
Brueckner, K. A., R. J. Eden, and N. C. Francis. Nuclear energy level fine structure and configuration mixing—76
Bruner, J. A. (see Fulbright, H. W.)—654(A)

Brysk, H. and M. E. Rose. Theoretical results on orbital capture—649(A)
Bube, Richard H. Infrared quenching and unified description of photoconductivity phenomena in CdS and CdSe—1105
Buechner, W. W., A. Sperduto, and Marcos Mazari. Magnetic analysis of protons from $Al^{27}(d,p)Al^{28}$—644(A)
—— (see Bockelman, C. K.)—655(A)
—— (see Sharp, R. D.)—632(A)
Bunker, M. E., J. P. Mize, and J. W. Starner. Decay of Rh^{106} and Rh^{106m}—659(A)
—— **and J. W. Starner.** Decay of Ti^{51} and Cr^{51}—1906(E)
—— (see Brolley, J. E., Jr.)—330(L)
—— (see Mize, J. P.)—671(A)
Bureau, A. J. (see Hammer, C. L.)—653(A)
Burford, A. O., J. F. Perkins, and S. K. Haynes. Relative intensities of radiations from Hf^{175}—3
Burgeson, J. W. (see Melvin, M. A.)—1663(A)
Burke, Edward, Jr. Isotope shift in first three spectra of B—1839
Burlew, John S. (see Potnis, V. R.)—671(A)
Burnett, C. R. Isotope shift in ionized spectrum of C—623(A)
Burson, S. B., J. M. LeBlanc, and D. W. Martin. Radiations from $_{50}Sn^{125}$ (9.7-day and 9.5-min)—660(A)
—— (see Martin, D. W.)—670(A)
Burstein, E. (see Lipson, H. G.)—1535(A); 444
Burwell, J. R. (see Kim, Y. B.)—642(A)
Butler, J. W. Deuteron capture by O^{16}—643(A)
—— **and H. D. Holmgren.** Energy levels in F^{19}—1649(A)
—— (see Holmgren, H. D.)—655(A)
Byatt, William J. Elastic scattering of slow electrons by atoms—1630(A)

Callaway, Joseph. Electronic energy bands in Fe—500
—— Ferromagnetism of Fe—627(A)
—— Interaction of π^- mesons with light nuclei—1628(A)
Callen, Herbert. Fluctuations and irreversibility—645(T)
Callendine, G. W., Jr. Radioactive isotopes in medicine—339(T)
Callihan, Dixon (see Williams, D. V. P.)—1626(A)
Camac, M., M. L. Halbert, and J. B. Platt. *L*-series x-rays from π-mesonic atoms—905
——, **A. D. McGuire, J. B. Platt, and H. J. Schulte.** *K*-series x-rays from π-mesonic atoms—897
Cameron, A. G. W. Evolution of elemental abundances resulting from neutron capture in stars—1653(A)
—— (see Katz, L.)—98
Caplan, P. J. (see Theissing, H. H.)—624(A)
Capps, R. H. Consequences of gauge invariance for electromagnetic transitions. II—926
—— **and W. G. Holladay.** Electromagnetic properties of nucleon in finite source theory—931
Carbone, R. J. (see Everhart, Edgar)—1287
Caretto, A. A., Jr., and G. Friedlander. Competition between (p,pn) and $(p,2p)$ reactions on Ce^{140}—1649(A)
Carleton, Nathaniel P. New type of lens for charged particles—664(A)
—— **and D. G. Bills.** Derivation relating pumping speed of ionization gauge to quantity of gas pumped—1662(A)
—— (see Bills, D. G.)—1662(A)
Carlson, R. R. (see Bashkin, S.)—107
Carmichael, Hugh and John F. Steljes. Cosmic-ray ionization bursts in unshielded 8-inch pressurized sphere at sea level—1542
Carmichael, J. H. (see Varnerin, L. J., Jr.)—1662(A)
Carothers, J. E. and C. G. Andre. π^+/π^- ratios produced by 340-Mev protons at 0°—651(A)
Carter, R. S., D. J. Hughes, and H. Palevsky. Energy distribution of cold neutrons scattered by lattice vibrations—611(A)
—— (see Harvey, J. A.)—10
Carver, J. G. and T. F. Godlove. Slow-neutron capture resonances in Te, W, and In—1634(A)
—— (see Godlove, T. F.)—1634(A)
Case, K. M. Wave equation for spin 0 in Hamiltonian form—1572
Cassatt, Wayne A. Jr., and W. Wayne Meinke. Decay scheme of Y^{88}—760
Castillo, Horace T. Radio detection of meteors using standard laboratory equipment—339(T)
Castle, J. G., Jr. Systematic g-shift for free electrons—341(A)
Cester, R. (see Kernan, A.)—640(A)
Cetlin, Beatrice B. (see Bozorth, R. M.)—1898(L)
Chamberlain, Joseph W. and Paul H. Roberts. Turbulence spectrum in Chandrasekhar's theory—1674
Chandler, D. C. (see Anderson, D. V.)—1639(A)
Chang, Roger. Relationship between activation energy for slip in crystalline solids and applied stress based on dislocation model—65(A)
—— (see Weissmann, Sigmund)—657(A)
Chanin, Lorne M. and Manfred A. Biondi. Temperature dependence of ionic mobilities: He^+ and He_2^+ in He—1658(A)
Chappelear, John. Photoproduction of mesons in deuterium—254
Chartres, B. A. and H. Messel. Angular distribution in electron-photon showers without Landau approximation—1604(L)
Chase, C. E. and Melvin A. Herlin. Ultrasonic measurements in magnetically-cooled liquid He—669(A)
Chase, David M. Inelastic scattering of nucleons by dynamic nuclear wall—629(A)
Chen, Francis F., Christopher P. Leavitt, and Anatole M. Shapiro. Attenuation cross sections for 860-Mev protons—857
Chesnut, W. G., E. M. Hafner, and R. Harding. Polarization of 210-Mev protons elastically scattered from C—639(A)
—— (see Hafner, E. M.)—639(A)
Chester, G. V. Behavior of Bose system—1062
Chiba, Ren (see McEllistrem, M. T.)—632(A)
Chidley, B. C. (see Johns, M. W.)—1645(A)
Chidley, B. G. and L. Katz. $N^{14}(\gamma,n)$ cross section near threshold—1646(A)
Childers, H. M. and J. D. Graves. Bipartition angles for Compton scattering by free electrons—343
Childs, H. R. (see Barnes, S. W.)—673(A)
Chin, J. (see DeJuren, J.)—191
Choppin, G. R. (see Harvey, B. G.)—337(L)
Chow, Richard H. and Byron T. Wright. Absolute angular distribution of 20-Mev protons elastically scattered by O and N—640(A)
Christensen, R. L. (see Reynolds, J. B.)—613(A)
Christofilos, N. C. (see Blewett, J. P.)—652(A)
Chupp, Warren W., Gerson Goldhaber, Sulamith Goldhaber, Stephen J. Goldsack, Joseph E. Lannutti, Frances M. Smith, and Francis H. Webb. Measurements on *K*-particles from Bevatron—335(L)
——, **Gerson Goldhaber, Sulamith Goldhaber, William R. Johnson, and Joseph E. Lannutti.** *K*-meson mass from *K*-hydrogen scattering event—1042(L)
—— (see Iloff, E. L.)—1617(L)
Chynoweth, A. G. Pyroelectric effect in $BaTiO_3$—1642(A)
—— (see McKay, K. G.)—1648(A)
Clancy, E. F. (see Sampson, John B.)—1657(A)

Clark, A. F. (see Kao, S. K.)—895
Clark, G. Experimental results on arrival times and lateral distribution of air-shower particles—609(A)
Clarke, Edward N. Nature of water-vapor-induced excess current on grown Ge p-n junctions—1656(A); 1899(L)
Clarke, R. L., E. Almqvist, and E. B. Paul. Reaction $P^{31}(p,\alpha)Si^{28}$—654(A)
Cleland, J. W. and J. H. Crawford, Jr. Radiation effects in GaSb—637(A)
——, **J. H. Crawford, Jr., and J. C. Pigg.** Fast neutron bombardment of p-type Ge—1170
Clement, J. D. (see Walton, R. B.)—1649(A)
Cloud, W. M. Isotope shift nonlinearities in spectrum of Cd—623(A)
Cobb, W. C. (see Browne, C. P.)—644(A)
Coburn, Horace H. and Sherman Frankel. Angular correlation measurements in Hg^{197}—671(A)
Cochran, D. R. F. (see Brolley, J. E., Jr.)—330(L)
Cochran, L. W. (see Kern, B. D.)—645(A)
Coester, F. Collective modes in nuclei—170; 648(A)
Cohen, Alvin J. Anisotropic color centers in α quartz—1636(A)
Cohen, Bernard L., H. G. Blosser, D. J. Coombe, G. M. McCormick, and E. Newman. (p,γ), (p,α), (p,He_3), (p,t), and (p,Be^7) cross sections—656(A)
—— **and Eugene Newman.** (p,pn) and $(p,2n)$ cross sections in medium weight elements—718
——, **E. Newman, and T. H. Handley.** $(p,pn)+(p,2n)$ and $(p,2p)$ cross sections in medium weight elements—723
Cohen, David. Proton bremsstrahlung—1629(A)
Cohen, M. H. and F. Keffer. Dipolar ferromagnetism at 0°K—1135
—— **and F. Keffer.** Dipolar sums in primitive cubic lattices—1128
Cohn, Hans O., J. K. Bair, J. D. Kington, and H. B. Willard. $Si^{28}(p,p'\gamma)Si^{28}$ reaction—644(A)
—— **and J. L. Fowler.** Elastic scattering of neutrons from Ne—1625(A)
—— (see Kington, J. D.)—1393
Coleman, G. H. and H. A. Tewes. Nuclear reactions of Cu with various high-energy particles—288
Coles, B. R. and W. R. Bitler. Effect of Al on saturation magnetic moments of Fe-Co alloys—627(A)
—— (see Taylor, J. C.)—614(A)
Colgate, Stirling A. Prediction of auroral γ rays—665(A)
Collington, D. J., A. N. Dellis, J. H. Sanders, and K. C. Turberfield. Magnetic moment of proton—1622(L)
Connelly, J. J., Jr., O. R. Harris, and J. W. Beams. Effect of centrifugal field on rate of diffusion in metals—1635(A)
Conwell, E. M. Hall effect and density of states in Ge—1195
Cook, M. J., K. Z. Morgan, and A. G. Barkow. Validity of current practice of using single-exposure date to calculate maximum permissible concentrations in air and water for continuous exposure to radioisotopes—1628(A)
Cook, W. S. (see Crysdale, J. H.)—1638(A)
Coombe, D. J. (see Cohen, B. L.)—656(A)
Coomes, E. A. (see Baldwin, G. J.)—1650(A)
——(see Davey, J. E.)—1651(A)
Cooper, John N. (see Milani, S.)—645(A)
—— (see Seiler, Milton R.)—340(A)
—— (see Smith, Robert T., Jr.)—340(A)
Corak, W. S. and C. B. Satterthwaite. Atomic heat of Sn in normal and superconducting states—1660(A)
—— (see Satterthwaite, C. B.)—1660(A)
Corbett, James W. and W. W. Watson. Maximizing separation factor of thermal diffusion column—634(A)
—— (see Schwartz, Robert, B.)—655(A)
Cork, J. M., M. K. Brice, and L. C. Schmid. Energies of radiations from Co^{57} and Co^{58}—703
—— (see Martin, D. W.)—670(A)
Cormack, D. V. (see Bernier, J. P.)—1640(A)
Corson, Dale R., William S. McDonald, and Vincent Z. Peterson. Neutral meson photoproduction at forward meson angles—652(A)
—— (see Davis, H. L.)—273
Couchman, James and C. D. Curtis. FM multichannel pulse-height analyzer—1626(A)
Courant, E. D. Nonlinearities in alternate-gradient synchrotron—652(A)
Courant, H. Associated photons in K-particle decays observed with multiplate cloud chamber—282
Cowan, Clyde L. Detection of neutrino—progress report—1623(T)
Cox, S. A. and R. M. Williamson. Angular distributions and angular correlations in $Be^9(d,p)Be^{10}$, and $B^{10}(d,p)B^{11}$—631(A)
—— (see Williamson, R. M.)—644(A)
Crandall, W. E., W. Birnbaum, G. P. Millburn, and R. V. Pyle. $C^{13}(p,pn)C^{12}$ cross section for 340-Mev protons—631(A)
Crane, W. W. T. (see Higgins, G. H.)—183
Crawford, G. J. B. Spin echoes with four pulses—600(L)
Crawford, G. W. (see Kendrick, N. S., Jr.)—1631(A)
—— (see Miller, J. E.)—1631(A)
Crawford, J. H., Jr., H. C. Schweinler, and D. K. Stevens. Magnetic indications of electronic structure of conduction band in Ge—1330(L)
—— (see Cleland, J. W.)—1170; 637(A)
—— (see Stevens, D. K.)—487
Crawford, M. F. Nuclear configurations from isotope shifts—1637(T)
Crawford, R. C. (see Harrison, G. R.)—1629(A)
Cross, W. G. and R. G. Jarvis. Elastic scattering of 14.6-Mev neutrons—621(A)
Crowe, K. M. Photopion production from nuclei—620(T)
——, **R. M. Friedman, and Hans Motz.** π^+ photoproduction in C—673(A)
——, **R. H. Helm, and G. W. Tautfast.** Preliminary data on measurement of $\mu^+ - \beta^+$ decay spectrum—872
—— (see Friedman, R. M.)—672(A)
—— (see Helm, R. H.)—650(A)
—— (see Motz, Hans)—673(A)
Crysdale, J. H., J. W. B. Day, and W. S. Cook. Experimental investigation of diffraction of electromagnetic waves by dominating ridge—1638(A)
Culler, Vaughn and R. W. Waniek. Total cross sections for high-energy neutrons—740
Cumming, James B. New Zn isotope, Zn^{65}—1645(A)
Curtis, C. D. (see Couchman, James)—1626(A)
Cutler, M. Forward characteristic of Ge point contact rectifiers—625(A)
Cutler, W. G., R. W. Schiessler, and W. Webb. Study of compressions of several high molecular weight hydrocarbons—638(A)

Dabbs, J. W. T., L. D. Roberts, and S. Bernstein. Direct polarization of In^{115} nuclei; J-value for 1.458 ev resonance—1652(A)
Daggett, E. H. and G. R. Grove. γ-ray spectrum of Po^{208}—1
Dahler, J. and J. O. Hirschfelder. Improved symmetrized cell theory of liquids—637(A)
Dalgarno, A. and G. W. Griffing. Quantum mechanical calculation on stopping cross section of H atoms for protons—1653(A)

Dalitz, R. H. Charge independence in light hyperfragments —1475
—— Pion production in electron-proton collisions—618(A)
—— Radiative τ-meson decay—915
—— **and F. J. Dyson.** Renormalization in new Tamm-Dancoff theory of meson-nucleon scattering—301
—— (see Kalos, M. H.)—617(A)
Dally, E. (see Klingensmith, R.)—340(A)
Danner, H. and R. Pepinsky. Specific heat anomaly of ferroelectric Cd niobate at Curie temperature—1215
Darden, S. E. Determination of strength function of nuclear energy levels—748
Darnell, F. J. and S. A. Friedberg. Magnetoresistance in Ge at low temperatures—636(A)
Das, T. P. and D. K. Roy. Spin-echoes with four pulses—an extension to n pulses—1906(E)
Dash, J. G. and R. Dean Taylor. Transition temperatures of He^3–He^4 solutions—598(L)
Dash, W. C. and R. Newman. Intrinsic optical absorption in single-crystal Ge and Si at 77°K and 300°K—1151
Daubin, Scott C. and Donald R. Hamilton. Perturbed γ-γ directional correlation in Cd^{114}—683
Davey, J. E. and E. A. Coomes. Thermionic properties of Th on W single crystals—1651(A)
Davidson, P. M. Growth of current between parallel plates —1072
Davis, H. L. and D. R. Corson. Elastic photo-production of π^0 mesons from deuterium at 270 Mev—273
Davis, R. E. (see Adams, E. N.)—625(A)
Davis, R. W. (see Ribe, F. L.)—331(L)
Davis, Raymond, Jr. Attempt to detect neutrinos by reaction $Cl^{37}(\bar{\nu},e^-)A^{37}$—664(A)
Dawson, W. K. Angular and energy distributions of photoprotons from Al, Cu, Rh, and Au—1648(A)
Day, J. W. B. (see Crysdale, J. H.)—1638(A)
Dean, Donald E. Using snooperscope tube with spectrometer —341(A)
DeBenedetti, S. (see Lang, G.)—596(L)
Dedrick, K. G. Deuteron-model calculation of high-energy nuclear photoeffect—1654(A)
Dehmelt, H. G. Atomic phosphorus paramagnetic resonance experiment employing universal dissociator—527
DeJuren, J. and J. Chin. Mn thermal neutron activation cross section—191
Dekker, A. J. Secondary electron emission and color centers —1647(A)
Dellis, A. N. (see Collington, D. J.)—1622(L)
de McMillan, Clara M. (see Mallmann, C. A.)—7
Demers, P. Work done with nuclear emulsions at Université de Montréal—1645(T)
Dempster, J. R. H. Simple results of Feynman field theory —674(A)
Denney, J. M. Magnetic susceptibility of Ti and substitutional Ti alloys—1640(A)
De Pangher, John. n-p scattering at 300 Mev—1447
Derbyshire, W. D. (see Yearian, H. J.)—626(A)
der Mateosian, E. (see Scharff-Goldhaber, Gertrude)—180
Desai, U. D. (see Sarabhai, V.)—1490
de Saussure, Gerard and L. S. Osborne. Elastic photoproduction of π^0 mesons in He and (γ,π) reaction on He at high energies—843
Deser, S. Functional integrals and adiabatic limits in field theory—325
d'Espagnat, Bernard and Jacques Prentki. Possible mathematical formulation of Gell-Mann model for new particles —328(L)
Dessler, Alexander J. and William M. Fairbank. Amplitude dependence of velocity of second sound—669(A)
DeStaebler, H., Jr., H. S. Bridge, B. Rossi, and B. V. Sreekantan. Recent results on S-particles—642(A)
Detenbeck, R. W. (see Braid, T. H.)—663(A)
Deutsch, M. (see Greenberg, J. S.)—665(A)
de Waard, H. Lifetime of 279-kev excited state of Tl^{208}—1045(L)
DeWire, J. W. (see Wolfe, B.)—268
Dexter, R. N. and Benjamin Lax. Microwave magnetoconductivity effects in InSb—635(A)
Diamond, H. (see Ghiorso, A.)—1048(L)
Dicke, R. H. (see Romer, R. H.)—532
Dickinson, W. C. (see Brolley, J. E., Jr.)—159
Dienes, G. J. (see Antal, J. J.)—1081
Dillon, J. A., Jr., and H. E. Farnsworth. Work function of (100) face of Ge single crystal as function of heat treatment and ion bombardment—1643(A)
Dingle, R. B. Theory of infrared absorption by carriers in semiconductors—1901(L)
Ditto, Steve J. (see Gordy, Walter)—1905(L)
Dixon, W. R. Energy and angular distributions of photoneutrons—1646(A)
—— (see Trainor, L. E. H.)—1655(A)
Dobrowolsky, W. (see Jones, R. V.)—646(A)
Doerner, R. K. and A. H. Weber. Internal conversion coefficients of Tl^{205} (parent, Hg^{205})—672(A)
Doggett, John A. (see Berger, Martin, J.)—663(A)
Donaldson, Robert E. and Hugh Bradner. Asymmetry in p-n and p-p scattering from targets bombarded with 285-Mev polarized protons—892
—— (see Bradner, Hugh)—890
Douglas, A. E. Recent work on ultraviolet spectra of simple molecules—1648(T)
Douglas, R. A. (see McEllistrem, M. T.)—632(A)
Downs, J. W. (see Kurbatov, J. D.)—340(A)
Drell, S. D. Nuclear radius and nuclear forces—619(A)
—— **and Kerson Huang.** Proton bremsstrahlung—686
—— **and L. Verlet.** Multiple scattering corrections in π^0-deuteron scattering—849
—— (see Huang, Kerson)—628(A)
Driscoll, Raymond L. Determination of current in absolute measure—634(A)
Dropesky, Bruce J. (see Sheline, Raymond K.)—1055(L)
Drosd, Ralph D. Gated multiple light pulse generator—1662(A)
Drummond, J. E. Masses of light nuclei. Method for correcting table of masses for new data—709
Duckworth, H. E. Present status of atomic-mass measurements—1638(T)
Dugdale, J. S. and D. K. C. MacDonald. Vibrational anharmonicity and lattice thermal properties—1905(E)
Dye, David L. Momentum spectrum from scattering in Pb of sea level penetrating shower secondaries—1458
Dyke, W. P., J. P. Barbour, E. E. Martin, and J. K. Trolan. T-F emission: experimental measurement of average electron current density from W—1192
Dyson, Freeman J. Second maximum in negative pion scattering cross section—1037(L)
—— **and H. Uberall.** Anisotropy of bremsstrahlung and pair production in single crystals—604(L)
—— (see Dalitz, R. H.)—301

Eades, R. G. Nuclear magnetic resonance spectrum of Al^{27} in euclase—1652(A)
Ebel, M. E. and M. H. Hull, Jr. Phase shifts for relativistic corrections in high-energy p-p scattering—1596
Eden, R. J. Nuclear saturation: Generalized Hartree-Fock method—1418
—— (see Brueckner, K. A.)—76
Eguchi, Tetsuo. Anomalous τ-meson decay—619(A)

Eichholz, G. G. Haeffner effect in Hg—1635(A)
Einbinder, Harvey. Expansion of two-dimensional wave fields in powers of $1/\rho$—676(A)
Eisberg, R. M., G. Igo, and H. E. Wegner. Elastic scattering of 40-Mev α particles from Al—1606(L)
—— (see Wegner, Harvey E.)—640(A); 825
Eisenschitz, R. "Virial theorem" for flow of energy—1059
Eisenstein, J. C. (see McCrum, N. G.)—1326(L)
Eisinger, J. T. (see Bonner, T. W.)—631(A)
Eisner, M. Canonical transformations of pseudovector field—675(A)
Ellis, J. A., M. B. Gottlieb, and L. H. Meredith. Double Geiger-tube study of soft radiation at northern latitude—609(A)
Ellis, Robert A. High-altitude rocket measurements with scintillation counters at northern latitudes—609(A)
—— (see McDonald, F. B.)—609(A)
Ellis, Robert E. and Larry Schecter. Elastic scattering of 48.2-Mev α particles—1044(L)
El-Mofty, Osman and Mohamed El-Nadi. Multiple meson production theories applied to cosmic-ray showers—921
El-Nadi, Mohamed (see El-Mofty, Osman)—921
El-Sum, Hussein M. A. and Albert V. Baez. Preliminary experiments on x-ray microscopy by reconstructed wave fronts—624(A)
Elwyn, Alexander J. (see McFarland, Charles E.)—655(A)
Engelkemeir, D. and L. B. Magnusson. Observation of 193-millimicrosecond metastable level in Pu^{239}—135
Epstein, S. (see Juretschke, H. J.)—636(A)
Evans, J. E. (see Joki, E. G.)—610(A)
—— (see Smith, M. S.)—611(A)
Everhart, Edgar, Gerald Stone, and R. J. Carbone. Classical calculations of differential cross section for scattering from Coulomb potential with exponential screening—1287

Fafarman, A. and M. H. Shamos. Mesonic x-rays from capture of cosmic-ray μ mesons in chemical compound—623(A)
Fairbank, William M. (see Dessler, Alexander J.)—669(A)
Falkoff, D. L. Noise fluctuations and irreversible processes—1657(A)
Fan, H. Y. (see Spitzer, W. G.)—1893(L)
Fang, P. H. Reciprocity theory of elementary particles—1658(A)
Fano, U. Application of operator calculus to irreversibility—660(A)
Faragó, P. S. and G. Marx. Quantum effects in interaction between free electrons and electromagnetic fields—1063
Farmer, Donald J. Decay of neutron-deficient Rh isotopes—659(A)
Farnsworth, H. E. Adsorption measurements using ion-bombardment cleaning and low-energy electron-diffraction techniques—1642(T)
—— (see Dillon, J. A., Jr.)—1643(A)
Farrelly, B., L. Koerts, N. Benczer, R. van Lieshout, and C. S. Wu. Radiations from Sb^{120}—1440
Farwell, G. W. (see Kerlee, D. D.)—1652(A)
Feenberg, Eugene. Superallowed β transitions in $N-Z=3$ series—71
—— (see Goldhammer, P.)—648(A)
Ferguson, A. J. and A. E. Litherland. Analysis of triple angular correlations in nuclear bombardment experiments—1654(A)
Ferrell, Richard A. Angular dependence of characteristic energy loss of electrons passing through metal foils—647(A)
—— (see Visscher, William M.)—649(A)
Feuer, Paula. Electronic states in perturbed periodic lattice—1092
Fey, R. L. and W. J. Graham. Ambipolar diffusion in Xe at 3-cm wavelength—1658(A)
Feynman, R. P. Theory of liquid He—656(T)
Fields, P. R. (see Ghiorso, A.)—1048(L)
Findley, Leon (see Koenigsberg, Ernest)—615(A)
Finkelstein, David. Dynamics of Klein particle—649(A)
Firth, K. (see Hunt, S. E.)—786
Fischbach, D. B. and A. S. Nowick. Deformation-induced charge flow in NaCl crystals—1333(L)
Fischer, Vera Kistiakowsky. Metastable states in Re^{180}, Ir^{181}, Au^{189}, Pb^{201}, and Pb^{209}—672(A); 764
—— (see Lidofsky, L. J.)—658(A)
Flanders, P. J. (see Otter, F. A., Jr.)—599(L)
Fleishman, B. A. One-dimensional dispersion of mass by molecular and turbulent diffusion—634(A)
—— (see Rubin, Robert J.)—656(A)
Fletcher, P. C. and L. C. Aamodt. Nuclear magnetic moment and mass of Cl^{38}—613(A)
Fletcher, W. H. (see Herndon, John A.)—1624(A)
Fluharty, R. G. (see Simpson, F. B.)—610(A)
Foldy, L. L. (see Nigam, B. P.)—675(A)
Foner, Simon. Hall effect in permalloys—1079
——, **H. J. Zeiger, R. L. Powell, and Benjamin Lax.** Microwave magnetoconductivity bridge for semiconductors—635(A)
Ford, J. and T. H. Berlin. Einstein-Bose gas below critical temperature—638(A)
Ford, Kenneth W. (see Hill, David L.)—649(A)
—— (see Levinson, Carl)—792
Forkman, Bengt (see Johansson, Sven A. E.)—1031(L)
Forrester, A. Theodore, Richard A. Gudmundsen, and Philip O. Johnson. Photoelectric mixing of incoherent light—1691.
Forstat, Harold and Charles A. Reynolds. Heat transfer in fine channels of He II—669(A)
Forster, H. H. and J. S. Wiggins. Radioactive decay of Cs^{134}—660(A)
Forster, Kurt H. Green's function for heat conduction-convection problems with given motion of boundaries—660(A)
Forsyth, P. A. Scattering of radio waves from aurora and meteors—1637(T)
—— (see Hines, C. O.)—1638(A)
Foster, J. S. Summary of recent research in physics at McGill University—1644(T)
Foster, K. W. (see Grove, G. R.)—340(A)
Fowler, J. L. (see Cohn, Hans O.)—1625(A)
Fowler, T. K. and J. I. Hopkins. Investigation of α resonances in Al—1629(A)
Fowler, W. A. (see Webb, T. S.)—138
Fowler, W. B. (see Block, M. M.)—261
Francis, N. C. (see Brueckner, K. A.)—76
Frank, R. M. and J. L. Gammel. Elastic scattering of protons by He^3 and T—1406
Frankel, Sherman. Effect of spin-orbit interaction on photonuclear electric dipole absorption—169
—— (see Coburn, Horace H.)—671(A)
Freden, Stanley C. and Harold K. Ticho. Capture of negative K mesons—1057(L)
Frederikse, H. P. R. and Eugenie V. Mielczarek. Thermoelectric power of InSb—1889(L)
Freedman, M. S., F. T. Porter, T. B. Novey, and F. Wagner, Jr. Nonunique first forbidden β transitions in Re^{186}—671(A)
—— (see Porter, F. T.)—671(A)
Freedman, S. J. (see Juretschke, H. J.)—636(A)
Freeman, Burton E. (see Hill, David L.)—649(A)
Freeman, Joan M. Inelastic neutron scattering in F^{19}—1446

Fregeau, Jerome H. and Robert Hofstadter. High-energy electron scattering and nuclear structure determinations. III. C^{12} nucleus—1503
Freier, P. S. (see Naugle, J. E.)—609(A)
French, J. B., E. C. Halbert, and Sudhir P. Pandya. Intermediate coupling shell model for Be^9—1387
Fretter, W. B., E. W. Friesen, G. E. Kepler, and L. Lagarrigue. Momentum and ionization measurements on charged V-particles—642(A)
Fried, Burton D. Covariant calculations of polarization in nucleon-nucleon scattering—675(A)
Fried, S. M. (see Ghiorso, A.)—1048(L)
Friedberg, S. A. (see Darnell, F. J.)—636(A)
Friedlander, G., J. Hudis, and R. L. Wolfgang. Disintegration of Al by protons in energy range 0.4 to 3.0 Bev —263
—— (see Caretto, A. A., Jr.)—1649(A)
Friedman, Abraham S. and Irwin Oppenheim. Statistical mechanical calculation of data of state of He isotopes at intermediate temperatures and densities—638(A)
—— (see Haar, Lester)—638(A)
Friedman, Jerome I. Phenomenological evidence for polarization of 310-Mev protons by elastic scattering in G5 emulsion—1047(L)
Friedman, M. H. and T. D. Lee. Scattering of pions by nucleons in intermediate coupling—618(A)
Friedman, R. M., K. M. Crowe, and Hans Motz. Pion pair production by photons—672(A)
—— (see Crowe, K. M.)—673(A)
—— (see Motz, Hans)—673(A)
Friesen, E. W. (see Fretter, W. B.)—642(A)
Fritzsche, H. Electrical properties of Ge semiconductors at low temperatures—406
—— **and K. Lark-Horovitz.** Electrical properties of p-type InSb at low temperatures—400
Frood, D. G. and J. R. Wait. Investigation of slot radiators in rectangular metal plates—1639(A)
Frost, R. T. and S. S. Hanna. α spectrum in decay of Li^8 —8
Fry, W. F., J. Schneps, G. A. Snow, and M. S. Swami. $\pi-\mu$ decay with associated electron pair—1055(L)
——, **J. Schneps, and M. S. Swami.** Disintegration of hyperfragments—1561
Frye, G. M., Jr., L. Rosen, and L. Stewart. Disintegration of C into three α particles by 12-20-Mev neutrons—1375
Fulbright, H. W. Variable-energy cyclotron at University of Rochester—1634(T)
——, **D. A. Bromley, and J. A. Bruner.** 8-Mev variable-energy cyclotron—654(A)
Fuller, C. S. and Howard Reiss. Ionization and solubility of impurities in semiconductors—624(A)
Fuller, E. G. Elastic scattering of photons from 5 to 30 Mev —639(T)
Furr, A. K. (see Rohrer, R. H.)—1626(A)
Fuson, Nelson, Marie-Louise Josien, and James R. Lawson. Effect of sample preparation upon infrared spectra of polynuclear hydrocarbons—1625(A)

Gaizauskas, V. and H. L. Welsh. Infrared absorption in gaseous, liquid, and solid CO_2 induced by intermolecular forces—1639(A)
Gallagher, J. D. (see Koontz, P. G.)—664(A)
Galonsky, A. and M. T. McEllistrem. Energy levels of Li^8 from deuteron-He differential cross sections—1906(E)
Galt, J. K. (see Bozorth, R. M.)—1898(L)
—— (see Yager, W. A.)—1203
Gammel, J. L. (see Frank, R. M.)—1406
Garfunkel, M. P. and L. J. Varnerin, Jr. Anomalous skin effect at low frequencies—1647(A)
Garrett, C. G. B. and W. H. Brattain. Physical theory of semiconductor surfaces—376
Garrido, L. (see Waniek, R. W.)—622(A)
Garstens, M. A. and J. I. Kaplan. Low-field magnetic resonance—459
Gartenhaus, S. Two-nucleon potential from cutoff Yukawa theory—619(A)
Geballe, T. H. (see Hrostowski, H. J.)—626(A)
—— (see Morin, F. J.)—467
Geffen, D. A. Simple nonrelativistic model for single meson production—1534
Geiger, Felix E., Jr. F' and K centers in additively colored KCl crystals—1075
Geiger, J. S. (see Graham, R. L.)—1646(A)
—— (see Hughes, V. W.)—666(A); 1842
Geiger, K. W. Neutron production by cosmic rays—1645(A)
Geller, S. Crystal structure of gadolinium orthoferrite, $GdFeO_3$—1641(A)
George, W. D. (see Barber, W. C.)—59
—— (see Brown, K. L.)—665(A)
Geusic, Joseph E. and Dudley Williams. Hfs in paramagnetic resonances in solutions of manganous salts—612(A)
Ghiorso, A. Transuranium elements—664(T)
——, **S. G. Thompson, G. H. Higgins, G. T. Seaborg, M. H. Studier, P. R. Fields, S. M. Fried, H. Diamond, J. F. Mech, G. L. Pyle, J. R. Huizenga, A. Hirsch, W. M. Manning, C. I. Browne, H. L. Smith, and R. W. Spence.** New elements einsteinium and fermium, atomic numbers 99 and 100—1048(L)
—— (see Harvey, B. G.)—337(L)
Giacomelli, G. (see Barnes, S. W.)—673(A)
Gianola, U. F. Noise characteristics of Si photovoltaic junctions—1656(A)
Gibbons, M. D. (see Stout, V. L.)—1643(A)
Giles, Frederick H. Use of characteristic curves in study of electrochemical systems—340(A)
Gilleo, M. A. Magnetic properties of $GdFeO_3$ crystal—1641(A)
Gilvarry, J. J. and G. H. Peebles. Solutions of temperature-perturbed Thomas-Fermi equation—550
Glasser, R. G., D. M. Haskin, Marcel Schein, and J. J. Lord. Analysis of properties of secondary particles in nucleon-nucleon collisions at very high energy—1555
—— (see Schein, Marcel)—643(A)
Glauber, R. J. Cross sections in deuterium at high energies —630(A)
—— Deuteron stripping processes at high energies—1515
—— (see Shapiro, I. I.)—629(A)
Glaubman, Michael J. Fast favored first forbidden β transition—659(A)
Glover, F. N. (see Barker, W. A.)—317
Glover, R. N. (see McNair, A.)—771
Godlove, T. F. and J. G. Carver. Neutron time-of-flight spectroscopy with linear electron accelerator—1634(A)
—— (see Carver, J. G.)—1634(A)
Gold, Louis. Hall theory in n-type Ge—596(L)
—— **and Laura M. Roth.** Galvanomagnetic theory of n-Ge and Si in saturation limit—1655(A)
Goldberg Colman (see Adams, E. N.)—625(A)
Goldberg, Irwin and Allen Janis. Transformation groups in configuration space—676(A)
Goldberg, Joshua N. Gravitational radiation—1873
Goldberger, Marvin L. Causality conditions and dispersion relations. I. Boson fields—979
——, **H. Miyazawa, and R. Oehme.** Application of dispersion relations to pion-nucleon scattering—986
Goldburg, W. I. Angular distribution of γ's from Coulomb excitation of thin Pt—617(A)

Goldemberg, J. and J. Leite Lopes. Shell effect on photonuclear reactions—1053(L)
Goldhaber, Gerson (see Chupp, Warren W.)—335(L); 1042(L)
—— (see Iloff, E. L.)—1617(L)
Goldhaber, Sulamith (see Chupp, Warren W.)—335(L); 1617(L)
—— (see Iloff, E. L.)—1617(L)
Goldhammer, P. and E. Feenberg. Coupling of $2s_{\frac{1}{2}}$ and $1d_{\frac{3}{2}}$ orbitals—648(A)
Goldman, J. E. (see Arrott, Anthony)—1641(A)
—— (see Pugh, Emerson William)—1641(A)
Goldsack, Stephen J. (see Chupp, Warren W.)—335(L)
Goloskie, R. (see Waniek, R. W.)—622(A)
Good, R. H., Jr. (see Murphy, E. L.)—1650(A)
Good, William B. (see Ruark, Arthur E.)—1628(A)
Goodman, B. B. (see Satterthwaite, C. B.)—1660(A)
Goodman, Clark (see Miyatake, Osamu)—1040(L)
Goodman, L. S. and S. Wexler. Nuclear spin and magnetic moment of 3.1-hr Cs^{134m}—192
Goodrich, Max (see Rojo, Onofre)—1629(A)
Gora, E. K. Microwave spectrum of ozone molecule—666(A)
Gordon, J. P. Hfs in inversion spectrum of $N^{14}H_3$ by a new high-resolution microwave spectrometer—1253
——, **H. J. Zeiger, and C. H. Townes.** The maser—new type of microwave amplifier, frequency standard, and spectrometer—1264
Gordon, M. M. Stripping theory and $Be^9(d,p)Be^{10}$ reaction—1625(A)
Gordy, Walter, Steve J. Ditto, James H. Wyman, and Roy S. Anderson. Three-millimeter wave radiation from sun—1905(L)
—— (see Ard, William B., Jr.)—612(A)
Gossett, C. R. (see Phillips, G. C.)—655(A)
—— (see Schiffer, J. P.)—655(A)
Gottlieb, M. B. (see Ellis, J. A.)—609(A)
—— (see McDonald, F. B.)—609(A)
—— (see Meredith, L. H.)—198
Gove, H. E. Elastic scattering of protons, deuterons, and α particles from heavy elements—1353
—— Measurements of properties of light nuclei, using Chalk River accelerator—1638(T)
——, **A. E. Litherland, E. B. Paul, and G. A. Bartholomew.** γ rays from reaction $Mg^{25}(p,p'\gamma)$—1649(A)
—— (see Bartholomew, G. A.)—1649(A)
—— (see Litherland, A. E.)—644(A)
—— (see Paul, E. B.)—644(A); 1339
Gow, James D. (see Ruby, Lawrence)—663(A)
Gowan, E. H. Ozone measurements over Edmonton (lat. N. 53°34′, long. W. 113°31′) 1951 to 1954—1637(A)
Graham, Martin. Precision vibrating-coil magnetic-gradient recorder—653(A)
Graham, R. L., R. E. Bell, L. Yaffe, and J. S. Geiger. Thermal neutron capture cross section of Au^{198} and half-life of 209-kev state in Hg^{199}—1646(A)
Graham, W. J. (see Fey, R. L.)—1658(A)
Grattidge, Walter. Properties of iron oxide-alumina system—1643(A)
Graves, J. D. (see Childers, H. M.)—343
Gray, Ernest P., Robert W. Hart, and William H. Guier. Statistical theory of atomic excitation by electron impact. II. Application to H and He—1661(A)
—— (see Hart, Robert W.)—1661(A)
Green, Alex E. S. Particle binding energies and diffuseness of nuclear boundary—1410
—— Particle binding energies in diffuse boundary IPM—1627(A)
—— **and Kiuck Lee.** Energy eigenvalues for spherical well with exponentially diffuse boundary—772
—— (see Lee, Kiuck)—1627(A)
—— (see Salacz-Dohnanyi, Julius)—1627(A)
—— (see Zankel, Kenneth L.)—1628(A)
Green, R. B. Theory of slip-band formation—1635(A)
Greenberg, J. Mayo. Scattering approximations using plane wave trial functions—630(A)
Greenberg, J. S. and M. Deutsch. Internal pair creation in negatron decay—665(A)
Greenberg, O. W. and A. S. Wightman. Re-examination of neutrino theory of light—675(A)
Griem, H. and S. F. Singer. Geomagnetic albedo at rocket altitudes at equator—608(A)
Griffin, James J. Variational approach to collective nuclear behavior—648(A)
Griffing, D. F. (see Wheatley, J. C.)—334(L)
Griffing, G. W. (see Dalgarno, A.)—1653(A)
Grilly, E. R. (see Mills, R. L.)—480
Gross, E. P. Theory of magnetic resonance saturation—622(A)
—— (see Lebowitz, Joel L.)—623(A)
Grosskreutz, J. C. Angular distribution of protons from $O^{18}(d,p)O^{17}$ reaction as function of bombarding energy—643(A)
—— (see Weller, C. E.)—655(A)
Grove, G. R. and L. N. Russell. Emission constant of Ac^{227}—340(A)
——, **K. W. Foster, and R. E. Vallee.** Gaseous thermal diffusion—340(A)
—— (see Daggett, E. H.)—1
Gudmundsen, Richard A. (see Forrester, A. Theodore)—1691
Guier, William H. (see Gray, Ernest P.)—1661(A)
—— (see Hart, Robert W.)—1661(A)
Gunn, S. R. (see Higgins, G. H.)—183
Gupta, Suraj N. Multiple bremsstrahlung—1015
Guthe, D. B. (see Bockelman, C. K.)—655(A)

Haar, Lester, Joe C. Bradley, and Abraham S. Friedman. Ideal gas thermodynamic functions of isotopic hydrogen sulfides—638(A)
Haddock, Roy P. (see Birge, Robert W.)—329(L)
—— (see Kerth, L. T.)—641(A)
Haeberli, W. Energy levels of Na^{23}—640(A)
Hafner, E. M. and W. Chestnut. Phase-shift analysis of 210-Mev proton polarization—639(A)
—— (see Chestnut, W. G.)—639(A)
Hagedorn, F. B. (see Webb, T. S.)—138
Hakeem, M. A. (see Rojo, Onofre)—1629(A)
Halbert, E. C. (see French, J. B.)—1387
Halbert, M. L. (see Camac, M.)—905
Hale, D. P. and R. D. Present. Mirror reactions $H^3(d,n)He^4$ and $He^3(d,p)He^4$—1366
Hall, D. (see Wightman, A. S.)—674(A)
Hallett, A. C. H. Viscosity of liquid He II—1660(T)
—— (see Benson, C. B.)—1660(A)
Halsted, R. E. Photoluminescent modulation in nonuniformly excited ZnS phosphors—1897(L)
Ham, F. S. and D. Mattis. Electrical properties of thin film semiconductors—1656(A)
Hamilton, Donald R. (see Daubin, Scott C.)—683
—— (see Reynolds, J. B.)—613(A)
Hamlin, Daniel A. (see Merritt, Jack)—1523
Hammer, C. L. and A. J. Bureau. Method for prompt destruction of electron beam in conventional synchrotron—653(A)
—— (see Pidd, R. W.)—1396

Handley, T. H. and W. S. Lyon. Long-lived isomer of Al^{28}—755
—— **and W. S. Lyon.** Neutron-deficient activities of Tb—1415
—— (see Cohen, B. L.)—723
—— (see Jones, W. H.)—184
Hanna, S. S. (see Frost, R. T.)—8
Harbottle, G. (see Scharff-Goldhaber, Gertrude)—180
Harding, R. (see Chestnut, W. G.)—639(A)
Hardwick, E. R. and W. G. McMillan. Energy transport in scintillation process—658(A)
Hare, W. F. J., Elizabeth J. Allin, and H. L. Welsh. Infrared absorption of liquid and solid H_2 with various ortho-para ratios—1887(L)
—— (see Allin, Elizabeth J.)—1639(A)
Harris, J. C. (see Milani, S.)—645(A)
—— (see Seiler, Milton R.)—340(A)
—— (see Smith, Robert T., Jr.)—340(A)
Harris, O. R. (see Connelly, J. J., Jr.)—1635(A)
Harrison, G. R., R. C. Crawford, and J. I. Hopkins. *K*-series fluorescence yield measurements of A, Cu^{65}, and In^{115}—1629(A)
Harrison, S. E. (see Kriessman, C. J.)—627(A)
Harrower, G. A. Energy spectra of secondary electrons from Mo and W for low primary energies—1650(A)
Hart, Robert W., Ernest P. Gray, and William H. Guier. Statistical theory of atomic excitation by electron impact. I. Theoretical development—1661(A)
—— (see Gray, Ernest P.)—1661(A)
Harth, E. M. (see Blevins, M. E.)—1628(A)
—— (see Block, M. M.)—261
—— (see Slaughter, G. G.)—1626(A)
Hartman, P. L. Optical absorption and reflectivity of alkali halides in far ultraviolet—1648(T)
—— (see Nelson, J. R.)—658(A)
Hartree, D. R. Atomic wave functions, with exchange, for some atoms of first long period—1637(T)
—— Interpolation of atomic wave functions and fields—1637(T)
Hartz, T. R. Radio star scintillations and ionosphere—1638(A)
Harvey, B. G. Systematics of neutron capture cross sections—333(L)
——, **S. G. Thompson, G. R. Choppin, and A. Ghiorso.** Nuclide 99^{254}—337(L)
Harvey, J. A., D. J. Hughes, R. S. Carter, and V. E. Pilcher. Spacings and neutron widths of nuclear energy levels—10
—— (see Hughes, D. J.)—1032(L)
—— (see Pilcher, V. E.)—611(A)
—— (see Stolovy, A.)—611(A)
Hasebe, K. and K. Yamamoto. Streamer theory and value of α/p—1331(L)
Haskin, D. M. and Marcel Schein. Analysis of properties of secondary particles in nucleon-nucleon collisions at very high energy—643(A)
—— (see Glasser, R. G.)—1555
—— (see Schein, Marcel)—643(A)
Hatcher, R. D. (see Klerer, M.)—675(A)
Haugerud, Ö. and S. O. Sörensen. Mesonic decay of $_3H^4$ nucleus—1046(L)
Hauver, George and Louis Zernow. Ultra high speed cine-microscopy and time resolved spectroscopy—635(A)
Haxby, Bernard V. Optical measurements on additively colored MgO single crystals—1636(A)
Hay, D. R. and R. C. Langille. Vhf and uhf propagation in central Canada—1638(A)
Hayashi, Izuo (see Kumagai, Hiroo)—1116
Haynes, J. R. New intrinsic recombination radiation from Ge—1656(A)
Haynes, S. K. (see Burford, A. O.)—3
—— (see Tidwell, Marvin)—1629(A)
Hayward, R. W. and D. D. Hoppes. Inner bremsstrahlung from V^{48}—659(A)
Hazen, W. E. Energy of electrons or photons from their cascade showers in Cu—911
Hazzaa, I. B. (see Sedra, R. N.)—1070
Hazzard, G. W. Education of physicists in engineering world—341(T)
Hector, L. Grant. New sintered-plate Ni-Cd storage battery—341(T)
Heikes, R. R. Magnetic transformation in MnBi—446
—— Relation of magnetic structure to electrical conductivity in NiO and related compounds—1232
Hein, R. A. Superconductivity of Hf—668(A)
Heinberg, M. (see Page, L. A.)—665(A)
Hellens, R. L. (see Weddell, J. B.)—621(A)
Helm, R. H., K. M. Crowe, and G. W. Tautfest. μ-e decay spectrum—650(A)
—— (see Crowe, K. M.)—872
Henkel, R. L., J. E. Perry, Jr., and R. K. Smith. Breakup of deuterons on H, T, He^3, and He^4—1050(L)
—— (see Brolley, J. E., Jr.)—159; 330(L); 616(L)
—— (see Nobles, R. A.)—616(A)
Henley, E. M. Model for multiple meson production—619(A)
Henry, Warren E. Intradomain magnetic saturation for Fe—668(A)
Herasymenko, P. Thermodynamic properties of α Ag-Cd and α Au-Cd alloys—614(A)
Hereford, Frank L. (see Wagner, Robert T.)—593(L); 665(A)
Herlin, Melvin A. (see Chase, C. E.)—669(A)
—— (see Jennings, L. D.)—668(A)
—— (see Kolm, Henry H.)—669(A)
—— Structure of energy bands in semiconductors—620(T)
Herman, Robert and Richard F. Wallis. Optical bleaching of *F* centers in x-rayed alkali halide crystals—435
Herndon, John A., A. H. Nielsen, and W. H. Fletcher. Infrared spectrum of SCl_2—1624(A)
Herring, D. F. Automatic pressure control system—634(A)
—— (see McEllistrem, M. T.)—632(A)
Hersh, Herbert N. Color centers in KI at liquid He temperatures—1636(A)
Herzberg, G. Lamb shifts in He^+ and He—1637(T)
Hess, F. G. and W. Opechowski. Theory of radiative β decay and electron capture—1654(A)
Heydenburg, N. P. and G. M. Temmer. Energy levels in Ti, Fe, Ge, and Mo by Coulomb excitation—617(A)
—— (see Temmer, G. M.)—617(A); 1609(L)
Hicks, D. A. (see Pyle, R. V.)—616(A)
Higgins, G. H., W. W. T. Crane, and S. R. Gunn. Average number of neutrons per spontaneous fission of Cm^{244}—183
—— (see Ghiorso, A.)—1048(L)
Hill, David L., Burton E. Freeman, and Kenneth W. Ford. Nuclear charge distribution in Pb^{208}—649(A)
Hill, R. D., E. O. Salant, and M. Widgoff. Heavy mesons produced by 2.2- and 3.0-Bev protons—229
—— (see Wheatley, J. C.)—334(L)
Hines, C. O., P. A. Forsyth, and E. L. Vogan. Diurnal variations in rate of meteor detection by forward scattering—1638(A)
Hirsch, A. (see Ghiorso, A.)—1048(L)
Hirschberg, Joseph G. Application of photomultiplier to interference spectroscope—623(A)

—— Emission spectroscopy at liquid He temperature—1898(L)
Hirschfelder, J. O. (see Dahler, J.)—637(A)
Ho, Kuo-Chu. Double interpolation and differentiation formulas—1627(A)
—— Focusing high-current electron beams by aperture effect—1627(A)
Hobson, J. P., J. C. Hubbs, W. A. Nierenberg, and H. B. Silsbee. Nuclear spin of Rb^{85}—method of measurement—612(A)
—— (see Hubbs, J. C.)—612(A)
Hoch, Michael. Reaction between BaO and C—1651(A)
Hodson, A. L. (see Ballam, J.)—1038(L)
Hoffman, J. G. Monte Carlo methods for study of cell populations—341(T)
Hofstadter, Robert (see Fregeau, Jerome H.)—1503
Hogg, Benjamin G. Energy available for β decay of Nd^{150}—175
Hok, Ong Ping. Rotational levels in the β decay of Pa isotopes—1613(L)
Holden, A. N., B. T. Matthias, W. J. Merz, and J. P. Remeika. Guanidine aluminum sulfate hexahydrate—626(A)
—— (see Merz, W. J.)—626(A)
Holladay, W. G. (see Capps, R. H.)—931
Holland, R. E., D. R. Inglis, R. E. Malm, and F. P. Mooring. Scarcity of low-energy levels of Be^9 appearing in two B reactions—92
Holmgren, H. D. and J. W. Butler. $O^{18}(d,n\gamma)F^{19}$ reaction—655(A)
—— (see Butler, J. W.)—1649(A)
Holroyd, L. V. (see Srinivasan, D.)—633(A)
Holstein, T. Optical absorption by conduction electrons in solids—1647(T)
Hoover, C. W., Jr. Transient response of cavity resonator—634(A)
Hopkins, J. I. (see Fowler, T. K.)—1629(A)
—— (see Harrison, G. R.)—1629(A)
Hoppes, D. D. (see Hayward, R. W.)—659(A)
Horie, Hisashi and Akito Arima. Configuration mixing and quadrupole moments of odd nuclei—778
Hornbostel, J. and E. O. Salant. Further observations of negative K mesons—338(L)
Hornyak, W. F. and R. Sherr. Inelastic scattering of 19-Mev protons by O^{16}: (B) γ radiation—632(A)
—— (see Sherr, R.)—632(A)
Hove, John E. Surface adsorption and migration energies for KCl—430
Howarth, D. J. Application of augmented plane wave method to Cu—469
Howland, P. R. and N. E. Scofield. Triggering fast two-crystal Compton scintillation spectrometer with iodine-escape x-rays from NaI(Tl) primary crystal—663(A)
Hrostowski, H. J., F. J. Morin, T. H. Geballe, and G. H. Wheatley. Hall effect and conductivity of InSb—626(A)
Huang, Kerson and S. D. Drell. Proton bremsstrahlung—628(A)
—— (see Drell, S. D.)—686
Hubbs, J. C., J. P. Hobson, W. A. Nierenberg, and H. B. Silsbee. Spin and magnetic moment of (4.7-hour) Rb^{84}—612(A)
—— (see Hobson, J. P.)—612(A)
Hudis, J. (see Friedlander, G.)—263
Hudson, George E. and Alfred Saenger. Periodic shock production in resonating gas columns—633(A)
Hudspeth, Emmett L., Ira L. Morgan, and Joseph T. Peoples. γ rays from proton bombardment of O^{18}—643(A)
—— (see Bostrom, Norman A.)—643(A)
Huggett, R. W. (see Kim, Y. B.)—642(A)
Hughes, D. J. Widths and spacings of nuclear energy levels—622(T)
—— **and J. A. Harvey.** Size distribution of neutron widths—1032(L)
—— (see Carter, R. S.)—611(A)
—— (see Harvey, J. A.)—10
—— (see Palevsky, H.)—611(A)
—— (see Pilcher, V. E.)—611(A)
Hughes, R. H. Isotope shift in first spectrum of atomic Li—1837
Hughes, V. W. and J. S. Geiger. Two-quantum transitions in microwave Zeeman spectrum of atomic oxygen—666(A); 1842
Hughes, W. T. (see Moore, George E.)—1643(A)
Huizenga, J. R. (see Ghiorso, A.)—1048(L)
Hull, M. H., Jr. (see Ebel, M. E.)—1596
Humphrey, James N. Sensitization of photoconductivity in PbSe—625(A)
Hunt, F. R. (see Brannen, Eric)—1658(A)
Hunt, S. E. and K. Firth. Resonant capture of protons by F in energy range 0.5 to 2.2 Mev—786
Hunten, D. M. Seasonal intensity variation of twilight Na emission—1637(A)
Huntington, H. B., G. A. Shirn, and E. S. Wajda. Calculation of entropies of lattice defects—1085
Hurwitz, H., Jr. (see Sampson, John B.)—1657(A)
Husain, A., C. J. D. Jarvis, and E. Pickup. Identification of cosmic-ray shower particles in emulsions—609(A)
——, **C. J. D. Jarvis, and E. Pickup.** Mass measurements of particles and existence of 1450 m_e mesons—1612(L)
—— (see Jarvis, C. J. D.)—1644(A)
Hutson, A. R. Studies of thermionic emission from single-crystal W—1650(T)
Hwang, Jenn-Lin. Revised Houston method for counting lattice frequencies—1098

Igo, G. Total neutron cross section of Re—610(A)
—— (see Eisberg, R. M.)—1606(L)
—— (see Wegner, Harvey E.)—640(A); 825
Iloff, E. L., W. W. Chupp, Gerson Goldhaber, S. Goldhaber, J. E. Lannutti, A. Pevsner, and D. Ritson. Mean lifetime of positive K mesons—1617(L)
Inglis, D. R. (see Holland, R. E.)—92
—— (see Lee, L. L., Jr.)—96
Ise, John, Jr. (see Pyle, R. V.)—616(A)
Iwanaga, Kenzo (see Kumagai, Hiroo)—1116

Jackson, J. David. Electron capture by positrons in gases—1653(A)
Jaffe, I. (see Ziegler, C. A.)—663(A)
Jakobson, Mark J. (see White, R. Stephen)—651(A)
James, H. M. (see Keenan, T. A.)—1660(A)
Janis, Allen (see Goldberg, Irwin)—676(A)
Jarmain, W. R. (see Nicholls, R. W.)—667(A)
Jarmie, Nelson. Mass measurement and excited states of F^{21}—1043(L)
Jarvis, C. J. D., A. Husain, and E. Pickup. Identification of cosmic-ray shower particles in emulsions. I. Ionization-scattering method—1644(A)
—— (see Husain, A.)—609(A); 1612(L)
Jarvis, R. G. (see Cross, W. G.)—621(A)
Jastrow, Robert. (see Block, Martin M.)—619(A)
Javan, Ali. Effects of bending mode of vibration on hfs of ICN—1302
Jeffries, C. D. (see Jones, R. V.)—646(A)
—— (see Sogo, P. B.)—613(A)
Jehle, Herbert, J. M. Yos, and W. L. Bade. Specific interaction between identical molecule pairs—1640(A)
Jenkins, H. B. (see Barr, T. A.)—1631(A)

Jennings, B. (see Weddell, J. B.)—621(A)
Jennings, L. D. and Melvin A. Herlin. Thermodynamic properties of chrome alum—668(A)
Jodra, Luis G. and Nathan Sugarman. High-energy fission of Bi. Proton energy dependence—1470
Johansson, Sven A. E. and Bengt Forkman. Fine structure in photoproton spectrum of oxygen—1031(L)
Johns, H. E. (see Bernier, J. P.)—1640(A)
Johns, M. W., B. C. Chidley, and I. R. Williams. Radioactive decay of Ga^{73}—1645(A)
Johnson, John L. and William S. Porter. Study of reactions $H^3(d,n)\alpha$ and $He^3(d,p)\alpha$—630(A)
Johnson, Philip O. (see Forrester, A. Theodore)—1691
Johnson, William R. Multiple meson production in emulsions exposed to Bevatron beam—1047(L)
—— (see Chupp, Warren W.)—1042(L)
Johnstone, C. W. (see Koontz, P. G.)—664(A)
Joki, E. G., L. G. Miller, and J. E. Evans. Total neutron cross sections of Na, K, and Rb, in 0.03- to 10-ev region—610(A)
—— (see Smith, M. S.)—611(A)
Jones, A. Vallence. Infrared spectrum of night sky near 10 000 A—1637(A)
Jones, R. V., W. Dobrowolsky, W. B. Kunkel, and C. D. Jeffries. Cyclotron resonance of free electrons in nitrogen afterglow—646(A)
Jones, W. H., A. Timnick, J. H. Paehler, and T. H. Handley. Bombardment energy and fission product yield pattern for protons on natural U and U^{235}—184
Jones, Ernest A. (see Akers, Lawrence K.)—1624(A)
Josien, Marie-Louise (see Fuson, Nelson)—1625(A)
Judek, B. and E. Pickup. Identification of cosmic-ray shower particles in emulsions. II. Range-scattering method—1644(A)
Juenker, D. W. Surface barrier analysis for metals by means of Schottky deviations—1155
——, **R. A. Meussner, and C. E. Birchenall.** Cavity formation in FeO—657(A)
Juretschke, H. J., S. J. Freedman, and S. Epstein. Galvanomagnetic effects in single crystals of Sb—636(A)

Kac, Mark. Theory of sound dispersion in dilute gases—645(T)
Kaempffer, F. A. Elementary particles as self-maintained excitations—1614(L)
—— Models of elementary particles—1637(T)
—— Simple model of elementary particles—1659(A)
Kahn, Bernd (see Lyon, W. S.)—728
Kaiser, H. F. Synchro-microtron requiring no static magnetic guide field—653(A)
Kallmann, Hartmut, Bernard Kramer, and Peter Mark. Impedance measurements on CdS crystals—1328(L)
——, **Bernard Kramer, and Arnold Perlmutter.** Infrared stimulation and quenching of photo conductivity in luminescent powders—391
Kalnajs, J. (see Smakula, A.)—1737; 1747
Kalos, M. H. and R. H. Dalitz. Numerical calculation of meson-nucleon scattering—617(A)
Kambe, K. Cohesive energy of noble metals—419
Kamei, Tohru. Quadrupole moments of Ta^{181} and Lu^{175}—789
Kammer, E. W. Effect of elastic strain upon electrical resistance when cold-work induced imperfections are present—594(L)
—— Effect of elastic strain upon electrical resistance when lattice imperfections are present—1630(A)
Kanzaki, Hiroshi. Electron traps in AgCl—1888(L)
Känzig, Werner. Electron spin resonance of V_1-centers—1890(L)
Kao, S. K. and A. F. Clark. p-p scattering in nuclear emulsions at 432 Mev—895
Kaplan, Jerome I. Calculation of spin resonance equation—622(A)
—— Spin resonance in metals as function of Overhauser effect—1322
—— Thermomagnetic anisotropy—1808
—— (see Garstens, M. A.)—459
Kaplon, M. F., J. Klarmann, and G. Yekutieli. β decay of K-mesons and classification of K-meson decays—1528
—— (see Klarmann, J.)—641(A)
—— (see Koshiba, M.)—641(A)
—— (see Yekutieli, G.)—641(A)
Katcoff, Seymour. Radiations from long-lived Tc^{99}—1618(L)
Katz, Ernst. Self-diffusion and ionic conduction in crystals—1334(L)
Katz, Leon. Photonuclear reactions: experimental results—1644(T)
——, **T. M. Kavanagh, A. G. W. Cameron, E. C. Bailey, and J. W. T. Spinks.** Photofission of U^{238}—98
—— (see Chidley, B. G.)—1646(A)
—— (see Pederson, E. C. B.)—1634(A)
Katzman, John. Directional intensity studies of cosmic rays—1645(A)
—— (see Rose, D. C.)—608(A)
Kavanagh, T. M. (see Katz, L.)—98
Keck, J. C. (see Tollestrup, A. V.)—220
Keenan, T. A. and H. M. James. Orientational transitions in CD_4—1660(A)
Keepin, G. R., Jr. (see Koontz, P. G.)—664(A)
Keesom, P. H. and N. Pearlman. Atomic heat of graphite between 1 and 20°K—1119
Keffer, F. (see Cohen, M. H.)—1128; 1135
Keller, Fred L. and Alvin H. Nielsen. High-dispersion measurement on ν_2 of NO_2 at 200°C—1624(A)
Keller, William E. PV isotherms of He^3 gas between 1.5 and 3.8°K—670(A)
Kelly, R. L. Technique for study of thin metallic films—615(A)
Kendrick, N. S., Jr., J. E. Miller, and G. W. Crawford. Design of oven for obtaining x-ray diffraction patterns of materials with low thermal conductivity—1631(A)
—— (see Miller, J. E.)—1631(A)
Kepler, G. E. (see Fretter, W. B.)—642(A)
Kerlee, D. D., J. S. Blair, and G. W. Farwell. Consistency of nuclear radius determinations from elastic scattering of alphas—1652(A)
Kern, B. D. and L. W. Cochran. γ rays from proton bombardment of P—645(A)
Kernan, A. and R. Cester. p-p interactions at 3 Bev—640(A)
Kerner, Edward H. Electric conductivity of composite media—1656(A)
—— Electronic band configuration of mixed linear lattices—1648(T)
Kerth, Leroy T., D. H. Stork, R. W. Birge, R. P. Haddock, and M. N. Whitehead. Production of heavy mesons at Bevatron—641(A)
—— (see Birge, Robert W.)—329(L)
Kerwin, L. Ionization-probability curves using electron selector—1661(T)
Keyes, Robert W. Effect of pressure on electrical conductivity of InSb—490
—— Effects of hydrostatic pressure on conductivity of InSb—626(A)
—— Elasto-galvanomagnetic effect in Ge—1655(A)
Keys, John E. Parallel-plate transmission line—1639(A)
Kikuchi, Ryoichi. Statistical mechanics of liquid He^3—1684

Kim, Y. B., J. R. Burwell, R. W. Huggett, and R. W. Thompson. Evidence for charge asymmetry of V^0-particles—642(A)
King, D. T. Multiplicity distribution of $0+N_s$ stars—642(A)
King, R. W. Supermultiplets and spin-dependent forces—67
Kingsbury, R. F. Oscillator strengths for transitions between $2p^53p$ and $2p^53s$ in O I, including configuration interaction—1846
Kington, J. D., J. K. Bair, Hans O. Cohn, and H. B. Willard. Proton-neutron threshold measurements—1393
—— (see Cohn, H. O.)—644(A)
Kinsey, B. B. Resonances in the elastic scattering of protons—332(L)
Kissinger, C. W. (see Perls, T. A.)—635(A)
Kivelson, D. and D. R. Lide. Internal motion in methyl amine—667(A)
Kjeldaas, T., Jr., and W. Kohn. Interpretation of Knight shift in metallic Na—622(A)
Klarmann, J., M. F. Kaplon, and G. Yekutieli. "V-particles" in nuclear emulsion—641(A)
—— (see Kaplon, M. F.)—1528
—— (see Yekutieli, G.)—641(A)
Klein, Abraham. Low-energy theorems for renormalizable field theories—998
—— **and Bruce H. McCormick.** Correlation of meson-nucleon scattering and nuclear forces—618(A)
—— (see Bernstein, Jeremy)—966
Klerer, M. and R. D. Hatcher. Approximately relativistic equations—675(A)
Klick, C. C. (see Russell, G. A.)—1639(A)
Klingensmith, R., E. Dally, and G. Arfken. Stability of transuranic elements—340(A)
Klokholm, E. (see Otter, F. A., Jr.)—599(L)
Kmetko, E. A. Effect of ambients on thermoelectric power and conductance of Ge particle aggregates—1642(A)
Knight, J. D. and E. W. Baker. Decay properties of Tl^{198}, Tl^{197}, and Tl^{198m}—1646(A)
Kobayashi, Jinzo and Ryuzo Ueda. X-ray study of phase transition of ferroelectric $PbTiO_3$ at low temperature—1900(L)
Koch, H. W., J. M. Wyckoff, and B. Petree. Response of NaI spectrometer to high-energy electrons—663(A)
—— (see Wyckhoff, J. M.)—616(A)
Koenigsberg, Ernest and Leon Findley. Conductivity of thin films in longitudinal magnetic field—615(A)
Koerts, L. (see Farrelly, B.)—1440
Koester, L. J., Jr. Neutral photomesons from H—651(A)
—— (see Mills, F. E.)—651(A)
Kofoed-Hansen, O. Alternative interpretations of slow-neutron cross sections—154
—— (see Margolis, B.)—611(A)
Kohn, Walter and Daniel Schechter. Theory of acceptor levels in Ge—1903(L)
—— (see Kjeldaas, T., Jr.)—622(A)
Kolm, Henry H. and Melvin A. Herlin. New method for measuring absolute viscosity of liquid He II—669(A)
—— **and George W. Pratt, Jr.** Field-induced surface effects—1644(A)
Komar, Arthur. Defining invariants of metric spaces—662(A)
Konopinski, E. β decay—630(T)
Koontz, P. G., C. W. Johnstone, G. R. Keepin, Jr., and J. D. Gallagher. New multichannel recording time-delay analyzer—664(A)
Korff, S. A. Prospective cosmic-ray observation during international geophysical year—1645(T)
—— (see Soberman, R. K.)—608(A)
Koshiba, M. and M. F. Kaplon. High-energy cosmic-ray soft showers in nuclear emulsion—641(A)
Kraichnan, Robert H. Special-relativistic derivation of generally covariant gravitation theory—1906(E)
Kramer, Bernard (see Kallmann, Hartmut)—391; 1328(L)
Krasner, Sol. Electron loss cross sections for He atoms passing through gases—520
Kraus, Alfred A., Jr. (see Bonner, T. W.)—631(A)
Kriessman, C. J. and S. E. Harrison. Ionic equilibrium in series of magnesium-manganese ferrites—627(A)
Krone, R. W., N. P. Baumann, and F. W. Prosser, Jr. Properties of some excited states in Mg^{24}—1649(A)
Krook, Max. Dynamics of rarefied gases—1896(L)
Kruger, Paul and Nathan Sugarman. High-energy fission of heavy elements. Nuclear charge dependence—1459
Krusemeyer, H. J. Influence of electric field on work function of oxide-coated cathode—1650(T)
Kuipers, George A. Infrared spectrum of HF—1624(A)
Kumagai, Hiroo, Hidetaro Abe, Kazuo Ôno, Izuo Hayashi, Junji Shimada, and Kenzo Iwanaga. Frequency dependence of magnetic resonance in α-Fe_2O_3—1116
Kunkel, W. B. (see Jones, R. V.)—646(A)
Kurath, Dieter. Intermediate coupling in $1p$ shell—648(A)
Kurbatov, J. D. and J. W. Downs. Relative stability of even-numbered isobars—340(A)
Kusch, P. (see Miller, R. C.)—1314

Lagarrigue, L. (see Fretter, W. B.)—642(A)
Lambertson, Glen R., C. Lasky, and Robert H. Phillips. Design studies for alternating-gradient magnets. II. Model measurements—653(A)
La Mer, V. K. Carnot's concept of entropy, and modern presentations of thermodynamics—656(T)
Landon, H. H. Radiation widths in slow-neutron resonances of Ir—610(A)
Lane, A. M. and C. F. Wandel. Imaginary part of potential in optical model of nucleus—647(A)
Lane, C. T. (see Wheeler, R. G.)—1667
Lane, R. O. (see Langsdorf, A., Jr.)—621(A)
Lang, G., S. DeBenedetti, and R. Smoluchowski. Measurement of electron momentum by positron annihilation—596(L)
Langford, F. L., R. A. Webb, and F. T. Rogers, Jr. Diffusion of uranyl nitrate activity through porous media—1631(A)
Langille, R. C. (see Hay, D. R.)—1638(A)
Langsdorf, A., Jr., and R. O. Lane. Angular distributions of scattering of moderate-energy neutrons—621(A)
Lannutti, Joseph E. (see Chupp, Warren W.)—335(L); 1042(L)
—— (see Iloff, E. L.)—1617(L)
Lark-Horovitz, K. (see Fritzche, H.)—400
Larson, Clarence E. Nuclear power reactor—1623(T)
Larson, Q. V. (see Boyd, G. E.)—1030(L)
Lasky, C. (see Lambertson, Glen R.)—653(A)
Laslett, L. Jackson. Betatron oscillations in fixed-field alternate-gradient accelerator with spirally-ridged poles—653(A)
Latter, Richard. Atomic energy levels for Thomas-Fermi and Thomas-Fermi-Dirac potential—510
—— Temperature behavior of Thomas-Fermi statistical model for atoms—1854
Lauff, G. H. (see Anderson, D. V.)—1639(A)
Lauritsen, C. C. (see Webb, T. S.)—138
Lawson, James R. (see Fuson, Nelson)—1625(A)
Lax, Benjamin and Laura M. Roth. Propagation and plasma oscillation in semiconductors—637(A)
—— (see Dexter, R. N.)—635(A)
—— (see Foner, Simon)—635(A)

—— (see Mavroides, J. G.)—1656(A)
Lax, Louis C. and Gerald A. Wrenshall. Simultaneous rates of P transfer between fifteen compartments within rat—1640(A)
Lax, M. (see Rosenberg, R.)—649(A)
Lazarus, A. J. (see Masek, G. E.)—650(A)
Leavitt, Christopher P. (see Chen, Francis F.)—857
LeBlanc, J. M. (see Burson, S. B.)—660(A)
Lebowitz, Joel L. and E. P. Gross. Quantum theory of dielectric relaxation—623(A)
—— (see Bergmann, Peter G.)—578
Ledbetter, Nasira F. (see Branson, Herman)—1643(A)
Leder, Lewis B. and L. Marton. Cross sections for characteristic energy loss of electrons—647(A)
Lederman, L. M. (see Rinehart, M. C.)—673(A)
—— (see Sargent, C. P.)—885
Lee, Kiuck and Alex E. S. Green. Diffuse boundary IPM mass surface—1627(A)
—— (see Green, Alex E. S.)—772
Lee, L. L., Jr., and D. R. Inglis. Energy levels in Be^9—96
—— **and Waldo Rall.** Angular distributions for $Ti^{46,48}(d,p)Ti^{47,49}$ reactions with 4.16-Mev deuterons—1384
Lee, Po and G. L. Weissler. Absorption cross section of He and A in extreme uv—540
Lee, T. D. Absorption experiments involving heavy mesons —337(L)
—— (see Friedman, M. H.)—618(A)
Leinhardt, T. E. and J. M. Reynolds. Small electromagnet for low-temperature magnetic measurements—1626(A)
Lemonick, A. (see Reynolds, J. B.)—613(A)
Levinson, Carl and Kenneth W. Ford. Independent particle model of nucleus. I. Interparticle forces and configuration mixing—792
Levitas, A. Electrical properties of Ge-Si alloys—1810
—— Mobility of holes in Ge-Si alloys—625(A)
Levitt, L., G. E. Tauber, and T. Y. Wu. Energy levels of H^-—1659(A)
Lewis, H. W. Surface energies in superconductors—669(A)
—— (see Bernstein, E. M.)—617(A)
—— (see Olness, J. W.)—654(A)
Lewis, M. B. and A. J. Siegert. Variant on Yang-Lee theory of condensation—661(A)
Lewis, R. R., Jr. Many-body effects in nuclear scattering of electrons—628(A)
Lichtenberg, D. B. Pion production in p-p scattering—618 (A)
Lide, D. R. (see Kivelson, D.)—667(A)
Lidofsky, L. J., N. Benczer, and V. K. Fischer. Radioactive decay of Ca^{47}—658(A)
Liebson, S. H. and E. J. West. Surface recombination of CdS—647(A)
Likely, J. G. (see Ajzenberg, F.)—654(A)
Lin, Chun C. Theory of fine structure of microwave spectrum of NO_2—666(A)
Lin, Lan-Ying and B. R. Russell. Change in length of alkali halide crystals caused by x-ray irradiation—657(A)
Lind, D. A. and J. J. Van Loef. Analysis of inelastic neutron scattering data for Mn, Fe, and I—621(A)
Lindemann, W. W. Cause and elimination of anomalous flicker effect—1650(A)
Linder, S. L. Nuclear magnetic relaxation in ethane derivatives—614(A)
Lindsay, Robert and John J. Banewicz. Conductivity of NiO as function of temperature and surrounding atmosphere —636(A)
Lipson, H. G., E. Burstein, and Paul L. Smith. Optical properties of plastically deformed Ge—444
Lipworth, Edgar (see Novick, Robert)—612(A)
Litherland, A. E., E. B. Paul, G. A. Bartholomew, and H. E. Gove. γ-ray cascades in Al^{28}—644(A)
—— (see Bartholomew, G. A.)—1649(A)
—— (see Ferguson, A. J.)—1654(A)
—— (see Gove, H. E.)—1649(A)
—— (see Paul, E. B.)—644(A); 1339
Long, Donald. Effect of pressure on electrical properties of InSb—388
Longini, R. L. Electronic interaction of imperfections in semiconductors and insulators—636(A)
—— (see McKelvey, J. P.)—1227
Lopes, J. Leite (see Goldemberg, J.)—1053(L)
Lord, J. J. (see Glasser, R. G.)—1555
Lorrain, Paul. Pressurized high-frequency Cockcroft-Walton accelerator—1634(T)
Loughhead, R. E. Solution of problems involving hydromagnetic flow of compressible ionized fluids—1678
Low, W. (see Steinberger, I. T.)—1217
Lowitz, D. A., W. Webb, and R. W. Schiessler. Temperature-pressure-structure effects on viscosity of several higher hydrocarbons—637(A)
Lurio, A. and A. G. Prodell. Hfs of Ga isotopes in ground state—613(A)
Lutes, O. S. and E. Maxwell. Superconductivity of Sn whiskers—668(A)
Lye, Robert G. Secondary electron emission from MgO single crystals—1647(A)
Lyon, W. S. and Bernd Kahn. Decay of Sc^{47}—728
—— (see Handley, T. H.)—755; 1415

MacDonald, A. D. Distribution functions in high-frequency gas discharges—1661(T)
MacDonald, D. K. C. Electron transport properties of solids at low temperatures—1647(T)
—— (see Dugdale, J. S.)—1905(E)
Madansky, L. and George E. Owen. Heavy particle stripping—1608(L)
Maenchen, George, Wilson M. Powell, George Saphir, and Robert W. Wright. π^--proton interactions at 4.5 Bev —1619(L)
Magnusson, L. B. (see Engelkemeir, D.)—135
Mallmann, C. A., A. H. W. Aten, Jr., D. R. Bes, and Clara M. de McMillan. γ rays of Te^{131} and Te^{132}—7
Malm, R. E. (see Holland, R. E.)—92
Mandel, M. (see Barrett, A. H.)—666(A)
Mandeville, C. E. (see Potnis, V. R.)—671(A)
Mandl, F. and T. Regge. Pion production for polarized protons—618(A)
—— **and T. Regge.** Reaction $p + p \rightarrow \pi^0 + d$ with polarized protons—1478
Mann, D. E., Janet Hawkins Meal, and Earle K. Plyler. Vibrational spectrum of tetrabromoethylene—667(A)
Mann, K. C., D. C. Milley, and J. A. L. Thompson. Ring-focus collection in thin-lens nuclear spectrometers—1634 (A)
Manning, W. M. (see Ghiorso, A.)—1048(L)
Marcus, J. A. (see Shafroth, S. M.)—664(A)
Margenau, Henry (see Meyeratt, Roland E.)—1851
Margolis, B., O. Kofoed-Hansen, and E. Nagel. Analysis of low-energy neutron-resonance cross sections—611(A)
Margulies, R. S. Positive pion scattering by H at 300 Mev —673(A)
Marion, J. B. (see Bonner, T. W.)—631(A)
Mark, Hans and George Paulissen. Cascade transitions between rotational levels in odd A nuclei—1654(A)
—— (see Paulissen, George)—617(A)
Mark, Peter (see Kallmann, Hartmut)—1325(L)
Markham, Jordan J. Comparison of Condon and adiabatic approximations for impurity center—636(A)

Marshall, J. F. (see Pomerantz, M. A.)—489
Marshall, L. Inelastic polarization and nucleon momentum distribution—1033(L)
Martin, D. W., J. M. Cork, and S. B. Burson. Radiations from Ce^{139}(33-hr)—670(A)
—— (see Burson, S. B.)—660(A)
Martin, E. E. (see Dyke, W. P.)—1192
Martius, Ursula M. Initial stages of oxidation of Ni—1635 (A)
Marton, L., J. Arol Simpson, and T. F. McCraw. Distribution of electrons scattered by Au—495
——, **J. Arol Simpson, and T. F. McCraw.** Distribution of electrons scattered in solids—1648(A)
—— (see Leder, Lewis B.)—647(A)
Marx, G. (see Farago, P. S.)—1063
Maryott, A. A. and G. Birnbaum. Microwave absorption in compressed O_2—1886(L)
Masek, G. E., A. J. Lazarus, and W. K. H. Panofsky. Electromagnetic production of μ mesons—650(A)
Mason, W. P. Dislocation relaxations at low temperatures and limiting shear stress in metals—615(A)
—— (see Bömmel, H. E.)—1894(L)
Massey, H. S. W. Research in gaseous electronics in the United Kingdom—1657(T)
Matossi, Frank. Dependence of light amplification in phosphors on light intensity—1332(L)
—— **and Sol Nudelman.** Electroluminescence excited by short field pulses—1100
Matthias, B. T. (see Holden, A. N.)—626(A)
—— (see Merz, W. J.)—626(A)
Mattis, D. (see Ham, F. S.)—1656(A)
Maunsell, C. D. Spectra of low-current-density glow discharges—1661(A)
Mavroides, J. G. and Benjamin Lax. Galvanomagnetic theory of holes in Ge and Si—1656(A)
Maxwell, E. (see Lutes, O. S.)—668(A)
Maxwell, L. H. (see Wachtman, J. B., Jr.)—657(A)
Mazari, Marcos (see Buechner, W. W.)—644(A)
McCarthy, Kathryn A. and Stanley S. Ballard. Thermal conductivity of Ge at ambient temperatures—1104
McCormick, Bruce H. (see Klein, Abraham)—618(A)
McCormick, G. H. (see Cohen, B. L.)—656(A)
McCrary, J. H. (see Bent, R. D.)—710
McCraw, T. F. (see Marton, L.)—495; 1648(A)
McCrum, N. G. and J. C. Eisenstein. Dipole fields and He film—1326(L)
McDonald, F. B., R. A. Ellis, and M. B. Gottlieb. Rocket observations on soft radiation at northern latitudes—609 (A)
McDonald, William S. (see Corson, Dale R.)—652(A)
McEllistrem, M. T., Ren Chiba, R. A. Douglas, D. F. Herring, and E. A. Silverstein. Differential cross sections for $C^{13}+d$ reactions—632(A)
—— (see Galonsky, A.)—1906(E)
McFarland, Charles E., Franklin B. Shull, Alexander J. Elwyn, and Benjamin Zeidman. Stripping reactions $Fe^{56}(d,p)Fe^{57}$ and $Fe^{57}(d,p)Fe^{58}$—655(A)
McGowan, F. K. and P. H. Stelson. Angular distribution of γ rays from Coulomb excitation—127
—— (see Stelson, P. H.)—112; 616(A)
McGruer, J. N., E. K. Warburton, and R. S. Bender. (d,p) Reactions from C^{12} and C^{13}—632(A)
McGuire, A. D. (see Camac, M.)—897
McIntosh, J. S. (see Aron, W.)—629(A)
McKay, K. G. and A. G. Chynoweth. Optical studies of avalanche breakdown in Si—1648(A)
—— (see Rose, D. J.)—1648(A)
McKelvey, J. P. and R. L. Longini. Recombination of injected carriers at dislocation edges in semiconductors—1227
McKeown, M. (see Scharff-Goldhaber, Gertrude)—180
McMillan, D. R. and Andrew Robeson. Comparison of ultrasonic velocities in series of carbonates and acetates—1631(A)
McMillan, W. G. Exchange in Thomas-Fermi-Dirac model —661(A)
—— (see Hardwick, E. R.)—658(A)
McNair, A., R. N. Glover, and H. W. Wilson. K^{40} branching ratio—771
Mead, F. C., Jr. Disposal of radioactive wastes—339(T)
Meal, Janet Hawkins (see Mann, D. E.)—667(A)
Mech, J. F. (see Ghiorso, A.)—1048(L)
Meek, J. H. Motions of auroral light forms—1637(A)
Meinke, W. Wayne (see Cassatt, Wayne A., Jr.)—760
Melamed, N. T. (see Bowers, R.)—1781
Melvin, M. A. Fractional occurrence numbers of eigenstates —1663(A)
—— Radiation flux field outside of stars and spherical reactors—371; 1663(A)
—— Simplification in finding symmetry-adapted eigenstates —1659(A)
—— **and J. W. Burgeson.** Resiliency of pure metals—1663 (A)
Merat, Parviz (see Anderson, James L.)—1871
Meredith, L. H., J. A. Van Allen, and M. B. Gottlieb. Cosmic-ray intensity above atmosphere at high latitudes—198
—— (see Ellis, J. A.)—609(A)
Merritt, F. R. (see Bozorth, R. M.)—1898(L)
—— (see Yager, W. A.)—1203
Merritt, Jack and Daniel A. Hamlin. Production of π^+-mesons at 0° by 335-Mev protons on deuterium and complex nuclei—1523
Merz, W. J., J. P. Remeika, A. N. Holden, and B. T. Matthias. Electrical properties of guanidine aluminum sulfate hexahydrate (G.A.S.H.) and some isomorphs—626(A)
—— (see Holden, A. N.)—626(A)
Merzbacher, E. (see Patterson, J. R.)—1625(A)
—— (see Toller, A. L.)—1625(A)
Messel, H. (see Chartres, B. A.)—1604(L)
Metzger, Franz R. Nuclear resonance fluorescence in Ge^{74} and Pr^{141}—613(A)
Meussner, R. A. (see Juenker, D. W.)—657(A)
Meyer, Peter and J. A. Simpson. Changes in low-energy particle cutoff and primary spectrum of cosmic radiation—1517
—— **and J. A. Simpson.** Changes in low-energy primary spectrum and low-energy particle cutoff of cosmic radiations—608(A)
Meyerott, Roland E. and Henry Margenau. Line broadening by electrons: Validity of simple theories—1851
Mielczarek, Eugenie V. (see Frederikse, H. P. R.)—1889(L)
Milani, S., John N. Cooper, and J. C. Harris. γ-ray resonances in reaction $Si^{29}(p,\gamma)P^{30}$—645(A)
Millburn, G. P. (see Crandall, W. E.)—631(A)
Miller, D. (see Barnes, S. W.)—673(A)
Miller, J. E., N. S. Kendrick, Jr., and G. W. Crawford. Preliminary investigation of crystal structure changes of S—1631(A)
—— (see Kendrick, N. S., Jr.)—1631(A)
Miller, L. G. (see Joki, E. G.)—610(A)
Miller, R. C. and P. Kusch. Velocity distributions in K and Tl atomic beams—1314
Miller, S. L. Avalanche breakdown in Ge—1234
Milley, D. C. (see Mann, K. C.)—1634(A)
Millman, P. M. Excitation and ionization produced by meteors—1637(T)

Mills, F. E. and L. J. Koester, Jr. Neutral photomesons from H—651(A)
Mills, R. L. and E. R. Grilly. Melting curves of He^3, He^4, H_2, D_2, Ne, N_2, and O_2 up to 3500 kg/cm²—480
Misner, C. W. Applications of topology to general relativity —662(A)
Mitler, Henri. Correlation energy of He—1835
Mitra, A. N. Pion-nucleon scattering at high energies—957
Miyatake, Osamu and Clark Goodman. Observations on the charge and mass distributions in nuclei—1040(L)
Miyazawa, Hironari. Feynman amplitudes and strong-coupling pion theory—944
—— **and Reinhard Oehme.** Decay of spin-zero mesons into two leptons—315
—— (see Goldberger, M. L.)—986
Mize, J. P., M. E. Bunker, and J. W. Starner. Radioactive decay of Yb^{175}—671(A)
—— (see Brolley, J. E., Jr.)—330(L)
—— (see Bunker, M. E.)—659(A)
Moore, George E. and W. T. Hughes. Dissociation of solid compounds by electron bombardment—1643(A)
Moore, J. Slow-neutron resonance scattering in In—610(A)
Mooring, F. P. (see Holland, R. E.)—92
Moravcsik, Michael J. and J. Michael Sellen, Jr. Scattering of electrons in strong-focusing synchrotron—653(A)
Morgan, Ira L. Interaction of 3.7-Mev neutrons with Al, S, Fe, and Cu—621(A)
—— (see Bostrom, Norman A.)—643(A)
—— (see Hudspeth, Emmett L.)—643(A)
Morgan, K. Z. (see Cook, M. J.)—1628(A)
Morin, F. J. and T. H. Geballe. Electrical conductivity and Seebeck effect in $Ni_{0.95}Fe_{2.05}O_4$—467
—— (see Hrostowski, H. J.)—626(A)
Morinaga, H. Reaction $Ni^{68}(\alpha,\gamma)Zn^{68}$—655(A)
—— (see Bleuler, E.)—658(A)
Morris, T. F. Elementary particle models—650(A)
Morrish, A. H. and S. P. Yu. Magnetic measurements on single microscopic particle—1641(A)
Morrison, P. Sun and cosmic rays—341(T)
Morrison, S. Roy. Generation of $1/f$ noise by levels in linear or planar array—1904(L)
—— Surface levels, their influence on field effect and $1/f$ noise—1655(A)
Moszkowski, Steven A. Particle states in spheroidal nuclei —803
—— Particle states in spheroidal potential—648(A)
Mottelson, B. R. and S. G. Nilsson. Classification of nucleonic states in deformed nuclei—1615(L)
Motz, Hans, K. M. Crowe, and R. M. Friedman. π^-/π^+ ratios in photoproduction—673(A)
—— (see Crowe, K. M.)—673(A)
—— (see Friedman, R. M.)—672(A)
Motz, Henry. γ-ray spectrum of $Cd^{113}(n,\gamma)Cd^{114}$—656(A)
Moulthrop, Peter H. Pion production by neutrons on He—651(A); 1509
Mower, Lyman. Variational calculation of electron scattering by static potential—1065
Moyer, Burton J. (see Bandtel, K. C.)—673(A)
—— (see Wilcox, John M.)—875
Muehlhause, C. O. (see Bloom, S. D.)—654(A)
Muench, Nils L. Effects of stress on superconducting Sn, In, Tl, and Al—1814
—— **and H. E. Rorschach, Jr.** Displacement of superconducting critical field by pressure—668(A)
Müller, Erwin W. and Kanwar Bahadur. Velocity distribution in field ion emission—1651(A)
Murphy, E. L. and R. H. Good, Jr. Transition between field and thermionic emission—1650(A)
Murray, R. B. and L. D. Roberts. Extension of molecular field theory to hexagonal lattice—1630(A)
—— (see Roberts, L. D.)—1630(A)
Nagel, E. (see Margolis, B.)—611(A)
Naugle, J. E., P. S. Freier, and E. P. Ney. Energy spectrum of medium and heavy primaries at $\lambda = 61°$—609(A)
Need, John L. Mechanism of reaction $C^{12}+p \rightarrow p+3\alpha$ at 29 Mev—1356
Neher, H. V. Cosmic-ray intensity near north magnetic pole in 1954—620(T)
Nelson, E. B. (see Bashkin, S.)—107
Nelson, James R. Optical absorption spectrum of MgO by reflectivity—1902(L)
——, **J. G. Siegfried, and P. L. Hartman.** Absorption of alkali-halides in far uv—658(A)
Neufeld, Jacob and R. H. Ritchie. Density effect in ionization energy loss of charged particles—1125
—— **and W. S. Snyder.** Number of vacancies created by heavy corpuscular radiation—1326(L)
Newman, Eugene (see Cohen, Bernard L.)—656(A); 718; 723
Newman, Ezra and Peter G. Bergmann. Lagrangians linear in "velocities"—587
Newman, R. Optical properties of In-doped Si—465
—— (see Dash, W. C.)—1151
Newson, H. W. (see Nichols, P. F.)—621(A)
—— (see Patterson, J. R.)—1625(A)
—— (see Toller, A. L.)—620(A); 1625(A)
Newstein, M. C. Variational treatment of elastic scattering of electrons from H—628(A)
Ney, E. P. (see Naugle, J. E.)—609(A)
Neynaber, R. H., W. G. Brammer, and W. W. Beeman. Small-angle x-ray scattering from cold-worked metals—615(A)
Nicholls, R. W. and W. R. Jarmain. "Average" internuclear separations arising in study of molecular band-systems—667(A)
—— (see Brannen, Eric)—1658(A)
Nichols, P. F., R. G. Smith, and H. W. Newson. Total neutron cross sections in kev region: Zr^{90}, Zr^{91}, and Zr^{92}—621(A)
Nielsen, Alvin H. (see Herndon, John A.)—1624(A)
—— (see Keller, Fred L.)—1624(A)
—— (see Smith, D. F.)—1624(A)
Nierenberg, W. A. (see Hobson, J. P.)—612(A)
—— (see Hubbs, J. C.)—612(A)
Niestlie, John W., Jr., and Arthur I. Berman. Neutron velocity distribution in infinite scattering medium with finite absorption—612(A)
Nigam, B. P. and L. L. Foldy. Space inversion and charge conjugation for fermion fields—675(A)
—— **and H. P. Noyes.** Quasi-bound states of pion-nucleon system in lowest Tamm-Dancoff approximation—989
Nilsson, S. G. (see Mottelson, B. R.)—1615(L)
Nobles, R. A., R. L. Henkel, and R. K. Smith. Neutron-induced fission excitation curve for Am^{241}—616(A)
Novey, T. B. α-γ directional correlation in Am^{241}—672(A)
—— (see Freedman, M. S.)—671(A)
—— (see Porter, F. T.)—671(A)
Novick, Robert, Edgar Lipworth, and Paul F. Yergin. Fine structure of singly ionized He—612(A)
Nowick, A. S. (see Fischbach, D. B.)—1333(L)
Noyes, H. P. Effective range analysis of pion-nucleon S-waves—618(A)
—— (see Nigam, B. P.)—989
Nudelman, Sol (see Matossi, Frank)—1100
O'Dell, F. W. and M. M. Shapiro. Comparison of ionization-range methods of mass estimation—641(A)

Odian, A. (see Weinstein, R. M.)—1621(L)
Oehme, Reinhard (see Goldberger, M. L.)—986
—— (see Miyazawa, Hironari)—315
O'Friel, Z. and A. H. Weber. Internal conversion coefficient of Cr^{51}—659(A)
Ogilvy, K. W. Cosmic-ray proton spectrum at sea level—1645(A)
Okazaki, Albert. Scattering of polarized neutrons by heavy nuclei—55
Olbert, S. Diffusion equation on nucleonic component of cosmic rays—661(A)
Oleson, Norman (see Watanabe, Satosi)—646(A); 1701
Olness, J. W. and H. W. Lewis. γ rays from protons on P^{31}—654(A)
Olsen, Haakon. Outgoing and ingoing waves in final states and bremsstrahlung—1335(L)
Ôno, Kazuo (see Kumagai, Hiroo)—1116
Opechowski, W. (see Hess, F. G.)—1654(A)
Oppenheim, Irwin (see Friedman, Abraham S.)—638(A)
O'Rourke, R. C. and A. Anderson. Problem in shower theory (Approximation A)—1484
Osborne, L. S. (see deSaussure, Gerard)—843
Otter, F. A., Jr., P. J. Flanders, and E. Klokholm. Ferromagnetism in noble metal allows containing Mn—599(L)
Overton, W. C., Jr., and Ted G. Berlincourt. Pressure dependence of de Haas-van Alphen parameters in Bi—1165
Owen, George E. (see Madansky, L.)—1608(L)

Paehler, J. H. (see Jones, W. H.)—184
Page, L. A., M. Heinberg, O. J. Wallace, and T. W. Trout. Angular correlation of two-quantum annihilation in condensed materials—665(A)
Pais, A. and R. Serber. Interaction between K-particles and nucleons—1551
Palevsky, H., D. J. Hughes, and R. L. Zimmerman. Inelastic scattering of cold neutrons by lattice vibrations of crystalline solids—611(A)
—— (see Carter, R. S.)—611(A)
Palmatier, E. D. (see Reeves, Tricia)—1628(A)
Pandya, Sudhir P. (see French, J. B.)—1387
Panofsky, W. K. H. and G. B. Yodh. Pion production from H by 600-Mev electrons—651(A)
—— (see Masek, G. E.)—650(A)
Pappis, J. (see Bickford, L. R., Jr.)—1210
Paquette, D. R. (see Perls, T. A.)—635(A)
Park, David. Radiations from spinning rod—1324
Parker, Eugene N. Hydromagnetic waves and acceleration of cosmic rays—241
Parmenter, R. H. Energy levels of crystal modified by alloying or by pressure—1759
—— Uniform strains and deformation potentials—1767
Parratt, L. G. Structure of thin evaporated Cu films by total reflection of x-rays—1635(A)
Passell, Thomas O. (see Rasmussen, John O.)—42
Patterson, J. R., H. W. Newson, and E. Merzbacher. Neutron resonances in kev region: F^{19} and P^{31}—1625(A)
—— (see Toller, A. L.)—620(A)
Paul, E. B., G. A. Bartholomew, H. E. Gove, and A. E. Litherland. γ rays from proton bombardment of Mg^{24}—644(A)
——, **H. E. Gove, A. E. Litherland, and G. A. Bartholomew.** Proton capture γ rays from reaction $P^{31}(p,\gamma)S^{32}$ leading to ground and first excited states of S^{32}—1339
—— (see Bartholomew, G. A.)—1649(A)
—— (see Clarke, R. L.)—654(A)
—— (see Gove, H. E.)—1649(A)
—— (see Litherland, A. E.)—644(A)
Paulissen, George and Hans Mark. Electric excitation of Pd, Cd, and Mo by protons—617(A)
—— (see Mark, Hans)—1654(A)
Pearlman, N. (see Keesom, P. H.)—1119
Pearson, Gerald. Solar battery—1623(T)
Pease, Jane (see Pease, Robert L.)—1600
Pease, Robert L. and Jane Pease. Necessary condition for positive definite energy—1600
Peaslee, D. C. "Normalized" β interactions—1654(A)
—— Nuclear oscillator potential—648(A)
Pederson, E. C. B. and L. Katz. Betatron energy control—1634(A)
Peebles, G. H. (see Gilvarry, J. J.)—550
Pellam, John R. Andronikashvilli disk measurements in liquid He^3–He^4 mixtures—1327(L)
Penfield, R. H. Attempt to geometrize electromagnetic theory—342(A)
Peoples, Joseph T. (see Hudspeth, Emmett L.)—643(A)
Pepinsky, R. (see Danner, H.)—1215
Percus, J. K. and G. J. Yevick. Exact new reformulation of many-body problem—661(A)
—— (see Yevick, G. J.)—661(A)
Peria, W. T. Photoelectric emission from metals into MgO—1647(A)
Perkins, J. F. Monte Carlo calculation of γ-ray reflection coefficients of concrete and Al—1629(A)
—— (see Burford, A. O.)—3
Perkins, R. B. (see Becker, R. L.)—1646(A)
Perlman, I. (see Asaro, Frank)—37
Perlman, Morris L. (see Wolfsberg, Max)—1833
Perlmutter, Arnold (see Kallmann, Hartmut)—391
Perls, T. A., C. W. Kissinger, and D. R. Paquette. Steady-state calibration of vibration transducers at accelerations up to ± 4000 g—635(A)
Perry, J. E., Jr., and S. J. Bame, Jr. $T(p,\gamma)He^4$ reaction—1368
—— (see Henkel, R. L.)—1050(L)
Petch, H. E. Location of H atoms in unit cell of portlandite $[Ca(OH)_2]$—1635(A)
Peter, M. and M. W. P. Strandberg. Molecular-beam microwave-absorption spectroscope—667(A)
Peterson, James R. (see Birge, Robert W.)—329(L)
Peterson, L. (see Winckler, J. R.)—608(A)
Peterson, R. W. Activation diffusion and thermionic emission in oxide coated cathodes—1651(A)
Peterson, Vincent Z. (see Corson, Dale R.)—652(A)
—— (see Walker, R. L.)—210
Petree, B. (see Koch, H. W.)—663(A)
Pevsner, A. (see Iloff, E. L.)—1617(L)
—— (see Sreekantan, B. V.)—642(A)
Phelps, A. V. Absorption studies of He metastable atoms and molecules—1307
—— Absorption studies of metastable states of Ne—1657(A)
Phillips, G. C., C. R. Gossett, J. P. Schiffer, and P. M. Windham. Inelastic scattering of protons from Fe^{56} and Fe^{58}—655(A)
—— (see Schiffer, J. P.)—655(A)
Phillips, Robert H. (see Lambertson, Glen R.)—653(A)
Pickup, E. (see Husain, A.)—609(A); 1612(L)
—— (see Jarvis, C. J. D.)—1644(A)
—— (see Judek, B.)—1644(A)
Pidd, R. W. and C. L. Hammer. Electron scattering on W at 31, 40, and 60 Mev—1396
Pierce, Louis. Centrifugal distortion effects in ozone—666(A)
Pigg, J. C. (see Cleland, J. W.)—1170
Pilcher, V. E., D. J. Hughes, and J. A. Harvey. Recent developments in analysis of neutron resonances and results of fast chopper measurements on Ta—611(A)
—— (see Harvey, J. A.)—10
Pines, David (see Bardeen, John)—1140

Pipkin, F. M. (see Reynolds, J. B.)—613(A)
Plano, Richard J. and Irwin A. Pless. Negative-pressure pentane bubble chamber used in high-energy experiments—639(A)
—— (see Pless, Irwin A.)—639(A)
Platt, J. B. Yields of mesonic K and L series x-rays—628(T)
—— (see Camac, M.)—897; 905
Pleasonton, Frances (see Snell, Arthur H.)—1625(A)
Pless, Irwin A. and Richard J. Plano. Study of 456-Mev proton interactions with H and C—639(A)
—— (see Plano, Richard J.)—639(A)
Plyler, Earle K. (see Mann, D. E.)—667(A)
Pomerantz, M. A., R. A. Shatas, and J. F. Marshall. Electrical conductivity induced in MgO crystals by 1.3-Mev electron bombardment—489
Porter, C. E. Elastic scattering of α particles and deuterons by complex nuclei—1400
Porter, F. T., M. S. Freedman, T. B. Novey, and F. Wagner, Jr. β-γ angular anisotropy in Re^{186}—671(A)
—— (see Freedman, M. S.)—671(A)
Porter, William S. (see Johnson, John L.)—630(A)
Potnis, V. R., C. E. Mandeville, and John S. Burlew. Radiations from Pt^{197}—671(A)
Pound, R. V. (see Rice, Michael)—1036(L)
Powell, R. L. (see Foner, Simon)—635(A)
Powell, Wilson M. (see Maenchen, George)—1619(L)
Pratt, George W., Jr. (see Kolm, Henry H.)—1644(A)
Prentki, Jacques (see d'Espagnat, Bernard)—328(L)
Present, R. D. (see Hale, D. P.)—1366
Preston, M. A. Coupling constants of β-decay interaction and decay of Rb^{87}—1654(A)
—— (see Shapiro, J.)—1654(A)
Price, P. J. Theorem on many-body quantum ground state—670(A)
Price, William J. Air Force Institute of Technology engineering curriculum—339(T)
Prigogine, Ilya. Statistical mechanics of irreversible processes—645(T)
Prince, M. B. Si conductivity-modulated diffused p-n junction rectifier—625(A)
Pringle, R. W. (see Taylor, H. W.)—1345
Prodell, A. G. (see Lurio, A.)—613(A)
Prosser, F. W., Jr. (see Krone, R. W.)—1649(A)
Pruett, Charles H., H. H. Bolotin, P. L. Roggenkamp, and R. G. Wilkinson. Excited states of Ce^{140}—670(A)
—— (see Bolotin, Herbert H.)—62
Pryor, M. J. Transmission-line demonstration—342(A)
Pugh, Emerson M. and F. E. Allison. Corrections to Hall potential in ferromagnetic materials—1642(A)
—— (see Allison, F. E.)—1642(A)
Pugh, Emerson William and J. E. Goldman. Magnetic susceptibility of metallic Li—1641(A)
Pyle, G. L. (see Ghiorso, A.)—1048(L)
Pyle, R. V., D. A. Hicks, and John Ise, Jr. Spontaneous-fission neutron multiplicities—616(A)
—— (see Crandall, W. E.)—631(A)

Rado, G. T. Spin-wave resonance in ferromagnetic metals—627(T)
Rall, Waldo (see Lee, L. L., Jr.)—1384
Ramanathan, K. G. and T. M. Srinivasan. Specific heat of Bi at liquid He temperatures—442
Rand, S. Photonuclear effect—1620(L)
Ranken, W. A. (see Bent, R. D.)—710
Raphael, R. B. Singlet S-state nucleon-nucleon potential—619(A)
Raridon, Richard and P. K. S. Wang. Tungsten L x-rays from Be-window tube—1629(A)
—— (see Wang, P. K. S.)—1639(A)
Rarita, William. Scattering analysis—630(A)
—— (see Serber, Robert)—629(A)
Rasmussen, John O., Hilding Slätis, and Thomas O. Passell. β emitter Np^{239}. I. β spectroscopy—42
——, **Frank S. Stephens, Jr., Donald Strominger, and Björn Aström.** β emitter Np^{239}. II. Scintillation spectroscopy and coincidence studies—47
Redfield, David. Recombination processes in Te—635(A)
Redlich, Martin G. Interactions between configurations of three nucleons in 1d, 2s shell—1427
—— Wave functions for nuclear shell theory by variation method—1421
Reekie, James. λ-point transition in relation to atomic distribution in liquid He—1660(T)
Reeves, Tricia and E. D. Palmatier. Interval distribution of cosmic-ray tracks in extensive air showers—1628(A)
Regge, T. (see Mandl, F.)—618(A); 1478
Reiss, Howard. Ionization and solubility of impurities in semiconductors—1642(T)
—— (see Fuller, C. S.)—624(A)
Remeika, J. P. (see Holden, A. N.)—626(A)
—— (see Merz, W. J.)—626(A)
Repp, Gordon W. (see White, R. Stephen)—651(A)
Reynolds, Charles A. Kinetic theory of liquid He II: heat transfer—669(A)
—— (see Forstat, Harold)—669(A)
Reynolds, George T. Recent results concerning hyperons and heavy mesons—620(T)
—— **and W. A. Aron.** Masses of S particles—1038(L)
—— (see Ballam, J.)—1038(L)
Reynolds, H. L. and A. Zucker. Differential cross sections for elastic scattering of N by N—640(A)
Reynolds, J. B., R. L. Christensen, D. R. Hamilton, A. Lemonick, F. M. Pipkin, and H. H. Stroke. Nuclear spins and hyperfine separations of Au^{195} and Au^{197}—613(A)
Reynolds, J. M. (see Leinhardt, T. E.)—1626(A)
Ribe, F. L. and R. W. Davis. 14-Mev (n,α) cross section in Zr. III—331(L)
Rice, Michael and R. V. Pound. Ratio of magnetic moments of stable Ga isotopes—1036(L)
Rice, William L. R. Use of clays for disposal of radioactive wastes—340(A)
Rinehart, M. C., K. C. Rogers, and L. M. Lederman. Scattering of negative pions near 15 Mev in H—673(A)
—— (see Sargent, C. P.)—884
Ring, J. (see Barnes, S. W.)—673(A)
Ring, Laurence S., Jr. Photodeuteron/photoproton yield from S—137
Ritchie, R. H. (see Birkhoff, R. D.)—647(A)
—— (see Neufeld, Jacob)—1125
Ritson, D. (see Iloff, E. L.)—1617(L)
Roberts, L. D. and R. B. Murray. Crystalline electric field splitting effects in antiferromagnetic transitions—1630(A)
—— (see Dabbs, J. W. T.)—1652(A)
—— (see Murray, R. B.)—1630(A)
Roberts, Paul H. (see Chamberlain, Joseph W.)—1674
Robertson, Harry S. Periodic phenomena in direct-current glow discharges—1662(A)
Robeson, Andrew (see McMillan, D. R.)—1631(A)
Robinson, Kenneth W. Electronic detection of heavy mesons—1606(L)
—— Timing measurements on penetrating cosmic-ray showers—642(A)
Robinson, R. F.—Food sterilization by radiation—339(T)
Robson, J. M. Experiment on angular correlation in β decay of neutron—1638(T)
Rogers, F. T., Jr. (see Langford, F. L.)—1631(A)
—— (see Rogers, Marguerite M.)—1632(A)

Rogers, K. C. (see Rinehart, M. C.)—673(A)
—— (see Sargent, C. P.)—885
Rogers, Marguerite M. and F. T. Rogers, Jr. Special stopping-power laws—1632(A)
Rogers, William A. and Manfred A. Biondi. Doppler broadening of spectral lines emitted during dissociative recombination—1657(A)
Roggenkamp, Paul L. (see Bolotin, Herbert H.)—62
—— (see Pruett, C. H.)—670(A)
Rohrer, R. H., J. B. Bailey, and A. K. Furr. Performance of cathode-ray tube coincidence discriminator—1626(A)
Rojo, Onofre, M. A. Hakeem, and Max Goodrich. Relative number of γ rays from Po^{210}—1629(A)
Romer, R. H. and R. H. Dicke. New technique for high resolution microwave spectroscopy—532
Rorschach, H. E., Jr. (see Muench, N. L.)—668(A)
Rosa, Richard J. Shock wave spectroscopy—633(A)
Rose, D. C. Cosmic-ray measurements at sea level over wide ranges of latitude—1645(T)
—— **and J. Katzman.** Latitude effect on nucleon and hard components of cosmic rays—608(A)
Rose, D. J. and K. G. McKay. Microplasmas in Si—1648(A)
Rose, M. E. Gauge problem in internal conversion—1628(A)
—— (see Brysk, H.)—649(A)
Rosen, Louis and Leona Stewart. Experimental checks of statistical theory of nuclear reactions—1052(L)
—— (see Frye, G. M., Jr.)—1375
Rosenberg, A. and W. C. Winegard. Crystal growth phenomena in high-purity Pb—1635(A)
Rosenberg, R. and M. Lax. Validity of deformation-potential theory in n-type Ge—649(A)
Rosenstock, Herbert B. Optical properties of solids—657(A)
Rossi, B. (see DeStaebler, H., Jr.)—642(A)
Rotenberg, A. and L. Spruch. Interaction contribution to nuclear isomerism—649(A)
Roth, Laura M. (see Gold, Louis)—1655(A)
—— (see Lax, Benjamin)—637(A)
Rothstein, Jerome. Monomolecular *vs* bimolecular relaxation kinetics in Cu_3Au and β brass—614(A)
Rowland, R. E. Cascade γ rays from $_{84}Po^{214}$ (RaC')—757
Roy, D. K. (see Das, T. P.)—1906(E)
Ruark, Arthur E. and William B. Good. Unstable combinations which can stimulate neutral mesons—1628(A)
Rubenstein, R. A. and J. N. Snyder. Theoretical analysis of charge distribution on recoil Cl ions from K capture in A^{37}—189
Rubin, F. A. (see Ajzenberg, F.)—654(A)
Rubin, Robert J. and B. A. Fleishman. Frequency spectrum of one-dimensional isotopic crystal mixture—656(A)
Ruby, Lawrence and James D. Gow. Occluded-gas ion source—663(A)
Rundle, R. E. (see Wilkinson, M. K.)—627(A)
Russek, A. Exchange moment contributions to modified shell model—834
—— (see Box, H. C.)—341(T)
Russell, B. R. (see Lin, Lan-Ying)—657(A)
Russell, G. A. and C. C. Klick. Experimentally determined configuration coordinate curves for F-centers in alkali-halide crystals—1636(A)
Russell, L. N. (see Grove, G. R.)—340(A)
Russell, R. D. Pb isotopes and earth's history—1644(T)
Rutledge, W. C. Determination of instantaneous Ba and BaO evaporation rates from thermionic cathodes—1651(A)

Sachs, R. G. Classification of fundamental particles—1573
Sackinger, J. P. Fused silica dielectric measurements at low frequencies—342(A)
Saenger, Alfred (see Hudson, George E.)—633(A)
Saenz, A. W. Derivation of quantum-statistical transport equation for dilute gases—638(A)
Sahni, R. C. Automatic computation of electronic wave functions of molecules—1639(A)
Salacz-Dohnanyi, Julius and Alex E. S. Green. Mixed Wigner-IPM mass surface—1627(A)
Salant, E. O. (see Hill, R. D.)—229
—— (see Hornbostel, J.)—338(L)
Salkovitz, Edward I. (see Schindler, Albert I.)—1251
Salter, L. Low-frequency vibrational spectrum of fcc lattice—656(A)
Salwen, Harold. Resonance transitions in molecular beam experiments. I. General theory of transitions in rotating magnetic field—1274
Salzman, George. Neutron-electron interaction—973
—— Structure of mesonic cloud associated with nucleon—619(A)
Sampson, John B., H. Hurwitz, Jr., and E. F. Clancy. Sensitivity of radiation damage to displacement probability—1657(A)
Sanders, J. H. (see Collington, D. J.)—1622(L)
Sandri, G. (see Sreekantan, B. V.)—642(A)
Sands, M., M. Bloch, J. G. Teasdale, and R. L. Walker. Search for photoproduction of meson pairs in H—652(A)
Sands, R. H. Paramagnetic resonance absorption in glass—1222
Sandweiss, Jack (see Birge, Robert W.)—329(L)
Saphir, George (see Maenchen, George)—1619(L)
Sarabhai, V., U. D. Desai, and D. Venkatesan. Solar influence on anisotropy of primary cosmic radiation. I. Studies at low latitudes—1490
Sargent, C. P., M. Rinehart, L. M. Lederman, and K. C. Rogers. Diffusion cloud-chamber study of very slow mesons. II. β decay of muon—885
Satterthwaite, C. B., W. S. Corak, B. B. Goodman, and Aaron Wexler. Specific heat of V in normal and superconducting states—1660(A)
—— (see Corak, W. S.)—1660(A)
Saunders, M. J. and A. G. Smith. Atmospheric turbulence—1627(A)
Scanlon, W. W. Polar semiconductors—620(T)
Scarf, Frederick L. Spectrum of Bethe-Salpeter equation—675(A)
Schachter, Harry (see Wrenshall, Gerald A.)—1640(A)
Schardt, A. W. and Joan P. Welker. Energy levels of As^{75}—810
Scharenberg, R. P. (see Stewart, M. G.)—691
Scharff-Goldhaber, Gertrude, E. der Mateosian, G. Harbottle, and M. McKeown. Decay of U^{233} (74 yr)—180
Schawlow, A. L. Structure of intermediate state in superconductors—656(T)
Schechter, Daniel (see Kohn, Walter)—1903(L)
Schecter, Larry (see Ellis, Robert E.)—1044(L)
Scheidegger, Adrian E. Gravitational radiation—1883
Schein, Marcel, D. M. Haskin, and R. G. Glasser. Further investigations on photon event—643(A)
—— (see Glasser, R. G.)—1555
—— (see Haskin, D. M.)—643(A)
Schiessler, R. W. (see Cutler, W. G.)—638(A)
—— (see Lowitz, D. A.)—637(A)
Schiff, Daniel. Numerical solution of integral transport equation—660(A)
Schiff, L. I. Low-energy physics from high-energy standpoint—628(T)
Schiffer, J. P., P. M. Windham, C. R. Gossett, and G. C. Phillips. Inelastic scattering of protons from isotopes of Mn, Ni, and Cu—655(A)
—— (see Phillips, G. C.)—655(A)

Schiller, Ralph. Particle motion in nonrelativistic quantum theory—662(A)
Schindler, Albert I. and Edward I. Salkovitz. Ferromagnetic Hall coefficient of Ni alloys—1251
Schmid, L. C. (see Cork, J. M.)—703
Schmitt, R. W. Effect of order-disorder on low-temperature resistance maximum—614(A)
Schneps, J. (see Fry, W. F.)—1561; 1055(L)
Schrank, G. Elastic scattering of 17-Mev protons by nuclei —640(A)
—— Energy control for external cyclotron beams—677(A)
—— (see Aron, W.)—629(A)
Schremp, E. J. Isotopic spin and group-space of proper Lorentz group—1603
Schulte, H. J. (see Camac, M.)—897
Schultz, H. L. and W. G. Wadey. Electronic instrumentation for Yale slow-neutron velocity selector—1634(A)
—— (see Wadey, W. G.)—1634(A)
Schulz, William Donald. Interaction of nonlocal and local fields—290
Schumacher, Berthold W. Pictures of gas-streams at low-gas density taken by means of electrons—1638(A)
Schwartz, Charles. Hfs anomaly in atomic P-states—1035 (L)
Schwartz, Robert B., James W. Corbett, and William W. Watson. Protons from α bombardment of A^{39} and A^{40}—655 (A)
Schwarz, E. G. K. Si analysis for B by thermal neutrons—625(A)
Schwarzmann, Gertrude T. Classical microphysics—662(A)
—— Physical significance of three quantum numbers—677 (A)
Schweinler, H. C. (see Crawford, J. H.)—1330(L)
Sclar, N. Impact ionization of impurities in Ge—620(T)
Scofield, N. E. (see Howland, P. R.)—663(A)
Scott, G. D. (see Aziz, R. A.)—1636(A)
Scott, G. G. Gyromagnetic ratio of Fe at low magnetic intensities—1241
—— Gyromagnetic ratio of Ni at low magnetic intensities—1824
Scott, Mary Jean and Ralph E. Segel. Fast-neutron reactions in KI(Tl) crystals—622(A)
Scott, William T. Multiple Coulomb scattering including nuclear size effects—629(A)
Seaborg, G. T. (see Ghiorso, A.)—1048(L)
Sedra, R. N. and I. B. Hazzaa. Effect of radiation from solar flares on ionosphere and earth's magnetic field—1070
Seeman, N. (see Stiller, B.)—641(A)
Segel, Ralph E. (see Scott, Mary Jean)—622(A)
Segrè, Emilio. Neutron physics—630(T)
Seiler, Milton R., John N. Cooper, and J. C. Harris. γ-ray yield from natural Si bombarded with protons—340(A)
Seitz, F. Fermi statistics and its applications—630(T)
Seliger, H. H. (see Ziegler, C. A.)—663(A)
Sellen, J. Michael, Jr. (see Moravcsik, Michael J.)—653 (A)
Senio, Peter (see Tucker, Charles W., Jr.)—1777
Serber, Robert and William Rarita. p-p scattering high energies—629(A)
—— (see Pais, A.)—1551
Shafroth, S. M. and J. A. Marcus. Annihilation radiation from positrons stopping in superconducting Pb—664(A)
Shamos, M. H. (see Fafarman, A.)—623(A)
Shapiro, Anatole M. (see Chen, Francis F.)—857
Shapiro, H. S. Virial series of ideal Bose-Einstein gas—1673
Shapiro, I. I. and R. J. Glauber. Nucleon scattering by nuclei at high energies—629(A)
Shapiro, J. and M. A. Preston. Calculations on charge independence with repulsive core potentials—1654(A)
Shapiro, M. M. K-mesons and hyperons in cosmic radiation —620(T)
—— (see O'Dell, F. W.)—641(A)
—— (see Stiller, B.)—641(A)
Sharp, R. D., A. Sperduto, and W. W. Buechner. Angular distribution of proton groups from $N^{14}(d,p)N^{15}$ reaction—632(A)
Shatas, R. A. (see Pomerantz, M. A.)—489
Sheldon, J. W. Use of statistical field approximation in molecular physics—1291
Sheline, Raymond K. and Joseph R. Wilkinson. Isobaric triplet Cr^{49}—V^{49}—Ti^{49}—165
—— **and Joseph R. Wilkinson.** New radioactivity Mn^{60}—1630(A)
——, **Joseph R. Wilkinson, Bruce J. Dropesky, and Theodore T. Shull.** Evidence against the existence of 23-hour V^{50}—1055(L)
—— (see Wilkinson, Joseph R.)—752
Sherr, R. and W. F. Hornyak. Inelastic scattering of 19-Mev protons by O^{16}: (A) proton groups—632(A)
—— (see Hornyak, W. F.)—632(A)
Shibuya, Motoichi. Hot electron problem in semiconductors with spheroidal energy surfaces—1189
Shilts, J. L. (see Baldwin, G. J.)—1650(A)
Shimada, Junji (see Kumagai, Hiroo)—1116
Shirn, G. A. (see Huntington, H. B.)—1085
Shull, C. G. (see Wilkinson, M. K.)—627(A)
Shull, Franklin B. (see McFarland, Charles E.)—655(A)
Shull, Theodore T. (see Sheline, Raymond K.)—1055(L)
Shutt, R. P. (see Block, M. M.)—261
Sidhu, S. S. and D. D. Zauberis. Mutual solubilities of Fe and Os—615(A)
Siegert, A. J. F. (see Lewis, M. B.)—661(A)
Siegfried, J. G. (see Nelson, J. R.)—658(A)
Sils, V. (see Smakula, A.)—1744; 1747
Silsbee, H. B. (see Hobson, J. P.)—612(A)
—— (see Hubbs, J. C.)—612(A)
Silver, E. G. (see Waniek, R. W.)—622(A)
Silverman, A. (see Wolfe, B.)—268
Silverstein, E. A. (see McEllistrem, M. T.)—632(A)
Simnad, M. and R. Smoluchowski. Effect of proton irradiation upon electrode potential of W—1891(L)
Simon, Albert. Ambipolar diffusion in magnetic field—646 (A)
Simpson, F. B., R. G. Fluharty, and O. D. Simpson. Resonance parameters in Ta—610(A)
Simpson, J. A. (see Meyer, Peter)—608(A); 1517
Simpson, J. Arol (see Marton, L.)—495; 1648(A)
Simpson, O. D. (see Simpson, F. B.)—610(A)
Sinclair, Rolf M. γ radiation from interaction of 4.4-Mev neutrons with Fe^{54} and Fe^{56}—1351
—— γ radiation from interaction of 4.4-Mev neutrons with Ge and W—621(A)
Singer, S. F. (see Griem, H.)—608(A)
Singh, Nand Lal. Emission bands in Cu_2—1624(A)
—— (see True, Tom T.)—1626(A)
Sippel, R. F. (see Bent, R. D.)—710
Sites, J. R. (see Boyd, G. E.)—1030(L)
Skinner, R. Photonuclear reactions: theoretical considerations—1644(T)
Skulski, R. W. and D. Weimer. Reflection of compression wave from symmetrical wedge—633(A)
Slätis, Hilding (see Rasmussen, John O.)—42
Slaughter, G. G., M. M. Block, and E. M. Harth. Chronotron for time-of-flight studies of cosmic rays—1626(A)
Slichter, Charles P. Concept of temperature and Overhauser nuclear polarization effect—1822
—— Spin resonance of impurity atoms in Si—479

Slonczewski, J. C. and P. R. Weiss. Combined tight binding and perturbation theory of graphite π states—636(A)
Smakula, A. and J. Kalnajs. Precision determination of lattice constants with Geiger-counter x-ray diffractometer —1737
——, **J. Kalnajs, and V. Sils.** Densities and imperfections of single crystals—1747
—— **and V. Sils.** Precision density determination of large single crystals by hydrostatic weights—1744
Smart, J. Samuel. Application of Bethe-Weiss method to ferrimagnetism—1642(A)
Smith, A. G. (see Saunders, M. J.)—1627(A)
Smith, Bernard and Henry A. Boorse. He II film transport. II. Role of surface finish—346
—— **and Henry A. Boorse.** He II film transport. III. Role of film height—358
—— **and Henry A. Boorse.** He II film transport. IV. Role of temperature—367
Smith, D. F., and A. H. Nielsen. Pure rotational spectrum of HF—1624(A)
Smith, Frances M. (see Chupp, Warren W.)—335(L)
Smith, H. L. (see Ghiorso, A.)—1048(L)
Smith, M. S., R. R. Smith, E. G. Joki, and J. E. Evans. Total neutron cross section of Np-237 in 0.02- to 3-ev region—611(A)
Smith, P. L. (see Lipson, H. G.)—1535(A); 444
Smith, R. G. (see Nichols, P. F.)—621(A)
Smith, R. K. (see Henkel, R. L.)—1050(L)
—— (see Nobles, R. A.)—616(A)
Smith, R. R. (see Smith, M. S.)—611(A)
Smith, Robert T., Jr., J. C. Harris, and John N. Cooper. Technique for detection of nuclear resonances by observing residual radioactivity—340(A)
Smith, S. J. and L. M. Branscomb. Threshold for photodetachment from OH^-—1657(A)
Smither, R. K. Measurement of coefficient of secondary electron emission with resonant cavity—646(A)
Smoluchowski, R. (see Lang, G.)—596(L)
—— (see Simnad, M.)—1891(L)
Snell, Arthur H. and Frances Pleasonton. Charge spectrum of Cl^{37} recoils from neutron emission in electron-capture decay of A^{37}—1625(A)
Snow, G. A. (see Fry, W. F.)—1055(L)
Snyder, J. N. (see Rubenstein, R. A.)—189
Snyder, W. S. (see Neufeld, J.)—1326(L)
Soberman, R. K., A. Beiser, and S. A. Korff. Variation of position of cosmic-ray neutron intensity maximum with geomagnetic latitude—608(A)
Sogo, P. B. and C. D. Jeffries. Spin, magnetic moment, and electric quadrupole moment of La^{139} and magnetic moment of Cl^{35}—613(A)
Solomon, I. Relaxation processes in system of two spins—559
Sörensen, S. O. (see Haugerud, Ö.)—1046(L)
Spence, R. W. (see Ghiorso, A.)—1048(L)
Spencer, L. V. Asymptotic spatial trend of electron penetration—661(A)
—— Theory of electron penetration—639(T)
Sperduto, A. (see Buechner, W. W.)—644(A)
—— (see Sharp, R. D.)—632(A)
Spicer, B. M. Photoprotons from oxygen—33
Spinks, J. W. T. (see Katz, L.)—98
Spital, Sidney (see Baskir, Emanuel)—639(A)
Spitzer, W. G. and H. Y. Fan. Infrared absorption in InSb —1891(L)
Spruch, L. (see Rotenberg, A.)—649(A)
Sreekantan, B. V., A. Pevsner, and G. Sandri. Angular correlations in V^0-particle decays—642(A)
—— (see DeStaebler, H., Jr.)—642(A)
Srinivasan, D. and L. V. Holroyd. Sonoluminescence of water—633(A)
Srinivasan, T. M. (see Ramanathan, K. G.)—442
Stanger, Philip C. Study of spectroscopic binary 5 Lacertae —339(T)
Starner, J. W. (see Brolley, J. E., Jr.)—330(L)
—— (see Bunker, M. E.)—659(A); 1906(E)
—— (see Mize, J. P.)—671(A)
Stearns, M. B. Intensities and energy shifts of transitions in π-mesonic atoms—628(T)
Steele, M. C. Oscillatory galvanomagnetic properties of Sb single crystals at liquid He temperatures—1751
Steffen, R. M. Attenuation of Cd^{111} directional correlation in liquid In^{111} sources—659(A)
—— **and J. N. Brazos.** Decay of 72-sec In^{114} ground state—1646(A)
—— (see Brazos, J. N.)—1645(A)
Stein, P. C. (see Weinstein, R. M.)—1621(L)
Steinberg, M. S. Radiation dosage from thermonuclear explosions—666(A)
Steinberger, I. T., W. Low, and E. Alexander. Influence of alternating electric fields on light emission of some phosphors—1217
Steljes, John F. (see Carmichael, Hugh)—1542
Stelson, P. H. and F. K. McGowan. Coulomb excitation of states in Tl and Pb—616(A)
—— **and F. K. McGowan.** γ-ray yields from Coulomb excitation—112
—— (see McGowan, F. K.)—127
Stephens, Frank S., Jr. (see Rasmussen, John O.)—47
Stephenson, C. V. Radial vibrations in short hollow cylinders of $BaTiO_3$—1631(A)
Stephenson, R. J. Principles of reactor operation—339(T)
Sternglass, E. J. and M. M. Wachtel. Measurement of low-energy electron absorption in metals and insulators—646(A)
Sternheimer, R. M. Energy distribution of γ rays from π^0 decay—277; 618(A)
Stevens, D. K. and J. H. Crawford, Jr. Magnetic susceptibility of InSb—487
—— (see Crawford, J. H.)—1330(L)
Stewart, A. T. Angular correlation of photons from positron annihilation in solids—594(L)
Stewart, Leona (see Frye, G. M., Jr.)—1375
—— (see Rosen, Louis)—1052(L)
Stewart, M. G., R. P. Scharenberg, and M. L. Wiedenbeck. Angular correlation of γ rays of Ba^{134}—691
Stier, P. M. and C. F. Barnett. Electron capture cross section for protons—1630(A)
Stiller, B., M. M. Shapiro, and N. Seeman. Stopped K-mesons observed near geomagnetic equator—641(A)
Stolovy, A. and J. A. Harvey. Fast-chopper measurements of radiation widths—611(A)
Stone, Gerald (see Everhart, Edgar)—1287
Stork, Donald H. and S. Whetstone. Cross section for $p+p \rightarrow \pi^+ + p + n$—651(A)
—— (see Birge, Robert W.)—329(L)
—— (see Kerth, L. T.)—641(A)
—— (see Whetstone, S.)—673(A)
Stout, V. L. and M. D. Gibbons. Thin film interference phenomena applied to study of gettering by Ti—1643(A)
Straley, Joseph W. (see True, Tom T.)—1624(A)
Strandberg, M. W. P. Electronic contribution to effective nuclear masses in molecules—667(A)
—— (see Peter, M.)—667(A)
—— (see Swan, P. R.)—667(A)
—— (see Tinkham, M.)—527
Strauch, Karl. Double scattering experiment with 96-Mev protons—150

Stroke, H. H. (see Reynolds, J. B.)—613(A)
Strominger, Donald (see Rasmussen, John O.)—47
Studier, M. H. (see Ghiorso, A.)—1048(L)
Stull, J. L. (see Bickford, L. R., Jr.)—1210
Sturm, W. J. (see Binder, D.)—603(L)
Sugarman, Nathan (see Jodra, Luis G.)—1470
—— (see Kruger, Paul)—1459
Sugawara, M. Electromagnetic properties of deuteron—1601
Summers, R. (see Barnes, S. W.)—673(A)
Sunyar, A. W. Electric quadrupole transitions in nuclei—628(T)
—— (see Alburger, D. E.)—695
Sutton, Paul M. Computation of mean Debye temperature of cubic crystals from elastic constants. II—1826
Suura, Hiroshi. Radiative correction to high-energy electron scattering—1020
Swami, M. S. (see Fry, W. F.)—1561; 1055(L)
Swan, P. R. and M. W. P. Strandberg. Excited torsional states in asymmetric hindered rotors—667(A)
Swann, W. F. G. Certain matters pertaining to internal structure of nucleons—650(A)
Swanson, John A. Saturation Hall constant of semiconductors—1799
Swanson, R. W. (see van Bavel, C. H. M.)—1626(A)
Swenson, C. A. Compression of alkali metals to 10 000 atmospheres at low temperature—423

Taft, E. and L. Apker. Photoelectric emission from polycrystalline graphite—1831
Takano, Y. and J. L. Anderson. Generalization of Feynman's integral-over-all-paths formulation of quantum mechanics—674(A)
Tanaka, Katsumi. Lee model—676(A)
Tannenwald, P. E. Multiple resonances in cobalt ferrite—463
Tauber, G. E. Energy levels of Pb^{208}—176
—— (see Levitt, L.)—1659(A)
Tautfest, G. W. and K. L. Brown. Precision monitor for electron beams—664(A)
—— (see Crowe, K. M.)—872
—— (see Helm, R. H.)—650(A)
Taylor, H. W. and R. W. Pringle. γ-γ directional correlation in Pt^{190}—1345
Taylor, J. C. and B. R. Coles. Thermoelectric powers of some Pd alloys—614(A)
Taylor, Julius. Pressure dependence of resistivity, Hall constant, and energy gap for InAs—1655(A)
Taylor, R. Dean (see Dash, J. G.)—598(L)
Teasdale, J. G. (see Sands, M.)—652(A)
—— (see Walker, R. L.)—210
Teasdale, Tom S. Permanent magnetic moments of superconducting sphere—1248
Temmer, G. M. and N. P. Heydenburg. Energy levels in Ru, Pd, and Cd by Coulomb excitation—617(A)
—— **and N. P. Heydenburg.** Fast *F2* transition probabilities from Coulomb excitation—1609(L)
—— (see Heydenburg, N. P.)—617(A)
Tendam, D. J. (see Bleuler, E.)—1652(A); 1605(L)
Tewes, H. A. (see Coleman, G. H.)—288
Theissing, H. H. and P. J. Caplan. Atmospheric attenuation of solar millimeter-wave radiation—624(A)
Theoclitus, Gregory and Homer C. Wilkins. Counting efficiency of electromechanical message registers—634(A)
Thieme, M. T. and E. Bleuler. Decay of Au^{196} and Au^{198}—1646(A)
Thode, H. G. Abnormal fission yields and nuclear shell structure—1638(T)
Thompson, J. A. L. (see Mann, K. C.)—1634(A)
Thompson, R. W. (see Kim, Y. B.)—642(A)
Thompson, S. G. (see Ghiorso, A.)—1048(L)
—— (see Harvey, B. G.)—337(L)
Thorndike, A. M. (see Block, M. M.)—261
Ticho, Harold K. (see Freden, Stanley C.)—1057(L)
Tidwell, Marvin, S. K. Haynes, and P. K. S. Wang. Energy spectrum of low-voltage x-ray tube—1629(A)
—— (see Wang, P. K. S.)—1639(A)
Tilden, Elizabeth F. (see Bozorth, R. M.)—1788
Timnick, A. (see Jones, W. H.)—184
Tinkham, M. and M. W. P. Strandberg. Line breadths in microwave magnetic resonance spectrum of O_2—537
Tinlot, John (see Baskir, Emanuel)—639(A)
Tobin, R. A. (see Bendel, W. L.)—672(A)
Toller, A. L., H. W. Newson, and E. Merzbacher. Neutron resonances in kev region: Na^{23} and Al^{27}—1625(A)
——, **J. R. Patterson, and H. W. Newson.** Neutron resonances in kev region: Cl^{35}, Cl^{37}, K^{39}, and K^{41}—620(A)
Tollestrup, A. V., J. C. Keck, and R. M. Worlock. Photoproduction of positive pions in hydrogen-counter telescope method—220
Tomboulian, D. H. (see Bedo, D. E.)—624(A)
Tomlinson, R. H. (see Wiles, D. M.)—188
Toms, M. E. (see Bendel, W. L.)—672(A)
Toppel, B. J., D. H. Wilkinson, and D. E. Alburger. 2^- state at 8.85 Mev in O^{18}—632(A)
Townes, C. H. (see Gordon, J. P.)—1264
Trainor, L. E. H. and W. R. Dixon. Possibility of nuclear change of phase—1655(A)
Treiman, S. B. and H. W. Wyld, Jr. γ stability of *K*-mesons—1039(L)
Trolan, J. K. (see Dyke, W. P.)—1192
Trout, T. W. (see Page, L. A.)—665(A)
True, Tom T., Nand Lal Singh, and Joseph W. Straley. Infrared intensity measurements in halogenated methanes—1624(A)
Tucker, Charles W., Jr., and Peter Senio. X-ray scattering effects due to localized static lattice defects—1777
Turberfield, K. C. (see Collington, D. J.)—1622(L)
Turner, E. B. Radiation from strong shock front in Kr—633(A)
Tweet, A. G. Electrical properties of plastically deformed Ge—1245
—— Properties of grain boundaries in Au-doped Ge—1182
Tyler, W. W. Photoconductivity in Ge—620(T)

Uberall, H. (see Dyson, F. J.)—604(L)
Ueda, Ryuzo (see Kobayashi, Jinzo)—1900(L)
Uhlir, A., Jr. Micromachining with virtual electrodes—615(A)
Underwood, Newton (see van Bavel, C. H. M.)—1626(A)

Vallee, R. E. (see Grove, G. R.)—340(A)
Van Allen, J. A. Interpretation of soft radiation observed at high altitudes in northern latitudes—609(A)
—— (see Meredith, L. H.)—198
van Bavel, C. H. M., Newton Underwood, and R. W. Swanson. Soil moisture determination by neutron measurements—1626(A)
van Lieshout, R. (see Farrelly, B.)—1440
Van Loef, J. J. (see Lind, D. A.)—621(A)
Van Vleck, J. H. Bloembergen spin reservoir temperature in paramagnetic resonance experiments—1659(A)
Varnerin, L. J., Jr., and J. H. Carmichael. Role of reemission in ionic pumping—1662(A)
—— (see Garfunkel, M. P.)—1647(A)
Vash, A. M. (see Blewett, J. P.)—652(A)
Venkatesan, D. (see Sarabhai, V.)—1490
Verlet, L. (see Drell, S. D.)—849
Vette, J. I. (see Walker, R. L.)—210

Visscher, William M. and Richard A. Ferrell. Nuclear forces and β decay of C^{14}—649(A)
Vogan, E. L. (see Hines, C. O.)—1638(A)
Volkoff, G. M. Radio-frequency spectra of nuclei in crystals—1648(T)
Voss, R. G. P. and R. Wilson. Neutron and proton distributions in heavy nuclei—1056(L)

Wachtel, M. M. (see Sternglass, E. J.)—646(A)
Wachtman, J. B., Jr., and L. H. Maxwell. Slip systems and creep in oxide crystals—657(A)
Wadey, W. G. and H. L. Schultz. Revised Yale linear electron accelerator and facilities—1634(A)
—— (see Schultz, H. L.)—1634(A)
Wagener, S. Adsorption measurements at very low pressures—1643(A)
Wagner, F., Jr. (see Freedman, M. S.)—671(A)
—— (see Porter, F. T.)—671(A)
Wagner, Robert T. and Frank L. Hereford. Temperature effects in annihilation of positrons—593(L)
—— **and F. L. Hereford.** Temperature effects in 3-quantum annihilation of positrons—665(A)
Wahl, Arthur G. Fission of U^{235} by 14-Mev neutrons: Nuclear charge distribution and yield fine structure—730
Wainfan, N., W. C. Walker, and G. L. Weissler. Photoionization efficiencies and cross sections in O_2, N_2, CO_2, A, H_2O, H_2, and CH_4—542
Wait, J. R. (see Frood, D. G.)—1639(A)
Wajda, E. S. (see Huntington, H. B.)—1085
Waldron, R. D. Infrared spectra of ferrites—1727
Walker, R. L. Photoproduction of mesons in H and deuterium—620(T)
——, **J. G. Teasdale, V. Z. Peterson, and J. I. Vette.** Photoproduction of positive pions in hydrogen-magnetic spectrometer method—210
—— (see Sands, M.)—652(A)
Walker, W. C. (see Wainfan, N.)—542
Wall, N. S. (see Bromley, D. A.)—1029(L)
Wallace, O. J. (see Page, L. A.)—665(A)
Wallace, R. W. (see Bandtel, K. C.)—673(A)
Wallis, G. and J. F. Battey. Modulation of Schottky emission from metal point contacts to Ge—625(A)
Wallis, Richard F. (see Herman, Robert)—435
Walton, R. B., R. L. Becker, J. D. Clement, and M. S. Zucker. $C^{13}(\alpha,n)$ reaction—1649(A)
Wandel, C. F. (see Lane, A. M.)—647(A)
Wang, P. K. S., R. J. Raridon, and Marvin Tidwell. Scintillation spectrometry of x-rays from Be-window tube—1639(A)
—— (see Raridon, Richard)—1629(A)
—— (see Tidwell, Marvin)—1629(A)
Wang, Tien-Chuan. Pure nuclear quadrupole spectra of Cl and Sb isotopes in solids—566
Waniek, R. W., L. Garrido, R. Goloskie, and E. G. Silver. Secondaries from high-energy neutron interactions with W—622(A)
—— (see Culler, Vaughn)—740
Warburton, E. K. (see McGruer, J. N.)—632(A)
Waring, R. K., Jr. He film transfer rate from 0.14 to 2.19°K—1704
Warner, A. W., Jr. (see Bömmel, H. E.)—1894(L)
Warren, Dana T. Altitude effect on cosmic-ray fine structure—608(A)
Watanabe, Satosi and Norman L. Oleson. Possible explanation of moving striations in discharge tube—646(A)
—— **and Norman L. Oleson.** Traveling density waves in positive columns—1701
Watson, William W. (see Corbett, J. W.)—634(A)
—— (see Schwartz, Robert B.)—655(A)
Wattenberg, A. (see Weinstein, R. M.)—1621(L)
Webb, Francis H. (see Chupp, Warren W.)—335(L)
Webb, R. A. (see Langford, F. L.)—1631(A)
Webb, T. S., F. B. Hagedorn, W. A. Fowler, and C. C. Lauritsen. Elastic scattering of protons by F^{19}—138
Webb, W. (see Cutler, W. G.)—638(A)
—— (see Lowitz, D. A.)—637(A)
Webeler, R. (see Allen, G.)—556
Weber, A. H. (see Doerner, R. K.)—672(A)
—— (see O'Friel, Z.)—659(A)
Weber, Marvin J. (see Brode, Robert B.)—610(A)
Weddell, J. B., B. Jennings, and R. L. Hellens. Scattering of 4.4-Mev neutrons by C, Ca, Fe, and Zr—621(A)
Wegner, Harvey E., R. M. Eisberg, and G. Igo. Elastic scattering of 40-Mev α particles from heavy elements—825
——, **R. M. Eisberg, and G. Igo.** Elastic scattering of 40-Mev α particles from heavy nuclei—640(A)
—— (see Bloom, S. D.)—654(A)
—— (see Eisberg, R. M.)—1606(L)
Weimer, D. (see Skulski, R. W.)—633(A)
Weinstein, R. M., A. Odian, P. C. Stein, and A. Wattenberg. Photoproton-proton coincidences from various nuclei—1621(L)
Weiss, P. R. (see Slonczewski, J. C.)—636(A)
Weiss, R. J. (see Antal, J. J.)—1081
Weissler, G. L. (see Lee, Po)—540
—— (see Wainfan, N.)—542
Weissmann, Sigmund and Roger Chang. X-ray diffraction studies of radiation damage of Ge single crystal—657(A)
Welker, Joan P. (see Schardt, A. W.)—810
Weller, C. E. and J. C. Grosskreutz. γ rays from proton bombardment of Cu^{63} and Cu^{65}—655(A)
Welmers, E. T. Information theory—bit by bit—341(T)
Welsh, H. L. (see Allin, Elizabeth J.)—1639(A)
—— (see Gaizauskas, V.)—1639(A)
—— (see Hare, W. F. J.)—1887(L)
Welton, Ted A. Fixed-frequency billion-volt proton cyclotron—1623(T)
Wessel, W. Quantum electrodynamics and mass operator—676(A)
West, E. J. (see Liebson, S. H.)—647(A)
Wexler, Aaron (see Satterthwaite, C. B.)—1660(A)
Wexler, S. (see Goodman, L. S.)—192
Wheatley, G. H. (see Hrostowski, H. J.)—626(A)
Wheatley, J. C., D. F. Griffing, and R. D. Hill. Ratio of magnetic moments of Co^{59} and Co^{60}—334(L)
Wheeler, John A. Scattering and potential—630(A)
Wheeler, R. G., C. H. Blakewood, and C. T. Lane. Second sound attenuation in rotating He II—1667
Whetstone, S. and D. Stork. Scattering of 22-Mev positive pions on protons—673(A)
—— (see Stork, D.)—651(A)
White, R. Stephen, Mark J. Jakobson, and Gordon W. Repp. π^+ photomeson production at 143°—651(A)
Whitehead, Marian N. (see Birge, Robert W.)—329(L)
—— (see Kerth, L. T.)—641(A)
Whittemore, W. L. (see Block, M. M.)—261
Widgoff, M. (see Hill, R. D.)—229
Widom, B. Inelastic molecular collisions near threshold—1658(A)
Wiedenbeck, M. L. (see Stewart, M. G.)—691
Wieder, H. H. Electrical behavior of $BaTiO_3$ single crystals at low temperatures—1161
Wiggins, J. S. (see Forster, H. H.)—660(A)
Wightman, A. S. and D. Hall. Universal singular functions in local relativistic quantum field theory—674(A)
—— (see Greenberg, O. W.)—675(A)
Wikner, N. F. (see Bandtel, K. C.)—673(A)

Wilcox, John M. and Burton J. Moyer. Nuclear internal momentum distributions—875
Wiles, D. M. and R. H. Tomlinson. Half-life of Cs^{137}—188
Wilkins, Homer C. (see Theoclitus, Gregory)—634(A)
Wilkinson, D. H. Energy dependence of cross sections for reactions $C^{13}(d,n)N^{14}$ and $C^{13}(d,t)C^{12}$ up to E_D=20 Mev —632(A)
—— Lowest state of surface osciliation of O^{16} at 14.7 Mev —1347
—— (see Toppel, B. J.)—632(A)
Wilkinson, Joseph R. and Raymond K. Sheline. New isotope Mn^{58}—752
—— (see Sheline, Raymond K.)—165; 1055(L); 1630(A)
Wilkinson, M. K., C. G. Shull, and R. E. Rundle. Ferromagnetic structure of UH_3—627(A)
Wilkinson, Roger G. (see Bolotin, Herbert H.)—62; 671 (A)
—— (see Pruett, C. H.)—670(A)
Willard, H. B. (see Cohn, H. O.)—644(A)
—— (see Kington, J. D.)—1393
Williams, Albert J. (see Bozorth, R. M.)—1788
Williams, D. V. P. and Dixon Callihan. Resolving time of Geiger-Mueller counters—1626(A)
Williams, Dudley. Recent spectroscopic studies of thermal radiation in atmosphere—1623(T)
—— (see Geusic, Joseph E.)—612(A)
Williams, I. R. (see Johns, M. W.)—1645(A)
Williams, R. W. (see Altman, L.)—609(A)
Williamson, R. M. and S. A. Cox. Angular distributions and angular correlations in $Mg^{24}(d,p)Mg^{25}$—644(A)
—— (see Cox, S. A.)—631(A)
Wilson, H. W. (see McNair, A.)—771
Wilson, R. (see Voss, R. G. P.)—1056(L)
Winckler, J. R. and L. Peterson. Azimuthal effect for cosmic-ray protons and α particles using Čerenkov counter —608(A)
Windham, P. M. (see Phillips, G. C.)—655(A)
—— (see Schiffer, J. P.)—655(A)
Winegard, W. C. (see Rosenberg, A.)—1635(A)
Winter, Rolf G. Search for double β decay in Cd and Mo—88
Witmer, Enos E. Electron mass as natural unit of mass for nuclei and elementary particles—1653(A)
—— Three-dimensionality of space and masses of nuclei and elementary particles—1663(A)
Woernley, D. L. Magnetic susceptibilities of biological material—341(T)
Wolfe, B., A. Silverman, and J. W. DeWire. Elastic photoproduction of π^0 mesons from deuterium—268
Wolfgang, R. L. (see Friedlander, G.)—263
Wolfsberg, Max and Morris L. Perlman. Multiple electron excitation in Auger processes—1833
Woods, Joseph F. Hall effect and resistivity study of photoconducting PbS films—658(A)
Worley, R. D., M. W. Zemansky, and H. A. Boorse. Heat capacities of V and Ta in normal and superconducting phases—447
Worlock, R. M. (see Tollestrup, A. V.)—220
Wrenshall, Gerald A. and Harry Schachter. Transfer rate measurements in hydrodynamic system containing nonuniformly mixing compartment—1640(A)
—— (see Lax, Louis C.)—1640(A)
Wright, Byron T. (see Chow, Richard H.)—640(A)
Wright, Robert W. (see Maenchen, George)—1619(L)
Wright, S. Courtenay. Phase shift formulas for nucleon-nucleon scattering—996
Wu, C. S. (see Farrelly, B.)—1440
Wu, T. Y. (see Levitt, L.)—1659(A)
Wyckoff, J. M. and H. W. Koch. Energy spectrum of delayed γ rays from U photofission—616(A)
—— (see Koch, H. W.)—663(A)
Wyld, H. W., Jr. (see Treiman, S. B.)—1039(L)
Wyman, James H. (see Gordy, Walter)—1905(L)

Yadoff, Oleg. Production of electrostatic charges by rotation of permanent magnet—677(A)
—— **and Sophie Yadoff.** Rotational oscillations of electrostatically charged conductors—635(A)
Yadoff, Sophie (see Yadoff, Oleg)—635(A)
Yaffe, L. (see Graham, R. L.)—1646(A)
Yager, W. A., J. K. Galt, and F. R. Merritt. Ferromagnetic resonance in two Ni-Fe ferrites—1203
—— (see Bozorth, R. M.)—1898(L)
Yagoda, Herman. Charge spectrum and zenith angle distribution of heavy primary nuclei entering atmosphere—1644(A)
—— Mesonic decay of ejected triton—651(A)
Yalow, Rosalyn S. and Solomon A. Berson. Kinetic analysis of thyroidal iodide trapping and binding in human subject—342(A)
Yamamoto, K. (see Hasebe, K.)—1331(L)
Yearian, H. J. and W. D. Derbyshire. Oxygen parameters of $FeFe_{(2-x)}Cr_xO_4$ spinel system—626(A)
Yekutieli, G., M. F. Kaplon, and J. Klarmann. β decay of K-mesons—641(A)
—— (see Kaplon, M. F.)—1528
—— (see Klarmann, J.)—641(A)
Yergin, Paul F. (see Novick, Robert)—612(A)
Yevick, G. J. and J. K. Percus. Exact classical and quantum mechanical equations of motion for N particles using collective coordinates—661(A)
—— (see Percus, J. K.)—661(A)
Yilmaz, Huseyin. Formulation of relativity—662(A)
Yodh, G. B. (see Panofsky, W. K. H.)—651(A)
Yos, J. M. (see Jehle, Herbert)—1640(A)
Young, J. R. Deterioration of luminescent phosphor under positive ion bombardment—1648(A)
Yu, S. P. (see Morrish, A. H.)—1641(A)

Zankel, Kenneth L. and Alex E. S. Green. Perturbations of semiempirical mass equation—1628(A)
Zauberis, D. D. (see Sidhu, S. S.)—615(A)
Zeidman, Benjamin (see McFarland, Charles E.)—655(A)
Zeiger, H. J. (see Foner, Simon)—635(A)
—— (see Gordon, J. P.)—1264
Zemansky, M. W. (see Worley, R. D.)—447
Zernow, Louis (see Hauver, George)—635(A)
Ziegler, C. A., H. H. Seliger, and I. Jaffe. Oxygen quenching and wavelength shifters in liquid scintillators—663(A)
Zimmerman, E. J. Scintillation response of anthracene to low-energy protons and He ions—1199
Zimmerman, R. L. (see Palevsky, H.)—611(A)
Zinn, W. H. Atomic energy—630(T)
Zuchelli, A. J. (see Berko, S.)—1652(A)
Zucker, A. (see Reynolds, H. L.)—640(A)
Zucker, M. S. (see Walton, R. B.)—1649(A)

Author Index to Volume 100

References with (A) are to abstracts of papers presented at meetings of the American Physical Society; references with (T) designate title only. References with (L) are to Letters to the Editor. References with (E) are to Errata.

Abraham, M. and S. J. Goldsack. Pi meson production in Pb and C—1799(A)

Adair, Robert K. Angular distribution of Λ^0 and θ^0 decays —1540(L)

Adams, A., Jr. (see Statz, H.)—1260(A)

Adkins, R. and J. G. Brennan. Intermediate coupling in odd-odd nuclei—1790(E)

Ahrens, T. Matrix element relations in β decay theory and nuclear forces—974(A)

—— (see Miller, M. M.)—974(A)

Ajzenberg, F., A. Rubin, G. D. Johnson, and M. Mazari. Neutrons from proton bombardment of B^{11}—960(A)

—— (see Rubin, A.)—961(A)

Akeley, Edward S. Determination of magnetic field strength H and its vector potential A in terms of magnetic field strength H_s on plane surface, with application to spiral ridged FFAG accelerator—972(A)

Alaga, G. New type of selection rules in β-decay of strongly deformed nuclei—432(L)

Alba Andrade, Fernando. Experimental nuclear physics in University of Mexico—954(T)

—— (see Mazari, M.)—972(A)

Alburger, D. E. and B. J. Toppel. Radioactive decays of Rh^{106} and Ag^{106}—1357

—— (see Toppel, B. J.)—1254(A)

Alexeff, Igor and Edward C. Peterson. Evapor-ion pump behavior with noble gases—1239(A)

Alger, R. S. (see Anderson, T. H.)—964(A)

Allen, William A. (see Mayfield, Earle B.)—1800(A)

Allis, W. P. (see Dreicer, H.)—1234(A)

Allison, B. (see Fabricand, B. P.)—1249(A)

Almqvist, E., R. L. Clarke, and E. B. Paul. (p,α) reactions in Cl and K—1265(A)

Alvarez, Luis W. Hydrogen bubble-chamber design and experiments—1255(T)

——, **Frank S. Crawford, Jr., Myron L. Good, and M. Lynn Stevenson.** K-meson lifetimes—1264(A)

Anderson, A. B. C. Dependence of discrete acoustic frequencies emitted by jet on vortex-ring coalescence at Reynolds numbers up to 7000—1800(A)

Anderson, C. D. (see Sorrels, J. D.)—1457

Anderson, H. L., W. C. Davidon, M. Glicksman, and U. E. Kruse. Scattering of positive pions by H at 189 Mev—279

——, **W. C. Davidon, and U. E. Kruse.** Causality in pion-proton scattering—339

—— **and M. Glicksman.** Scattering of pions by H at 165 Mev—268

Anderson, J. D., R. W. Kenney, and C. A. McDonald. Yield of π^0 photomesons as function of atomic number—1798(A)

Anderson, J. M. and L. Goldstein. Interaction of electromagnetic waves of rf in isothermal plasmas: Collision cross section of He atoms and ions for electrons—1037

—— **and L. Goldstein.** Microwave studies of slow electron collision processes in He plasmas—1229(A)

—— (see Goldstein, L.)—1229(A)

Anderson, P. W. Electromagnetic theory of cyclotron resonance in metals—749(L)

—— **and H. Hasegawa.** Considerations on double exchange —675

—— **and H. Suhl.** Instability in motion of ferromagnets at high microwave power levels—1788(L)

Anderson, T. H., R. D. Jordan, and R. S. Alger. Irradiation effects in some organic compounds—964(A)

Antes, L. L. (see Marburger, R. E.)—978(A)

Apfel, J. H. and L. N. Hadley. Exciton absorption in cuprous oxide—1689

Argo, H. V. (see Holm, Dale M.)—1244(A)

Armstrong, Baxter H. High-energy pion-proton cross sections—1798(A)

Arnold, W. H., Jr., J. Ballam, M. Grisaru, C. McGrew, and H. W. Wyld. Anomalous V^0-particles—1804(A)

——, **J. Ballam, and George T. Reynolds.** Cloud-chamber observations on charged V particles—295

——, **W. Martin, and H. W. Wyld.** Anomalous neutral V-particles—1545(L)

Arnowitt, R. and S. Deser. Renormalization of derivative coupling theories—349

Aron, Jack and Gerhart Groetzinger. Longitudinal photomagnetoelectric effect in Ge—1128

—— (see Groetzinger, Gerhart)—978(A)

Artman, J. O. Microwave resonance relations in anisotropic single crystal ferrites—1243(A)

Asaro, Frank, F. S. Stephens, Jr., W. M. Gibson, R. A. Glass, and I. Perlman. α-decay properties of Am^{239}—1541(L)

——, **Frank S. Stephens, Jr., B. G. Harvey, and I. Perlman.** Complex α and γ spectra of $Cf^{250,252}$—137

—— (see Stephens, F. S., Jr.)—1543(L)

Auer, Peter L. Semiempirical calculation of Townsend α—1228(A)

Austerman, Stanley B. Stored energy release in graphite irradiated at low temperatures—1807(A)

—— **and John E. Hove.** Irradiation of graphite at liquid He temperatures—1214(L)

Austern, N. Isobar role in two-nucleon processes: Deuteron photoeffect—1522

Austin, Alfred E. and Ralph J. Harrison. Interpretation of stored energy of irradiated graphite in terms of elastic energy associated with microscopic strain—1225(L)

Autler, S. H. and C. H. Townes. Stark effect in rapidly varying fields—703

Axel, Peter (see Fox, John D.)—1249(A)

—— (see Vegors, Stanley H., Jr.)—1238(A)

Ayres, R. U. and R. H. Tredgold. Crystal structure of solid rare gases—1257(A)

Ayres, W. P., P. H. Vartanian, and J. L. Melchor. Frequency doubling in ferrites—1791(A)

Backus, John. Alternative interpretation of magnetic forces between moving charges—1808(A)

Bader, M. (see Pixley, R. E.)—1805(A)

Baggerly, L. L., P. Marmier, F. Boehm, and J. W. M. DuMond. Decay of Ir^{188}—1364

Bailey, T. L. and E. E. Muschlitz. Scattering of low-energy H^- ions in He—1231(A)

Bair, J. K., J. D. Kington, and H. B. Willard. γ-ray and neutron yields from proton bombardment of B—21

Baker, E. W. (see Knight, J. D.)—1334

Baldwin, John (see Fischer, David)—1445

Ball, William P. (see MacGregor, M. H.)—1793(A)

Ballam, J. (see Arnold, W. H.)—295; 1804(A)

Ballard, Stanley S. (see McCarthy, Kathryn A.)—969(A)

Baños, Alfredo, Jr. Normal modes characterizing magnetoelastic plane waves—1801(A)

Barbour, J. P. (see Trolan, J. K.)—1646
Barkas, Walter H., Paul H. Barrett, Pierre Cuer, Harry H. Heckman, Frances M. Smith, and Harold K. Ticho. High-velocity particle ranges in emulsion—1797(A)
—— (see Heckman, Harry H.)—1803(A)
—— (see Smith, Frances M.)—1802(A)
Barker, Paul B. Cosmic-ray electrons near sea level and at mountain altitudes—860
Barker, W. A. and A. Mencher. Thermodynamics of irreversible processes and Overhauser nuclear polarization effect—1224(L)
Barnes, C. A. and R. W. Kavanagh. 15-Mev γ radiation from $B^{11}+d$—1796(A)
—— (see Mills, W. R., Jr.)—1794(A)
Barnett, C. F. and P. M. Stier. Electron loss cross section for fast He atoms—1268(A)
Barredo, Joseph G. Interaction of elementary particles—970(A)
Barrett, Paul H. (see Barkas, Walter H.)—1797(A)
Barschall, H. H. and S. E. Darden. Strength function of nuclear energy levels—1242(A)
Bart, W. L. (see Beams, J. W.)—1657
Barton, M. Q. (see Smith, J. H.)—1265(A)
Bashkin, S. (see Carlson, R. R.)—1254(A)
Baskin, Y. and L. Meyer. Lattice constants of graphite at low temperatures—544
Bath, H. M. and M. Cutler. Measurement of bulk and surface recombination by photoconductance—1259(A)
Battey, J. F. and R. M. Baum. Carrier capture probabilities in Ni-doped Ge—1550(A); 1634
Baum, R. M. (see Battey, J. F.)—1550(A); 1634
Baumann, N. P., F. W. Prosser, Jr., and R. W. Krone. Elastic scattering of protons from Na^{23}—1244(A)
Bay, Z., V. P. Henri, and H. Kanner. Statistical theory of delayed-coincidence experiments—1197
Beams, J. W., J. B. Breazeale, and W. L. Bart. Mechanical strength of thin films of metals—1657
Bean, C. P. (see Jacobs, I. S.)—1060
Becker, R. A. (see Gove, Norwood)—1236(A)
Bederson, B. (see Hammer, J.)—1229(A)
Bedo, D. E. and D. H. Tomboulian. Soft x-ray emission spectrum of Ge—1257(A)
Beers, Yardley (see Sterzer, Fred)—1174
Behrends, R. E., R. J. Finkelstein, and A. Sirlin. Radiative corrections to decay processes—1809(A)
Beiser, A. (see Soberman, R. K.)—859
Belinfante, F. J. Attempts at quantization of gravitational field—967(T)
—— Bending of light and falling rotators—1250(A)
Bemski, G. Lifetime of electrons in p-type Si—523
Benczer, N., B. Farrelly, L. Koerts, and C. S. Wu. Investigation of I^{128}—955(A)
Bender, R. S. (see McGruer, J. N.)—235
Benedek, George B., William Paul, and Harvey Brooks. Conductivity, Hall effect, and magnetoresistance in n-type Ge, and their dependence on pressure—1129
Benedict, F. D. and G. Tice. Angular distribution of γ rays in Coulomb excitation—1545(L)
—— (see Breit, G.)—429(L)
Bennett, H. E. (see Rank, D. H.)—993
Bennett, J. M. (see Rank, D. H.)—993
Bent, R. D., T. W. Bonner, J. H. McCrary, and W. A. Ranken. γ-rays from deuteron bombardment of Al^{27} and P^{31}—774
——, **T. W. Bonner, J. H. McCrary, and W. A. Ranken.** γ-rays from reactions $Be^9(\alpha,n\gamma)C^{12}$, $C^{13}(d,p\gamma)C^{14}$, $N^{14}(d,p\gamma)N^{15}$, and $N^{14}(d,n\gamma)O^{15}$—771
Berberet, J. A. and K. C. Clark. Resonance irradiation of Hg vapor in N—506
Beringer, R. Yale heavy ion accelerator—1548(T)
—— (see Quinton, A. R.)—1549(A)
Bernstein, E. M. and H. W. Lewis. First excited state of Mn^{55}—1367
—— **and H. W. Lewis.** Internal conversion electrons from electric excitation of Ta^{181}, Au^{197}, and Pt^{195}—1345
Bersohn, R. (see Das, T. P.)—1792(A)
Biedenharn, L. C. and C. M. Class. Soluble problem in theory of Coulomb excitation—1790(E)
——, **J. L. McHale, and R. M. Thaler.** Quantum calculation of Coulomb excitation—376
—— (see Goldstein, M.)—436(L)
Bielecki, A. J. (see Meister, A. G.)—1267(A)
Biondi, Manfred A. and Lorne M. Chanin. Deviations from Blanc's law of ionic mobilities: Ne^+ in Ne-H mixtures—1230(A)
—— (see Chanin, Lorne M.)—1230(A)
Birge, R. W., J. R. Peterson, D. H. Stork, and M. N. Whitehead. Mass values of K-mesons—430(L)
Birkhoff, R. D. (see Blackstock, A. W.)—1078
Bitter, Francis and John F. Waymouth. Radiation temperature of a plasma—1230(A)
Björnerud, E. K. Ionization of cloud-chamber tracks—972(A)
Blackstock, A. W., R. H. Ritchie, and R. D. Birkhoff. Mean free path for discrete electron energy losses in metallic foils—1078
Blair, J. M. (see Hill, H. A.)—961(A)
Blakewood, C. H. (see Mobley, R. C.)—1242(A)
Blatt, F. J. Effect of point imperfections on electrical properties of Cu. II. Thermoelectric power—666
Blatt, J. M. and S. T. Butler. Superfluidity of ideal Bose-Einstein gas—476
——, **S. T. Butler, and M. R. Schafroth.** Statistical mechanics of rotating buckets—481
—— (see Butler, S. T.)—495
—— (see Lustig, Harry)—777
—— (see Schafroth, M. R.)—1221(L)
Bleakney, Walker. Transient surface temperatures in shock tube—958(T)
Bledsoe, M. D. and V. G. Szebehely. Hydrodynamic impact of curved surfaces—968(A)
Bleuler, E. (see Blue, J. W.)—1324
—— (see Morinaga, H.)—1236(A)
Blevins, Gilbert S., Walter Gordy, and William M. Fairbank. Superconductivity at mm wave frequencies—1215(L)
Blevins, M. E. (see Block, M. M.)—959(A)
—— (see Fairbank, W. M.)—971(A)
Block, M. M., E. M. Harth, and M. E. Blevins. Evidence for β decay of neutral V-particles—959(A)
——, **E. M. Harth, and R. M. Sternheimer.** Energy distribution of K mesons produced in nuclei—324
—— (see Harth, E. M.)—959(A)
Blodgett, K., III (see Gebbie, H. A.)—970(A)
Bloom, S. D., G. N. Glasoe, C. O. Muehlhause, and H. E. Wegner. Inelastic and elastic scattering of 1.7-Mev neutrons—1248(A)
Blosser, H. G., C. D. Goodman, T. H. Handley, and M. L. Randolph. 14-Mev (n,α) cross-section measurement—429(L)
—— **and T. H. Handley.** (p,n) reactions at 12 Mev—1340
Bloxsom, D. E. (see Perry, R. W.)—968(A)
Bludman, Sidney A. Extended isotopic spin invariance and meson-nucleon coupling—372
Blue, J. W. and E. Bleuler. Radioactivity of Sc^{44}—1324
Blunt, R. F., H. P. R. Frederikse, and W. R. Hosler. Electrical and optical properties of intermetallic compounds. IV. Mg_2Sn—663
Boehm, F. (see Baggerly, L. L.)—1364

Bollinger, L. M., R. E. Coté, and J. M. LeBlanc. Characteristics of new Argonne fast neutron chopper—1239(A)
——, **D. A. Dahlberg, R. R. Palmer, and G. E. Thomas.** Slow neutron resonances of Mn, Bi, and Se—126
—— (see LeBlanc, J. M.)—1248(A)
Bömmel, H. E. Ultrasonic attenuation in superconducting and normal-conducting Sn at low temperatures—758(L)
Bondelid, R. O. (see Fagg, L. W.)—1299
Bonner, T. W. (see Bent, R.D.)—771; 774
—— (see Brugger, R. M.)—84
—— (see Marion, J. B.)—46; 91; 847
—— (see Taylor, H. L.)—174
Booth, Rex (see MacGregor, M. H.)—1793(A)
Bornstein, L. A. and L. H. Fisher. Formative time lags of positive point-to-plane corona in N_2 and A—1228(A)
Borst, L. B. Design considerations for research reactors—971(T)
Bostick, Winston H. Hypothesis for origin of magnetic fields and angular rotations of stars and planets—1007
—— Torus model of elementary particles in which stability may be achieved by gravitational forces resulting from concentrated electromagnetic field—1250(A)
Bostrom, Norman A., Emmett L. Hudspeth, and Ira L. Morgan. Neutron detection with BaF_2 scintillator—973(A)
Bowe, Joseph C. Measurement of electron mobilities in gases—1268(A)
Bowen, D. B. Electronic structure of heaviest metals—1802(T)
Bowen, L. O. (see Lowe, I. J.)—1243(A)
Bowers, Raymond. Magnetic susceptibility of Na metal—1141
Bowyer, J. M. and L. Talbot. Drag in rotating cylinder apparatus near conditions of free molecule flow—968(A)
Boyle, W. S. (see Germer, L. H.)—1232(A)
Braams, C. M. (see Buechner, W. W.)—1387
Brabant, John M. (see Wallace, Roger W.)—962(A)
Brachman, Malcolm K. and J. Ross Macdonald. New linear-system integral transform relations—966(A)
Bracken, J. T., E. A. Rollor, and J. A. Mohrbacher. Effects of operating proportional counters in high γ fields—972(A)
Brandt, Werner. Intermolecular force fields in high polymers composed of alternating dipole chains—969(A)
Branson, Herman and L. B. Garner, II. Electron impact studies with trimethylamine—964(A)
Bray, Ralph. Electrical breakdown in InSb at low temperature—1262(A)
—— Minority carrier extraction in Ge—1047
Breazeale, J. B. (see Beams, J. W.)—1657
Breit, G. Possibilities of heavy ion bombardment—1548(T)
——, **M. E. Ebel, and F. D. Benedict.** Angular distribution of γ-rays in Coulomb excitation—429(L)
—— **and J. P. Lazarus.** Effects of finite amplitude in Coulomb excitation—942(L)
Breitenbecher, D. V. Gated phototube for fast pulse operation—978(A)
Brennan, J. G. (see Adkins, R.)—1790(E)
Brice, M. K. (see Cork, J. M.)—188; 955(A); 1237(A)
Bridge, H. S. Charged K mesons—967(T)
Brinkman, J. A. New method for determination of activation energies—1807(A)
Brock, Ernest G. Field emission microscopy of allotropic transformation: α-β titanium—1619
Brockhouse, B. N. and H. P. Myers. New magnetic transition in Mn_2ZnC—1242(A)
—— **and A. T. Stewart.** Scattering of neutrons by phonons in Al single crystal—756(L)
Broder, J. D. (see Wolff, G. A.)—1144
Brody, T. A. Apparent length of tracks in nuclear emulsions—972(A)
Broer, J. W. (see Chiba, Ren)—1253(A)
—— (see Douglas, R. A.)—1253(A)
Brooks, F. L. (see Silvidi, A. A.)—979(A)
Brooks, Harvey (see Benedek, George B.)—1129
Brophy, James J. Excess noise in plastically deformed Ge—1261(A)
—— **and Norman Rostoker.** Hall effect noise—754(L)
Brosi, A. R. and B. H. Ketelle. Radioactivity of Ce^{137} isomers—169
Brown, H. A. and J. M. Luttinger. Ferromagnetic and antiferromagnetic Curie temperatures—685
Brown, K. L. Z-dependence of bremsstrahlung in case of complete screening—1798(A)
Brown, L. Carlton and Paul M. Parker. Nuclear magnetic dipole and electric quadrupole energy relations—1764
Brown, Sanborn C. (see Persson, Karl-B.)—729
Brown, W. L. Surface potential and surface charge distribution from semiconductor field effect measurements—590
—— (see Penman, S.)—1259(A)
Browne, C. P. Isotopic spin-selection rule violation in $O^{18}(d,\alpha)N^{16}$—1253(A)
Browne, M. E. (see Owen, J.)—965(A)
Broyles, A. A. Stark fields from ions in plasma—1181
Brueckner, K. A. Many-body problem for strongly interacting particles. II. Linked cluster expansion—36
——, **R. J. Eden, and N. C. Francis.** Theory of neutron reactions with nuclei at low energy—891
Brugger, Robert M., T. W. Bonner, and J. B. Marion. Nuclear reactions $Sc^{45}(p,n)Ti^{45}$, $Cu^{63}(p,n)Zn^{63}$—84
—— (see Marion, Jerry B.)—46; 69
—— (see Simpson, O. D.)—1249(A)
Brun, E., W. E. Meyerhof, and J. J. Kraushaar. Excited states of Ge^{72}—1795(A)
Buechner, W. W. Nuclear energy levels observed from inelastic proton scattering experiments—954(T)
——, **C. M. Braams, and A. Sperduto.** Inelastic proton scattering from V—1387
—— (see Paris, C. H.)—1317
—— (see Sperduto, A.)—961(A)
Buerger, M. J. Arrangement of atoms in wollastonite-type crystals—970(A)
Bullis, W. M. and W. E. Krag. Hall effect and magnetoresistance in n-type Ge—1258(A)
Bullock, M. L. (see Holmgren, H. D.)—436(L); 1253(A)
Bunker, M. E. (see Duffield, R. B.)—1236(A)
—— (see Mize, J. P.)—1390
Burch, D. S., G. H. Dunn, R. Geballe, and V. M. Madsen. Failure of Schottky theory for positive column of O_2—1235(A)
Burgess, J. H. and R. E. Norberg. Double-frequency magnetic resonance in free radical—752(L)
Burkhardt, J. L. Nuclear scattering of low-energy photons—192
——, **E. J. Winhold, and T. H. Dupree.** Photoexcitation of isomeric state of In^{115}—199
Burkig, J. W., Glen E. Schrank, and J. Reginald Richardson. p-p scatterings at 19.6 Mev—1805(A)
Burkig, V. C. and K. R. MacKenzie. Relative stopping power of some metallic elements for 20-Mev protons—1805(A)
Burson, S. Bradley (see Martin, David W.)—1236(A)
Burstein, Elias (see Lax, Melvin)—592
Butler, J. W. (see Kunz, W. E.)—1252(A)
Butler, S. T. and J. M. Blatt. Nonequilibrium nature of superfluid state—495
—— (see Blatt, J. M.)—476; 481

Byram, E. T., T. A. Chubb, and H. Friedman. γ-ray absorption measurements of density of upper atmosphere—963(A)

Caldwell, David O. Range-energy relation and masses of new particles—291
—— **and Yash Pal.** Photometric mass determinations in multiplate cloud chamber—1803(A)
Caldwell, R. S. and H. Y. Fan. Infrared properties of Se—1251(A)
Callaway, J. and R. D. Woods. Nucleon distribution in Ca^{40}—956(A)
Cameron, J. R. (see Weinman, J. A.)—1239(A)
Cano-Corona, O. and R. Pepinsky. Present limitations of x-ray analyses of organic natural products—970(A)
Carlson, R. O. Electrical properties of near-degenerate B-doped Si—1075
Carlson, R. R. and S. Bashkin. Excited states of O^{16} from proton bombardment of N^{15}—1254(A)
Carrillo, Nabor. Hundimienta de ciudades (sinking of cities)—962(T)
Carter, David. Phase centers of microwave antennas—966(A)
Case, K. M. Hamiltonian form of integral spin wave equations—1513
—— (see Mendlowitz, H.)—1551
Caspari, M. E. (see Rau, Richard R.)—632
Cassatt, Wayne A., Jr., and W. Wayne Meinke. Decay scheme of In^{109}—1372
Cavanaugh, R. E., D. M. Haskin, and Marcel Schein. Nuclear collisions of 5.7-Bev protons and 3.0-Bev π^--mesons—1263(A)
Cester, R., T. F. Hoang, and A. Kernan. p-p interactions at 3 Bev—940(L)
Cetlin, B. B. (see Galt, J. K.)—748(L)
Chamberlain, Owen, Emilio Segrè, Clyde Wiegand, and Thomas Ypsilantis. Observation of antiprotons—947(L)
—— Velocity-selecting Čerenkov counter—1801(T)
Champion, K. S. W. and A. B. de Saint Maurice. Ion diffusion in uniform magnetic field—1233(A)
Chandrasekhar, S. Astrophysical questions and galactic origin of cosmic rays—1247(T)
Chang, W. Y. (see Gupta, I. C.)—1264(A)
—— (see Snyder, A.)—1264(A)
Chanin, Lorne M. and Manfred A. Biondi. Temperature dependence of ionic mobilities: Ne^+ and Ne_2^+ in Ne—1230(A)
—— (see Biondi, Manfred A.)—1230(A)
Chapman, R. A. (see Marion, J. B.)—1795(A)
Cheng, L. S. Sargent diagram and comparative half-lives for allowed K-capture transitions of nuclides with $Z \leqslant 60$—979(A)
Chester, G. V. λ transition in liquid He—455
—— Statistical mechanics of mixtures of isotopes—446
Chiba, Ren, R. A. Douglas, J. W. Broer, D. F. Herring, and E. A. Silverstein. Electrostatic analysis of nuclear reaction energies. IV—1253(A)
—— (see Douglas, R. A.)—1253(A)
—— (see Herring, D. F.)—1239(A)
Chinowsky, W. and J. Steinberger. Reaction $\pi^- + d \rightarrow 2n + \pi^0$; parity of neutral meson—1476
Chou, A. (see Kerker, M.)—977(T)
Christian, J. W. Stripline or microwave printed circuits—1549(A)
Christian, R. (see Friedman, M. H.)—1494
Christian, Schuyler M. (see Dresselhaus, G.)—1218(L)
Christofilos, N. C. (see Cottingham, J. G.)—1269(A)
Chubb, T. A. (see Byram, E. T.)—963(A)
Chupp, Warren W., Gerson Goldhaber, Sulamith Goldhaber, and Francis H. Webb. Interactions of negative K-particles at rest—959(A)
Church, E. L. and J. Weneser. Electric-monopole transitions in atomic nuclei—943(L); 1241(A)
Clark, K. C. (see Berberet, J. A.)—506
Clarke, Edward N. (see Hopkins, Robert L.)—1786(L)
Clarke, R. L. (see Almqvist, E.)—1265(A)
Class, C. M. (see Biedenharn, L. C.)—1790(E)
Cleland, J. W. and J. H. Crawford, Jr. Fast-neutron bombardment of GaSb—1614
—— (see Stevens, D. K.)—1084
Clement, J. R., J. K. Logan, and J. Gaffney. Liquid He vapor pressure equation—743
Cohen, Bernard L. (p,γ) cross sections—206
Cohen, S. G. and S. Ofer. Spectrum of internal bremsstrahlung from Cr^{51}—856
Cole, F. T. and D. W. Kerst. Small model FFAG betatron. II. Design calculations—1246(A)
—— (see Terwilliger, K. M.)—1246(A)
Coleman, Bernard D. Time dependence of mechanical breakdown phenomena—1257(A)
Coles, Donald. Similarity laws for nonequilibrium turbulent boundary layer—958(T)
Connell, R. A. and J. A. Marcus. Hall effect and magnetoresistance of Bi single crystals at He temperatures—1256(A)
Connors, D. R., W. C. Miller, and B. Waldman. Energy determination of Au^{198} conversion electrons—1237(A)
Conzett, Homer E. Inelastic scattering of protons from Li^7, C^{12}, Mg^{24}, and Si^{28}—1794(A)
Cook, C. F. (see Marion, J. B.)—91; 847
Cook, C. S. (see Tomnovec, F. M.)—1254(A)
Coomes, E. A. (see Haas, G. A.)—640
Cooper, H. (see Schwed, P.)—978(A)
Cooper, Leon N. Nonrenormalizable field theory—362
Corenzwit, E. (see Matthias, B. T.)—626
Cork, Bruce and W. A. Wenzel. Elastic p-p scattering in Bev range—962(A)
Cork, James M., M. K. Brice, D. W. Martin, L. C. Schmid, and R. G. Helmer. Nuclear levels in Tm^{169}, Lu^{175}, and Lu^{177} as derived from radioactive isotopes of Yb—1237(A)
——, **M. K. Brice, L. C. Schmid, and R. G. Helmer.** γ energies in Tc^{97} following K capture in Ru^{97}—955(A)
——, **M. K. Brice, L. C. Schmid, and R. G. Helmer.** Radioactive decay of Ru^{97}—188
—— (see Martin, David W.)—1236(A)
Corson, Dale R. (see McDonald, W. S.)—1799(A)
Coté, R. E. (see Bollinger, L. M.)—1239(A)
—— (see LeBlanc, J. M.)—1248(A)
Cottingham, J. G., N. C. Christofilos, M. Plotkin, E. C. Raka, and R. H. Rhéaume. Electrical analog—electrical system—1269(A)
—— (see Spiro, J.)—1269(A)
Courant, E. D., R. R. Kassner, E. C. Raka, Lloyd Smith, and J. Spiro. Electron analog—performance and interpretation. II.—1269(A)
—— (see Green, G. K.)—1268(A)
—— (see Raka, E. C.)—1269(A)
—— (see Spiro, J.)—1269(A)
Cox, Everett F. Proposed change in scaling laws for explosive phenomena—967(A)
Cranberg, L. and J. S. Levin. Inelastic scattering of neutrons from Fe by time-of-flight—434(L)
Crawford, Frank S., Jr. (see Alvarez, Luis W.)—1264(A)
Crawford, J. H., Jr. (see Cleland, J. W.)—1614
—— (see Stevens, D. K.)—1084
Crawford, R. C. (see Harrison, G. R.)—841

Critchfield, C. L. and Robert Lowen. Model for potential between nucleon and nucleus—956(A)
Crowe, K. M., R. M. Friedman, and D. C. Hagerman. π^+ photoproduction ratio of D to H—1799(A)
—— (see Friedman, R. M.)—1799(A)
—— (see Hagerman, Donald C.)—869
Cuer, Pierre (see Barkas, Walter H.)—1797(A)
Cunningham, W. J. Nonlinear oscillators with constant time delay—1549(A)
Cutler, M. (see Bath, H. M.)—1259(A)

Dabbs, J. W. T. (see Roberts, L. D.)—1100
Dahlberg, D. A. (see Bollinger, L. M.)—126
Dail, H. W., Jr. (see Galt, J. K.)—748(L)
Dalitz, R. H. (see Kalos, M. H.)—1515
D'Altroy, F. and H. Y. Fan. Polarization of impurities in Ge—1260(A)
Danielson, G. C. (see Redin, R. D.)—1252(A)
—— (see Whitsett, C. R.)—1261(A)
Danner, H. R. (see Frazer, B. C.)—745(L)
Darden, S. E., R. B. Perkins, and R. B. Walton. Small-angle scattering of neutrons by intermediate and heavy nuclei—1315
—— (see Barschall, H. H.)—1242(A)
Das, T. P. and R. Bersohn. Quadrupole polarization of charge-clouds in ions—1792(A)
D'Asaro, L. A. Use of field emission microscope for investigating surface conditions on alloy—1258(A)
Davidon, W. C. (see Anderson, H. L.)—279; 339
Davidson, J. M. Experimental thermal conductivities of gases and gaseous mixtures—966(A)
Davis, L., Jr. (see Statz, H.)—1260(A)
Davis, Leverett, Jr. Interplanetary magnetic fields and cosmic rays—958(A); 1440
—— Origin of cosmic rays—1806(T)
Davis, Robert H., Ajay S. Divatia, R. D. Moffat, and D. A. Lind. Coulomb excitation of Re, In, and Hg by protons—1266(A)
—— (see Divatia, Ajay S.)—1266(A)
Day, M. C., Jr., G. W. Eakins, and A. F. Voigt. Disintegration schemes of Te^{127} and Te^{129} ground states—796
De Bitetto, D. J. and L. H. Fisher. First and second Townsend coefficients in H_2 and N_2—1227(A)
Dedrick, K. G. Deuteron-model calculation of high-energy nuclear photoeffect—58
DeMars, G. A. (see Statz, H.)—1260(A)
Dempsey, D. F., W. C. Miller, and B. Waldman. Third-order aberration and focusing with sector-shaped magnetic field—1240(A)
De Oyarzabal, Juan. Pion-pair production—974(A)
De Pangher, J. and W. C. Roesch. Neutron dosimeter with uniform sensitivity from 0.1 to 3.0 Mev—1793(A)
de Saint Maurice, A. B. (see Champion, K. S. W.)—1233(A)
Deser, S. (see Arnowitt, R.)—349
DeWitt, Bryce S. State vector normalization in formal scattering theory—905
Dexter, D. L. Absorption cross section for light in perfect solids—964(A)
——, **C. C. Klick, and G. A. Russell.** Criterion for occurrence of luminescence—603
—— (see Klick, C. C.)—964(A)
Dexter, R. N. and Benjamin Lax. Cyclotron absorption in Bi—1216(L)
Dickey, J. E. (see Huntington, H. B.)—1117
Dieckamp, H. Influence of lattice defects on Young's modulus of Cu—1807(A)
Dieke, G. H. and L. Heroux. Zeeman effects and magnetic properties of Nd salts—965(A)
Dillon, J. F., Jr., S. Geschwind, and V. Jaccarino. Ferrimagnetic resonance in single crystals of Mn ferrite—750(L)
Divatia, Ajay S., Robert H. Davis, R. D. Moffat, and D. A. Lind. Coulomb excitation of In^{115}, I^{127}, Ta^{181}, Th^{232}, and U^{238}—1266(A)
—— (see Davis, Robert H.)—1266(A)
Dobovišek, B. (see Havliček, F. I.)—1355
Doggett, W. O. (see Mead, S. W.)—1794(A)
Donnelly, R. J. Liquid He *II* in rotation—1548(T)
Douglas, R. A., J. W. Broer, and Ren Chiba. $C^{14}+d$ reactions—1253(A)
—— (see Chiba, Ren)—1253(A)
—— (see Herring, D. F.)—1239(A)
Dousmanis, G. C., T. M. Sanders, Jr., and C. H. Townes. Microwave spectra of free radicals OH and OD—1735
Dowling, J. M. Normal coordinate treatment for out-of-plane vibrations of ethylene type molecules—1267(A)
—— (see Meister, A. G.)—1267(A)
Dreicer, H. and W. P. Allis. Inclusion of Coulomb interactions in Boltzmann equations—1234(A)
Drell, S. D. Nuclear radius and nuclear forces—97
Dresselhaus, G. Energy-band structure of solids with ZnS-type lattices—1251(T)
—— Spin-orbit coupling effects in Zn blende structures—580
——, **A. F. Kip, and C. Kittel.** Plasma resonance in crystals: Observations and theory—618
——, **A. F. Kip, and C. Kittel.** Plasma resonance in semiconductor crystals—1262(A)
——, **A. F. Kip, Han-Ying Ku, G. Wagoner, and Schuyler M. Christian.** Cyclotron resonance in Ge-Si alloys—1218(L)
Dropesky, B. J. and A. W. Schardt. Decay of Ne^{24}—954(A)
Drost-Hansen, W. and H. W. Neill. Temperature anomalies in properties of liquid water—1800(A)
Drummond, J. E. and L. Wilcox. Resonant power transfer within plasma in magnetic field—1233(A)
Duffield, R. B., M. E. Bunker, J. P. Mize, and J. W. Starner. Decay of Cs^{129}—1236(A)
Duffus, H. J. Observations of geomagnetic micropulsations—966(A)
DuMond, J. W. W. (see Baggerly, L. L.)—1364
Dunlap, W. Crawford, Jr. Amphoteric impurity action in Ge—1629
Dunn, G. H. (see Burch, D. S.)—1235(A)
Dunning, K. L. (see Fagg, L. W.)—1299
Dupree, T. H. (see Burkhardt, J. L.)—199
Duvall, G. E. Linearized flow theory and shock waves in metals—967(A)
Dyke, W. P. (see Trolan, J. K.)—1646
Dyson, Freeman J. Scattering of mesons by fixed scatterer—344

Eakins, G. W. (see Day, M. C., Jr.)—796
Easterday, H. (see Imhof, William)—1798(A)
Ebel, M. E. (see Breit, G.)—429(L)
Ecker, G. Influence of electron emission on cathode processes of arc—1232(A)
Edelsack, E. A. and W. E. Kreger. Thick target bremsstrahlung spectra for 1.00-, 1.50-, and 2.00-Mev electrons—973(A)
Eden, R. J. (see Brueckner, K. A.)—891
Edwards, Palmer L. Magnetic properties of murdochite, Cu_6PbO_8—1242(A)
Einstein, H. A. Dynamic model for viscous sublayer of turbulent flow along smooth boundary—958(T)

Eisberg, R. M., G. Igo, and H. E. Wegner. Protons from bombardment of several elements with 40-Mev α particles —961(A); 1309
—— (see Igo, G.)—1244(A)
—— (see Palevsky, H.)—1266(A)
Ekstein, Hans and Norman Rostoker. Quantum theory of fluctuations—1023
Elliott, J. F., S. Legvold, and F. H. Spedding. Magnetic properties of Er metal—1595
Ellis, R. E. (see Schecter, Larry)—1805(A)
Ellis, S. G. Electrolytic etching at small-angle grain boundaries in Ge—1140
Elsasser, W. M. Progress in hydromagnetism—957(T)
Endt, P. M. (see Paris, C. H.)—1317
Engelkemeir, D. W. (see Magnusson, L. B.)—1237(A)
English, W. N. (see Stewart, R. W.)—969(A)
Epstein, S. Remarks on strangeness—1809(A)
Erickson, Roger D. Minimum quenching times of low voltage, nonself-quenching Geiger counters—1234(A)
Erkman, J. O. Free surface motion due to obliquely incident shock waves—1801(A)
Escobar, I. (see Harris, F. B.)—255
Estrada, L. Electric quadrupole moment and corrections to magnetic moment of deuteron for velocity-dependent tensor forces—956(A)
Etzel, H. W. Detection of vacancies created by x-rays in NaCl—1643
Evans, J. S. and R. H. Tredgold. Positional correlation study for system of two electrons—1250(A)
Everett, A. E. and M. J. Glaubman. γ-γ directional correlations in Cs^{128}—955(A)
Ewald, A. W. (see Kohnke, E. E.)—1252(A)
Ewing, Maurice. Earthquake surface waves in period range 1–500 seconds—957(T)
—— Earthquake waves as tool for exploring ocean basins—1796(T)

Fabricand, Burton P., B. Allison, and J. Halpern. Photoneutron angular distribution from C—1249(A)
—— (see Yergin, Paul F.)—1249(A); 1269(A)
Fafarman, A. and M. H. Shamos. Mesonic x-rays from capture of cosmic-ray μ mesons in chemical compound—874
Fagg, L. W., E. A. Wolicki, R. O. Bondelid, K. L. Dunning, and S. Snyder. Coulomb excitation of Te and Ag—1299
—— (see Wolicki, E. A.)—1265(A)
Fairbank, William M., E. M. Harth, M. E. Blevins, and G. G. Slaughter. Liquid He bubble chamber—971(A)
—— (see Blevins, Gilbert S.)—1215(L)
Faire, A. C. and George W. Griffing. Low-pressure afterglow studies in N_2—1231(A)
Famularo, K. F. (see Simmons, B. E.)—1265(A)
Fan, H. Y. (see Caldwell, R. S.)—1251(A)
—— (see D'Altroy, F.)—1260(A)
Farrelly, B. (see Benczer, N.)—955(A)
Feher, G., R. C. Fletcher, and E. A. Gere. Exchange effects in spin resonance of impurity atoms in Si—1784(L)
Feld, Bernard T. Effects of angular momentum on τ-decay schemes—1263(A)
——, **A. C. Odian, D. M. Ritson, and A. Wattenberg.** Spin of τ^+ meson—1539(L)
—— (see Odian, Allen)—1241(A)
—— (see Ritson, D. M.)—1263(A)
Feldman, David (see Ohnuma, Shoroku)—1241(A)
Feldmann, W. L. (see Pearson, G. L.)—1251(A)
Felix, B. R., L. Passell, and H. B. Silsbee. Thermal conductivity of superconducting Pb below 1°K—1808(A)
—— (see Passell, L.)—1808(A)
Ferguson, G. A., C. W. Peters, and F. E. Jablonski. Boron trimethyl counters—1239(A)
Fernandez, Carlos Graef. Theory of gravitation—967(T)
Ferrell, Richard A. Coulomb enhancement of positron annihilation in metals—973(A)
—— **and W. M. Visscher.** Nuclear compressibility and O^+ states of O^{16} and C^{12}—1796(A)
Feynman, R. P. Remarks on problem of superconductivity —1802(T)
Field, L. M. Modern trends in interaction of electron beams with high-frequency fields—1794(T)
Fields, P. R., J. E. Gindler, A. L. Harkness, M. H. Studier, J. R. Huizenga, and A. M. Friedman. Electron capture decay of Am^{244} and spontaneous fission half-life of Pu^{244}—172
Fields, T., E. J. Schillinger, and J. Kenski. Pulse characteristics of CdSe crystals—964(A)
Filosofo, I. Čerenkov counter as high-energy photon spectrometer—1246(A)
Finkelstein, David. Internal structure of spinning particles —924
Finkelstein, R. J. and M. Moe. Scattering by symmetric potential—1775
—— (see Behrends, R. E.)—1809(A)
Fischer, David and John Baldwin. p-p polarization at 170 Mev—1445
Fisher, J. C. Developments in crystal growth—1802(T)
Fisher, L. H. (see Bornstein, L. A.)—1228(A)
—— (see De Bitetto, D. J.)—1227(A)
Fletcher, R. C., W. A. Yager, and F. R. Merritt. Observation of quantum effects in cyclotron resonance—747(L)
—— (see Feher, G.)—1784(L)
Fluharty, R. G. (see Simpson, O. D.)—1249(A)
Foote, H. L., Jr. Slow neutron resonance scattering of U^{238} —1248(A)
Forbush, Scott E. Absence of meteorological effects on world-wide sunspot variation in cosmic-ray ionization—958(A)
Ford, Kenneth W. and Carl Levinson. Independent-particle model of nucleus. II. Weak surface coupling—1
—— (see Levinson, Carl)—13
Fowler, Charles A., Jr., and Edward M. Fryer. Magnetic domains in thin films of Ni-Fe—746(L)
Fowler, R. G. (see Lee, R. J.)—1234(A)
Fowler, W. A. Nuclear reactions and element synthesis in stars—1791(T)
Fowler, William B. (see Maenchen, George)—1802(A)
—— (see Wright, Robert W.)—1802(A)
Fox, John D. and Peter Axel. Photoneutron effect in $Zr^{90}(\gamma,n)Zr^{89}$ and $Zr^{90}(\gamma,n)Zr^{89m}$—1249(A)
Fox, R. E. Negative-ion formation in iodine by electron capture—1229(A)
Francis, N. C. (see Brueckner, K. A.)—891
Frank, R. M. and J. F. Gammel. t-t interaction—973(A)
Frankel, Sherman (see Goldberg, Norman)—1350
Frankl, D. R. Electroluminescence of ZnS single crystals—1105; 1790(E)
Franzen, W., P. Huber, and L. Schellenberg. Recoil-coincidence method for producing monoenergetic d-d neutrons—1239(A)
Frazer, B. C., H. R. Danner, and R. Pepinsky. Single crystal neutron analysis of tetragonal $BaTiO_3$—745(L)
Frederikse, H. P. R. (see Blunt, R. F.)—663
—— (see Hosler, W. R.)—1261(A)
Freedman, M. S. (see Magnusson, L. B.)—1237(A)
Freier, G. D. (see Simmons, B. E.)—1265(A)
Frenkiel, François N. Fluid dynamics problems in geophysical sciences—957(T)
Fretter, W. B. Heavy mesons and hyperons: Progress report—967(T)
Freund, R. E. Thermoluminescence measurements of electroluminescent ZnS:Mn films—760(L)

Friedman, A. M. (see Fields, P. R.)—172
Friedman, H. (see Byram, E. T.)—963(A)
Friedman, Marvin H., T. D. Lee, and R. Christian. Scattering of pions by nucleons in intermediate coupling—1494
—— (see Haller, Kurt)—1501
Friedman, R. M. and K. M. Crowe. Pion pair photoproduction—1799(A)
—— (see Crowe, K. M.)—1799(A)
Friesen, E. W. Cloud-chamber ionization measurement and applications—1247(T)
Frisch, D. H. (see Gomez, R.)—1245(A)
—— (see Janes, G. S.)—1245(A)
—— (see Pugh, G. E.)—1245(A)
Fronsdal, C. Wave equations for arbitrary spin—1810(A)
Frost, L. S. and A. V. Phelps. Production and loss of excited atoms in He positive column—1234(A)
Fry, W. F., J. Schneps, G. A. Snow, and M. S. Swami. Nuclear capture of negative K mesons in emulsion—1448
——, **J. Schneps, G. A. Snow, and M. S. Swami.** Nuclear interaction in flight of Σ hyperon—939(L)
——, **J. Schneps, G. A. Snow, and M. S. Swami.** Observations of negative K mesons and charged hyperons—950(L)
—— (see Schneps, J.)—1263(A)
Fryer, Edward M. (see Fowler, Charles A., Jr.)—746(L)
Fuller, C. S. and H. Reiss. Compound formation between Li and B dissolved in single crystal Si—1806(A)
—— (see Morin, F. J.)—1807(A)

Gaffney, J. (see Clement, J. R.)—743
Gallagher, C. J. Thermal defects in Si—1259(A)
Galonsky, A. and J. P. Judish. Angular distribution of n-p scattering at 17.9 Mev—121
—— (see Johnson, C. H.)—1252(A)
Galt, J. K., W. A. Yager, F. R. Merritt, B. B. Cetlin, and H. W. Dail, Jr. Cyclotron resonance in metals: Bi—748(L)
Gambling, W. A. Glow-to-arc transitions in column of high-pressure glow in H_2—1232(A)
Gammel, J. F. (see Frank, R. M.)—973(A)
Garner, L. B., II (see Branson, Herman)—964(A)
Gartenhaus, Solomon. Two-nucleon potential from cutoff Yukawa theory—900
Geballe, R. (see Burch, D. S.)—1235(A)
Geballe, T. H. (see Hrostowski, H. J.)—1672
Gebbie, H. A. and K. Blodgett, III. Surface trapping in Ge—970(A)
Geer, E. H., E. B. Nelson, and E. A. Wolicki. α-α angular correlations in $B^{11}(p,\alpha\alpha)He^4$—215
—— (see Wolicki, E. A.)—1265(A)
Gelbard, Ely M. Three-body contributions to triton binding energy—1530
Gelinas, R. W. and S. S. Hanna. Search for states in Li^7 and Be^8—1253(A)
—— (see Lavier, E. C.)—1252(A)
Geller, Z. and W. Low. Attenuation of 1-cm microwaves by abnormal dc discharge in He—1240(A)
Gell-Mann, M. Causality and scattering—1795(T)
Geltman, Sydney. Theory of ionization probability near threshold—1231(A)
Gere, E. A. (see Feher, G.)—1784(L)
Gerhart, J. B. (see Sherr, R.)—945(L)
Germer, L. H. and W. S. Boyle. Short arcs—1232(A)
Gerritsen, H. J. (see Meijer, Paul H. E.)—742
Gerson, N. C. Fluid motions in terrestrial atmosphere—957(T)
Geschwind, S. (see Dillon, J. F., Jr.)—750(L)
Gibbons, J. H., R. L. Macklin, and H. W. Schmitt. $V^{51}(p,n)Cr^{51}$ reaction as 5–120-kev neutron source—167
Gibson, W. M. (see Asaro, Frank)—1541(L)
Gilbert, F. C., Charles E. Violet, and R. Stephen White. Negative K-particle interactions in nuclear emulsion. II—1803(A)
—— (see Violet, Charles E.)—1803(A)
—— (see White, R. Stephen)—1803(A)
Gilbert, Richard S. (see Hicks, Harry G.)—1284; 1286
Gilbert, T. L. Lagrangian formulation of gyromagnetic equation of magnetization field—1243(A)
Gilden, M. and L. Goldstein. Cyclotron resonance of electrons in gaseous discharge plasmas—1233(A)
Gindler, J. E. (see Fields, P. R.)—172
Givens, M. Parker, Charles J. Koester, and William L. Goffe. Soft x-ray absorption of Te and vitreous and metallic Se—1112
Glasoe, G. N. (see Bloom, S. D.)—1248(A)
Glass, R. A. (see Asaro, Frank)—1541(L)
Glauber, R. J. Cross sections in deuterium at high energies—242
Glaubman, M. J. (see Everett, A. E.)—955(A)
Glicksman, Maurice. Magnetoresistance and mobility of Ge-Si alloys—1258(A)
—— Magnetoresistance of Ge-Si alloys—1146
—— (see Anderson, H. L.)—268; 279
Goebel, Charles J., Robert Karplus, and Malvin A. Ruderman. Momentum dependence of phase shifts—240
Goering, H. L. (see Harman, T. C.)—1262(A)
Goffe, William L. (see Givens, M. Parker)—1112
Goldberg, Jean Snover, Hartland S. Snyder, and William T. Scott. Mean-value calculations for spatial multiple scattering—1013
Goldberg, Norman and Sherman Frankel. Angular correlation measurements in Te^{125} and Te^{125m}—1350
Goldhaber, Gerson. Interaction of K-particles from Bevatron—1806(T)
—— Properties of heavy mesons produced at Bevatron—1262(T)
—— (see Chupp, Warren W.)—959(A)
Goldhaber, Sulamith (see Chupp, Warren W.)—959(A)
Goldsack, S. J. (see Abraham, M.)—1799(A)
Goldstein, L. and J. M. Anderson. Collision cross section of N_2 molecules with slow electrons—1229(A)
—— Origin of λ transition in liquid He—966(A)
—— (see Anderson, J. M.)—1037; 1229(A)
—— (see Gilden, M.)—1233(A)
Goldstein, Louis. Interatomic correlations in liquid He^4—981
Goldstein, M., J. L. McHale, R. M. Thaler, and L. C. Biedenharn. Coulomb excitation directional correlation—436(L)
Goldwasser, E. L. and L. J. Koester, Jr. Photoproduction of π^0 mesons in He—1255(A)
Gomer, R. Experiments in field and ion emission—1794(T)
Gomez, R., G. E. Pugh, D. H. Frisch, and G. S. Janes. γ-ray scattering by complex nuclei—1245(A)
—— (see Janes, G. S.)—1245(A)
—— (see Pugh, G. E.)—1245(A)
Good, Myron L. K-meson counter experiments—1806(T)
—— (see Alvarez, Luis W.)—1264(A)
Goodenough, John B. Theory of role of covalence in perovskite-type manganites $[(La,M(II)]MnO_3$—564
Goodman, B. R. (see Luttinger, J. M.)—673
Goodman, C. D. (see Blosser, H. G.)—429(L)
Goodman, E. (see Haskin, D. M.)—1263(A)
Goodman, L. S. and S. Wexler. Nuclear spin and magnetic moment of 50-day In^{114m}—1245(A)
—— **and S. Wexler.** Nuclear spin and magnetic moment of 54-min In^{116m}—1796(A)
Gordy, Walter (see Blevins, Gilbert S.)—1215(L)

Gossett, C. R., G. C. Phillips, J. P. Schiffer, and P. M. Windham. Magnetic analysis of $Be^9(p,p')Be^{9*}$ and $Be^9(p,pn)Be^8$ reactions—203
Gould, C. L. (see Jacobus, D. D.)—1268(A)
Gould, F. T., T. I. Taylor, and W. W. Havens, Jr. Absorption cross section of Au for slow neutrons measured on single crystal spectrometer—1248(A)
Gove, Norwood, Fred A. Smith, and R. A. Becker. Radiations from Mo^{93}—1236(A)
Grad, Harold. Stochastic aspects of classical dynamics—958(T)
Graves, William E. and Allan C. G. Mitchell. Disintegration of Te^{130}—1236(A)
Green, G. K., E. D. Courant, L. J. Haworth, and H. S. Snyder. Electron analog—1268(A)
Greenberg, D. H. (see Van Lieshout, R.)—223
Greene, Lawrence C. CdS photorectifier—978(A)
Greene, R. E. (see Lamphere, R. W.)—763
Griffing, George W. (see Faire, A. C.)—1231(A)
Grimes, D. M. and J. W. Kuiper. Effect of V_2O_5 on spinel formation—1256(A)
Grisaru, M. (see Arnold, W. H.)—1804(A)
Grisoli, J. J. (see Jacobus, D. D.)—1268(A)
Grodzins, Lee and Henry Motz. Decay of 72-second and 49-day In^{114}—1236(A)
Groetzinger, Gerhart and Jack Aron. Longitudinal photomagnetoelectric effect in Ge—978(A)
—— (see Aron, Jack)—1128
Gross, E. P. Small oscillation theory of interaction of particle and scalar field—1571
Groves, Gordon W. Dynamics of equatorial waves in ocean—957(T)
Gupta, I. C., W. Y. Chang, and A. Snyder. Double-plate cloud chamber study of V^0-particles. I. Classification—1264(A)
—— (see Snyder, A.)—1264(A)
Gupta, U. C. (see Miller, D. W.)—1253(A)
—— (see Rasmussen, V. K.)—851

Haas, G. A. and E. A. Coomes. Schottky effect for SrO films on Mo—640
Haber-Schaim, U. Proton-nucleus collisions at 6 Bev—1263(A)
Hack, M. N. Theory of multiple quantum transitions—975(A)
Haddock, Roy. One hundred Bevatron τ^+'s—1803(A)
Hadley, L. N. (see Apfel, J. H.)—1689
Hagedorn, F. B. Preparation of thin N^{14} targets—1793(A)
Hagerman, Donald C. and K. M. Crowe. Measurement of high-energy end of bremsstrahlung spectrum—869
—— (see Crowe, K. M.)—1799(A)
Hagstrum, Homer D. Formation of metastable A^+, Kr^+, and Xe^+ by electron impact—1231(A)
Haller, Kurt and Marvin H. Friedman. Anomalous magnetic moment of nucleon—1501
Halpern, J. (see Fabricand, B. P.)—1249(A)
—— (see Weinstock, E. V.)—1293
Ham, Frank S. Ionized impurity scattering in semiconductors—1251(A)
Hammel, J. E. and J. F. Kephart. Distribution of number of prompt neutrons from spontaneous fission of Pu^{240}—190
Hammer, J., H. Malamud, and B. Bederson. Low-energy scattering of electrons by atoms—1229(A)
Handley, T. H. (see Blosser, H. G.)—429(L); 1340
—— (see Lyon, W. S.)—1280
Hanna, S. S. (see Gelinas, R. W.)—1253(A)
—— (see Lavier, E. C.)—1252(A)
—— (see Severiens, J. C.)—1254(A)
Hans, H. S. (see Rothman, M. A.)—83
Hanson, A. O. (see Scott, M. B.)—209
Hanson, H. P. X-ray absorption edges and chemical binding—958(T)
Hanson, R. J. (see Moore, D. C.)—972(A)
Harkness, A. L. (see Fields, P. R.)—172
Harman, T. C., S. E. Miller, and H. L. Goering. Preparation and electrical properties of Bi_2Te_3—1262(A)
Harris, F. B. and I. Escobar. East-west asymmetry of positive and negative mesons at geomagnetic equator—255
Harris, G., J. Orear, and S. Taylor. Lifetimes of τ^+ and K_L^+-mesons—932(L)
Harrison, Don E., Jr. Statistical mechanics of cathode sputtering—1234(A)
Harrison, G. R., R. C. Crawford, and J. I. Hopkins. K-series fluorescence yields of A^{40}, Cu^{65}, and In^{115}—841
Harrison, Melvin A. Townsend's first ionization coefficient in N_2—1800(A)
Harrison, Ralph J. (see Austin, Alfred E.)—1225(L)
Harth, E. M. and M. M. Block. Decay of anomalous charged K-meson—959(A)
—— (see Block, M. M.)—324; 959(A)
—— (see Fairbank, W. M.)—971(A)
Harvey, B. G. (see Asaro, Frank)—137
Harvey, J. A. (see Pilcher, V. E.)—1248(A)
Hasegawa, H. (see Anderson, P. W.)—675
Haskin, D. M., D. B. Williams, E. Goodman, and Marcel Schein. Analysis of capture stars of K^--mesons from Berkeley Bevatron—1263(A)
—— (see Cavanaugh, R. E.)—1263(A)
—— (see Leenov, Daniel)—1263(A)
—— (see Schein, Marcel)—1263(A); 1455
—— (see Williams, D. B.)—1547(L)
Hatch, Albert J. and H. Bartel Williams. Pressure limits of high-frequency secondary electron resonance breakdown mechanism—1228(A)
Hatton, J. Effect of pressure on electrical resistance of metals at liquid He temperatures—681
—— Effect of pressure on superconducting transition temperature of Tl—1784(L)
Havliček, F. I. and B. Doboviśek. Photodisintegration of C^{13} and O^{16}—1355
Haven, Y. (see Van Doorn, C. Z.)—753(L)
Havens, W. W., Jr. (see Gould, F. T.)—1248(A)
Haworth, L. J. (see Green, G. K.)—1268(A)
Haxby, R. O. (see Terwilliger, K. M.)—1246(A)
Haynes, J. R. Recombination radiation from Si—1259(A)
—— **and J. A. Hornbeck.** Trapping of minority carriers in Si. II. n-type Si—606
Heckman, Harry H., Frances M. Smith, and Walter H. Barkas. Masses of positive K-particles. II. Method, analysis, and results—1803(A)
—— (see Barkas, Walter H.)—1797(A)
—— (see Smith, Frances M.)—1802(A)
Hefferan V, J. (see Romero-Juárez, A.)—965(A)
Heft, Robert E. and W. F. Libby. Absolute cross sections for deuterons on Be—799
Helmer, R. G. (see Cork, J. M.)—188; 955(A); 1237(A)
Henderson, R. S. Electron spin coupling in polyatomic molecules—723
Hennig, G. R. (see Montet, G. L.)—1261(A)
Henri, V. P. (see Bay, Z.)—1197
Henry, Warren E. Ferrimagnetic interaction and remanence in $CoCO_3$—1791(A)
Henshaw, D. G. (see Hurst, D. G.)—994
Henyey, L. G. Numerical calculations of stellar evolution—1795(T)
Herb, R. G. (see Weinman, J. A.)—1239(A)
Herbert, R. A. (see Wolff, G. A.)—1144
Herman, Robert, M. C. Wallis, and R. F. Wallis. Frequencies and relative intensities of R_1 and R_2 bands in KCl—1267(A)

Heroux, L. (see Dieke, G. H.)—965(A)
Herring, D. F., R. A. Douglas, E. A. Silverstein, and Ren Chiba. Energy resolution obtainable with 2-Mev H_2^+ beam—1239(A)
—— (see Chiba, Ren)—1253(A)
Heusinkveld, Myron, Mark Jakobson, Lawrence Ruby, Bob H. Smith, and Byron T. Wright. Studies with three-dee three-phase proton cyclotron—1804(A)
Heydenburg, N. P. and G. M. Temmer. Coulomb excitation of rare-earth nuclei with α particles—150
—— (see Temmer, G. M.)—961(A)
Hicks, Harry G. and Richard S. Gilbert. Radiochemical studies of high-energy fission process—1286
——, **Peter C. Stevenson, Richard S. Gilbert, and William H. Hutchin.** Fission product yields of U bombarded with deuterons of various energies (20–190 Mev)—1284
Hildebrand, R. H. (see Nagle, D. E.)—959(A)
Hill, E. L. Relativistic theory of discrete momentum space and discrete space-time—1780
Hill, H. A. and J. M. Blair. Energy levels in F^{19}—961(A)
Hilton, H. H., III (see Mills, W. R., Jr.)—1794(A)
Hines, R. L. Reduction of optical reflectivity of glass by positive ion bombardment—1267(A)
Hintz, Norton M. Elastic scattering of protons at 9.9 Mev—1794(A)
Hjalmar, Elis, Hilding Slätis, and Stanley G. Thompson. Energy spectrum of neutrons from spontaneous fission of Cf^{252}—1542(L)
Hoang, T. F. (see Cester, R.)—940(L)
Hoff, R. W., H. Jaffe, T. O. Passell, F. S. Stephens, E. K. Hulet, and S. G. Thompson. Radioactive decay of isomers of Am^{242}—1403
Hogan, R. S. (see Marburger, R. E.)—978(A)
Hollander, J. M., W. G. Smith, and J. W. Mihelich. Energy levels of Pu^{239} populated by β decay of Np^{239}—1238(A)
Holliday, J. E. and E. J. Sternglass. New method for determining range of low-energy electrons in solids—1238(A)
Holm, Dale M. and H. V. Argo. *t-t* elastic scattering from 1.6 to 2.0 Mev—1244(A)
Holmes, John R. (see McClung, Fred)—1792(A)
Holmgren, H. D., M. L. Bullock, and W. E. Kunz. Angular distributions of protons from $Be^9(He^3,p)B^{11}$—436(L)
——, **W. E. Kunz, and L. Bullock.** Angular distribution of protons from $Be^9(He^3,p)B^{11}$ reaction—1253(A)
—— (see Kunz, W. E.)—1252(A)
Holstein, T. Mobility of positive ions in gas mixtures—1230(A)
Hopkins, J. I. (see Harrison, G. R.)—841
Hopkins, Robert L. and Edward N. Clarke. Thermal acceptors in vacuum heat-treated Ge—1786(L)
Horie, H. (see Sherr, R.)—945(L)
Hornbeck, J. A. (see Haynes, J. R.)—606
Hornyak, W. F. and R. Sherr. Inelastic scattering of 19-Mev protons by O^{16}—1409
—— (see Sherr, R.)—945(L)
Horowitz, M. (see Silvidi, A. A.)—979(A)
Hosler, W. R. and H. P. R. Frederikse. Electrical properties of Mg_2Sn at low temperatures—1261(A)
—— (see Blunt, R. F.)—663
Houston, W. V. and H. E. Rorschach. Motion of nuclei in liquid He—1003
—— (see Rorschach, H. E., Jr.)—966(A)
Hove, John E. Magnetic susceptibility of neutron-damaged graphite—1806(A)
—— Theory of magnetic susceptibility of graphite—645
—— (see Austerman, Stanley B.)—1214(L)
—— (see Rasor, Ned S.)—1806(A)
Hrostowski, H. J., F. J. Morin, T. H. Geballe, and G. H. Wheatley. Hall effect and conductivity of InSb—1672
—— (see Shulman, R. G.)—1792(A)
Huber, P. (see Franzen, W.)—1239(A)
Hudspeth, Emmett L. Neutron experiments with Van de Graaff generator—954(T)
—— (see Bostrom, Norman A.)—973(A)
—— (see Sattar, Abdul R.)—960(A)
Hughes, D. J. and V. E. Pilcher. Measurement of $\bar{\Gamma}_n^0/D$ ratio by average cross sections—1249(A)
—— (see Palevsky, H.)—1266(A)
Huibregtse, E. J. Electromechanical behavior of single crystals of $BaTiO_3$—977(T)
Huizenga, J. R. (see Fields, P. R.)—172
Hulet, E. K. (see Hoff, R. W.)—1403
Huntington, H. B., J. E. Dickey, and Robb Thomson. Dislocation energies in NaCl—1117
Hurst, D. G. and D. G. Henshaw. Atomic distribution in liquid He by neutron diffraction—994
Hutchin, William H. (see Hicks, Harry G.)—1284

Igo, G. Slow neutron resonances in Re—1338
—— **and H. E. Wegner.** Anomaly in nuclear energy level density measurements—1796(A)
——, **H. E. Wegner, and R. M. Eisberg.** Elastic scattering of 40-Mev α particles from light nuclei—1244(A)
—— (see Eisberg, R. M.)—961(A); 1309
Imhof, William, V. Perez-Mendez, and H. Easterday. π^+ photomeson production from various nuclei at 135°—1798(A)
Ingersoll, L. R. and D. H. Liebenberg. Faraday effect in gases—Experiment and theory—963(A)
Inglis, D. R. Origin of nuclear moments of inertia—1795(T)
Ise, John, Jr., Andre Lagarrigue, and Robert V. Pyle. Inelastic cross sections from 5-Bev π^- Bevatron beam in Pb and Al—1799(A)
Iselin, C. O'D. General circulation of ocean—1796(T)

Jablonski, F. E. (see Ferguson, G. A.)—1239(A)
Jaccarino, V. (see Dillon, J. F., Jr.)—750(L)
Jacobs, I. S. and C. P. Bean. Approach to elongated fine particle magnets—1060
Jacobs, Ira. Perturbation calculation of volume exclusion effect—1257(A)
Jacobsohn, B. A. Current problems in collective nuclear models—1795(T)
Jacobus, D. D., C. L. Gould, J. J. Grisoli, and I. J. Polk. Electron analog—construction—1268(A)
Jaffe, H. (see Hoff, R. W.)—1403
Jakobson, Mark (see Heusinkveld, Myron)—1804(A)
James, Hubert M. (see Lehman, Guy W.)—1658
Janes, G. S., R. Gomez, G. E. Pugh, and D. H. Frisch. γ-ray scattering by H—1245(A)
—— (see Gomez, R.)—1245(A)
—— (see Pugh, G. E.)—1245(A)
Jastram, P. S. (see Wood, G. T.)—1237(A)
Jaumot, F. E., Jr. (see Sawatzky, A.)—1627
Jenkins, F. A. and D. R. Speck. Nuclear moments of Gd from optical hfs—973(A)
Jensen, E. N. (see Nichols, R. T.)—1407
Jesse, William P. and John Sadauskis. Ionization by α particles in mixtures of gases—1755
Jester, Malvern H. L. (see Wallace, Roger W.)—962(A)
Johansson, Sven A. E. Rotational states in Tm^{169}—835
John, Walter. Excitation functions for α-induced reactions on Pb—1265(A)
Johnson, C. H. and A. Galonsky. $T(d,n)He^4$ reaction, 1–5 Mev—1252(A)

Johnson, G. D. (see Ajzenberg, F.)—960(A)
Johnson, V. A. Thermoelectric power in semiconductor showing high-temperature degeneracy—1251(A)
Jones, K. W. (see Williamson, R. M.)—960(A)
Jones, L. W. and K. M. Terwilliger. Small model FFAG betatron. III. Preliminary experimental results—1247(A)
—— (see Terwilliger, K. M.)—1246(A)
Jones, W. M. Half-life of T—124
Jordan, R. D. (see Anderson, T. H.)—964(A)
Joseph, J. Multiple photon production from electron pair annihilation—1241(A)
—— (see Rohrlich, F.)—1241(A)
Judd, David L. Theoretical study of relativistic constant-frequency cyclotrons—1804(A)
Judish, J. P. (see Galonsky, A.)—121

Kaiser, H. F. Microtron injector for electron synchrotrons—1246(A)
Kalos, M. H. and R. H. Dalitz. Pion-nucleon scattering calculations in Tamm-Dancoff theory—1515
Kammer, E. W., E. I. Salkovitz, and A. I. Schindler. Brillouin zone studies. V. Thermoelectric power of dilute Mg alloys—1257(A)
Kammerer, Otto F. (see Levy, Paul W.)—1787(L)
Kanner, H. (see Bay, Z.)—1197
Kaplan, J. I. Spin resonance in metals as altered by Overhauser effect—965(A)
Kaplan, Selig N. (see Millburn, George P.)—1793(A)
Kaplon, M. F. (see Koshiba, M.)—327
Karplus, Robert (see Goebel, Charles J.)—240
Kassner, R. R. (see Courant, E. D.)—1269(A)
—— (see Raka, E. C.)—1269(A)
—— (see Spiro, J.)—1269(A)
Katz, Samuel. Deformation zones produced by explosive shocks in ferrous metals—1800(A)
Kavanagh, R. W. (see Barnes, C. A.)—1796(A)
Keffer, Frederic. Temperature dependence of ferromagnetic anisotropy in cubic crystals—1692
Keller, William E. Pressure-volume isotherms of He^4 below 4.2°K—1790(E)
—— Second virial coefficients of He^3-He^4 mixtures between 2 and 4°K—1021
Kelly, Elmer (see Pyle, Robert V.)—1804(A)
Kenney, R. W. (see Anderson, J. D.)—1798(A)
Kenski, J. (see Fields, T.)—964(A)
Kenty, Carl. Continuum of Xe Hg′ molecule—1231(A)
Kephart, J. F. (see Hammel, J. E.)—190
Kerker, M. and A. Chou. Refractive index of colloidal solutions—977(T)
Kernan, A. (see Cester, R.)—940(L)
Kerr, Donald E. and Eldred F. Tubbs. Transient behavior following breakdown and its relation to afterglow processes—1231(A)
Kerst, D. W. (see Cole, F. T.)—1246(A)
—— (see Scott, M. B.)—209
—— (see Terwilliger, K. M.)—1246(A)
Ketelle, B. H. (see Brosi, A. R.)—169
Keyes, Robert W. Temperature dependence of elastoresistance in *n*-type Ge—1104
—— **and R. J. Sladek.** Reduction of charge carrier concentration in InSb at 4.2°K by strong magnetic field—1262(A)
Kikuchi, Chihiro. Doublet structure in paramagnetic absorption spectra of Mn^{++} in calcite—1243(A)
—— (see Matarrese, Lawrence M.)—1243(A)
Kinderman, Edwin M. (see Lefevre, Harlan W.)—1374
King, R. W. Hole-particle relations and *j-j* coupling—1240(A)
Kington, J. D. (see Bair, J. K.)—21
Kip, A. F. (see Dresselhaus, G.)—618; 1218(L); 1262(A)
—— (see Owen, J.)—965(A)
Kirkwood, J. G. (see Mazo, R. M.)—1787(L)
Kisslinger, L. S. *L-S* interaction in nuclei—1240(A)
Kittel, Charles. Cyclotron resonance in semiconductor crystals—958(T)
—— (see Dresselhaus, G.)—618; 1262(A)
Klein, Z. (see Moellering, W. M.)—441(L)
Kleitman, David and T. A. Longo. Deuteron irradiation of Ge at 90°K—1261(A)
—— (see Longo, Thomas A.)—1260(A)
Klema, Ernest D. γ-γ angular correlation in Ba^{131}—66
—— (see Osborn, R. K.)—822
Klick, C. C., G. A. Russell, and D. L. Dexter. Criterion for occurrence of luminescence—964(A)
—— (see Dexter, D. L.)—603
Knight, J. D. and E. W. Baker. Radiochemical study of Tl^{196}, Tl^{197}, and Tl^{198m}—1334
Koehler, W. C. (see Wollan, E. O.)—545
Koerts, L. A. Ch. (see Benczer, N.)—955(A)
—— (see Van Lieshout, R.)—223
Koester, Charles J. (see Givens, M. Parker)—1112
Koester, L. J., Jr. (see Goldwasser, E. L.)—1255(A)
Kohler, F. and O. K. Rice. Critical phenomena in triethylamine-water system—965(A)
Kohnke, E. E. and A. W. Ewald. Hall effect in gray Sn filaments—1251(A)
Korff, S. A. (see Soberman, R. K.)—859; 959(A)
Koshiba, M. and M. F. Kaplon. High-energy electromagnetic phenomena in cosmic radiation—327
—— **and Marcel Schein.** Time variation of primary heavy nuclei flux in cosmic radiation—1247(A)
—— (see Williams, D. B.)—1547(L)
Kottwitz, David. Magnetic superexchange interaction—1242(A)
Krag, W. E. (see Bullis, W. M.)—1258(A)
Kraushaar, J. J. (see Brun, E.)—1795(A)
Kreger, W. E., L. D. McIsaac, J. L. Mackin, and J. R. Lai. Radioactive decay of W^{181} and W^{185}—955(A)
—— (see Edelsack, E. A.)—973(A)
Krone, R. W. (see Baumann, N. P.)—1244(A)
Kruse, U. E. (see Anderson, H. L.)—279; 339
Ku, Han-Ying (see Dresselhaus, G.)—1218(L)
Kuiper, J. W. (see Grimes, D. M.)—1256(A)
Kulp, J. L. Present status of radio-carbon dating—962(T)
Kunz, W. E., J. W. Butler, and H. D. Holmgren. γ rays from He^3 bombardment of deuterium—1252(A)
—— (see Holmgren, H. D.)—436(L); 1253(A)
Kurbatov, J. D. Relative stability of even mass-number isobars—954(T)
Kurs, A. F. (see Montet, G. L.)—1261(A)
Kusch, P. Redetermination of hyperfine splittings of H and D in ground state—1188

Lagarrigue, Andre (see Ise, John, Jr.)—1799(A)
Lai, J. R. (see Kreger, W. E.)—955(A)
Lambe, John. CdS with Ag activator—1586
Lamphere, R. W. and R. E. Greene. Neutron-induced fission cross sections of U^{235} and U^{238}—763
Landé, Alfred. Quantum theory from nonquantal principles—979(A)
Landon, H. H. Radiation widths in slow neutron resonances—1414
Lane, A. M. and L. Verlet. Polarization in theory of giant resonances of neutron scattering—956(A)
LaRocca, E. W. Phase transformations in microstructure of explosively loaded Fe and steel—1800(A)
Laslett, L. J. (see Raka, E. C.)—1269(A)
Lavier, E. C., S. S. Hanna, and R. W. Gelinas. α spectrum from $Li^7(p,\gamma)Be^{8*}(\alpha)He^4$—1252(A)

Lawrence, E. O. Recent experiments with Bevatron—962 (T)
Lawson, R. D. Electric multipole moments in *j-j* coupling —845
—— Low-energy neutron scattering and bound state problem —957(A)
Lax, Benjamin and J. G. Mavroides. Statistics and galvanomagnetic effects in Ge and Si with warped energy surfaces—1650
—— (see Dexter, R. N.)—1216(L)
Lax, Melvin. Generalized theory of mobility—1808(A)
—— **and Elias Burstein.** Broadening of impurity levels in Si —592
Lazarus, John P. and S. Sack. Agreement of classical and quantum Coulomb excitation integrals—370
—— (see Breit, G.)—942(L)
LeBlanc, J. M., L. M. Bollinger, and R. E. Coté. Neutron transmission measurements on Br and Se—1248(A)
—— (see Bollinger, L. M.)—1239(A)
Lederman, L. M. (see Rinehart, M. C.)—883
Lee, R. J. and R. G. Fowler. Electrical characteristics of low-pressure spark discharges—1234(A)
Lee, T. D. and J. Orear. Speculations on heavy mesons—932(L)
—— (see Friedman, M. H.)—1494
Leenov, Daniel, D. M. Haskin, and Marcel Schein. Hyperfragments in light elements produced by Berkeley Bevatron—1263(A)
—— (see Schein, Marcel)—1455
Lefevre, Harlan W., Edwin M. Kinderman, and Harold H. Van Tuyl. New γ rays in the Np^{239} decay—1374
Legvold, S. (see Elliott, J. F.)—1595
Lehman, Guy W. Energy band calculations in f.c.c. Th—1791(A)
—— **and Hubert M. James.** Interaction of impurities and mobile carriers in semiconductors—1698
Leighton, R. B. (see Sorrels, J. D.)—1457; 1484
—— (see Trilling, G. H.)—1468
Levin, J. S. (see Cranberg, L.)—434(L)
Levinson, Carl and Kenneth W. Ford. Independent-particle model of nucleus. III. Ca isotopes—13
—— (see Ford, Kenneth W.)—1
Levy, Paul W. and Otto F. Kammerer. Radiation-induced amorphism in diamond—1787(L)
Lewis, H. W. Search for Hall effect in superconductor. II. Theory—641
Lewis, H. W. (see Bernstein, E. M.)—1345; 1367
Li, Yin-Yuan. Magnetic moment arrangements and magnetocrystalline deformations in antiferromagnetic compounds—627
Libby, W. F. (see Heft, Robert E.)—799
Lichtenberg, D. B. Pion production in p-p collisions—303
Liebenberg, D. H. (see Ingersoll, L. R.)—963(A)
Lin, Chun C. and Masataka Mizushima. Theory of hfs of NO molecule. II. Errata and some additional discussion—1726
Lind, D. A. (see Davis, Robert H.)—1266(A)
—— (see Divatia, Ajay S.)—1266(A)
Lindenbaum, Seymour J. and Luke C. L. Yuan. Total cross section of H for 150-750-Mev positive and negative pions—306
—— (see Pevsner, Aihud)—1419
Lindqvist, Torsten and Chien-Shiung Wu. Inner bremsstrahlung from A^{37}—145
Lipworth, Edgar (see Novick, Robert)—1153
Loebner, E. E. Bistable solid state opto-electronic devices —1239(A)
Loferski, Joseph (see Rappaport, Paul)—1261(A)
Logan, J. K. (see Clement, J. R.)—743
Logan, R. A. Precipitation of Cu in Ge—615
Longo, Thomas A. and David Kleitman. Neutron-irradiated Si—1260(A)
—— (see Kleitman, D.)—1261(A)
Lönsjö, O. (see Taylor, H. L.)—174
Low, Francis E. Effective-range theory of meson-nucleon scattering—1250(T)
—— (see Moellering, W. M.)—441(L)
Low, W. (see Geller, Z.)—1240(A)
Lowe, I. J., L. O. Bowen, and R. E. Norberg. Nuclear magnetic relaxation times in polyethylene—1243(A)
Lowen, Robert (see Critchfield, C. L.)—956(A)
Loyd, C. M. (see Ward, J. K.)—963(A)
Lozano, Juan Manuel. Poles of S-matrix for cloudy crystal ball model—956(A)
Luborsky, F. E. (see Paine, T. O.)—1055
Lustig, Harry and J. M. Blatt. Phase-shift analysis of single-channel reactions—777
Luttinger, J. M. and B. R. Goodman. Classical theory of cyclotron resonance for holes in Ge—673
—— (see Brown, H. A.)—685
Lyon, W. S. and T. H. Handley. Radioactive Ca^{47}—1280
—— **and R. R. Rickard.** γ-ray branching in Sr^{89}—112

Macdonald, J. Ross (see Brachman, Malcolm K.)—966(A)
MacDonald, William M. Isotopic spin impurity in light nuclei—51
MacGregor, M. H., William P. Ball, and Rex Booth. Nonelastic cross sections at 14 Mev—1793(A)
Macke, Wilhelm. Wave mechanical treatment of Fermi gas —992
MacKenzie, K. R. (see Burkig, V. C.)—1805(A)
—— (see Sonett, C. P.)—734
Mackin, J. L. (see Kreger, W. E.)—955(A)
Mackinnon, L. Relative absorption of 10 Mc/sec longitudinal sound waves in superconducting polycrystalline Sn rod—655
Macklin, R. L. (see Gibbons, J. H.)—167
Madsen, V. M. (see Burch, D. S.)—1235(A)
Maenchen, George, William B. Fowler, Wilson M. Powell, George Saphir, and Robert W. Wright. Production of unstable particles in 4.5-Bev π^--p collisions—1802(A)
—— (see Wright, Robert W.)—1802(A)
Magleby, E. H. (see Smith, J. R.)—1266(A)
Magnusson, L. B., D. W. Engelkemeir, M. S. Freedman, F. T. Porter, and F. Wagner, Jr. α decay of Np^{237}—1237 (A)
Malamud, H. (see Hammer, J.)—1229(A)
Maldonado, C. D. and R. C. Retherford. Semirandom sparking in short air gap—1228(A)
Malpica, José Mireles. Semiabsolute electrostatic voltmeter—967(A)
—— Semiabsolute measurements of voltage and current—975 (A)
Mandeville, C. E. (see Rothman, M. A.)—83
Marburger, R. E., D. C. Reynolds, L. L. Antes, and R. S. Hogan. Quantum yield of CdS photovoltaic cell—978 (A)
Marcus, J. A. (see Connell, R. A.)—1256(A)
Margulies, R. S. Positive pion scattering by H at 260, 300, and 400 Mev—1255(A)
Marion, Jerry B., T. W. Bonner, and C. F. Cook. (d,n) reactions on B and C—847
——, **T. W. Bonner, and C. F. Cook.** Reactions $T^3(p,n)He^3$, $Li^7(p,n)Be^7$, $Be^9(p,n)B^9$, and $F^{19}(p,n)Ne^{19}$—91
—— **and Robert M. Brugger.** Neutron-induced reactions in F—69
——, **R. M. Brugger, and T. W. Bonner.** (d,n) reactions in O^{18} and N^{14}—46

—— **and R. A. Chapman.** Low-lying level structure of Zn^{66} nucleus—1795(A)
—— (see Brugger, R. M.)—84
Mark, Hans and George T. Paulissen. Electric excitation of certain rare-earth nuclei by protons—813
—— (see Rubin, A.)—961(A)
Marmier, P. (see Baggerly, L. L.)—1364
Marshak, R. (see Okubo, S.)—1809(A)
—— (see Regge, T.)—1810(A)
Marshall, J. F. (see Pomerantz, M. A.)—964(A)
Martin, David W., S. Bradley Burson, and James M. Cork. Decay of Ca^{45}—1236(A)
—— (see Cork, J. M.)—1237(A)
Martin, E. E. (see Trolan, J. K.)—1646
Martin, W. (see Arnold, W. H., Jr.)—1545(L)
Marton, L. Perdida de energia por electrones en cuerpos solidos—958(T)
Martz, D. E. and R. S. Witte. Transverse field effects in PbS—1808(A)
Matarrese, Lawrence M. and Chihiro Kikuchi. Anisotropic paramagnetic absorption spectrum of manganous ion in cubic ZnS—1243(A)
Matthias, B. T. and E. Corenzwit. Superconductivity of Zr alloys—626
Maudlin, L. Z. (see Weissler, G. L.)—1800(A)
Maurer, R. D. Light scattering by optical glasses—977(T)
Mavroides, J. G. (see Lax, Benjamin)—1650
Mayer, Joseph E. Electron correlation—1579
Mayfield, Earle B., Harvey L. Morrison, and William A. Allen. Projectile penetration into sand—1800(A)
Mays, J. M. (see Shulman, R. G.)—692
Mazari, M., F. Alba, and V. Serment. Neutron total cross section measurements between 13.0 and 16.2 Mev—972(A)
—— (see Ajzenberg, F.)—960(A)
Mazo, R. M. and J. G. Kirkwood. Atomic distribution in liquid He^3—1787(L)
McCall, D. W. (see Shulman, R. G.)—692
McCarthy, Kathryn A. and Stanley S. Ballard. Variation with temperature of thermal conductivity of seven alkali halides—969(A)
McClelland, J. D. Field dependence of Hall potential and magnetoresistance of irradiated graphite—1807(A)
McClung, Fred and John R. Holmes. Isotope shift in spectra of Hg^{198}-Hg^{202}—1792(A)
McClure, B. T. Formative breakdown delays in noble gases at small overvoltages—1228(A)
McClure, John J. (see Urban, John S.)—1797(A)
McCombie, C. W. Fluctuations on damped transmission line—444
McCrary, J. H. (see Bent, R. D.)—771; 774
McDonald, C. A. (see Anderson, J. D.)—1798(A)
McDonald, Frank B. (see Webber, William R.)—1460
McDonald, W. S., Vincent Peterson, and Dale R. Corson. Photoproduction of neutral pions from protons at forward pion angles—1799(A)
McEllistrem, M. T. Analysis of C^{12}+d reactions—1253(A)
McGrew, C. (see Arnold, W. H.)—1804(A)
McGruer, J. N., E. K. Warburton, and R. S. Bender. (d,p) reactions from C^{12} and C^{13}—235
McHale, J. L. (see Biedenharn, L. C.)—376
—— (see Goldstein, M.)—436(L)
McIsaac, L. D. (see Kreger, W. E.)—955(A)
McLachlan, Dan, Jr. Neglected mathematics in solution of vibration problems—975(A)
McLeod, R. R. Coulomb excitation of In^{115m} by α particles—1265(A)
Mead, S. W., M. D. Petroff, and W. O. Doggett. Half-life of Sn^{119}—1794(A)
Medicus, Gustav. Pronounced deviations from Maxwellian velocity distribution of electrons in hollow hot cathode diodes with Ne filling—1232(A)
Medina, Alejandro. Divergences in field theory—967(T)
Meechan, C. J. Effect of low-temperature electron irradiation on electrical resistivity of Cu—1807(A)
Meijer, Paul H. E. and H. J. Gerritsen. Magnitude of splitting of lowest level in chromium alum—742
Meinke, W. Wayne (see Cassatt, Wayne A., Jr.)—1372
Meister, A. G., J. M. Dowling, A. N. Takata, and A. J. Bielecki. Potential constants for $CHDClBr$, CH_2F_2, CD_2F_2, and $CHDF_2$ molecules—1267(A)
Melchor, J. L. (see Ayres, W. P.)—1791(A)
Melkanoff, Michel A., John Nodvik, and David S. Saxon. Analysis of elastic scattering of 31.5-Mev protons—1805(A)
Mencher, A. (see Barker, W. A.)—1224(L)
Mendelsohn, L. I. (see Paine, T. O.)—1055
Mendlowitz, H. and K. M. Case. Double scattering of electrons with magnetic interaction. II. Depolarization—1551
Merritt, F. R. (see Fletcher, R. C.)—747(L)
—— (see Galt, J. K.)—748(L)
Metzger, F. R. (see Swann, C. P.)—1329
Meyer, L. (see Baskin, Y.)—544
Meyerhof, W. E. (see Brun, E.)—1795(A)
Meyer-Schützmeister, L. and V. L. Telegdi. Inelastic scattering of photons from Au^{197}—961(A)
Mihelich, J. W. (see Hollander, J. M.)—1238(A)
Millburn, George P., Burton J. Moyer, Yuin-Kwei Tai, and Selig N. Kaplan. Neutron yields from 32-Mev protons on thick targets—1793(A)
Miller, D. W., V. K. Rasmussen, M. B. Sampson, and U. C. Gupta. Reactions $Be^9(d,d')$ and $Be^9(\alpha,\alpha')$—1253(A)
—— (see Rasmussen, V. K.)—851
Miller, M. M. and T. Ahrens. Possibility of interpreting β decay spectra in terms of nuclear forces—974(A)
Miller, S. E. (see Harman, T. C.)—1262(A)
Miller, W. C. (see Connors, D. R.)—1237(A)
—— (see Dempsey, D. F.)—1240(A)
Miller, D. W. (see Rasmussen, V. K.)—181
Miller, W. C. (see Spiegel, V., Jr.)—1244(A)
—— (see Waldman, B.)—1244(A)
Mills, C. B. High-intensity ion sources—1233(A)
Mills, W. R., Jr., H. H. Hilton, III, and C. A. Barnes. Internal conversion coefficients of low excited states of F^{19}—1794(A)
Mitchell, Allan C. G. (see Graves, William E.)—1236(A)
Mize, J. P., M. E. Bunker, and J. W. Starner. Nuclear levels of Lu^{175}—1390
—— (see Duffield, R. B.)—1236(A)
Mizushima, Masataka (see Lin, Chun C.)—1726
Mobley, R. C., C. H. Blakewood, and D. C. Ralph. Low voltage magnet and regulated power supply—1242(A)
Moe, Mildred M. and David S. Saxon. Variational methods in scattering problems—1809(A)
—— (see Finkelstein, R. J.)—1775
Moellering, W. M., A. C. Zemach, A. Klein, and F. E. Low. Spatial extension of proton magnetic moment from hfs of H—441(L)
Moffat, R. D. (see Davis, Robert H.)—1266(A)
—— (see Divatia, Ajay S.)—1266(A)
Mohrbacher, J. A. (see Bracken, J. T.)—972(A)
Mondragón, A. Scattering length and effective range for velocity-dependent tensor forces—956(A)
Montet, G. L., A. F. Kurs, and G. R. Hennig. Tracer studies on radiation-damaged graphite—1261(A)
Montroll, Elliott W. and Renfrey B. Potts. Effect of defects on lattice vibrations—525

—— **and R. B. Potts.** Effect of impurities on lattice vibrations—969(A)
Moore, D. C. and R. J. Hanson. Čerenkov counter for high-energy cosmic rays—972(A)
Moore, G. E. Dissociation of solid compounds by electron impact—1794(T)
Mooser, E. Magnetic susceptibility of impurity-trapped electrons and holes in semiconductors—1589
Moravcsik, Michael J. Coulomb scattering of electrons at very small angles—1009
Morgan, Ira L. (see Bostrom, Norman A.)—973(A)
—— (see Sattar, Abdul R.)—960(A)
Morin, F. J., Howard Reiss, and C. S. Fuller. Ion pairing involving Li in Ge and Si—1807(A)
—— (see Hrostowski, H. J.)—1672
Morinaga, H. New radioactive isotope Sc^{47}—431(L)
—— **and E. Bleuler.** Sc^{50}—1236(A)
Morrison, Harvey L. (see Mayfield, Earle B.)—1800(A)
Moshinsky, Marcos. Collective motions and nuclear reactions—967(T)
Mosqueira R., Salvador. Teaching of physics in Mexico—954(T)
Motz, Henry (see Grodzins, Lee)—1236(A)
Motz, J. W. Bremsstrahlung differential cross-section measurements for 0.5- and 1.0-Mev electrons—1560
Moyer, Burton J. (see Millburn, George P.)—1793(A)
—— (see Squire, Robert K.)—1798(A)
Muehlhause, C. O. and S. Oleksa. β^- energy distribution from thermal fission of U^{235}—1266(A)
—— (see Bloom, S. D.)—1248(A)
Munick, Raymond J. Electrical conduction in Plexiglas—1256(A)
Murakawa, Kiyoshi. Nuclear moments of Mo^{95}, Mo^{97}, Zr^{93}, I^{127}, Sb^{121}, and Sb^{123}—1369
Murray, J. J. Observations on negative particles of protonic-mass stopping in Čerenkov counter—1801(T)
Murray, R. B. Magnetic and thermal properties of $MnCl_2$ at liquid He temperatures. II. Specific heat—1071
—— **and L. D. Roberts.** Magnetic and thermal properties of $MnCl_2$ at liquid He temperatures. I. Magnetic susceptibility—1067
—— (see Roberts, L. D.)—650; 1100
Muschlitz, E. E. (see Bailey, T. L.)—1231(A)
Musulin, Boris (see Wertz, John E.)—1810(A)
Myers, H. P. (see Brockhouse, B. N.)—1242(A)

Nagle, D. E. Pion-proton scattering observed with liquid-H_2 bubble-chamber—1255(T)
—— **and R. H. Hildebrand.** Observations on pion tracks in liquid H_2 bubble chamber—959(A)
Nambu, Yoichiro. Structure of Green's functions in quantum field theory—394
Naumann, R. A. (see Tomlinson, E. P.)—955(A)
Neher, H. V. Change with time of low-energy part of cosmic-ray spectrum—959(A)
Neill, H. W. (see Drost-Hansen, W.)—1800(A)
Nelson, E. B. (see Geer, E. H.)—215
Nesbet, R. K. Localized orbitals in nuclear structure—228
Neufeld, J. (see Snyder, W. S.)—969(A)
Newcomb, W. A. Magnetohydrodynamic waves in ionized plasma—968(A)
Newman, Roger. Visible light from a Si p-n junction—700
Newson, H. W. Li(p,n) reaction near threshold—960(A)
Newton, Roger G. Connection between S-matrix and tensor force—412
—— Relation of a potential to S-matrix—1250(T)
Ney, E. P. Low-energy end of primary cosmic-ray spectrum—971(T)
—— Recent experiments on primary cosmic rays—1806(T)
Nichols, R. T. and E. N. Jensen. Decay scheme of Sc^{47}—1407
Nier, A. O. (see Quisenberry, K. S.)—1245(A)
—— (see Scolman, T. T.)—1245(A)
Noble, L. M. and R. M. Steffen. Directional correlation with gaseous In^{111} sources—955(A)
Nodvik, John (see Melkanoff, Michel A.)—1805(A)
Norberg, R. E. (see Burgess, J. H.)—752(L)
—— (see Lowe, I. J.)—1243
Nottingham, W. B. Application of space-charge theory to determination of electron emitter properties—964(A)
Novick, Robert, Edgar Lipworth, and Paul F. Yergin. Fine structure of singly ionized He—1153

Odian, Allen C., Bernard Feld, William Rankin, Peter Stein, Albert Wattenberg, and Roy Weinstein. High-energy photoneutron-proton ejection from nuclei—1241(A)
—— (see Feld, B. T.)—1539(L)
—— (see Ritson, D. M.)—1263(A)
Oehme, Reinhard. Dispersion relations for pion-nucleon scattering. I. Spin-flip amplitude—1503
Ofer, S. (see Cohen, S. G.)—856
Ohkawa, Tihiro. FFAG electron cyclotron—1247(A)
Ohnuma, Shoroku and David Feldman. Phase shift analysis of nucleon-nucleon scattering at 150 Mev—1241(A)
Okaya, Y. (see Saito, Y.)—970(A)
Okubo, S. and R. Marshak. Difference in lifetimes of θ^0 and θ^- mesons—1809(A)
—— (see Regge, T.)—1810(A)
Oleksa, S. (see Muehlhause, C. O.)—1266(A)
Ore, A. (see Skoglund, A.)—1549(A)
Orear, Jay. Energy dependence of phase shifts in pion-proton scattering—288
—— (see Harris, G.)—932(L)
—— (see Lee, T. D.)—932(L)
Osborn, R. K. and E. D. Klema. Empirical correlation of nuclear magnetic moments—822
Osborne, W. Z. (see Skeen, C. H.)—1797(A)
Oskam, H. J. High-frequency gas discharge breakdown in Ne-A mixtures—1228(A)
Owen, G. E. (see Stewart, A. B.)—1235(A)
Owen, J., M. E. Browne, and A. F. Kip. Electron spin resonance in Cu-Mn and Ag-Mn alloys—965(A)
Oxley, C. L. and V. L. Telegdi. Scattering of 30-90 Mev γ-rays by protons—962(A)
—— **and V. L. Telegdi.** Scattering of 30-95 Mev photons by protons—435(L)

Pack, J. L. and A. V. Phelps. Drift velocity of electrons in He and H_2 at low fields—1229(A)
Paine, T. O., L. I. Mendelsohn, and F. E. Luborsky. Effect of shape anisotropy on coercive force of elongated single-magnetic-domain Fe particles—1055
Pais, A. and O. Piccioni. Decay and absorption of θ^0—1487
Pal, Yash (see Caldwell, David O.)—1803(A)
Palevsky, H., R. L. Zimmerman, R. M. Eisberg, and D. J. Hughes. Measurement of energy variation of neutron multiplication, η, for U^{233}, U^{235}, and Cu^{239} in thermal region—1266(A)
Palfrey, T. R., Jr. (see Tatro, C. A.)—1265(A)
Palmer, R. R. (see Bollinger, L. M.)—126
Paris, C. H., W. W. Buechner, and P. M. Endt. Energy levels of S^{33}, S^{35}, Cl^{36}, Cl^{38}, and Ba^{139}—1317
Parker, Paul M. (see Brown, L. Carlton)—1764
Parmenter, R. H. Energy levels of crystal modified by alloying or by pressure—573
Passell, L., B. R. Felix, and H. B. Silsbee. Thermal conductivity of Al at low temperatures—1808(A)
—— (see Felix, B. R.)—1808(A)

Passell, T. O. (see Hoff, R. W.)—1403
Paul, E. B. (see Almqvist, E.)—1265(A)
Paul, William (see Benedek, George B.)—1129
Paulissen, George T. (see Mark, Hans)—813
Pearson, G. L. Silicon solar battery—958(T)
——, **W. T. Read, Jr., and W. L. Feldmann.** Mechanical properties of Si, Ge, and ZnO whiskers—1251(A)
Peaslee, A. T., Jr. Production of pairs in capture of slow neutrons by protons—974(A)
Peaslee, D. C. Higher-spin particle formalism—1250(T)
Peed, William F. (see Rogosa, George L.)—1763
Pellam, J. R. Normal fluid excitation in liquid He II—1802(T)
Penfold, A. S. and B. M. Spicer. Detailed study of $O^{16}(\gamma,n)O^{15}$ reaction—1377
—— (see Spicer, B. M.)—1375
Penman, S. and W. L. Brown. Field effect in Si—1259(A)
Penning, J. R. and F. H. Schmidt. Decay of Ne^{20}—954(A)
Pepinsky, Ray. Crystal engineering: New concept in crystallography—971(A)
—— Neutron crystallography—971(T)
—— (see Cano-Çorona, O.)—970(A)
—— (see Frazer, B. C.)—745(L)
—— (see Saito, Y.)—970(A)
—— (see Vand, V.)—970(A)
Percus, J. K. Inadmissible auxiliary conditions in quantized linear systems—1208
Perez-Mendez, V. (see Imhof, William)—1798(A)
Perkins, R. B. (see Darden, S. E.)—1315
Perlman, I. (see Asaro, Frank)—137; 1541(L)
—— (see Stephens, F. S., Jr.)—1543(L)
Perlman, M. L. and Joan P. Welker. Disintegration scheme of Rb^{86}—81
—— (see Welker, Joan P.)—74
Perry, R. W. and D. E. Bloxsom. Use of electric arc heating in ultra-high temperature aerodynamics—968(A)
Persson, Karl-B. and Sanborn C. Brown. Electron loss in hydrogen afterglow—729
Peter, M. (see Strandberg, M. W. P.)—963(A)
Peters, C. W. (see Ferguson, G. A.)—1239(A)
Peterson, Edward C. (see Alexeff, Igor)—1239(A)
Peterson, James R. Mass values of identified K-mesons—1803(A)
—— (see Birge, R. W.)—430(L)
Peterson, Vincent (see McDonald, W. S.)—1799(A)
Petroff, M. D. (see Mead, S. W.)—1794(A)
Pevsner, Aihud. Photoplate studies on K-meson family—967(T)
—— **and James Rainwater.** Phase shift optical model calculations for elastic scattering of pions on Al—1431
——, **James Rainwater, Ross E. Williams, and Seymour J. Lindenbaum.** Elastic scattering of positive and negative pions on Al—1419
Phelps, A. V. Lifetime of imprisoned resonance radiation in Ne—1230(A)
—— (see Frost, L. S.)—1234(A)
—— (see Pack, J. L.)—1229(A)
Phillips, G. C., J. L. Russell, and C. W. Reich. Scattering of α particles from He and 3-Mev state in Be^8—960(A)
—— (see Gossett, C. R.)—203
Phillips, Norman E. Thermal conductivity of In-Tl alloys in normal and superconducting states—1719
Piccioni, O. (see Pais, A.)—1487
Pierce, W. M. A certain blindness in physicists—979(A)
Pilcher, V. E., J. A. Harvey, and K. K. Seth. Neutron total cross section of $_{92}U^{235}$ in ev region—1248(A)
—— (see Hughes, D. J.)—1249(A)
Pines, David and Charles P. Slichter. Relaxation times in magnetic resonance—1014
Piotrowski, Edward A. and Joseph S. Ziomek. Normal coordinate treatments and thermodynamic properties of $PFCl_2$ and $POFCl_2$—1267(A)
Piper, W. W. and J. S. Prener. Hartree-Fock wave functions for Mn^{+4}—1250(A)
Pixley, R. E., M. Bader, and Ward Whaling. Energy loss of protons in metals—1805(A)
Pleasonton, Frances (see Snell, Arthur H.)—1396
Plotkin, M. (see Cottingham, J. G.)—1269(A)
Polk, I. J. (see Jacobus, D. D.)—1268(A)
Pollard, E. C. Physics of cellular processes—1548(T)
Pomerantz, M. A., J. F. Marshall, and R. A. Shatas. Post-bombardment conductivity of MgO crystals—964(A)
Porter, C. E. Cross sections and complex potential—935(L)
Porter, F. T. (see Magnusson, L. B.)—1237(A)
Portis, A. M. Rapid passage effects in electron spin resonance—1219(L)
Potts, Renfrey B. (see Montroll, Elliott W.)—525; 969(A)
Powell, Wilson M. π-p, p-p, and n-p collisions at Bevatron energies—1791(T)
—— (see Maenchen, George)—1802(A)
—— (see Wright, Robert W.)—1802(A)
Prener, J. S. (see Piper, W. W.)—1250(A)
Prieto, C., Fernando E. Field of Bhabha equation—974(A)
Primak, William. Kinetics of processes distributed in activation energy—1677
Prosser, F. W., Jr. (see Baumann, N. P.)—1244(A)
Pruett, Charles H. and Roger G. Wilkinson. Electron capture decay of Os^{185} and excited states of Re^{185}—1237(A)
Pugh, G. E., R. Gomez, D. H. Frisch, and G. S. Janes. Nuclear γ-ray scattering techniques—1245(A)
—— (see Gomez, R.)—1245(A)
—— (see Janes, G. S.)—1245(A)
Pyle, Robert V., Elmer L. Kelly, J. Reginald Richardson, and Robert L. Thornton. Electron models of relativistic constant-frequency cyclotrons—1804(A)
—— (see Ise, John, Jr.)—1799(A)

Quinton, A. R. and R. Beringer. Determination of surface resistivity of metal surfaces by Q measurement—1549(A)
Quisenberry, K. S., T. T. Scolman, and A. O. Nier. Atomic masses of H^3, D^3, C^{13}, and S^{33}—1245(A)
—— (see Scolman, T. T.)—1245(A)

Rainwater, James (see Pevsner, Aihud)—1419; 1431
Raka, E. C., E. D. Courant, R. R. Kassner, L. J. Laslett, H. S. Snyder, and J. Spiro. Electron analog—performance and interpretation. I—1269(A)
—— (see Cottingham, J. G.)—1269(A)
—— (see Courant, E. D.)—1269(A)
Ralph, D. C. (see Mobley, R. C.)—1242(A)
Ramsey, Norman F. Resonance transitions induced by perturbations at two or more different frequencies—1191
Randolph, M. L. (see Blosser, H. G.)—429(L)
Rank, D. H., H. E. Bennett, and J. M. Bennett. Improved value of velocity of light derived from band spectrum method—993
Ranken, W. A. (see Bent, R. D.)—771; 774
Rankin, William (see Odian, Allen)—1241(A)
Rappaport, Paul and Joseph J. Loferski. Thresholds for electron-bombardment-induced lattice displacements in Si and Ge—1261(A)
Rarita, William. p-p scattering at 1 Bev—1241(A)
Rasmussen, J. O. (see Strominger, D.)—844
Rasmussen, V. K., D. W. Miller, and M. B. Sampson. Scattering of 22-Mev α particles by C^{12}—181
——, **D. W. Miller, M. B. Sampson, and U. C. Gupta.** Reactions $Be^9(\alpha,\alpha')$, $Be^9(\alpha,d)$, and $Be^9(d,d')$—851
—— (see Miller, D. W.)—1253(A)

Rasor, Ned S. and John E. Hove. Thermal conductivity of neutron-damaged graphite—1806(A)
Rau, Richard R. and M. E. Caspari. Faraday effect in Ge at room temperature—632
Ravenhall, D. G. Inelastic electron scattering by C—1797(A)
Read, W. T., Jr. (see Pearson, G. L.)—1251(A)
Reagan, Daryl. Photonuclear yields of N^{17}—113
Redfield, David. Recombination processes in Te—1094
Redin, R. D. and G. C. Danielson. Measurement of magnetic field gradients by Hall effect—1252(A)
Regge, T., S. Okubo, and R. Marshak. Remarks on antiproton—1810(A)
Reich, C W. (see Phillips, G. C.)—960(A)
Reier, Melvin and Morris H. Shamos. Neutron-capture gamma-ray spectra of V, Co, Ti, Fe, Cr, Au, Mn, and I—1302
Reif, F. Nuclear magnetic resonance studies of imperfect ionic crystals—1597
Reiss, Howard. Ionization of H in Ge and Si—1806(A)
—— (see Fuller, C. S.)—1806(A)
—— (see Morin, F. J.)—1807(A)
Rekers, R. G. and D. S. Villars. Flame zone spectroscopy of solid propellants. II—963(A)
Renero, Ignacio. Scattering by velocity-dependent potential—956(A)
Retherford, R. C. (see Maldonado, C. D.)—1228(A)
Revelle, R. Heat flow through ocean bottom—1796(T)
Reynolds, Charles A. Kinetic model of He II—1548(A)
Reynolds, D. C. (see Marburger, R. E.)—977(A)
Reynolds, George T. (see Arnold, W. H.)—295
Reynolds, H. L. and A. Zucker. Excitation function for reaction $Be^9(N^{14},\alpha n)F^{18}$—226
Rhéaume, R. H. (see Cottingham, J. G.)—1269(A)
Rhein, W. J. Efficiency of ZnS—plastic counters for fast neutrons—972(A)
Ribe, F. L. Pickup reactions $F^{19}(n,d)O^{18}$—1254(A)
Rice, O. K. (see Kohler, F.)—965(A)
Richards, Paul I. Multiple isotropic scattering—517
Richardson, J. Reginald (see Burkig, J. W.)—1805(A)
—— (see Pyle, Robert V.)—1804(A)
Rickard, R. R. (see Lyon, W. S.)—112
Rinehart, M. C., K. C. Rogers, and L. M. Lederman. Diffusion chamber study of very slow mesons. III. Scattering of negative pions in H—883
Ritchie, R. H. (see Blackstock, A. W.)—1078
Ritson, D. M., A. Odian, B. T. Feld, and A. Wattenberg. Spin of τ^+-meson—1263(A)
—— (see Feld, B. T.)—1539(L)
Robbins, A. B. $Li^7(\alpha,n)B^{10}$ reaction—1549(A)
Roberts, B. W. Neutron diffraction study of VD_x—1257(A)
Roberts, L. D. and R. B. Murray. Magnetic and thermal properties of UI_3 at liquid He temperatures—650
——, **R. B. Murray, and J. W. T. Dabbs.** Influence of crystalline electric fields on antiferromagnetic transitions—1100
—— (see Murray, R. B.)—1067
Roberts, S. Interpretation of optical properties of metal surfaces—1667
Robinson, Hugh G. Quadrupole spectrum of $BiCl_3$—1731
Robson, J. M. Angular correlation in β decay of neutron—933(L)
Roesch, W. C. (see De Pangher, J.)—1793(A)
Rogers, K. C. (see Rinehart, M. C.)—883
Rogosa, George L. and William F. Peed. Tc K x-ray spectrum—1763
Rohrlich, Fritz. Recent developments in theory of atomic spectra—1258(T)
—— **and J. Joseph.** Contribution of electron to pair production in atomic H—1241(A)
Rollor, E. A. (see Bracken, J. T.)—972(A)
Romero-Juárez, A. and J. Hefferan V. Systematic application of physical and mathematical methods to exploitation of Mexican oil fields—965(A)
Roos, Charles E. Auger effect in Fe, Ni, Cu, and Zn—1267(A)
Roothaan, C. C. Impact of electronic digital computers on molecular quantum-mechanical calculations—1258(T)
Rorschach, H. E., Jr., and W. V. Houston. Nuclear paramagnetism of liquid He^3—966(A)
—— (see Houston, W. V.)—1003
Rosenbaum, B. M. (see Welber, B.)—978(A)
Ross, Marc. Theory of pion photoproduction—1250(T)
Rostoker, Norman (see Brophy, James J.)—754(L)
—— (see Ekstein, Hans)—1023
Rotenberg, M. Nuclear Hartree-Fock calculations—439(L)
Roth, Wilfred. Vibratory gyro mass flowmeter—1549(A)
Rothman, M. A., H. S. Hans, and C. E. Mandeville. γ rays excited by inelastic scattering of neutrons in various elements—83
Rothstein, Jerome. Significance of nuclear spin echo experiments for foundation of statistical mechanics—1791(A)
Rouse, C. A. Cloud-chamber observations of μ-meson-induced electron showers—1797(A)
Royden, Herbert N. and Byron T. Wright. Small-angle p-p scattering at 20 Mev—1805(A)
Rubin, A., F. Ajzenberg, and Hans Mark. Energy levels of Si^{29}—961(A)
—— (see Ajzenberg, F.)—960(A)
Ruby, Lawrence (see Heusinkveld, Myron)—1804(A)
Ruderman, Malvin A. (see Goebel, Charles J.)—240
Russell, G. A. (see Dexter, D. L.)—603
—— (see Klick, C. C.)—964(A)
Russell, J. L. (see Phillips, G. C.)—960(A)

Sachs, A. M., H. Winick, and B. A. Wooten. Scattering of 38-Mev positive pions in H—1255(A)
Sack, S. (see Lazarus, John P.)—370
Sadauskis, John (see Jesse, William P.)—1755
Saenz, A. W. Quantum-statistical derivation of transport equation for mixtures of dilute gases with molecules of arbitrary spins—975(A)
Sailor, V. L. Neutron resonances in U^{233} and U^{235}—1249(A)
Saito, Y., Y. Okaya, and R. Pepinsky. Direct x-ray determination of absolute configurations of optically active molecules—970(A)
Salkovitz, E. I. (see Kammer, E. W.)—1257(A)
Sampson, M. B. (see Miller, D. W.)—1253(A)
—— (see Rasmussen, V. K.)—181; 851
Samson, J. A. R. (see Vollrath, R. E.)—1793(A)
Sanders, T. M., Jr. (see Dousmanis, G. C.)—1735
Saphir, George (see Maenchen, George)—1802(A)
—— (see Wright, Robert W.)—1802(A)
Sattar, Abdul R., Ira L. Morgan, and Emmett L. Hudspeth. Excitation curve for $Be^9(n,\alpha)He^6$—960(A)
Sawatzky, A. and F. E. Jaumot, Jr. Diffusion of Zn in single crystals of Ag—1627
Saxon, David S. Optical model of the nucleus—1795(T)
—— Tensor scattering matrix for electromagnetic field—1771
—— (see Melkanoff, Michel A.)—1805(A)
—— (see Moe, Mildred M.)—1809(A)
Scalettar, Richard. Schrödinger-like equation for measurement process—1808(A)
Scarf, Frederick L. Spectrum and nonrelativistic limit of Bethe-Salpeter equation—912
Schafroth, M. R. Connection between superfluidity and superconductivity—502
—— Superconductivity of charged ideal Bose gas—463
—— **and J. M. Blatt.** Phenomenological equations for superconductors—1221(L)

—— (see Blatt, J. M.)—481
Schardt, A. W. (see Dropesky, B. J.)—954(A)
Schawlow, A. L. and C. H. Townes. Effect on x-ray fine structure of deviations from a Coulomb field near nucleus—1273
Schecter, Larry and R. E. Ellis. Elastic scattering of 48-Mev α particles—1805(A)
Schein, Marcel and D. M. Haskin. Production of hyperons and K-mesons in high energy π^- beam of Berkeley Bevatron—1263(A)
——, **D. M. Haskin, and Daniel Leenov.** Unstable $_1H^4$ fragment from capture of a Σ^- hyperon—1455
—— (see Cavanaugh, R. E.)—1263(A)
—— (see Haskin, D. M.)—1263(A)
—— (see Koshiba, M.)—1247(A)
—— (see Leenov, Daniel)—1263(A)
—— (see Williams, D. B.)—1547(L)
Schellenberg, L. (see Franzen, W.)—1239(A)
Schiffer, J. P. (see Gossett, C. R.)—203
Schillinger, E. J. (see Fields, T.)—964(A)
Schindler, A. I. (see Kammer, E. W.)—1257(A)
Schmid, L. C. (see Cork, J. M.)—188; 955(A); 1237(A)
—— (see Cork, J. M.)—955(A)
—— (see Cork, J. M.)—1237(A)
Schmidt, Fred H. (see Penning, J. R.)—954(A)
—— (see Yavin, Avivi I.)—171
Schmitt, H. W. (see Gibbons, J. H.)—167
Schneps, J., M. S. Swami, and W. F. Fry. Disintegration of hyperfragments—1263(A)
—— (see Fry, W. F.)—939(L); 950(L); 1448
Schoepfle, G. K. (see Silvidi, A. S.)—979(A)
Schrank, Glen E. (see Burkig, J. W.)—1805(A)
Schubauer, G. B. New light on boundary layer transition problem—958(T)
Schultz, Cramer and Ross D. F. Thompson. Polarization effects in electron-photon interactions—1809(A)
Schwartz, H. M. Theory of atomic perturbation in α decay—135
Schwed, P., H. Cooper, and R. W. Webeler. Thermoelectric power of AuCu in nonequilibrium states—978(A)
Schweinler, H. C. (see Stevens, D. K.)—1094
Scolman, T. T., K. S. Quisenberry and A. O. Nier. Preliminary mass doublet measurements with Minnesota 16-in. mass spectrometer—1245(A)
—— (see Quisenberry, K. S.)—1245(A)
Scott, M. B., A. O. Hanson, and D. W. Kerst. Electro- and photo-disintegration cross sections of Cu^{63}—209
Scott, Mary Jean and Ralph E. Segel. Polarization in p-α elastic scattering—1244(A)
Scott, William T. (see Goldberg, Jean Snover)—1013
Seeman, Nathan, Maurice M. Shapiro, and Bertram Stiller. Nonmesonic decay of a He hyperfragment—1480
—— (see Stiller, B.)—959(A)
Segel, Ralph E. (see Scott, Mary Jean)—1244(A)
Segrè, Emilio. Properties of antiproton—1801(T)
—— (see Chamberlain, Owen)—947(L)
Seliger, H. H. Transmission of positrons and electrons—1029
Sengupta, S. Nuclear moments in jj-coupling—939(L)
Serber, R. Theoretical background of antiproton—1801(T)
Serment, V. (see Mazari, M.)—972(A)
Seth, K. K. (see Pilcher, V. E.)—1248(A)
Severiens, J. C. and S. S. Hanna. Lifetimes of first excited states of Al^{28} and B^{10}—1254(A)
Shamos, Morris H. (see Fafarman, A.)—874
—— (see Reier, Melvin)—1302
Shapiro, Maurice M. (see Seeman, Nathan)—1480
—— (see Stiller, B.)—959(A)
Shatas, R. A. (see Pomerantz, M. A.)—964(A)
Shephard, W. D. and W. D. Walker. Production of heavy unstable particles in π^--p collisions at 1.0 Bev—1264(A)
—— (see Walker, W. D.)—1264(A)
Sherman, H. Properties of halogen-quenched Geiger counters—972(A)
Sherr, R., J. B. Gerhart, H. Horie, and W. F. Hornyak. Decay rates of C^{14}, N^{14*}, and O^{15}—945(L)
—— (see Hornyak, W. F.)—1409
Shockley, W. Recent developments in transistor physics—1802(T)
Shulman, R. G. Valence bond calculations of acceptor energies in Si and Ge—1260(A)
——, **J. M. Mays, and D. W. McCall.** Nuclear magnetic resonance in semiconductors. I. Exchange broadening in InSb and CaSb—692
——, **B. J. Wyluda, and H. J. Hrostowski.** Quadrupole broadening of NMR lines by reversible axial stress—1792(A)
—— (see Wyluda, B. J.)—1258(A)
Sidhu, S. S. Neutron diffraction studies of metal-H systems—971(T)
Sidles, P. H. Thermal diffusivity of U from room temperature to 1000°C—1256(A)
Siegel, K. M. and A. L. Maffett. Slow motions—968(A)
Siegel, Robert T. Polarization of 350-Mev neutrons elastically scattered from nuclei—437(L)
Silsbee, H. B. (see Felix, B. R.)—1808(A)
—— (see Passell, L.)—1808(A)
Silverstein, E. A. (see Chiba, Ren)—1253(A)
—— (see Herring, D. F.)—1239(A)
Silvidi, A. S., G. K. Schoepfle, K. L. Warren, F. L. Brooks, and M. Horowitz. Instrument for measurement of information stored in photographic film—979(A)
Simmons, B. E., K. F. Famularo, and G. D. Freier. Coulomb excitation of Sm—1265(A)
Simon, Albert. Diffusion of like particles across magnetic field—1557
Simpson, F. B. (see Simpson, O. D.)—1249(A)
Simpson, J. A. Primary radiation and origin of its changes with time—1247(T)
—— Studies of extra-terrestrial phenomena during International Geophysical Year—971(T)
Simpson, O. D., R. G. Fluharty, F. B. Simpson, and R. M. Brugger. Neutron resonance parameters and total cross sections in U^{235}—1249(A)
Sirlin, A. (see Behrends, R. E.)—1809(A)
Sivertsen, J. and C. Wert. Young's modulus of Au-Ni alloys—1256(A)
Skeen, C. H. and W. Z. Osborne. Strange cosmic-ray event—1797(A)
Skoglund, A. and A. Ore. Radiation-induced dielectric changes in phosphorescent material—1549(A)
Sladek, R. J. (see Keyes, R. W.)—1262(A)
Slater, J. C. Recent progress in energy-band theory—958(T)
Slätis, Hilding (see Hjalmar, Elis)—1542(L)
Slaughter, G. G. (see Fairbank, W. M.)—971(A)
Slepian, Joseph. Angular momentum and energy of ions in magneto-ionic isotope separator—1238(A)
—— Isotopic separation by magneto-ionic expansion—1233(A)
Slichter, Charles P. (see Pines, David)—1014
Smith, Bob H. (see Heusinkveld, Myron)—1804(A)
Smith, Frances M., Harry H. Heckman, and Walter H. Barkas. Masses of positive K-particles. I. Identification of K-particles and analysis of secondaries—1802(A)
—— (see Barkas, Walter H.)—1797(A)
—— (see Heckman, Harry H.)—1803(A)
Smith, Fred A. (see Gove, Norwood)—1236(A)

Smith, George F. Velocity analysis of thermionic emission from single-crystal W—1115
Smith, J. H. and M. Q. Barton. Photodisintegration of Li and He near 200 Mev—1265(A)
Smith, J. R. and E. H. Magleby. Energy dependence of η for U^{235} in region 0.04–1.0 ev—1266(A)
Smith, Lloyd (see Courant, E. D.)—1269(A)
Smith, R. W. Edge electroluminescence from ZnS single crystals—760(L)
Smith, W. G. (see Hollander, J. M.)—1238(A)
Snell, Arthur H. and Frances Pleasonton. Spectrometry of neutrino recoils of A^{37}—1396
Snow, G. A. (see Fry, W. F.)—939(L); 950(L); 1448
Snyder, A., W. Y. Chang, and I. C. Gupta. Double-plate cloud chamber study of V^0-particles. II. Mean decay times of θ^0- and Λ^0-particles—1264(A)
—— (see Gupta, I. C.)—1264(A)
Snyder, Hartland S. (see Goldberg, Jean Snover)—1013
—— (see Green, G. K.)—1268(A)
—— (see Raka, E. C.)—1269(A)
Snyder, S. (see Fagg, L. W.)—1299
Snyder, W. S. and J. Neufeld. Computation of vacancies created by heavy corpuscular radiation—969(A)
Soberman, R. K., A. Beiser, and S. A. Korff. Variation of position of cosmic-ray neutron intensity maximum with geomagnetic latitude—859
—— **and S. A. Korff.** High-altitude cosmic-ray neutron intensity variations—959(A)
Sonder, E. Effect of Sb impurity on self-diffusion of Ag—1662
Sonett, C. P. and K. R. MacKenzie. Relative stopping power of various metals for 200-Mev protons—734
Sorrels, J. D., R. B. Leighton, and C. D. Anderson. Associated production of Ξ^- with two θ^0 particles—1457
——, **G. H. Trilling, and R. B. Leighton.** Λ^0-fragment decay in cloud chamber—1484
Speck, D. R. (see Jenkins, F. A.)—973(A)
Spedding, F. H. (see Elliott, J. F.)—1595
Sperduto, A. and W. W. Buechner. (p,p') and (p,α) reactions of K—961(A)
—— (see Buechner, W. W.)—1387
Spicer, B. M. (γ,p) reaction in A^{40}—791
—— **and A. S. Penfold.** $C^{12}(\gamma,n)$ curve near threshold—1375
—— (see Penfold, A. S.)—1377
Spiegel, V., Jr., B. Waldman, and W. C. Miller. Absolute cross sections for Coulomb scattering of 1.00-, 1.75-, and 2.50-Mev electrons—1244(A)
—— (see Waldman, B.)—1244(A)
Spiro, J., J. G. Cottingham, E. D. Courant, and R. R. Kassner. Electron analog—initial setup—1269(A)
—— (see Courant, E. D.)—1269(A)
—— (see Raka, E. C.)—1269(A)
Squire, Charles F. Apparatus for new magnetism laboratory—966(A)
—— Magnetic properties of superconductors—971(T)
Squire, Robert K. and Burton J. Moyer. Neutral pion production in p-p collisions—1798(A)
Stanley, R. W. Standards of length and wavelength—977(T)
Starner, J. W. (see Duffield, R. B.)—1236(A)
—— (see Mize, J. P.)—1390
Statz, H., G. A. deMars, L. Davis, Jr., and A. Adams, Jr. Surface states on Si—1260(A)
Steffen, R. M. Measurement of magnetic moments of excited nuclear states—1258(T)
—— (see Noble, L. M.)—955(A)
Stehle, P. Particle transport, electric currents, and pressure balance in a magnetically immobilized plasma—443
Stein, Peter (see Odian, Allen)—1241(A)
Steinberger, J. and Harry B. Wolfe. Electrons from muon capture—1490
—— (see Chinowsky, W.)—1476
Stephens, Frank S., Jr., Frank Asaro, and I. Perlman. Radiations from 1− states in even-even nuclei—1543(L)
—— (see Asaro, Frank)—137; 1541(L)
—— (see Hoff, R. W.)—1403
Stern, Frank and Robert M. Talley. Impurity band in semiconductors with small effective mass—1638
Sternglass, E. J. and M. M. Wachtel. Transmission secondary electron multiplication for high resolution counting and imaging—1238(A)
—— (see Holliday, J. E.)—1238(A)
Sternheimer, R. M. Polarization of protons elastically scattered from nuclei—886
—— (see Block, M. M.)—324
Sterzer, Fred and Yardley Beers. Pure quadrupole spectra of CH_3I and CF_3I vapors—1174
Stevens, D. K., J. W. Cleland, J. H. Crawford, Jr., and H. C. Schweinler. Magnetic susceptibility of Ge—1084
Stevenson, M. Lynn (see Alvarez, Luis W.)—1264(A)
Stevenson, Peter C. (see Hicks, Harry G.)—1284
Stewart, A. B. and G. E. Owen. Oscillating glow discharge plasma—1235(A)
Stewart, A. T. (see Brockhouse, B. N.)—756(L)
Stewart, R. W. and W. N. English. Fluctuation of sound transmitted in ocean—969(A)
Stier, P. M. (see Barnett, C. F.)—1268(A)
Stiller, Bertram, N. Seeman, and M. M. Shapiro. Nonmesonic decay of He hyperfragment—959(A)
—— (see Seeman, Nathan)—1480
Stine, Howard A. and Warren Winovich. Application of light-scattering theory to measurement of density fluctuations in turbulent fluids—968(A)
St. John, Robert (see Zei, Dino)—1232(A)
Stork, D. H. Properties of positive K-mesons—1806(T)
—— (see Birge, R. W.)—430(L)
Strandberg, M. W. P. and M. Peter. Precision of microwave spectrographs—963(A)
Streib, J. F. Elastic scattering of electrons by Li^6 and Li^7—1797(A)
Strominger, D. and J. O. Rasmussen. 4.1×10^{-8} second metastable state in Pa^{233}—844
Studier, M. H. (see Fields, P. R.)—172
Stump, R. Angular correlation of annihilation radiation in superconducting Pb—1256(A)
Sugawara, Tadashi. Nuclear spin-lattice relaxation in solid H_2—759(L)
Suhl, H. (see Anderson, P. W.)—1788(L)
Summers-Gill, R. G. Differential cross sections for scattering of charged particles by Be—1795(A)
Sun, C. R. and Byron T. Wright. Double-channel magnetic β-ray spectrometer for short-lived activities—1793(A)
Swami, M. S. (see Fry, W. F.)—939(L); 950(L); 1448
—— (see Schneps, J.)—1263(A)
Swann, C. P. and F. R. Metzger. Production of Y^{89m}, Ba^{137m}, and Hg^{199m} by inelastic neutron scattering—1329
Swenson, C. A. Properties of In and Tl at low temperatures—1607
Swiatecki, W. J. Systematics of fission asymmetry—936(L)
—— Systematics of spontaneous fission half-lives—937(L)
Symon, Keith R. General theory of orbits in FFAG accelerators—1247(A)
Szebehely, V. G. (see Bledsoe, M. D.)—968(A)

Tai, Yuin-Kwei (see Millburn, George P.)—1793(A)
Takata, A. N. (see Meister, A. G.)—1267(A)
Takeda, Gyo. Strong pion-pion interaction model applied to pion-nucleon scattering in 1-Bev region—440(L)

Talbot, L. (see Bowyer, J. M.)—968(A)
Talley, Robert M. (see Stern, Frank)—1638
Tannenwald, P. E. Ferromagnetic resonance in Mn ferrite single crystals—1713
Tatro, C. A. and T. R. Palfrey, Jr. High-energy photoproton emission at 175°—1265(A)
Tauber, G. E. and T. Y. Wu. Self-consistent treatment of nuclear independent-particle model—1240(A)
—— (see Wu, Ta-You)—1767
Tauer, K. J. and R. J. Weiss. Magnetic second order transitions—1223(L)
Taylor, H. L., O. Lönsjö, and T. W. Bonner. Nonelastic scattering cross sections for fast neutrons—174
Taylor, Julius H. Pressure dependence of resistivity, Hall coefficient, and energy gap for InAs—1593
Taylor, S. (see Harris, G.)—932(L)
Taylor, T. I. (see Gould, F. T.)—1248(A)
Telegdi, V. L. (see Meyer-Schützmeister, L.)—961(A)
—— (see Oxley, C. L.)—435(L); 962(A)
Teller, E. Velocity dependence of nuclear potential—1795(T)
Temmer, G. M. and N. P. Heydenburg. Coulomb excitation of Cu, Zn, As, Se, and Ru—961(A)
—— (see Heydenburg, N. P.)—150
Teng, L. C. Billion-volt injection into high-energy accelerators—1247(T)
Terwilliger, K. M., L. W. Jones, F. T. Cole, D. W. Kerst, and R. O. Haxby. Small model FFAG betatron. I. General description—1246(A)
—— (see Jones, L. W.)—1247(A)
Thaler, R. M. (see Biedenharn, L. C.)—376
—— (see Goldstein, M.)—436(L)
Thomas, G. E. (see Bollinger, L. M.)—126
Thomas, R. G. Collision matrix for (n,d) and (p,d) reactions—25
Thompson, Ross D. F. (see Schultz, Cramer)—1809(A)
Thompson, Stanley G. (see Hjalmar, Elis)—1542(L)
—— (see Hoff, R. W.)—1403
Thomson, Robb (see Huntington, H. B.)—1117
Thorndike, A. M. Nucleon-nucleon interactions—1791(T)
Thornton, Robert L. (see Pyle, Robert V.)—1804(A)
Thornton, W. A. Electroluminescence in ZnS—1268(A)
Tice, G. (see Benedict, F. D.)—1545(L)
Ticho, Harold K. (see Barkas, Walter H.)—1797(A)
Tinkham, M. Magnetic resonance demonstration of charge transfer in Fe group fluorides—1792(A)
Tomboulian, D. H. Experimental study of electromagnetic spectrum emitted by high-energy electrons accelerated in synchrotron—977(T)
—— (see Bedo, D. E.)—1257(A)
Tomlinson, E. P. and R. A. Naumann. Decay of Pt^{191}—955(A)
Tomnovec, F. M. and C. S. Cook. 5.3-Mev energy level in Mg^{24} following decay of Na^{24}—1254(A)
Toppel, B. J., D. H. Wilkinson, and D. E. Alburger. Inelastic scattering of protons from F^{19}—1254(A)
—— (see Alburger, D. E.)—1357
Townes, C. H. (see Autler, S. H.)—703
—— (see Dousmanis, G. C.)—1735
—— (see Schawlow, A. L.)—1273
Tredgold, R. H. (see Ayres, R. U.)—1257(A)
—— (see Evans, J. S.)—1250(A)
Treiman, S. B. and H. W. Wyld, Jr. Angular correlation effects in V-particle decay—879
Trilling, G. H. Recent studies of V particle production—967(T)
—— **and R. B. Leighton.** Cloud-chamber investigation of charged V particles—1468
—— (see Sorrels, J. D.)—1484
Trolan, J. K., J. P. Barbour, E. E. Martin, and W. P. Dyke. Electron emission from lattice step on clean W—1646
Tseng, T. P. Vapor pressure of solution of He^3 in liquid He^4—977(T)
Tubbs, Eldred F. (see Kerr, Donald E.)—1231(A)
Tweet, A. G. Precipitation of Cu in plastically deformed Ge—1260(A)
Tyler, W. W. and H. H. Woodbury. Scattering of carriers from doubly charged impurity sites in Ge—1259(A)
—— (See Woodbury, H. H.)—659; 1259(A)

Urban, John S. and John J. McClure. Analysis of nuclear emulsion tracks by scattering measurements—1797(A)
Utiyama, Ryoyu. A theory of new particles—248

Vallarta, Manuel Sandoval. Origin of knee of latitude effect of cosmic rays—971(T)
Vand, V. and R. Pepinsky. Developments in statistical approach to x-ray crystal analysis—970(A)
Van Doorn, C. Z. and Y. Haven. Dichroism of F and M absorption bands in KCl—753(L)
Van Dyke, Karl S. Vibrations of quartz plate—1550(A)
Van Lieshout, R., D. H. Greenberg, L. A. Ch. Koerts, and C. S. Wu. Decay of Cr^{49}—223
Van Tuyl, Harold H. (see Lefevre, Harlan W.)—1374
VanZandt, T. E. Derivation from Boltzmann's equation of similarity laws for ionized gases—1235(A)
Vartanian, P. H. (see Ayres, W. P.)—1791(A)
Vegors, Stanley H., Jr., and Peter Axel. γ-ray induced isomers with half-lives between 10^{-6} and 10^{-1} sec—1238(A)
Verlet, L. (see Lane, A. M.)—956(A)
Villars, D. S. (see Rekers, R. G.)—963(A)
Violet, Charles E., F. C. Gilbert, and R. Stephen White. Negative K-particle interactions in nuclear emulsion. I—1803(A)
—— (see Gilbert, F. C.)—1803(A)
—— (see White, R. Stephen)—1803(A)
Visscher, W. M. (see Ferrell, R. A.)—1796(A)
Vivo, Juana L. (see Wertz, John E.)—1792(A); 1810(A)
Vogt, Erich. Nucleon-nucleus interaction with polarization—957(A)
Voigt, A. F. (see Day, M. C., Jr.)—796
Vollrath, R. E. and J. A. R. Samson. Obtaining high temperatures for nuclear fusion—1793(A)
Volman, David H. Excited states of oxygen from energy transfer and light absorption—963(A)
von Engel, A. Past and present ideas about cold arcs—1232(T)

Wachtel, M. M. (see Sternglass, E. J.)—1238(A)
Wadey, W. G. Laboratory vacuum fittings and standardization of vacuum fittings—1549(A)
Wagner, F., Jr. (see Magnusson, L. B.)—1237(A)
Wagoner, G. (see Dresselhaus, G.)—1218(L)
Waldman, B., V. Spiegel, Jr., and W. C. Miller. Plural scattering of fast electrons—1244(A)
—— (see Connors, D. R.)—1237(A)
—— (see Dempsey, D. F.)—1240(A)
—— (see Spiegel, V., Jr.)—1244(A)
Walker, W. C. and G. L. Weissler. Light absorption and photoionization in NO and N_2O—1231(A)
Walker, W. D. and W. D. Shephard. π^--p collisions at 1.0 Bev—1264(A)
—— (see Shephard, W. D.)—1264(A)
Wallace, P. R. Annihilation of positrons in condensed materials—738

Wallace, Roger W., Malvern H. L. Jester, and John M. Brabant. Total-absorption spectrometer measurements of γ rays emitted from targets bombarded with 6.2-Bev protons—962(A)
Wallenmeyer, W. A. Meson production in n-p collisions by Cosmotron-produced neutrons with energies up to 1.5 Bev—1255(A)
Wallis, M. C. (see Herman, Robert)—1267(A)
Wallis, R. F. (see Herman, Robert)—1267(A)
Walsh, J. M. Dynamic compressions for some twenty-five solids and liquids at explosively attainable pressures—954(T)
Walton, R. B. (see Darden, S. E.)—1315
Wannier, Gregory H. Possibility of a Zener effect—1227(L)
—— Threshold law for multiple ionization—1180
Warburton, E. K. (see McGruer, J. N.)—235
Ward, J. K. and C. M. Loyd. Intensity of vibronic bands in 3000–5000 A absorption system of ClO_2—963(A)
Warren, K. L. (see Silvidi, A. A.)—979(A)
Wattenberg, Albert (see Feld, B. T.)—1539(L)
—— (see Odian, Allen)—1241(A)
—— (see Ritson, D. M.)—1263(A)
Waymouth, John F. (see Bitter, Francis)—1230(A)
Webb, Francis H. (see Chupp, Warren W.)—959(A)
Webber, William R. and Frank B. McDonald. Intensities of low-Z components of primary cosmic radiation at $\lambda=41°$ using Čerenkov detector—1460
Webeler, R. W. (see Schwed, P.)—978(A)
Wegner, H. E. (see Bloom, S. D.)—1248(A)
—— (see Eisberg, R. M.)—961(A); 1309
—— (see Igo, G.)—1244(A); 1796(A)
Weinman, J. A., J. R. Cameron, and R. G. Herb. Negative H ion source—1239(A)
Weinstein, Roy (see Allen, Odian)—1241(A)
Weinstock, E. V. and J. Halpern. Bremsstrahlung spectrum from internal target of 22-Mev betatron—1293
Weiss, R. J. (see Tauer, K. J.)—1223(L)
Weissler, G. L. and L. Z. Maudlin. Absorption of vacuum ultraviolet radiation by thin plastic films—1800(A)
—— (see Walker, W. C.)—1231(A)
Welber, B. and B. M. Rosenbaum. State of order of Cd-poor $MgCd_x$—978(A)
Welker, Joan P. and M. L. Perlman. K-capture-positron ratios for first forbidden transitions of Rb^{86} and relative probability of L- to K-electron capture—74
—— (see Perlman, M. L.)—81
Weneser, J. (see Church, E. L.)—943(L); 1241(A)
Wenzel, W. A. (see Cork, Bruce)—962(A)
Wert, C. (see Sivertsen, J.)—1256(A)
Wertz, John E. and Juana L. Vivo. Electron spin resonance of defect centers in Mg oxide—1792(A)
——, **Juana L. Vivo, and Boris Musulin.** Electron spin resonance of impurities in Mg oxide—1810(A)
Westendorp, W. F. Recent cathode-ray developmental work—977(T)
Wexler, S. (see Goodman, L. S.)—1245(A); 1796(A)
Whaling, Ward (see Pixley, R. E.)—1805(A)
Wheatley, G. H. (see Hrostowski, H. J.)—1672
Wheelon, Albert D. Single-meson production in nucleon-nuclei collisions—974(A)
White, R. Stephen, F. C. Gilbert, and Charles E. Violet. Negative K-particle interactions in nuclear emulsion. III—1803(A)
—— (see Gilbert, F. C.)—1803(A)
—— (see Violet, Charles E.)—1803(A)
Whitehead, M. N. (see Birge, R. W.)—430(L)
Whitsett, C. R. and G. C. Danielson. Electrical properties of semiconductors Mg_2Si and Mg_2Ge—1261(A)
Wiegand, Clyde. Mass determination of antiproton—1801(T)
—— (see Chamberlain, Owen)—947(L)
Wiewall, Miguel, Jr. Observations of ionospheric drifts over Puerto Rico—968(A)
Wight, H. M. Ultrasonic investigation of vibrational energy transitions in N_2O induced by molecular collisions with H_2O and D_2O—977(T)
Wilcox, L. (see Drummond, J. E.)—1233(A)
Wilkinson, D. H. Reactions $C^{12}(d,n)N^{13}$ ground state and $C^{13}(d,t)C^{12}$ up to $E_d=20$ Mev—32
—— (see Toppel, B. J.)—1254(A)
Wilkinson, Roger G. (see Pruett, Charles H.)—1237(A)
Willard, H. B. (see Bair, J. K.)—21
Williams, D. B., D. M. Haskin, M. Koshiba, and Marcel Schein. Capture of K^--meson with emission of high-energy electron as only visible prong—1547(L)
—— (see Haskin, D. M.)—1263(A)
Williams, H. Bartel (see Hatch, Albert J.)—1228(A)
Williams, Ross E. (see Pevsner, Aihud)—1419
Williamson, R. M. and K. W. Jones. $Li^7(p,p'\gamma)$ and $Li^7(p,\gamma)$ reactions—960(A)
Wilson, R. R. Initial performance of Cornell strong-focusing synchrotron—962(T)
Winans, J. G. (see Zei, Dino)—1232(A)
Windham, P. M. (see Gossett, C. R.)—203
Winhold, E. J. (see Burkhardt, J. L.)—199
Winick, H. (see Sachs, A. M.)—1255(A)
Winovich, Warren (see Stine, Howard A.)—968(A)
Winter, Rolf G. Double K capture and single K capture with positron emission—142
Witte, R. S. (see Martz, D. E.)—1808(A)
Wolfe, Harry B. (see Steinberger, J.)—1490
Wolff, G. A., R. A. Herbert, and J. D. Broder. Electroluminescence of GaP—1144
Wolicki, E. A., L. W. Fagg, and E. H. Geer. Coulomb excitation of energy levels in Br and Re—1265(A)
—— (see Fagg, L. W.)—1299
—— (see Geer, E. H.)—215
Wollan, E. O. and W. C. Koehler. Neutron diffraction study of magnetic properties of series of perovskite type compounds $[(1-x)La, xCa]MnO_x$—545
Wood, G. T. and P. S. Jastram. Directional and polarization-direction correlations in Pb^{208} γ-γ cascades—1237(A)
Woodbury, H. H. Electronic effects of Ge containing double acceptor impurities—1794(T)
—— **and W. W. Tyler.** Properties of Ge doped with Mn—659
—— **and W. W. Tyler.** Properties of Zn-doped Ge—1259(A)
—— (see Tyler, W. W.)—1259(A)
Woods, R. D. (see Callaway, J.)—956(A)
Wooten, B. A. (see Sachs, A. M.)—1255(A)
Wright, Byron T. (see Heusinkveld, Myron)—1804(A)
—— (see Royden, Herbert N.)—1805(A)
—— (see Sun, C. R.)—1793(A)
Wright, G. T. Fluorescence excitation spectrum of anthracene—587
—— Scintillation response of anthracene crystals to short-range electrons—588
Wright, Robert W., George Saphir, Wilson M. Powell, George Maenchen, and William B. Fowler. p-p interactions at 5.3 Bev—1802(A)
—— (see Maenchen, George)—1802(A)
Wu, Chien Shiung (see Benczer, N.)—955(A)
—— (see Lindqvist, Torsten)—145
—— (see Van Lieshout, R.)—223
Wu, Ta-You. Electron affinity of B, C, N, and O atoms—1195

—— **and G. E. Tauber.** "Contact interaction" in relativistic energy of two-electron atoms—1767
—— (see Tauber, G. E.)—1240(A)
Wyld, H. W. (see Arnold, W. H., Jr.)—1545(L); 1804(A)
—— (see Treiman, S. B.)—879
Wyluda, B. J. and R. G. Shulman. Cu in Ge; Recombination center and trapping center—1258(A)
—— (see Shulman, R. G.)—1792(A)

Yager, W. A. (see Fletcher, R. C.)—747(L)
—— (see Galt, J. K.)—748(L)
Yamagata, Taketora and Megumu Yoshimine. Monte Carlo calculation on Čerenkov counters—1246(A)
Yavin, Avivi I. and Fred H. Schmidt. Precision energy measurements of γ rays following decay of Bi^{207}—171
Yennie, D. R. Interactions of electrons and nucleons—1795(T)
Yergin, Paul F. and Burton P. Fabricand. $Mg(\gamma,n)$ cross section—1249(A)
—— **and Burton P. Fabricand.** $Sr^{88, 87, 86}$, Y^{89}, $Zr^{92}(\gamma,n)$ cross sections—1269(A)
—— (see Novick, Robert)—1153
Yilmaz, Huseyin. Wave functions and transition probabilities for light atoms—1148
Yodh, G. B. Pion production by inelastic scattering of electrons in H—1791(T)
Yoshimine, Megumu (see Yamagata, Taketora)—1246(A)
Yoshinaga, Hiroshi. Reflectivity of several crystals in far infrared region between 20 and 200 microns—753(L)
Ypsilantis, Thomas (see Chamberlain, Owen)—947(L)
Yuan, Luke C. L. (see Lindenbaum, S. J.)—306

Zachariasen, F. Photoproduction of π-meson pairs in H—1809(A)
Zandy, Hassan F. M_{IV} and M_V absorption lines and edges of $_{64}$Gd, $_{66}$Dy and $_{70}$Yb—1549(A)
Zei, Dino, Robert St. John, and J. G. Winans. Properties of arc cathode spots in magnetic fields—1232(A)
Zemach, A. C. (see Moellering, W. M.)—441
Zimmerman, R. L. (see Palevsky, H.)—1266(A)
Ziomek, Joseph S. (see Piotrowski, Edward A.)—1267(A)
Zollweg, Robert J. X-ray lattice constant of BaO—671
Zucker, A. (see Reynolds, H. L.)—226

Analytic Subject Index to Volume 100

References with (A) are to abstracts of papers presented at meetings of the American Physical Society; references with (L) are to Letters to the Editor; references with (E) are to Errata. Items are listed under the following categories:

Acoustics
Astrophysics
Atomic and Molecular Beams
Atomic Mass and Abundance
Atomic Structure and Spectra
Biophysics
Chemical Effects and Properties
Constants, Standards, Units
Cosmic Radiation
Crystalline State
Dielectrics and Dielectric Properties
Diffraction
Diffusion
Elasticity and Plasticity
Electrical Conductivity and Resistance
Electrical Discharges
Electrical Properties
Electromagnetic Theory and Electrodynamics
Electrons and Positrons
Elementary Particle Interactions
Errata
Field Theory
Films, Properties
Fluid Dynamics
Gamma Rays
Gases
Geophysics
Helium, Liquid
Imperfections in Solids
Ionization
Ions
Ions and Electrons, Mobility
Liquids
Luminescence
Magnetic Properties
Magnetic Resonance
Mathematical Methods
Mechanics
Mesons and Hyperons
Methods and Instruments
Microwaves
Miscellaneous
Molecular Aggregates
Molecular Structure and Spectra
Neutrino
Noise
Nuclear Fission
Nuclear Moments and Spin
Nuclear Photoeffects
Nuclear Reactions, General
Nuclear Reactions Induced by α Particles and He^4
Nuclear Reactions Induced by Deuterons and Tritons
Nuclear Reactions Induced by Mesons
Nuclear Reactions Induced by Neutrons
Nuclear Reactions Induced by Protons
Nuclear Spectra
Nuclear Structure Theory
Optical Properties
Proceedings of the American Physical Society
Quantum Electrodynamics
Quantum Mechanics
Radiation
Radioactivity
Range and Energy Loss of Particles
Relativity and Gravitation
Scattering, General
Scattering of α Particles
Scattering of Deuterons and Tritons
Scattering of Electrons and Positrons
Scattering of Mesons
Scattering of Neutrons
Scattering of Protons
Semiconductors
Spectra, General
Statistical Mechanics and Thermodynamics
Superconductivity
Thermal Properties
X-Rays

Absorption of Radiation (see **Radiation**)

Acoustics

Fluctuation of sound transmitted in ocean, R. W. Stewart and W. N. English—969(A)

Relative absorption of 10-Mc/sec longitudinal sound waves in a superconducting polycrystalline Sn rod, L. Mackinnon—655

Ultrasonic attenuation in superconducting and normal-conducting Sn at low temperature, H. E. Bömmel—758(L)

Adsorption (see **Gases**)

Aerodynamics (see **Fluid Dynamics**)

Afterglow (see **Electrical Discharges**)

Alloys (see **Crystalline State**)

Annihilation (see **Electrons and Positrons**)

Antiferroelectric Phenomena (see **Dielectrics and Dielectric Properties**)

Antiferromagnetism (see **Magnetic Properties**)

Antiprotons (see **Elementary Particle Interactions**)

Arcs (see **Electrical Discharges**)

Astrophysics

Hypothesis for origin of magnetic fields and angular rotations of stars and planets, Winston H. Bostick—1007

Interplanetary magnetic fields and cosmic rays, Leverett Davis, Jr.—958(A); 1440

Atmosphere (see **Geophysics**)

Atomic and Molecular Beams

Electron loss cross section for fast He atoms, C. F. Barnett and P. M. Stier—1268(A)

Low-energy scattering of electrons by atoms, J. Hammer, H. Malamud, and B. Bederson—1229(A)

Nuclear spin and magnetic moment of 50-day In^{114m}, L. S. Goodman and S. Wexler—1245(A)

Nuclear spin and magnetic moment of 54-min In^{116m}, L. S. Goodman and S. Wexler—1796(A)

Redetermination of hyperfine splittings of H and D in ground state, P. Kusch—1188

Resonance transitions induced by perturbations at two or more different frequencies, Norman F. Ramsey—1191

Theory of multiple-quantum transitions, M. N. Hack—975(A)

Atomic Mass and Abundance

Atomic masses of H^1, D^2, C^{12}, and S^{32}, K. S. Quisenberry, T. T. Scolman, and A. O. Nier—1245(A)

Mass doublet measurements with Minnesota 16-in. mass spectrometer, T. T. Scolman, K. S. Quisenberry, and A. O. Nier—1245(A)

Atomic Structure and Spectra

Effect on x-ray fine structure of deviations from a Coulomb field near the nucleus, A. L. Schawlow and C. H. Townes—1273

Electron affinity of B, C, N, and O atoms, Ta-You Wu—1195

Fine structure of singly ionized He, Robert Novick, Edgar Lipworth, and Paul F. Yergin—1153

Hartree-Fock wave functions for Mn^{+4}, W. W. Piper and J. S. Prener—1250(A)

Isotope shift in spectra of Hg^{198}-Hg^{202}, Fred McClung and John R. Holmes—1792(A)

Lifetime of imprisoned resonance radiation in Ne, A. V. Phelps—1230(A)

Mesonic x-rays from capture of cosmic-ray μ mesons in chemical compound, A. Fafarman and M. H. Shamos—874

Nuclear moments of Gd from optical hfs, F. A. Jenkins and D. R. Speck—973(A)

Nuclear moments of Mo^{95}, Mo^{97}, Zr^{93}, I^{127}, Sb^{121}, and Sb^{123}, Kiyoshi Murakawa—1369

Redetermination of hyperfine splittings of H and D in ground state, P. Kusch—1188
Resonance irradiation of Hg vapor in nitrogen, J. A. Berberet and K. C. Clark—506
Spatial extension of proton magnetic moment from hfs of hydrogen, W. M. Moellering, A. C. Zemach, A. Klein, and F. E. Low—441(L)
Tc K x-ray spectrum, George L. Rogosa and William F. Peed—1763
Theory of atomic perturbation in α decay, H. M. Schwartz—135
Wave functions and transition probabilities for light atoms, Huseyin Yilmaz—1148
Auger Effect (see **Atomic Structure and Spectra; X-Rays**)
Aurora (see **Astrophysics; Geophysics**)

Barkhausen Effect (see **Magnetic Properties**)
Biophysics
Present limitations of x-ray analyses of organic natural products, O. Cano-Corona and R. Pepinsky—970(A)
Boson Theory (see **Field Theory**)
Bremsstrahlung (see **Radiation**)
Broadening of Spectral Lines (see **Atomic Structure and Spectra; Molecular Structure and Spectra; Spectra, General**)

Capture Cross Sections (see **Electrons and Positrons; Nuclear Reactions; Radiation**)
Čerenkov Effect (see **Radiation**)
Chemical Effects and Properties
Chemical Reactions (see **Chemical Effects and Properties**)
Chemiluminescence (see **Luminescence**)
Cold Emission (see **Electrical Properties**)
Colloids (see **Chemical Effects and Properties; Molecular Aggregates**)
Compton Effect (see **Radiation**)
Conductivity, Electrical (see **Electrical Conductivity and Resistance**)
Conductivity, Thermal (see **Thermal Properties**)
Constants, Standards, Units
Improved value of velocity of light derived from band spectrum method, D. H. Rank, H. E. Bennett, and J. M. Bennett—993
Cosmic Radiation (see also **Mesons and Hyperons**)
Absence of meteorological effects on world-wide sunspot variation in cosmic-ray ionization, Scott E. Forbush—958(A)
Čerenkov counter for high-energy cosmic rays, D. C. Moore and R. J. Hanson—972(A)
Change with time of low-energy part of cosmic-ray spectrum, H. V. Neher—959(A)
Cloud-chamber investigation of charged V particles, G. H. Trilling and R. B. Leighton—1468
Cloud-chamber observations of μ-meson-induced electron showers, C. A. Rouse—1797(A)
Cosmic-ray electrons near sea level and at mountain altitudes, Paul B. Barker—860
East-west asymmetry of positive and negative mesons at geomagnetic equator, F. B. Harris and I. Escobar—255
High-altitude cosmic-ray neutron intensity variations, R. K. Soberman and S. A. Korff—959(A)
High-energy electromagnetic phenomena in cosmic radiation, M. Koshiba and M. F. Kaplon—327
Intensities of low-Z components of primary cosmic radiation at λ=41° using Čerenkov detector, William R. Webber and Frank B. McDonald—1460
Interplanetary magnetic fields and cosmic rays, Leverett Davis, Jr.—958(A); 1440
Strange cosmic-ray event, C. H. Skeen and W. Z. Osborne—1797(A)
Time variation of primary heavy nuclei flux in cosmic radiation, M. Koshiba and Marcel Schein—1247(A)
Variation of position of cosmic-ray neutron intensity maximum with geomagnetic latitude, R. K. Soberman, A. Beiser, and S. A. Korff—859
Cosmology (see **Astrophysics; Relativity and Gravitation**)
Coulomb Excitation (see **Nuclear Reactions; Nuclear Spectra**)
Critical Potentials (see **Atomic Structure and Spectra; Molecular Structure and Spectra**)
Cross Section (see **Electrons and Positrons; Nuclear Reactions; Radiation; Scattering**)
Crystal Counters (see **Methods and Instruments**)
Crystalline State (see also **Electrical Properties; Imperfections in Solids; Magnetic Properties; Semiconductors; etc.**)
Absorption cross section for light in perfect solids, D. L. Dexter—964(A)
Annihilation of positrons in condensed materials, P. R. Wallace—738
Arrangement of atoms in wollastonite-type crystals, M. J. Buerger—970(A)
Brillouin zone studies. V. Thermoelectric power of dilute Mg alloys, E. W. Kammer, E. I. Salkovitz, and A. I. Schindler—1257(A)
Coulomb enhancement of positron annihilation in metals, Richard A. Ferrell—973(A)
Crystal engineering: New concept in crystallography, R. Pepinsky—971(A)
Crystal structure of solid rare gases, R. U. Ayres and R. H. Tredgold—1257(A)
Cyclotron absorption in Bi, R. N. Dexter and Benjamin Lax—1216(L)
Detection of vacancies created by x-rays in NaCl, H. W. Etzel—1643
Developments in statistical approach to x-ray crystal analysis, V. Vand and R. Pepinsky—970(A)
Dichroism of F and M absorption bands in KCl, C. Z. van Doorn and Y. Haven—753(L)
Direct x-ray determination of absolute configurations of optically active molecules, Y. Saito, Y. Okaya, and R. Pepinsky—970(A)
Dislocation energies in NaCl, H. B. Huntington, J. E. Dickey, and Robb Thomson—1117
Effect of defects on lattice vibrations, Elliott W. Montroll and Renfrey B. Potts—525
Effect of impurities on lattice vibrations, Elliott W. Montroll and R. B. Potts—969(A)
Electron correlation, Joseph E. Mayer—1579
Energy band calculations in f.c.c. Th, G. W. Lehman—1791(A)
Energy levels of crystal modified by alloying or by pressure, R. H. Parmenter—573
Exciton absorption in cuprous oxide, J. H. Apfel and L. N. Hadley—1689
Field emission microscopy of allotropic transformation: α-β titanium, Ernest G. Brock—1619
Frequencies and relative intensities of R_1 and R_2 bands in KCl, Robert Herman, M. C. Wallis, and R. F. Wallis—1267(A)
Interpretation of optical properties of metal surfaces, S. Roberts—1667
Interpretation of stored energy of irradiated graphite in terms of elastic energy associated with microscopic strain, Alfred E. Austin and Ralph J. Harrison—1225(L)

Crystalline State (Continued)
Irradiation of graphite at liquid He temperatures, Stanley B. Austerman and John E. Hove—1214(L)
Kinetics of processes distributed in activation energy, William Primak—1677
Lattice constants of graphite at low temperatures, Y. Baskin and L. Meyer—544
Neutron diffraction study of magnetic properties of series of perovskite-type compounds $[(1-x)\mathrm{La}, x\mathrm{Ca}]\mathrm{MnO}_3$, E. O. Wollan and W. C. Koehler—545
Neutron diffraction study of VD_x, B. W. Roberts—1257(A)
New method for determination of activation energies, J. A. Brinkman—1807(A)
Nuclear magnetic resonance studies of imperfect ionic crystals, F. Reif—1597
Phase transformations in microstructure of explosively loaded Fe and steel, E, W. LaRocca—1800(A)
Possibility of Zener effect, Gregory H. Wannier—1227(L)
Precipitation of Cu in Ge, R. A. Logan—615
Present limitations of x-ray analyses of organic natural products, O. Cano-Corona and R. Pepinsky—970(A)
Radiation-induced amorphism in diamond, Paul W. Levy and Otto F. Kammerer—1787(L)
Scattering of neutrons by phonons in Al single crystal, B. N. Brockhouse and A. T. Stewart—756(L)
Small-oscillation theory of interaction of particle and scalar field, E. P. Gross—1571
Spin-orbit coupling effects in Zn blende structures, G. Dresselhaus—580
State of order of Cd-poor $MgCd_x$, B. Welber and B. M. Rosenbaum—978(A)
Stored-energy release in graphite irradiated at low temperatures, S. B. Austerman—1807(A)
Theory of role of covalence in perovskite-type manganites $[\mathrm{La}, M(\mathrm{II})]\mathrm{MnO}_3$, John B. Goodenough—564
Tracer studies on radiation-damaged graphite, G. L. Montet, A. F. Kurs, and G. R. Hennig—1261(A)
Use of field emission microscope for investigating surface conditions on an alloy, L. A. D'Asaro—1258(A)
X-ray lattice constant of BaO, Robert J. Zollweg—671
Young's modulus of Au-Ni alloys, J. Sivertsen and C. Wert—1256(A)

Diamagnetism (see **Magnetic Properties**)
Dielectrics and Dielectric Properties
Radiation-induced dielectric changes in phosphorescent material, A. Skoglund and A. Ore—1549(A)
Single crystal neutron analysis of tetragonal $BaTiO_3$, B. C. Frazer, H. R. Danner, and R. Pepinsky—745(L)
Vibrations of quartz plate, Karl S. Van Dyke—1550(A)
Diffraction (see also **Scattering**)
Arrangement of atoms in wollastonite-type crystals, M. J. Buerger—970(A)
Atomic distribution in liquid He by neutron diffraction, D. G. Hurst and D. G. Henshaw—994
Crystal engineering: New concept in crystallography, R. Pepinsky—971(A)
Developments in statistical approach to x-ray crystal analysis, V. Vand and R. Pepinsky—970(A)
Direct x-ray determination of absolute configurations of optically active molecules, Y. Saito, Y. Okaya, and R. Pepinsky—970(A)
Interatomic correlations in liquid He^4, Louis Goldstein—981
Neutron diffraction study of magnetic properties of series of perovskite-type compounds $[(1-x)\mathrm{La}, x\mathrm{Ca}]\mathrm{MnO}_3$, E. O. Wollan and W. C. Koehler—545
Neutron diffraction study of VD_x, B. W. Roberts—1257(A)
Present limitations of x-ray analyses of organic natural products, O. Cano-Corona and R. Pepinsky—970(A)
Single-crystal neutron analysis of tetragonal $BaTiO_3$, B. C. Frazer, H. R. Danner, and R. Pepinsky—745(L)
Diffusion
Diffusion of like particles across magnetic field, Albert Simon—1557
Diffusion of Zn in single crystals of Ag, A. Sawatzky and F. E. Jaumot, Jr.—1627
Effect of Sb impurity on self-diffusion of Ag, E. Sonder—1662
Ion diffusion in a uniform magnetic field, K. S. W. Champion and A. B. de Saint Maurice—1233(A)
Thermal diffusivity of U from room temperature to 1000°C, P. H. Sidles—1256(A)
Discharge of Electricity in Gases (see **Electrical Discharges**)
Disintegration and Excitation of Nucleus (see **Nuclear Reactions**)
Dynamics (see **Mechanics**)

Elasticity and Plasticity
Influence of lattice defects on Young's modulus of Cu, H. Dieckamp—1807(A)
Interpretation of stored energy of irradiated graphite in terms of elastic energy associated with microscopic strain, Alfred E. Austin and Ralph J. Harrison—1225(L)
Mechanical properties of Si, Ge, and ZnO whiskers, G. L. Pearson, W. T. Read, Jr., and W. L. Feldmann—1251(A)
Mechanical strength of thin films of metals, J. W. Beams, J. B. Breazeale, and W. L. Bart—1657
Properties of In and Tl at low temperatures, C. A. Swenson—1607
Time dependence of mechanical breakdown phenomena, Bernard D. Coleman—1257(A)
Young's modulus of Au-Ni alloys, J. Sivertsen and C. Wert—1256(A)
Electrical Breakdown (see **Dielectrics and Dielectric Properties; Electrical Discharges**)
Electrical Conductivity and Resistance (see also **Semiconductors; Superconductors**)
Determination of surface resistivity of metal surfaces by Z measurement, A. R. Quinton and R. Beringer—1549(A)
Effect of low-temperature electron irradiation on electrical resistivity of Cu, C. J. Meechan—1807(A)
Effect of pressure on electrical resistance of metals at liquid He temperatures, J. Hatton—681
Electrical and optical properties of intermetallic compounds. IV. Mg_2Sn, R. F. Blunt, H. P. R. Frederikse, and W. R. Hosler—663
Electrical conduction in Plexiglas, Raymond J. Munick—1256(A)
Electrical properties of Mg_2Sn at low temperatures, W. R. Hosler and H. P. R. Frederikse—1261(A)
Field dependence of Hall potential and magnetoresistance of irradiated graphite, J. D. McClelland—1807(A)
Generalized theory of mobility, Melvin Lax—1808(A)
Hall effect and conductivity of InSb, H. J. Hrostowski, F. J. Morin, T. H. Geballe, and G. H. Wheatley—1672
Hall effect and magnetoresistance of Bi single crystals at He temperatures, R. A. Connell and J. A. Marcus—1256(A)
Hall effect in gray Sn filaments, E. E. Kohnke and A. W. Ewald—1251(A)
Hall effect noise, James J. Brophy and Norman Rostoker—754(L)

Measurement of magnetic field gradients by Hall effect, R. D. Redin and G. C. Danielson—1257(A)
Post-bombardment conductivity of MgO crystals, M. A. Pomerantz, J. F. Marshall, and R. A. Shatas—964(A)
Pressure dependence of resistivity, Hall coefficient, and energy gap for InAs, Julius H. Taylor—1593
Properties of In and Tl at low temperatures, C. A. Swenson—1607
Recombination processes in Te, David Redfield—1094
Reduction of charge carrier concentration in InSb at 4.2°K by strong magnetic field, R. W. Keyes and R. J. Sladek—1262(A)
Search for Hall effect in superconductor. II. Theory, H. W. Lewis—641
Transverse field effects in PbS, D. E. Martz and R. S. Witte—1808(A)

Electrical Discharges

Attenuation of 1-cm microwaves by abnormal dc discharge in He, Z. Geller and W. Low—1240(A)
Collision cross section of N_2 molecules with slow electrons, L. Goldstein and J. M. Anderson—1229(A)
Cyclotron resonance of electrons in gaseous discharge plasmas, M. Gilden and L. Goldstein—1233(A)
Derivation from Boltzmann's equation of similarity laws for ionized gases, T. E. VanZandt—1235(A)
Diffusion of like particles across magnetic field, Albert Simon—1557
Drift velocity of electrons in He and H_2 at low fields, J. L. Pack and A. V. Phelps—1229(A)
Electrical characteristics of low-pressure spark discharges, R. J. Lee and R. G. Fowler—1234(A)
Electron loss in hydrogen afterglow, Karl-B. Persson and Sanborn C. Brown—729
Electron mobilities in gases, Joseph C. Bowe—1268(A)
Failure of Schottky theory for positive column of O_2, D. S. Burch, G. H. Dunn, R. Geballe, and V. M. Madsen—1235(A)
First and second Townsend coefficients in H_2 and N_2, D. J. De Bitetto and L. H. Fisher—1227(A)
Formative breakdown delays in noble gases at small overvoltages, B. T. McClure—1228(A)
Formative time lags of positive point-to-plane corona in N_2 and A, L. A. Bornstein and L. H. Fisher—1228(A)
Glow-to-arc transitions in column of high-pressure glow in H_2, W. A. Gambling—1232(A)
High-frequency gas discharge breakdown in Ne-A mixtures, H. J. Oskam—1228(A)
Inclusion of Coulomb interactions in Boltzmann equations, H. Dreicer and W. P. Allis—1234(A)
Influence of electron emission on cathode processes of arc, G. Ecker—1232(A)
Ion diffusion in uniform magnetic field, K. S. W. Champion and A. B. de Saint Maurice—1233(A)
Lifetime of imprisoned resonance radiation in Ne, A. V. Phelps—1230(A)
Low-pressure afterglow studies in N_2, A. C. Faire and George W. Griffing—1231(A)
Magnetohydrodynamic waves in ionized plasma, W. A. Newcomb—968(A)
Microwave studies of slow-electron collision processes in He plasmas, J. M. Anderson and L. Goldstein—1229(A)
Minimum quenching times of low-voltage, nonself-quenching Geiger counters, Roger D. Erickson—1234(A)
Negative-ion formation in iodine by electron capture, R. E. Fox—1229(A)
Oscillating glow discharge plasma, A. B. Stewart and G. E. Owen—1235(A)
Particle transport, electric currents, and pressure balance in a magnetically immobilized plasma, P. Stehle—443
Pressure limits of high-frequency secondary electron resonance breakdown mechanism, Albert J. Hatch and H. Bartel Williams—1228(A)
Production and loss of excited atoms in He positive column, L. S. Frost and A. V. Phelps—1234(A)
Pronounced deviations from Maxwellian velocity distribution of electrons in hollow hot cathode diodes with Ne filling, Gustav Medicus—1232(A)
Properties of arc cathode spots in magnetic fields, Dino Zei, Robert St. John, and J. G. Winans—1232(A)
Radiation temperature of plasma, Francis Bitter and John F. Waymouth—1230(A)
Resonance irradiation of Hg vapor in nitrogen, J. A. Berberet and K. C. Clark—506
Resonant power transfer within plasma in magnetic field, J. E. Drummond and L. Wilcox—1233(A)
Semiempirical calculation of Townsend α, Peter L. Auer—1228(A)
Semirandom sparking in short air gap, C. D. Maldonado and R. C. Retherford—1228(A)
Short arcs, L. H. Germer and W. S. Boyle—1232(A)
Townsend's first ionization coefficient in N_2, Melvin A. Harrison—1800(A)
Transient behavior following breakdown and its relation to afterglow processes, Donald E. Kerr and Eldred F. Tubbs—1231(A)
Uv continuum of $XeHg'$ molecule, Carl Kenty—1231(A)

Electrical Properties (see also **Dielectrics and Dielectric Properties; Electrical Conductivity and Resistance; Semiconductors; Superconductors**)

Application of space-charge theory to determination of electron emitter properties, W. B. Nottingham—964(A)
Brillouin zone studies. V. Thermoelectric power of dilute Mg alloys, E. W. Kammer, E. I. Salkovitz, and A. I. Schindler—1257(A)
CdS photorectifier, Lawrence C. Greene—978(A)
Effect of point imperfections on electrical properties of Cu. II. Thermoelectric power, F. J. Blatt—666
Electrical breakdown in InSb at low temperature, Ralph Bray—1262(A)
Electron emission from lattice step on clean tungsten, J. K. Trolan, J. P. Barbour, E. E. Martin, and W. P. Dyke—1646
Field effect in Si, S. Penman and W. L. Brown—1259(A)
Field emission microscopy of allotropic transformation: α-β titanium, Ernest G. Brock—1619
Interaction of elementary particles, Joseph G. Barredo—970(A)
Longitudinal photomagnetoelectric effect in Ge, Gerhart Groetzinger and Jack Aron—978(A); Jack Aron and Gerhart Groetzinger—1128
Preparation and electrical properties of Bi_2Te_3, T. C. Harman, S. E. Miller, and H. L. Goering—1262(A)
Pressure limits of high-frequency secondary electron resonance breakdown mechanism, Albert J. Hatch and H. Bartel Williams—1228(A)
Quantum yield of CdS photovoltaic cell, R. E. Marburger, D. C. Reynolds, L. L. Antes, and R. S. Hogan—978(A)
Schottky effect for SrO films on Mo, G. A. Haas and E. A. Coomes—640
Statistical mechanics of cathode sputtering, Don E. Harrison, Jr.—1234(A)
Thermoelectric power in semiconductor showing high-temperature degeneracy, V. A. Johnson—1251(A)
Thermoelectric power of AuCu in nonequilibrium states, P. Schwed, H. Cooper, and R. W. Webeler—978(A)
Use of field emission microscope for investigating surface conditions on alloy, L. A. D'Asaro—1258(A)
Velocity analysis of thermionic emission from single-crystal tungsten, George F. Smith—1115

Electrodynamics (see **Electromagnetic Theory and Electrodynamics**)
Electrolysis (see **Chemical Effects and Properties**)
Electromagnetic Theory and Electrodynamics
Alternative interpretation of magnetic forces between moving charges, John Backus—1808(A)
Determination of magnetic field strength H and its vector potential A in terms of magnetic field strength H_s on plane surface, with application to spiral ridged FFAG accelerator, Edward S. Akeley—972(A)
Fluctuations on damped transmission line, C. W. McCombie—444
Interaction of electromagnetic waves of rf in isothermal plasmas: Collision cross section of He atoms and ions for electrons, J. M. Anderson and L. Goldstein—1037
Tensor scattering matrix for electromagnetic field, David S. Saxon—1771
Theory of orbits in FFAG accelerators, Keith R. Symon —1247(A)
Third-order aberration and focusing with sector-shaped magnetic field, D. F. Dempsey, W. C. Miller, and B. Waldman—1240(A)
Electron Diffraction (see **Diffraction; Scattering of Electrons and Positrons**)
Electron Optics (see **Electromagnetic Theory and Electrodynamics**)
Electronic Tubes (see **Methods and Instruments**)
Electrons and Positrons (see also **Electromagnetic Theory and Electrodynamics; Elementary Particle Interactions; Scattering of Electrons and Positrons**)
Angular correlation of annihilation radiation in superconducting Pb, R. Stump—1256(A)
Annihilation of positrons in condensed materials, P. R. Wallace—738
Contribution of electron to pair production in atomic hydrogen, F. Rohrlich and J. Joseph—1241(A)
Coulomb enhancement of positron annihilation in metals, Richard A. Ferrell—973(A)
Multiple photon production from electron pair annihilation, J. Joseph—1241(A)
Electrons, Mobility (see **Ions and Electrons, Mobility**)
Electrons, Scattering of (see **Scattering of Electrons and Positrons**)
Electrons, Secondary (see **Electrical Properties**)
Electrons, Thermionic (see **Electrical Properties**)
Electro-Optical Effects (see **Optical Properties**)
Electrostriction (see **Dielectrics and Dielectric Properties**)
Elementary Particle Interactions
Analysis of capture stars of K^--mesons from Berkeley Bevatron, D. M. Haskin, D. B. Williams, E. Goodman, and Marcel Schein—1263(A)
Angular distribution of Λ^0 and θ^0 decays, Robert K. Adair —1540(L)
Angular distribution of n-p scattering at 17.9 Mev, A. Galonsky and J. P. Judish—121
Anomalous magnetic moment of nucleon, Kurt Haller and Marvin H. Friedman—1501
Causality in pion-proton scattering, H. L. Anderson, W. C. Davidon, and U. E. Kruse—339
Diffusion chamber study of very slow mesons. III. Scattering of negative pions in hydrogen, M. C. Rinehart, K. C. Rogers, and L. M. Lederman—883
Dispersion relations for pion-nucleon scattering. I. Spin-flip amplitude, Reinhard Oehme—1503
Elastic p-p scattering in Bev range, Bruce Cork and W. A. Wenzel—962(A)
Electric quadrupole moment and corrections to magnetic moment of deuteron for velocity-dependent tensor forces, L. Estrada—956(A)
Electrons from muon capture, J. Steinberger and Harry B. Wolfe—1490
Energy dependence of phase shifts in pion-proton scattering, Jay Orear—288
Extended isotopic spin invariance and meson-nucleon coupling, Sidney A. Bludman—372
γ-ray scattering by hydrogen, G. S. Janes, R. Gomez, G. E. Pugh, and D. H. Frisch—1245(A)
High-energy pion-proton cross sections, Baxter H. Armstrong—1798(A)
Hyperfragments in light elements produced by Berkeley Bevatron, Daniel Leenov, D. M. Haskin, and Marcel Schein—1263(A)
Internal structure of spinning particles, David Finkelstein —924
Isobar role in two-nucleon processes; deuteron photoeffect, N. Austern—1522
Meson production in n-p collisions by Cosmotron-produced neutrons with energies up to 1.5 Bev, W. A. Wallenmeyer—1255(A)
Neutral pion production in p-p collisions, Robert K. Squire and Burton J. Moyer—1798(A)
Observation of antiprotons, Owen Chamberlain, Emilio Segrè, Clyde Wiegand, and Thomas Ypsilantis—947(L)
Phase-shift analysis of nucleon-nucleon scattering at 150 Mev, Shoroku Ohnuma and David Feldman—1241(A)
Photoproduction of neutral pions from protons at forward pion angles, W. S. McDonald—1799(A)
Photoproduction of π-meson pairs in hydrogen, F. Zachariasen—1809(A)
π^+ photoproduction ratio of deuterium to hydrogen, K. M. Crowe, R. M. Friedman, and D. C. Hagerman—1799(A)
Pion-nucleon scattering calculations in Tamm-Dancoff theory, M. H. Kalos and R. H. Dalitz—1515
Pion pair photoproduction, R. M. Friedman and K. M. Crowe—1799(A)
Pion production in p-p collisions, D. B. Lichtenberg—303
π^--p collisions at 1.0 Bev, W. D. Walker and W. D. Shephard—1264(A)
Positive pion scattering by H at 260, 300, and 400 Mev, R. S. Margulies—1255(A)
p-p interactions at 3 Bev, R. Cester, T. F. Hoang, and A. Kernan—940(L)
p-p interactions at 5.3 Bev, Robert W. Wright, George Saphir, Wilson M. Powell, George Maenchen, and William B. Fowler—1802(A)
p-p polarization at 170 Mev, David Fischer and John Baldwin—1445
p-p scattering at 1 Bev, William Rarita—1241(A)
p-p scatterings at 19.6 Mev, J. W. Burkig, Glen E. Schrank, and J. Reginald Richardson—1805(A)
Production of heavy unstable particles in π^--p collisions at 1.0 Bev, W. D. Shephard and W. D. Walker—1264(A)
Production of hyperons and K-mesons in high-energy π^- beam of Berkeley Bevatron, Marcel Schein and D. M. Haskin—1263(A)
Production of pairs in capture of slow neutrons by protons, A. T. Peaslee, Jr.—974(A)
Production of unstable particles in 4.5-Bev π^--p collisions, George Maenchen, William B. Fowler, Wilson M. Powell, George Saphir, and Robert W. Wright—1802 (A)
Reaction $\pi^-+d\rightarrow 2n+\pi^0$; parity of neutral meson, W. Chinowsky and J. Steinberger—1476
Remarks on antiproton, T. Regge, S. Okubo, and R. Marshak—1810(A)
Scattering length and effective range for velocity-dependent tensor forces, A. Mondragón—956(A)
Scattering of pions by H at 165 Mev, H. L. Anderson and M. Glicksman—268

Scattering of pions by nucleons in intermediate coupling, M. H. Friedman, T. D. Lee, and R. Christian—1494
Scattering of positive pions by H at 189 Mev, H. L. Anderson, W. C. Davidon, M. Glicksman, and U. E. Kruse—279
Scattering of 30–95 Mev γ rays by protons, C. L. Oxley and V. L. Telegdi—962(A)
Scattering of 30–95 Mev photons by protons, C. L. Oxley and V. L. Telegdi—435(L)
Scattering of 38-Mev positive pions in hydrogen, A. M. Sachs, H. Winick, and B. A. Wooten—1255(A)
Small-angle p-p scattering at 20 Mev, Herbert N. Royden and Byron T. Wright—1805(A)
Strong pion-pion interaction model applied to pion-nucleon scattering in 1-Bev region, Gyo Takeda—440(L)
Torus model of elementary particles in which stability may be achieved by gravitational forces resulting from concentrated electromagnetic field, Winston H. Bostick—1250(A)
Total cross section of H for 150–750-Mev positive and negative pions, S. J. Lindenbaum and Luke C. L. Yuan—306
Two-nucleon potential from cutoff Yukawa theory, Solomon Gartenhaus—900
Unstable $_1H^4$ fragment from capture of Σ^- hyperon, Marcel Schein, D. M. Haskin, and Daniel Leenov—1455
Elements (see **Atomic Mass and Abundance**)
Energy Loss of Particles (see **Range and Energy Loss**)
Energy States of Atoms (see **Atomic Structure and Spectra**)
Energy States of Molecules (see **Molecular Structure and Spectra**)
Energy States of Nucleus (see **Nuclear Reactions; Nuclear Spectra; Nuclear Structure Theory**)
Equations of State (see **Chemical Effects and Properties**)
Errata
Electroluminescence of ZnS single crystals, D. R. Frankl—1790(E)
Intermediate coupling in odd-odd nuclei, R. Adkins and J. G. Brennan—1790(E)
Pressure-volume isotherms of He^4 below 4.2°K, William E. Keller—1790(E)
Soluble problem in theory of Coulomb excitation, L. C. Biedenharn and C. M. Class—1790(E)
Errors of Measurement (see **Methods and Instruments**)
Evaporation (see **Liquids**)
Excitation of Atoms (see **Atomic Structure and Spectra**)
Excitation of Molecules (see **Molecular Structure and Spectra**)
Excitation of Nucleus (see **Nuclear Reactions; Nuclear Spectra; Nuclear Structure Theory**)
Explosion Phenomena (see **Fluid Dynamics**)

Faraday Effect (see **Optical Properties**)
Ferroelectric Phenomena (see **Dielectrics and Dielectric Properties**)
Ferromagnetism (see **Magnetic Properties**)
Field Emission (see **Electrical Properties**)
Field Theory (see also **Quantum Electrodynamics**)
Anomalous magnetic moment of nucleon, Kurt Haller and Marvin H. Friedman—1501
Connection between S-matrix and tensor force, Roger G. Newton—412
Dispersion relations for pion-nucleon scattering. I. Spin-flip amplitude, Reinhard Oehme—1503
Extended isotopic spin invariance and meson-nucleon coupling, Sidney A. Bludman—372
Field of Bhabha equation, Fernando E. Prieto C.—974(A)
Hamiltonian form of integral spin wave equations, K. M. Case—1513
Isobar role in two-nucleon processes: Deuteron photoeffect, N. Austern—1522
Momentum dependence of phase shifts, Charles J. Goebel, Robert Karplus, and Malvin A. Ruderman—240
Nonrenormalizable field theory, Leon N. Cooper—362
Pion-nucleon scattering calculations in Tamm-Dancoff theory, M. H. Kalos and R. H. Dalitz—1515
Radiative corrections to decay processes, R. E. Behrends, R. J. Finkelstein, and A. Sirlin—1809(A)
Renormalization of derivative coupling theories, R. Arnowitt and S. Deser—349
Scattering of pions by nucleons in intermediate coupling, M. H. Friedman, T. D. Lee, and R. Christian—1494
Spectrum and nonrelativistic limit of Bethe-Salpeter equation, Frederick L. Scarf—912
State vector normalization in formal scattering theory, Bryce S. DeWitt—905
Structure of Green's functions in quantum field theory, Yoichiro Nambu—394
Two-nucleon potential from cutoff Yukawa theory, Solomon Gartenhaus—900
Wave equations for arbitrary spin, C. Fronsdal—1810(A)
Films, Properties
Absorption of vacuum uv radiation by thin plastic films, G. L. Weissler and L. Z. Maudlin—1800(A)
Mechanical strength of thin films of metals, J. W. Beams, J. B. Breazeale, and W. L. Bart—1657
Schottky effect for SrO films on Mo, G. A. Haas and E. A. Coomes—640
Fine Structure (see **Atomic Structure and Spectra**)
Fission of Nucleus (see **Nuclear Fission**)
Fluctuation Phenomena (see **Noise**)
Fluid Dynamics
Application of light-scattering theory to measurement of density fluctuations in turbulent fluids, Howard A. Stine and Warren Winovich—968(A)
Dependence of discrete acoustic frequencies emitted by jet on vortex-ring coalescence at Reynolds numbers up to 7000, A. B. C. Anderson—1800(A)
Drag in rotating cylinder apparatus near conditions of free molecule flow, J. M. Bowyer and L. Talbot—968(A)
Free surface motion due to obliquely incident shock waves, J. O. Erkman—1801(A)
Hydrodynamic impact of curved surfaces, M. D. Bledsoe and V. G. Szebehely—968(A)
Linearized flow theory and shock waves in metals, G. E. Duvall—967(A)
Magnetohydrodynamic waves in ionized plasma, W. A. Newcomb—968(A)
Normal modes characterizing magneto-elastic plane wave, Alfredo Baños, Jr.—1801(A)
Proposed change in scaling laws for explosive phenomena, Everett F. Cox—967(A)
Slow motions, K. M. Siegel and A. L. Maffett—968(A)
Use of electric arc heating in ultra-high temperature aerodynamics, R. W. Perry and D. E. Bloxsom—968(A)
Fluorescence (see **Luminescence**)
Friction (see **Mechanics**)

Galvanomagnetic Effect (see **Magnetic Properties**)
Gamma Rays (see also **Nuclear Reactions; Nuclear Spectra; Radiation Range and Energy Loss**)
γ-ray scattering by complex nuclei, R. Gomez, G. E. Pugh, D. H. Frisch, and G. S. Janes—1245(A)
γ-ray scattering by hydrogen, G. S. Janes, R. Gomez, G. E. Pugh, and D. H. Frisch—1245(A)
Nuclear γ-ray scattering techniques, G. E. Pugh, R. Gomez, D. H. Frisch, and G. S. Janes—1245(A)
Polarization effects in electron-photon interactions, Cramer Schultz and Ross D. Thompson—1809(A)

Gamma Rays (Continued)
Scattering of 30-90 Mev γ rays by protons, C. L. Oxley and V. L. Telegdi—962(A)
Scattering of 30-95 Mev photons by protons, C. L. Oxley and V. L. Telegdi—435(L)
Gases
Derivation from Boltzmann's equation of similarity laws for ionized gases, T. E. VanZandt—1235(A)
Electron mobilities in gases, Joseph C. Bowe—1268(A)
Inclusion of Coulomb interactions in Boltzmann equations, H. Dreicer and W. P. Allis—1234(A)
Quantum-statistical derivation of transport equation for mixtures of dilute gases with molecules of arbitrary spins, A. W. Saenz—975(A)
Geophysics
Absence of meteorological effects on world-wide sunspot variation in cosmic-ray ionization, Scott E. Forbush—958(A)
Fluctuation of sound transmitted in ocean, R. W. Stewart and W. N. English—969(A)
γ-ray absorption measurements of density of upper atmosphere, E. T. Byram, T. A. Chubb, and H. Friedman—963(A)
Geomagnetic micropulsations, H. J. Duffus—966(A)
Ionospheric drifts over Puerto Rico, Miguel Wiewall, Jr.—968(A)
Systematic application of physical and mathematical methods to exploitation of Mexican oil fields, A. Romero-Juárez and J. Hefferan V—965(A)
Glasses (see **Molecular Aggregates**)
Gravitation (see **Relativity and Gravitation**)
Gyromagnetization (see **Magnetic Properties**)

Hall Effect (see **Electrical Conductivity and Resistance; Semiconductors**)
Heat Capacity (see **Thermal Properties**)
Heat Conduction (see **Thermal Properties**)
Heat of Dissociation and Formation (see **Molecular Structure and Spectra**)
Heat of Fusion (see **Thermal Properties**)
Heat of Vaporization (see **Thermal Properties**)
Helium, Liquid
Atomic distribution in liquid He by neutron diffraction, D. G. Hurst and D. G. Henshaw—994
Atomic distribution in liquid He^3, R. M. Mazo and J. G. Kirkwood—1787(L)
Interatomic correlations in liquid He^4, Louis Goldstein—981
Kinetic model of He II, Charles A. Reynolds—1548(A)
λ transition in liquid He, G. V. Chester—455
Liquid He bubble chamber, W. M. Fairbank, E. M. Harth, M. E. Blevins, and G. G. Slaughter—971(A)
Liquid He vapor pressure equation, J. R. Clement, J. K. Logan, and J. Gaffney—743
Motion of nuclei in liquid He, W. V. Houston and H. E. Rorschach—1003
Nuclear paramagnetism of liquid He^3, H. E. Rorschach, Jr., and W. V. Houston—966(A)
Origin of λ transition in liquid He, Louis Goldstein—966(A)
Pressure-volume isotherms of He^4 below 4.2°K, William E. Keller—1790(E)
Second virial coefficients of He^3-He^4 mixtures between 2 and 4°K, William E. Keller—1021
Statistical mechanics of mixtures of isotopes, G. V. Chester—446
High-Voltage Tubes in Machines (see **Methods and Instruments**)
Hydrodynamics (see **Fluid Dynamics**)

Hyperfine Structure (see **Atomic Structure and Spectra; Molecular Structure and Spectra; Nuclear Moments and Spin**)
Hyperons (see **Mesons and Hyperons**)

Imperfections in Solids (see also **Crystalline State; Electrical Conductivity and Resistance; Luminescence; Semiconductors**)
Computation of vacancies created by heavy corpuscular radiation, W. S. Snyder and J. Neufeld—969(A)
Deformation zones produced by explosive shocks in ferrous metals, Samuel Katz—1800(A)
Detection of vacancies created by x-rays in NaCl, H. W. Etzel—1643
Deuteron irradiation of Ge at 90°K, D. Kleitman and T. A. Longo—1261(A)
Dichroism of F and M absorption bands in KCl, C. Z. van Doorn and Y. Haven—753(L)
Dislocation energies in NaCl, H. B. Huntington, J. E. Dickey, and Robb Thomson—1117
Effect of defects on lattice vibrations, Elliott W. Montroll and Renfrey B. Potts—525
Effect of impurities on lattice vibrations, Elliott W. Montroll and R. B. Potts—969(A)
Effect of low-temperature electron irradiation on electrical resistivity of Cu, C. J. Meechan—1807(A)
Effect of point imperfections on electrical properties of Cu. II. Thermoelectric power, F. J. Blatt—666
Effect of Sb impurity on self-diffusion of Ag, E. Sonder—1662
Electrolytic etching at small-angle grain boundaries in Ge, S. G. Ellis—1140
Electron spin resonance of defect centers in MgO, John E. Wertz and Juana L. Vivo—1792(A)
Electron spin resonance of impurities in MgO, John E. Wertz, Juana L. Vivo, and Boris Musulin—1810(A)
Energy levels of crystal modified by alloying or by pressure, R. H. Parmenter—573
Excess noise in plastically deformed Ge, James J. Brophy—1261(A)
Fast-neutron bombardment of GaSb, J. W. Cleland and J. H. Crawford, Jr.—1614
Field dependence of Hall potential and magnetoresistance of irradiated graphite, J. D. McClelland—1807(A)
Frequencies and relative intensities of R_1 and R_2 bands in KCl, Robert Herman, H. C. Wallis, and R. F. Wallis—1267(A)
Influence of lattice defects on Young's modulus of Cu, H. Dieckamp—1807(A)
Interpretation of stored energy of irradiated graphite in terms of elastic energy associated with microscopic strain, Alfred E. Austin and Ralph J. Harrison—1225(L)
Irradiation effects in some organic compounds, T. H. Anderson, R. D. Jordan, and R. S. Alger—964(A)
Irradiation of graphite at liquid He temperatures, Stanley B. Austerman and John E. Hove—1214(L)
Kinetics of processes distributed in activation energy, William Primak—1677
Lattice constants of graphite at low temperatures, Y. Baskin and L. Meyer—544
Magnetic susceptibility of neutron-damaged graphite, John E. Hove—1806(A)
Neutron-irradiated Si, Thomas A. Longo and David Kleitman—1260(A)
New method for determination of activation energies, J. A. Brinkman—1807(A)
Nuclear magnetic resonance studies of imperfect ionic crystals, F. Reif—1597

Post-bombardment conductivity of MgO crystals, M. A. Pomerantz, J. F. Marshall, and R. A. Shatas—964(A)
Precipitation of Cu in Ge, R. A. Logan—615
Precipitation of Cu in plastically deformed Ge, A. G. Tweet—1260(A)
Radiation-induced amorphism in diamond, Paul W. Levy and Otto F. Kammerer—1787—(L)
Radiation-induced dielectric changes in phosphorescent material, A. Skoglund and A. Ore—1549(A)
Reduction of optical reflectivity of glass by positive ion bombardment, R. L. Hines—1267(A)
Stored energy release in graphite irradiated at low temperatures, S. B. Austerman—1807(A)
Thermal acceptors in vacuum heat-treated Ge, Robert L. Hopkins and Edward N. Clarke—1786(L)
Thermal conductivity of neutron-damaged graphite, Ned S. Rasor and John E. Hove—1806(A)
Thermal defects in Si, C. J. Gallagher—1259(A)
Thresholds for electron-bombardment-induced lattice displacements in Si and Ge, Paul Rappaport and Joseph J. Loferski—1261(A)
Tracer studies on radiation-damaged graphite, G. L. Montet, A. F. Kurs, and G. R. Hennig—1261(A)

Inelastic Scattering (see **Nuclear Reactions; Scattering**)
Instruments (see **Methods and Instruments**)
Internal Conversion (see **Nuclear Spectra**)
Ionization (see also **Electrical Discharges; Range and Energy Loss of Particles**)
Ionization by α particles in mixtures of gases, William P. Jesse and John Sadauskis—1755
Ionization of cloud-chamber tracks, E. K. Björnerud—972(A)
Ionization of H in Ge and Si, Howard Reiss—1806(A)
Light absorption and photoionization in NO and N_2O, W. C. Walker and G. L. Weissler—1231(A)
Theory of ionization probability near threshold, Sydney Geltman—1231(A)
Threshold law for multiple ionization, G. H. Wannier—1180

Ionization Potentials of Atoms (see **Atomic Structure and Spectra**)
Ionization Potentials of Molecules (see **Molecular Structure and Spectra**)
Ionosphere (see **Geophysics**)
Ions (see also **Electrical Discharges**)
Angular momentum and energy of ions in magneto-ionic isotope separator, Joseph Slepian—1238(A)
Energy resolution obtainable with 2-Mev He^+ beam, D. F. Herring, R. A. Douglas, E. A. Silverstein, and Ren Chiba—1239(A)
Formation of metastable A^+, Kr^+, and Xe^+ by electron impact, Homer D. Hagstrum—1231(A)
High-intensity ion sources, C. B. Mills—1233(A)
Ion diffusion in uniform magnetic field, K. S. W. Champion and A. B. de Saint Maurice—1233(A)
Negative H ion source, J. A. Weinman, J. R. Cameron, and R. G. Herb—1239(A)
Negative-ion formation in iodine by electron capture, R. E. Fox—1229(A)
Resonance irradiation of Hg vapor in nitrogen, J. A. Berberet and K. C. Clark—506
Scattering of low-energy H^- ions in He, T. L. Bailey and E. E. Muschlitz—1231(A)
Stark fields from ions in plasma, A. A. Broyles—1181
Statistical mechanics of cathode sputtering, Don E. Harrison, Jr.—1234(A)

Ions and Electrons, Mobility (see also **Semiconductors**)
Deviations from Blanc's law of ionic mobilities: Ne^+ in Ne-H mixtures, Manfred A. Biondi and Lorne M. Chanin—1230(A)
Electron mobilities in gases, Joseph C. Bowe—1268(A)
Generalized theory of mobility, Melvin Lax—1808(A)
Mobility of positive ions in gas mixtures, T. Holstein—1230(A)
Temperature dependence of ionic mobilities: Ne^+ and Ne_2^+ in Ne, Lorne M. Chanin and Manfred A. Biondi—1230(A)

Isobars (see **Atomic Mass and Abundance**)
Isomers, Molecular (see **Molecular Structure and Spectra**)
Isomers, Nuclear (see **Nuclear Spectra**)
Isotopes (see **Atomic Mass and Abundance; Radioactivity**)

Kerr Effect (see **Optical Properties**)
Kinetic Theory of Gases (see **Gases**)

Liquid Helium (see **Helium, Liquid**)
Liquids
Temperature anomalies in properties of liquid water, W. Drost-Hansen and H. W. Neill—1800(A)

Luminescence
CdS with Ag activator, John Lambe—1586
Criterion for occurrence of luminescence, C. C. Klick, G. A. Russell, and D. L. Dexter—964(A); D. L. Dexter, C. C. Klick, and G. A. Russell—603
Edge electroluminescence from ZnS single crystals, R. W. Smith—760(L)
Electroluminescence in ZnS, W. A. Thornton—1268(A)
Electroluminescence of GaP, G. A. Wolff, R. A. Herbert, and J. D. Broder—1144
Electroluminescence of ZnS single crystals, D. R. Frankl—1105; 1790(E)
Fluorescence excitation spectrum of anthracene, G. T. Wright—587
Radiation-induced dielectric changes in phosphorescent material, A. Skoglund and A. Ore—1549(A)
Scintillation response of anthracene crystals to short-range electrons, G. T. Wright—588
Thermoluminescence measurements of electroluminescent ZnS:Mn films, R. E. Freund—760(L)

Magnetic Fields (see **Electromagnetic Theory and Electrodynamics**)
Magnetic Properties
Approach to elongated fine particle magnets, I. S. Jacobs and C. P. Bean—1060
Considerations on double exchange, P. W. Anderson and H. Hasegawa—675
Deformation zones produced by explosive shocks in ferrous metals, Samuel Katz—1800(A)
Effect of shape anisotropy on coercive force of elongated single-magnetic-domain Fe particles, T. O. Paine, L. I. Mendelsohn, and F. E. Luborsky—1055
Effect of V_2O_3 on spinel formation, D. M. Grimes and J. W. Kuiper—1256(A)
Ferrimagnetic interaction and remanence in $CoCO_3$, Warren E. Henry—1791(A)
Ferrimagnetic resonance in single crystals of Mn ferrite, J. F. Dillon, Jr., S. Geschwind, and V. Jaccarino—750(L)
Ferromagnetic and antiferromagnetic Curie temperatures, H. A. Brown and J. M. Luttinger—685
Ferromagnetic resonance in Mn ferrite single crystals, P. E. Tannenwald—1713
Frequency doubling in ferrites, W. P. Ayres, P. H. Vartanian, and J. L. Melchor—1791(A)
Influence of crystalline electric fields on antiferromagnetic transitions, L. D. Roberts, R. B. Murray, and J. W. T. Dabbs—1100

Magnetic Properties (Continued)
Instability in motion of ferromagnets at high microwave power levels, P. W. Anderson and H. Suhl—1788(L)
Lagrangian formulation of gyromagnetic equation of magnetization fields, T. L. Gilbert—1243(A)
Magnetic and thermal properties of $MnCl_2$ at liquid He temperatures. I. Magnetic susceptibility, R. B. Murray and L. D. Roberts—1067; II. Specific heat, R. B. Murray—1071
Magnetic and thermal properties of UI_3 at liquid He temperatures, L. D. Roberts and R. B. Murray—650
Magnetic domains in thin films of Ni-Fe, Charles A. Fowler, Jr., and Edward M. Fryer—746(L)
Magnetic moment arrangements and magnetocrystalline deformations in antiferromagnetic compounds, Yin-Yuan Li—627
Magnetic properties of Er metal, J. F. Elliott, S. Legvold, and F. H. Spedding—1595
Magnetic properties of murdochite, Cu_4PbO_6, Palmer L. Edwards—1242(A)
Magnetic second order transitions, K. J. Tauer and R. J. Weiss—1223(L)
Magnetic superexchange interaction, David Kottwitz—1242(A)
Magnetic susceptibility of Ge, D. K. Stevens, J. W. Cleland, J. H. Crawford, Jr., and H. C. Schweinler—1084
Magnetic susceptibility of impurity-trapped electrons and holes in semiconductors, E. Mooser—1589
Magnetic susceptibility of Na metal, Raymond Bowers—1141
Magnetic susceptibility of neutron-damaged graphite, John E. Hove—1806(A)
Magnitude of splitting of lowest level in chromium alum, Paul H. E. Meijer and H. J. Gerritsen—742
Microwave resonance relations in anisotropic single crystal ferrites, J. O. Artman—1243(A)
Neutron diffraction study of magnetic properties of series of perovskite type compounds $[(1-x)\mathrm{La}, x\mathrm{Ca}]MnO_3$, E. O. Wollan and W. C. Koehler—545
New magnetic transition in Mn_3ZnC, B. N. Brockhouse and H. P. Myers—1242(A)
Nuclear paramagnetism of liquid He^3, H. E. Rorschach, Jr., and W. V. Houston—966(A)
Phase transformations in microstructure of explosively loaded Fe and steel, E. W. LaRocca—1800(A)
Temperature dependence of ferromagnetic anisotropy in cubic crystals, Frederic Keffer—1692
Theory of magnetic susceptibility of graphite, John E. Hove—645
Theory of role of covalence in perovskite-type manganites $[\mathrm{La}, M(\mathrm{II})]MnO_3$, John B. Goodenough—564
Zeeman effects and magnetic properties of Nd salts, G. H. Dieke and L. Heroux—965(A)
Magnetic Resonance (see also **Nuclear Moments and Spin**)
Anisotropic paramagnetic absorption spectrum of manganous ion in cubic ZnS, Lawrence M. Matarrese and Chihiro Kikuchi—1243(A)
Classical theory of cyclotron resonance for holes in Ge, J. M. Luttinger and B. R. Goodman—673
Cyclotron absorption in Bi, R. N. Dexter and Benjamin Lax—1216(L)
Cyclotron resonance in Ge-Si alloys, G. Dresselhaus, A. F. Kip, Han-Ying Ku, G. Wagoner, and Schuyler M. Christian—1218(L)
Cyclotron resonance in metals: Bi, J. K. Galt, W. A. Yager, F. R. Merritt, B. B. Cetlin, and H. W. Dail, Jr.—748(L)
Cyclotron resonance of electrons in gaseous discharge plasmas, M. Gilden and L. Goldstein—1233(A)
Double-frequency magnetic resonance in free radical, J. H. Burgess and R. E. Norberg—752(L)
Doublet structure in paramagnetic absorption spectra of Mn^{++} in calcite, Chihiro Kikuchi—1243(A)
Electromagnetic theory of cyclotron resonance in metals, P. W. Anderson—749(L)
Electron spin resonance in Cu-Mn and Ag-Mn alloys, J. Owen, M. E. Browne, and A. F. Kip—965(A)
Electron spin resonance of defect centers in MgO, John E. Wertz and Juana L. Vivo—1792(A)
Electron spin resonance of impurities in MgO, John E. Wertz, Juana L. Vivo, and Boris Musulin—1810(A)
Exchange effects in spin resonance of impurity atoms in Si, G. Feher, R. C. Fletcher, and E. A. Gere—1784(L)
Ferrimagnetic resonance in single crystals of Mn ferrite, J. F. Dillon, Jr., S. Geschwind, and V. Jaccarino—750(L)
Ferromagnetic resonance in Mn ferrite single crystals, P. E. Tannenwald—1713
Frequency doubling in ferrites, W. P. Ayres, P. H. Vartanian, and J. L. Melchor—1791(A)
Instability in motion of ferromagnets at high microwave power levels, P. W. Anderson and H. Suhl—1788(L)
Magnetic resonance demonstration of charge transfer in Fe group fluorides, M. Tinkham—1792(A)
Magnitude of splitting of lowest level in chromium alum, Paul H. E. Meijer and H. J. Gerritsen—742
Microwave resonance relations in anisotropic single crystal ferrites, J. O. Artman—1243(A)
Nuclear magnetic dipole and electric quadrupole energy relations, L. Carlton Brown and Paul M. Parker—1764
Nuclear magnetic relaxation times in polyethylene, I. J. Lowe, L. O. Bowen, and R. E. Norberg—1243(A)
Nuclear magnetic resonance in semiconductors. I. Exchange broadening in InSb and GaSb, R. G. Shulman, J. M. Mays, and D. W. McCall—692
Nuclear magnetic resonance studies of imperfect ionic crystals, F. Reif—1597
Nuclear spin and magnetic moment of 50-day In^{114m}, L. S. Goodman and S. Wexler—1245(A)
Nuclear spin and magnetic moment of 54-min In^{130m}, L. S. Goodman and S. Wexler—1796(A)
Nuclear spin-lattice relaxation in solid H_2, Tadashi Sugawara—759(L)
Observation of quantum effects in cyclotron resonance, R. C. Fletcher, W. A. Yager, and F. R. Merritt—747(L)
Plasma resonance in crystals: Observations and theory, G. Dresselhaus, A. F. Kip, and C. Kittel—618
Plasma resonance in semiconductor crystals, G. Dresselhaus, A. F. Kip, and C. Kittel—1262(A)
Pure quadrupole spectra of CH_3I and CF_3I vapors, Fred Sterzer and Yardley Beers—1174
Quadrupole broadening of NMR lines by reversible axial stress, R. G. Shulman, B. J. Wyluda, and H. J. Hrostowski—1792(A)
Quadrupole spectrum of $BiCl_3$, Hugh G. Robinson—1731
Rapid-passage effects in electron spin resonance, A. M. Portis—1219(L)
Relaxation times in magnetic resonance, David Pines and Charles P. Slichter—1014
Resonance transitions induced by perturbations at two or more different frequencies, Norman F. Ramsey—1191
Resonant power transfer within plasma in magnetic field, J. E. Drummond and L. Wilcox—1233(A)
Significance of nuclear spin echo experiments for foundation of statistical mechanics, Jerome Rothstein—1791(A)
Spin resonance in metals as altered by Overhauser effect, J. I. Kaplan—965(A)

Theory of hfs of NO molecule. II. Errata and some additional discussion, Chun C. Lin and Masataka Mizushima —1726
Theory of multiple-quantum transitions, M. N. Hack—975 (A)
Thermodynamics of irreversible processes and Overhauser nuclear polarization effect, W. A. Barker and A. Mencher—1224(L)
Magneto-Optical Effects (see **Optical Properties**)
Magnetoresistance (see **Electrical Conductivity and Resistance; Semiconductors**)
Magnetostriction (see **Magnetic Properties**)
Mass Defects (see **Atomic Mass and Abundance**)
Mass Spectroscopy (see **Atomic Mass and Abundance; Methods and Instruments**)
Mathematical Methods
Neglected mathematics in solution of vibration problems, Dan McLachlan, Jr.—975(A)
New linear-system integral transform relations, Malcolm K. Brachman and J. Ross Macdonald—966(A)
Quantum theory of fluctuations, Hans Ekstein and Norman Rostoker—1023
Statistical theory of delayed-coincidence experiments, Z. Bay, V. P. Henri, and H. Kanner—1197
Measurements (see **Methods and Instruments**)
Mechanics
Neglected mathematics in solution of vibration problems, Dan McLachlan, Jr.—975(A)
Projectile penetration into sand, Earle B. Mayfield, Harvey L. Morrison, and William A. Allen—1800(A)
Mechanics, Quantum—Atomic Structure and Spectra (see **Atomic Structure and Spectra**)
Mechanics, Quantum—General (see **Quantum Mechanics**)
Mechanics, Quantum—Molecular Structure and Spectra (see **Molecular Structure and Spectra**)
Mechanics, Quantum—Nuclear (see **Nuclear Structure Theory**)
Mechanics, Quantum—of Solid Bodies (see **Crystalline State**)
Mechanics, Statistical (see **Statistical Mechanics and Thermodynamics**)
Meson Field Theory (see **Field Theory**)
Mesons and Hyperons (see also **Cosmic Radiation; Elementary Particle Interactions; Nuclear Reactions Induced by Mesons and Hyperons; Scattering of Mesons and Hyperons**)
A theory of new particles, Ryoyu Utiyama—248
Analysis of capture stars of K^--mesons from Berkeley Bevatron, D. M. Haskin, D. B. Williams, E. Goodman, and Marcel Schein—1263(A)
Angular correlation effects in V-particle decay, S. B. Treiman and H. W. Wyld, Jr.—879
Angular distribution of Λ^0 and θ^0 decays, Robert K. Adair —1540(L)
Anomalous neutral V-particles, W. H. Arnold, Jr., W. Martin, and H. W. Wyld—1545(L)
Anomalous V^0-particles, H. W. Arnold, J. Ballam, M. Grisaru, C. McGrew, and W. H. Wyld—1804(A)
Associated production of Ξ with two θ^0 particles, J. D. Sorrels, R. B. Leighton, and C. D. Anderson—1457
Capture of K^--meson with emission of high-energy electron as only visible prong, D. B. Williams, D. M. Haskin, M. Koshiba, and Marcel Schein—1547(L)
Cloud-chamber investigation of charged V particles, G. H. Trilling and R. B. Leighton—1468
Cloud-chamber observations of μ-meson-induced electron showers, C. A. Rouse—1797(A)
Cloud-chamber observations on charged V particles, W. H. Arnold, J. Ballam, and George T. Reynolds—295
Decay and absorption of θ^0, A. Pais and O. Piccioni—1487
Decay of anomalous charged K-meson, E. M. Harth and M. M. Block—959(A)
Difference in lifetimes of θ^0 and θ^+ mesons, S. Okubo and R. Marshak—1809(A)
Disintegration of hyperfragments, J. Schneps, M. S. Swami, and W. F. Fry—1263(A)
Double-plate cloud-chamber study of V^0-particles. I. Classification, I. C. Gupta, W. Y. Chang, and A. Snyder—1264 (A); II. Mean decay times of θ^0- and Λ^0-particles, A. Snyder, W. Y. Chang, and I. C. Gupta—1264(A)
East-west asymmetry of positive and negative mesons at geomagnetic equator, F. B. Harris and I. Escobar—255
Effects of angular momentum on τ-decay schemes, Bernard T. Feld—1263(A)
Energy distribution of K mesons produced in nuclei, M. M. Block, E. M. Harth, and R. M. Sternheimer—324
Evidence for β decay of neutral V-particles, M. M. Block, E. M. Harth, and M. E. Blevins—959(A)
Hyperfragments in light elements produced by Berkeley bevatron, Daniel Leenov, D. M. Haskin, and Marcel Schein—1263(A)
Interactions of negative K-particles at rest, Warren W. Chupp, Gerson Goldhaber, Sulamith Goldhaber, and Francis H. Webb—959(A)
K-meson lifetimes, Luis W. Alvarez, Frank S. Crawford, Jr., Myron L. Good, and M. Lynn Stevenson—1264(A)
Λ^0-fragment decay in cloud chamber, J. D. Sorrels, G. H. Trilling, and R. B. Leighton—1484
Lifetimes of τ^+ and K_1^+-mesons, G. Harris, J. Orear, and S. Taylor—932(L)
Mass values of identified K-mesons, James R. Peterson—1803(A)
Mass values of K-mesons, R. W. Birge, J. R. Peterson, D. H. Stork, and M. N. Whitehead—430(L)
Masses of positive K-particles. I. Identification of K-particles and analysis of secondaries, Frances M. Smith, Harry H. Heckman, and Walter H. Barkas—1802(A); II. Method, analysis, and results, Harry H. Heckman, Frances M. Smith, and Walter H. Barkas—1803(A)
Meson production in n-p collisions by Cosmotron-produced neutrons with energies up to 1.5 Bev, W. A. Wallenmeyer—1255(A)
Mesonic x-rays from capture of cosmic-ray μ mesons in chemical compound, A. Fafarman and M. H. Shamos—874
Negative K-particle interactions in nuclear emulsion. I, Charles E. Violet, F. C. Gilbert, and R. Stephen White —1803(A); II, F. C. Gilbert, Charles E. Violet, and R. Stephen White—1803(A); III, R. Stephen White, F. C. Gilbert, and Charles E. Violet—1803(A)
Neutral pion production in p-p collisions, Robert K. Squire and Burton J. Moyer—1798(A)
Nonmesonic decay of He hyperfragment, B. Stiller, N. Seeman, and M. M. Shapiro—959(A); Nathan Seeman, Maurice M. Shapiro, and Bertram Stiller—1480
Nuclear capture of negative K mesons in emulsion, W. F. Fry, J. Schneps, G. A. Snow, and M. S. Swami—1448
Nuclear interaction in flight of Σ hyperon, W. F. Fry, J. Schneps, G. A. Snow, and M. S. Swami—939(L)
Observations of negative K mesons and charged hyperons, W. F. Fry, J. Schneps, G. A. Snow, and M. S. Swami —950(L)
Observations on pion tracks in liquid H_2 bubble chamber, D. E. Nagle and R. H. Hildebrand—959(A)
One hundred Bevatron τ^+'s, Roy Haddock—1803(A)
Photometric mass determinations in multiplate cloud chamber, David O. Caldwell and Yash Pal—1803(A)
Photoproduction of neutral pions from protons at forward pion angles, W. S. McDonald, Vincent Peterson, and Dale R. Corson—1799(A)

Mesons and Hyperons (Continued)
Photoproduction of π-meson pairs in hydrogen, F. Zachariasen—1809(A)
Photoproduction of π^0 mesons in He, E. L. Goldwasser and L. J. Koester, Jr.—1255(A)
π^0 photomeson production from various nuclei at 135°, William Imhof, V. Perez-Mendez, and H. Easterday—1798(A)
π^0 photoproduction ratio of deuterium to hydrogen, K. M. Crowe, R. M. Friedman, and D. C. Hagerman—1799(A)
Pi-meson production in lead and carbon, M. Abraham and S. J. Goldsack—1799(A)
Pion-pair photoproduction, R. M. Friedman and K. M. Crowe—1799(A)
Pion-pair production, Juan De Oyarzabal—974(A)
Pion production in p-p collisions, D. B. Lichtenberg—308
p-p interactions at 3 Bev, R. Cester, T. F. Hoang, and A. Kernan—940(L)
Production of hyperons and K-mesons in high-energy π^- beam of Berkeley Bevatron, Marcel Schein and D. M. Haskin—1263(A)
Range-energy relation and masses of new particles, David O. Caldwell—291
Reaction $\pi^-+d\rightarrow 2n+\pi^0$; parity of neutral meson, W. Chinowsky and J. Steinberger—1476
Remarks on antiproton, T. Regge, S. Okubo, and R. Marshak—1810(A)
Remarks on strangeness, S. Epstein—1809(A)
Single-meson production in nucleon-nuclei collisions, Albert D. Wheelon—974(A)
Speculations on heavy mesons, T. D. Lee and J. Orear—932(L)
Spin of τ^+ meson, D. M. Ritson, A. Odian, B. T. Feld, and A. Wattenberg—1263(A); B. T. Feld, A. C. Odian, D. M. Ritson, and A. Wattenberg—1539(L)
Strange cosmic-ray event, C. H. Skeen and W. Z. Osborne—1797(A)
Unstable $_1H^4$ fragment from capture of a Σ^- hyperon, Marcel Schein, D. M. Haskin, and Daniel Leenov—1455
Yield of π^0 photomesons as function of atomic number, J. D. Anderson, R. W. Kenney, and C. A. McDonald—1798(A)
Metals (see **Crystalline State**)
Metastable Atoms (see **Atomic Structure and Spectra**)
Metastable Molecules (see **Molecular Structure and Spectra**)
Meteorology (see **Geophysics**)
Methods and Instruments
Analysis of nuclear emulsion tracks by scattering measurements, John S. Urban and John J. McClure—1797(A)
Angular momentum and energy of ions in magneto-ionic isotope separator, Joseph Slepian—1238(A)
Apparatus for new magnetism laboratory, Charles F. Squire—966(A)
Apparent length of tracks in nuclear emulsion, T. A. Brody—972(A)
Bistable solid state opto-electronic devices, E. E. Loebner—1239(A)
Boron trimethyl counters, G. A. Ferguson, C. W. Peters, and F. E. Jablonski—1239(A)
CdS photorectifier, Lawrence C. Greene—978(A)
Čerenkov counter as high-energy photon spectrometer, I. Filosofo—1246(A)
Čerenkov counter for high-energy cosmic rays, D. C. Moore and R. J. Hanson—972(A)
Characteristics of new Argonne fast-neutron chopper, L. M. Bollinger, R. E. Coté, and J. M. LeBlanc—1239(A)
Crystal engineering: New concept in crystallography, R. Pepinsky—971(A)
Determination of magnetic field strength H and its vector potential A in terms of magnetic field strength H_0 on plane surface, with application to spiral ridged FFAG accelerator, Edward S. Akeley—972(A)
Determination of surface resistivity of metal surfaces by Q measurement, A. R. Quinton and R. Beringer—1549(A)
Developments in statistical approach to x-ray crystal analysis, V. Vand and R. Pepinsky—970(A)
Double-channel magnetic β-ray spectrometer for short-lived activities, C. R. Sun and Byron T. Wright—1793(A)
Effects of operating proportional counters in high γ fields, J. T. Bracken, E. A. Rollor, and J. A. Mohrbacher—972(A)
Efficiency of ZnS—plastic counters for fast neutrons, W. J. Rhein—972(A)
Electron analog, G. K. Green, E. D. Courant, L. J. Haworth, and H. S. Snyder—1268(A)
Electron analog—construction, D. D. Jacobus, C. L. Gould, J. J. Grisoli, and I. J. Polk—1268(A)
Electron analog—electrical system, J. G. Cottingham, N. C. Christofilos, M. Plotkin, E. C. Raka, and R. H. Rhéaume—1269(A)
Electron analog—initial setup, J. Spiro, J. G. Cottingham, E. D. Courant, and R. R. Kassner—1269(A)
Electron analog—performance and interpretation. I., E. C. Raka, E. D. Courant, R. R. Kassner, L. J. Laslett, H. S. Snyder, and J. Spiro—1269(A); II., E. D. Courant, R. R. Kassner, E. C. Raka, Lloyd Smith, and I. Spiro—1269(A)
Electron models of relativistic constant-frequency cyclotrons, Robert V. Pyle, Elmer L. Kelly, J. Reginald Richardson, and Robert L. Thornton—1804(A)
Energy resolution obtainable with 2-Mev H_2^+ beam, D. F. Herring, R. A. Douglas, E. A. Silverstein, and Ren Chiba—1239(A)
Evapor-ion pump behavior with noble gases, Igor Alexeff and Edward C. Peterson—1239(A)
FFAG (fixed field alternating gradient) electron cyclotron, Tihiro Ohkawa—1247(A)
Gated phototube for fast pulse operation, D. V. Breitenbecher—978(A)
High-intensity ion sources, C. B. Mills—1233(A)
Instrument for measurement of information stored in photographic film, A. S. Silvidi, G. K. Schoepfle, K. L. Warren, F. L. Brooks, and M. Horowitz—979(A)
Ionization of cloud-chamber tracks, E. K. Björnerud—972(A)
Isotopic separation by magneto-ionic expansion, Joseph Slepian—1233(A)
Laboratory vacuum fittings and standardization of vacuum fittings, W. G. Wadey—1549(A)
Liquid He bubble chamber, W. M. Fairbank, E. M. Harth, M. E. Blevins, and G. G. Slaughter—971(A)
Low-voltage magnet and regulated power supply, R. C. Mobley, C. H. Blakewood, and D. C. Ralph—1242(A)
Measurement of magnetic field gradients by Hall effect, R. D. Redin and G. C. Danielson—1252(A)
Microtron injector for electron synchrotrons, H. F. Kaiser—1246(A)
Monte Carlo calculation on Čerenkov counters, Taketora Yamagata and Megumu Yoshimine—1246(A)
Negative H ion source, J. A. Weinman, J. R. Cameron, and R. G. Herb—1239(A)
Neutron detection with BaF^2 scintillator, Norman A. Bostrom, Emmett L. Hudspeth, and Ira L. Morgan—973(A)
Neutron dosimeter with uniform sensitivity from 0.1 to 3.0 Mev, J. De Pangher and W. C. Roesch—1793(A)

New method for determining range of low-energy electrons in solids, J. E. Holliday and E. J. Sternglass—1238(A)
Nonlinear oscillators with constant time delay, W. J. Cunningham—1549(A)
Nuclear γ-ray scattering techniques, G. E. Pugh, R. Gomez, D. H. Frisch, and G. S. Janes—1245(A)
Observations on pion tracks in liquid hydrogen bubble chamber, D. E. Nagle and R. H. Hildebrand—959(A)
Obtaining high temperatures for nuclear fusion, R. E. Vollrath and J. A. R. Samson—1793(A)
Phase centers of microwave antennas, David Carter—966(A)
Photometric mass determinations in multiplate cloud chamber, David O. Caldwell and Yash Pal—1803(A)
Precision of microwave spectrographs, M. W. P. Strandberg and M. Peter—963(A)
Preparation of thin N^{16} targets, F. B. Hagedorn—1793(A)
Present limitations of x-ray analyses of organic natural products, O. Cano-Corona and R. Pepinsky—970(A)
Properties of halogen-quenched Geiger counters, H. Sherman—972(A)
Pulse characteristics of CdSe crystals, T. Fields, E. J. Schillinger, and J. Kenski—964(A)
Quantum yield of CdS photovoltaic cell, R. E. Marburger, D. C. Reynolds, L. L. Antes, and R. S. Hogan—978(A)
Recoil-coincidence method for producing monoenergetic *d-d* neutrons, W. Franzen, P. Huber, and L. Schellenberg—1239(A)
Semiabsolute electrostatic voltmeter, José Mireles Malpica—967(A)
Semiabsolute measurements of voltage and current, José Mireles Malpica—975(A)
Small model FFAG (fixed field alternating gradient) Betatron. I. General description, K. M. Terwilliger, L. W. Jones, F. T. Cole, D. W. Kerst, and R. O. Haxby—1246(A); II. Design calculations, F. T. Cole and D. W. Kerst—1246(A); III. Preliminary experimental results, L. W. Jones and K. M. Terwilliger—1247(A)
Stripline or microwave printed circuits, J. W. Christian—1549(A)
Studies with three-dee three-phase proton cyclotron, Myron Heusinkveld, Mark Jakobson, Lawrence Rudy, Bob H. Smith, and Byron T. Wright—1804(A)
Systematic application of physical and mathematical methods to exploitation of Mexican oil fields, A. Romero-Juárez and J. Hefferan V—965(A)
Theoretical study of relativistic constant-frequency cyclotrons, David L. Judd—1804(A)
Theory of orbits in FFAG (fixed field alternating gradient) accelerators, Keith R. Symon—1247(A)
Third-order aberration and focusing with sector-shaped magnetic field, D. F. Dempsey, W. C. Miller, and B. Waldman—1240(A)
Total-absorption spectrometer measurements of γ rays emitted from targets bombarded with 6.2-Bev protons, Roger W. Wallace, Malvern H. L. Jester, and John M. Brabant—962(A)
Transmission secondary electron multiplication for high resolution counting and imaging, E. J. Sternglass and M. M. Wachtel—1238(A)
Use of electric arc heating in ultra-high temperature aerodynamics, R. W. Perry and D. E. Bloxsom—968(A)
Use of field emission microscope for investigating surface conditions on alloy, L. A. D'Asaro—1258(A)
Vibratory gyro mass flowmeter, Wilfred Roth—1549(A)

Microwaves (see also **Atomic Structure and Spectra; Magnetic Resonance; Molecular Structure and Spectra; Nuclear Moments and Spin**)
Attenuation of 1-cm microwaves by abnormal dc discharge in He, Z. Geller and W. Low—1240(A)
Interaction of electromagnetic waves of rf in isothermal plasmas: Collision cross section of He atoms and ions for electrons, J. M. Anderson and L. Goldstein—1037
Phase centers of microwave antennas, David Carter—966(A)
Precision of microwave spectrographs, M. W. P. Strandberg and M. Peter—963(A)
Superconductivity at mm wave frequencies, Gilbert S. Blevins, Walter Gordy, and William M. Fairbank—1215(L)

Miscellaneous
A certain blindness in physicists, W. M. Pierce—979(A)

Mobility of Ions and Electrons (see **Ions and Electrons, Mobility**)

Molecular Aggregates
Electrical conduction in Plexiglas, Raymond J. Munick—1256(A)
Intermolecular force fields in high polymers composed of alternating dipole chains, Werner Brandt—969(A)
Perturbation calculation of volume exclusion effect, Ira Jacobs—1257(A)
Reduction of optical reflectivity of glass by positive ion bombardment, R. L. Hines—1267(A)
Soft x-ray absorption of Te and vitreous and metallic Se, M. Parker Givens, Charles J. Koester, and William L. Goffe—1112
Time dependence of mechanical breakdown phenomena, Bernard D. Coleman—1257(A)

Molecular Beams (see **Atomic and Molecular Beams**)

Molecular Structure and Spectra
Continuum of XeHg′ molecule, Carl Kenty—1231(A)
Electron impact studies with trimethylamine, Herman Branson and L. B. Garner, II—964(A)
Electron spin coupling in polyatomic molecules, R. S. Henderson—723
Excited states of oxygen from energy transfer and light absorption, David H. Volman—963(A)
Improved value of velocity of light derived from band spectrum method, D. H. Rank, H. E. Bennett, and J. M. Bennett—993
Intensity of vibronic bands in 3000–5000 A absorption system of ClO_2, J. K. Ward and C. M. Loyd—963(A)
Light absorption and photoionization in NO and N_2O, W. C. Walker and G. L. Weissler—1231(A)
Microwave spectra of free radicals OH and OD, G. C. Dousmanis, T. M. Sanders, Jr., and C. H. Townes—1735
Normal coordinate treatment for out-of-plane vibrations of ethylene type molecules, J. M. Dowling—1267(A)
Normal coordinate treatments and thermodynamic properties of $PFCl_3$ and $POFCl_3$, Edward A. Piotrowski and Joseph S. Ziomek—1267(A)
Perturbation calculation of volume exclusion effect, Ira Jacobs—1257(A)
Potential constants for $CHDClBr$, CH_3F_3, CD_3F_3, and $CHDF_2$ molecules, A. G. Meister, J. M. Dowling, A. N. Takata, and A. J. Bielecki—1267(A)
Pure quadrupole spectra of CH_3I and CF_3I vapors, Fred Sterzer and Yardley Beers—1174
Quadrupole spectrum of $BiCl_3$, Hugh G. Robinson—1731
Stark effect in rapidly varying fields, S. H. Autler and C. H. Townes—703
Theory of hfs of NO molecule. II. Errata and some additional discussion, Chun C. Lin and Masataka Mizushima—1726

Moments, Nuclear (see **Nuclear Moments and Spin**)

Moments of Molecules (see **Molecular Structure and Spectra**)

Neutrino (see also **Nuclear Spectra; Radioactivity**)
Spectrometry of neutrino recoils of A^{37}, Arthur H. Snell and Frances Pleasonton—1396
Neutron Diffraction (see **Diffraction; Scattering of Neutrons**)
Neutrons (see **Elementary Particle Interactions**)
Noise
Excess noise in plastically deformed Ge, James J. Brophy—1261(A)
Fluctuations on damped transmission line, C. W. McCombie—444
Hall effect noise, James J. Brophy and Norman Rostoker—754(L)
Quantum theory of fluctuations, Hans Ekstein and Norman Rostoker—1023
Nuclear Fission
β^- energy distribution from thermal fission of U^{235}, C. O. Muehlhause and S. Oleksa—1266(A)
Distribution of number of prompt neutrons from spontaneous fission of Pu^{240}, J. E. Hammel and J. F. Kephart—190
Electron capture decay of Am^{254} and spontaneous fission half-life of Pu^{244}, P. R. Fields, J. E. Gindler, A. L. Harkness, M. H. Studier, J. R. Huizenga, and A. M. Friedman—172
Energy dependence of η for U^{235} in region 0.04–1.0 ev, J. R. Smith and E. H. Magleby—1266(A)
Energy spectrum of neutrons from spontaneous fission of Cf^{252}, Elis Hjalmar, Hilding Slätis, and Stanley G. Thompson—1542(L)
Fission product yields of U bombarded with deuterons of various energies (20–190 Mev), Harry G. Hicks, Peter C. Stevenson, Richard S. Gilbert, and William H. Hutchin—1284
Measurement of energy variation of neutron multiplication, η, for U^{233}, U^{235}, and Cu^{239} in thermal region, H. Palevsky, R. L. Zimmerman, R. M. Eisberg, and D. J. Hughes—1266(A)
Neutron-induced fission cross sections of U^{234} and U^{236}, R. W. Lamphere and R. E. Greene—763
Radiochemical studies of high-energy fission process, Harry G. Hicks and Richard S. Gilbert—1286
Systematics of fission asymmetry, W. J. Swiatecki—936(L)
Systematics of spontaneous fission half-lives, W. J. Swiatecki—937(L)
Nuclear Forces (see **Elementary Particle Interactions; Field Theory; Nuclear Structure Theory**)
Nuclear Induction (see **Magnetic Resonance; Nuclear Moments and Spin**)
Nuclear Isomers (see **Nuclear Spectra; Radioactivity**)
Nuclear Moments and Spin
Anomalous magnetic moment of nucleon, Kurt Haller and Marvin H. Friedman—1501
Electric quadrupole moment and corrections to magnetic moment of deuteron for velocity-dependent tensor forces, L. Estrada—956(A)
Empirical correlation of nuclear magnetic moments, R. K. Osborn and E. D. Klema—822
Nuclear moments in *jj*-coupling, S. Sengupta—939(L)
Nuclear moments of Gd from optical hfs, F. A. Jenkins and D. R. Speck—973(A)
Nuclear moments of Mo^{95}, Mo^{97}, Zr^{91}, I^{127}, Sb^{121}, and Sb^{123}, Kiyoshi Murakawa—1369
Nuclear spin and magnetic moment of 50-day In^{114m}, L. S. Goodman and S. Wexler—1245(A)
Nuclear spin and magnetic moment of 54-min In^{116m}, L. S. Goodman and S. Wexler—1796(A)
Pure quadrupole spectra of CH_3I and CF_3I vapors, Fred Sterzer and Yardley Beers—1174
Quadrupole broadening of nuclear magnetic resonance lines by reversible axial stress, R. G. Shulman, B. J. Wyluda, and H. J. Hrostowski—1792(A)
Quadrupole polarization of charge-clouds in ions, T. P. Das and R. Bersohn—1792(A)
Quadrupole spectrum of BiCl$_3$, Hugh G. Robinson—1731
Spatial extension of proton magnetic moment from hfs of hydrogen, W. M. Moellering, A. C. Zemach, A. Klein, and F. E. Low—441(L)
Thermodynamics of irreversible processes and Overhauser nuclear polarization effect, W. A. Barker and A. Mencher—1224(L)
Nuclear Photoeffects
$C^{12}(\gamma,n)$ curve near threshold, B. M. Spicer and A. S. Penfold—1375
Detailed study of $O^{16}(\gamma,n)O^{15}$ reaction, A. S. Penfold and B. M. Spicer—1377
Deuteron-model calculation of high-energy nuclear photoeffect, K. G. Dedrick—58
Electro- and photodisintegration cross sections of Cu^{63}, M. B. Scott, A. O. Hanson, and D. W. Kerst—209
(γ,p) reaction in A^{40}, B. M. Spicer—791
High-energy photoneutron-proton ejection from nuclei, Allen Odian, Bernard Feld, William Rankin, Peter Stein, Albert Wattenberg, and Roy Weinstein—1241(A)
High-energy photoproton emission at 175°, C. A. Tatro and T. R. Palfrey, Jr.—1265(A)
Inelastic scattering of photons from Au^{197}, L. Meyer-Schützmeister and V. L. Telegdi—961(A)
Isobar role in two-nucleon processes: Deuteron photoeffect—1522
$Mg(\gamma,n)$ cross section, Paul F. Yergin and Burton P. Fabricand—1249(A)
Nuclear scattering of low-energy photons, J. L. Burkhardt—192
Photodisintegration of C^{12} and O^{16}, F. I. Havliček and B. Dobovišek—1355
Photodisintegration of Li and He near 200 Mev, J. H. Smith and M. Q. Barton—1265(A)
Photoexcitation of isomeric state of In^{115}, J. L. Burkhardt, E. J. Winhold, and T. H. Dupree—199
Photoneutron angular distribution from carbon, B. P. Fabricand, B. Allison, and J. Halpern—1249(A)
Photoneutron effect in $Zr^{90}(\gamma,n)Zr^{89}$ and $Zr^{96}(\gamma,n)Zr^{95m}$, John D. Fox and Peter Axel—1249(A)
Photonuclear yields of N^{17}, Daryl Reagan—113
Photoproduction of neutral pions from protons at forward pion angles, W. S. McDonald, Vincent Peterson, and Dale R. Corson—1799(A)
Photoproduction of π-meson pairs in hydrogen, F. Zachariasen—1809(A)
Photoproduction of π^0 mesons in He, E. L. Goldwasser and L. J. Koester, Jr.—1255(A)
π^+ photomeson production from various nuclei at 135°, William Imhof, V. Perez-Mendez, and H. Easterday—1798(A)
π^+ photoproduction ratio of deuterium to hydrogen, K. M. Crowe, R. M. Friedman, and D. C. Hagerman—1799(A)
Pion-pair photoproduction, R. M. Friedman and K. M. Crowe—1799(A)
$Sr^{86,87,88}$, Y^{89}, Zr^{90} (γ,n) cross sections, Paul F. Yergin and Burton P. Fabricand—1269(A)
Yield of π^0 photomesons as function of atomic number, J. D. Anderson, R. W. Kenney, and C. A. McDonald—1798(A)
Nuclear Reactions, General (see also **Elementary Particle Interactions; Scattering**)
Agreement of classical and quantum Coulomb excitation integrals, John P. Lazarus and S. Sack—376

Angular distribution of γ rays in Coulomb excitation, G. Breit, M. E. Ebel, and F. D. Benedict—429(L); F. D. Benedict and G. Tice—1545(L)
Anomaly in nuclear energy level density measurements, G. Igo and H. E. Wegner—1796(A)
Collision matrix for (n,d) and (p,d) reactions, R. G. Thomas—25
Coulomb excitation directional correlation, M. Goldstein, J. L. McHale, R. M. Thaler, and L. C. Biedenharn—436(L)
Cross sections and complex potential, C. E. Porter—935(L)
Cross sections in deuterium at high energies, R. J. Glauber—242
Effects of finite amplitude in Coulomb excitation, G. Breit and J. P. Lazarus—942(L)
Electro- and photodisintegration cross sections of Cu^{63}, M. B. Scott, A. O. Hanson, and D. W. Kerst—209
Excitation function for reaction $Be^9(N^{14},\alpha n)F^{18}$, H. L. Reynolds and A. Zucker—226
Nucleon-nucleus interaction with polarization, Erich Vogt—957(A)
Phase-shift analysis of single-channel reactions, Harry Lustig and J. M. Blatt—777
Quantum calculation of Coulomb excitation, L. C. Biedenharn, J. L. McHale, and R. M. Thaler—376
Scattering by velocity-dependent potential, Ignacio Renero—956(A)
Scattering length and effective range for velocity-dependent tensor forces, A. Mondragón—956(A)
Soluble problem in theory of Coulomb excitation, L. C. Biedenharn and C. M. Class—1790(E)

Nuclear Reactions Induced by α Particles and He^3 (see also **Scattering of α Particles**)

Angular distribution of protons from $Be^9(He^3,p)B^{11}$ reaction, H. D. Holmgren, W. E. Kunz, and M. L. Bullock—1253(A)
Angular distributions of protons from $Be^9(He^3,p)B^{11}$, H. D. Holmgren, M. L. Bullock, and W. E. Kunz—436(L)
$Be^9(\alpha,\alpha')$, $Be^9(\alpha,d')$ reactions, V. K. Rasmussen, D. W. Miller, M. B. Sampson, and U. C. Gupta—851
$Be^9(d,d')$ and $Be^9(\alpha,\alpha')$ reactions, D. W. Miller, V. K. Rasmussen, M. B. Sampson, and U. C. Gupta—1253(A)
Coulomb excitation of Cu, Zn, As, Se, and Ru, G. M. Temmer and N. P. Heydenburg—961(A)
Coulomb excitation of energy levels in Br and Re, E. A. Wolicki, L. W. Fagg, and E. H. Geer—1265(A)
Coulomb excitation of In^{115}, I^{127}, Ta^{181}, Th^{232}, and U^{238}, Ajay S. Divatia, Robert H. Davis, R. D. Moffat, and D. A. Lind—1266(A)
Coulomb excitation of In^{115m} by α particles, R. R. McLeod—1265(A)
Coulomb excitation of rare-earth nuclei with α particles, N. P. Heydenburg and G. M. Temmer—150
Coulomb excitation of Te and Ag, L. W. Fagg, A. Wolicki, R. O. Bondelid, K. L. Dunning, and S. Snyder—1299
Differential cross sections for scattering of charged particles by Be, R. G. Summers-Gill—1795(A)
Electrostatic analysis of nuclear reaction energies, IV, Ren Chiba, R. A. Douglas, J. W. Broer, D. F. Herring, and E. A. Silverstein—1253(A)
Excitation functions for α-induced reactions on Pb, Walter John—1265(A)
γ rays from He^3 bombardment of deuterium, W. E. Kunz, J. W. Butler, and H. D. Holmgren—1252(A)
γ rays from reactions $Be^9(\alpha,n\gamma)C^{12}$, $C^{12}(d,p\gamma)C^{13}$, $N^{14}(d,p\gamma)N^{15}$, and $N^{14}(d,n\gamma)O^{15}$, R. D. Bent, T. W. Bonner, J. H. McCrary, and W. A. Ranken—771
Internal conversion electrons from electric excitation of Ta^{181}, Au^{197}, and Pt^{198}, E. M. Bernstein and H. W. Lewis—1345
$Li^7(\alpha,n)B^{10}$ reaction, A. B. Robbins—1549(A)
Protons from bombardment of several elements with 40-Mev α particles, R. M. Eisberg, G. Igo, and H. E. Wegner—961(A); 1309

Nuclear Reactions Induced by Deuterons and Tritons (see also **Scattering of Deuterons and Tritons**)

Absolute cross sections for deuterons on Be, Robert E. Heft and W. F. Libby—799
Analysis of $C^{13}+d$ reactions, M. T. McEllistrem—1253(A)
$Be^9(\alpha,\alpha')$, $Be^9(\alpha,d)$, and $Be^9(d,d')$ reactions, V. K. Rasmussen, D. W. Miller, M. B. Sampson, and U. C. Gupta—851
$Be^9(d,d')$ and $Be^9(\alpha,\alpha')$ reactions, D. W. Miller, V. K. Rasmussen, M. B. Sampson, and U. C. Gupta—1253(A)
$C^{14}+d$ reactions, R. A. Douglas, J. W. Broer, and Ren Chiba—1253(A)
Differential cross sections for scattering of charged particles by Be, R. G. Summers-Gill—1795(A)
(d,n) reactions in O^{16} and N^{14}, J. B. Marion, R. M. Brugger, and T. W. Bonner—46
(d,n) reactions on boron and carbon, J. B. Marion, T. W. Bonner, and C. F. Cook—847
(d,p) reactions from C^{12} and C^{13}, J. N. McGruer, E. K. Warburton, and R. S. Bender—235
Electrostatic analysis of nuclear reaction energies, IV, Ren Chiba, R. A. Douglas, J. W. Broer, D. F. Herring, and E. A. Silverstein—1253(A)
Energy levels of S^{32}, S^{33}, Cl^{35}, Cl^{37}, and Ba^{137}, C. H. Parjs, W. W. Buechner, and P. M. Endt—1317
15-Mev γ radiation from $B^{11}+d$, G. A. Barnes and R. W. Kavanagh—1796(A)
γ rays from deuteron bombardment of Al^{27} and P^{31}, R. D. Bent, T. W. Bonner, J. H. McCrary, and W. A. Ranken—774
γ rays from reactions $Be^9(\alpha,n\gamma)C^{12}$, $C^{12}(d,p\gamma)C^{13}$, $N^{14}(d,\gamma)N^{16}$, and $N^{14}(d,n\gamma)O^{15}$, R. D. Bent, T. W. Bonner, J. H. McCrary, and W. A. Ranken—771
Isotopic spin-selection rule violation in $O^{16}(d,\alpha)N^{14}$, C. P. Browne—1253(A)
Lifetimes of first excited states of Al^{28} and B^{10}, J. C. Severiens and S. S. Hanna—1254(A)
Reactions $C^{13}(d,n)N^{14}$ ground state and $C^{13}(d,t)C^{11}$ up to $E_d=20$ Mev, D. H. Wilkinson—32
Search for states in Li^7 and Be^9, R. W. Gelinas and S. S. Hanna—1253(A)
Si^{29} energy levels, A. Rubin, F. Ajzenberg, and Hans Mark—961(A)
$T(d,n)He^4$ reaction, 1–5 Mev, C. H. Johnson and A. Galonsky—1252(A)

Nuclear Reactions Induced by Mesons and Hyperons (see also **Elementary Particle Interactions; Mesons and Hyperons; Scattering of Mesons and Hyperons**)

Analysis of capture stars of K^--mesons from Berkeley Bevatron, D. M. Haskin, D. B. Williams, E. Goodman, and Marcel Schein—1263(A)
Capture of K^--meson with emission of high-energy electron as only visible prong, D. B. Williams, D. M. Haskin, M. Koshiba, and Marcel Schein—1547(L)
Cross sections in deuterium at high energies, R. J. Glauber—242
Electrons from muon capture, J. Steinberger and Harry B. Wolfe—1490
High-energy pion-proton cross sections, Baxter H. Armstrong—1798(A)
Hyperfragments in light elements produced by Berkeley Bevatron, Daniel Leenov, D. M. Haskin, and Marcel Schein—1263(A)

Nuclear Reactions Induced by Mesons and Hyperons (Continued)
Inelastic cross sections from 5-Bev π^- Bevatron beam in Pb and Al, John Ise, Jr., Andre Lagarrigue, and Robert V. Pyle—1799(A)
Interactions of negative K-particles at rest, Warren W. Chupp, Gerson Goldhaber, Sulamith Goldhaber, and Francis H. Webb—959(A)
Negative K-particle interactions in nuclear emulsion. I, Charles E. Violet, F. C. Gilbert, and R. Stephen White—1803(A); II, F. C. Gilbert, Charles E. Violet, and R. Stephen White—1803(A); III, R. Stephen White, F. C. Gilbert, and Charles E. Violet—1803(A)
Nuclear capture of negative K mesons in emulsion, W. F. Fry, J. Schneps, G. A. Snow, and M. S. Swami—1448
Nuclear collisions of 5.7-Bev protons and 3.0-Bev π^- mesons, R. E. Cavanaugh, D. M. Haskin, and Marcel Schein—1263(A)
π^--p collisions at 1.0 Bev, W. D. Walker and W. D. Shephard—1264(A)
Production of heavy unstable particles in π^--p collisions at 1.0 Bev, W. D. Shephard and W. D. Walker—1264(A)
Production of hyperons and K-mesons in high-energy π^- beam of Berkeley Bevatron, Marcel Schein and D. M. Haskin—1263(A)
Production of unstable particles in 4.5-Bev π^--p collisions, George Maenchen, William B. Fowler, Wilson M. Powell, George Saphir, and Robert W. Wright—1802(A)
Reaction $\pi^-+d\rightarrow 2n+\pi^0$; parity of neutral meson, W. Chinowsky and J. Steinberger—1476
Total cross section of H for 150-750 Mev positive and negative pions, S. J. Lindenbaum and Luke C. L. Yuan—306

Nuclear Reactions Induced by Neutrons (see also **Elementary Particle Interactions; Scattering of Neutrons**)
Absorption cross section of Au for slow neutrons measured on single crystal spectrometer, F. T. Gould, T. I. Taylor, and W. W. Havens, Jr.—1248(A)
Collision matrix for (n,d) and (p,d) reactions, R. G. Thomas—25
Cross sections in deuterium at high energies, R. J. Glauber—242
Excitation curve for $Be^9(n,\alpha)He^6$, Abdul R. Sattar, Ira L. Morgan and Emmett L. Hudspeth—960(A)
14-Mev (n,α) cross-section measurement, H. G. Blosser, C. D. Goodman, T. H. Handley, and M. L. Randolph—429(L)
γ rays excited by inelastic scattering of neutrons in various elements, M. A. Rothman, H. S. Hans, and C. E. Mandeville—83
Inelastic and elastic scattering of 1.7-Mev neutrons, S. D. Bloom, G. N. Glasoe, C. O. Muehlhause, and H. E. Wegner—1248(A)
Inelastic scattering of neutrons from Fe by time of flight, L. Cranberg and J. S. Levin—434(L)
Low-energy neutron scattering and bound state problem, R. D. Lawson—957(A)
Measurement of $\bar{\Gamma}_n^0/D$ ratio by average cross sections, D. J. Hughes and V. E. Pilcher—1249(A)
Meson production in n-p collisions by Cosmotron-produced neutrons with energies up to 1.5 Bev, W. A. Wallenmeyer—1255(A)
Neutron-capture gamma-ray spectra of V, Co, Ti, Fe, Cr, Au, Mn, and I, Melvin Reier and Morris H. Shamos—1302
Neutron detection with BaF_2 scintillator, Norman A. Bostrom, Emmett L. Hudspeth, and Ira L. Morgan—973(A)
Neutron-induced fission cross sections of U^{234} and U^{238}, R. W. Lamphere and R. E. Greene—763
Neutron-induced reactions in F, Jerry B. Marion and Robert M. Brugger—69
Neutron resonance parameters and total cross sections in U^{238}, O. D. Simpson, R. G. Fluharty, F. B. Simpson, and R. M. Brugger—1249(A)
Neutron resonances in U^{238} and U^{235}, V. L. Sailor—1249(A)
Neutron total cross-section measurements between 13.0 and 16.2 Mev, M. Mazari, F. Alba, and V. Serment—972(A)
Neutron total cross section of $_{92}U^{235}$ in ev region, V. E. Pilcher, J. A. Harvey, and K. K. Seth—1248(A)
Neutron transmission measurements on Br and Se, J. M. LeBlanc, L. M. Bollinger, and R. E. Coté—1248(A)
Nonelastic cross sections at 14 Mev, M. H. MacGregor, William P. Ball, and Rex Booth—1793(A)
Nonelastic scattering cross sections for fast neutrons, H. L. Taylor, O. Lönsjö, and T. W. Bonner—174
Pickup reactions $F^{19}(n,d)O^{18}$, F. L. Ribe—1254(A)
Polarization in theory of giant-resonances of neutron scattering, A. M. Lane and L. Verlet—956(A)
Poles of S-matrix for cloudy crystal ball model, Juan Manuel Lozano—956(A)
Production of pairs in capture of slow neutrons by protons, A. T. Peaslee, Jr.—974(A)
Production of Y^{88m}, Ba^{137m}, and Hg^{199m} by inelastic neutron scattering, C. P. Swann and F. R. Metzger—1329
Radiation widths in slow-neutron resonances, H. H. Landon—1414
Slow-neutron resonances in Re, G. Igo—1338
Slow-neutron resonances of Mn, Bi, and Se, L. M. Bollinger, D. A. Dahlberg, R. R. Palmer, and G. E. Thomas—126
Theory of neutron reactions with nuclei at low energy, K. A. Brueckner, R. J. Eden, and N. C. Francis—891

Nuclear Reactions Induced by Protons (see also **Elementary Particle Interactions; Scattering of Protons**)
α spectrum from $Li^7(p,\gamma)Be^{8*}(\alpha)He^4$, E. C. Lavier, S. S. Hanna, and R. W. Gelinas—1552(A)
α-α angular correlations in $B^{11}(p,\alpha\alpha)He^4$, E. H. Geer, E. B. Nelson, and E. A. Wolicki—215
Angular distribution of γ rays in Coulomb excitation, G. Breit, M. E. Ebel, and F. D. Benedict—429(L); F. D. Benedict and G. Tice—1545(L)
Collision matrix for (n,d) and (p,d) reactions, R. G. Thomas—25
Coulomb excitation directional correlation, M. Goldstein, J. L. McHale, R. M. Thaler, and L. C. Biedenharn—436(L)
Coulomb excitation of energy levels in Br and Re, E. A. Wolicki, L. W. Fagg, and E. H. Geer—1265(A)
Coulomb excitation of In^{115}, I^{127}, Ta^{181}, Th^{232}, and U^{238}, Ajay S. Divatia, Robert H. Davis, R. D. Moffat, and D. A. Lind—1266(A)
Coulomb excitation of Re, In, and Hg by protons, Robert H. Davis, Ajay S. Divatia, R. D. Moffat, and D. A. Lind—1266(A)
Coulomb excitation of Sm, B. E. Simmons, K. F. Famularo, and G. D. Freier—1265(A)
Coulomb excitation of Te and Ag, L. W. Fagg, E. A. Wolicki, R. O. Bondelid, K. L. Dunning, and S. Snyder—1299
Cross sections in deuterium at high energies, R. J. Glauber—242
Differential cross sections for scattering of charged particles by Be, R. G. Summers-Gill—1795(A)
Electric excitation of certain rare-earth nuclei by protons, Hans Mark and George T. Paulissen—813

Excited states of O^{18} from proton bombardment of N^{15}, R. P[illegible]con and S. Bashkin—1254(A)
5.3-M[illegible]rgy level in Mg^{24} following decay of Na^{24}, F. M[illegible]nnovec and C. S. Cook—1254(A)
F^{19} energy levels, H. A. Hill and J. M. Blair—961(A)
γ-ray and neutron yields from proton bombardment of boron, J. K. Bair, J. D. Kington, and H. B. Willard—21
Inelastic proton scattering from V. W. W. Buechner, C. M. Braams, and A. Sperduto—1387
Inelastic scattering of 19-Mev protons by O^{16}, W. F. Hornyak and R. Sherr—1409
Inelastic scattering of protons from F^{19}, B. J. Toppel, D. H. Wilkinson, and D. E. Alburger—1254(A)
Inelastic scattering of protons from Li^7, C^{12}, Mg^{24}, and Si^{28}, Homer E. Conzett—1794(A)
Internal conversion electrons from electric excitation of Ta^{180}, Au^{197}, and Pt^{195}, E. M. Bernstein and H. W. Lewis—1345
$K(p,p')$ and $K(p,\alpha)$ reactions, A. Sperduto and W. W. Buechner—961(A)
$Li(p,n)$ reaction near threshold, H. W. Newson—960(A)
$Li^7(p,p'\gamma)$ and $Li^7(p,\gamma)$ reactions, R. M. Williamson and K. W. Jones—960(A)
Magnetic analysis of $Be^9(p,p')Be^{9*}$ and $Be^9(p,pn)Be^8$ reactions, C. R. Gossett, G. C. Phillips, J. P. Schiffer, and P. M. Windham—203
Neutral pion production in p-p collisions, Robert K. Squire and Burton J. Moyer—1798(A)
Neutron yields from 32-Mev protons on thick targets, George P. Millburn, Burton J. Moyer, Yuin-Kwei Tai, and Selig N. Kaplan—1793(A)
Neutrons from proton bombardment of B^{11}, F. Ajzenberg, A. Rubin, G. D. Johnson, and M. Mazari—960(A)
Nuclear collisions of 5.7-Bev protons and 3.0-Bev π^- mesons, R. E. Cavanaugh, D. M. Haskin, and Marcel Schein—1263(A)
Nuclear reactions $Sc^{45}(p,n)Ti^{45}$, $Cu^{63}(p,n)Zn^{63}$, R. M. Brugger, T. W. Bonner, and J. B. Marion—84
(p,α) reactions in chlorine and potassium, E. Almqvist, R. L. Clarke, and E. B. Paul—1265(A)
(p,γ) cross sections, Bernard L. Cohen—206
(p,n) reactions at 12 Mev, H. G. Blosser and T. H. Handley—1340
p-p interactions at 3 Bev, R. Cester, T. F. Hoang, and A. Kernan—940(L)
p-p interactions at 5.3 Bev, Robert W. Wright, George Saphir, Wilson M. Powell, George Maenchen, and William B. Fowler—1802(A)
Proton-nucleus collisions at 6 Bev, U. Haber-Schaim—1263(A)
$T^3(p,n)He^3$, $Li^7(p,n)Be^7$, $Be^9(p,n)B^9$, and $F^{19}(p,n)N^{19}$ reactions, J. B. Marion, T. W. Bonner, and C. F. Cook—91
Total-absorption spectrometer measurements of γ rays emitted from targets bombarded with 6.2-Bev protons, Roger W. Wallace, Malvern H. L. Jester, and John M. Brabant—962(A)
$V^{51}(p,n)Cr^{51}$ reaction as 5- to 120-kev neutron source, J. H. Gibbons, R. L. Macklin, and H. W. Schmitt—167
Zn^{65} low-lying level structure, J. B. Marion and R. A. Chapman—1795(A)
Nuclear Scattering (see **Scattering**)
Nuclear Spectra (see also **Nuclear Reactions; Radioactivity**)
Am^{239} α-decay properties, Frank Asaro, F. S. Stephens, Jr., W. M. Gibson, R. A. Glass, and I. Perlman—1541(L)
Am^{242} isomers, radioactive decay, R. W. Hoff, H. Jaffe, T. O. Passell, F. S. Stephens, E. K. Hulet, and S. G. Thompson—1403
Am^{244} electron capture decay and spontaneous fission half-life of Pu^{244}, P. R. Fields, J. E. Gindler, A. L. Harkness, M. H. Studier, J. R. Huizenga, and A. M. Friedman—172
Angular correlation in β decay of neutron, J. M. Robson—933(L)
Angular distribution of γ rays in Coulomb excitation, G. Breit, M. E. Ebel, and F. D. Benedict—429(L); F. D. Benedict and G. Tice—1545(L)
Au^{198} conversion electrons, energy determination, D. R. Connors, W. C. Miller, and B. Waldman—1237(A)
Ba^{136} γ-γ angular correlation, Ernest D. Klema—66
C^{14}, N^{14*}, and O^{15} decay rates, R. Sherr, J. B. Gerhart, H. Horie, and W. F. Hornyak—945(L)
Ca^{47} decay, W. S. Lyon and T. H. Handley—1280
Ca^{49} decay, David W. Martin, S. Bradley Burson, and James M. Cork—1236(A)
Ce^{139} isomers, radioactivity, A. R. Brosi and B. H. Ketelle—169
$Cf^{250, 252}$ complex α and γ spectra, Frank Asaro, Frank S. Stephens, Jr., B. G. Harvey, and I. Perlman—137
Coulomb excitation directional correlation, M. Goldstein, J. L. McHale, R. M. Thaler, and L. C. Biedenharn—436(L)
Coulomb excitation of Cu, Zn, As, Se, and Ru, G. M. Temmer and N. P. Heydenburg—961(A)
Coulomb excitation of energy levels in Br and Re, E. A. Wolicki, L. W. Fagg, and E. H. Geer—1265(A)
Coulomb excitation of In^{115}, I^{127}, Ta^{181}, Th^{232}, and U^{238}, Ajay S. Divatia, Robert H. Davis, R. D. Moffat, and D. A. Lind—1266(A)
Coulomb excitation of In^{115m} by α particles, R. R. McLeod—1265(A)
Coulomb excitation of rare-earth nuclei with α particles, N. P. Heydenburg and G. M. Temmer—150
Coulomb excitation of Re, In, and Hg by protons, Robert H. Davis, Ajay S. Divatia, R. D. Moffat, and D. A. Lind—1266(A)
Coulomb excitation of Sm, B. E. Simmons, K. F. Famularo, and G. D. Freier—1265(A)
Coulomb excitation of Te and Ag, L. W. Fagg, E. A. Wolicki, R. O. Bondelid, K. L. Dunning, and S. Snyder—1299
Cr^{48} decay, R. van Lieshout, D. H. Greenberg, L. A. Ch. Koerts, and C. S. Wu—223
Cr^{51} spectrum of internal bremsstrahlung, S. G. Cohen and S. Ofer—856
Cs^{130} γ-γ directional correlations, A. E. Everett and M. J. Glaubman—955(A)
Cs^{130} decay, R. B. Duffield, M. E. Bunker, J. P. Mize, and J. W. Starner—1236(A)
Directional and polarization-direction correlations in Pb^{206} γ-γ cascades, G. T. Wood and P. S. Jastram—1237(A)
Directional correlation with gaseous In^{111} sources, L. M. Noble and R. M. Steffen—955(A)
Double K capture and single K capture with positron emission, Rolf G. Winter—142
Effects of finite amplitude in Coulomb excitation, G. Breit and J. P. Lazarus—942(L)
Electric excitation of certain rare-earth nuclei by protons, Hans Mark and George T. Paulissen—813
Electric-monopole transitions in atomic nuclei, E. L. Church and J. Weneser—943(L); 1241(A)
Electric multipole moments in j-j coupling, R. D. Lawson—845
Electron capture decay of Am^{244} and spontaneous fission half-life of Pu^{244}, P. R. Fields, J. E. Grindler, A. L. Harkness, M. H. Studier, J. R. Huizenga, and A. M. Friedman—172

Nuclear Spectra (Continued)
Energy levels of S^{30}, S^{35}, Cl^{38}, Cl^{38}, and Ba^{139}, C. H. Paris, W. W. Buechner, and P. M. Endt—1317
5.3-Mev energy level in Mg^{26} following decay of Na^{24}, F. M. Tomnovec and C. S. Cook—1254(A)
15-Mev γ radiation from $B^{11}+d$, C. A. Barnes and R. W. Kavanagh—1796(A)
F^{19} energy levels, H. A. Hill and J. M. Blair—961(A)
γ energies in Tc^{97} following K capture in Ru^{97}, J. M. Cork, M. K. Brice, L. C. Schmid, and R. G. Helmer—955(A)
γ-ray induced isomers with half-lives between 10^{-6} and 10^{-4} sec, Stanley H. Vegors, Jr., and Peter Axel—1238(A)
Ge^{73} excited states, E. Brun, W. E. Meyerhof, and J. J. Kraushaar—1795(A)
I^{128} investigation, N. Benczer, B. Farrelly, L. Koerts, and C. S. Wu—955(A)
In^{107} decay, Wayne A. Cassatt, Jr., and W. Wayne Meinke—1372
In^{114} 72-sec and 49-day decay, Lee Grodzins and Henry Motz—1236(A)
Inner bremsstrahlung from A^{37}, Torsten Lindqvist and Chien-Shiung Wu—145
Intermediate coupling in odd-odd nuclei, R. Adkins and J. G. Brennan—1790(E)
Internal conversion coefficients of low excited states of F^{19}, W. R. Mills, Jr., H. H. Hilton, III, and C. A. Barnes—1794(A)
Internal conversion electrons from electric excitation of Ta^{181}, Au^{197}, and Pt^{195}, E. M. Bernstein and H. W. Lewis—1345
Ir^{192} decay, L. L. Baggerly, Marmier F. Boehm, and J. W. M. DuMond—1364
K-series fluorescence yields of A^{38}, Cu^{65}, and In^{113}, G. R. Harrison, R. C. Crawford, and J. I. Hopkins—841
Lifetimes of first excited states of Al^{28} and B^{10}, J. C. Severiens and S. S. Hanna—1254(A)
Lu^{175} nuclear levels, J. P. Mize, M. E. Bunker, and J. W. Starner—1390
Matrix element relations in β decay theory and nuclear forces, T. Ahrens—974(A)
Mn^{56} first excited state, E. M. Bernstein and H. W. Lewis—1367
Mo^{91} disintegration, Norwood Gove, Fred A. Smith, and R. A. Becker—1236(A)
Ne^{20} decay, J. R. Penning and F. H. Schmidt—954(A)
Ne^{24} decay, B. J. Dropesky and A. W. Schardt—954(A)
Neutron-capture gamma-ray spectra of V, Co, Ti, Fe, Cr, Au, Mn, and I, Melvin Reier and Morris H. Shamos—1302
New type of selection rules in β decay of strongly deformed nuclei, G. Alaga—432(L)
Np^{237} α decay, L. B. Magnusson, D. W. Engelkemeir, M. S. Freedman, F. T. Porter, and F. Wagner, Jr.—1237(A)
Np^{239} decay, new γ rays, Harlan W. Lefevre, Edwin M. Kinderman, and Harold H. Van Tuyl—1374
Nuclear compressibility and the 0^+ states of O^{16} and C^{12}, R. A. Ferrell and W. M. Visscher—1796(A)
Os^{185} electron capture decay and Re^{185} excited states, Charles H. Pruett and Roger G. Wilkinson—1237(A)
Pa^{231} 4.1×10^{-9} second metastable state, D. Strominger and J. O. Rasmussen—844
Photoexcitation of isomeric state of In^{115}, J. L. Burkhardt, E. J. Winhold, and T. H. Dupree—199
Possibility of interpreting β-decay spectra in terms of nuclear forces, M. M. Miller and T. Ahrens—974(A)
Precision energy measurements of γ rays following decay of Bi^{207}, Avivi I. Yavin and Fred H. Schmidt—171
Pt^{191} decay, E. P. Tomlinson and R. A. Naumann—955(A)
Pu^{239} energy levels populated by β decay of Np^{239}, J. M. Hollander, W. G. Smith, and J. W. Mihelich—1238(A)
Radiations from 1− states in even-even nuclei, F. S. Stephens, Jr., Frank Asaro, and I. Perlman—1543(L)
Rb^{86} disintegration scheme, M. L. Perlman and Joan P. Welker—81
Rb^{84} K-capture-positron ratios for first forbidden transitions and relative probability of L- to K-electron capture, Joan P. Welker and M. Perlman—74
Rh^{106} and Ag^{106} decays, D. E. Alburger and B. J. Toppel—1357
Ru^{97} decay, J. M. Cork, M. K. Brice, L. C. Schmid, and R. G. Helmer—188
Sargent diagram and comparative half-lives for allowed K-capture transitions of nuclides with $Z\leqslant60$, L. S. Cheng—979(A)
Sc^{42}, new radioactive isotope, H. Morinaga—431(L)
Sc^{44} radioactivity, J. W. Blue and E. Bleuler—1324
Sc^{47} decay scheme, R. T. Nichols and E. N. Jensen—1407
Sc^{50}, H. Morinaga and E. Bleuler—1236(A)
Si^{28} energy levels, A. Rubin, F. Ajzenberg, and Hans Mark—961(A)
Sn^{110} half-life, S. W. Mead, M. D. Petroff, and W. O. Doggett—1794(A)
Soluble problem in theory of Coulomb excitation, L. C. Biedenharn and C. M. Class—1791(E)
Spectrometry of neutrino recoils of A^{37}, Arthur H. Snell and Frances Pleasonton—1396
Sr^{85} γ-ray branching, W. S. Lyon and R. R. Rickard—112
Statistical theory of delayed-coincidence experiments, Z. Bay, V. P. Henri, and H. Kanner—1197
Te^{125} and Te^{128} angular correlation measurements, Norman Goldberg and Sherman Frankel—1350
Te^{127} and Te^{129} ground-state disintegration schemes, M. C. Day, Jr., G. W. Eakins, and A. F. Voigt—796
Te^{129} disintegration, William E. Graves and Allan C. G. Mitchell—1236(A)
Tl^{195}, Tl^{197}, and Tl^{199m} radiochemical study, J. D. Knight and E. W. Baker—1334
Tm^{169}, Lu^{175}, and Lu^{177} nuclear levels as derived from radioactive isotopes of Yb, J. M. Cork, M. K. Brice, D. W. Martin, L. C. Schmid, and R. G. Helmer—1237(A)
Tm^{169} rotational states, Sven A. E. Johansson—835
W^{181} and W^{185} decay, W. E. Kreger, L. D. McIsaac, J. L. Mackin, and J. R. Lai—955(A)
Nuclear Structure Theory (see also **Nuclear Reactions**; **Nuclear Spectra**)
Anomaly in nuclear energy level density measurements, G. Igo and H. E. Wegner—1796(A)
C^{14}, N^{14*}, and O^{15} decay rates, R. Sherr, J. B. Gerhart, H. Horie, and W. F. Hornyak—945(L)
Deuteron-model calculation of high-energy nuclear photoeffect, K. G. Dedrick—58
Effect on x-ray fine structure of deviations from Coulomb field near nucleus, A. L. Schawlow and C. H. Townes—1273
Electric-monopole transitions in atomic nuclei, E. L. Church and J. Weneser—943(L); 1241(A)
Electric quadrupole moment and corrections to magnetic moment of deuteron for velocity-dependent tensor forces, L. Estrada—956(A)
Empirical correlation of nuclear magnetic moments, R. K. Osborn and E. D. Klema—822
Hole-particle relations and j-j coupling, R. W. King—1240(A)
Independent-particle model of nucleus. II. Weak surface coupling, Kenneth W. Ford and Carl Levinson—1; III. Ca isotopes, Carl Levinson and Kenneth W. Ford—13
Intermediate coupling in odd-odd nuclei, R. Adkins and J. G. Brennan—1790(E)

Isotopic spin impurity in light nuclei, William M. MacDonald—51
Localized orbitals in nuclear structure, R. K. Nesbet—228
Low-energy neutron scattering and bound state problem, R. D. Lawson—957(A)
L-S interaction in nuclei, L. S. Kisslinger—1240(A)
Many-body problem for strongly interacting particles. II. Linked cluster expansion, K. A. Brueckner—36
Matrix element relations in β-decay theory and nuclear forces, T. Ahrens—974(A)
Model for potential between nucleon and nucleus, C. L. Critchfield and Robert Lowen—956(A)
New type of selection rules in β decay of strongly deformed nuclei, G. Alaga—432(L)
Nuclear compressibility and 0^+ states of O^{16} and C^{12}, R. A. Ferrell and W. M. Visscher—1796(A)
Nuclear Hartree-Fock calculations, M. Rotenberg—439(L)
Nuclear moments in *jj*-coupling, S. Sengupta—939(L)
Nuclear radius and nuclear forces, S. D. Drell—97
Nucleon distribution in Ca^{40}, J. Callaway and R. D. Woods—956(A)
Nucleon-nucleus interaction with polarization, Erich Vogt—957(A)
Polarization in theory of giant resonances of neutron scattering, A. M. Lane and L. Verlet—956(A)
Poles of *S*-matrix for cloudy crystal ball model, Juan Manuel Lozano—956(A)
Possibility of interpreting β decay spectra in terms of nuclear forces, M. M. Miller and T. Ahrens—974(A)
Self-consistent treatment of nuclear independent-particle model, G. E. Tauber and T. Y. Wu—1240(A)
Strength function of nuclear energy levels, H. H. Barschall and S. E. Darden—1242(A)
Three-body contributions to triton binding energy, Ely M. Gelbard—1530

Optical Instruments (see **Methods and Instruments**)
Optical Properties (see also **Luminescence**)
Absorption cross section for light in perfect solids, D. L. Dexter—964(A)
Absorption of vacuum uv radiation by thin plastic films, G. L. Weissler and L. Z. Maudlin—1800(A)
CdS with Ag activator, John Lambe—1586
Detection of vacancies created by x-rays in NaCl, H. W. Etzel—1643
Dichroism of *F* and *M* absorption bands in KCl, C. Z. van Doorn and Y. Haven—753(L)
Electrical and optical properties of intermetallic compounds. IV. Mg_2Sn, R. F. Blunt, H. P. R. Frederikse, and W. R. Hosler—663
Electroluminescence of GaP, G. A. Wolff, R. A. Herbert, and J. D. Broder—1144
Faraday effect in gases—experiment and theory, L. R. Ingersoll and D. H. Liebenberg—963(A)
Faraday effect in Ge at room temperature, Richard R. Rau and M. E. Caspari—632
Frequencies and relative intensities of R_1 and R_2 bands in KCl, Robert Herman, M. C. Wallis, and R. F. Wallis—1267(A)
Infrared properties of Se, R. S. Caldwell and H. Y. Fan—1251(A)
Interpretation of optical properties of metal surfaces, S. Roberts—1667
Irradiation effects in some organic compounds, T. H. Anderson, R. D. Jordan, and R. S. Alger—964(A)
Light absorption and photoionization in NO and N_2O, W. C. Walker and G. L. Weissler—1231(A)
Longitudinal photomagnetoelectric effect in Ge, Gerhart Groetzinger and Jack Aron—975(A); Jack Aron and Gerhart Groetzinger—1128
Quantum yields of CdS photovoltaic cell, R. E. Marburger, D. C. Reynolds, L. I. Antes, and R. S. Hogan—978(A)
Reduction of optical reflectivity of glass by positive-ion bombardment, R. L. Hines—1267(A)
Reflectivity of several crystals in far infrared region between 20 and 200 microns, Hiroshi Yoshinaga—753(L)
Soft x-ray absorption of Te and vitreous and metallic Se, M. Parker Givens, Charles J. Koester, and William L. Goffe—1112
Visible light from Si *p-n* junction, Roger Newman—700
Zeeman effects and magnetic properties of Nd salts, G. H. Dieke and L. Heroux—965(A)

Pair Production (see **Electrons and Positrons**)
Phosphors and Phosphorescence (see **Luminescence; Semiconductors**)
Photoconductivity (see **Electrical Conductivity and Resistance**)
Photodisintegration (see **Nuclear Photoeffects**)
Photoelasticity (see **Elasticity and Plasticity**)
Photoelectric Effect (see **Electrical Properties**)
Photography and Photographic Emulsions (see **Methods and Instruments; Optical Properties**)
Photometry (see **Methods and Instruments; Optical Properties**)
Photons (see **Radiation**)
Photovoltaic Effect (see **Electrical Properties; Semiconductors**)
Piezoelectric Effect (see **Dielectrics and Dielectric Properties**)
Plasticity (see **Elasticity and Plasticity**)
Polarization, Electrical (see **Dielectrics and Dielectric Properties**)
Polymers (see **Molecular Aggregates**)
Positrons (see **Electrons and Positrons**)
Probability (see **Mathematical Methods**)
Proceedings of the American Physical Society
Meeting Held at Mexico City, Mexico, August 29–31, 1955 [Bull. Am. Phys. Soc. **30**, No. 5 (1955)]—952
Fall Meeting of the New York State Section at Clarkson College of Technology, Potsdam, New York, October 7 and 8, 1955—977
Fall Meeting of the Ohio Section at Wright-Patterson Air Force Base, Ohio, October 14 and 15, 1955—977
Eighth Annual Gaseous Electronics Conference at Schenectady, New York, October 20–22, 1955—1227
Fall Meeting of the New England Section at Yale University, New Haven Connecticut, November 12, 1955—1548
Thanksgiving Meeting at the University of Chicago, Chicago, Illinois, November 25 and 26, 1955 [Bull. Am. Phys. Soc. **30**, No. 7 (1955)]—1235
Winter Meeting on the Pacific Coast at Los Angeles, California, December 28, 29, and 30, 1955 [Bull. Am. Phys. Soc. **30**, No. 8 (1955)]—1790
Protons (see **Elementary Particle Interactions**)

Quantum Electrodynamics (see also **Field Theory**)
"Contact interaction" in relativistic energy of two-electron atoms, Ta-You Wu and G. E. Tauber—1767
Contribution of electron to pair production in atomic hydrogen, F. Rohrlich and J. Joseph—1241(A)
Internal structure of spinning particles, David Finkelstein—924
Multiple photon production from electron pair annihilation, J. Joseph—1241(A)
Radiative corrections to decay processes, R. E. Behrends, R. J. Finkelstein, and A. Sirlin—1809(A)
Spatial extension of proton magnetic moment from hfs of hydrogen, W. M. Moellering, A. C. Zemach, A. Klein, and F. E. Low—441(L)

Quantum Mechanics
Agreement of classical and quantum Coulomb excitation integrals, John P. Lazarus and S. Sack—370
Hamiltonian form of integral-spin wave equations, K. M. Case—1513
Hartree-Fock wave functions for Mn^{+4}, W. W. Piper and J. S. Prener—1250(A)
Inadmissible auxiliary conditions in quantized linear systems, J. K. Percus—1208
Phase-shift analysis of single-channel reactions, Harry Lustig and J. M. Blatt—777
Positional correlation study for system of two electrons, J. S. Evans and R. H. Tredgold—1250(A)
Quantum theory from nonquantal principles, Alfred Landé —979(A)
Quantum theory of fluctuations, Hans Ekstein and Norman Rostoker—1023
Schrödinger-like equation for measurement process, Richard Scalettar—1808(A)
Stark effect in rapidly varying fields, S. H. Autler and C. H. Townes—703
Theory of multiple-quantum transitions, M. N. Hack— 975(A)
Wave equations for arbitrary spin, C. Fronsdal—1810(A)
Wave functions and transition probabilities for light atoms, Huseyin Yilmaz—1148
Wave mechanical treatment of Fermi gas, Wilhelm Macke —992
Quenching of Radiation (see **Radiation**)

Radar (see **Methods and Instruments; Radiation**)
Radiation (see also **Gamma Rays; Range and Energy Loss; X-Rays**)
Application of light-scattering theory to measurement of density fluctuations in turbulent fluids, Howard A. Stine and Warren Winovich—968(A)
Bremsstrahlung differential cross-section measurements for 0.5- and 1.0-Mev electrons, J. W. Motz—1560
Bremsstrahlung spectrum from internal target of 22-Mev betatron, E. V. Weinstock and J. Halpern—1293
Čerenkov counter as high-energy photon spectrometer, I. Filosofo—1246(A)
Čerenkov counter for high-energy cosmic rays, D. C. Moore and R. J. Hanson—972(A)
γ-ray scattering by hydrogen, G. S. Janes, R. Gomez, G. E. Pugh, and D. H. Frisch—1245(A)
High-energy end of bremsstrahlung spectrum, Donald C. Hagerman and K. M. Crowe—869
Inner bremsstrahlung from A^{37}, Torsten Lindqvist and Chien-Shiung Wu—145
Monte Carlo calculation on Čerenkov counters, Taketora Yamagata and Megumu Yoshimine—1246(A)
Nuclear scattering of low-energy photons, J. L. Burkhardt—192
Polarization effects in electron-photon interactions, Cramer Schultz and Ross D. F. Thompson—1809(A)
Recombination radiation from Si, J. R. Haynes—1259(A)
Resonance irradiation of Hg vapor in nitrogen, J. A. Berberet and K. C. Clark—506
Scattering of 30- to 90-Mev γ rays by protons, C. L. Oxley and V. L. Telegdi—962(A)
Scattering of 30- to 95-Mev photons by protons, C. L. Oxley and V. L. Telegdi—435(L)
Tensor scattering matrix for electromagnetic field, David S. Saxon—1771
Thick-target bremsstrahlung spectra for 1.00-, 1.50-, and 2.00-Mev electrons, E. A. Edelsack and W. E. Kreger —973(A)
Z-dependence of bremsstrahlung in case of complete screening, K. L. Brown—1798(A)

Radio Waves (see **Radiation**)
Radioactivity (see also **Nuclear Spectra**)
Am^{239} α-decay properties, Frank Asaro, F. S. Stephens, Jr., W. M. Gibson, R. A. Glass, and I. Perlman— 1541(L)
Am^{244} electron capture decay, and spontaneous fission half-life of Pu^{244}, P. R. Fields, J. E. Gindler, A. L. Harkness, M. H. Studier, J. R. Huizenga, and A. M. Friedman —172
Angular correlation in β decay of neutron, J. M. Robson —933(L)
$Cf^{249, 250}$ complex α and γ spectra, Frank Asaro, Frank S. Stephens, Jr., B. G. Harvey, and I. Perlman—137
Double K capture and single K capture with positron emission, Rolf G. Winter—142
Matrix element relations in β-decay theory and nuclear forces, T. Ahrens—974(A)
New type of selection rules in β decay of strongly deformed nuclei, G. Alaga—432(L)
Np^{239} decay, new γ rays, Harlan W. Lefevre, Edwin M. Kinderman, and Harold H. Van Tuyl—1374
Pa^{231} 4.1×10^{-4} second metastable state, D. Strominger and J. O. Rasmussen—844
Possibility of interpreting β-decay spectra in terms of nuclear forces, M. M. Miller and T. Ahrens—974(A)
Sn^{119} half-life, S. W. Mead, M. D. Petroff, and W. O. Doggett—1794(A)
Theory of atomic perturbation in α decay, H. M. Schwartz —135
Tritium half-life, W. M. Jones—124
Raman Spectra (see **Molecular Structure and Spectra**)
Range and Energy Loss of Particles (see also **Scattering**)
Apparent length of tracks in nuclear emulsion, T. A. Brody—972(A)
Electron loss cross section for fast He atoms, C. F. Barnett and P. M. Stier—1268(A)
Energy loss of protons in metals, R. E. Pixley, M. Bader, and Ward Whaling—1805(A)
High-velocity particle ranges in emulsion, Walter H. Barkas, Paul H. Barrett, Pierre Cuer, Harry H. Heckman, Frances M. Smith, and Harold K. Ticho—1797(A)
Mean free path for discrete electron energy losses in metallic foils, A. W. Blackstock, R. H. Ritchie, and R. D. Birkhoff—1078
New method for determining range of low-energy electrons in solids, J. E. Holliday and E. J. Sternglass—1238(A)
Photometric mass determinations in multiplate cloud chamber, David O. Caldwell and Yash Pal—1803(A)
Range-energy relation and masses of new particles, David O. Caldwell—291
Relative stopping power of some metallic elements for 20-Mev protons, V. C. Burkig and K. R. MacKenzie— 1805(A)
Relative stopping power of various metals for 200-Mev protons, C. P. Sonett and K. R. MacKenzie—734
Transmission of positrons and electrons, H. H. Seliger —1029
Recombination (see **Molecular Structure and Spectra**)
Rectifiers (see **Electrical Conductivity and Resistance; Semiconductors**)
Relativity and Gravitation
Bending of light and falling rotators, F. J. Belinfante— 1250(A)
Relativistic theory of discrete momentum space and discrete space-time, E. L. Hill—1780
Torus model of elementary particles in which stability may be achieved by gravitational forces resulting from concentrated electromagnetic field, Winston H. Bostick— 1250(A)

Resistance, Electrical (see **Electrical Conductivity and Resistance**)
Resonance Radiation (see **Radiation**)

Scattering, General (see also **Diffraction; Elementary Particle Interactions; Nuclear Reactions; Range and Energy Loss of Particles**)
Analysis of nuclear emulsion tracks by scattering measurements, John S. Urban and John J. McClure—1797(A)
Mean-value calculations for spatial multiple scattering, Jean Snover Goldberg, Hartland S. Snyder, and William T. Scott—1013
Multiple isotropic scattering, Paul I. Richards—517
Nuclear scattering of low-energy photons, J. L. Burkhardt—192
Scattering by symmetric potential, R. J. Finkelstein and M. Moe—1775
Scattering by velocity-dependent potential, Ignacio Renero —956(A)
State vector normalization in formal scattering theory, Bryce S. DeWitt—905
Tensor scattering matrix for electromagnetic field, David S. Saxon—1771
Variational methods in scattering problems, Mildred M. Moe and David S. Saxon—1809(A)
Scattering of α Particles (see also **Nuclear Reactions Induced by α Particles and He⁴**)
Elastic scattering of 40-Mev α particles from light nuclei, G. Igo, H. E. Wegner, and R. M. Eisberg—1244(A)
Elastic scattering of 48-Mev α particles, Larry Schecter and R. E. Ellis—1805(A)
Scattering of α particles from He and 3-Mev state in Be^8, G. C. Phillips, J. L. Russell, and C. W. Reich—960(A)
Scattering of 22-Mev α particles by C^{12}, V. K. Rasmussen, D. W. Miller, and M. B. Sampson—181
Scattering of Atoms and Molecules (see **Atomic and Molecular Beams**)
Scattering of Deuterons and Tritons (see also **Nuclear Reactions Induced by Deuterons and Tritons**)
t-t elastic scattering from 1.6 to 2.0 Mev, Dale M. Holm and H. V. Argo—1244(A)
t-t interaction, R. M. Frank and J. F. Gammel—973(A)
Scattering of Electrons and Positrons (see also **Electrons and Positrons**)
Absolute cross sections for Coulomb scattering of 1.00-, 1.75-, and 2.50-Mev electrons, V. Spiegel, Jr., B. Waldman, and W. C. Miller—1244(A)
Collision cross section of N_2 molecules with slow electrons, L. Goldstein and J. M. Anderson—1229(A)
Coulomb scattering of electrons at very small angles, Michael J. Moravcsik—1009
Double scattering of electrons with magnetic interaction. II. Depolarization, H. Mendlowitz and K. M. Case—1751
Elastic scattering of electrons by Li^6 and Li^7, J. F. Streib —1797(A)
Formation of metastable A^+, Kr^+, and Xe^+ by electron impact, Homer D. Hagstrum—1231(A)
Inelastic electron scattering by carbon, D. G. Ravenhall —1797(A)
Interaction of rf electromagnetic waves in isothermal plasmas: Collision cross section of He atoms and ions for electrons, J. M. Anderson and L. Goldstein—1037
Low-energy scattering of electrons by atoms, J. Hammer, H. Malamud, and B. Bederson—1229(A)
Mean free path for discrete electron energy losses in metallic foils, A. W. Blackstock, R. H. Ritchie, and R. D. Birkhoff—1078
Microwave studies of slow electron collision processes in He plasmas, J. M. Anderson and L. Goldstein—1229(A)
Plural scattering of fast electrons, B. Waldman, V. Spiegel, Jr., and W. C. Miller—1244(A)
Theory of ionization probability near threshold, Sydney Geltman—1231(A)
Threshold law for multiple ionization, G. H. Wannier— 1180
Transmission of positrons and electrons, H. H. Seliger —1029
Scattering of Mesons and Hyperons (see also **Mesons and Hyperons; Nuclear Reactions Induced by Mesons and Hyperons**)
Causality in pion-proton scattering, H. L. Anderson, W. C. Davidon, and U. E. Kruse—339
Diffusion chamber study of very slow mesons. III. Scattering of negative pions in hydrogen, M. C. Rinehart, K. C. Rogers, and L. M. Lederman—883
Dispersion relations for pion-nucleon scattering. I. Spin-flip amplitude, Reinhard Oehne—1503
Elastic scattering of positive and negative pions on Al, Aihud Pevsner, James Rainwater, Ross E. Williams, and Seymour J. Lindenbaum—1419
Energy dependence of phase shifts in pion-proton scattering, Jay Orear—288
Phase-shift optical model calculations for elastic scattering of pions on Al, Aihud Pevsner and James Rainwater— 1431
Pion-nucleon scattering calculations in Tamm-Dancoff theory, M. H. Kalos and R. H. Dalitz—1515
Positive pion scattering by H at 260, 300, and 400 Mev, R. S. Margulies—1255(A)
Scattering of mesons by fixed scatterer, Freeman J. Dyson —344
Scattering of pions by H at 165 Mev, H. L. Anderson and M. Glicksman—268
Scattering of pions by nucleons in intermediate coupling, M. H. Friedman, T. D. Lee, and R. Christian—1494
Scattering of positive pions by H at 189 Mev, H. L. Anderson, W. C. Davidon, M. Glicksman, and U. E. Kruse—279
Scattering of 38-Mev positive pions in hydrogen, A. M. Sachs, H. Winick, and B. A. Wooten—1255(A)
Strong pion-pion interaction model applied to pion-nucleon scattering in 1-Bev region, Gyo Takeda—440(L)
Total cross section of H for 150- to 750-Mev positive and negative pions, S. J. Lindenbaum and Luke C. L. Yuan —306
Scattering of Neutrons (see also **Nuclear Reactions Induced by Neutrons**)
Angular distribution of n-p scattering at 17.9 Mev, A. Galonsky and J. P. Judish—121
Atomic distribution in liquid He by neutron diffraction, D. G. Hurst and D. G. Henshaw—994
γ rays excited by inelastic scattering of neutrons in various elements, M. A. Rothman, H. S. Hans, and C. E. Mandeville—83
Inelastic and elastic scattering of 1.7-Mev neutrons, S. D. Bloom, G. N. Glasoe, C. O. Muehlhause, and H. E. Wegner—1248(A)
Inelastic scattering of neutrons from Fe by time of flight, L. Cranberg and J. S. Levin—434(L)
Interatomic correlations in liquid He^4, Louis Goldstein— 981
Low-energy neutron scattering and bound state problem, R. D. Lawson—957(A)
Nonelastic cross sections at 14 Mev, M. H. MacGregor, William P. Ball, and Rex Booth—1793(A)
Nonelastic scattering cross sections for fast neutrons, H. L. Taylor, O. Lönsjö, and T. W. Bonner—174
Phase-shift analysis of nucleon-nucleon scattering at 150 Mev, Shoroku Ohnuma and David Feldman—1241(A)

Scattering of Neutrons (Continued)
Polarization in theory of giant resonances of neutron scattering, A. M. Lane and L. Verlet—956(A)
Polarization of 350-Mev neutrons elastically scattered from nuclei, Robert T. Siegel—437(L)
Production of Y^{88m}, Ba^{137m}, and Hg^{199m} by inelastic neutron scattering, C. P. Swann and F. R. Metzger—1329
Radiation widths in slow neutron resonances, H. H. Landon—1414
Scattering of neutrons by phonons in Al single crystal, B. N. Brockhouse and A. T. Stewart—756(L)
Slow neutron resonance scattering of U^{238}, H. L. Foote, Jr.—1248(A)
Slow neutron resonances in Re, G. Igo—1338
Slow neutron resonances of Mn, Bi, and Se, L. M. Bollinger, D. A. Dahlberg, R. R. Palmer, and G. E. Thomas—126
Small-angle scattering of neutrons by intermediate and heavy nuclei, S. E. Darden, R. B. Perkins, and R. B. Walton—1315
Scattering of Protons (see also **Nuclear Reactions Induced by Protons**)
Analysis of elastic scattering of 31.5-Mev protons, Michel A. Meklanoff, John Nodvik, and David S. Saxon—1805(A)
Elastic p-p scattering in Bev range, Bruce Cork and W. A. Wenzel—962(A)
Elastic scattering of protons at 9.9 Mev, Norton M. Hintz—1794(A)
Elastic scattering of protons from Na^{23}, N. P. Baumann, F. W. Prosser, Jr., and R. W. Krone—1244(A)
Inelastic proton scattering from vanadium, W. W. Buechner, C. M. Braams, and A. Sperduto—1387
Inelastic scattering of 19-Mev protons by O^{18}, W. F. Hornyak and R. Sherr—1409
Inelastic scattering of protons from F^{19}, B. J. Toppel, D. H. Wilkinson, and D. E. Alburger—1254(A)
Inelastic scattering of protons from Li^7, C^{13}, Mg^{26}, and Si^{28}, Homer E. Conzett—1794(A)
Phase-shift analysis of nucleon-nucleon scattering at 150 Mev, Shoroku Ohnuma and David Feldman—1241(A)
Polarization in p-α elastic scattering, Mary Jean Scott and Ralph E. Siegel—1244(A)
Polarization of protons elastically scattered from nuclei, R. M. Sternheimer—886
p-p polarization at 170 Mev, David Fischer and John Baldwin—1445
p-p scattering at 1 Bev, William Rarita—1241(A)
p-p scatterings at 19.6 Mev, J. W. Burkig, Glen E. Schrank, and J. Reginald Richardson—1805(A)
Small-angle p-p scattering at 20 Mev, Herbert N. Royden and Byron T. Wright—1805(A)
Scattering of Radiation (see **Gamma Rays; Radiation; X-Rays**)
Scintillation Counters (see **Methods and Instruments**)
Secondary Emission (see **Electrical Properties**)
Semiconductors
Amphoteric impurity in Ge, W. Crawford Dunlap, Jr.—1629
Broadening of impurity levels in Si, Melvin Lax and Elias Burstein—592
Carrier capture probabilities in Ni-doped Ge, J. F. Battey and R. M. Baum—1550(A); 1634
CdS photorectifier, Lawrence C. Greene—978(A)
Classical theory of cyclotron resonance for holes in Ge, J. M. Luttinger and B. R. Goodman—673
Compound formation between Li and B dissolved in single crystal Si, C. S. Fuller and H. Reiss—1806(A)
Conductivity, Hall effect, and magnetoresistance in n-type Ge, and their dependence on pressure, George B. Benedek, William Paul, and Harvey Brooks—1129
Cu in Ge; recombination center and trapping centers, B. J. Wyluda and R. G. Shulman—1258(A)
Cyclotron resonance in Ge-Si alloys, G. Dresselhaus, A. F. Kip, Han-Ying Ku, G. Wagoner, and Schuyler M. Christian—1218(L)
Deuteron irradiation of Ge at 90°K, D. Kleitman and T. A. Long—1261(A)
Electrical and optical properties of intermetallic compounds. IV. Mg_2Sn, R. F. Blunt, H. P. R. Frederikse, and W. R. Hosler—663
Electrical breakdown in InSb at low temperature, Ralph Bray—1262(A)
Electrical properties of Mg_2Sn at low temperatures, W. R. Hosler and H. P. R. Frederikse—1261(A)
Electrical properties of near-degenerate B-doped Si, R. O. Carlson—1075
Electrical properties of semiconductors Mg_2Si and Mg_2Ge, C. R. Whitsett and G. C. Danielson—1261(A)
Electrolytic etching at small-angle grain boundaries in Ge, S. G. Ellis—1140
Excess noise in plastically deformed Ge, James J. Brophy—1261(A)
Exchange effects in spin resonance of impurity atoms in Si, G. Feher, R. C. Fletcher, and E. A. Gere—1784(L)
Faraday effect in Ge at room temperature, Richard R. Rau and M. E. Caspari—632
Fast-neutron bombardment of GaSb, J. W. Cleland and J. H. Crawford, Jr.—1614
Field effect in Si, S. Penman and W. L. Brown—1259(A)
Hall effect and conductivity of InSb, H. J. Hrostowski, F. J. Morin, T. H. Geballe, and G. H. Wheatley—1672
Hall effect and magnetoresistance in n-type Ge, W. M. Bullis and W. E. Krag—1258(A)
Hall effect in gray Sn filaments, E. E. Kohnke and A. W. Ewald—1251(A)
Hall effect noise, James J. Brophy and Norman Rostoker—754(L)
Impurity band in semiconductors with small effective mass, Frank Stern and Robert M. Talley—1638
Infrared properties of Se, R. S. Caldwell and H. Y. Fan—1251(A)
Interaction of impurities and mobile carriers in semiconductors, Guy W. Lehman and Hubert M. James—1698
Ion pairing involving Li and Ge and Si, F. Morin, Howard Reiss, and C. S. Fuller—1807(A)
Ionization of H in Ge and Si, Howard Reiss—1806(A)
Ionized impurity scattering in semiconductors, Frank S. Ham—1251(A)
Lifetime of electrons in p-type Si, G. Bemski—523
Longitudinal photomagnetoelectric effect in Ge, Gerhart Groetzinger and Jack Aron—978(A); Jack Aron and Gerhart Groetzinger—1128
Magnetic susceptibility of Ge, D. K. Stevens, J. W. Cleland, J. H. Crawford, Jr., and H. C. Schweinler—1084
Magnetic susceptibility of impurity-trapped electrons and holes in semiconductors, E. Mooser—1589
Magnetoresistance and mobility of Ge-Si alloys, M. Glicksman—1258(A)
Magnetoresistance of Ge-Si alloys, Maurice Glicksman—1146
Measurement of bulk and surface recombination by photoconductance, H. M. Bath and M. Cutler—1259(A)
Mechanical properties of Si, Ge, and ZnO whiskers, C. L. Pearson, W. T. Read, Jr., and W. L. Feldman—1251(A)
Minority carrier extraction in Ge, Ralph Bray—1047

Neutron-irradiated Si, Thomas A. Longo and David Kleitman—1260(A)
Nuclear magnetic resonance in semiconductors. I. Exchange broadening in InSb and CaSb, R. G. Shulman, J. M. Mays, and D. W. McCall—692
Observation of quantum effects in cyclotron resonance, R. C. Fletcher, W. A. Yager, and F. R. Merritt—747(L)
Plasma resonance in crystals: Observations and theory, G. Dresselhaus, A. F. Kip, and C. Kittel—618
Plasma resonance in semiconductor crystals, G. Dresselhaus, A. F. Kip, and C. Kittel—1262(A)
Polarization of impurities in Ge, F. D'Altroy and H. Y. Fan—1260(A)
Precipitation of Cu in Ge, R. A. Logan—615
Precipitation of Cu in plastically deformed Ge, A. G. Tweet—1260(A)
Quantum yield of CdS photovoltaic cell, R. E. Marburger, D. C. Reynolds, L. L. Antes, and R. S. Hogan—978(A)
Preparation and electrical properties of Bi_2Te_3, T. C. Harman, S. E. Miller, and H. L. Goering—1262(A)
Pressure dependence of resistivity, Hall coefficient, and energy gap for InAs, Julius H. Taylor—1593
Properties of Ge doped with Mn, H. H. Woodbury and W. W. Tyler—659
Properties of Zn-doped Ge, H. H. Woodbury and W. W. Tyler—1259(A)
Pulse characteristics of CdSe crystals, T. Fields, E. J. Schillinger, and J. Kenski—964(A)
Recombination of radiation from Si, J. R. Haynes—1259(A)
Recombination processes in Te, David Redfield—1094
Reduction of charge carrier concentration in InSb at 4.2°K by strong magnetic field, R. W. Keyes and R. J. Sladek—1262(A)
Reflectivity of several crystals in far infrared region between 20 and 200 microns, Hiroshi Yoshinaga—753(L)
Scattering of carriers from doubly charged impurity sites in Ge, W. W. Tyler and H. H. Woodbury—1259(A)
Spin-orbit coupling effects in zinc blende structures, G. Dresselhaus—580
Statistics and galvanomagnetic effects in Ce and Si with warped energy surfaces, Benjamin Lax and J. G. Mavroides—1650
Surface potential and surface charge distribution from semiconductor field effect measurements, W. L. Brown—590
Surface states on Si, H. Statz, G. A. deMars, L. Davis, Jr., and A. Adams, Jr.—1260(A)
Surface trapping in Ge, H. A. Gebbie and K. Blodgett III—970(A)
Temperature dependence of elastoresistance in *n*-type Ge, Robert W. Keyes—1104
Thermal acceptors in vacuum heat-treated Ge, Robert L. Hopkins and Edward N. Clarke—1786(L)
Thermal defects in Si, C. J. Gallagher—1259(A)
Thermoelectric power in semiconductor showing high-temperature degeneracy, V. A. Johnson—1251(A)
Thresholds for electron-bombardment-induced lattice displacements in Si and Ge, Paul Rappaport and Joseph J. Loferski—1261(A)
Transverse field effects in PbS, D. E. Martz and R. S. Witte—1808(A)
Trapping of minority carriers in Si. II. *n*-type Si, J. R. Haynes and J. A. Hornbeck—606
Valence bond calculations of acceptor energies in Si and Ge, R. G. Shulman—1260(A)
Visible light from Si *p-n* junction, Roger Newman—700

Shock Waves (see **Fluid Dynamics**)

Solid State (see **Crystalline State**)
Solutions (see **Liquids**)
Sound (see **Acoustics**)
Spallation (see **Nuclear Reactions**)
Spark Discharge (see **Electrical Discharges**)
Specific Heat (see **Thermal Properties**)
Spectra, Atomic (see **Atomic Structure and Spectra**)
Spectra, General
Flame zone spectroscopy of solid propellants. II, R. Rekers and D. S. Villars—963(A)
Stark fields from ions in plasma, A. A. Broyles—1181
Spectra, Molecular (see **Molecular Structure and Spectra**)
Spectra, Nuclear (see **Nuclear Spectra**)
Spectroscopy Technique (see **Methods and Instruments**)
Spinor Fields (see **Field Theory**)
Standards (see **Constants, Standards, Units**)
Stark Effect (see **Atomic Structure and Spectra**)
Statistical Mechanics and Thermodynamics
Connection between superfluidity and superconductivity, M. R. Schafroth—502
Critical phenomena in triethylamine-water system, F. Kohler and O. K. Rice—965(A)
Derivation from Boltzmann's equation of similarity laws for ionized gases, T. E. VanZandt—1235(A)
Electron correlation, Joseph E. Mayer—1579
Fluctuations on damped transmission line, C. W. McCombie—444
Inclusion of Coulomb interactions in Boltzmann equations, H. Dreicer and W. P. Allis—1234(A)
Magnetic second-order transitions, K. J. Tauer and R. J. Weiss—1223(L)
Nonequilibrium nature of superfluid state, S. T. Butler and J. M. Blatt—495
Quantum-statistical derivation of transport equation for mixtures of dilute gases with molecules of arbitrary spins, A. W. Saenz—975(A)
Second virial coefficients of He^3-He^4 mixtures between 2 and 4°K, William E. Keller—1021
Significance of nuclear spin echo experiments for foundation of statistical mechanics, Jerome Rothstein—1791(A)
Statistical mechanics of cathode sputtering, Don E. Harrison, Jr.—1234(A)
Statistical mechanics of mixtures of isotopes, G. V. Chester—446
Statistical mechanics of rotating buckets, J. M. Blatt, S. T. Butler, and M. R. Schafroth—481
Superconductivity of charged ideal Bose gas, M. R. Schafroth—463
Superfluidity of ideal Bose-Einstein gas, J. M. Blatt and S. T. Butler—476
Thermodynamics of irreversible processes and Overhauser nuclear polarization effect, W. A. Barker and A. Mencher—1224(L)

Statistical Methods (see **Mathematical Methods**)
Superconductivity
Angular correlation of annihilation radiation in superconducting Pb, R. Stump—1256(A)
Connection between superfluidity and superconductivity, M. R. Schafroth—502
Effect of pressure on superconducting transition temperature of Tl, J. Hatton—1784(L)
Phenomenological equations for superconductors, M. R. Schafroth and J. M. Blatt—1221(L)
Properties of In and Tl at low temperatures, C. A. Swenson—1607
Relative absorption of 10 Mc/sec longitudinal sound waves in superconducting polycrystalline Sn rod, L. Mackinnon—655
Search for Hall effect in superconductor. II. Theory, H. W. Lewis—641

Superconductivity (Continued)
Superconductivity at mm wave frequencies, Gilbert S. Blevins, Walter Gordy, and William M. Fairbank—1215(L)
Superconductivity of charged ideal Bose gas, M. R. Schafroth—463
Superconductivity of Zr alloys, B. T. Matthias and E. Corenzwit—626
Thermal conductivity of In-Tl alloys in normal and superconducting states, Norman E. Phillips—1719
Thermal conductivity of superconducting Pb below 1°K, B. R. Felix, L. Passell, and H. B. Silsbee—1808(A)
Ultrasonic attenuation in superconducting and normal-conducting Sn at low temperature, H. E. Bömmel—758(L)
Supersonics (see **Fluid Dynamics**)

Thermal Conductivity (see **Thermal Properties**)
Thermal Diffusion (see **Diffusion**)
Thermal Expansion (see **Thermal Properties**)
Thermal Properties
Magnetic and thermal properties of UI_3 at liquid He temperatures, I. D. Roberts and R. B. Murray—650
Properties of In and Tl at low temperatures, C. A. Swenson—1607
Stored energy release in graphite irradiated at low temperatures, S. B. Austerman—1807(A)
Temperature anomalies in properties of liquid water, W. Drost-Hansen and H. W. Neill—1800(A)
Thermal conductivities of gases and gaseous mixtures, J. M. Davidson—966(A)
Thermal conductivity of Al at low temperatures, L. Passell, B. R. Felix, and H. B. Silsbee—1808(A)
Thermal conductivity of In-Tl alloys in normal and superconducting states, Norman E. Phillips—1719
Thermal conductivity of neutron-damaged graphite, Ned S. Rasor and John E. Hove—1806(A)
Thermal conductivity of superconducting Pb below 1°K, B. R. Felix, L. Passell, and H. B. Silsbee—1808(A)
Thermal diffusivity of U from room temperature to 1000°C, P. H. Sidles—1256(A)
Variation with temperature of thermal conductivity of seven alkali halides, Kathryn A. McCarthy and Stanley S. Ballard—969(A)

Thermal Radiation (see **Radiation**)
Thermionic Emission (see **Electrical Properties**)
Thermodynamics (see **Statistical Mechanics and Thermodynamics**)
Thermoelectric Effect (see **Electrical Properties; Semiconductors**)
Thermoluminescence (see **Luminescence**)
Thermomagnetic Effect (see **Magnetic Properties**)
Total Cross Sections (see **Electrons and Positrons; Nuclear Reactions**)
Transmutation (see **Nuclear Reactions**)

Uncertainty Principle (see **Quantum Mechanics**)
Units (see **Constants, Standards, Units**)

Vacuum Tubes (see **Methods and Instruments**)
Van der Waals Forces (see **Molecular Structure and Spectra**)
Viscosity (see **Liquids**)

Wave Mechanics (see **Quantum Mechanics**)
Work Function (see **Electrical Properties**)
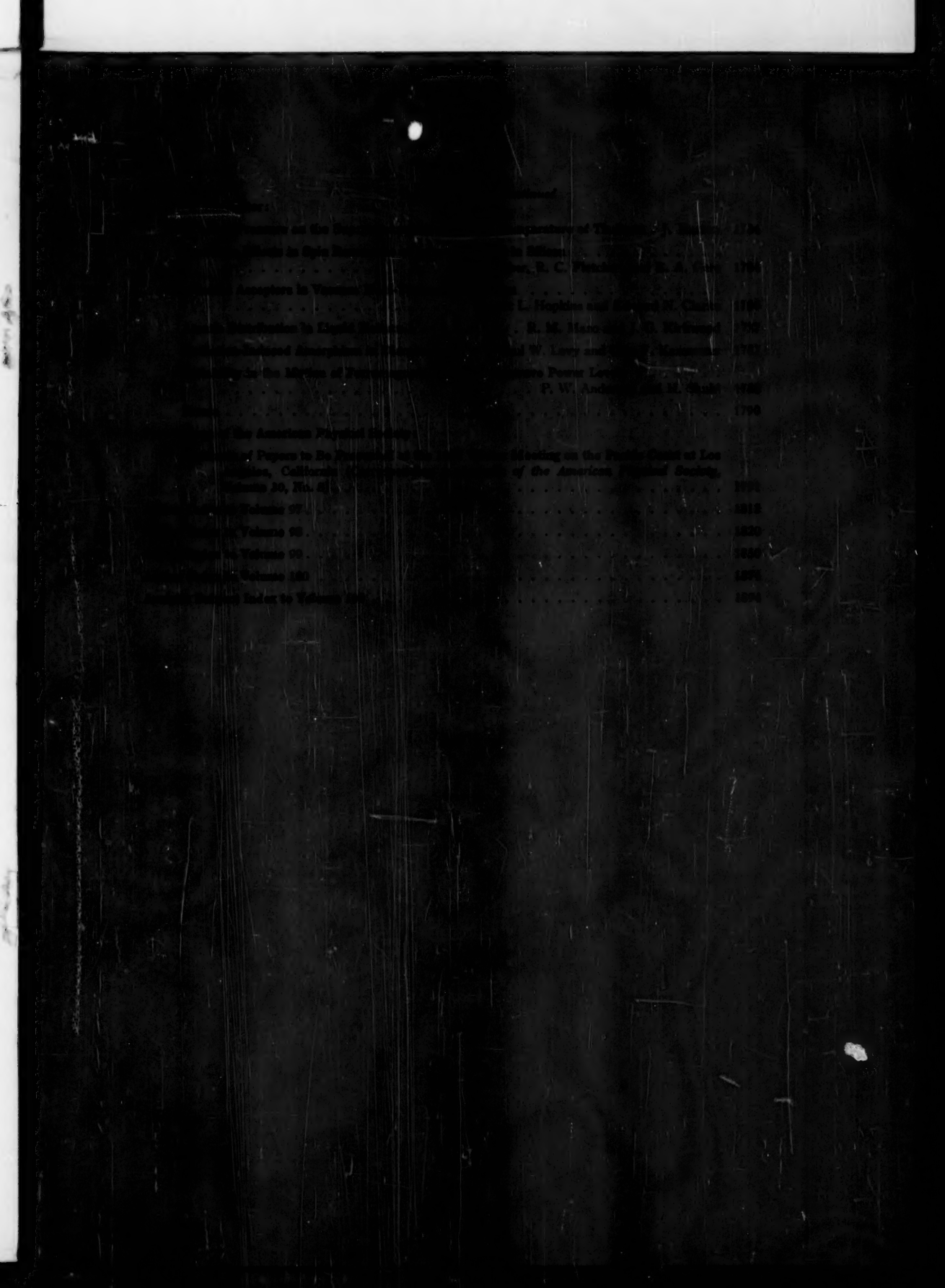
X-Rays
Auger effect in Fe, Ni, Cu, and Zn, Charles E. Roos—1267(A)
Effect on x-ray fine structure of deviations from a Coulomb field near nucleus, A. L. Schawlow and C. H. Townes—1273
K-series fluorescence yields of A^{39}, Cu^{65}, and In^{115}, G. R. Harrison, R. C. Crawford, and J. I. Hopkins—841
M_{IV} and M_V absorption lines and edges of $_{64}$Gd, $_{66}$Dy, and $_{70}$Yb, Hassan F. Zandy—1549(A)
Mesonic x-rays from capture of cosmic-ray μ mesons in chemical compound, A. Fafarman and M. H. Shamos—874
Soft x-ray absorption of Te and yitreous and metallic Se, M. Parker Givens, Charles J. Koester, and William L. Goffe—1112
Soft x-ray emission spectrum of Ge, D. E. Bedo and D. H. Tomboulian—1257(A)
Tc *K* x-ray spectrum, George L. Rogosa and William F. Peed—1763
X-ray lattice constant of BaO, Robert J. Zollweg—671